Report on Pilots

CHPM2030 Deliverable D6.2

Version: May 2019

CHPM2030

This project has received funding from the European Union's Horizon 2020 research and innovation programme under grant agreement nº 654100.

Author contact
Tamás Miklovicz
La Palma Research Centre
El Fronton 37.
38787 Garafia
Spain
Email: tamas.miklovicz@lapalmacentre.eu

Published by the CHPM2030 project, 2018
University of Miskolc
H-3515 Miskolc-Egyetemváros
Hungary
Email: foldshe@uni-miskolc.hu

CHPM2030 DELIVERABLE D6.2

Report on Pilots (compiled from 5 reports)

Summary:

This report presents an evaluation framework that facilitates the investigation of study areas for CHPM technology. The same methodology was applied to five areas (South West England, Portuguese Iberian Pyrite Belt, Romania Beius basin and Bihor mountains, Nautanen and Kristineberg in Sweden) evaluating their CHPM potential and characteristics. A European outlook for CHPM prospective locations has also been prepared, covering 24 countries.

Authors:

Tamas Miklovicz, *Engineering Geologists*, La Palma Research Centre, Spain.

Paul A J Lusty, *Principal Economic Geologist*, Richard B Haslam, *Structural Geologist*, Richard A Shaw, *Economic Geologist*, Eimear A Deady, *Minerals Geoscientist*, Paul Williamson, *Senior Geophysicist*, British Geological Survey.

Elsa Cristina Ramalho, *Geological Engineer*, João Xavier Matos, *Economic Geologist,* João Gameira Carvalho, *Geophysicist*, Portuguese National Laboratory of Energy and Geology.

Diana Perșa, *Researcher*, Ștefan Marincea, *Senior Researcher*, Delia Dumitraș, *Senior Researcher,* Cătălin Simion, *Researcher*, Geological Institute of Romania

Gerhard Schwarz, *Geophysicist*, Benno Kathol, *Geologist,* Magnus Ripa, *Geologist*, Bo Thunholm, *Hydrogeologist* Edward P Lynch, *Geologist,* Johan Jönberger, *Geophysicist*, Geological Survey of Sweden.

Domenico Marchese, *Project Officer*, Anita Demény, *Project Officer*, Isabel Fernandez, *Executive Director*, European Federation of Geologist

This project has received funding from the European Union's Horizon 2020 research and innovation programme under grant agreement nº 654100.

TABLE OF CONTENT

LIST OF FIGURES

LIST OF TABLES

LIST OF ABBREVIATIONS

CHPM: Combined Heat Power and Metal extraction technology
CHPM2030: The EU Horizon 2020 funded project under Grant Agreement nº 654100
EFG: European Federation of Geologists
LTP: Linked Third Parties
TRL: Technology Readiness Level
EC: European Commission
HS: Horizon Scanning
BGS: British Geological Survey
SGU: Geological Survey of Sweden
LNEG: Portuguese Geological Survey
IGR: Geological Institute of Romania
LPRC: La Palma Research Centre
RBINS: Royal Belgian Institute of Natural Sciences
EGS: Enhanced or Engineered Geothermal System
HDR: Hot Dry Rock
WP: Work Package

0. Preface

CHPM technology is a low-TRL, novel concept that needs further nurturing and future-oriented thinking. WP6 coordinates these forward-looking efforts and aims to set the ground for subsequent pilot implementation by working on three future-oriented tasks: mapping convergent technology areas, study pilot areas, develop research roadmaps. These three areas of study are grouped under three WP6 subtasks: Task 6.1 Horizon scanning & Visions; Task 6.2 Preparation for pilots; Task 6.3 Roadmapping.

The objective of Task 6.1 task is to start up a technology visioning process for the further development of the CHPM concepts with the help of horizon scanning, a Delphi survey and a Visioning process. The outcome of this combined exercise will be the identification of trends and new concepts defining plausible targets where the CHPM technology could evolve in the future. The realisation of these targets will be made plausible with the help of an array of convergent technologies that can support their implementation by 2030/2050.

The aim of Task 6.2 is to support the development of technology and economic feasibility for a pilot implementation of such system, by evaluating potential pilot areas according to a harmonized framework. This evaluation will also be used for starting up discussions on the financing of such investments. The potential areas, or study areas are: SW England, Portuguese Iberian Pyrite Belt, Romania Beius area, Sweden (Nautanen, Kristineberg). In addition, EFG has been working on EU level in order to set up a spatial database on prospective locations for CHPM technology with the help of EFG' Linked Third Parties (LTPs).

Task 6.3 is focusing on the development of a roadmap from 2019 through 2030 to 2050. The short-term, 2030 aspect is to prepare for early implementation and to provide a timeline and direct support to the first pilots. The long-term aspects aim to provide revision and updates in response to unforeseen, emerging phenomena, supporting breakthrough research for future CHPM development.

1. Executive summary

There are many innovative geothermal or mineral related projects in the EU, but CHPM2030 is unique for tackling both mineral raw material dependency and sustainable energy supply of the EU, under a single interlinked process. The concepts that have been developed within the framework of this project aim to increase the economics of deep geothermal, especially Enhanced Geothermal Systems, projects by extracting valuable metals from the geothermal brine. The first pilot applications are envisioned by 2030 and the full-scale applications by 2050.

The Roadmapping and Preparation for Pilots Work Package (WP6) utilises the synergetic combination of foresight methods (Deliverable 6.1) and evaluates study areas (Deliverable 6.2) in order to deliver a roadmap, a strategic plan, an agenda for 2030 and 2050 (Deliverable 6.3), that leads to the desired end-state of the CHPM technology.

This report, compiled from 6 documents, presents 1) an evaluation framework that facilitates the investigation of study areas for CHPM technology; 2) the description of areas from 4 countries, concerning their CHPM potential and characteristics: Cornwall in South West England, Portuguese Iberian Pyrite Belt, Beius basin and Bihor mountains in Romania, Nautanen and Kristineberg in Sweden; 3) an European outlook for CHPM prospective locations, covering 24 countries.

The baseline for this study was presented in WP1, Task 1.2 Knowledge Gaps and Updating Information: CHPM2030 Deliverable 1.2 Report on Data Availability (Schwarz et al. 2016). Here the focus was on data availability, whereas in Task 6.2 the focus was on the detailed evaluation of data. In Task 6.2 the first activity was the development of a harmonised study area evaluation template. This was an iterative process with the involvement of the technology developers and the study area representatives at consortium meetings, workshops and fieldtrips.

The final evaluation template outlines a group of important topics that must be taken into account when evaluating the CHPM potential at a given area. The topics are the following: geology and geophysics of the prospective area, deep metal enrichment, EGS potential integrated 3D-4D model, information for CHPM technological elements (underground heat

exchanger (deep metal enrichment + potential reservoir), production and injection wells, Electrolytic metal recovery and gas diffusion electro-precipitation, power plant, salt gradient power generation), operational characteristics (environmental, social and political background, financial aspects), with numerous subtopics and a short description.

The report on south-west England, considered the availability of geoscience information, the geological environment, geothermal characteristics, potential for deep metal enrichment, and technical, environmental, social and regulatory factors that could influence the future development of CHPM extraction technology in the region. South-west England was selected as the UK CHPM2030 study area as it is a major magmatic province, with high heat production, and hosts extensive polymetallic mineralisation. The study area is extensively mineralised, hosting the highly productive Camborne-Redruth mining district. The Carnmenellis granite was the focus of a major geothermal experiment, the UK hot dry rock (HDR) research and development programme that ran for more than 15 years, and produced a huge amount of data and analysis on the geothermal energy potential of south-west England. A contemporary project, operated by Geothermal Engineering Ltd, is the United Downs Deep Geothermal Power (UDDGP) project, located near Redruth. The temperature of the Carnmenellis granite at 5 km depth is estimated to be 200^{o}C. Cornish granites typically have very low primary permeability, but relatively high hydraulic conductivity as a result of faults and joints. Fluid circulation is evident in the local mines where thermal, saline brines discharge from cross-course structures. It is concluded that a dynamic system driven by convective and hydrodynamic forces has allowed continuous water-rock reaction to occur within the upper 3–4 km of the currently exposed Carnmenellis granite. These brines contain reported lithium concentrations of up to 125 mg/l^{-1}, probably as a result of the breakdown of mica during fluid-rock interaction. Preliminary modelling of the Cornubian Batholith has been undertaken to improve understanding of its properties relevant to geothermal energy development. A regional model was constructed to understand the spatial relationship of key geological parameters that were used for the development of subsequent site-scale models. One of the site-scale models is based on data from the HDR project site, and has a depth range of -1000 to -3000 mbsl. The model is centred on the HDR project boreholes, incorporating fracture data from two of the deep boreholes and site-specific hydrological properties. Data and assumptions about the fracture network were used to generate three discreet fracture

network (DFN) models for the HDR project reservoir. These were up-scaled to include porosity and permeability in order to understand the potential flow pathways within the reservoir. The second site-scale model considers an area located to the NW of the Carnmenellis granite, where the current UDDGP project is located. The target geothermal reservoir is still considered to be the Carnmenellis granite, and the model covers a volume of 12 km^3, with a depth range of -1500 to -5500 mbsl. In summary south-west England, and specifically Cornwall, is an excellent location for a pilot-scale CHPM system. It has the essential prerequisites of a proven geothermal energy resource and abundant polymetallic mineralisation. It is one of the best surveyed and most data-rich parts of the UK, with a long history of mineral development and geothermal research. The local government and communities appear supportive of deep geothermal resource development, and it has a major, active co-funded deep geothermal project.

The report from Portugal provides an update of the geoscientific data and information on the South-West Iberian Pyrite Belt (IPB), a Variscan metallogenic province with massive sulphides deposits. This active mining region, with vast amount of geological information available, has a good prospect of mineralization at deeper levels, therefore of interest for CHPM technology. The chosen study area is Never-Corvo Mine due to the available 3D geological, geophysical models and its relation with EGS potential. The deposit consists of 7 massive sulphide ore lenses with copper, zinc, and lead mineralizations. The report presents the relevant geological, geophysical, mineralogical characteristics of the area to investigate the feasibility of the implementation of CHPM technology at Never-Corvo. The main interest is the existence of the deep mineralization, near the operating mine. The coproduction of energy and minerals would extend the lifetime of the mine operation. The study also presents emerging factors, such as the energy transition, financial requirements and possibilities, advancement in 3D modelling of the deposit, challenges to generate data about the deeper levels (>1.2 km), environmental, social and political background, and the possible future agreements between the mining management and the Portuguese government. There was also a synergy with the ongoing mining operations, parallel EU funded projects (SmartExploration, Explora), and the CHPM study are evaluation.

At the Romanian study areas, the Beius basin and the Bihor Mountains were investigated by IGR due to the favourable geothermal and mineral potential of the areas for CHPM

technology. In the Beius Basin, the geothermal potential is high due to the thin crust, as a result of a regional extension in the Pannonian Basin, resulting high heat flow (above 80mW/m2) and elevated geothermal gradient (5.6-6.2 °C/100 m). Deep mineralization is also expected due to intrusive magmatic bodies within the Beius Basin. On the other hand, the Bihor mountains are also of interest due to the mineral deposits, which is part of the Banatitic Magmatic and Metallogenetic Belt metallogenic province. The granodiorite – granite plutonic body, formed skarn mineralisation at the contact with Mid- and Upper Triassic limestones. The identified deposit types of interest are 1) iron, boron, bismuth, molybdenum bearing skarns, and related vein occurrences with copper, zinc, lead sulphides, 2) Brucite deposits from Budureasa and Pietroasa, 3) Borate deposit from the contact of aureole of the Pietroasa granitoid body through metasomatic processes, 4) tungsten bearing and base metal skarns at Baita Bihor. Furthermore, there is an ongoing district heating system in Beius town, whose operator showed interest for the CHPM technology in the future. This shows public support for geothermal applications, indicated geological potential for heat and metals, and industry interest for the additional metal extraction technology.

In Sweden, two CHPM test sites are proposed for further investigations: These are the Kristineberg area in the Skellefte district and the Nautanen area in the Northern Norrbotten ore province. The Kristineberg area is known for its volcanogenic massive sulphide deposits (VMS). Zinc is the main target, though in some areas copper and gold ores are mined. The area was studied by geophysical methods down to 12 km and by drilling down to about 1400 m below surface. High resolution reflection seismic data outlined the VMS ore bodies and associated structures. However, the completed seismic surveys also have shown that considerable efforts were needed to acquire high quality data, preferably by 3D surveys. The operations in the Kristineberg mine have reached a depth of 1200 m, 31 million tons of ore were mined, reserves are 5 million tons and resources about 13 million tons. The combined grades of mined ore, reserves and resources are 3.9 % zinc, 0.7 ppm gold, 44 ppm silver, 0.9 % copper and 0.4 % lead. Mineralisation in the Nautanen area are part of several hydrothermal copper-gold occurrences related to the ironoxide-copper-gold (IOCG) mineral deposits. The “Nautanen North” deposit has an indicated resource of 9.6 million tons of ore grading at 1.7 % copper, 0.8 ppm gold, 5.5 ppm silver and 76 ppm molybdenum, with additional inferred resources of 6.4 million tons grading at 1 % copper, 0.4 ppm gold, 4.6 ppm

silver and 41 ppm molybdenum. In both mining areas, the installation of a CHPM system is highly challenging. The low geothermal gradient of only about 16 °C/km and heat flow density of about 50 mW/m^2, typical to the Fennoscandian Shield, demand large borehole depths of at least 5 to 7 km. At such depths, there is very limited information available about geological structures, deep-seated fluids, and hydraulic conductivity of the crystalline bedrock. However, with the help of integrated geophysical studies, i.e., deep seismic and magnetotelluric measurements and in cooperation with the mining industry, many advancements were made facilitating the CHPM potential in future projects.

The European outlook for prospective CHPM potential has been prepared with the help of the EFG's Linked Third Parties, the national geological associations. In total there were 24 countries covered: Belgium, Czech Republic, Finland, France, Germany, Greece, Hungary, Ireland, Italy, Netherlands, Poland, Portugal, Serbia, Slovenia, Spain, Switzerland, Ukraine, Austria, Croatia, Cyprus, Luxembourg, Slovakia, Sweden the United Kingdom. In each country, there were 3 tasks: 1) Area selection: define an area most likely to be a future CHPM candidate; 2) Basic area evaluation: the task continued with the evaluation of the basic characteristics of the selected areas; 3) CHPM characteristics: this task considered a deeper investigation and data evaluation of the most likely CHPM sites. This was a rough screening for areas that may be further CHPM site. Areas selected as "type B", has the potential for "CHM" technology and use the delivered metal extraction technological couples with direct heating application. Areas selected as "type A" may be actual areas for a full "CHPM" application, after a thorough geological, geophysical exploration that can show the ultra-deep mineral enrichment. This work has shown a number of areas that has potential to develop a CHPM site, but the lack of publicly available data may still represent a bottleneck to improve the knowledge needed implement CHPM technology at any of the selected sites. The identified areas have been gathered in a publicly available online database: http://bit.ly/CHPMinfoplatform.

It has been found that a new type of exploration mindset is required for undertaking such survey. Exploration at areas for combined heat, power and metal extraction will have to use the traditional surveying and interpretation methods, but it must improve on them, and combine tools from both geothermal and mineral exploration campaigns, to create a comprehensive strategy. The first step for that was the creation of the evaluation template,

which served as a “checklist” for important characteristics to consider when looking into CHPM potential. The 5 study areas from 4 countries have been evaluated according to this new strategy and each area has the potential to develop actual CHPM pilots in the future. Each area has its unique characteristics, and all have substantial amount of information available publicly from the top 1 km of the crust, providing a good understanding of the near surface. The next challenge thus is to extend this understanding at deeper levels, run new, preferably 3D surveys, further advance each predictive 3D models for a downwards continuation. With the help of these study reports and the European outlook study, the following items have now been clarified: 1) the information available at each area, 2) the CHPM potential based on this geoscientific data, 3) remaining gaps to be overcome in the future. Based on this knowledge, the idea of pilot implementation can be further advanced through concrete recommendations in the CHPM2030 roadmaps (CHPM2030 Deliverable 6.3). The next exploration/research projects can continue, based on these recommendations and the CHPM pilot readiness level can be achieved by 2030.

2. Introduction

Work Package 6 Roadmapping and Preparation for Pilots aims to set the ground for CHPM pilot implementation following the EC-funded period. Such follow-up planning is necessary, because CHPM2030 is a low-TRL research project, based on a novel idea that needs further nurturing and support beyond the immediate duration of the project. This is done through the creation of a technology roadmap that outlines desired future visions and targets and the actions that will need to be made in order to arrive to this vision (pilot and commercial readiness level by 2030 and 2050 respectively). This is the main result of the work package. In order to deliver this roadmap document, several complementary steps needed to be undertaken along Task 6.1 and Task 6.2 (Figure 1).

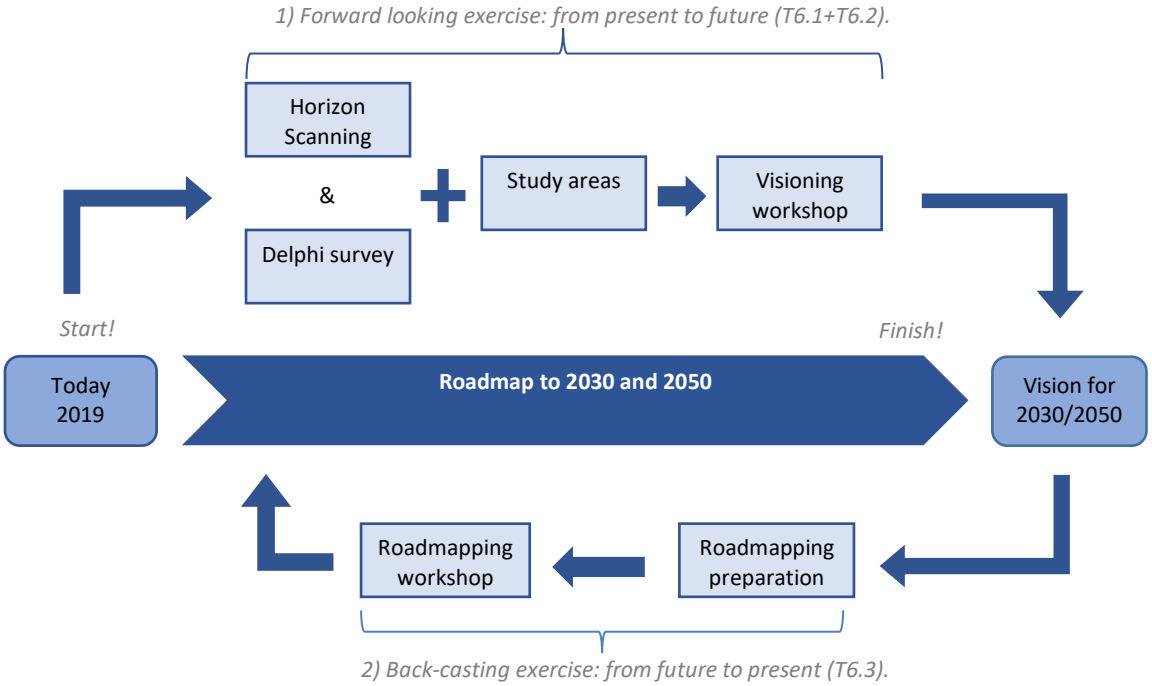

Figure 1: WP6 Roadmapping and Preparation for Pilots workflow

The first forward looking exercise started from the present technological baseline towards the future, with the help of Horizon Scanning, Delphi survey, Visioning. Horizon Scanning provided the present technological baseline, with an expert workshop on mapping key interest areas and gap analysis. The results have been formulated into Delphi statements covering various aspects of the technology. The 2-round Delphi provided more pieces of the puzzle of what the future may be at key interest areas. The next step was the organisation of

a Visioning workshop where the Experts defined preferred targets for two timeframes to enable the technology implementation at TRL6-7 by 2030, and TRL8-9 by 2050. The sum of the targets is the Vision that describes the desired targets in the future. This line of activities includes Task 6.2, investigating potential pilot areas (Cornwall in South West England, Portuguese Iberian Pyrite Belt, Beius basin and Bihor mountains in Romania, Nautanen and Kristineberg in Sweden), with a European outlook for the application of CHPM technology in the future, with the development of a harmonised study area evaluation template document.

The second line of activities started at the desired vision in the future, and used a roadmapping workshop and back-casting exercise to identify, what actions need to be taken in order to arrive to the desired future destination (Vision), with the pre-assessed study areas and other prospective locations across Europe (as identified by EFG LTPs), through emerging issues (Delphi) from the technology baseline of today (HS). The roadmap document is building on Deliverables 6.1 and 6.2.

In WP6, the two main lines of activities were the preparation and implementation the Horizon Scanning, the 2-round CHPM2030 Delphi survey, Visioning workshop; and the formulation of a CHPM area evaluation template and framework to investigate study areas and to select and evaluate European areas for CHPM potential, with parallel development at each study areas and the review and integration of *WP1 Methodology framework definition* baseline.

3. Methodology and objectives

3.1. Summary of WP1 findings

In WP1, under Task 1.2 Knowledge gaps, updating information the focus was on data availability and screening for potential areas. In Deliverable 1.2 Report on Data Availability (Schwarz et al. 2016), a brief overview was provided about the four major ore districts in Europe: SW England, Southern Portugal, NW Romania and Central and Northern Sweden.

The report aimed at setting the ground for identifying future CHPM sites through investigating the following points: previous research and unprocessed data (drilling, geophysics); structural settings, geometry, composition of ore deposits; current 3D metallogenic (predictive) models; extending existing models to greater depth; understanding knowledge gaps and limitations; mineralisation, deep seated faults, fracture zones; past and present tectonics, deep fluid flow,

heat flow, temperature. Nevertheless, some major questions left to be answered, mostly related to the uncertainties coming from the CHPM relevant depths, spatial distribution of structures and lithologies, details of mineralisation, physical properties and their characterization (temperature, electrical conductivity, seismic velocity).

The four country reports (*Appendices D1.2.1 to D1.2.4*) describes that the general geology of each selected study area, future potential pilots, are well known and documented. These selected areas are located in three large metallogenic provinces in Europe:

- Precambrian Fennoscandian Shield province, as for the Swedish study area;
- Late Paleozoic Variscan province, as for Cornwall and southern Portuguese study areas;
- Mesozoic-Cenozoic Alpine province, as for NW Romanian study area.

These selected areas have been investigated according to the CHPM technology objectives, focusing on the geothermal potential geological data and description of the mineralized areas. The second also includes description of ongoing geophysical efforts for increasing resolution at CHPM relevant depths (3-6 km) at the mineralised zones.

Beside the four study areas, the Linked Third Parties (LTPs) of the European Federation of Geologists (EFG) attempted to create an inventory of drill holes where temperatures exceeded 100°C and/or metal enrichment was encountered at depth. This investigation was performed at 24 European Countries. The National Associations collected publicly available geological data at national level on deep drilling programs, geophysical and geochemical explorations and other relevant geo-scientific data on geothermal potential and deep mineral enrichment (Appendix D1.2.5 Report on Data Collection by the EFG Linked Third Parties).

As a general observation, geological data at deeper levels (>1km) is very limited. However, at shallower levels, the geology, mineralisation, fluids, geothermal potential is well documented at the investigated sites, which is freely and openly available. It was identified that the structural information and the knowledge of the physical state of the upper crust have significant improvement in order meet CHPM requirements.

In WP6, under *Task 6.2 Preparation for pilots* the focus shifts towards Data Evaluation for CHPM potential of the study areas and Europe wide. Since there was already a good

description on the geology, mineralization, geothermal potential and CHPM relevant data availability of the study areas and LTPs (D1.2 Report on Data Availability), the core question in Task 6.2 was the following: how to advance the study area evaluation from the solid baseline which has been provided in WP1.

In addition to the previous point, there has been new advancements in the CHPM technology by the Consortium, with better understanding on the data requirements of the technological components (metal mobilisation and extraction, baseline economics, environmental considerations and system integration). Parallel to the technological development, there has been also new insight from the foresight process from Task 6.1.

Since many of the study areas are at active mining and/or geothermal development areas, since the submission of D1.2, new results and geological data become available, that has been used in this study.

Therefore, in Task 6.2 the first objective here was to gather ideas, strategies on the core question of T6.2: how to advance the study area evaluation from the solid baseline which has been provided in WP1.

3.2 Developing the evaluation template

This subtask represents the short-term planning to "set the ground for subsequent pilot implementation" and builds on the result of D1.2 Report on Data Availability (including South West England, Portugal, Iberian Pyrite Belt, Romania, Sweden, Report on data availability of drill holes: Europe integrated Annexes) and D2.4 Report on Overall System Dynamics. In Task 6.2 Preparation for Pilots the focus is on Data Evaluation for CHPM potential of the Study Areas and Europe wide. The objective of Task 6.2 is to support the development of technology and economic feasibility for pilot implementation of such system, in order to generate discussion on financing such project. This objective is engaged through the following actions:

- Developing a framework that harmonise and guide the area evaluation for CHPM prospect,
- In-depth evaluation of of four areas according to the evaluation framework,
- Selection and basic evaluation of European potential areas by the EFG LTPs

- Creation of a spatial database on European scale of prospective CHPM areas, including information from the study areas and LTPs.

The first task, parallel to continue working at the study areas by British Geological Survey, Portuguese National Laboratory of Energy and Geology, Geological Institute of Romania, Geological Survey of Sweden, was the development of a common framework, a template for evaluating a study area for CHPM potential. Due to the novelty of the task, a common framework or template is required in order to 1) evaluate the areas according to the CHPM2030 consortium common knowledge, 2) harmonized work: structured reports and better area comparison and compatibility. This document outlines the topics that are important to cover when evaluating an area for CHPM potential.

After internal preparation at LPRC, the work started with email communication and online meetings between LPRC, UNIM and the four study area representatives during December, January and February 2018. It was important to discuss this with the partners in this subtask and build a common strategy, since such kind of evaluation/exploration work has not been done before.

Work meetings and field trips

By the time of the Lanzarote Consortium meeting (22-23 March 2018), a draft template was prepared by LPRC, based on partners input. On the second day at the T6.2 workshop, all partners participated in the refining of this template. In WP1 the main objective was to survey data availability on these areas, whereas in WP6 the effort shifts to data evaluation. In order to create a consistent assessment of each site, an evaluation framework has to be set up, which was the aim of this workshop. The idea was to generate meaningful discussion between the technology developers (VITO, KU Leuven, UNIM, USZ, ÍSOR, MinPol) and the study area representatives (IGR, SGU, LNEG, BGS, EFG), in a matchmaking exercise. The former represented a set of requirements on what they want to know about an area, before deploying CHPM technology, the latter represented data availability from a concrete site. The discussion was following the themes of the template, and it reflected at each point on the study areas. The work has been split into two groups and facilitated by the moderators from LPRC.

Figure 2: Lanzarote Consortium meeting and workshop participants (22-23 March 2018)

The results of the Lanzarote T6.2 workshop has been used to update the template with the input from both technology representatives and study area representatives. The updated template was again presented at the EFG orientation workshop for the Linked Third Parties in Brussels (12 April 2018). The objective for the LTPs is to develop a study and a spatial database on European scale of prospective CHPM areas. EFG LTPs assess the geological data on suitable ore-bearing formations and geothermal projects- collected in WP1, in relation with the potential application of the CHPM technology.

The aim of the one-day workshop was to update the LTPs about the recent development of the project and to create guidelines and instructions for CHPM prospective areas selection & evaluation. The LTPs were introduced to the scope of their involvement through presentations from UNIM (Éva Hartai: general project presentation, Tamas Madarász: Technological elements and system dynamics), SGU (Gerhard Schwarz: Data Availability,

Summary of the Country Reports), LPRC (Tamas Miklovicz: Aim and Structure of WP6) and EFG (Anita Demény: CHPM Site Selection, Investigation Framework and Data Assessment). After the presentations, interactive group work followed.

Figure 3: Brussels workshop participants (12 April 2018)

The workshop was divided in two parts: area selection and area evaluation for CHPM technology application. The first part was an example-led discussion, while the LTPs were given incomplete information about different geological cases and they were asked to decide whether it was of interest for the project or not. During the second exercise, the discussion was about the evaluation template, and the LTPs were asked to gather ideas/comments and gaps/limitations related to the topics. The workshop was facilitated by EFG and LPRC.

Table 1: Countries included in the European outlook for prospective locations

EFG LTPs involved in CHPM2030 (16+1)			Data collected by RBINS (7)
• Belgium • Czech Republic • Finland • France (by EFG) • Germany • Greece	• Hungary • Ireland • Italy • The Netherlands • Poland • Portugal	• Serbia • Slovenia • Spain • Switzerland • Ukraine	• Austria • Croatia • Cyprus • Luxembourg • Slovakia • Sweden • United Kingdom

After the workshop the template was finalised and the three LTP tasks were outlined:

1. area selection of prospective CHPM areas

EFG Linked Third Parties were asked to define at minimum 1, but maximum 6 prospective CHPM areas in their country, and have to indicate the requested information on these areas in the Prospective CHPM areas table. If more than 6 areas were identified in the country, all of them can be indicated into the prospective CHPM areas table, but the area assessment, which was the upcoming task, had been done only for the 6 most suitable areas. The main parameters have to be taken into consideration during the prospective CHPM area(s) selection are 1) the existence of deep metal enrichment(s): degree of the mineralization, and type of mineralization; 2) the temperature: considering the possibility of heat and power production (type A: T > 100 °C) or only heat production (type B: 100 °C > T > 50 °C).

However, it is important to mention that this area selection for prospective areas, was a rough screening for areas that may be further investigated in the future. Areas selected as “type B”, has the potential for use “CHM” technology and use the delivered metal extraction technological couples with direct heating application. Areas selected as “type A” may be actual areas for a full “CHPM” application, after a thorough geophysical exploration that can show the ultra-deep mineral enrichment. On the other hand, if the requirements were set too high (T > 170 °C + indicated metal enrichment), many potential areas would have been ruled out due to the lack of information or direct evidence at such depths.

2. evaluation of basic characteristics of prospective CHPM areas

The second task was to describe prospective CHPM areas in their country. EFG Linked Third Parties reported on the 6 most suitable areas (from the previously identified list), and completed the evaluation of the basic characteristics of the areas. During the evaluation, LTPs to followed the template (Template for evaluation of basic characteristics of prospective CHPM areas), provided by EFG.

3. evaluation of CHPM characteristics of prospective CHPM areas

All EFG Linked Third Parties defined prospective CHPM areas in their country and filled out the Prospective CHPM areas table in the Guidelines for the selection of prospective CHPM areas. During task 2 and 3, EFG LTPs provided input according to Figure 4.

Evaluation of basic characteristics	Evaluation of CHPM characteristics
CHPM geology → local geology (in regional context) → target formation → available cross sections, geological maps, geochemical results, lithological information	**Operational characteristics: expected design parameters** → **Expected design parameters of the CHPM technological building blocks** • underground heat exchanger • production + injection wells • electrolytic metal recovery • gas diffusion electro-precipitation • power plant (heat exchanger) • local heat and electricity demand • salt gradient power generation → **Environmental, social and political background** • gaseous and solids emissions • water and noise pollution • land and water use • induced seismicity/landslides, subsidence • public acceptance • political support • legislation, regulatory framework → **Financial aspects** • local demand for heat and electricity
CHPM geophysics → previous geophysical measurement (in CHPM relevance) → what measurements can be used and how to locate/define the ultradeep orebody/heat exchanger → available geophysical maps, cross sections, logs, etc.	
Deep metal enrichment → (expected) metal enrichment based on available geophysical, geological, drill data, samples information, geochemistry	
Integrated 3D-4D model → existing 3D models of the target area and of the deep metal enrichment	
EGS geothermal potential → EGS potential (heat & energy) of the area → geothermal characteristics (temperature gradient, heat flux, stress field, water availability, EGS geology) → presence of deep fluids/brines, fracture system, crustal permeability	

Figure 4: EFG LTP evaluation template chapters.

Parallel to the EFG LTP area selection and evaluation, the partners were working on the in-depth evaluation of the 4 selected study areas. The CHPM2030 partners met in Cornwall

between the 22-24th of May, to study the Cornubian granite province, which is a potential CHPM site in the future. The field trip was led and hosted by Eimear Deady and Richard Shaw from the British Geological Survey. The field trip was a good opportunity to further develop the evaluation template through informal discussion after the field activity.

The first day started at the United Downs geothermal project site. This site is being prepared for a geothermal drilling operation. The well doublet goes into the Carnmenellis granite body and the produced hot water will fuel a demonstration power plant with 1 megawatt of electric power. The next stop from the field trip was at the Carn Brea viewpoint where the tectonic setting, geology and mineralization in the area around the Camborne-Redruth mining district was explained. Next, the partners visited the famous Crowns engine houses at Botallack and had a guided tour at the Geevor tin mine, including ore processing facilities and underground tunnels. In the evening, the CHPM2030 partners had the opportunity to network with industry representatives in Cornwall, including the Cornish Lithium, GeoScience Limited, Avalon Science Limited, Camborne School of Mines and EGS Energy.

On the second day, the group visited the old HDR site at Rosemanowes Quarry in the Carnmenellis Granite. The deep drill holes, (>2000 meters), are still open and perfect for Avalon Science Limited to test and calibrate their latest cutting edge equipments. The next stop was at the Wheal Jane mine water treatment plant. Wheal Jane was a tin mine, which closed in 1991. The water is currently being pumped from the mine and treated in surface facilities. During the afternoon the partners studied the porphyritic biotite granite at Cligga head. Sheeted greisen tin-tungsten (Sn-W) and tin-tungsten-copper (Sn-W-Cu) can be observed with sulphide mineralization.

Figure 5: Participants of the Cornwall field trip (22-24th of May 2018)

The second day finished with a discussion about the study area's evaluation strategies related to WP6 – Roadmapping and Preparation to Pilots. It was concluded that it is important to integrate all available "geo" data into an existing/new 3D/4D model for better understanding the picture as a whole, to help the deeper extrapolation, for better conceptual understanding, test the theories from the area, visualize data, create new and tangible results of the area. Many other aspects have been discussed, including the importance of deep water availability, surface fresh water for the GDEx technology, social and political acceptance and support locally, access to grid, local heat/electricity demand, potential environmental risks, targeting for micas as geological sink for many elements, and more. The field trip was closed with the visit to Rinsey Cove, where it could be observed how the Tregonning-Godolphin Granite intruded into the local metasedimentary rocks, and their interaction.

The CHPM2030 project participants visited the second study area for WP6 in Beius Basin, Romania (25-26 July 2018). The field trip was organised by Diana Persa and Stefan Marincea from the Geological Institute of Romania, with the focus was on the Romanian banatitic magmatic and metallogenic belt.

The participants first visited the town hall of Beius, located on the Northwest of Romania, where the local geothermal district heating system and its instrumentations was explained. The field program included visits to several skarn related exposures of the banatitic magmatism, including Budureasa (Valea Mare, quarry with brucite bearing granodiorite-dolomite contact), Pietroasa (Dealul Gruiului, adit for exploiting magnesian borate bearing altered dolomite) and Baita (marble quarry, calcic skarns with base metal sulphides) in the Bihor Mts. and at Cazanesti (Cerboaia Valley, gehlenite bearing high temperature contact zone) in the Magureaua Vatei area. These skarns are especially interesting, as these are expected to be present 3-5 km depth at the host rock and magmatic intrusion contact zones. Since many of the surface exposure skarns were mineralised, it is expected to see similar processes at depth, being a special interest area for simultaneous geothermal energy and mineral extraction, the aim of the CHPM technology. In the end of the field day, the Romanian team presented the current stage of their 3D modelling efforts. Besides the field exposures, the participants had the opportunity to visit the Turda salt mine, the Bears' Cave at Chiscau and the Gold Museum in Brad.

Figure 5: Participants of the Romania field trip (25-26 July 2018)

Beside personal meetings, Task 6.2 participants kept continuous online communication to finalise the evaluation template, share the progress of the study area reports and to agree on the submission/review process.

Internal submission

It was agreed that the reports will be submitted in phases, in order to avoid review overload. The first part of the evaluation template was submitted for internal review at the end of December, the second half was submitted before the end of February, and the last part was be submitted by the end of March:

- 1st end of December 2018: basic characterization, chapters: Geology of the prospective area; Geophysics of the prospective area; Deep metal enrichment; EGS potential.
- 2nd end of February 2019: advanced evaluation, chapters:
    - Information for CHPM technological elements, incl. Underground heat exchanger (deep metal enrichment + potential reservoir); Production and injection wells; Electrolytic metal recovery and gas diffusion electro-precipitation; Power plant; Salt gradient power generation.
    - Operational characteristics incl. Environmental, social and political background; Financial aspects; Site-specific requirements according to the Grant Agreement
- 3rd end of March: 3D modeling results (Integrated 3D-4D model).

All previous chapters were updated when needed by the end of March. The submission of D6.2 Report on Pilots was in May.

Mitigation measures

During the project review meeting, it has been identified that there is a “The risk of not having enough data and detailed and comprehensive information for the preparation of study areas (WP6), to clearly show the potential of the CHPM2030 technological solution and allow for future advances in the TRL building on the results of CHPM2030, has to be addressed and mitigation measures put in place before end of December 2018”. This is a general risk that was anticipated in the beginning. The established mitigation measures included:

- Developing a study area evaluation template and framework (Lanzarote and Brussels workshops, Cornwall & Romania field trips)
- October 3. online workshop on 3D modelling status and evaluation template qualitative (good, mixed or gaps & recommendations) review of different chapters at each study area.
- Online follow-up meeting with the study areas to discuss the mitigation measures plan, and updated accordingly (Mid December).
- multiphase internal submission and review process of the study area reports (December 31, February 28, March 30), to ensure consistency of the different study area reports.
- Review each part of the documents provided by BGS, IGR, LNEG, and update it before April (January - April).
- Online meeting for the status of the reports, submission timing and review process. (mid-March 2019).
- Identified gaps & recommendations (to be addressed in the roadmap) discussed between the study areas in the online workshop (April 2019).

3.3 Explanation of the chapters in the final evaluation template

The evaluation template outlines the topics that are important to cover when evaluating an area for CHPM potential with the aim to be used as:

- aid for evaluating the study areas;
- guideline for the EFG LTPs for the EU spatial database on prospective CHPM locations;
- assistance and instruction on how to select and assess any other location, beyond the project for the first pilots;
- input for the Roadmap 2030.

The final evaluation template has been finished and circulated within the study area representatives. It contains the 9 chapters.

1) Geology of the prospective area

CHPM geology: description of the local geology in the regional context, but focusing on the target formation.

Including the following aspects:

- local geology (in regional context), tectonic development;
- focus on CHPM target formation;
- interpretation from surface indication to deeper structures;
- interest is originally fractured systems (skarn, VMS, etc.);
- list of available cross sections, geological maps, geochemical results, lithological information and other geological data resources.

Notes: Many of these issues has been described in WP1 and reported in Deliverable 1.2., therefore study areas were asked shortly summarized, update and reference the results presented in D1.2. The same true for the next chapters in the template: Geophysics of the prospective area.

Keywords: local geology, stratigraphy, lithology, cross section.

2) Geophysics of the prospective area

CHPM geophysics: Description of previous geophysical measurements and findings on the area, in CHPM relevance. What measurements can be used and how to locate/define the deep metal enrichment. Presenting available geophysical maps, cross sections, logs, other measurements in the Annex.

- Previous geophysical measurements (in CHPM relevance).
- Geophysical results that can be used for locating/defining the deep metal enrichment.
- List of available geophysical maps, cross sections, logs and other measurements.

Notes: already done in WP1, therefore shortly summarized and referenced to D1.2 and other detailed studies,

Keywords: geophysical data, interpretation.

3) Deep metal enrichment

Mineralization: Description of the (expected) deep metal enrichment based on available geophysical, geological and samples information, geochemistry, etc.

Including:

- Type of mineralization, metals.
- Applicable leaching agents based on WP2.

Keywords: mineralization, deep metal enrichment, applicable leaching agents.

4) EGS potential

EGS Geothermal potential: Description of the EGS potential (heat & energy) of the area; Geothermal characteristics (temperature gradient, heat flux, stress field, thermal conductivity, water availability, EGS geology); Presence of deep fluids/brines, fracture system, crustal permeability. As CHPM is a geothermal technology at its core, the precondition for such application is a functioning geothermal system. At this point the geothermal/EGS potential is investigated through the following points:

- EGS potential (heat & energy) of the area.
- Geothermal characteristics (temperature gradient, heat flux, stress field, water availability, EGS geology).
- Presence/indication of deep fluids/brines, fracture system, crustal permeability.
- Deep water availability.
- Output parameters of the reservoir at the production well.
- Petrophysical parameters.

Keywords: EGS, reservoir, water availability, geothermal energy.

5) Integrated 3D-4D model

Integrated 3D model: from geological and geophysical results compile 3D model of the target area and deep mineralization zone. During the working meetings in WP6, it has been established that an important point for advancing the study area understanding, compared what has been delivered in WP1, is the development of an integrated 3D, potentially 4D model. This could be a major advancement compared to what has been presented in WP1 Deliverable 1.2. Developing new 3D model would be the answer to the initial core question of Task 6.2: How can we advance the study area evaluation from the solid baseline which has been already provided in WP1?

- 3D integration of geological and geophysical results.
- Already existing 3D-4D models of the target area and the deep metal enrichment.
- Integrate all available “geo” data into existing/new 3D/4D model for better understanding the picture as a whole, to help the deeper extrapolation, for better conceptual understanding, test the theories we have from the area, visualize data, create new and tangible results of the area.
- The model ideally includes geological structures, mineralization, hydrogeological flow, stress field, reservoir and hydrodynamical parameters, fluid losses, etc.

Notes: CHPM2030 is a TRL4-5 research project and the first pilots are set for 2030, therefore, it is not expected to deliver fully developed, “commercial” 3D models by the end of the project. The goal is to set the direction, create the first models and tackle the remaining gaps with structured recommendations in the Deliverable 6.3 Roadmap 2030 document.

Keywords: 3D modelling, visualization, interpretation, depth continuation, deep metal enrichment.

6) Information for CHPM technological elements

The following subchapters are focusing on the CHPM technological components and describes the available information regarding each study areas. These are the expected range of parameters at the future CHPM building blocks: underground heat exchanger, production wells, electrolytic metal recovery, heat exchanger, gas diffusion electro-precipitation, salt gradient power generation and injection wells (based on D2.4 Overall system dynamics). Environmental mitigation strategies, social and political background, financial aspects are also considered here.

For future pilots, all these aspects required to be fully described and elaborated. However, due to current knowledge gaps and limitations, actions and recommendations are going to be formulated to reach that level of understanding at the study area in the future. These next steps will be summaries in the Deliverable 6.3 Roadmap 2030 document.

6.1) Underground heat exchanger (deep metal enrichment + potential reservoir)

- extension of the metal enrichment (volumetric interpretation);

- expected type and porosity/permeability (fractured, porous, etc.) of the reservoir;
- type of mineralization and expected metals.

Keywords: mineralization, reservoir.

6.2) Production and injection wells

- depth of potential wells;
- conceptual drill and well design (based on the stress field and the area specifics);
- wells connection;
- expected temperature/pressure at the bottom/wellhead.

Notes: on a conceptual level, what can we expect for these aspects.

Keywords: Drilling depth, well design.

6.3) Electrolytic metal recovery and gas diffusion electro-precipitation

- potential target metals/products to be recovered;
- brine: foreseen chemical composition and physical parameters.

Keywords: target metals, potential products.

6.4) Power plant

- local heat and electricity demand (industrial, municipal, agricultural, etc.);
- access to the grid.

Keywords: demand for heat & electricity, grid availability.

6.5) Salt gradient power generation

- salinity of expected geothermal brine;
- fresh water supply from the surface (water sources).

Keywords: fresh water supply, brine salinity,

7) Operational characteristics: Environmental, social and political background

Environmental:

- list of potential environmental risks and mitigation strategies (gaseous and solids emissions, water and noise pollution, induced seismicity, land use/subsidence, induced seismicity/landslides, water use, thermal pollution, etc.);
- in-line with D2.4 and WP5 integrated environmental assessment;
- local competition for land and water availability;
- risk of mobilizing radioactive/toxic materials.

Social**:**

- Social Licence to Operate,
- public acceptance for geothermal applications.

Political:

- political support on renewable/geothermal energy:
- licensing: how to get the licence for the technology, it can get difficult;
- presence of supporting legislation, regulatory framework.

Notes: Due diligence, de-risk a project before the start.

Keywords: environmental risks and mitigation strategies, SLO, licencing.

8) Financial aspects

Financial aspects: applying the financial tools developed in WP5. Local demand for heat (green houses, industry, residential, greenhouses, illustrated with Lindal diagram, etc.) and electricity (proximity of electric grid, residential/industrial needs etc..).

- Use of economic tools developed in WP5 (shifted to the roadmapping document).
- List of potential local stakeholders (community, political, companies).
- Local demand for heat and electricity.
- Potential investors.

Keywords: WP5 financial tools, local investors, geothermal energy utilization/demand.

9) Site-specific requirements according

Is has been also agreed to include specific site-specific aspects, outside of the evaluation template, at the end of the report. Each study area interpreted and summarized these issues shortly according to the Grant Agreement, while the evaluation template covered the larger picture.

Considering that CHPM2030 is a research project at TRL 4-5 and the first pilots are set for 2030, this template is not expected to be completed with all details and aspects of the presented topics. This is not possible at the moment, mainly due to lack of data from CHPM target depth. Instead, the template is to set a common framework and direction to evaluate the study areas according to the available data, collected in WP1, and then tackle the remaining gaps with structured recommendations, that can be fully elaborated in Deliverable 6.3 Roadmap 2030 and 2050. Some of the topics, such as social, political, environmental background, therefore are covered with short qualitative reflection, ensuring that all important aspects are considered.

4. Executive summaries of the study area reports

4.1 South West England

Full report in Appendix 6.2.1: Report on Pilots: South West England. Authors: Paul A J Lusty, *Principal Economic Geologist*, Richard B Haslam, *Structural Geologist*, Richard A Shaw, *Economic Geologist*, Eimear A Deady, *Minerals Geoscientist*, Paul Williamson, *Senior Geophysicist*, British Geological Survey.

This report covers south-west England, considering the availability of geoscience information, the geological environment, geothermal characteristics, potential for deep metal enrichment, and technical, environmental, social and regulatory factors that could influence the future development of CHPM extraction technology in the region.

The geothermal energy potential of the UK was investigated by research funded by the UK government and European Commission between 1977 and 1994. The UK has a fairly uniform background heat flow field, with areas of greater heat flow associated with the radiogenic Permian granites in south-west England, buried Caledonian granites of northern England and the batholith in the Eastern Highlands of Scotland. South-west England was selected as the UK CHPM2030 study area as it is a major magmatic province, with high heat production, and

hosts extensive polymetallic mineralisation. Its long history of metal production, and economic geology research means it is a data-rich region. It is also the focus for contemporary deep geothermal research and development in the UK.

South-west England forms an integral part of the European Variscides and has been influenced by rifting, convergence and passive margin inversion and extensional reactivation. Crustal extension and orogenic collapse during the late Carboniferous and lower Permian resulted in extensive granitic magmatism in the region, forming the Cornubian Batholith. The granites were emplaced into largely Devonian sedimentary rocks, hosted in fault-bound basins. Crustal extension and shortening resulted in large-scale faulting and folding across the region. A major structural feature of south-west England is approximately NW-SE-trending fracture systems, locally termed 'cross-courses', which are considered to play a significant role in the overall permeability of the region. Extensive, internationally renowned granite-related mineralisation occurred during the early to mid-Permian, which contains metals including tin, tungsten, copper, zinc, and arsenic. A separate, Mid-Triassic phase of mineralisation related to basinal fluids, and containing lead, zinc, silver, fluorite and barite developed in the cross-course fractures.

This review whilst considering the broader scale geological context, principally focuses on a study area covering the northern part of the Carnmenellis granite, one of the six exposed granite plutons that form the Cornubian Batholith. At surface the Carnmenellis granite is roughly circular in shape and covers an area of some 135 km2. However, in common with the other plutons its shape at depth and thickness remains uncertain. This project used borehole data in conjunction with existing gravity models to better constrain the position of the upper granite surface.

Geological research in south-west England spans over two hundred and fifty years and has been greatly enhanced by geophysical surveys. Gravity modelling of the Cornubian Batholith has resulted in variable estimates of its thickness. The most recent interpretation suggests that the batholith consists of two sheets, with an upper granite, with a base at 6–8 km, and a lower more extensive granite sheet, with a base at 12–15 km. This is supported by the magnetotelluric (MT) and seismic data. Modelling of the Carnmenellis granite suggests it may have a centrally located feeder zone. Seismic surveys have been conducted across south-west

England and its adjacent areas. However, no reflectors were identified in the granite, the granite/country rock contact was not imaged, and it was concluded that the granite is seismically featureless. MT data from the Carnmenellis granite indicates a very homogenous body, with joint closure by a depth of 7 km, and a change to pore-dominated resistivity below this depth. High resolution magnetic and radiometric datasets for south-west England were obtained during the recent Tellus South West survey. This data has been widely used in research projects, resulting in new structural interpretations, improved correlations of stratigraphic units and a re-evaluation of the heat production across the batholith.

The study area is extensively mineralised, hosting the highly productive Camborne-Redruth mining district. The granite-related mineralisation can be broadly defined as quartz–wolframite and tourmaline–quartz–cassiterite veins, with subordinate copper, arsenic, and minor bismuth, silver, and lead, which typically occur in swarms in both the granite and the metasedimentary country rock. Grade and tonnage of these deposits are comparable to significant vein-stockwork tin-tungsten deposits globally. Cobalt has been produced from this type of mineralisation in the Redruth area. The Mid-Triassic, variably metalliferous, cross-course veins cross-cut and displace the granite-related mineralisation in this area. They are primarily lead, zinc, silver, fluorite and baryte-bearing, and virtually all the mineralised veins occur in the metasedimentary rocks.

The Carnmenellis granite was the focus of a major geothermal experiment, the UK hot dry rock (HDR) research and development programme that ran for more than 15 years, and produced a huge amount of data and analysis on the geothermal energy potential of south-west England. The project, based at Rosemanowes Quarry, near Penryn in west Cornwall, aimed to demonstrate the feasibility of establishing a ‘full-scale prototype’ HDR power station in Cornwall. A contemporary project, operated by operated by Geothermal Engineering Ltd (GEL), is the United Downs Deep Geothermal Power (UDDGP) project, located near Redruth and about 7 km north of the old HDR project site. The HDR project focussed on engineering an underground heat exchanger in the low porosity and permeability rock mass using reservoir stimulation. In contrast the UDDGP project is based on a new concept of exploiting the natural permeability that may exist in major fault zones in Cornwall, eliminating the requirement for artificial stimulation of the rock mass. Much of the data, information and analysis presented this review arises from these two deep geothermal development projects.

The temperature of the Carnmenellis granite at 5 km depth is estimated to be 200°C. This estimate is consistent with the actual temperatures measured in the HDR project boreholes. Heat production maps define clear zones of greater heat production in the Carnmenellis granite outcrop. In the United Downs project area, heatflow modelling predicts that at a vertical depth of 4500 m the temperature will be between 180–220°C.

Cornish granites typically have very low primary permeability, but relatively high hydraulic conductivity as a result of faults and joints. The latter are particularly important for controlling fluid flow in Cornish granites. Fluid circulation has been a continuous feature of the Carnmenellis granite and its host rocks since emplacement. Fluid circulation is evident in the local mines where thermal, saline brines discharge from crosscourse structures. It is concluded that a dynamic system driven by convective and hydrodynamic forces has allowed continuous water-rock reaction to occur within the upper 3–4 km of the currently exposed pluton. It is thought that a large reservoir of probable diluted palaeobrines exists at depth in this area. However, these are not viewed as static, trapped palaeofluids, but rather part of a dynamic system of fluid circulation, involving continuous mixing of saline and meteoric waters, and water-rock reaction that continues today. These brines contain lithium concentrations of up to 125 mg/l^{-1}, probably as a result of the mica breakdown during fluid-rock interaction.

An extensive programme of both direct and indirect stress measurement was undertaken in the Carnmenellis granite during the HDR project in an attempt to understand how the stress regime would influence the shape, extent and orientation of the growth of a geothermal reservoir. Initial tests to develop a ‘commercial-scale’ heat exchanger at the Rosemanowes site were largely unsuccessful, as when water circulation commenced fluids losses were excessive and the pumping pressures required to maintain circulation were excessive, due to the poor connectivity between the boreholes. A configuration, involving a third borehole orientated to maximise the number of joint intersections and use of viscous gel to open up the rock volume had lower impedance and water losses, and injection and production flow rates in the system were measured over a continuous four-year period. It was concluded that the ‘optimum hydraulic performance’ that could be achieved at the Rosemanowes site was an injection flow rate of 24l/s, with impedance of 0.6 MPa per l/s and with a water loss of 21 per cent. A decline in the thermal performance of the system was also observed over the

monitoring period, due to a short circuit between the boreholes. The UDDGP project is currently working on the basis that if the PTFZ is assumed to have a width of about 200 m and two fractures occur every metre that have an aperture of 90 µm, the entire zone would have a transmissivity of 123 mD, resulting in a transmissivity of about 25 Dm. Based on this and heat flow modelling the project aims to produce water at the surface at about 175°C, with a circulation flow rate of between 20–60 l/s.

It has been demonstrated that the stress regime in Cornwall means fluid injected into a deep borehole will migrate downwards, along favourably orientated joints, hence the requirement for the injection borehole to be shallower than the production hole. The UDDGP project boreholes have a large (c. 2000 m) separation, in order to exploit a sufficiently large heat exchanger and reduce the risk of short-circuiting of flow, and will be driven by a downhole pump that will create a pressure sink above the production well. It is predicted that even at moderate injection pressures shearing will occur on favourably orientated fractures.

Preliminary modelling of the Cornubian Batholith has been undertaken to improve understanding of its properties relevant to geothermal energy development. A regional model was constructed to understand the spatial relationship of key geological parameters that were used for the development of subsequent site-scale models. One of the site-scale models is based on data from the HDR project site, and covers a volume of 2.6 km^3, with a depth range of -1000 to -3000 mbsl. The model is centred on the HDR project boreholes, incorporating fracture data from two of the deep boreholes and site-specific hydrological properties. Data and assumptions about the fracture network were used to generate three discreet fracture network (DFN) models for the HDR project reservoir. These were up-scaled to include porosity and permeability in order to understand the potential flow pathways within the reservoir. The second site-scale model considers an area located to the NW of the Carnmenellis granite, where the current UDDGP project is located. The target geothermal reservoir is still considered to be the Carnmenellis granite, and the model covers a volume of 12 km^3, with a depth range of -1500 to -5500 mbsl. In the absence of any published data on the fracture network in the UDDGP project target reservoir and given the consistency of fractures mapped at surface in the Carnmenellis granite the two fracture sets identified and characterised in the HDR project site model were also used in this model. Due to the uncertainty associated with the location and scale of the fault that the UDDGP project is

targeting it was represented in the model as a fractured volume of rock, based on DFN modelling methods. An additional fracture set that is parallel to the fault strike was added to the two regional fracture sets in the UDDGP project site model. Compared to the HDR site project model the modelled volume shows a clear increase in permeability within the fault zone, despite the background permeability being similar. However, the model is likely to overestimate the permeability in the UDDGP project reservoir as the fracture apertures used in the modelling are based on the measured flow within the shallower HDR project boreholes. Although this modelling informs our understanding of the properties of two potential deep geothermal reservoirs in contrasting structural settings in the Carnmenellis granite, there are a number of uncertainties and limitations to these models, which future research will have to address.

The presence of mineralisation at EGS depths (≥4 km) in Cornwall is highly uncertain due to a lack of direct evidence. The deepest mine workings in Cornwall extend to about 1000 m depth, and until 2019 the deepest drilling in Cornwall reached about 2600 m, with only trace quantities of sulfide identified in the core. Significantly, the drilling at the UDDGP project has encountered a number of mineral lodes and cross-course structures. However, the CHPM concept does not necessarily rely an ore body in the traditional sense. Any metal enriched geological formation is a potential target for leaching. The Cornubian Batholith is notable globally for its high bismuth concentrations and the granite is strongly enriched in lithium. Disseminated niobium and tantalum phases also occur in some of the granites. The Carnmenellis granite predominantly comprises quartz, orthoclase feldspar, biotite and muscovite. Micas represent sinks for many minor metals. Preliminary leaching experiments on a mica concentrate produced from a Carnmenellis granite sample were disappointing in terms of the concentrations of metals recovered.

The UDDGP project provides the best indications of the potential environmental impacts of future geothermal resource development in Cornwall. There is a strong preference for new developments to utilise brownfield sites in the region. Proximity to the National Grid and network availability to connect new generation projects will also be a major consideration in the location of future developments. The planning permission application for geothermal exploration and development on the UDDGP project site received no objections from both statutory consultees and local residents. Private housing exists along the western, northern

and eastern perimeters of the industrial estate, and the nearest village is less than 1 km away. Background monitoring and predictive modelling was undertaken to predict the noise levels in the area surrounding the site. The drilling rig being used has been designed to minimise environmental impact in urban and noise-sensitive environments, and a range of noise mitigation and attenuation measures have been implemented at the drilling site. Induced seismicity is a concern in all projects that involve deep drilling and water circulation through fractures. During the HDR project tens of thousands of micro-events were recorded, however, very few were felt at surface. In the planning consent for the project the local planning authority included a requirement for both seismic monitoring and a control protocol. Data from the monitoring system is made publically available. Mining in south-west England stretches back millennia, and the mining landscape is testament to the impact mineral extraction has had on the development of the region. The last decade has seen a renewed interest in metals and mining in south-west England. The extent of mineral extraction in south-west England and its impact on the heritage of the region probably means local communities have a relatively receptive attitude towards natural resource development. GEL have undertaken an extensive education and community outreach programme targeting the full cross-section of potential stakeholders. The UDDGP project consultation programme suggests that the local community and politicians are supportive of deep geothermal power development in Cornwall. Plymouth University, in south-west England are researching the issues relating to public perception of geothermal energy exploitation in the UK.

Geothermal heat is considered to have the potential to make a significant contribution to meeting the emissions targets set out in the UK Climate Change Act. One of the key challenges with ownership and regulation of geothermal heat in the UK is that it is regarded as a physical property, not a recoverable material such as a metallic mineral ore. As such, ‘heat’ is not a legally-defined entity and this causes some difficulties for assigning legal ownership and regulating it. Revision of geothermal regulations is one of a number of measures required to encourage the exploitation of geothermal resources in the UK. The current regulatory approach in the UK for deep geothermal developments requires environmental permissions and licences from the Environment Agency. Development falls under environmental permitting and groundwater regulations, as defined by the Water Framework Directive.

The National Planning Policy Framework in England states that Local Planning Authorities should develop positive strategies to help increase the use and supply of renewables and low carbon energy and heat. The Overarching National Policy Statement for Energy, sets out national policy for the delivery of major energy infrastructure, and indicates that the Government is committed to increasing dramatically the amount of renewable generation capacity. It includes a list of generic impacts that must be considered by energy development proposals. Cornwall Council are keen to understand the potential for geothermal resource development in the county, and strategies it could take to stimulate the deep geothermal sector. Cornwall has produced a 'Sustainable Energy Action Plan', which describes the importance of supporting and promoting geothermal opportunities. The Cornwall 'Local Plan' contains a specific 'Renewable and low carbon energy' policy, which seeks to increase the use and production of renewables and low carbon energy generation. The Council is particularly supportive of developments that 'create opportunities for co-location of energy producers with energy users, in particular heat, and facilitate renewable and low carbon energy innovation.

The mineral ownership situation in Great Britain could present a challenge for the CHPM2030 concept of recovering metals from a geothermal system. The rights to non-energy minerals in Great Britain, with the exception of gold and silver, are mainly in private ownership, and only the mineral rights owner can legally grant rights to explore and mine. Hence a critical stage in the exploration and development process is determination of mineral ownership. This can be difficult and time consuming in Great Britain, particularly in regions with a long history of mineral extraction such as Cornwall.

During the HDR project analysis was undertaken on the economic costs of HDR systems. The capital costs associated with a 'post-prototype' commercial-scale HDR power station in south-west England was estimated to be in the range of £71–100 million (equivalent 2018 prices). If an operational geothermal system can be established at the UDDGP project there are plans to construct a demonstration power plant to supply power to the UK national grid. Demand for renewables (and bio-fuels) is projected to increase in Cornwall, reaching 101 ktoe in 2030. Previous estimates of the electricity generation potential of deep geothermal in south-west England range from 100MW to 4GW, with significant by-product heat. It is suggested that development of this deep geothermal resource could result in Cornwall becoming an

attractive destination for power dependent industries. The electricity grid in Cornwall has spare capacity on the network to take more locally generated renewable energy. However, there is very little capacity available for new connections.

In summary south-west England, and specifically Cornwall, is an excellent location for a pilot-scale CHPM system. It has the essential prerequisites of a proven geothermal energy resource and abundant polymetallic mineralisation. It is one of the best surveyed and most data-rich parts of the UK, with a long history of mineral development and geothermal research. The local government and communities are supportive of deep geothermal resource development, and it has a major, active co-funded deep geothermal project.

4.2 Iberian Pyrite Belt, Portugal

Full report in Appendix 6.2.2: Report on Pilots: Portugal, Iberian Pyrite Belt. Authors: Elsa Cristina Ramalho, *Geological Engineer*, João Xavier Matos, *Economic Geologist,* João Gameira Carvalho, *Geophysicist*, Portuguese National Laboratory of Energy and Geology.

This report provides an update of geoscientific data and information relating south-west Iberian Pyrite Belt (IPB), Portugal. The IPB massive sulphides deposits is a Variscan metallogenic province located in the SW of Portugal and Spain that hosts the largest concentration of massive sulphide deposits worldwide, covering about 250 km long and 30–50 km wide and are associated with volcano-sedimentary sequences present in sea floor environment (http://geoportal.lneg.pt). This geographical area, with particular geological volcanic and sedimentary sequences of Carboniferous and Devonian ages, identified in the southwest of the Iberian Peninsula runs from NW to SE, from Alcácer do Sal (Portugal) to Seville (Spain), and, in the Portuguese side, it covers two active mines: Neves-Corvo mine, owned by Lundin Mining (www.lundinmining.com), and at the Aljustrel mine, owned by Almina (www.almina.pt). For its potentialities and full mining operation with good prospective of increasing in depth the research and exploitation, Neves-Corvo Mine was chosen for test site, to be studied for CHPM purposes, because of its depth of exploitation and undergoing research projects (SmartExploration and Explora UE projects). Because of these projects a deep 3D geological and geophysical model is being reviewed, with old mining data and recent acquired geophysical acquisition, reprocessing and reinterpretation. At the same time, its relation with EGS potentialities will be considered. The Neves-Corvo mine area

includes presently 7 massive sulphide ore lenses and is mainly a copper and zinc mine, producing copper, zinc and lead concentrates. The operation is owned and operated by Lundin Mining's Portuguese subsidiary Somincor (http://www.lundinmining.com). Although this mine does not explore any ultra-deep orebodies that allow the application of the CHPM technology yet, prospecting in depth is underway to check for the continuity of the Lombador orebody, so far. Lombador is the deepest orebody that is identified in the Lundin permit area. Geophysical modelling and reflection seismics were conducted under the scope of H2020 SmartExploration (H2020) (https://smartexploration.eu/) and Explora (Alentejo2020) projects and a more refined model will turn out with the available data.

This report will cover the main parameters regarding the feasibility of the implementation of the CHPM technology in Neves-Corvo, that will complement the CHPMD1.2.2. report, namely in the possibility of existence of ultra-deep boreholes in the future and in the geothermal gradient that allows reaching adequate temperatures to produce energy (~70 °C) at relatively shallow depths (~2.5-3 km), compatible with both energy production and metal recovery in the geothermal brine to increase mining production.

An overall look upon the external requirements to the implementation of CHPM technology was studied. Emergent external factors such as energy transition, financial requirements and possibilities, and environmental, social and political backgrounds and future prospects are also referred in the report, as well as possible future agreements between the mining management and the Portuguese government.

Finally, some new data is incorporated into a GoCad 3D model as an update to the GoCad model published in ProMine (EU FP7, Carvalho et al., 2016). This update includes supplementary information, such as deeper and all other recent boreholes information, from 2012 to 2018, to cross-check with geophysical data, reprocessed gravimetric, magnetic, electromagnetic and surface and deep reflection seismic data.

4.3 Beuis Basin, Romania

Full report in Appendix 6.2.3: Report on Pilots: Romania. Authors: Diana Perșa, *Researcher*, Ștefan Marincea, *Senior Researcher*, Delia Dumitraș, *Senior Researcher,* Cătălin Simion, *Researcher*, Geological Institute of Romania.

The purpose of this study is to provide relevant information that leads to the selection of a pilot site, an area that has favorable preconditions for the existence of deep mineralization and high geothermal potential at the same place. In Romania the the Beiuș Basin – Bihor Mountains has been selected as study areas. The site is situated at the convergence of two major structural units and has characteristics similar those. Thus, the Beiuș Basin, which is a part of the Pannonian Basin, has high geothermal potential. At the same time, Bihor Mountains' structural unit is a part of the North Apuseni Mountains, and it is part of the metallogenic province Banatitic Magmatic and Metallogenetic Belt.

Both Pannonian Basin (Romanian part) and Beiuș Basin have the following characteristics:

- The thin crust, (which is estimated at 25-27 km), and the thin lithosphere (60 -70 km) that resulted during regional extensional processes of Pannonian Basin that started in Miocene;
- Below Neogene deposits, Triassic deposits host a geothermal aquifer;
- The existence of intrusive magmatic bodies in the depth.

Both North Apuseni Mountains and Bihor Mountains have the following characteristics:

- Existence of a granodiorite - granite pluton with regional extension that has been extruded during Late Cretaceous.
- The existence of important mineralized areas, specific to the Banatitic Magmatic and Metallogenetic Belt, among which we mention the skarns that have been formed at the contact between the pluton and the Mid-Triassic and Upper Triassic limestones.
- Existence of a large geothermal aquifer recharge area that is represented by karst deposits of mainly by Triassic deposits

Geothermal potential

For the eastern limit of the Pannonian Basin, Rădulescu and Dimitrescu (1982) estimated the mean heat flow of 96 mWm-2. Geothermal gradients for Pannonian Basin are high, varying from 6.2 to 5.6 ^{o}C/100 m at 500 m and at 2000 m b.s.w.l respectively. Due to the thin crust and the thin lithosphere, Beiuș Basin is characterized by high heat flow, with values up to 90 mWm-2.

In Apuseni Mountains, in areas affected by Tertiary tectogeneses usually referred to terrains younger than 50 Ma, the three components of the regional heat flow: crustal radiogenic, thermal transient perturbation, and background heat flow from deeper sources, contributes with 36, 27 and 27 mWm^{-2}, respectively, to the mean value 90 mWm^{-2}.

Thermal conductivity [10-3cal/cm x ^{o}C x s] of the rocks belonging to the Romanian part of the Pannonian Basin and the surrounding areas has been determined through laboratory methods, and has high values varying from 3,5 – 12 for granites, 4.8 – 5.0 for diorites and 6 – 7 for dolomitized limestone.

Based on these data the conclusion is that in Bihor Mountains, the heat flow of granitic – granodioritic bodies from Pietroasa and Budureasa are supposed to have high values in the depth. Also the heat flow of the rocks that host the geothermal aquifer (limestone, dolomite and quartzite, marble) has high values. But an important cooling agent is represented by the continuous circulation of the surface water through the karst areas of Bihor Mountains into the geothermal aquifer from Beiuș Basin. It is expected that in the depth of 4 km, where the access of water is prevented by the aquiclude Lower Triassic layers the heat flow of the batholith to be considerable.

Deep metal enrichment

Mineralization is widespread in the mountainous area and is expected to be found in the basin area. In Bihor Mountains the mineralization is generated during the banatitic calcalkaline magmatism (Post-Lower Masstrichtian-Palaeogene), which is represented by bodies of intrusive rocks, generally hypabyssal as well as plutonic ones, which are widely developed in the depth. Plutons of granodiorite-granite rocks, to which the main sulphide mineralization is genetically linked, constitute main mass of banatitic bodies in the Apuseni Mountains; in Bihor Mountains they crop out on small areas, but they develop in the depth.

Magmatic bodies intruded Permian-Mesozoic sequences and produced contact-metamorphic aureoles, at Pietroasa, Budureasa and, most extended at Baita Bihor. In the contact aureoles of the granodiorite-granites plutons, skarns with Fe, B, Bi, Mo have been formed. At Valea Seacă, Valea Mare-Budureasa etc., the skarns are overlapped by sulphide mineralization.

Brucite deposits from Budureasa and Pietroasa were investigated by surface pits, drillings and underground galleries. They have been formed at the contact of granodiorites with the Anisian dolomites and have a structure with four zones, ranging from granodiorites to pure dolomites containing holocrystalline hypidiomorphic granodiorites, magnesian skarns, Brucite-bearing zones, recrystallized Anisian dolomite.

Borate deposit is situated in the middle basin of the Aleului Valley (Bihor Mountains), at its confluence with the Sebisel Valley, at the Gruiului Hill. The formation of the borates from the contact aureole of the Pietroasa granitoid body is the result of an infiltration metasomatic process.

W-bearing and base metal skarns are characteristic only for Baita Bihor. At Baița Bihor, some magnesian skarn bodies or ore pipes such as those at Antoniu, Bolfu-Tony, Hoanca Motului, Baia Roșie are boron-bearing skarns and represents well-defined metasomatic columns. A sole similar body, or metasomatic column, that from Dealul Gruiului was identified at Pietroasa.

Laboratory experiments performed during the implementation of this project lead to promising results.

- Two rock samples from Romania were used for leaching experiments by Chris Rochelle et al., in 2017 (CHPM2030 Project Deliverable 2.2): a skarn from Pietroasa and a mineralized rock from Cacova Ierii. The experiments used a range of fluid types and pressure/temperature conditions to identify fluid-rock reactions and quantify the potential for enhancing metal release. For conditions of temperature/ pressure of 100 °C, and 200 bar the efficient substances proved to be 0.6 M NaCl, and HCl/HNO3 mix for both samples. The main elements recovered are: Co, Sr, Mo, Sb, Mn, Zn, W.
- In 2018, using GDEx technology, Xochitl Dominguez et al. (CHPM2030 Deliverable 3.3) completed the experiments to recover metals from the geothermal brine provided by a Beiuș Basin well. According to this study, the results are promising. Especially the content of Sr in one of the brine samples and the content of Sr recovered are remarkable.
- A considerable enrichment of magnesium minerals was highlighted in the precipitate resulted from the geothermal water extracted from a Beiuș Basin well compared with

spring and water coming from a mine. Thus, the magnesium content is less than 5% in surface, and at least 13% in the geothermal waters.

3D model

Integrating all the data available in a 3D geological database and creating the 3D geological model provided an overview on the spatial distribution and the geometry of the middle and upper Triassic sedimentary deposits within Beiuș Basin and their contact with the Upper-Cretaceous intrusive body, from Bihor Mountains.

The 3D model shows the extension of Upper Triassic deposits, both in Beiuș Basin and in Bihor Mountains, linking the two structural units, generating magnesian skarns on one side and transporting geothermal water on the other. This dual role in the perimeter explains an increased content of magnesium in geothermal waters from Beiuș Basin.

The 3D model revealed the fact that there is a region bordering Beiuș Basin where the batholith is extended: at Budureasa, where there is an increased possibility to have both mineralisation and high geothermal potential within a small area.

The 3D model emphasizes the large areas on which Triassic deposits outcrop. Being represented by highly fissured karst deposits they, on one side, assure a continuous recharge of the geothermal aquifer, but, on the other side, they have an important contribution to the decrease of the geothermal potential of the rocks, being a cooling agent.

The batholith's apophyses that were detected by complex geophysical methods within Beiuș Basin, and can be taken into consideration for further investigations are represented by the model.

The 3D model helped to visualize and understand the spatial relations at the border between the basin and the mountains and provides new data that are needed to set the parameters for planning new exploration works.

At the same time the 3D model helps us to reduce the original area for new future investigations to a smaller area with an increased probability that it is suitable for a CHPM system.

Hydrogeology

The geothermal aquifer from Beiuș and Ștei is hosted in fractured Triassic dolomites that have a regional extension. Triassic aquifer from Beiuș Basin is a confined aquifer with negative piezometric levels (- 18.48 m 3001 H Beiuş and unstable – 45m 3003 H Beiuş) or artesian (3002 H Ştei), depending on the position of the tectonic block. Beiuș aquifer is an open geothermal system, where recharge equilibrates with the mass extraction and its reservoir pressure stabilizes. Its recharge can be both hot deep recharge and colder shallow recharge. The latter can eventually cause reservoir temperature to decline and production wells to cool down. In fact, this second alternative was demonstrated when the increase of the volume of injected water was accompanied by the decrease of the water temperature within aquifer. More research is needed to improve the knowledge on this subject. The aquifer is exploited by 2 extraction wells and one injection well in Beiuș, and one extraction well in Ștei, situated at a distance of 18 km from Beiuș. The most productive well is 3001, from Beiuș, that has a wellhead temperature of 88^{o}C, coming from 2460 m depth.

Geothermal district heating system

Beiuş town has an extensive geothermal heating system (GDHS), which provides heat for approximately 70% of the population, covering about 60% of the urban heating demand. The previous system that used coal as a source of energy was completely replaced by GDHS. The geothermal heat energy is delivered to the consumers either indirectly via substations with heat exchangers feeding double closed loop distribution pipe networks, one for Domestic Heating (DH) and the other for Hot Sanitary Water (HSW), or directly to the individual buildings with their own heat exchangers. The exploitation license of Beiuș geothermal reservoir perimeter is owned by Transgex S.A.

In 2016 the energy of 74,452 of GJ/year has been delivered to the population. The value of water production was higher than 1 million m3. In 2018 a partnership formed by the City Hall and private company submitted project proposals in order to get EU funding for the extension of the GDHS. They also showed their interested for the results of CHPM2030 project and expressed their will to be part of a consortium that could consider a CHPM installation in Beiuș in the future.

4.4 Nautanen, Kristineberg, Sweden

Full report in Appendix 6.2.4: Report on Pilots: Sweden. Authors: Gerhard Schwarz, *Geophysicist*, Benno Kathol, *Geologist,* Magnus Ripa, *Geologist*, Bo Thunholm, *Hydrogeologist* Edward P Lynch, *Geologist,* Johan Jönberger, *Geophysicist*, Geological Survey of Sweden.

There are four major ore provinces in Sweden, i.e., Bergslagen, the Skellefte district, the Northern Norrbotten ore province and the Caledonian orogen. In these, we have chosen the areas around the Kristineberg mine in the Skellefte district and the abandoned Nautanen mine in Northern Norrbotten for further screening the applicability of the CHPM technology there.

The Kristineberg area in the southwestern part of the Skellefte district is known for its volcanogenic massive sulphide deposits (VMS). Based on their age and geological history of rock sequences, the bedrock in the Skellefte district and surrounding areas in northern Västerbotten and southern Norrbotten counties can be divided and assigned to three major lithotectonic units. These are the Svecokarelian orogen, the Ediacaran to Cambrian sedimentary cover sequence and the Caledonian orogen. The Skellefte district sensu stricto belongs entirely to the Svecokarelian orogen.

The bedrock in the Skellefte district was formed or reworked by Svecokarelian orogenic processes, which lasted from about 1.96 to 1.75 Ga. This time interval includes subduction-related processes, collision, and extension-related collapse of the thickened crust. The peak of Svecokarelian deformation and metamorphism occurred between 1.85 and 1.80 Ga, but earlier phases of deformation at 1.89 – 1.87 Ga have been reported under the last decade. The Svecokarelian orogen comprises Svecokarelian intrusive rocks, formed by orogenic processes and Svecofennian supracrustal rocks, i.e. early orogenic sedimentary and volcanic rocks, the latter hosting the VMS deposits of the Skellefte district and thus the Kristineberg mine.

The Kristineberg mine is the oldest and largest massive sulphide mine in the Skellefte district and in continuous operation until today. Mining began in the year 1940 at the ore body outcropping at surface. Since then, production has reached down to around 1 200 m making Kristineberg to one of the deepest mines in Sweden. The ore is a complex massive sulphide

with zinc being the main metal, although in some areas copper-gold ores are mined. Until year 2017, 31 million tons have been mined, reserves are 5 million tons and resources about 13 million tons. The combined grades of mined ore, reserves and resources are 3.9 % zinc, 0.7 g/t gold, 44 g/t silver, 0.9 % copper and 0.4 % lead.

The rocks surrounding the Kristineberg deposit have been strongly hydrothermally altered and are multiphase folded and strongly sheared. The schistose rocks are now dominated by quartz–muscovite–chlorite–pyrite in varying proportions, and exhibit marked sodium depletion and co-enrichment of magnesium and potassium. Cordierite, phlogopite and andalusite occur in considerable amounts. Kyanite has rarely been observed, mainly associated with quartz veins. In general, the iron–magnesium alteration minerals are magnesium-rich, and the modal chlorite content increases towards the Kristineberg ore horizon, which is surrounded by a halo of more muscovite-rich rocks.

The Geological Survey of Sweden has a long-standing tradition in geological mapping of the country with the support from airborne geophysics, motivated by the low degree of bedrock exposures. Magnetic properties, electrical resistivity and gamma radiation of shallow crustal rocks were thus studied in the Skellefte district and the Nautanen area, complemed by ground surveys on these rock properties and on gravity.

During the last two decades, reflection seismic investigations were introduced in Sweden in larger extent by academia in cooperation with the mining industry for prospecting after minerals and ores in the Earth's uppermost crust. The Kristineberg area in the western Skellefte district was studied at depth down to 12 km by seismic methods, complimented by drillhole data down to ca 1400 m below surface. High resolution reflection seismic data provided detailed images of an VMS ore body and associated structures. However, the seismic experiments have also shown that considerable efforts need to be undertaken in geologically complex areas to properly acquire data, i.e., preferably by 3D instead of 2D surveys.

The Nautanen deposit is situated in the Northern Norrbotten ore province in northernmost Sweden. At this historical mining location, intermittent exploration has been carried out for over 100 years. Approximately 72 000 tonnes of copper and iron ore were extracted between 1902 and 1907. Further exploration in the 1970s and 80s produced a pre-regulatory total resource estimate for the "old" Nautanen deposit of approxi¬mately 2.94 Mt grading 0.78%

Cu and 0.52 ppm Au. Present-day exploration by Boliden Mines ral AB has resulted in the discovery of an additional copper-gold mineralisation approximately 1.6 km north-northwest of the old Nautanen mine along the trend of the Nautanen deformation zone (NDZ). This "Nautanen North" deposit has an indicated resource of 9.6 Mt grading 1.7% Cu, 0.8 ppm Au, 5.5 ppm Ag and 73 ppm Mo, with an additional inferred resource of 6.4 Mt grading 1.0% Cu, 0.4 ppm Au, 4.6 ppm Ag and 41 ppm Mo.

The bedrock in Northern Norrbotten is part of the 2.0–1.8 Ga old Svecokarelian orogen. The orogen comprises both pre-orogenic rocks formed in the Archaean and early Palaeoproterozoic, as well as rocks formed during the orogeny itself. The bedrock in the Nautanen area consists of a partly conformable succession of syn-orogenic, Palaeoprote¬rozoic volcano-sedimentary rocks. This supracrustal sequence is generally of calc-alkaline, basaltic andesite to andesite composition and has undergone extensive de¬formation, metamorphism, recrystallisation and hydrothermal alteration. Intrusive rocks, including deformed gabbroic, syenitic and dioritic bodies and younger, deformed to massive granitic and gabbroic-doleritic plutons and dykes, occur in the area.

The mineralisations at Nautanen are part of several hydrothermal copper-gold occurrences assigned to the iron oxide-copper-gold (IOCG) mineral deposit class which occur within the regional approximately north-northwest-trending Nautanen deformation zone (NDZ). The NDZ represents the most conspicuous structural feature in the area and is clearly delineated on magnetic anomaly maps as a somewhat dilational, linear zone of sub-parallel and tightly banded magnetic susceptibility anomalies. The coupling of high-strain deformation and magnetic banding reflects episodic metasomatic-hydrothermal fluid flow, probably enhanced by increased permeability associated with protracted and focused deformation. Two general styles of mineralisation are recognised in the area: (1) an inferred older phase of disseminated to semi-massive (replacement-style) sulphide mineralisation forming sub-vertical lenses and linear zones mainly within the NDZ; and (2) mineralisation associated with quartz ± tourmaline ± amphibole veins occurring mainly east of the NDZ or as a late-stage brittle overprint within the high-strain zone.

Geophysical surveys, mostly using potential field and electrical methods in the Nautanen area were concentrated on the shallow sub-surface down to some hundred metres depth, being

of economic interest. No investigations are known in the surroundings of Nautanen that are covering deeper seated structures and formations.

Our understanding of deep-seated fluids in the crystalline bedrock is still rudimentary. Hydraulic conductivity decreases with depth at a high degree of variability. Investigations in boreholes indicate that hydraulic conductivity below 650 m depth varies between 10^{-7} and 10^{-12} m/s. Data on the composition of fluids indicate that brines (> 5 % TDS/l) occur far inland at several 1000 metres depth. Their residence time was estimated at the order of some hundred millions of years by the analysis of He-isotopes. Corrected geothermal heat flow density is about 50 mW/m^2. Data on heat production do not show large differences between rock types related to their content in radioactive elements.

The generally low geothermal gradient of less than 20 °C/km in the crystalline basement of the Fenno-scandian Shield was verified by sensing temperature in deep boreholes in the Skellefte district and adjacent to the Nautanen mine. The temperature gradient measured here to about 16 °C/km should allow for low- to mid-enthalpy geothermal systems as part of a possible CHPM unit.

5. Extended summary of European Prospective Locations

Full report in Appendix 6.2.5: Report on European Prospective Locations. Authors: Domenico Marchese, *Project Officer*, Anita Demény, *Project Officer*, Isabel Fernandez, *Executive Director*, European Federation of Geologist

This work has put together the data collected with the results of the most recent predictive metallogenical models. The report provides a "European perspective" on the potential areas of CHPM development.

The Linked Third Parties, following the guidelines and indications provided by the European Federation of Geologists, have evaluated the existing geological data relating to mineral formations and geothermal projects, previously collected in WP1 (Work Package), according to the potential application of CHPM technology. This work has put together the data collected with the results of the most recent predictive metallogenical models.

The task of the LTPs were three-fold:

1. Area selection: this task was concerning with the selection of a limited number of sites where drill holes showed the entry characteristics to define an area most likely to be a future CHPM candidate (Temperature, Metal enrichments, fluids, etc.).
2. Basic area evaluation: the task continued with the evaluation of the basic characteristics of the selected areas by taking into account geological and geophysical data with a CHPM relevance, mineralisation, integrated 3D models, EGS potential info and so forth.
3. CHPM characteristics: this task considered a deeper investigation and data comprehension of the most likely CHPM candidate sites where some operational characteristics and well capacity were taken into account as well as the related environmental and social impacts that may arise from such CHPM systems.

The area selection was a screening process, looking for areas for future CHPM application, that is intended to be further investigated in the future, as interest for CHPM technology arise. Areas selected as type B, has the potential for metal extraction and direct heating systems ("CHM"), while areas type A has the potential for heat, power and metal extraction ("CHPM"). In either case the next step if further geophysical/geological exploration at the identified areas.

16 of the LTPs have been involved in the task, investigating CHPM potential in the following countries: Belgium, Czech Republic, Finland, France (investigation conducted by EFG), Germany, Greece, Hungary, Ireland, Italy, Netherlands, Poland, Portugal, Serbia, Slovenia, Spain, Switzerland, Ukraine. Besides, the "Institut Royal des Sciences Naturelles de Belgique" (IRSBN), collected and evaluated the data provided by 8 other countries that were not directly involved in the Project (e.g. Austria, Croatia, Cyprus, Luxembourg, Slovakia, Sweden the United Kingdom).

As a summary, 34 over 50 places have been identified with "Type A = T>100°C" and more than 22 with "Type B = T>40/50°C", that have future potential for applying CHPM technology in the future. In the selected areas several kinds of mineralisation have been identified: Hydrothermal, Epithermal and Porphyry are those most commonly reported. The depth of mineralisation, as well as the correspondence temperature, vary considerably site by site (exhaustive reports of each selected site have been collected in Annex where the reader may

find a list of commodities and the degree of mineralisation expressed in % or ppm when provided by the LTPs).

The study has supported the development of a spatial database of European prospective locations for CHPM technology. The data collected on a European Scale was delivered on the web-based interactive platform, with OpenStreetMap (OSM). All the outputs, visualised in the spatial database, have been made accessible to the public: http://bit.ly/CHPMinfoplatform.

6. Conclusions

Task 6.2 objective of setting "the ground for subsequent pilot implementation", has been completed by the 1) development of a common evaluation template, that facilitated the investigation of the study areas according to the consortium's common understanding; 2) evaluation of five European study areas: SW England, IPB, Romanian Beius area, Sweden (Nautanen, Kristineberg), according to the harmonised evaluation template; 3) creation of a European outlook on prospective location, including a publicly available spatial database.

The baseline for this study was developed in WP1, Task 1.2 Knowledge gaps and updating information. In CHPM2030 Deliverable 1.2 Report on Data Availability (Schwarz et al. 2016) a brief overview was presented about the four major ore districts in Europe: SW England, Southern Portugal, NW Romania and Central and Northern Sweden. Beside these focused reports, a trans-European inventory was also created of drill holes where temperature exceeded 100 °C and metal enrichment was encountered. Here the focus was on data availability, whereas in Task 6.2 the focus was on the detailed evaluation of data.

In Task 6.2 the first activity was the development of a harmonised study area evaluation template. This guideline was created with the involvement of the entire consortium, through workshops (Lanzarote study area workshop with the consortium: 22-23 March 2018, Brussels workshop with the Linked Third Parties: 12 April 2018), online meetings and fieldtrips (Cornwall field trip: 22-24th of May 2018, Romania field trip: 25-26 July 2018). This was an iterative process with the involvement of the technology developers and the study area representatives.

The final evaluation template outlines a group of important topics that must be taken into account when evaluating the CHPM potential at a given area. The topics are the following:

Geology and geophysics of the prospective area, Deep metal enrichment, EGS potential Integrated 3D-4D model, information for CHPM technological elements (underground heat exchanger (deep metal enrichment + potential reservoir), Production and injection wells, Electrolytic metal recovery and gas diffusion electro-precipitation, Power plant, Salt gradient power generation), Operational characteristics (environmental, social and political background, financial aspects), with numerous subtopics and a short description.

The evaluation guideline is to be used as 1) an aid for evaluating the study areas; 2) a guideline for the EFG LTPs for the EU spatial database on prospective CHPM locations, 3) assistance and instruction on how to select and assess any other location for the first pilots; 4) input for the Roadmap2030.

Now that all available information, provided in D1.2, has been updated and evaluated (D6.2) for CHPM potential, the next step is to plan ahead and see what actions needs to be done, in order to arrive to pilot readiness level by 2030, in the form of a roadmap.

The roadmapping activity for CHPM aims to directly support the early implementation of the technology at the pilot sites, follow-up on the technology components, and the definition of how overall geothermal technology may evolve. These aspects may be developed together, but given the current available resources, it is split to three actions corresponding to the three layers of the D6.3 Roadmap for 2030 and 2050 document.

Part 1 is the continuation of WP6 T6.1 foresight exercise, building on the results from the Horizon Scanning, Delphi survey, and Visioning workshop, at the initially identified topics. This part will use the Roadmapping workshop to develop actions and timeline, with the addition of signposts and wildcards, in order to arrive the Vision described in T6.1. This exercise identified the overall trends and opportunities at important but uncertain areas for CHPM development in the future.

- → Testing the overall CHPM concept
- Input from Roadmapping workshop in Las Palmas
- Output: actions and timeline for reaching the vision described in D6.1.

Part 2 is going to be the direct follow-up of the technological components, with the contribution from the responsible partners, providing short-, mid- and long-term research

plan. This includes a one paragraph description of the current state-of-the-art, immediate research plan, mid-term (2030) requirements for pilot readiness level (TRL 6-7), and long term (2050) objectives for the commercial level (TRL 8-9) application, for each technological component: Integrated reservoir management, Metal content mobilisation using mild leaching and with nanoparticles, GDEx, HPHT electrolytic metal recovery, Reverse osmosis electrodialysis, System integration. This aspect gives concrete guidance and direction at the technology component level.

- → Testing the current CHPM schematics,
- Input from the CHPM component follow-up roadmap,
- Output: the State-of-the-art, Immediate research plan, Pilot research plan (2030), Long term objectives, goals (2050), for the current CHPM components.

Part 3 is dealing with the study areas, giving instructions, needs, exploration plan for the next 10 years about how to arrive to pilot readiness level or to actual pilots by 2030, based on the gaps and recommendation, identified during T6.2. This part aims for direct support for the first pilot to be implemented at the study areas.

- → Testing the potential areas for applying current CHPM concept,
- Input from the study area roadmapping online meeting in early May and study area reports,
- Output: actions, needs, exploration plan, agenda, for the next 10 years' timeline, in order to reach pilot readiness level or first "CHPM plug-in" ready pilots.

All CHPM2030 study areas had very different geological, geothermal and mineral characteristics. This provided a complementary coverage of the type of areas that may be of interest in Europe for the future. However, due to the same reason, the reports reached different levels of maturity, and the recommendations, to be formulated as part of the roadmap, are also going to be specific for the individual areas.

The report on south-west England, considered the availability of geoscience information, the geological environment, geothermal characteristics, potential for deep metal enrichment, and technical, environmental, social and regulatory factors that could influence the future development of CHPM extraction technology in the region. Preliminary modelling of the

Cornubian Batholith has been undertaken to improve understanding of its properties relevant to geothermal energy development. A regional model was constructed to understand the spatial relationship of key geological parameters. This data was used for the development of two site-scale models that aimed to improve understanding of the fracture network and flow pathways at the reservoir-scale. In summary south-west England, and specifically Cornwall, is an excellent location for a pilot-scale CHPM system. It has the essential prerequisites of a proven geothermal energy resource and abundant polymetallic mineralisation. It is one of the best surveyed and most data-rich parts of the UK, with a long history of mineral development and geothermal research. The local government and communities appear supportive of deep geothermal resource development, and it has a major, active co-funded deep geothermal project.

The report from Portugal provides an update of the geoscientific data and information on the South-West Iberian Pyrite Belt (IPB), a Variscan metallogenic province with massive sulphides deposits. This active mining region, with vast amount of geological information available, has a good prospect of mineralization at deeper levels, therefore of interest for CHPM technology. The chosen study area is Never-Corvo Mine due to the available 3D geological, geophysical models and its relation with EGS potential. The deposit consists of 7 massive sulphide ore lenses with copper, zinc, and lead mineralisations. The report presents the relevant geological, geophysical, mineralogical characteristics of the area to investigate the feasibility of the implementation of CHPM technology at Never-Corvo. The main interest is the existence of the deep mineralization, near the operating mine. The coproduction of energy and minerals would extend the lifetime of the mine operation. The study also presents emerging factors, such as the energy transition, financial requirements and possibilities, advancement in 3D modelling of the deposit, challenges to generate data about the deeper levels (>1.2 km), environmental, social and political background, and the possible future agreements between the mining management and the Portuguese government. There was also a synergy with the ongoing mining operations, parallel EU funded projects (SmartExploration, Explora), and the CHPM study are evaluation.

At the Romanian study areas, the Beius basin and the Bihor Mountains were investigated by IGR due to the favourable geothermal and mineral potential of the areas for CHPM technology. In the Beius Basin, the geothermal potential is high due to the thin crust, as a

result of a regional extension in the Pannonian Basin, resulting high heat flow (above 80mW/m^2) and elevated geothermal gradient (5.6-6.2 ^{o}C/100 m). Deep mineralization is also expected due to intrusive magmatic bodies within the Beius Basin. On the other hand, the Bihor mountains are also of interest due to the mineral deposits, which is part of the Banatitic Magmatic and Metallogenetic Belt metallogenic province. The granodiorite – granite plutonic body, formed skarn mineralization at the contact with Mid- and Upper Triassic limestones. The identified deposit types of interest are 1) iron, boron, bismuth, molybdenum bearing skarns, and related vein occurrences with copper, zinc, lead sulphides, 2) Brucite deposits from Budureasa and Pietroasa, 3) Borate deposit from the contact of aureole of the Pietroasa granitoid body through metasomatic processes, 4) wolfram bearing and base metal skarns at Baita Bihor. Furthermore, there is an ongoing district heating system in Beius town, whose operator showed interest for the CHPM technology in the future. This shows public support for geothermal applications, indicated geological potential for heat and metals, and industry interest for the additional metal extraction technology.

In Sweden, two CHPM test sites are proposed for further investigations: These are the Kristineberg area in the Skellefte district and the Nautanen area in the Northern Norrbotten ore province. The Kristineberg area is known for its volcanogenic massive sulphide deposits (VMS). Zinc is the main target, though in some areas copper and gold ores are mined. The area was studied by geophysical methods down to 12 km and by drilling down to about 1400 m below surface. High resolution reflection seismic data outlined the VMS ore bodies and associated structures. However, the completed seismic surveys also have shown that considerable efforts were needed to acquire high quality data, preferably by 3D surveys. The operations in the Kristineberg mine have reached a depth of 1200 m, 31 million tons of ore were mined, reserves are 5 million tons and resources about 13 million tons. The combined grades of mined ore, reserves and resources are 3.9 % zinc, 0.7 ppm gold, 44 ppm silver, 0.9 % copper and 0.4 % lead. Mineralisations in the Nautanen area are part of several hydrothermal copper-gold occurrences related to the ironoxide-copper-gold (IOCG) mineral deposits. The “Nautanen North” deposit has an indicated resource of 9.6 million tons of ore grading at 1.7 % copper, 0.8 ppm gold, 5.5 ppm silver and 76 ppm molybdenum, with additional inferred resources of 6.4 million tons grading at 1 % copper, 0.4 ppm gold, 4.6 ppm silver and 41 ppm molybdenum. In both mining areas, the installation of a CHPM system is

highly challenging. The low geothermal gradient of only about 16 ^{o}C/km and heat flow density of about 50 mW/m^2, typical to the Fennoscandian Shield, demand large borehole depths of at least 5 to 7 km. At such depths, there is very limited information available about geological structures, deep-seated fluids, and hydraulic conductivity of the crystalline bedrock. However, with the help of integrated geophysical studies, i.e., deep seismic and magnetotelluric measurements and in cooperation with the mining industry, many advancements were made facilitating the CHPM potential in future projects.

The European outlook for prospective CHPM potential has been prepared with the help of the EFG's Linked Third Parties, the national geological associations. In total there were 24 countries covered: Belgium, Czech Republic, Finland, France, Germany, Greece, Hungary, Ireland, Italy, Netherlands, Poland, Portugal, Serbia, Slovenia, Spain, Switzerland, Ukraine, Austria, Croatia, Cyprus, Luxembourg, Slovakia, Sweden the United Kingdom. In each country, there were 3 tasks: 1) Area selection: define an area most likely to be a future CHPM candidate; 2. Basic area evaluation: the task continued with the evaluation of the basic characteristics of the selected areas; 3) CHPM characteristics: this task considered a deeper investigation and data evaluation of the most likely CHPM sites. This was a rough screening for areas that may be further CHPM site. Areas selected as "type B", has the potential for "CHM" technology and use the delivered metal extraction technological couples with direct heating application. Areas selected as "type A" may be actual areas for a full scale CHPM application, after a thorough geophysical exploration that can show the ultra-deep mineral enrichment. This work has shown a number of areas that has potential to develop a CHPM site, but the lack of publicly available data may still represent a bottleneck to improve the knowledge needed implement CHPM technology at any of the selected sites. The identified areas have been gathered in a publicly available online database: http://bit.ly/CHPMinfoplatform.

It has been found that a new type of exploration mindset is required for undertaking such survey. Exploration at areas for combined heat, power and metal extraction will have to use the traditional surveying and interpretation methods, but it must improve on them, and combine tools from both geothermal and mineral exploration campaigns, to create a comprehensive strategy. The first step for that was the creation of the evaluation template, which served as a "checklist" for important characteristics to consider when looking into

CHPM potential. The 5 study areas from 4 countries have been evaluated according to this new strategy and each area has the potential to develop actual CHPM pilots in the future. Each area has its unique characteristics, but overall, they all have substantial amount of information available publicly from the top 1 km of the crust, providing a good understanding of the near surface. The next challenge thus is to extend this understanding at deeper levels, run new, preferably 3D surveys, further advance each predictive 3D models for a downwards continuation. With the help of these study reports and the European outlook study, the following items have now been clarified: 1) the information available at each area, 2) the CHPM potential based on this geoscientific data, 3) remaining gaps to be overcome in the future. Based on this knowledge, the idea of pilot implementation can be further advanced through concrete recommendations in the CHPM2030 roadmaps (CHPM2030 Deliverable 6.3). The next exploration/research projects can continue, based on these recommendations and the CHPM pilot readiness level can be achieved by 2030.

References

Gerhard Schwarz, Magnus Ripa, Bo Thunholm, Richard A Shaw, Keith Bateman, Eimear Deady, Paul Lusty, Elsa Cristina Ramalho, João Xavier Matos, João Gameira Carvalho, Diana Perșa, Ștefan Marincea,, Albert Baltreș, Constantin Costea, Delia Dumitraș, Gabriel Preda, Vanja Bisevac,, Isabel Fernandez, 2016: Report on data availability, CHPM2030 project Deliverable D1.2, link:

https://www.chpm2030.eu/wp-content/uploads/2017/02/CHPM2030_D1.2_public_small.pdf

List of Appendices: Report on Pilots

A6.2.1: Report on Pilots: South West England.

A6.2.2: Report on Pilots: Portugal, Iberian Pyrite Belt.

A6.2.3: Report on Pilots: Romania.

A6.2.4: Report on Pilots: Sweden.

A6.2.5: Report on European Prospective Locations.

CHPM2030

CHPM2030 DELIVERABLE D6.2.1.

REPORT ON PILOTS: EVALUATION OF THE CHPM POTENTIAL OF CORNWALL, SOUTH WEST ENGLAND

Summary:
This report investigates the potential for combined heat and metal production from south-west England, considering availability of legacy geoscience information, the geological environment, geothermal characteristics, potential for deep metal enrichment, and technical, environmental, social and regulatory factors that could influence the future development of this technology in the region.

Authors:

Paul A J Lusty, British Geological Survey, Principal Economic Geologist
Richard B Haslam, British Geological Survey, Structural Geologist
Richard A Shaw, British Geological Survey, Economic Geologist
Eimear A Deady, British Geological Survey, Minerals Geoscientist
Paul Williamson, British Geological Survey, Senior Geophysicist

This project has received funding from the European Union's Horizon 2020 research and innovation programme under grant agreement nº 654100.

TABLE OF CONTENTS

LIST OF FIGURES

LIST OF TABLES

1 Executive summary

The CHPM2030 project aims to develop a novel technological solution of Combined Heat, Power and Metal (CHPM) extraction from ultra-deep ore bodies, which will pave the way for pilot-scale systems to be operational by 2030. This technology will help increase the attractiveness of renewable geothermal energy and also reduce Europe's dependency on the import of metals and fossil fuels. In the envisioned technology, an engineered geothermal system (EGS) is established within a metal-bearing geological formation at depths of 4 km or greater, which will be manipulated in such a way that the co-production of energy and metals will be possible. Critical to this, is an understanding of the natural networks of hydraulically-conductive mineral veins that could function as heat-exchange surfaces, and sources of metals. If metals can be leached from the orebodies in high concentrations, and over a prolonged period of time, then their recovery may substantially influence the economics of engineered geothermal systems. Furthermore, leaching of metals from subsurface pathways in a controlled way has the potential to improve fluid flow, and so increase system performance over time.

The CHPM2030 project examined the potential of four areas in Europe for CHPM systems, namely the Precambrian Fennoscandian Shield province, in Sweden; the late Palaeozoic Variscan province, of south-west England and southern Portugal; and the Mesozoic-Cenozoic Alpine province, in north-west Romania. This report covers south-west England, considering the availability of geoscience information, the geological environment, geothermal characteristics, potential for deep metal enrichment, and technical, environmental, social and regulatory factors that could influence the future development of CHPM extraction technology in the region.

The geothermal energy potential of the UK was investigated by research funded by the UK government and European Commission between 1977 and 1994. The UK has a fairly uniform background heat flow field, with areas of greater heat flow associated with the radiogenic Permian granites in south-west England, buried Caledonian granites of northern England and the batholith in the Eastern Highlands of Scotland. South-west England was selected as the UK CHPM2030 study area as it is a major magmatic province, with high heat production, and hosts extensive polymetallic mineralisation. Its long history of metal production, and economic geology research means it is a data-rich region. It is also the focus for contemporary deep geothermal research and development in the UK.

South-west England forms an integral part of the European Variscides and has been influenced by rifting, convergence and passive margin inversion and extensional reactivation. Crustal extension and orogenic collapse during the late Carboniferous and lower Permian resulted in extensive granitic magmatism in the region, forming the Cornubian Batholith. The granites were emplaced into largely Devonian sedimentary rocks, hosted in fault-bound basins. Crustal extension and shortening resulted in large-scale faulting and folding across the region. A major structural feature of south-west England is approximately NW-SE-trending fracture systems, locally termed 'cross-courses', which are considered to play a significant role in the overall permeability of the region. Extensive, internationally renowned granite-related mineralisation occurred during the early to mid-Permian, which contains metals including tin, tungsten, copper, zinc, and arsenic. A separate, Mid-Triassic phase of mineralisation related to basinal fluids, and containing lead, zinc, silver, fluorite and barite developed in the cross-course fractures.

This review whilst considering the broader scale geological context, principally focuses on a study area covering the northern part of the Carnmenellis granite, one of the six exposed granite plutons that form the Cornubian Batholith. At surface the Carnmenellis granite is roughly circular in shape and covers an area of

some 135 km^2. However, in common with the other plutons its shape at depth and thickness remains uncertain. This project used borehole data in conjunction with existing gravity models to better constrain the position of the upper granite surface.

Geological research in south-west England spans over two hundred and fifty years and has been greatly enhanced by geophysical surveys. Gravity modelling of the Cornubian Batholith has resulted in variable estimates of its thickness. The most recent interpretation suggests that the batholith consists of two sheets, with an upper granite, with a base at 6–8 km, and a lower more extensive granite sheet, with a base at 12–15 km. This is supported by the magnetotelluric (MT) and seismic data. Modelling of the Carnmenellis granite suggests it may have a centrally located feeder zone. Seismic surveys have been conducted across south-west England and its adjacent areas. However, no reflectors were identified in the granite, the granite/country rock contact was not imaged, and it was concluded that the granite is seismically featureless. MT data from the Carnmenellis granite indicates a very homogenous body, with joint closure by a depth of 7 km, and a change to pore-dominated resistivity below this depth. High resolution magnetic and radiometric datasets for south-west England were obtained during the recent Tellus South West survey. This data has been widely used in research projects, resulting in new structural interpretations, improved correlations of stratigraphic units and a re-evaluation of the heat production across the batholith.

The study area is extensively mineralised, hosting the highly productive Camborne-Redruth mining district. The granite-related mineralisation can be broadly defined as quartz–wolframite and tourmaline–quartz–cassiterite veins, with subordinate copper, arsenic, and minor bismuth, silver, and lead, which typically occur in swarms in both the granite and the metasedimentary country rock. Grade and tonnage of these deposits are comparable to significant vein-stockwork tin-tungsten deposits globally. Cobalt has been produced from this type of mineralisation in the Redruth area. The Mid-Triassic, variably metalliferous, cross-course veins cross-cut and displace the granite-related mineralisation in this area. They are primarily lead, zinc, silver, fluorite and baryte-bearing, and virtually all the mineralised veins occur in the metasedimentary rocks.

The Carnmenellis granite was the focus of a major geothermal experiment, the UK hot dry rock (HDR) research and development programme that ran for more than 15 years, and produced a huge amount of data and analysis on the geothermal energy potential of south-west England. The project, based at Rosemanowes Quarry, near Penryn in west Cornwall, aimed to demonstrate the feasibility of establishing a 'full-scale prototype' HDR power station in Cornwall. A contemporary project, operated by operated by Geothermal Engineering Ltd (GEL), is the United Downs Deep Geothermal Power (UDDGP) project, located near Redruth and about 7 km north of the old HDR project site. The HDR project focussed on engineering an underground heat exchanger in the low porosity and permeability rock mass using reservoir stimulation. In contrast the UDDGP project is based on a new concept of exploiting the natural permeability that may exist in major fault zones in Cornwall, eliminating the requirement for artificial stimulation of the rock mass. Much of the data, information and analysis presented this review arises from these two deep geothermal development projects.

The temperature of the Carnmenellis granite at 5 km depth is estimated to be 200°C. This estimate is consistent with the actual temperatures measured in the HDR project boreholes. Heat production maps define clear zones of greater heat production in the Carnmenellis granite outcrop. In the United Downs project area, heatflow modelling predicts that at a vertical depth of 4500 m the temperature will be between 180–220°C.

Cornish granites typically have very low primary permeability, but relatively high hydraulic conductivity as a result of faults and joints. The latter are particularly important for controlling fluid flow in Cornish granites. Fluid circulation has been a continuous feature of the Carnmenellis granite and its host rocks since emplacement. Fluid circulation is evident in the local mines where thermal, saline brines discharge from

crosscourse structures. It is concluded that a dynamic system driven by convective and hydrodynamic forces has allowed continuous water-rock reaction to occur within the upper 3–4 km of the currently exposed pluton. It is thought that a large reservoir of probable diluted palaeobrines exists at depth in this area. However, these are not viewed as static, trapped palaeofluids, but rather part of a dynamic system of fluid circulation, involving continuous mixing of saline and meteoric waters, and water-rock reaction that continues today. These brines contain lithium concentrations of up to 125 mg/l^{-1}, probably as a result of the mica breakdown during fluid-rock interaction.

An extensive programme of both direct and indirect stress measurement was undertaken in the Carnmenellis granite during the HDR project in an attempt to understand how the stress regime would influence the shape, extent and orientation of the growth of a geothermal reservoir. Initial tests to develop a 'commercial-scale' heat exchanger at the Rosemanowes site were largely unsuccessful, as when water circulation commenced fluids losses were excessive and the pumping pressures required to maintain circulation were excessive, due to the poor connectivity between the boreholes. A configuration, involving a third borehole orientated to maximise the number of joint intersections and use of viscous gel to open up the rock volume had lower impedance and water losses, and injection and production flow rates in the system were measured over a continuous four year period. It was concluded that the 'optimum hydraulic performance' that could be achieved at the Rosemanowes site was an injection flow rate of 24l/s, with impedance of 0.6 MPa per l/s and with a water loss of 21 per cent. A decline in the thermal performance of the system was also observed over the monitoring period, due to a short circuit between the boreholes. The UDDGP project is currently working on the basis that if the PTFZ is assumed to have a width of about 200 m and two fractures occur every metre that have an aperture of 90 µm, the entire zone would have a transmissivity of 123 mD, resulting in a transmissivity of about 25 Dm. Based on this and heat flow modelling the project aims to produce water at the surface at about 175°C, with a circulation flow rate of between 20–60 l/s.

It has been demonstrated that the stress regime in Cornwall means fluid injected into a deep borehole will migrate downwards, along favourably orientated joints, hence the requirement for the injection borehole to be shallower than the production hole. The UDDGP project boreholes have a large (c. 2000 m) separation, in order to exploit a sufficiently large heat exchanger and reduce the risk of short-circuiting of flow, and will be driven by a downhole pump that will create a pressure sink above the production well. It is predicted that even at moderate injection pressures shearing will occur on favourably orientated fractures.

Preliminary modelling of the Cornubian Batholith has been undertaken to improve understanding of its properties relevant to geothermal energy development. A regional model was constructed to understand the spatial relationship of key geological parameters that were used for the development of subsequent site-scale models. One of the site-scale models is based on data from the HDR project site, and covers a volume of 2.6 km^3, with a depth range of -1000 to -3000 mbsl. The model is centred on the HDR project boreholes, incorporating fracture data from two of the deep boreholes and site-specific hydrological properties. Data and assumptions about the fracture network were used to generate three discreet fracture network (DFN) models for the HDR project reservoir. These were up-scaled to include porosity and permeability in order to understand the potential flow pathways within the reservoir. The second site-scale model considers an area located to the NW of the Carnmenellis granite, where the current UDDGP project is located. The target geothermal reservoir is still considered to be the Carnmenellis granite, and the model covers a volume of 12 km^3, with a depth range of -1500 to -5500 mbsl. In the absence of any published data on the fracture network in the UDDGP project target reservoir and given the consistency of fractures mapped at surface in the Carnmenellis granite the two fracture sets identified and characterised in the HDR project site model were

also used in this model. Due to the uncertainty associated with the location and scale of the fault that the UDDGP project is targeting it was represented in the model as a fractured volume of rock, based on DFN modelling methods. An additional fracture set that is parallel to the fault strike was added to the two regional fracture sets in the UDDGP project site model. Compared to the HDR site project model the modelled volume shows a clear increase in permeability within the fault zone, despite the background permeability being similar. However, the model is likely to overestimate the permeability in the UDDGP project reservoir as the fracture apertures used in the modelling are based on the measured flow within the shallower HDR project boreholes. Although this modelling informs our understanding of the properties of two potential deep geothermal reservoirs in contrasting structural settings in the Carnmenellis granite, there are a number of uncertainties and limitations to these models, which future research will have to address.

The presence of mineralisation at EGS depths (≥4 km) in Cornwall is highly uncertain due to a lack of direct evidence. The deepest mine workings in Cornwall extend to about 1000 m depth, and until 2019 the deepest drilling in Cornwall reached about 2600 m, with only trace quantities of sulfide identified in the core. Significantly, the drilling at the UDDGP project has encountered a number of mineral lodes and cross-course structures. However, the CHPM concept does not necessarily rely an ore body in the traditional sense. Any metal enriched geological formation is a potential target for leaching. The Cornubian Batholith is notable globally for its high bismuth concentrations and the granite is strongly enriched in lithium. Disseminated niobium and tantalum phases also occur in some of the granites. The Carnmenellis granite predominantly comprises quartz, orthoclase feldspar, biotite and muscovite. Micas represent sinks for many minor metals. Preliminary leaching experiments on a mica concentrate produced from a Carnmenellis granite sample were disappointing in terms of the concentrations of metals recovered.

The UDDGP project provides the best indications of the potential environmental impacts of future geothermal resource development in Cornwall. There is a strong preference for new developments to utilise brownfield sites in the region. Proximity to the National Grid and network availability to connect new generation projects will also be a major consideration in the location of future developments. The planning permission application for geothermal exploration and development on the UDDGP project site received no objections from both statutory consultees and local residents. Private housing exists along the western, northern and eastern perimeters of the industrial estate, and the nearest village is less than 1 km away. Background monitoring and predictive modelling was undertaken to predict the noise levels in the area surrounding the site. The drilling rig being used has been designed to minimise environmental impact in urban and noise-sensitive environments, and a range of noise mitigation and attenuation measures have been implemented at the drilling site. Induced seismicity is a concern in all projects that involve deep drilling and water circulation through fractures. During the HDR project tens of thousands of micro-events were recorded, however, very few were felt at surface. In the planning consent for the project the local planning authority included a requirement for both seismic monitoring and a control protocol. Data from the monitoring system is made publically available. Mining in south-west England stretches back millennia, and the mining landscape is testament to the impact mineral extraction has had on the development of the region. The last decade has seen a renewed interest in metals and mining in south-west England. The extent of mineral extraction in south-west England and its impact on the heritage of the region probably means local communities have a relatively receptive attitude towards natural resource development. GEL have undertaken an extensive education and community outreach programme targeting the full cross-section of potential stakeholders. The UDDGP project consultation programme suggests that the local community and politicians are supportive of deep geothermal power development in Cornwall. Plymouth University, in south-west England are researching the issues relating to public perception of geothermal energy exploitation in the UK.

Geothermal heat is considered to have the potential to make a significant contribution to meeting the emissions targets set out in the UK Climate Change Act. One of the key challenges with ownership and regulation of geothermal heat in the UK is that it is regarded as a physical property, not a recoverable material such as a metallic mineral ore. As such, 'heat' is not a legally-defined entity and this causes some difficulties for assigning legal ownership and regulating it. Revision of geothermal regulations is one of a number of measures required to encourage the exploitation of geothermal resources in the UK. The current regulatory approach in the UK for deep geothermal developments requires environmental permissions and licences from the Environment Agency. Development falls under environmental permitting and groundwater regulations, as defined by the Water Framework Directive.

The National Planning Policy Framework in England states that Local Planning Authorities should develop positive strategies to help increase the use and supply of renewables and low carbon energy and heat. The Overarching National Policy Statement for Energy, sets out national policy for the delivery of major energy infrastructure, and indicates that the Government is committed to increasing dramatically the amount of renewable generation capacity. It includes a list of generic impacts that must be considered by energy development proposals. Cornwall Council are keen to understand the potential for geothermal resource development in the county, and strategies it could take to stimulate the deep geothermal sector. Cornwall has produced a 'Sustainable Energy Action Plan', which describes the importance of supporting and promoting geothermal opportunities. The Cornwall 'Local Plan' contains a specific 'Renewable and low carbon energy' policy, which seeks to increase the use and production of renewables and low carbon energy generation. The Council is particularly supportive of developments that 'create opportunities for co-location of energy producers with energy users, in particular heat, and facilitate renewable and low carbon energy innovation.

The mineral ownership situation in Great Britain could present a challenge for the CHPM2030 concept of recovering metals from a geothermal system. The rights to non-energy minerals in Great Britain, with the exception of gold and silver, are mainly in private ownership, and only the mineral rights owner can legally grant rights to explore and mine. Hence a critical stage in the exploration and development process is determination of mineral ownership. This can be difficult and time consuming in Great Britain, particularly in regions with a long history of mineral extraction such as Cornwall.

During the HDR project analysis was undertaken on the economic costs of HDR systems. The capital costs associated with a 'post-prototype' commercial-scale HDR power station in south-west England was estimated to be in the range of £71–100 million (equivalent 2018 prices). If an operational geothermal system can be established at the UDDGP project there are plans to construct a demonstration power plant to supply power to the UK national grid. Demand for renewables (and bio-fuels) is projected to increase in Cornwall, reaching 101 ktoe in 2030. Previous estimates of the electricity generation potential of deep geothermal in south-west England range from 100MW to 4GW, with significant by-product heat. It is suggested that development of this deep geothermal resource could result in Cornwall becoming an attractive destination for power dependent industries. The electricity grid in Cornwall has spare capacity on the network to take more locally generated renewable energy. However, there is very little capacity available for new connections.

In summary south-west England, and specifically Cornwall, is an excellent location for a pilot-scale CHPM system. It has the essential prerequisites of a proven geothermal energy resource and abundant polymetallic mineralisation. It is one of the best surveyed and most data-rich parts of the UK, with a long history of mineral development and geothermal research. The local government and communities appear supportive of deep geothermal resource development, and it has a major, active co-funded deep geothermal project.

2 Introduction

2.1 Objectives and role of the CHPM2030 project

The strategic objective of the CHPM2030 project is to develop a novel technological solution (Combined Heat, Power and Metal extraction from ultra-deep ore bodies), which will help reduce Europe's dependency on the import of metals and fossil fuels, and at the same time, lower the environmental impact of the energy supply.

In the envisioned technology, an Enhanced Geothermal System (EGS) is established on a metal-bearing geological formation, which will be manipulated in a way that the co-production of energy and metals will be possible. At a laboratory scale, the project intends to prove the concept that the composition and structure of ore bodies have certain characteristics that could be advantageous when developing an EGS.

2.2 UK CHPM2030 study area selection

Geological mapping of the UK commenced in the 1800s, and digital geological maps at a scale of 1:50 000 exist for all of the UK and 1:10 000 scale mapping is widely available. This information has supported extensive onshore exploration for metallic minerals, industrial minerals, coal, oil and gas, and geothermal resources. A 'National Geological Model' (NGM) has been constructed for the UK, and comprises an accurate, multi-scaled geospatial model of the subsurface geology. The NGM comprises a bedrock 'fence diagram' (UK3D) and a number of other 3D geological models. In terms of geophysical data, seismic data coverage is relatively good for regions underlain by sedimentary basins. Land gravity survey data covers all of Great Britain at an approximate resolution of one observation per 1.6 km^2. A series of regional aeromagnetic surveys of Great Britain provide complete coverage, typically at a flying height of about 300 m, with a 2 km line separation. More than a million onshore boreholes exist in Great Britain, with about 1760 boreholes that are over 1 km deep. Many bore holes have associated geochemical data, geophysical downhole log data and other records. There are 544 sites with a downhole temperature from 1 km or deeper. The geothermal energy potential of the UK was investigated by research funded by the UK government and European Commission between 1977 and 1994. This appraised heat flow, the potential for exploitation of radiothermal granites as hot dry rock (HDR) reservoirs and hot brines in deep sedimentary aquifers (Busby, 2010).

The United Kingdom is located on stable basement and is devoid of the active volcanism and high heat flows associated with tectonic activity. The average UK geothermal gradient is 26 °C km^{-1}, but locally it can exceed 35 °C km^{-1} (Busby, 2010). Temperatures at depth are determined by the heat flow and the thermal conductivities of the strata. The distribution of heat flow measurements across the UK is very uneven, and many of the boreholes from which data is derived were drilled for other purposes. The heat flow map of the UK is based on 212 observed heat flow measurements based on equilibrium temperatures and laboratory thermal conductivities, augmented by 504 heat flow estimates based on core borehole temperatures and estimated thermal conductivities (Figure 1A) (Busby and Terrington, 2017). There is a fairly uniform background heat flow field of about 55 mW m^{-2} with areas of greater heat flow associated with the radiogenic Permian granites in south-west England (117 ± 8 mW m^{-2}) and buried Caledonian granites of northern England (maximum values of 101 mW m^{-2}) (Figure 1A). Heat flow values also exceed the regional background over the batholith in the Eastern Highlands of Scotland (maximum values of 76 mW m^{-2}) (Beamish and Busby, 2016) (Figure 1B).

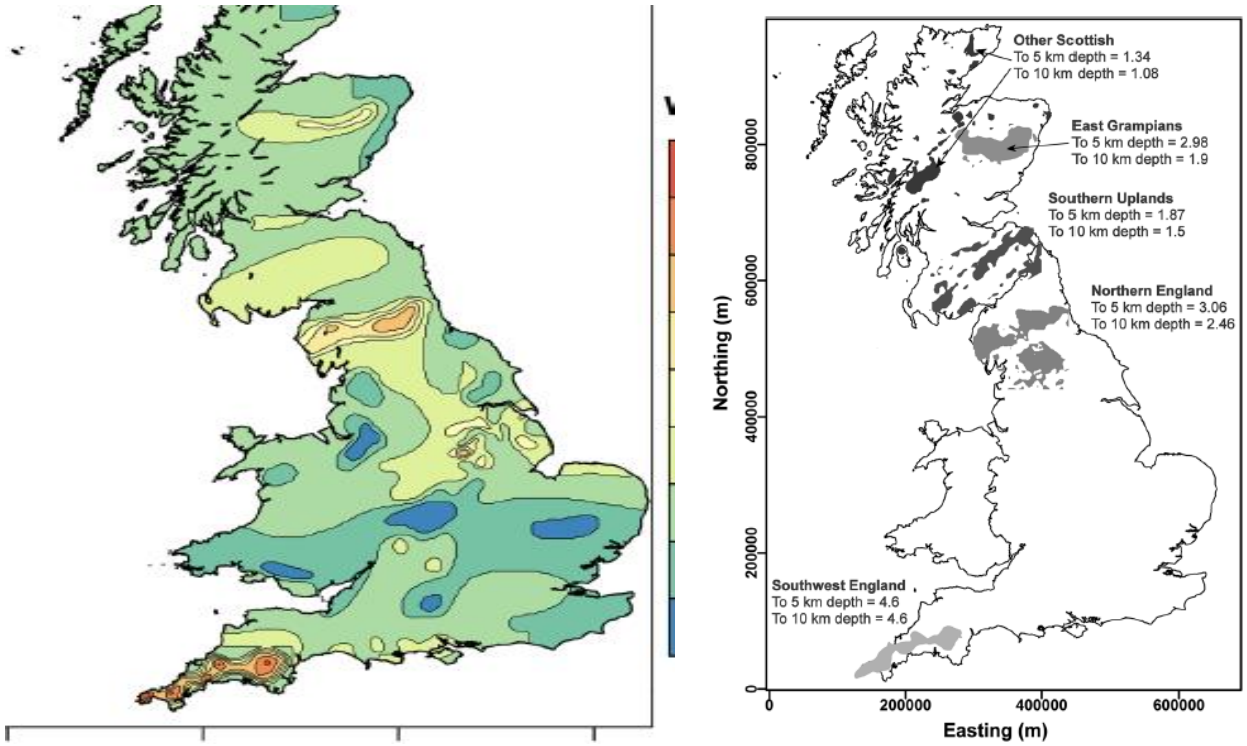

Figure 1: The deep geothermal energy potential of Great Britain. A. Surface heat flow map. B. The locations of significant high-level heat producing granites. Reproduced, unmodified from Busby and Terrington (2017), under Creative Commons Attribution 4.0 International License (http://creativecommons.org/licenses/by/4.0/). © The Author(s) 2017.

2.2.1 South-west England

An assessment of the EGS resource base for Great Britain identifies south-west England as having the greatest amount of 'technical potential power' at each 'depth slice' evaluated and in total, of all the English regions (Busby and Terrington, 2017). The high heat production of the region is associated with the Cornubian granite batholith, which extends across Devon and Cornwall (Figure 2). The Cornubian Batholith was the focus of a major geothermal experiment, the UK hot dry rock (HDR) research and development programme that ran from 1977 until the early 1990s (MacDonald et al., 1992; Richards et al., 1991) (Figure 3). There is currently significant renewed interest in the deep geothermal resource in Cornwall, with two advanced geothermal power projects in the county.

In addition to being one of the most prospective regions of Great Britain for deep geothermal heat south-west England hosts the Cornubian Orefield, part of the globally important Variscan metallogenic province (Figure 4). The orefield is a world-class Sn-W-Cu province and also contains As, Fe, Pb-Zn-Ag, U-Ni-Co and Sb-Au-rich mineralisation (Figure 5). It was a globally significant tin and copper producer during the late eighteenth century, and tin production continued up to late 1990s (Figure 6). During the last decade there has been a revival of interest in mineral exploration in the region, stimulated by the acquisition of high resolution airborne geophysical data, a LiDAR survey and geochemical sampling of soils and stream sediments (Yeomans, 2017), and development of the world-class Hemerdon W-Sn deposit (Shail et al., 2017). Growing interest in the security of supply of raw materials has stimulated research on the 'critical' metal potential the region, with an emphasis on tungsten, antimony, indium, cobalt and lithium (Simons et al., 2013a, b, 2014; 2017).

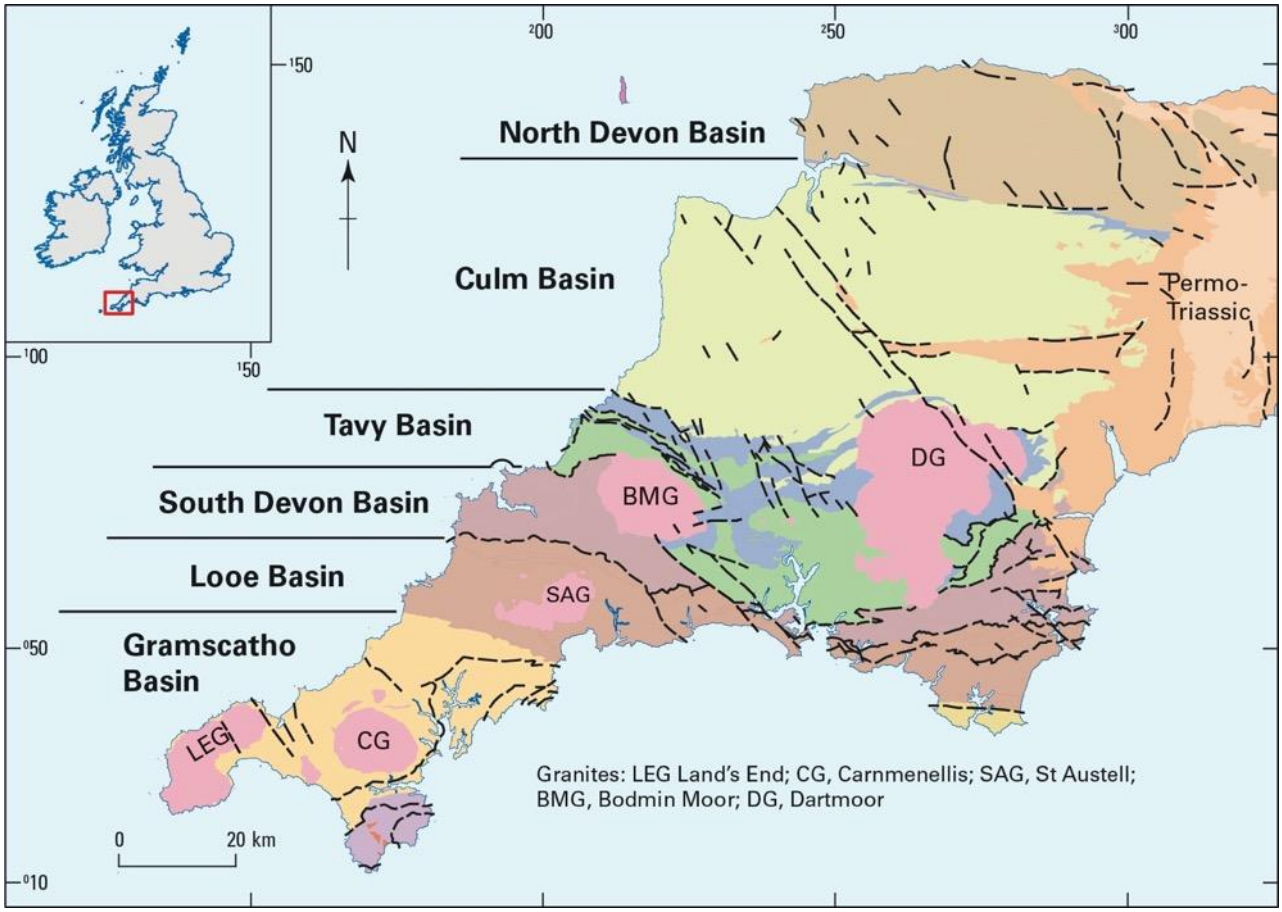

Figure 2: Simplified geological map of south-west England showing the distribution of sedimentary basins and the location of the granites of the Cornubian Batholith. The sedimentary basins typically comprise undifferentiated siltstones, mudstones and sandstones, with subordinate conglomerate. Modified from Shail and Leveridge (2009) with additional BGS data.

In summary the rationale for selection of south-west England as the UK CHPM2030 study area is due to a coincidence of geological phenomena and data availability:

i) The extensive exposed Permian granites result in it being one of the main high heat production and flow provinces in the UK;
ii) It hosts a major polymetallic ore field that is spatially associated and intrinsically linked to the granitic magmatism (Figure 5);
iii) It has a long history of metal production (surface and underground mining greatly enhance the geoscience knowledge base) and geothermal and economic geology research (geological research in south-west England has been undertaken for >250 years), meaning it is one of the best surveyed parts of the UK, and resulting in extensive data availability; and
iv) It is the focus for deep geothermal research and development in the UK, with ongoing mineral exploration programmes.

Figure 3: Rosemanowas Quarry, Cornwall, the Hot Dry Rock (HDR) project drilling site. A. Pump infrastructure used in the hydraulic stimulation experiments. B. Equipment used in the viscous fluid hydraulic stimulation experiments. Images reproduced from the HDR project photo archive held by the British Geological Survey. C. The quarry in 2017, which is used for testing geophysical equipment. D. The three HDR project borehole collars. E. Core from HDR project borehole RH12. F. Core from HDR project borehole RH15. British Geological Survey © UKRI.

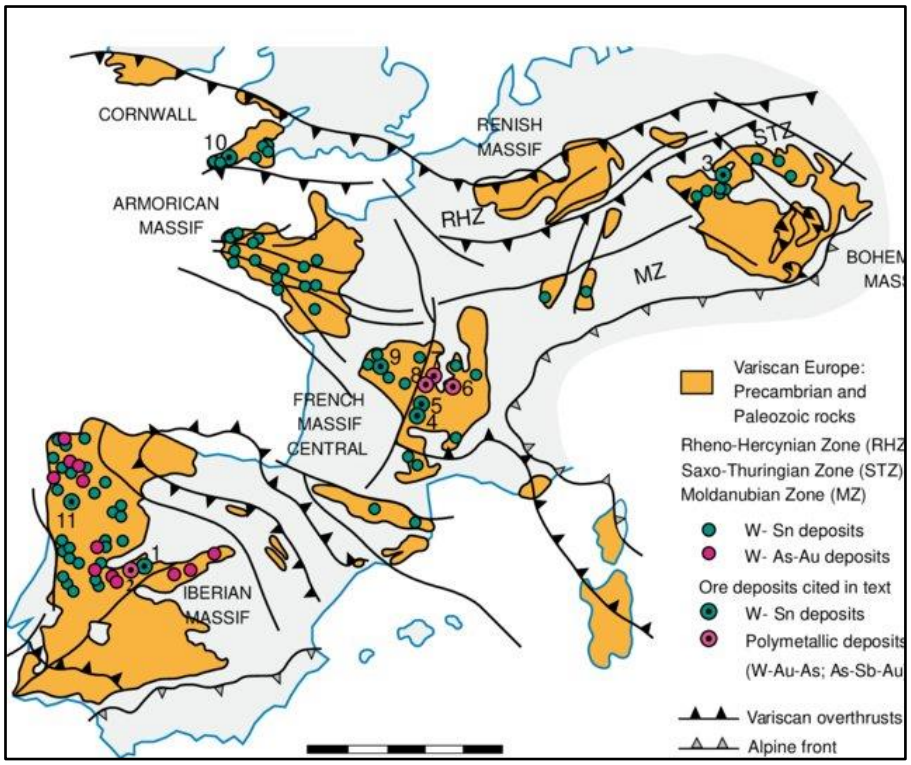

Figure 4: The Variscan belt in central and western Europe and major W-Sn and polymetallic minerals deposits. Reproduced, unmodified from Timón et al. (2019), under Creative Commons Attribution 4.0 International License (http://creativecommons.org/ licenses/by/4.0/).

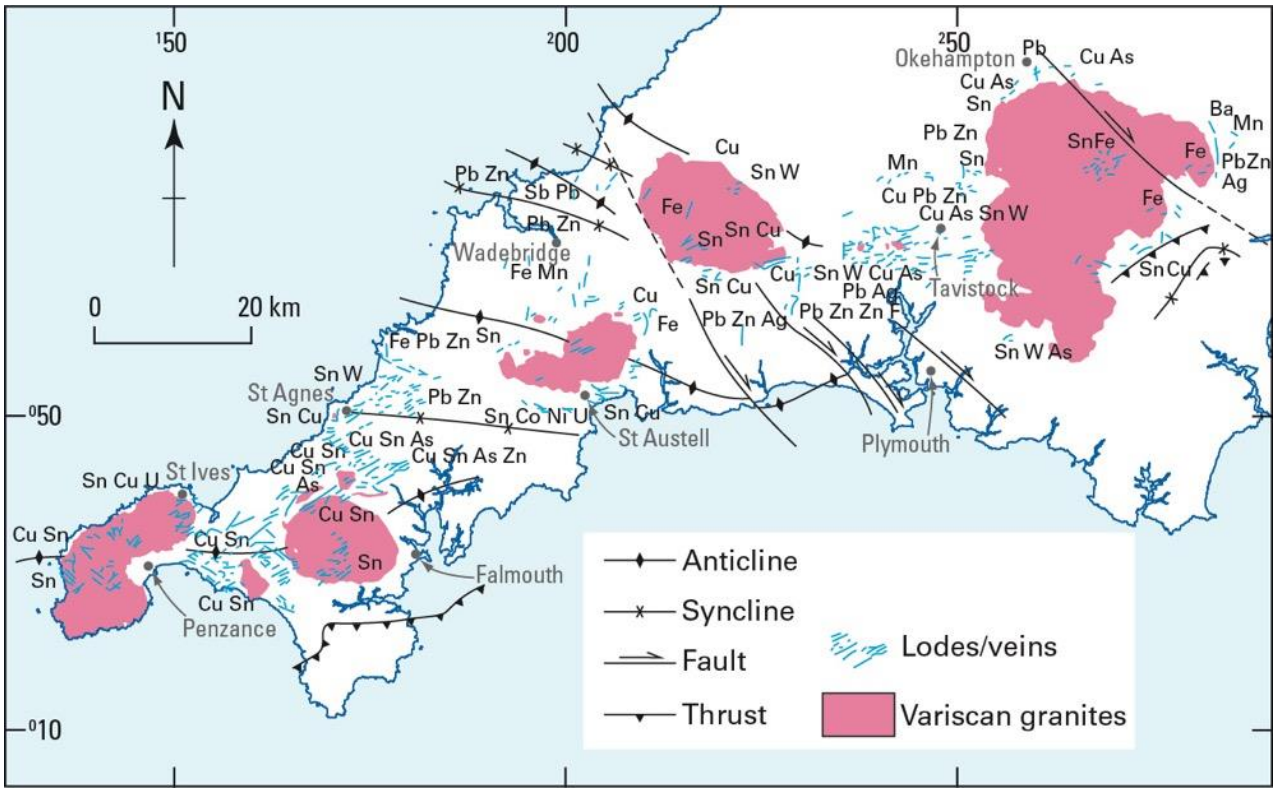

Figure 5: The Cornubian Orefield of south-west England. Modified from Dunham et al. (1978).

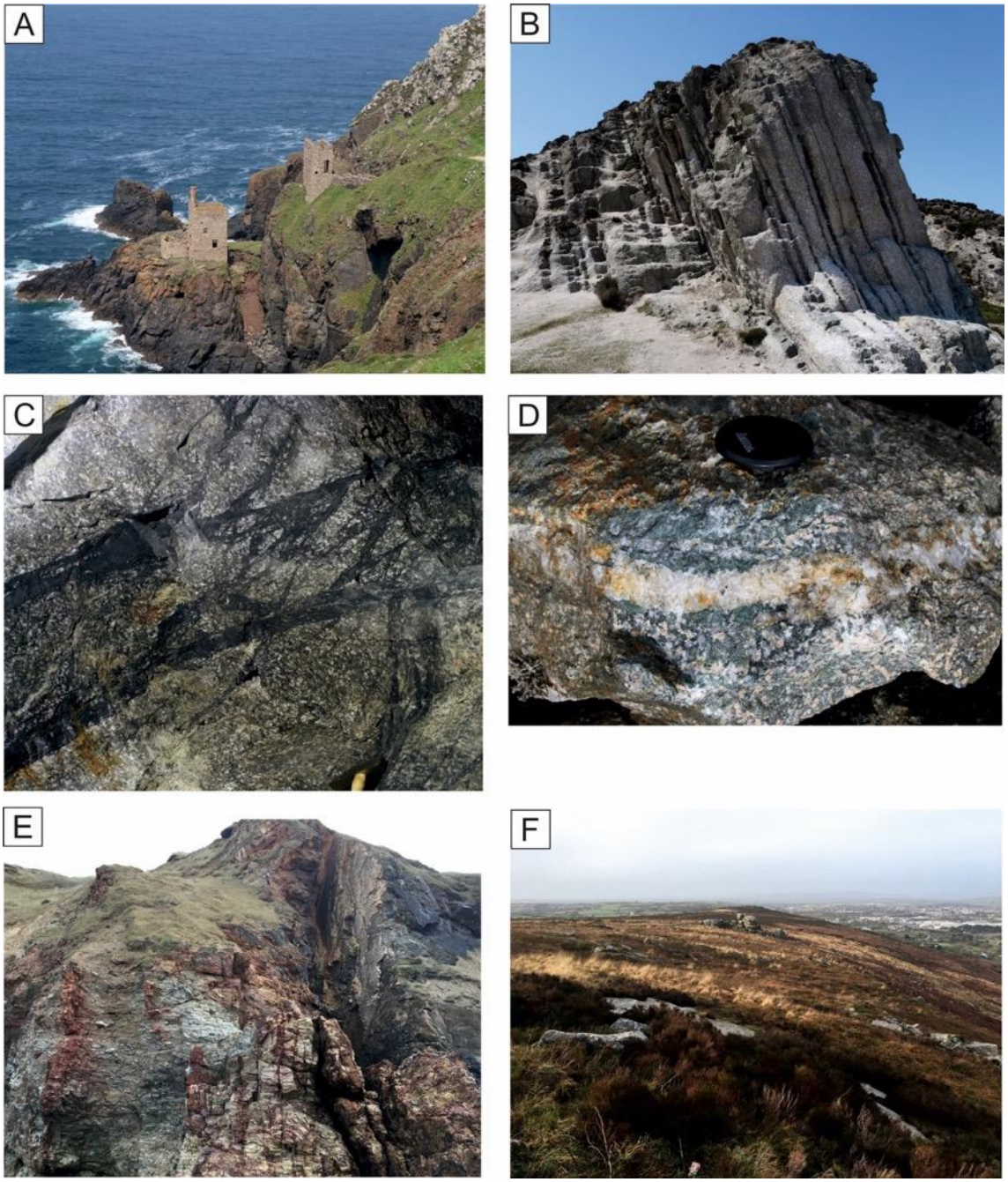

Figure 6: Typical Cornish mineralisation and exposures of granite. A. The Crowns Engine house, Botallack, Cornwall, evidence of the long history of mining in the region. B. Greisen bordered sheeted tin-tungsten veins occur in granite at Cligga Head on the north coast of Cornwall. C. South Crofty Mine, Robinson's Section, 380 fm. level, No. 4 lode west. Cassiterite/tourmaline filled fractures forming No. 4 lode seen in the roof of a drive in megacrystic, coarse-grained, biotite-granite. D. Main-stage mineralisation collected from a mine dump in the Minions area of Cornwall. E. A major zone of N-S-trending cross-course mineralisation, Cotty's Point, near Perranporth, north Cornwall. F. View westwards from close to the Carn Brea monument the along the exposure of the Carn Brea granite (a satellite granite of the Carnmenellis pluton), overlooking Camborne. British Geological Survey © UKRI.

2.2.2 The northern Carnmenellis CHPM2030 study area

The entire Cornubian Batholith is prospective for deep geothermal heat, with predicted average temperatures, at a depth of 5 km, ranging between 185 °C to 221 °C (Beamish and Busby, 2016). Mineralisation, the second criteria for CHPM, also occurs across much of the peninsula (Figure 6A). However, this pilot area assessment whilst considering the broader scale geological context and drawing on data from across Cornwall, principally focuses on a study area, of about 50 km^2, covering the northern part of the Carnmenellis granite (Figure 7). The reasons for selecting this area were:

i) The average temperature of the Carnmenellis granite, at 5 km depth, is predicted to be 200 °C (Beamish and Busby, 2016);
ii) Its hosts a well-defined mineralised belt, the Camborne-Redruth mining district, which passes along the northern edge of the Carnmenellis granite;
iii) Its complex structural geology, including major faults zones that are likely to enhance reservoir permeability, and a rheological contrast along the granite-country rock contact and metamorphic aureole;
iv) The presence of the legacy HDR research site (Figure 3), the boreholes from which provide the only published deep temperature measurements for the batholith, and confirm that the Carnmenellis granite has temperatures of 79 °C and 100 °C at 2.1 km and 2.6 km depeth, respectively; and
v) It contains the recently established United Downs Deep Geothermal Power (UDDGP) project, which is drilling two new deep boreholes into the granite.

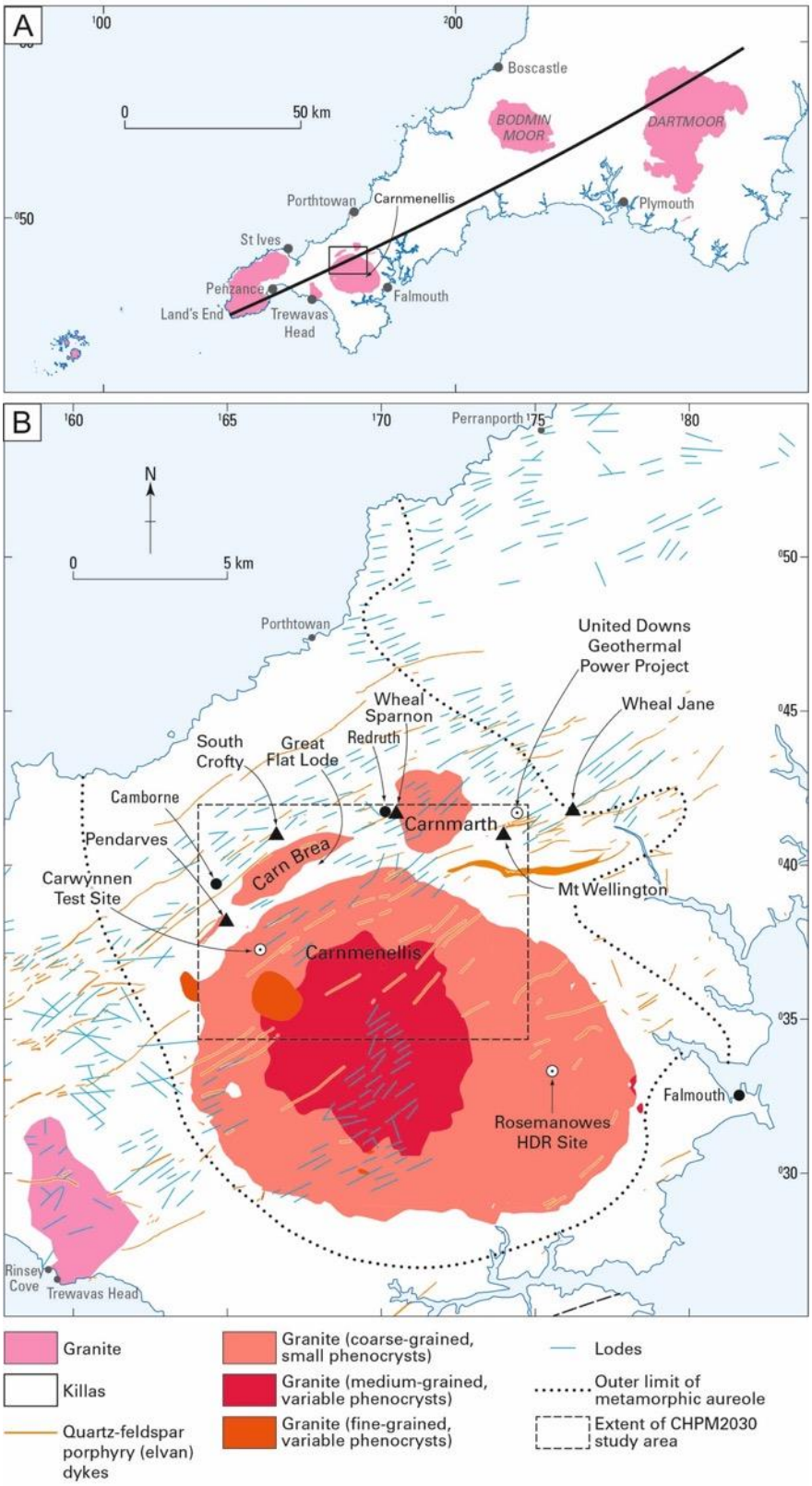

Figure 7: Location of the CHPM2030 south-west England study area. A. The position of the study area on the Cornubian peninsula of south-west England, with the major granite plutons shown. The black continuous line represents the approximate location of the cross-section shown in Figure 9. B. Simplified geology of the study area and its immediate surroundings, and key localities referred to in the text. British Geological Survey © UKRI.

3 Geology of the prospective area

3.1 Regional geological history

For a detailed review of the geology of the south-west England region the reader is referred to Westhead et al. (2017) and references herein. A brief chronology of major geological events in south-west England, from oldest to youngest, includes:

i) The development of a series of middle Palaeozoic (410–345 Ma), E–W-trending volcano-sedimentary basins (Figure 2) that have been inverted, deformed and subjected to low-grade metamorphism (Parker, 1989; Shail et al., 2014);
ii) Variscan continental collision, during the mid-Carboniferous (331–329 Ma), resulted in significant crustal shortening and the development of NNW-trending thrust sheets (Parker, 1989; Shail et al., 2014);
iii) Crustal extension and orogenic collapse during the late Carboniferous and lower Permian that resulted in extensive granitic magmatism (295–270 Ma) (Figure 2) and associated hypothermal (300–600°C) W-Sn greisens (Figure 6B), and mesothermal (200–300°C) Sn-Cu mineralisation hosted by E–W-trending mineral lodes (Figure 6C,D). Following granite emplacement widespread Pb-Zn-Ba-F-U mineralisation developed in N–S-trending cross-courses (Figure 6E), many of which are re-activated NNW-trending thrust sheets (LeBoutillier, 2002; Parker, 1989; Shail et al., 2014) (Table 1) and;
iv) Cyclic periods of uplift, erosion and sedimentation throughout the Jurassic and Cretaceous (Parker, 1989; Shail et al., 2014) resulting in the current landscape (e.g. exposure of granite roof zones at the existing land surface, Figure 6G).

3.1.1.1 Early Permian post-Variscan magmatism

The current surface expression (Figure 6F) of the Cornubian Batholith comprises six large granite plutons. From west to east these are: the offshore Isles of Scilly (120 km^2), Land's End (190 km^2), Carnmenellis (135 km^2), St Austell (85 km^2), Bodmin (220 km^2) (Figure 8A), and Dartmoor (650 km^2) (Figure 2, Figure 9). The subsurface extent of the Cornubian Batholith is estimated to be about 250 km in length and it has an approximate width of between 40–60 km (Scrivener, 2006; Willis-Richards and Jackson, 1989). However, there is uncertainty about the true size of the Cornubian Batholith because current models are based on limited geophysical data and very few deep drill holes. Similarly, there is some uncertainty about the true thickness and shape of the granite plutons. 2D-gravity modelling of the Carnmenellis, St Austell and Bodmin granites indicates they are tabular bodies with an estimated thickness of between three and four kilometres, whilst the larger Dartmoor pluton is estimated to be about nine kilometres thick (Taylor, 2007). However, seismic refraction data (discussed in Section 4.1.2.2) suggest that the depth of the base of the batholith (i.e. its lower contact with the killas) is variable, ranging from about 7–8 km beneath the Bodmin and Carnmenellis granites, respectively, to about ten kilometres beneath the Dartmoor granite (Brooks et al., 1984; Shail et al., 2014).

Radiometric dating (U-Pb in monazite and zircon) suggests that the extensive granitic magmatism in south-west England occurred over a period of about 20 million years, between about 293–274 Ma, although separate intrusive episodes can be identified in some of the individual plutons (Chen et al., 1993; Chesley et al., 1993; Clark et al., 1994). In terms of age, the plutons can be broadly divided into two groups: (i) the older (>290 Ma) Bodmin Moor, Isles of Scilly and Carnmenellis granites and; (ii) the younger (<286 Ma) Land's End, St Austell and Dartmoor granites (Figure 10).

Table 1: Summary of mineralisation styles in the south-west England. Adapted from Andersen et al. (2016).

Pre-granite mineralisation	Main ore minerals				
1) Rifting and passive margin development (early Devonian- Carboniferous) sedimentary-exhalative (SedEx) mineralisation	Haematite	Siderite	Galena	Sphalerite	
2) Variscan convergence and continental collision (late Devonian-Carboniferous) shear zone hosted Au-Sb + base metal mineralisation	Gold	Bournonite	Sphalerite	Chalcopyrite	Tetrahedrite
Granite-related mineralisation					
3) Early post-Variscan extension and magmatism (early Permian)					
a) Magnetite-silicate skarns developed in metabasaltic hosts	Magnetite	Cassiterite			
b) Sulfide-silicate skarns developed in calc-silicate granite hosts	Cassiterite	Arsenopyrite	Pyrite	Chalcopyrite	Pyrrhotite
c) Greisen-bordered sheeted vein complexes	Wolframite	Cassiterite	Chalcopyrite	Sphalerite	Bismuthinite
d) Quartz-tourmaline veins and breccias	Cassiterite	Haematite			
e) Polymetallic sulfide lodes	Cassiterite	Chalcopyrite	Wolframite	Arsenopyrite	Sphalerite
Post-granite mineralisation					
4) Episodic intraplate rifting and inversion (late Permian – Cenozoic)					
a) Crosscourse Pb-Zn ± F, Ba mineralisation	Galena	Sphalerite	Arsenopyrite	Chalcopyrite	

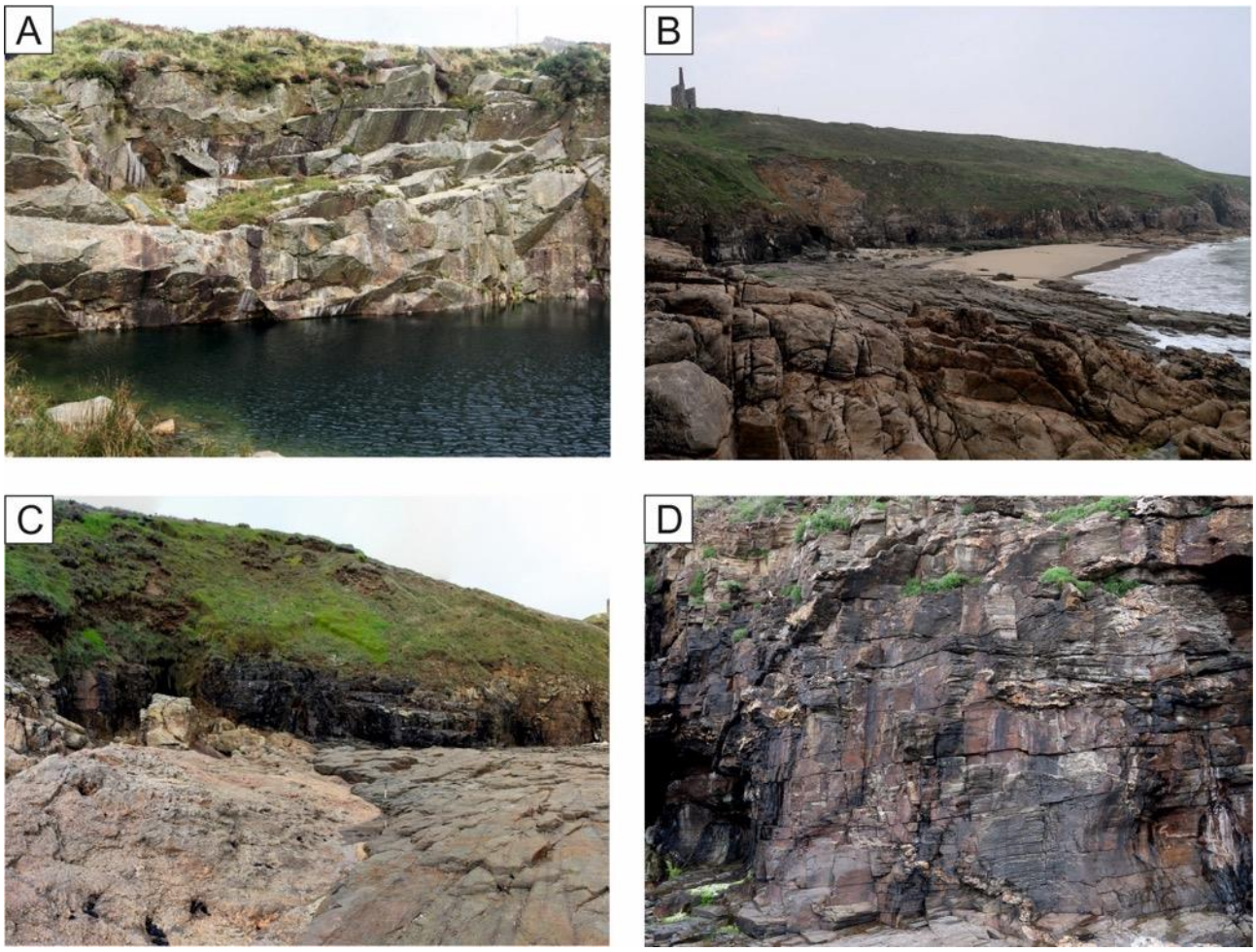

Figure 8: Typical exposures of granite and their country rocks in Cornwall. A. Quarried exposure in the Bodmin granite close to Minions, Cornwall. B. Exposure of granite intrusion (foreground), with rocks of the Mylor Slate Formation, locally termed 'killas' forming the wave-cut platform, at Rinsey Cove, south-west Cornwall. C. Contact between the granite and metasedimentary rocks (Mylor Slate Formation), at Rinsey Cove, south-west Cornwall. Deformed quartz veins in the metasedimentary rocks (Mylor Slate) at Rinsey Cove, south-west Cornwall. British Geological Survey © UKRI.

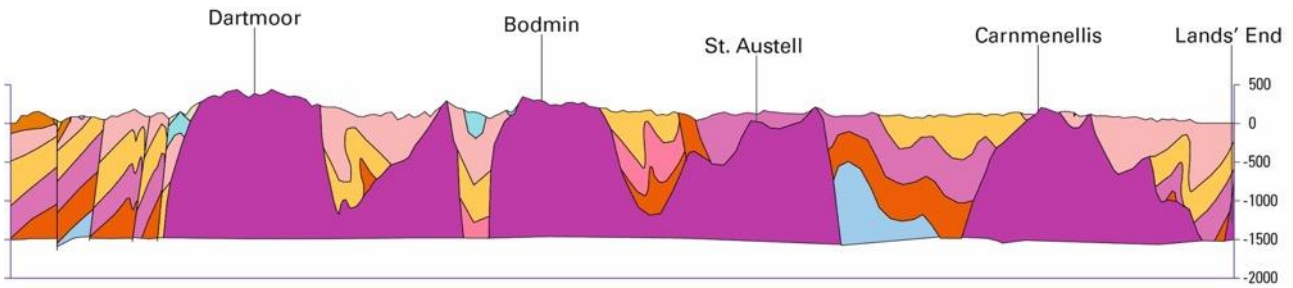

Figure 9: Schematic cross-section of the geology of the south-west region from St Just to Crewkerne. The major granite plutons are labelled and shown in purple with adjacent sedimentary basins. Adapted from Westhead et al. (2017).

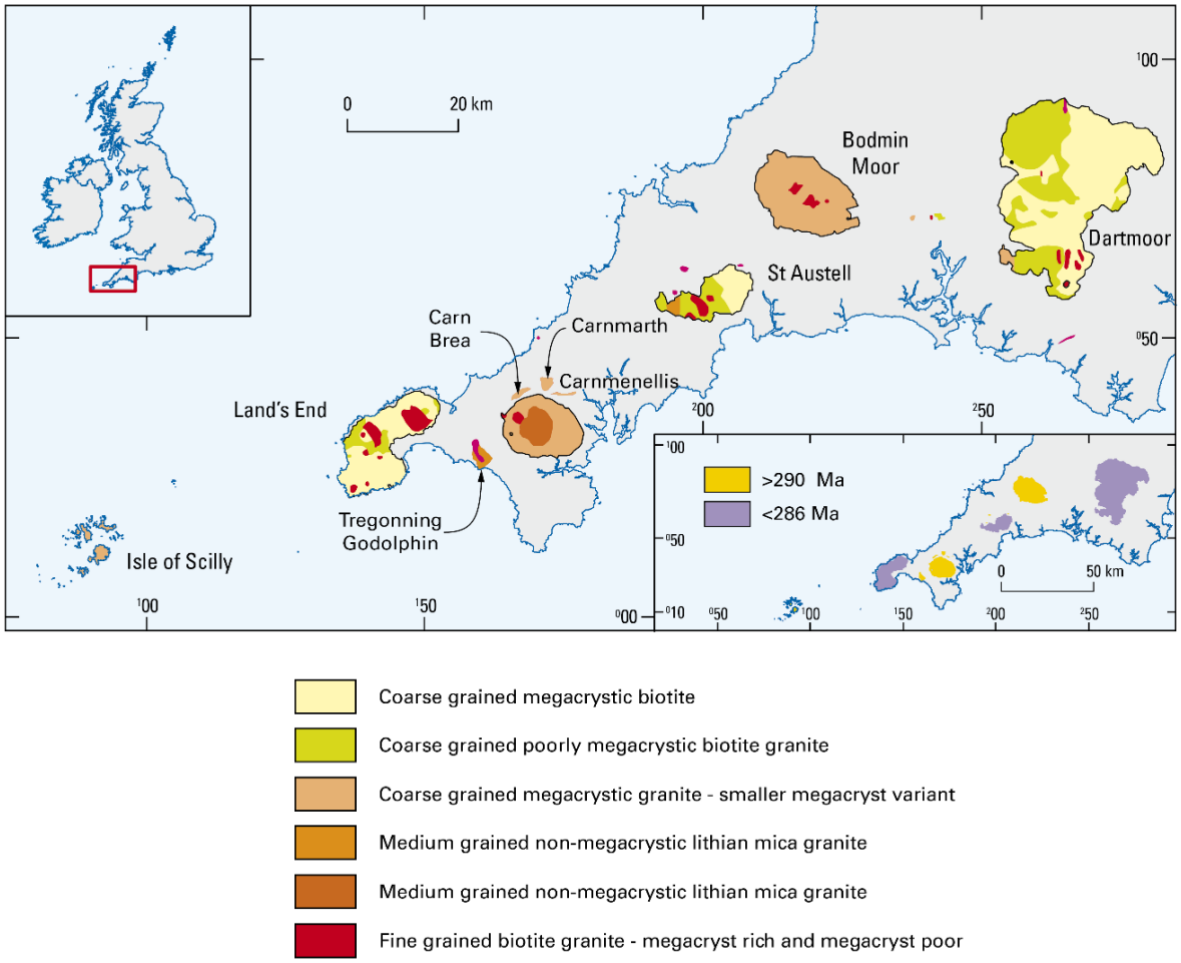

Figure 10: Map showing the principal mineralogical and textural variations in the Cornubian Batholith. It combines subdivisions into biotite and Li-mica granites with a textural scheme based primarily on mean matrix grainsize and the size and abundance of alkali feldspar megacrysts. Compiled from Bott and Scott (1964); Brooks et al. (1983); Dangerfield and Hawkes (1981); Exley and Stone (1982); Floyd et al. (1993), Hawkes and Dangerfield (1978); Manning (1998); Manning et al. (1996); Shail et al. (2014); Stone and Exley (1985); and Simons et al. (2016). In-set map shows the distribution of granite ages: Dartmoor, St Austell and Land's End (in purple) are <286 Ma, whereas Bodmin, Carnmenellis and Isle of Scilly (in yellow) are older (>290 Ma), based on Chen et al. (1993); Chesley et al. (1993); Clark et al. (1994); Darbyshire and Shepherd (1987). British Geological Survey © UKRI.

Compositionally the granites are all peraluminous, S-type granites that are enriched in elements such as K, B, F, Li, U, Th, Sn, Rb and Pb. A notable feature of Cornubian granites is their high uranium content (with an average content of about 12 ppm for all plutons), which is largely controlled by the distribution of accessory minerals such as uraninite and monazite (Chappell and Hine, 2006; Scrivener, 2006). Importantly it is the radioactive decay of uranium, thorium and potassium in the Cornubian granites that is responsible for their high heat production (Chappell and Hine, 2006). There have been many attempts to produce classification schemes, which describe the mineralogical and textural variations observed in the Cornish granites (Brooks et al., 1983; Floyd et al., 1993; Ghosh, 1934). The granites of south-west England have most recently been categorised by Simons et al. (2016) into five groups based on their mineralogy. These comprise the: two-mica granites such as Bodmin and Carnmenellis (G1); muscovite granites such as Hemerdon Ball and Cligga Head

(G2); biotite granites such as Land's End, St Austell and Dartmoor (G3); tourmaline granites that comprise parts of the St Austell granite (G4); and topaz granites such as Tregonning-Godolphin (G5). Other minor variants also exist, including Li-mica granite and fluorite granite (Brooks et al., 1983; Busby, 2010; Floyd et al., 1993; Manning et al., 1996). The older granites (Bodmin Moor, Isles of Scilly, and Carnmenellis) can be distinguished from the younger granites (Land's End, St Austell and Dartmoor) by their texture, composition (peraluminosity), isotopic signature ($^{\varepsilon}$Nd) and rare earth element (REE) patterns. These differences may reflect increased mantle-melting and possibly increased amounts of crustal melting during formation of the younger granites, probably in response to higher temperatures in the lower crust. However, it remains unclear why temperatures increased, and if this change was transitional, or an abrupt change in response to a discrete tectonic event (Shail et al., 2014; Stone, 1995, 1997, 2000a, b).

3.1.1.2 Country rocks

Emplacement of the Cornubian Batholith into largely Devonian sedimentary rocks caused large-scale heating and thermal alteration (Figure 8B,C). The resulting metamorphic rocks in south-west England are locally known as 'killas' (Figure 8D). Although these rocks are not economically important in themselves, fractures within them host a significant proportion of the region's mineral deposits (e.g. polymetallic mineral veins, or 'lodes'). The killas comprises a series of Devonian (410–355 Ma), marine deposited sandstones, siltstones, mudstones and rare carbonates that were regionally metamorphosed to sub-green schist facies during the Variscan Orogeny. As a result of granite emplacement, the low-grade regional metamorphism has been locally overprinted by higher-grade contact metamorphism, to produce a series of aluminosilicate and/or cordierite-bearing slates (Selwood et al., 1998).

3.2 Tectonic framework

The majority of the following section is based on Westhead et al. (2017). South-west England is located in the Variscan orogenic belt, which extends across southern England, a small part of southern Wales and Ireland, and across extensive areas of Europe (Figure 4). The region forms part of the Rhenohercynian Zone, which is interpreted as an oceanic collision belt (Franke, 1989; Holder and Leveridge, 1986). The sedimentary rocks of Devonian and Carboniferous age were deposited in fault-bounded basins (Figure 11), which are recognised as forming part of a passive margin sequence (Holder and Leveridge, 1994). The correlation of these rocks across north-western Europe (Holder and Leveridge, 1986) is indicative of a pattern of extensive E–W-trending sedimentary basins forming the northern passive margin of a laterally extensive Rhenohercynian oceanic basin (Franke, 1989). Remnants of oceanic crust and active margin sequences from this basin are preserved in southern Cornwall as the Lizard ophiolite. The sequence of extension and basin opening, followed by inversion and deformation within the Variscan rocks of the south-west England is considered to be related to the continental rifting and growth of the Rhenohercynian Ocean, followed by its closure during continental collision. Rifting of the passive margin occurred over a period of approximately 65 Ma, from the Early Devonian to the early Carboniferous, with extensional faulting becoming progressively younger northwards (Leveridge, 2002) (Figure 11).

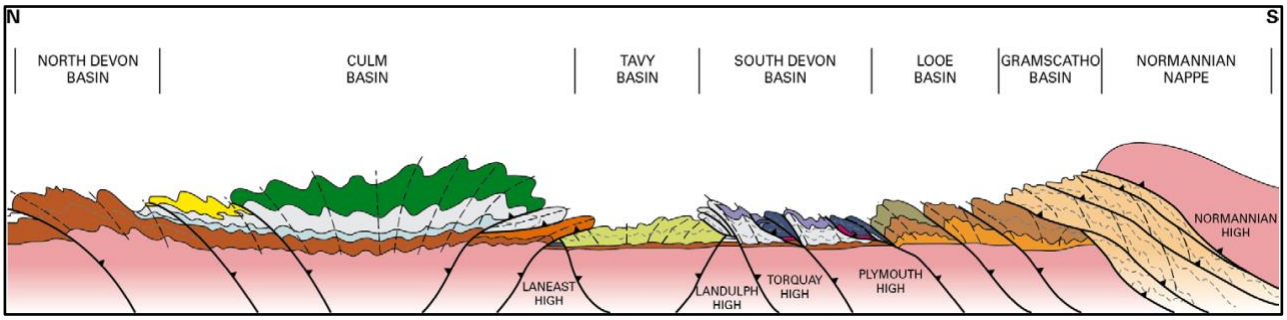

Figure 11: Sketch cross-section of the Variscan belt of south-west England, late Carboniferous. The sequence comprises six major E–W-trending fault-bounded basins: the Gramscatho, Looe, south Devon, Tavy, Culm and north Devon basins, with extensional faulting and intervening highs, getting progressively younger northwards. Redrawn from Leveridge and Hartley (2006).

The Rhenohercynian passive margin sequence within south-west England consists of six major E–W-trending fault-bounded basins: from east to west these are the: North Devon Basin; Culm Basin; Tavy Basin; South Devon Basin; Looe Basin and; Gramscatho Basin, together with the intervening highs (Figure 2, Figure 11). The synrift basin fill of the Gramscatho Basin is largely covered by sedimentation, resulting from subsequent Late Devonian synconvergence. To the north, the Looe Basin is overthrust to the south by sedimentary rocks of the Gramscatho Basin (Holder and Leveridge, 1986). Its northern boundary is defined by the interbasinal high deposits of the Plymouth Limestone Formation (Leveridge, 2002). The strata of the Looe basin constitute three major thrust nappes. At each thrust front, large-scale antiformal folding is present in the hanging wall, which suggests that internally the Looe Basin comprises three sub-basins with half-graben geometries.

The latest stages of the Carboniferous and the Permian are marked by a number of tectonic events related to a post-Variscan phase of regional extension (Holder and Leveridge, 1994). Extension and pressure release led to the melting of the lower crust–mantle boundary and the intrusion of the Dartmoor and Bodmin granites between 290 and 280 Ma (Chen et al., 1993; Chesley et al., 1993; Darbyshire and Shepherd, 1985). Related acid volcanic activity along the main NW-trending strike-slip faults, including the associated high-level quartz-feldspar porphyry dykes, which are locally termed ‘elvans’, and the intrusion of similar felsitic magma into E–W fractures, is compatible with N–S extension at the time. Similarly the formation of the E–W-trending, main stage, mineral veins, dated at 280 ± 20 Ma (Moorbath, 1962), indicates that the crust was undergoing N–S extension. The magnitude of this latest Carboniferous to Permian extension is indicated by the formation of sedimentary basins, containing several kilometres’ thickness of Permian sediments, above extensionally reactivated Variscan thrusts in Plymouth Bay (Evans, 1990), the Haig Fras, Melville and St Marys basins in the South-west Approaches (Hillis and Chapman, 1992), and the Crediton trough in Devon (Durrance, 1985b). Within south-west England, a number of gently dipping thrusts exhibit significant extensional reactivation, most of which can be ascribed to Permian extension.

Post-Variscan movements include sinistral fault displacements on the NW-trending faults during N–S extension in the Permian, the Late Triassic to Jurassic or the early Palaeogene. The dextral displacements of the NW-trending faults are related to N–S compression most probably of Late Cretaceous, late Palaeogene–Neogene or Miocene age (Leveridge, 2002) (Figure 8D).

3.2.1 Structural geology

South-west England is a structurally complex region whose geological past has been dominated by Variscan tectonics (Figure 2 and Figure 12). British Geological Survey (BGS) mapping, academic research and seismic surveys have led to the identification of three main deformational phases associated with Variscan orogenesis. Two phases are related to crustal shortening (D_1 and D_2) whilst the third (D_3) is associated with crustal extension during orogenic collapse (Alexander and Shail, 1996; Leveridge, 2002). The D_1 deformation event (c. 385 Ma) is characterised by: i) large-scale (10s km), NW-SE-trending strike-slip faults; ii) a NNW-trending mineral lineations; and iii) E-W-trending folds. Structures associated with the second deformation event (D_2) are similar to those formed during D_1, but D_2 structures are generally more steeply dipping. The D_3 event (c. 305–300 Ma) occurred in response to orogenic collapse and associated crustal extension. It resulted in the development of steep to gently inclined WNW-ESE-trending extensional faults (Alexander and Shail, 1996; Leveridge, 2002) (Figure 13). Regionally extensive NNW-SSE-trending cross-course structures formed during the Permian in response to a period of crustal extension (Scrivener et al., 1994; Shail and Alexander, 1997).

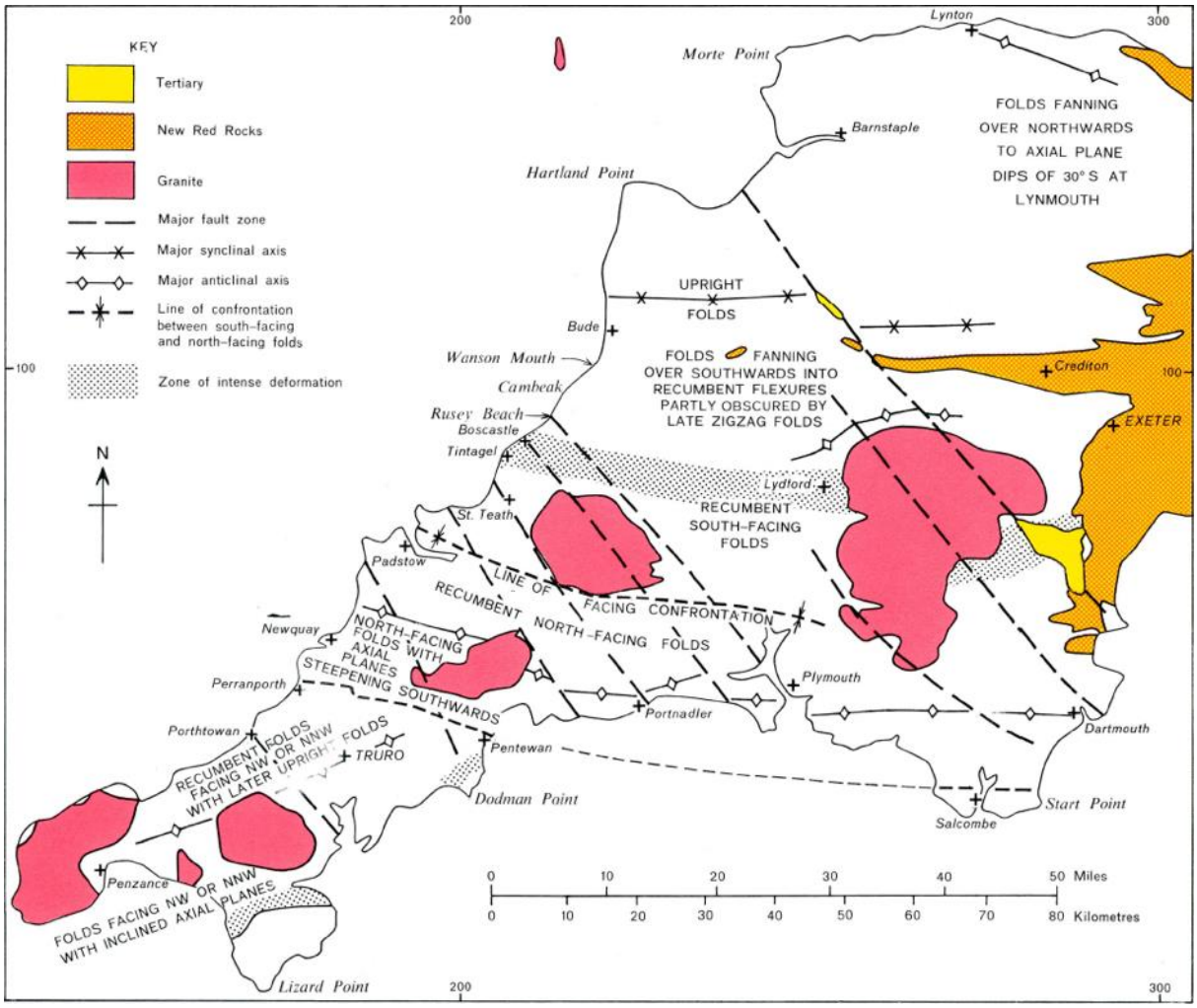

Figure 12: The major structures in south-west England, including the significant NW-SE-trending cross-courses. Reproduced from Edmonds et al. (1985).

Figure 13: Extensional fault (dashed white line) in the cliff at Gooden Heane Cove, near Portreath. British Geological Survey © UKRI.

In south-west England both granite and the killas have inherently poor permeability (Heath, 1985). Accordingly, fluid circulation in the region is largely controlled by regional-scale structures (e.g. NW-SE-trending faults) (Figure 2) and fractures (Bromley et al., 1989; Heath, 1985; Smedley et al., 1989). Fractures in the granite are primarily the result of magma chamber processes, for example cooling and hydro-fracturing (caused by the movement of magmatic fluids). In contrast fractures in the killas are principally the result of granite emplacement. Local zones of high-fracture density, in both granite and killas, may also be associated with episodes of late faulting. However, the permeability and connectivity of these fractures, particularly at depth, remains enigmatic (Heath, 1985).

3.3 Geology of the CHPM2030 study area

The geology of the south-west England study area (Figure 7) is dominated by the following lithologies: i) Devonian metasedimentary rocks of the Mylor Slate Formation; ii) the younger (Permian) Carnmenellis granite; and subordinate, iii) NE-SW-trending quartz-feldspar porphyry dykes (elvans). A description of these lithologies is provided below.

3.3.1 CHPM target formations

3.3.1.1 Mylor Slate Formation

The Mylor Slate Formation (MSF) (Figure 8B, C, D), or Mylor Series as it was previously known, extends over a large area of southern Cornwall, including the area around the northern edge of the Carnmenellis granite. The formation comprises two distinct sedimentary facies, which include interbedded slates and siltstones, and a breccia facies (the Porthleven Breccia Member, PBM). The MSF also includes a significant igneous component in the form of metamorphosed basic lavas and volcanic breccias (greenstones) that occur towards the base of the formation. The MSF typically comprises well-bedded dark grey slates with thin (c. 5 mm), finely spaced, siltstone laminae. Locally within the formation thin beds of siltstone (up to 15 cm thick) and fine-grained sandstone (up to 30 cm thick) are interbedded with the slate (Leveridge et al., 1990). The MSF was interpreted by Wilson and Taylor (1976) to be a low-energy, marine basinal sequence that contains distal turbidites, whereas the PBM formed in a higher energy environment, and is thought to represent a marine mass flow deposit (Middleton and Hampton, 1976).

The rocks of the MSF were initially regionally metamorphosed to greenschist facies at about 355 Ma (Hawkes, 1981), at a temperature of about 300°C and a pressure of at least 3 kbars (Barnes and Andrews, 1981), representing a burial depth of about 12 km (Holder and Leveridge, 1986). Emplacement of the Carnmenellis granite during the Permian (c. 313±3) (Neace et al., 2016) resulted in high-temperature contact metamorphism of the MSF, which resulted in the formation of hornfelsed slates and siltstones that typically contain coarse-grained andalusite. The metamorphic aureole around the northern edge of the Carnmenellis granite extends for approximately 1 km at its widest point (Leveridge et al., 1990) (Figure 7).

3.3.1.2 Carnmenellis granite

The Carnmenellis granite is a large (135 km^2), roughly circular granite body, with two satellite granites (the Carn Marth and Carn Brae granites) on its' northern edge (Figure 7). Emplacement of the Carnmenellis granite into the MSF occurred during the Permian (c. 293 Ma) (Chen et al., 1993; Chesley et al., 1993). It is a two-mica granite (G1), which exhibits variation in both grain size (coarse, medium and fine-grained), and the abundance and size of feldspar phenocrysts (Figure 10, Figure 14). The smaller of the two satellite granite bodies found at the northern edge of the Carnmenellis granite is also a coarse-grained, two-mica granite (G1), whereas the larger one is a fine- to coarse-grained muscovite granite (G2) (Simons et al., 2016). The Carnmenellis granite predominantly comprises alkali feldspar, plagioclase, quartz, biotite and muscovite, with accessory tourmaline, andalusite, ilmenite, apatite, monazite, zircon, xenotime and uraninite (Bromley et al., 1989). It is chemically similar to other Cornubian granites, being a peraluminous (A/CNK >1), S-type granite, enriched relative to the upper continental crust, in elements such as Li, Be, In, Sn, As, Pb and W (Bromley et al., 1989; Simons et al., 2016). The observed chemical and mineralogical characteristics of the Carnmenellis granite indicate formation by partial melting of a muscovite and biotite-rich greywacke source rock (Simons et al., 2016).

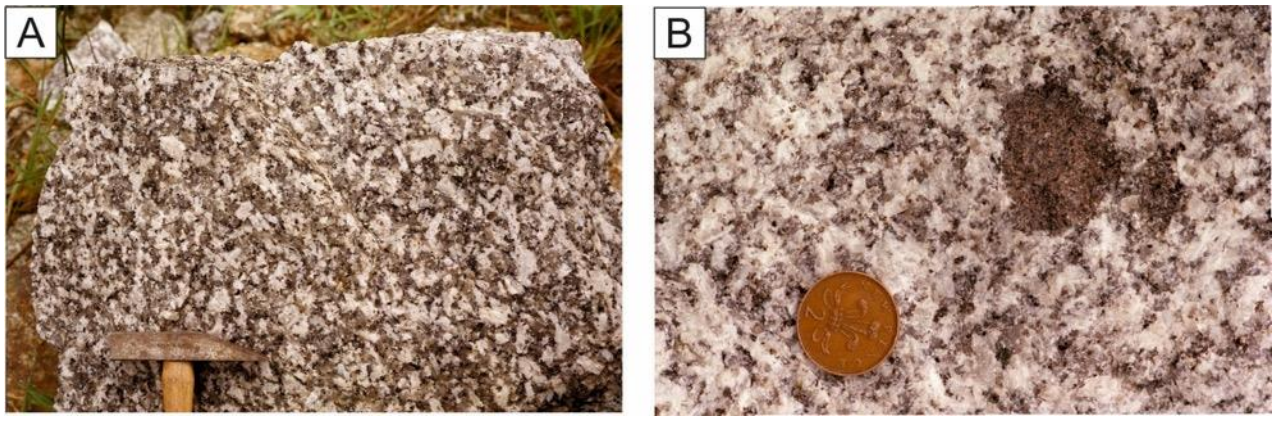

Figure 14: Carnmenellis granite. A. Trevone Quarry, near Longdowns. Unfoliated Carnmenellis granite. Carnmenellis Granite showing no significant alignment of the megacrysts. B. Carnsew Quarry, Penryn. A xenolith in the Carnmenellis granite. A biotite-rich xenolith of sedimentary origin lying within the Carnmenellis granite. British Geological Survey © UKRI.

The shape, thickness and size of the Cornubian Batholith has been the subject of significant scientific debate for almost 60 years. Early land-based gravity surveys confirmed (Bott et al., 1958) that the individual granite bodies exposed at surface are connected at depth. 2D-gravity modelling has been used to define the extent of the granite at depth (Beer et al., 1975; Rollin, 1988; Rollin et al., 1982; Tombs, 1977), and to define the thickness and shape of the individual plutons (Bott and Scott, 1964; Brooks et al., 1983; Edwards, 1984; Willis-

Richards and Baria, 1989). The most recent re-interpretation of gravity data by Taylor (2007) predicts that the Carnmenellis granite is an asymmetrical, tabular body approximately 3–4 km thick (Figure 15). The asymmetry of the Carnmenellis granite is mirrored in the width of the metamorphic aureole, which is significantly wider on the northern edge of the granite, where it can be up to 3 km wide. On the southern and eastern edges where the contact with the country rocks is steeper, the aureole rarely exceeds 1 km in width (Leveridge et al., 1990; Westhead et al., 2017). There are only limited seismic refraction data that cover the onshore extent of the Cornubian Batholith. However, these seismic refraction data do provide an indication of the depth of the base of the batholith (i.e. its lower contact with the killas), which is variable, and ranges between about seven and eight kilometres beneath the Carnmenellis granite (Brooks et al., 1984; Shail et al., 2014).

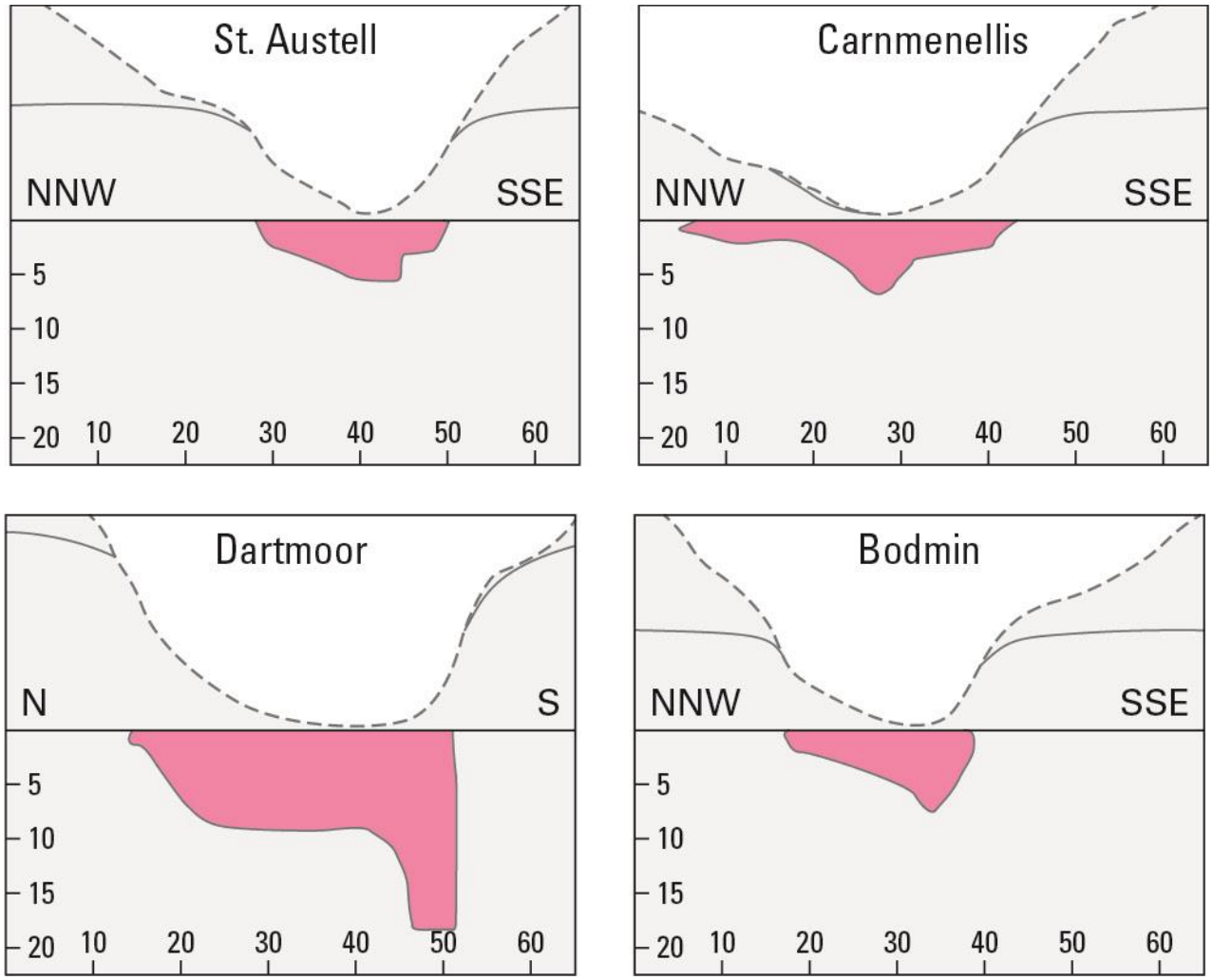

Figure 15: 2D gravity models for the St Austell, Carnmenellis, Dartmoor and Bodmin. Depths are in kilometres and horizontal scale has tick marks at 10 km intervals. Redrawn from Taylor (2007) Geological Society of London ©.

However, there is significant uncertainty about the actual shape and thickness of the Carnmenellis granite, and other plutons in south-west England, because of assumptions made during modelling (e.g. density contrasts) and the limited amount of data the models are based on. It is important to note that very few boreholes have been drilled to validate these models. However, two deep (2–2.5 km) boreholes in the

Carnmenellis granite, drilled during the HDR Programme, confirm that the granite extends to at least this depth and that it is chemically and mineralogically consistent over this depth range (Burgess et al., 1982a).

Constraining the Carnmenellis granite surface using borehole records

The BGS single onshore borehole database (SOBI) contains records produced by geologists or geotechnical engineers from drilling and site investigations. BGS holds a total of 2293 borehole records for the counties of Devon and Cornwall in south-west England (Figure 16). Of these records, 1414 have been digitised and 879 paper records are not yet available digitally. In an attempt improve the current topographic model for the granite surface, digital records of bore holes were reviewed and data on the depth of granite intersection were recorded (Appendix 1). For the purposes of this study only bore holes with a total depth greater than 100 m (500 in total) were considered (Figure 17). Of these, 88 boreholes encountered granite, with 37 being drilled directly into the granite at surface, and with the remaining 51 intersecting granite at depth. The following information was compiled for each of the bore holes: borehole name, BGS ID, hyperlink, approximate granite intersection depth in metres, total depth of bore hole, azimuth, inclination, easting and northing. The azimuth, inclination and depth of granite intersection have been used to define a revised granite surface for the modelling work (Section 7). All data are freely available from https://www.bgs.ac.uk/products/onshore/sobi.html.

3.3.1.3 Other rock types

Quartz-feldspar porphyry dykes (‘elvans’) are a relatively common intrusive feature found in the Carnmenellis granite and in the MSF around the northern-edge of the granite, especially in the mineralised zone around Camborne and Redruth (Figure 7). The dykes are typically steeply dipping and vary in thickness between a few tens of centimetres to more than 40 metres (Figure 18). They generally trend ENE-WSW, which is parallel to the strike direction of the hydrothermal mineral veins in the mineralised zone around Camborne and Redruth (Leveridge et al., 1990). Elvans are mineralogically simple, typically comprising alkali feldspar, quartz and plagioclase, and commonly display evidence of alteration of varying intensity, which resulted in the formation of secondary white mica, biotite and tourmaline. Geochemically elvans are granitic in composition, but with an enrichment in potassium. The similarity in mineralogy and chemistry of the elvans and granites has led some researchers to suggest a genetic link between the two (Shepherd et al., 1985).

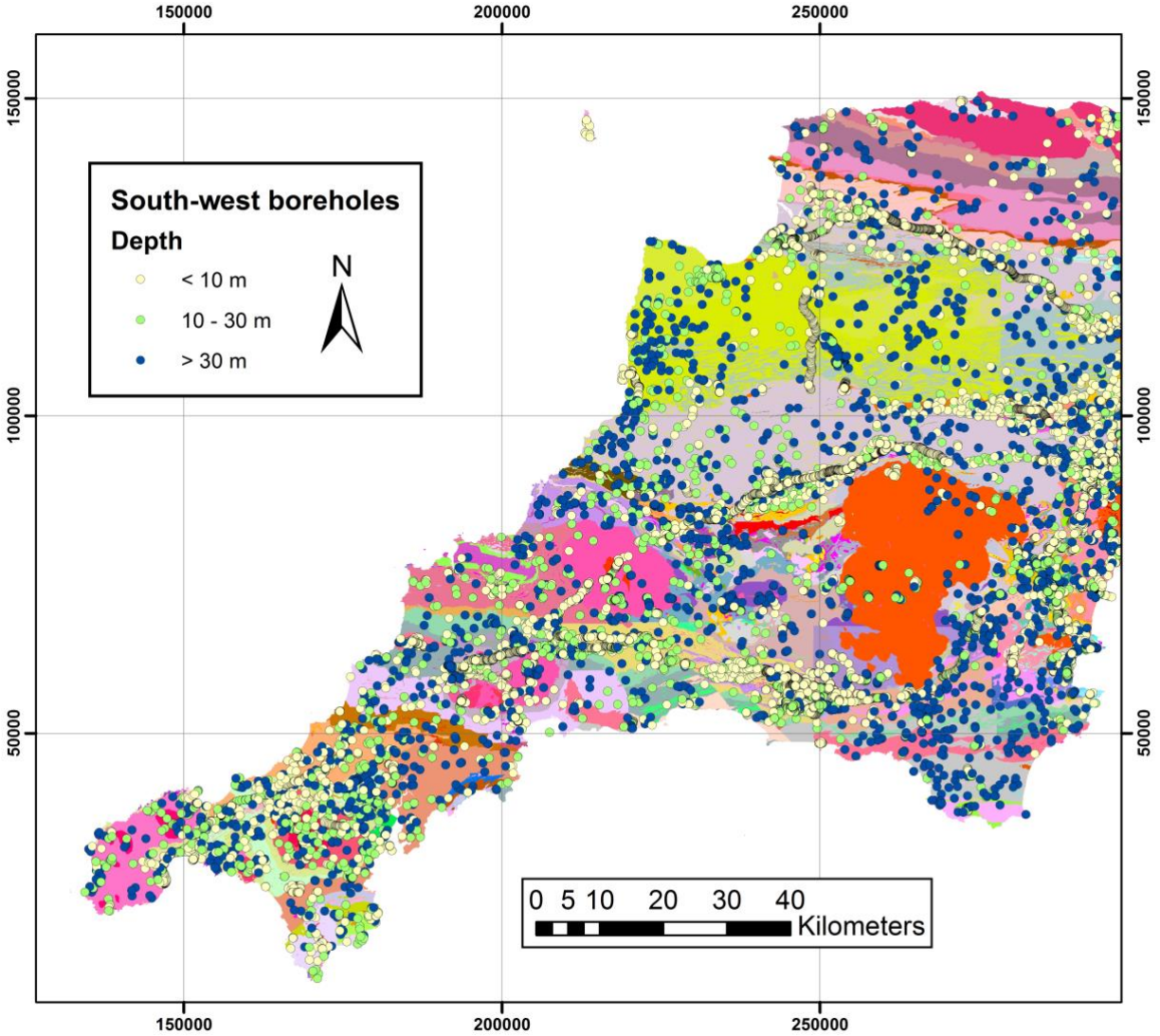

Figure 16: Distribution of bore holes that have been drilled in south-west England. Data for these bore holes are held at the British Geological Survey. British Geological Survey © UKRI.

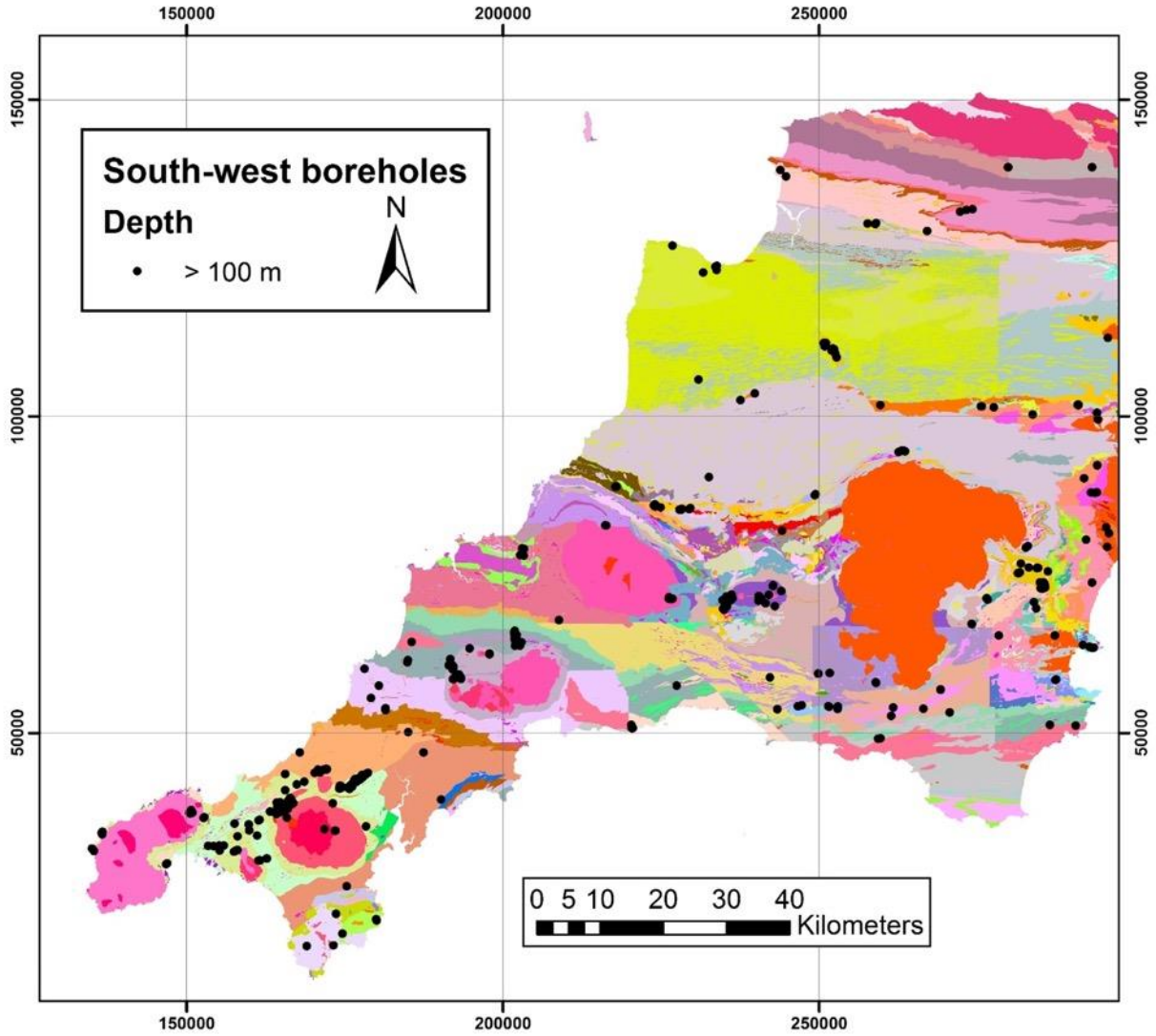

Figure 17: Boreholes deeper than 100 m (500 in total) that were reviewed in this study. British Geological Survey © UKRI.

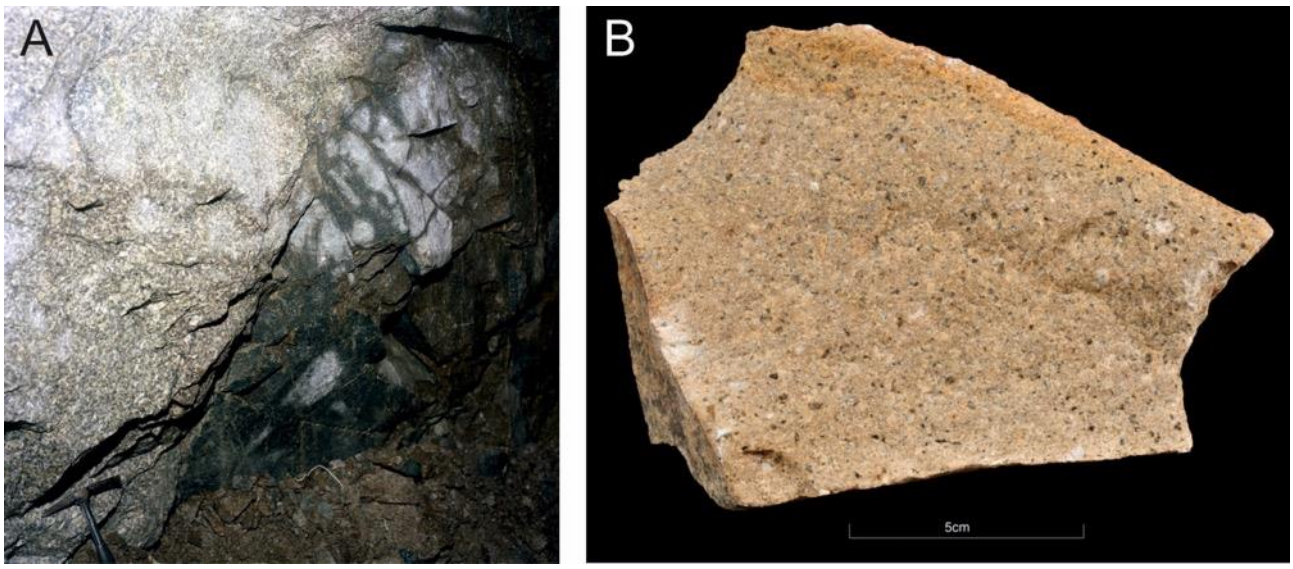

Figure 18: Quartz-feldspar porphyry dykes, which are locally termed 'elvans' in south-west England. A: South Crofty Mine, Robinson's Section, cross cut N. from No. 4 to No. 6 lode. Megacrystic, coarse-grained, biotite-granite/elvan contact in cross-cut. B: An elvan from DeLank Quarry, Bodmin, Cornwall. British Geological Survey © UKRI.

3.3.2 Key structural features

Cornish granites, including the Carnmenellis granite, typically have very low primary permeability, in the order of 10^{-8} to 10^{-10} D (Batchelor, 1978), but relatively high hydraulic conductivity (c. 20 mD;) according to Durrance (1985a) . The high hydraulic conductivity is driven by geological features in the granite such as joints, fractures, faults, mineral veins and heavily-fractured elvan dykes (Heath, 1985; Smedley et al., 1989).

3.3.2.1 Jointing in the granite

Jointing is particularly important for controlling fluid flow in Cornish granites (Figure 19), and the following four joint sets have been identified in the Carnmenellis granite (Bromley et al., 1989; Heath, 1985; Leveridge et al., 1990) (Figure 20):

i) Major joint set 1 is characterised by a set of steeply-dipping (60–85°) ENE-WSW-trending joints that contain tourmaline and quartz. They are parallel to the elvan dykes and hydrothermal mineral veins observed in the mineralised zone around Camborne and Redruth;
ii) Major joint set 2 is characterised by a set of vertical, variably mineralised (with galena and fluorspar) NNW-SSE-trending joints that are perpendicular to major joint set 1, but parallel to regional 'cross-course' structures;
iii) A subordinate set of unmineralised, vertical, NNE-SSW-trending joints; and
iv) A second set of subordinate, unmineralised, vertical E-W-trending joints.

Figure 19: Typical jointing in the Godolphin granite, exposed at Rinsey Cove, SW Cornwall. British Geological Survey © UKRI.

There are a number of lines of evidence to suggest that the joints in the Carnmenellis granite formed in response to externally applied regional stress: i) fractures in the country rock have a similar trend to that of the major joints sets in the granite; ii) joint sets with a similar orientation have been observed in the other major granite bodies in Cornwall; iii) a general lack of radial or concentric cooling joints in the granite; and iv) about 95 per cent of steeply-dipping joints in all granite bodies lie within a few tens of degrees of the dominant NNW-SSE trend (Bromley et al., 1989; Leveridge et al., 1990). It is also the regional stress field, orientated NNW-SSE that controls fluid flow, predominantly along stress-field parallel features such as joints and cross-courses. The horizontal stress regime ensures that these features remain dilated, permitting fluid movement. Evidence for this has been reported by a number of studies (Alderton and Sheppard, 1977; Smedley et al., 1989) that have sampled warm, saline fluids from springs issuing from NNW-SSE-trending features in the deep-mines at the northern edge of the Carnmenellis granite. Work by Batchelor (1978), as part of the HDR programme, also indicated that NNW-SSE-trending features occur at depths of 2.6 km in the Carnmenellis granite.

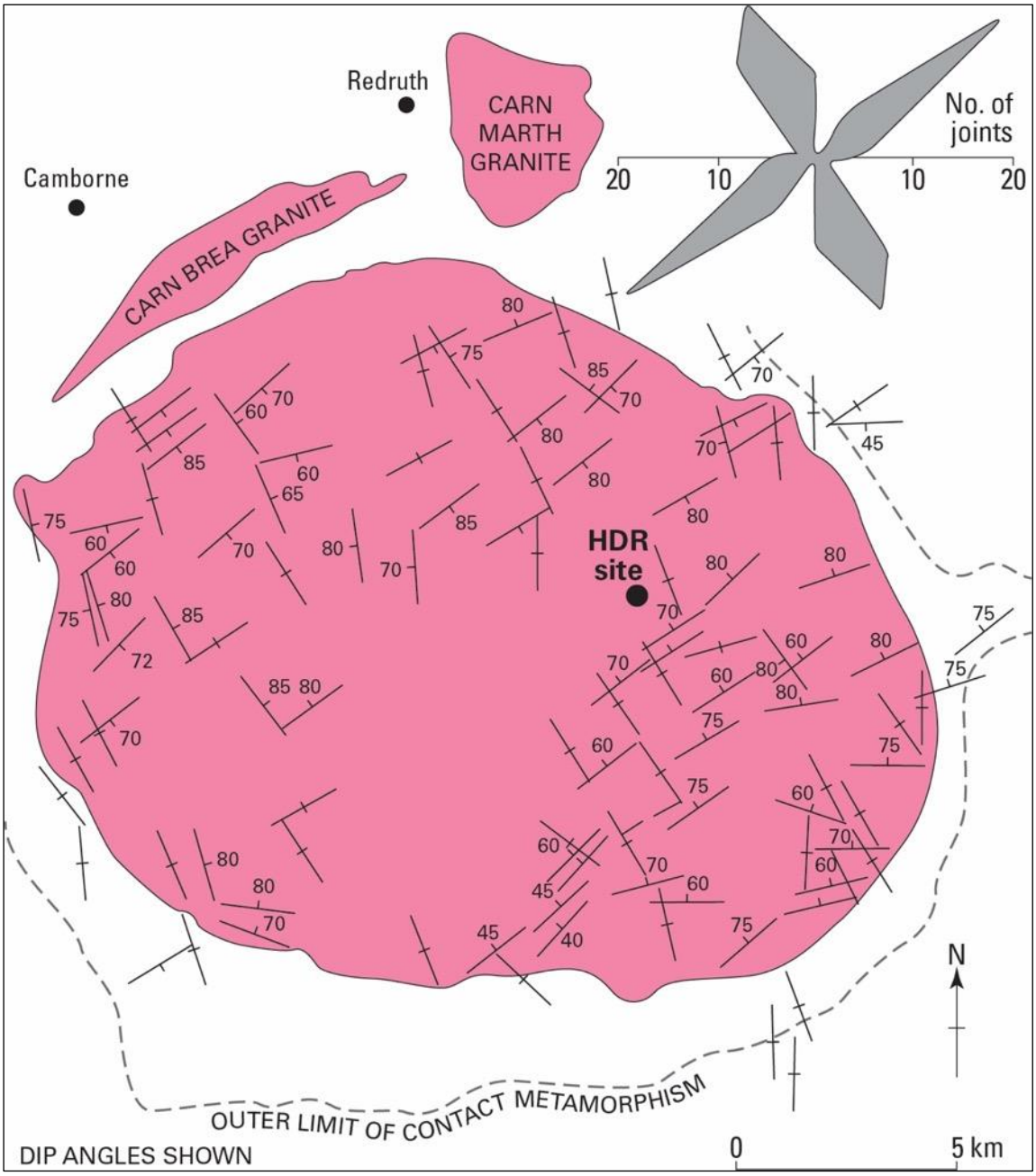

Figure 20: Sketch map of the Carnmenellis granite showing the strike and dip of the major joint sets Redrawn from Batchelor and Pine (1986), Figure 2, ©International Society for Rock Mechanics.

3.3.2.2 Faulting

A major feature of the region is the oblique dextral strike-slip faulting, striking between NW and NNW, which is locally associated with a subordinate complementary fault set striking between NNE and NE. In the CHPM2030 study area there is evidence for a period of N–S shearing followed by E–W crustal extension, which led to the development of extensive NW to N–S-trending fracture systems, throughout the Cornubian Orefield, locally termed 'cross-courses' (as strictly, they offset or cut across the earlier formed lode structures) (Figure 12). The Great Cross-course, the principal cross-course structure in the South Crofty Mine, is considered to represent a pre-granite strike-slip fault which was episodically reactivated during the Late Permian/Early

Triassic (Edmonds et al., 1985). The cross-course structures are likely to play a significant role in the overall permeability of the region. They are variably mineralised, with the vast majority of mineralised cross-courses occurring in the country rock, rather than granite (pers. comm.). The continuity of these structures in the study area remains ambiguous. BGS mapping from the mid-1800s shows these structures extending from the coast west of Porthtowan to the area SE of the Carn Marth granite (Figure 21A). However, subsequent revision of the mapping by the BGS (1990) whilst retaining inferred NW to N–S-trending faults, suggests these structures have more limited strike extent (Figure 21B). Whilst the cross-course structures can be clearly observed in coastal sections along the north Cornwall coast (Figure 22), and inland in underground mines exposures e.g. South Crofty (Figure 23), their position and continuity in the intervening zones remains conjectural.

Figure 21: Mapped cross-course structures to the north of the Carnmenellis granite. (A) NW-SE-trending cross-course structures are shown in white on the 1846 BGS map (de la Beche, 1846). (B) More recent BGS mapping (1990) of the same area depicts the cross-course structures as less continuous inferred faults (dashed black lines) (British Geological Survey, 1990). British Geological Survey © UKRI.

3.3.3 Data availability

The BGS is the world's longest established national geological survey, and is the UK's premier provider of objective and authoritative geoscientific data. It has been gathering geoscience data and information about the subsurface in the UK and other countries for more than 180 years. It is a data-rich organisation with more than 500 datasets in its care, including environmental monitoring data, digital databases, physical collections (e.g. borehole core, rocks and minerals), records and archives. Importantly, a great many of these datasets are openly available, many of which provide complete, seamless UK coverage at a number of scales. Certain other

datasets may be subject to confidentiality clauses and/or licencing fees. Information about how to access these datasets can be found here: http://www.bgs.ac.uk/data/home.html?src=topNav.

These national datasets are available to the CHPM2030 project, and can provide a very useful starting point to assess CHPM potential in south-west England. Many of the datasets cover much of the UK, whereas others are specific to south-west England (e.g. geophysical data conducted as part of the TELLUS project (http://www.tellusgb.ac.uk/). Most of the data stored relate to surface exposures or the near-surface environment. Although, the datasets do contain much information about a large number of boreholes and mines, most does not extend below 100 m, and there is limited data below 1,000 m. This places significant constraints on predictions when extrapolating the data to EGS depths (i.e. 4–6 km). The datasets are also of differing ages and levels of detail - reflecting changing national priorities over the past decades. In terms of geothermal development, much of the data are derived from a national programme of work in the 1980s and early 1990s. Therefore, the data reflect monitoring technology and ideas at that time, and much of the data are in analogue format. Details of BGS' data holdings are outlined CHPM2030 Deliverable D1.2 (Shaw et al., 2016).

Figure 22: Major cross-course structures exposed in the cliffs on the north Cornwall coast. A. Cross-course in the bay is traceable from water line up the beach and into the cliff face (dashed line) at Gooden Heane Cove, near Portreath. B. Cross-course viewed from the cliff top west of Porthtowan. This structure is shown on Figure 21B extending southward from the coast west of Porthtowan for a strike distance of about 2 km. C. Mineralised cross-course in the cliff face at St Agnes. The vein has multiple stage of development, open space and contains quartz-tourmaline-pyrite and minor chalcopyrite. D. Mineralised cross-course in the cliff at Cotty's Point, near Perranporth. The mineralisation comprises numerous episodes of chalcedonic and coarse quartz infill, which are evidence of multiple fluid flow events. Significant reddening of the host killas may be related to iron-rich fluids. British Geological Survey © UKRI.

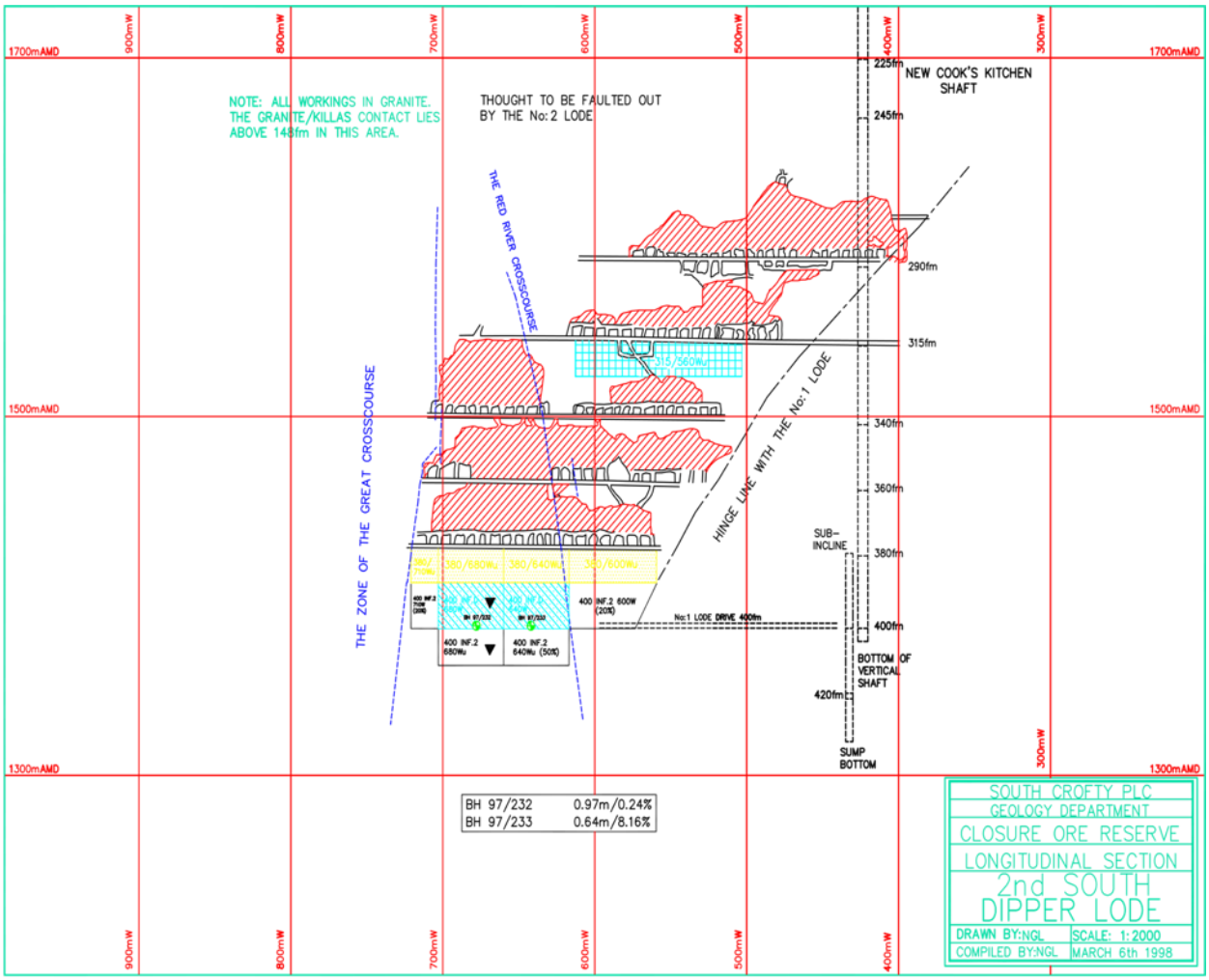

Figure 23: South Crofty Mine plan showing cross-courses identified in the mine. Reproduced with permission of Cornish Mines; credit: Dr Nick Le Boutillier (BSc PhD MCSM EurGeol CGeol FGS).

4 Geophysics of the prospective area

4.1 Previous work and data availability

4.1.1 Airborne data

In 1955 the British Geological Survey commenced the national aeromagnetic survey of the UK (altitude of 305 m and flight lines at 2 km). However, because of the mineral resource potential of south-west England, it was decided to combine the aeromagnetic survey with the UK Atomic Energy Agency uranium exploration programme and fly a more detailed co-funded survey over the region (Kimbell et al., 2003). The first part of the survey was flown in 1957, covering west and central Cornwall and used magnetic, electromagnetic (EM) and radiometric sensors. The EM results are strongly affected by cultural noise and equipment failure. The second phase, continuing eastward to cover the rest of Cornwall, most of Devon and part of Somerset, was flown in 1958–59 with only magnetic and radiometric sensors. The flight lines were flown parallel to the N–S National Grid lines and spaced 400 m (±200 m) apart and at an altitude of 150 m (± 30m). The principal aim of the radiometric survey was to identify vein-style uranium mineralisation. However, little attention was given to regional interpretation or other applications of the data (Kimbell et al., 2000; Kimbell et al., 2003). Iso-rad maps show a good correlation with the geology over the granites, surficial concentrations of radioactive minerals and mine dump material. The results of the aeromagnetic data have been included in published BGS maps of the region. The EM data has not been comprehensively interpreted, but many of the anomalies were considered topographical in origin or due to power infrastructure (Cornwell et al., 1995). In 1996 a decision was made to digitise the radiometric data from the 1957 survey to see if any new information could be gained (Kimbell et al., 2000). The digital data (Figure 24) provided new insights into the geology of the region, including the influence of granite mineralogy and alteration on the radiometric response, the characteristics of the Lizard Peninsula, changes in radiometric levels related to lithological units in the sedimentary rocks and the occurrences of uranium mineralisation (Kimbell et al., 2003).

This data has been superseded by that collected during the Tellus South West (TellusSW) survey (2013–2014), which encompasses the counties of Cornwall and parts of Devon and Somerset. The TellusSW survey had a number of components, but the most relevant to this review are a high resolution airborne geophysical survey, an airborne LiDAR survey, and geochemical sampling of soils and stream sediments. The maps and data produced show the soils, rocks and landscape at unprecedented depth and detail, and augment existing data to provide the two counties with among the best and most comprehensive environmental datasets anywhere in the world (www.tellusgb.ac.uk). The airborne geophysical data acquired during the second half of 2013 comprised a high resolution magnetic/magnetic gradient survey (Figure 25) combined with a multichannel (256 channel) radiometric survey (Figure 26). The survey was carried out using 200 m (N–S) line separations at a mean elevation of 91 m. Encompassing the counties of Cornwall and parts of Devon and Somerset, the survey provided 60,323 line-kilometres of data (www.tellusgb.ac.uk). The data is free to download and full details of the survey are provided in Beamish and White (2014). The LiDAR survey covers the same area as the geophysics and was flown during July to August 2013. Details of the survey can be found in Gerard (2014) and a high resolution digital terrain model was produced from the data by Ferraccioli et al. (2015) (see Appendix A in Gerard, 2014).

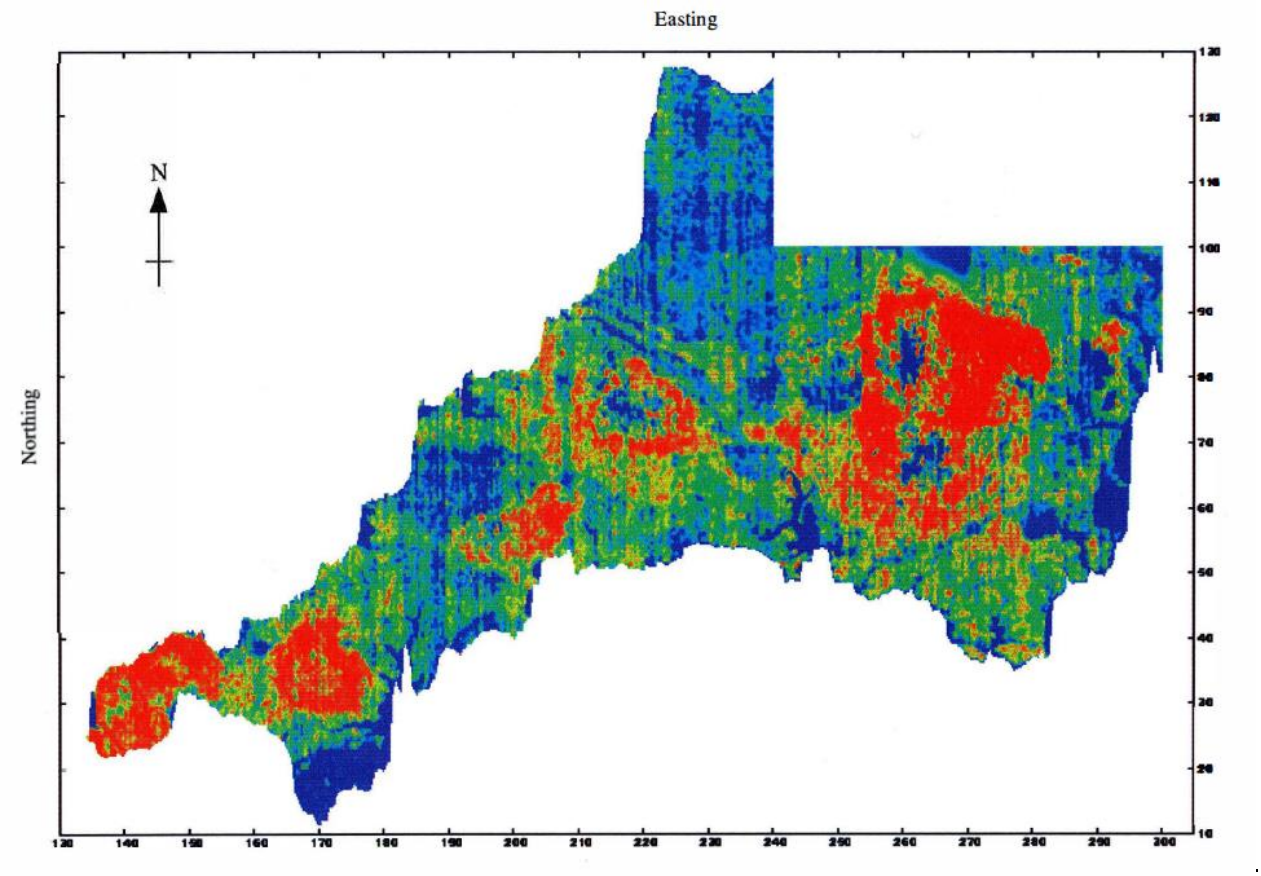

Figure 24: Total radiometric count map for south-west England. Red = high count, blue = low count. Shaded-relief map of the 1950s airborne radiometric data over south-west England. Reproduced from (Kimbell et al., 2000). British Geological Survey © UKRI.

Yeomans (2017) provides a summary of the potential applications of the TellusSW data for advancing our knowledge of the geology of south-west England. Simons et al. (2016) produced a new map for the Cornubian Batholith. However, it is based on mineralogical, geochemical and field relationships from a limited number of samples and selected areas of granite outcrop. Yeomans (2017) emphasises how the continuous nature of the airborne radiometric data (Figure 26) means it could be used for re-mapping these composite granites in a more objective way using their radioelement variation (which is a function of their geochemistry). This could be particularly valuable for enhancing our understanding in areas that may have low or no outcrop exposure. Yeomans (2018) used a machine learning approach (machine learning combine's statistical analyses and computer science to undertake automated pattern recognition in datasets), employing a range of algorithms to re-map and classify different granite types based on the airborne radiometric data and subsequently integrating the Tellus stream-sediment data. As the radiometric (gamma ray) data provide ground concentration estimates of the heat-producing radioelements it has also been used to revaluate heat production across the batholith (Beamish and Busby, 2016), which is discussed in Section 6.1.1. The TellusSW magnetic and LiDAR data have proved particularly useful for defining lineaments. This has permitted new structural interpretations in some areas and improved correlation of lithostratigraphic units across some map sheet boundaries (Yeomans, 2017). Yeomans et al. (2019) used the TellusSW magnetic, radiometric and LiDAR data and Object-Based Image Analysis (OBIA) (a tool for analysing spatially correlated groups of pixels) for semi-automated geological lineament detection in south-west England. This approach has generated a new comprehensive lineament network for the region (Figure 27).

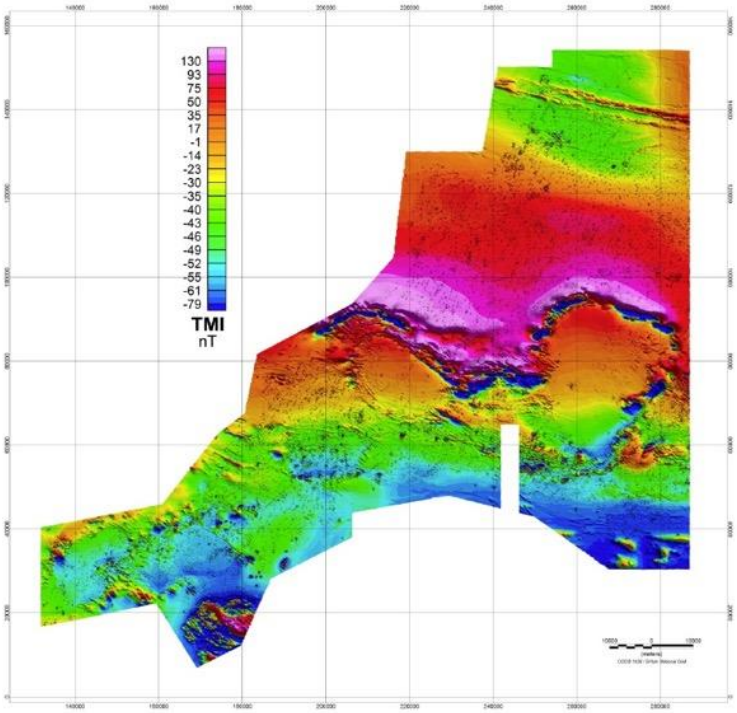

Figure 25: Total Magnetic Intensity (TMI), IGRF corrected to provide the final TMI anomaly data. Equal-area colour normalisation. Reproduced from Beamish and White (2014). British Geological Survey © UKRI.

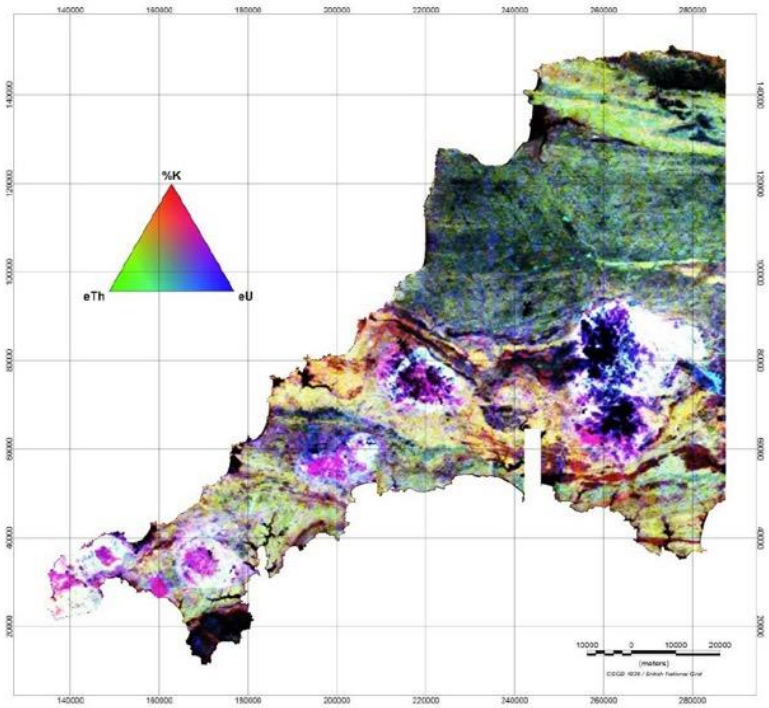

Figure 26: Ternary radiometric image formed from the Potassium (%K), Thorium (eTh) and Uranium (eU) ground concentration estimates. Reproduced from Beamish and White (2014). British Geological Survey © UKRI.

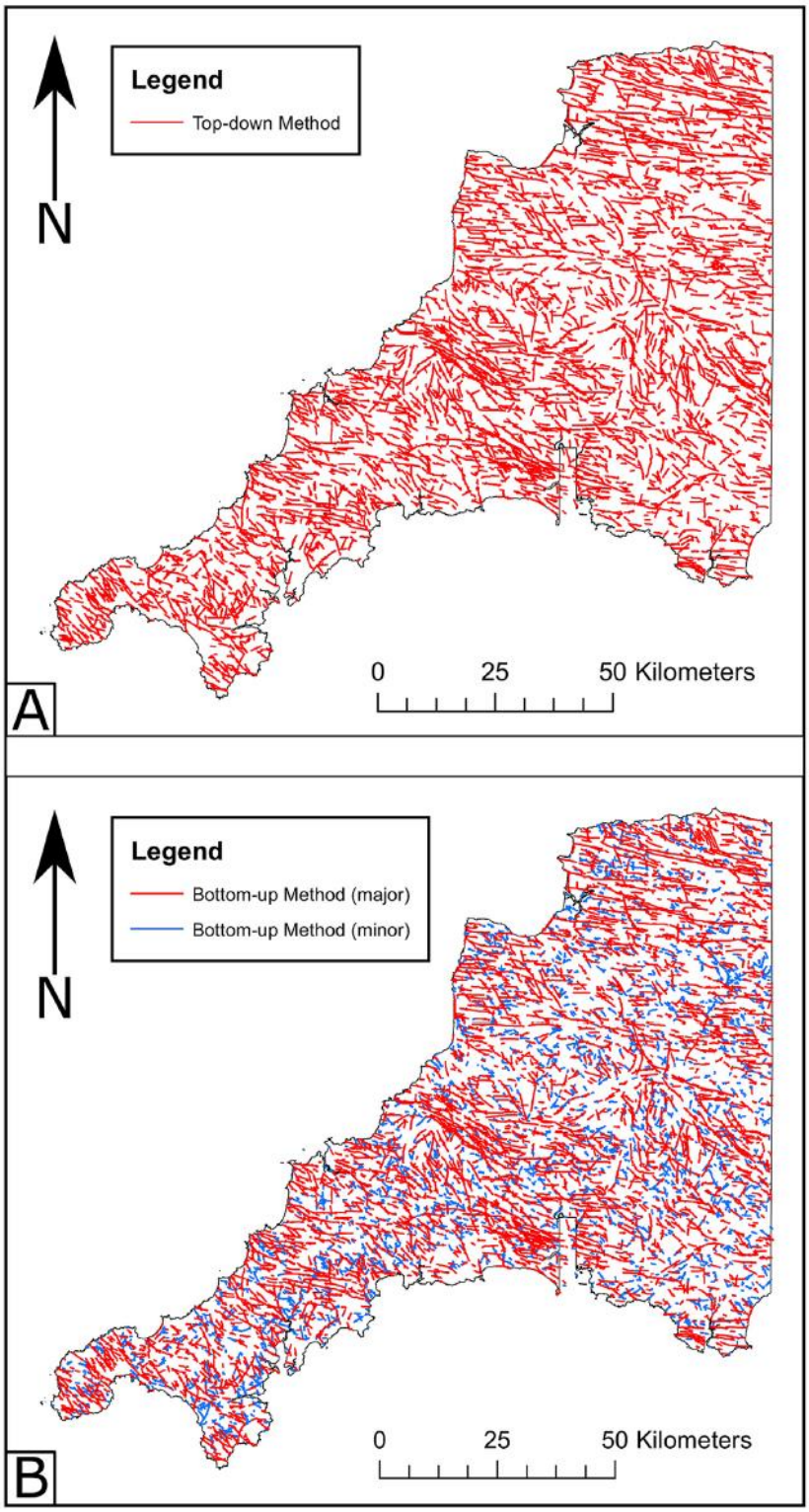

Figure 27: Regional lineament maps for south-west England. A. top-down methodology. B. Bottom-up methodology, see Yeomans et al. (2019) for a description of the lineament detection methodology. Reproduced from Yeomans et al. (2019), under Creative Commons Attribution 4.0 International License(http://creativecommons.org/ licenses/by/4.0/).

4.1.2 Ground-based data

4.1.2.1 Gravity data

There has been a long held view that the outcropping granites in south-west England were interconnected at depth (de la Beche, 1839). This was confirmed by gravity data derived in the 1950s, and the Bouguer gravity anomaly field in south-west England was first described and interpreted by Bott et al. (1958). Negative Bouguer gravity anomalies define the Cornubian peninsula, with significant lows associated with the exposed granite plutons (Figure 28). Bott et al. (1958) concluded that the exposed granites represented cupolas on a single elongated batholith that extended to a depth of at least 8 km and possibly as deep as 20 km. They considered the contacts between the granite and country rocks to typically slope outwards. Tombs (1977) used the gravity data to produce a three-dimensional model of the Cornubian Batholith, which suggested westward thinning of the batholith and the presence of shallow ridges connecting the exposed granite bodies.

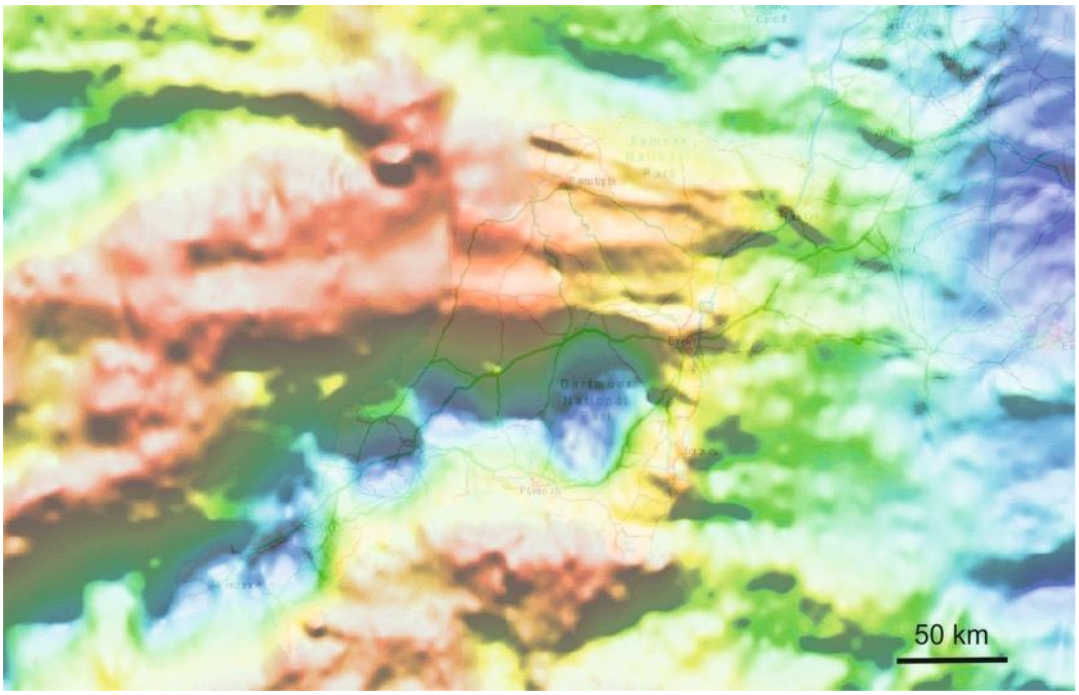

Figure 28: BGS gravity anomaly map over south-west England. The measured gravity values have been corrected in order to show the anomalies attributable to variations in crustal density. In broad terms the blues are attributable to large volumes of low density rocks, the reds to high density rocks. Significant lows occur, for instance, over areas of thick, low density sedimentary rocks, or large granites. Contains Ordnance Data © Crown Copyright and database rights [2019]. Ordnance Survey Licence no. 100021290. Contains British Geological Survey materials © NERC [2019].

The 'Camborne Geothermal Energy Project' carried out under contract as part of the Departments of Energy's Renewable Energy Research and Development Programme produced a three dimensional model of the shape of the Cornubian Batholith from gravity, density and wide angle seismic surveys (Willis-Richards et al., 1989). The gravity data (Figure 28 and Figure 29) were used to produce a three dimensional model covering the major granite outcrops from Dartmoor to Lands End (Willis-Richards and Jackson, 1989) (Figure 30). Details of the gravity modelling are described in Willis-Richards and Baria (1989) and summarised in Willis-Richards et al. (1989). Gravity derived estimates of batholith thickness are dependent on a number of assumptions, however,

the average batholith thickness under Lands End, Carnmenellis and the St Austell area was modelled to be about 13.5 km. The most significant features identified from the model were: i) that the batholith can be divided into two 'compartments', separated by a 3000 m deep, fault-bounded trough, extending between Carnmenelis and St Austell area; ii) all the major plutons are connected by saddles of granite in the roof of the batholith that are generally concealed by less than 2 km of cover rocks; iii) a buried granite ridge, under several hundred meters of cover rocks, extends northwards from the Carnmanellis granite towards Cligga Head; iv) a south-sloping base to the batholith, indicative of post-emplacement tilting to the south; and v) an estimated total volume of the batholith of about 68,000 km^3 (Figure 30) (Willis-Richards et al., 1989). A limitation with the gravity data is its spatial resolution, which makes features of less than about 2 km wavelength challenging to resolve. Despite this the model provided a limit to the total area and volume of the batholith (Willis-Richards et al., 1989). However, it was acknowledged that the estimated volume, based on the gravity modelled dimensions was significantly larger than previous estimates (Willis-Richards and Jackson, 1989). In fact the Cornubian Batholith appeared unusually thick relative most other granites globally, and more recent modelling of the gravity anomaly by Taylor (2007) has resulted in a significant reduction in the thickness of the Bodmin, St Austell and Carnmenellis plutons, and the confirmation of deeper, possible feeder zones towards the south of the Bodmin, St Austell and Dartmoor granites (Figure 15).

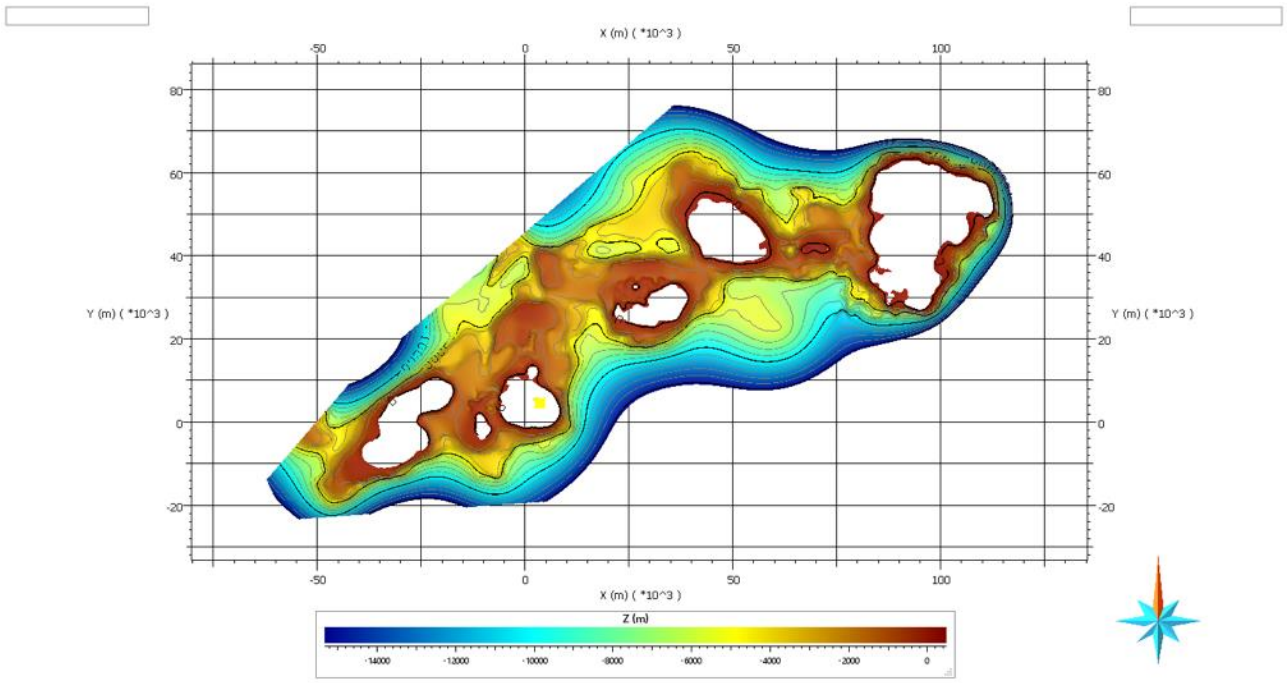

Figure 29: Plan view of the modelled top surface of the Cornubian Batholith (revised from CSM Report 2C-7, 1988; Willis-Richards and Baria, 1989; Tombs, 1980; Rollin, 1988 and Tombs, 1977). British Geological Survey © UKRI.

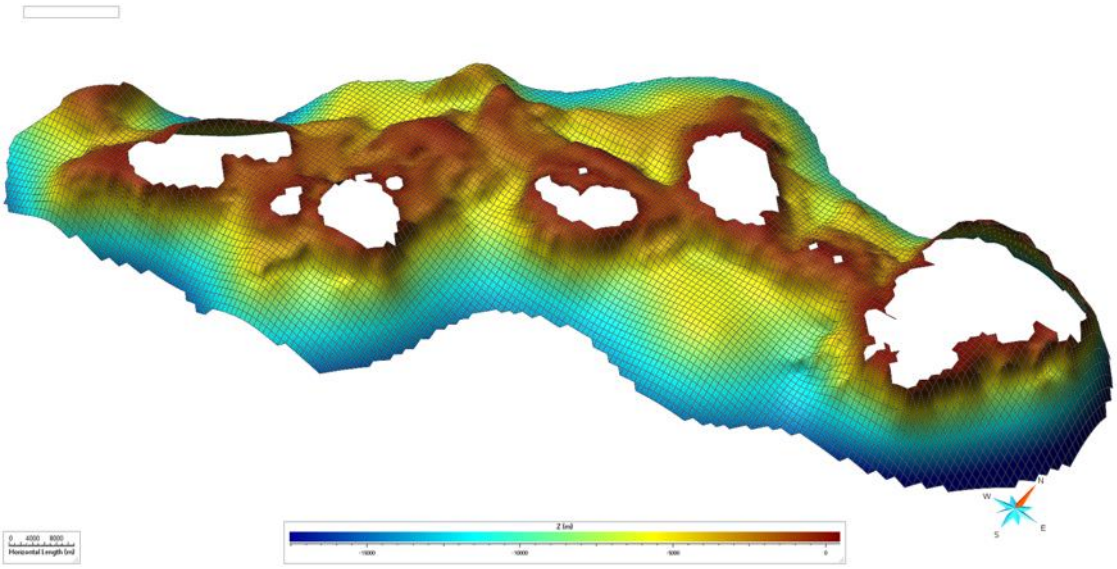

Figure 30: Perspective 3 dimensional view of the modelled top surface of the Cornubian Batholith (revised from CSM Report 2C-7, 1988; Willis-Richards and Baria, 1989; Tombs, 1980; Rollin, 1988 and Tombs, 1977). British Geological Survey © UKRI.

4.1.2.2 Seismic data

A seismic refraction experiment was undertaken in south-west England in 1966. One line was along the granite batholith and its seaward extension towards the WSW. The crustal structure along this line was initially described by Bott et al. (1970) and is discussed in detail by Holder and Bott (1971). The granite was interpreted to represents a 10–12 km thick upper crustal layer with a uniform velocity of 5.85 kms^{-1}. However, a near surface lower velocity layer of 2–3 km thickness can be distinguished. There is no sudden increase in velocity at the base of the upper crustal layer, but between 9–13 km velocity gradually increases, reaching 6.9 kms^{-1} at the base of the crust at 27 km (Figure 31).

A subsequent large-scale crustal refraction/wide angle reflection experiment (the Southwest England Seismic Experiment, SWESE) was carried out in 1979. The survey comprised a series of recording lines spanning the Cornubian peninsula (see Figure 1 in Brooks et al., 1984). Three crustal reflectors were identified (see Figure 6 in Brooks et al., 1984 and Figure 1.2 in Jones et al., 1989). The upper reflector (R1) lies at a depth of about 8 km ±1.15 km, and appears to be restricted to the interior of the granite batholith. It was considered to potentially represent the boundary between different intrusive phases of the granite, a zone of thrusting in the granite, or stoped blocks within the pluton. A deeper reflector (R2) is located at a depth of 10–15 km, and was interpreted to gradually shallow northwards. Although it coincides locally with the base of the granite as predicted by gravity modelling, this reflector extends well beyond the northern limit of the granite body. Accordingly, rather than representing the base of the batholith it was considered more likely that the R2 reflector was a thrust surface that is locally coincident with the gravity modelled base. The third reflector (R3) is located at a depth of 27–30 km and interpreted to represent the base of the crust. The experiment also imaged some shallow reflectors that coincide with the roof of the granite based on gravity modelling (Brooks et al., 1984). Rather than an internal batholith reflector, Shail et al. (2014) subsequently interpreted R1 to represent the lower contact of the granite with the host rock (i.e. the base of the batholith), which lies at a depth of c. 8 km below the southern parts of Carnmenellis.

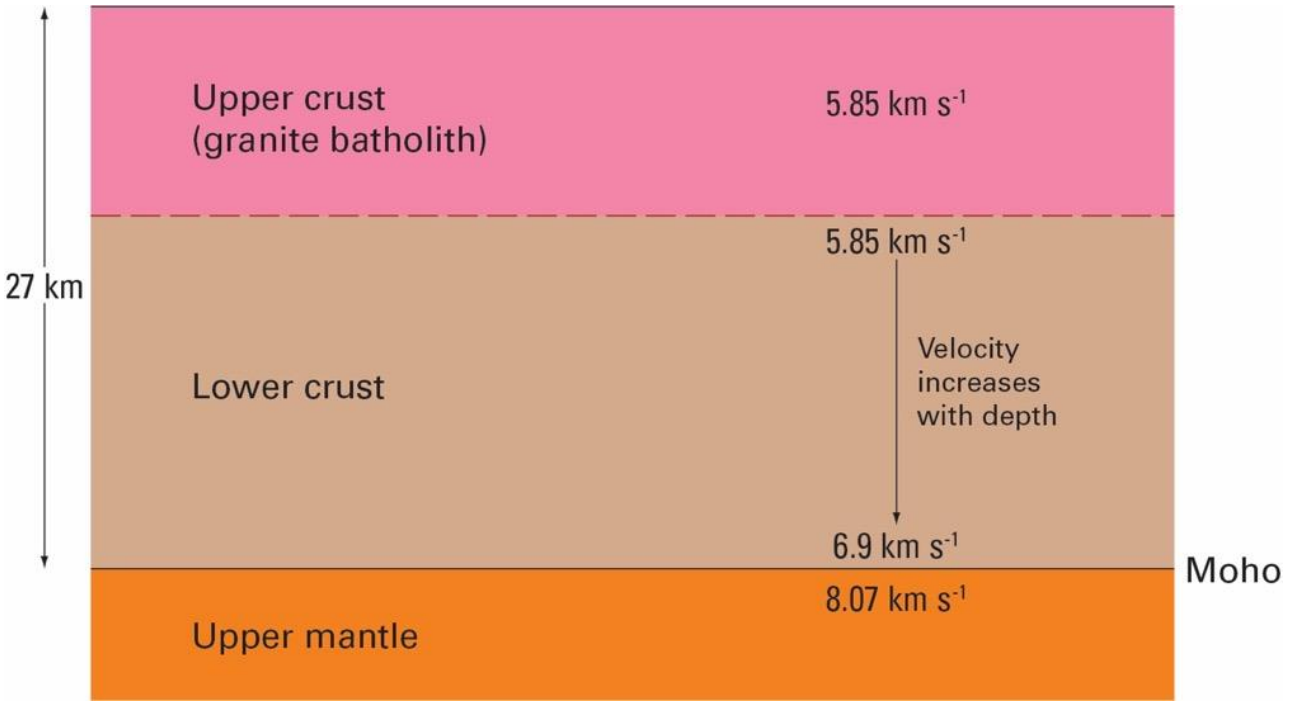

Figure 31: Model of the crustal structure for the seismic refraction line along the granite batholith. Reproduced from Fig 9. A. P. Holder & M. H. P. Bott. Crustal Structure in the Vicinity of South-west England. Geophysical Journal International (1971) 23 (5): 465-489, doi: 10.1111/j.1365-246X.1971.tb01838.x. By permission of Oxford University Press on behalf of the Royal Astronomical Society. Please visit: https://academic.oup.com/gji/article/23/5/465/677462. This figure is not included under the Creative Commons CC-BY license of this publication. For permissions, please contact journals.permissions@oup.com

Deep offshore seismic reflection profiles from the South West Approaches Traverse (SWAT) crossed south-west England. SWAT 6 crossed the Cornubian Batholith (Prive, 1986). A normal incidence seismic reflection survey was conducted over two lines to investigate the internal structure of the Cornubian Batholith (Willis-Richards et al., 1989). The two lines cross at the Rosemanowes site, passing over the HDR reservoir (see Figure 3.1 in Willis-Richard et al., 1989). The purpose of the survey was to investigate the structure of the granite between 4–8 km and determine the size and shape of the granite. The seismic section displays many short reflectors within the killlas where it reaches a thickness of >0.5 km (Jones, 1989). This was as anticipated, based on its known compositional variation (Willis-Richards et al., 1989). These reflectors are apparent down to about 4.5 km in the killas or appear to stop at the killas/granite boundary if it is shallower than this (Jones, 1989). However, the actual granite/killas contact was not imaged, as it is not reflective. This is because the seismic reflection technique is based on measurements of acoustic impedance. Acoustic impedance is a product of the density and the seismic velocity. The killas has a significantly higher density than the granite (making gravity modelling a good technique for determining the shape of the granite), but the granite has a much higher seismic velocity than the killas, therefore the acoustic impedance is very similar for both lithologies (Willis-Richards et al., 1989). There are no reflectors in the granite, which appears to be seismically featureless to a depth of 14 km (Jones, 1989; Willis-Richards et al., 1989) (see Figure 3 in Jones, 1991). Despite the normal incidence reflection data containing no evidence of structures at depths of 4–8 km, the wide angled reflection interpretation i.e. Brooks et al. (1984) does identify a feature (R1) at a depth of between 6–8 km (Jones, 1991). Resistivity data from Beamish (1990) (see below) suggests this depth represents a change from

an interconnected joint/pore network at hydrostatic pressures to a regime of isolated pores at lithostatic pressures. This could cause a decrease in seismic velocity, consistent with the presence of the R1 reflector in the wide angled data. This change would occur over too large a depth interval to produce a normal-incidence reflection, hence its absence in this dataset (Jones, 1991).

4.1.2.3 Magnetotellurics

A magnetotelluric (MT) survey was undertaken over the Carnmenellis granite in 1988 by BGS. MT uses natural variations in the earths EM field as its source. The way in which the EM source is modified by the rocks being surveyed is used to determine the resistivity of the rock as a function of depth. The most significant findings were that the granite appears very homogenous on a broad scale and that below a depth 1 km resistivity values increase down to a depth of about 6 km. Below 6 km the resistivity values remain fairly consistent down to 12–14 km. Importantly, it was concluded that the results are consistent with joint closure by a depth of 7 km, with a change to pore-dominated resistivity below this depth (see Figure 6 in Beamish, 1990). The electrical base of the granite was modelled at 14 km, which is consistent with gravity modelling (Beamish, 1990).

4.1.2.4 Natural seismicity

The British Geological Survey has monitored natural seismicity in Cornwall since 1980. Natural seismicity can be used to confirm the direction of the regional principal stresses and provide information on stress anisotropy at depth. Based upon events monitored between 1981–1987, those within the granite batholith cluster between 4–6 km depth, with some recorded at a depth of in excess of 8 km. Hypocentres located in the killas do not have a similar depth grouping. Focal mechanisms, are consistent with the maximum compressive stress being directed from the SE (Willis-Richards et al., 1989). Willis-Richards et al. (1989) notes that the magnitude of deviatoric stress in a deep (6 km) geothermal reservoir is an important parameter that will influence stimulation of the reservoir. It is considered unlikely that deviatoric stresses will exist in a granite for geologically significant time periods at temperatures above 200–220°C. It is suggested that this corresponds well with the observations based on natural seismicity. It is concluded that the transition from brittle to ductile conditions is probably occurring 'within the region of interest for geothermal exploitation', and at reservoir temperatures and over human time-scales the granite will behave elastically (Willis-Richards et al., 1989).

4.2 Tellus magnetics data reassessment

Given the importance of structure to EGS the TellusSW magnetics data was reassessed during this review. Figure 32 shows the geology and corresponding TellusSW aeromagnetic data over the north-eastern margin of the Carnmenellis granite. The country rocks are predominantly hornfelsed slates and siltstones of the MSF, with some metabasaltic rocks present. In the extreme NE of the district, metamorphosed mudstones and sandstones of the Gramscatho Formation are also present. Both granites and country rocks are intruded by a predominantly NE-trending suite of felsite dykes (Figure 32A).

The magnetic anomaly map (Figure 32B) shows that areas of granite are generally magnetically 'quiet', with little evidence of coherent features. Those magnetic features that are present over the granite are generally bullseye features that can be correlated with cultural structures (for example farm buildings) identified on Ordnance Survey (OS) topographic maps. Such anomalies that do not relate to cultural features are considered likely to arise from unmapped sources, which are potentially shallowly-buried. Comparison of the geology map with the magnetic anomaly map shows that the felsite dykes are, as would be expected on compositional grounds, not associated with linear magnetic anomalies. In areas that are not underlain by granite, there is a

good correlation between magnetic anomalies and mapped metabasaltic rocks, with additional anomalies that have no obvious geological correlation, potentially reflecting unmapped or buried magnetic units. The NE margin of the Carnmenellis granite is associated with a fairly broad NW-SE-trending linear feature (Figure 32B).

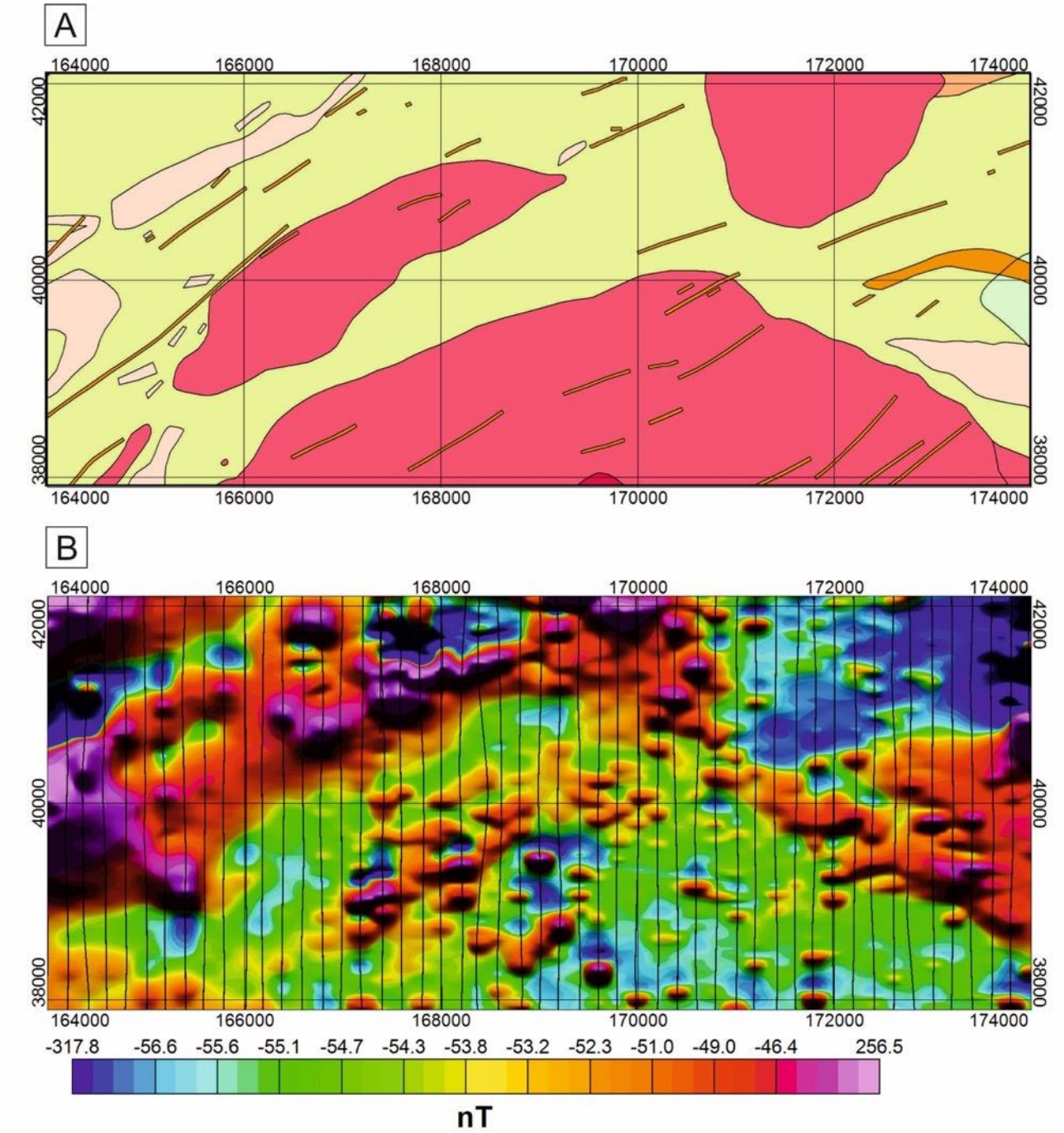

Figure 32: Geology and magnetic response over the north-eastern margin of the Carnmenellis granite. A. 1:50 000 scale solid geology. B. The TellusSW aeromagnetic data of the same area, with N-S flight lines displayed, produced from the TellusSW airborne geophysical survey data (Beamish et al., 2014). British Geological Survey © UKRI.

In order to examine this linear feature in a regional context, the TellusSW data for a 40 km x 40 km area enclosing the primary area of interest were examined. Figure 33 shows the reduced-to-pole total magnetic

intensity (TMI) anomaly and illustrates that the NW-SE-trending feature along the NE margin of the Carnmenellis granite forms part of a longer, regional NW-SE-trending feature that crosses Cornwall. Figure 34 shows the tilt-derivative of the TMI anomaly (Miller and Singh, 1994), further illustrating this linear magnetic feature.

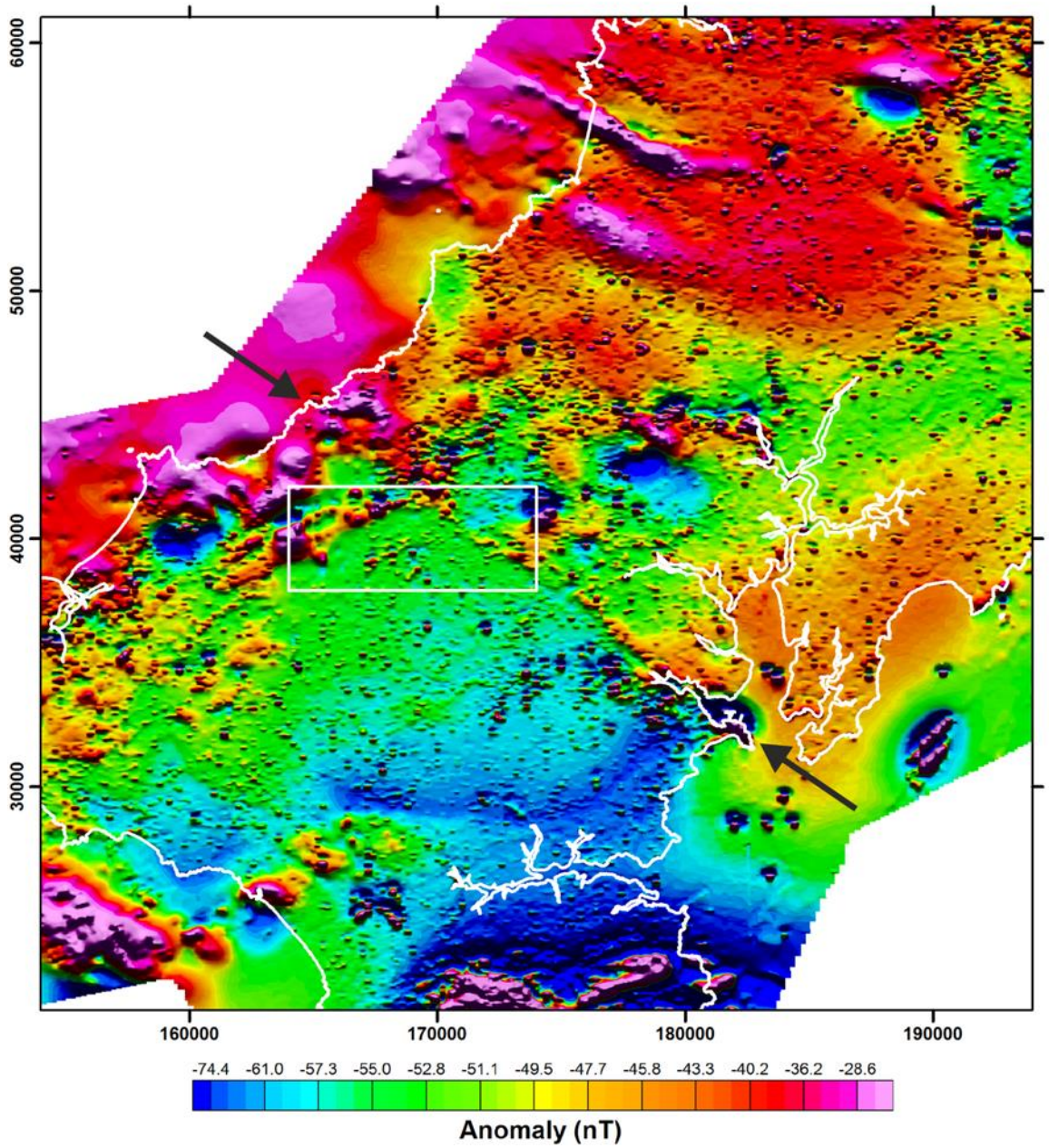

Figure 33: Regional reduced-to-pole total magnetic intensity anomaly from the Tellus SW aeromagnetic data. The white rectangle shows the area shown in Figure 32, and the two arrow indicate the regional magnetic lineament described in the text. Contains Ordnance Data © Crown Copyright and database rights [2019]. Ordnance Survey Licence no. 100021290. Contains British Geological Survey materials © NERC [2019].

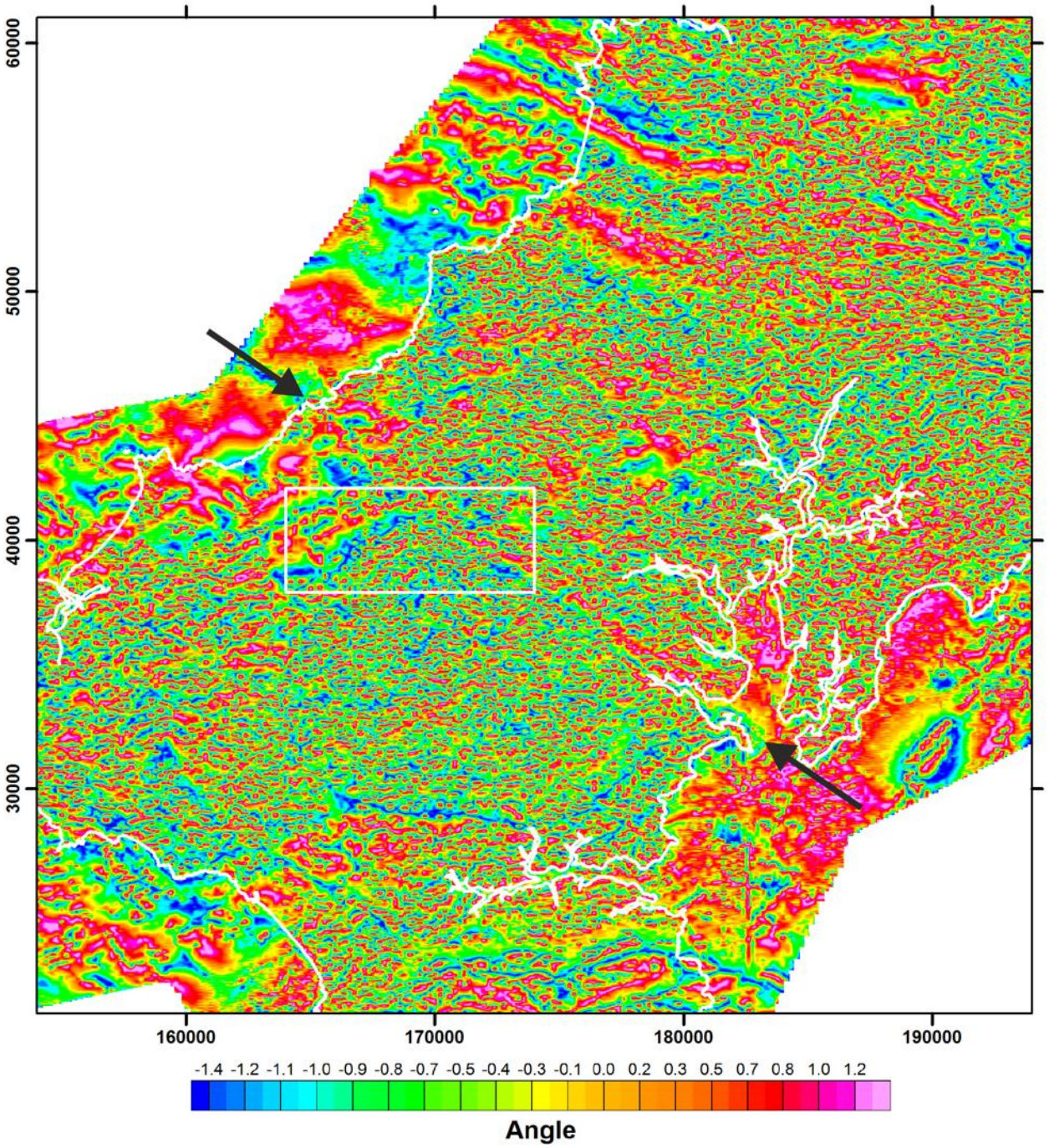

Figure 34: Tilt-derivative of the regional TMI anomaly. The two arrows indicate two arrows indicate the regional NW-SE-trending magnetic lineament described in the text. Contains Ordnance Data © Crown Copyright and database rights [2019]. Ordnance Survey Licence no. 100021290. Contains British Geological Survey materials © NERC [2019].

In common with the aeromagnetic data, cultural interference and associated anomalies are a challenge for interpretation of the TellusSW radiometric data (Figure 35). This is illustrated by the radiometric (potassium) data to the east of Redruth. A significant anomaly coincides with an area of made ground on the OS map. This is a landfill site that has been covered by china clay waste, which results in the elevated potassium signal (Figure 35).

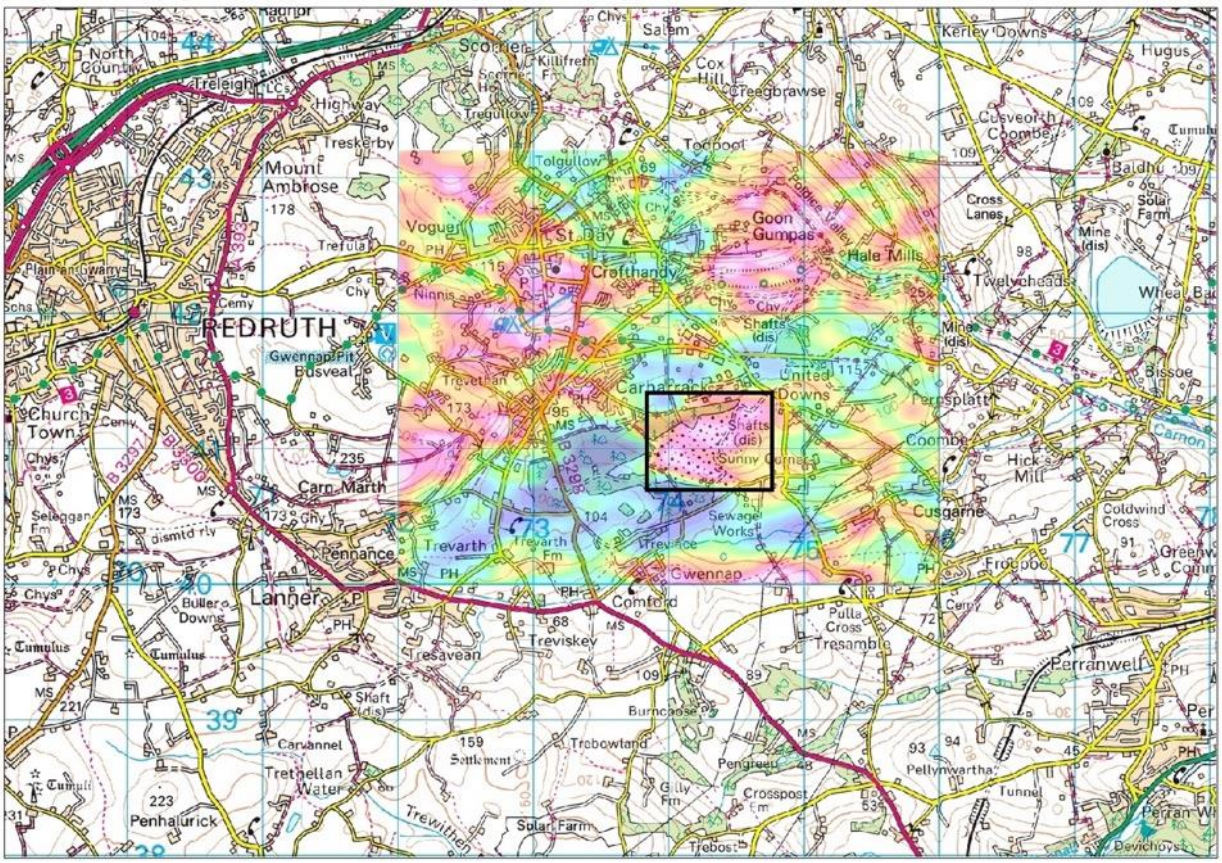

Figure 35: An example of a cultural artefact seen in airborne radiometric (potassium) data. The area in the rectangle is a historic landfill site that has been capped with china clay, which results in a strong positive signal. Contains Ordnance Data © Crown Copyright and database rights [2019]. Ordnance Survey Licence no. 100021290. Contains British Geological Survey materials © NERC [2019].

5 Deep metal enrichment

5.1 Types of mineralisation in the CHPM2030 study area

The CHPM2030 study area hosts two principal types and phases of mineralisation: i) granite-related mineralisation, which was largely formed during the Early to Mid-Permian; and ii) Mid-Triassic mineralisation, resulting from fracture-controlled migration of basinal brines from the Permo-Triassic basins into older rocks, which formed the so called 'cross-course' veins. Both types are abundant in the Camborne-Redruth area of Cornwall, which is located in the study area (Figure 7).

5.1.1 Granite-related mineralisation

Granite-related mineralisation, also termed 'main stage' mineralisation, is abundant in the study area (Figure 7). It primarily resulted from the migration and mixing of magmatic hydrothermal and other fluids within fractures in the granites and metasedimentary host rocks. It is considered a globally important, type example, of mineralisation associated with granitic magmatism, and has been termed 'Cornwall-type' mineralisation.

The majority of metal production, including tin, copper, zinc, arsenic and tungsten, from the Cornubian orefield has been obtained from exploitation of these large syn-granite fissure veins, termed 'lodes'. The term lode implies that both the vein and the altered wall-rock that hosts it are mineralised. Many of the endogranitic systems can be described as lode zones, which often contain multiple, inter-related veins rather than a single continuous vein structure (Dominy and Camm, 1998). This mineralisation style can be broadly defined as quartz–wolframite and tourmaline–quartz–cassiterite veins (Figure 6C), with subordinate Cu, As, and minor Bi, Ag, and Pb that is related to high-level, high-heat producing granites (Romer and Kroner, 2016). The lodes generally have exploitable strike lengths of a few hundred to a thousand metres (and exceptionally up to 6000 m e.g. the Great Flat lode) and dip lengths of 100–500 m (up to 2000 m e.g. Dolcoath Main lode). Lode widths range from a few tens of centimetres to 20 m, but are typically in the range 0.5–2 m. The lodes typically occupy steeply-dipping (more than 65°) faults or fractures, however, shallow-dipping (less than 50°) structures may also carry significant mineralisation. Lodes typically occur in swarms, for example, over 30 subparallel lodes occur in the Camborne-Redruth district (Figure 7) (Jackson et al., 1989). The Great Flat Lode (Figure 36) is a very large ore-bearing body, situated to the south of Carn Brea, and tilted at an angle of about 45°. Typically lodes are found perpendicular to the ground surface or at angles of about 60°. The low angle of the Great Flat lode meant that mines could be placed at the optimum locations to extract the tin or copper ore whilst minimising the amount of waste removed.

It is thought that 90–100 per cent of the total Sn, Cu, and As production of the region is derived from within 1500 m of a granite contact (Willis-Richards and Jackson, 1989). Lodes in which quartz ± chlorite ± fluorite form the principal gangue minerals, and which host variable combinations of cassiterite, chalcopyrite, arsenopyrite, sphalerite, galena and sporadic wolframite are the dominant type of lode mineralisation in the country rock surrounding the granites, but also occurs within the granite plutons XX. These lodes were the main source of Cu and As, as well as substantial Sn, occasionally present as stannite. Lodes with a primary tourmaline-quartz-cassiterite ± rutile ± arsenopyrite ± fluorite ± specular hematite assemblage have been a significant source of Sn production from granites and, to a lesser extent, from the metasedimentary rocks. Examples include the lower parts of Dolcoath Main Lode, the Great Flat Lode, and the 'numbered' lodes at the South Crofty Mine (Edmonds et al., 1985).

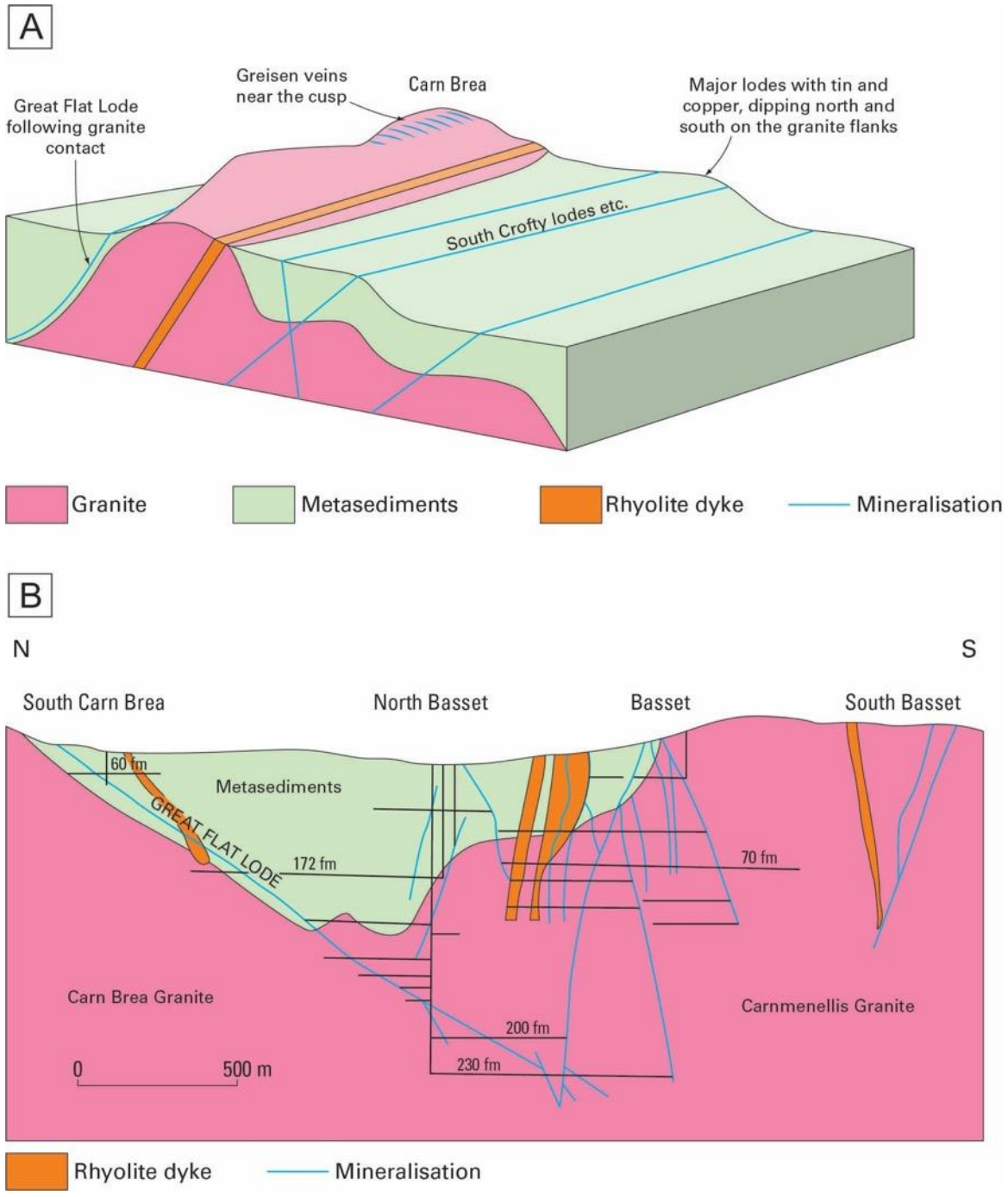

Figure 36: The Carn Brea area and its mineralisation. (A) Schematic diagram of the geology of the Carn Brea area, identifying the major lodes in the region. (B) Schematic cross-section through the Great Flat Lode, which is predominantly hosted in metasedimentary rocks between the Carn Brea granite to the north and the Carnmenellis granite to the south. Redrawn from webpages accessed July 2017 (no longer accessible online). Credit: Dr Nick Le Boutillier (BSc PhD MCSM EurGeol CGeol FGS).

In some areas as the mines deepened, copper production from near surface quartz-chlorite-fluorite sulfide assemblages transitioned in to tin production from tourmaline-dominated assemblages. The change from a 'copper zone' to 'tin zone' typically occurs in the vicinity of the granite–host rock boundary, but can be significantly higher or lower, and include a mixed zone containing both Cu and Sn assemblages (Figure 37).

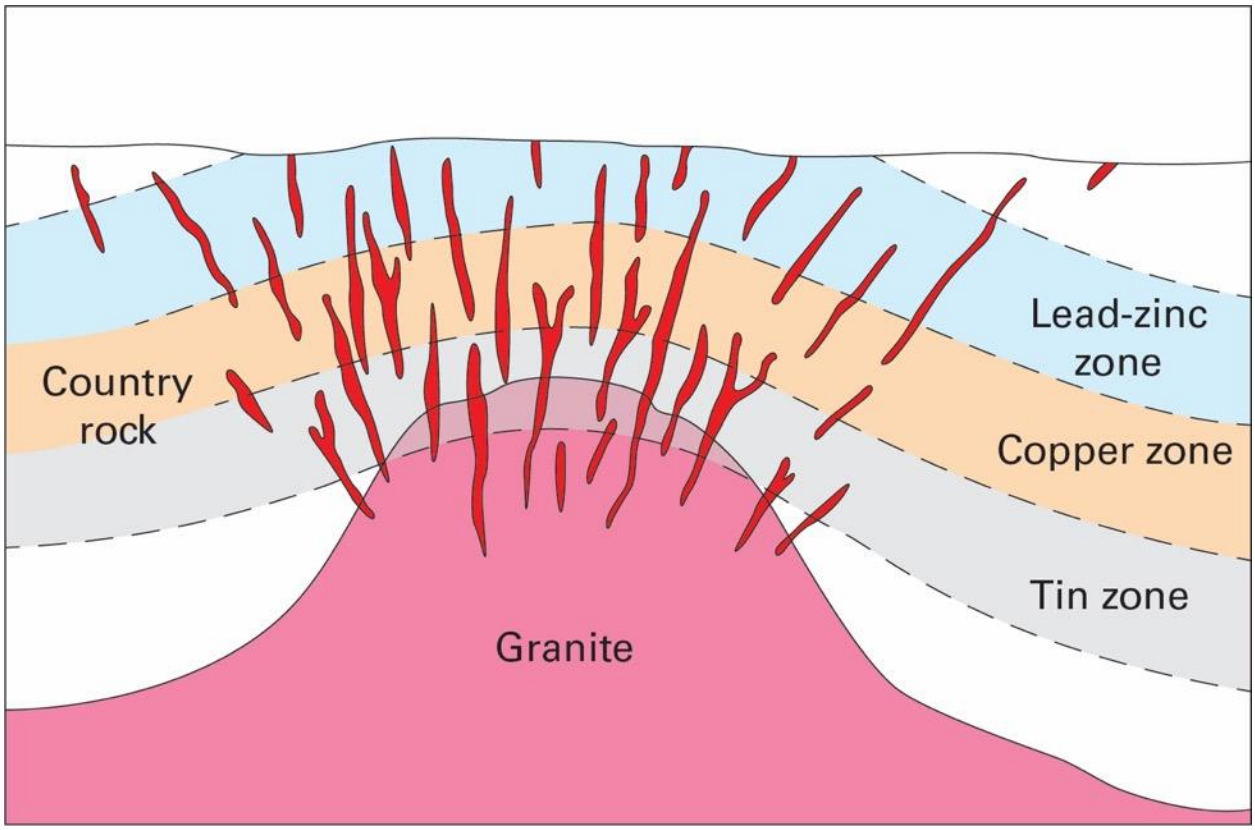

Figure 37: Schematic diagram illustrating the regional zonation of metals in vein deposits in south-west England. Redrawn from Sinclair (1995). Copy of the version available at [http://publications.gc.ca/collections/collection_2016/rncan-nrcan/M40-49-8-23-eng.pdf].

In addition to the Sn and Cu that dominated metal production in the region, cobalt was produced from Wheal Sparnon, located in Redruth town. This is one of few known mines that solely produced cobalt, with intermittent production between 1808–1827 (Jenkin, 1979). Little information is available on the deposit, however, cobalt was hosted in a range of mineral phases, including cobaltite, erythrite, skutterudite and safflorite (Tindle, 2008), with mineralisation extending to a depth of >120 m (NAMHO, 2013).

The Camborne-Redruth district was the most productive in the region, with hundreds of mines being developed from the mid-19th Century onwards. It also includes some mines with the longest life span in the region. In the Carn Brea area, some of the larger mines represent an amalgamation of hundreds of once independent workings. These larger mines were often also consolidated, for example Dolcoath and East Pool were later merged (in 1936) with South Crofty to form the South Crofty Mine. Figure 38 shows a grade–tonnage diagram to illustrate the size and grade of the major mines of south-west England, relative to tin-tungsten deposits globally.

In Cornwall between 1852–1914 more than 210 000 tonnes of contained copper metal was produced, and between 1848–1920 about 800 000 tonnes of tin ore was mined (Burt et al., 2014). Many mines closed in the early 20th Century and with declining tin prices the deposits became increasingly uneconomic, with the last mine in the region, the South Crofty Mine, ceasing operation in 1998.

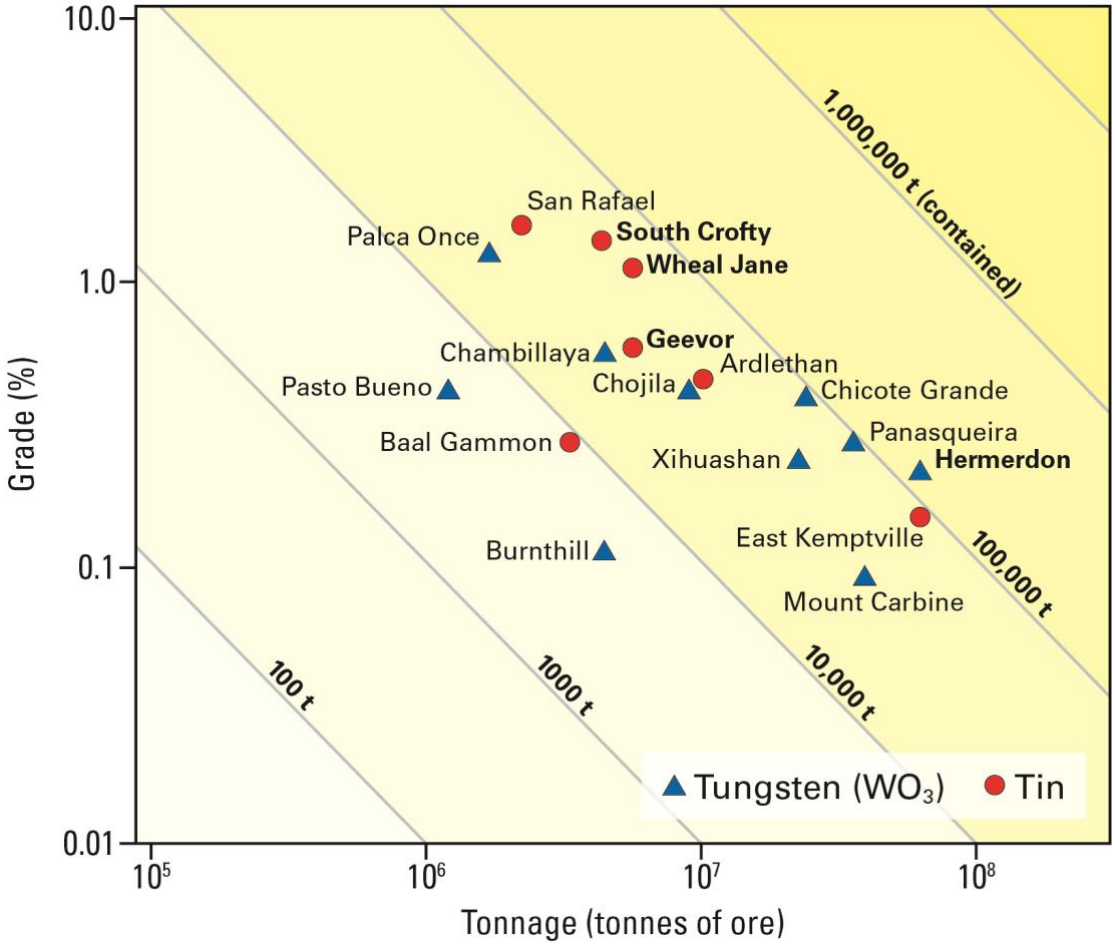

Figure 38: Grade versus tonnage diagram for vein-stockwork tin-tungsten deposits from south-west England and globally. Modified from Sinclair (1995). Copy of the version available at [http://publications.gc.ca/collections/collection_2016/rncan-nrcan/M40-49-8-23-eng.pdf].

5.1.2 Triassic 'cross-course' mineralisation

In the area to the NW of the Carnmenellis granite there are significant NNW-trending structures that cross-cut the granite-related mineralisation (Figure 22, Figure 39). Their structural characteristics are described in Section 3.3.2.2. These structures are variably mineralised (barren, non-metalliferous veins are commonly associated with the Mid-Triassic mineralising event), which means they have produced less total metal than the granite-related, main-stage mineralisation. They have been primarily exploited for lead, zinc, silver, fluorite and barite. In the Camborne-Redruth area these structures are vertical- to sub-vertical (Figure 22) and displace the 'main-stage' mineralisation by up to 100 m (Dines, 1956). There are two types of cross-course structure in the area: i) fracture zone cross-courses; and ii) extensional cross-courses. The 100 m wide Great Cross-course

represents a fracture zone cross-course that comprises networks of intense micro fractures and quartz veins with variable amounts of argillic and haematitic alteration (Dominy et al., 1994). The extensional cross-courses are the most common type in this area, with veins ranging in width from a few centimetres to about 2 m. With the exception of a small amount of localised silicification and kaolinisation there is little wallrock alteration associated with these veins. These fissures, contain open-space, and are principally filled by quartz and chalcedony, with variable quantities of fluorite, pyrite, chlorite, siderite, calcite and haematite (Dominy et al., 1994) (Figure 40).

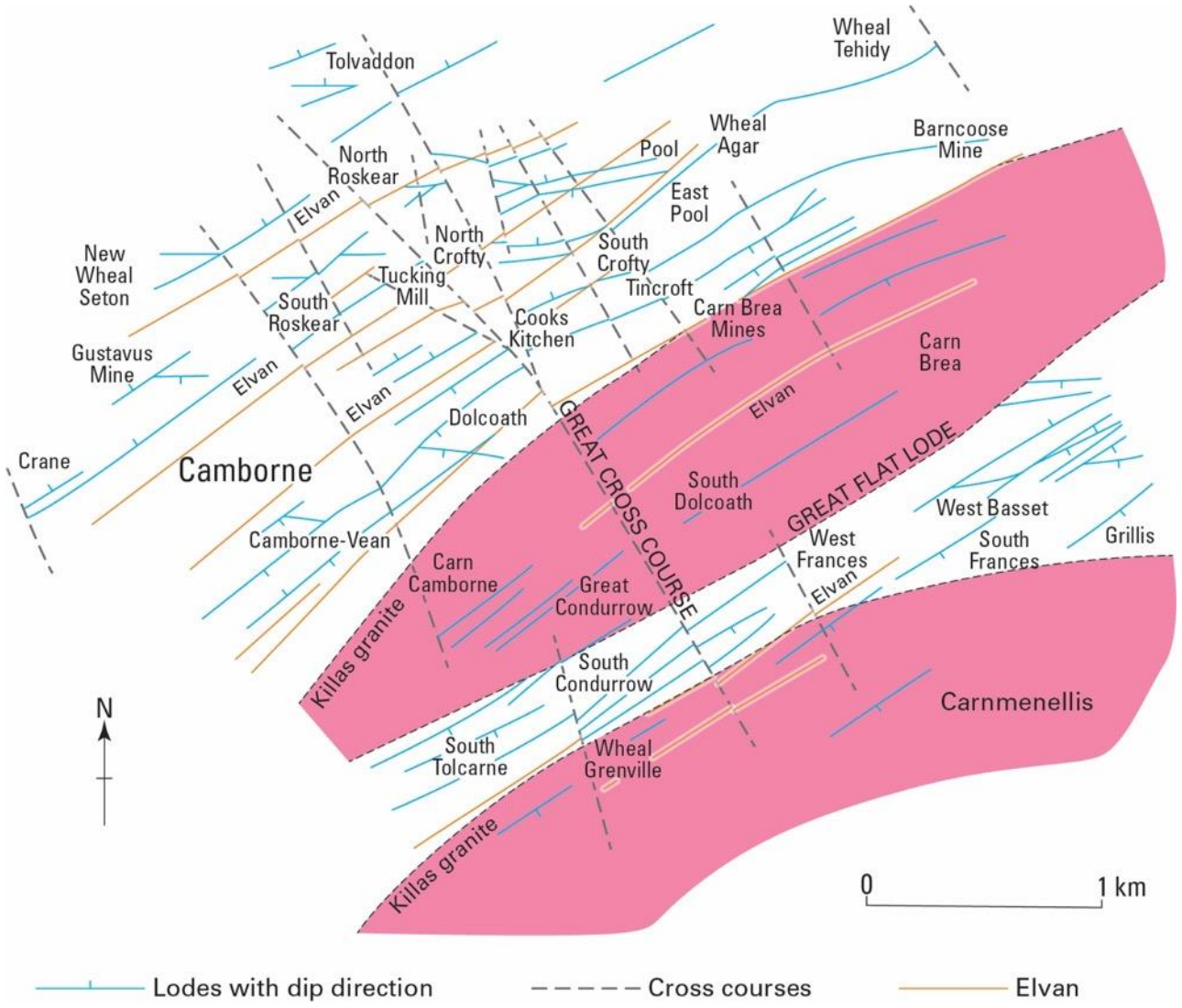

Figure 39: Map of the main lodes and cross-course veins in the area NW of the Carnmenellis granite. Redrawn from Dominy et al. (1994).

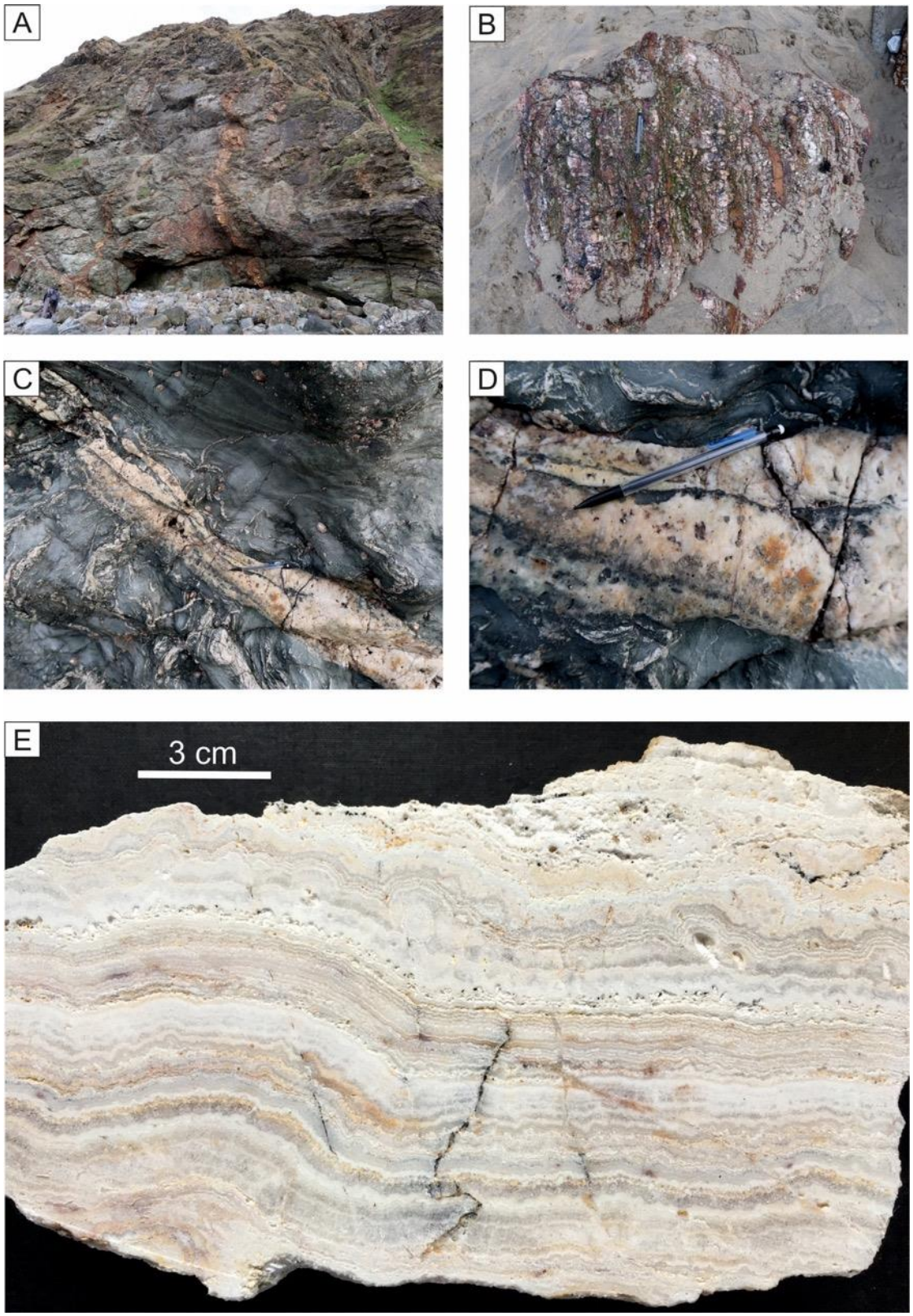

Figure 40: Typical cross-course mineralisation. A. Mineralisation in the cliff near Cotty's Point, Perranporth. B. Block of cross-course mineralisation on the beach at Cotty's Point. C. Mineralised cross-course vein in the metasedimentary rocks at St Agnes. D. Detail of the vein shown in C, which contains abundant pyrite. E. A cut vein sample, from Cotty's Point, primarily composed of multiple layers of quartz and chalcedony. British Geological Survey © UKRI.

5.2 Controls on mineralisation

In the Camborne-Redruth area over 35 sub-parallel veins, or lodes, are present (Dines, 1956). Both single in-filled fractures and composite systems are present in the area, with the latter being more common (Dominy and Camm, 1998). Lodes are typically orientated E–W and the strong preferred orientation of the lode vein systems is a clear indication that the host fractures were produced within a regional confining stress field. The weakest principal stress appears to be oriented normal to the axis of each portion of the batholith, and the maximum principal stress oriented between the vertical and the horizontal, in a plane parallel to the axial trace of the batholith (Jackson et al., 1989). Fracturing is thought to result from hydraulic stresses related to individual plutons (Moore, 1975). Moore (1975) suggested that the magmatic fluids exited the granite via pre-existing faults, and enlarged primary igneous joints and extensional fractures and faults created by the emplacement of the intrusion. Once developed, the fracture systems acted as high permeability corridors exerting a profound control on the movement of fluids around and through the batholith (Jackson et al., 1989). Fluids were drawn into active fault zones during the dilation phase prior to faulting and were transmitted along the faults after the seismic event (Sibson et al., 1975). Controls on ore localisation are complex and related to the many stages of structural reactivation that are present within a vein. A number of variable factors, including host-rock fracture geometry, lithology and physiochemical conditions of the wall rocks and fluids exerted control on the formation of mineralisation (Dominy and Camm, 1998).

5.3 Potential for deep metal enrichment

The deepest mine in south-west England is the Dolcoath mine, located in the area north of Carn Brea (Figure 7), where mine workings reached a depth of approximately 1000 m. Zonation of the mineralisation in the mine (copper in the upper zone and tin in the deeper zone) resulted in initial production of copper with subsequent production of tin. This zoning is attributed to pressure-temperature regimes along the granite metasediment contact (Dominy and Camm, 1998), and is supported by fluid inclusion data which demonstrate that the deeper tin zone is related to generally higher temperature fluids (Scrivener et al., 1986). The Dolcoath Main Lode was the largest tin-bearing structure in the region at 12 m wide (Dines, 1956). The mine produced some 2.5–3 million tonnes of ore, at a grade of about 1.6 per cent Sn (40,000 tonnes Sn metal) (Dominy and Camm, 1998). Between 800–900 m the lode consists of tourmaline-cassiterite veins. These comprise cassiterite, hydrothermal schorl-buergerite tourmaline (LeBoutillier et al., 2002 and reference therein), fluorspar and quartz, and quartz tourmaline breccia, which is crosscut by veins of clear quartz and fluorspar. At greater depths the schorl-buergerite tourmaline is replaced by a tourmalinised breccia. Vein paragenesis comprises: i. quartz + cassiterite + tourmaline; ii. multiple generations of brecciation with influxes of cassiterite and tourmaline; and iii. cementation by quartz with chalcopyrite (Dines, 1956). The wall rock for 1.5 m on either side of the lode fissures is brecciated, with localised areas being completely chloritised or tourmalinised and impregnated with cassiterite (Dines, 1956). In the deepest part of the mine tourmaline lodes varied in width from 5–30 m (Dominy and Camm, 1998).

The deepest drilling in Cornwall was undertaken during the HDR research programme. Three holes were drilled at the Rosemanowes Quarry in the Carnmenellis granite. The deepest hole reached 2610 m and a review of the single, partial, log (only one borehole has an available log, BH RH15 available digitally from the BGS, see Appendix 2 for further details) was undertaken as part of this project. Three mentions of sulfide are made in the log between 2213 and 2610 m (core samples are available for review, Figure 3E,F), and these are described as being associated with vein structures. However, no further details on the ‘sulphide mineralisation’ are described in the log. The CHPM concept does not necessarily require an ore body in the traditional sense. Any

metal enriched geological formation or reservoir of metals is a potential target for leaching. Accordingly, the following section provides a general overview of the distribution of metals in the Cornish granites.

5.4 The batholith as a metal reservoir

5.4.1 Granite geochemistry

The most recent geochemical analyses of the granites in south-west England has been undertaken by Simons et al. (2017; 2016), and the resulting new categorisation into five groups (types G1 to G5), based on their mineralogy, is described in Section 3.1.1.1. Simons et al. (2016) present data on the major elements (SiO_2, Al_2O_3, TiO_2, Fe_2O_3, MnO, MgO, CaO, Na_2O, K_2O, P_2O_5), trace elements (Ba, Pb, Rb, Sr, Nb, Th, U, Zr), and the rare earth elements (REE). Simons et al. (2017) includes new geochemical data on the fractionation of Li, Be, Ga, Nb, Ta, In, Sn, Sb, W and Bi in the G1–G5 granites of the Cornubian Batholith (Simons et al., 2017). The Cornubian granite has previously been identified as bismuth enriched, with Bi concentrations in south-west England granites two orders of magnitude higher than world average estimates for granites. The average concentration of Bi in south-west England granites ranges from 1–2ppm, whilst the global mean concentration of Bi in granites is about 0.05ppm (Ball et al., 1982). Regionally, there is a strong enrichment in Li in all the granites, whereas the G2 and G5 granites are enriched in W. Gallium, In and Sb plot towards expected UCC abundances. Beryllium, Nb, Ta, Sn and Bi are slightly enriched in the least evolved G1 and G3 granites, typically increasing for the G2, G4 and G5 granites. Average values for the peri-Gondwanan Devonian Gramscatho Basin (GB) plot around average UCC abundances (Simons et al., 2017). Examination of trace trace element distribution across the granites, highlights the abundance of many of the metals in the G5 (topaz) granites and the enrichment of Be in G2 (muscovite) granites. The enrichment of Li, Ga, Nb, Ta, Sn and W in the G5 (topaz) granites is explained by the high-F content of these granites.

5.4.2 Disseminated mineralisation

Granites that evolve towards or have high-F contents may contain disseminated magmatic mineralisation, depending on depth of intrusion, with limited partitioning of metals such as Sn and W into fluids exsolved from the melt (Pollard et al., 1987; Simons et al., 2017). With increased fractionation, the distribution of less compatible elements such as Tb and Nb is controlled by accessory phases such as rutile and columbite, which can occur as common magmatic phases, disseminated throughout a granite body with high levels of fractionation (Simons et al., 2017). Disseminated Nb and Ta phases have been found in the G4 (tourmaline) and G5 (topaz) granites (Simons et al., 2017). The G5 (topaz) granites of the batholith evolve towards very low-grade disseminated Sn–Ta–Nb–(W) magmatic mineralisation, which to date, has not been exploited (Simons et al., 2017).

5.4.3 Silicate-hosted metals

Fractionation, dominated by biotite and feldspars, increases Be, Nb, Ta, In, Sn, W and Bi in the G1 (two-mica) and G2 (muscovite) granites. Lithium is dominantly hosted by trioctahedral micas (i.e. biotite, lepidolite and zinnwaldite) in all the granites of the Cornubian Batholith. Gallium is fairly evenly distributed between all major silicates. Niobium and tantalum partition into muscovite in the G1–G2 granites; biotite, lepidolite and zinnwaldite micas into the G3 (biotite) granites, and accessory minerals into the G4 (tourmaline) and the G5 (topaz) granites. Fe-Ti oxides are an important host of these metals in all the south-west England granite types, and columbite-tantalite host Nb and Ta in the G5 (topaz) granites. Indium, Sn and W follow Nb and Ta, with the exception of the G4 (tourmaline) granites, in which they are incorporated into trioctahedral micas (Simons

et al., 2017). In the G2 (muscovite) granites the metals partition dominantly into muscovite, with limited disseminated magmatic mineralisation (Simons et al., 2017).

Although very limited data exists on deep (>1000 m) metal enrichment in the Cornubian orefield, the short review above indicates that some of the host rocks (i.e. the granite) to the hydrothermal mineralisation contain either disseminated metal-bearing phases, most common in the younger, more fractionated granites, or metals are incorporated into the structure of common silicate minerals, such as biotite and feldspar. Preliminary research to assess the potential for mobilising these metals from rock-forming minerals in the granites, in a CHPM-types system, is described in Section 5.5.

The Carnmenellis granite is a two-mica granite that predominantly comprises quartz, orthoclase feldspar, biotite (5–10 modal %), muscovite (up to 6 modal %) and about 1 modal per cent tourmaline. Accessory minerals typically include zircon, monazite, xenotime, andalusite, apatite, ilmenite, fluorite and topaz (Simons et al., 2017). However, disseminated sulfides are extremely rare, meaning the potential for extracting metals from sulfides contained in the Carnmenellis granite during circulation of an EGS fluid is limited. Another potential 'target' mineral that may host appreciable concentrations of minor and rare metals is mica. Micas are known to be important sinks for many minor metals, especially in granitic rocks. For example, Simons et al. (2017) showed that biotite in the Carnmenellis granite is enriched in Li (up to 3,450 ppm), Ga (105 ppm), and Nb (up to 182 ppm). Whereas, muscovite from the same study contains less lithium (up to 1,300 ppm), Ga (up to 170 ppm) and Nb (up to 73 ppm), but is more enriched in Sn (up to 60 ppm) and W (up to 69 ppm).

5.4.3.1 Preliminary leaching experiments

Based on the results of the study by Simons et al. (2017) and the abundance of mica (between 11 and 16 modal %) in the Carnmenellis granite, leaching experiments were conducted at the British Geological Survey to evaluate the potential for recovering metals such as Li, Ga, Nb and Sn from micas in the Carnmenellis granite. A large (approximately 8 kg) sample of fresh Carnmenellis granite was jaw crushed to a nominal grain size of 10 mm and then sieved to produce a sub-sample with a grain size of 500–250 µm. A rough mixed mica (biotite and muscovite) concentrate was extracted from an approximately 750 g sample of the 500–250 µm sieved material using an automated panning machine. After drying overnight at 40°C about 9 g of mica concentrate was loaded into a titanium reaction vessel with 350 ml of 0.1 M acetic acid. The vessel was pressurised to 200 bar with N2 and held at a constant temperature of 200°C for approximately six weeks. After six weeks the fluid in the vessel was sampled and analysed by ICP-MS at the BGS for a range of major and trace elements, including lithium.

ICP-MS results (Table 2) show that acetic acid at a concentration of 0.1 M is not particularly effective for leaching metals from mica at a temperature of 200°C and a pressure of 200 bar. With the exception of Si and Na the concentrations of the other major elements (i.e. Ca, Mg, and K) in the leachate do not exceed 50 ppm, whereas the concentrations of the minor and trace elements in the leachate are typically very low (i.e. <0.5 ppm). However, only one lixiviant was tested under fixed conditions (i.e. concentration, temperature and pressure), and it is possible that using alternative lixiviants (e.g. EDTA) and/or a different set of experimental conditions would liberate a higher concentration of metals.

Table 2: ICP-MS data (ppm) for a sample of Carnmenellis granite analysed during the CHPM2030 project.

Element	Ca	Na	K	Si	Cu	Li	Sn	Ga	Nb
Concentration in ppm	50.0	67.0	33.6	239	0.184	0.007	0.089	0.01	0.008

5.5 Applicable leaching agents based on WP2

A key aspect of the CHPM2030 concept is that metals can be transported in solution and extracted at the surface. The extraction process will be more efficient with higher dissolved metals concentrations, but this could result in problems with precipitation in the production boreholes and surface infrastructure. An entire work package (WP2) in the CHPM2030 project was devoted to investigating metal mobilisation using mild leaching agents (Kilpatrick et al., 2017). Three mineralised samples from Cornwall were used in the experimental work: i) from the South Caradon Mine, which is located on Bodmin Moor. This was one of the major copper producing mines in Cornwall. The sample was dominated by quartz, containing pyrite and arsenopyrite, and was selected to represent the 'main-stage' mineralisation; ii) a composite sample from Herodsfoot Pb-Ag-Zn-Cu mine, SE of Bodmin, composed of metasedimentary rock and quartz vein material. This sample, represents 'cross-course' mineralisation, and was dominated by quartz. Galena was the dominant sulfide mineral, with minor pyrite and sphalerite also present. Antimony is associated with the base metals, predominantly occurring in bournonite (Deady and Moore, 2015; Knight et al., 2016); and iii) from Cligga Head to represent tin-tungsten mineralisation (Moore and Jackson, 1977). This sample was dominated by quartz, but contained cassiterite, columbite and ferberite.

Seven experiments using acetic acid at concentrations of 0.1 M and of 0.001 M, at 70°C in a rotating mixer, and at 150°C in a pressurised batch vessel were conducted on the Cornish samples of mineralisation. For the sample of 'main-stage' mineralisation the spread of elements extracted during both experiments are broadly similar, with detectable concentrations of some elements considered 'critical', along with a broader range of elements that are associated with mineralisation in south-west England. It was concluded that acetic acid concentration and pH had very little influence on the concentration of elements liberated during the experiments. Three experiments were carried out using the sample of 'cross-course' mineralisation. Two used acetic acid at a concentration of 0.1 M, and the other an acid concentration of 0.001 M. Experiments employed the following varying conditions: 70 °C, atmospheric pressure, and 150 °C/200 bar. Acid concentration significantly affected the number of elements recovered in the leachate and their concentration, with the stronger acid performing best. Cobalt, gallium, molybdenum and antimony were detected in the leachates. Notably, concentrations of cobalt, gallium, lead and some REE were greater in the leachate produced by the 70°C experiment, than in the 150°C experiment, possibly indicating that formation of a precipitate occurred during the higher temperature experiment, which resulted in scavenging of some of these elements (Figure 41). All of the experiments on the sample of 'cross-course' mineralisation leached a greater number of elements than was achieved from the other sample types. Experiments on the tin-tungsten mineralised sample, resulted in notable differences in the concentrations of metals liberated from the sample depending on the acetic acid concentration used. The number of elements detected in the leachate were limited, but a greater number of elements at higher concentrations were detected in the 0.001 M experiment. However, with the exception of tungsten, no other critical metals were detectable in the leachates arising from either experiment on the tin-tungsten mineralisation. Copper, arsenic, tungsten and iron were relatively abundant in the leachates, reaching concentrations of about 2E-5 M, 2E-6 M, 8E-7 M, 7E-7 M and 1E-4 M, respectively,

in the experiment that used the more concentrated acid. Complete details of the experimental methods and results can be found in Kilpatrick et al. (2017).

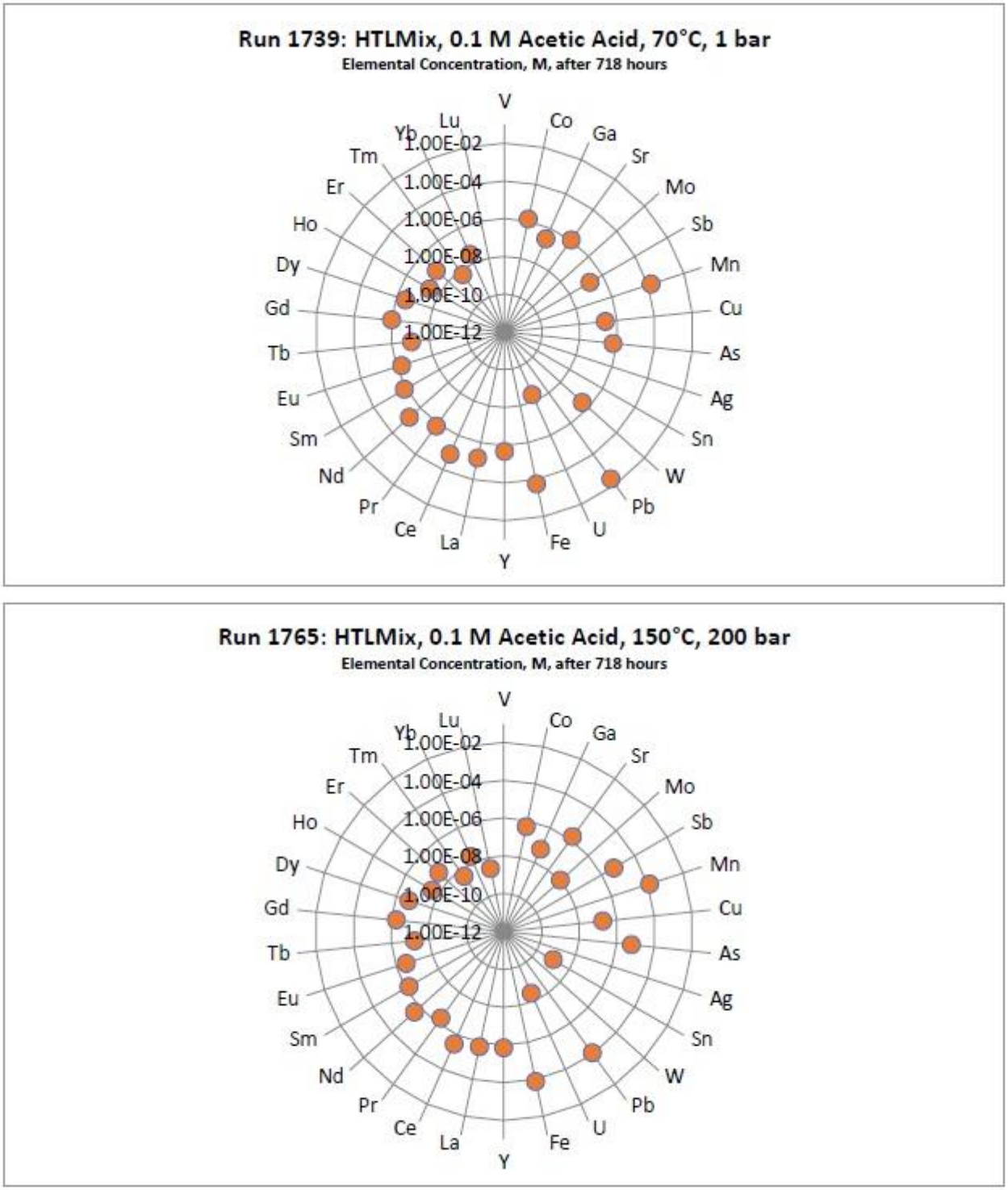

Figure 41: Concentration of selected metals in the leachates arising from experiments on a sample of 'cross-course' mineralisation from Cornwall (Kilpatrick et al., 2017). British Geological Survey © UKRI.

6 EGS potential

6.1 Geothermal characteristics of the area

6.1.1 Temperature gradient and heat flux

The mean heat flow of the Cornubian Batholith is 117 ± 8 mW m^{-2} (Beamish and Busby, 2016). A programme of relatively shallow (100–303 m, the majority 100 m deep) borehole measurements were undertaken across the Cornubian Batholith during the 1980s, as part of the HDR research programme. The heat production and heat flow data obtained are presented in Wheildon et al. (1981) and Thomas-Betts et al. (1989). The locations of the boreholes on the Cornubian Batholith are shown in Figure 42. Deeper heat flow values are also available from the South Crofty (650 m) and Geevor mines (403 m) (Downing and Gray, 1986; Tammemagi and Wheildon, 1974). This data is reviewed in Downing and Gray (1986) and Lee et al. (1987).

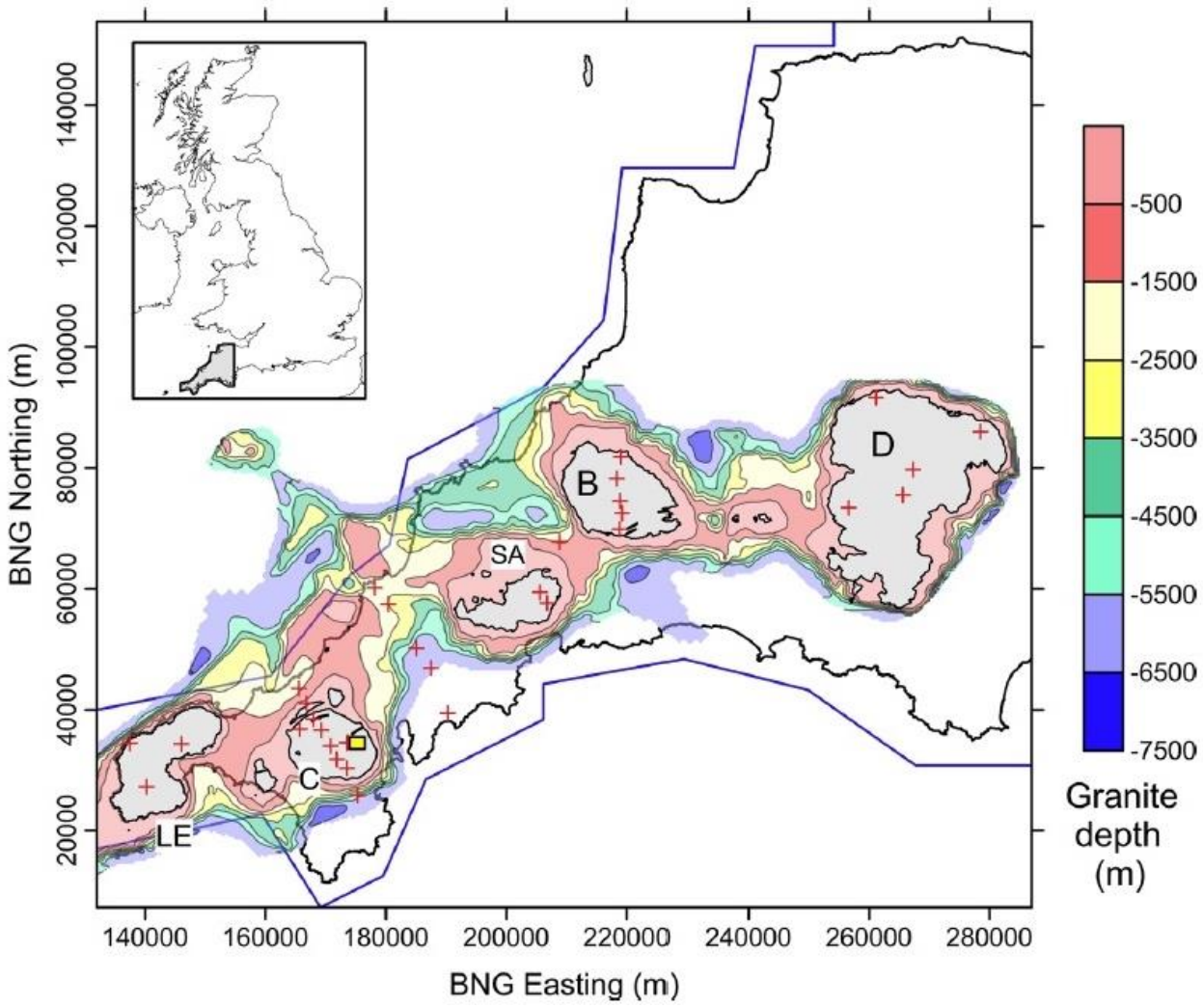

Figure 42: South-west England and geothermal borehole locations. Coloured contours show the depts. Below ground of a model of the batholith obtained from the 3D gravity model. Granite outrcrops are shown in grey with labels, LE (Land's End), C (Carnmenellis), SA (St Austell), B (Bodmin) and D (Dartmoor). Reproduced, unmodified from Beamish and Busby (2016), under Creative Commons Attribution 4.0 International License (http://creativecommons.org/ licenses/by/4.0/). © Beamish and Busby. 2016.

Beamish and Busby (2016) reassessed the published data on heat flow values and heat production from 34 boreholes, using the latest paleoclimate reconstruction, and provide revised estimates of heat at depth. They discard the data from the two mine sites as the temperature gradient is likely to have been affected by the extensive period of mining activity. The recalculated heat flows and borehole-derived heat production data have been used to estimate temperatures at 5 km depth for each of the granites. The temperatures at 5 km depth range from 185°C for the Dartmoor granite to 221°C for the St Austell granite. The temperature of the Carnmenellis granite at 5 km depth was estimated to be 200°C (Beamish and Busby, 2016) (Figure 43).

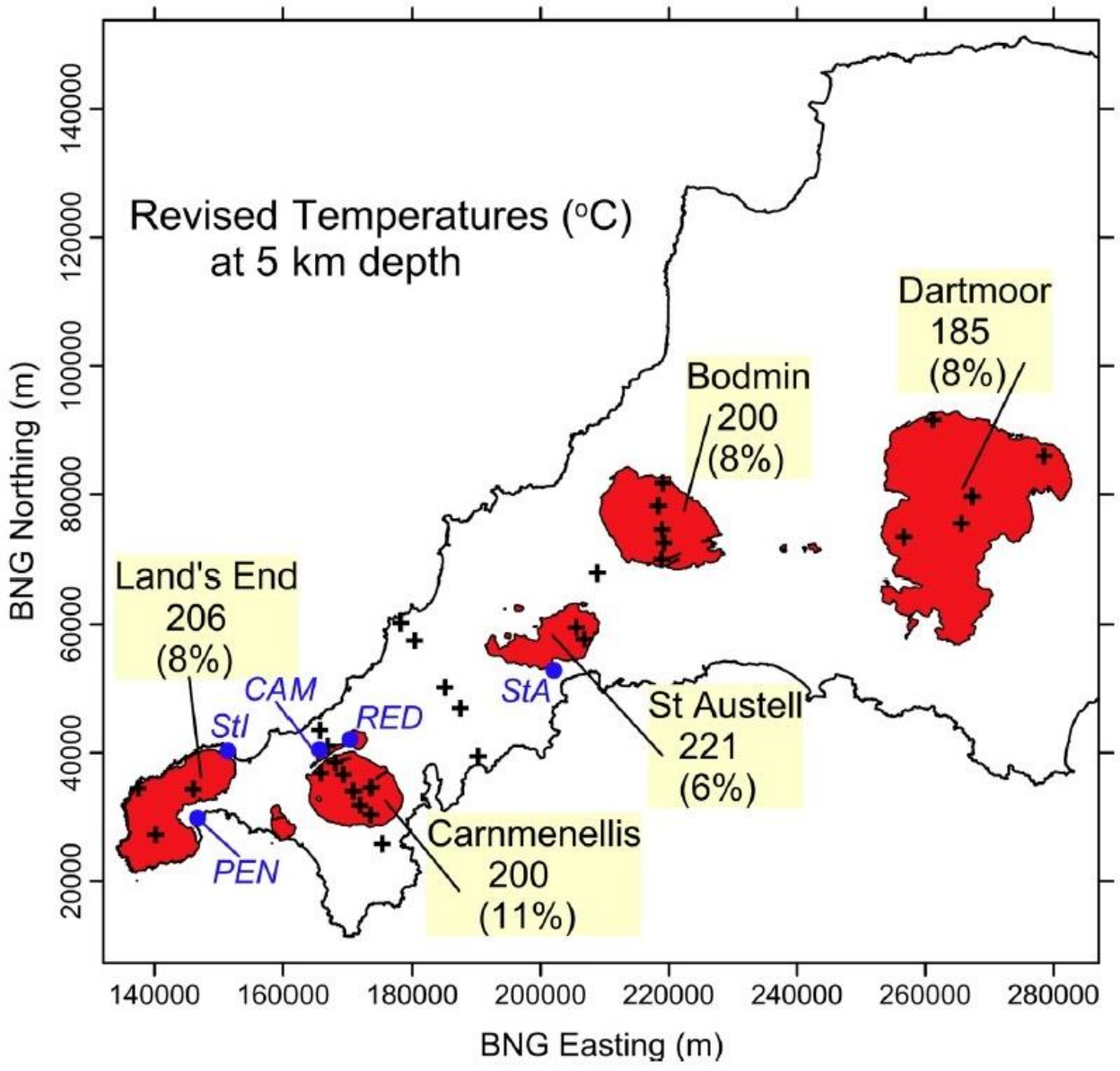

Figure 43: Revised granite-average tempetures (in °C) at a depth of 5 km and percentage increases (in brackets) over previously publicshed estimates. Reproduced, unmodified from Beamish and Busby (2016), under Creative Commons Attribution 4.0 International License (http://creativecommons.org/licenses/by/4.0/). © Beamish and Busby. 2016.

For validation purposes, the only deep temperature measurements that exist for the Cornubian Batholith are those from the HDR boreholes at the Rosemanowas quarry in the Carnmenellis granite. RH12 reached a depth of 2.1 km at which the rock temperature was 79°C. A subsequent drill hole (RH15) extended to 2.6 km, at which depth the rock temperature was 100°C (Barker et al., 2000). The revised heat flow estimates for the shallow holes at the Rosemanowas site are consistent with this, as the constant heat production with depth model, returns subsurface temperatures that are only slightly higher than the temperatures measured in the deep holes, of about 84°C and 102°C at 2.1 km and 2.6 km, respectively (Beamish and Busby, 2016). Beamish and Busby (2016) also consider the borehole heat production values in the context of the TellusSW radiometric data, which provides ground concentration estimates of the heat-producing radioelements. They use the relatively sparse borehole data as a control to correct the airborne estimates. The corrected airborne heat production estimates provide a heat production map, based on uniformly acquired data, in which it is possible to identify zones of high heat production at a detailed scale (Figure 44). Previous observations based on the borehole data alone suggested that the greatest areas of heat production within the granites was towards the granite/country rock contact. Using the heat production maps it is possible to define clear zones with the highest values (Figure 45). Whilst these zones have associations with the granite margins they also extend across the granite bodies (Beamish and Busby, 2016). The expected temperature of 200°C at 5 km depth in the Carnmenellis granite is too low to have a significant effect on the granite strength and brittle behaviour (Pine and Kwakwa, 1989).

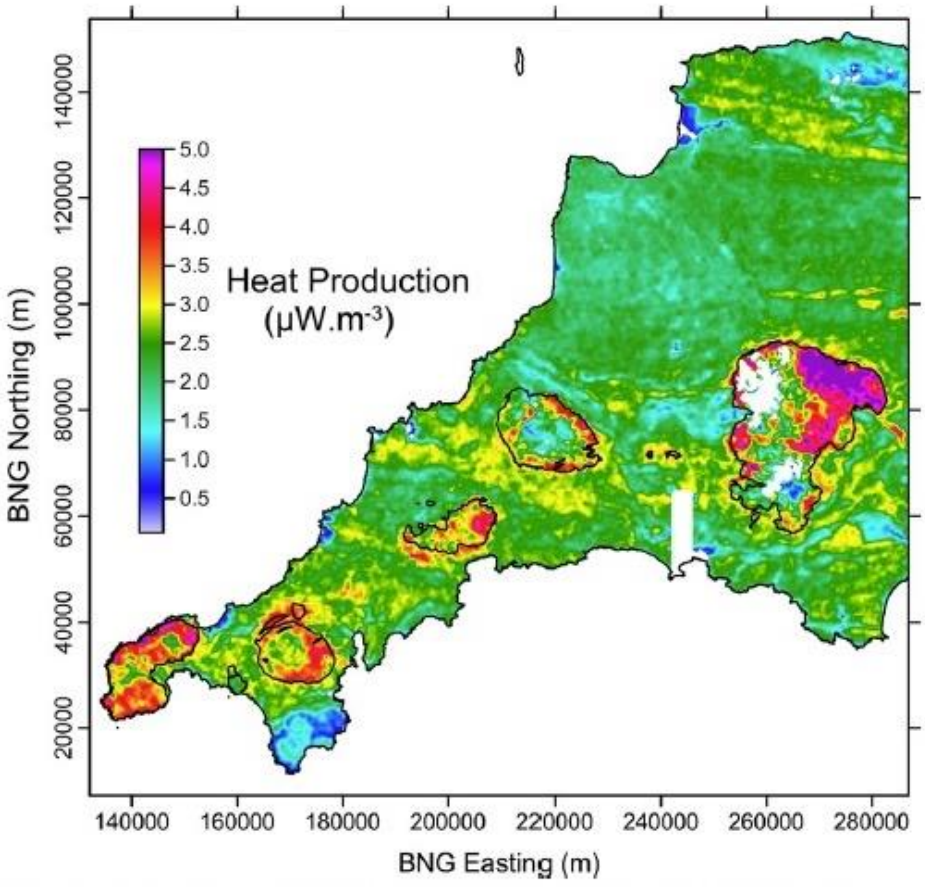

Figure 44: Revised heat production estimates for south-west England. Reproduced, unmodified from Beamish and Busby (2016), under Creative Commons Attribution 4.0 International License (http://creativecommons.org/ licenses/by/4.0/). © Beamish and Busby. 2016.

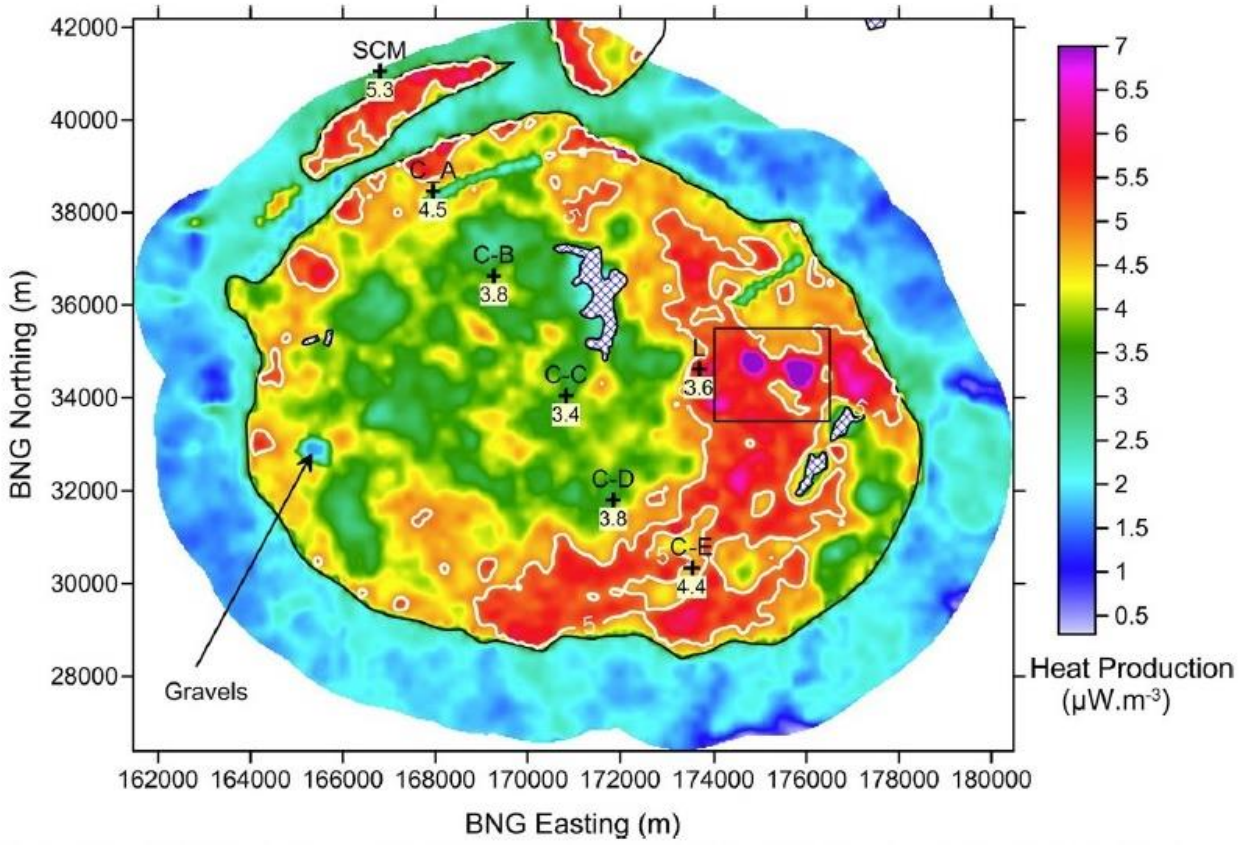

Figure 45: Area of the Carnmenellis granite outcrop, radially extended by 2 km. Continuous colour image of BH-correct heat production. Reproduced, unmodified from Beamish and Busby (2016), under Creative Commons Attribution 4.0 International License (http://creativecommons.org/ licenses/by/4.0/). © Beamish and Busby. 2016.

6.1.2 Stress field

The magnitude and orientation of the in-situ stresses exert the dominant control on the shape, extent and orientation of the growth of a HDR reservoir (Pine et al., 1983b). An extensive programme of both direct and indirect stress measurement was undertaken in the Carnmenellis granite during the HDR project. Hydraulic fracture or hydrofracture stress tests were conducted in borehole RH 12, at progressively deeper levels to a maximum depth of 2550 m, in the Carnmenellis granite at Rosemanowes quarry. The tests provides values for the minimum horizontal stress and estimates of the maximum horizontal stress, and its variation with depth. Stress anisotropy was very significant in the parts of the hole tested, with maximum and minimum horizontal stresses at a vertical depth of 2000 m of about 70 and 30 MPa, respectively. The overburden stress at this depth was estimated to be 52 MPa (Batchelor and Pine, 1986; Pine et al., 1983a). The results of the hydrofracture measurements gave the following trends with depth: maximum horizontal stress (MPa) = 15 + 27.5 d; minimum horizontal stress (MPa) = 6 + 11.8 d; and vertical stress (MPa) = 26 d. The maximum shear stress was found to increase rapidly with depth, and this stress condition was considered vital for strike slip shearing during hydraulic stimulation at Rosemanowes quarry. If the stress field at depth is compared with Mohr's envelope for the intact granite, it shows that that compressive failure of the borehole wall should not occur. In contrast, if 'effective' stress conditions apply (i.e. borehole pressure equals the pore fluid pressing the surrounding rock), then shear failure of the rock is predicted. Examination of the boreholes with dip-meter,

four-arm calliper and borehole televiewer did not identify any breakouts prior to the wells being exposed to the high hydraulic pressures (Batchelor and Pine, 1986).

Overcoring rock stress measurements were conducted at the South Crofty mine (about 10 km from the Rosemanowes test site), at a depth of 790 m. Two types of overcoring technique were used, but the average principal stress directions, based on the four best tests using the Commonwealth Scientific and Industrial Research Organisation of Australia (CSIRO) system are shown in Table 3. The direction of maximum principal stress was 130–320°. A significant anisotropy exists between the two horizontal principal stresses, and the conditions were mainly attributed to tectonics arising from the Alpine orogeny. The direction of maximum principal stress, of about 130°, and the stress magnitudes determined by overcoring measurements (Table 3) were close to those measured by the hydrofracture tests at the same depth (~770 m) (Batchelor and Pine, 1986; Pine et al., 1983a).

Table 3: Average principal stress directions based on the four best CSIRO overcoring tests undertaken in South Crofty mine. σ_1 = maximum principal stress; σ_3 = minimum principal stress (Pine et al., 1983b).

Stress	Magnitude (MPa)	Azimuth (°)	Dip (°)
σ_1	37.7	129.8	5.0
σ_2	18.5	−13.1	84.4
σ_3	11.3	40. 5	−3.2

However, Evans et al. (1992) urge caution regarding the direction of maximum horizontal stress reported in earlier publications arising from the HDR project (e.g. Pine and Batchelor, 1984). This is due to their reliance on over coring data from the South Crofty Mine (which is located well outside the main Carnmenellis pluton) as it was not possible to image the fractures that developed during the hydrofracture stress measurements in RH12 (Evans et al., 1992). Subsequent data collection, including imaging of induced fractures in RH15 (N156°E±10), hydraulic fracture measurements at the Carwynnen test site in the Carnmenellis granite (N147°E±7) (Haimson et al., 1989), and data arising from inversion of focal mechanism solutions of induced seismicity at the Rosemanowas site (143–180°) (Pine et al., 1990) suggest that N150°E±10° is a more appropriate orientation for the direction of maximum horizontal stress in the Carnmenellis pluton (Evans et al., 1992).

The differential strain analysis (DSA) technique can be used to derive strain orientation data from orientated core. However, during the HDR drilling programme it was not possible to obtain orientated core. Hence the available core could not be used to derive true orientation data. Despite this, the principal strain directions can be estimated if it is assumed that one of the principal strains is vertical. Granite cubes were cut from the cores taken from depths ranging from 1500–2400 m. Figure 46 shows the stresses based on the DSA measurements compared with the results from the hydrofracturing and over-coring tests. The stress measurements from the cubes at about 1500 m are similar to those from the hydraulic stress tests. However, at greater depths the results from the DSA did not agree with the overall trend. Some of the deeper cores obtained were heavily 'disked' and the data obtained from cubes containing disking would give excessive strain values parallel to the core axis and an underestimate of the horizontal stresses. This appears to be the case at depths below 1700 m, where the data from the DSA is not consistent with the results from the other techniques (Batchelor and Pine, 1986).

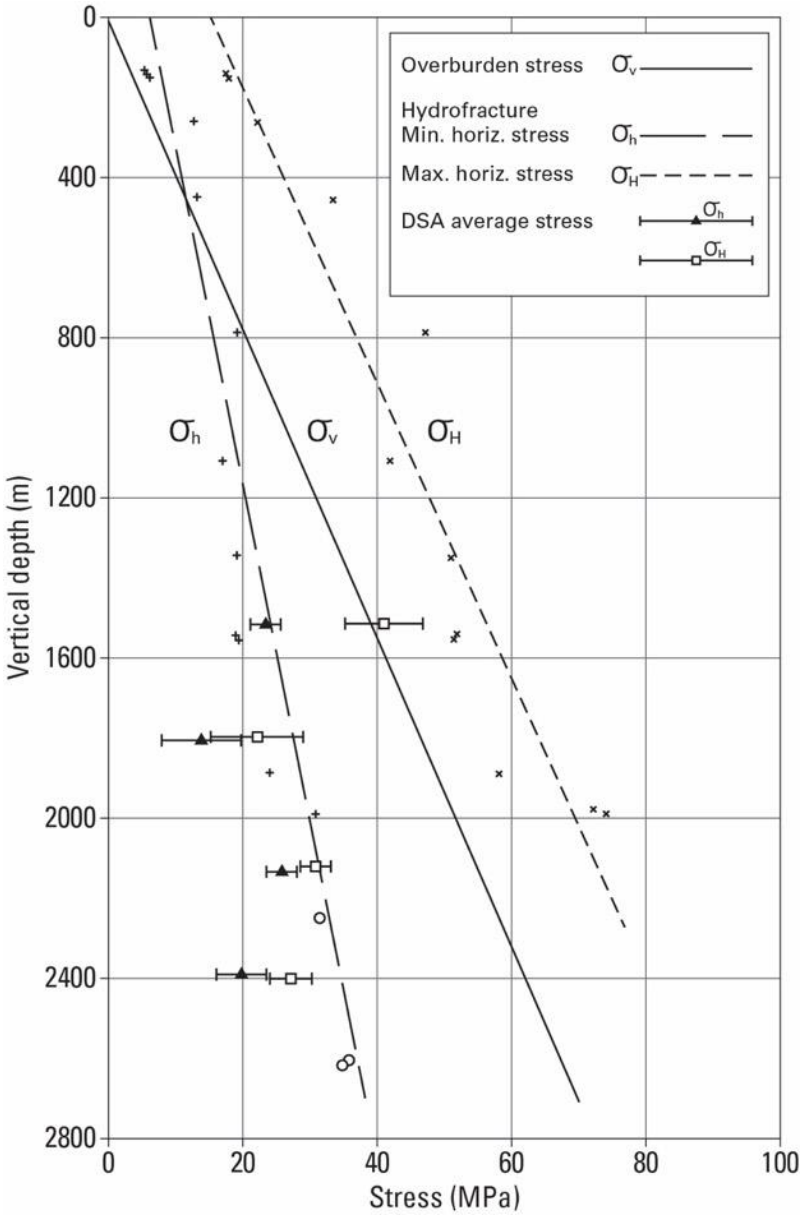

Figure 46: Depth vs. stress plot for the three principal stresses, showing data obtained from DSA, hydrofracturing and over-coring measurements. Redrawn from Batchelor and Pine (1986), Figure 4, ©International Society for Rock Mechanics.

The relationship between injection flow rate and injection pressure was studied during the hydraulic injection tests at the HDR site. During one test, involving repeated pressurisation of a single feature in a short packed off section of well, a significant increase in flow rate occurred above 8 MPa. The open hole lengths of the three HDR project holes were 357 m, 722 m and 575 m. Flow measurements and temperature logging over these intervals indicated that water entered or exited the well on joints that were within 30° of the direction of the maximum principal stress. However, not all joints at this orientation permit water to leave or enter the well. The threshold pressure of joint opening was determined by plotting pressure change as a function of the square root of the flow rate, and for RH12 this indicated a minimum effective stress of 7.0 MPa at 1800 m depth (Batchelor and Pine, 1986).

A major hydraulic stimulation operation was undertaken on HDR well RH15 to produce a fracture at a depth of 2370 m. This involved pumping 5500 m^3 of viscous fluid into the well over a period of 8 hours. Following the injection, the well was closed (shut in), and the pressure decay was observed over a 24 hour period (Figure 47). The well closure pressure (minimum pressure required to keep fractures open) was determined to be 30.25 MPa, after about 5 hours of closure. The hydrostatic pressure at 2370 m was 20.55 MPa, which means closure occurred at a well head pressure of 9.7 MPa (Batchelor and Pine, 1986).

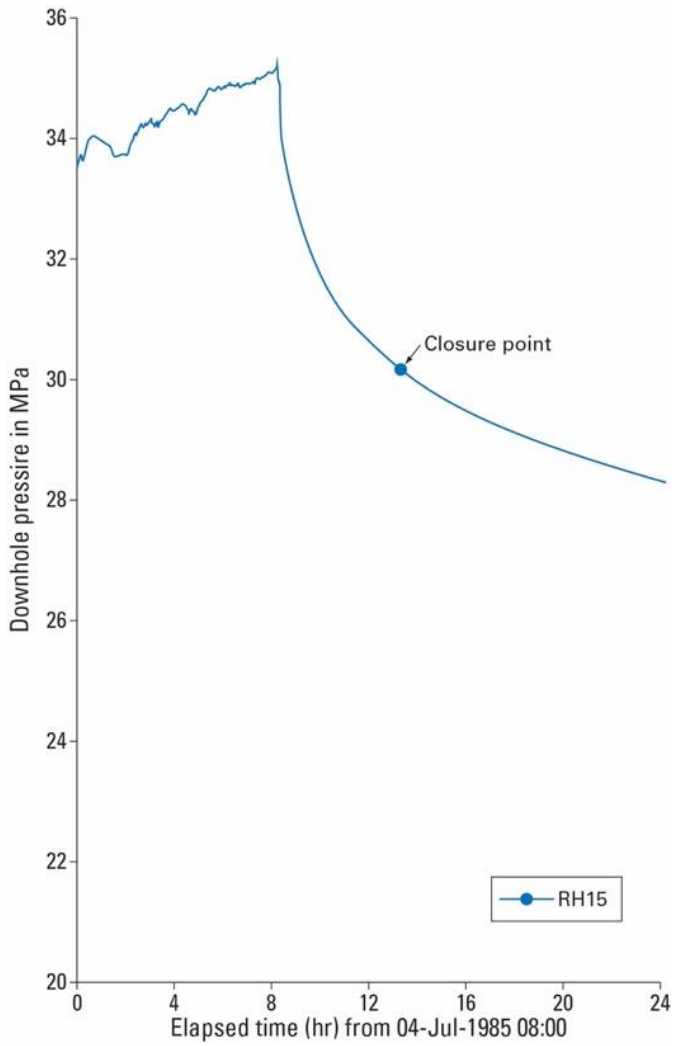

Figure 47: Downhole pressure for 24 hours covering the 8 hours of injection and the first 16 hours of well shut in. Redrawn from Batchelor and Pine (1986), Figure 7, ©International Society for Rock Mechanics.

A microseismic network was established to monitor the injection operations at the HDR site. It was active throughout the Phase 2A (studies at intermediate depths, 2500 m, focussed on assessing the feasibility of creating a subsurface heat exchanger; MacDonald et al. 1992) injections and recorded about 30 000 events. 5260 events were located and provided information on the reservoir geometry. Figure 48 shows that most of the events occurred beneath the wells. This was attributed to the shearing along natural joints, in response to the highly anisotropic stress field (Mines, 1988).

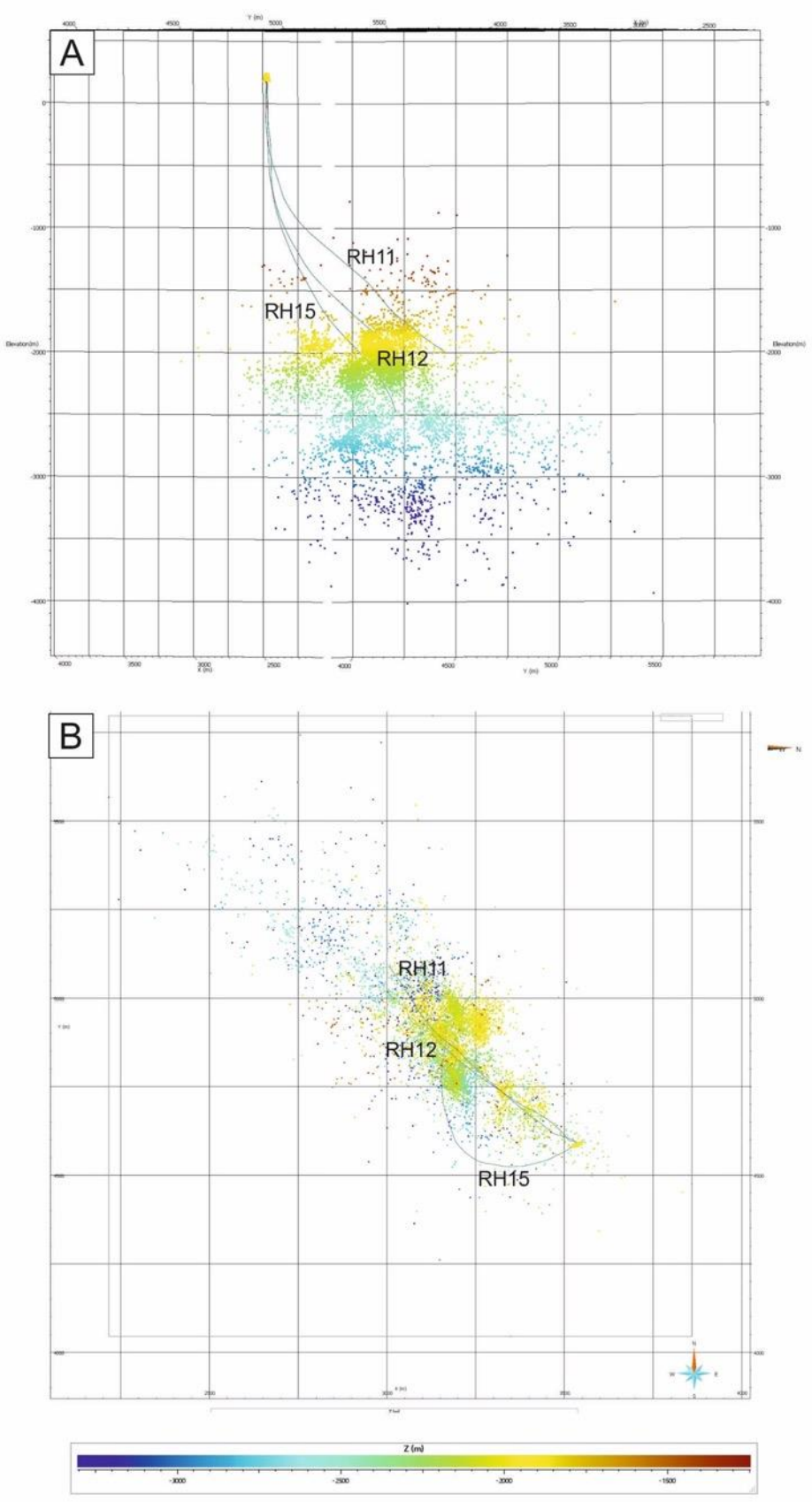

Figure 48: Microseismic event locations and well trajectories. A. View in the plane. B. Plan view. British Geological Survey © UKRI.

P-wave first motion data collected by seismic networks can be used to determine fault plane solutions (a way of showing the fault and the direction of slip on it from a seismic event). P-wave first motions, based on a 'double couple' mechanism will define two orthogonal planes. The monitoring network at the HDR site had insufficient sensors to determine faults plane solutions for individual seismic events. However, the complete data set collected was used to generate a composite solution to determine the predominant fault mechanism. The seismic data collected during the major, viscous hydraulic stimulation experiment in HDR well RH15 (described above) is presented in Baria et al. (1985). The fault plane solution based on this data indicates that either left or right lateral strike slip motion on close to vertical faults planes has occurred. The two planes defined have strike orientations of 353° and 263°. The plane at 353° has an orientation similar to one of the major joint sets observed at 2000 m depth using a borehole televiewer. It was concluded that 353° is the orientation of the majority of the 'mobile joints'. Fault plane solutions based on data from other injection experiments are consistent with these findings. The fault plane solutions indicate that the maximum principal stress direction is located to the west of 353°, in the dilatational quadrant. More than 80 per cent of the events measured indicate a strike slip motion and if the friction between joint surfaces is assumed to be at an angle of 35–45° it results in a stress direction of 320–330°. This agrees with the directions measured by the overcoming experiments described above (Batchelor and Pine, 1986).

When plotted the microseismic events form a cloud with a general strike of 135–315°. The combination of the orientations of the major joint sets and the stress regime shown in Figure 49, limited the growth of the hydraulically stimulated reservoir to a direction that predominantly lies between the maximum principal stress direction and the joint set that strikes at about 330°. However, detailed examination of the reservoirs internal structure indicates groups of planes strike at about 350°, but have an overall pattern more comparable to the stress direction (Batchelor and Pine, 1986).

Rock stress measurements have also been made at the Carwynnen experimental site, close to the NW margin of the Carnmenellis granite. This location has vertical boreholes to a depth of 700 m (Tunbridge et al., 1989). Two series of hydraulic fracturing stress measurements were made here in the late 1980s, one at a shallow level (74–134 m) and the other at a deeper level (602–685 m). They calculated the principal horizontal stresses, which were indicative of a compressive stress regime with a NW maximum horizontal stress direction, and a ratio greater than 2:1 between the horizontal stresses. The relative principal stress magnitudes in the deeper level zone would favour strike-slip faulting. The stress directions and relative stress magnitudes obtained from the Carwynnen experiment were consistent with the existing stress measurements for the Carnmenellis granite (Rosemanowes site and South Crofty Mine). They conclude that the stress measurements obtained from the Carwynnen site represent the regional stress regime and the conditions in the upper kilometre of the Carnmenellis granite. Additionally, agreement between the independent measurements (see Figure 7 in Haimson et al., 1989), are indicative of the reliability of the data and the uniformity of the stress field in the Carnmenellis granite (Haimson et al., 1989).

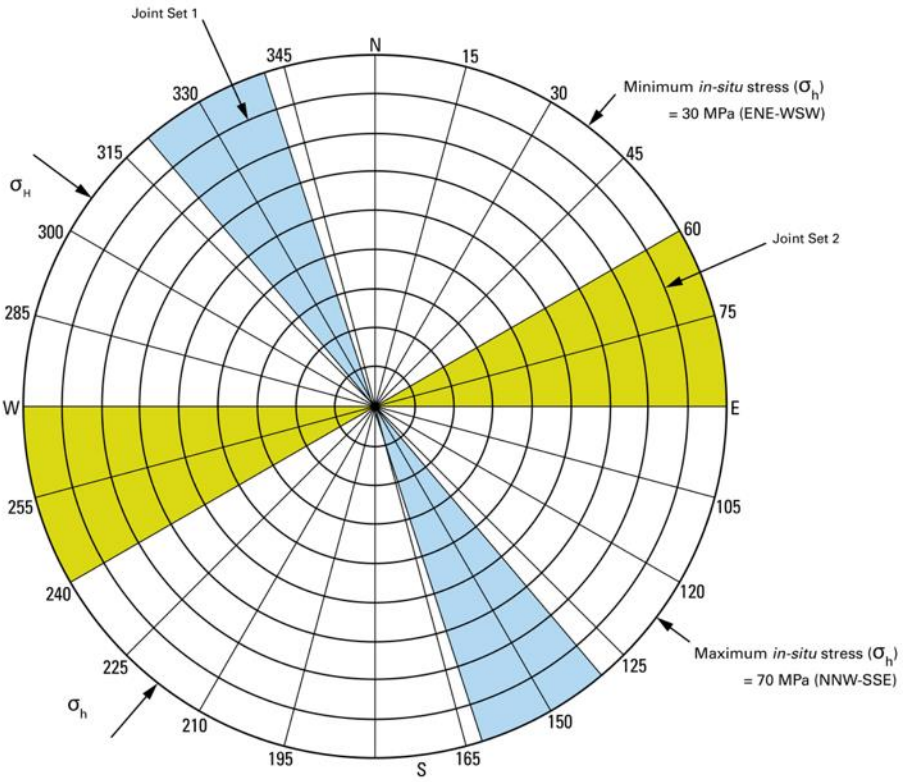

Figure 49: Strike directions of the major joint sets and principal stress orientation (note a more recent review i.e. Evans et al., 1992 suggests a more appropriate orientation for the direction of maximum horizontal stress in the Carnmenellis pluton is N150°E±10°, see Section 6.1.2) and magnitude in the Carnmenellis granite as determined by in-situ hydraulic fracture tests at the Rosemanowes HDR test site. Redrawn from Batchelor and Pine (1986), Figure 10, ©International Society for Rock Mechanics.

6.1.2.1 Implications for fracture systems at greater depth and crustal permeability

It was originally calculated that the microseismic events extended to depths of over 4 km (Figure 48) and no significant changes in their directions were apparent. It was concluded that this is evidence that there is no significant rotation of the stress field at depth (up to 6 km; Pine and Kwakwa, 1989) in the Carnmenellis granite, major structures extend to these depths, and the stress field is 'critically anisotropic', with fluids occurring in near vertical structures. However, the researchers note that even with the 'substantial and comprehensive data set there can be no great confidence in the extrapolation of all aspects of the stress tenor [to much greater depth]'. Despite this uncertainty they conclude that the 'persistence of the serve anisotropy and the direction of the stresses can be predicted and minimum horizontal stress trend may well persist in the 3000–7000 m depth range' (Batchelor and Pine, 1986). Pine and Kwakwa (1989) reviewed the hydrofracture stress measurements (HFSM) made during the HDR project, to assess the implications for measuring stress at depths of up to 6 km. They considered there to be too few data points at 2.6 km to be confident about stress magnitudes at this depth and extrapolating these values to depths of great than 3–4 km is high-risk. Despite this they indicate that extrapolation to 6 km depth based on data from the 0–4 km depth range in the same rock type (i.e. Carnmenellis granite) the measurements were made in 'should be sufficiently accurate'.

However, this assumes that no major stress discontinuity exists at depth, but they postulate that such as discontinuity would be the result of a major lithological change, or the occurrences of a major structure, which should be obvious from surface geophysics or drilling (Pine and Kwakwa, 1989). It is important to note that a more recent reassessment of the microseismic data, using information from an additional measurement station, which improved vertical accuracy to less than 20 m, relocates the seismic events to a maximum depth of the 3 km (Evans et al., 1992).

6.2 Evidence for deep fluids

6.2.1 Deep-saline fluids

Warm (up to 55°C), high-salinity groundwaters have been found at depths of up to 820 metres, primarily issuing from NNW-SSE-trending cross-courses and lodes in mines at the northern edge of the Carnmenellis granite. These flows occur in mines in both the granite and in the killas. Some of the cross-course flows have been discharging for more than 30 years. Crosscourse bines typically discharge at about 1–10 l/s at temperatures between 40–45°C, and with salinities of about 2000 mg/l, suggesting that a large reservoir of saline, thermal water exists at depth. These deep spring waters are mildly acidic to neutral (pH 5.4–7.7), and compositionally they are dominated by Na, Ca and Cl (Smedley et al., 1989) (Table 4).

The Na/K geothermometer indicates an equilibrium temperature of 54 °C for the water, which suggests a depth of origin of 1.1 to 1.2 km, or some 440 m below the depth of discharge into the South Crofty Mine (Burgess et al., 1982b). Stable oxygen ($\delta^{18}O$) and hydrogen ($\delta^{2}D$) isotope studies indicate that these waters are not derived from seawater, but are more likely diluted palaeobrines, which have flowed through cross-course structures within the granite and killas. Their chemical and isotopic signatures also indicate mixing and dilution by circulation of local meteoric water (Alderton and Sheppard, 1977; Smedley et al., 1989). Isotope (^{4}He and U series) studies by Burgess et al. (1982b), Edmunds et al. (1984), and Smedley and Allen (2004) identify components of the deep-brines with ages of between 10000 and 1000000 years old. The presence of tritium and $\delta^{14}C$ isotopes indicate that up to 40 per cent of the deep-brines, by volume, comprise more recent (1953–1978) meteoric water, which indicates mixing of fluids (Burgess et al., 1982a). The mixing of these waters also points to percolation of modern waters to a depth of at least 700 metres below ground level, where it mixed with older, deeper saline fluids (Burgess et al., 1982b; Downing, 1986; Smedley and Allen, 2004). Historically these waters have only been analysed for a limited suite of major and minor elements, which means that the concentration of metals of economic interest in these deep fluids remains enigmatic. One exception is lithium. The concentration of lithium, up to 125 mg/l^{-1} in deep spring waters from South Crofty (Edmunds et al., 1984), is of current interest to Cornish Lithium Ltd., a private company actively exploring south-west England for brine-hosted lithium resources. It is thought that the relatively high concentrations of lithium in these waters is a function of mica breakdown during fluid-rock reaction (Edmunds et al., 1984). This is also of interest to future geothermal projects in south-west England, as lithium may be a metal that could be leached, and recovered, by CHP operations.

Table 4: Summary of deep, mine water compositions from mines around the northern edge of the Carnmenellis granite, including South Crofty (1, 2 and 3), Clifford United (4), and Wheal Seton (5). Data from Alderton and Shepherd (1977) and Smedley et al. (1989). *Tr.* = trace and *n.d.* = not determined.

	1	2	3	4	5
	mg l^{-1}				
Na	2000	3210	457	2043	230
K	87.6	138	25.1	111	83
Ca	1070	1670	287	1166	2,,490
Mg	33.2	51.6	24.7	32	44
Fe	1.92	1.82	0.1	*Tr.*	2
Al	<0.4	<0.4	<0.1	*Tr.*	182
Si	14.4	19.6	12	24	13
Mn	2.58	3.03	1.2	*Tr.*	*Tr.*
Sr	17.6	27.6	1.3	*n.d.*	*n.d.*
Li	59.6	97.2	9.9	61	80
Cl	5800	8750	1260	5,628	9,168
Br	*n.d.*	*n.d.*	*n.d.*	*n.d.*	*Tr.*
HCO3	*n.d.*	*n.d.*	126	*n.d.*	*n.d.*
F	*n.d.*	*n.d.*	3.6	*n.d.*	*n.d.*
SO4	126	107	92	124	21
B	7.60	*12.2*	0.8	*n.d.*	*n.d.*
TDS	9,226	14,099	2,306	9,189	14,441
pH	6.61	6.79	6.85	*n.d.*	*n.d.*
Depth (m)	690	690	618	448	330
Temp (°C)	41.6	45.3	35	52	33

6.2.2 Fluid circulation models

Palaeo-fluid flow in and around the Carnmenellis granite can be divided in to four main stages (Figure 50): (i) Expulsion of early magmatic fluids associated with the emplacement of the granite, which led to the formation of sheeted Sn-W greisens in the granite roof zone and overlying metasedimentary rocks. Hydrothermal convection of formation waters starts to occur in response to the thermal anomaly created by the granite emplacement; (ii) Copper, zinc and sulphur are leached from the host rocks. Formation waters are drawn down through the granite as the system begins to cool, resulting in the deposition of Cu-Zn- sulfides in veins; (iii) Main-stage, polymetallic lodes are emplaced within the granite roof zone by further expulsion of magmatic fluids; and (iv) Formation waters start to circulate through the granite in response to cooling of the system, resulting in the deposition of Cu-Zn- sulfides in steeply dipping fissures (Smedley et al., 1989). Post-magmatism basinal brines circulate through N–S-trending structures within the granite and killas, mixing with meteoric waters. These fluids deposited Pb-Zn-rich mineralisation within the so-called cross-course veins (Gleeson et al., 2000; Gleeson et al., 2001; Scrivener et al., 1994).

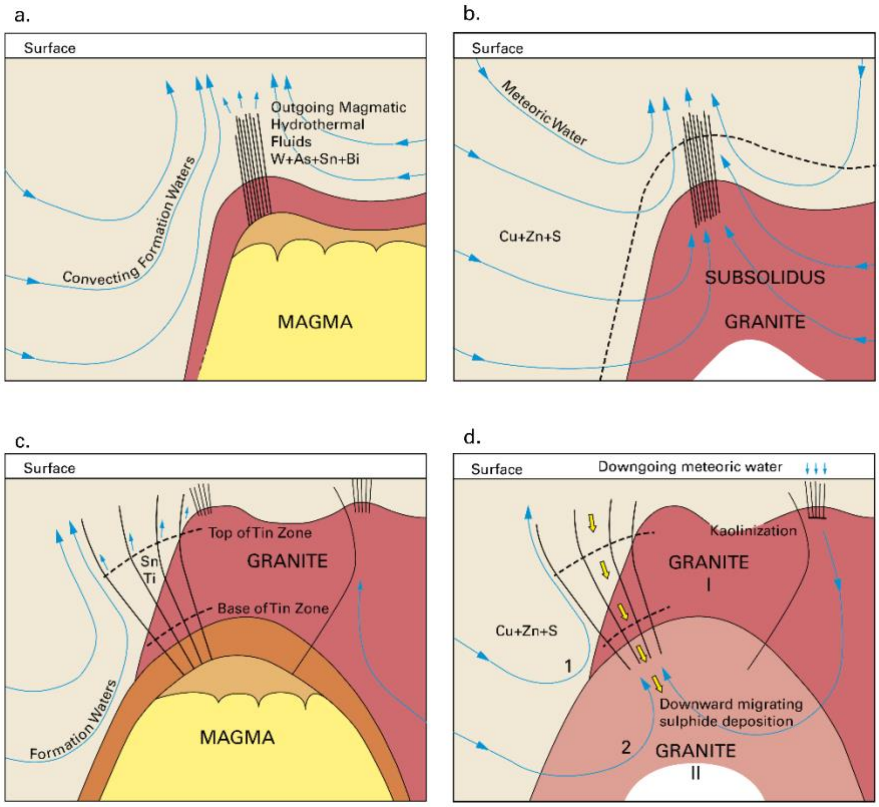

Figure 50: Schematic diagram illustrating fluid flow regimes in relation to emplacement of the Carnmenellis granite. (A) Expulsion of magmatic fluids forming Sn-W greisen's and generation of hydrothermal convection in the overlying groundwater. (B) Leaching of metals and sulphur from the host rocks. Cooling of the system permits meteoric waters to move down into the granite pluton. (C) Main stage, polymetallic lodes form in the roof zone of the granite pluton from expulsion of magmatic fluids. (D) Meteoric waters circulate through the granite as the system cools. Cu-Zn sulfides are deposited in a series of lodes. Re-drawn from Smedley et al. (1989). British Geological Survey © UKRI.

7 Integrated modelling

Modelling of the Cornubian Batholith was undertaken as part of the CHPM2030 project to improve understanding of its geothermal properties. This work involved the development of three models: a regional model, and two site-specific models, one based on the HDR project site, and the other on the ongoing United Downs Deep Geothermal Power (UDDGP) project. Here we outline the data used, methodology and limitations of the three models. The models were developed in a range of modelling software packages, including Fracman, Move4D, Petrel, and SKUA-GoCAD, with each piece of software bringing its own strengths to the modelling.

7.1 Regional model

The regional model was constructed to understand the spatial relationship of key geological parameters that feed directly into the site-scale models. The model covers the Cornubian Batholith, including the Dartmoor, Bodmin, Carnmenellis, St. Austell, and Lands' End granites, but excludes the Scilly Isles (Figure 51). It consists of a 3D Geospatial Information Dataset, containing the most relevant information for this project and future research in the region.

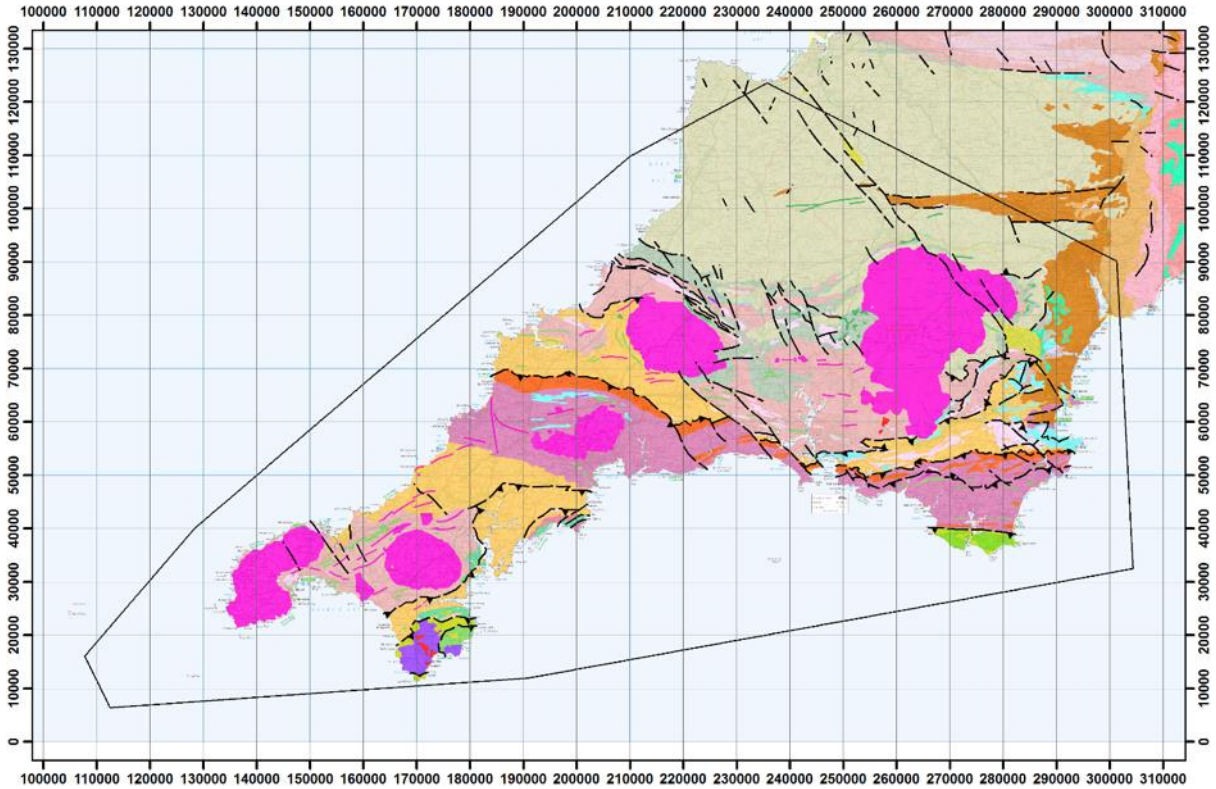

Figure 51: Geological map showing the extent of the regional model (black line) covering Cornwall and southern Devon, and the mapped location of the granite (pink). Contains Ordnance Data © Crown Copyright and database rights [2019]. Ordnance Survey Licence no. 100021290. Contains British Geological Survey materials © NERC [2019].

The model consists of two geological units: granite and killas. The granite surface was derived from the regional gravity model (Camborne School of Mines, 1988; Willis-Richards and Baria, 1989) and enhanced with five higher resolution gravity models for south-west Dartmoor (Tombs, 1977), the area between Dartmoor and Bodmin Moor (Rollin, 1988), Hayle-Leedstown (Tombs, 1977), and St. Agnes (Tombs, 1977) and St. Austell (Tombs, 1977), and the top granite contact based on 50 boreholes records (see Section 3.3.1.2 and Figure 17) (Figure 52). The surface extent of the granite was based on BGS 1:50 000 scale onshore mapping data and 1:250 000 offshore mapping data for the Land's End granite. Properties were calculated on the surface, including curvature, slope and aspect.

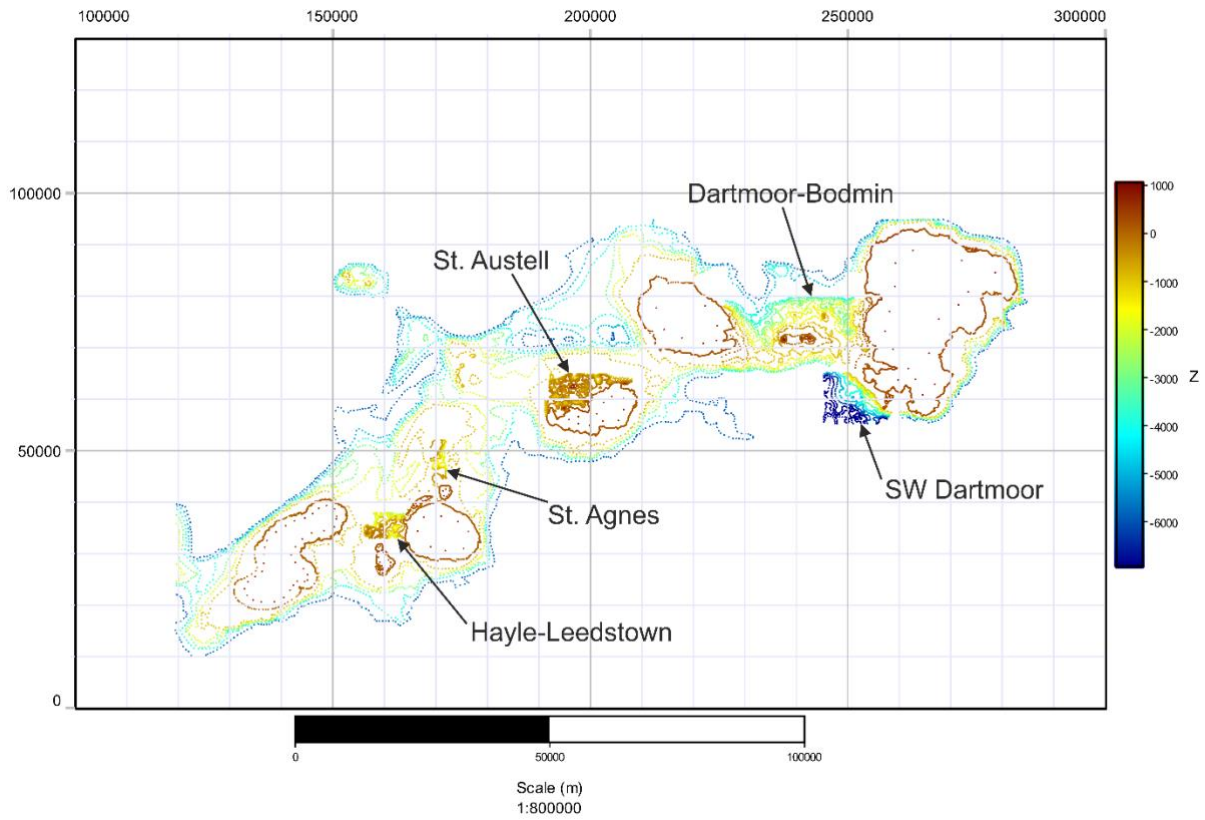

Figure 52: Points of the top granite contact used for modelling the top granite surface. Arrows indicate the location of the additional higher resolution gravity models mentioned in the text. British Geological Survey © UKRI.

The land surface and bathymetry data is derived from the General Bathymetric Chart of the Oceans (GEBCO; The GEBCO_2014 Grid, version 20150318, http://www.gebco.net) and was used as the capping surface to the model (Figure 53). Additionally this surface was used to drape the boundary polygons, and fault network. Using the GEBCO bathymetry data allowed the offshore Lands' End granite to be modelled. The base of the granite has been investigated through seismic (Brooks et al., 1984; Jones, 1991), MT (Beamish, 1990), and gravity modelling (Taylor, 2007; Willis-Richards and Baria, 1989). There is ambiguity regarding the exact location of the base of the granite. The seismic data identify a seismically homogeneous granite with three reflectors at a depth of; 6–8km, 12–15 km and 30 km; the latter reflecting the Moho (Brooks et al., 1984). The magnetotelluric survey shows resistivity increasing to a depth of 6 km, at which point joints and cracks close, and by 7 km pore-related resistivity dominates (Beamish, 1990). The electrical base of the granite lies at 14 km.

Gravity modelling by Willis-Richards and Baria (1989) suggests the base of the granite is located at between 12–15 km. Taylor (2007) suggests that the granite consists of two sheets, with an upper granite, with a base at 6–8 km, and a lower more extensive granite sheet, with a base at 12–15 km. This is supported by the magnetotelluric and seismic data. Based on the seismic data of Brooks et al. (1984), both the upper granite base and the lower granite base have been modelled (Figure 54). The base of the lower granite has been interpolated across the model extent and forms the base of the model. The surfaces of the base of the granite show a general deepening to the SE, and the lower granite thins towards the north. However, the surfaces are based on limited data and further work is required to improve understanding of the base of the granites and the shape of the two granite sheets if deeper geothermal reservoirs are to be explored.

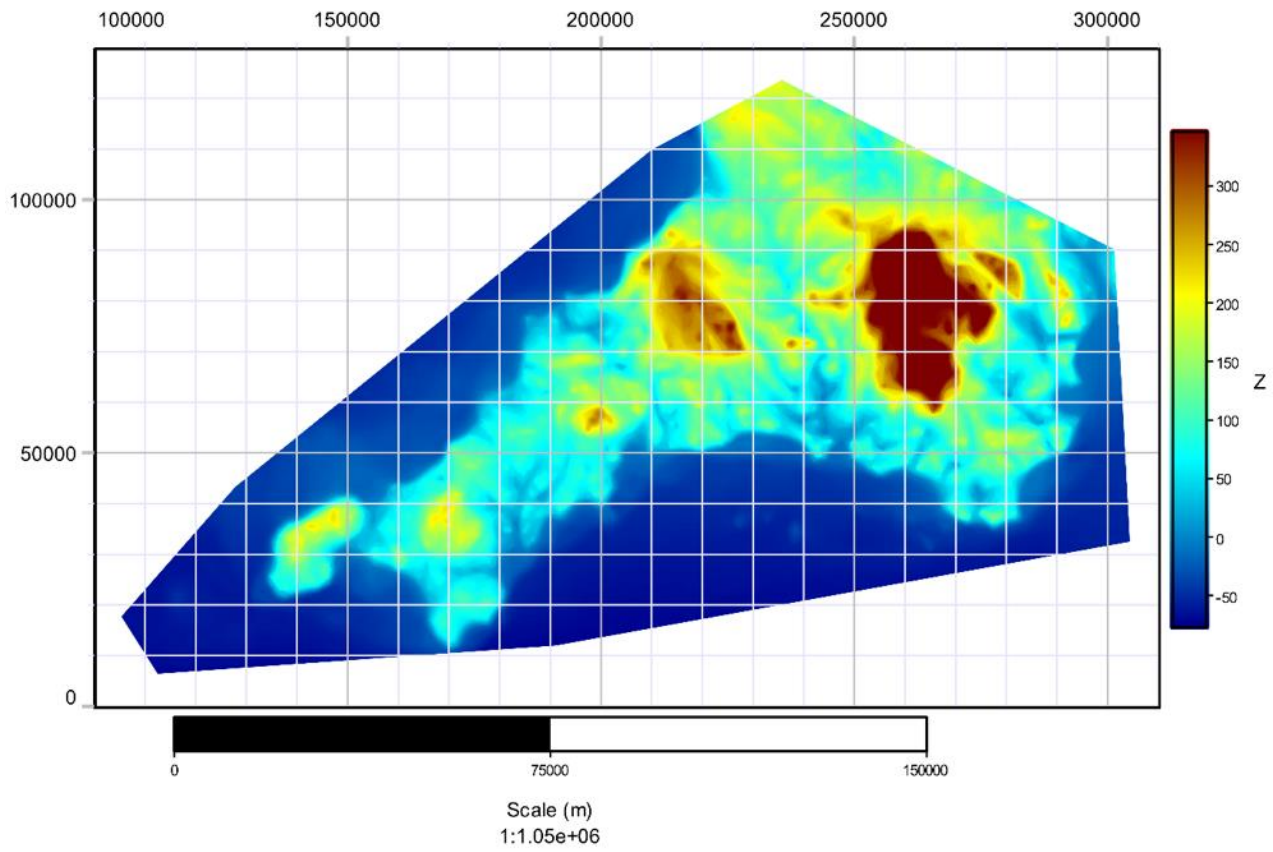

Figure 53: Modelled topographic surface. The granite intrusions can be identified as higher ground. British Geological Survey © UKRI.

Modelled surfaces were constructed using the GoCAD/SKUA implicit method with a spatial sampling of 500 m. The relative difference between the input data and output surfaces were calculated to estimate the error and uncertainty associated with the modelled surface (Table 5). There was good agreement between the modelled topography and input data, but the top granite surface had a larger error. The top granite surface is based on the interpretation of geophysical models and relatively sparse data, and given the scale of the regional model and the surface resolution (>500 m) the error is not considered to present an issue.

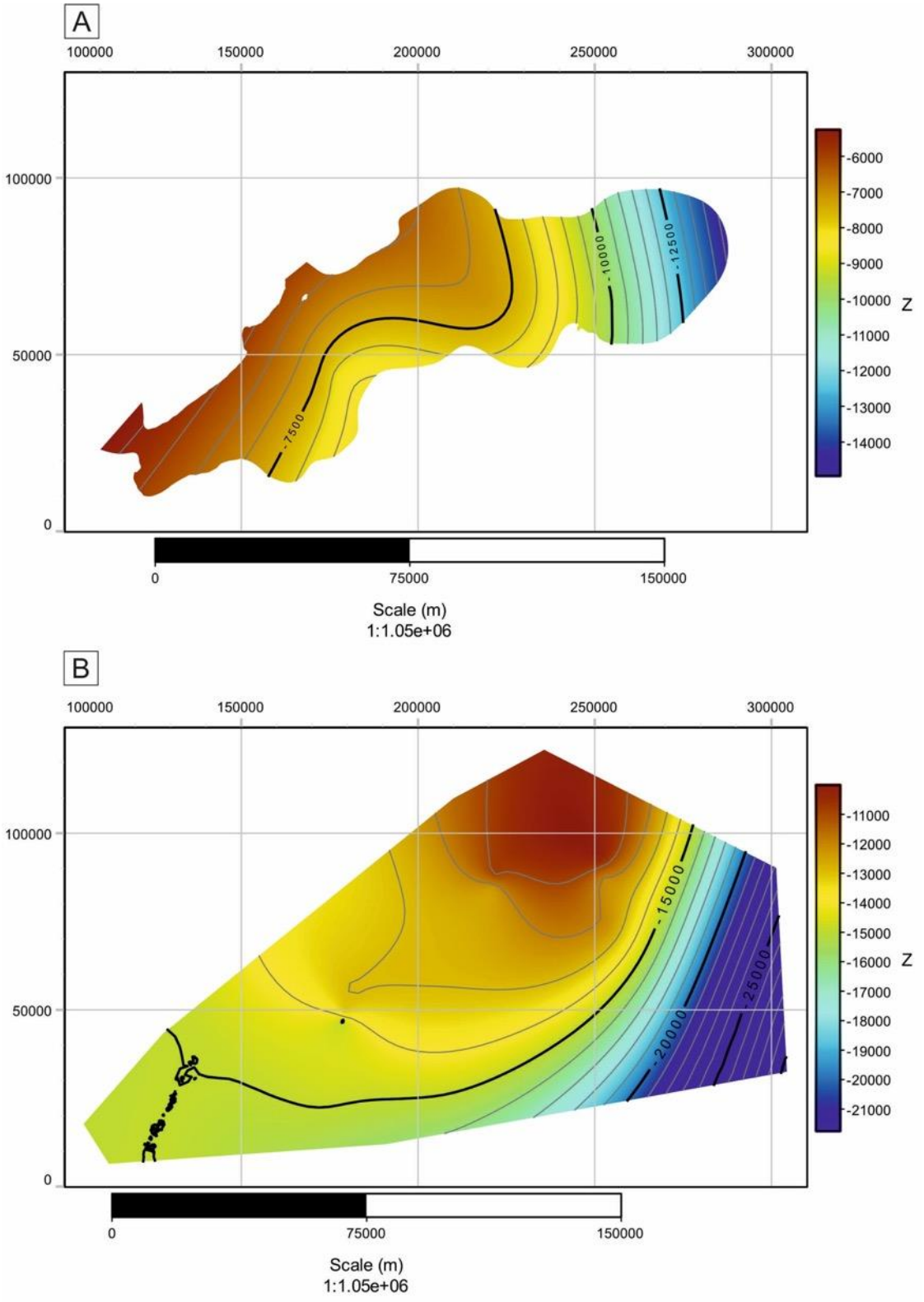

Figure 54: The granite surface used in the model. A. Upper granite surface. B. Lower surface granite surface, which has been extended across the model and also represents the base of the model. British Geological Survey © UKRI.

Table 5: Computed difference between input data and modelled granite surfaces.

Data	Error
Topography	Mean = -0.149066 m SD = 4.80127
Granite	Mean = 12.1854 m SD = 111.487

The model area is crosscut by numerous faults that would be impractical to model at a regional scale and it was therefore decided that only larger faults would be modelled (Figure 55). Major structural orientations across Cornwall include NE-SW-trending thrusts, E–W-trending thrusts, E–W-trending normal faults, and NE-SW-trending and NW-SE-trending strike-slip faults. The Cornubian granite is primarily affected by the NW-SE-trending strike-slip faults and the 19 most prominent faults identified in Camborne School of Mines (1988) were included in the regional model. These faults were modelled as vertical structures that transect the model from the topographic surface to the base of the model. Although additional faults could be incorporated into the model, for the purpose of this study, the number used were considered sufficient to show the general trend of the structures that cut the granite.

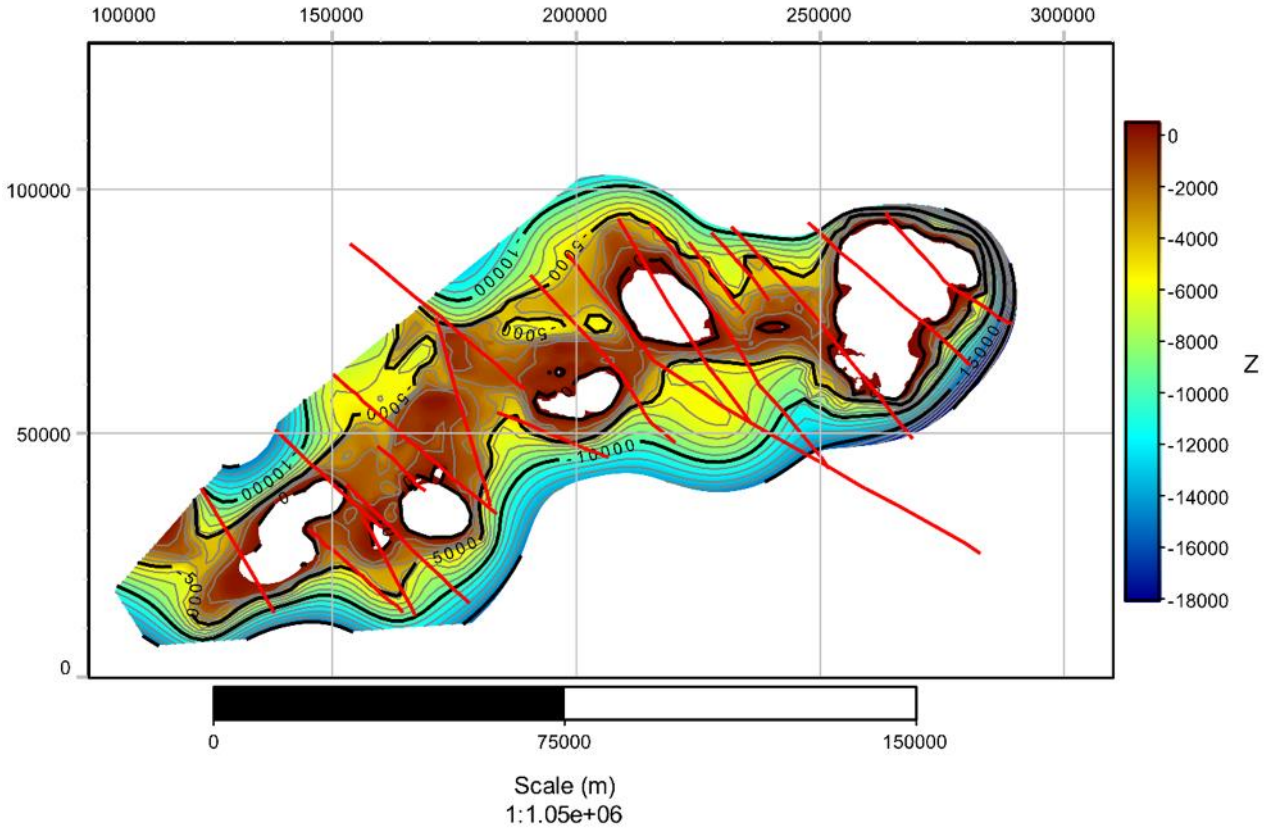

Figure 55: Map view of the top granite surface and principal large faults (red lines; after CSM, 1988). British Geological Survey © UKRI.

Once the geometrical model was established and built the model was voxelated and properties assigned. The voxel model represents an area of 207,543 km^3 with a voxel size of 1065x639x160 m (XxYxZ) resulting in 1,906,068 voxels (Figure 56). With the framework built, physical properties, including heat production, heat flow, and temperature were interpolated or simulated into the voxelated volume (Appendix 3).

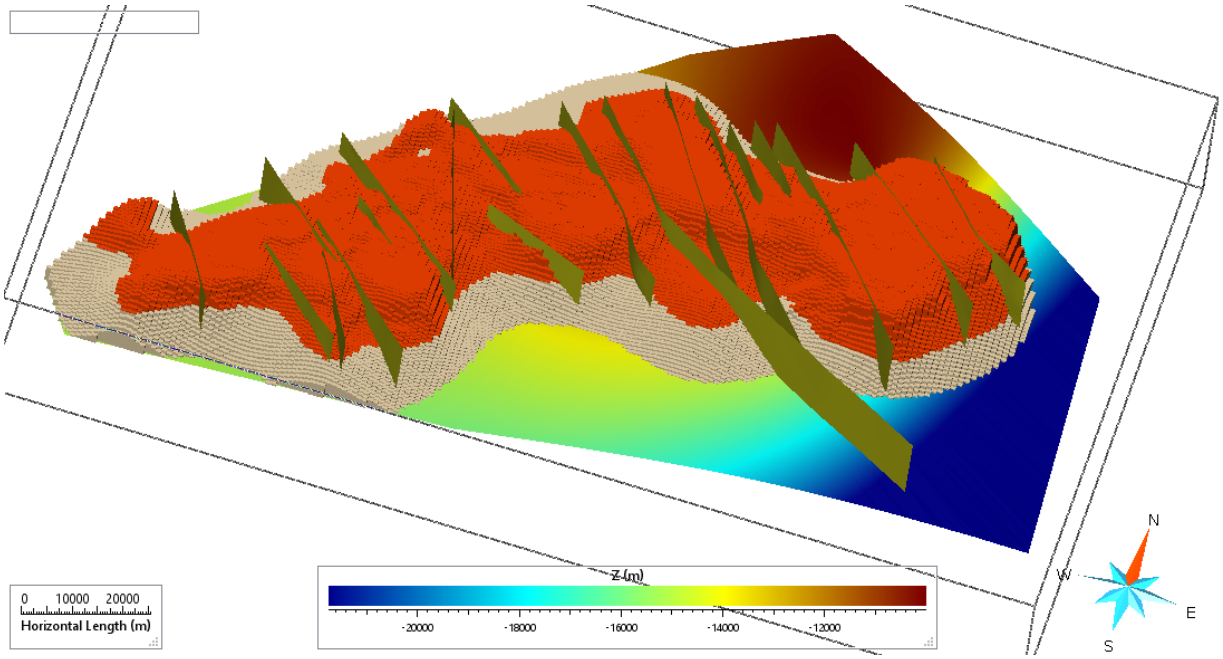

Figure 56: 3D view of the voxelated granite model showing the two granite sheets and the SE dipping base of the granite. British Geological Survey © UKRI.

7.1.1 Fracture data

Fractures are the predominant flow pathway within the granite and understanding the spatial properties of the fracture network is important for modelling the fracture network and upscaling the network for flow simulations (

Figure 57). The fracture modelling focuses on the Carnmenellis granite as the two site-scale models are both located within this pluton. However, there is a requirement to extend the fracture characterisation across the extent of the Cornumbian Batholith if the entire geothermal potential of the granite is to be examined. A number of studies on the fractures in the Carnmenellis granite have shown that there are three dominant fracture sets; two near vertical and one that is sub-horizontal (Camborne School of Mines, 1986). The two high angle fracture sets trend NNW-SSE and ENE-WSW, and dip at 80–90 degrees (Figure 20). The sub-horizontal fracture set is limited to the near surface and therefore at reservoir depths is unlikely to be a contributing factor in the reservoir flow model, and is therefore not included in the model. The two principal fracture sets are identifiable in the downhole image logs from RH12 and RH15 (Figure 58). RH12 was drilled towards the NW and therefore there is a bias in the data towards the ENE-aligned fracture set. In contrast RH15 was drilled in a spiral to intersect the microsesimic cloud resulting from the stimulation of RH12. Terzaghi (1965) correction was applied to both wells to reduce the bias within the dataset. Fracture intensity (fracture per m) was calculated from the fracture logs and upscaled to 5 m intervals for each fracture set (Figure 59). There is no indication of a mechanical stratigraphy with the cumulative frequency plot showing a uniform slope. Therefore, there was no need to subdivide the granite into discreet fracture stratigraphy.

Figure 57: Coastal exposure of fractured Lands' End granite. British Geological Survey © UKRI.

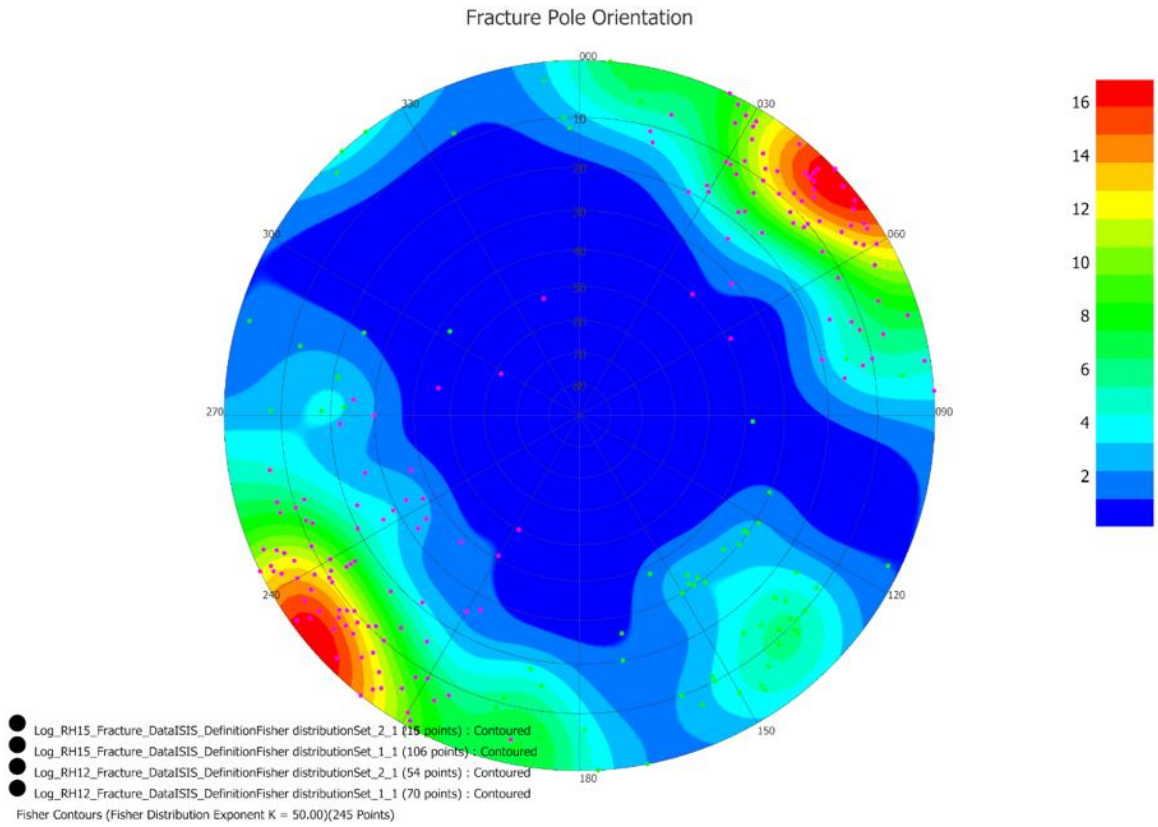

Figure 58: Lower hemisphere stereonet showing the poles to fractures from the downhole image logs for RH12 and RH15. Two primary fracture sets can be identified striking NW-SE and NE-SW, which matches with the known surface fracture orientations for the Carnmenellis granite. British Geological Survey © UKRI.

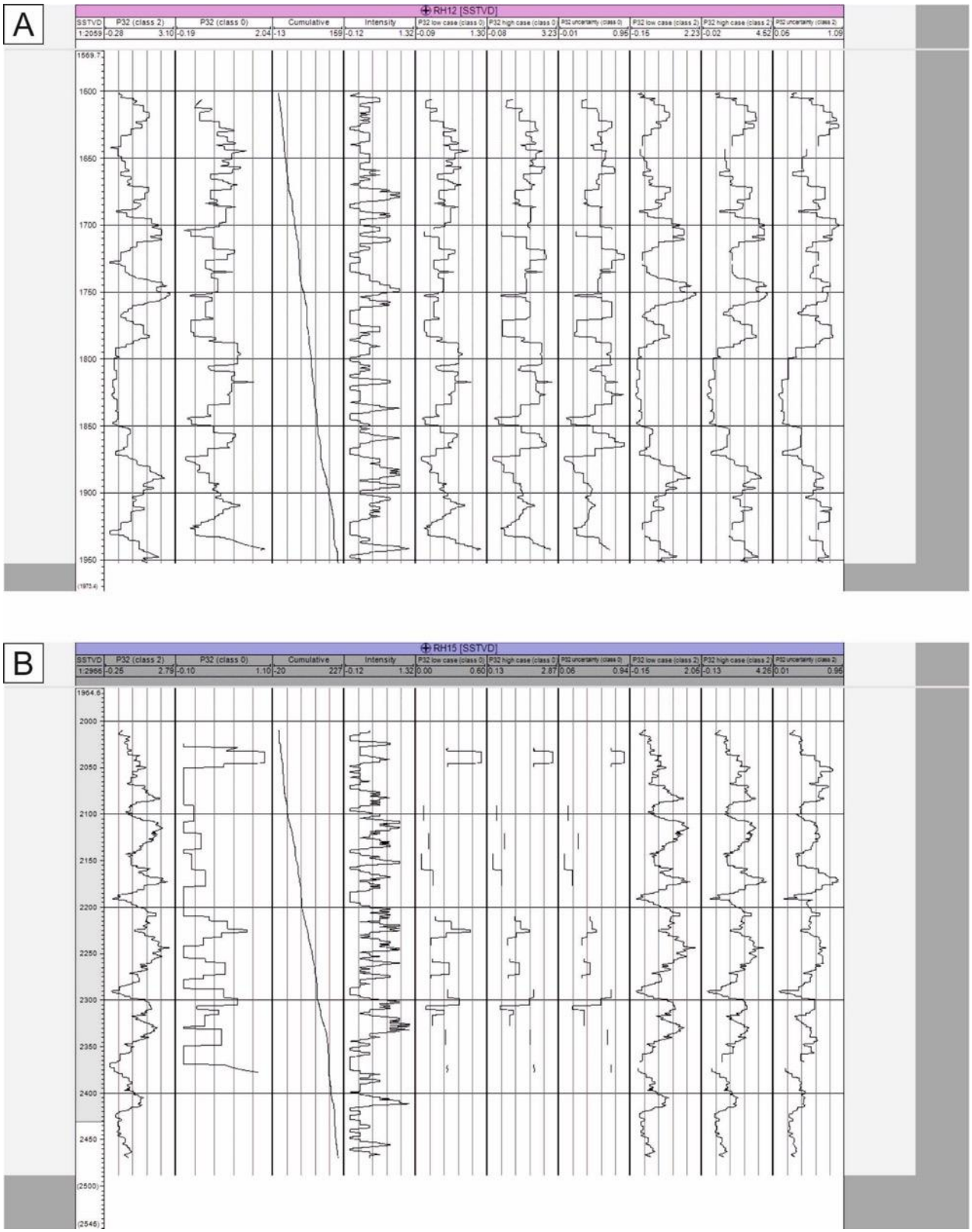

Figure 59: Derived fracture intensity, cumulative frequency, density, and uncertainty for the two fracture sets identified from the downhole image logs. A. RH 12. B. RH 15. British Geological Survey © UKRI.

The fracture density (P32; m^2/m^3) was calculated from the intensity providing a mean density per 5 m interval. Low (P10) and high (P90) confidence intervals were also calculated, providing three models that account for the recorded fracture intensity (Appendix 4). There is no direct evidence to account for the changes in fracture density and therefore it is assumed that density is random within the granite, at least at the site scale. Histograms of the computed fracture density reflect a truncated normal distribution. Fracture density within the model was randomly drawn from the corresponding distribution, with a given mean, standard deviation and upper and lower limits.

In addition to the fracture set definition, orientation and density, it is necessary to estimate the fracture length, shape and aperture for Discrete Fracture Network (DFN) modelling. Although the fracture azimuth and dip are relatively well constrained within the granite there is limited information on the fracture length or fracture aperture distribution, especially at reservoir depths.

Fracture lengths were measured in four quarries and are reported in Camborne School of Mines (1986). If all fractures are considered, both the horizontal and vertical length fit a lognormal distribution (Figure 60) with a maximum recorded length of 300 m.

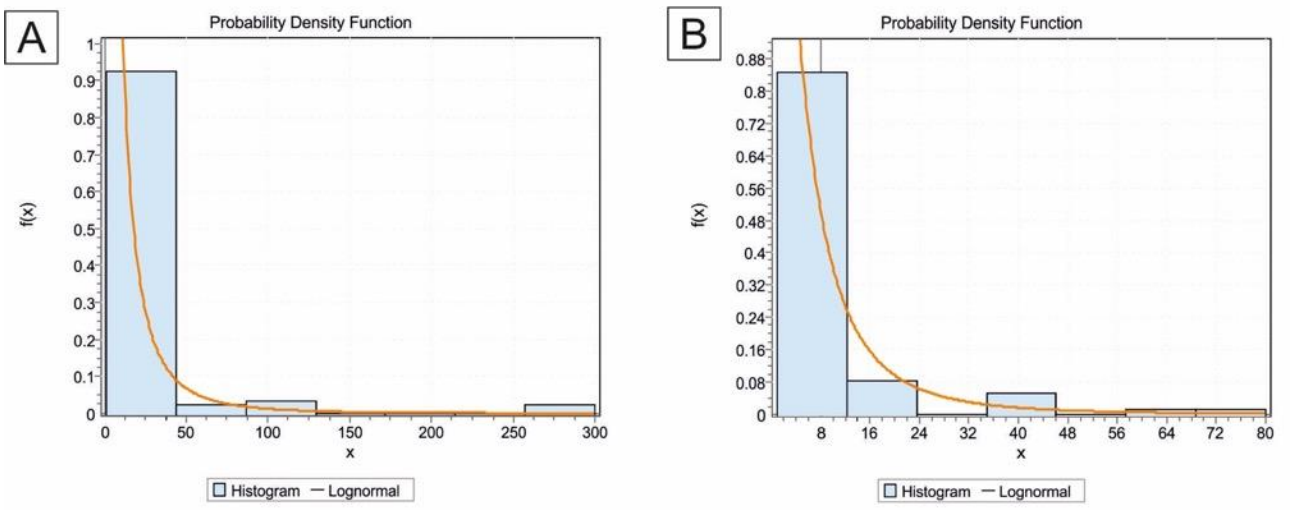

Figure 60: Lognormal horizontal fracture length distributions for all fractures. A. Left. B. Right. British Geological Survey © UKRI.

If each fracture set is considered independently, assuming that length still follows a lognormal distribution, we can calculate the mean and standard deviation for each fracture set (Figure 61). The aspect ratio for each fracture set was calculated by dividing the mean horizontal length by the mean vertical length. Fracture aperture is very poorly constrained and data on fracture aperture only exists from the surface or relatively near-surface mines, which will over estimate fracture aperture. However, results from numerical modelling and hydraulic testing at the HDR project site provide estimates for fracture aperture at reservoir depths, which ranges between 5–50 µm with a mean of 10 µm (Pine and Nicol, 1993). Additionally, it is known that

permeability prior to stimulation was 10^{-6} µm^2 but post stimulation this increased to $0.5*10^{-3}$ µm^2. Given a flow fracture spacing of 10 m (based on data from flow logging data), the hydraulic aperture is 40 µm (Evans et al., 1992).

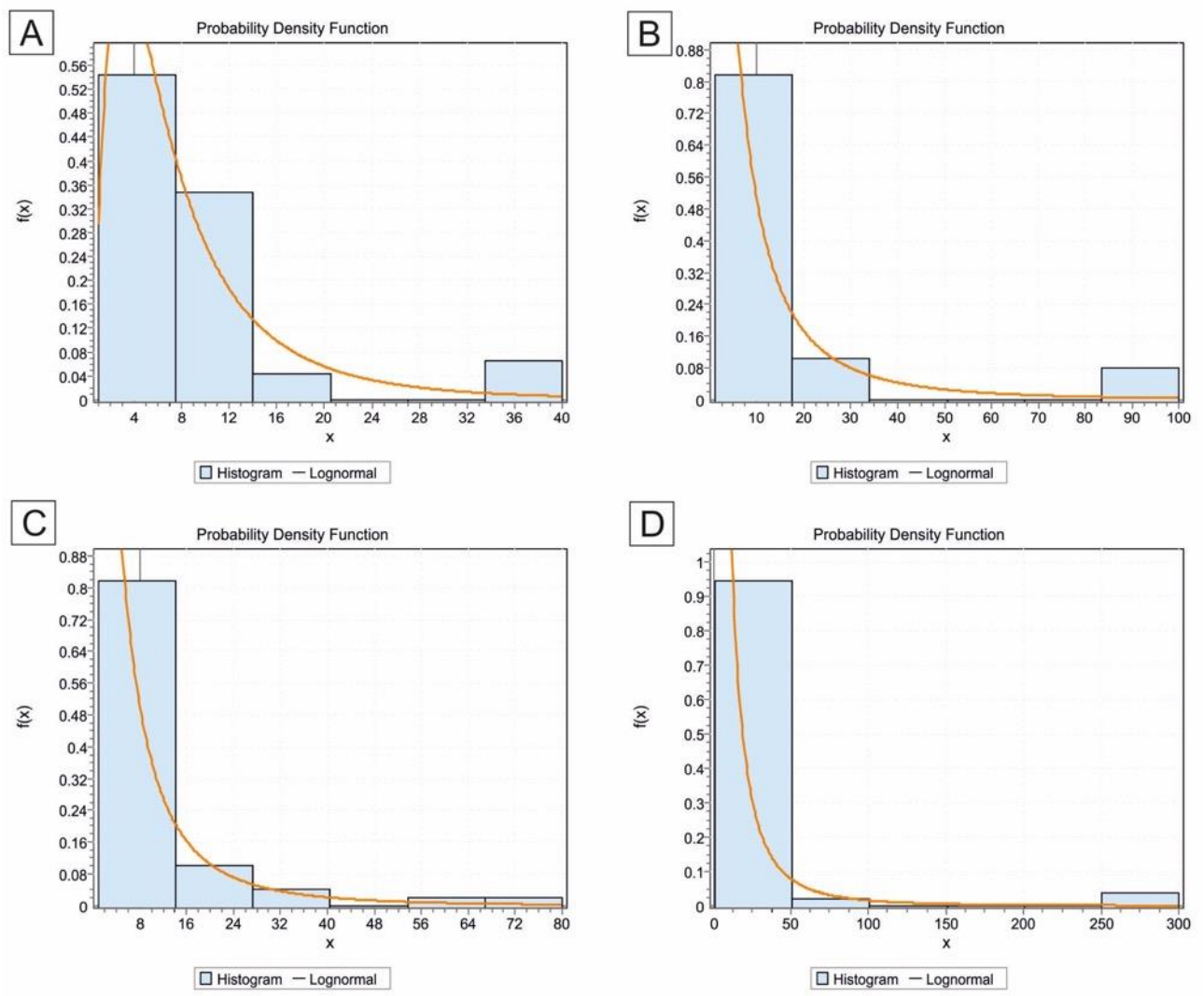

Figure 61: Calculated lognormal distributions for two fracture sets. A. Fracture set 1 for vertical lengths. B. Fracture set 1 for horizontal lengths. C. Fracture set 2 for vertical lengths. D. Fracture set 2 for horizontal lengths. British Geological Survey © UKRI.

It is also known that the flow is predominantly along the NNW-SSE-trending fractures (Evans et al., 1992). Given that these are approximately parallel to the maximum compressive direction, they will have a higher dilation tendency (Ferrill and Morris, 2003; Morris et al., 1996) (Figure 62) and therefore a larger aperture. Low flow rate hydraulic tests at low injection pressures indicated permeabilities between 1–10 µD at up to 0.7 MPa fluid overpressure. Permeability subsequently increased to 60 µD at a pressure of 3 MPa, prior to the onset of significant discontinuous behaviour at pressures over 5 MPa (Parker, 1999). The pumping test data show that the aperture is strongly controlled by the in-situ stress conditions. This supports the dilation tendency results, with fractures aligned parallel to the direction of maximum compression becoming

increasingly open as injection pressure increases. It is assumed that fractures perpendicular to the maximum compressive stress direction will have an aperture in the order of a tenth of the fractures parallel to the maximum compressive stress direction (Figure 63).

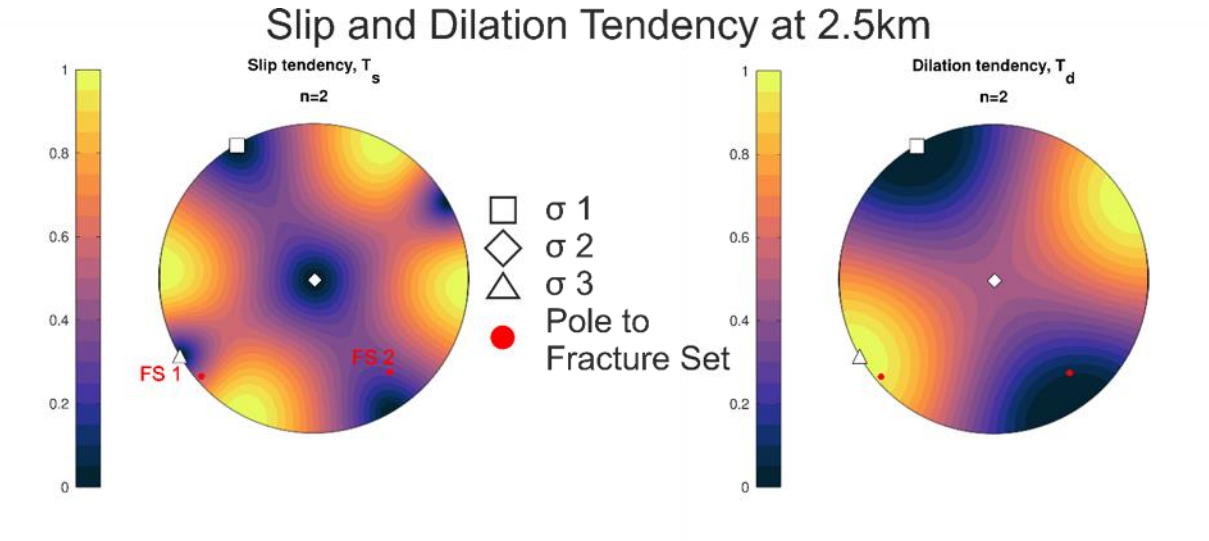

Figure 62: Slip tendency and dilation tendency analysis and the two fracture sets (FS1 and FS2) based on insitu stress equivalent to 2 km at the Hot Dry Rock project site and the revised direction of maximum compression as measured in RH 15 of 150 degrees ± 10 degrees. Note that fracture set 1 is optimally aligned for dilation. Neither fracture set are preferentially aligned for slip reactivation. British Geological Survey © UKRI.

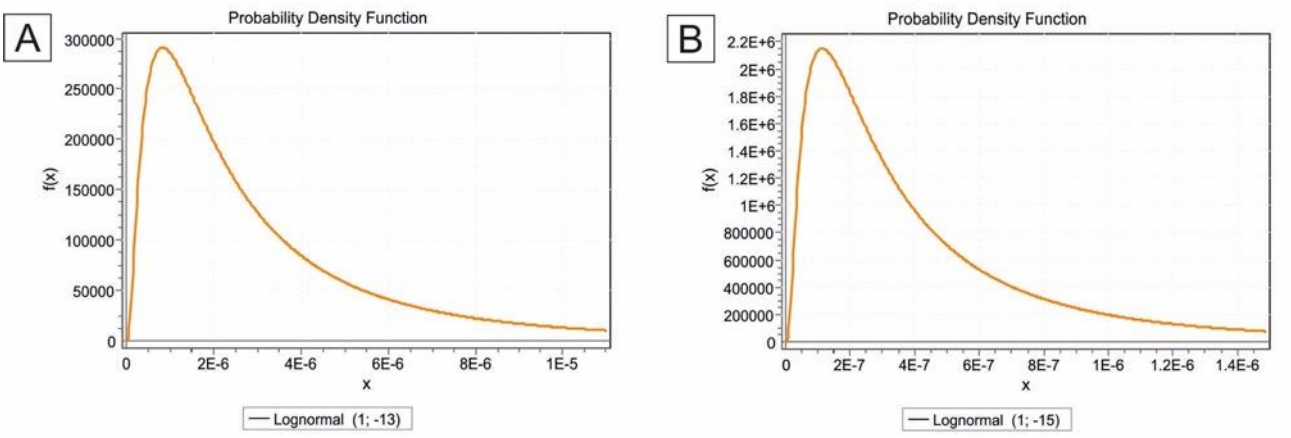

Figure 63: Assumed aperture distribution. A. Fracture set 1 (parallel to maximum compressive direction). B. Fracture set 2. British Geological Survey © UKRI.

7.2 Hot dry rock project site model

The HDR project site model is a site-scale model that includes fracture data from two of the three deep boreholes drilled as part of the HDR project; RH 12 and RH 15. The model covers a volume of 2.6 km^3, centred on the wells and has a depth range of -1000 to -3000 mbsl (

Figure 64). The region was gridded with a cell size of 13x10x10m and properties were transferred from the regional model. The HDR project site model also includes site-specific parameters related to the hydrological properties of the system. As previously discussed, fracture flow is the predominant flow mechanism within the granite. Therefore the statistics and assumptions on the fracture network described above were used to generate three discreet fracture network models for the HDR reservoir. These were up scaled to include porosity and permeability to understand the likely flow pathways within the reservoir. In order to facilitate future geomechanical modelling the model was orientated parallel to the regional direction of maximum horizontal compressive stress.

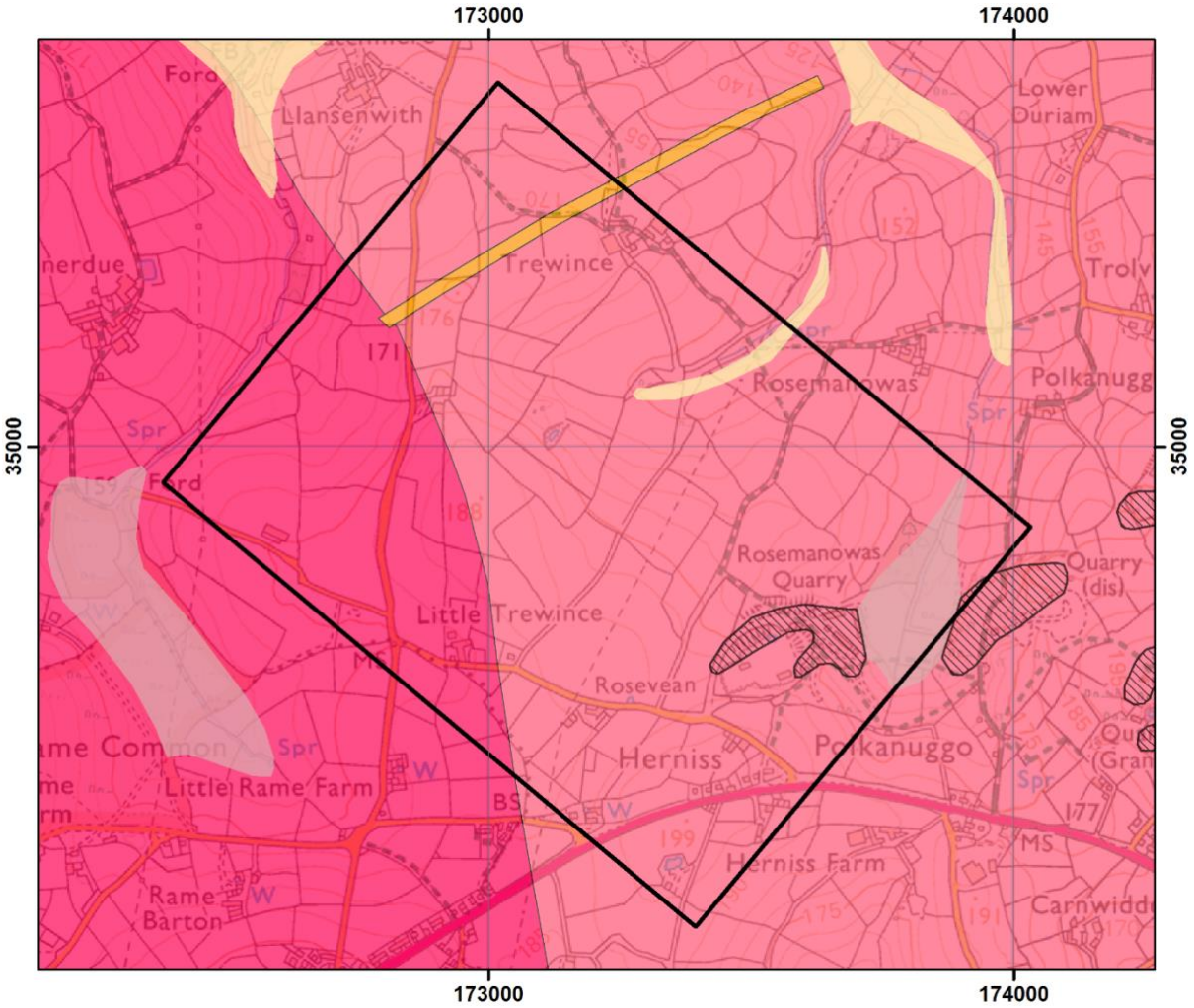

Figure 64: 1:50 000 scale geological map of the HDR project site showing the lack of faults and uniform geology. The area covered by the HDR project site model is shown by the black outline. Contains Ordnance Data © Crown Copyright and database rights [2019]. Ordnance Survey Licence no. 100021290. Contains British Geological Survey materials © NERC [2019].

The modelling parameters for the stochastic simulation of the DFN are presented in Appendix 5 and are based on the above discussion. Evans et al. (1992) state that only 10 per cent of the imaged fractures had appreciable flow, and a spacing of approximately 10–15 m. Given the focus on the dominant flow pathways, fracture permeability and porosity was calculated for fractures with a length greater than 150 m, but less than 300 m,

resulting in a spacing of about 10–15m. The resulting permeability is within good agreement with the 1–10uD reported by Parker (1999).

Once the fracture network was generated, the resulting DFNs were upscaled into the voxel volume (Appendix 6). A number of methods are available for upscaling including the Oda method (Oda, 1985), the flow-based method (Lough et al., 1997), and a corrected Oda method (Ghahfarokhi, 2017). The Oda method is considered a good first pass for upscaling DFN for porosity and permeability, as it is quick to calculate but it tends to overestimate the permeability and porosity as it does not take into account the connectivity of the fracture network. The flow-based method is more accurate, but very slow especially when the model contains a large number of voxels. To reduce the over estimation the corrected Oda method can be applied, which up scales the fracture network using the faster Oda method, but corrects the results based on a subsample of cells to which the flow-based method is applied. This has the advantage of being relatively quick and reducing the over estimation issue associated with the classical Oda method.

7.3 United Downs Deep Geothermal Power project site model

The UDDGP project site model considers an area located to the NW of the Carnmenellis granite. However, the target reservoir is still considered to be within the Carnmenellis granite. The site is located near historical mine workings and the area is cut by a number of NNW-SSE-trending faults and ENE-WSW-trending mineralised zones. The site-scale model covers a volume of 12 km^3, including the drilling pad and the SW extent of the drilling with a depth range of -1500 to -5500 mbsl (Figure 65). The region was voxelated with a voxel size of 15x20x10 m and properties were transferred from the regional model.

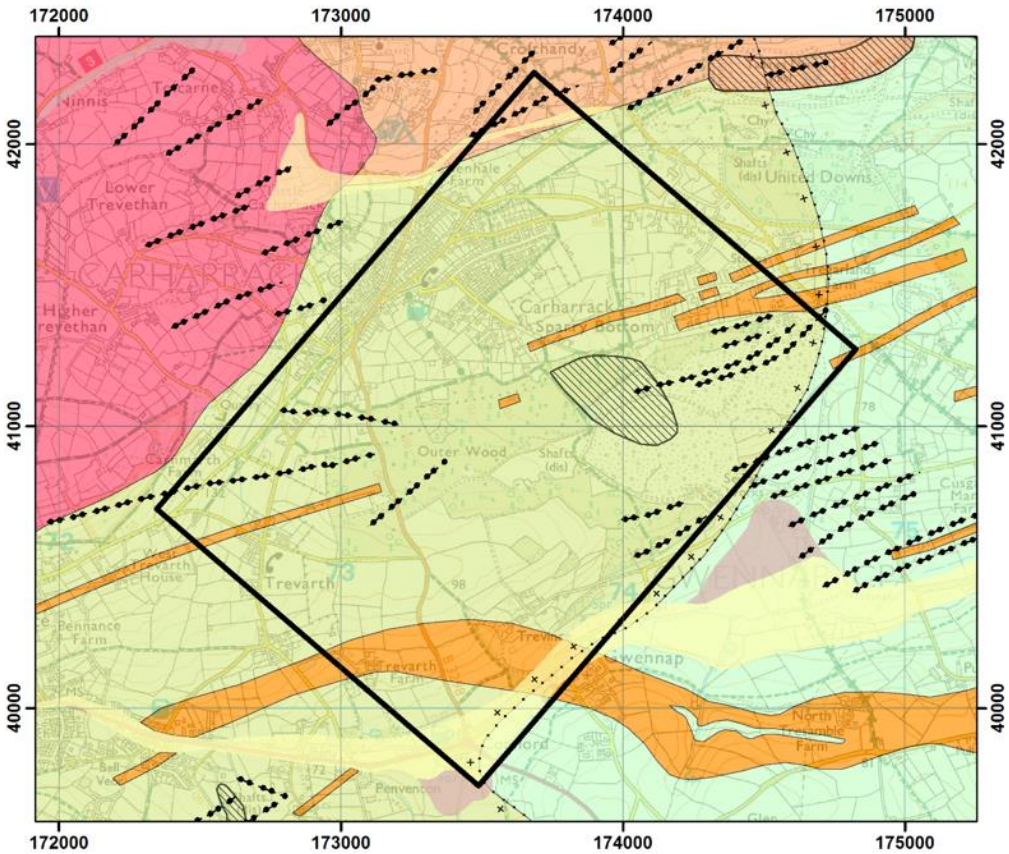

Figure 65: BGS 1:50 000 scale geological map of the UDDGP project site model area (thick black line) showing the general structure with NE-SW-trending mineral veins (dotted lines) and felsic intrusions (orange polygons) in the killas (green and blue). Note that no faults are shown on this map. Granite is coloured red and orange. Contains Ordnance Data © Crown Copyright and database rights [2019]. Ordnance Survey Licence no. 100021290. Contains British Geological Survey materials © NERC [2019].

There is not currently any published data on the fracture network in the UDDGP project target reservoir. However, given the consistency of the mapped fractures at surface across the Carnmenellis granite it was assumed that the fracture parameters will be similar to those used in the HDR project site model that is described above (Appendix 7). The workflow for the UDDGP project site model replicates that of the HDR project site model except for the addition of a fault zone, which is discussed in more detail below. In order to facilitate future geomechanical modelling the model was orientated so that it was parallel to the regional direction of maximum horizontal compressive stress. The UDDGP project is targeting a fault zone within the granite that may be more densely fractured, resulting in higher permeability and flow rates that will be sufficient development of a geothermal system, without the need for hydraulic stimulation of the reservoir.

The UDDGP project drilling target is an inferred 500 m wide fault zone located to the south-west of the site, and termed the Porthtowan Fault Zone (PTFZ). The faults have been mapped at surface as a series of smaller faults forming a board fault zone. The fault zone trends NNW-SSE and is aligned with the general trend of the cross-courses and strike-slip faults, such as the Sticklepath-Lustleigh fault zone near Dartmoor. These faults are considered to have been active during the Cenozoic and represent the most recent recorded fault movement within the area. However, there are inconsistencies between the mapped extent of the faults shown on the published 1:10 000 scale geological map (Figure 66) and a map published by Geothermal Engineering Ltd (Figure 67). The latter has been used in the modelling. The PTFZ is modelled as a volume of rock between two bounding fault surfaces located to the east and west, respectively. There is limited information on the vertical extent of the faults and the PTFZ has been modelled by the vertical projection of surface fault traces through the model. There is a large uncertainty regarding the presence, location and nature of the fault zone at reservoir depths that only drilling can reduce.

As the target reservoir for the UDDGP project is the Carnmenellis granite, and surface mapping has shown consistent fracture patterns across the granite, it is assumed that the two fracture sets used in the HDR project site model will persist across the UDDGP project site. This includes consistency in fracture density, length, aperture distributions and aspect ratio. However, the target fault zone adds additional complexity to this area.

Considering the uncertainty associated with the location of the faults within the PTFZ it was considered more appropriate to consider the fault zone and associated damage zone as a fractured volume of rock and therefore DFN modelling methods can be applied to attempt to represent the fault zone within the model. In addition to the two primary fracture sets identified in the HDR project site model, a third fracture set that is parallel to the fault strike was introduced. Studies of faults have shown that they tend to characterised by a fault core, surrounded by a region of damaged rock before transitioning into host rock. The density of fractures will be greatest close to the fault plane, reducing away from the fault. It was assumed that the fracture density within the fault zone is equivalent to the maximum density observed within well RH12 and RH15, which was 4.14 m^2/m^3. It was also assumed that the fault-related fracture density will reduce with distance from the fault. Accordingly, the inverse of the cube root of the distance from the fault scaled by 4.14 was used so that the maximum fracture density is at the fault plane and reduces smoothly away from the fault zone (Figure 68).

This is a conceptual model of the potential fracture density of the fault zone, which needs to be validated with additional data.

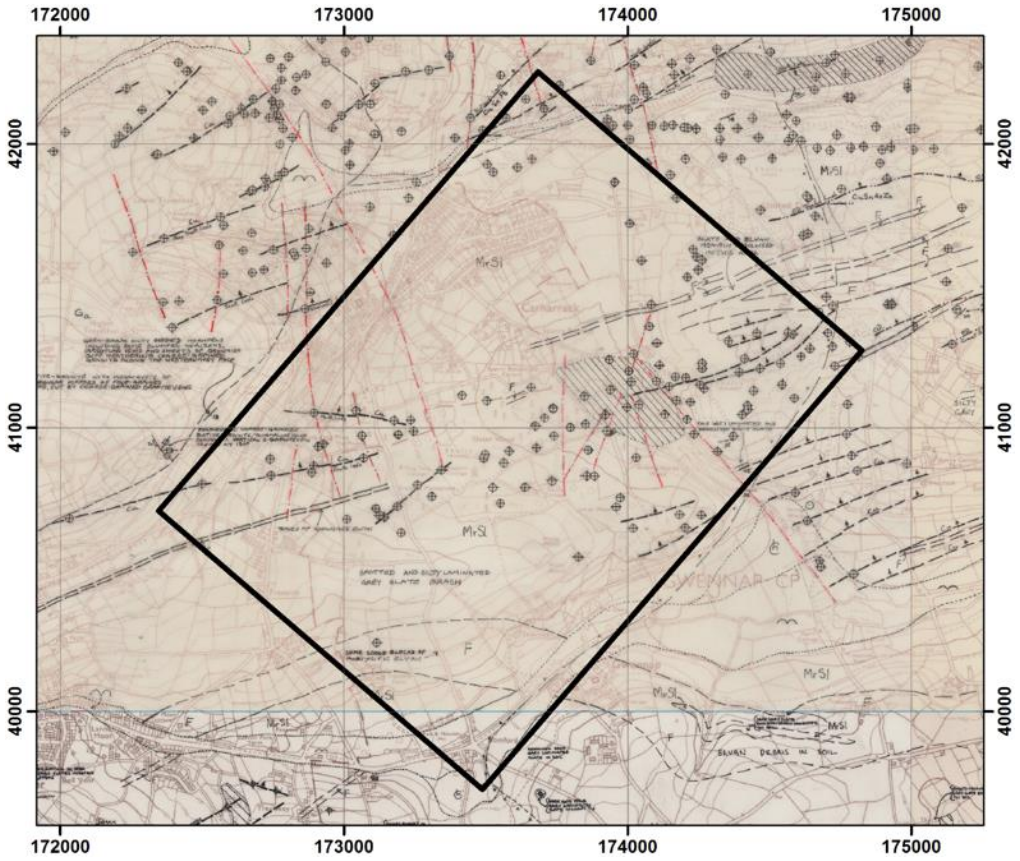

Figure 66: BGS published 1:10 000 scale mapped faults and veins across the area covered by the UDDGP project site model. Contains Ordnance Data © Crown Copyright and database rights [2019]. Ordnance Survey Licence no. 100021290. Contains British Geological Survey materials © NERC [2019].

Once the fracture network was generated, the resulting DFNs were up scaled into the voxel volume (Appendix 8) using the same approach described above for the HDR site project model. The up scaled permeabilities show a clear increase within the fault zone relative to the HDR site project model, despite the background permeability being similar. However, the model is likely to overestimate the permeability in the deeper reservoir as the fracture apertures used in the modelling are based on the measured flow within the shallower HDR wells. As previously discussed the fracture permeability is strongly controlled by the insitu stress, which increases with depth and may result in smaller effective apertures and therefore reduced permeability.

7.4 Uncertainties and limitations

There are a number of uncertainties and limitations to the current models. These include the range of assumptions used during the modelling workflow and the generalisation of the data. In terms of the regional model the greatest uncertainty remains the shape and extent of the granite. Although a revised top granite

surface has been developed, this is still largely based on the original gravity inversion with only minor corrections based on the additional data. At the borehole-scale there is likely to be a significant difference between the modelled granite surface and the depth at which granite is intersected. However, the top granite surface was only ever intended to be used for regional studies and at this scale it is considered to be adequate.

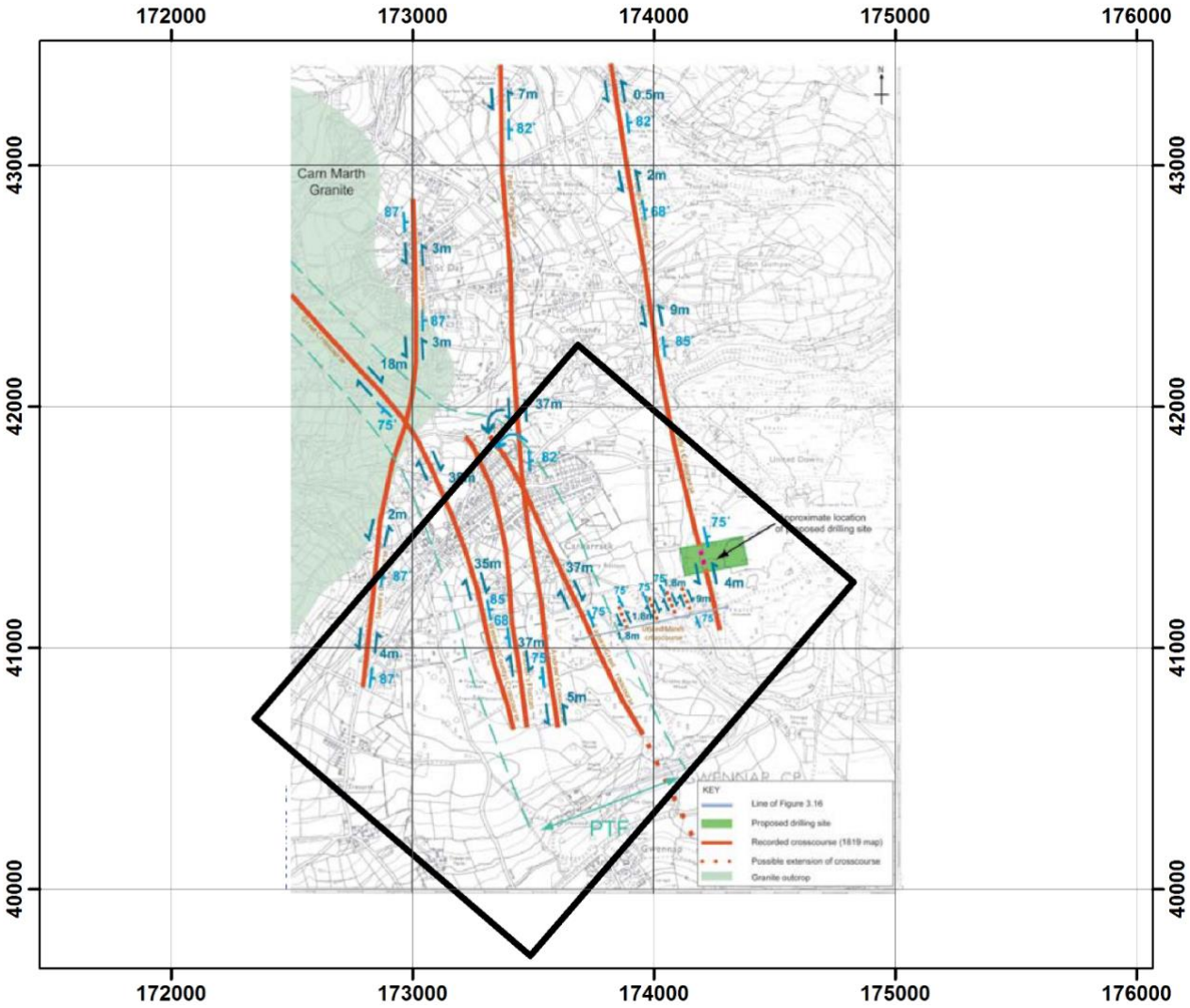

Figure 67: Map of the area of the UDDGP project site showing a number of NNE-SSW faults (orange) and the interpreted position of the Porthtowan Fault Zone (PTZ; Blue). Reproduced with permission of Geothermal Engineering Ltd 2018.

There are still large uncertainties regarding the depth of the base of the granite and the nature of the contact between the granites. A conservative depth to the base of the granite, of 12–15 km, was used in the modelling, which is based on one of the interpreted seismic reflectors. Additional research is required to better constrain the base of the granite, as future geothermal drilling in Cornwall may target even deeper, potentially higher temperature zones in the granite. If the base of the granite is shallower than predicted there is a risk that these deeper wells could extend through the base of the granite. In the current modelling the Cornubian Batholith is modelled as one contiguous granite body. However, it is known from surface mapping that the granite

consists of a number of distinct plutons. It is unclear what the shape of the individual granites is or how they potentially connect at depth. Only detailed exploration is likely resolve this.

Based on the modelled properties it is apparent that there is limited information on heat flow and heat production with depth, both of which have a significant impact on the assessment of the potential heat resource that could be extracted. The current drilling at the UDDGP project site and the associated data produced, including radiometric downhole surveys should significantly improve understanding of heat production at depths greater than 2.6 km in the Cornubian Batholith. The location of the UDDGP project boreholes on the flanks of the granite will also provide information on the thermal blanketing effect of the killas. The new data should also improve understanding of the consistency of the geothermal gradient across a larger area, and whether it is valid to extrapolate these values across the Cornubian granite, as has been done in the CHPM2030 project modelling.

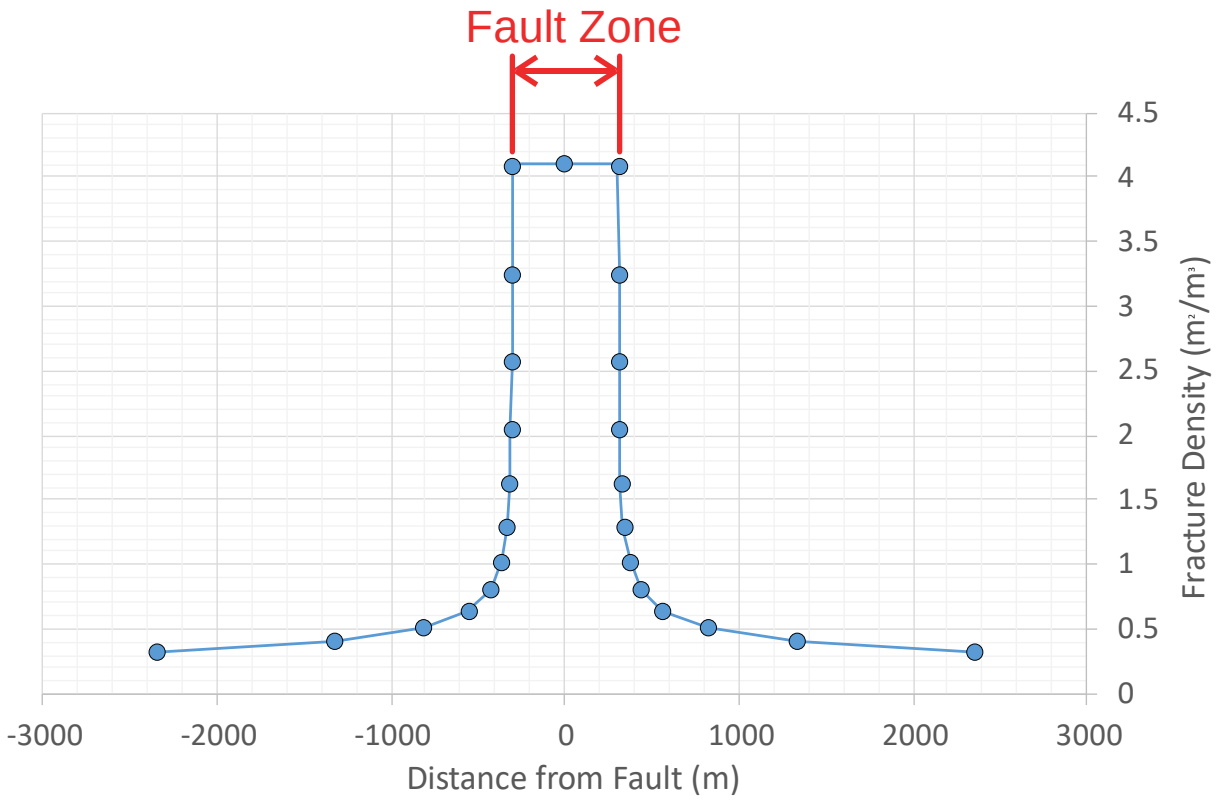

Figure 68: Idealised model of the change in fracture density with distance from the Porthtowan Fault Zone. British Geological Survey © UKRI.

At a regional scale the large faults in Cornwall are relatively well understood, however, their frequency and effect on the granite at depth is unknown. In the current modelling the faults are projected through the granite and over the full depth of the model, however, this may not be valid. It is possible that the faults may interact differently with the granite at depth, contrasting with how they behave in the near surface environment or in the metasedimentary country rocks.

For the site-scale models the greatest uncertainty relates to the position and properties of structures at depth. The nature of the fault-related fracturing has not been measured, and the data used in the UDDGP project site model represents an idealised system. Additional investigation is required to improve understanding of fault-related fracture systems and spatial relationships with the fault zone. This is considered essential for the concept on which the UDDGP project is based on (i.e. exploiting the natural permeability of a fault zone) to become widely accepted by the geothermal community.

Although the fracture system within the Carnmenellis granite is reasonably well understood the regional fracture system across the south-west is poorly defined. The least well understood fracture parameters include density, length and aperture. Further studies of fracture systems in granites across south-west England are essential for informing regional geothermal exploration. Although the site-scale models provide a qualitative assessment of the reservoirs, detailed numerical simulations are required to calibrate the models in order to understand how the reservoirs will evolve during production and to optimise development of the resource. This information could be used to better predict the thermal drawdown and the life expectancy of the reservoir. Flow and pumping data exists from the HDR project. This could be used to validate the models produced, providing confidence in the methodology and assumption used. As additional data becomes available this will need to be integrated into the UDDGP project site model, and calibration and validation can be undertaken.

8 Information for CHPM technology development

The UK HDR project, based at Rosemanowes Quarry, near Penryn in west Cornwall, aimed to demonstrate the feasibility of establishing a 'full-scale prototype' HDR power station in Cornwall. The project comprised three phases: i) focussed on experiments at shallow depth (300 m) that aimed to improve the permeability of the reservoir; ii) deeper (2500 m) studies focussed on the development of a HDR subsurface heat exchanger; and iii) development of a 'commercial depth' (~6 km deep) HDR prototype system. Phase 3A is particularly relevant to CHPM2030 as it examined the feasibility of creating an underground HDR heat exchanger, techniques for enhancing hydraulic performance and addressing the challenge of 'short circuits' in these systems, and modelling system performance, resource size and economic criteria (MacDonald et al., 1992).

8.1 Underground heat exchanger and metal enrichment

8.1.1 Expected reservoir characteristics

The philosophy for developing HDR systems in Cornwall has evolved substantially since the HDR research project, particularly the type of geological environment being targeted for the development of these systems and the requirement for artificial stimulation of the rock mass. The Rosemanowes test site is located in the eastern part of the Carnmenellis granite, away from any identified geological structures, in what was considered to be 'virgin' rock. Initial experimental work during the HDR project (Phase 1) focussed on enhancing the permeability of the rock mass surrounding the boreholes. Tests on boreholes at a depth of 300 m, employing a combination of explosives, hydraulic fracturing and water circulation, demonstrated that the impedance of the system could be reduced by a factor of 50 relative to the natural rock mass. The lowest flow impedance achieved at Rosemanowes was about 0.1 MPa per 1/s. However, it was noted at the time that the shallow level of the testing was unrepresentative of a deeper system (>400 m depth), in which the minimum principal stress would typically be horizontal, causing fractures to preferentially develop in the vertical plane.

Phase 2 in the HDR project, extending over an eight year period, focussed on development of a 'commercial-scale' heat exchanger. At the time, it was considered necessary to drill to a depth of 6 km to establish a 'commercial' system. However, to reduce drilling costs two boreholes to a depth of about 2 km were drilled. It was hoped that the results of this study would have relevance to the geological conditions at 6 km depth, but the limitations of these relatively shallow holes were acknowledged. During this phase defined as '2A', two holes (RH11 and RH12), deviated from the vertical by 30° were drilled to 2 km depth, and maintained at a separation of 300 m apart (Figure 69). Hydraulic fracturing was conducted in the lower borehole, with the aim of opening near-vertical joints that potentially rose upwards, joining it to the upper borehole.

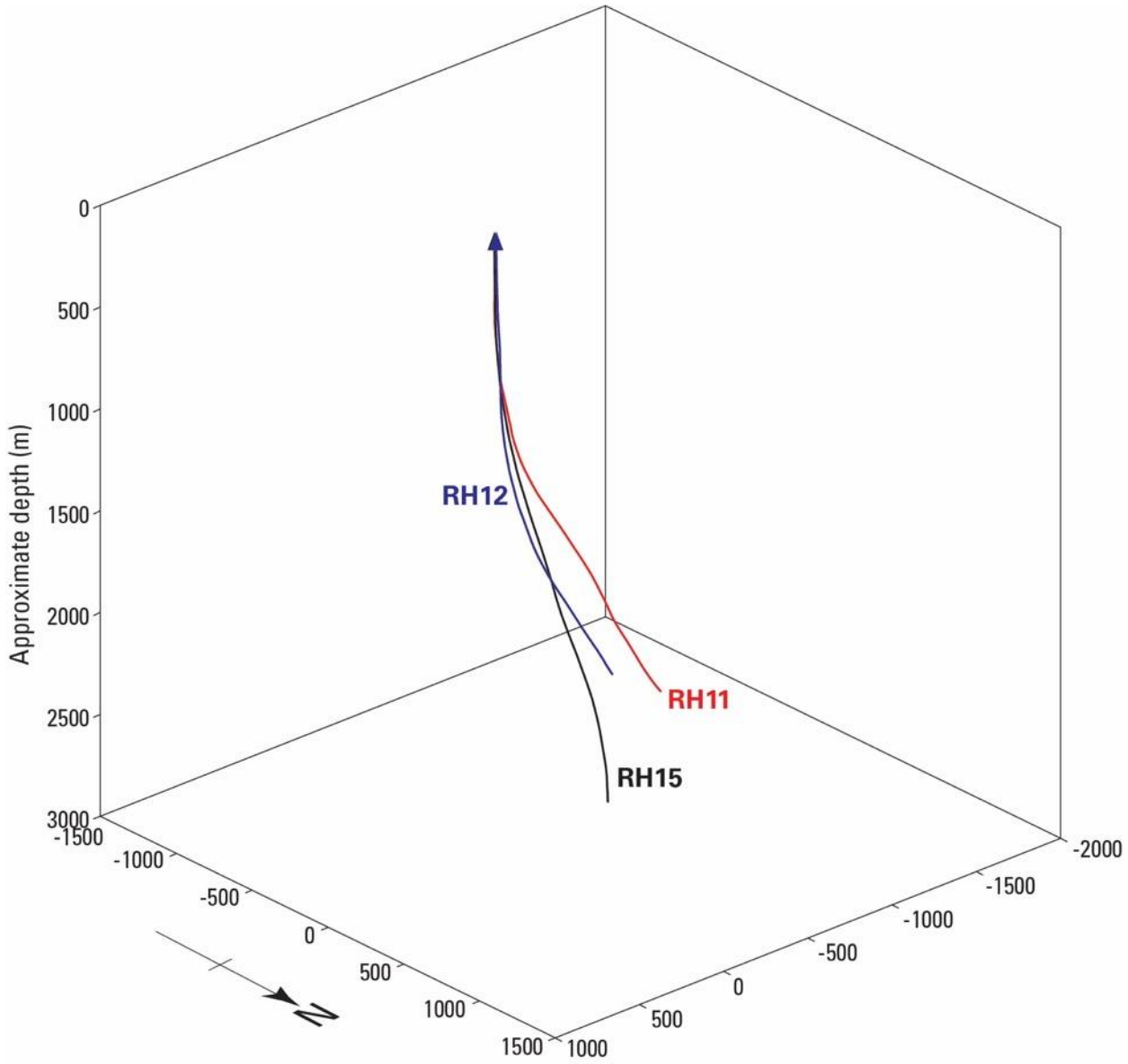

Figure 69: Configuration of the HDR project boreholes. Based on information supplied by Avalon Geoscience Ltd. British Geological Survey © UKRI.

However, when water circulation commenced fluids losses were excessive and the pumping pressures required to maintain circulation were excessive. It is reported that it was not possible 'to get within a factor of ten of the target production flow rate of 75 l/s. The poor connectivity between the boreholes was confirmed from pumping and tracer tests. Subsequent stress measurements indicated that the direction of maximum principal stress in the granite was closely aligned with the borehole deviation, the least desirable combination for intersecting joints that could easily be opened by hydraulic stimulation. As a result the project moved into Phase 2B, in which another borehole (RH15) was drilled to 2600 m depth. In an attempt to maximise the number of joint intersections, its trajectory crossed the microsesimic cloud (measured beneath each of the shallower boreholes during the stimulation and circulation tests, Figure 48), and was perpendicular to the vertical plane of the first two boreholes. A medium-viscosity gel was used to try and open up the volume of rock between borehole RH15 and the deeper of the two earlier holes (RH12). Using this new configuration

injection and production flow rates in the system were measured over a continuous four year period (Figure 70).

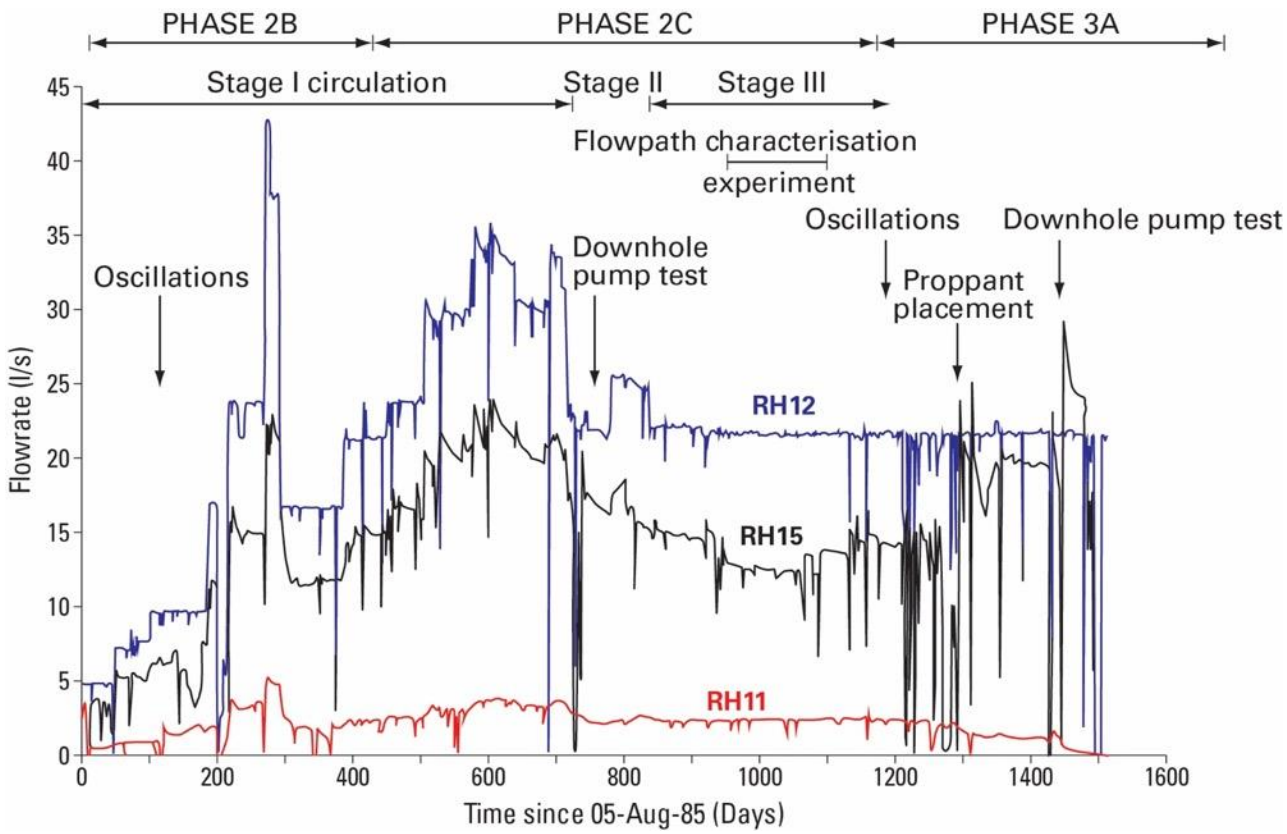

Figure 70: Injection and production flow rate measured in the Rosemanowes system, during the HDR project. Modified from Parker (1990), Contains public sector information licensed under the Open Government Licence v3.0.

The data showed that during Phase 2B there was a gradual increase in the injection flow rate (Figure 70). As the project progressed into Phase 2C and the injection pressure and flow rate increased, impedance in the system declined. It also demonstrated that at injection pressures exceeding 10 MPa above hydrostatic pressure water losses from the system were too great. It was concluded that the 'optimum hydraulic performance' that could be achieved at the Rosemanowes site was an injection flow rate of 24l/s, with impedance of 0.6 MPa per l/s and with a water loss of 21 per cent. This level of hydraulic performance was considerably lower than that considered desirable for a 'commercial' prototype. A further concern was that although the RH12/RH15 system had lower impedance and water losses than the previous configuration (circulation between RH11 and RH12) there was a decline in thermal performance. Over a three year period the temperature at the top of the of production borehole declined from 80°C to 55°C. Flow path modelling of the system using tracer and subsequent thermal modelling showed that a 'short circuit' existed between the boreholes, significantly reducing its effectiveness as a heat exchanger. It was concluded that the granite surrounding the area of the short circuit had cooled more quickly than the rest of the reservoir causing cooler water to enter the production borehole. Towards the end of Phase 2 a review of the programme examined the status of HDR technology in south-west England, and identified the following specific issues: i) the size of the subsurface heat exchanged available was considerably smaller than required for a 'commercial' system; ii) short circuiting reduced the thermal efficiency of the heat exchanger and water losses were too great; iii) the

experimental work had not managed to demonstrate the concept of being able to engineer a underground heat exchanger; and iv) a 'commercial'-scale system may require the development of a number of underground 'modules' operated in parallel. Despite these problems the experimental work continued into a third phase (3A). An experiment in Phase 3A involved injecting sand, as a proppant material, into the joints surrounding the production well. The sand was introduced into the system using a high viscosity (700 cP) gel during a secondary stimulation stage. This stimulation reduced water loss and impedance of the system, but exacerbated the short circuiting and caused a further decline in the water temperature from the production borehole (Figure 71). Another experiment attempted to address the short circuiting by shutting off the problematic section of the production borehole using a temporary packer assembly. Subsequent flow testing showed that the short circuit had been sealed off, but a very low flow rate resulted, which was not be corrected by further stimulation. It was concluded that this stimulation failed to establish a connection with the previously stimulated zone that ran parallel to it. Phase 3A of the project also resulted in a conceptual design for a 6 km deep, 'commercial' HDR prototype power station and cost modelling for a HDR power station are described in Section 9.2 (MacDonald et al., 1992).

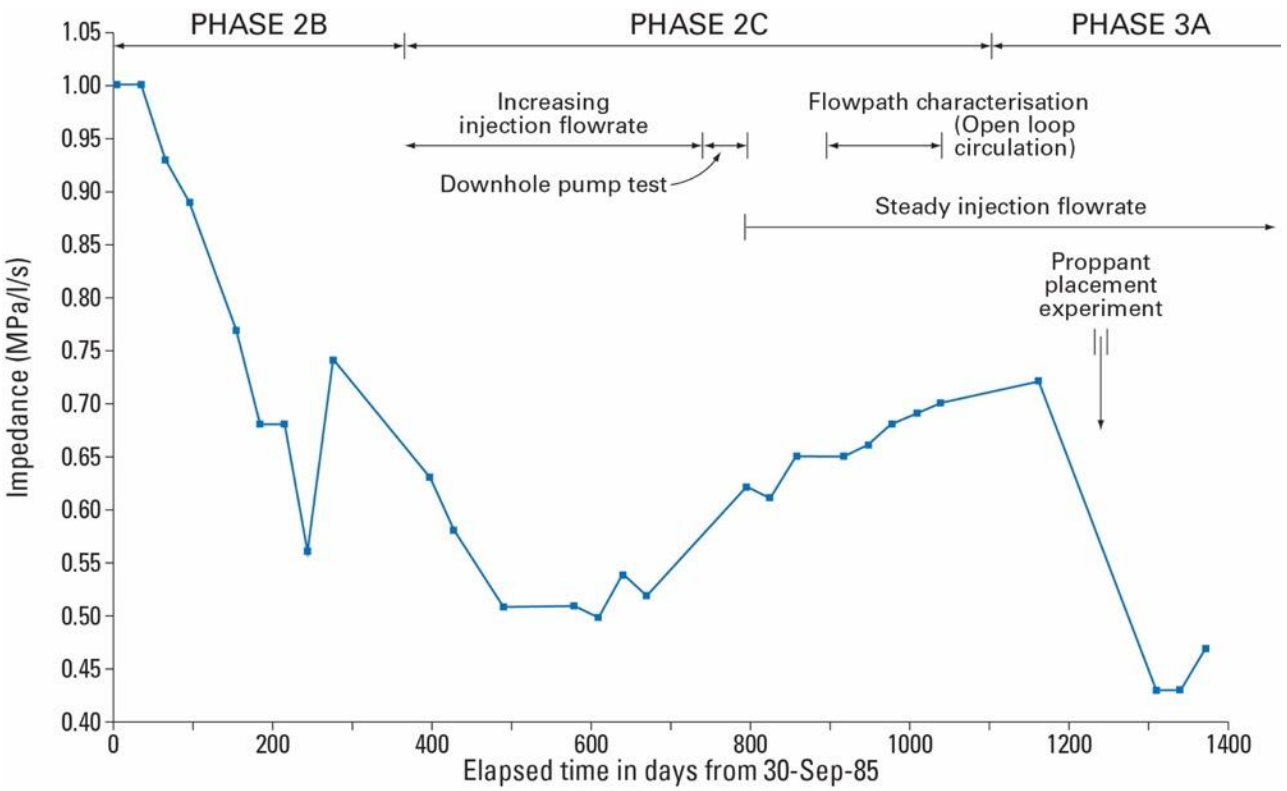

Figure 71: Impedance in the RH12/RH15 system. Modified from Parker (1990), Contains public sector information licensed under the Open Government Licence v3.0.

Whilst building on the experience and expertise developed during the HDR project the current (drilling commenced in November 2018) United Downs Deep Geothermal Power (UDDGP) project, operated by Geothermal Engineering Limited (GEL) plans to test a new concept for EGS development in Cornwall. From the reconnaissance stage it was assumed that the rock matrix being targeted for an EGS in Cornwall would have

low to very low porosity and permeability. In fact there is little evidence for the granite in south-west England having sufficient transmissivity for geothermal circulation without reservoir stimulation. However, it is acknowledged that the existing lack of evidence largely results from limited deep subsurface investigation, which could identify fault, fracture and weathered zones creating natural permeability that is exploitable as a geothermal reservoir (Atkins, 2013). Accordingly, development of a geothermal reservoir in the Cornubian Batholith would be dependent on the presence of fracture-controlled permeability, and this would have to be of an adequate size to host a commercial-scale heat exchanger, and extend deep enough to reach sufficient temperatures (Ledingham et al., 2019).

The UDDGP, located to the east of the Carnmarth granite (Figure 7), is actively targeting a structurally complex zone, with the objective of exploiting the natural permeability that exists in the fracture system to circulate water between two boreholes. The target geological structure is termed the 'Porthtowan Fault Zone' (PTFZ), which is located about 800 m to the west of the United Downs drilling site (Geothermal Engineering Ltd, 2018e). GEL describe the PTFZ as 'a geological structure which extends across Cornwall from Porthtowan on the north coast to Falmouth on the south coast. It is no longer active but it should contain a concentration of natural fractures…' (Geothermal Engineering Ltd, 2018b). It is a >15 km long NNW-SSE orientated strike-slip fault. It unlikely to represent a discreet structure, but rather a 200–500 m wide feature, comprised of several anastomosing faults. It is assumed to be near-vertical and extend to EGS depths, based upon its linearity. It is reportedly mapped along the NE side of the Carnmenellis granite and has been identified in some of the mines in the area. Cross-course structure identified in the mines, which have the same orientation as the PTFZ frequently result in bad ground, as a result of fracturing and are zones of fluid flow. It is hoped that the PTFZ shares these characteristics (Ledingham et al., 2019). Estimates of the permeability and transmissivity of the PTFZ have been made based on a number of assumptions. Ledingham et al. (2019) indicate that if the PTFZ is assumed to have true width of 200 m and two fractures occur every metre that have an aperture of 90 µm, the entire zone would have a transmissivity of 123 mD, resulting in a transmissivity of about 25 Dm. It is acknowledged that this transmissivity value is relatively low for a productive geothermal reservoir (Ledingham et al., 2019). For comparison, drilling for geothermal exploration in the Weardale granite of northern England, also targeting a major, linear, sub-vertical structure encountered a highly permeable zone at a depth of about 400 m and a transmissivity of 4000 Dm (= 3×10^{-9} m^2 m) was obtained from a 21 m interval in the borehole. This is more than 20 times greater than maximum value reported elsewhere from granites and other crystalline rocks. However, in terms of the entire granite sequence drilled (almost 600 m) more than 99 per cent of the total transmissivity is accounted for by the fracture zone in the 21 m interval (Younger and Manning, 2010).

GEL conducted heat flow modelling of the United Downs area, and at a vertical depth of 4500 m (the bottom of the production well) it is predicted that the temperature will be between 180–220°C (at a 90 per cent confidence level). Based on this, and the expected transmissivity the project aims to produce water at the surface at about 175°C, with a circulation flow rate of between 20–60 l/s (Ledingham et al., 2019).

8.1.2 Expected types of mineralisation and metal enrichment

The only information available on the potential for deep (>1 km) metal enrichment in Cornwall comes from drilling and logs from the HDR experiments, and the current UDDGP project. Minor sulfide was logged in RH15 at depths in excess of 2200 m. Limited published information is available on the UD-1 well to a depth of about 2000 m. The initial 210 m of the hole was dominated by killas. Persistent, steeply dipping quartz veins were encountered in this section. Granite was first intersected at a depth of 210–230 m. It was a fine-grained

kaolinised microgranite. It is reported that in the upper 1000 m of UD-1 'a number of predicated mineral lodes and cross-course structures….were encountered.' (Ledingham et al., 2019). These were presumably 'predicted' on the basis of the known abundance of mineralisation in the United Downs area. Below 250 m depth the near-bit gamma log showed peaks that corresponded with the observation of 'mineralization' in the drill chippings. A chlorite-rich zone at 750 m correlates with a gamma ray peak and is described in the evaluation log as a 'hydrothermal quartz-chlorite lode', containing 50–75 per cent quartz, with accessory phases including chlorite, tourmaline, muscovite, arsenopyrite, chalcopyrite and cassiterite, and no oxidation present. A feature described as a 'sulphide-rich lode' was also encountered at 1325–1335 m depth. Apparently mineralised chippings coincided with an increase in the rate of drilling progress, a peak in the gamma log and decline in the weight on bit. In the drill evaluation log this 'hydrothermal lode' is described as containing pyrite, cassiterite, tourmaline, quartz, biotite, and muscovite, with no evidence of mineral oxidation (Ledingham et al., 2019). Despite this encouraging information, at the time of writing, no direct evidence exists for the existence of substantial mineralisation at EGS reservoir depths (4–5 km) in Cornwall. However, equally there is currently no reason to conclude that it does not extend to these depths. There is a growing body of global of evidence to suggest that fracture-controlled fluid flow, and therefore the potential for mineral deposit formation, can occur at depths of several to tens of kilometres (Barnes, 1997). Assuming the abundant near-surface, metallic mineralisation of the Cornubian orefield (Section 5.1) is stable under the pressures and temperature at 4–5 km, in order to proceed with the CHPM concept and other components of the design, it should be assumed that any mineralisation occurring at reservoir depths is most likely to be of similar style and composition. The release of additional data from the UDDGP project may help to verify this.

8.2 Production and injection wells

In the original design for the HDR project the injection borehole (RH12) was below the production borehole (RH11), because it was assumed that the injected water would move upwards (Figure 69). In contrast this experiment demonstrated that the water migrated downwards, along favourably orientated joints. The position of RD15, below RH12 attempted to correct for this issue. The stress regime at the UDDGP project location will be the same as at Rosemanowes, therefore, downward migration of injected water is expected, although if necessary this could be facilitated by temporary increases of the injection pressure (Ledingham et al., 2019).

The UDDGP project aims to drill two boreholes that will both intersect the PTFZ (Figure 72). A borehole to about 2500 m will be used for water injection, whilst a deeper hole extending to about 4500 m will be used for production (Geothermal Engineering Ltd, 2018e). A downhole pump in the production well will drive the UDDGP system. This will result in a pressure sink around the production well, causing water to migrate towards it from the injection well and the broader rock mass. It is predicted that even moderate injection pressures will result in shearing on favourably orientated fractures, which likely to occur at pressures as low as 5 Mpa (Ledingham et al., 2019).

Well spacing is a major consideration in EGS design and is dependent on range of factors, including the expected permeability of the reservoir. The UDDGP project concept is based on the assumption that the natural fracture-controlled permeability, resulting from the PTFZ, will be sufficient to permit fluid circulation over a large vertical distance. High permeability coupled with a large (c. 2000 m) separation between the injection and production wells is hoped to result in a sufficiently large natural heat exchanger for a commercial-

scale operation. The large separation should also reduce the risk of short-circuiting of flow from the injector to producer wells, which is detrimental to system performance (Ledingham et al., 2019).

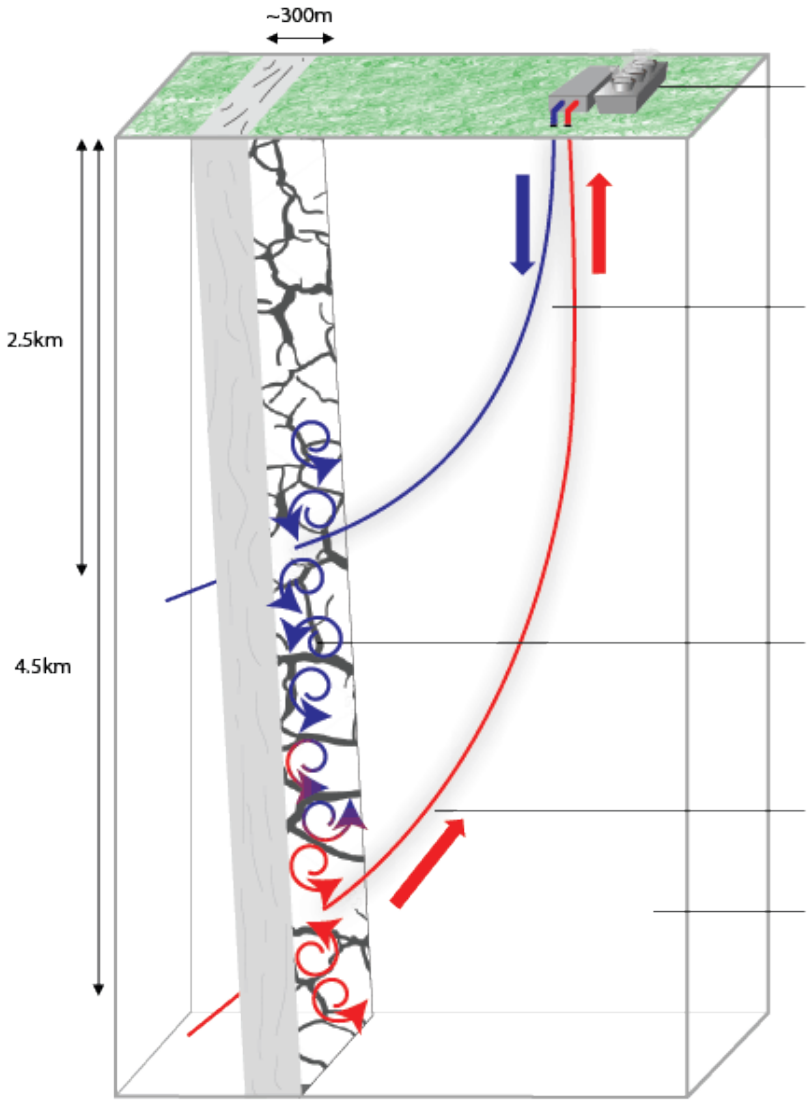

Figure 72: Schematic representation of the planned EGS system for the United Downs Deep Geothermal Power project. Water will be injected into the ground through the shallower injection well (blue), obtain heat from the rocks and return to the surface up a deeper production well (red), fed through a heat exchanger and then re-injected into the ground to collect more heat in a continuous cycle. The extracted heat will be used to supply a demonstration power plant. Reproduced with permission of Geothermal Engineering Ltd 2018.

At surface the well centres are only 8 m apart, which is a function of the space limitations on the site. Initially the wells will be 24 inches (609.6 mm) in diameter and vertical, but as they become deeper they will be deviated towards the SW to try and intersect the PTFZ (predicted to be about 700 m way from the well centres), and gradually narrowed in diameter (Table 6) (Geothermal Engineering Ltd, 2018a). The kickoff points for the wells will be 1110 m and 3400 m for the injection and production wells, respectively (Ledingham et al.,

2019). The two holes will be steel cased for the majority of their length, with the last few hundred metres being open hole, with a terminal diameter of 8.5 inches (Geothermal Engineering Ltd, 2018a).

Table 6: The planned completions for the two wells that will be drilled at the United Downs Deep Geothermal Power project. Reproduced from Ledingham et al. (2019).

Injection well			Production well		
Drilled diameter (mm)	Depth	Casing size (mm)	Drilled diameter (mm)	Depth	Casing size (mm)
24" (609.6)	250 m	18 5/8" (473.07)	24" (609.6)	250 m	18 5/8" (473.07)
17 ½" (444.5)	900 m	13 5/8" (346.07)	17 ½" (444.5)	900 m	13 5/8" (346.07)
12 ¼" (311.15)	4000 m	9 5/8" (244.47)	12 ¼" (311.15)	4000 m	9 5/8" (244.47)
8 ½" (215.9)			8 ½" (215.9)		

8.3 Power plant and local energy demand

If establishing an operational geothermal system is successful the UDDGP project plans to construct a demonstration power plant to supply power to the UK national grid. Initial plans are to establish a 1MWe plant, whilst considering the potential to expand the size to 3MWe (this limit of the available grid connection), subject to system performance and availability of further funding. Preliminary plans for plant design involve the use of a binary power plant (Geothermal Engineering Ltd, 2018d). Cornwall Council published a technical paper on energy projection for the county. Total final energy demand in Cornwall (excluding aviation and shipping) was projected to fall by nine per cent from 1,030 kilo tonnes of oil equivalent (ktoe) in 2007 to 939 ktoe in 2030. Considering increases in population, final energy demand per person in Cornwall was projected to decrease from 1.954 toe in 2007 to 1.490 toe in 2030. Final energy demand per household was projected to decrease from 4.496 toe in 2007 to 3.172 toe in 2030. Demand for renewables and bio-fuels was projected to increase in Cornwall from 5 ktoe in 2007 to 101 ktoe in 2030 (Table 7) (Cornwall Council, 2013b).

8.4 Salt gradient power generation

The concept of salinity gradient power relies on the existence of two solutions with large differences in salt concentration. Freshwater represents a low salinity solution that could be used in this process. The south-west of England experiences average annual rainfall values in the range of 1000 and 1500 mm, meaning access to water in the CHPM study area is unlikely to be a problem. Surface drainage in the study area is characterised by a radiating pattern of small rivers that drain off the high-ground of the granite (c. 300 m above sea-level) towards the coast (c. 60 m above sea level). The majority of water used in the study area is derived from surface water sources, for example Stithians Reservoir, which has a capacity of about 5 million litres. Very little water is sourced from underground aquifers (i.e. groundwaters), because the rocks that comprise the study area have very low-primary permeability and are therefore classified as low productivity aquifers. Historically water has been drawn from disused mine shafts and adits for public supply and agricultural uses, although it is unclear if this practice still takes place. Similarly, shallow (10–15 m deep) groundwaters held in weathered and fractured granite and country rock (killas) has also been used as a local water source; however, borehole yields are typically very low. For example, the average yield from 73 boreholes in the Carnmenellis granite was about 37 m^3 per day (Leveridge et al., 1990).

Table 7: Energy demand by final user in kilo tonnes of oil equivalent. For details of the calculations and data sources used and table notes see (Cornwall Council, 2013b). Reproduced from Cornwall Council (2013b).

		2007	2010	2015	2020	2025	2030
Domestic	Electricity	116	114	90	87	94	105
	Gas	146	160	131	126	132	139
	Petroleum	65	73	29	17	18	15
	Coal/ Manufactured fuels	5	5	5	5	5	7
	Renewables	0	4	28	35	36	37
	TOTAL	**332**	**356**	**283**	**270**	**285**	**303**
Industrial and commercial	Electricity	131	123	132	136	141	149
	Gas	113	107	100	81	77	80
	Petroleum	102	78	74	60	56	54
	Coal/ Manufactured fuels	5	5	4	4	3	3
	Renewables	5	8	18	57	57	57
	TOTAL	**356**	**327**	**331**	**326**	**323**	**332**
Transport	Electricity	0	1	1	2	1	1
	Petroleum (Rail)	10	9	10	10	9	9
	Petroleum (Road)	336	312	294	280	282	276
	Bio-fuel	0	3	9	16	6	7
	TOTAL	**346**	**325**	**314**	**308**	**298**	**293**
TOTAL	Electricity	247	238	223	225	236	255
	Gas	259	266	232	207	209	219
	Petroleum	513	472	407	367	365	355
	Coal/ Manufactured fuels	10	10	9	9	8	9
	Renewables and bio-fuels	5	15	55	108	99	101
	TOTAL	**1,034**	**1001**	**926**	**916**	**917**	**939**

The composition of shallow groundwater in the study area is largely controlled by the bedrock lithology, and to a lesser extent metallic mineralisation and farming practices. The groundwaters are typically low-salinity, mildly acidic and have relatively low total dissolved solids (TDS) content. However, groundwaters from the country rock (killas) have a higher TDS content and major ion concentration than those from the granite. Groundwaters from both rock types are typically soft, with $CaCO_3$ contents of between 24 and 116 mg l^{-1}. However, groundwaters from the granite tend to have lower $CaCO_3$ contents (24–43 mg l^{-1}) and are therefore more acidic (pH between 4 and 7), than those from the country rock (pH between 5 and 8) (Leveridge et al., 1990) (Table 8). Further details about groundwater and surface water chemistry can be found in Smedley et al. (1989).

Table 8: A summary of selected parameters for granite-hosted and country rock (killas) hosted groundwaters. Data from Leveridge et al. (1990).

	Granite groundwaters			Country rock (killas) groundwaters		
Temperature (°C)	15.6	10.8	14.5	12.5	18.5	13.8
pH	6.78	5.13	5.70	6.94	6.62	6.32
SEC (µS/cm)	200	210	112	210	120	340
TDS (mg l^{-1})	97.2	70.2	83.4	92.5	128	198
Total hardness (mg l^{-1} $CaCO_3$)	43	24	37	45	58	116
Sodium (mg l^{-1})	13.4	13.7	18.8	13.9	30.9	20.6
Chloride (mg l^{-1})	24	22	28	23	41	36
Silica (mg l^{-1})	1.0	4.1	4.1	2.2	11.4	2.5

9 Operational characteristics

9.1 Environmental, social and political background

9.1.1 Environmental

The HDR project took place in a quarry, which was chosen because it was on the exposed Carnmenellis granite and no major structural features were evident at the surface (Parker, 1991). The quarry is principally surrounded by arable farmland, traversed by a number of minor roads, with the A394 to its immediate south. A number of villages and smaller settlements are located within a 1 km radius of the site. Three reservoirs are located less than 3.5 km from the quarry (Figure 73). Although it is unclear whether it was a criteria for site selection at the time, the quarry setting represented a brownfield site, and would have significantly shielded the operations that took place for some 14 years. The location in the base of the quarry would have helped to reduce the visual impact of the drilling rig and well towers (Figure 3A and Figure 74).

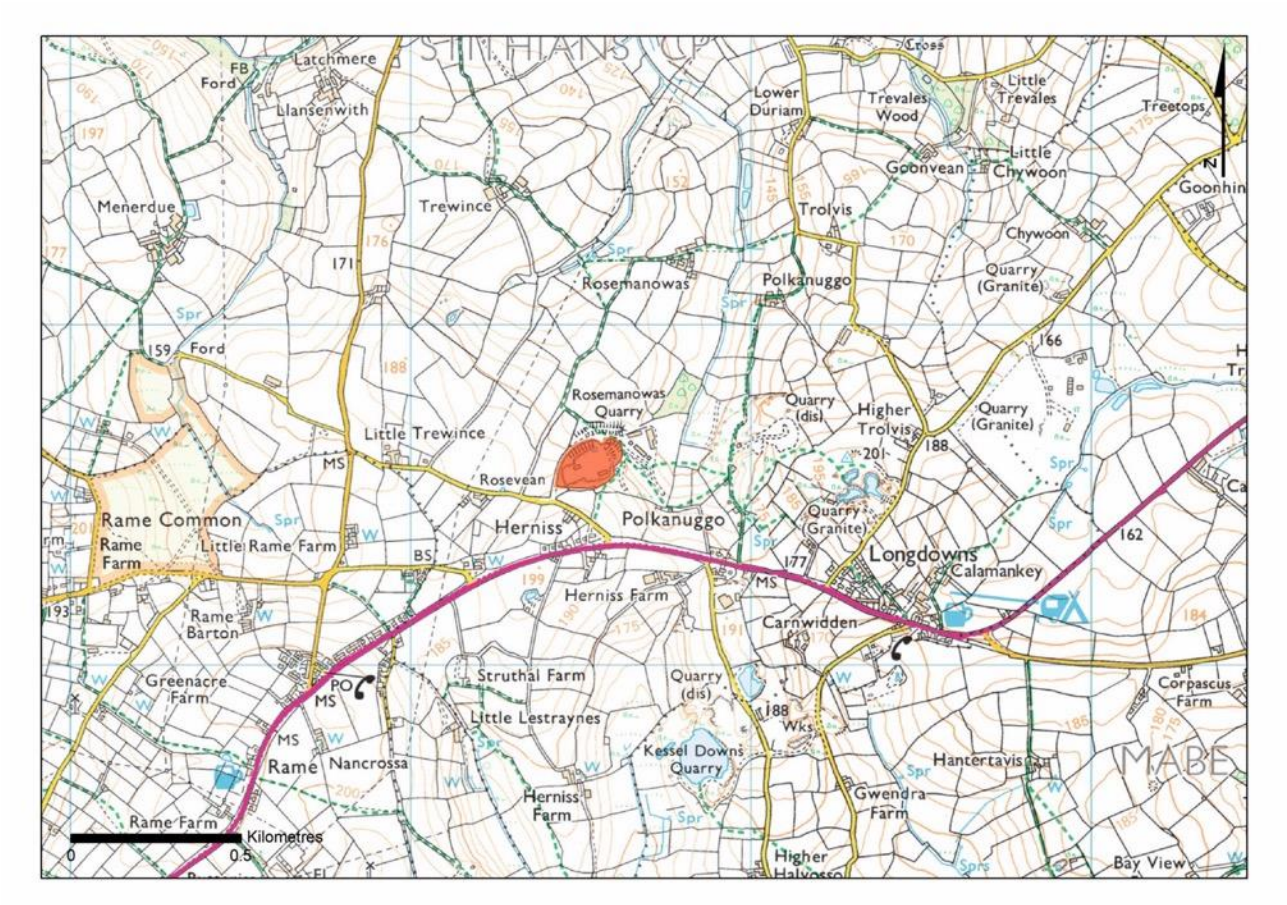

Figure 73: Location of Rosemanowes Quarry (shaded red) and the surrounding land use and infrastructure. Contains Ordnance Data © Crown Copyright and database rights [2019]. Ordnance Survey Licence no. 100021290. British Geological Survey © UKRI.

The location of the UDDGP project site, its extent and the current development provide the best indications of the potential environmental impacts of future geothermal resource development in Cornwall. The UDDGP project site is located 4.1 km east of Redruth and about 7 km north of the old HDR project site (Figure 7 and Figure 75).

Figure 74: Operations at the Rosemanowes HDR project site during the 1980s and 1990s. A/B. Aerial view of the quarry during drilling operations. C. View across the quarry and of the two towers. D. Steamy water being generated at a wellhead. E. Construction of the cistern for the boreholes. F. The cascade and water lagoon at the site. Images reproduced from the HDR project photo archive held by the British Geological Survey.

There were several locations in the area from which the PTFZ could have been targeted with drilling. However, with the exception of the United Downs Industrial Estate these were all greenfield sites. Given the existence of a brownfield site strong justification would be required for selection of an alternative (pers. comm.). Geothermal Engineering Ltd (2018) indicate that other considerations were good road access, sufficient space for the drilling rig, a relatively flat site, proximity to the National Grid and availability of services.

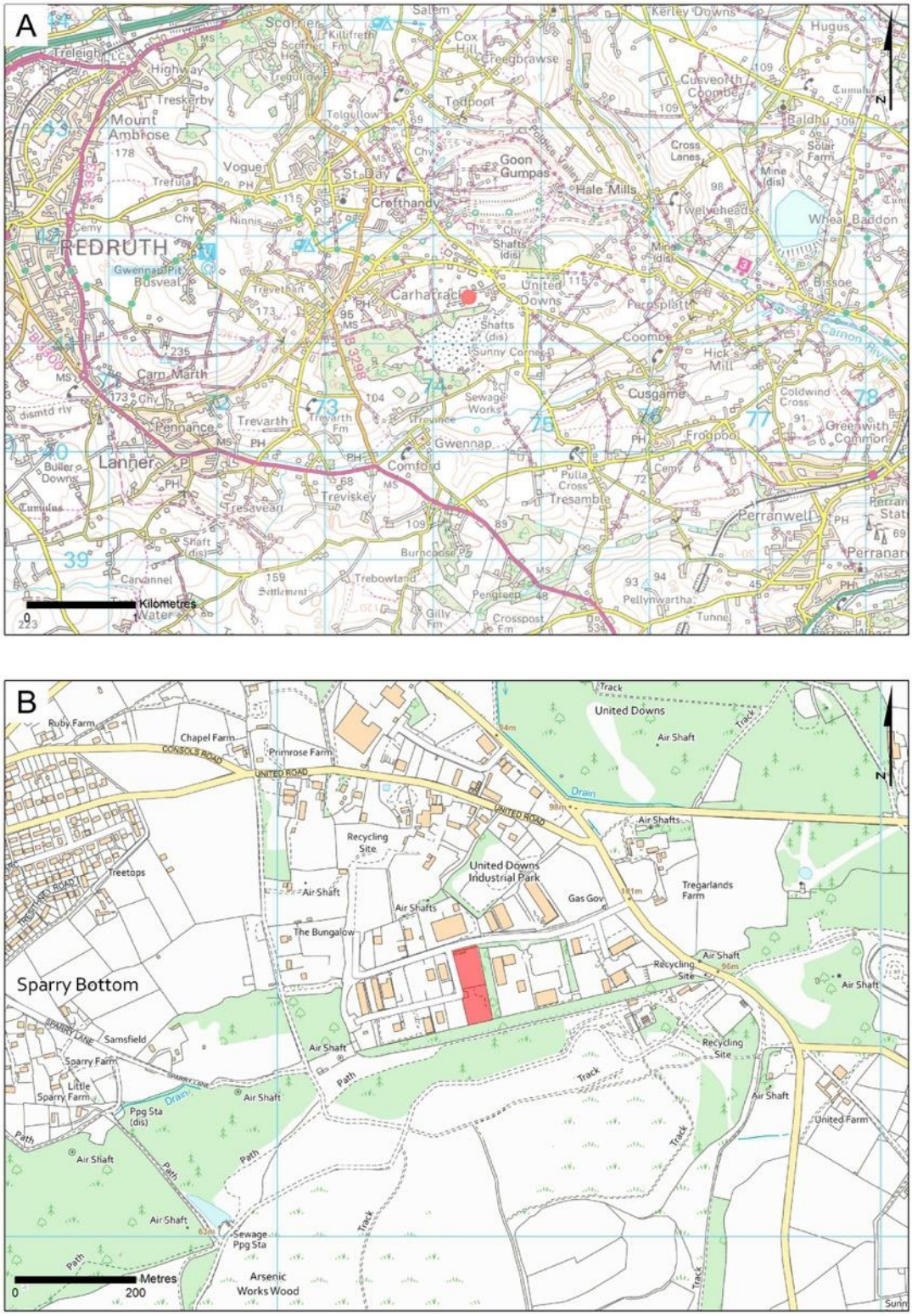

Figure 75: Location of the United Downs Deep Geothermal Power project and the surrounding land use and infrastructure. A. General location of the site (red circle) east of Redruth. B. Position of the site on the United Down Industrial Park. Contains Ordnance Data © Crown Copyright and database rights [2019]. Ordnance Survey Licence no. 100021290. British Geological Survey © UKRI.

In March 2010 Geothermal Engineering Ltd (GEL) submitted a 'hybrid' (comprising part detail, part 'outline') planning permission application (NR/10/00056/GEO) to Cornwall Council for geothermal exploration and development on, on an unoccupied plot on the United Downs Industrial Estate (Figure 76). The 'detailed' part of the application covered the drilling of the wells and associated pumping and test equipment. Whilst only 'outline' information was provided for the development of a power generating plant, pumping equipment and electrical infrastructure etc. The scheme received no objections from both statutory consultees and local residents, and planning permission was granted in October 2010 (Cornwall Council, 2012). All planning application documents are available online from Cornwall Council (Cornwall Council, 2019). These include specific documents relating to ecology, landscape and visual impact, geology and hydrology, noise and vibration and public consultation.

Figure 76: Nature of the land use surrounding the United Downs Deep Geothermal Power project site (outlined in red). British Geological Survey © UKRI.

9.1.1.1 Noise and microseismic monitoring at the UDDGP project

Geothermal Engineering Ltd (2018b) indicate that the principal environmental impacts associated with the UDDGP project relate to the exploration of the geothermal resource, which requires the drilling of two boreholes. The drilling rig and its diesel power generators represent a potential source of noise and it has a visual impact. The industrial site on which the drilling rig is located is noisy during the day, but not active over night or at weekends. Private housing exists along the western, northern and eastern perimeter of the industrial estate. The closest properties are about 300 m from the site, and the nearest village of Carharrach is less than 1 km to the west (Figure 75

Figure 75). The planning consent specifies the maximum acceptable noise levels during day and night. Background monitoring and predictive modelling was undertaken to predict the noise levels in the area surrounding the site (Ledingham et al., 2019). The drilling rig being used for the UDDGP project is a new generation semi-automated hydraulic rig. The H. Anger's Söhne Innova rig was constructed in 2007 and according to the manufacturer it has been designed to minimise environmental impact, as the space required to install the rig is much smaller than is necessary for conventional rigs; and it produces considerably less noise, making it beneficial for use in urban and noise-sensitive environments (H. Anger's Söhne, 2019), such as United Downs. In addition a range of noise mitigation and attenuation measures have been implemented at the drilling site, including the use of acoustic barriers. Continuous noise monitoring is taking place during the drilling phase, with sensors positioned on site and remotely (Ledingham et al., 2019). GEL have published a project 'noise management information sheet' (Geothermal Engineering Ltd, 2018f). Ledingham et al. (2019) indicates that only on a 'handful' of occasions have noise levels from drilling approached or exceeded the pre-set limits. GEL have established a noise reporting system, and it is reported that some local residents have complained about noise resulting from the drilling rig, despite the noise levels being below the threshold set in the planning consent (Ledingham et al., 2019).

The drilling rig comprises a mast, substructure, top drive, substructure, generators, pumps, drilling mud system, waste handling and data recording and has sufficient drill pipe to drill to more than 5000 m. The height of the mast of the rig is 51.8 m above ground level, meaning it is visible for some distance from the site (Figure 77). Drilling the two wells is anticipated to take six to seven months, operating 24 hours a day, 7 days a week (Geothermal Engineering Ltd, 2018b), therefore these specific impacts associated with the rig are short-term in nature. A further impact arising from the rig relates to its transportation to the UDDGP project site by road. This means during mobilisation and demobilisation of the rig there will be many (~70) large transport vehicles accessing the site over a 10–14 day period (Geothermal Engineering Ltd, 2018f).

Induced seismicity is a concern in all projects that involve deep drilling and water circulation through fractures. Geothermal Engineering Ltd (2018b) indicate that 'Testing and operating the geothermal reservoir will cause some micro-earthquakes but nearly all will be too small to be felt at surface.' During the HDR project tens of thousands of micro-events were recorded, however, it is reported that only two were felt at the surface (Geothermal Engineering Ltd, 2018b). In the planning consent for the project the local planning authority included a requirement for both seismic monitoring and for a monitoring and control protocol. A monitoring network has been installed on and around the site that combines microseismic and ground vibration monitoring systems. This will be capable of detecting seismic events down to magnitude 0.0 at a depth of 5 km around the reservoir, and to magnitude of 1.0 across a wider, 10 km x 10 km area. Background monitoring commenced several months before the drilling started. Data is transmitted from each station to a central processing centre, where a system automatically detects events. Data from the monitoring system is transferred to the British Geological Survey who make them publically available via their website (Ledingham et al., 2019).

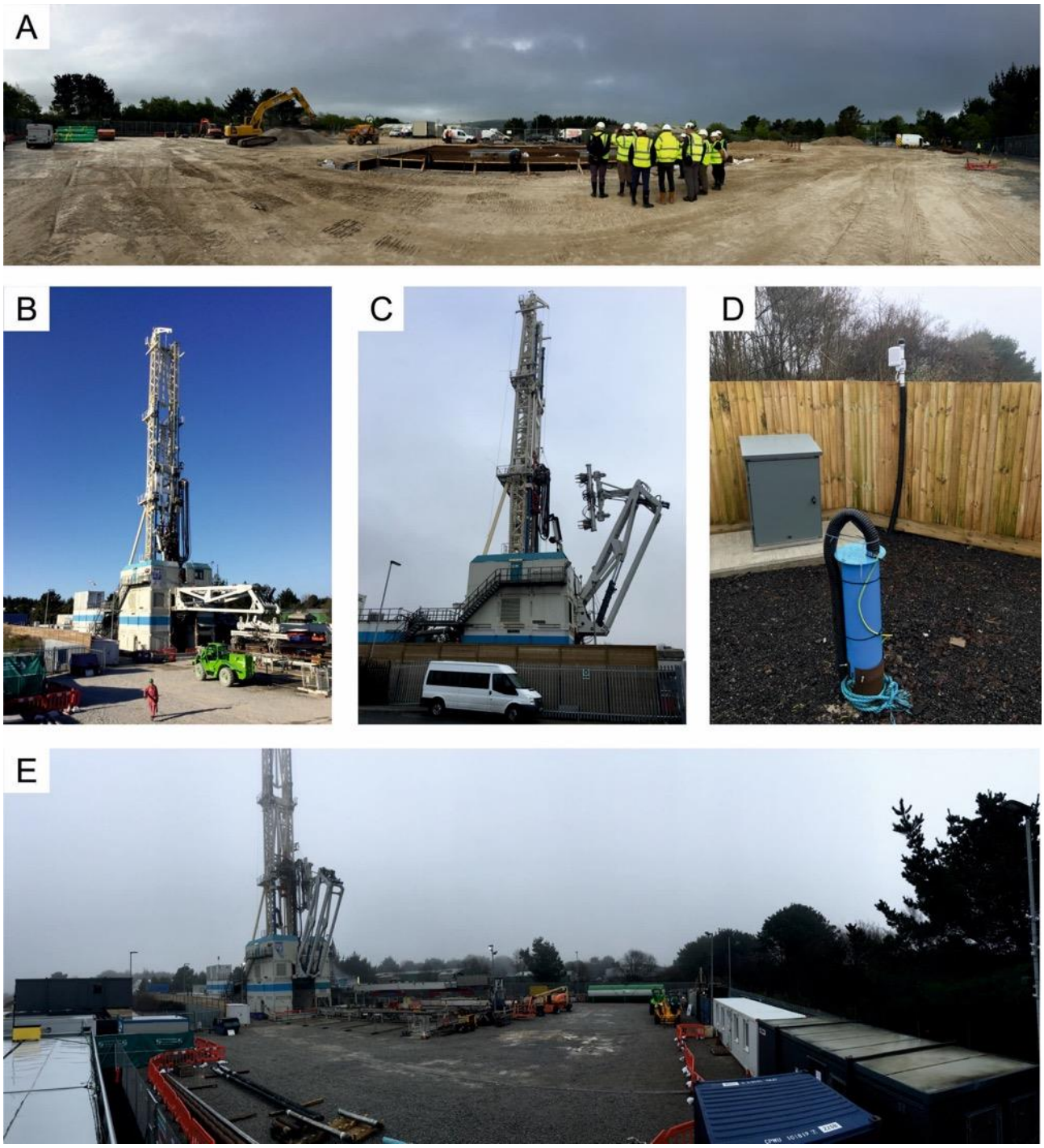

Figure 77: The United Downs Deep Geothermal Power project site. A. Site preparation and construction of the concrete drill pad in May 2018. H. Anger's Söhne Innova rig installed on the site. C. The height of the mast of the rig is more than 50 m above ground level, meaning it is visible for some distance from the site. D. Part of the ground vibration monitoring system at the site. E. View across the site. The trees to the right of the image mark the southern boundary of the site (Figure 76). British Geological Survey © UKRI.

9.1.2 Social

The history of mining in south-west England stretches back for millennia (Figure 78). The fact that UNESCO World Heritage Site status has been granted to the Cornwall and West Devon mining landscape is testament to the impact mineral extraction has had on the development of the region. The landscape of Cornwall and West Devon was transformed during the 18th and early 19th centuries as the copper and tin mining industry developed. The extensive underground mine workings, engine houses, which litter the landscape, new towns, ports and harbours and their associated industries reflect the importance of the region in terms of its 19th century metal production and the contribution it made to supplying raw materials for the Industrial Revolution in Great Britain (UNESCO, 2006). Of all the counties in the England Cornwall has experienced the most metalliferous mining. In addition the UK was the ninth largest producer of kaolin in the world in 2017 and made a more significant contribution to global supply in the past (Brown et al., 2019). Koalin resources in Great Britain are confined to the granites of south-west England and the deposits are world class in terms of size and quality. All the main granite intrusion have been worked to some extend in the past, but production has historically been based on the central and western parts of the St Austell granite and south-western margin of the Dartmoor granite. The kaolin production has had a strong impact on the Cornish landscape (Figure 79). Kaolinisation on the south-western part of the Dartmoor granite is adjacent to and extends into the Dartmoor National Park. In 2001, the two companies working in the area announced their intention to relinquish their planning permissions within the National Park because of the impact that these workings would have on a sensitive area. There are several SSSIs (mainly geological) located within the operational area in Cornwall. Goss and Tregoss Moor Special Area of Conservation is located just to the NE of the main kaolin extraction area (Bloodworth and Wrighton, 2009) (Figure 79). The last decade has seen a renewed interest in metals in south-west England. The most notable development, is the Drakelands Mine, formerly known as the Hemerdon Mine, near Plymouth. Hemerdon is one of the world's largest tungsten deposits and an open-pit mining operation was established here in 2015 to primarily produce tungsten and tin. There are also plans to reopen the South Crofty Mine. The South Crofty project is fully permitted, with an underground mining licence valid until 2071, planning permission to construct a new process plant and a permit from the Environment Agency to dewater the historical mine workings. The extent of mineral extraction in south-west England and its impact on the heritage of the region means local communities probably have a relatively receptive attitude towards natural resource development, mining projects and geothermal operations. Furthermore, factors such as income, unemployment levels, health, education, skills and training, and living environment can have an influence on local attitudes to developments that could have potential socio-economic benefits. Cornwall has a number of area with consistently high levels of deprivation (Cornwall Council, 2017b). It is noted that the Camborne and Redruth community network has the highest number of neighbourhoods in the most deprived 20 per cent in England. The number of deprived neighbourhoods in Cornwall has increased since 2010. This is attributed to a number of factors, including income and employment and a slight delay between the economic recovery in Cornwall and the rest of the country (Cornwall Council, 2015).

The most up to date information on the attitudes of communities in Cornwall to deep geothermal power development are provided by the consultation programme that was undertaken to support the proposed development of the UDDGP project. The consultation process involved disseminating information on geothermal energy to local stakeholders, outlining the plans for the geothermal power plant development, providing the community with an opportunity to discuss and interrogate the proposal, assessing the views and concerns of the community, and communicating the benefits and local impacts of the proposed plan.

Figure 78: Evidence of the strong influence of mining on the landscape of south-west England. A. There is extensive evidence of Cornwall's long mining history along the coastline. View along the coast towards Cligga Head. B/C. The Crowns mine at Botallack forms one of the most spectacular historic mining scenes in Cornwall with the engine house perched precariously on the rocks just above the sea (Figure 6A). D. The Wheal Jane water treatment facility, which was constructed to treat the polluted water from this underground mine. E. China clay workings, Great Pit, Lee Moor, south Dartmoor. F. Part of the old china clay workings in the kaolinised granite of Tregonning Hill, on or near the site of the first china clay workings in Cornwall. Steep narrow quartz and greisen veins cut the altered granite. G. Development works during the construction of the Drakelands Mine, formerly known as the Hemerdon Mine in 2014. British Geological Survey © UKRI.

Figure 79: China clay working to the NE of St Austell, Cornwall. Towns are labelled for reference. British Geological Survey © UKRI.

The Planning Application Document on the public consultation concluded that: 'The overwhelming response from the community consultation programme has been positive.' and 'The local politicians have been supportive.' It is also indicate that based on a consultation questionnaire completed by 88 people 'There was overwhelming support for geothermal energy with 89 per cent supporting the development of geothermal energy in the locality and only 6 per cent objecting'. Concerns about the project primarily focussed on traffic and noise, although it is emphasised that 'many people listed no concerns at all.' (Wardell Armstrong, 2010b).

Plymouth University, in south-west England are studying the issues relating to public perception of geothermal energy exploitation in the UK. The research will consider both the psychological and social factors that influence public opinion, and the influence of the media. The latter will examine how to improve communications between resource companies and affected residents that live close to potential geothermal sites (Geothermal Engineering Ltd, 2018g). GEL have undertaken an extensive education and community outreach programme targeting the full cross-section of potential stakeholders. More details can be found in Ledingham et al. (2019)

9.1.3 Political and regulatory framework

Geothermal heat has the potential to make a significant contribution to meeting the UK's legally binding emissions targets set out in the UK Climate Change Act (Abesser et al., 2018).

9.1.3.1 National context

Heat

Abesser et al. (2018) indicate that geothermal heat needs to be managed and regulated in a similar way to other natural resources such as oil, gas, coal and water. This requires clear definition of the term 'geothermal energy' as well as a clear understanding of ownership. One of the key challenges with ownership and regulation of geothermal heat in the UK is that it is regarded as a physical property, not a recoverable material such as a metallic mineral ore. As such, 'heat' is not a legally-defined entity and this causes some difficulties for assigning legal ownership and regulating it. Abesser et al. (2018) suggest that revision of geothermal regulations is one of a number of measures required to encourage exploitation of geothermal resources in the UK. Regulations enact the law, and a change to UK law is needed so that it better defines heat, and thereby allows implementation of such regulations. Currently, heat is not dealt with in UK law, except as a pollutant. Such cases are covered by the EU Water Framework Directive and UK groundwater regulations. Detrimental impact of geothermal schemes on other users (e.g. neighbouring schemes) are covered by 'private nuisance', i.e. they are a civil issue (Abesser et al., 2018). Abesser et al. (2018) indicate that early development risks are one of the main reasons why so few geothermal energy projects have been implemented in the UK to date.

In terms of the current regulatory approach in the UK for deep geothermal, the same requirements for environmental permissions and licences from the Environment Agency apply as for the open-loop, shallow geothermal systems (which abstract groundwater and return discharge it to the ground after it has been used for heating or cooling). They fall under environmental permitting and groundwater regulations, as defined by the Water Framework Directive, in EU countries. In the UK, the regulatory control of abstraction and discharges, required for open-loop systems, is solely aimed at protecting groundwater, not regulating heat (Abesser et al., 2018).

Minerals

Mineral exploration of fluctuating intensity has been undertaken in Great Britain over the last fifty years and there are several areas where exploration has identified potentially economic resources of a number of metals. Although many significant discoveries were made during this period, the last tin mine in Great Britain, South Crofty, in Cornwall, closed in 1998 (Colman and Cooper, 2000), and with the exception of a small gold deposit in Northern Ireland and the Drakelands tin-tungsten mine in Devon no new operations have since been commissioned.

The rights to non-energy minerals in Great Britain, with the exception of gold and silver, are mainly in private ownership although a significant proportion is owned by the Crown and by Government departments and agencies (Colman and Cooper, 2000). In Great Britain only the mineral rights owner can legally grant rights to explore and mine (Robertson, 1983). Hence a critical stage in the exploration and development process is determination of mineral ownership. Great Britain has no minerals title registry or system and although mineral rights in Great Britain are typically held by the surface landowner, they may have been retained by previous landowners when the surface freehold was sold. The beneficiaries of such rights are often unknown

to the surface owners and the titles to the mineral rights may have been lost or destroyed. In some regions, particularly those with a long history of mineral extraction such as Cornwall this issue can be compounded by several parties potentially having interests in the mineral rights of a particular area (undivided interests). The process of determining mineral ownership in Great Britain can be time consuming and costly and is a potential deterrent to investment. In Great Britain granting of an exploration agreement confers not rights of entry and the applicant has to negotiate access with surface rights owners. Severed land and mineral rights ownership in Great Britain can result in access problems.

The National Planning Policy Framework (NPPF) establishes the overarching context for the development of Local Planning policy and guidance in England. In relation to renewables and low carbon energy and heat it states that Local Planning Authorities should develop positive strategies to help increase the use and supply. It states that local planning policies should be designed to maximise deployment of renewables and low carbon energy, while ensuring that adverse impacts are addressed satisfactorily. The NPPF contains support for community-led initiatives for renewable and low carbon energy (Cornwall Council, 2016b). The National Planning Practice Guidance adds further context to the NPPF, and helps local councils in developing policies to support the framework. Whilst the NPPG reinforces the role that planning has in the delivery of renewable and low energy infrastructure, it states that renewable energy developments should be acceptable for their proposed location (Cornwall Council, 2016b). The Guidance on 'Renewable and low carbon energy' states that 'Community initiatives are likely to play an increasingly important role and should be encouraged as a way of providing positive local benefit from renewable energy development.' (Ministry of Housing Communities & Local Government, 2015). The Overarching National Policy Statement (NPS) for Energy (EN-1) sets out national policy for the delivery of major energy infrastructure. It states that 'As part of the UK's need to diversify and decarbonise electricity generation, the Government is committed to increasing dramatically the amount of renewable generation capacity'. It emphasises that renewable energy generation is 'essential to enable the UK to meet its commitments under the EU Renewable Energy Directive', and 'will also help improve our energy security by reducing our dependence on imported fossil fuels'. The NPS includes a list of generic impacts that must be considered by energy development proposals (Department of Energy and Climate Change, 2011). Whilst the NPS specifically identifies a range of technologies from which future large-scale renewable energy generation is likely to come, geothermal energy is not mentioned.

9.1.3.2 Cornwall future growth and energy strategy

Cornwall Council became a signatory of the 'Nottingham Declaration' on climate change in 2010. Cornwall Council commissioned a study that was published in 2012 to better understand the potential for geothermal resource development in the county. It considered technology, policy and commercial considerations that impact the sector. It identified a number of reasons for the slow development of deep geothermal in Cornwall, strategies the Council could take to stimulate the deep geothermal sector and presented three options for future development (ARUP, 2012). In 2013 Cornwall Council released the 'Sustainable Energy Action Plan (SEAP)'. This indicates that Cornwall has an annual energy demand estimated to be about £1.4 billion. It states that 'Cornwall Council has the responsibility to lead by example and inspire the businesses and communities in Cornwall to drive down emission and energy demand.' It describes the importance of 'Supporting and promoting geothermal opportunities' and how the Council is seeking to better understand the potential of the resource, and if appropriate, to support development of this sector in line with the green energy aspirations of the county (Cornwall Council, 2013a). Since 2015 Cornwall has had devolved powers. In 2018 the Council released a 'New Frontiers' plan, which describes how 'Cornwall…will continue their economic, social and environmental transformation…'. It emphasises the importance of clean growth and environmental

management, and states 'Our peninsula is energy rich, with strong established and emerging renewable energy sectors including solar, wind and geothermal.' (Cornwall Council, 2018).

9.1.3.3 Planning policy in Cornwall

The Cornwall Local Plan was formally adopted on 22 November 2016. It provides the overarching planning policy framework for Cornwall, and covers the period up to 2030. The Cornwall Local Plan Strategic Policies 2010–2030 ('The Local Plan') sets out the Council's vision and strategy for Cornwall until 2030 and policies that will be used in determining planning applications. The Plan contains a specific 'Renewable and low carbon energy' policy, which seeks to increase the use and production of renewables and low carbon energy generation. In terms of context it states that more than 14 per cent of households in Cornwall spend more than 10 per cent of their income on fuel for domestic heating and that the county uses an estimated £500 million of energy annually. It emphasises that renewable and low carbon electricity and heat generation is reliant on continued access to the natural resources. With respect to geothermal it states that careful management is necessary to ensure that new developments do not harm the integrity of deep geothermal reservoirs. This is supported by another specific policy on 'Safeguarding renewable energy' that states 'New development, where appropriate, should show that it does not significantly harm the performance of any existing facility…or the availability of their resource (where the operation is dependent on uninterrupted flow of energy to the installation).' (Cornwall Council, 2016a). Cornwall Council also provides planning policy guidance, commonly referred to as Supplementary Planning Documents (SPD), which provide more detailed advice and guidance to supplement policies and proposals contained in the Local Plan. In 2016 the Council published the SPD: 'Cornwall Renewable Energy Planning Advice'. The Planning Advice contains general guidance, which is relevant to planning for all renewable energy technologies. The general guidance considers 'community energy' i.e. a model focussed on a 'local energy economy', with a shift of ownership to local people. The Council believes this model of renewable energy deployment should receive particular support at the planning decision stage. It also focuses on 'optimising renewable energy' i.e. minimising its impact by maximising its efficiency (Cornwall Council, 2016b). The Local Plan specifically states that renewable energy development will be supported where they 'maximise the use of the available resource by deploying installations with the greatest energy output practicable' (Cornwall Council, 2016a). The general guidance also emphasises the importance of 'co-location' (Cornwall Council, 2016b), since the Local Plan is particularly supportive of developments that 'create opportunities for colocation of energy producers with energy users, in particular heat, and facilitate renewable and low carbon energy innovation.' (Cornwall Council, 2016a). The SPD indicates that examples where co-location between heat generation and consumption is likely to be encouraged include geothermal energy (Cornwall Council, 2016b). A section of the SPD is devoted to 'deep geothermal', which discusses the importance of optimisation and co-location, and potential impacts, including on landscape, ecology and biodiversity, the historic environment, and noise emissions. In terms of used of land it indicates that 'whenever geological and thermal conditions allow, geothermal development should be sited on previously developed/brownfield sites, contaminated land…and industrial land.' It 'should avoid significant loss of Best and Most Versatile agricultural land.' It also provides more detailed advice and guidance on flood management, rights of way and highways, traffic, and the impacts of drilling and the requirement for seismic hazard assessment (Cornwall Council, 2016b). The SPD describes the importance of 'safeguarding' renewable energy resources, in line with the specific policy in the Local Plan (see above). However, it indicates that 'Deep geothermal operations may also conflict with the interests of minerals safeguarding areas' (Cornwall Council, 2016b), for which there is also a specific policy ('Minerals safeguarding') in the Local Plan, which states 'Important mineral resources and reserves…shall be safeguarded from sterilisation by other forms of

incompatible development.' (Cornwall Council, 2016a). The SPD indicates that 'Where deep geothermal developments are proposed within, or near to minerals safeguarding areas, it is recommended that the issue be addressed as part of the pre-application process with the Council and, if necessary, through engagement with the land owner and relevant mineral operator.' (Cornwall Council, 2016b).

9.2 Financial aspects

MacDonald et al. (1992) indicates that cumulative expenditure (to April 1991) on phases 1 to 3A of the HDR project was more than £35 million. When this historical price is converted into equivalent present-day prices (2018) by using historical inflation rates, the expenditure is more than £73 million. An alternative source estimates that government and European Union support for this project was about £50 million (Law, 2011). During Phase 3A of the HDR project work was undertaken on the economic costs of HDR systems. The capital cost associated with a 'post-prototype' commercial-scale HDR power station was estimated to be about £45 million in 1990. An alternative cost model estimated it be £35 million (MacDonald et al., 1992). Conversion of these historical prices to 2018 prices places current capital cost at between about £71–100 million.

A study commissioned by the Department of Energy and Climate Change, included a review of the costs associated with exploration, exploitation and potential investment returns for deep geothermal. The research took a case study-based approach, with the low permeability granites of south-west England being selected as one of the case studies. A high level techno-economic model was developed to assess the expected financial returns. This report concluded that south-west of England has a development potential of 100MW of electricity generation (Atkins, 2013). A previous study by Sinclair Knight Merz (2012) concluded that Cornwall's generating capacity could be up to 4GW of electricity, with a by-product of 13GW of heat (ERDF, 2016). ERDF (2016) indicate that a 100MW geothermal resource could provide electricity to about 150 000 homes and 4GW would be greater than Cornwall's total energy demand. It is emphasised how development of geothermal resources could result in more affordable heat and power. This could result in Cornwall becoming an attractive destination for power dependent industries and those seeking to lower energy costs. It is suggested that development of a geothermal industry will produce 'high value' jobs resulting in both direct and indirect employment, arising from down-stream industries (ERDF, 2016). For the UDDGP project the Planning Application Document on the 'Socio-economic and environmental benefits' indicates that Geothermal Engineering are seeking a partner to utilise a portion of the renewable heat that is generated from the power plant, and would be provided 'at a very low cost'. It indicates that potential industrial partners include: agriculture for glasshouses, industrial drying facilities, laundry services, breweries and industries with significant cooling requirements e.g. IT data centres (Wardell Armstrong, 2010a).

The electricity grid in Cornwall has spare capacity on the network to take more locally generated renewable energy. However, because of existing connection agreements, which are yet to be used, and the time required to make upgrades to the grid, there is very little capacity actually available for new connections. The Council indicates that delivering geothermal in the capacities that appear achievable will take many years, because each 5–10 MW project will require 4–6 years of construction time. They suggest that potential solutions include reviewing connection agreements, improved network management, energy storage schemes, as well as general infrastructure improvements. The UDGP project has secured a grid connection (Cornwall Council, 2017a).

The costs associated with the UNDGP project provide the most recent estimates of the expenditure associated with geothermal exploration and development in Cornwall. The project has a total cost of £18 million, which has obtained from three funding sources. The European Regional Development Fund has provided £10.6 million under its Priority Axis 4 ('Supporting the Shift Towards a Low Carbon Economy in All Sectors'). Cornwall Council has provided £2.4 million in support of its economic development programme and its vision for a low carbon energy future. The remaining £5 million has been provided by private investors (Geothermal Engineering Ltd, 2018c). The Planning Application Document on the 'Socio-economic and environmental benefits' of the UDDGP project outlines the level of economic investment required to establish a 10 MWe geothermal plant. It was estimated the geothermal power plant would annually generate more than 55,188 MWh of electrical output (sufficient to supply the electrical requirements of more than 9000 homes) and 65,043 MWh of thermal output. In 2010 it was estimated that the total investment required for the project would be about £44 million. At this time the borehole drilling and exploration was estimated to be in the order of £8 million (then GEL were proposing to develop up to three wells). It is indicated that once operational the power station would provide 4–5 permanent jobs (Wardell Armstrong, 2010a).

10 References

ABESSER, C, SCHOFIELD, D, BUSBY, B, BONSOR, B, AND WARD, R. 2018. Who owns (geothermal) heat? *British Geological Survey*.

ALDERTON, D, AND SHEPPARD, S. 1977. Chemistry and origin of thermal waters from southwest England. *Transactions of the Institute of Mining and Metallurgy Section B-Applied Earth Science*, Vol. 86, B191-B194.

ALEXANDER, A, AND SHAIL, R. 1996. Late-to post-Variscan structures on the coast between Penzance and Pentewan, South Cornwall. *Proceedings of the Ussher Society*, Vol. 9, 6.

ANDERSEN, J, STICKLAND, R, ROLLINSON, G, AND SHAIL, R. 2016. *Indium mineralisation in SW England: Host parageneses and mineralogical relations*. No. 78.

ARUP. 2012. Cornwall Geothermal Options Report. *Ove Arup & Partners Ltd* (London, United Kingdom).

ATKINS. 2013. Deep Geothermal Review Study Final Report.

BALL, T, BASHAM, I, BLANK, D, AND SMITH, T. 1982. Aspects of the geochemistry of bismuth in South-West England. *Proceedings of the Ussher Society*, Vol. 5, 376-382.

BARIA, R, HEARN, K C, LANYON, G N, AND BATCHELOR, A S. 1985. Microseismic Results

BARKER, J A, DOWNING, R A, GRAY, D A, FINDLAY, J, KELLAWAY, G A, PARKER, R H, AND ROLLIN, K E. 2000. Hydrogeothermal studies in the United Kingdom. *Quarterly Journal of Engineering Geology and Hydrogeology*, Vol. 33, 41-58.

BARNES, H L. 1997. *Geochemistry of hydrothermal ore deposits*. (New York: Wiley.) ISBN 047157144X 9780471571445

BARNES, R, AND ANDREWS, J. 1981. Pumpellyite-actinolite grade regional metamorphism in south Cornwall. *Proceedings of the Ussher Society*, Vol. 5, 139-146.

BATCHELOR, A. 1978. The engineering properties of the southwestern granites related to artificial geothermal exploitation. *Proc. Ussher Soc*, Vol. 4, 355-361.

BATCHELOR, A, AND PINE, R. 1986. The results of in situ stress determinations by seven methods to depths of 2500 m in the Carnmenellis granite. *ISRM International Symposium*, International Society for Rock Mechanics.

BEAMISH, D. 1990. *A deep geoelectric survey of the Carnmenellis granite*. No. 102.

BEAMISH, D, AND BUSBY, J. 2016. The Cornubian geothermal province: heat production and flow in SW England: estimates from boreholes and airborne gamma-ray measurements. *Geothermal Energy*, Vol. 4, 4.

BEAMISH, D, HOWARD, A, WARD, E K, WHITE, J, AND YOUNG, M E. 2014. Tellus South West airborne geophysical data (British Geological Survey).

BEAMISH, D, AND WHITE, J. 2014. TellusSW : airborne geophysical data and processing report. . *British Geological Survey* (Keyworth, Nottingham).

BEER, K E, BURLEY, A J, AND TOMBS, J M C. 1975. The concealed granite roof in south-west Cornwall. *Institute of Geological Sciences*, 1 (Keyworth, Nottingham).

BLOODWORTH, A, AND WRIGHTON, C. 2009. Mineral Planning Factsheet Kaolin.

BOTT, M H P, DAY, A A, MASSON-SMITH, D, AND DUNHAM, K C. 1958. The geological interpretation of gravity and magnetic surveys in Devon and Cornwall. *Philosophical Transactions of the Royal Society of London. Series A, Mathematical and Physical Sciences*, Vol. 251, 161-191.

BOTT, M H P, HOLDER, A P, LONG, R E, AND LUCAS, A L (editors). 1970. *Crustal structure beneath the granites of south-west England. In Mechanism of igneous intrusion*. Geol. J., special issue.

BOTT, M H P, AND SCOTT, P (editors). 1964. *Recent geophysical studies in south-west England*. Present view of some aspects of the geology of Cornwall. (Truro: Blackford.)

BRITISH GEOLOGICAL SURVEY. 1990. Geological Survey of England and Wales 1:63,360/1:50,000 geological map series, New Series. Falmouth. Sheet number 352. 1:50 000.

BROMLEY, A V, THOMAS, L J, SHEPHEARD, T J, AND DARBYSHIRE, D P F. 1989. Geochemistry in relation to Hot Dry Rock development in Cornwall, Volume 5. Mineralogy and geochemistry of the Carnmenellis Granite. *British Geological Survey*, British Geological Survey Research Report SD/89/2.

BROOKS, M, DOODY, J J, AND AL-RAWI, F R J. 1984. Major crustal reflectors beneath SW England. *Journal of the Geological Society*, Vol. 141, 6.

BROOKS, M, MECHIE, J, AND LLWELLYN, D J (editors). 1983. *Geophysical investigations in the Variscides of Southwest Britain*. The Variscan foldbelt in the British Isles. (Bristol: Adam Hilger Ltd.)

BROWN, T, IDOINE, N, RAYCRAFT, E, HOBBS, S, SHAW, R, EVERETT, P, KRESSE, C, DEADY, E, AND BIDE, T. 2019. World Mineral Production 2013-2017. *British Geological Survey*.

BURGESS, W G, EDMUNDS, W M, ANDREWS, J N, AND KAY, R L F. 1982a. The origin and circulation of grounwater in the Carnmenellis Granite: the hydrogeochmeical evidence. *British Geological Survey*, WJ/GE/82/004.

BURGESS, W G, EDMUNDS, W M, ANDREWS, J N, KAY, R L F, AND LEE, D J. 1982b. origin and circulation of groundwater in the Carnmenellis granite: the hydrogeochemical evidence. *nstitute of Geological Sciences* (London).

BURT, R, BURNLEY, R, GILL, M, AND NEILL, A. 2014. *Mining in Cornwall and Devon: Mines and Men*. (University of Exeter Press.) ISBN 085989889X

BUSBY, J. 2010. Geothermal Prospects in the United Kingdom. Proceedings World Geothermal Congress Bali, Indonesia.

BUSBY, J, AND TERRINGTON, R. 2017. Assessment of the resource base for engineered geothermal systems in Great Britain. *Geothermal Energy*, Vol. 5, 7.

CAMBORNE SCHOOL OF MINES. 1986. Jointing in the Carnmenellis granite (Report 2A-59). 2A-46 (Camborne, United Kingdom).

CAMBORNE SCHOOL OF MINES. 1988. Resource evaluation (Report 2C-7). 2A-46 (Camborne, United Kingdom).

CHAPPELL, B W, AND HINE, R. 2006. The Cornubian Batholith: an Example of Magmatic Fractionation on a Crustal Scale. *Resource Geology*, Vol. 56, 203-244.

CHEN, Y, CLARK, A H, FARRAR, E, WASTENEYS, H A H P, HODGSON, M J, AND BROMLEY, A V. 1993. Diachronous and independent histories of plutonism and mineralization in the Cornubian Batholith, southwest England. *Journal of the Geological Society*, Vol. 150, 1183-1191.

CHESLEY, J T, HALLIDAY, A N, SNEE, L W, MEZGER, K, SHEPHERD, T J, AND SCRIVENER, R C. 1993. Thermochronology of the Cornubian batholith in southwest England: Implications for pluton emplacement and protracted hydrothermal mineralization. *Geochimica et Cosmochimica Acta*, Vol. 57, 1817-1835.

CLARK, A, CHEN, Y, FARRAR, E, AND NORTHCOTE, B. 1994. Refinement of the time/space relationships of intrusion and hydrothermal activity in the Cornubian Batholith. *Abstracts Volume, Ussher Society Annual Meeting, Minehead*.

COLMAN, T B, AND COOPER, D C. 2000. Exploration for metalliferous and related minerals in Britain: a guide. *British Geological Survey*.

CORNWALL COUNCIL. 2012. Renewable Energy Planning Guidance Note 8 The Development of deep geothermal.

CORNWALL COUNCIL. 2013a. Sustainable Energy Action Plan (SEAP) for a Green Cornwall. *Cornwall Council* (Cornwall, United Kingdom).

CORNWALL COUNCIL. 2013b. Technical Paper E1 (b) Energy Projections for Cornwall. *Cornwall Council* (Cornwall, United Kingdom).

CORNWALL COUNCIL. 2015. Indices of Multiple Deprivation 2015. Cornwall, Cornwall Council 6.

CORNWALL COUNCIL. 2016a. Cornwall Local Plan - Strategic Policies 2010-2030. *Cornwall Council* (Cornwall, United Kingdom).

CORNWALL COUNCIL. 2016b. Cornwall Renewable Energy Planning Advice. *Cornwall Council* (Cornwall, United Kingdom).

CORNWALL COUNCIL. 2017a. Deep geothermal FAQ's. https://www.cornwall.gov.uk/media/16892627/faqs-210617.pdf

CORNWALL COUNCIL. 2017b. Deprivation. [cited 03 April]. https://www.cornwall.gov.uk/council-and-democracy/data-and-research/data-by-topic/deprivation

CORNWALL COUNCIL. 2018. New Frontiers - An inclusive approach to an economy, environment and society that works for everyone in Cornwall and the Isles of Scilly. *Cornwall Council* (Cornwall, United Kingdom).

CORNWALL COUNCIL. 2019. Planning – Planning Application Documents. http://planning.cornwall.gov.uk/online-applications/applicationDetails.do?activeTab=documents&keyVal=KYLN1FFG0DT00

CORNWELL, J D, KIMBELL, S F, EVANS, A D, AND COOPER, D C. 1995. A review of detailed airborne geophysical surveys in Great Britain. *British Geological Survey* (Keyworth, Nottingham).

DANGERFIELD, J, AND HAWKES, J. 1981. The Variscan granites of south-west England: additional information. *Proceedings of the Ussher Society*, Vol. 5, 116-120.

DARBYSHIRE, D, AND SHEPHERD, T. 1987. Chronology of magmatism in south-west England: the minor intrusions. *Proceedings of the Ussher Society*, Vol. 6, 431-438.

DARBYSHIRE, D P F, AND SHEPHERD, T J. 1985. Chronology of granite magmatism and associated mineralization, SW England. *Journal of the Geological Society*, Vol. 142, 1159-1177.

DE LA BECHE, H T. 1839. Report On the Geology of Cornwall, Devon and West Somerset.

DE LA BECHE, H T. 1846. Geological Survey of England and Wales 1:63,360 geological map series [Old Series]. [South Coast, from Polperro to St. Neverne, N. Coast, St. Agnes Head to Portreath, Truro, Falmouth, the Mining Districts of St. Austell, Fowey, Camborne, Redruth, showing Lodes.] Sheet number 31. 1:63 360.

DEADY, É, AND MOORE, K R. 2015. The Key to Understanding Antimony Mineralisation in South West England — the North Herodsfoot Mine? Applied Earth Science, Taylor & Francis. **124** 20-59.

DEPARTMENT OF ENERGY AND CLIMATE CHANGE. 2011. Overarching National Policy Statement for Energy (EN-1). (London, United Kingdom).

DINES, H G. 1956. *The metalliferous mining region of south-west England*. No. 1. (HM Stationery Office.)

DOMINY, S, AND CAMM, G. 1998. Controls on ore localization in tin-bearing veins: a review. *PROCEEDINGS-USSHER SOCIETY*, Vol. 9, 241-249.

DOMINY, S, SCRIVENER, R, LE BOUTILLIER, N, BUSSELL, M, AND HALLS, C. 1994. Crosscourses in South Crofty Mine, Cornwall: further studies of paragenesis and structure. *Proceedings-Ussher Society*, Vol. 8, 237-237.

DOWNING, R A. 1986. *Geothermal energy: The potential in the United Kingdom*. (HMSO.)

DOWNING, R A, AND GRAY, D A. 1986. *Geothermal energy : the potential in the United Kingdom*. (London: H.M.S.O.) ISBN 0118843664 9780118843669

DUNHAM, K, BEER, K E, ELLIS, R A, GALLAGHER, M J, NUTT, M J C, AND WEBB, B C. 1978. United Kingdom. *Mineral deposits of Europe*. HASLAM, H W, KVALHEIM, A, AND BOWIE, S H U (editors). Volume 1 (Northwest Europe). (London: Institution of Mining and Metallurgy and Mineralogical Society.) ISBN 0900488441

DURRANCE, E M. 1985a. Hydrothermal circulation and isostasy, with particular reference to the granites of southwest England. . *Institution of Mining and Metallurgy Conference on High heat production (HHP) granites, hydrothermal circulation and ore genesis; St. Austell (UK); 22-25 Sep 1985*.

DURRANCE, E M. 1985b. A possible major Variscan thrust along the southern margin of the Bude Formation, south-west England. *Proceedings of the Ussher Society*, Vol. 6, 173-179.

EDMONDS, E A, MCKEOWN, M C, WILLIAMS, M, AND DEWEY, H. 1985. *British Regional Geology. South-west England. Fourth edition. Reprinted 1985 with additional references*.

EDMUNDS, W, ANDREWS, J, BURGESS, W, KAY, R, AND LEE, D. 1984. The evolution of saline and thermal groundwaters in the Carnmenellis granite. *Mineralogical Magazine*, Vol. 48, 407-424.

EDWARDS, J. 1984. Interpretations of seismic and gravity surveys over the eastern part of the Cornubian platform. *Geological Society, London, Special Publications*, Vol. 14, 119-124.

ERDF. 2016. Vision for geothermal energy in Cornwall. European Regional Development Fund Convergence http://www.erdfconvergence.org.uk/_userfiles/files/GrowthProgramme/Geothermalvisionjan2016update.pdf

EVANS, C D R. 1990. The geology of the western English Channel and its western approaches. *British Geological Survey*, United Kingdom offshore regional report (London).

EVANS, K F, KOHL, T, HOPKIRK, R J, AND RYBACH, L. 1992. Modelling of energy production from Hot Dry Rock systems. *Eidgenössische Technische Hochschule (ETH)* (Zürich, Switzerland).

EXLEY, C S, AND STONE, M (editors). 1982. *Hercynian intrusive rocks*. Igneous rocks of the British Isles. (Chichester: Wiley.)

FERRACCIOLI, F, GERARD, F, ROBINSON, C, JORDAN, T, BISZCZUK, M, IRELAND, L, BEASLEY, M, VIDAMOUR, A, BARKER, A, ARNOLD, R, DINN, M, FOX, A, AND HOWARD, A. 2015. LiDAR based Digital Terrain Model (DTM) data for South West England. CENTRE, N E I D.

FERRILL, D A, AND MORRIS, A P. 2003. Dilational normal faults. *Journal of Structural Geology*, Vol. 25, 183-196.

FLOYD, P A, EXLEY, C S, AND STYLES, M. 1993. The igneous rocks of south-west England. 1-7 in *Igneous Rocks of South-West England*. (Springer).

FRANKE, W. 1989. Tectonostratigraphic units in the Variscan belt of central Europe. *Geol Soc Am Spec Pap*, Vol. 230, 67-90.

GEOTHERMAL ENGINEERING LTD. 2018a. Drilling the wells. https://www.uniteddownsgeothermal.co.uk/drilling-the-wells

GEOTHERMAL ENGINEERING LTD. 2018b. Frequently asked questions. https://www.uniteddownsgeothermal.co.uk/frequently-asked-questions

GEOTHERMAL ENGINEERING LTD. 2018c. Funding. https://www.uniteddownsgeothermal.co.uk/funding-objectives

GEOTHERMAL ENGINEERING LTD. 2018d. Generating Electricity. https://www.uniteddownsgeothermal.co.uk/generating-electricity

GEOTHERMAL ENGINEERING LTD. 2018e. Project Overview. https://www.uniteddownsgeothermal.co.uk/project-overview

GEOTHERMAL ENGINEERING LTD. 2018f. UDDGP Noise Management Information Sheet 2.

GEOTHERMAL ENGINEERING LTD. 2018g. University of Plymouth research. [cited 03 April]. https://www.uniteddownsgeothermal.co.uk/plymouth-university-research

GERARD, F. 2014. PROJECT: PM_1478 Processing of LIDAR data for the South West TELLUS Project.

GHAHFAROKHI, P K. 2017. The structured gridding implications for upscaling model discrete fracture networks (DFN) using corrected Oda's method. *Journal of Petroleum Science and Engineering*, Vol. 153, 70-80.

GHOSH, P K. 1934. The Carnmenellis Granite: Its Petrology, Metamorphism and Tectonics. *Quarterly Journal of the Geological Society*, Vol. 90, 240-276.

GLEESON, S, WILKINSON, J, SHAW, H, AND HERRINGTON, R. 2000. Post-magmatic hydrothermal circulation and the origin of base metal mineralization, Cornwall, UK. *Journal of the Geological Society*, Vol. 157, 589-600.

GLEESON, S, WILKINSON, J, STUART, F, AND BANKS, D. 2001. The origin and evolution of base metal mineralising brines and hydrothermal fluids, South Cornwall, UK. *Geochimica et Cosmochimica Acta*, Vol. 65, 2067-2079.

H. ANGER'S SÖHNE. 2019. HAS Innova rig. [cited 23/03]. http://www.angers-soehne.com/?page_id=4793&lang=en

HAIMSON, B C, TUNBRIDGE, L W, LEE, M Y, AND COOLING, C M. 1989. Measurement of rock stress using the hydraulic fracturing method in Cornwall, U.K.—Part II. Data reduction and stress calculation. *International Journal of Rock Mechanics and Mining Sciences & Geomechanics Abstracts*, Vol. 26, 361-372.

HAWKES, J. 1981. A tectonic 'watershed'of fundamental consequence in the post-Westphalian evolution of Cornubia. *Proceedings of the Ussher Society*, Vol. 5, 128-131.

HAWKES, J, AND DANGERFIELD, J. 1978. The Variscan granites of south-west England: a progress report. *Proceedings of the Ussher Society*, Vol. 4, 158-171.

HEATH, M J. 1985. Geological control of fracture permeability in Carnmenellis granite, Cornwall: implications for radionuclide migration. *Mineralogical Magazine*, Vol. 49, 233-244.

HILLIS, R, AND CHAPMAN, T. 1992. Variscan structure and its influence on post-Carboniferous basin development, Western Approaches Basin, SW UK Continental Shelf. *Journal of the Geological Society*, Vol. 149, 413-417.

HOLDER, A P, AND BOTT, M H P. 1971. Crustal Structure in the Vicinity of South-west England. *Geophysical Journal of the Royal Astronomical Society*, Vol. 23, 465-489.

HOLDER, M T, AND LEVERIDGE, B. 1986. Correlation of the Rhenohercynian Variscides. *Journal of the Geological Society*, Vol. 143, 141-147.

HOLDER, M T, AND LEVERIDGE, B E. 1994. A framework for the European Variscides. *British Geological Survey*, Technical Report WA/94/24 (Keyworth, Nottingham).

JACKSON, N J, WILLIS-RICHARDS, J, MANNING, D A, AND SAMS, M S. 1989. Evolution of the Cornubian ore field, Southwest England; Part II, Mineral deposits and ore-forming processes. *Economic Geology*, Vol. 84, 1101-1133.

JENKIN, A K H. 1979. *Mines and miners of Cornwall (Vol. 10 Camborne and Illogan)*. (Truro Bookshop.)

JONES, R H. 1989. Camborne Geothermal Energy Project 2C-7 Resource Evaluation: Seismic Reflection Survey. *Camborne School of Mines*.

JONES, R H. 1991. A seismic reflection survey as part of a geophysical investigation of the Carnmenellis Granite. Annual Conference of the Ussher Society, January 1991 418-420.

KILPATRICK, A, ROCHELLE, C, RUSHTON, J, LACINSKA, A, FŰZÉRI, D, CHENERY, S, MARRIOT, A, HAMILTON, E, WATTS, M, MOUNTNEY, I, AND KEMP, S. 2017. Report on metal content mobilisation using mild leaching.

KIMBELL, S F, COOPER, D C, AND SCRIVENER, R C. 2000. *The digitisation and interpretation of data from the 1957/9 airborne radiometric survey of south-west England: British Geological Survey, Regional Geophysics Series, Technical Report WK/00/04*.

KIMBELL, S F, COOPER, D C, AND SCRIVENER, R C. 2003. *The digitisation and geological interpretation of data from the 1957-9 airborne radiometric survey of south-west England*. No. 10.

KNIGHT, H, DEADY, É, GUNN, A G, MOORE, K, AND NADEN, J. 2016. Ore fluid characteristics of antimony deposits in South West England: new insights into ore genesis in Wadebridge-Port Isaac and Herodsfoot. *Applied Earth Science*, Vol. 125, 89-89.

LAW, R. 2011. Deep geothermal UK - United Downs Project, Redruth. Ground Source Live June 8th 2011.

LeBoutillier, N, Camm, G, Shail, R, Bromley, A, Jewson, C, and Hoppe, N. 2002. Tourmaline-quartz-cassiterite mineralization of the Land's End Granite at Nanjizal, west Cornwall.

LeBoutillier, N G. 2002. The Tectonics of Variscan Magmatism and Mineralisation in South West England. University of Exeter.

Ledingham, P, Cotton, L, and Law, R. 2019. The United Downs Deep Geothermal Power Project. 44th Workshop on Geothermal Reservoir Engineering. Stanford University, Stanford, California 1-11.

Lee, M K, Brown, G C, Webb, P C, Wheildon, J, and Rollin, K E. 1987. Heat flow, heat production and thermo-tectonic setting in mainland UK. *Journal of the Geological Society*, Vol. 144, 35-42.

Leveridge, B, and Hartley, A. 2006. *0 The Variscan Orogeny: the development and deformation of Devonian/Carboniferous basins in SW England and South Wales The Variscan of SW England*.

Leveridge, B E. 2002. *Geology of the Plymouth and south-east Cornwall area: memoir for 1:50 000 geological sheet 348*. (London: H.M.S.O.) ISBN 0118845608 9780118845601

Leveridge, B E, Holder, M T, Goode, A J J, Scrivener, R C, and Monkhouse, R A. 1990. *Geology of the country around Falmouth: memoir for the 1:50000 geological sheet 352*. (London: H.M.S.O.) ISBN 0118844679 9780118844673

Lough, M F, Lee, S H, and Kamath, J. 1997. A New Method To Calculate Effective Permeability of Gridblocks Used in the Simulation of Naturally Fractured Reservoirs. *SPE Reservoir Engineering*, Vol. 12, 219-224.

MacDonald, P, Stedman, A, and Symons, G. 1992. The UK geothermal hot dry rock R&D programme. Proceedings, Seventeenth Workshop on Geothermal Reservoir Engineering. Stanford University, Stanford, California 5-11.

Manning, D A C. 1998. Granites and associated igneous activity. 15 in *The Geology of Cornwall and the Isles of. Scilly*. Selwood, E B, Durrance, E M, and Bristow, C M (editors). (Exeter: Exeter University Press.)

Manning, D A C, Hill, P I, and Howe, J H. 1996. Primary lithological variation in the kaolinized St Austell Granite, Cornwall, England. *Journal of the Geological Society*, Vol. 153, 827-838.

Middleton, G V, and Hampton, M A. 1976. Subaqueous sediment transport and deposition by sediment gravity flows. 21 in *Marine sediemnt transport and environmental management*. Stanley, D J, and Switt, D J P (editors). (New York: John Wiley.)

Miller, H G, and Singh, V. 1994. Potential field tilt—a new concept for location of potential field sources. *Journal of Applied Geophysics*, Vol. 32, 213-217.

Mines, C S o. 1988. Camborne Geothermal Energy Project Viscous Stimulation of Hot Dry Rock Reservoir.

Ministry of Housing Communities & Local Government. 2015. Guidance Renewable and low carbon energy. (London, United Kingdom).

MOORBATH, S E. 1962. Lead isotope abundance studies on mineral occurrences in the British Isles and their geological significance. *Phil. Trans. R. Soc. Lond. A*, Vol. 254, 295-360.

MOORE, J M. 1975. A mechanical interpretation of the vein and dyke systems of the SW England orefield. *Mineralium Deposita*, Vol. 10, 374-388.

MOORE, J M, AND JACKSON, N. 1977. Structure and mineralization in the Cligga granite stock, Cornwall. *Journal of the Geological Society*, Vol. 133, 467-480.

MORRIS, A, HENDERSON, D B, AND FERRILL, D A. 1996. Slip-tendency analysis and fault reactivation. *Geology*, Vol. 24, 275-278.

NAMHO. 2013. The Archeology of Cobalt Mining - Cobalt assessment.

NEACE, E R, NANCE, R D, MURPHY, J B, LANCASTER, P J, AND SHAIL, R K. 2016. Zircon LA-ICPMS geochronology of the Cornubian Batholith, SW England. *Tectonophysics*, Vol. 681, 332-352.

ODA, M. 1985. Permeability tensor for discontinuous rock masses. *Géotechnique*, Vol. 35, 483-495.

PARKER, R H (editor). 1989. *Hot Dry Rock Geothermal Energy, Phase 2B Final Report of the Camborne school of Mines Project*. (Pergamon Press.)

PARKER, R H (editor). 1990. *Progress in hot dry rock technology for application in south west England (1987-1989)*.

PARKER, R H. 1991. Problems in the development of artificial geothermal energy exploitation in Cornwall. Annual Conference of the Ussher Society 316-320.

PARKER, R H. 1999. The Rosemanowes HDR project 1983–1991. *Geothermics*, Vol. 28, 603-615.

PINE, R J, JUPE, A, AND TUNBRIDGE, L W. 1990. An evaluation of in situ stress measurements affecting different volumes of rock in the Carnmenellis granite.
effects in rock masses. Loen. Norway. June 1990. International Society for Rock Mechanics first international workshop on scale.

PINE, R J, AND KWAKWA, K A. 1989. Experience with hydrofracture stress measurements to depths of 2.6 km and implications for measurements to 6 km in the Carnmenellis granite. *International Journal of Rock Mechanics and Mining Sciences & Geomechanics Abstracts*, Vol. 26, 565-571.

PINE, R J, LEDINGHAM, P, AND MERRIFIELD, C M. 1983a. In-situ stress measurement in the Carnmenellis granite—II. Hydrofracture tests at Rosemanowes quarry to depths of 2000 m. *International Journal of Rock Mechanics and Mining Sciences & Geomechanics Abstracts*, Vol. 20, 63-72.

PINE, R J, AND NICOL, D A C. 1993. Analytical and Numerical Modeling of High Pressure Fluid-Rock Mechanical Interaction in HDR Geothermal Energy Reservoirs. 523-546 in *Surface and Underground Project Case Histories*. HOEK, E (editor). (Oxford: Pergamon.) ISBN 978-0-08-042068-4

PINE, R J, TUNBRIDGE, L W, AND KWAKWA, K. 1983b. In-situ stress measurement in the Carnmenellis granite—I. Overcoring tests at South Crofty mine at a depth of 790 m. *International Journal of Rock Mechanics and Mining Sciences & Geomechanics Abstracts*, Vol. 20, 51-62.

POLLARD, P, PICHAVANT, M, AND CHAROY, B. 1987. Contrasting evolution of fluorine-and boron-rich tin systems. *Mineralium Deposita*, Vol. 22, 315-321.

PRIVE, E. 1986. Sesimic interpretation and gravity modelling of BIRPS SWAT lines 5 and 6. *British Geological Survey*.

RICHARDS, H G, WILLIS-RICHARDS, J, AND PYE, J. 1991. A review of geological investigations associated with the UK Hot Dry Rock programme
Annual Conference of the Ussher Society.

ROBERTSON, K F. 1983. Obtaining Mineral Prospecting Permissions in Southwest England. *Occasional Papers of the Institution of Mining and Metallurgy*, Vol. Legal aspects of prospecting in the United Kingdom, 1-6.

ROLLIN, K. 1988. A detailed gravity survey between Dartmoor and Bodmin Moor: the shape of the Cornubian granite ridge and a new Tertiary basin. *Proceedings of the Geologists' Association*, Vol. 99, 15-25.

ROLLIN, K E, O'BRIEN, C F, AND TOMBS, J M C. 1982. Seismic and gravity surveys over the concealed granite ridge at Bosworgy, Cornwall. *Institute of Geological Sciences*, 49 (Keyworth, Nottingham).

ROMER, R L, AND KRONER, U. 2016. Phanerozoic tin and tungsten mineralization—tectonic controls on the distribution of enriched protoliths and heat sources for crustal melting. *Gondwana Research*, Vol. 31, 60-95.

SCRIVENER, R, DARBYSHIRE, D, AND SHEPHERD, T. 1994. Timing and significance of crosscourse mineralization in SW England. *Journal of the Geological Society*, Vol. 151, 587-590.

SCRIVENER, R C (editor). 2006. *Cornubian Granites and Mineralisation of SW England*. The Geology of England and Wales. (London: The Geological Society.)

SCRIVENER, R C, SHEPHERD, T J, AND GARRIOCH, N. 1986. Ore genesis at Wheal Pendarves and South Crofty Mine, Cornwall—a preliminary fluid inclusion study. *Proceedings of the Ussher Society*, Vol. 6, 412-416.

SELWOOD, E B, DURRANCE, E M, AND BRISTOW, C M (editors). 1998. *The Geology of Cornwall and the Isles of. Scilly.* (Exeter: Exeter University Press.)

SHAIL, R, MCFARLANE, J, HASSALL, L, THIEL, H, STOCK, T, SMETHURST, M, TAPSTER, S, SCRIVENER, R, LEVERIDGE, B, AND SIMONS, B. 2017. The geological setting of the Hemerdon W–Sn deposit. *Applied Earth Science*, Vol. 126, 92-92.

SHAIL, R K, AND ALEXANDER, A C. 1997. Late Carboniferous to Triassic reactivation of Variscan basement in the western English Channel: evidence from onshore exposures in south Cornwall. *Journal of the Geological Society*, Vol. 154, 163-168.

SHAIL, R K, ANDERSEN, J O, SIMONS, B, AND WILLIAMSON, B. 2014. EUROGRANITES 2014 – Granites and mineralisation of SW England. *University of Exeter* (United Kingdom).

SHAIL, R K, AND LEVERIDGE, B E. 2009. The Rhenohercynian passive margin of SW England: Development, inversion and extensional reactivation. *Comptes Rendus Geoscience*, Vol. 341, 140-155.

SHAW, R A, DEADY, E, BATEMAN, K, AND LUSTY, P. 2016. Report on data availability: South-west England.

SHEPHERD, T, MILLER, M, SCRIVENER, R, AND DARBYSHIRE, D. 1985. Hydrothermal fluid evolution in relation to mineralization in southwest England with special reference to the Dartmoor-Bodmin area. *High Heat Production (HHP) Granites, hydrothermal circulation and ore genesis*, 345-364.

SIBSON, R, MOORE, J M M, AND RANKIN, A. 1975. Seismic pumping—a hydrothermal fluid transport mechanism. *Journal of the Geological Society*, Vol. 131, 653-659.

SIMONS, B, ANDERSEN, J, AND SHAIL, R. 2013a. *Concentrations of critical metals in the Carnmenellis biotite granite, Cornwall, UK*.

SIMONS, B, ANDERSEN, J, AND SHAIL, R. 2013b. *Distribution of critical metals in biotite and Li mica granite from Cornwall, UK*.

SIMONS, B, ANDERSEN, J, AND SHAIL, R. 2014. *Fractionation of critical metals in the granites of SW England*.

SIMONS, B, ANDERSEN, J C, SHAIL, R K, AND JENNER, F E. 2017. Fractionation of Li, Be, Ga, Nb, Ta, In, Sn, Sb, W and Bi in the peraluminous Early Permian Variscan granites of the Cornubian Batholith: precursor processes to magmatic-hydrothermal mineralisation. *Lithos*, Vol. 278, 491-512.

SIMONS, B, SHAIL, R K, AND ANDERSEN, J C Ø. 2016. The petrogenesis of the Early Permian Variscan granites of the Cornubian Batholith: Lower plate post-collisional peraluminous magmatism in the Rhenohercynian Zone of SW England. *Lithos*, Vol. 260, 76-94.

SINCLAIR KNIGHT MERZ. 2012. Geothermal Energy Potential in Great Britain and Northern Ireland. 174.

SINCLAIR, W. 1995. Vein-stockwork tin, tungsten. 409-420 in *Geology of Canadian Mineral Deposit Types*. ECKSTRAND, O R, SINCLAIR, W D, AND THORPE, R I (editors). (Geological Survey of Canada.)

SMEDLEY, P, AND ALLEN, D. 2004. Baseline report series. 16, the granites of south-west England.

SMEDLEY, P L, BROMLEY, A V, SHEPHEARD, T J, EDMUNDS, W M, AND KAY, R L F. 1989. Geochemistry in relation to Hot Dry Rock development in Cornwall, Volume 4. Fluid circulation in the Carnmenellis granite: hydrogeological, hydrogeochemical and palaeofluid evidence. *British Geological Survey*, British Geological Survey Research Report SD/89/2.

STONE, M. 1995. The main Dartmoor granites: Petrogenesis and comparisons with the Cammenellis and Isles of Scilly granites. *Proceedings-Ussher Society*, Vol. 8, 379-379.

STONE, M. 1997. A geochemical dichotomy in the Cornubian batholith. *Proceedings-Ussher Society*, Vol. 9, 206-210.

STONE, M. 2000a. The early Cornubian plutons: A geochemical study, comparisons and some implications. *Geoscience in South-West England*, Vol. 10, 37-41.

STONE, M. 2000b. Petrogenetic implications from biotite compositional variations in the Cornubian granite batholith. *Mineralogical Magazine*, Vol. 64, 729-735.

STONE, M, AND EXLEY, C S (editors). 1985. *High heat production granites of south-west England and their associated mineralisation: a review*. High Heat Production (HHP) Granites, hydrothermal circulation and ore genesis. (London: Institution of Mining and Metallurgy.)

TAMMEMAGI, H Y, AND WHEILDON, J. 1974. Terrestrial Heat Flow and Heat Generation in South-west England. *Geophysical Journal of the Royal Astronomical Society*, Vol. 38, 83-94.

TAYLOR, G K. 2007. Pluton shapes in the Cornubian Batholith: new perspectives from gravity modelling. *Journal of the Geological Society*, Vol. 164, 525-528.

TERZAGHI, R D. 1965. Sources of Error in Joint Surveys. *Géotechnique*, Vol. 15, 287-304.

THOMAS-BETTS, A, WHEILDON, J, AND SAMS, M S. 1989. Further heatflow measurement and geothermal modelling in the vicinity of Carnmenellis granite. . *Camborne School of Mines*.

TIMÓN, S, LÓPEZ MORO, F J, L. ROMER, R, RHEDE, D, FERNÁNDEZ-FERNÁNDEZ, A, AND MORO BENITO, M C. 2019. Late-Variscan multistage hydrothermal processes unveiled by chemical ages coupled with compositional and textural uraninite variations in W-Au deposits in the western Spanish Central System Batholith. No. 17.

TINDLE, A G. 2008. *Minerals of Britain and Ireland*. (Terra Publishing.) ISBN 190354422X

TOMBS, J M C. 1977. A study of the space form of the Cornubian granite batholith and its application to detailed gravity surveys in Cornwall. *Institute of Geological Sciences*, 11 (Keyworth, Nottingham).

TUNBRIDGE, L W, COOLING, C M, AND HAIMSON, B C. 1989. Measurement of rock stress using the hydraulic fracturing method in Cornwall, U.K.—Part I. field measurements. *International Journal of Rock Mechanics and Mining Sciences & Geomechanics Abstracts*, Vol. 26, 351-360.

UNESCO. 2006. Nomination of the Cornwall and West Devon Mining Landscape for inclusion on the World Heritage List.

WARDELL ARMSTRONG. 2010a. 4 Socio-economic and environmental benefits NR/10/00056/GEO. Planning Application Documents. cornwall.gov.uk.

WARDELL ARMSTRONG. 2010b. 11 Public consultation NR/10/00056/GEO. Planning Application Documents. cornwall.gov.uk.

WESTHEAD, K, HOLDEN, A, SCHOFIELD, D, HASLAM, R, LOVELESS, S, BLOOMFIELD, J P, LEE, J R, BAPTIE, B, SHAW, R P, BIDE, T, AND MCEVOY, F M. 2017. National Geological Screening: South-

west England region. *British Geological Survey*, Commissioned Report CR/17/095 (Keyworth, Nottingham).

WHEILDON, J, M.F., F, J.R.L, E, AND A., T-B. 1981. Investigation of the S.W. England thermal anomaly zone. CEC Final Report, Contract No 097-76 EGUK, 568-78-1 EGUK. (Brussels).

WILLIS-RICHARDS, J, AND BARIA, R. 1989. Camborne Geothermal Energy Project 2C-7 Resource Evaluation: Gravity and Themal Modelling. *Camborne School of Mines*.

WILLIS-RICHARDS, J, AND JACKSON, N J. 1989. Evolution of the Cornubian ore field, Southwest England; Part I, Batholith modeling and ore distribution. *Economic Geology*, Vol. 84, 1078-1100.

WILLIS-RICHARDS, J, JONES, R H, AND BARIA, R. 1989. Camborne Geothermal Energy Project 2C-7 Resource Evaluation: Overview. *Camborne School of Mines*.

WILSON, A, AND TAYLOR, R. 1976. *Stratigraphy and sedimentation in west Cornwall*.

YEOMANS, C. 2017. *Tellus South West data usage: a review (2014–2016)*. No. 3.

YEOMANS, C. 2018. Enhancing the Geological Understanding of Southwest England Using Machine Learning Algorithms. University of Exeter.

YEOMANS, C M, MIDDLETON, M, SHAIL, R K, GREBBY, S, AND LUSTY, P A J. 2019. Integrated Object-Based Image Analysis for semi-automated geological lineament detection in southwest England. *Computers & Geosciences*, Vol. 123, 137-148.

YOUNGER, P L, AND MANNING, D A C. 2010. Hyper-permeable granite: lessons from test-pumping in the Eastgate Geothermal Borehole, Weardale, UK. *Quarterly Journal of Engineering Geology and Hydrogeology*, Vol. 43, 5-10.

Appendix 1 Borehole data used to determine the depth to granite surface.

Bore hole name	BGS ID	Hyperlink	Granite intersection depth m	**Total depth**	Azimuth	Inclination	Easting	Northing
Baltrink 11	658977	http://bgsintranet/ImageConverter/ScanToPdf?group_id=658977&type=0	0	244	314	-55	150470	37420
Bosworgy 1	622890	http://bgsintranet/ImageConverter/ScanToPdf?group_id=622890&type=0	170.76	214		vertical	158060	33670
CLV 17	702987	http://bgsintranet/ImageConverter/ScanToPdf?group_id=702987&type=0	155.83	695.4	301	-45	164200	37170
CM1	689090	http://bgsintranet/ImageConverter/ScanToPdf?group_id=689090&type=0	205	346	327.5	-45	165276	37859
CM3	689091	http://bgsintranet/ImageConverter/ScanToPdf?group_id=689091&type=0	33	1040.7	327	-45	165733	38078
CTL 18	689068	http://bgsintranet/ImageConverter/ScanToPdf?group_id=689068&type=0	217	236.22	330	-55	165470	38060
CTL10	689064	http://bgsintranet/ImageConverter/ScanToPdf?group_id=689064&type=0	2.5	663	338	-55	166660	39180
CTL11	689065	http://bgsintranet/ImageConverter/ScanToPdf?group_id=689065&type=0	21.5	121.92	328	-50	166480	39060
CTL13	689066	http://bgsintranet/ImageConverter/ScanToPdf?group_id=689066&type=0	0	144.78	330	-55	165950	37950
CTL17	689067	http://bgsintranet/ImageConverter/ScanToPdf?group_id=689067&type=0	0	124.96	338	-75	166660	39180
CTL19	689069	http://bgsintranet/ImageConverter/ScanToPdf?group_id=689069&type=0	0	647.09	338	-55	166580	39400
CTL22	689070	http://bgsintranet/ImageConverter/ScanToPdf?group_id=689070&type=0	214	459.02	330	-55	165470	37710
CTL27	689073	http://bgsintranet/ImageConverter/ScanToPdf?group_id=689073&type=0	0	429.15	330	-60	165990	38010

CTL27	689059	http://bgsintranet/ImageConverter/ScanToPdf?group_id=689059&type=0	0	217.32	328	-50	166780	38870
CTL4	689060	http://bgsintranet/ImageConverter/ScanToPdf?group_id=689060&type=0	0	193.54	328	-49	166550	38710
CTL6	689061	http://bgsintranet/ImageConverter/ScanToPdf?group_id=689061&type=0	0	121.92	309	-48	16690	38940
CTL7	689062	http://bgsintranet/ImageConverter/ScanToPdf?group_id=689062&type=0	0	171.6	328	-50	166660	38810
D3	618452	http://bgsintranet/ImageConverter/ScanToPdf?group_id=618452&type=0	556	793	358	-50	242740	73320
East pool new shaft Taylors	714113	http://bgsintranet/ImageConverter/ScanToPdf?group_id=714113&type=0	353	573	unknown	unknown	167420	41870
GFL1	689087	http://bgsintranet/ImageConverter/ScanToPdf?group_id=689087&type=0	114.24	340		vertical	165630	38160
GFL2	689088	http://bgsintranet/ImageConverter/ScanToPdf?group_id=689088&type=0	191.23	330		vertical	165470	38040
IMS 14	610069	http://bgsintranet/ImageConverter/ScanToPdf?group_id=610069&type=0	25.6	159.1	357	-45	226280	71430
IMS 16	610070	http://bgsintranet/ImageConverter/ScanToPdf?group_id=610070&type=0	6	237.74	0	-55	226240	71190
IMS 6	618442	http://bgsintranet/ImageConverter/ScanToPdf?group_id=618442&type=0	0	238.65	164.5	-50	242090	71840
IMS20	610071	http://bgsintranet/ImageConverter/ScanToPdf?group_id=610071&type=0	0	134.25	0	-45	226820	71210
IMS22	610072	http://bgsintranet/ImageConverter/ScanToPdf?group_id=610072&type=0	0	160.02	180	-50	226740	71150
IMS30	610073	http://bgsintranet/ImageConverter/ScanToPdf?group_id=610073&type=0	0	124.96	180	-45	226640	71220
IMS7 Calstock	618443	http://bgsintranet/ImageConverter/ScanToPdf?group_id=618443&type=0	249	481.58	147	-45	240460	71650

KB 83-1A	658491	http://bgsintranet/scripts/ida/boreholescan/dispBorehole.cfm?bgsID=658491	456	429		-90	236020	71490
KB85-3	658437	http://bgsintranet/ImageConverter/ScanToPdf?group_id=658437&type=0	265.7	400	True north	-45	236320	71270
KB86-4	658438	http://bgsintranet/scripts/IDA/boreholescan/dispBorehole.cfm?bgsid=658438	317	493.25	177	-45	236130	71880
MENNOR 1	658973	http://bgsintranet/ImageConverter/ScanToPdf?group_id=658973&type=0	43	150.57	358	-45	152690	36600
Pendarves P4	689078	http://bgsintranet/ImageConverter/ScanToPdf?group_id=689078&type=0	155	172	147	-45	165040	37550
Pendarves B1	702962	http://bgsintranet/ImageConverter/ScanToPdf?group_id=702962&type=0	64	304.8	147	-45	165810	39050
Pendarves B2	702963	http://bgsintranet/ImageConverter/ScanToPdf?group_id=702963&type=0	128	257.25	147	-45	164910	38920
Pendarves B9	702956	http://bgsintranet/ImageConverter/ScanToPdf?group_id=702956&type=0	150	243.23	147	-45	164580	38590
Pendarves DDH 200	689092	http://bgsintranet/ImageConverter/ScanToPdf?group_id=689092&type=0	0	261	151.5	1	165020	38010
Pendarves DDH 201	689093	http://bgsintranet/ImageConverter/ScanToPdf?group_id=689093&type=0	0	152.37	151.5	36	165020	38010
Pendarves DDH 202	689094	http://bgsintranet/ImageConverter/ScanToPdf?group_id=689094&type=0	0	271	141	-1	165160	38090
Pendarves DDH 208	689096	http://bgsintranet/ImageConverter/ScanToPdf?group_id=689096&type=0	0	210	95.5	21	165160	38090
Pendarves E1	702960	http://bgsintranet/ImageConverter/ScanToPdf?group_id=702960&type=0	182	203	333	-45	164480	38730
Pendarves F1	702957	http://bgsintranet/ImageConverter/ScanToPdf?group_id=702957&type=0	0	151.48	327	-45	164820	38160
Pendarves F2	702966	http://bgsintranet/ImageConverter/ScanToPdf?group_id=702966&type=0	97	142.95	327	-45	164780	38250
Pendarves F4	702983	http://bgsintranet/ImageConverter/ScanToPdf?group_id=702983&type=0	185	316.38	329	-45	164550	38130

Pendarves G1	702967	http://bgsintranet/ImageConverter/ScanToPdf?group_id=702967&type=0	340.5	343.2	147	-45	164260	39000
Pendarves G2	702980	http://bgsintranet/ImageConverter/ScanToPdf?group_id=702980&type=0	257.18	265	147	-45	166440	38860
Pendarves Q2	702946	http://bgsintranet/ImageConverter/ScanToPdf?group_id=702946&type=0	94	161.54	147	-45	164930	37980
Pendarves Q3	702947	http://bgsintranet/ImageConverter/ScanToPdf?group_id=702947&type=0	23	170	327	-45	164880	38070
Pendarves Q4	702943	http://bgsintranet/ImageConverter/ScanToPdf?group_id=702943&type=0	36	152.7	327	-45	164550	37730
Pendarves Q5	702944	http://bgsintranet/ImageConverter/ScanToPdf?group_id=702944&type=0	30.5	151.79	327	-45	164500	37700
Pendarves Q6	702945	http://bgsintranet/ImageConverter/ScanToPdf?group_id=702945&type=0	25	150.57	327	-45	164450	37670
Pendarves R4	702952	http://bgsintranet/ImageConverter/ScanToPdf?group_id=702952&type=0	125	152.7	147	-45	164600	38560
Pendavres DH 203	689095	http://bgsintranet/ImageConverter/ScanToPdf?group_id=689095&type=0	0	351	115	-1	165160	38090
RADNOR 16	657228	http://bgsintranet/ImageConverter/ScanToPdf?group_id=657228&type=0	362	850	337	-75	172000	44300
RADNOR 3	657226	http://bgsintranet/ImageConverter/ScanToPdf?group_id=657226&type=0	428.5	609.6	329	-50	172160	44300
RADNOR 5	657230	http://bgsintranet/ImageConverter/ScanToPdf?group_id=657230&type=0	439	467.56	343	-50	171720	44230
RH15	625306	http://bgsintranet/ImageConverter/ScanToPdf?group_id=625306&type=0	0	2610.5	357.7	29.4	173555	34590
RH6	625300	http://bgsintranet/ImageConverter/ScanToPdf?group_id=625300&type=0	0	309	unknown assume vertical		173464	34548
RH8(B)	625301	http://bgsintranet/ImageConverter/ScanToPdf?group_id=625301&type=0	0	304	unknown assume vertical		173468	34567
RH9(D)	625302	http://bgsintranet/ImageConverter/ScanToPdf?group_id=625302&type=0	0	305	unknown assume vertical		173484	34569

RM80-11	658489	http://bgsintranet/ImageConverter/ScanToPdf?group_id=658489&type=0	482.15	500	356	-45	360700	71130
RM82-29	658481	http://bgsintranet/ImageConverter/ScanToPdf?group_id=658481&type=0	522	699.5	177	-50	235990	71440
Roughter D2	608638	http://bgsintranet/ImageConverter/ScanToPdf?group_id=608638&type=0	50.55	114	unknown	-60	216350	82770
Roughtor D4	608640	http://bgsintranet/ImageConverter/ScanToPdf?group_id=608640&type=0	89.85	117	unknown	-74	216210	82810
S.C. 1	689054	http://bgsintranet/ImageConverter/ScanToPdf?group_id=689054&type=0	0	416.05	330	-50	166520	39530
S.C. 3	689056	http://bgsintranet/ImageConverter/ScanToPdf?group_id=689056&type=0	0	422.14	330	-60	166230	39380
S.C. 4	689057	http://bgsintranet/ImageConverter/ScanToPdf?group_id=689057&type=0	0	403.86	335	-60	166090	39320
S.C.2	689055	http://bgsintranet/ImageConverter/ScanToPdf?group_id=689055&type=0	0	354.17	330	-60	166310	39530
S.C.5	689058	http://bgsintranet/ImageConverter/ScanToPdf?group_id=689058&type=0	0	533.09	330	-50	166360	39760
SJ1	615290	http://bgsintranet/ImageConverter/ScanToPdf?group_id=615290&type=0	421.17	846.98	251	-45	135070	31770
SJ2	615291	http://bgsintranet/ImageConverter/ScanToPdf?group_id=615291&type=0	0	557.78	247	-45	135380	31380
SJ3	615292	http://bgsintranet/ImageConverter/ScanToPdf?group_id=615292&type=0	649.41	355.32	267	-45	136580	34220
SJ4	615293	http://bgsintranet/ImageConverter/ScanToPdf?group_id=615293&type=0	133.01	322	44	-45	136660	34010
SJ5	615294	http://bgsintranet/ImageConverter/ScanToPdf?group_id=615294&type=0	1161	1192	267	-45	136690	34390
Stithians	625307	http://bgsintranet/ImageConverter/ScanToPdf?group_id=625307&type=0	0	309	unknown assume vertical		173460	34540
TRDD2013001	19905551	http://bgsintranet/ImageConverter/ScanToPdf?group_id=19905551&type=0	484	544.5	294	-65	191920	60741

Trebowland Manor	618330	http://bgsintranet/ImageConverter/ScanToPdf?group_id=618330&type=0	0	110	No data	No data	173100	38900
TS1	658962	http://bgsintranet/ImageConverter/ScanToPdf?group_id=658962&type=0	0	271.27	306.5	-75	150540	37350
TS12	658972	http://bgsintranet/ImageConverter/ScanToPdf?group_id=658972&type=0	0	198	314	-50	150720	37660
TS3	658964	http://bgsintranet/ImageConverter/ScanToPdf?group_id=658964&type=0	0	375.51	306.5	-72	150580	37280
TS4	658965	http://bgsintranet/ImageConverter/ScanToPdf?group_id=658965&type=0	0	223.11	306.5	-65	150750	37830
TS5	658966	http://bgsintranet/ImageConverter/ScanToPdf?group_id=658966&type=0	0	375.81	306.5	-72	150690	37340
TS6	658967	http://bgsintranet/ImageConverter/ScanToPdf?group_id=658967&type=0	43	308.15	306.5	-72	150800	37390
TS7	658968	http://bgsintranet/ImageConverter/ScanToPdf?group_id=658968&type=0	0	366.36	313	-72	150920	37430
Wheal Grenville No 25	689072	http://bgsintranet/ImageConverter/ScanToPdf?group_id=689072&type=0	78.5	436.77	330	-60	165960	38370
Wheal Vor CTL 15	612498	http://bgsintranet/ImageConverter/ScanToPdf?group_id=612498&type=0	330	347.77		vertical	161510	29900
Wheal Vor CTL 35	612500	http://bgsintranet/ImageConverter/ScanToPdf?group_id=612500&type=0	350	429.15	155	-50	161650	29880

Appendix 2 Extracts from the RH15 core log.

7356 3459

HOT DRY ROCK GEOTHERMAL ENERGY PROJECT
CAMBORNE SCHOOL OF MINES

Measured Depth (MD) 2274.4 - 2284.7 m
Trud Depth (TD) 2185.4 - 2194.4 m

WELL RH15
Core L
Sheet 1 of 3

Machine National 80UE, Kenting Rig K31
Core Barrel Hycalog 6½ in x 2⅜ in x 45 ft, double swivel
Bit Design Security H99F, 8½ x 2⅜ in 6-cone TC insert

Wellhead Coordinates SW 173555 34594
Wellhead Elevation 161.83 m AOD
Inclination 28.6° Azimuth 359.5°

Core Photograph	Fracture/Vein Relative Dip (vein width)	Fracture/Vein Relative Azimuth	Physical Description of Discontinuities	Symbolic Fracture Log	Lengths of Matching Core	Core Length (m)	Geological Description: Rock Fabric	Geological Description: Alteration	Geological Description: Vein/Fracture Mineralogy
			smooth to rough, rounded drilling break			0.00			
	1: 75° (<0.5 mm)	Ref	1 vein				Fine-medium grained equigranular granite		1: Reddened vein
			2 fresh, hackled drilling break						
	3: 75°	0°	3 smooth to rough, planar						3: Reddened
			4 smooth, rounded, drilling break					Slight Reddening	
			5 rough drilling break, some grinding			0.50			
			6 fresh, hackled drilling break						
	7: 85°	Ref	7 rough, planar						7: Chlorite
	8: 20°	+180°	8 rough drilling break, some grinding						
			9 smooth, planar drilling break					Reddening decreases	
	10: 90° (1 mm)		10 vein						10: Quartz/Chlorite
	11: 70° (1 mm)	Ref	11 vein						11: Quartz/Chlorite
	12: 70° (1 mm)	0°	12 vein			1.00			12: Quartz/Chlorite
	13: 50°	-150°	13 rough, planar drilling break?						13: None
	14: 75°	+90°	14 rough, planar						14: Trace light green mineral
	15: 40°	+30°	15 fresh, hackled drilling break					Trace Reddening	
			16 rough drilling break, some grinding						
	17: 55°	Ref	17 rough, angular						17: Reddened
	18: 85° (<0.5 mm)	-150°	18 vein						18: Chlorite
	19: 85° (<0.5 mm)	-150°	19 vein			1.50			19: Chlorite
			20 fresh, angular drilling break						
	21: 90°		21 smooth, planar						21: None
			22 fresh, hackled drilling break						
	23: 90°	Ref	23 fresh, hackled drilling break						
			24 smooth, planar drilling break						
	25: 80° (2 mm)	Ref	25 vein						25: Tourmaline?
	26: 80° (1 mm)	-140°	26 vein			2.00			26: Quartz/Chlorite Sulphides
	27: 30°	-140°	27 fresh, planar drilling break?						27: None
			28 rough to smooth, planar drilling break						
			29 fresh, hackled drilling break						
	30: 70°	+90°	30 rough, planar						30: None
			31 rough to smooth, planar drilling break						
	32: 80° (1 mm)	-140°	32 vein						32: Chlorite/Quartz
			33 fresh, hackled drilling break			2.50			
	34: 70°	-40°	34 rough, planar						34: None
	35: 80° (1 mm)	-140°	35 vein						35: Chlorite/Quartz
	36: 80° (1 mm)	-140°	36 vein						36: Chlorite/Quartz
			37 vein						
	38: 80°	-140°	38 rough, some grinding						3: Chlorite
			39 smooth, rounded, drilling break			2.90			

Total Solid Recovery (%) 64

Logged by RMcC
Date Jan 1985

SW 73 SW/11
7356 3459

HOT DRY ROCK GEOTHERMAL ENERGY PROJECT
CAMBORNE SCHOOL OF MINES

Measured Depth (MD) 2274.4 - 2284.7 m
True Depth (TD) 2185.4 - 2194.4 m

WELL RH15
Core L
Sheet 2 of 3

Machine National 80UE, Kenting Rig K31
Core Barrel Hycalog 6½ in x 2⅝ in x 45 ft, double swivel
Bit Design Security H99F, 8⅜ x 2⅝ in 6-cone TC insert

Wellhead Coordinates SW 173555 34594
Wellhead Elevation 161.83 m AOD
Inclination 28.6° Azimuth 359.5°

Core Photograph	Fracture/Vein Relative Dip (vein width)	Fracture/Vein Relative Azimuth	Physical Description of Discontinuities	Symbolic Fracture Log	Lengths of Matching Core	Core Length (m)	Geological Description: Rock Fabric	Geological Description: Alteration	Geological Description: Vein/Fracture Mineralogy
						2.90			
	40: 85° (0.5 mm)	Ref	40 vein	40			Fine-medium grained equigranular granite		40: Chlorite/Quartz
			41 fresh, hackled drilling break	41					
			42 fresh, hackled drilling break	42					
			43 fresh, hackled drilling break						
	44: 70°	-100°	44 smooth, planar	43					44: Chlorite
			45 rough, drilling break						
			46 rough drilling break, some grinding	44		3.50			
			47 rough drilling break, some grinding	45 47 46					
			48 smooth, planar drilling break	48					
			49 smooth, planar drilling break	49					
			50 rough to smooth, drilling break	50					
	51: 70°	Ref	51 rough, planar			4.00		Trace Reddening	51: Chlorite with silicified margin
			52 rough drilling break, some grinding	51					
			53 smooth, rounded, drilling break	52 53					
	54: 70° (1 mm)	0°	54 vein	54					54: Chlorite/ Sulphides
			55 rough to smooth, rounded, drilling break						
	56: 30°	Ref	56 rough to smooth, rounded, drilling break	55 56		4.50			
			57 rough drilling break, some grinding	57 58					
	58: 75°	Ref	58 rough, planar					Slight Reddening	Brown 58: Carbonate
			59 smooth, planar drilling break						
			60 rough, drilling break	59		5.00			
			61 smooth, planar drilling break	60 61					
	62: 60° (1 mm)	Ref	62 vein	62				Slight Reddening with silicified zone	62: Chlorite
	63: 60° (1 mm)	+10°	63 vein	63					63: Chlorite
			64 smooth, planar drilling break	65 64		5.50			
			65 smooth, planar drilling break						
	66: 50°	Ref	66 rough, planar	66				Trace Reddening	66: None
			67 smooth, planar drilling break	67		5.70			

Total Solid Recovery (%) 64

Logged by RMcC
Date Jan 1985

7356 3459

HOT DRY ROCK GEOTHERMAL ENERGY PROJECT
CAMBORNE SCHOOL OF MINES

Measured Depth (MD) 2274.4 - 2284.7 m
True Depth (TD) 2185.4 - 2194.4 m

WELL RH15
Core L
Sheet 3 of 3

Machine National 80UE, Kenting Rig K31
Core Barrel Hycalog 6½ in x 2⅝ in x 45 ft, double swivel
Bit Design Security H99F, 8⅜ x 2⅝ in 6-cone TC insert

Wellhead Coordinates SW 173555 34594
Wellhead Elevation 161.83 m AOD
Inclination 28.6° Azimuth 359.5°

Core Photograph	Fracture/Vein Relative Dip (vein width)	Fracture/Vein Relative Azimuth	Physical Description of Discontinuities	Symbolic Fracture Log	Lengths of Matching Core	Core Length (m)	Geological Description: Rock Fabric	Geological Description: Alteration	Geological Description: Vein/Fracture Mineralogy
	68: 75°	Ref	68 rough, planar drilling break			5.70	Fine-medium grained equigranular granite		
	69: 75° (2 mm)	-90°	69 vein					Silification	69: Chlorite
	70: 60°	+180°	70 rough, planar drilling break						
			71 smooth, planar drilling break						
			72 smooth, drilling break					Slight Reddening	
						6.00			
	73: 65°	Ref	73 rough, planar						Brown 73: Carbonate
			74 smooth, planar drilling break				Low mafic content	Trace Reddening	
			75 smooth, rounded, drilling break						
			76 angular rough to smooth drilling break					Medium Reddening	
								Strong Reddening	
	77: 65°	Ref	77 smooth, rounded, drilling break			6.50			
			78 smooth, planar drilling break						
	79: 70° (<0.5 mm)	Ref	79 vein						79: Chlorite
	80: 70°	0°	80 rough, angular						80: Chlorite
			81 smooth, rounded, drilling break						
	82: 70°		82 smooth, angular drilling break						
	83: 70° (5 mm)	Ref	83 vein						83: Chlorite/Quartz
			84 smooth, rounded, drilling break						

Total Solid Recovery (%) 64

Logged by RMk
Date Jan 198[illegible]

Appendix 3 Properties simulated, interpolate or calculated through the model volume.

Property	Source	Units	Method
BrazillianTensileStrength	CSM Report 2A-46 Mechanical Properties of the Carnmenellis Granite HDR Report 3,3,1	MPa	BrazillianTensileStrength = 10.6 + 1.1 * (DepthBelowSurface / 1000)
DepthBelowSurface		m	Calculated from model
DistancetoFault		m	Calculated from model
DistancetoGranite		m	Calculated from model
GraniteDensity	CSM Report 2A-46 Mechanical Properties of the Carnmenellis Granite HDR Report 3,3,1	Kg/m^3	Granite = 2640
GraniteThickness		m	Calculated from model
HeatFlow	Wheildon and Rollins 1986. eq 2.5 and 2.6	mWm^{-2}	For depths Greater than 300m below ground level HeatFlow= (2 * 833.33 * ThermalConductivityMean * log ((TemperatureHDRGradient + 823.33) / 833.33) + (HeatProductionBeamishCoKrig * pow((DepthBelowSurface / 1000), 2)))/(2 * (DepthBelowSurface / 1000))
HeatFlowInverse	Wheildon and Rollins 1986. eq 2.5 and 2.14	mWm^{-2}	For depths Greater than 300m below ground level HeatFlowInverse = (ThermalConductivityMean * 833.33 * log(((TemperatureHDRGradient + 823.33) / 833.3))+(HeatProductionBeamishCoKrig / pow(0.1,2) * (1-(0.1 * (DepthBelowSurface / 1000) + 1)*(1 - (log(0.1 * (DepthBelowSurface / 1000) + 1))))))/(DepthBelowSurface / 1000);}
HeatFlowMeanNormDistCorrAFrancis1980	Francis (1980)	mWm^{-2}	Simulated from a Normal Distribution Granite – Mean = 116 SD=9 Killas – Mean =59 SD=10

HeatFlowRichardsonOxburgh1979	In Francis (1980) eq5.6 (after Richardson and Oxburgh 1979)	mWm^{-2}	HeatFlowRichardsonOxburgh1979= 27 + (16.6 * HeatProductionBeamishCoKrig); This is known to under estimate the heat flow (Beamish and Busby, 2016)
HeatProductionBeamishCoKrig	Beamish and Busby (2016)	uWm^{-3}	Co-Kriging simulation of the Heat production model from beamish cross correlated with log of the inverse distance from granite with a correlation coefficient of 0.5. The variogram had sill of 0.501789, exponential, R1 = 14422.9, R2 = 18585.6, R3 = 262196 and an azimuth of 3.15886 and nugget of 0.
HeatProductionBeamishCoKrigExpoDecrease	Wheildon and Rollins 1986. eq 2.9	uWm^{-3}	HeatProductionBeamishCoKrigExpoDecrease = HeatProductionBeamishCoKrig * exp(-(DepthBelowSurface / 1000) / 16.6);
HeatProductionBeamishCoKrigInverse	Wheildon and Rollins 1986. eq 2.13	uWm^{-3}	HeatProductionBeamishCoKrigInverse = HeatProductionBeamishCoKrig / (0.1 * (DepthBrlowSurface / 1000) +1);
PoissonsRation	Parker 1991		For granite only. PoissonsRatio = urand(0.22 ,0.27);
PoissonsRationTemperatureYu2014	Yu 2014		Change in Poissons Ratio in response to increase in temperature PoissonsRatioTemperatureYu2014 = 0.0004 * TemperatureKHDRGeothermalGradient + 0.22;

Regions			Calculated from model 1=Killas 2=Upper Granite 3=Lower Granite
SHMaxAzimuth		°	Based on SHINE (Carafa et al., 2014) interpolation of World Stress Map 2016 data (Heidbach et al. 2016)
SHMaxMagnitude	Parker 1991	MPa	SHmax = 15 + 28 * (DepthBelowSurface / 1000)
ShminAzimuth		°	Based on SHINE (Carafa et al, 2014) interpolation of World Stress Map 2016 data (Heidbach et al. 2016)
ShminMagnitude	Parker 1991	MPa	Shmin = 6 + 12*(DepthBelowSurface / 1000)
SpecificHeatCapacity	Lindroth and Krawza 1971 in Jackson et al. 1989	$Jg^{-1}K^{-1}$	SpecificHeatCapacity= 4.186 * (0.209334 + 0.000131034 * TemperatureHDRGradient);
SurfaceTemperature	Francis 1980	°C	11
SvMagnitude	Parker 1991	MPa	SvMagnitude = 26 * (DepthBelowSurface / 1000)
TemperatureHDRGradient	Parker 1991	°C	TemperatureHDRGradient = 0.035 * DepthBelowSurface + 12;
TemperatureHaenel1980	Haenel 1980 (Francis 1980 eq5.1)	°C	TemperatureHaenel1980 = SurfaceTemp + (HeatFlowMeanNormDistCorrAFrancis1980 * (-1 * (DepthBelowSurface / 1000)) / ThermalConductivityMean) - (HeatProductionBeamishCoKrig * (-1 * DepthBelowSurface / 1000)/(2 * ThermalConductivityMean));
TemperatureHaenel1980RichardsonOxbughHeatFlow	Francis 1980 eq5.4	°C	Change in Temperature with constant heat production but with temperature dependant thermal conductivity TemperatureHaenel1980Richardson = SurfaceTemperature + ((HeatFlowRichardsonOxburgh1979 * (DepthBelowSurface / 1000)) / ThermalConductivity) - ((HeatProductionBeamishCoKrig * pow(DepthBelowSurface / 1000,2)) / (2 * ThermalConductivity));
TemperatureKHDRGradient	Parker 1991	K	Temperature at depth in Kelvin based on HDR geothermal gradient TemperatureKHDRGradient = TemperatureHDRGradient + 273.15;
ThermalDiffusivity	Vosteen and Schellschmidt 2003 Eq. 3	m^2s^{-1}	ThermalDiffusivity = ThermalConductivity / (GraniteDensity * SpecificHeatCapacity);

ThermalConductTempKappelmyerHaenel1974	Kappelmeyer and Haenel, 1974 in Wheildon and Rollins 1986	$Wm^{-1}K^{-1}$	ThermalConductTempKappelmyerHaenel1974 = ThermalConductivityMean * 833.33 / (823.33 + TemperatureHDRGradient);
ThermalConductivity	Granite – Francis 1980 Killas - Kappelmeyer and Haenel, 1974	$Wm^{-1}K^{-1}$	Granite ThermalConductivity = -0.41 * log(TemperatureHDRGradient) + 4.0; Killas - Perpendicular to bedding ThermalConductivity= -0.056 * log(TemperatureHDRGradient) + 2.0302;
ThermalConductivityMean	Francis 1980	$Wm^{-1}K^{-1}$	Granite – ThermalConductivity = 3.33 Killas – ThermalConductivity = 2.5
ThermalConductivitySartori1983	Sartori 1983 in Jackson et al. 1989	$Wm^{-1}K^{-1}$	Granite ThermalConductivitySartori1983 = 574.8 / TemperatureKHDRGradient + 1.30;
ThermalExpansionCoefficientHeuze1983	Heuze 1983 in Jackson et al. 1989	K-1	Granite ThermalExpansionCoefficientHeuze1983 = 0.000005 + (TemperatureHDRGradient / 920) * 0.000018;
ThicknessLowerGranite		m	Calculated from model
ThicknessUpperGranite		m	Calculated from model
TriaxialCompressiveStrength	Mechanical Properties of the Carnmenellis Granite HDR Report 3,3,1	MPa	Granite TriaxialCompressiveStrength = 132 + (37 * (DepthBelowSurface / 1000));
UniaxialCompressiveStrength	Mechanical Properties of the Carnmenellis Granite HDR Report 3,3,1	MPa	Granite UniaxialCompressiveStrength = 32 * (DepthBelowSurface / 1000) + 103:
UniaxialCompressiveStrengthTemperatureYu2014	Yu et al. 2014	MPa	Granite UniaxialCompressiveStrengthTemperatureYu2014 = -0.0001 * pow(TemperatureHDRGradient,2) - 0.0284 * TemperatureHDRGradient + 103;
YoungsModulus	Mechanical Properties of the Carnmenellis Granite HDR Report 3,3,1	GPa	Granite YoungsModulus = 54 + (4 * (DepthBelowSurface / 1000));

YoungsModulusTemperatureHeuze1983	Heuze 1983 in Jackson et al. 1989	GPa	Granite YoungsModulusTemperatureHeuze1983 = ((90 + (4 * (DepthBelowSurface / 1000))) * (1000 - TemperatureKHDRGradient)) / 1000;
YoungsModulusTemperatureYu2014	Yu et al. 2014	GPa	Granite YoungsModulusTemperatureYu2014 = -0.0002 * pow(TemperatureHDRGradient,2) + 0.0515 * TemperatureHDRGradient + 54;

Appendix 4 Fracture density statistics and histograms from calculated fracture density.

Property	Mean	SD	Low Cut off	High Cut off	
FS1 Low	0.354883	0.222659	0	1.18521	

					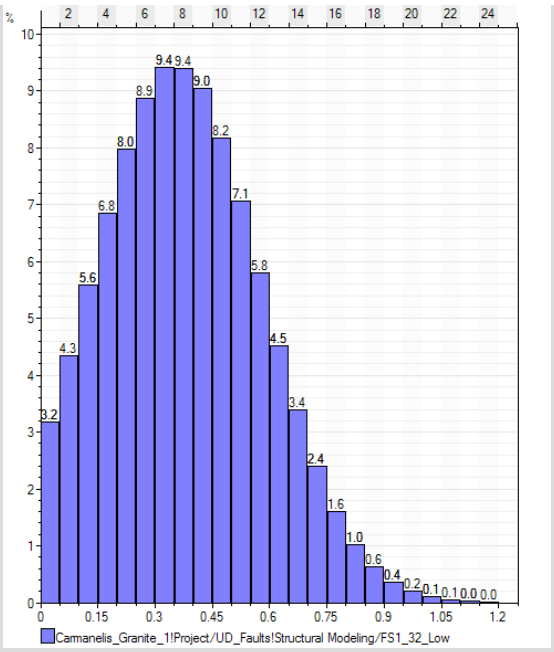
FS1 Mean	0.493334	0.403768	0	1.85008	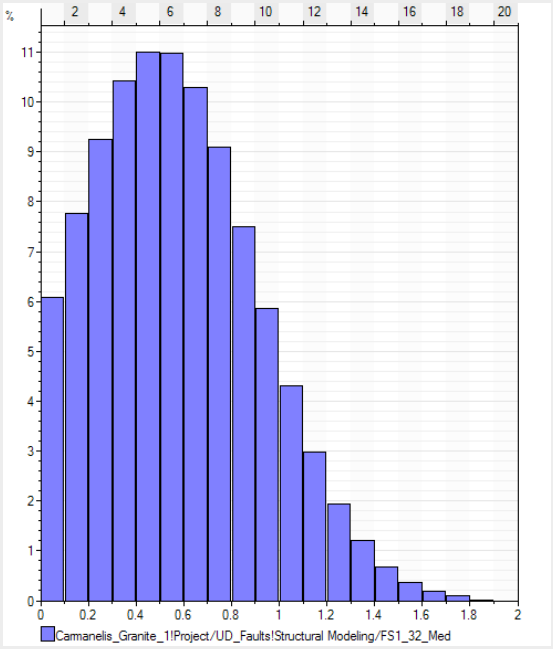
FS1 High	1.51089	0.64597	0	2.9548	

					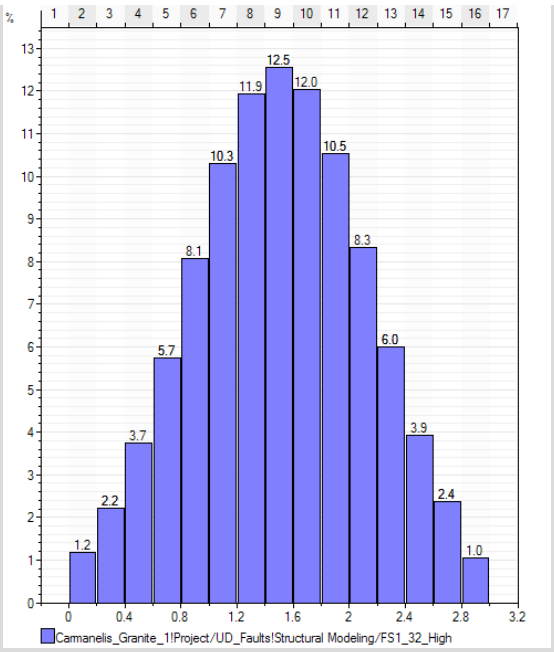
FS2 Low	0.732625	0.435894	0	2.02774	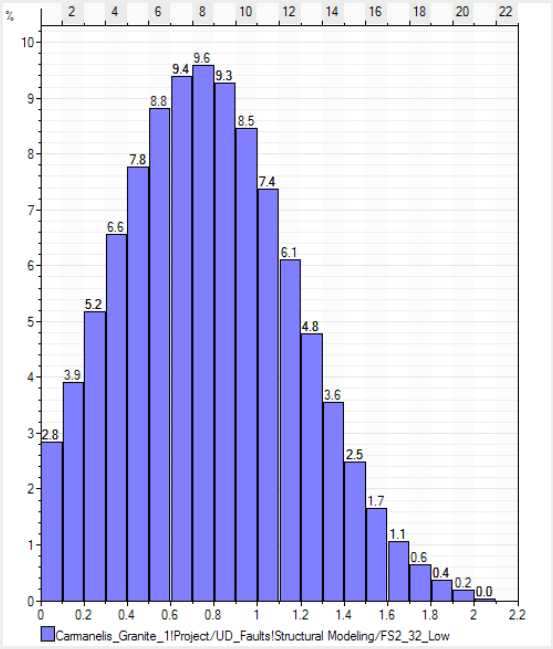

FS2 Mean	1.11078	0.614915	0	2.8212	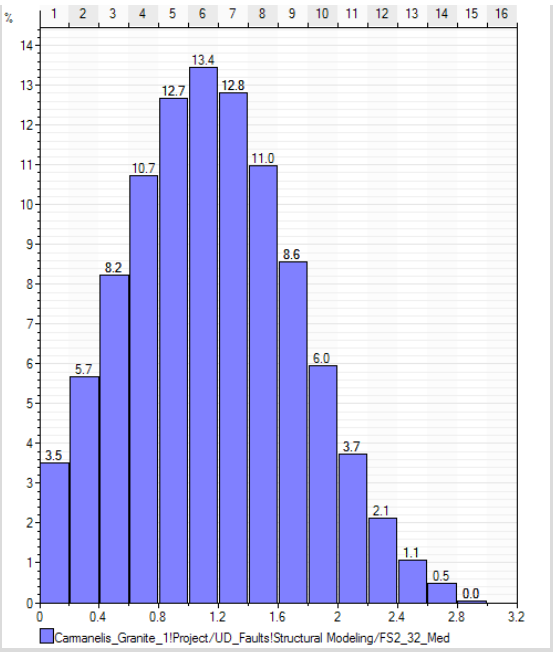
FS2 High	2.030668	0.862203	0	4.14364	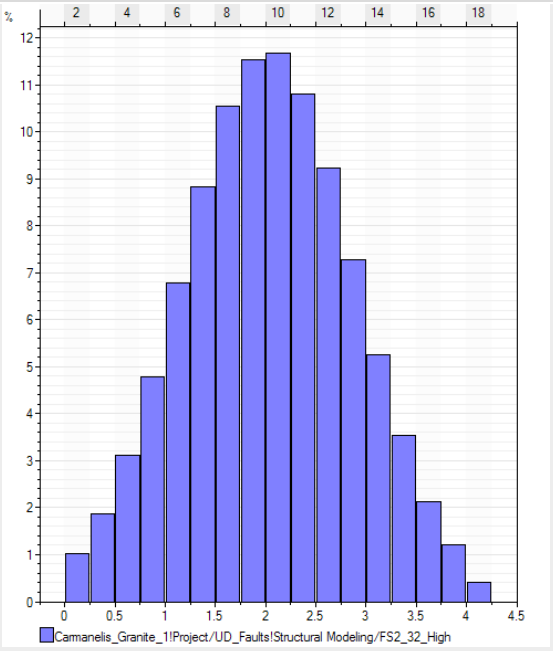

Appendix 5 The parameters used for the three DFN models for the HDR site. Note the three density models used in the three models.

	FS1	FS2
Density	P32 Low, Med, High	P32 Low, Med, High
Sides	4	4
Elongation ratio	2	1.7
Length Distribution	Lognormal	Lognormal
Length Distribution – Mean	13.925	13.357
Length Distribution - SD	33.89	25.018
Maximum Length of Implicit	150m	150m
Maximum Length	300m	300m
Orientation – Dip Azimuth	49.49	321.75
Orientation – Dip	86.36	67.22
Orientation – Concentration	15.91	8.40
Aperture Distribution	Lognormal	Lognormal
Aperture Distribution – Mean	3.7267E-6	5.0435E-7
Aperture Distribution – SD	4.885E-6	6.6112E-7
Aperture Distribution - Max	0.00005	0.000025
Aperture Distribution - Min	0	0

Appendix 6 Calculated permeability in each of the principal grid orientations (i, j, k) and for each of the HDR model based on the corrected Oda method for fractures with a horizontal length greater than 150m.

Model	Direction	Mean Permeability (mD)	SD		
HDR Low	Ki	0.0051	0.0279	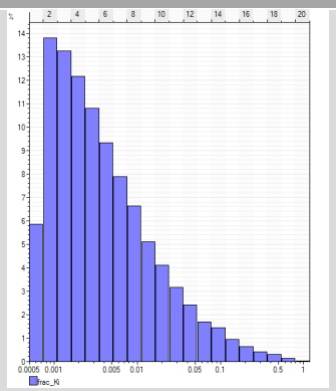	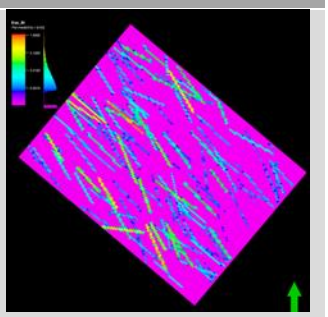
	Kj	0.0009	0.0068	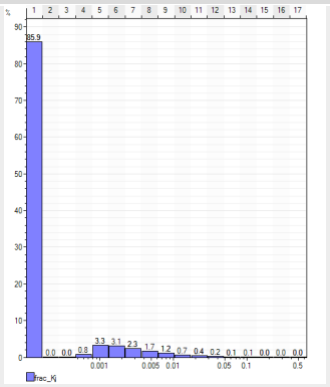	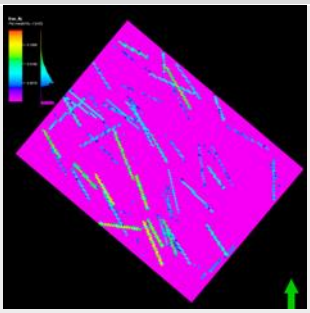
	Kk	0.0070	0.0375	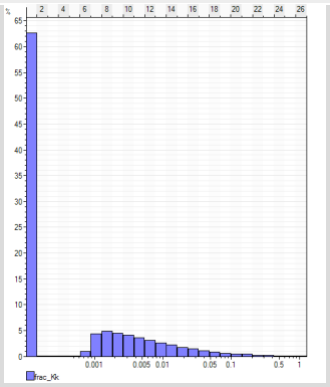	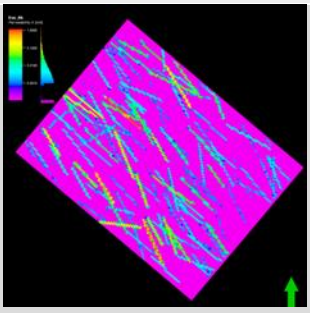

HDR Mean	Ki	0.0082	0.0346	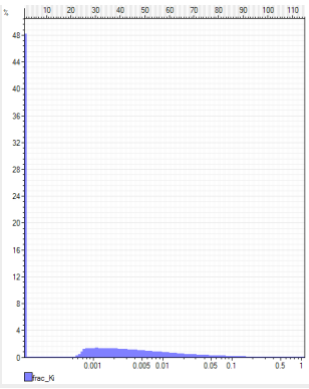	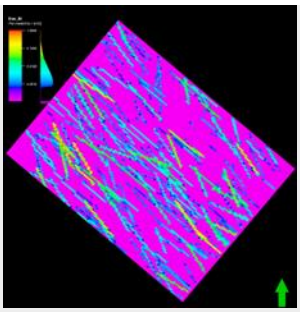
	Kj	0.0014	0.0081	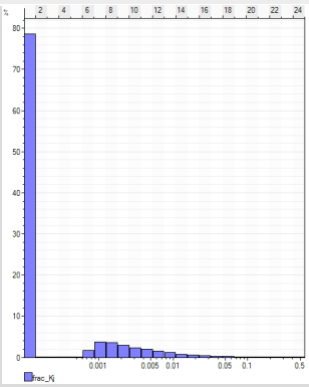	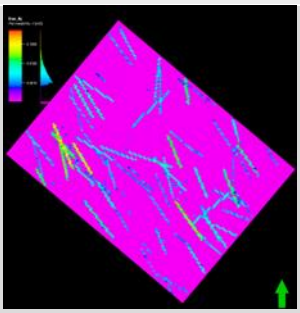
	Kk	0.0110	0.0468	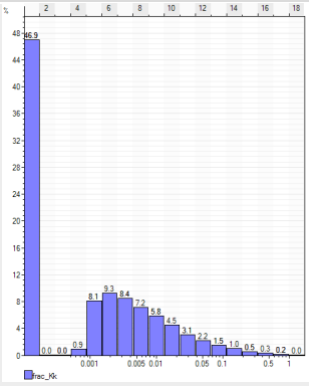	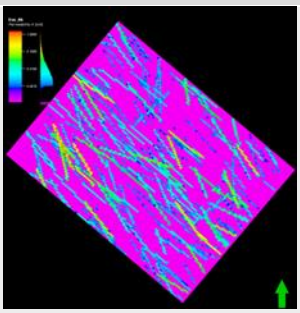
HDR High	Ki	0.0230	0.0592	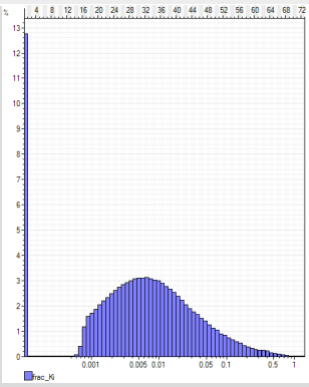	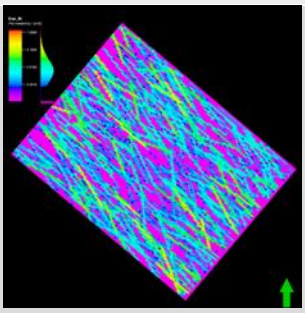

	Kj	0.0038	0.0130	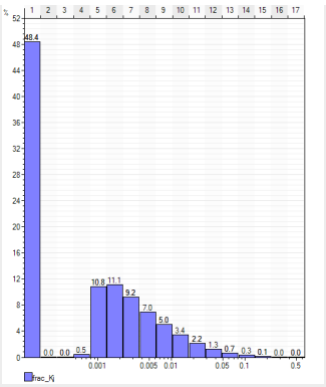	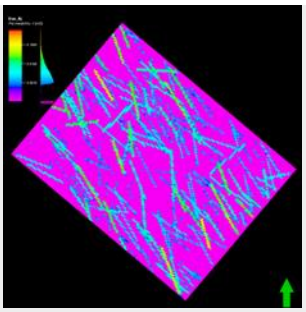
	Kk	0.0280	0.0703	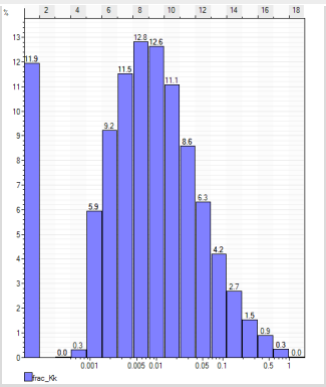	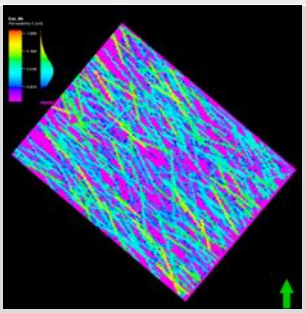

Appendix 7 Calculated permeability in each of the principal grid orientations (i, j, k) and for each of the UD model based on the corrected Oda method for fractures with a horizontal length greater than 150m.

	FS1	FS2	Fault Zone
Density	P32 Low, Med, High	P32 Low, Med, High	P32 = 4.14 within the fault zone and the inverse of the cube root of the distance to fault multiplied by the 4.14
Sides	4	4	4
Elongation ratio	2	1.7	2
Length Distribution	Lognormal	Lognormal	Lognormal
Length Distribution – Mean	13.925	13.357	13.925
Length Distribution - SD	33.89	25.018	33.89
Maximum Length of Implicit	150m	150m	150m
Maximum Length	300m	300m	300m
Orientation – Azimuth	49.49	321.75	Perpendicular to the fault strike
Orientation – Dip	86.36	67.22	85
Orientation – Concentration	15.91	8.40	50
Aperture Distribution	Lognormal	Lognormal	Log-Normal
Aperture Distribution – Mean	3.7267E-6	5.0435E-7	3.7267E-6
Aperture Distribution – SD	4.885E-6	6.6112E-7	4.885E-6
Aperture Distribution - Max	0.00005	0.000025	0.00005
Aperture Distribution - Min	0	0	0

Appendix 8 Modelled permeabilaties for the UD model

Model	Direction	Mean Permeability (mD)	SD		
UD Low	Ki	0.0242	0.0499	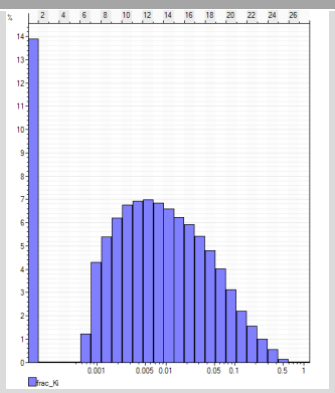	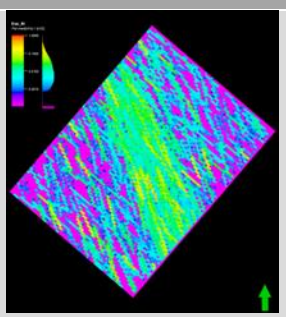
	Kj	0.0047	0.0112	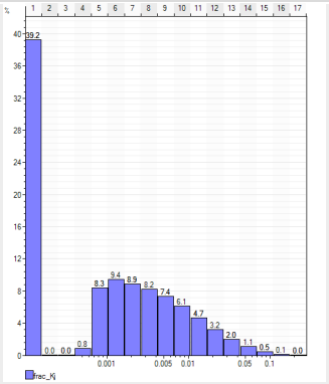	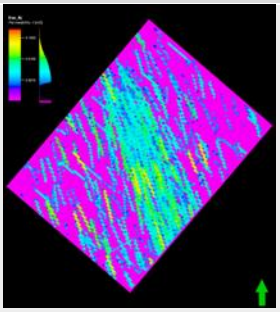
	Kk	0.0323	0.0646	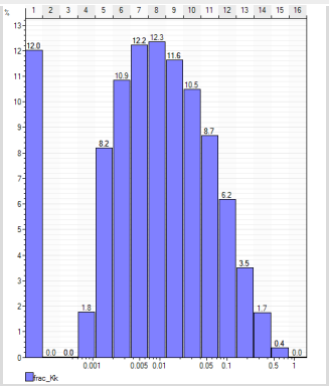	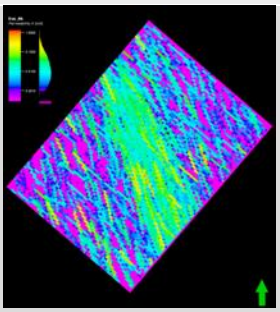
UD Mean	Ki	0.0274	0.0524	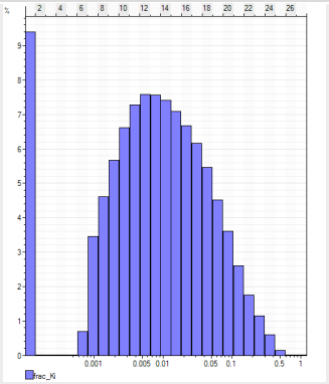	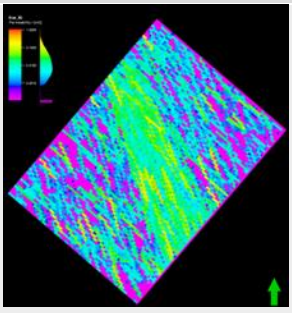

	Kj	0.0055	0.0123	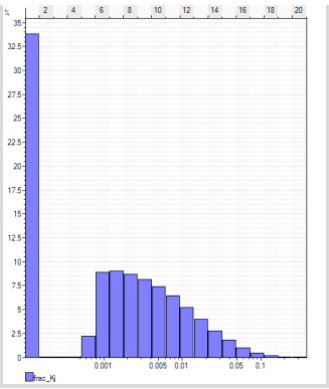	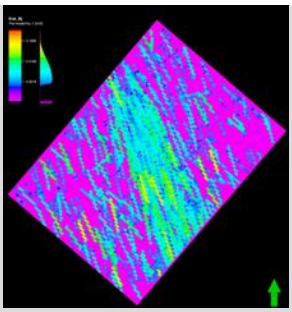
	Kk	0.0355	0.0665	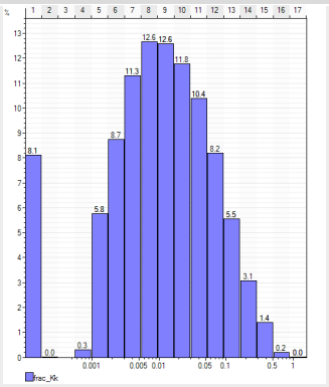	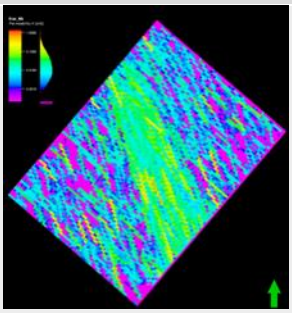
UD High	Ki	0.0449	0.0671	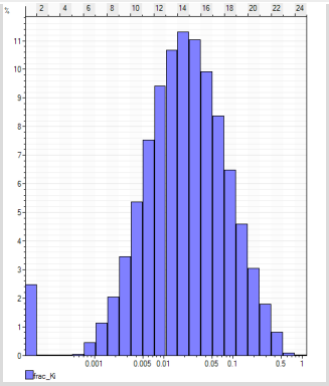	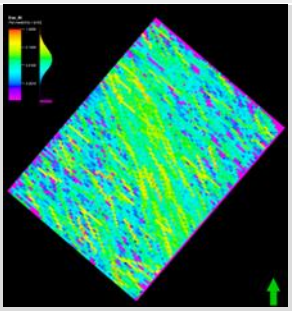
	Kj	0.0083	0.0150	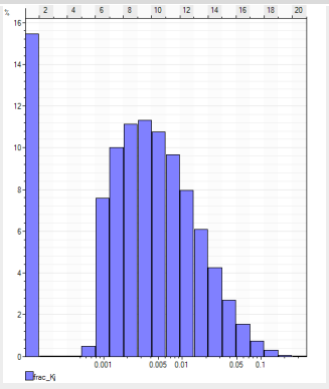	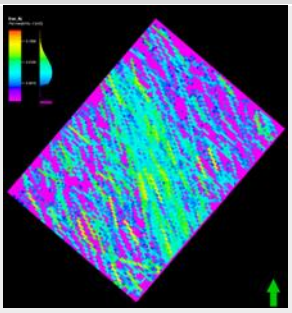

	Kk	0.0530	0.0788	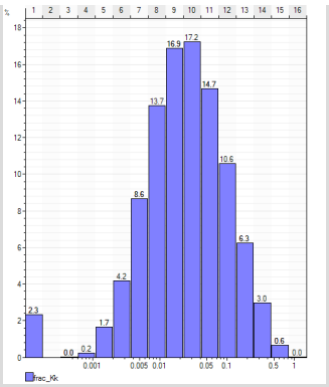	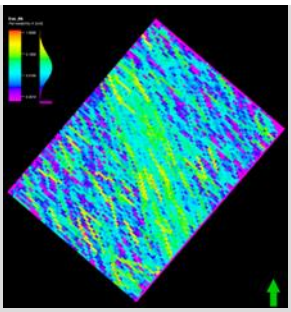

CHPM2030 Deliverable D6.2.2

Report on PILOTS:

Portugal Iberian Pyrite Belt

Summary:

This report provides an update of geoscientific data and information relating south-west Iberian Pyrite Belt, Portugal, and its relation with EGS potentialities, by updating information and possibilities on the following aspects of a potential CHPM application: underground heat exchanger, production/injection wells, metal recovery, power plant, SGPG, environmental, social, political background, financial, stakeholder requirements. The report also highlights the relevant updates of the 3D geological and geophysical modelling of the Lombador orebody of Neves-Corvo.

Authors:

Elsa Cristina Ramalho, Laboratório Nacional de Energia e Geologia, Geological Engineer

João Xavier Matos, Laboratório Nacional de Energia e Geologia, Economic Geologist

João Gameira Carvalho, Laboratório Nacional de Energia e Geologia, Geophysicist

This project has received funding from the European Union's Horizon 2020 research and innovation programme under grant agreement no 654100.

TABLE OF CONTENT

INDEX OF FIGURES

INDEX OF TABLES

EXECUTIVE SUMMARY

This report provides an update of geoscientific data and information relating south-west Iberian Pyrite Belt (IPB), Portugal. The IPB massive sulphides deposits is a Variscan metallogenic province located in the SW of Portugal and Spain that hosts the largest concentration of massive sulphide deposits worldwide, covering about 250 km long and 30–50 km wide and are associated with volcano-sedimentary sequences present in sea floor environment (http://geoportal.lneg.pt). This geographical area, with particular geological volcanic and sedimentary sequences of Carboniferous and Devonian ages, identified in the southwest of the Iberian Peninsula runs from NW to SE, from Alcácer do Sal (Portugal) to Seville (Spain), and, in the Portuguese side, it covers two active mines: Neves-Corvo mine, owned by Lundin Mining (www.lundinmining.com), and at the Aljustrel mine, owned by Almina (www.almina.pt). For its potentialities and full mining operation with good prospective of increasing in depth the research and exploitation, Neves-Corvo Mine was chosen for test site, to be studied for CHPM purposes, because of its depth of exploitation and undergoing research projects (SmartExploration and Explora UE projects). Because of these projects a deep 3D geological and geophysical model is being reviewed, with old mining data and recent acquired geophysical acquisition, reprocessing and reinterpretation. At the same time, its relation with EGS potentialities will be considered. The Neves-Corvo mine area includes presently 7 massive sulphide ore lenses and is mainly a copper and zinc mine, producing copper, zinc and lead concentrates. The operation is owned and operated by Lundin Mining's Portuguese subsidiary Somincor (http://www.lundinmining.com). Although this mine does not explore any ultra-deep orebodies that allow the application of the CHPM technology yet, prospecting in depth is underway to check for the continuity of the Lombador orebody, so far. Lombador is the deepest orebody that is identified in the Lundin permit area. Geophysical modelling and reflection seismics were conducted under the scope of H2020 SmartExploration (H2020) (https://smartexploration.eu/) and Explora (Alentejo2020) projects and a more refined model will turn out with the available data.

This report will cover the main parameters regarding the feasibility of the implementation of the CHPM technology in Neves-Corvo, that will complement the CHPMD1.2.2. report, namely in the possibility of existence of ultra-deep boreholes in the future and in the geothermal gradient that allows reaching adequate temperatures to produce energy (~70 °C) at relatively shallow depths (~2.5-3 km), compatible with both energy production and metal recovery in the geothermal brine to increase mining production.

An overall look upon the external requirements to the implementation of CHPM technology was studied. Emergent external factors such as energy transition, financial requirements and possibilities, and environmental, social and political backgrounds and future prospects are also referred in the report, as well as possible future agreements between the mining management and the Portuguese government.

Finally, some new data is incorporated into a GoCad 3D model as an update to the GoCad model published in ProMine (EU FP7, Carvalho et al., 2016). This update includes supplementary information, such as deeper and all other recent boreholes information, from 2012 to 2018, to cross-check with geophysical data, reprocessed gravimetric, magnetic, electromagnetic and surface and deep reflection seismic data.

1. INTRODUCTION

This report is part of the tasks of the WP6 of the CHPM2030 "Combined Heat, Power and Metal extraction from ultra-deep orebodies" project, complementing report D1.2.2 Report on pilots and concerns mostly an update of geoscientific data and information relating south-west Iberian Pyrite Belt, Portugal, regarding a 3D geological and geophysical model and its relation with EGS potentialities, for implementing the project. Only in Azores Islands geothermal energy is produced, about 14 GW/y, and a significant part of it comes from the high enthalpy energy produced by the volcanoes. However, Mainland Portugal is geologically different without active volcanism, with geothermal energy produced only in the spa complexes, e.g. for swimming pools, located in the crossing of regional faults. Geothermal is used mainly to house heating and Sanitary Hot Waters (SHW). In the rest of the country geothermal gradient is normal, from about 17°C/km until 30°C/km (CHPM2030 D1.2.2), and adequate temperatures for energy production are only found deeper than 2 km. Some crucial points are focused in this report and their feasibility is discussed. Neves-Corvo and other mines located in the IPB VMS province are indicated in Fig. 1.

As described in the deliverable CHPM2030 D1.2.2, the Iberian Pyrite Belt (IPB) is a Variscan metallogenic province located in the SW of Portugal and Spain that hosts the largest concentration of massive sulphide deposits worldwide (Inverno et al., 2015), covering about 250 km long and 30–50 km wide (

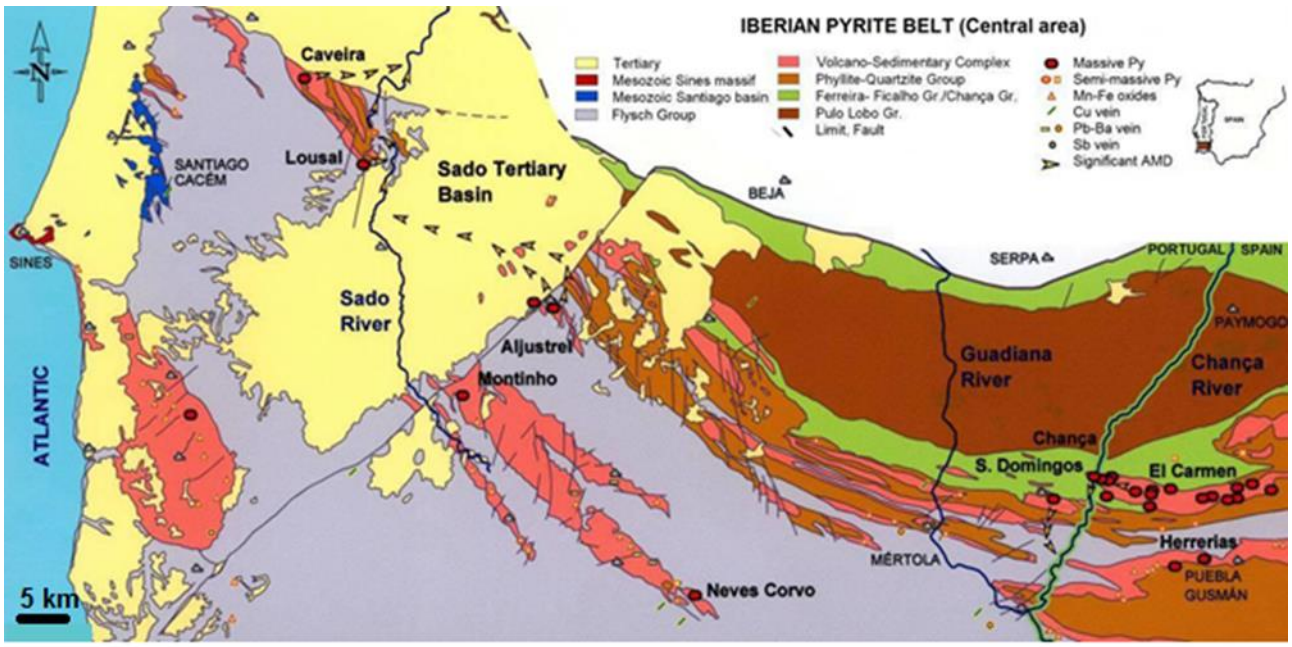

Figure 1). The Neves-Corvo Mine is marked in red. This geographical area, with particular geological volcanic and sedimentary sequences of Carboniferous and Devonian ages, identified in the southwest of the Iberian Peninsula (Oliveira et al., 2013) runs from NW to SE, from Alcácer do Sal (Portugal) to Seville (Spain).

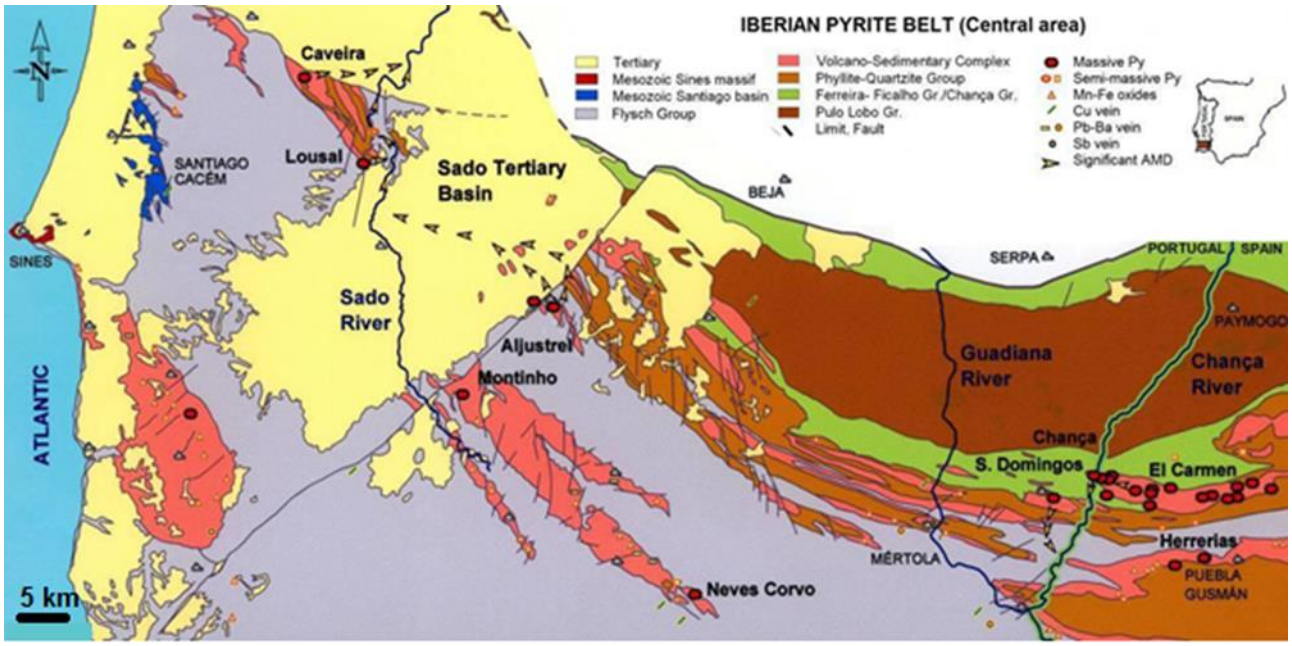

Figure 1. Location of the central area of the IPB Portuguese sector within the scope of the Iberian Peninsula and main geological groups. Location of the IPB massive sulphide deposits and intense acid mine drainage (Inverno et al., 2015, Abreu et al., 2010). Active mining: Neves-Corvo (Somincor-Lundin Mining) and Aljustrel (Almina). Scale (line): 5 km.

Since the 1960's intense geophysical exploration has been done allowing discovering new hidden massive sulphide orebodies (like Neves-Corvo (Albouy et al., 1981, Relvas et al., 2006, see

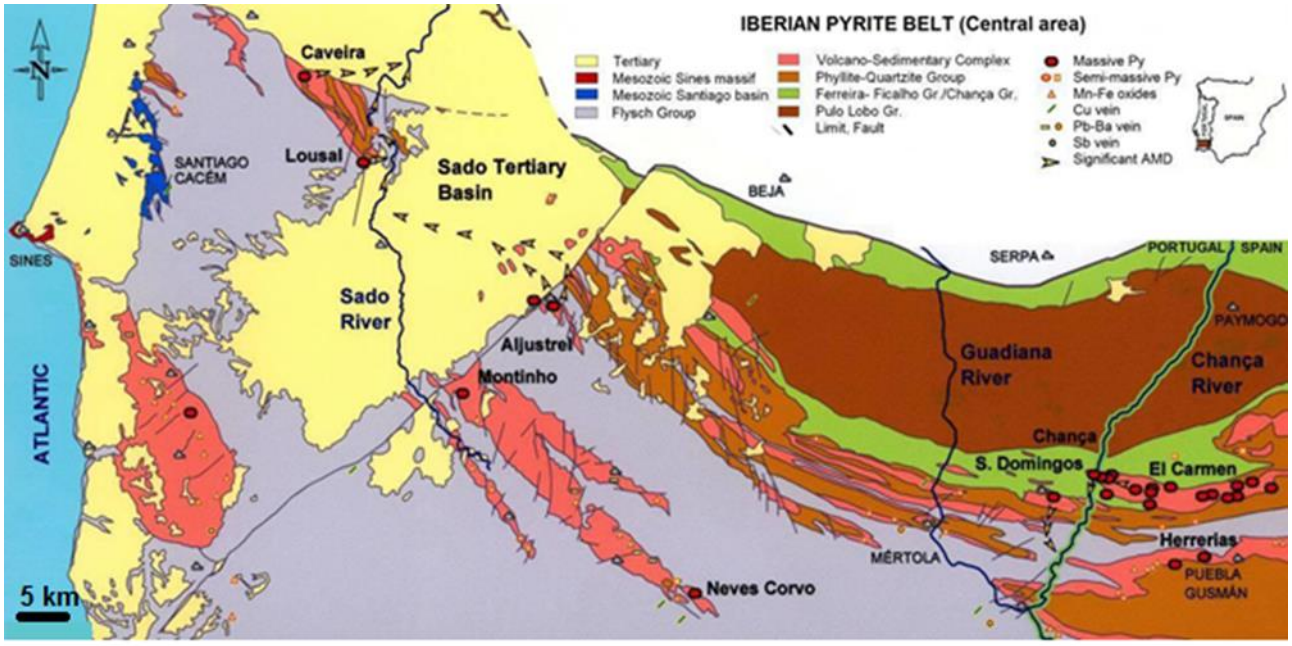

Figure 1), Las Cruces (Doyle, 1996) and Lagoa Salgada (Oliveira et al., 1998)). Schematically, the ore deposits in the IPB are shown in Figure 2.

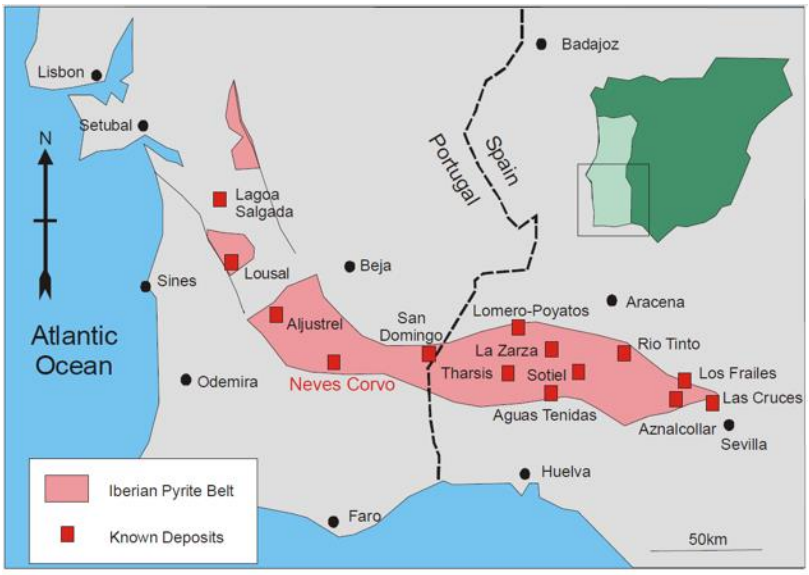

Figure 2. Location of Neves-Corvo and other VMS Deposits within the IPB (www.lundinmining.com).

Finally, an update of geoscientific data and information relating the Mine of Neves Corvo in south-west Iberian Pyrite Belt (IPB), Portugal, is made, regarding the 3D geological and geophysical model and its relation with EGS potentialities, for implementing the project.

2. GEOLOGY

Geology was described in detail in the report CHPM2030 D.1.2.2. Due to the large amount of mineral deposits in southern Portugal (Figure 3) and because of the intensive deep mining prospecting, a dense boreholes network was created, drilled by mining companies (see example of exploration drillhole distribution in the IPB Portuguese sector. Looking at the ore distribution when its overimposed by geology, the considerable amount of mineral deposits are concentrated in some areas with particular features, like identified ore deposits, geological thrusts and the possibility of dipping of knowing ore lenses, as referred in report CHPM2030 D1.2.2 and as seen again in Figure 3.

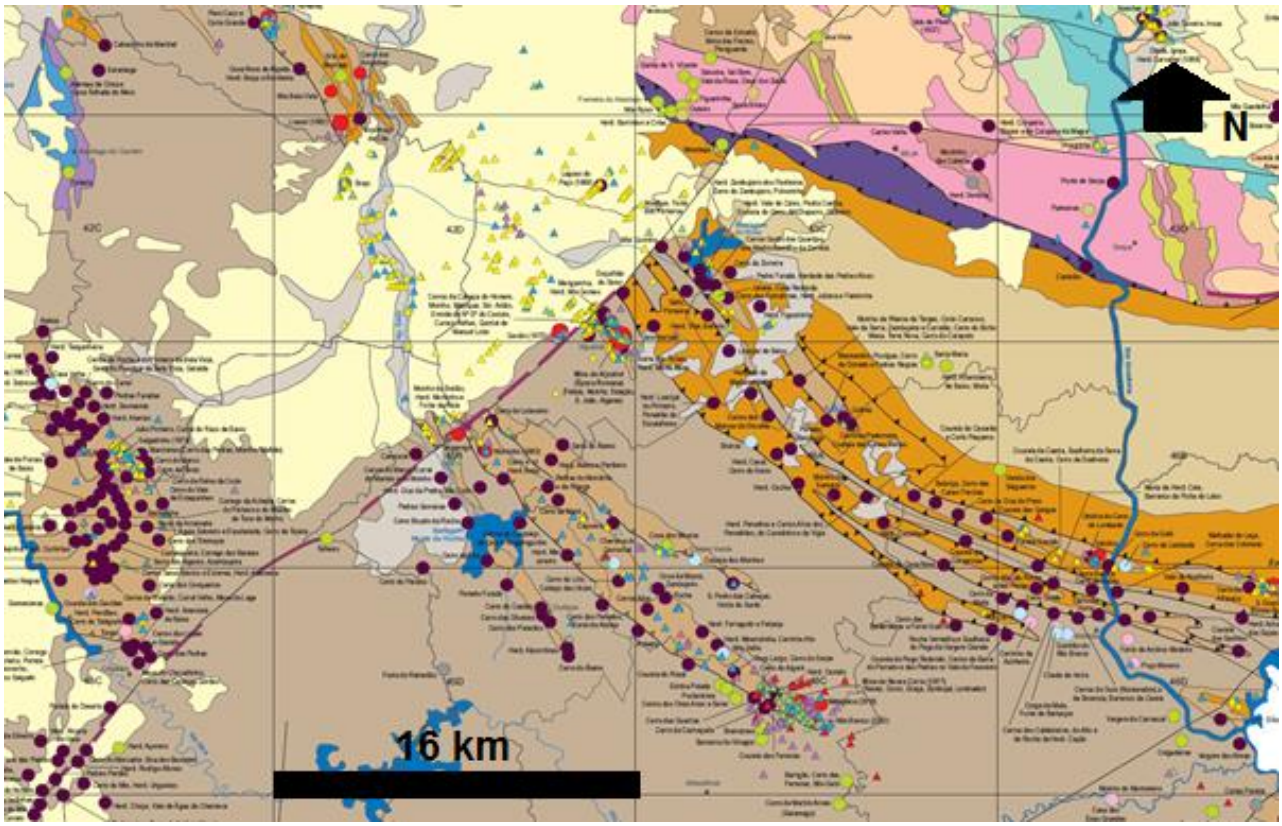

Figure 3. Central area of the geology of the IPB Portuguese sector (ad. Matos and Filipe Eds., LNEG 2013): mineral occurrences - circles: red - massive sulphides, dark purple - Mn, green - Cu, blue – Ba(Pb) and exploration drill holes (triangles). Map grid: 1/25,000 scale maps (16 km x 10 km).

The southern part of the country shows excellent logistics for exploration and mining, namely in the Neves-Corvo Mine. Considering the CHPM2030 objectives, the Neves-Corvo deposit was selected.

Figure 4 shows the geographic distribution of the known ore deposits for this mine deposits as they are known today.

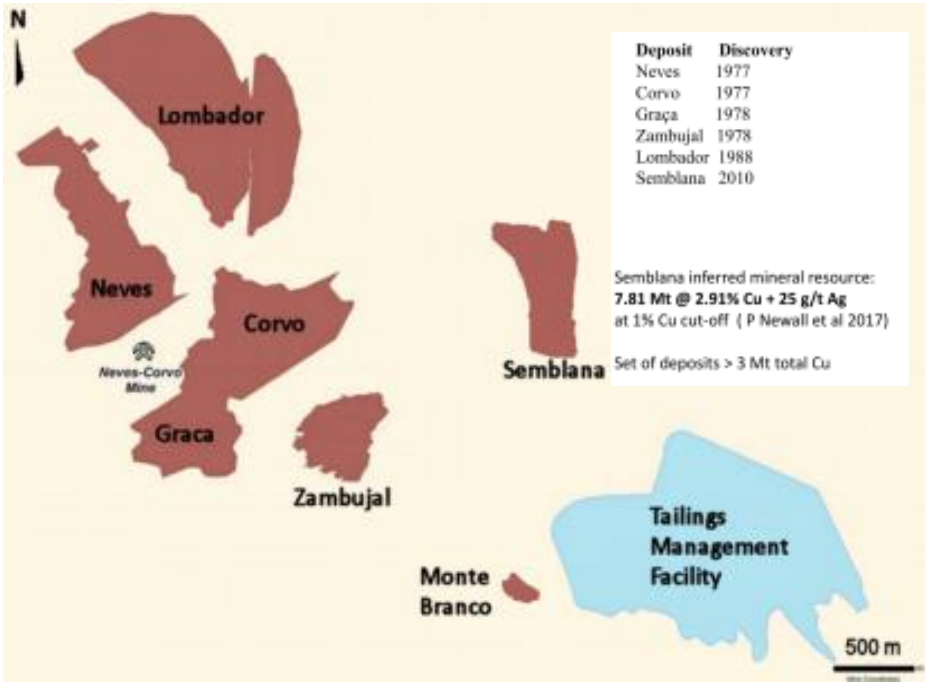

Figure 4. Ore deposits schematic geographic distribution in Neves-Corvo (Scale (line): 500 m).

Neves-Corvo Mine is owned by Lundin Mining who has become a stakeholder for the project, considering the deep mining operations (until 900 m depth) and available exploration drill hole data, until 1,800 m depth in the Cotovio sector, located SE of the Neves-Corvo mine. Selected drill core samples were studied within CHPM2030 and other undergoing projects (EXPLORA and SmartExploration) are conducting a geochemical, geophysical and therefore geological reanalysis, to increase the accuracy of the previous characterization of the improvement of the geological scenario in depth. The model analysis published will be complemented with inferred deep geophysical model, based in the LNEG seismic profiles (data up to 10 km depth) performed in the EU FP7 PROMINE project and Lundin Mining. Some of the new results, obtained in hydrogeologic surveys in Neves-Corvo, and the projects Explora (Alentejo2020) and SmartExploration (H2020) are included in this report. Either Neves-Corvo or Aljustrel mines produce copper ore concentrates from mined massive and stockwork sulphide ores. In the case of the Neves-Corvo mine, zinc and lead concentrates are produced in addition.

To understand the rock-mechanical and geochemical properties of the IPB ore bodies, such as electrical resistivity, thermal conductivity, magnetic susceptibility in basic volcanic rocks with magnetite and pyrrhotite and jaspers with magnetite, rock density in in massive sulphide, stockworks veins and volcanic and sedimentary host rocks and geotechnical properties within the scope of CHPM2030 were carried out in exploration drillhole cores, related with different mineralogical, geochemical and mechanical characteristics of the mineralization and related host

rocks. Different geological scenarios were identified in CHPM2030 D1.2.2 report, considering the presence of sedimentary and volcanic rocks of the IPB Volcano-Sedimentary Complex (VSC) and sedimentary rocks of the Phyllite-quartzite Group (PQG). Considering the IPB geology the following lithological units were considered:

- Mineralization: massive sulphides and stockwork (sulphide vein network);
- Upper VSC sediments - siliceous shales, grey shales, green shales, purple shales, cherts, jaspers and volcanogenic sediments;
- Lower VSC sediments – black pyritic shales, black cherts;
- VSC felsic volcanics (with and without hydrothermal alteration);
- VSC basic volcanics;
- PQG sediments – shales, silts and quartzites, forming the IPB basal siliciclastic basement.

The IPB massive sulphides deposits are associated with volcano-sedimentary sequences present in sea floor environment. Genetic models are present in literature (see for instance Barriga et al., 1997; Leistel et al., 1998; Carvalho et al., 1999; Tornos, 2006; Relvas et al., 2006, Rosa et al., 2008) considering hydrothermal events formed by circulation of sea water in the host rock sequences and later discharge of mineralized fluids. By that time, a Neves-Corvo general geological section was constructed (see figure 5), adapted from Relvas et al. (2006).

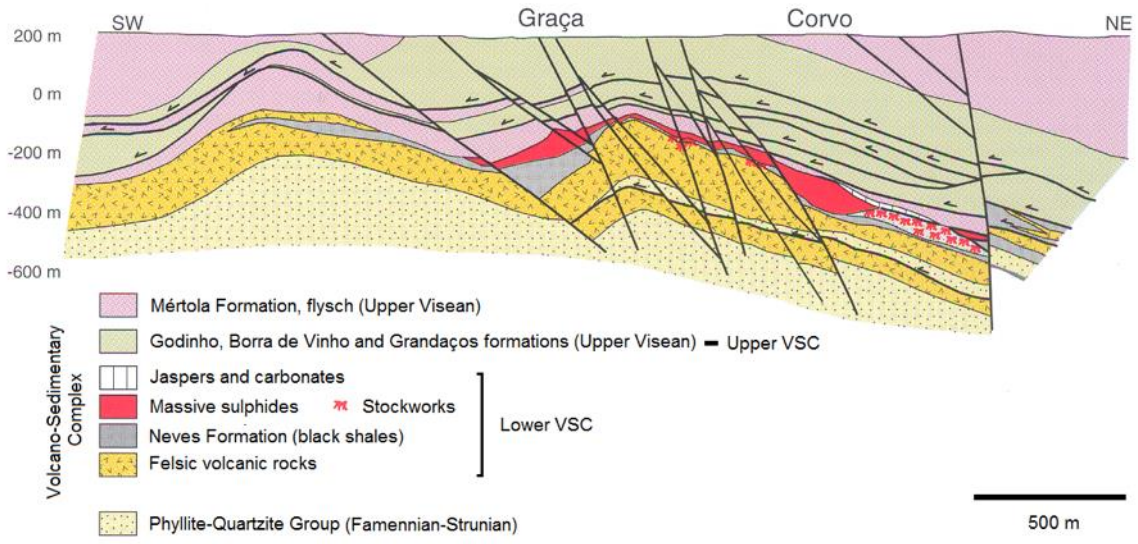

Figure 5. Neves-Corvo general geological section (adapted from Relvas et al., 2006). Location of the lower sector of the Corvo massive ore lens (blue arrow).

Regional and hydrothermal alteration occurs, the second represented by silica and chlorite in the inner zones and silica + sericite in the external zones. A significant number of deposits is directly associated with felsic volcanic rocks formed in the late Devonian (Matos et al., 2011) and early Carboniferous (Barrie et al., 2002; Tornos, 2006), see Neves-Corvo section, figure 5. The deposits generally present a lenticular shape with up to 2 km of length and thickness usually < 150 m. The stockwork structures are commonly present in the root of the hydrothermal system. Variscan tectonics can change the original geometry by folding and faulting, including thrust generation, promoting the existence of complex structures. The deposits are formed mainly by massive pyrite. Other minerals occur like chalcopyrite, sphalerite, galena and sulphossalts locally with economic importance. Present near mining exploration projects, like the Lundin Mining Neves-Corvo DGEG Exploration Permit Area, are being developed and focused in the research of new metal rich massive and stockwork mineralizations and LNEG is cooperating with them.

The next chapter will show in detail the geophysical methods that were applied to get this new geological cross-section of the Neves-Corvo area. However, geophysical magnetic and gravimetric inversion along with borehole lithology to provide calibrations was very important to construct a 2D geogilocal model. According with these new geophysical processed data and with the data from CHPM2030 D.1.2.2, the 2D model for the Neves-Corvo ore based on geology and the response of magnetics and gravimetric data is represented in figure 6.

As described in report CHPM2030 D1.2.2, the IPB regional structure is conditioned by a SW tectonic vergence. Globally, the geological structures present an E-W direction in Spain and close to the Portuguese/Spanish border and a NW-SE direction in the western Portuguese IPB sector. Several complex antiforms are defined, forming VSC-PQG outcropping lineaments (see in the Portuguese sector the 1:200,000 SGP geological maps, Sheets 7 and 8, Oliveira et al., 1988 and 1992, Oliveira et al., 2013, Inverno et al., 2015). These structures are present in depth, under Flysch BAFG sediments and/or Cenozoic age sediments (*e.g*. Sado Basin, Oliveira et al., 1998). In the northern IPB regions allochtonous structures are dominant. In the southern IPB branch the complexity is lower.

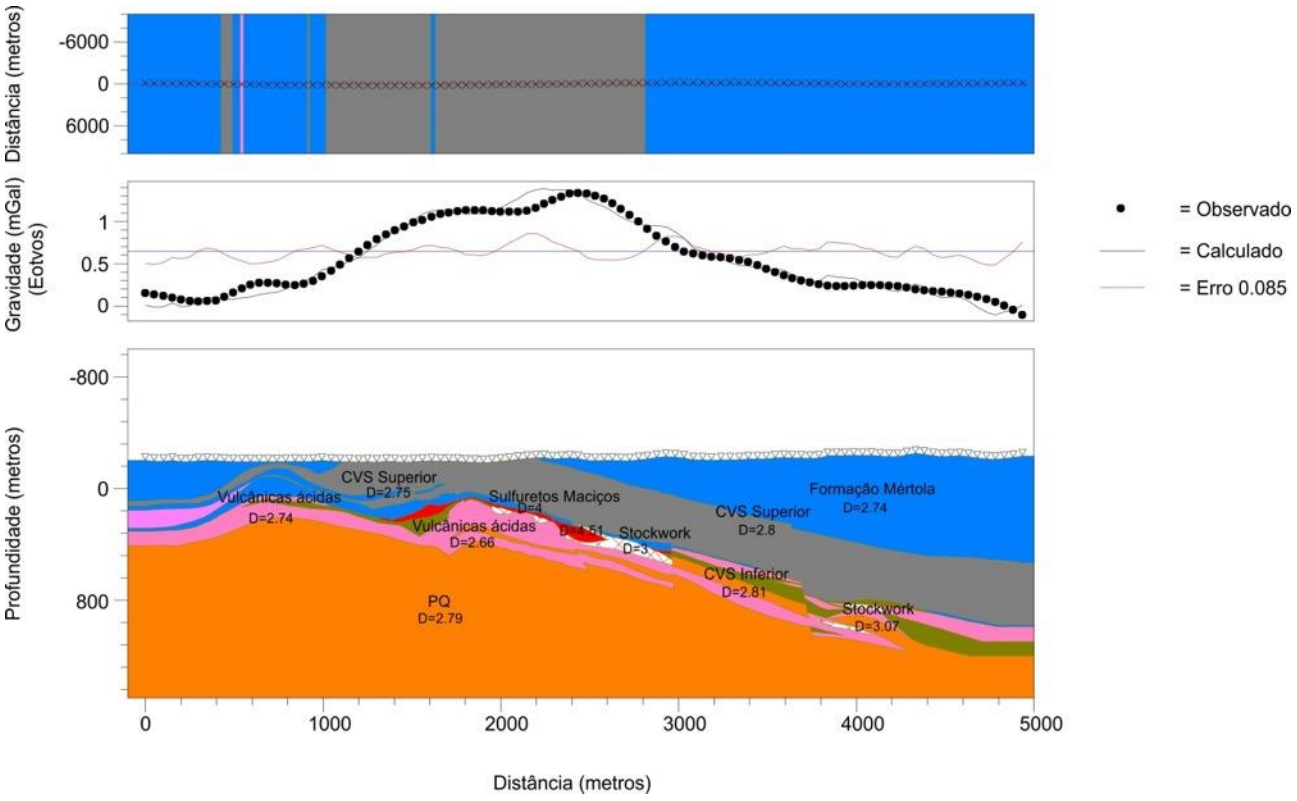

Figure 6. 2D geological model of Neves-Corvo ore body based on gravimetric inverted data. Orange: PQ; Pink: Vulcânicas ácidas (acidic volcanic); Green: CVS inferior (Lower CVS); Red: Sulfuretos Maciços (Massive Sulfides); White with crosses: Stockwork; Blue: Formação de Mértola (Mértola Fm); Grey: CVS superior (Upper CVS);

3. NEW GEOPHYSICAL ACHIEVMENTS IN THE IPB

The LNEG EXPLORA/Alentejo2020 research project promoted recently regional geophysical mapping focused in the IPB Portuguese sector.

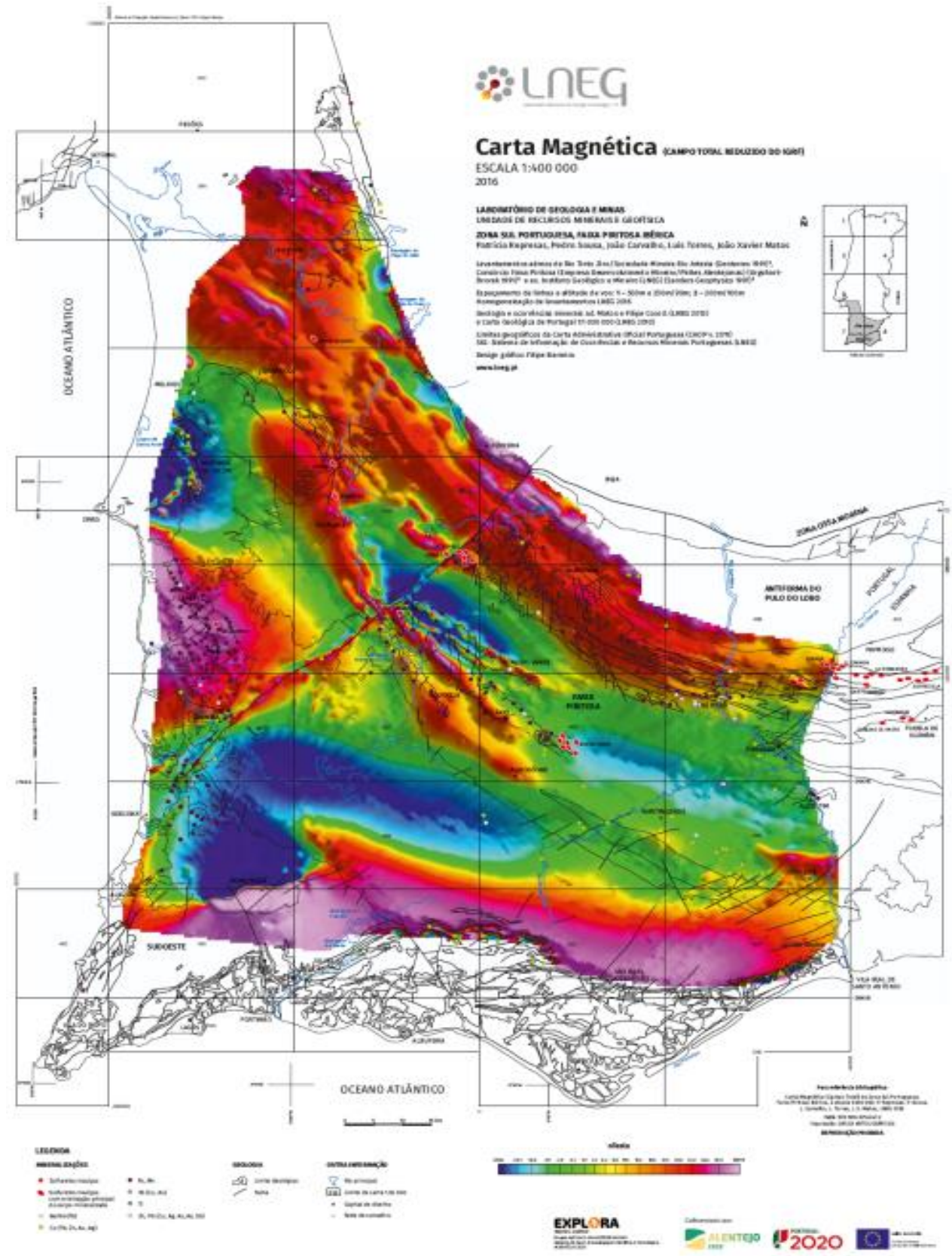

Figure 7. Magnetic (Total field IGRF reduction) South Portuguese Zone 1/400,000 scale maps, Represas et al., LNEG 2016, EXPLORA/Alentejo2020 Project.

These maps allow a better understanding of the Volcano-Sedimentary Complex structures and lineaments (Matos et al. 2018; Batista et al., 2014; Represas et al., 2016).

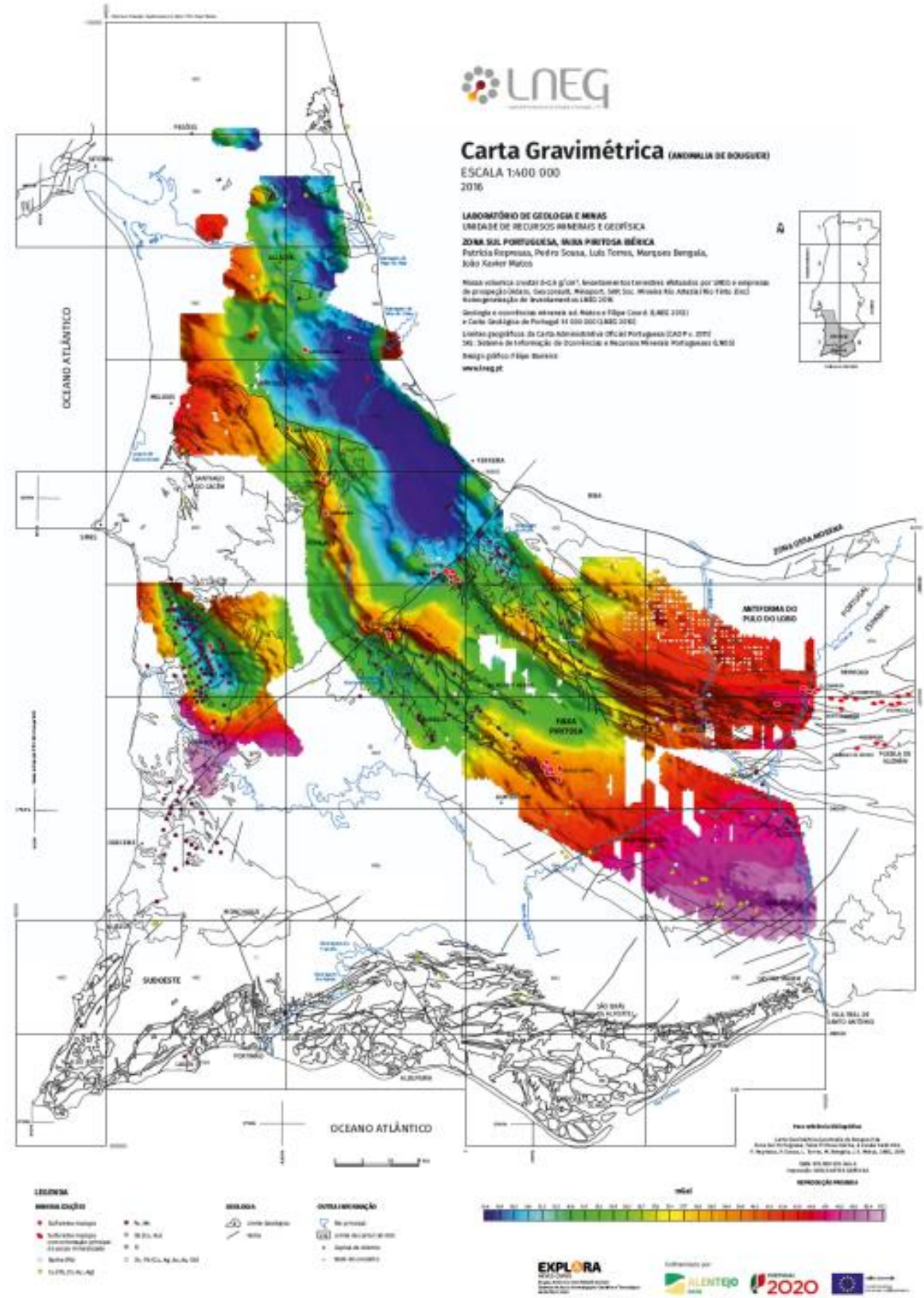

Figure 8. Gravimetry (Bouguer 2.6) South Portuguese Zone 1/400,000 scale maps, Represas et al., LNEG 2016, EXPLORA/Alentejo2020 Project.

Magnetic (Total field IGRF reduction) and Gravimetry (Bouguer 2.6) South Portuguese Zone 1/400,000 scale maps were released (Represas et al., 2016), in the EXPLORA/Alentejo2020 Project are represented respectively in figures 7 and 8.

These maps are the homogenization of decades of airborne and regular field surveys.

The map in figure 7, showing the total magnetic field with IGRF reduction clearly shows some features, from which can be highlighted the long dike related with the Messejana regional fault, that crosses the entire map in the NE-SW direction. Neves-Corvo is located in the edge of the Rosário anticline, seen in the magnetic map with a negative anomaly reaching about -15 nT. The same area corresponds to a strong gravimetric anomaly, as seen in figure 8. 3D models of the residual Bouguer Anomaly Map from Neves-Corvo have been constructed.

Aerospectrometry of the study area, Scale 1:50.000, is represented in Figure 9.

The area has more than 204,000 drillhole densities, 163 magnetic susceptibilities measurements in outcrop, 5500 measurements of magnetic susceptibilities in drillhole and about 60 electrical conductivities measurements in outcrop.

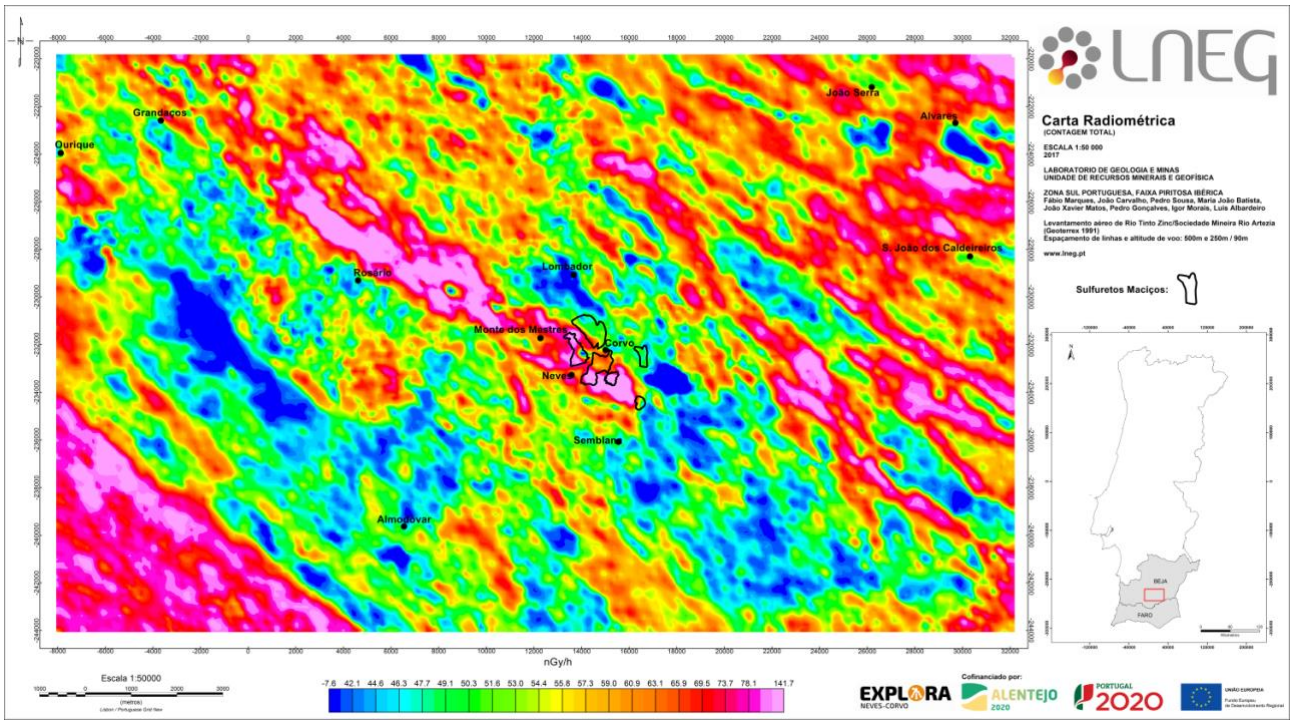

Figure 9. Aeroradiometry (Total Count) of the study area. Scale 1:50,000 the orebodies projection at surface (Courtesy of Explora project, F. Marques, LNEG 2018).

The 2nd vertical derivative of the gravimetric map was used in Neves-Corvo to highlight low wavelength anomalies related small orebodies. The aeroradiometry of the study area shows a surface weakness in Total count related with the presence of large areas covered with shales and greywackes flysch sediments of the Mértola Formation. Outcropping VSC felsic volcanic rocks are reflected by intense anomalies (Total Count) Neves-Corvo. The three types of data were plotted in 2D SW-NE cross-section (figure 10).

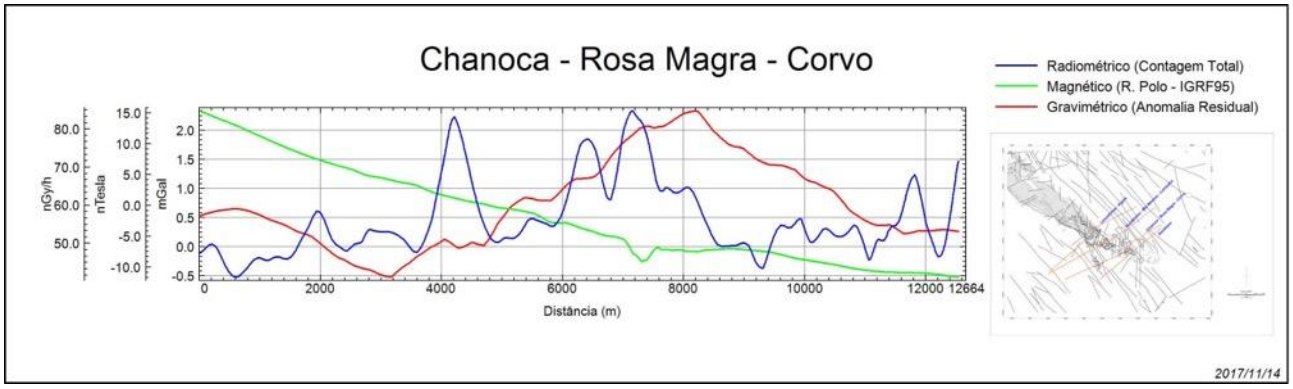

Figure 10. Response of gravity, magnetic and aerospectrometric data for Neves-Corvo orebody (courtesy of Explora project, F. Marques, LNEG 2018).

The 3D location of the known massive ore bodies in the Neves-Corvo mine is the one depicted in Figure 11 (Lundin Mining). The ore lenses present a lenticular shape like other IPB VHMS deposits. The ore lenses located near the surface are directed linked with the Neves-Corvo gravity anomaly (Leca 1983, Carvalho et al., 1999, Matos et al. in press, Explora Project, 2018).

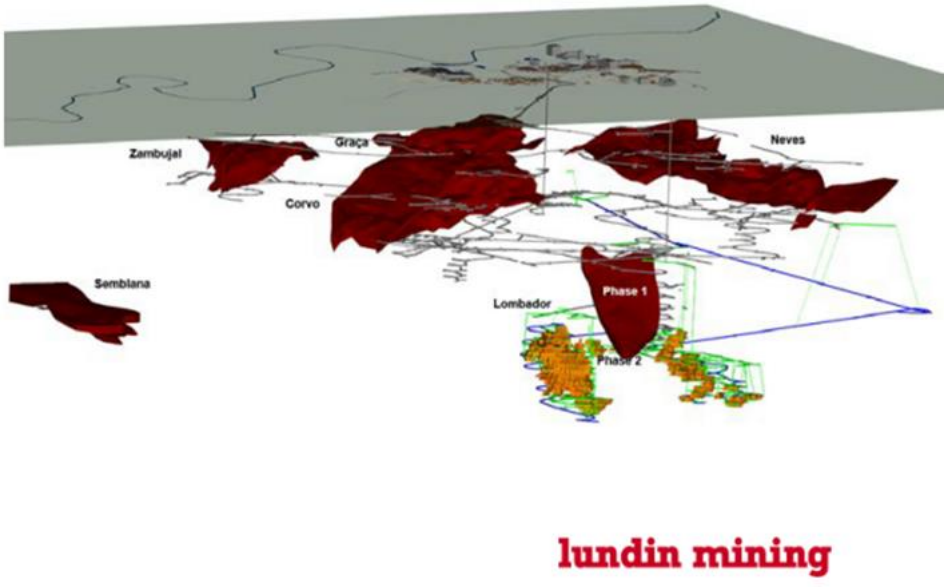

Figure 11. 3D location of the known ore bodies in Neves-Corvo (Lundin Mining).

Metal zonation can be correlated with rock density as shown by the 3D geochemical and gravity inversion maps of the Corvo and Graça ore lenses in figure 12 (Batista et al., 2014). Even though the calculated geochemistry and density models indicate that the places where high rock density and high Cu concentration coincide, are places where the predictability values are considered to be the highest. This corresponds to the known massive sulphide ore lenses.

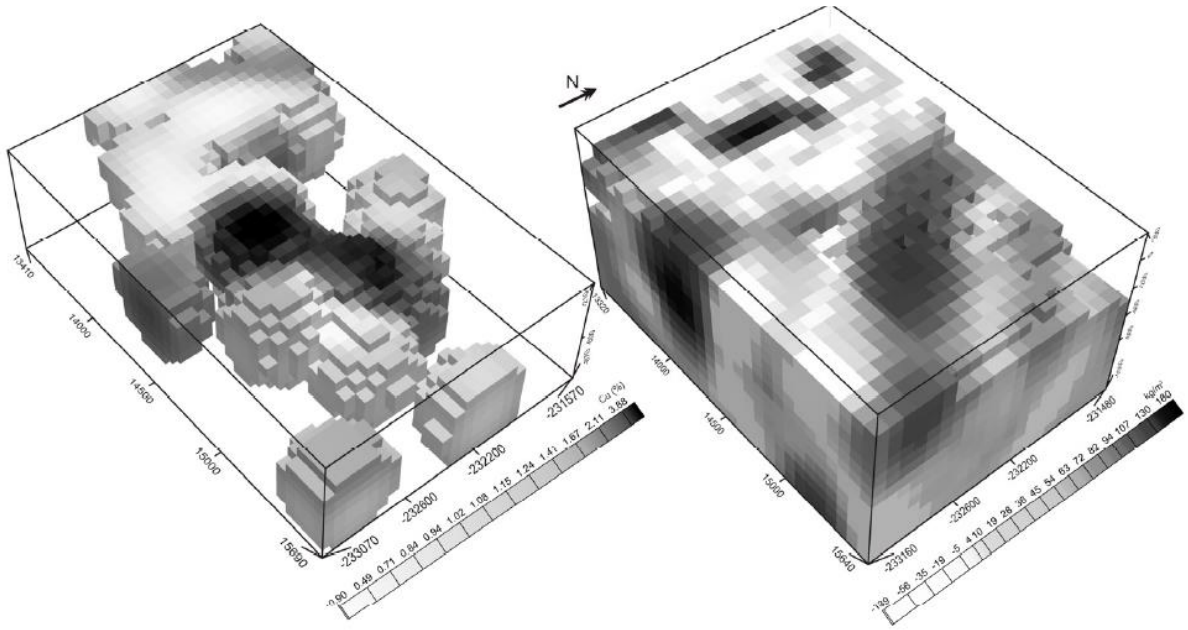

Figure 12. Neves-Corvo 3D geochemical and gravity inversion model (Batista et al. 2014).

Some gravimetric anomalies (residual anomaly) were located at the Neves-Corvo orebody were 2D modelled (figure 13).

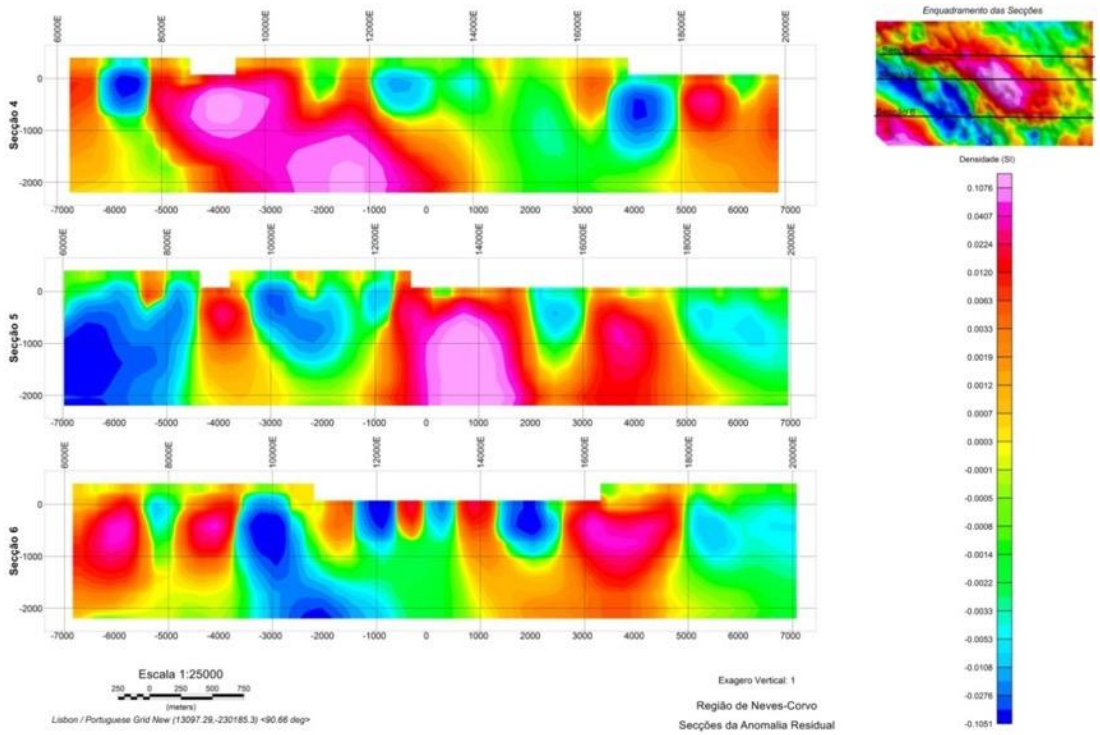

Figure 13. 2D gravity models of the Corvo sector of the Neves-Corvo mine. Sections of Residual Anomaly (courtesy of Explora project, F. Marques, LNEG 2019).

2D modelling showed higher density materials in the area of the orebody masses that dips about 45°SW towards depth and show good prospective of deepening of those materials below the 200 meters depth. In fact, the 2D modelling of the residual gravimetric anomaly shows several denser masses in depth that are coincident with the presence of identified orebodies.

As seen in figure 13, the 2D geological model of Neves-Corvo orebody based on gravimetric inverted data shows the presence of mineralized stockwork located deeper than 1000 meters. Reflection seismics conducted inside the mine at 600 m depth at the moment of this report will allow us to compose the 2D geological model as the identified reflectors will be visible in depth or not (Project SmartExploration, H2020 budget, Lundin Mining current exploration program).

4. DEEP METAL ENRICHMENT

In each massive sulphide orebody metal zonation occurs related with the hydrothermal system developed in the area. Commonly hanging walls present high values of Zn and Pb, while footwall areas are copper rich. The stockwork mineralization present a particular metal zonation

distributed in different host rocks that include VSC felsic volcanic rocks and sediments (Neves and Corvo formations) and the basal siliciclastic unit the Phyllite-Quartzite Formation (Relvas et al., 2006; Oliveira et al., 2013). The Neves-Corvo metal zonation can be observed in the map of the figure 14.

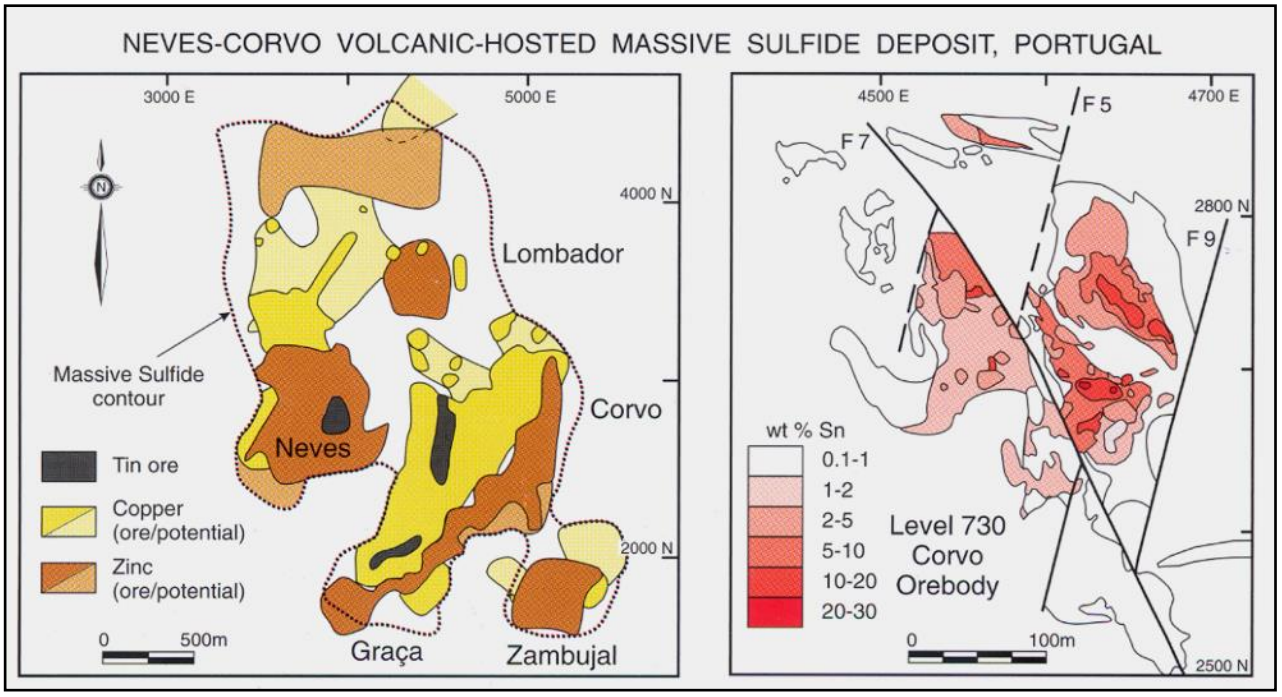

Figure 14. Metal zonation maps of the Neves-Corvo deposit (Relvas et al. 2006, SEG).

As mentioned before, the Neves-Corvo mine area includes presently 7 massive sulphide ore lenses. The 3D location of the known ore bodies in Neves-Corvo is the one depicted in figure 15.

Further work of the Promine Project is allowing correlation between seismic reflectors and conductive bodies TEM, thrust faults and orebodies, improving therefore the knowledge in depth of the study area.

These 3D geophysical models are being improved as new data are being acquired. The 3D models include new reflection seismics surveys at ~-600m, TEM modelling, gravimetric and magnetic modelling.

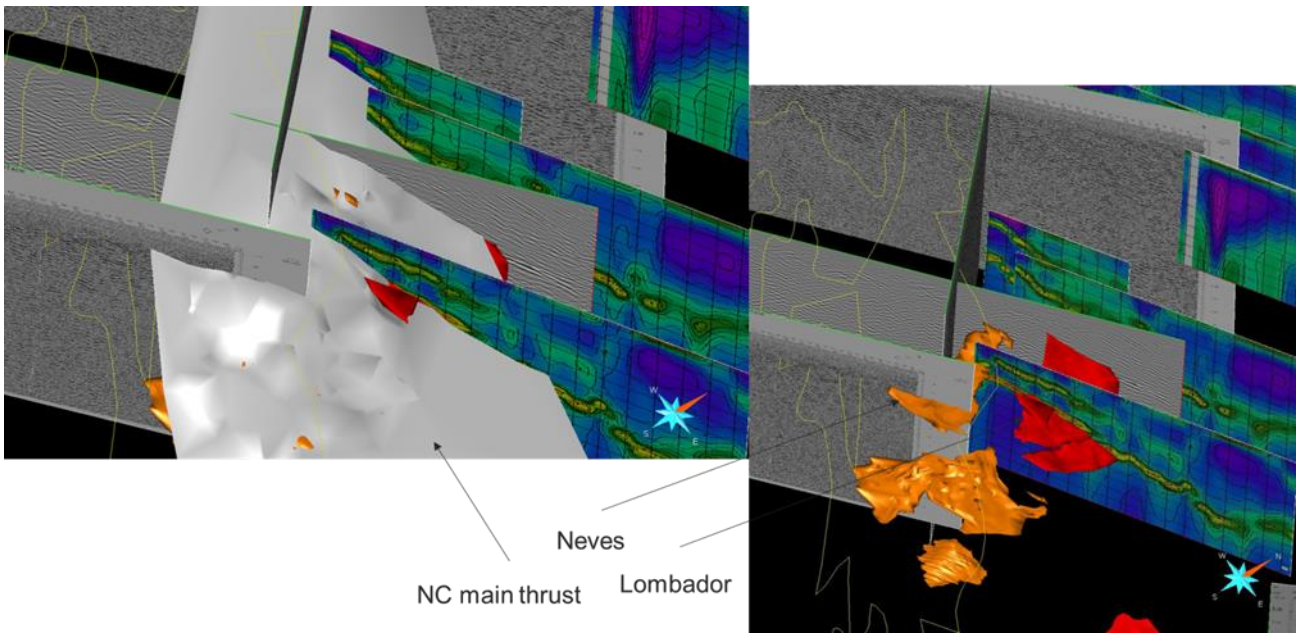

Figure 15. Improvement of the 3D geophysical models of the PROMINE Project, showing EM conductors in deep and massive sulphide mineralization (Courtesy of Smart Exploration project).

Regarding electromagnetic (TEM) data, the profiles are being reprocessed so that a 3D model is being built within the scope of SmartExploration to integrate other sources of information (Figs. 15 and 16).

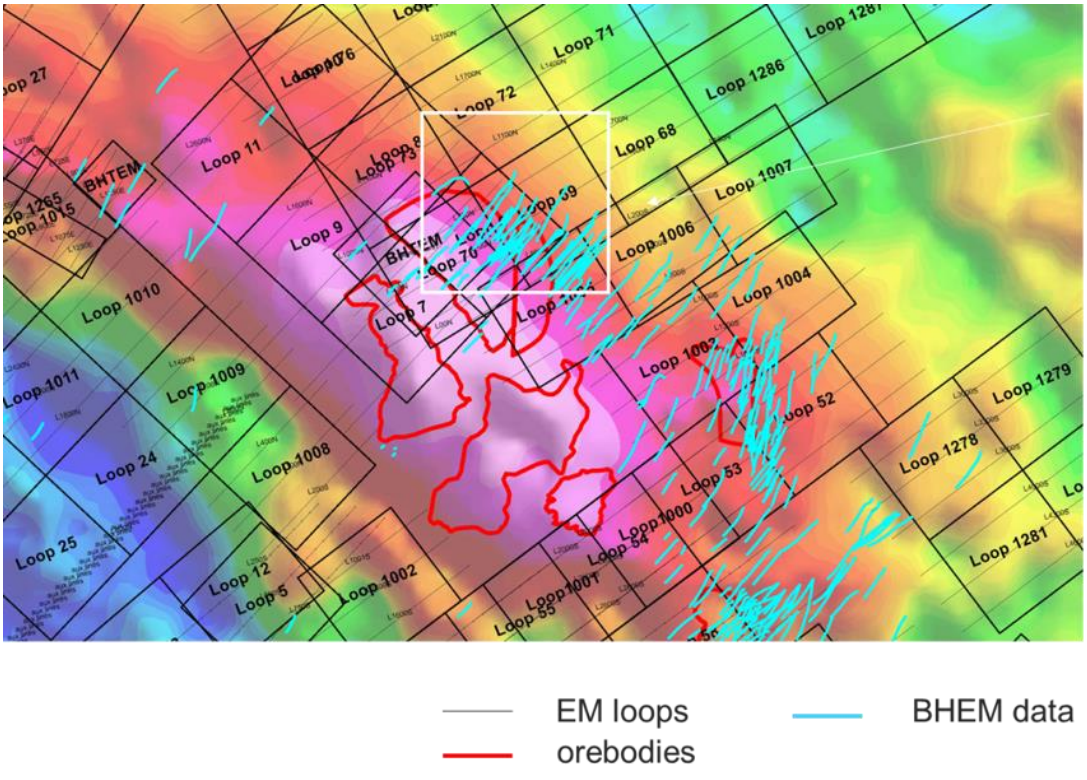

Figure 16. EM profiles and loops carried out in Neves-Corvo Mine permit (Courtesy of Smart Exploration project).

Geophysical seismic surveys conducted in the Promine project show a deep-rooted faults (> 5 km) that controls the Paleozoic basement block units, like in the case study of Cotovio (Carvalho et al., 2016, see figure 19). These fault systems can promote deep water circulation and eventual metal leaching in depth. In the Neves-Corvo mine region several copper veins are present, related with late-Variscan strike-slip faults, like the Brancanes, Porteirinhos and Barrigão old mines (Matos et al., 2003; Reiser et al., 2011, Fig. 18). These veins present chalcopyrite + pyrite + sulphossalts associated with quartz and carbonates.

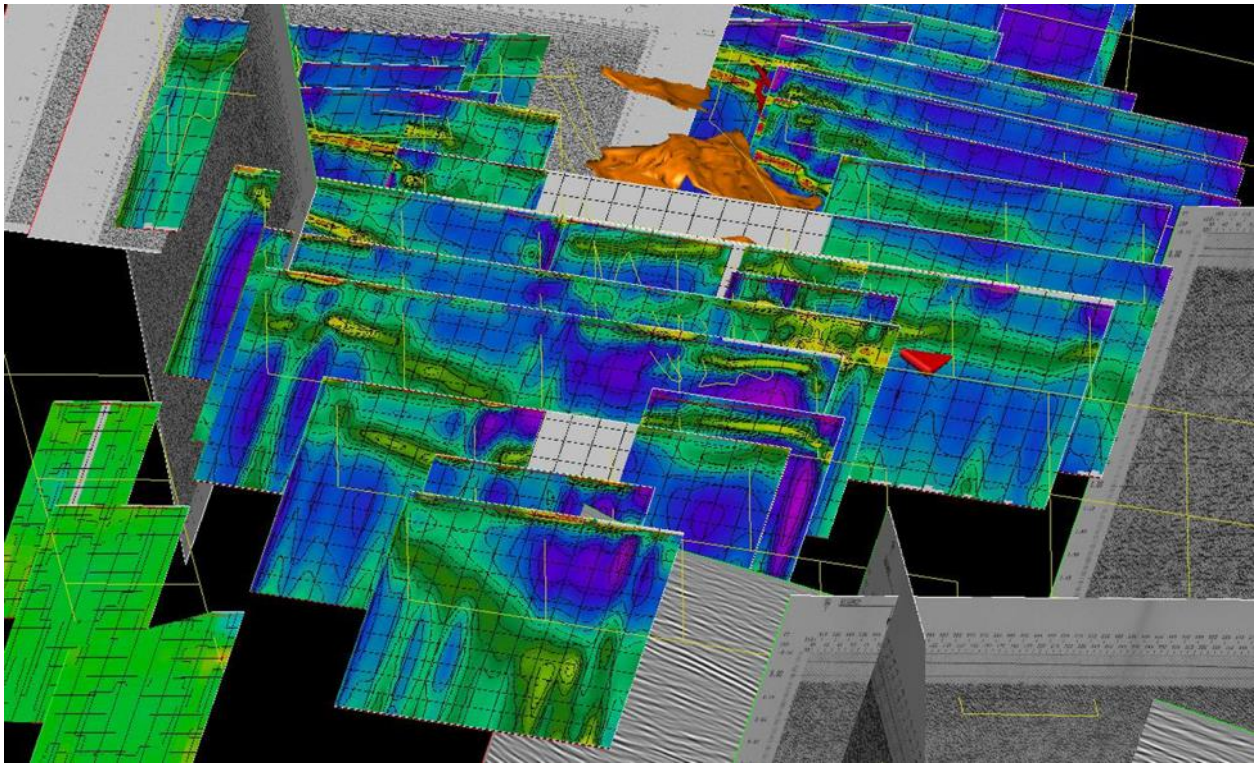

Figure 17. TEM profiles and loops carried out in Neves-Corvo Mine permit (Courtesy of Smart Exploration project).

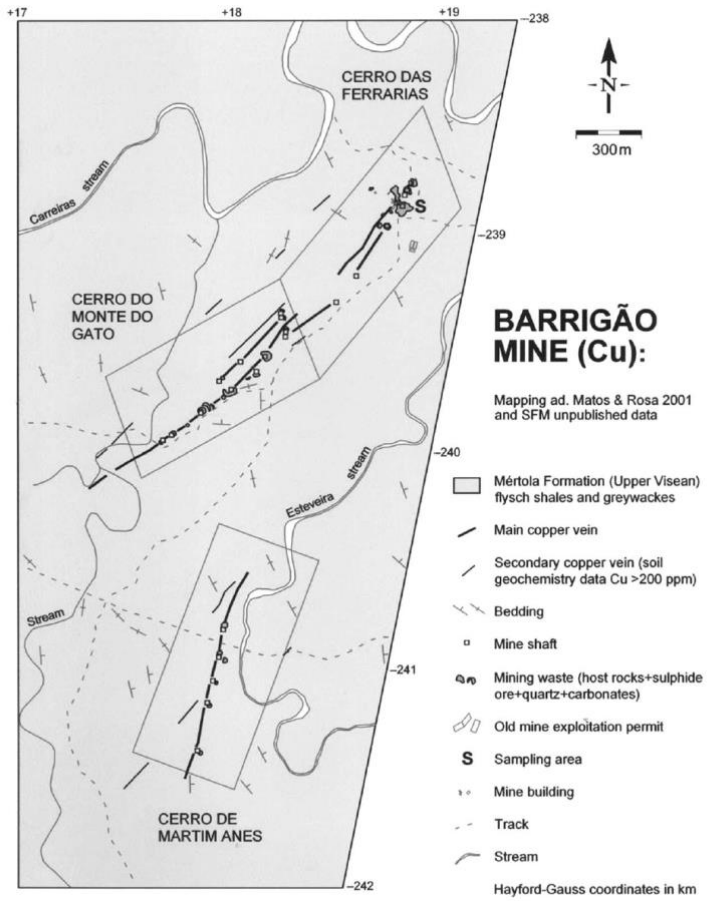

Figure 18. Structural map of the Barrigão copper mine, SE of Neves-Corvo (in Reiser et al., 2011)

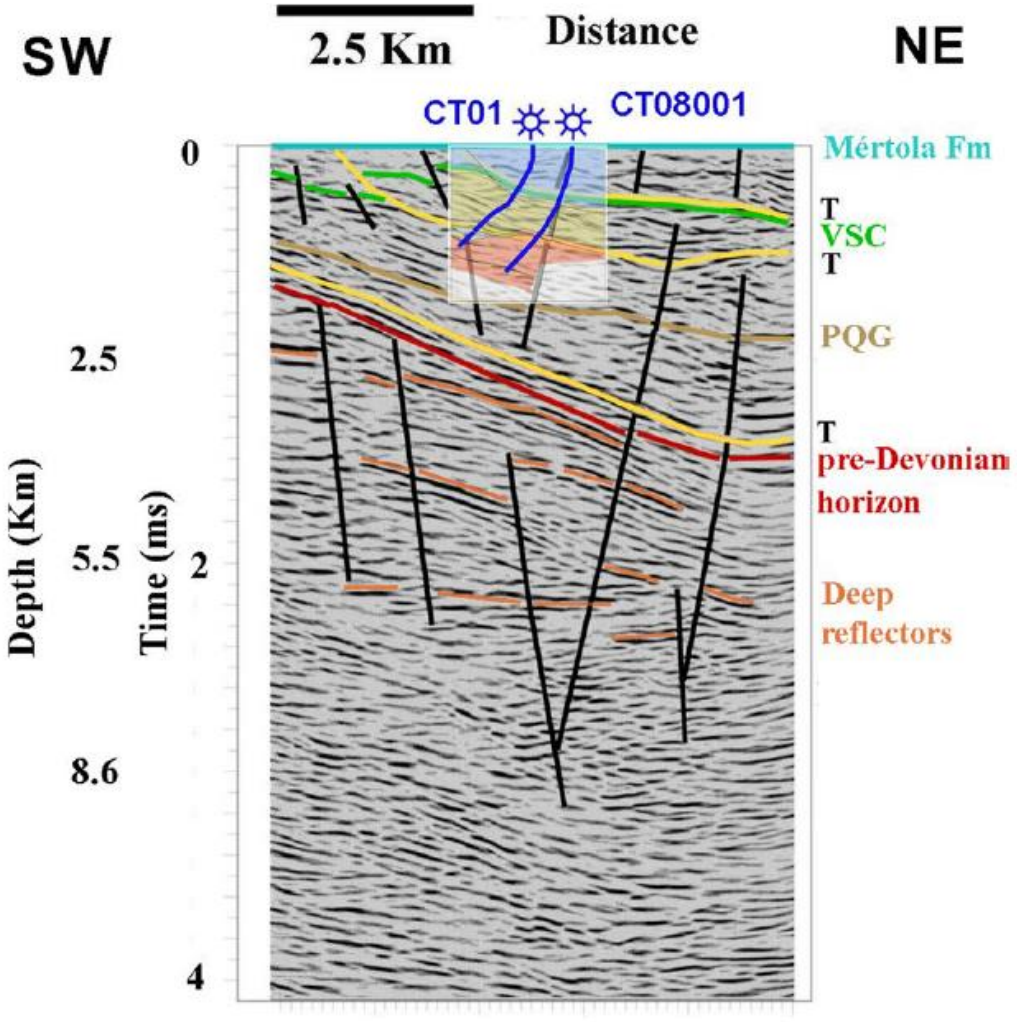

Figure 19. Deep late Variscan faults reflected in seismic surveys, performed at the Cotovio sector, SE of the Neves-Corvo mine. Boreholes CT01 and CT8001 cut the mineralization and are being used to calibrate time domain electromagnetics (TEM).

5 EGS POTENTIAL

The economic feasibility of EGS projects in the IPB jointly used to generate combined heat and metal extraction can indeed be a reality. Some studies consider that, with adequate investment in research and development over the next few years, EGS technology will become competitive and an important contribution to the energy-mix by 2050 or even earlier and if metals would be extracted at the same time, it would be a competitive advantage.

5.1 Hydraulic properties, deep fluid flow

According with Batista (2003), water pumping tests performed in the Neves-Corvo IPB area (See Fig. 1) and surroundings, conducted by Bertrand et al. (1982) in eight wells with maximum depth of 261 m and drill holes with depths ranging from 100 to 645 m, and concluded that drawdowns to

the nearby wells range between 0.88 and 21.6 m and to the drillholes directly between 6 and 43.4 m. Transmissivities have values respectively of between 9.1 x 10^{-6} and 1.1 x 10^{-4} to the wells and between 1.86 and 64.6 x 10^{-6} m^2/s to the drillholes. (Batista, 2003). This is representative for the upper aquifer. For the intermediate and deeper aquifers hydraulic parameters are not available, since they reflect the interest of the company in orebodies and groundwater studies are not the major priority.

In the Variscan Massif terrains (north and centre of Portugal) the permeability is higher, reaching dozens of meters per second and is associated to fracturing zones. In these fracturing zones, decompression and terrain alteration allow a permeability that averagely ranges from 0.1 and 2 x 10^{-6} m/s. At bigger depths, and away from the fracturing zones, permeability diminishes, and is lower than 0.01 x 10^{-6} m/s.

Some conclusions could be taken from these hydrogeological data:

1. The possibility to find an important aquifer in this compact unit pile with low permeability and with low effective porosity is very low.
2. The deep fractures opened to water circulation are found in the top of the pyrite ore lenses, in the flysch greywackes from the base and not in the interior of the sulphide ore. These greywackes show more permeable fractured zones that, instead, can make groundwater circulation easier. Its depth depends on the orebody. Lombador, the orebody in study, here has an indicated downward continuation.

This last conclusion may be important, if these more permeable zones are near the sub-vertical faults that put the sulphide ore in contact with surface waters. Since the ductile shales are above these greywackes are much less permeable, making groundwater circulation towards the surface possible only in fracture zones. Zones with the contact between surface and mineralized ores are located in the Graça Hill and in the main meander of Ribeira de Oeiras, S of the Neves-Corvo Mine.

Through monitoring and surface water control, Fernandez-Rubio y Associados (1994), the hydrogeological system of Neves-Corvo identified three hydrogeological units:

- Upper Shallow System – This system is considered to be an aquifer or an aquitard, free to semi-confined, relatively heterogenous with permeability decreasing in depth, extends from surface to 100 to 200 meters depth.

- Intermediate system – Considered a semi-confined defined in the limit of the previous aquifer, until the top of the mineralization.
- Deep mining system – Confined aquifer composed by the mineralized deposits and overimposed rocks.

The chemical groundwater analysis has origin mostly from this deep mining system, since they often cross mineralized deposits. They were collected in the mine. However, they are considered as pristine groundwater.

5.2 Fluid composition, brines, meteoric waters

Regular analyses from two different groundwater surveys in the deep mining system of Neves-Corvo Mine have been conducted. Most of them are collected at a depth of ~600 meters. One of chosen the surveys was conducted in July 2017 and the other in April 2018 to compare. All the samples come from water from deep aquifer that crosses the ore. Most groundwaters have hydrogeological Na-Cl-HCO_3 or Na-Mg-SO_4 facies. Values reported here are maximum limit values. These values come from different groundwater sources as referred from its name and location and as far as possible, contain the important information for the project, as referred in Reikjavique meeting.

- Fluid composition (fO_2, CO_2, salinity NaCl eq.)
- Redox conditions (Eh or pKe)
- pH (acid or alcaline)
- T range (°C)
- Pressure (bar)
- Flowrate (L/s)
- Amount of oxidizing compound
- Concentration of suspended solids (mg/l)
- Salinity (mg/l)

Tables 1 and 3 are referred to measured *in situ* parameters in different groundwater sources, collected in Neves-Corvo Mine, in the Lombador mass in two surveys carried out in July 2017. Tables 2 and 4 are referred Major parameters in different groundwater sources from Neves-Corvo, in the Lombador mass in April 2018. For depths reaching the bottom of the mine at 1,000 m (m.a.s.l.), although there is not a regular survey programme, the fluid temperature ranges from 30

to 39 °C with dissolved solids dried at 105 °C ranging from 800 to 23,200 mg/L (confidential information).

Table 1 – *Main parameters in different groundwater sources from Neves-Corvo, in the Lombador mass in July 2017. ORP=Oxi-reduction potential, EC=Electrical Conductivity µS/cm, RES=resistivity (ohm.cm), Resist=Resistivity (ohm.m), TDS= Total Dissolved Solids (ppm), D.O.=Dissolved Oxygen (%).*

ID	Depth Z [m]	Temp. [°C]	pH campo	ORP [mV]	Eh (V)	EC [µS/cm]	RES [Ohm-cm]	Resist (ohm.m)	TDS [ppm]	Press. [psi]	D.O. [%]
PH116	625	36.89	5.4	12.7	0.2172	14780	68	0.91	7393	15.735	41
PH114	740	36.87	7.8	8.3	0.2128	18380	54	16.69	9193	15.926	51.1
PH109	740	36.69	6.56	-123	0.0815	5784	173	1.36	2892	15.914	21.9
PH103	625	36.14	7.5	85.1	0.2896	2582	387	17.15	1291	15.723	54.9
PH115	625	35.35	3.46	287.5	0.492	8865	113	3	4432	15.725	53.5
PH104	625	33.68	8.02	68.9	0.2734	4113	243	21.6	2057	15.721	53.9
PH106	740	32.47	7.94	11.5	0.216	3169	316	2.41	1585	15.929	49.4
PH107	740	32.22	6.83	0.5	0.205	19900	50	6.86	9954	15.926	42
PH102	410	29.45	8.37	117.6	0.3221	1497	668	10.02	748	15.336	51.8

Table 2 – Main parameters in different groundwater sources from Neves-Corvo, in the Lombador mass in July 2017.

ID	m Z De-pth	Cu mg/L <0,002 Copper	Fe mg/L <0,005 Iron	Pb mg/L <0,01 Lead	Li mg/L <0,002 Lithium	Mg mg/L <0,02 Magne sium	Mn mg/L <0,0005 Mangane se	Si mg/L <0,6 Silicon	Ag mg/L <0,005 Silver	Na mg/L <0,03 Sodium	Sr mg/L <0,001 Stronti um	Sn mg/L <0,01 Tin	W µg/L 1.0 Tung sten	U µg/L 0.10 Urani um	Zn mg/L <0,003 Zinc
PH116	625	0.02	1050	1.34	1.88	1880	129	7.89	0.05	1130	3.19	0.1	2	1.19	797
PH114	740	0.0083	1.39	0.01	3.02	264	1.16	8.1	0.005	3570	10.3	0.01	1.6	0.1	2.32
PH109	740	0.002	94.8	0.01	0.441	86.2	4.26	5.11	0.005	804	1.89	0.01	1	0.22	60.7
PH103	625	0.002	0.171	0.01	0.26	52.2	0.0137	8.11	0.005	413	1.8	0.01	1.7	0.1	0.0218
PH115	625	0.002	408	0.01	0.904	670	26.3	8.05	0.005	854	4	0.01	1	2.68	166
PH104	625	0.0041	0.125	0.01	0.522	67.6	0.0488	6.79	0.005	783	1.52	0.01	1.2	1.36	0.0348
PH106	740	0.002	0.318	0.01	0.298	98.5	0.111	8.08	0.005	460	2.79	0.01	3.3	0.12	0.0564
PH107	740	0.0203	1.63	0.01	2.96	2600	49.8	7.2	0.005	2390	8.94	0.01	3.2	0.15	46.4
PH102	410	0.002	0.0495	0.01	0.0585	54.6	0.00797	8.48	0.005	208	0.762	0.01	1.4	0.1	0.003

Table 3 – Main parameters in different groundwater sources from Neves-Corvo, in the Lombador mass in April 2018. ORP=Oxi-reduction potential , EC=Electrical Conductivity µS/cm , RES=resistivity ohm.cm , Resist=Resistivity ohm.m , TDS= Total Dissolved Solids ppm, D.O.=Dissolved Oxygen %.

ID	Depth Z (m)	Temp.[°C]	pH	ORP [mV]	Eh (V)	EC [µS/cm]	RES [Ohm-cm]	TDS [ppm]	Press. [psi]	D.O. [%]
PH122	625	39.16	7.29	2.0	0.2	2278	439	1139	15.646	7.5
PH115	625	35.76	3.30	198.4	0.4	8287	121	4144	15.653	58.0
PH103	625	35.41	7.23	47.8	0.3	2802	357	1401	15.636	47.9
PH116	625	33.21	5.71	14.4	0.2	13110	76	6555	15.658	33.3
PH114	740	32.58	6.71	-58.8	0.1	17100	58	8552	15.819	46.3
PH109-1	1000	31.93	6.07	11.1	0.2	11150	90	5576	15.807	32.0
PH107	740	31.92	6.37	-19.8	0.2	17940	56	8970	15.825	21.4
PH133	765	30.98	6.66	-20.0	0.2	8036	124	4018	15.789	26.5
PH137	381.7	30.90	7.92	-63.9	0.1	2280	439	1140	15.270	11.4
PH136	380.4	30.44	7.86	-25.6	0.2	3405	294	1703	15.276	57.1
PH102	410	30.17	6.93	-31.4	0.2	1762	568	881	15.301	49.2

Table 4 – Main parameters in different groundwater sources from Neves-Corvo, in the Lombador mass in April 2018.

ID	(m) Z De-pth	Cu mg/L 0.002 Copper	Fe mg/L 0.005 Iron_	Pb mg/L 0.01 Lead	Li mg/L 0.002 Lithium	Mg mg/L 0.02 Magne sium	Mn mg/L 0.0005 Mangane se	Ni mg/L 0.005 Nickel	Si mg/L 0.6 Silico n	Ag mg/L 0.005 Silver	Na mg/L 0.03 Sodiu m	Sr mg/L 0.001 Stron tium	Sn mg/L <0,01 Tin	U µg/L 0.10 Urani um	Zn mg/L <0,003 Zinc
PH122	375	0.002	0.0593	0.01	0.112	53.4	0.024	0.005	8.28	0.005	365	1.16	0.01	0.10	0.003
PH115	375	0.0297	264	0.022	0.792	578	24.8	0.159	8.19	0.005	894	3.81	0.01	0.11	0.003
PH103	375	0.0043	0.0124	0.01	0.323	93.7	0.849	0.0051	8.14	0.005	565	2.03	0.01	1.37	132
PH116	375	0.002	490	0.024	1.27	1390	59.6	0.375	8.55	0.005	1360	5.64	0.01	0.1	1.77
PH114	260	0.002	25.9	0.01	1.81	500	7.22	0.0336	7.69	0.005	2880	9.43	0.01	0.46	466
PH109-1		0.002	155	0.174	0.633	638	24.3	0.0784	7.92	0.005	1580	2.01	0.01	0.14	17.2
PH107	260	0.0705	42.8	0.01	2.02	1300	20.3	0.104	8.09	0.005	2790	8.53	0.01	0.34	191
PH133	235	1.04	0.224	0.01	0.982	230	3.39	0.0437	6.42	0.005	1390	5.42	0.01	0.18	40.6
PH137	618.3	0.002	0.0877	0.01	0.206	12.4	0.00687	0.005	6.4	0.005	429	0.284	0.01	0.51	13.6
PH136	619.6	0.002	0.141	0.01	0.339	43	0.0196	0.005	7.02	0.005	651	0.946	0.01	0.1	0.003
PH102	590	0.0025	0.0049	0.01	0.0559	94.5	2.37	0.0166	7.4	0.005	253	1.03	0.01	0.1	0.003

5.3 Temperatures in depth

This sub-chapter summarizes the sub-chapter 4.5. Temperatures in depth, in CHPM2030 D1.2.2. It deals in detail with all the parameters used to draw an estimated Heat Flow Density map for mainland Portugal, with special emphasis to southern Portugal. At the moment of this report its importance lies on the deep relation between temperatures in depth with mineralized orebodies. Although the Heat Flow Density (HFD) values for mainland Portugal vary from 40 mW/m^2 to 115 mW/m^2, as reported in CHPM2030 D1.2.2., with an average value of about 75 mW/m^2, HFD values for the Centro Iberian Zone (CIZ) (up north) of the Hesperic Massif range from 65 mW/m^2 to 80

mW/m^2. In the South Portuguese Zone (SPZ), with location of our zone of interest, however, regional HFD values reach about 90 mW/m^2. A map of HFD in Mainland Portugal as reported in http://geoportal.lneg.pt, is shown in Figure 20.

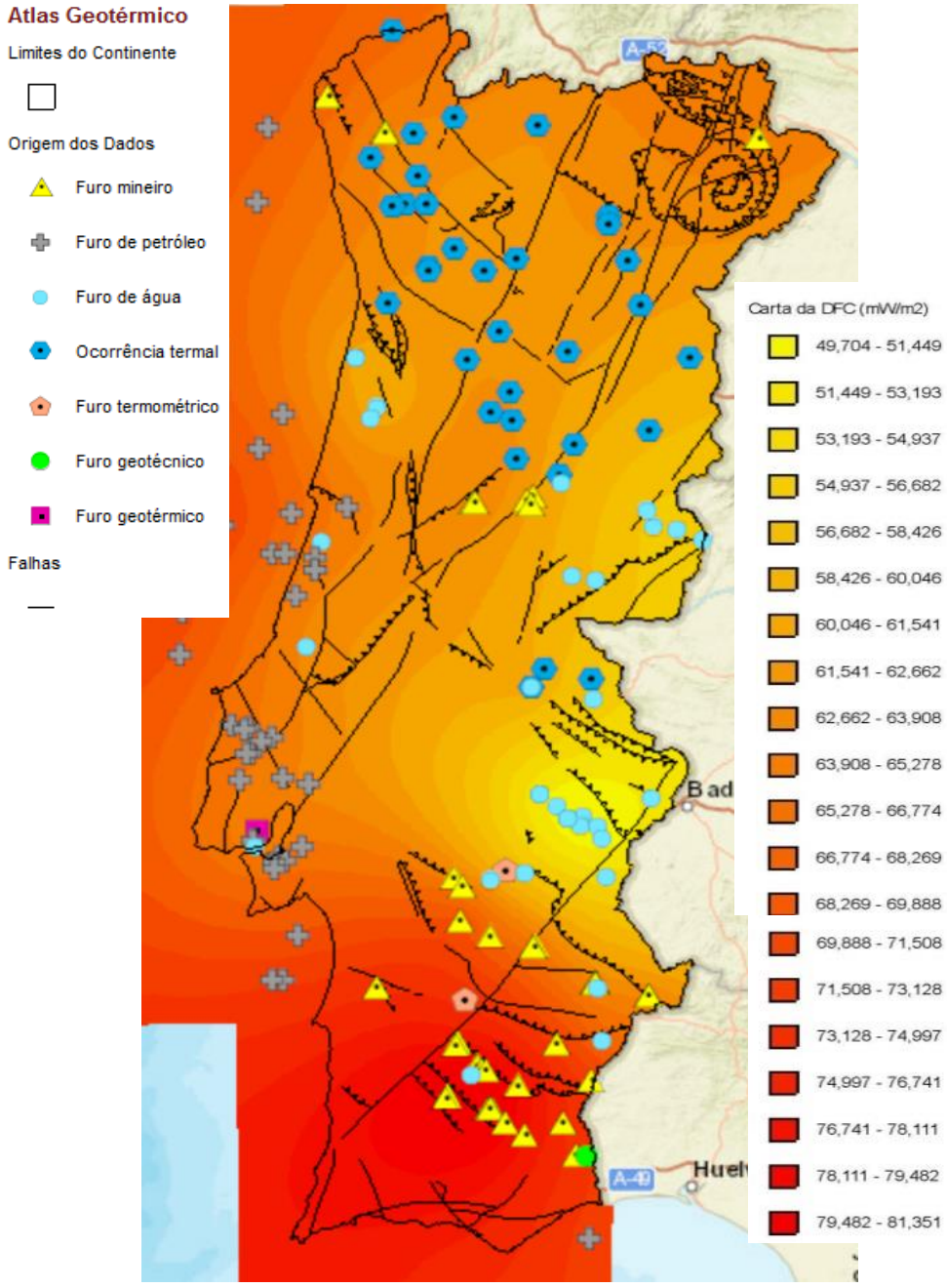

Figure 20. Heat flow map (DFC in Portuguese) for mainland Portugal, from the Portuguese Geothermal Atlas (Atlas Geoérmico) (http://geoportal.lneg.pt). Furo mineiro = mining well; furo de petróleo = oil well; furo de água = water well; ocorrência termal = thermal occurrence; furo termométrico = thermometric well; furo geotécnico =geotechnical well; furo geotérmico = geothermal well, falhas = faults). Units (mW/m^2).

Figure 21shows the heat flow map for the Iberian Pyrite Belt (http://geoportal.lneg.pt). As seen there is an increase of the HFD regional values in the South Portuguese Zone, more specifically in the Neves-Corvo area.

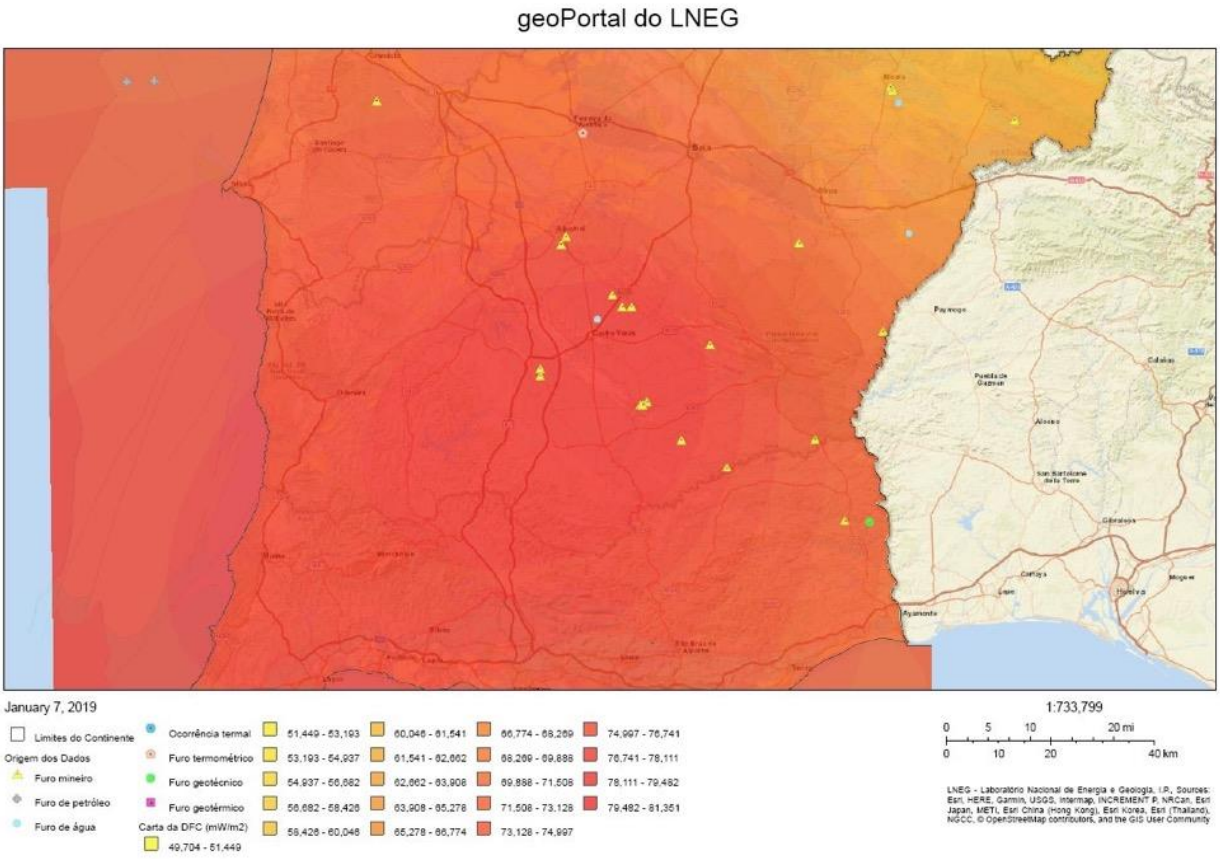

Figure 21. Surface Heat flow map (DFC in Portuguese) for the Iberian Pyrite Belt (http://geoportal.lneg.pt, from the Portuguese Geothermal Atlas (Atlas Geotérmico) (http://geoportal.lneg.pt). Furo mineiro = mining well; furo de petróleo = oil well); furo de água = water well; ocorrência termal = thermal occurrence; furo termométrico = thermometric well; furo geotécnico = geotechnical well; furo geotérmico = geothermal well, falhas = faults). Units (mW/m^2).

A map of the geothermal gradient for Mainland Portugal is shown in figure 22 and in the IPB is represented in figure 23 (http://geoportal.lneg.pt).

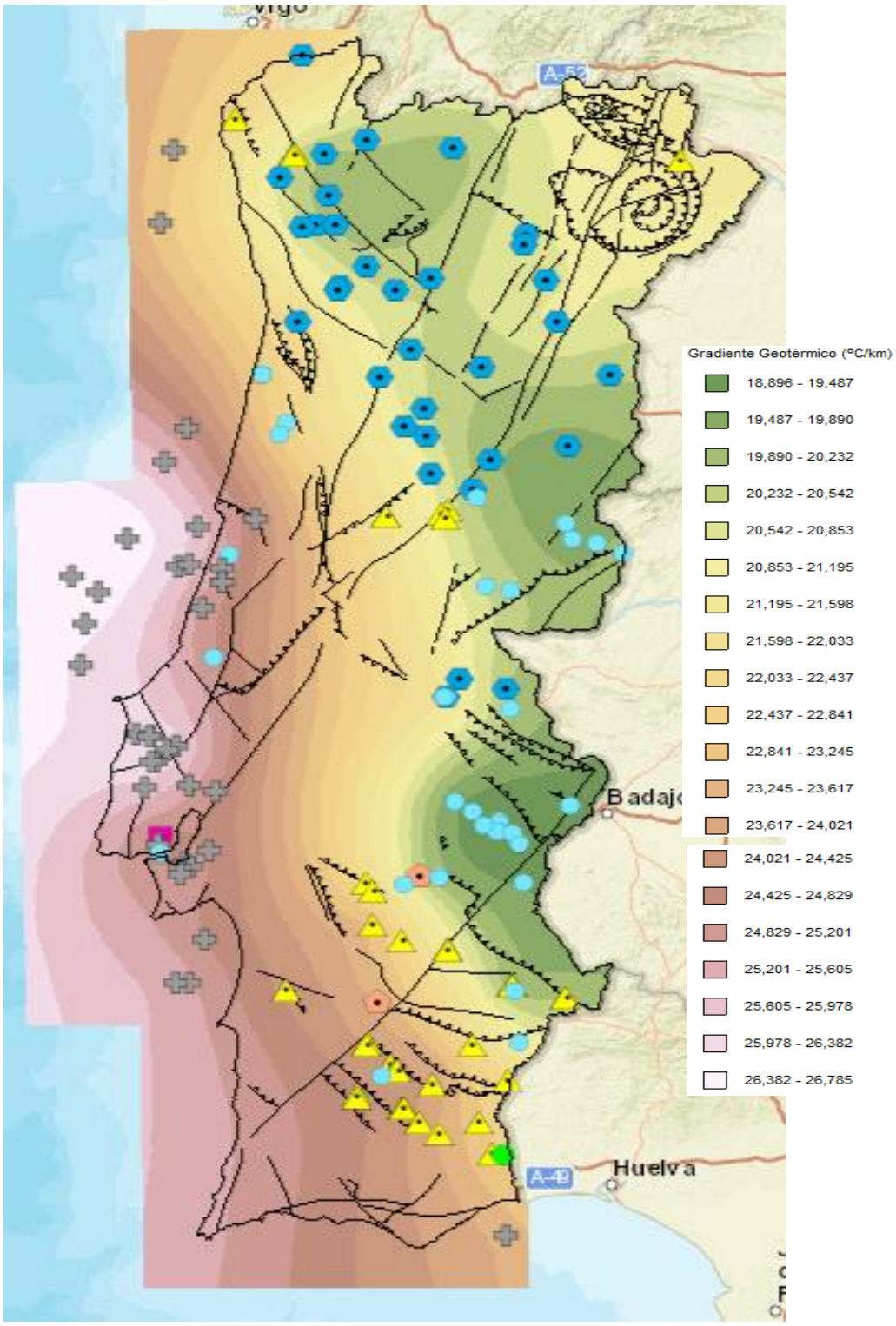

Figure 22. Geothermal gradient (Gradiente geotérmico in Portuguese) for Mainland Portugal with the IPB sector, [http://geoportal.lneg.pt,](http://geoportal.lneg.pt) from the Portuguese Geothermal Atlas (Atlas Getoérmico) (http://geoportal.lneg.pt). Furo mineiro = mining well; furo de petróleo = oil well); furo de água = water well; ocorrência termal = thermal occurrence; furo termométrico=thermometric well; furo geoténcico = geotechnical well; furo geotérmico = geothermal well, falhas = faults). Units °C/km.

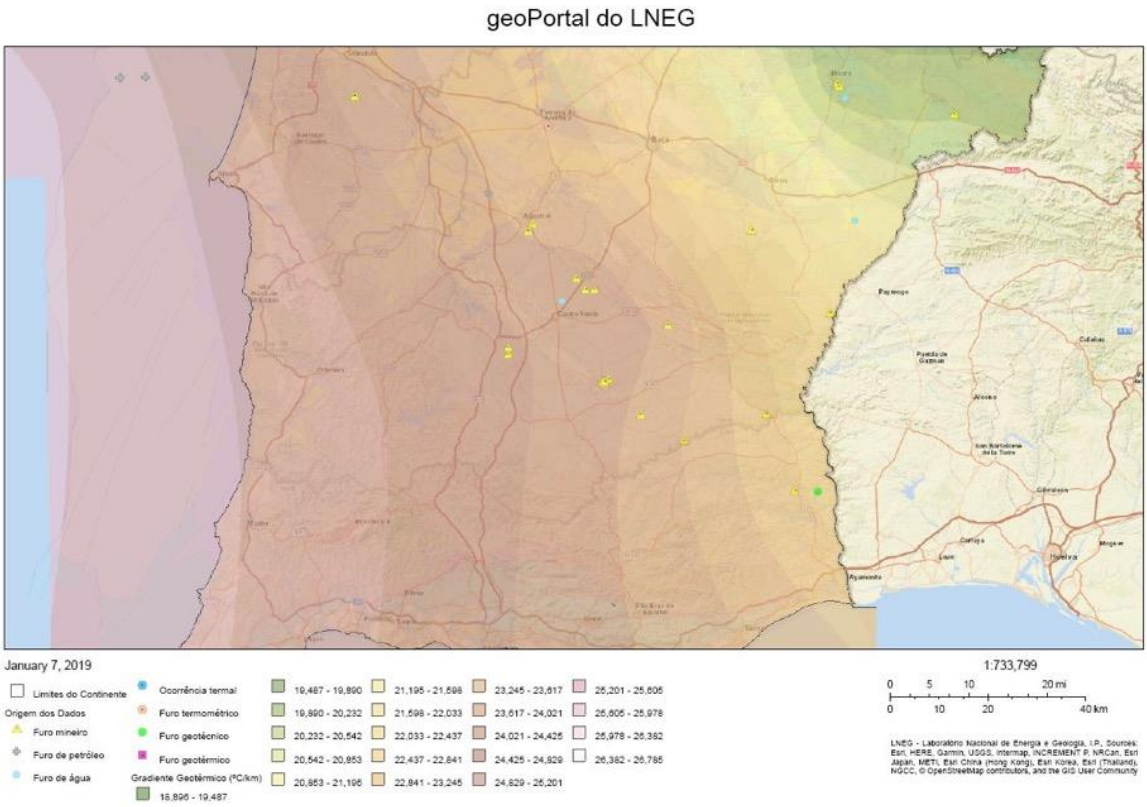

Figure 23. Geothermal gradient (Gradiente geotérmico in Portuguese) for the Iberian Pyrite Belt (http://geoportal.lneg.pt). from the Portuguese Geothermal Atlas (Atlas Getoérmico) (http://geoportal.lneg.pt). Furo mineiro=mining well; furo de petróleo=oil well); furo de água=water well; ocorrência termal=thermal occurrence; furo termométrico=thermometric well; furo geoténcico=geotechnical well; furo geotérmico=geothermal well, falhas=faults). Units °C/km.

As exhaustively reported in CHPM2030 D1.2.2, temperature in depth maps obtained with geothermal mapping together with thickness, transmissivity, and fluid chemical characteristics also in depth have a significant importance in the entire process to evaluate areas with more accurate methods and additional resources. Therefore, temperatures at 1,000, 2,000 and 5,000 m are estimated, following heat flow density estimations (from average thermal conductivity and geothermal gradient) and heat production values (A) (Haenel et al., 1980), based on spectrometric concentrations of U, Th and K, mostly from Rybach and Cermak (1982), Correia (1995) and aerospectrometric surveys for mining prospecting.

In this case, the step model was used.

$$T(z) - T_0 = \frac{q\,z}{k} + \frac{A\,z^2}{2\,k} \qquad (1)$$

where T(z) is the temperature at depth z (°C), T_0 is the average surface temperature on Earth (°C), z is the depth (m), A is the heat production per unit of volume ($Wm^{-1}K^{-1}$), q is the surface heat flow density (Wm^{-2}) and k is the thermal conductivity ($Wm^{-1}K^{-1}$)

Whenever possible, considered temperature was the measured temperature or interpolated between two measured temperatures, such as the case of onshore and offshore boreholes. In case of its inexistence, temperatures were extrapolated to bigger depths from shallower depths. The first was used only in several oil wells, after bottom bole temperatures correction for thermal disturbances caused by drilling (Haenel et al., 1988).

Heat Flow Density inferred from silica geothermometers (Ramalho and Correia, 2015) was not used for the IPB area, although its values were considered at national level, since there was information enough about k and A. Generally, temperatures in depth are higher in the Lusitanian Basin and in the SPZ, where the IPB is located.

Temperatures at 1000 m depth for the IPB are represented in http://www.geoportal.pt, in the Atlas de Geotérmico de Portugal Continental group of layers, reaching about 40 °C in the IPB, estimated with the methods described previously. According to Pacheco (2018, pers.com.) temperatures depth reach circa 40 °C in the lower levels of the Neves-Corvo Mine, about 900 m deep (CHPM2030 D1.2.2).

Temperatures at 2,000 m depth for the IPB are depicted in Figure 24, and can reach about 63 °C in the IPB. Estimated temperature in the area for 5,000 m deep, using the previously described methods for geothermal investigation is about 132 °C (Figure 25). EGS technology can therefore represent a huge renewable energy resource that could provide a significant base-load electric power if technical improvements in drilling technologies, rock fracturing techniques, and thermodynamic cycles were achieved

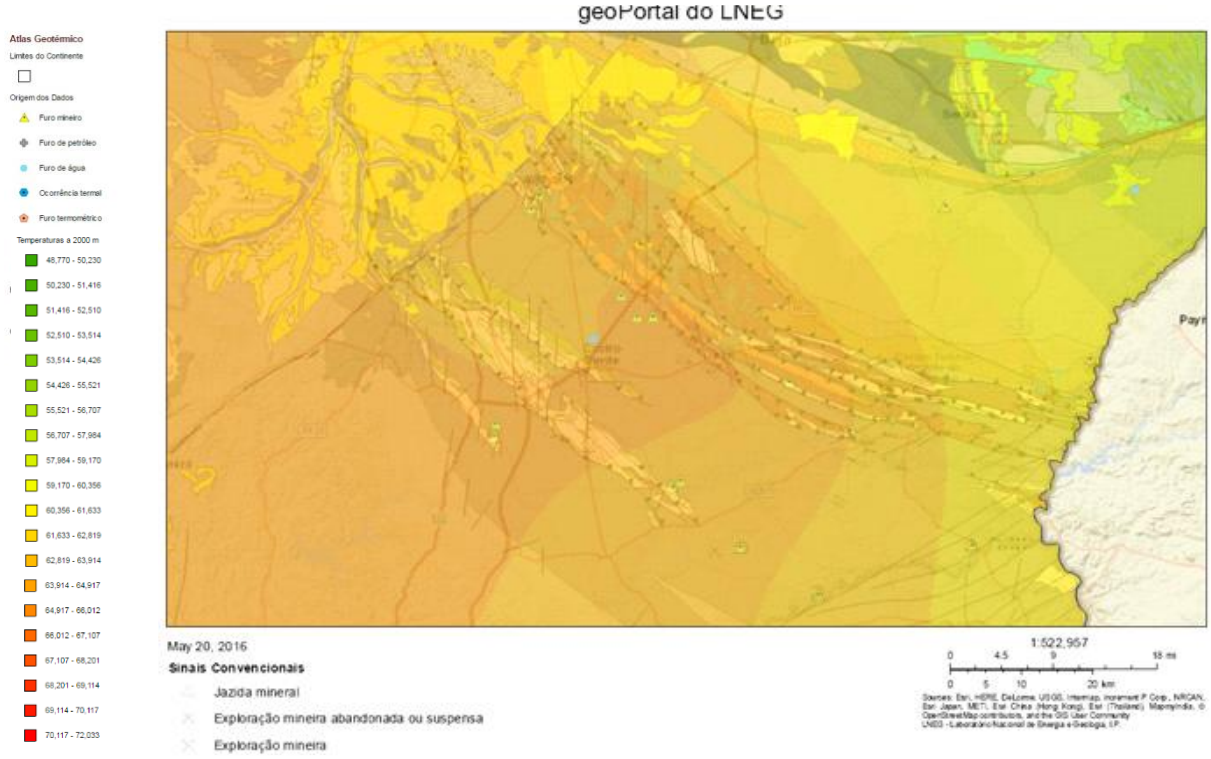

Figure 24. Temperature estimation (°C) at 2,000 m deep in the IPB Portuguese sector from the Portuguese Geothermal Atlas (Atlas Geotérmico) (http://geoportal.lneg.pt). Geology ad. from http://geoportal.lneg.pt. Furo mineiro = mining well; furo de petóleo = oil well); furo de água = water well; ocorrência termal = thermal occur rence; furo termométrico = thermometric well; jazida mineral = deposit ore; Exploração mineira abandonada ou suspense=abandoned or suspended mining exploitation; Exploração mineira = Mining exploitation).

Existing temperature in depth models and structural models in IPB will be jointly interpreted according with the 3D modelling that is being built.

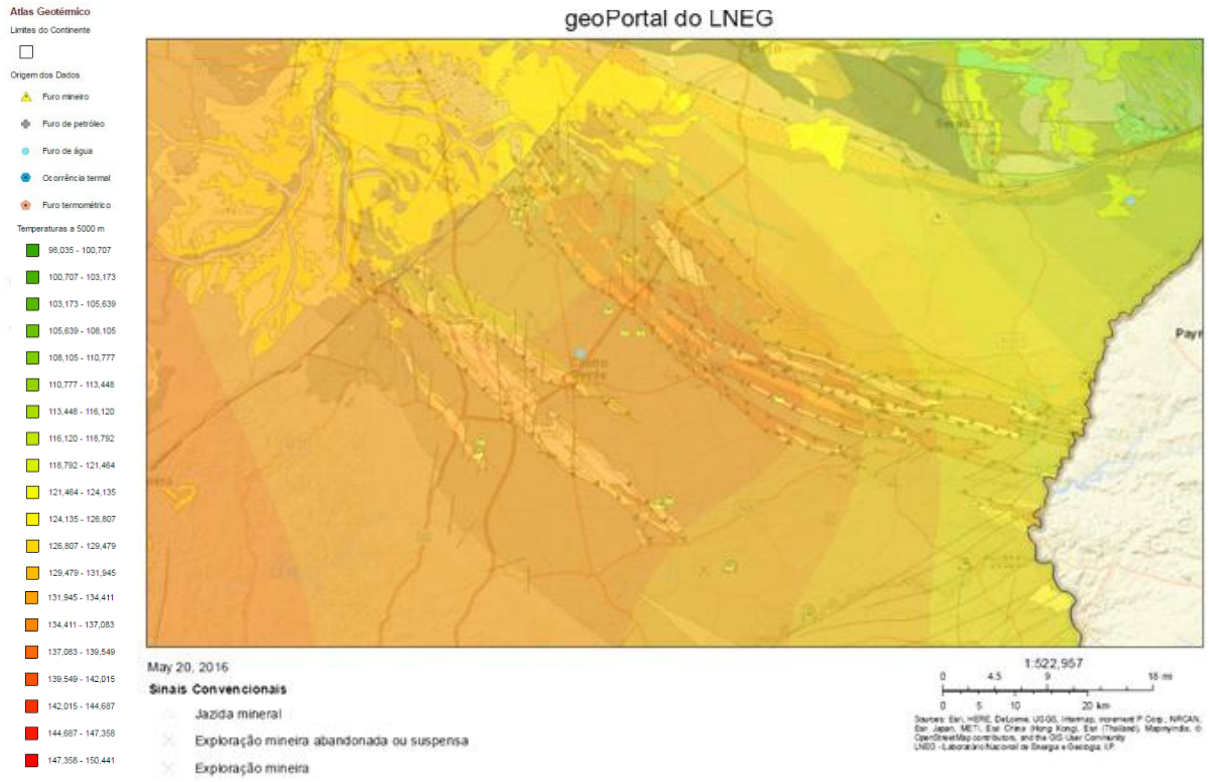

Figure 25. Temperature estimation (°C) at 5,000 m deep in the IPB Portuguese sector from the Portuguese Geothermal Atlas (Atlas Geotérmico) (http://geoportal.lneg.pt). Geology ad. from http://geoportal.lneg.pt. Furo mineiro=mining well; furo de petóleo=oil well); furo de água = water well; ocorrência termal = thermal occurrence; furo termométrico=thermometric well; jazida mineral = deposit ore; Exploração mineira abandonada ou suspense=abandoned or suspended mining exploitation; Exploração mineira = Mining exploitation).

6 INFORMATION FOR CHPM BUILDING BLOCKS

The following subchapters are focusing on the CHPM technological components and describes the available information regarding the study area. For future pilots, these aspects required to be fully described and elaborated. However, due to current knowledge gaps and limitations, actions and recommendations are going to be formulated to reach that level of understanding at the study area in the future. These next steps will be summaries in the Deliverable 6.3 Roadmap 2030 document.

6.1 Underground heat exchanger

Previous geothermal studies refer heat flow density values (HFD) of about 80 mW/m^2, in the area of Neves-Corvo Mine (Fig. 23). Although not the most attractive values for CHPM purposes, they are far from being disposable, and a well with 2500 meters depth may be enough for reaching the required temperatures for energy production.

6.2 Production/injection wells

At this moment, there are not available wells deep enough to ensure the duplet required by the method. Only if the new research data obtained through the Smart Exploration (H2020) and Explora (Alentejo2020) projects show good perspectives of the existence of a deeper orebody to exploit, deeper wells will be drilled by the mining company. The investment in these drill holes will be associated to the current VMS mineral exploration to be performed by Lundin Mining. Besides the presence of exploration drill holes conducted in the Neves-Corvo region up to 2,006 m length, that crossed mineralized stockwork at about 1,200-1,300 meters deep (Explora project, confidential information), so far, the deepest drill hole only achieve to a vertical depth of 1,645 m. However, at this particular depth the maximum reached temperature is of about 60 °C. Fig. 24 shows the temperature estimation (°C) at 2,000 m deep in the IPB Portuguese sector.

If recent reflection seismic surveys conducted at level -600 m of the mine and at the surface over the Lombador orebody provide good results concerning the prolongation of mineralization to deeper levels than the present one (-1,200 m), deeper wells will be drilled and therefore CHPM may be a feasible possibility to implement. So far, surface 1D loop transient electromagnetic (TEM) data suggests this possibility and, as stated above, stockwork mineralization has been intersected at 1200-1300m depth.

6.3 Metal recovery

Neves-Corvo extracts Cooper (Cu), Lead (Pb), Zinc (Zn) and Silver (Ag) only through an underground mine. Nowadays it produces about 45 000 tons of Cu and 75 000 tons of Zn per year. The deposits located within the Neves-Corvo Mining Concession consist of seven orebodies: Neves, Corvo, Graça, Zambujal, Lombador, Monte Branco and Semblana, the last two still in exploration phase, as referred in CHPM2030 D1.2.2 report. To date, a total of 1,037 surface drill holes for 822,266 m and a total of 5,928 underground drillholes for 591557m have been completed. The drilling, together with geophysical data has defined the seven mineralized zones of Neves, Corvo, Graça, Zambujal, Lombador, Monte Branco and Semblana with a combined total strike length of over 5,000 m and to depths of up to 1400m from surface (https:\\www.lundinmining.com).

6.4 Power plant

Neves-Corvo is located about 15 km away from Almodôvar and about 20 km southeast of the town of Castro Verde (Fig. 26) and approximately 220 km southeast of Lisbon. Almodôvar and Castro

Verde have about the same amount of population, with about 7,500 inhabitants in the county. The small town of Aljustrel, presently with IPB active mining (Almina company) and located slightly further away (42 km) has a population of around 9,200. Neves-Corvo has good connections to the national road network and a dedicated railway link into the Portuguese railway network and to the port of Setúbal (actual ore concentrate export area). There are no major centres of population close to the mine, although there are many small villages with populations numbered in the hundreds in the vicinities of the Neves Corvo Mine, many of them with inhabitants working in the mine. Energy may be used to supply these villages and the surface Mine facilities. The mine is connected to the national grid by a single 150 kV, 50 MVA rated, overhead power line 22.5 km long. The Neves-Corvo Mining Concession provides sufficient surface rights to accommodate the existing mine infrastructure and allow expansion as contemplated by ZEP.

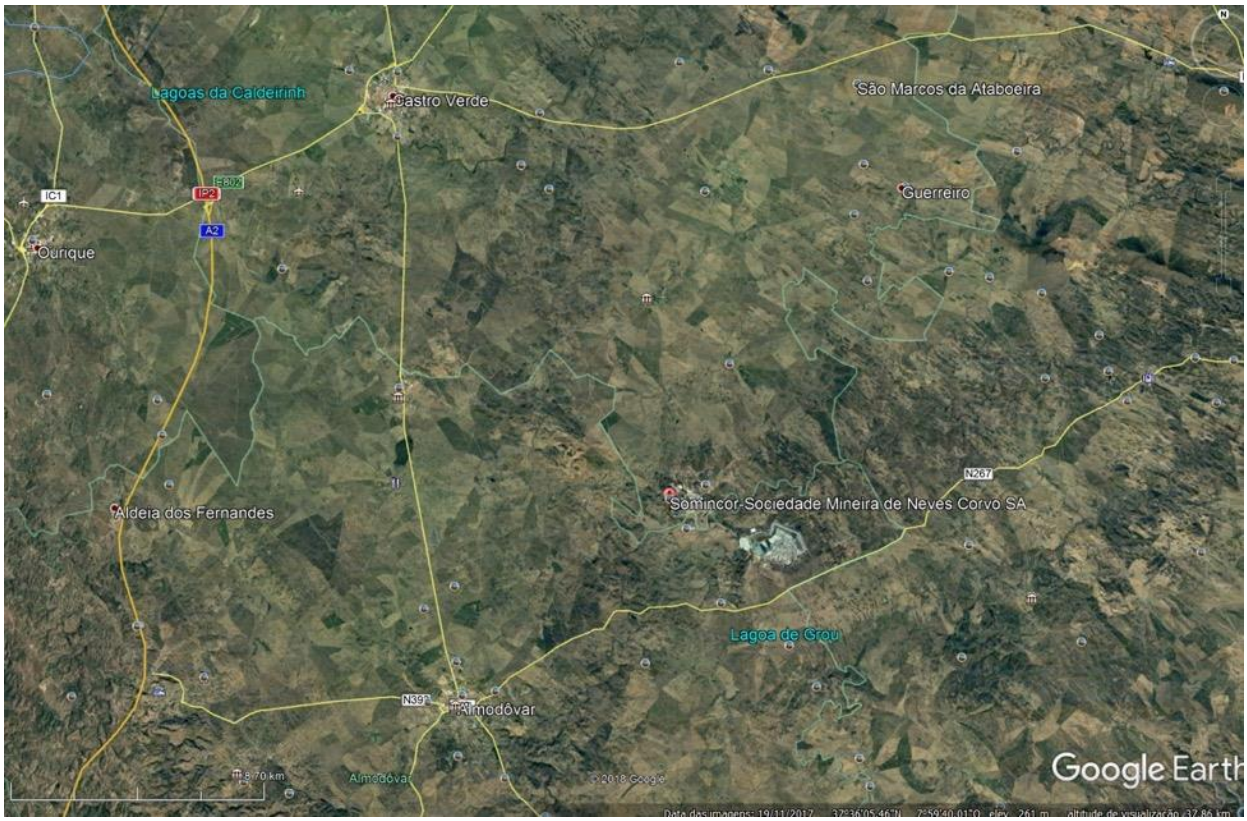

Figure 26. Location of Mina de Neves-Corvo and both major villages nearby, Almodôvar and Castro Verde (GoogleEarth@).

6.5 Salt Geothermal Power Generation

Although Neves-Corvo does not have deep enough drill holes to extract geothermal brine, there is a stream nearby named Ribeira de Oeiras, containing freshwater above the mine. The Oeiras stream valley cross cut several vertical faults taking water towards depth. In the mining area the stream floor is cemented to avoid and control water infiltration in the area where are located the

mining infrastructures (shafts and galleries). As common in the south of Portugal the water flow is very low and seasonal (long dry season). Considering the landscape and geological settings it cannot be considered as an option for salt geothermal power generation.

Fresh water is supplied to the mine via a 400 mm diameter pipeline from the Santa Clara reservoir, approximately 40 km west of the mine. Supply capacity is 600 m^3/h whilst storage facilities close to the mine hold 30 days' requirements. The current total fresh water requirement for the mine and plant is approximately 180m^3/h with as much as 75 % of the volume being reused (www.lundinmining.com).

6.6 Environmental, social, political background

Portugal, like many other countries is facing the challenge of changing the energy paradigm. Renewable energies, especially geothermal energy, play an important role in this subject since its use is not limited in time and is available 24/7. Geothermal energy being ecological, with reduced gas emissions towards the atmosphere, safe and easy to control has also the possibility of being jointly used with other energy sources to increase its efficiency.

This type of energy is economically sustainable although there is a significant initial investment, either for small or medium size installations.

Able of being used at regional level is therefore an increasing factor of industrial competitively, bringing positive effects in the economy development and job creation.

However, these types of energies have a weak dissemination in public opinion and there is a total absence of tradition in this type of geothermal exploitations, in opposition of their strong dissemination in northern Europe. Nevertheless, the fact that Portugal has had so far no commercial oil-discovery and several public contestation and protest against oil exploration in Portuguese mainland and offshore, opens the ways to alternative energy sources, such as geothermal exploration.

In spite of this, legislation in Portugal is still very low focused. Indeed, there is a lack of legislation adapted to the new reality of shallow geothermal installations. Geothermal resources are generally ruled by the Portuguese Law 15/2015 of June 22nd and the Decree-Law 87/90, from March 16th. Having a mixed technical component in the Geology and Energy areas, there are not many companies with skills to ensure the quality of these projects and to implement this type of energy. Synergies must be assured if this type of technology will ever be implemented.

Specifically, in the Mine of Neves-Corvo SOMINCOR has developed a corporate and site strategy for reducing energy use and GHG are monitored and reported as part of the Air Quality Greenhouse Gas Management Plan ("AQGHGMP"), although this system has only recently been put in place. To meet water quality discharge thresholds, the water management system has been recently redesigned and reengineered. Portuguese discharge quality standards have been met since the introduction of these new systems. Overall water consumption and discharge into surface water bodies is expected to increase as a result of the Zinc Expansion Project (ZEP), but will stay well within the permitted requirements due to improvements in water recycling and water management on site.

6.7 Financial

At this moment the Portuguese government does not contribute continuously to private initiatives regarding the implementation and use of any renewable energy or any innovative projects regarding the paradigm of energy transition. Special calls with special objectives are therefore at the moment launched in a non-periodical way. Anyway, the Fundo de Apoio à Inovação (FAI) (http://fai.pt/) is one of the national governmental organizations that can provide some financial aid to the implementation of new concepts of generating heat in a renewable and clean way.

6.8 Meeting stakeholder requirements

The Pilot mission objective at the Portuguese Iberian Pyrite Belt, Task 6.2.2, was twofold, serving the overall objective of setting the ground for subsequent pilot implementation. The first, and main goal was developing the evaluation template and investigating the Portuguese Iberian Pyrite Belt according to it. The result of this subtask is this report. The second objective was to develop a surveying program covering simultaneously stakeholder requirements from the mining and geothermal sectors, eventually combining the two agendas under the same program. This summary describes the beginning of this effort.

So far, the knowledge about the existence of deep orebodies is restrained to about 1500 m depth. Since mineral exploration is the major activity that brings local and national economy into life, only if new deeper orebodies will be found under the scope of mineral exploration may bring the two agendas (mineral and geothermal) together. Keeping in mind that working together on mineral exploration and on geothermal exploration, a CHPM exploration campaign or a complex survey for CHPM, would be dependent on new deeper orebodies discoveries and the evolution of technical capabilities for exploitation at such large depths. The combination of the tools and approaches

from mineral and geothermal exploration will therefore be a target to reach if that scenario will become a reality. If so, a CHPM pilot technology involving the mine can be included in the roadmapping for 2030, if the Portuguese Government and Lundin Mining will accept to sign a Grant Agreement that involves mineral and geothermal stakeholder requirements for geo-data acquisition.

This subtask will be further explained in the Deliverable 6.3 Roadmap document, and will provide future recommendation on this line of activities.

7. 3D MODELLING

This 3D modelling chapter was deliberately left for last because it contains the information that will be used in first stages of Roadmapping. In fact, due to unfinished character of this subject, it is an important part of the Roadmapping. So far, Oasis Montaj and GoCad are being used to build a 3D model of the joint geological, geophysical and mining information gathered in Neves-Corvo Mine concession area. Besides the drillholes data, superficial geological mapping and underground mining data were considered in the generation of key surfaces related with the major geological units. These data are crucial to constrains the geological and geophysical models and to infer the existence of deeper mineral orebodies that can be useful for CHPM purposes. Special focus is on the Lombador orebody, that shows good prospects of continuity at depth. This orebody that may serve simultaneously the goals of the ultra-deep mining activity and temperatures in depth high enough to produce energy (http://geoportal.lneg.pt). Therefore, taking as basis the Promine project "Nano-particle products from new mineral resources in Europe" (https://cordis.europa.eu/project/rcn/93327/reporting/en), further developments were undertaken and included as information to develop in CHPM technology. Some non-crucial, but confidential, selected 3D models were introduced in this report so that a quick look at the models can be foreseen as the possible prolongation in depth of the Lombador orebody. Figures 27 and 28 show the 3D model of the Neves-Corvo mine region depicting major stratigraphic boundaries, orebodies and location of drillholes.

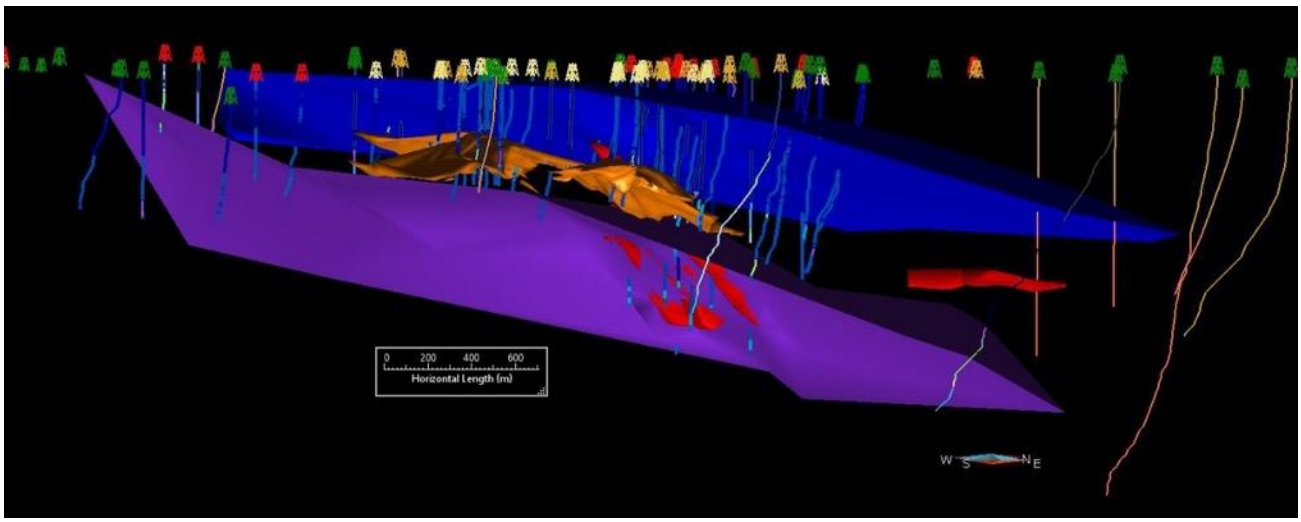

Figure 27. 3D model of the Neves-Corvo mine region showing major stratigraphic boundaries, orebodies and location of drillholes in GoCad. Legend: Blue - Top of ore-bearing Volcanic-Sedimentary Complex (VSC) geol ogical unit. Purple - top of the basement unit Phyllite - Quartzite (PQ) Formation. Red - Semblana and Lombador orebodies. Orange - Neves, Corvo and Graça orebodies. Drillholes are plotted in different colours because they belong to different surveys. White boreholes have no information.

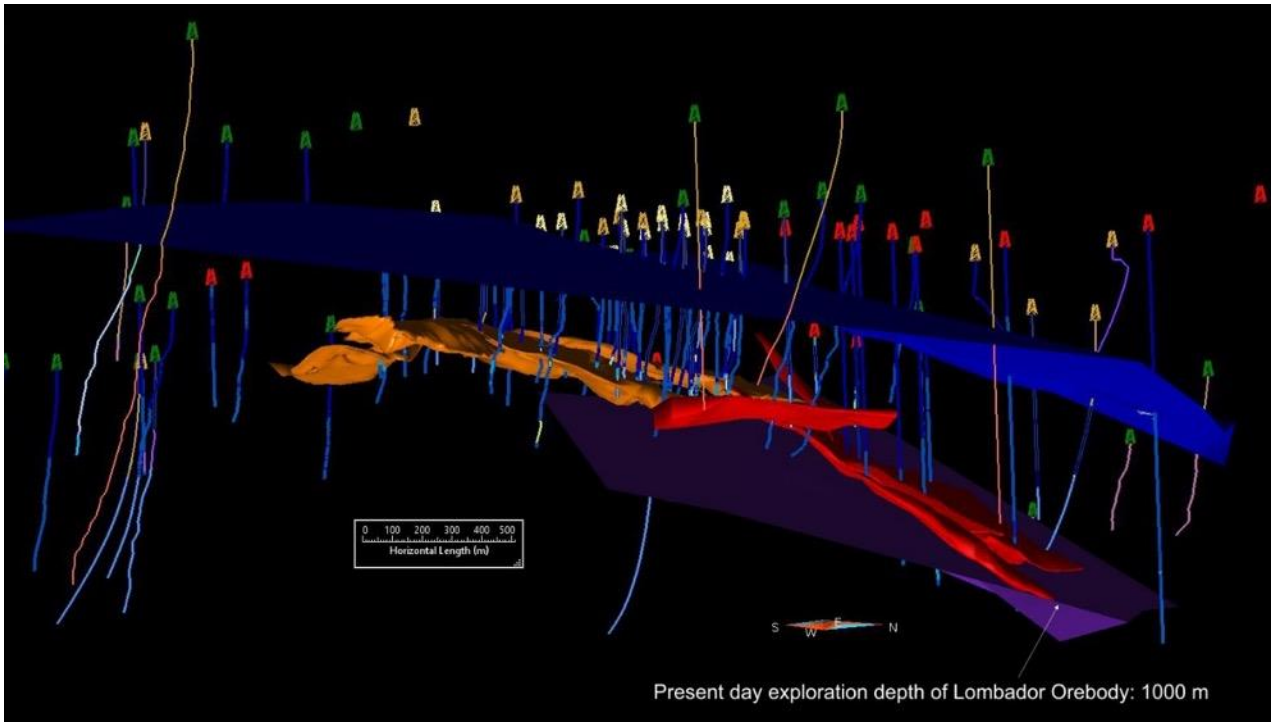

Figure 28: A different view of the 3D model of the Neves-Corvo mine region showing major stratigraphic boundaries, orebodies and location of drillholes in GoCad. Legend: Blue - Top of ore-bearing Volcanic-Sedimentary Complex (VSC) geological unit. Purple - top of the basement unit Phyllite-Quartzite Formation. Red - Semblana and Lombador orebodies. Orange - Neves, Corvo and Graça orebodies. Drillholes are plotted in different colours because they belong to different surveys. White boreholes have no information.

The Lombador strikes in depth, but it was crossed by very few drillholes at the time of the Promine project. Figure 30 shows a close-up view of the 3D model and recent drill holes showing present exploitation depth of the Lombador orebody.

The inclusion of transient electro-magnetic (TEM) cross-section resulting from the inversion of 1D surface loops, overlapped to the 3D geological model shows the prolongation of the Lombador orebody host rocks till at least 1600 m, as suggested by TEM data and confirmed by a drillhole (in Figure 31). The existence of 3 loops with 3 lines inside of it, with 3000 meters long and 23 cross sections as the inversion of 1D surface loops to be processed with Maxwell, will allow a much more detailed view of the Lombador orebody, based on its electromagnetic characteristics.

The result of the inverted 1D surface loop, chosen by crossing the recent borehole shown in Fig. 29, clearly shows a distinctive layer with higher electrical conductivities that may correspond the prolonging in depth of Lombador orebody. The same Figure 30 shows an area where a borehole, drilled from the mine gallery at 600 meters depth intercepted a stockwork mineralization at 1400-1500 meters depth, a suggested by the figure. This leaves good prospects to the 3D modelling that will be carried out in the TEM inverted sections, to build the 3D model, including the recently acquired reflection seismics in the mine.

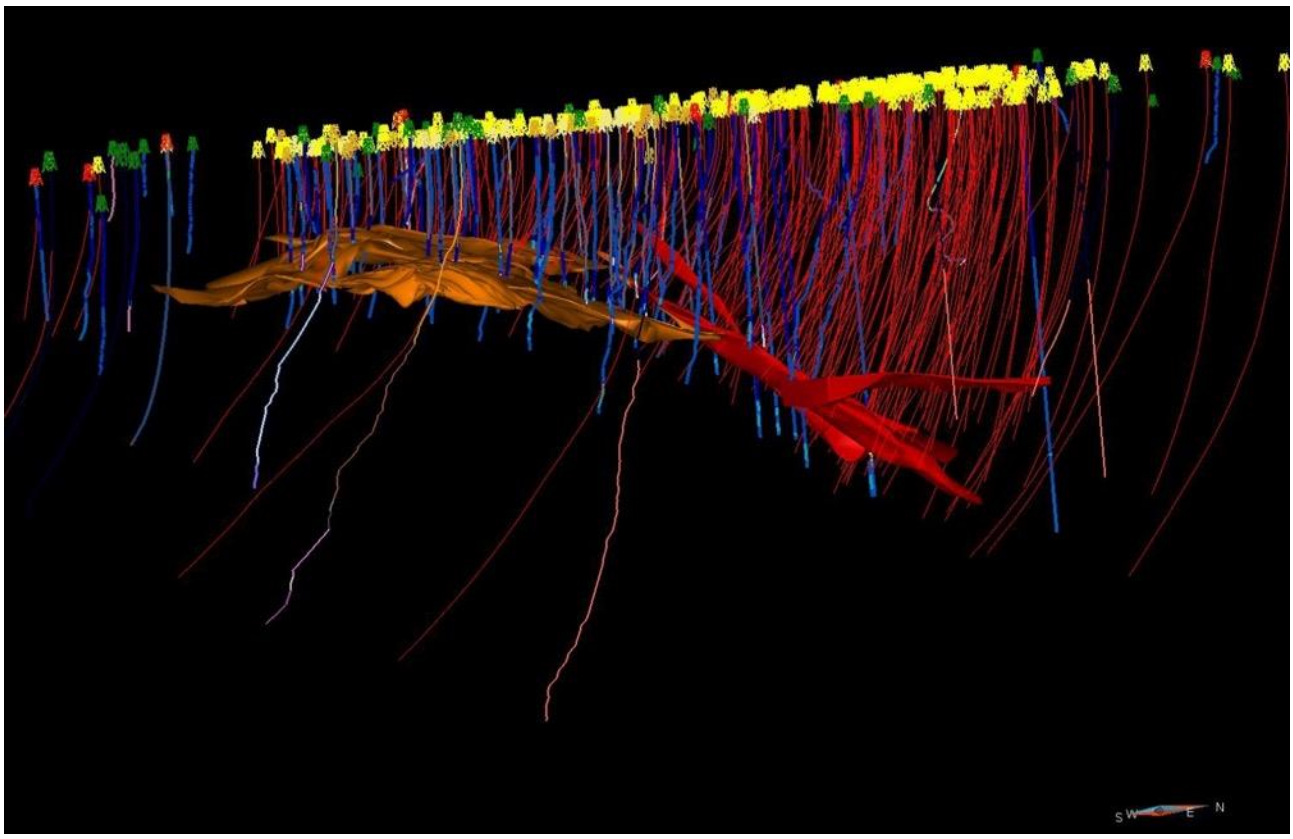

Figure 29. Close-up view in a different perpective of the 3D GoCad model showing present exploitation depth of the Lombador orebody. Legend: Red - Semblana and Lombador orebodies. Orange - Neves, Corvo and Graça orebodies. Yellow corresponds to new drillhole data drilled after Promine project. Notice deep drillholes cutting across Lombador orebody and going much deeper. Drillholes are plotted in different colours because they belong to different surveys.

Reprocessing 2D seismic profiles overlapped to the 3D geological model are part of the Smart Exploration project (Fig. 31). The prolongation of the Lombador orebody host rocks till at least 1600 m is also suggested by 2D seismic data conducted by Promine.

The mine galleries intersecting the Neves-Corvo and Lombador orebodies are depicted in Fig. 32. In this figure, purple parts correspond to location of receivers that were used to collect the in-mine recent seismic data, at the level 640 m. The purpose was to investigate how deep mineralization extends down dip.

As it can also be seen from Fig. 32, there are good prospects that the Lombador orebody extends in depth, but only with the data processing that will be carried out by Smart Exploration and Explora projects, further information can be added to CHPM purposes.

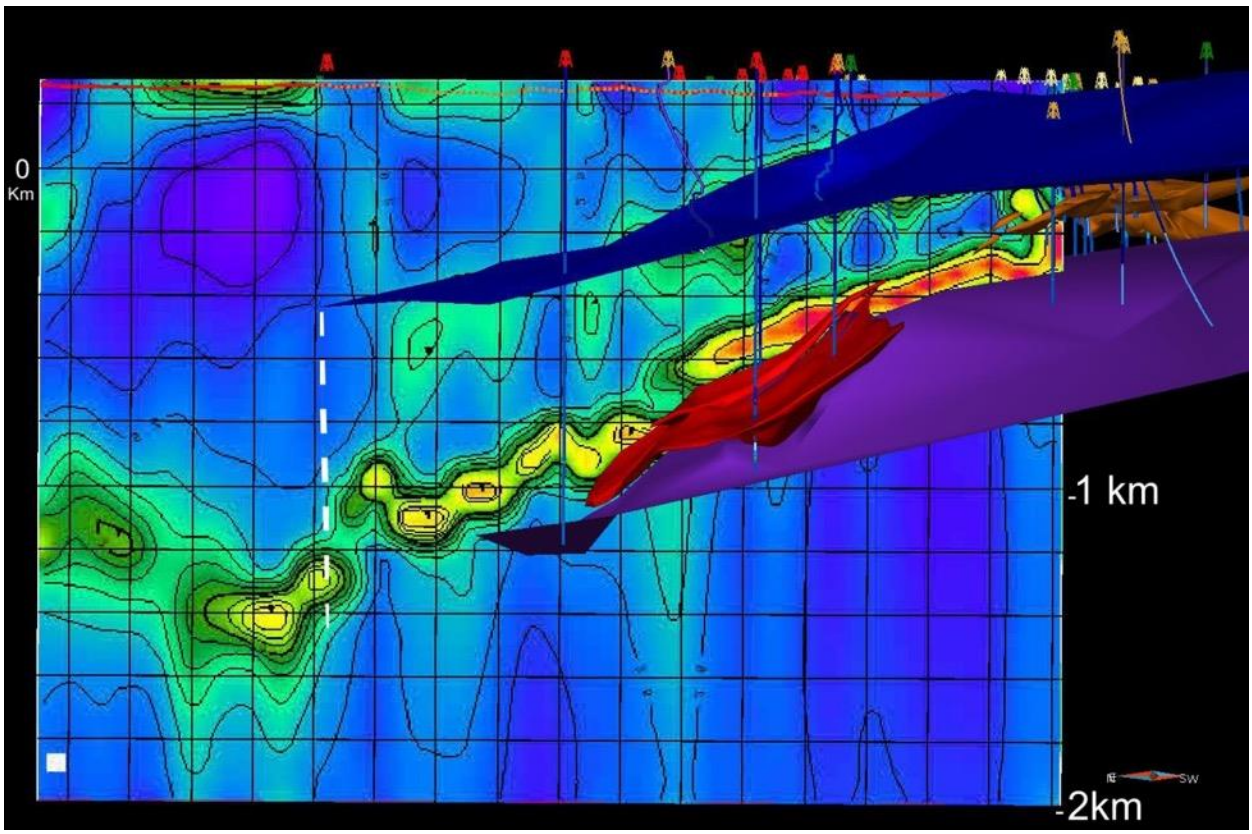

Figure 30. Transient electro-magnetic (TEM) cross-section resulting from the inversion of 1D surface loops, overlapped to the 3D geological model. Legend: Blue - Top of ore-bearing Volcanic-Sedimentary Complex (VSC) geological unit. Purple - top of the basement unit Phyllite-Quartzite Formation. Red - Semblana and Lombador orebodies. Orange - Neves, Corvo and Graça orebodies. The prolongation of the Lombador orebody host rocks till at least 1600 m is suggested by TEM data. Dash white line represent approximate location of recent borehole that intersected stockwork mineralization at 1400-1500 m depth. Blue corresponds to low electrical electrical conductivities, yellow and finally red correspond to high and very high electrical conductivities. Drillholes are plotted in different colours because they belong to different surveys.

8 CONCLUDING REMARKS

The last edition of the "Geothermal Resources Atlas of Europe" (Hurter and Haenel, 2002), incorporates this dataset and added some thermometric boreholes drilled with specific geothermal purposes near the IPB. According with Heat Flow Density Commission the geothermal information approach is reliable and quality of data is improved as more information is acquired. The geothermal database followed the format described in Ramalho (1999) and follows as much as possible the standards defined by the International Heat Flow Commission (Jessop, 1990). For the reached studied depths (~1,000 m) the temperatures (~40°C) cannot allow questioning the implementation of a CHPM facility. But at 2,000 m depth, estimated temperature of about 70 °C, may be interesting for the implementation of this technique. The existence in depth of further

orebodies yet to be exploited may be considered as promising and therefor, with a good potential for the use of CHPM.

Nevertheless, Southern Portugal may show good prospects to implement CHPM technology. However, it still lacks the co-existence of deep wells, able of producing energy and the absolute knowledge of ultra-deep orebodies that supply brines with adequate characteristics.

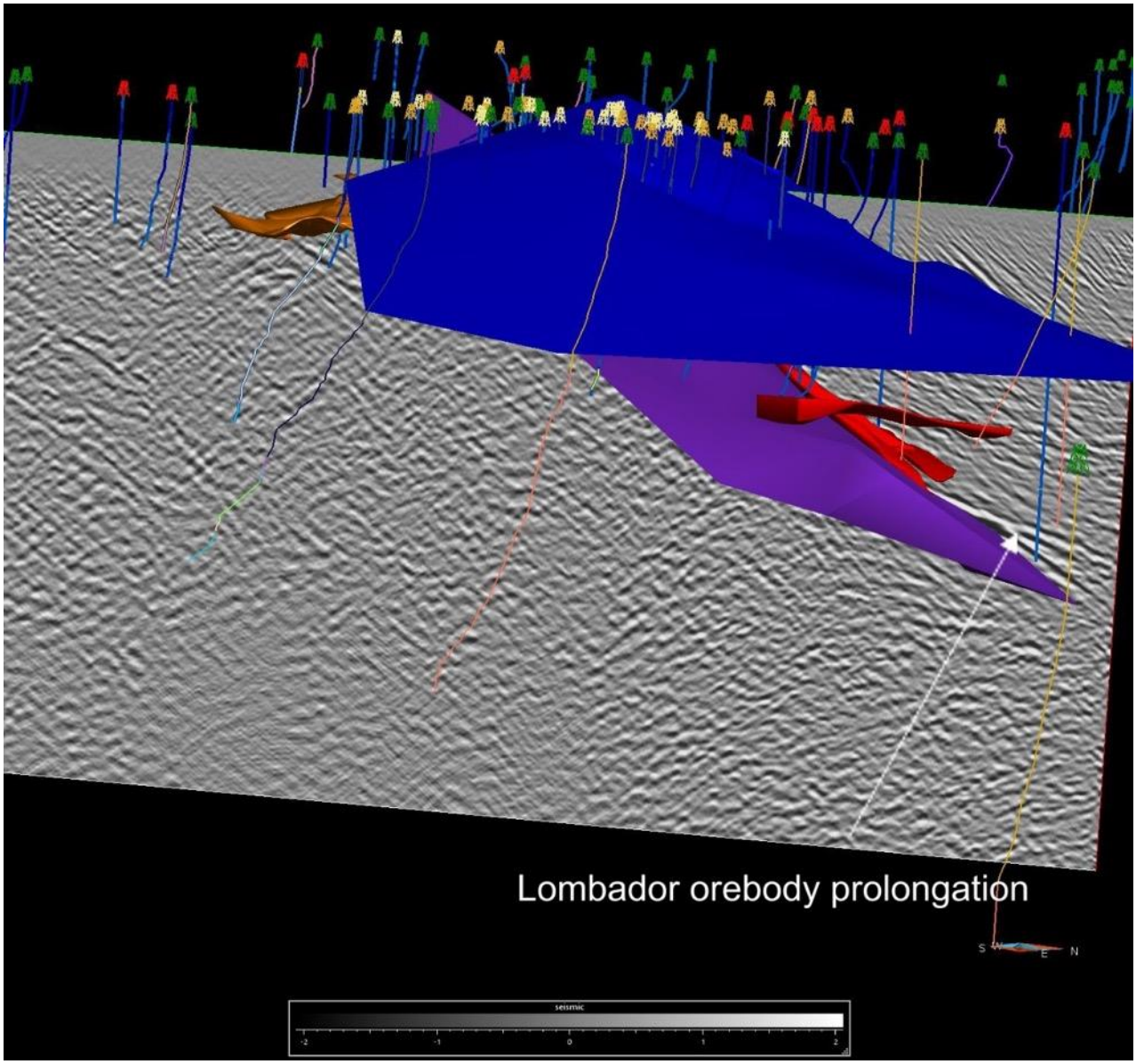

Figure 31. Reprocessed 2D seismic profile overlapped to the 3D geological model. Legend: Blue - Top of ore-bearing Volcanic-Sedimentary Complex (VSC) geological unit. Purple - top of the basement unit Phyllite-Quartzite Formation. Red - Semblana and Lombador orebodies. Orange - Neves, Corvo and Graça orebodies. The prolongation of the Lombador orebody host rocks till at least 1600 m is suggested by seismic data. Drillholes are plotted in different colours because they belong to different surveys.

So far, the deepest well drilled by Neves-Corvo reaches about 2 km and maximum temperature is about 65 °C. This leaves us with a big gap between the necessary depths for CHPM technology and the dataset which is currently available.

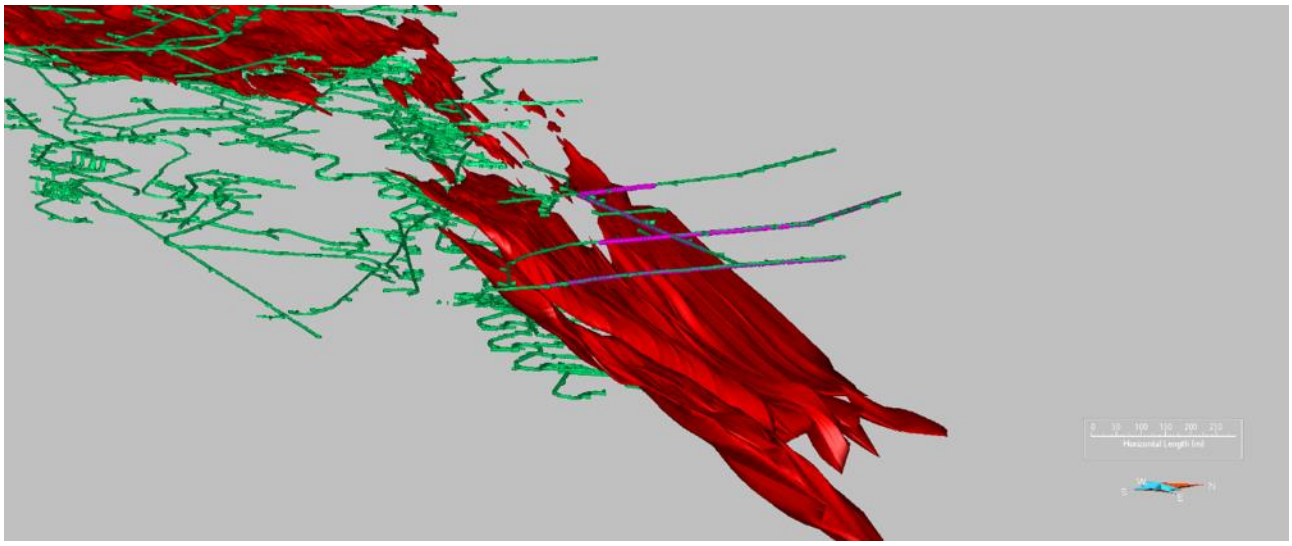

Figure 32. Mine galleries intersecting the Neves-Corvo and Lombador orebodies (green). Purple parts correspond to location of receivers that were used to collect in-mine seismic data, at the level 640 m. The purpose was to investigate how deep mineralization extends down dip..

Very recent geophysical and drilling results suggest the possibility of the existence of mineralization at least at 1.5 km, possibly at bigger depths, decreasing the gap between present mineralization and CHPM required depths.

Although 3D modelling of the orebodies is still underway. The studied data also allow to consider the future development of EGS facilities. The Roadmapping for 2030 document will aim to highlight some important issues to implement in such a time horizon CHPM.

ACKNOWLEDGEMENTS

The authors of this document wish to thank to Lundin Mining, specially Nelson Pacheco, Chief Geologist of the Neves-Corvo mine and Mafalda Oliveira, all the technical support to the CHPM 2030 LNEG team. Portuguese CH2030 team also thanks Judite Fernandes in the hydrogeology, Augusto Filipe for sharing figures related with SIORMIN database. The team thanks Patrícia Represas and Fábio Marques from LNEG, the project EXPLORA (Alentejo 2020) and the project SmartExploration (H2020) team, Pedro Dias source of the new data presented here.

REFERENCES

ALBOUY, L., CONDE, L.N., FOGLIERINNI, F., LECA, X., MORIKIS, A., CALLIER, L., CARVALHO, P., SONGY, J.C., 1981. *Le gisement de sulfures massifs polymétalliques de Neves-Corvo, Baixo Alentejo, Portugal*. Chronique de La Recherche Minière, nº 460, BRGM: 5-27.

BARRIGA, F.J.A.S., CARVALHO, D., RIBEIRO, A., 1997. Introduction to the Iberian Pyrite Belt. In: Barriga, F.J.A.S., Carvalho, D. (eds.). Geology and VMS deposits of the Iberian Pyrite Belt. Society of Economic Geologists Neves-Corvo Field Conference, Guidebook Series, 27:

BATISTA, M. J., 2003. Comportamento de elementos químicos no sistema rocha-solo-sedimento-planta na área mineira de Neves-Corvo: Implicações Ambientais. PhD thesis, University of Aveiro, 393p.

BATISTA, M.J., REPRESAS, P., MATOS, J.X., INVERNO, C.M.C., 2014. 3D predictive modelling using drillhole geochemistry and gravity inversion. First approach using data from Neves-Corvo mining area, Iberian Pyrite Belt. Comunicações Geológicas 101, Esp. II, p. 747-752, IX CNG/2º CoGePLiP, Porto, ISSN:0873-948X, e-ISSN: 1647-581X.

BERTRAND, L., CARRARA, M., DELPONT, G., FEUGA, B., LANDRY, J. AND WOJTKOWIAK, F., 1982. "Reconnaissance Hydrogeologique du Gisement de Neves-Corvo". Somincor, Sociedade Mineira de Neves-Corvo. *Bureau de Recherches Geologiques et Minieres, Agence d'Interventions a l'Etranger.*

CARVALHO, D., BARRIGA, F. J. A. S., MUNHÁ, J., 1999. *Bimodal-siliciclastic systems – the case of the Iberian Pyrite Belt.* Reviews in Economic Geology 8: 375-408.

CARVALHO, J., INVERNO, C., MATOS, J.X., ROSA, C., GRANADO, I., BRANCH, T., REPRESAS, P., CARABANEANU, L., MATIAS, L., SOUSA, P., 2016. Subsurface Mapping in the Iberian Pyrite Belt Using Seismic Reflection Profiling and Potential Field Data. International Journal of Earth Sciences, Geol Rundschau, Ed. Springer Verlag, DOI 10.1007/s00531-016-1340-1, 19p.

CORREIA, A., 1995. Determinação da produção de calor em amostras rochosas. Aplicação a amostras portuguesas, *Comunicações do Instituto Geológico e Mineiro*, T. 81, pp.39-46.

DOYLE, M., 1996. Las Cruces Copper Deposit, Pyrite Belt, Spain. *Bol. Geologico y Minero ITGE*, v. 107 (5-6), Madrid, 201-204.

Haenel, R., Legrand, R., Balling, N., Saxov, S., Brow, K., Goble, R., Meunier, J. Fanelli, M., Rori, A., Solomone, M., Taffi, L., Prins, S., Berley, A. J., Edmunds, W. M., Oxburgh, E. R., Richardson, S. W.

and Wheildon, 1980. Atlas of Subsurface Temperature in the European Community, Th. Schafer Druckerei GmbH, Hannover, 36p., 43 maps.

HAENEL, R., RYBACH, L. and STEGENA, L., 1988. Handbook of terrestrial heat flow determination: with guidelines and recommendations of the International Heat Flow Commission. Springer, 486p.

Inverno, C., Díez-Montes, A., Rosa, C., García-Crespo, J., Matos, García-Lobón, J. L., Carvalho, J, Bellido, F., Castello-Branco, J.M., Ayala, C., Batista, M. J., Rubio, F., Granado, I., Tornos, F., Oliveira, J. T., Rey, C., Araújo, V., Sánchez-García, T., Pereira, Z., Represas, P., Solá, A. R. and Sousa, P., 2015. – Chap. 9. Introduction and Geological Setting of the Iberian Pyrite Belt, pp. 191-207. 3D, 4D and Predictive Modelling of Major Mineral Belts in Europe, Mineral Resource Reviews, DOI 10.1007/978-3-319-17428-0_9.

JESSOP, A. M. , 1990. Thermal Geophysics. Developments in solid Earth Geophysics. Elsevier. 306p.

LEISTEL, J., MARCOUX, E., THIEBLEMONT, D., QUESADA, C., SANCHEZ, A., ALMODOVAR, G., PASCUAL, E., SAEZ, R, 1998. The volcanic-hosted massive sulphide deposits of the Iberian Pyrite Belt. Review and preface to the special issue. *Mineralium Deposita*, 33, pp.2-30.

MATOS, J. X., MARTINS, L., ROSA, C., 2003. Parque Mineiro da Cova dos Mouros – IGM contribute for the sustainable development of the mining park. IGME, Pub. Museo Geom., nº2, p. 487-494.

MATOS, J.X., FILIPE, A., Coordenadores, 2013. Carta de Ocorrências Mineiras do Alentejo e Algarve à escala 1:400 000, versão digital. Edição LNEG/ATLANTERRA, Lisboa. ISBN: 978-989-675-029-9, Colaboração: D. Oliveira, C. Inverno, C. Rosa, M.J. Batista, Z. Pereira, R. Salgueiro, T. Cunha, F. Barreira. http://www.lneg.pt/download/7904/.

MATOS, J.X., MENDES, M., ALBARDEIRO, L., MORAIS, I., MARQUES, F., PEREIRA, Z., SOLÁ, R., BATISTA, M.J., CARVALHO, J., SALGUEIRO, R., SOUSA, P., INVERNO, C., OLIVEIRA, D.P.S, 2018. Projeto EXPLORA. Encontro Ciência, FCT 2018. Resumo, Sessão Industrialização e Processos e Materiais Avançados, 2 p.

MATOS, J.X., PEREIRA, Z., ROSA, C.J.P., ROSA, D.R.N., OLIVEIRA, J.T., RELVAS, J.M.R.S., 2011. Late Strunian age: a key time frame for VMS deposit exploration in the Iberian Pyrite Belt. *11TH SGA Biennial Meeting*, Autofagasta, Chile, pp. 790-792.

OLIVEIRA, J. T., coord., 1992. Notícia Explicativa Carta Geológica de Portugal, esc. 1/200 000, fl. 8, Serv. Geológicos de Portugal.

OLIVEIRA, J. T., ROSA, C. J. P., PEREIRA, Z., ROSA D. R. N., MATOS, J. X., INVERNO, C. M. C. and ANDERSEN, T., 2013. Geology of the Rosário–Neves-Corvo antiform, Iberian Pyrite Belt, Portugal: new insights from physical volcanology, palynostratigraphy and isotope geochronology studies. Mineralium Deposita, 48: 749-766.

OLIVEIRA, J., QUESADA, C., 1998. A comparison of stratigraphy, structure and paleogeography of the South Portuguese Zone and Southwest England, European Variscides. *Annual Conference of the Ussher Society*, Geoscience in south-west England 9, 141-150.

OLIVEIRA, J.T., ROSA, C., ROSA, D., PEREIRA, Z., MATOS, J.X., INVERNO, C., ANDERSEN, T., 2013. Geology of the Neves-Corvo antiform, Iberian Pyrite Belt, Portugal: New insights from physical volcanology, palynostratigraphy and isotope geochronology studies. Mineralium Deposita 48: DOI 10.1007/s00126-012-0453-0, pp. 749-766.

OLIVEIRA, V., MATOS, J. X., BENGALA, M., SILVA, N., SOUSA, P. and TORRES, L., 1998. Geology and geophysics as successful tools in the discovery of the Lagoa Salgada orebody (Sado Tertiary Basin - Iberian Pyrite Belt), Grândola, Portugal. Mineralium Deposita, 33: 170-187.

RAMALHO, E. C. and CORREIA, A. (2015) – Estimativa da densidade de fluxo de calor à superfície em Portugal Continental: aplicação de geotermómetros de SiO_2 em águas de circulação profunda. Actas do X Congresso Ibérico de Geoquímica, Lisboa, Portugal.

RAMALHO, E. C., 1999. O "Atlas de Recursos Geotérmicos da Europa" como impulso da inventariação da informação geotérmica existente em Portugal Continental', *Actas do Encontro sobre Sistemas de Informação Geográfica e Geológica de Base Regional, 23 Setembro 1999, Beja*, Painel 1 – Projectos Europeus e Transfronteiriços, pp.1.41-1.44.

REISER, F. K. M., ROSA, D. R. N., PINTO, A. M., CARVALHO, J. R. S., MATOS, J. X., GUIMARÃES, F., ALVES, L. C., de OLIVEIRA, D.P.S., 2011. Mineralogy and geochemistry of tin- and germanium bearing copper ore from the Barrigão remobilised vein deposit, Iberian Pyrite Belt, Portugal. International Geology Review, Taylor & Francis Ed., Vol. 53, n. 10, 1212–1238 p.

RELVAS J. M. R. S., BARRIGA, F. J. A. S, FERREIRA, A., NOIVA, P. C.S, FERREIRA, A, NOIVA, PC, PACHECO, N., BARRIGA, G., 2006. Hydrothermal alteration and mineralization in the Neves-Corvo volcanic-hosted massive sulfide deposit, Portugal: I. Geology, Mineralogy, and Geochemistry. *Economic Geology*, 101-4: 753-790.

REPRESAS, P., SOUSA, P., CARVALHO, J., TORRES, L., MATOS, J.X., 2016. Carta Magnética (Campo Total Reduzido Do Igrf) Da Zona Sul Portuguesa, Faixa Piritosa Ibérica, ESC. 1/400 000. EDIÇÃO LNEG/URMG, LISBOA, ISBN: 978-989-675-047-3.

REPRESAS, P., SOUSA, P., TORRES, L., BENGALA, M., MATOS, J.X., 2016. Carta Gravimétrica (anomalia de Bouguer, densidade 2,6) da Zona Sul Portuguesa, Faixa Piritosa Ibérica, esc. 1/400 000. Edição LNEG/URMG, Lisboa, ISBN: 978-989-675-046-6.

ROSA, C.J.P., MCPHIE, J., RELVAS, J., PEREIRA, Z., OLIVEIRA, T., PACHECO, N. 2008. Volcanic setting of the giant Neves-Corvo massive sulfide deposit, Iberian Pyrite Belt, Portugal. Mineralium Deposita, 43: 449-466.

RYBACH, L. and CERMAK, V., 1982. Radioactive heat generation in rocks. In: G. Angenheister (Editor), Landolt-Bornstein. Numerical data and functional relationships in science and technology. *New Series,* Group V, vol. 1a, Springer-Verlag, Berlin, pp. 353-371.

TORNOS, F., 2006. Environment of formation and styles of volcanogenic massive sulfides: The Iberian Pyrite Belt. Ore Geology Reviews, 28: 259-307.

TORNOS, F., BARRIGA, F., MARCOUX, E., PASCUAL, E., PONS, J. M., RELVAS, J., VELASCO, F., 2000. The Iberian Pyrite Belt, in Large, R., Blundell, D. (eds.). Database on global VMS districts: CODES-GEODE, p. 19-52.

CHPM2030 DELIVERABLE D6.2.3

REPORT ON PILOTS: EVALUATION OF THE CHPM POTENTIAL OF THE STUDY SITE, ROMANIA

Summary:

This report presents the data related to the Beius Basin - Bihor Mountains study area, evaluating for the potential of becoming a CHPM pilot area according to the concept presented in the CHPM2030 project; this pilot area has both geothermal potential and mineralization to enable their combined exploitation in a CHPM plant. In order to reach this goal, based on these data, further research can be initiated.

Authors:

Diana Perșa, Geological Institute of Romania, Researcher

Ștefan Marincea, Geological Institute of Romania, Senior Researcher

Delia Dumitraș, Geological Institute of Romania, Senior Researcher

Cătălin Simion, Geological Institute of Romania, Researcher

List of figures

List of tables

Table of content

Executive summary

The purpose of this study is to provide relevant information that leads to the selection of a pilot site, an area that has favorable preconditions for the existence of deep mineralization and high geothermal potential at the same place. In Romania the the Beiuș Basin – Bihor Mountains has been selected as study areas. The site is situated at the convergence of two major structural units and has characteristics similar those. Thus, the Beiuș Basin, which is a part of the Pannonian Basin, has high geothermal potential. At the same time, Bihor Mountains' structural unit is a part of the North Apuseni Mountains, and it is part of the metallogenic province Banatitic Magmatic and Metallogenetic Belt.

Both Pannonian Basin (Romanian part) and Beiuș Basin have the following relevant elements:

- The thin crust, (which is estimated at 25-27 km), and the thin lithosphere (60 -70 km) that resulted during regional extensional processes of Pannonian Basin that started in Miocene;
- Below Neogene deposits, Triassic deposits host a geothermal aquifer;
- The existence of intrusive magmatic bodies in the depth.

Both North Apuseni Mountains and Bihor Mountains have the following relevant elements:

- Existence of a granodiorite - granite pluton with regional extension that has been extruded during Late Cretaceous.
- The existence of important mineralized areas, specific to the Banatitic Magmatic and Metallogenetic Belt, among which we mention the skarns that have been formed at the contact between the pluton and the Mid-Triassic and Upper Triassic limestones.
- Existence of a large geothermal aquifer recharge area that is represented by karst deposits of mainly by Triassic deposits

Geothermal potential

For the eastern limit of the Pannonian Basin, Rădulescu and Dimitrescu (1982) estimated the mean heat flow of 96 mWm^{-2}. Geothermal gradients for **Pannonian Basin** are high, varying from 6.2 to 5.6 $^{o}C/100$ m at 500 m and at 2000 m b.s.w.l respectively. Due to the thin crust and the thin lithosphere, Beiuș Basin is characterized by high heat flow, with values up to 90 mWm^{-2}.

In **Apuseni Mountains**, in areas affected by Tertiary tectogeneses usually referred to terrains younger than 50 Ma, the three components of the regional heat flow: crustal radiogenic, thermal transient perturbation, and background heat flow from deeper sources, contributes with 36, 27 and 27 mWm^{-2}, respectively, to the mean value 90 mWm^{-2}.

Thermal conductivity [10^{-3}cal/cm x ^{o}C x s] of the rocks belonging to the Romanian part of the Pannonian Basin and the surrounding areas has been determined through laboratory methods, and has high values varying from 3,5 – 12 for granites, 4.8 – 5.0 for diorites and 6 – 7 for dolomitized limestone.

Based on these data the conclusion is that in Bihor Mountains, the heat flow of granitic – granodioritic bodies from Pietroasa and Budureasa are supposed to have high values in the depth. Also the heat flow of the rocks that host the geothermal aquifer (limestone, dolomite and quartzite, marble) has high values. But an important cooling agent is represented by the continuous circulation of the surface water through the karst areas of Bihor Mountains into the geothermal aquifer from Beiuș Basin. It is expected that in the depth of 4 km, where the access of water is prevented by the aquiclude Lower Triassic layers the heat flow of the batholith to be considerable.

Deep metal enrichment

Mineralization is widespread in the mountainous area and is expected to be found in the basin area. In Bihor Mountains the mineralization is generated during the banatitic calcalkaline magmatism (Post-Lower

Masstrichtian-Palaeogene), which is represented by bodies of intrusive rocks, generally hypabyssal as well as plutonic ones, which are widely developed in the depth. Plutons of granodiorite-granite rocks, to which the main sulphide mineralization is genetically linked, constitute main mass of banatitic bodies in the Apuseni Mountains; in Bihor Mountains they crop out on small areas, but they develop in the depth.

Magmatic bodies intruded Permian-Mesozoic sequences and produced contact-metamorphic aureoles, at Pietroasa, Budureasa and, most extended at Baita Bihor. In the contact aureoles of the granodiorite-granites plutons, skarns with Fe, B, Bi, Mo have been formed. At Valea Seacă, Valea Mare-Budureasa etc., the skarns are overlapped by sulphide mineralization.

Brucite deposits from Budureasa and Pietroasa were investigated by surface pits, drillings and underground galleries. They have been formed at the contact of granodiorites with the Anisian dolomites and have a structure with four zones, ranging from granodiorites to pure dolomites containing holocrystalline hypidiomorphic granodiorites, magnesian skarns, Brucite-bearing zones, recrystallized Anisian dolomite.

Borate deposit is situated **i**n the middle basin of the Aleului Valley (Bihor Mountains), at its confluence with the Sebisel Valley, at the Gruiului Hill. The formation of the borates from the contact aureole of the Pietroasa granitoid body is the result of an infiltration metasomatic process.

W-bearing and base metal skarns are characteristic only for Baita Bihor. At Baița Bihor, some magnesian skarn bodies or ore pipes such as those at Antoniu, Bolfu-Tony, Hoanca Motului, Baia Roșie are **boron-bearing skarns** and represents well-defined metasomatic columns. A sole similar body, or metasomatic column, that from Dealul Gruiului was identified at Pietroasa.

Laboratory experiments performed during the implementation of this project lead to promising results.

- Two rock samples from Romania were used for **leaching experiments** by Chris Rochelle et al., in 2017 (CHPM2030 Project Deliverable 2.2): a skarn from Pietroasa and a mineralized rock from Cacova Ierii. The experiments used a range of fluid types and pressure/temperature conditions to identify fluid-rock reactions and quantify the potential for enhancing metal release. For conditions of temperature/ pressure of 100 °C, and 200 bar the efficient substances proved to be 0.6 M NaCl, and HCl/HNO3 mix for both samples. The main elements recovered are: **Co, Sr, Mo, Sb, Mn, Zn, W.**
- In 2018, using GDEx technology, Xochitl Dominguez et al. (CHPM2030 Deliverable 3.3) completed the experiments to **recover metals from the geothermal brine** provided by a Beiuș Basin well. According to this study, the results are promising. Especially the content of Sr in one of the brine samples and the content of Sr recovered are remarkable.
- A considerable enrichment of magnesium minerals was highlighted in the precipitate resulted from the geothermal water extracted from a Beiuș Basin well compared with spring and water coming from a mine. Thus, the magnesium content is less than 5% in surface, and at least 13% in the geothermal waters.

Integrated 3D model

Integrating all the data available in a 3D geological database and creating the 3D geological model provided an overview on the spatial distribution and the geometry of the middle and upper Triassic sedimentary deposits within Beiuș Basin and their contact with the Upper-Cretaceous intrusive body, from Bihor Mountains.

The 3D model shows the extension of Upper Triassic deposits, both in Beiuș Basin and in Bihor Mountains, linking the two structural units, generating magnesian skarns on one side and transporting geothermal water on the other. This dual role in the perimeter explains an increased content of magnesium in geothermal waters from Beiuș Basin.

The 3D model revealed the fact that there is a region bordering Beiuș Basin where the batholith is extended: at Budureasa, where there is an increased possibility to have both mineralisation and high geothermal potential within a small area.

The 3D model emphasizes the large areas on which Triassic deposits outcrop. Being represented by highly fissured karst deposits they, on one side, assure a continuous recharge of the geothermal aquifer, but, on the other side, they have an important contribution to the decrease of the geothermal potential of the rocks, being a cooling agent.

The batholith's apophyses that were detected by complex geophysical methods within Beiuș Basin, and can be taken into consideration for further investigations are represented by the model.

The 3D model helped us to visualize and understand the spatial relations at the border between the basin and the mountains and provides new data that are needed to set the parameters for planning new exploration works.

At the same time the 3D model helps us to reduce the original area for new future investigations to a smaller area with an increased probability that it is suitable for a CHPM system.

Hydrogeology

The geothermal aquifer from Beiuș and Ștei is hosted in fractured Triassic dolomites that have a regional extension. Triassic aquifer from Beiuș Basin is a confined aquifer with negative piezometric levels (- 18.48 m 3001 H Beiuş and unstable – 45m 3003 H Beiuş) or artesian (3002 H Ştei), depending on the position of the tectonic block. Beiuș aquifer is an open geothermal system, where recharge equilibrates with the mass extraction and its reservoir pressure stabilizes. Its recharge can be both hot deep recharge and colder shallow recharge. The latter can eventually cause reservoir temperature to decline and production wells to cool down. In fact, this second alternative was demonstrated when the increase of the volume of injected water was accompanied by the decrease of the water temperature within aquifer. More research is needed to improve the knowledge on this subject. The aquifer is exploited by 2 extraction wells and one injection well in Beiuș, and one extraction well in Ștei, situated at a distance of 18 km from Beiuș. The most productive well is 3001, from Beiuș, that has a wellhead temperature of 88^{o}C, coming from 2460 m depth.

Geothermal district heating system

Beiuş town has an extensive geothermal heating system (GDHS), which provides heat for approximately 70% of the population, covering about 60% of the urban heating demand. The previous system that used coal as a source of energy was completely replaced by GDHS. The geothermal heat energy is delivered to the consumers either indirectly via substations with heat exchangers feeding double closed loop distribution pipe networks, one for Domestic Heating (DH) and the other for Hot Sanitary Water (HSW), or directly to the individual buildings with their own heat exchangers. The exploitation license of Beiuș geothermal reservoir perimeter is owned by Transgex S.A.

Currently, the geothermal energy exploitation system consists of 2 geothermal water production wells drilled to a TVD of 2576 m and 2700 m, with a production capacity of 450 m^3 / h, and one re-injection well having a TVD over 2,000 m. The geothermal water transport network in the city includes 18 km pipelines. The GDHS has the following users: 120 block stairs connected to the centralized distribution of heat; public institutions are heated with geothermal energy (colleges, schools, kindergartens, municipal hospital, community centre, pharmacies, medical offices and laboratories, churches and places of worship, gymnasiums); undertakings with more than 1000 employees; 200 individual homes with their own thermal units connected to the transmission geothermal water.

In 2016 the energy of 74,452 of GJ/year has been delivered to the population. The value of water production was higher than 1 million m^3. In 2018 a partnership formed by the City Hall and private company submitted project proposals in order to get EU funding for the extension of the GDHS. They also showed their interested for the results of CHPM2030 project and expressed their will to be part of a consortium that could consider a CHPM installation in Beiuș in the future.

1. Overview of CHPM2030 study area in Romania

1.1 Objectives and role of the CHPM2030 project

The pilot mission objective of Task 6.2 in Work Package 6 is to "Combine metallogenic models with geothermal datasets to develop a database of suitable areas in selected case-study areas in Europe where such developments could be feasible". One of these study-case areas is Beiuș Basin - Bihor Mountains in Romania.

1.2 Selection of the CHPM2030 study area in Romania

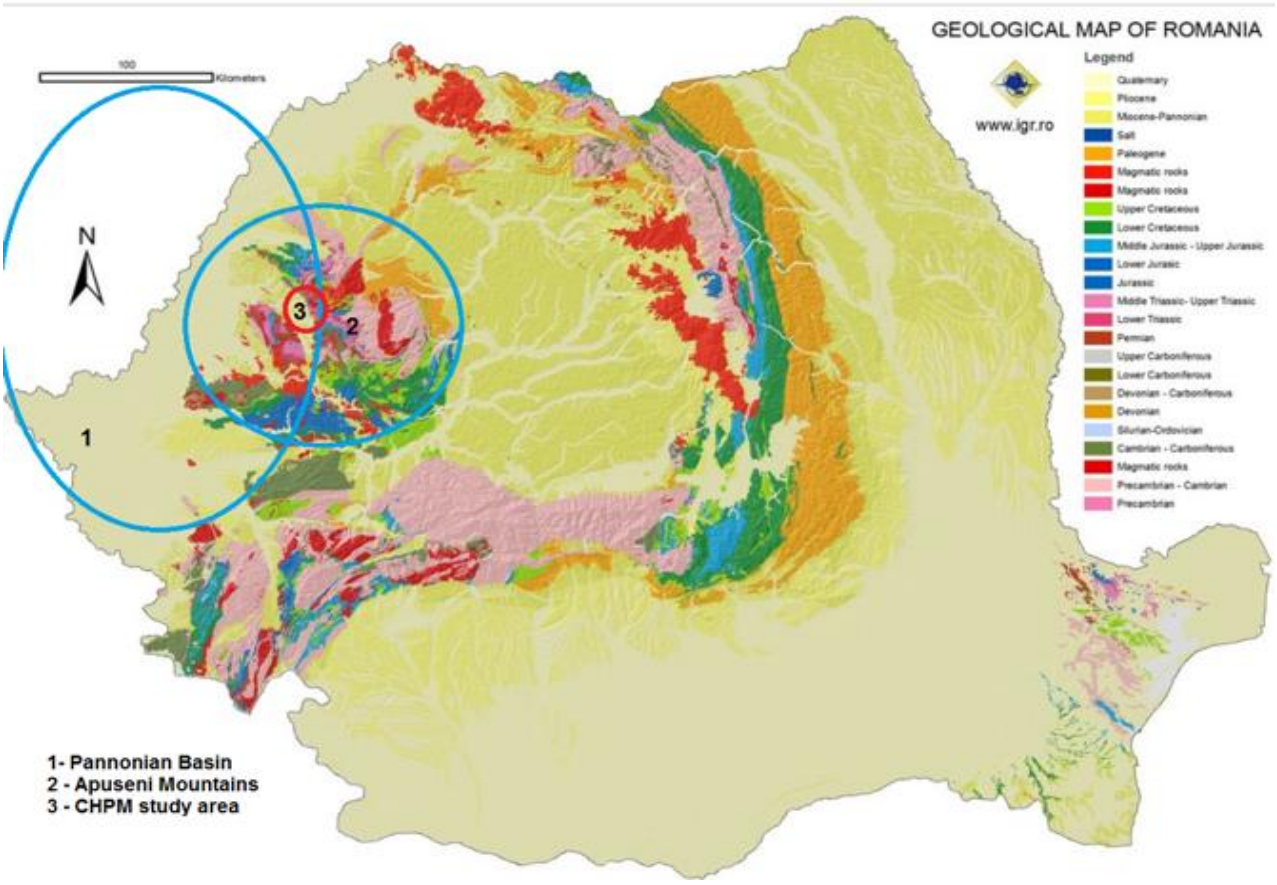

Figure 1 Location of the region Pannonian Basin – Apuseni Mountains

The CHPM study area, which includes Beiuș Basin and Bihor Mountains, is situated at the convergence of two major structural units and takes traits from each of them. Thus, the Beius Basin, which is an extension of the Pannonian Basin, has a geothermal potential similar to it. At the same time, Bihor Mountains structural unit is a part of the North Apuseni Mountains, and is included into the metallogenic province Banatitic Magmatic and Metallogenetic Belt (Figure 1).

The reasons why the study area was chosen in the junction region of the Pannonian Basin and the Apuseni Mountains (Figure 2) are:

- The high geothermal potential of the Pannonian Basin, being the highest in Romania, also found in the Beiuș Basin;
- Existence of a mineralization associated with the upper Cretaceous magmatism described both in the North Apuseni Mountains and in the Bihor Mountains;
- The existence of a granite – granodiorite batholith that outcrops in North Apuseni Mountains, but whose presence was also reported both in Beiuș Basin, at depth;

A map showing the relation between regional and local structural units we are referring to is given in Figure 2.

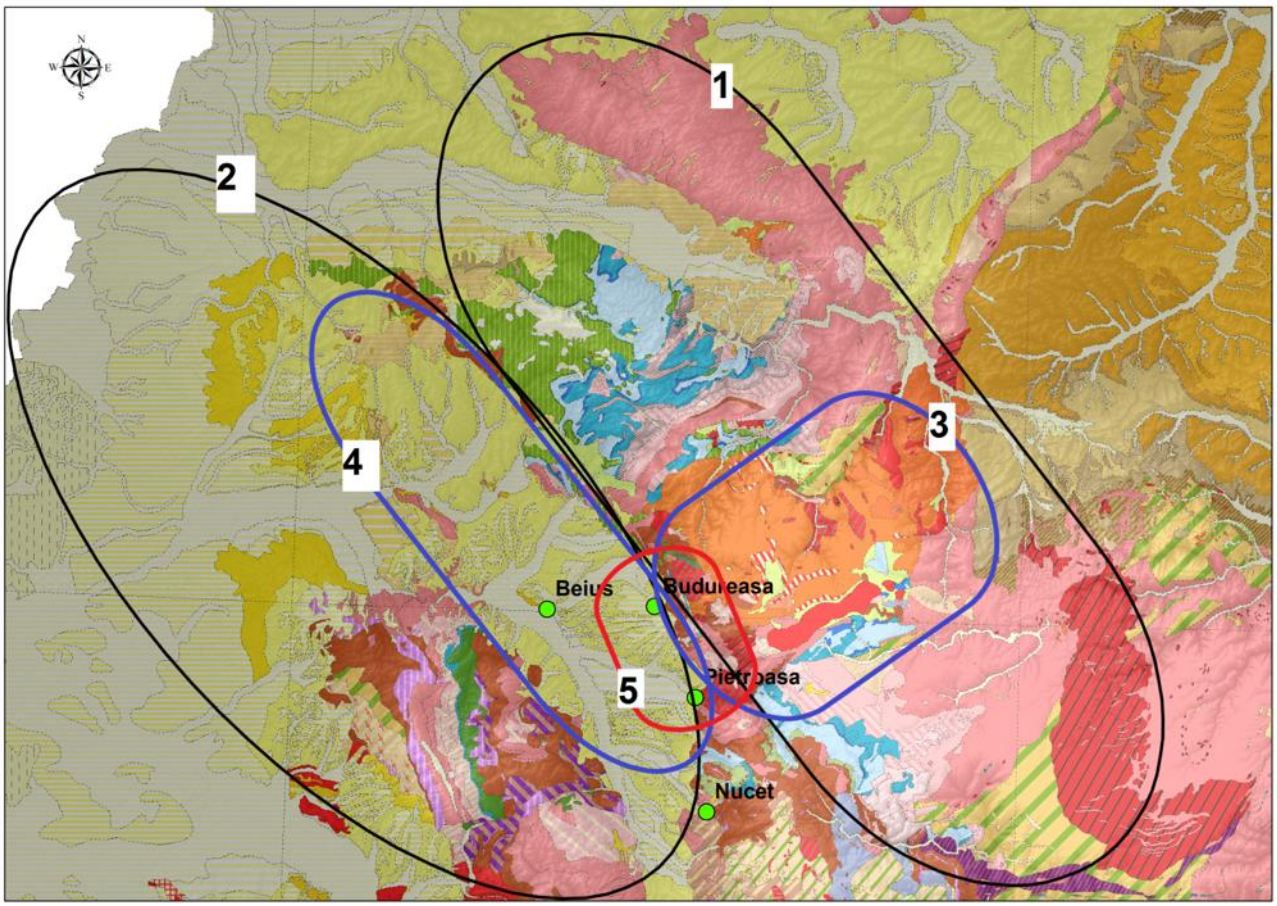

Figure 2 Relation between regional and local structural units that are described within the study. 1-North Apuseni Mountains; 2- Pannonian Basin; 3 – Bihor Mountains; 4 – Beius Basin; 5 – Potential pilot site.

1.3 Description of relevant features at regional level

Describing regional features leads to a better understanding of the study area situation.

1.3.1 Pannonian Basin

Pannonian Basin (Western Plain) is the largest area in Romania that exhibits heat flow density values exceeding 100 W/m^2. Here numerous hydrothermal systems exist, which are characterized by well-head temperatures of 60 - 120^o C and by flow rates of 10 – 20 l/s. The regional high heat flow density was explained mainly by the thinning of the lithosphere as a result of the extension process produced since the Miocene time. Crustal fractures and also positive magnetic anomalies as reflecting the presence of pre-neogenic or neogenic volcanic masses have been considered too as having an important influence on the heat flow (Airinei et Pricăjan, 1976).

According to the lithology and structure of the water-bearing formations, in the eastern limit of the Romanian part of the Pannonian Basin (Western Plain) there have been distinguished four main hydrothermal systems with a regional extent exceeding 8600 km^2. Three of the structures have been formed owing to the sedimentation of a thick sequence constituted by sands and sandstones, within a post - Sennonian depression with deposits of maximum depth of 2000 m. Within these geothermal structures a decreasing of pressure has been observed during simultaneous exploitation of five or seven wells. , it is not the case of the Oradea and Beiuș geothermal systems which are hosted in fissured limestone and dolomites.

The central part of the Western Plain (Oradea and Beiuș zone) is underlain by the carbonate Mesozoic age which constitutes a distinct hydrogeologic unit. Here an active water recharge maintains the pressure in aquifer, and no pressure drop has been reported, even during intensive exploitation of geothermal wells.

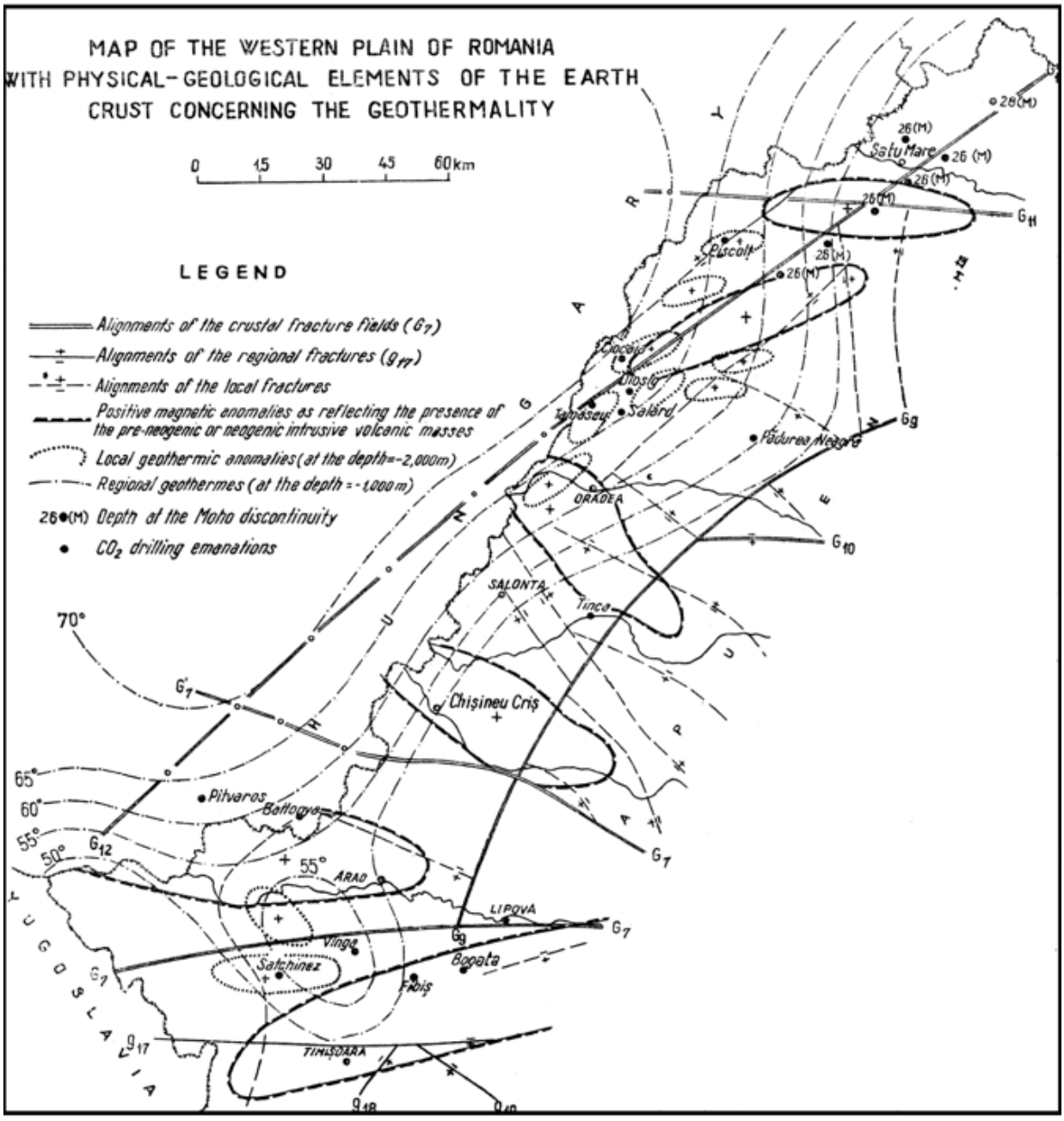

Figure 3 Map of Western Plain of Romania showing, reproduced after Airinei et Pricăjan, 1976:
- Isotherms at 1 000 m depth;
- Positive magnetic anomalies indicating the presence of intrusive masses;

- Local geothermic anomalies at 2000 m depth;
- Alignments of fractures (local and crustal).

1.3.2 Apuseni Mountains

Apuseni Mountains a sector of the Late Cretaceous Banatitic Magmatic and Metallogenetic belt (BMMB) is subdivided into three zones: Vlădeasa (Pb-Zn ores of restricted metallogenetic potential); Gilău-Bihor (Fe, Bi, Mo, Cu, W, Au, Ni, Co, Pb, Zn, Ag, U, B ores / conspicuous peri-batholitic arrangement) and South Apuseni (only one minor Fe-skarn occurrence) (Figure 4).

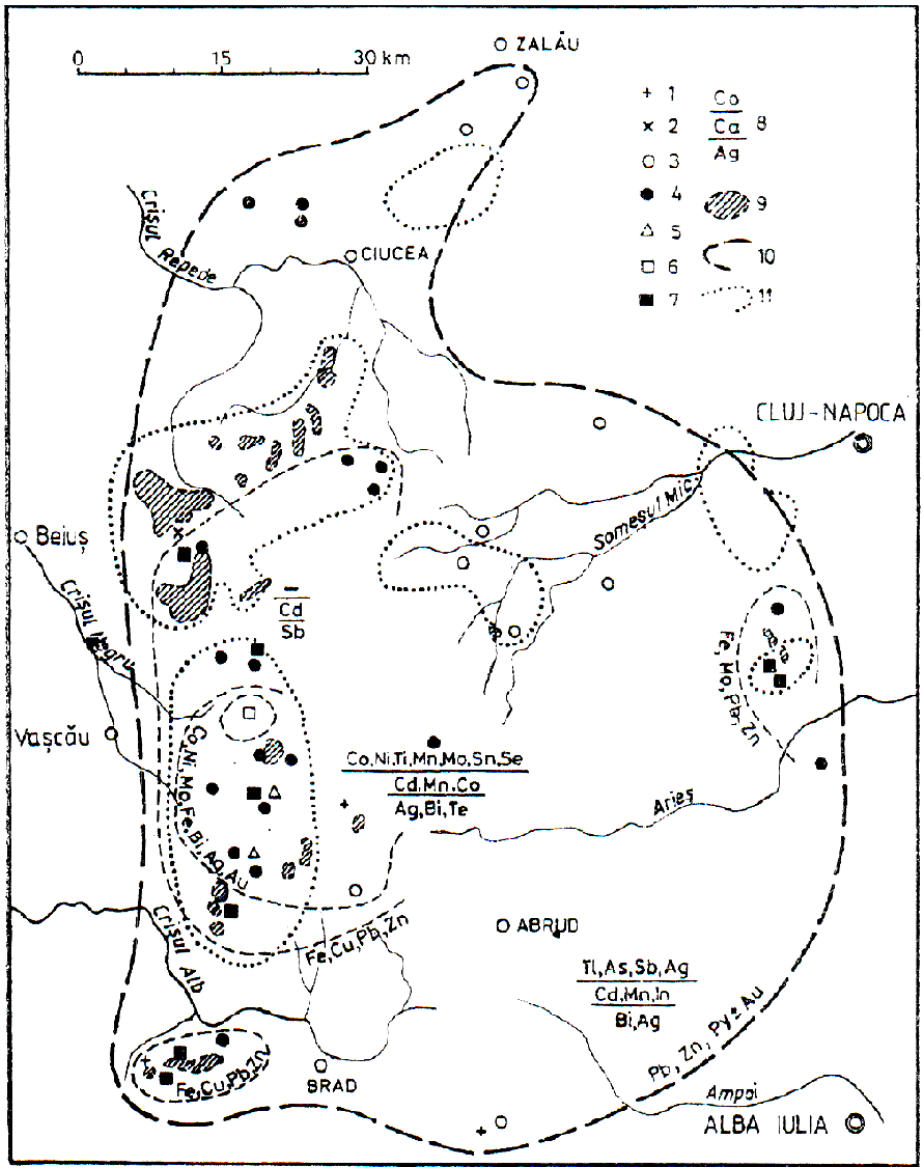

Figure 4 Sketch with regional distribution of the mineralization types in the Apuseni Mountains (Stefan et al, 1986).

1. Baritine occurrences;
2. Brucite occurrences;
3. Pyrite occurrences with, or without gold;
4. polymetalic occurrences (Cu, Pb, Zn);
5. occurrences with Co, Ni, As, Bi, Ag ore;
6. Bi, Mo, W, B, Cu, Pb, Zn occurrences;
7. Fe with, or without Cu occurrences;
8. minor elements characteristic (downwards) in pyrite, spalerite, galena;
9. outcrop, areas with hollocrystalline, equigranular rocks;
10. zones contours;
11. geophysical anomalies.

The sketch indicates mineralized areas according to the geological map of Figure 5.

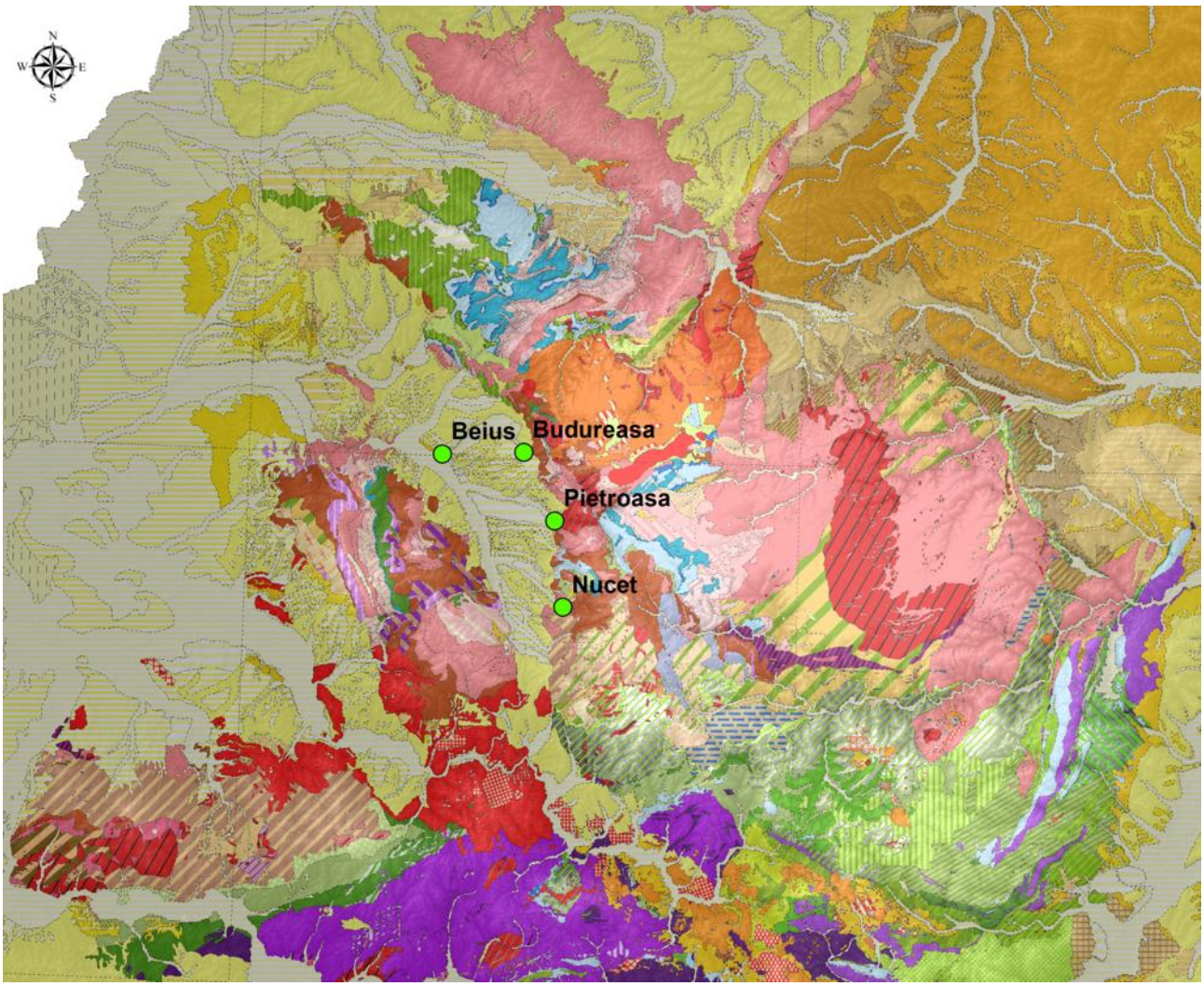

Figure 5 Geological Map of Apuseni Mountains, scale 1: 200 000. Source, Geological Institute of Romania. The legend is the same with that of Figure 6.

1.4 The CHPM study are Beiuș Basin – Bihor Mountains

Beiuș Basin – Bihor Mountains area, having the general features of the region, has, in a limited space the potential for the installation of a CHPM system, namely the existence of geothermal potential and mineralization. For this, it was selected as the CHPM study area. The arguments that led to this conclusion are as follows:

- Having temperatures of 84^{o}C at TVD 2460 m, it is expected that, at 5 km depth, the temperature can be above 150^{o}C.
- Mineralization is widespread in the mountainous area and is expected to be found in the basin area.
- It has already been demonstrated in WP3 that geothermal water contains metals that can be extracted.
- The existence of a geothermal energy exploitation system that could be extended.
- Both local authority and the economic agent that runs the geothermal water system expressed their interested for this.

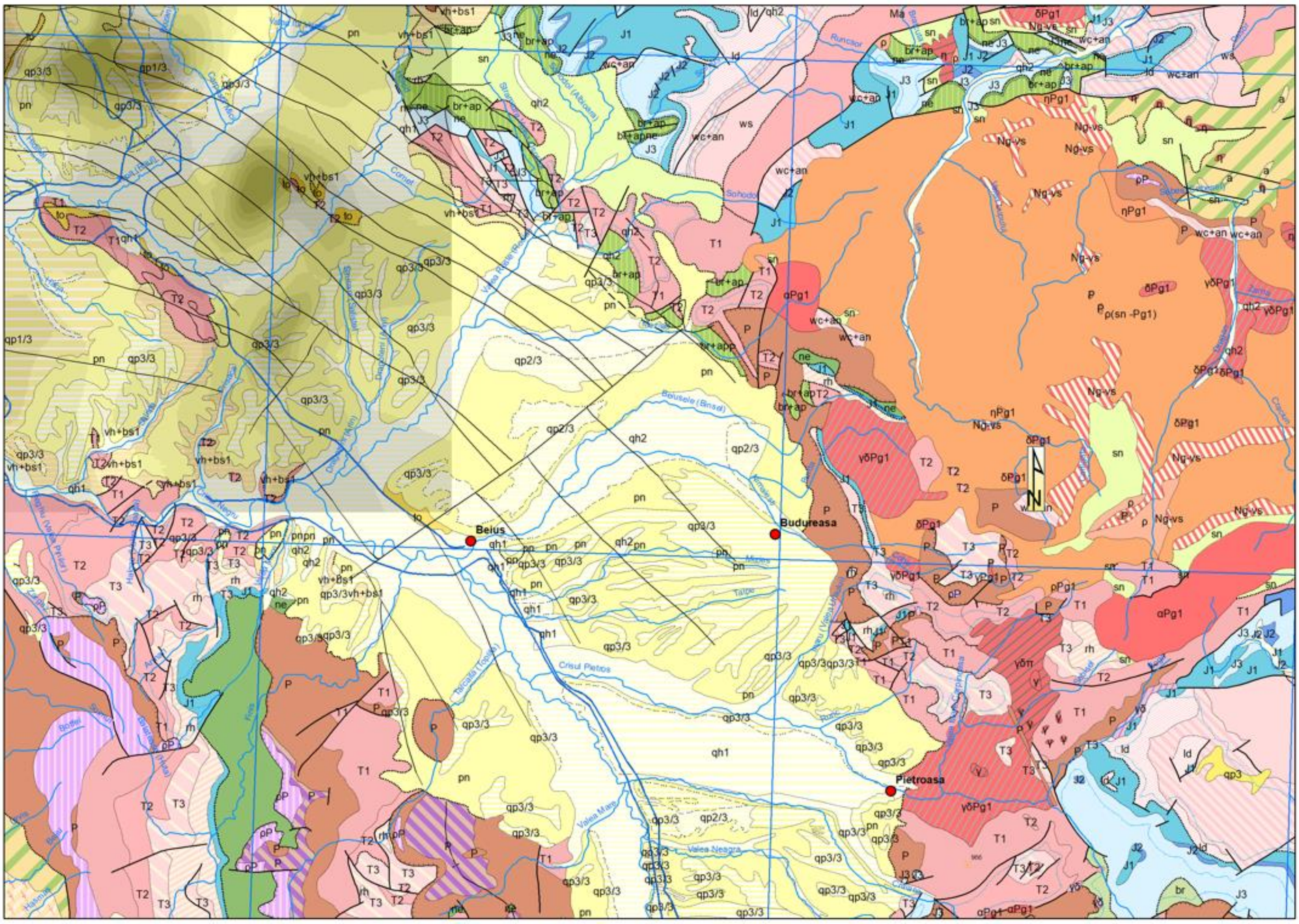

Figure 6 Map of the CHPM study area. Granite and granodiorite bodies outcrop in the eastern part, and aeromagnetic anomalies showing a magmatic intrusion are shown in the western part

Figure 6 bis Legend of CHPM Study area

2. Geology of the prospective area

2.1 Regional geological history

Since Bihor Mountains are part of the North Apuseni Mountains and Beius Basin is a prolongation of the Pannonian Basin, their tectonic evolution is linked to a wider area containing the two major structural units mentioned above.

2.1.1 Geological and structural history of the Apuseni Mountains

The major geological events in North Apuseni Mountains are:

Formation of various basement tectonic units, made up of Early Proterozoic metamorphic rocks (mostly from high-grade metamorphic sequences) and associated granites (Late Cambrian 502–490 Ma, Middle to Late Devonian 372–364 Ma and Early Permian 278–264 Ma), with a Permo-Mesozoic sedimentary and volcanic cover (e.g., Stan, 1987; Dallmeyer *et al.*, 1999, Pana *et al.*, 2002a); The delineation of system of nappes (Bihor, Codru, Highis-Drocea, Biharia, Baia de Aries), named the Inner Dacides (Sandulescu, 1984), which have been juxtaposed during Late Paleozoic (Variscan) orogenic activity (when they recorded three distinct tectonic phases at mid-crustal levels); Crustal shortening within Alpine tectonic activity during the Turonian; Intra-Turonian ('Mediterranean') westward back-vergent thrusting, creating the retro-vergent side of the orogen in a series of four main nappe units: Mecsek, Bihor, Codru and Biharia (e.g., Săndulescu, 1984; Balintoni, 1994; Haas and Pero, 2004; Schmid et al., 2008); Deposition of formations within Gosau-type basins during the Senonian; Deformation was coeval with and followed by latest Cretaceous intrusive and extrusive (sub-) volcanic Banatitic magmatism.

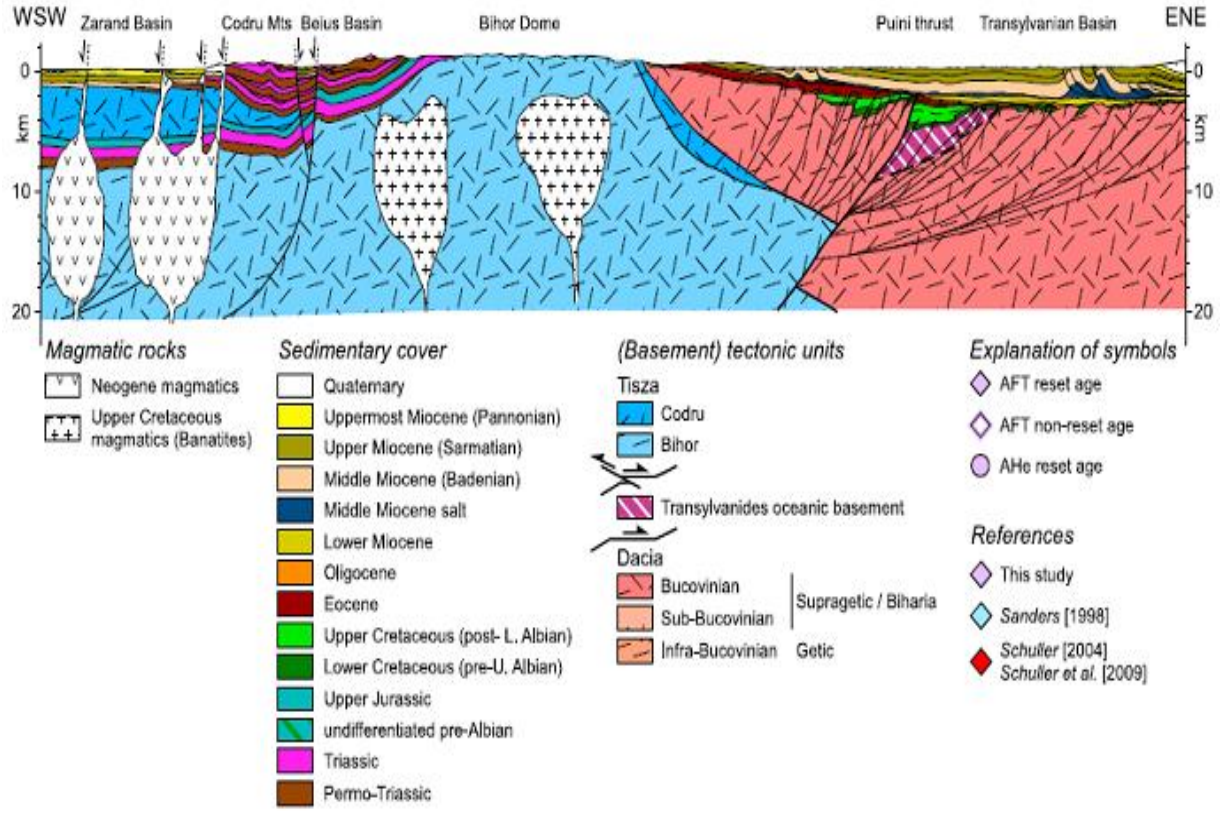

Figure 7 Cross – section illustrating magmatism processes within Apuseni Mountains, (Merten et al, 2011).

Re-Os ages of Banatitic magmatic activity range between 84–72 Ma for the Apuseni area (Zimmerman et al., 2008). For the Apuseni Mountains, K-Ar and 40Ar/39Ar ages indicate latest Cretaceous–Eocene cooling of the Banatites (Bleahu et al., 1981; Wiesinger et al., 2005). Based on 40Ar/39Ar amphibole and biotite ages ranging between 89 Ma in the South Carpathians to 61 Ma in the Apuseni Mountains, Wiesinger et al. (2005) suggested three consecutive magmatic events: Turonian–Santonian, Campanian and Maastrichtian.

The bulk of the Paleocene – Eocene ages are derived from older K-Ar measurements (Bleahu et al., 1981) and represent cooling ages.

2.1.2 Neogene structure of the Romanian sector of the Pannonian Basin

The structure of the Romanian sector of the Pannonian Basin was studied based on seismic research and borehole data (Visarion et al., 1979, Polonic, 1985). It is a subsidence and sedimentation basin; its formation began in the Middle Miocene. During the Miocene and Pannonian in the eastern part of the basin the sediments were deposited in shallow-marine environments. The faults affect both the basement and the sedimentary cover of Pannonian Basin, some of the blocks forming a graben-horst like structure. In the vicinity of Apuseni Mountains the Neogene formations lie directly on the crystalline or eruptive basement in the southern part, whereas in the northern part, they cover a more complex Mesozoic basement. The thickness of the Neogene sediments is shown up to 2000 m.

2.2. Tectonic framework

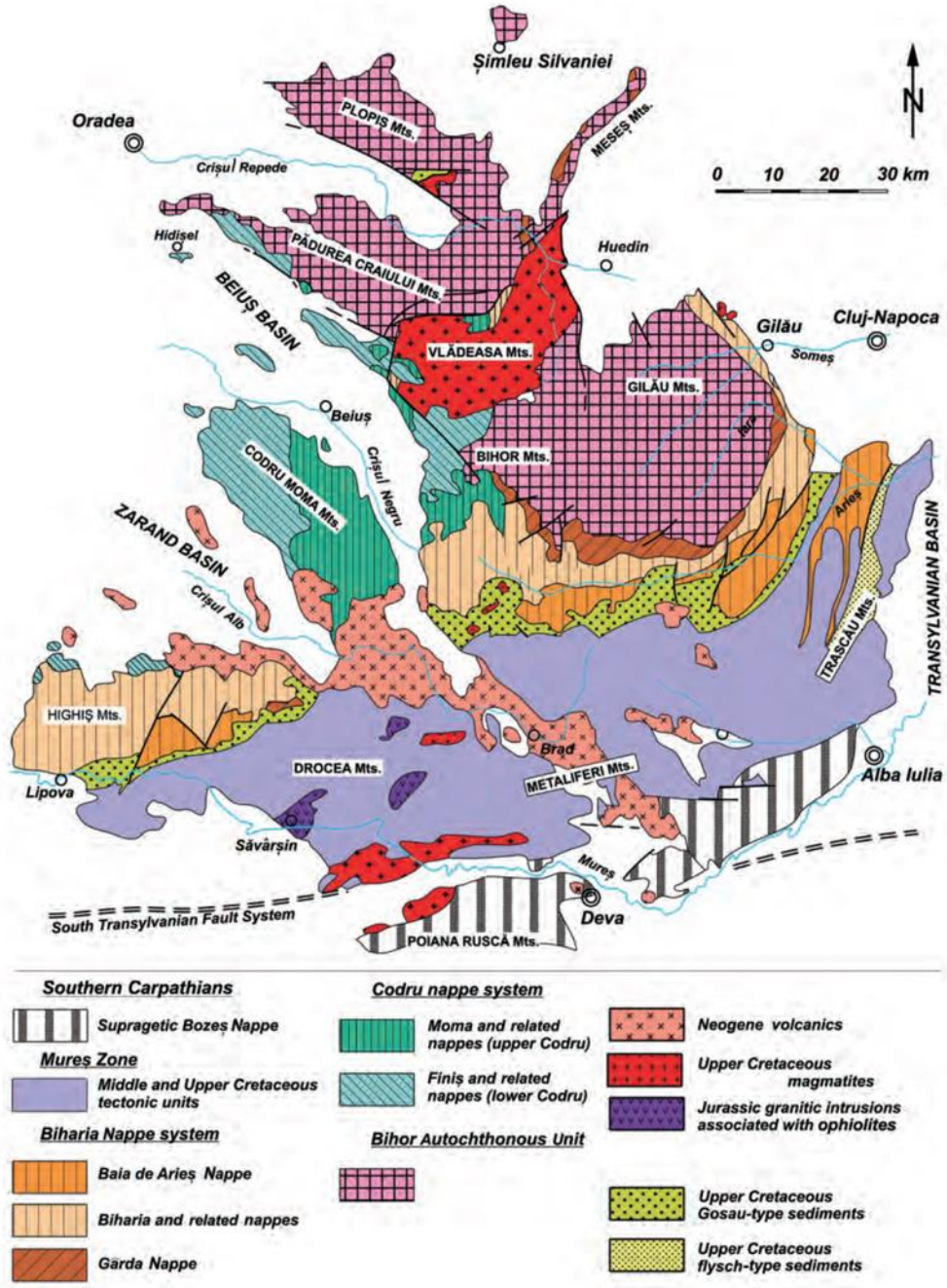

Figure 8 Simplified Alpine structure of the Apuseni Mt, from Ionescu et al. (2009) compiled by C. Balica from papers by Ianovici et al. (1976), Bleahu et al. (1981), Săndulescu (1984), Kräutner (1996), and Balintoni & Puşte (2002).

2.2.1. North Apuseni Mountains

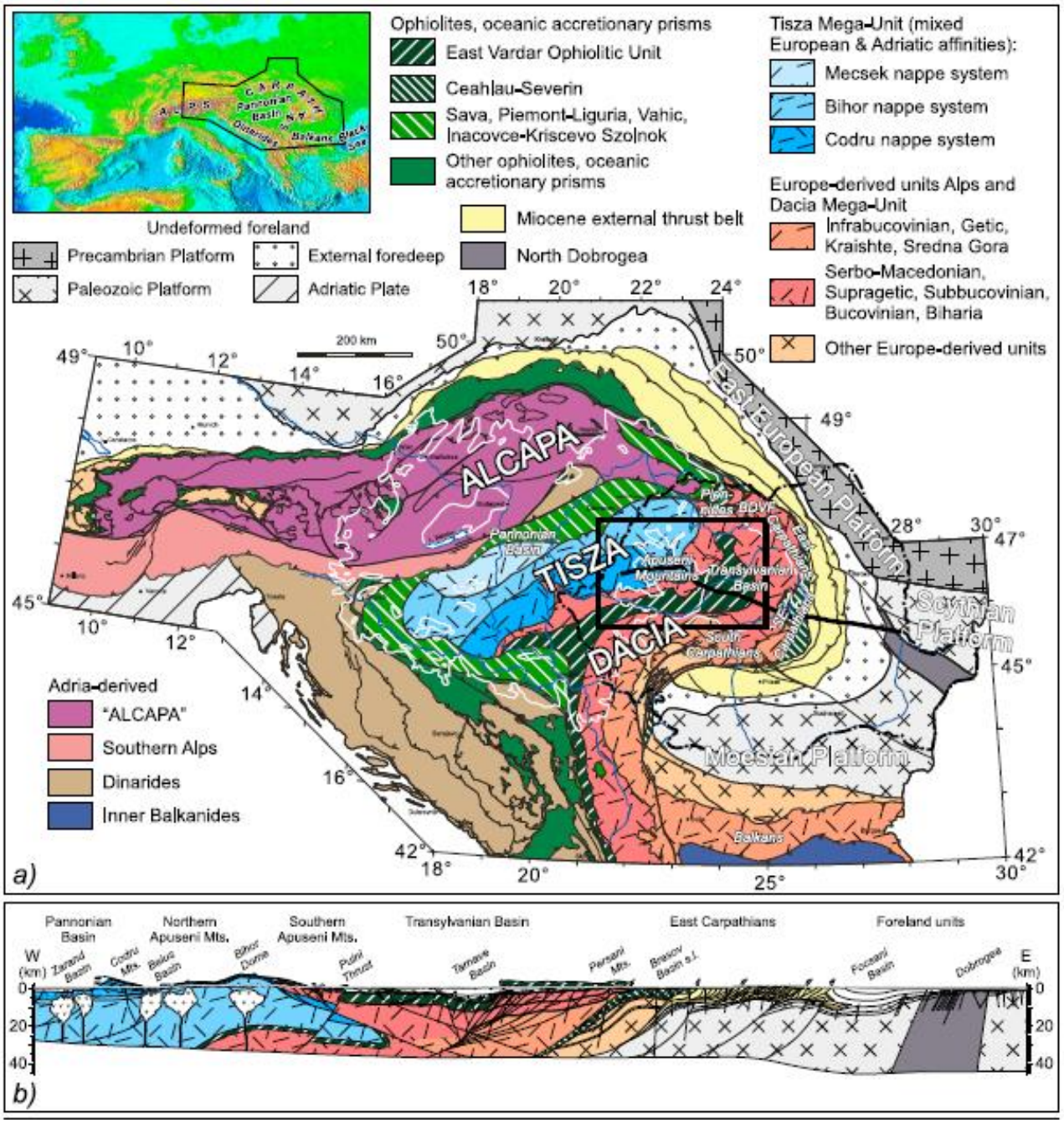

Figure 9 (a) Tectonic map of the Eastern Alps-Carpathians-Dinarides-Balkans region (simplified after work by Schmid et al. [2008]) and its location in the topographic map of Europe. Solid black line indicates the location of the cross-section and solid box indicates the location of the Apuseni Mountains. White lines indicate the outlines of the Pannonian and Transylvanian Basins and dashed black line indicates the border of Romania. (b) Conceptual cross-section through the Apuseni Mountains, Transylvanian Basin and SE Carpathians (simplified after work by Schmid et al. [2008]). Reproduced after Merten et al, 2011.

The tectonic units that build up the northern segment of the Apuseni Mountains are termed as *Apusenides* and are part of the Tisia unit (Kovács, 1982; Fülöp et al., 1987; Csontos, 1995; Csontos & Vörös, 2004; Császár, 2006). Tisia unit is built up of a crystalline basement and a Permo-Mesozoic sedimentary sequence ranging up to the Late Cretaceous. The architecture of the North Apuseni Mountains contains, as the structurally deepest unit, the “Bihor Autochthonous Unit” or the “Bihor Unit”. It is of a regional extent and has a relative autochthonous position in respect to the higher nappe systems. The structurally higher units

can be grouped, according to their origin and lithological content, in two nappe systems, thrust on top of the "Bihor Autochthonous Unit": the deeper Codru nappe system and the tectonically higher Biharia nappe system. Each system is believed to originate in different areas of the Tisia micro-continent.

During Mesozoic to Tertiary plate movements several mountain belts have been formed within the Alpine–Carpathian orogen. The Apuseni Mountains as part of this mountain belt have been formed during Cretaceous times as a result of the convergence and collision of the two microplates Tisia and Dacia.

In North Apuseni Mountains two main igneous stages of rocks belonging to Banatite Magmatic and Metallogenetic Belt are recognized (Ștefan et al., 1988, 1992): phase I having volcanic character, and phase II with intrusive character. The volcanic phase includes andesites, dacites and rhyolites, developed in time as follows: andesitic lavas at the beginning, followed by dacitic lavas. Rhyolites, sometimes with ignimbritic character, end the volcanic activity. The intrusive phase is represented by small bodies of diorite and quartz diorite as well as by granodiorite (+ granite) plutons (Budureasa, Drăganului Valley and Pietroasa). During the second phase of Ștefan et al. (1988, 1992), rhyolite, rhyodacite, aplite, microgranite, porphyrytic microgranite and micropegmatite dykes were emplaced along NW–SE faults. Towards the south, in the Băiţa Bihor area basic rocks (basalts, lamprophyres), probably originating from a deeper source, crosscut the main magmatic suite.

2.2.2. Pannonian Basin

According to Demetrescu (1989) the Romanian part of the Pannonian Depression is characterized by high heat flow (Demetrescu, 1978; Horvath et al., 1979), the lithosphere being hotter and thinner than in the surrounding areas. The lithosphere thickness was estimated at 60-70 km using magnetotelluric and heat flow data (Stegena et al., 1975; Adam, 1980; Demetrescu et al., 1984). Thinning of the lithosphere seems to occur in the entire depth interval, including the crust: deep seismic sounding studies indicate values of 25-27 km for the crustal thickness (Rădulescu et al., 1976). The extensional tectonics of Romanian part of the Pannonian Basin (Western Plain) is well documented by seismological data (Polonic, 1985).

In 1989 Demetrescu and Polonic described the formation and evolution of the Romanian part of Pannonian Basin as a result of a complex thermo mechanical phenomenon of lithosphere extension. As a result of the extension by tectonic forces, the lithosphere is thinned and, for reasons of isostasy, an initial subsidence occurs. Thinning of the lithosphere is accompanied by heating as a result of the elevation of the asthenosphere. The thermal anomaly induced by extension then tends to dissipate by conduction and the cooling lithosphere contracts, resulting in thermal subsidence. If these phenomena take place below the sea level, as the basin subsides sediments are deposited. The sedimentary load enhances the subsidence, the actual subsidence of the basin being larger than the tectonic subsidence-the sum of the initial and thermal subsidence.

Many studies referring to the evolution of Pannonian Depression confirmed the above mentioned theories and data. Horvath et al (2015) summarizes the current ideas on the evolution of Pannonian – Carpathian region with the following phrases: 'Alcapa and Tisza-Dacia as orogenic wedges detached from their mantle lithosphere in the Alpine and Adriatic/Dinaric collision zone during the Late Oligocene to Early Miocene. They suffered a dramatic thermal impact leading to crustal melting during extrusion, when these crustal flakes could have been directly superimposed on the asthenosphere in the Carpathian embayment. Since then, the large part of the Pannonian has been cooling and a new mantle lithosphere growing. Geothermal data show that the Pannonian basin with cessation of volcanic activity in the Late Miocene is still very hot and Miocene to Quaternary clastic basin fill, together with karstified Mesozoic carbonates form good geothermal reservoirs of regional extent. In addition to these gravity-driven aquifer systems, a strongly

overpressured reservoir can be found below a regional pressure seal in synrift strata and fractured basement rocks.'

According to Matenco, and Matenco et al (2012) the Pannonian Basin is made up of a large number of Miocene (half-) grabens distributed in a wide area, from the Apuseni Mountains to the Alps in the west, Western Carpathians in the north and Dinarides in the south. In the east three basins were formed, Borod, Beiuș and Zarand. Matenco published a transect connecting the Apuseni Mountains with the SE part of the basin Pannonan Basin (Figure 10) that indicates that the extensional mechanics was asymmetric and the deformation migrated in space and time across the basin, from Early Miocene to early Pontian and in space the extension started near the Dinarides during Early Miocene times, continued everywhere in the basin during the Middle Miocene and finished in the area close to the Apuseni Mountains and South Carpathians during the late Miocene.

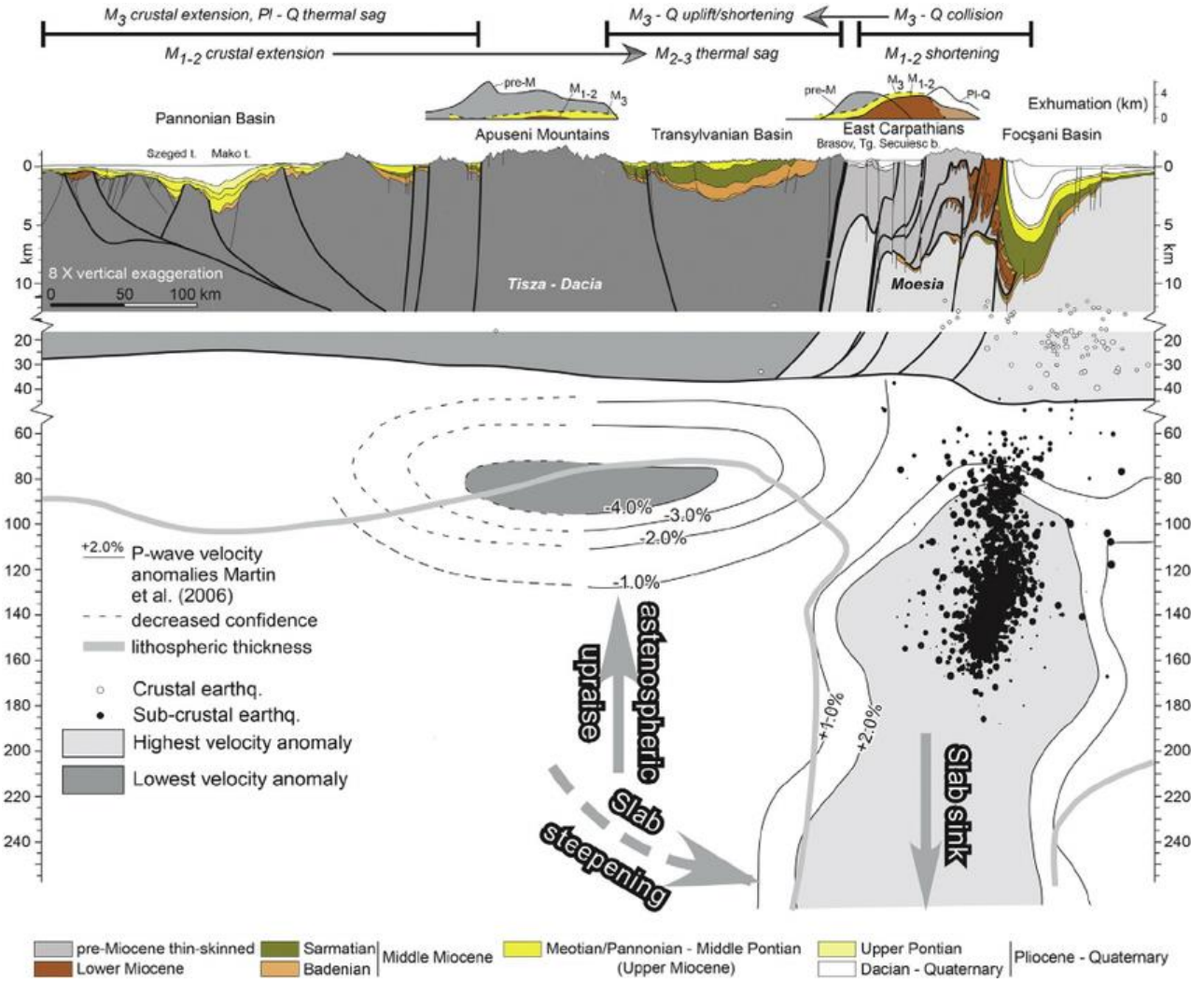

Figure 10 Simplified lithospheric scale cross section across the SE part of the Pannonian Basin, Apuseni Mountains, Transylvanian Basin and SE Carpathians and amounts of exhumation over the Apuseni Mountains and SE Carpathians derived from low-temperature thermochronology (modified from Matenco and Radivojević , 2012). The geological cross section displays only Miocene – Quaternary sediments geometries and faults patterns. All pre-Miocene structures were ignored. The location of the cross section is displayed in Fig. 1. pre-M = pre-Miocene; M 1 = Early Miocene; M 2 = Middle Miocene; M 3 = Late Miocene; Pl = Pliocene; Q = Quaternary. The lower part of the figure is the crustal and upper mantle structure beneath the western Pannonian Basin – Carpathian Mountains with underlying the seismicity and the anomalies detected by high resolution, local teleseismic tomography.

Assessments of the crust and lithosphere thickness have been done in the 'Atlas of the present-day geodynamics of the Pannonian basin' ***http://geophysics.elte.hu/atlas/geodin_atlas.htm*.** According to Horváth et al, (Figures 11, 12) the thickness of the crust is below 25 km, and thickness of the lithosphere is below 60 km in Apuseni Mountains.

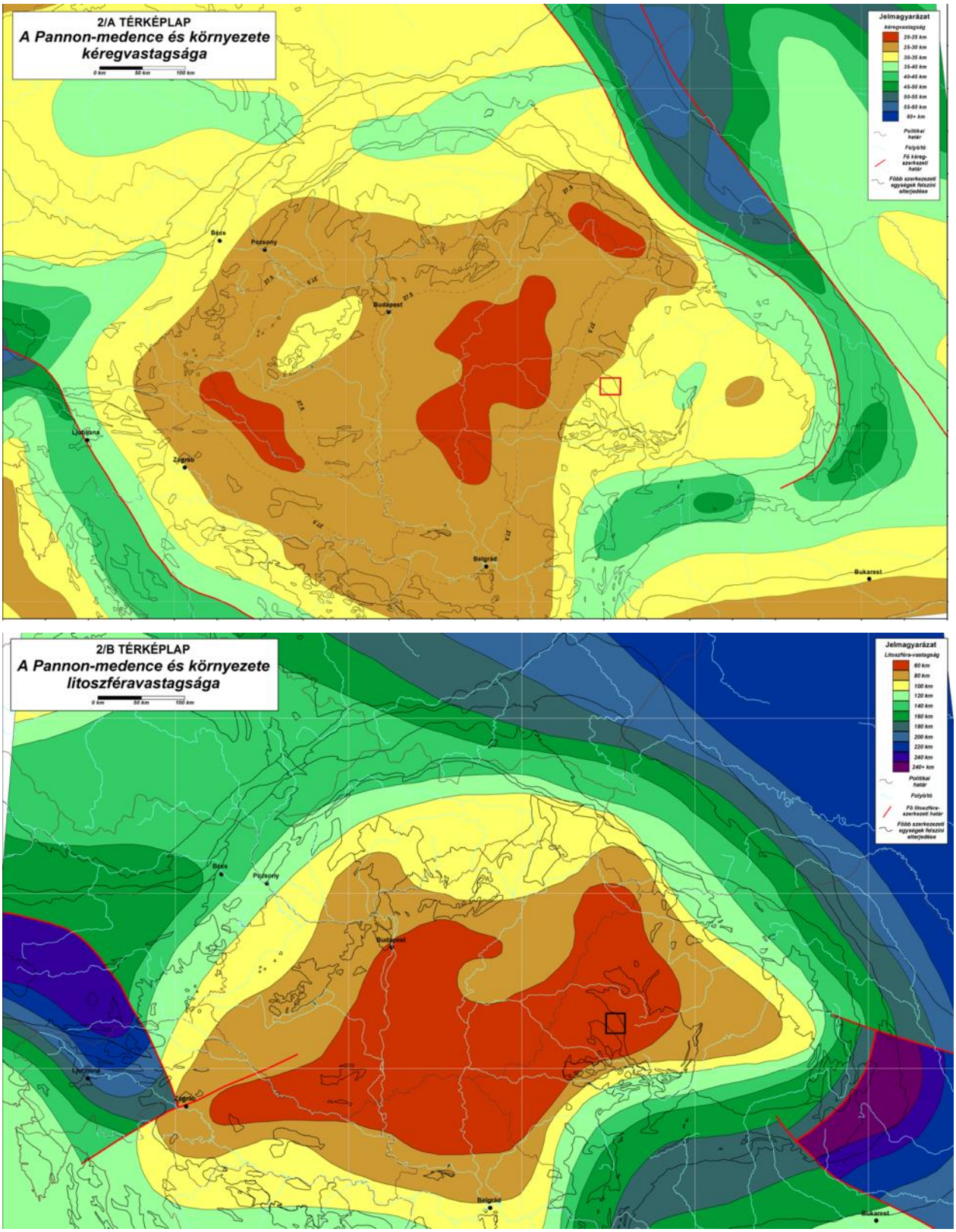

Figures 11, 12 Maps of crustal and lithosphere thicknesses, reproduced after Horváth et al.,(2001 – 2004).

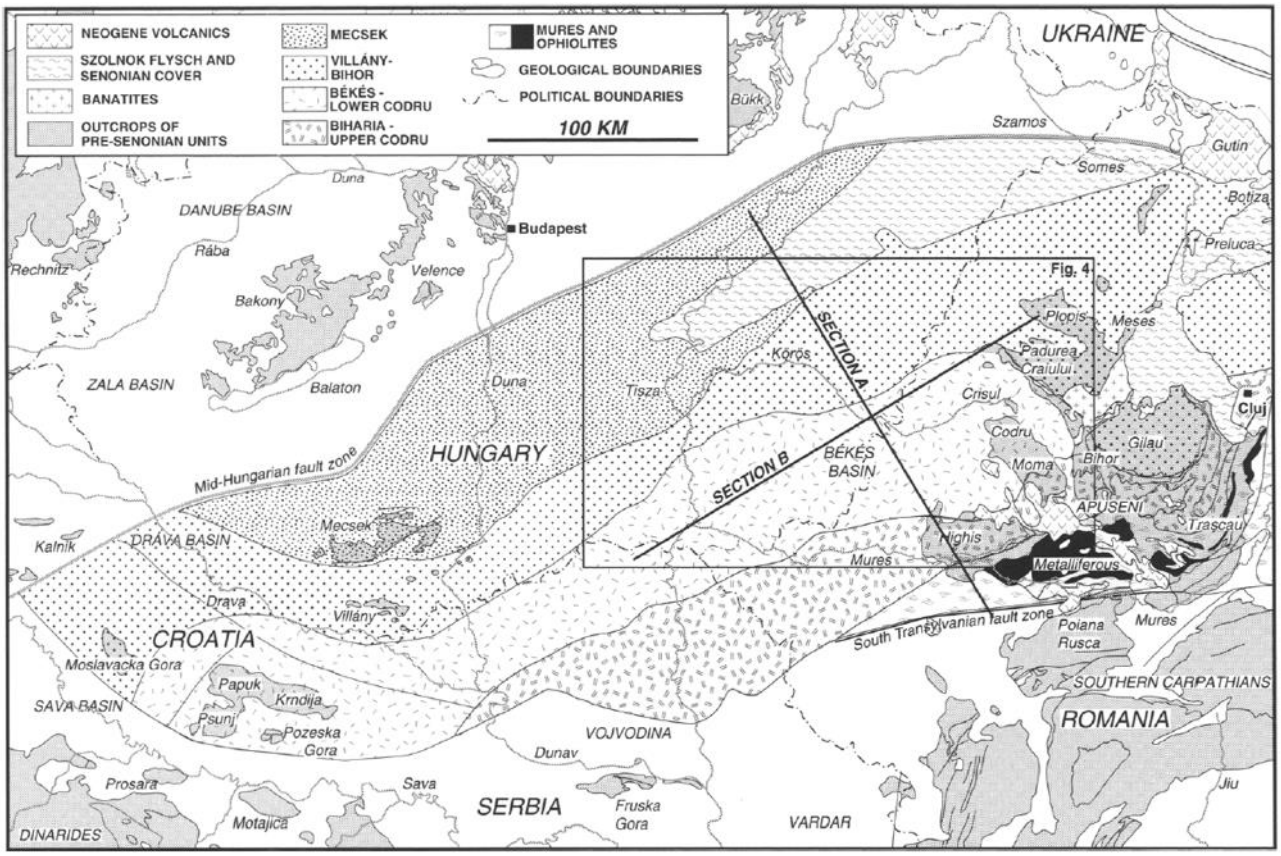

Figure 13 Regional geologic subcrop map of the SE Pannonian basin, modified from Csontos et al. (1992). Locations of a detailed map (Fig. 4) and structure transects A and B are shown.

Finally, Tari *et al*, (2015) based on seismic data, estimated that the thicknesses of the crust and lithosphere in the region of North Apuseni Mountains are of around 20 km, and almost between 60 and 80 km, respectively (Figure 13, 13 bis).

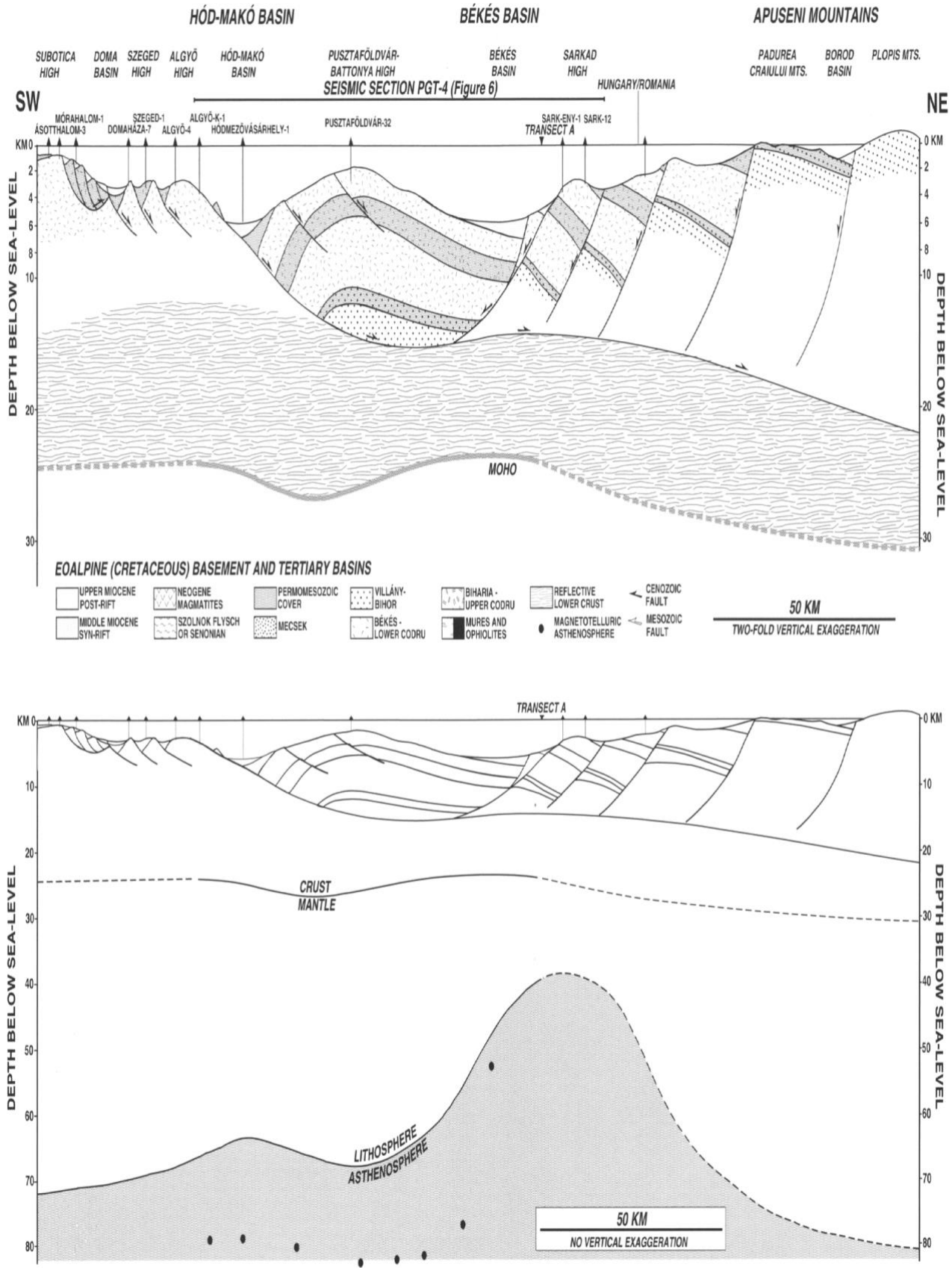

Figure 13bis Transect B with crustal and lithosphere thicknesses, reproduced after Tari et al, 2015.

2.3. Geology of CHPM2030 study area

2.3.1. Bihor Mountains

Bihor Mountains structural unit consists of "Bihor Autochthonous Unit" and two nappe systems, thrust on top of it: the deeper Codru Nappe system and the higher Biharia Nappe system.

- "Bihor Autochthonous Unit" consists of a metamorphic basement and a sedimentary cover. The basement is a lithostratigraphic unit comprising medium-grade micaschists and quartzites, gneisses, amphibolites and ultramafic rocks. One of its dominant features is the frequent occurrence of pegmatites, large-scale migmatization and the presence of large granitic intrusions such as the Codru and Muntele Mare plutons. The cover is represented by Permo-Mesozoic siliciclastic and calcareous sediments.
- The Codru nappe system comprises seven tectonic subunits, and, except for the Finiș Nappe subunit, contains only Permo-Mesozoic sedimentary sequences (Ianovici et al., 1976; Bleahu et al., 1981; Săndulescu, 1984).
- The Biharia nappe system is best exposed at south-western margin of the Bihor Mountains. It includes six tectonic units, which are built of metamorphic basement rocks. Only two units show a Permo-Mesozoic sedimentary cover.

During Late Cretaceous with the formation of the so called "banatites" took place. These comprise a sequence of calcalkaline intrusions ranging from granite to diorite, accompanied often by volcanic rocks. The banatitic magmatism gives rise to some important mineralization, for example in skarns which formed along the contact of the intrusions with mainly Mid-Triassic limestones (Ilinca, 2010). A characteristic feature of the banatites and in particular granodiorites is the frequency of the xenoliths of metamorphic, sedimentary and magmatic nature of various sizes, ranging from 1-2 cm to several cubic meters.

At the end of Cretaceous, during the "Laramian" orogenic phase, widespread intrusive, subvolcanic, as well as volcanic bodies were formed (Figure 14).

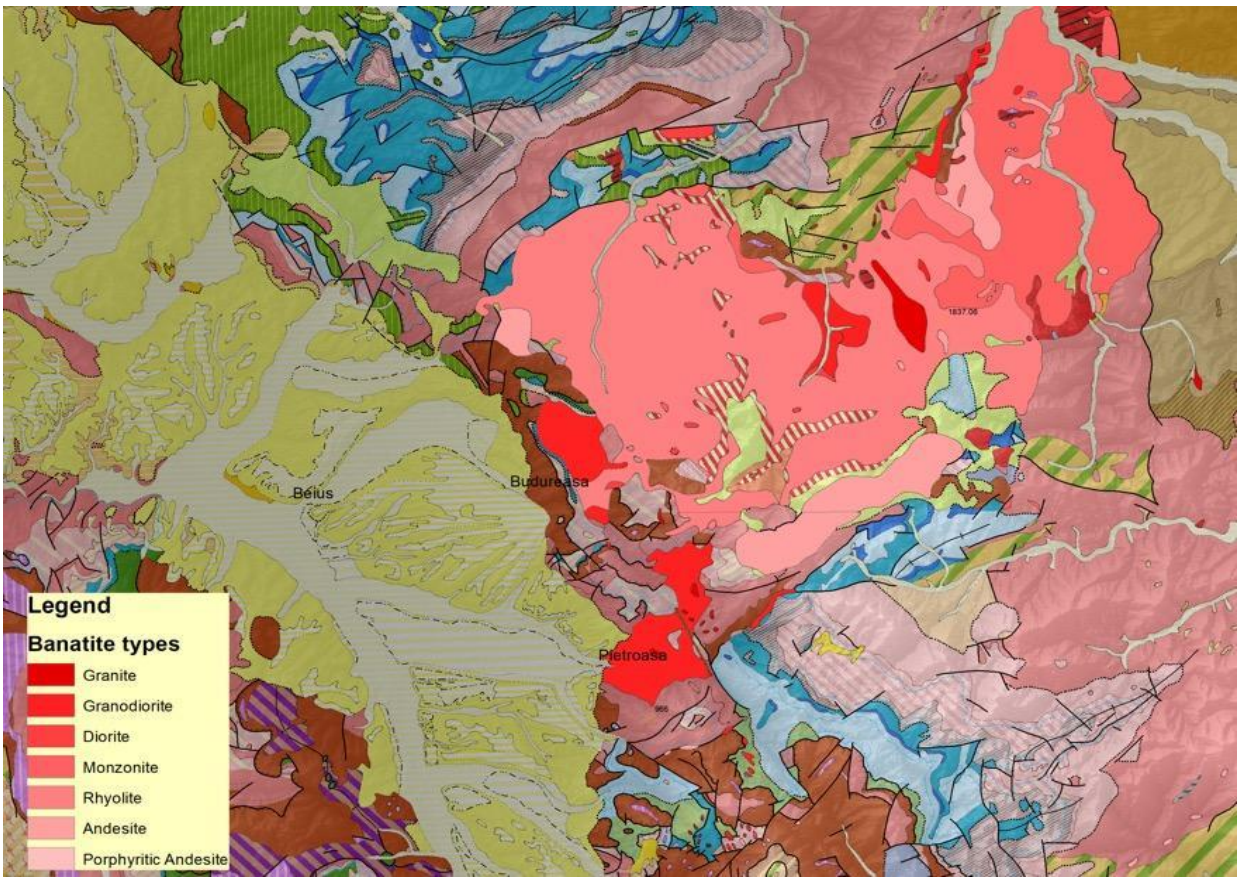

Figure 14 Types of banatites from Bihor Mountains

The batholitic body, which is of hypoabissal origin, extends within Bihor Mountains, both at the surface and in the underground, up to the Galbena fault. At the surface, within the Pietroasa - Aleului valley area, and further north, up to Budureasa, granodiorites outcrop. Associated with this banatitic intrusion, apophyses and bodies, of andesitic or basaltic composition, have been documented, especially in the upper reaches of Crișu Bãița along the valleys Hoanca Moțului, Corlatu and Fleșcuța, as well as in the Valea Seacã catchment area.

The intrusion of the banatites has resulted in contact processes that concerned the sedimentary deposits being traversed. At the contact of the banatites with the limestones, marbles and various types of calcic skarns have been formed, while at the contact with the detritic and pelitic rocks, hornfels, garnet skarns, etc. are met (I. Orășeanu, 2010).

Regional extension of a granodioritic batholith, as well as the existence of the extensive contact areas between magmatic intrusions and Triassic deposits are illustrated in Figure 15. Within these areas described in Bihor Mountains as well as in many other regions of the North Apuseni Mountains contact aureoles have been generated.

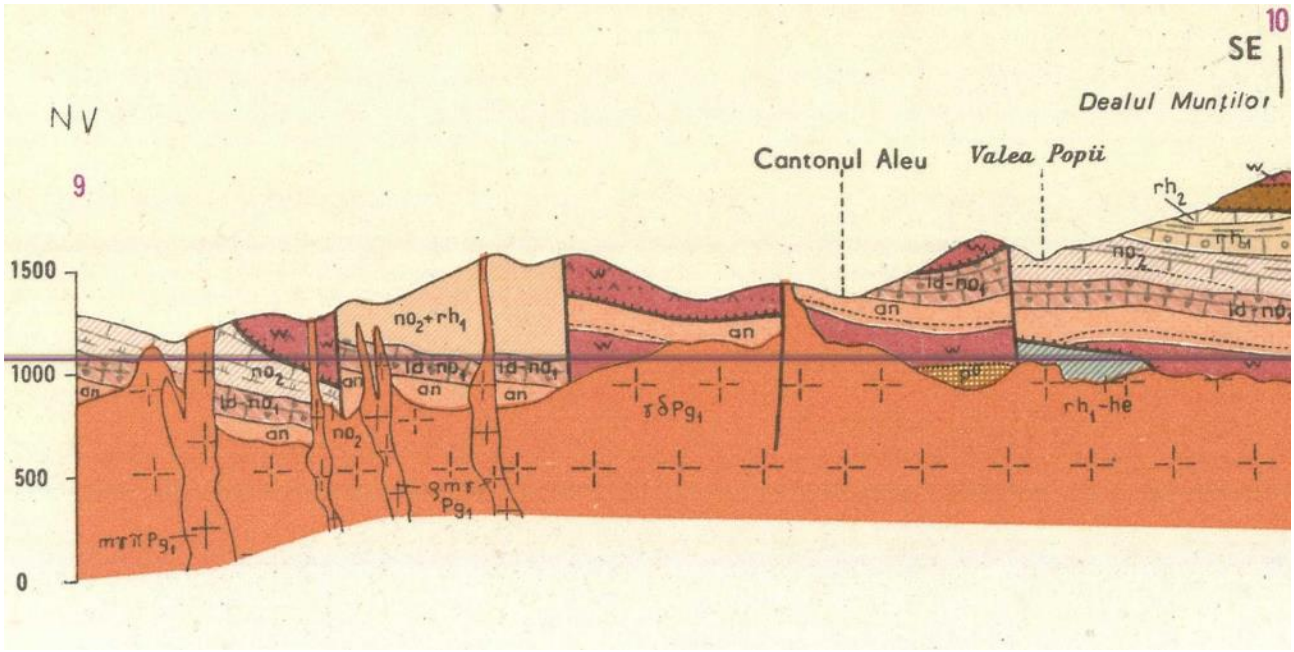

Figure 15 Bihor Mountains – cross section, reproduced after Bleahu et al, published with the map of Pietroasa, scale 1:50 000, 1985.

2.3.2. Beiuș Basin

A result of Neogene processes is Beiuș Basin. In 1991, based on geological and geophysical prospection (seismic, gravimetric, aeromagnetic), and *in situ* gravimetric measurements and geothermic measurements in boreholes, Dinu et al (1991), elaborated the structural map at the contact between the pre-Neogene and Neogene deposits of Beiuș Basin, that was accompanied by the isobaths map of the basis of Neogene deposits, and with isopachs map of Neogene deposits (Figures 16, 17).

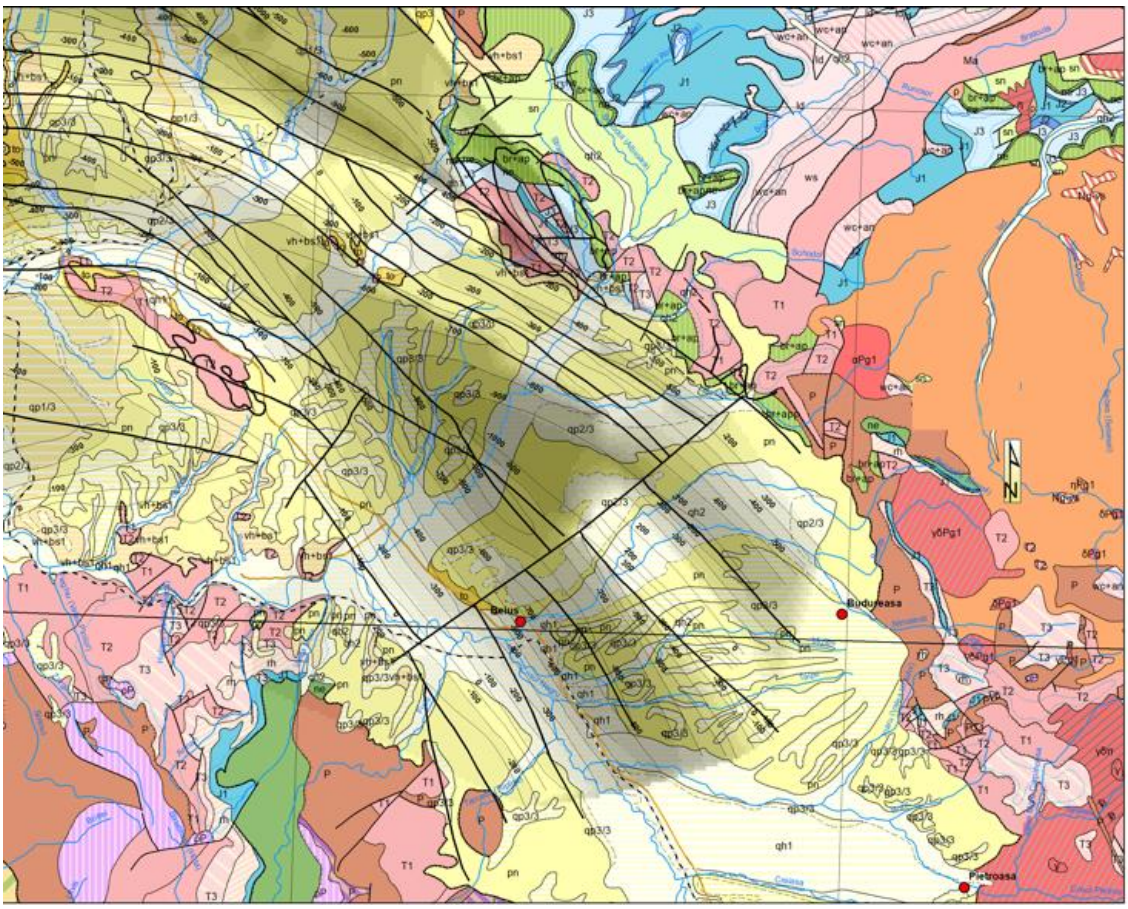

Figure 16 Isobaths map at the contact between pre Neogene and Neogene deposits from Beiuș Basin, modified after Dinu et al, 1991.

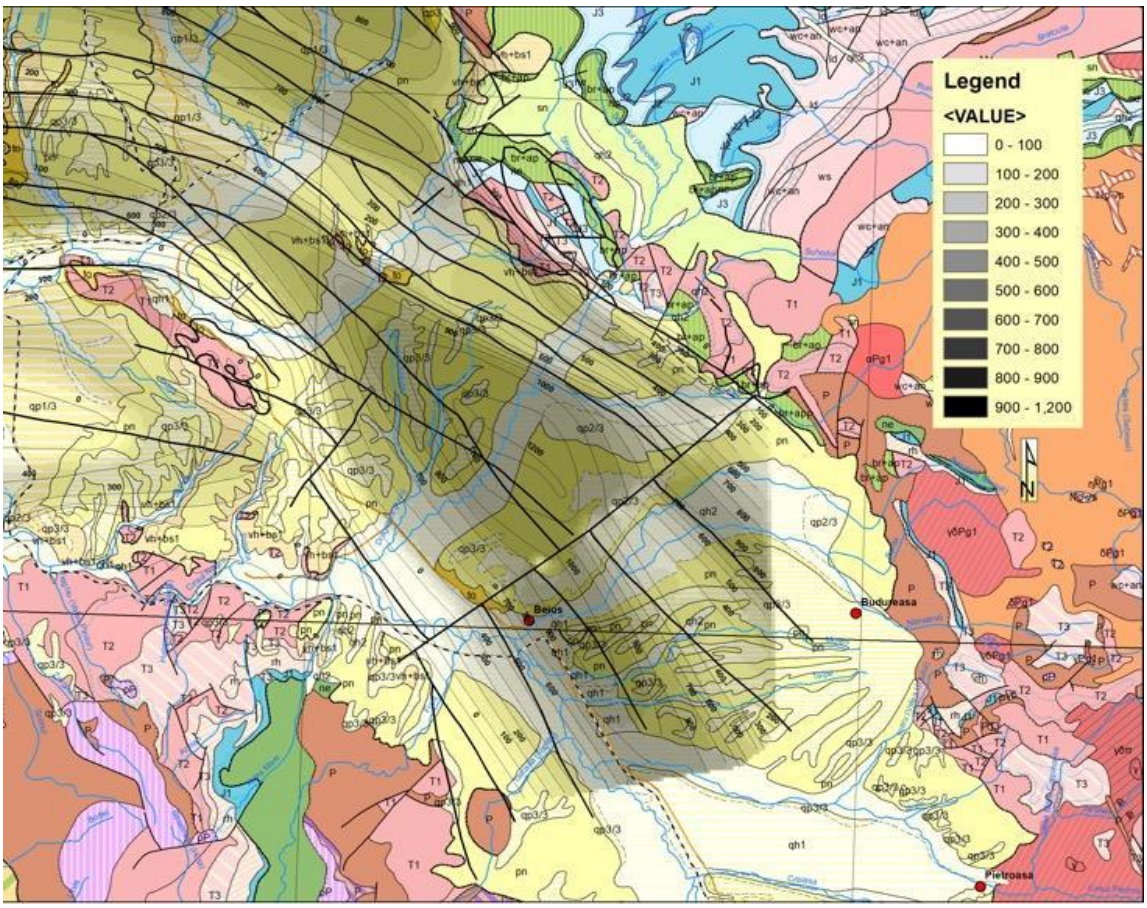

Figure 17 Isopachs map of Neogene deposits from Beiuș Basin, modified after Dinu et al, 1991.

Based on these data the following conclusions were drawn as a result: the overall structure of the Beiuș Basin is of collapse post-tectonic basin type, made by down going at the high-angle faults; there are many faults which give some particular features with uplift and down going sectors.
The structural map reveals two distinct sectors (in the north-west and south-east) separated by an uplift central zone with a transverse trend, which separates the basement of the Pannonian Basin and the basement of the Apuseni Mountains.

In the north-western sector, the basin is broadened, the trend of fractures and structures is east-westwards and the basin is sinking towards the Pannonian Basin where it has the tendency to bend and to connect with this basin`s structures. The structure of this sector is very complicated due to the great number of faults specific to extensional basins and to the existence of intrusive magmatic bodies in the depth (Figure 17).

In the south-eastern sector, the basin has a graben structure type, with the central part down going to isobathic values of about – 1000 m (Drăgoieni – Beiuș zone). The main down going sector rises gradually towards the orogenic belt. An important transverse strike-slip fault is to be mentioned to the North of Beiuș city.

The main structural trends are the same as the main trends of the eruptions centres in Apuseni Mountains, having north-eastern – south-western directions, showing that Beiuș Basin is the result of the collapse sectors due to important magma extrusions.

The isopachs of Neogene deposits map emphasize the sectors with thick sedimentary deposits which correspond to the basin axis.

In Beiuș Basin the faults system is well documented. Most of them, that disturbed both pre - Neogene and Neogene deposits, are considered to be (S. Bordea, Gh.Mantea, 1999) old fractures reactivated during the Neogene diastrophism phases. Old Austrian or intra-Turonian fractures have been reactivated and determined the individualization of Beiuș Basin, during the Styrian movements.

Many of the faults are marked by mesothermal waters, springs of mineralized (ferro-sulphurous) having between 17°C to 24°C have been reported at Răbăgani, Dobrești, Rotărești, Coșdeni, Holod.

The most important faults are to be menioned:

- Galbena fault – has about 100 km in length, being traced in Padurea Craiului, Bihor, and Metaliferi Mountains; it is accompanied by a system of parallel faults trending NW – SE; some of them are penetrated by the Banatitic magmatites of the Alpine subsequent magmatism, which form veins of 2 km length. Galbena strike slip fault, is a regional fracture, that is represented on the Deep Structure Map of Romania, scale 1:1 500 000. At the same time this fracture is a prolongation of a line of magnetic maximum that is linked to banatitic eruptions (Gavăt et al).
- Dobrești fault, along which Crișu Negru River runs;
- Beiuș – Răbăgani fault follows the axis of Beiuș Basin.

Many authors highlighted the existence of intrusive magmatic bodies in Beiuș Basin (Figure 18). Some of them consider that they are a banatites, manifestation of Upper Cretaceous magmatism like in North Apuseni Mountains, and others (Dinu et al, 1991, Seghedi et al, 2011) rather assume that they represent magmatic intrusions into an extensional basin during Neogene, similar with the ones from South Apuseni Mountains. Magnetic anomalies indicating intrusive magmatic bodies have been reported since the seventies in Pannonian Basin near the border with Hungary too (Figure 3). It means the intrusions from

Beiuș Basin are not singular appearances, and they are worth to be subject of investigations for EGS installation purposes in the future.

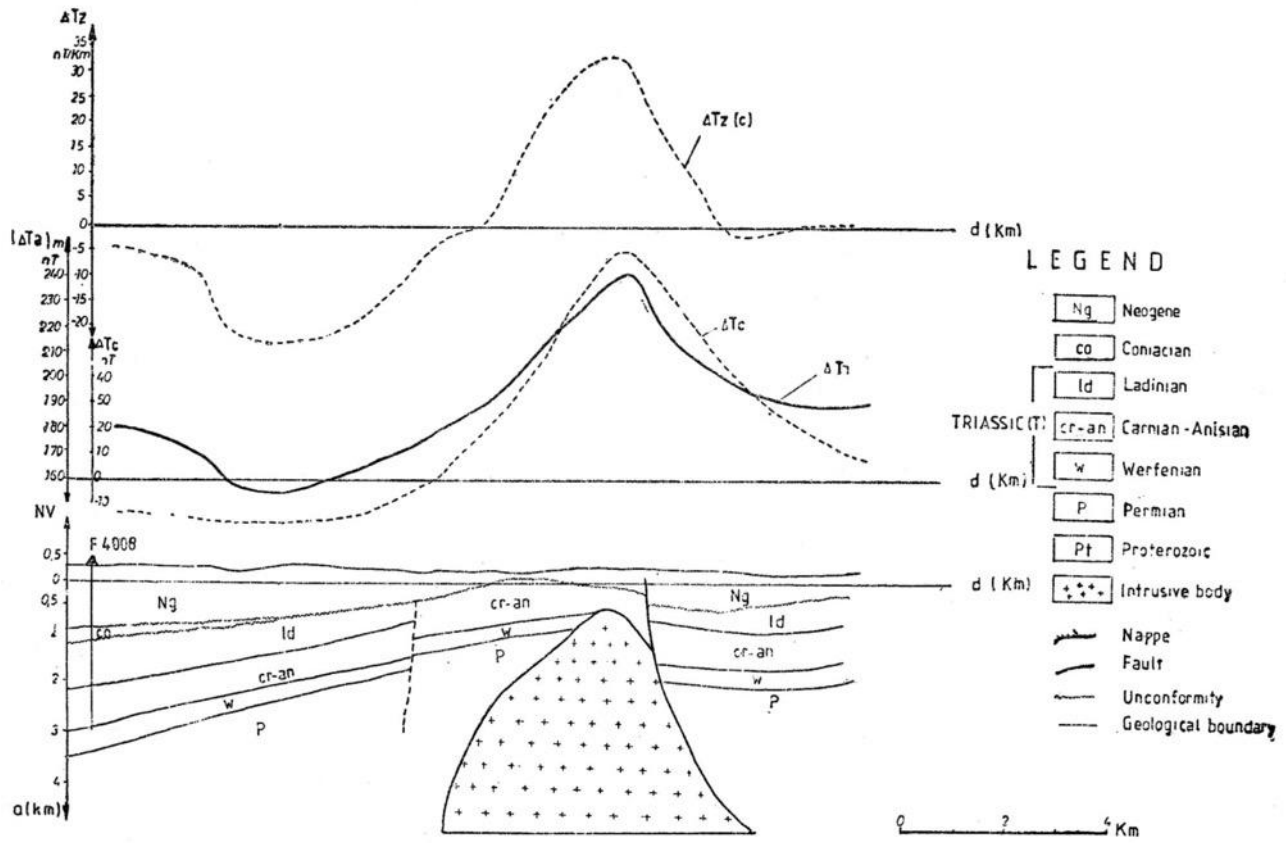

Figure 18 Beiuș Basin – longitudinal cross – section, correlated with aeromagnetic data, reproduced after Dinu et al, 1991.

3. Geophysics of the prospective area

3.1. Airborne data

For delineation of the regional batholith from Bihor Mountains we used ***Earth Magnetic Anomaly Grid*** *(https://www.ngdc.noaa.gov/geomag/emag2.html)* compiled from satellite, ship, and airborne magnetic measurements; the image has a 4 km altitude from the Earth surface (Figure 19). The image afferent to the batholith from Bihor Mountains was downloaded from the website, was georeferenced and than was included into GIS together with the countours of the batholiths, as defined by Andrei et al (1989). As can be seen the Romanian ground-based vertical component of geomagnetic anomaly data, which is used to define the countours of the batholiths, is consistent with the international data for example EMAG2v3, which highlights (by the red colour) the presence of the batholith in this location. In Figure 19 there is a continuous line with white circles that indicates the contour of the batholiths in the depth, and other contours that indicate the regions where the batholiths outcrops, or is near the surface.

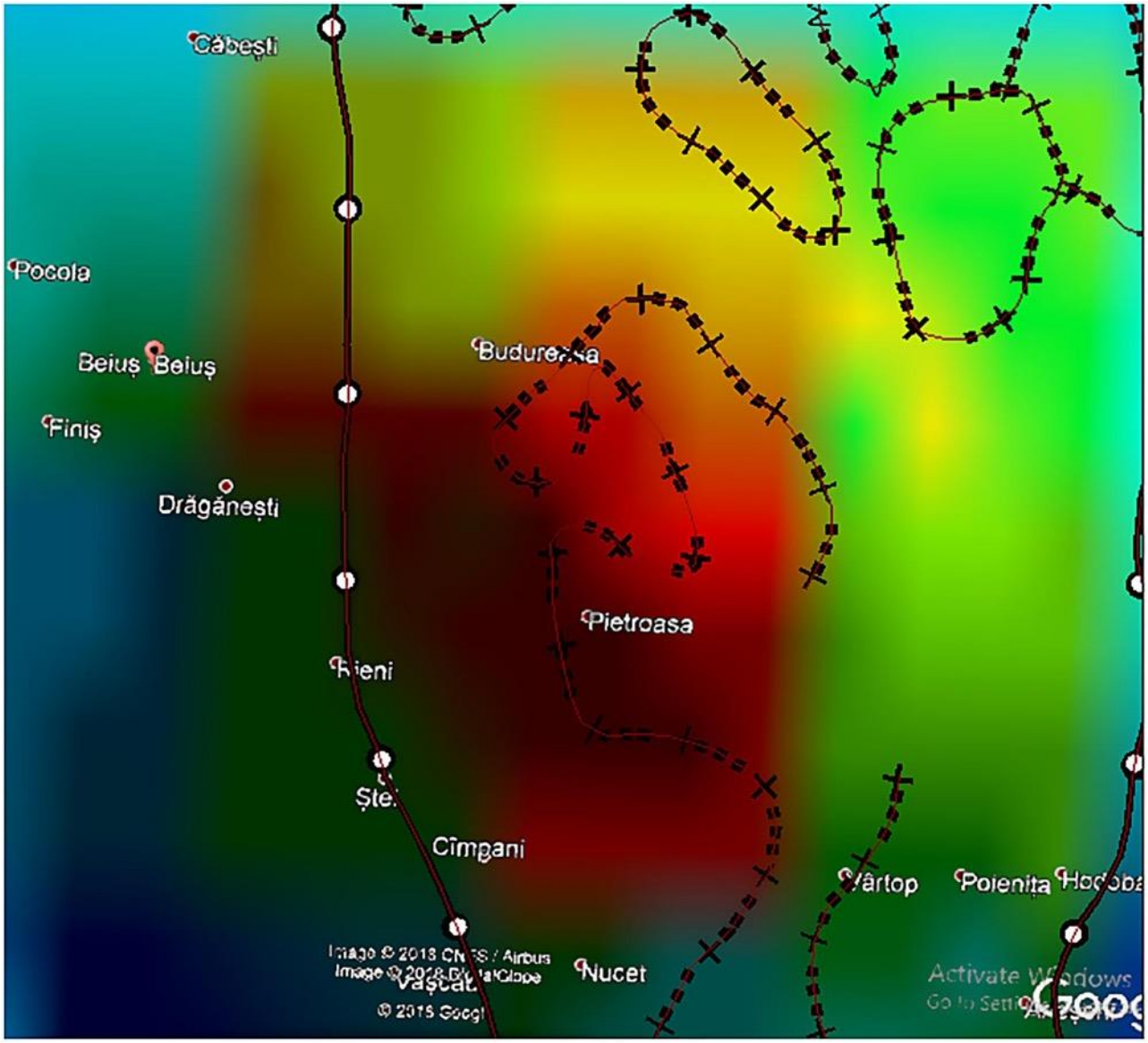

Figure 19 A fragment of Earth Magnetic Anomaly Grid compiled from satellite, ship, and airborne magnetic measurements; the image has a 4 km altitude from the Earth surface. The figure contains the contour of the batholith as defined by Andrei et al, (1989.)

In recent years Romanian researchers analyze the degree of confidence of older data integrating them in international datasets. For example, in 2012, Bețuțiu et al realized a critical analysis of Romanian geomagnetic data for the WDMAM Project purposes (http://geomag.org/models/WDMAM/WDMAM_NGDC_V1.1.pdf). 'Total intensity scalar geomagnetic anomaly for the 2007.5 epoch at the 3000 m altitude' map (Figure 20) is one of the results.

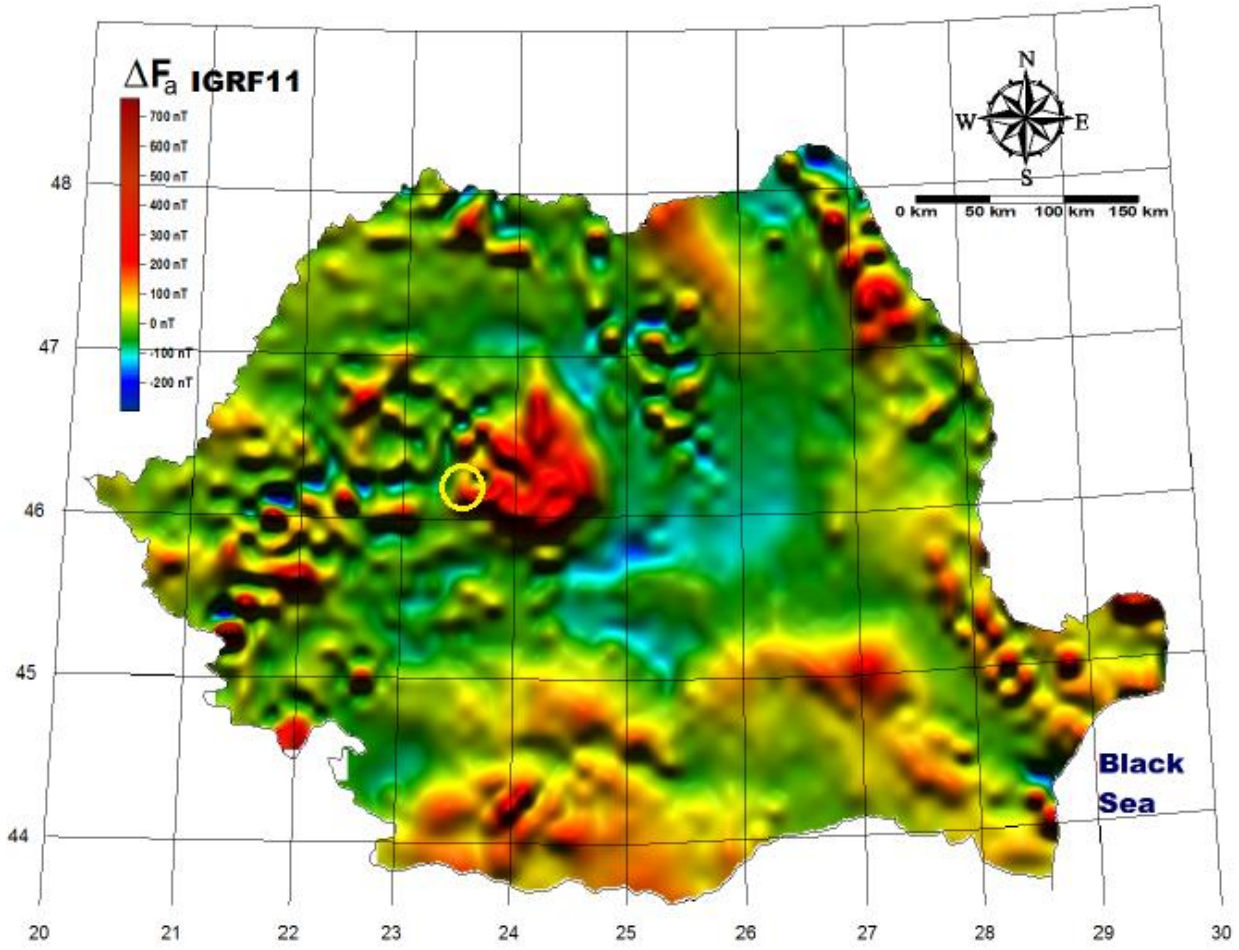

Figure 20 'Total intensity scalar geomagnetic anomaly for the 2007.5 epoch at the 3000 m altitude' map, reproduced after Beșuțiu et al, 2012. Location of study area is indicated.

Remote sensing research has been developed since 1975 (S.Veliciu et al., 1975, 1976, V. Vîjdea et al., 1977 – 1996, A.Vîjdea et al. 1996 – 2018). For Apuseni Mountains studies have been developed by A.Vîjdea, which emphasized that, for, North Apuseni Mountains, the system of lines representing faults has N 60^{o} - 70^{o} E as a major dominant direction, that suggest the over thrusting of two nappes systems (Figure 21). The 6-line systems groups have been confronted with geophysical maps, and the conclusion was that 80% of gravimetric and magnetometric anomalies have a correspondent in the maps with linear elements.

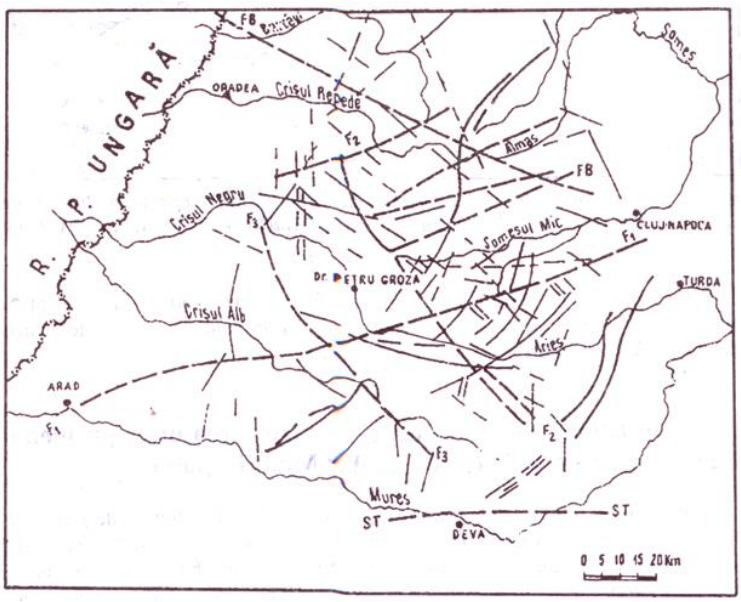

Figure 21 Sketch with major liniar elements deciphered on sattelite images. Reproduced after Visarion, 1997.

3.2. Ground-based data

The detailed interpretation of the magnetic anomalies situated on Romania's territory has been made by several authors (Gavăt et al., 1965; Constantinescu et al., 1972; Airinei, 1985; Visarion et al., 1988, 1998; Beşuţiu, 2001). The map of anomaly of the vertical component of the magnetic field and Bouguer Anomaly map were compiled and the values of ϒ isolines (or mgal isolines) were transposed to a grid with 200 meters cells. These compiled maps are to be found on the IGR's website, at to following address: http://harti.igr.ro/geofizica-v1/. Figures 22 and 23 show fragments of these maps selected for Beiuș Basin and Bihor Mountains.

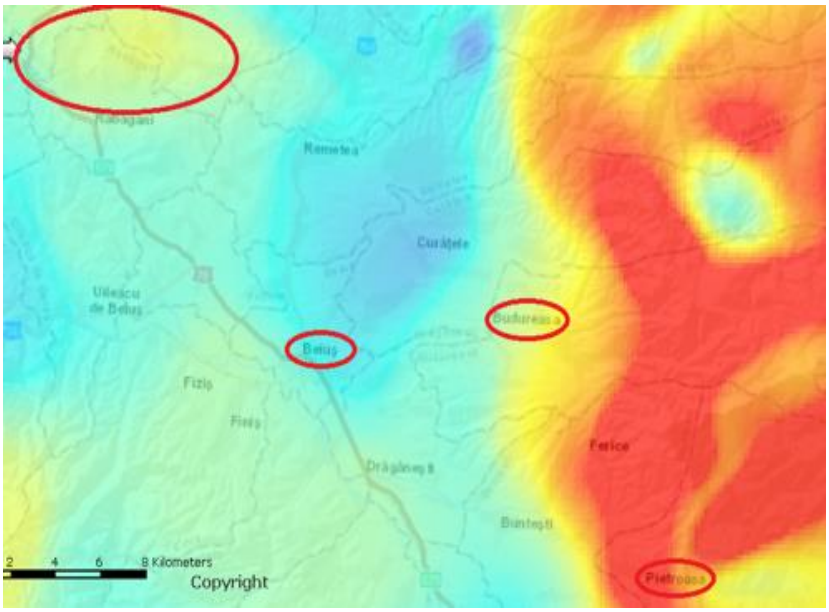

Figure 22 Fragment of vertical component of the geomagnetic anomaly map (DZa), (Authors Airinei et al, (1983) *published by IGR. Locations of Beiuș, Budureasa and Pietroasa are indicated, as well as the location of the anomaly from Beiuș Basin.*

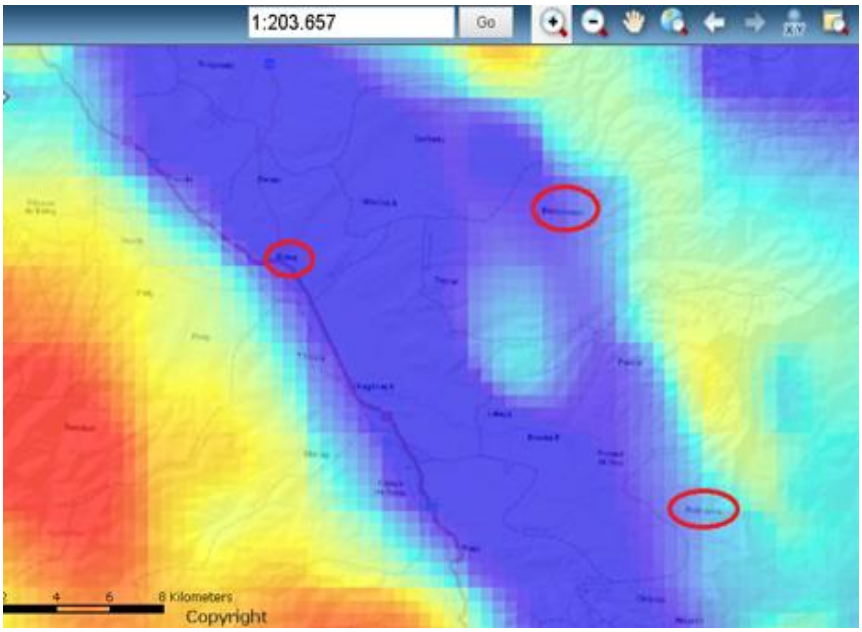

*Figure 23 Fragment of local gravimetric anomaly map, (*Bouguer Anomaly for δ = 2.67 g / cm3, Source: Nicolescu et al, 1991) *resulted from interpretation in ArcGIS Spatial Analyst by using Bouguer anomaly and regional gravimetric anomaly. Values are given in mgal. Locations of Beiuș, Budureasa and Pietroasa are indicated.*

In 2005 Ioane and Ion, elaborated a 3D crustal gravity modelling of the Romanian territory. The completion of the Bouguer gravity map for the Romanian territory, as well as the calculation of the mean gravity dataset in a 5' x 7.5' grid, enabled a 3D modelling approach for the crustal structure. The geophysical model has been built using information derived from published crustal models based on refraction seismic and borehole data, each layer getting a mean density value describing the main density contrasts. The 3D stripped gravity map was derived from the above mentioned gravity maps (Figure 24).

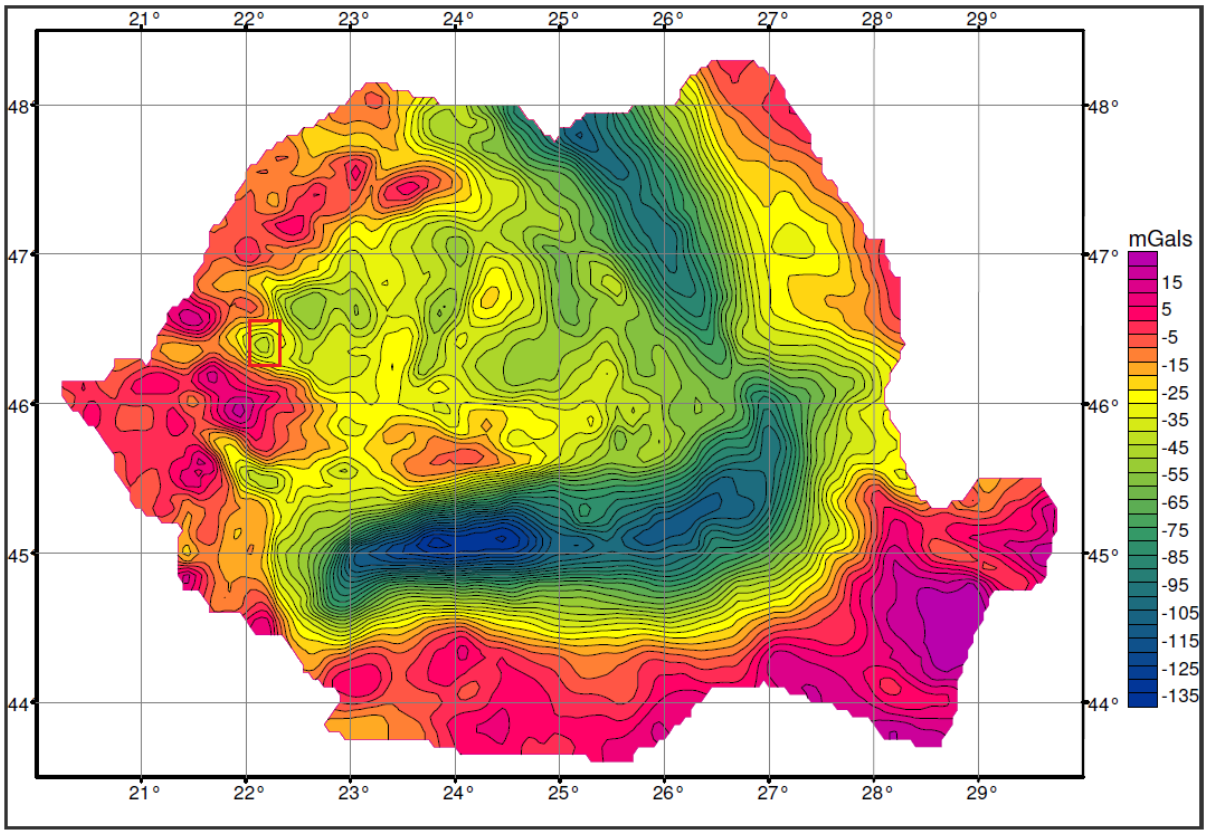

Figure 24 Bouguer gravity anomalies (Romania)

The delineation of the Bihor – Vlădeasa banatitic batholith is showed by the Vertical component of the geomagnetic anomaly map (ΔZa), on the scale 1: 1 000 000, published in 1983 by IGR (Figure 22). According to Bețuțiu et al (2012), for the study case region, the aeromagnetic survey was realized at 1000 m altitude.

Moreover, local gravimetric anomaly data (Figure 23) are available on the IGR's map scale 1:1 000 000, for the interpretation.

In most cases the structures of Bihor – Vlădeasa Mountains, being of acid composition (granite – granodorite) are pointed out by maximum aeromagnetic anomalies coupled with gravity minima. For Bihor – Vlădeasa, one of the most important banatitic structures in Romania, gravity and magnetic simulation models have been realised, showing an extension along north – south direction over 60 km, with a mean width around 25 km. The etimated hight of the intrusive mass is 7 – 10 km.

The banatitic structures from the Bihor – Vlădeasa pluton have been identified by drilligs reaching as far as 1300 m depth. At the same time mining works have been realised but at smaller depths. Cross-sections have been elaborated too.

For Bihor Mountains, in IGR's archive there are regional and also local maps at 1:25 000 and 1:5 000 scales, which are based on gravimetric and magnetometry measurements. They have been elaborated in search for ore deposits.

The most important results of research on banatitic magmatites (Upper Cretaceous – Paleogene), that has been carried out since 1962, are the geological maps, scale 1:50.000, the afferent profiles, and the profiles scale 1: 200.000 published by M. Ștefănescu et al, e.g. the one showed in Figure 25.

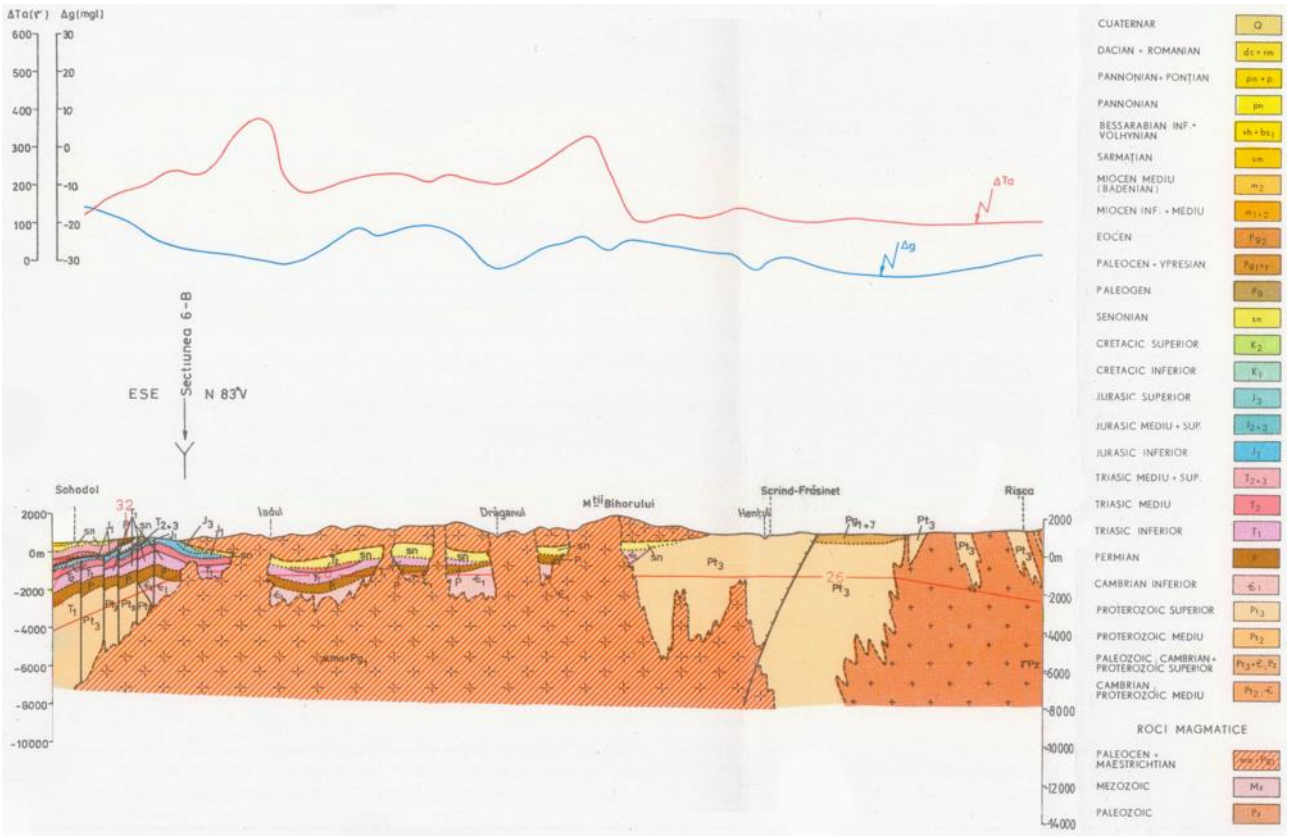

Figure 25 Bihor Mountains – cross section, scale 1:200.000; reproduced after Ștefănescu et al, – IGR's cross sections, 1988.

The above mentioned input is the primary data for the 3D model of Bihor – Vlădeasa batholith distribution that is realized within the project and will be reported in another chapter. An example of the contour of the batholith is given in the Figure 26.

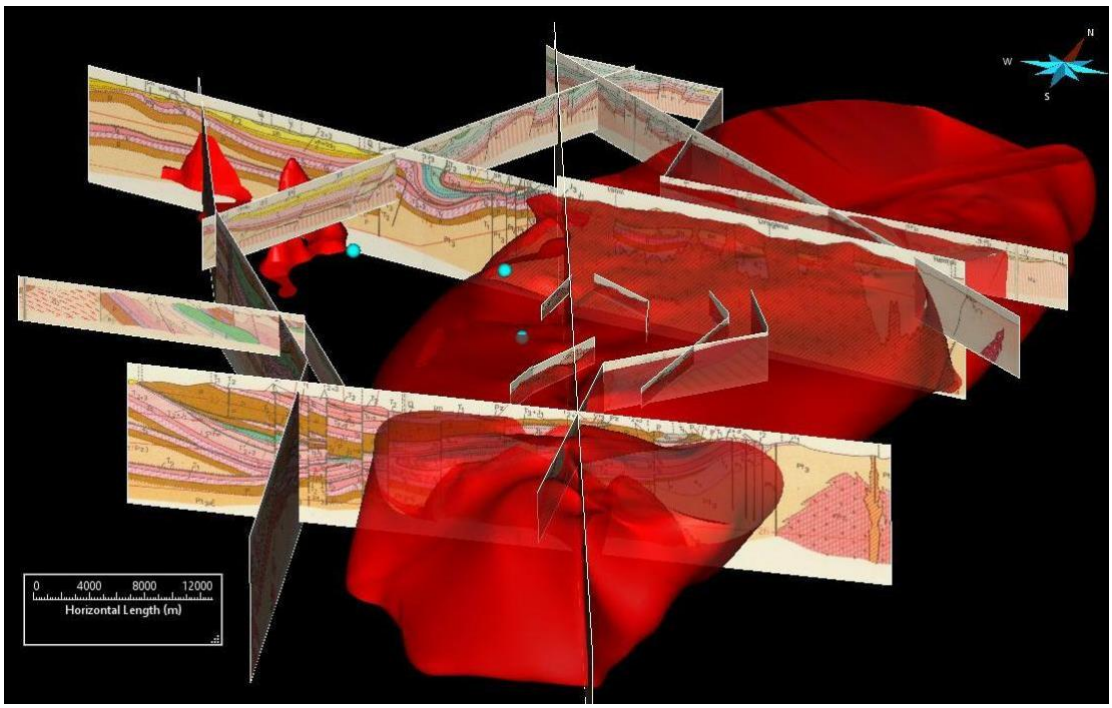

Figure 26 3D model of the batholith contoured based on cross-sections and magnetometry maps.

For the purpose of 3D modelling for Bihor Mountains, the maps scale 1:25 000, contained in the following report is used: ***'Report on geological, geochemical, magnetometric and electrometric prospection works in Budureasa - Bihor Mountains'***, authors: Manea el al, 1973, that contains maps at 1:25 000 scales.

Seismic refraction prospecting has been developed in order delineate the areas that contain mineral deposits. For example, since the seventies it has been revealed the existence of a batolith in Apuseni Mountains (Figure 27).

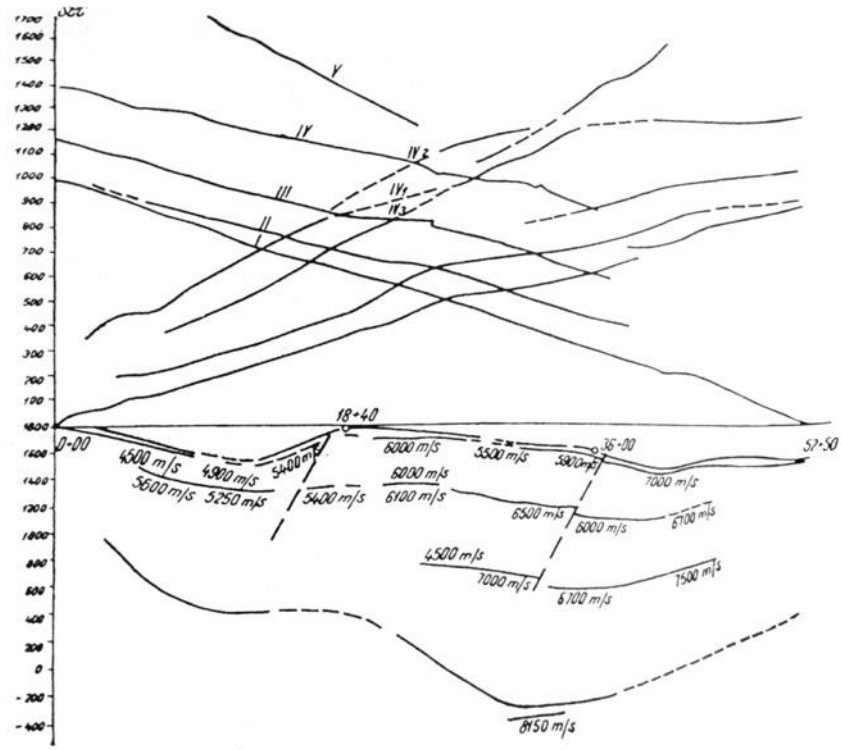

Figure 27 Refraction seismic profile in Apuseni Mountains that show a grandioritic body intruded into crystalline schists. Reproduced after Paicu and Patrichi, 1961.

Based on north-west part of the regional crustal profile XI in Romania, continue seismic surveys of the Romanian National Seismic Network and punctual seismic recording, a joint inversion method of receiver function and Rayleigh wave dispersion was employed by Bala et al, in order to derive the 1D seismic velocity models for several seismic station locations in western part of Romania. The study uses new data emerged from permanent network of broadband stations in Romania, as well as data from temporary networks established during the joint projects with European partners in the last decades.

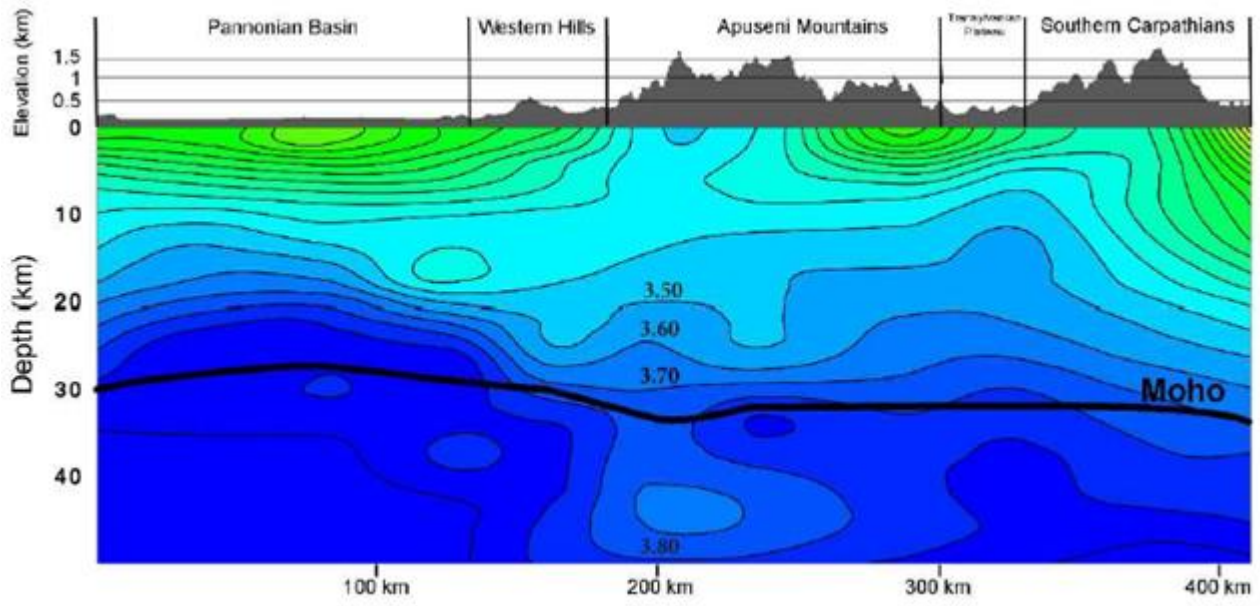

Figure 27 bis Seismic profile across Pannonian Basin and Apuseni Mountains. Reproduced after Bala et al, 2018.

In Figure 27 bis the profile is crossing an important section of Pannonian basin, the contact with Apuseni Mountains and crossing even the Southern Carpathians. The Moho depth is at about 29-30 km in the west, then a section with reduced velocities of 27- 28 km. In the central part of Apuseni Mountains the Moho is at 31-32 km depth followed by a flat section and decreasing to 33 km depth in the Southern Carpathians. The authors stress that comparing the data with crustal thickness determined in other areas belonging to Carpathian Orogeny, the Apuseni Mountains shows unusually reduced crustal depths. This bring up the hypothesis according to which these mountains represent in the Carpathian geosyncline zone, an area with an independent tectonic crustal structure with low crustal depths, compared to other areas belonging to Carpathian Orogeny.

4. Deep metal enrichment

North Apuseni Mountains Alpine magmatism is integrated within a broader context, defined by the term **Banatitic Magmatic and Metallogenic Belt – BMMB**, which represents a series of discontinuous magmatic and metallogenic occurrences of Upper Cretaceous age, which are discordant in respect to Mid-Cretaceous nappe structures of the region (Cioflica & Vlad, 1973; Ciobanu et al., 2002). The metalogenesis of Bihor Mountains is closely linked to the evolution of banatitic magmatism in the North Apuseni Mountains.

The data on **evolution of banatitic magmatism and the metallogenesis of North Apuseni Mountains**, were adapted from Ștefan et al, (1992), which synthetised the works conducted in the region before 1989 by:

Mureșan, 1971; Lazăr et al., 1972; Istrate, Bratosin, 1976; Istrate, 1978; Ştefan, 1980; Udubașa et al., 1980; Istrate, Udubașa, 1981; Ştefan el. al., 1985, 1986, 1988; Ştefan et al., 1989, unpublished report.

The banatitic calcalkaline magmatism (Post-Lower Masstrichtian-Palaeogene) which is widely developed in the Bihor Mountains was emplaced within two important cycles. **The first cycle** is characterized by lava flows (Vlădeasa) sometimes accompanied by pyroclastics (Vlădeasa); simultaneously superficial subvolcanic bodies have been emplaced (Vlădeasa, Bihor). The typical development area of the first cycle volcanism – the Vlădeasa Mts – contains the greatest volume of rhyolites forming the volcano-plutonic massif of Vlădeasa (Giușcă et al., 1969). The rocks of the Vlădeasa main eruptive body cut and include andesites, dacites and two older rhyolite rock types producing contact breccias with them.

Within **the second cycle** there have been emplaced bodies of intrusive rocks, generally hypabyssal as well as plutonic ones which are widely developed in the depth (Proca, Proca, 1972; Cioflica et al., 1982). Late alkaline vein differentiation products of granodiorite-granitic magma were reported too. Magmatic banatitic activity in the Bihor Mts ends with dykes of basic rocks (very abundant in Bihor).

The second cycle of banatitic magmatism contains a large range of quartz-diorites rocks and granodiorite - granitic rocks, accompanied and proceeded in crystallization succession by their porphyritic varieties, which are placed at the periphery of plutons, both as marginal facies of big bodies and as their apophyses. Swarms of subvolcanic bodies of porphyritic, quartz-diorite, granodioritic or granitic rocks are supposed to be associated to some profound plutonic bodies; such a supposition which is on account of geophysical data was confirmed by deep drillings, which have done in the area of Hălmăgel - Valea Seacă pluton (Cioflica et al., 1982).

Petrographically, the intrusive banatitic rocks in the Budureasa and Pietroasa areas range from granites to quartz diorites, with a prevalence of monzogranites and granodiorites (Istrate & Udubașa, 1981; Ionescu, 1996a; Ionescu & Har, 2001). Quartz monzonites, quartz monzodiorites and diorites occur as well (Istrate & Udubașa, 1981). Granodiorites are hypidiomorphic-granular, whereas porphyritic textures are restricted to the marginal facies. Granodiorites have a grayish to yellowish or pinkish color and consist of K-feldspar, quartz, plagioclase (mostly oligoclase or oligoclase/andesine), biotite, magnesiohornblende and rare clinopyroxene. Titanite, zircon, apatite and allanite-(Ce) occur as accessory minerals.

In Bihor Mountains diorites and their porphyritic varieties are displayed at the periphery of a granitic pluton or in its cover. In Pietroasa, Budureasa and Western Vlădeasa massif, quartz- dioritic rocks occur either as some independent bodies or at the periphery of granodiorite – granitic - monzodioritic rocks. Porphyritic micro diorites are also met in the northern extremity of eastern Vlădeasa eruptive massif, north of Crișul Repede River, at the periphery and in the cover of a granodiorite porphyry dyke.

Granodiorite-granites, to which the main sulphide mineralization is genetically linked, constitute main mass of banatitic bhey crop out on small areas; their development in the depth was emphasized (in Bihor Mountains).
Based on complex studies and reserves calculations performed by Cioflică et al (1989) the table given below was published (Table 1):

Table 1 Ore deposits connected to laramian magmatism

Location	Rock samples	Mineralization
Băița Bihor – Valea Seacă	Ca skarns; Mg skarns; granodiorites	Mo-Bi, B, Cu–Bi–W, Pb-Zn-Cu, Cu-Py
Borod – Cornițel	Rhyolites	Pb - Zn

Rănușa, Zimbru	Metarhyolites; meta conglomerates	Cu; Cu-Mo
Avram Iancu	Epimetamorphic rocks (limestones)	Cu-Ni-Co
Brusturi – Luncșoara	Epimetamorphic rocks (limestones)	Pb-Zn-Cu
Băișoara	Ca skarns	Fe (Pb-Zn)
Măgureaua Vaței	Ca skarns	Fe (Cu)
Săvârșin	Granites	Mo
Cerbia	Granites	Mo (Pb-Zn)
Căzănești	Basalts	Cu-Py

Source: Map of the distribution of the ore deposits in the Apuseni Mountains after Cioflică et al.

Budureasa - Valea Fagului is also added to this list by Borcoș (1997) who mention the following comodities: Pb+Zn, Cu, Au+Ag, Fe.

A map showing the location of these mineralization areas within Apuseni Mountains is given in Figure 28.

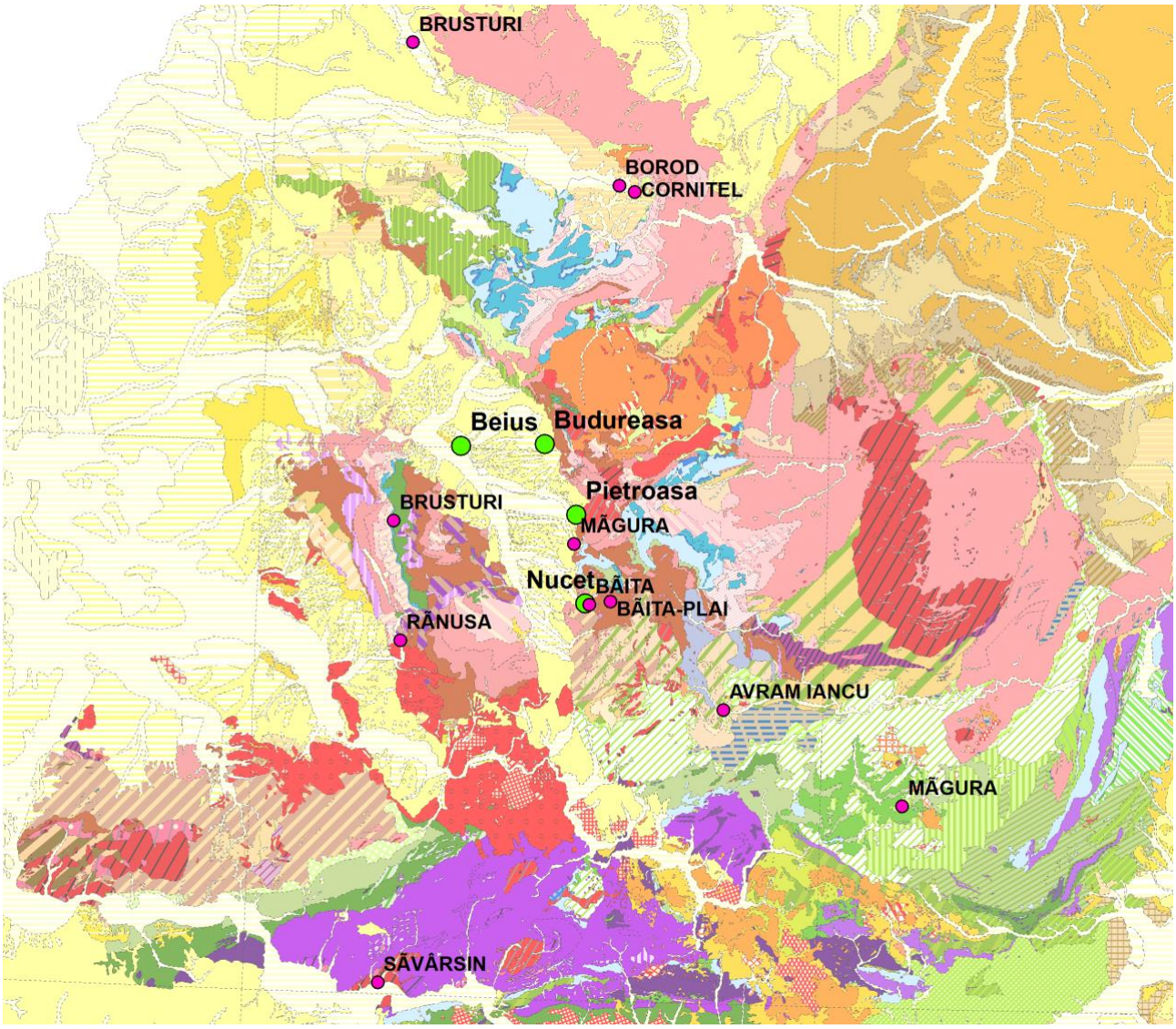

Figure 28 Apuseni Mountains and locations of mineralization areas.

Ştefan *et al.* (1992) has studied in detail the petrochemical and geochemical features of the banatites from the North Apuseni Mountains. In 2001 a study by Ionescu and Har, described the global geochemical characteristics of the rocks from this region. Some results of this study for granodiorites (chemical analyses and trace-elements and RE contents) are given below:

Table 2 Chemical analyses of the granodiorites from Budureasa and Pietroasa

Sample location	Chemical composition %											
	SiO2	Al2O3	Fe2O3	FeO	CaO	MgO	K2O	Na2O	TiO2	P2O5	MnO	H2O
BUDUREASA												
Gallery 8	70.83	14.79	2.55	0	2.73	0.85	3	3.64	0.24	0.41	0.59	0.37
Gallery 8	72.1	13.82	1.91	0	2.31	1.12	2.84	3.6	0.24	1.74	0.36	0.06
Gallery 8	70.69	14.6	2.76	0	2.13	1.37	2.92	3.08	0.38	1.05	0.57	0.45
Gallery 6 bis	69.8	14.51	2.68	0	2.87	1.3	3.08	3.04	0.32	1.78	0.69	0.08
Lateral drift no. 350/Gallery 6 bis	69.31	14.01	2.7	0	2.75	1.7	3.4	2.8	0.46	0.6	0.58	1.69
Gallery 6 bis	69.6	14.61	2.9	0	2.42	1.5	3.2	3.2	0.46	0.66	0.59	0.86
Lateral drift no.250/Gallery 6 bis	69.04	14.54	2.8	0	2.61	1.3	3.3	2.9	0.52	0.58	0.85	1.56
Lateral drift no. 350/ Gallery 8	70.06	14.37	2.55	0	2.08	1.7	3.8	2.8	0.52	0.04	0.41	1.7
Gallery 8	69.84	14.93	2.8	0	2.33	1.5	3	3.5	0.52	0.18	0.46	0.94
PIETROASA												
Sebisel Valley	66.13	12	4.2	1.81	3.4	3.2	2.79	3.93	0.75	0.16	0.09	1.01
Sebisel Valley	66.82	12.35	3.57	1.67	3.08	2.8	2.72	3.31	0.75	0.16	0.09	1.71
Sebisel Valley	67.53	13.06	3.43	1.81	2.46	2.3	3.39	4.25	0.8	0.16	0.1	0.25
Gallery 3	67.83	11.42	3.18	1.67	3.01	2.4	3.88	4.12	0.9	0.16	0.11	0.8
Gallery 3	66.35	13.22	3.81	1.81	3.4	2.4	3.49	3.31	0.75	0.16	0.09	0.71
Gallery 3	66.86	12.54	3.73	1.54	2.41	2.3	3.66	3.69	0.8	0.15	0.08	1.22
Gallery 3	67.07	13.04	3.42	1.81	2.71	2.4	3.56	3.69	0.65	0.14	0.07	0.94
Gallery 3	66.25	12.14	3.73	2.23	3.18	3	3.32	3.82	0.85	0.2	0.08	1
Gallery 3	66.33	12.52	3.65	1.95	2.76	3.1	3.37	3.93	0.85	0.2	0.09	0.86
Gallery 3	67.37	11.34	3.57	1.67	3.37	2.5	3.54	3.93	0.75	0.16	0.08	0.7
Aleu Valley	67.45	11.82	3.72	2.09	2.67	2.6	3.61	4.58	0.75	0.18	0.09	0.31
Aleu Valley	63.53	11.9	3.65	1.95	2.08	3.5	3.06	3.18	0.8	0.18	0.08	2.18
Prislop Hill	66.76	12.8	3.65	1.96	2.44	2.9	3.18	3.63	0.8	0.16	0.07	0.93
Prislop Hill	66.73	12.54	4.03	1.96	2.99	2.6	3.23	3.66	0.85	0.19	0.1	0.31
Aleu Valley	65.72	12.47	4.03	1.96	2.82	3.3	3.01	3.93	0.8	0.2	0.1	0.35
Aleu Valley	64.4	11.68	3.81	1.11	3.51	2.9	3.9	3.63	0.8	0.16	0.09	0.35

Table 3 Trace-elements and REE contents of the granodiorites and diorite from Budureasa-Pietroasa area*

Sample location	TiO2	Cu	Zn	Ga	Rb	Sr	Y	Zr	Nb	Ba	La	Ce	Hf	Pb	Th
	%	ppm													
Limit of detection	0.1	5	3	5	2	2	2	2	3	15	15	15	3	3	5
Budureasa granodiorite Sârca Valley	0.8	uld*	67	20	38	535	31	712	8	346	18	52	17	49	uld
Budureasa granodiorite Sârca	0.4	6	41	17	178	133	35	203	11	577	43	78	10	20	uld

Valley															
Pietroasa diorite Quarry	0.9	19	48	21	164	290	37	287	19	567	40	86	10	24	uld
Pietroasa granodiorite Quarry	0.6	21	44	19	149	273	21	202	8	945	43	81	6	29	uld

** Chemical analyses for trace elements were made by ED-XRFA (the X-ray Fluorescence Neutronic Thermic Activation method) by Prof. dr. Doris Stüben (Institut für Petrographie und Geochemie, Karlsruhe University, Germany).*

The granodiorites acidity varies between 63.53 % and 70.83 % SiO2. The Na2O contents range between 2.80 % and 4.58 %, while K2O range between 2.72 and 3.90 %. A quite obvious difference can be noticed between the rocks of the two areas: granodiorites from Budureasa are a little more acid and contain more Al and Mn than those of the Pietroasa body. In return, they are poorer in Fe, Ca, alkalies and Ti (Ionescu and Hae, 2001).

The above mentioned study emphasizes the main conclusions with a special reference to Pietroasa and Budureasa intrusive bodies:

- The banatites from the North Apuseni Mountains are the result of the oceanic crust subduction in the western basin (Rădulescu, 1974).
- The Budureasa and Pietroasa banatite bodies belong to the second stage (Istrate and Udubaşa, 1980; Ştefan *et al*., 1988) of the Laramian magmatism, which has a calco-alkalin character.
- The petrochemical studies show some differences between the Budureasa and Pietroasa igneous bodies: generated in the same structural frame (continental arc granitoids), the Budureasa magmas preceded in time the more alkaline Pietroasa magmas.
- The petrochemical differences observed between the Budureasa and Pietroasa banatitic bodies are at variance with the presence of a single, deep situated, batholith with large apophyses (as the Budureasa and Pietroasa bodies were considered).
- The magma genesis begun closer to the subduction front (the Budureasa body) and continued further in time with the Pietroasa body.
- The rocks from Budureasa area reveal a long-time evolution, emplacement and crystallization of the diorite-granodiorite-granite magmas: from 88 to even 54.5 Ma.

Around big bodies of granodiorite-granitic composition, **phenomena of thermal metamorphism are reported.** Their extension around the pluton is 1500 m as in the Bihor Mountains (Cioflică et al., 1974). Although products of thermal metamorphism are widely spread in the Bihor, intensity of thermal metamorphism reached only the facies of hornfels.

Under geologically favorable conditions, i.e. in the contact aureole of the granodiorite-granites plutons, Fe, B, Bi, Mo bearing skarns have been formed, locally overlapped by sulphide mineralization, sometimes independently developed, such as the vein occurrences with Cu, Zn and Pb sulphides at Valea Seacă, Valea Mare-Budureasa etc.

Skarns often accompanied by magnetite concentration occur almost everywhere at the contact between diorite and carbonate rocks, sometime base metal sulphides associate with the skarns. So, at Măgureaua Vaței skarns of a very rich paragenesis (gehlenite, spurrite, tilleyite, garnets, pyroxenes, wollastonite, and vesuvianite) are associated to Fe ± Ba metasomatic mineralization in the western extremity of quartz-mondozodioritic body and sulphide veins in the eastern extremity on the magmatic body, where granites - granodiorite prevail. On Martin hill at Sârbi-Hălmăgel, in the aureole of dioritic body, which is crossed by

granodiorites, iron oxides and sulphide mineralization occur. Magnetite associated with banatitic magmatites are also found at the spring of Arieșul Mic, Valea Seacă and Budureasa; at Valea Seacă and Budureasa, sulphide mineralization overlies this kind of mineralization.

Magmatic bodies intruded Permian-Mesozoic sequences and produced contact-metamorphic aureoles, at Pietroasa, Budureasa and, most extended at Baita Bihor, where the surface exposure of the contact rocks reach many square kilometers, being the largest in Romania.

Brucite deposits

Between 1982 and 1990 the **brucite deposits** from Budureasa and Pietroasa were investigated by surface pits, drillings and underground galleries. A schematic and idealized view of the contact of granodiorites with the Anisian dolomites shows a structure with four zones, ranging from granodiorites to pure dolomites (Ionescu & Hoeck, 2005):

- Granodiorites are holocrystalline hypidiomorphic, sometimes porphyritic, with large feldspar phenocrysts. Various magmatic, metamorphic and sedimentary xenoliths are common at the periphery of the intrusion.
- Magnesian skarns, forming the innermost zone of the contact aureole, consist mainly of forsterite, garnet (andradite) and clinopyroxene (diopside, hedenbergite). Periclase and spinel occur as well. A wealth of hydrated minerals mainly serpentine minerals, phlogopite, talc, chlorite, epidote–zoisite, apatite, tremolite–actinolite and subordinately hydrogarnet, vesuvianite, chondrodite, clinohumite, hydrotalcite, brucite, hydromagnesite and pyrophyllite were also formed. Younger veins with quartz, magnesite, sepiolite, calcite, pyrite, pyrrhotite, sphalerite, chalcopyrite, galenobismutite, and galena are common. The skarn thickness around the granodioritic body is relatively small, ranging from 0.5 up to maximum 7 m. The first occurrence of hydrogarnet and magnesioferrite in Romania was described from the Budureasa area by Ghergari & Ionescu (2000).
- Brucite-bearing zones occur only at some distances (0.5 to 7 m) from the contact. The irregular, sometimes lens-shaped brucite-bearing zones range from several metres up to tens of metres in width and from tens to several hundreds of metres in length, respectively. The thickness of the brucite-bearing zone can significantly vary within the short distance. The variation of brucite content across the contact aureola around the granodioritic intrusion is highly inhomogeneous, ranging from brucite-rich, with up to 40 wt% brucite to brucite-poor domains, with less than 5 wt% brucite. The average content of brucite is around 10.5 wt% in the Budureasa area and 7.5 wt% in the Pietroasa area, respectively (Ionescu, 1999).
- Recrystallized Anisian dolomite, without or with only very low Si and Al content, follows the brucite-rich zones. Brucite forms small lamellae of 20×20×2 µm up to 80×50×6 µm (length, width, thickness). Large individual lamellae, over 1 mm in length are only exceptionally found. Brucite lamellae group in clusters of various shapes and sizes (in average from 0.05 to 1.3 mm). Fillings of small veinlets or isolated lamellae are rare.

Borate deposit

In the middle basin of the Aleului Valley (Bihor Mountains), at its confluence with the Sebisel Valley, at the Gruiului Hill, an important endogene borate deposit, including ludwigite and szaibelyite, pointing to the kotoite presence, was identified. The mineralized site is situated at about 4 km NE of the locality of Pietroasa (Bihor District). The occurrence, investigated by mine workings, had also been pointed out (Stoicovici, Stoici, 1969; Stoici, 1974). In 1992 this deposit constitutes the study object of a thorough mineralogical study, realised by S. Marincea.

The ore deposit is hosted in a zone with magnesian hornfels (sensu Turner, Verhoogen, 1960), at the contact of the Pietroasa banatitic pluton with Anisian dolomite limestone of the Ferice Nappe (see Bordea, 1973, for details).

The data analysed by Marincea, (1992) consisting of mineralogical and physico-chemical study of szaibelyite and associated minerals in the Gruiului Hill occurrence, correlated with general geological aspects led as to the following conclusions:

- The formation of the borates from the contact aureole of the Pietroasa granitoid body is the result of an infiltration metasomatic process. This process explains the frequency of the occurrence of ludwigite in other parts of the contact aureole of the body (Rafalet, 1963). In case of the Gruiului Hill occurrence the significant boron-fluorine supply implies large metasomatic processes compatible only with an intense diffusion metasomatism.
- The hypothesis of a diffusion metasomatism implies the tectonic control of the boron minerals disposition in case of the Gruiului Hill occurrence. This hypothesis, also supported by Stoicovici and Stoici (1969), is based on the location of the mineralized zone nearby a Major fault of the Galbenii fracture system (with a NW-SE disposition): Tirău-Măgura Guranilor Fault, at its intersection with a network of conjugated fractures.
- The presence of minerals with potential fluorine contents (clinohumite can contain up to 4 per cent F according to Aleksandrov, 1982) makes plausible the hypothesis of the boron transport as fluoro-boric compounds with alkaline solutions as an age. (Barsukov, Egorov, 1957). The interaction with the dolomitic background makes possible the decrease of the alkalinity of such solutions, necessary for borate precipitation.
- Iron seems to be the primary precipitant of boron, as indicated by ludwigite formation before the pure magnesian borates. The iron deficit in the system would make possible the synchronous crystallization of such borate (that is of suanite or fluoborite) as well as the later crystallization of kotoite (Barsukov, Egorov, 1957).
- Boron-(fluorine) metasomatic supply is unique, influencing the preservation of the pure magnesian character of the primary borates, imprinted by the paleosome origin. The character of these borates, highly susceptible to the acceptance into the network of cations like Mn^{+}, Sn^{4+}, Ti^{4+}, induces the extreme magnesian character of the Gruiului Hill szaibelyite, for which the secondary genesis has been admitted.
- The constancy of the magnesian contents in calcites occurring in areas with hornfels affected or unaffected by the boron metasomatism leads to the conclusion of the extension of this metasomatism in zones where the limited development of the silicate minerals made possible the formation of an "excess" of magnesium available in the carbonate phases. The reverse correlation between the abundance of the silicates and the abundance of the boron minerals implies the active role of the lithologic control in the location of the Gruiului Hill mineralization.

W-bearing and base metal skarns

W-bearing and base metal skarns are characteristic only for Baita Bihor. Triassic dolostones, that discordantly overlies the Permian — Lower Triassic quartz sandstones and micro-conglomerates, form in both cases the protolith of the **magnesian skarns**. At Baița Bihor, some magnesian skarn bodies or ore pipes such as those at Antoniu, Bolfu-Tony, Hoanca Motului, Baia Roșie are **boron-bearing skarns** and represents well-defined metasomatic columns. A sole similar body, or metasomatic column, that from Dealul Gruiului was identified at Pietroasa.

The magnesian skarns are hosted by Anisian — Carnian or Carnian — Norian dolostones at Băița Bihor (Bordea et al. 1988) and by Anisian dolostones of the Ferice unit at Pietroasa (Bleahu et al. 1985); the

country rock is folded by traversing faults, which are more evident at Băița Bihor. The skarn bodies crop out on very small areas, but were extensively investigated by mining works.

*

Two rock samples from Romania were used for leaching experiments by Chris Rochelle et al., in 2017 as part of the CHPM2030 project's laboratory work: a skarn from Pietroasa **(HTL320)** and a mineralized rock from Cacova Ierii **(HTL321)**. The experiments used a range of fluid types and pressure/temperature conditions to identify fluid-rock reactions and quantify the potential for enhancing metal release. For the 2 samples the results are showed in Figures 29 – 32. We can see that for conditions of temperature/ pressure of 100 °C, and 200 bar the efficient substances proved to be 0.6 M NaCl, and HCl/HNO3 mix for both samples. The main elements recovered are: Co, Sr, Mo, Sb, Mn, Zn, and W.

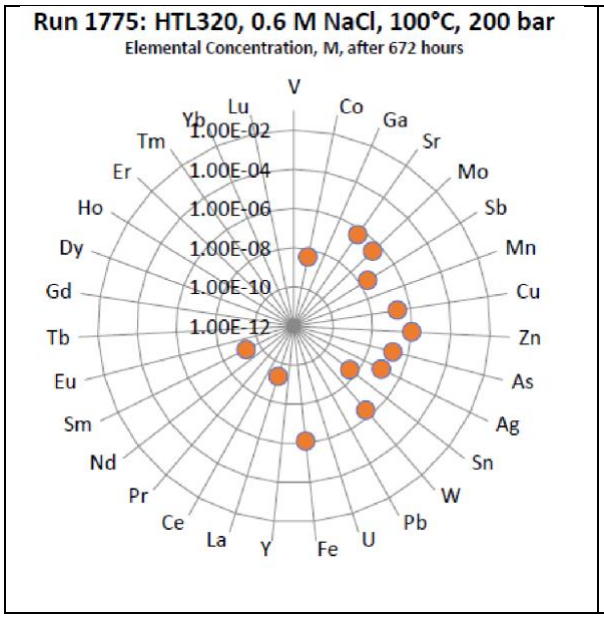

Figure 29 Selected metal concs. For Run 1775 final fluid (partner sample HTL320: 0.6 M NaCl, 100 °C, 200 bar)

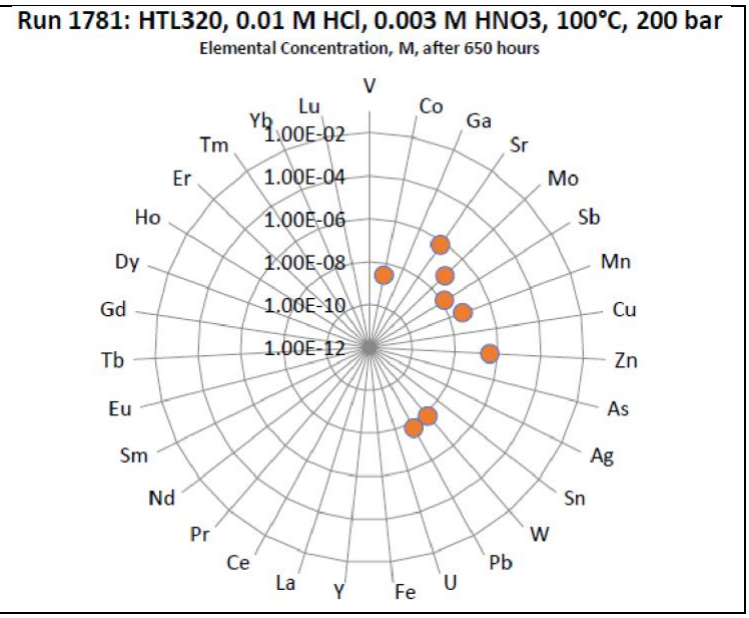

Figure 30 Selected metal concs. For Run 1781 final fluid (partner sample HTL320: HCl/HNO3 mix, 100 °C, and 200 bar).

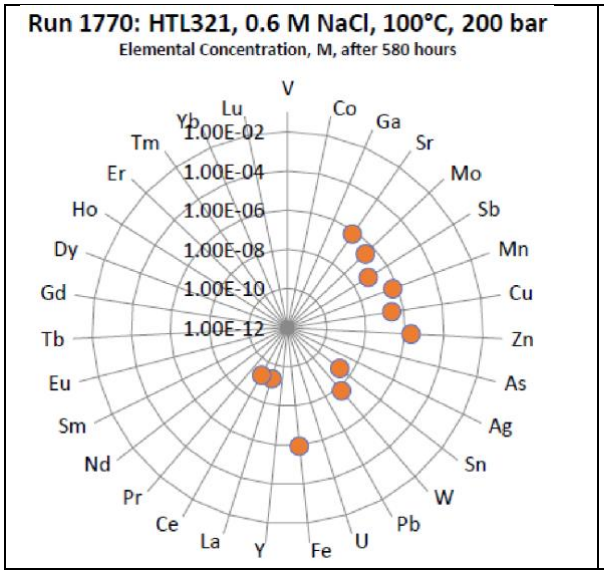

Figure 31 Selected metal concs. For Run 1770 final fluid (partner sample HTL321: 0.6 M NaCl, 100 °C, and 200 bar).

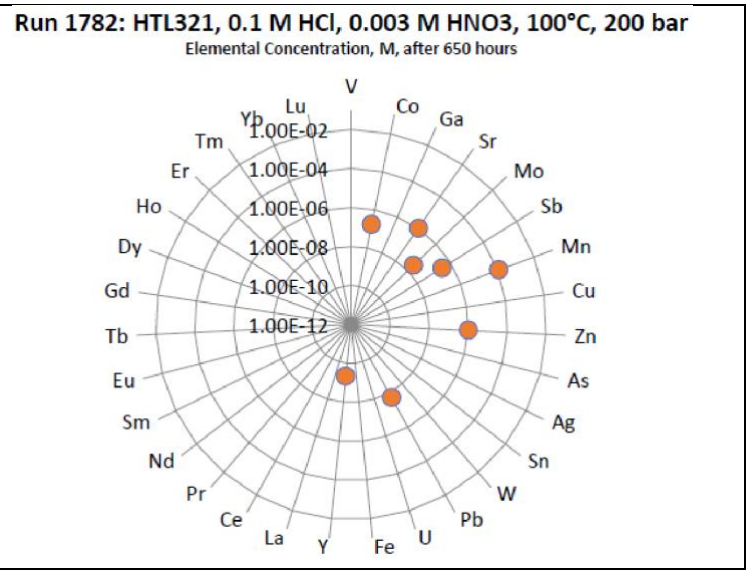

Figure 32 Selected metal concs. For Run 1782 final fluid (partner sample HTL321: HCl/HNO3 mix, 100 °C, and 200 bar).

5. EGS potential

The heat flow map of Romania and the map of temperatures at 3000 meters depth are based on temperature measurements in 4000 deep wells, the determination of thermal conductivity of the rocks, thermometric prospection and thermometry of ground waters. Also information on deep geological structure, the heterogeneity of the subsoil, the basement faults, the intrusive masses, the structures liable to underground accumulations, have been considered (Figures 33,34). For the study-case area the heat flow map indicates around 90 mW/m^2 and the temperature at 3000 m depth map is around 85^{o}C.

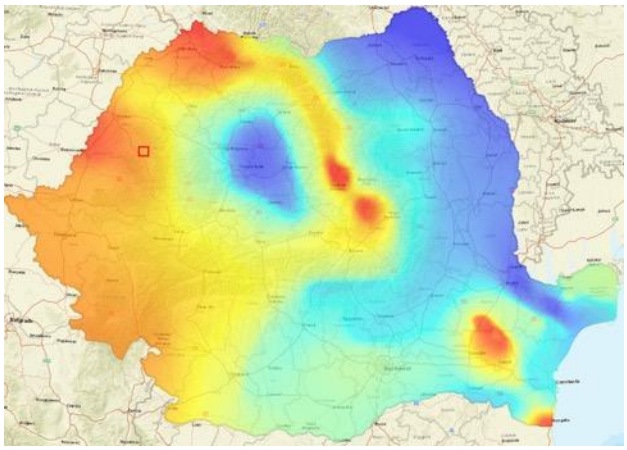

Figure 33 Heat flow in Romania (Raster resulted by interpolation of heat flow isolines - mW/m^2 -from Map of heat flow, Visarion et al, 1985)

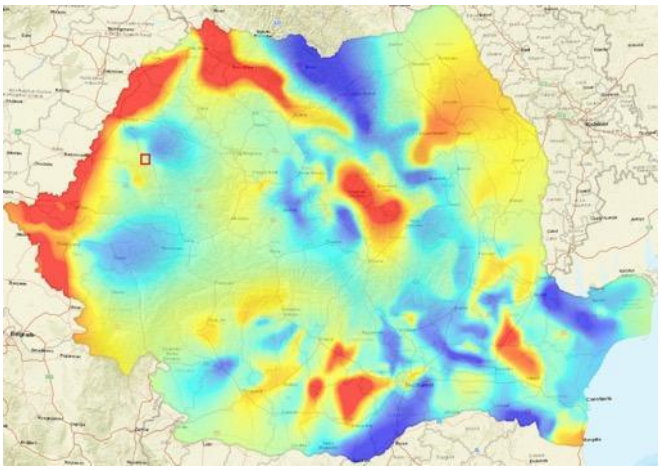

Figure 34 Map of temperatures at 3000 meters depth (Raster resulted by interpolation of geoisotherms - °C - from Map of heat flow, Visarion et al, 1985)

Previous to 2006 153 new reliable heat flow density determinations, 100 measurements in thermally stabilized boreholes (deeper than 1000 m), collection and interpretation of temperature from oil industry boreholes lead to the improvement of knowledge on geothermal potential for each region (Veliciu *et al,* 2006).

In Romania the mean heat flow varies between 21 and 120 mW/m^2 and the estimated temperature at 3000 meters depth varies between 44 and 163^o C. There are over 250 wells drilled with depths down to 3,500 m, which show the presence of low enthalpy geothermal resources (40-120°C). In Romania, the average thermal gradient is 2.5 ^{o}C/100 m, and it can exceed 6.6^o C/km in Pannonian Basin (Paraschiv et Cristian, 1976). In Romania three main areas having a high geothermal potential are to be mentioned, in East Carpathians, Moesian Platform and, the most important, Pannonian Basin.

In Bihor Mountains a regional batholith of banatitic origin outcrops and has been contoured in the depth. At the same time geophysical measurements highlighted the existence of a batholith in Beiuș Basin.

Beiuș Basin is a part of the Pannonian Basin being formed by the same thermochronological processes that transformed the whole region during Neogene. That is why Beiuș Basin is expected to share the general favorable conditons as regards to the high heat flow, and temperature in the depth as Pannonian Basin. On the other hand Bihor Mountains, which are bordering the Pannonian Basin differ both in structure and termocronological processes history from the basin. Consequently, a special attention has to be given to local conditions.

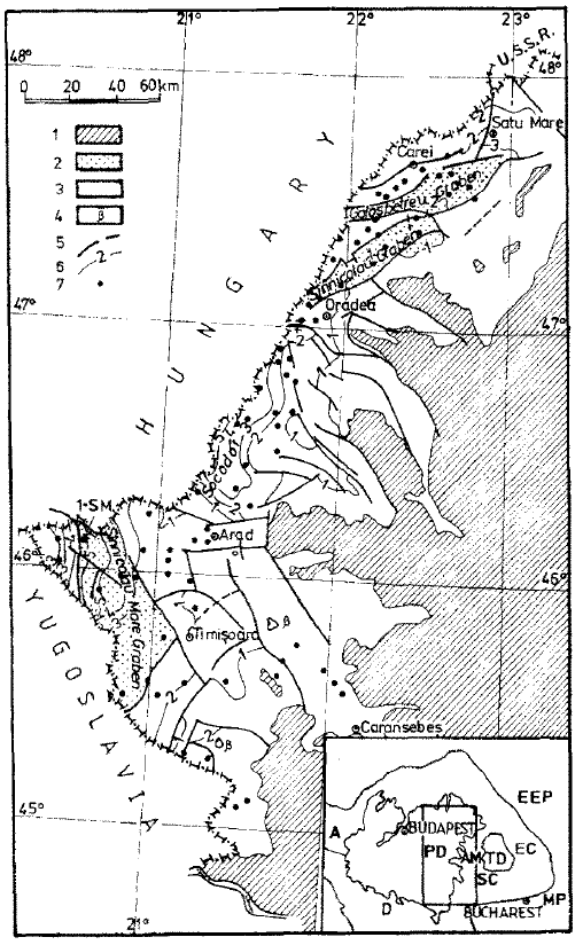

Figure 35 Location of geothermal wells; Reproduced after Demetrscu and Polonic

For the estimation of geothermal potential for Beiuș Basin and Bihor Mountains we will review the Romanian studies on these two areas. Then, as local data have been integrated into regional and European analyses offering a larger perspective on this theme, we shall refer to some of these studies.

In 1989 Demetrescu and Polonic described the formation and evolution of Romanian part of Pannonian Basin as a result of a complex thermomechanical phenomenon of lithospheric extension. The connection between heat flow, subsidence and sedimentation has been studied by Demetrescu based on data from 75 boreholes generally uniformly distributed over the study area (35). The conclusions are given below:

- The water-loaded tectonic subsidence in the Romanian part of Pannonian Depression at the end of the Badenian, Sarmatian and Early Pannonian until present is registered. The formation of the basin began in the Badenian, reaching depths of 300-400 m, and continued in the Sarmatian. The deepening of the basin extended to the east and south in the Pannonian and Quaternary. The present tectonic subsidence reaches values of 1200-1400 m.

- The quasi-linear time dependence of the tectonic subsidence suggests a finite rate extension since the Badenian, with extensional strain rates of 1-2%/m.y. Pre-Badenian instantaneous extension followed by a Badenian-Present thermal subsidence (Slater et al., 1980) can be accommodated with extension factors of 1.2-1.4 if initial altitudes were up to 1 km.

- Heat flow data suggest a contribution to the surface heat flow of 15-30 mWm^{-2}. This contribution is due to the heat coming from the convective transfer of heat by lithosphere material ascending during extension.

To compensate for the lack of measurements, Demetrescu used different types of data to produce patterns that would lead to the estimation of heat flow for the various structural structures, including the Pannonian Basin and the Apuseni Mountains. Thus, he was able to estimate that in areas of the Carpathians, affected by Tertiary tecto - geneses, usually referred to terrains younger than 50 Ma, the three components of the regional heat flow: crustal radiogenic, thermal transient perturbation and background heat flow from deeper sources, contribute with 36, 27 and 27 mWm^{-2}, respectively, to the mean value 90 mWm^{-2}.

Time - dependent history of the Neogene sedimentary formations chart used by Demetrescu for his models is given below (Figure 36).

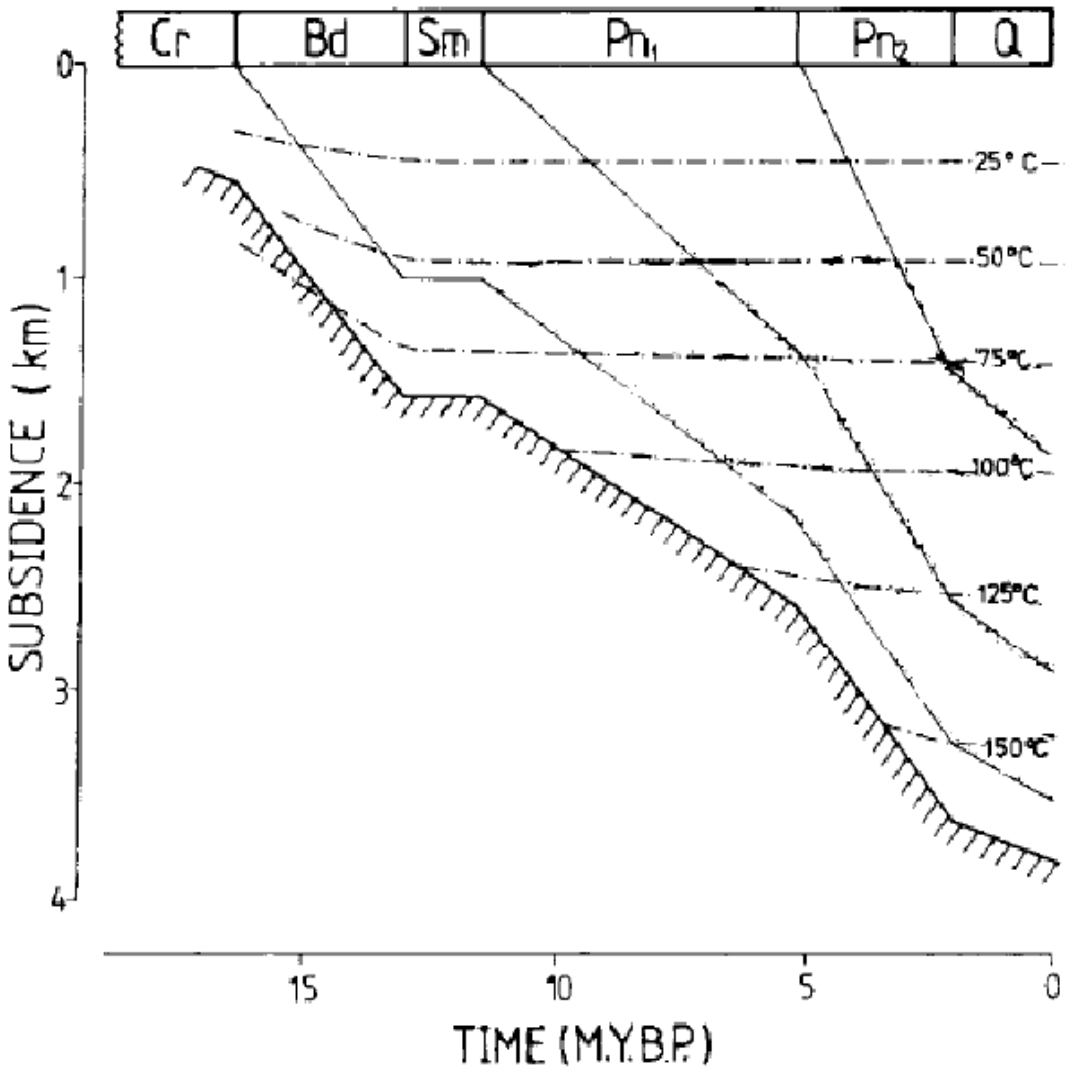

Figure 36 Time - dependent history of the Neogene sedimentary formations. Reproduced after Demetrescu and Polonic, 1989; Data were acquired from a borehole that is considered representative for Pannonian Basin.Continuous line – depositional isochron; dashed and dotted line – temperature; Cr. Cretaceous; Bd – Badenian; Sm – Sarmatioan; Pn_1 – Lower Pannonian; Pn_2 – Upper Pannonian; Q – Quarternary.

Rădulescu and Dimitrescu (1982) highlighted a correlation with the age of the last tectono-thermal event that mobilized the region in which the heat flow values were determined. For the eastern limit of the Pannonian Basin, where last tectono-thermal event was Post-Miocene extension (age 10 – 25 Ma) the mean heat flow is 96 mWm^{-2} (standard deviation 8).

The radiogenic heat generation of the region, for each type of rock was calculated by Veliciu, (1987), using the heat generation constants revised by Rybach (1976). Table 4 lists the average heat generation values from the Carpathians grouped according to the petrographic facies. For comparison, characteristic values for the Swiss Alps (Rybach 1976) are given. In terms of the surface radiogenic heat generation of the rocks, the differences found between these two Alpine orogenic regions are minor.

Table 4 Heat generation values for the Carpatians (Reproduced from Veliciu, 1987)

Rock Type	Romanian Carpathians (Veliciu 1987)			Swiss Alps (Rybach 1976)		
	Number of samples	Range (μWm^{-3})	Mean	Number of samples	Range (μWm^{-3})	Mean
Granitic rocks:						
Granite	50	1.94 – 3.10	2.52	8	1.88 – 6.06	2.50
Granodiorite	41	1.71 – 1.99	1.87			1.50
Andesite	61	0.52 – 1.18	0.85			1.10
Basalt	53	0.14 - 0.57	0.35	8	0.08 – 1.05	0.30
Metamorphic rocks:						
Green schists facies (epizone)	22	0.70 – 1.49	1.09	18	0.25 – 2.42	1.50
Amphibolites facies (mezozone)	391	1.74 – 3.11	2.43	55	0.86 – 5.02	2.42
Sedimentary rocks:						
Cretaceous flysch (sandstones)	91	0.86 – 1.31	1.09			
Carbonate rocks				12	0.03 – 0.92	0.33
Continental crust			0.72			0.80

In 1986 Neguț and Pauca determined the thermal conductivity of the rocks belonging to the Romanian part of the Pannonian Basin and the surrounding areas through laboratory methods. The results for the rock encountered in our perimeter are given in the Table 5:

Table 5 Thermal conductivity of the rocks from Pannonian Basin

The rock	Thermal conductivity (10^{-3}cal/cm x ^{o}C x s)
Magmatic rocks	
Granite	3.5 - 12
Granodiorite	3.5 – 7.8
Diorite	4.8 – 5.0
Basalt	2.0 – 8.0
Gabbros	4.0 – 9.4
Metamorphic rocks	
Quartzite	8.2 – 19.0
Marble	6.0 – 8.0
Sedimentary rocks	
Limestone	1.5 – 7.0
Dolomitize limestone	6.0 – 7.0
Dolomite	2.0 – 12.0
Geothermal water	1.0 – 1.2
Water (0 - 100^{o}C)	0.9

Based on these data the conclusion is that in Bihor Mountains, the heat flow of granitic – granodioritic bodies from Pietroasa and Budureasa are supposed to have high values in the depth. Also the heat flow of the rocks that host the geothermal aquifer (limestone, dolomite and quartzite, marble) has high values. But an import cooling agent is represented by the continuous circulation of the water that comes from the karst areas of Bihor Mountains into the geothermal aquifer from Beiuș Basin. It is expected that in the depth of 4 km, where the access of water is prevented by the aquiclude Lower Triassic layers the heat flow of the batholith to be considerable.

Paraschiv and Cristian (1976) realised measurements in a stabilized regime at 3000 oil exploration drilling and in unstabilized regime at 170 more. For Pannonian Basin (Romanian part) the following results are given below:

Table 6 Geothermal gradients for Pannonian Basin

Pannonian Basin	No. of oil structures	No. of temperature measurements	Depth of 500 m b.s.w.l.		Depth of 1000 m b.s.w.l.		Depth of 2000 m b.s.w.l.	
			Gradient (°C/100 m)	T (m/°C)	G(°C/100 M)	T (m/°C)	G (°C/100 m)	T (m/°C)
South	8	300	6.2	16.3	5.8	17.4	5.6	18.1
North	10	259	6.9	15.2	6.5	16.5	5.8	17.8

The following chart expresses the difference that exist between the Pannonain Basin and the other important basins from Romania (Figure 37)

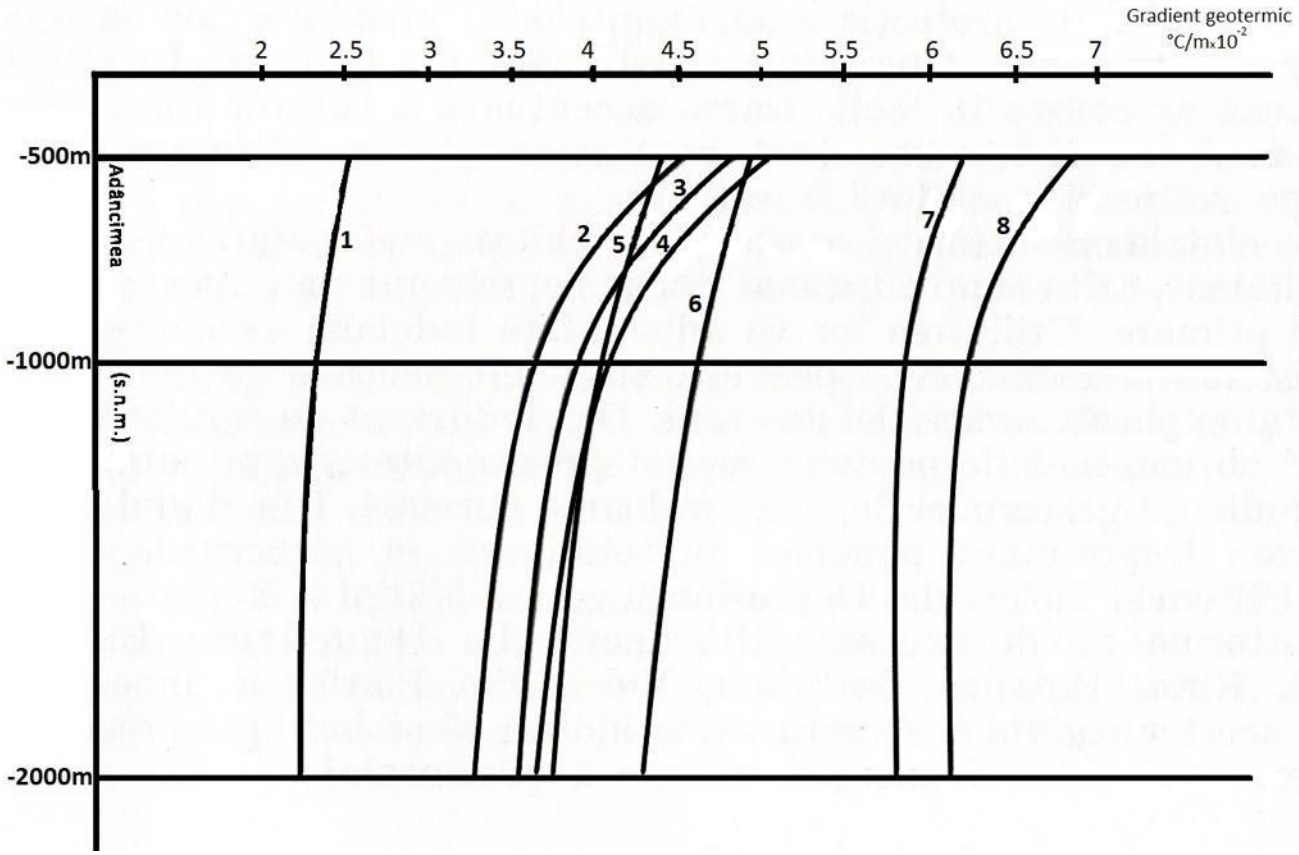

Figure 37 Geothermal gradient of different basins from Romania, reproduced after Paraschiv and Cristian (1976); 7 and 8 are the values afferent to Pannonian Basin

In the volume *Terrestrial Heat Flow and the Lithosphere Structure* edited by V. Cermak, and L. Rybach the international profile running WNW-ESE Romania has been published. The thermal structure of the lithosphere was considered by Demetrescu (1984) and Rădulescu (1985). As far as the crust alone is concerned, steady – state conduction models are justified for the most of the Romanin territory considering the age of the last thermal event affecting the various tectonic units (Figure 38).

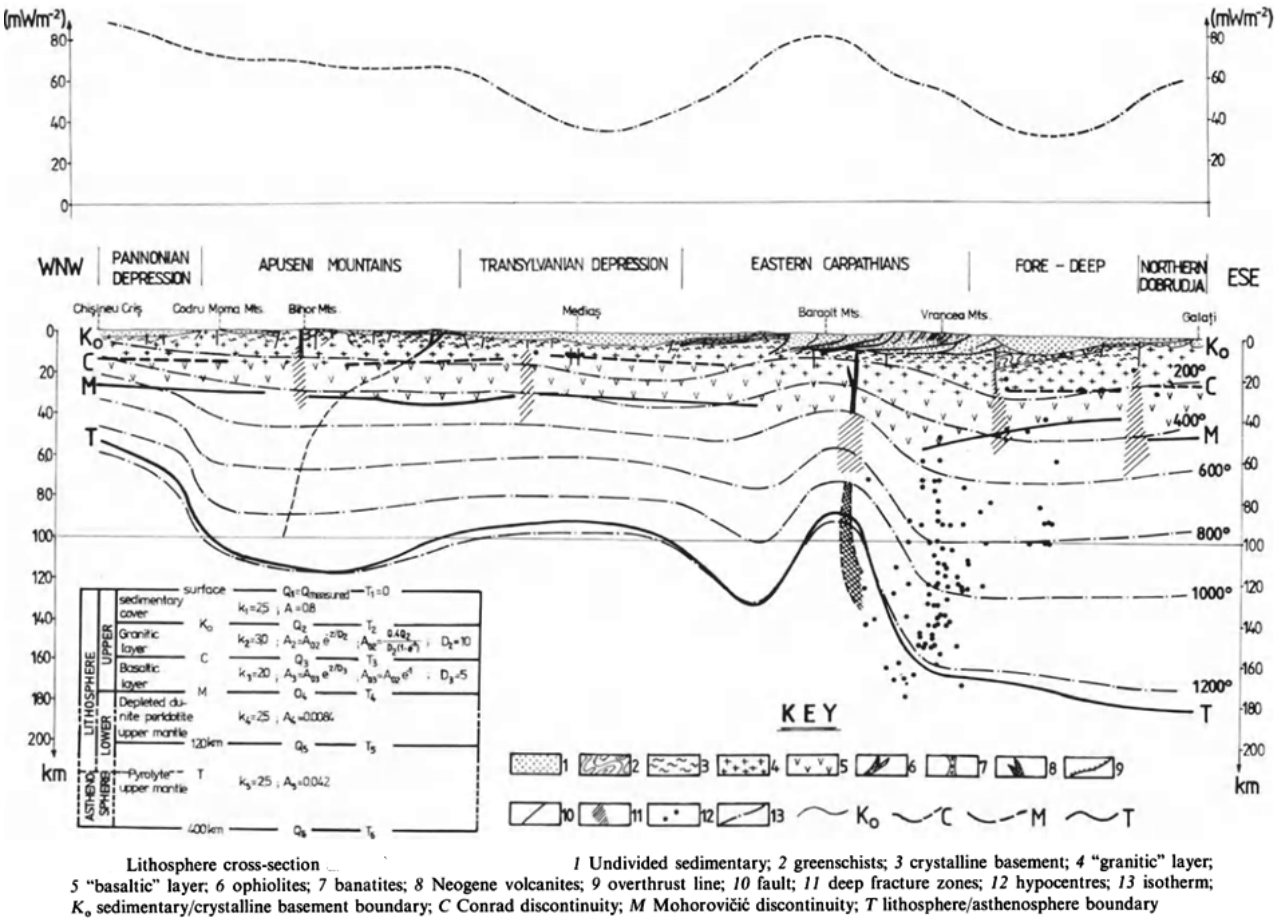

Lithosphere cross-section ... *1* Undivided sedimentary; *2* greenschists; *3* crystalline basement; *4* "granitic" layer; *5* "basaltic" layer; *6* ophiolites; *7* banatites; *8* Neogene volcanites; *9* overthrust line; *10* fault; *11* deep fracture zones; *12* hypocentres; *13* isotherm; K_o sedimentary/crystalline basement boundary; *C* Conrad discontinuity; *M* Mohorovičić discontinuity; *T* lithosphere/asthenosphere boundary

Figure 38 Lithosphere cross – section of Romanian structural units – reproduced after Demetrescu (1984) and Rădulescu (1985).

According to the Demetrescu and Rădulescu for Beiuș Basin values above 80 mWm^{-2} and for Apuseni Mountains values are above 70 mWm^{-2} for the heat flow have been estimated.

These values have been confirmed by researchers that, using different multidisciplinary approaches, reached similar results. We want to give some examples. In 2006 Dererova *et al* applied integrated lithospheric modelling combining the interpretation of surface heat flow, geoid, gravity, and topography data for the determination of the lithospheric thermal structure along four transects crossing the eastern Carpathians from the European Platform to the Pannonian Basin and propose a new map of lithospheric thicknesses. The heat flow values for Beiuș Basin and Bihor Mountains that are represented in these transects, are around, or above 80 mWm^{-2}. For densities and thermal properties values from the Table 7 have been used.

Table 7 Densities and Thermal properties

Densities and Thermal Properties of the Different Bodies Used in the Transects[a]

No.	Unit	HP	TC	ρ_0
1	Neogene sediments	3.0–3.5	2.0–2.5	2400–2550
2	flysch, foreland basin, sedimentary cover of European Platform	1.0–2.5	2.0–2.5	2550–2650
3	volcanics	2.0–3.5	2.5–3.0	2600–2800
4	Carpathian and Pannonian upper crust	1.0–3.5	2.0–3.0	2740–2750
5	European Platform upper crust	1.5–2.5	2.0–2.5	2650–2820
6	European Platform lower crust	0.2	2.0	2950–2980
7	Carpathian and Pannonian lower crust	0.2	2.0	2930
8	Carpathian and Pannonian mantle lithosphere	0.05	3.40	3200
9	European mantle lithosphere	0.05	3.40	3200
10	mantle lithosphere anomalous body	0.05	3.40	3210
11	main suture zone	0.1	2.50	3000

[a]No., reference number in Figure 3; HP, heat production ($\mu W/m^3$); TC, thermal conductivity (W/(m K)); ρ_0, density at room temperature (kg/m^3).

In 2013 in his PhD thesis Grinc focused on the application of integrated modelling of the lithosphere in the Carpathian - Pannonian Basin region to study and clarify the tectonic evolution and lithospheric structure. He used joint interpretation of 4 geophysical data sets at the same time: potential field data (gravity–Bouguer or free air–and geoid), topography and corrected heat flow data, and corroborated them with the results of the seismic interpretation and borehole data. One of the profiles that resulted from this analysis showed the heat flow value for Bihor Mountains higher than 70 mWm^{-2} (Figure 39).

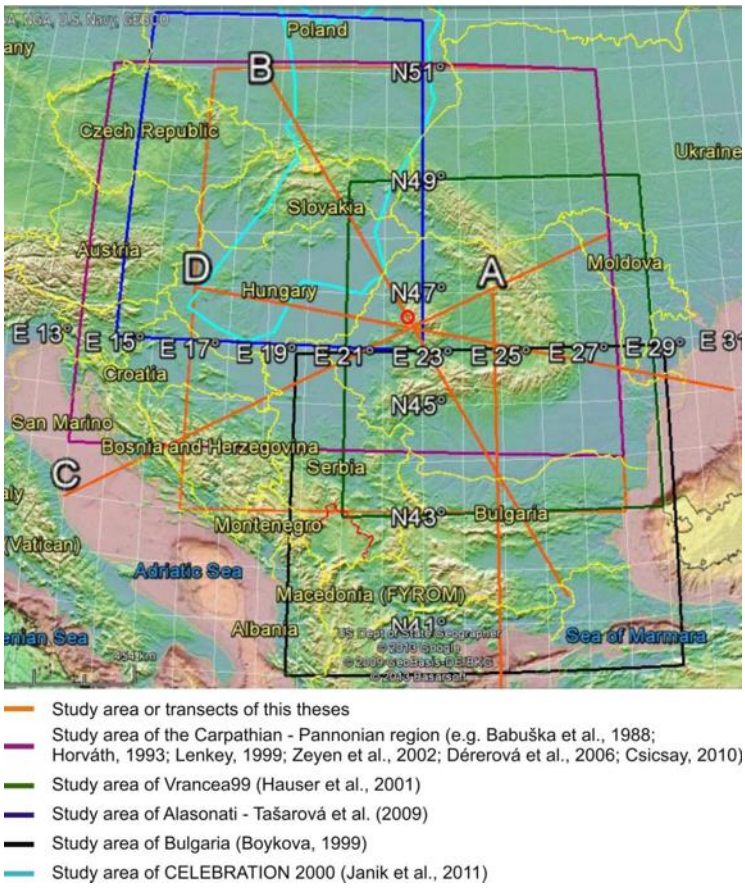

Figure 39 - 1) Topographic map of central Europe and Balkan shows the geographical location of the previous and current geophysical investigations. Position of the Transect B-B' is indicated. Reproduced from Grinc, 2013.

2) Lithospheric model for transect B. (a) Surface heat flow density, (b) free-air gravity anomaly, (c) geoid, (d) topography with dots corresponding to measured data with uncertainty bars and solid lines to calculated values; (e) lithospheric structure; In the lithospheric mantle, isotherms are drawn every 200°C. Numbers in the figure title indicate the starting and endpoint coordinates of the transects. The black dashed lines correspond to the results of a model with flat lower-upper-crustal limit and Moho underneath the Moesian Platform. Dotted lines and dots show positions of interfaces obtained from different seismic experiments. Black fat capital letters denote crossing points with the other interpreted transects. Reproduced from Grinc, 2013. Heat Flow of Bihor Mountains is indicated with a red line

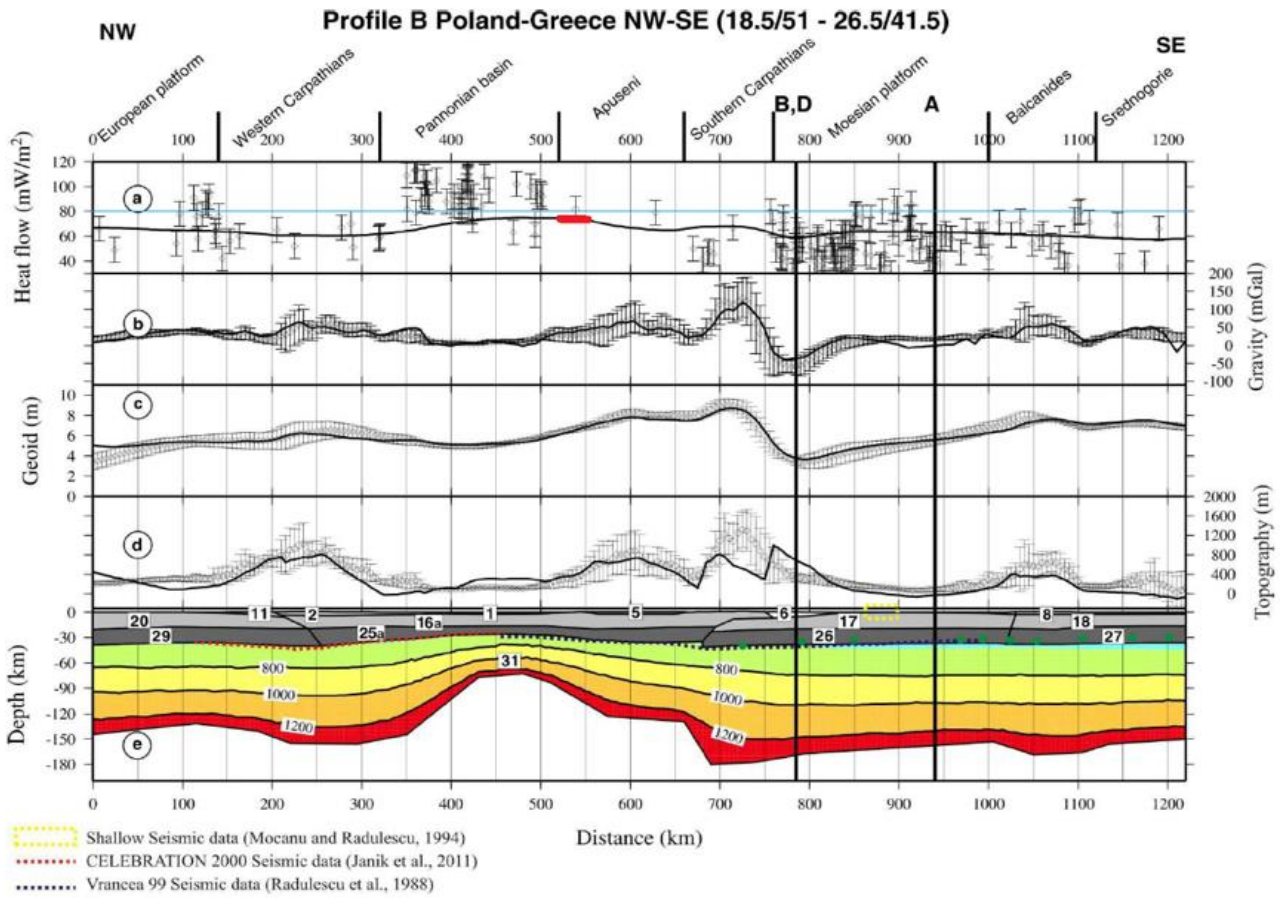

6. Hydrogeology and ground district heating system

The geothermal aquifer from Beiuș and Ștei is hosted in fractured Triassic dolomites that have a regional extension. These Triassic rocks are intercepted at different depth, the blocks being separated by fractures. There is a hydrodynamic link between the blocks, which is confirmed by dynamic level stabilisation in a relatively short time after the beginning of drilling or groundwater pumping (Figure 40).

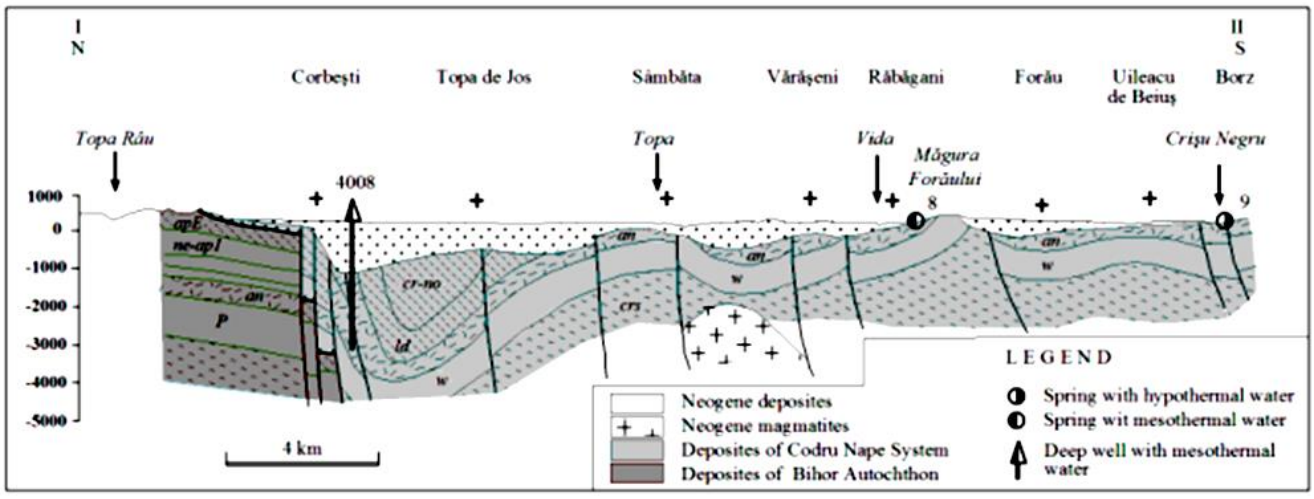

Figure 40 Beiuș Basin transverse ladinian – anisian deposits host the geothermal aquifer - reproduced after Orășenu, 2015.

The 3 wells, 3001 H Beius (TVD 2576 m), 3003 H Beius and 3002 H Ştei (TVD 2790m) that intercepted the Triassic collector encountered two types of faults reversed (Mesozoic) and normal gravitational (Neozoic). Reversed faults were generated during over thrusting processes, while normal faults were formed at the same time with the deepening of the Beiuș Basin. Between 3001 H and 3003 H drillings there is at least one normal faults going down towards SE, in a NE-SW direction with amplitude of approximately 360 m (Figure 41).

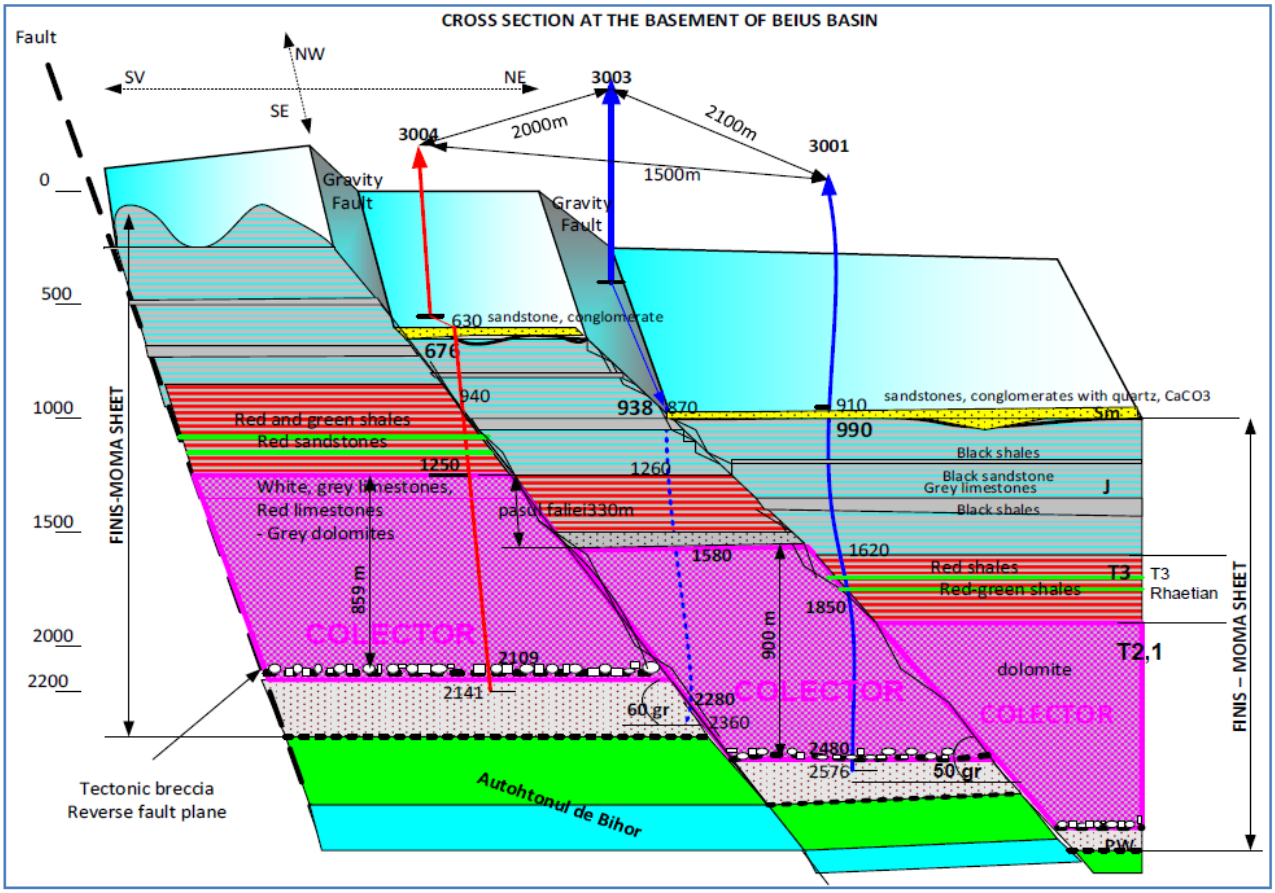

Figure 41 A SW-NE cross-section through the part of the Beius basin lying directly below the town of Beius, showing the location and trajectories of wells F-3001, F-3003 and F-3004 (Transgex, 2015)

Reversed faults system usually follows the W-E direction, while normal gravitational faults system with influence over the reversed ones has both NW-SE (basin frame) and W-E (central area of the basin) directions. The two types of fractures as well as the accompanying fissures represent the main water flow channels.

Triassic aquifer from Beiuș Basin is a confined aquifer with negative piezometric levels (- 18.48 m 3001 H Beiuş and unstable – 45m 3003 H Beiuş) or artesian (3002 H Ştei), depending on the position of the tectonic block.

The map of piezometric contours of the Triassic thermal aquifer of Beiuş Basin basement was elaborated by Oraseanu, (2015) on the basis of the thermal emergence elevations from the basin border and central part and of the water level elevations measured in the wells from Corbeşti, Beiuş and Ştei after drilling operations.
The general flowing direction is from south – west to north - east, from Bihor Mountains to Beiuș city (Figure 42).

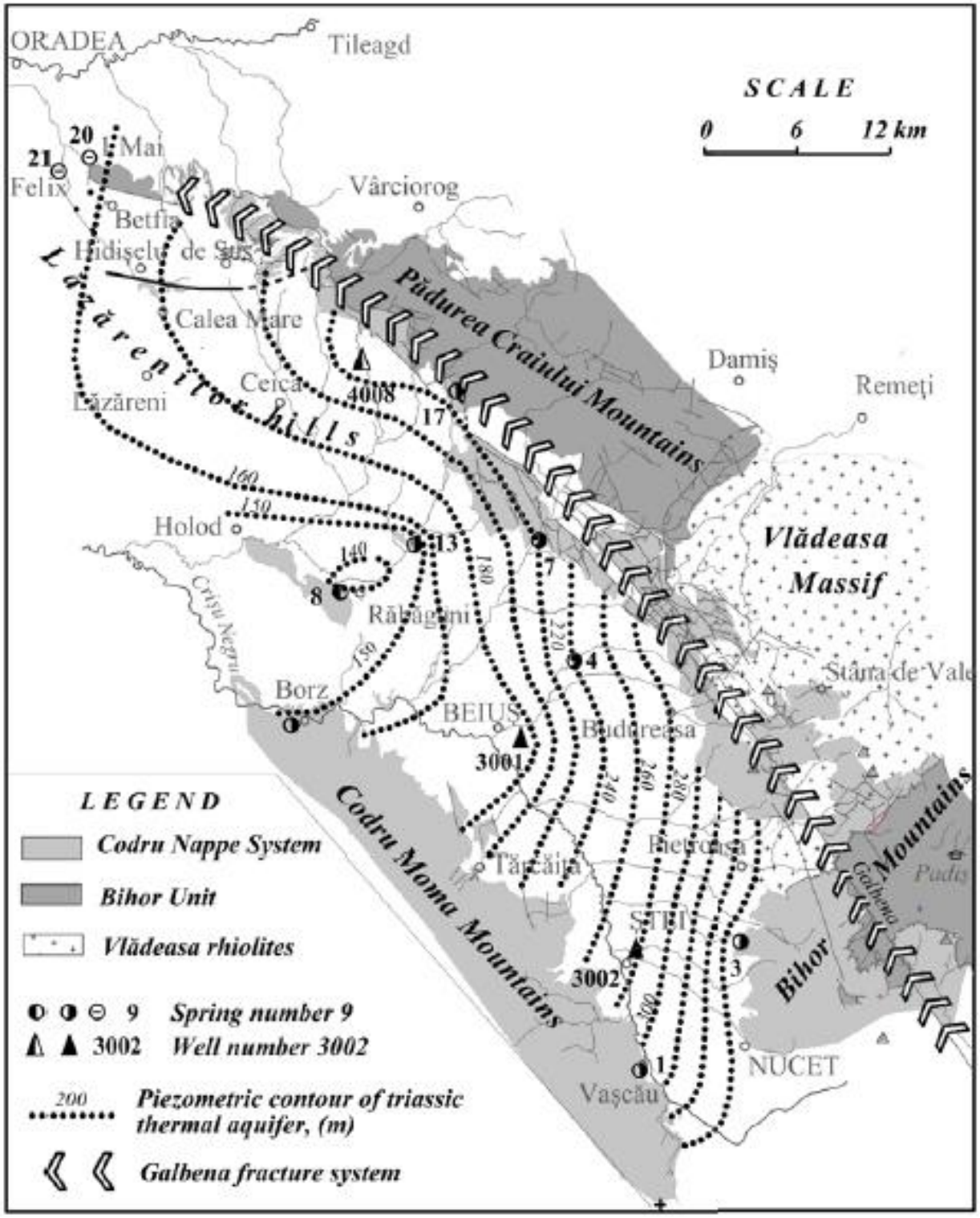

Figure 42 Piezometric contour of the Triassic aquifer in the Beiuș Basin basement. Reproduced after Oreseanu, 2015.

The calculation of hydro-geologic parameters has been carried out by processing the data in efficacy and performance tests, as well as by base measurements.

Hydro-geologic parameters for 3001 H well	Hydro-geologic parameters for 3003 H well
- TVD 2576 m - Stabilised hydrostatic level NH = - 18.48m - Transmissivity T=132.46 mc/m/day - Hydraulic conductivity K=0.64m/day - Average static pressure per resource Ps=196.73at - Flow capacity kh=47 Darcy/m. - Drilling hydrodynamic efficiency 3001 H E=77.5%. - Base temperature measured at 2460 m depth is 88°C, while temperature at well head is 84°C.	- TVD 2500 m - Unstable hydrostatic level NH = - 45m - Flow rate obtained Q = 7 l/s - Unstable dynamic level Nd = - 27m - Unstable temperature T = 600C - Clear water PH = 7 - The water type is bicarbonate-sulpho-sodium of low mineralisation with no significant sediments.

In the 3001 H Beius drilling equipped with a high capacity long axis pump (Qmax=50 l/s). The parameters show a good potential of the Triassic aquifer.
In the 3003 H drilling, pumping has been made with a low capacity submersible electric pump (Qmax=10l/s). Up to this flow rate, there is an increase of the dynamic level due to the thermolift generated by increasing temperature. The phenomenon persists until reaching maximum temperature at exploitation head (approximately 80°C) obtained with flow rates exceeding 15 l/s.

The pumped geothermal water has been analysed in authorised laboratories – Institute of Physical Medicine and Balneoclimatology Bucharest, A.P.M. Oradea, Radiation Hygiene Laboratory Oradea – from the point of view of both chemical reactions and radioactivity.

Physical characterisation:	Chemical characterisation:
- Base temperature 83°- 88°C - Specific weight 970 – 972 Kgf/m3 - Clear aspect	- Water type bicarbonate-sulpho-sodium - Low mineralisation 0.4-0.9 g/l - Total hardness 12 - 13G - Bicarbonate 250 - 300 mg/l - PH = 7

The springs water of the Mesozoic carbonate deposits is of the Ca(Mg)-HCO3 type, and the water of springs and wells drilled in the Neogene deposits is Na-HCO3 type. Most of the waters from thermal sources of the basin range between these two types, indicating a mixed genesis. The warmer waters, which are in contact with the batholith, and come from the depth, are mixed with colder waters coming from precipitation that pass through the karst Triassic deposits. The waters coming from the surface represent a cooling agent for the aquifer. Also, the presence of radioactivity may be explained by contamination in contact with Banatitic and Neogene magmatic rocks in the area.

6.1 Fresh water supply from the surface

According to Orășeanu, the rainfall across Bihor Mountains area has an uneven distribution. Multiannual average values display an increase of the annual amounts from the Beiuș basin (Budureasa - 941.3 mm, Pietroasa - 948.6 mm, Băița - 884.2 mm) eastward, up to the Stâna de Vale - Piatra Graitoare ridge area (Stâna de Vale - 1608.5 mm).
The fresh supply will be assured by Crișu Negru River and its tributaries, as Table 8 indicates.

Table 8 Morphometric and hydrometric data for main rivers

No.	River	Gauging station		F km²	H m	Q m³/s	q l/s/km²	Bf	ME, days	RT, days	TF
1	2	3	4	5	6	7	8	9	10	11	12
1	Someşu Cald	Beliş	1950-1967	320	1247	6.22	19.4	0.24	48	37.1	0.196
2	Someşu Cald	Smida		110	1293	2.35	21.4	0.25			
3	Beliş	Beliş		119	1249	2.32	19.5	0.27	47	34.2	0.208
4	Beliş	Poiana Horea		83	1259	1.69	20.4	0.28			
5	Drăgan	P. Crucii am.		119	1228	3.74	31.4	0.25			
6	Sebişel	P. Crucii		39.4	1172	1.19	30.2	0.25	123	81	0.092
7	Iad	Leşu		101	979	2.83	28.0	0.20			
8	Iad	Stâna de Vale		27	1210	1.10	40.9	0.25	24	24.7	0.192
9	Crişu Pietros	Pietroasa		123	956	4.15	33.7	0.21	15	21.4	0.208
10	Crişu Băiţa	Băiţa		36	892	0.86	23.9	0.19			
11	Arieş	Scărişoara		200	1099	5.45	27.25	0.27	35	29.8	0.232
12	Crişu Pietros	Pietroasa	X.1984-IX.1985			4.28	34.8	0.30			
13	Crişu Băiţa	Băiţa				0.80	22.2	0.27			
14	Sighiştel	Sighiştel				0.46		0.26			
15	Crăiasa	Giuleşti upstream				0.41		0.18			
16	Galbena	Intre Ape				1.92		0.29			
17	Bulz	Canton silvic				0.92		0.25			
18	Arieş	Scărişoara				5.34	26.7	0.28			
19	Beliş	Poiana Horea				1.83	22.0	0.30			
20	Someşu Cald	Smida				3.34	30.4	0.28			

F - surface of hydrographic basin (h.b.); H - mean altitude of h.b.; Q - mean multiannual discharge;
q - mean multiannual specific discharge; Bf - base flow index; EM - memory effect. TR - Regulation time;
FT - truncation frequency (EM, TR and FT computed for 1971-1975 period).
Note: Data in columns 5-9 after "Râurile României". 1950-1967 time period

6.2 Salinity of expected geothermal brine

The type of the geothermal water is bicarbonate-sulpho-sodium, with low mineralisation 0.4-0.9 g/l. Total hardness is 12 - 13G, bicarbonate is between 250 - 300 mg/l, and pH=7. It is expected that the salinity of the brine that will circulate inside the CHPM system to have much higher values.

*

In 2017, from 3 extraction wells from Beiuș geothermal aquifer water samples were collected. A spring and the water coming from a mine were sampled too. The residuum which precipitated after evaporation was studied by scanning electron microscopy (SEM-EDAX), FTIR and X-ray powder diffraction. This study led to the following conclusions:

The mineralogy of geothermal samples is characterized by the presence of aragonite, brucite, dolomite, clay minerals and probably amorphous hydrated silica. This conclusion is based on:

- the broad hump registered between 15 and 20° 2 theta on the XRD patterns,
- the characters and intensities of the bands centered around 3350 and 1630 cm^{-1} in the FTIR spectra.

The SEM analysis of the dried samples shows the presence of needle-shaped crystals of bassanite with parallel accretion of trigonal crystals of aragonite or brucite. Hydroboracite, nitrocalcite, epsomite and halite were also identified. Fig. 28 shows the images of minerals resulted from geothermal brine precipitate and Figure 43 shows SEM images and the chemical composition of a sample of geothermal brine precipitate from 3001 well from Beiuș. A considerable enrichment of magnesium minerals was highlighted in the geothermal water as compared with spring and water coming from mine. Thus, the magnesium content is less than 5% in surface, and at least 13% in the geothermal waters (Table 9**).**

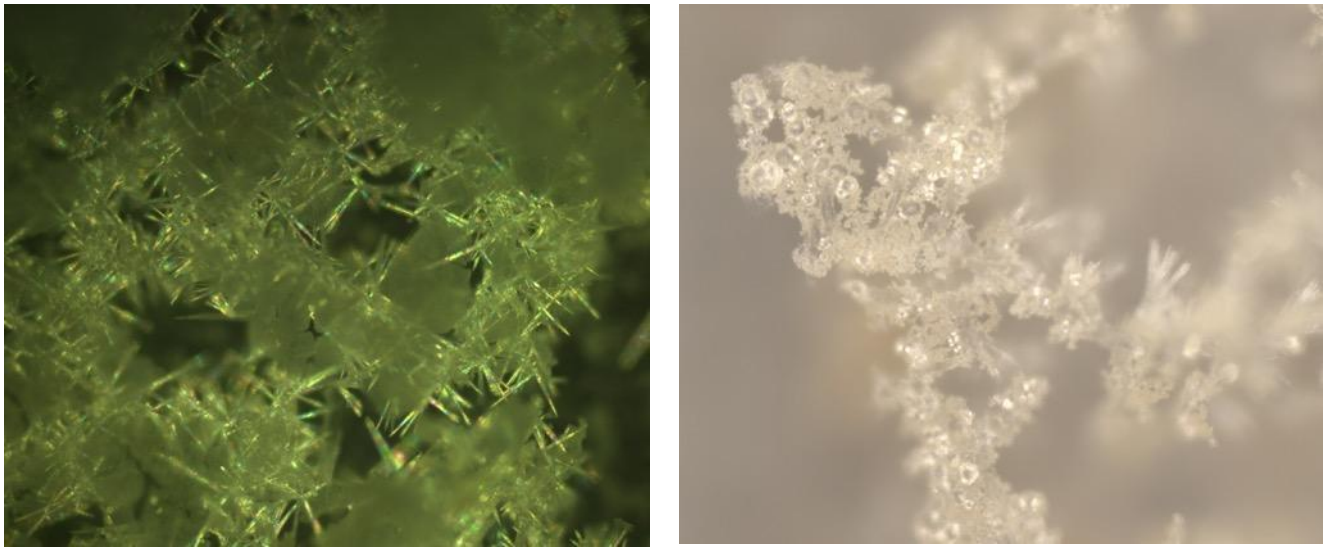

Figure 43 Images of the minerals precipitated from the geothermal brine – optical microscope

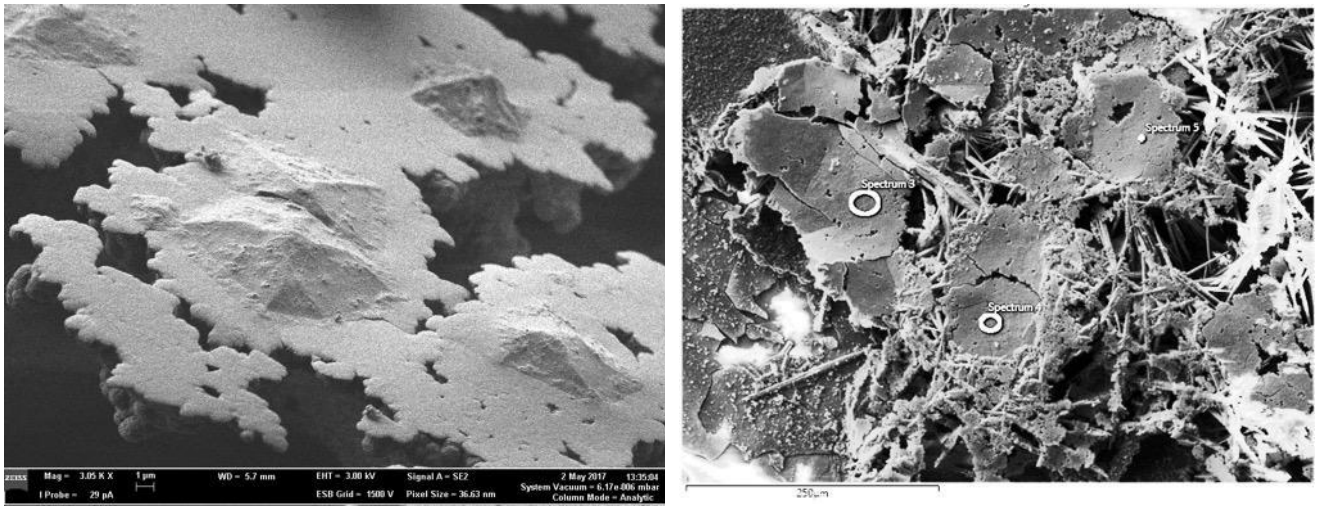

Figure 44 SEM images 1 and 2 of the precipitate of the geothermal brines of Beiuș

Table 9 Elements content for 3 analysed points of image 2

Result Type	Weight %		
Spectrum Label	Spectrum 3	Spectrum 4	Spectrum 5
O	46.63	47.94	48.85
Mg	22.45	22.05	22.16
Si	30.93	29.41	28.45
Ca		0.59	0.53
Total	100.00	100.00	100.00

In 2018, using GDEx technology, Xochitl Dominguez et al., also as part of the CHPM2030 projects's laboratory experiments, completed experiments for the recover of metals from the geothermal brine provided by a Beiuș Basin well. The results are showed in the Figures 45 - 48. According to this study, that compared the results for Beiuș with the international ones, the results are promising. Especially the content of Sr in one of the brine samples and the content of Sr recovered are remarkable.

Real brine	Energy used (kWh m^{-3})	Energy used (kWh kg^{-1} metal rem.)	Current efficiency (%)
Sample 1	10.26	0.04	44.48
Sample 2	16.86	0.05	52.06

Figure 45 Energy balance during experiments using GDEx for the treatment of real geothermal brines (i.e., sample 1 and sample 2) from Romania.

Parameter	Units	Sample 1		Sample 2		Parameter	Units	Sample 1		Sample 2	
		Total	Filtered	Total	Filtered			Total	Filtered	Total	Filtered
						Metals					
Ph		7.9		8.2		Sr	µm L^{-1}	12040	12040	760	760
Sulfate	mg L^{-1}	1100	1100	60	59	Fe	µm L^{-1}	2300	<10	33	<10
NO_2-N	mg N L^{-1}	<0.1	<0.1	<0.1	<0.1	Li	µm L^{-1}	129	129	33	33
NO_3-N	mg N L^{-1}	<2.5	<2.5	<2.5	<2.5	Al	µm L^{-1}	44	<10	<10	<10
Bromide	mg L^{-1}	<0.5	<0.5	<0.5	<0.5	Mn	µm L^{-1}	40	39	<1	<1
Fluoride	mg L^{-1}	1	1	0.52	0.52	Ba	µm L^{-1}	32	32	81	81
Chloride	mg L^{-1}	<5	<5	<5	<5	Rb	µm L^{-1}	16	16	14	14
Ca	µm L^{-1}	303000	303000	50900	50800	As	µm L^{-1}	9	3.8	5.7	5.7
K	µm L^{-1}	12800	12800	5790	5760	Cs	µm L^{-1}	2.5	2.5	2.3	2.3
Mg	µm L^{-1}	85600	85600	20500	20500	Zn	µm L^{-1}	1.5	1.5	62	62
Na	µm L^{-1}	29600	29600	12100	12100	Mo	µm L^{-1}	1.3	1.3	1	1
Sr	µm L^{-1}	12400	12400	727	727	Cu	µm L^{-1}	<1	<1	8	8
REE	µm L^{-1}	<1	<1	<1	<1	Os	µm L^{-1}	<10	<10	<10	<10
						Be	µm L^{-1}	<10	<10	<10	<10
						Ni	µm L^{-1}	<1	<1	13	12
						Pb	µm L^{-1}	<1	<1	1.3	<1

Figure 46 Chemical characterization from real geothermal brines from Romania

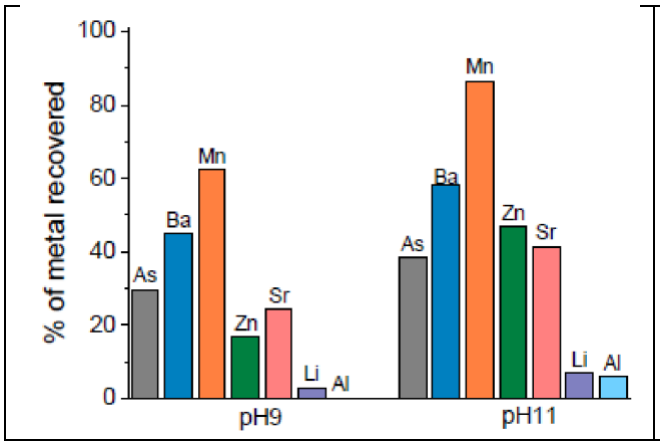

Figure 47 Percentage (%) of the initial metal recovered in the precipitated product from sample 1 at different pH values.

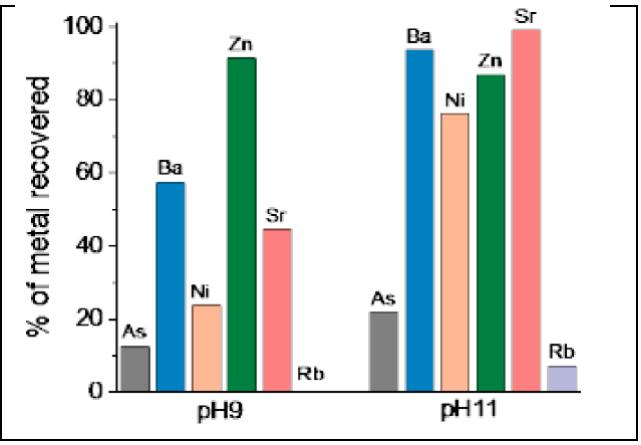

Figure 48 Percentage (%) of the initial metal recovered in the precipitated product from sample 2 at different pH values.

6.3 GDHS

It is very important to refer to the extensive presence in Bihor Mountains of Mesozoic carbonates series, and Palaeozoic limestones and dolomites, highly fractured and karstified, having a very high effective infiltration and porosity, that host the geothermal aquifer which has a regional extension and with intensive groundwater flow. Beiuș aquifer is an open geothermal system, where recharge equilibrates with the mass extraction and its reservoir pressure stabilizes. Its recharge can be both hot deep recharge and colder shallow recharge. The latter can eventually cause reservoir temperature to decline and production wells to cool down. In fact, this second alternative was demonstrated when the increase of the volume of injected water was accompanied by the decrease of the water temperature within aquifer. More research is needed to improve the knowledge on this subject.

The Beiuș city has an extensive geothermal district heating system (GDHS) that supplies heat to about 70 % of the population, covering around 60% of the city heating demand. The old system has been entirely replaced by GDHS.

The geothermal heat energy is delivered to the consumers either indirectly via substations with heat exchangers feeding double closed loop distribution pipe networks, one for Domestic Heating (DH) and the other for Hot Sanitary Water (HSW), or directly to the individual buildings with their own heat exchangers. The biggest individual closed loop distribution systems are old, remains from the time when the central part of the city was heated by three oil fired heat stations. Additionally, around 35 modern compact micro modular substations have been installed. The layout of the main district heating pipe system in the city is shown on street map in Figure 49. The exploitation license of Beiuș geothermal reservoir perimeter is owned by Transgex S.A.

Currently, according to Transgex S.A the geothermal energy exploitation system consists of:

- 2 geothermal water production wells drilled at 2576 m and 2700 m respectively, with a production capacity of 450 m^3 / h;
- 1 re-injection drilling depth of over 2,000 m;
- 18 km from geothermal water transport network in the city;
- 120 block stairs connected to the centralized distribution of heat;
- Public institutions are heated with geothermal energy (colleges, schools, kindergartens, municipal hospital, culture house, pharmacies, medical offices and laboratories, churches and places of worship, gymnasiums);
- undertakings with more than 1000 employees;
- 200 individual homes with their own thermal units connected to the transmission geothermal water.

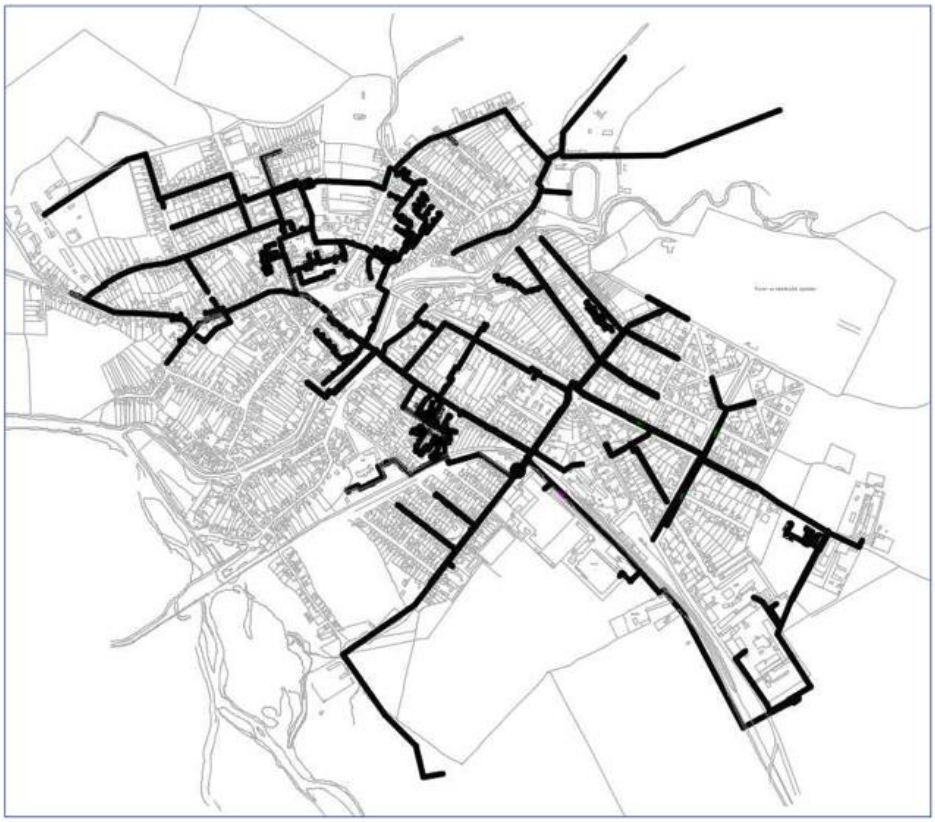

Figure 49 Map of the GDHS pipeline of Beiuș; reproduced after Orkustofnun, 2017

In 2017 Orkustofnun published a pre-feasibility study that, besides a description of the existing situation, contains the financial analysis for the necessary investments that can lead to the optimal use of energy for the whole city and for the surrounding areas.

The supply of geothermal heat to the GeoDH system in 2016, measured at the end users, is summarized in Table 10:

Table 10 Operational parameters of the GeoDH system in 2016

Year	Production well	Energy delivered 2016		Volume delivered	2016 production/ well	2016 production/ well	2016 average / well
Beius Geothermal		[GJ/year]	[m3/year] calculated	[m3/year]	[m3]	[GJ/year]	[l/s]
2016	3001	49 591	305 144	338 038	643 182	104 529	20,4
	3003	24 861	202 713	193 084	395 797	48 541	12,6
TOTAL		74 452	507 857	531 122	1 038 979	153 070	32,9

Solutions for extend the GDHS have been proposed within the pre-feasibility study. According to this study estimated annual heat consumption in Beius is 246 TJ/year which corresponds to annual burning of wood around 25,600 [m3/year], emitting 27,000 [t CO2/year]. Also, with current market prices for wood for heating and GeoDH state regulated heating tariffs the citizens of Beius enjoy between 30% - 50% reduction in annual heating cost, when connected to the GDH system.

In Beiuș the production of geothermal water increased (Figure 50), partially due to the utilization of the reinjection well (F-3004), that has only been utilized at the nominal flow-rate of 1 – 3 l/s.

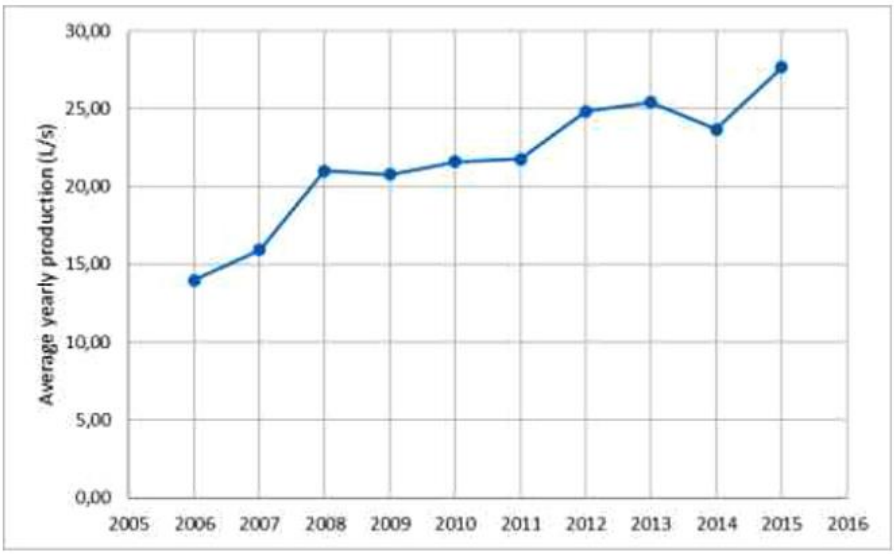

Figure 50 Production of geothermal water in Beiuș

7. Integrated 3D Model

The main reason for creating a 3D model is to integrate all available geo-data (geological, structural, and geophysical) for Beiuș Basin and its adjacent area. The 3D model is meant to illustrate the main features that are important in order to decide to what extent the chosen perimeter is proper for a CHPM system installation. The model focuses on the geometry of the middle and upper Triassic sedimentary deposits within Beiuș Basin and their contact with an Upper Cretaceous – Paleogene intrusive body where contact aureoles have been formed.

The 3D geological model of both the batholith and Triassic deposits was built using Paradigm™ GOCAD® 17 in order to observe their spatial distribution and to know if the requirements of the CHPM system are met (existence of heat and mineralisation in the same place).

7.1. Input dataset

- Creating the 3D geological database and building the three-dimensional model requires the integration, digitalisation, organisation and visualisation of all types of input data available such as geological maps and cross-sections, lithological columns, geophysical maps, wells, etc. The existing national datasets that are used in creating the 3D model are:
- Geological map, Brad and Șimleul Silvanei sheets, scale 1:200 000 with theirs cross sections, 1967, Giușcă et Bleahu
- Geological map, Pietroasa sheet, scale 1:50 000 and its cross sections, 1985, Bleahu et al.,
- lithological columns of 1 injection and 2 geothermal water extraction wells from Beiuș up to 2500 m depth
- Geological cross sections A1, A2, B6, scale 1:200 000, elaborated by M. Ștefănescu et al
- Structural map at the contact between the pre-Neogene and Neogene deposits of Beiuș Basin, accompanied by the isobaths map of the basis of Neogene deposits, and with isopach map of Neogene deposits, 1991, Dinu et al,.
- Geological sketch map of the distribution of the depth banatitic structure of Romania deduced from aeromagnetic and gravity data.

7.2. Methodology

The key input information for building the 3D model was the geological and geophysical maps and sections. The first step, before the modelling itself, was georeferencing the geological, geophysical and structural maps in ArcMap 10.3 using the Dealul Piscului 1970/ Stereo 70 coordinate system. Dealul Piscului 1970/ Stereo 70 is suitable for use in Romania – onshore and offshore and uses the Dealul Piscului 1970 geographic 2D CRS as its base CRS and the Stereo 70 (Oblique Stereographic) as its projection. The next step was to create the project in GOCAD defining the coordinate system and the bounding box of the study area. After that, the georeferenced maps were imported in GOCAD

After importing the georeferenced maps in GOCAD, a digital elevation model was created using ASTER Global Digital Elevation Model from USGS database (https://earthexplorer.usgs.gov/). The ASTER GDEM has been downloaded as tiff file and converted to the Dealul Piscului 1970/ Stereo 70 coordinate system using ArcMap and after that, the dataset containing the elevation has been imported in GOCAD.

Before importing the geological cross-sections, they have been rectified in a photo editing software in order to fit them to the coordinate system. The sections were imported and placed in GOCAD according to geological maps and digital elevation model.

The modelling started with digitalization of the tops of middle and upper Triassic sedimentary deposits within Beiuș Basin and their contact with the intrusive body, the faults and the intrusive body itself reported on the vertical cross-sections. Also, the outcropping middle and upper Triassic deposits, the upper Cretaceous – Paleogene intrusive body and the faults were digitalised on the geological maps and projected on digital elevation model.

The next step was the creation of fault planes using the Fault Construction Wizard application from GOCAD. The modelling of the layer horizons started with the digitalization of the layer boundaries on the geological cross sections. The creation of the horizon surfaces has been done with the Faulted Horizon Construction Wizard from GOCAD.

Building the intrusive body started with the digitalization of the intrusion boundary on the geological cross-sections and geological maps. The depth extension of the intrusive body was delineated from the map of banatitic structures from Romania as inferred from aeromagnetic and gravity structures, elaborated by Andrei et at., (1989) and from Earth Magnetic Anomaly Grid (https://www.ngdc.noaa.gov/geomag/emag2.html) compiled from satellite, ship, and aiborne magnetic measurements. Beside those data, for modelling the batholith, we used the maps 1:25 000, contained in *'Report on geological, geochemical, magnetometric and electrometric prospection works in Budureasa - Bihor Mountains'*, authors: Manea el al, 1973.

The presence of the intrusive body within Beiuș Basin was identified based on aeromagnetic, surface magnetic, gravimetric and seismic (refraction methods) data by Dinu et al., 1991. The creation of the intrusive body started with the digitalisation of the magnetic anomaly from the map. Then, the data was extrapolated in depth and correlated with the longitudinal cross sections from the map of vertical gradient of magnetic anomaly (Tz) from the Beiuș Basin.

7.3. 3D modelling results

Integrating all the data available in a 3D geological database and creating the 3D geological model provided an overview on the spatial distribution and the geometry of the middle and upper Triassic sedimentary deposits within Beiuș Basin and their contact with the upper-Cretaceous intrusive body, from Bihor Mountains.

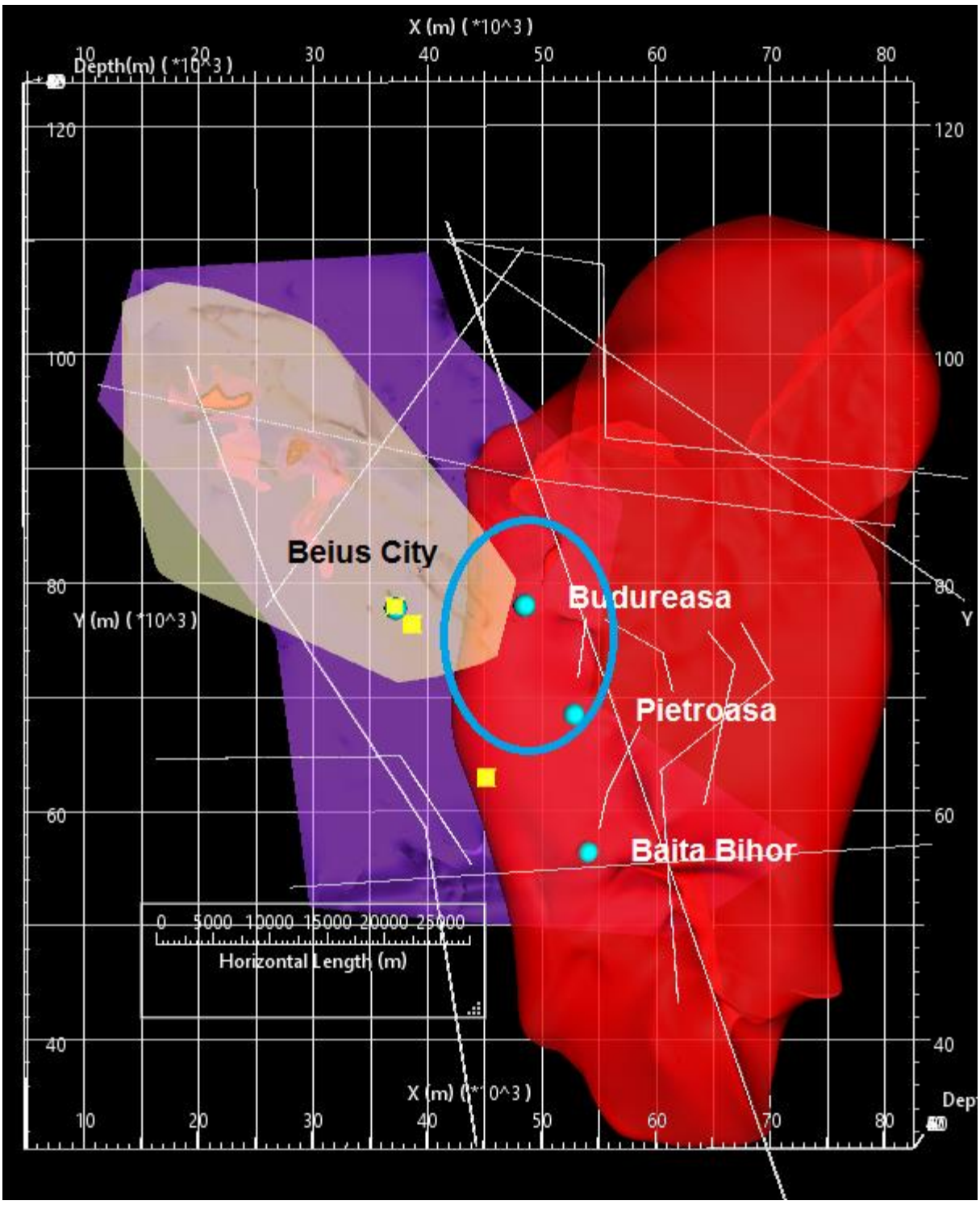

Figure 51 Spatial distribution of Batholith (red), Triassic deposits (violet) and Neogene deposits (beige); blue bullets are sites with mineralization, plus Beius city; yellow squares represent the geothermal wells from Beiuș and Ștei. The blue circle is the selected pilot site.

As can be seen in Figure 51, there is a region bordering Beiuș Basin where the batholith is extended: at Budureasa. The same is showed in Figure 52.

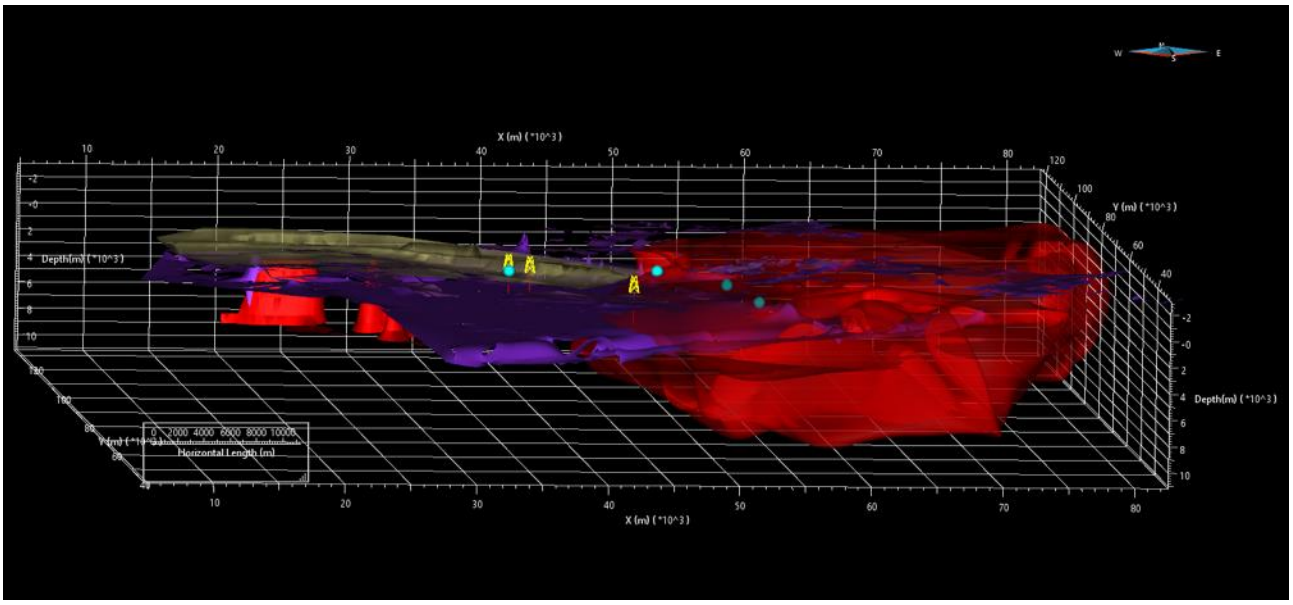

Figure 52 Areas where the batholith (red), Upper Triassic deposits (violet) and Neogene deposits (beige) interact; blue bullets are Pietroasa, Budureasa and Baita Bihor sites with mineralization, plus Beius city; yellow squares represent the geothermal wells from Beiuș and Ștei.

From the structural point of view, an increased possibility to have both mineralisation and high geothermal potential within a small area exists at Budureasa.

Figures 52 and Figure 53 show the extension of Upper Triassic deposits, both in Beiuș Basin and in Bihor Mountains, linking the two structural units, generating magnesian skarns on one side and transporting geothermal water on the other. This dual role in the perimeter explains an increased content of magnesium in geothermal waters from Beiuș Basin.

Figure 53 emphasizes the large areas on which Triassic deposits outcrop. Being represented by highly fissured karst deposits they, on one side, assure a continuous recharge of the geothermal aquifer, but, on the other side, they have an important contribution to the decrease of the geothermal potential of the rocks, being a cooling agent.

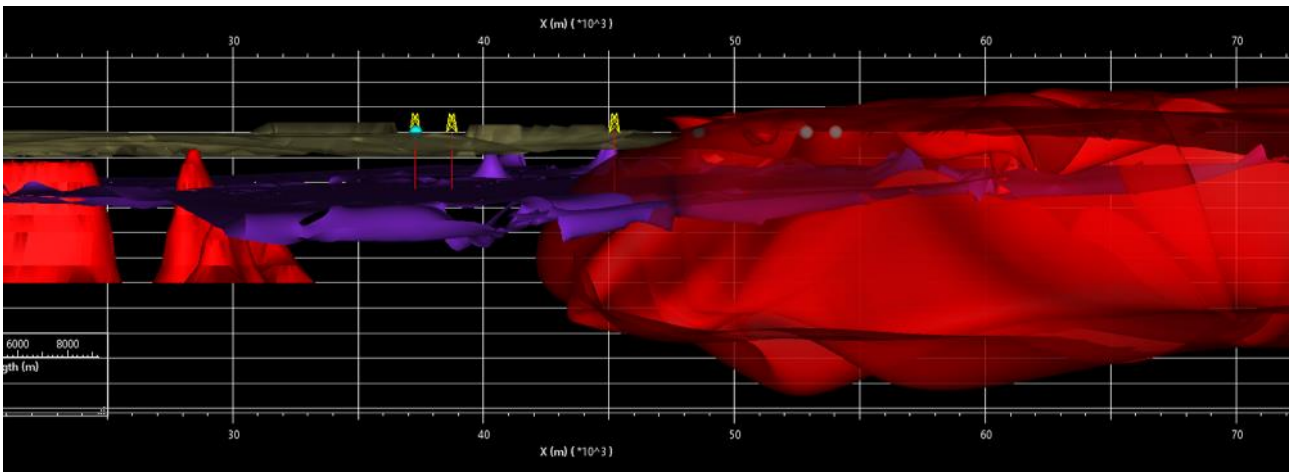

Figure 53 Existence of batholith's apophyses within Beiuș Basin. The legend is like in Figure 52.

The batholith's apophyses that were detected by complex geophysical methods within Beiuș Basin, and can be taken into consideration for further investigations are shown in Figures 52 and 53.

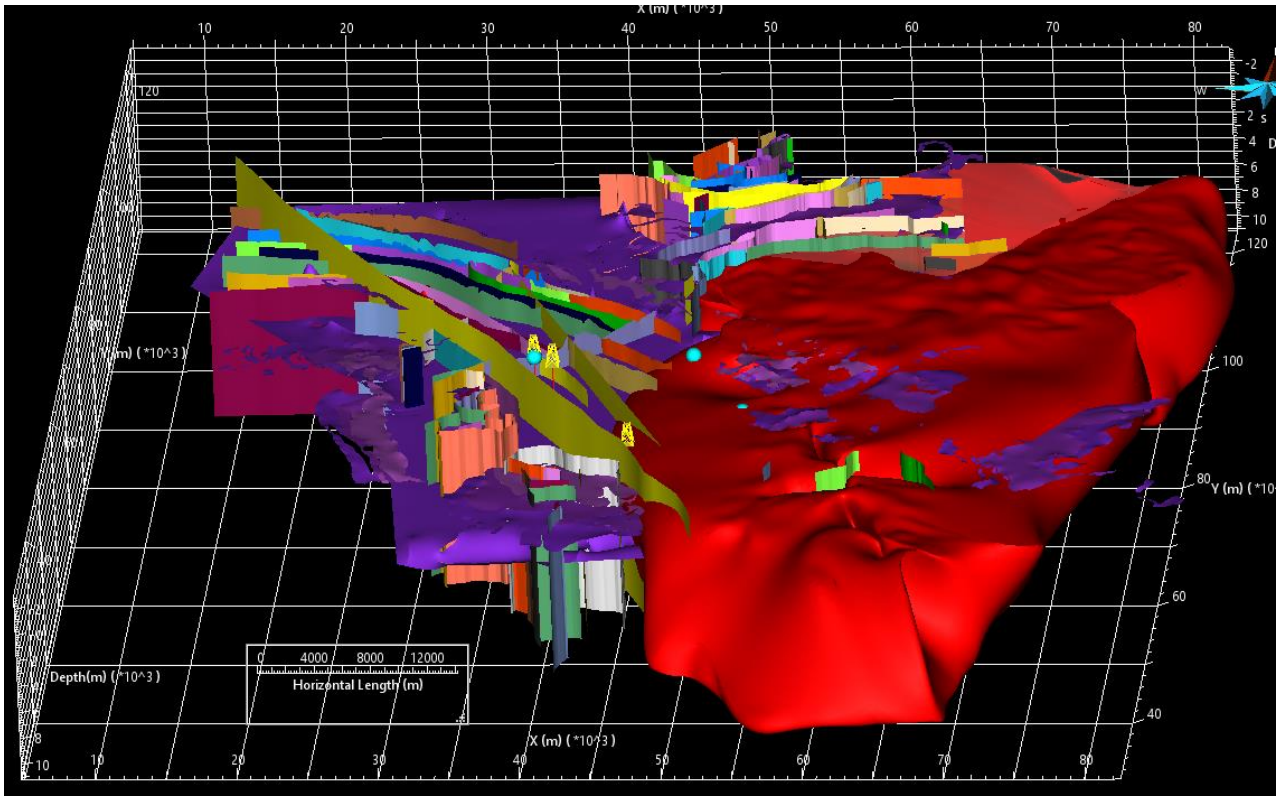

Figure 54 Main faults reported in the region; in red is the batholiths that outcrops in Bihor Mountains; in violet Upper Triassic layer is represented.

Many faults afferent to Beiuș Basin are inventoried and reported, and very few for Bihor Mountains, as Figure 54 shows.
These numerous faults are explainded by the extension processes of the entire Pannonian Basin during its Miocene evolution. Galbena strike slip fault is a deep structure fracture, which is reported in Bihor Mountains.

The 3D model helped us to visualize and understand the spatial relations at the border between the basin and the mountains and provides new data that are needed to set parameters for planning new exploration works.

At the same time the 3D model helps us to reduce the area of new planned investigations to a smaller area with an increased probability that fits conditions of a CHPM system.

8. Information for CHPM technological elements

The integration of all the available data afferent to Beiuș Basin – Bihor Mountains and performing the 3D modelling of the region led to the selection of a restricted area compared to the initial one proposed for the project, an area where further research need to be developed (Figure 55). It is estimated that this pilot site offers the possibility to find geothermal potential and metals in a single place.

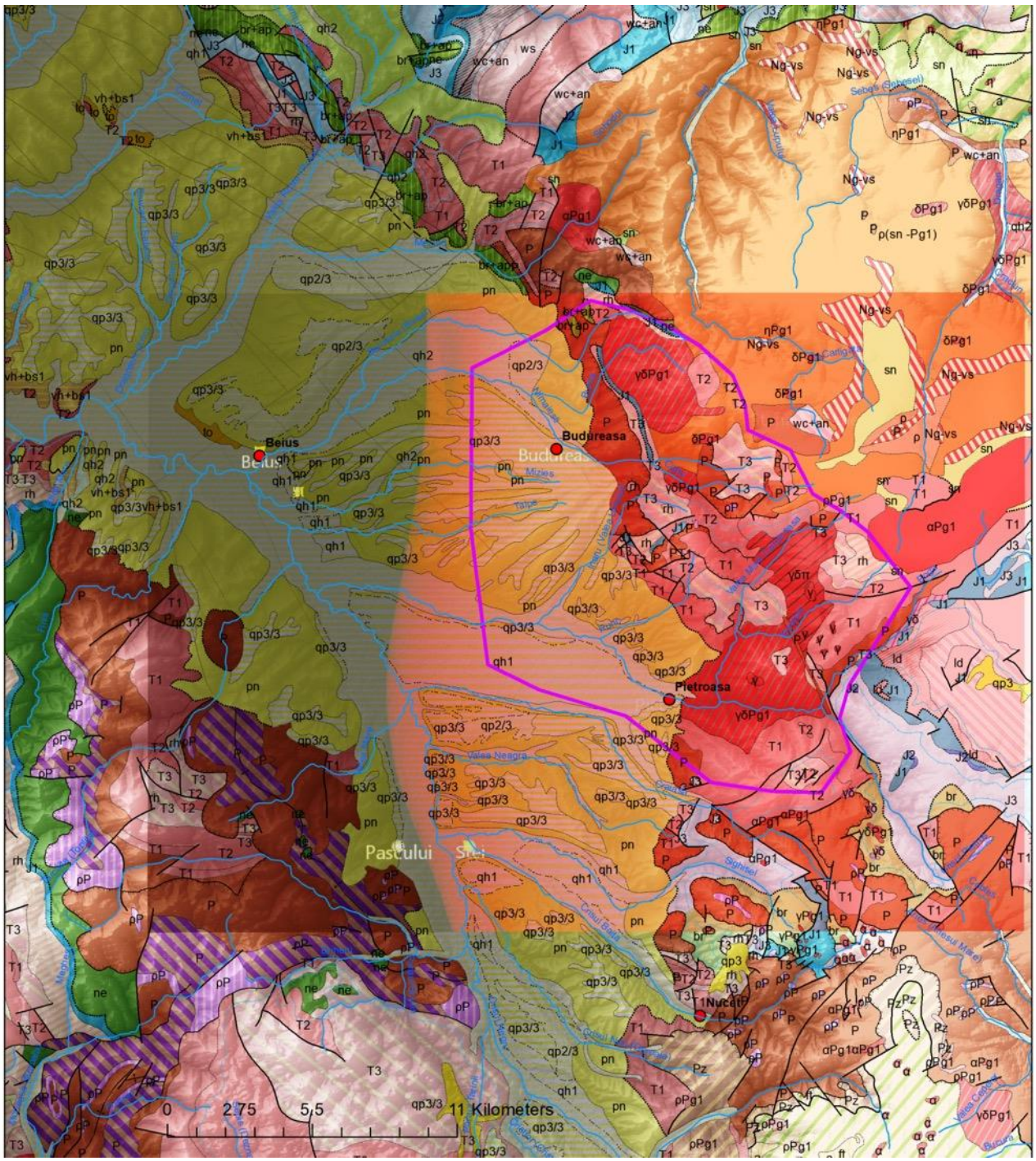

Figure 55 Initial perimeter and the pilot site contour (violet line)

One of the main findings of the project is that, although it was not intercepted by drillings, there is a great probability that the batholith, which outcrops in the mountains, to be intercepted in the Beiuș Basin, where the hydrothermal energy is already exploited.

The new CHPM technology determines us to look for additional sites, other than classical ones, from where it is possible to extract metals. In Romania's case the selected site is at the margin of a sedimentary basin, where in the depth a batholith it is possible to be intercepted, and where geothermal potential is higher. For this, magnetometric and gravimetric studies have been used that helped us to delineate the contour of the batholith at a distance of cca 8 km from the city of Beiuș (Figure 56).

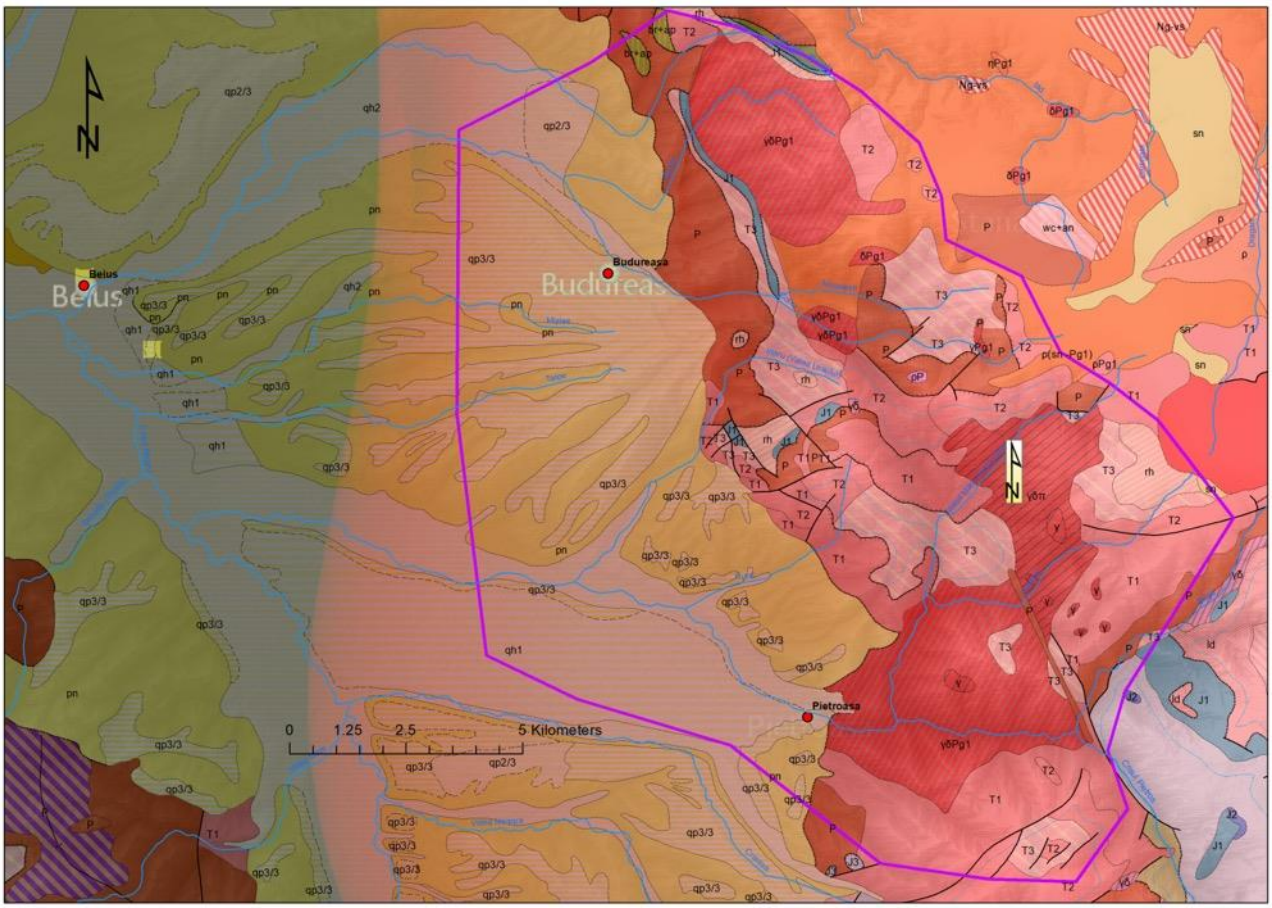

Figure 56 Contour of the batholith in Beiuș Basin. The shape of the batholith is modeled by the measurements synthesized by Proca (1979) and Andrei (1989).

In the situation that further research confirms these presumptions, a near-field EGS could be created, which by association with metal extraction would become profitable in the long run. The new pilot site, being situated near the perimeter for which Transgex S.A. has the geothermal water exploitation license, has a surface of almost 150 sqkm.

8.1 Underground heat exchanger (deep metal enrichment + potential reservoir)

Extension of the metal enrichment

At more than 4 km depth the contact between the granodiorite - granite extensional batholith with the Codru Nappe System (Finiș or Vălani Nappe) is probably to be encountered, or, even the contact of the batholiths with the Bihor Autochtonous Unit. In the first case, *Finiș-Gârda Nappe* is represented mainly by mezozoic rocks and has a metamorphic basement consisting of the Codru Granitoids and Migmatites, which are the oldest basic intrusions being pre-Hercynian, according to Dallmeyer et al. (1994). As specific lithostratigraphic features, the following are to be mentioned:

- large development of the Permian, with felsic ignimbritic volcanism;
- complete development of the Triassic sequence, with Carpathian Keuper and Kössen facies in the Late and latest Triassic;
- marine, marly-calcareous facies of the Lower Jurassic;
- development of a flysch-type sequence in the Tithonian-Neocomian;

In the second case *The Bihor Unit* is represented by a crystalline basement, and a sedimentary cover. The basement consists of the medium-grade Somes Series (micaschists, amphibolites, leptynites) and the

retrogressive Arada Series (chlorite-sericite-albite schists, metarhyolites), both intruded by the Muntele Mare granitic massif. The ages of the metamorphism and of the intrusion are Paleozoic. The sedimentary sequence of the Bihor Unit includes, (besides very scarce Permian) Triassic, Jurassic and pre-Senonian Cretaceous formations. The following specific lithostratigraphic features must be underlined:

- development of a carbonatic platform series from the Upper Werfenian to the base of the Carnian;
- absence of the major part of the Upper Triassic;
- Gresten paralic facies of the Lower Jurassic;
- marine sequence of the Middle Jurassic and of the base of the Upper Jurassic;
- development of a carbonatic platform in the Kimmeridgian and the Tithonic;
- lag of sedimentation at the base of the Cretaceous, marked by bauxites;
- calcareous neritic lithofacies of the Barremian and Aptian, passing into a marly sedimentation which continues in the Turonian;

The post-tectonic cover formed of Senonian formations in Gosau facies masks the thrust contacts of the Codru Nappes, especially in Bihor Mts.

Expected type and porosity/permeability of the reservoir;

The reservoir that hosts the geothermal aquifer was intercepted up to 2700 m depth where there is the Werfenian impermeable layer forming the bed of the aquifer, and where the drilling of the wells stopped. The transmissivity for Middle and Upper Triassic deposits in the well 3001 is T=132.46 mc/m/day, and hydraulic conductivity is K=0.64m/day. There is no information on deeper layers from Beiuș Basin. No studies regarding the fissures systems have been found for this pilot site, they are to be included into the research plans for the future.

Type of mineralization and expected metals

The granodioritic – granite rocks of the batholith itself have a high content of elements such as: Sr, Ba, Rb, Cs (see Table 3). Also, the boron content is as follows:

Table 11 Boron content of the magmatic rocks in the Bihor Mountains

Rock type	Location	Boron (g/t)
Granodiorite	Valea Seacă	10
Granite	Băița Plai (foraj struct.)	20
Porphyry granite	Budureasa	30
Granite with orthoclase	Budureasa	10
Granodiorite with biotite	Pietroasa	20
Porphyry granite	Gârda	50
Diorite	Valea Seacă	10

Quantitatively, Alpine ores are the most important, and represent 80% of the Romanian national resource estimates (mined out/ and present resources/reserves). The main stages are connected with the Laramian (Banatitic) magmatic products especially skarn deposits and porphyry deposits (Vlad, Borcoș, 1997). In the pilot site metallogenesis in subduction – related setting is represented. Widespread westward subduction during the Upper Cretaceous – Paleocene gave rise to polyphase calc-alkaline magmatism (Laramian magmatism, known also as Banatitic). The major intrusive event in the region has a granodiorite – granite evolutionary trend, the magmatism of this granodiorite – granite type generally yielded base – metal ores in non-porphyry environment: skarn deposits predominate, whereas vein deposits are rare.

The inner zone corresponding to a northwestward direction of subduction exhibits a complex metallogenesis in Bihor – Gilău Mountains.

The area we envisage contains skarn deposits and prospects related to granodiorite – granite plutons.

- When wall rocks are mainly calcareous, Fe-Cu skarn deposits occur near the contact zones, and Pb – Zn skarn deposits occur far from the contact zone.
- When wall rocks are various sedimentary rock and coeval or older ingenous rocks, magnesian and calcic skarns with Mo, W, Bi, Cu, Pb, Zn and B mineralization are found near and away from the pluton.

The main types of deposits reported within the pilot site are: skarns, brucite deposits and borate deposits.

Table 12 Chemical composition of Skarns*****

	Skarn calcic-magnesian	**Skarn magnesian**
SiO_2	23,72	40,82
TiO_2	0,03	0,01
Al_2O_3	1,36	0,31
Fe_2O_3	2,07	3,86
FeO	0,82	1,23
CaO	26,82	16,83
MgO	17,18	19,68
MnO	0,55	0,93
Na_2O	0,48	0,51
K_2O	0,21	0,30
P_2O_3	0,05	0,04
p.p.c.	26,31	15,98
Total	99,60	99,49

Analist: L. Stoici

According to Stoicovici et Soici, magnesian and also calcic – magnesian skarns from Triassic dolomites contain the following metallic elements: Zn – 0,26%; Ga – 0,0005%; Pb – 0,68%; In – 0,034%; Bi– 0,06%; Sn – 0,0005%; Cu – 0,83%; W – 0,001%; Mo – 0,001%.

8.2 Production and injection wells

Production and injection wells

The two production and one injection wells that are used in Beiuș Basin for the exploitation of the geothermal aquifer have been described in the chapter 6. A new information must be added as follows: in April 2019, SC Transgex SA announced the public about the Environmental Impact Assessment (EIA) revision in Beiuș determined by the project '**Increasing the production of geothermal water in Beiuş by drilling a production well and interconnecting it to the geothermal water transport network N. Cristescu street intersection St. Gen. L.Mociulski**' which is located in Beiuș city. Given the close cooperation with this company, we hope to get rock samples and other information belonging to this new well.

Depth of potential wells

Based on geophysics and geological cross – sections, there is the possibility to intercept the metal – bearing intrusive – body at a depth of cca 4 km. The main condition, this of having a temperature higher of 150 ^{o}C for the fluids extracted from this ore-body determines us to create a geothermal model specific to this area, before knowing which is the depth of the two (injection and extraction) wells. We hope that data obtained from the new well of Beiuș to help us with this model.

Conceptual drill and well design (based on the stress field and the area specifics)

Data obtained from the new well of Beiuș can provide valuable information for the new projected EGS system. Before drilling, research must be developed in many domains, including stress field. After the necessary preliminary data are obtained the construction of the wells follows 3 s**tages:** drilling and casing the wells, development of the wells and testing the wells.

Wells connection

Beiuş town, with 12,000 inhabitants, is one of the few cities from Europe that are heated entirely with geothermal water. There are two production wells at Beiuş which are equipped with Icelandic line shaft pumps and 1 re-injection well (Figure 57). A new geothermal extraction well is going to be drilled starting with 2019.

Expected temperature/pressure at the bottom/wellhead

The location of the pilot site is at the border between Beiuș Basin and Bihor Mountains, and both structural units are characterised by thin crust and litosphere. Also, other elements, like geothermal gradient of the region, or radiogenic type of the batholith encourage us to expect that at 5-6 km depth to obtain temperatures higer than 150^{o}C. A geothermal model is necessary for a better estimation.

Figure 57 Pumping installation from Beiuș

8.3 Electrolytic metal recovery and gas diffusion electro-precipitation

Potential target metals/products to be recovered

During the CHPM2030 project's implementation by using GDEx technology VITO succeeded to recover **high content of Sr** from a geothermal brine of the well 30001 from Beiuș.

Also, during the CHPM2030 project's implementation **a high content of Magnesium** has been highlighted in the precipitate resulted from the evaporation of the geothermal brine from Beiuș.

Based on these data at least an enrichment of the fluid with magnesium and strontium is to be expected.

Brine: foreseen chemical composition and physical parameters

Laboratory leaching experiments performed by BGS on 2 samples from the pilot site during the CHPM2030 project implementarion indicate that by adding ***0.6 M NaCl, 100 °C, at a preassure of 200 bar, or adding HCl/HNO3 mix, 100 °C, at a preassure of 200 bar*** good results are obtained for Co, Sr, Mo, Sb, Mn, Zn, and W.

In the future, by using mild leaching substances it is expcted that the above mentioned elements to be found in the fluid that is extracted.

8.4 Power plant

Figures 58, 59 District modules belonging to GeoDHsys of Beiuș.

In Beiuș there are 20 thermal modules, where the geothermal water is led to the heat exchanger and heat is produced. The total heat supplied to consumers overpass 40,000 Gcal/year (Figures 58 – 59). These modules replaced an old coal-fired thermal power plant.

Local heat and electricity demand (industrial, municipal, agricultural, etc.)

There are no known administrative or resource-based barriers, for further extension of the geothermal district heating system in Beiuș city. At present the combined capacity of the deep well pumps in both production wells cannot sustain further increase of the GeoDH system. During winter months 2016 its capacity was not enough during peak demand of the system. Connection of new consumers to the system has been put on hold until its geothermal production capacity has been increased.

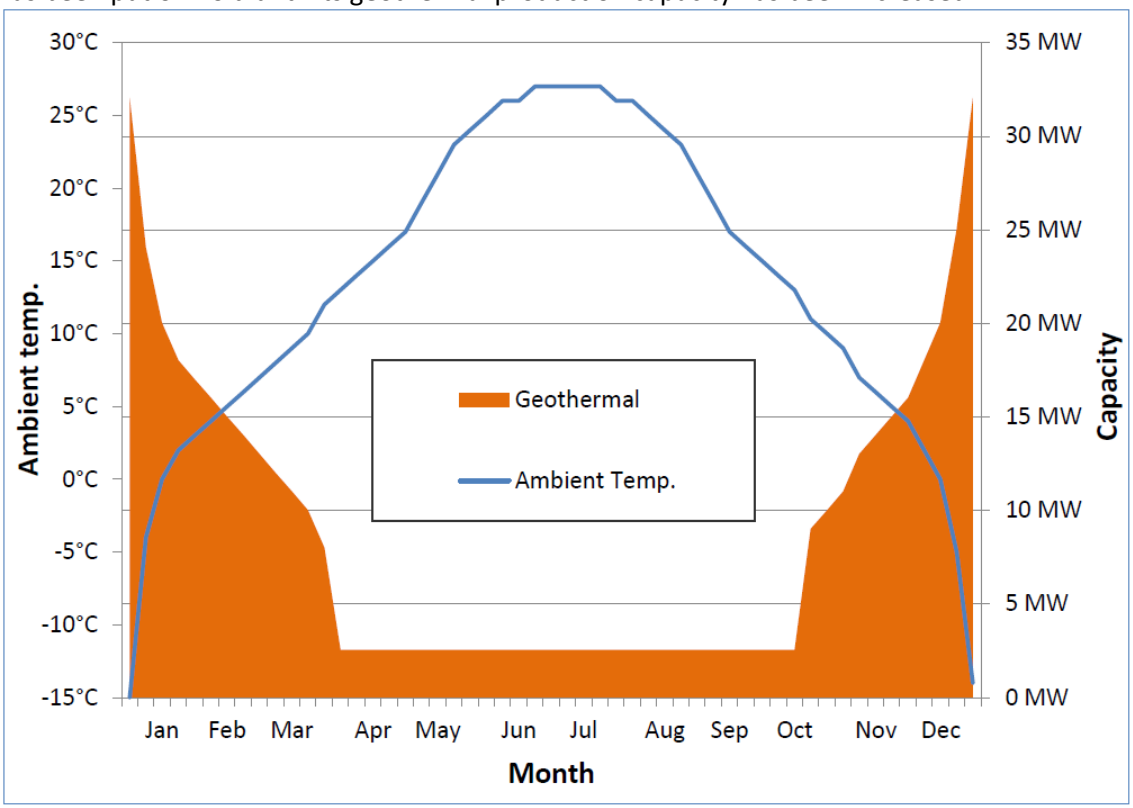

Figure 60 Monthly GeoDH heat demand MWth based on ambient temperature

According to the Pre-Feasibility study elaborated by Gunnarsson (2017), there is no central gas supply system in the city. Some single houses use gas for heating of hot sanitary water (HSW) but major heat source for HSW and domestic heating (DH) is wood burning.

Their estimated annual heat demand is 93 TJ/year to be compared to 153 TJ/year consumption of geothermal heat delivered (measured at consumers) in 2016 in existing GeoDH system. For the existing GeoDH system to serve those not yet connected it needs to increase its annual production by 60 %.

Table 13 Estimated heat demand for potential new GeoDH consumers

Houses not yet connected to GeoDH Heated with wood	Annual heat demand TJ/year	Annual wood consumption m3/year (wood)	Annual CO_2 emission t CO_2/year
733 single houses	72,6	7 559	7 982
One block house with 12 apartments	0,8	81	86
10 Warehouses and institutions	19,2	2 000	2 112
Total	92,5	9 640	10 621

In 2019 a solution for expansion of the GeoDH by drilling an additional production well has been chosen. But still the need for geothermal energy remains for the neighboring villages:

Table 14 Villages around Beiuș city

Distance between Beius and surrounding villages		Population
Beius – Delani:	3 km	369
Beius – Draganesti:	5 km	2 800
Beius – Curatele:	7 km	2 700
Beius – Pocola:	6 km	1 600
Beius – Budureasa:	12 km	2 600
Beius – Finis:	4 km	3 600
Beius – Tarcaia:	5 km	2 100
Beius – Remetea:	9 km	3 100

A new potential CHPM plant that can be located at Budureasa, would be able to provide geothermal energy for the neighboring villages, or electricity to the national grid.

Access to the grid

There are clear laws that allow and encourage the production of electricity from renewables. Among other incentives there are the Green Certificates. The Law **220/2008 stipulates the inclusion in the consumer's invoices the payments for green certificates. In Romania each consumer pays 11Eur/MWh/month for green certificates.**

9. Environmental, social and political background:

In 2017 a Pre-Feasibility study on Beiuș GeoDHsys extension (Gunnarsson et al, 2017) has been completed. In this chapter we took data from this study and would like to thank the authors.

Environmental

The use of low temperature geothermal energy in Beius has very limited CO2 equivalent emission, coming indirectly mainly from the production of the electricity used for its pump operations, in case it is produced by burning fossil fuel. Limited amount of GHG follow the geothermal water and leave it during utilisation.
It must only be a question of short time for Beius city to reach its goal of being 100% heated with geothermal water from its geothermal reservoir underneath its grounds. When accomplished, the local air pollution from district heating will come to an end in the city with enormous improvement in air quality, especially during the heating season. Estimated annual heat consumption in Beius is 246 TJ/year which corresponds to annual burning of wood around 25,600 [m3/year], emitting 27,000 [t CO2/year].
Multidisciplinary studies must be done in order to prevent environmental risks such as: water and noise pollution, induced seismicity, land use/subsidence, induced seismicity/landslides, water use, thermal pollution, etc.
An issue for the future to be considered will be local competition for water availability. Local community has the right to decide how to manage this problem, based on correct information.
The risk of mobilizing radioactive/toxic materials exists especially at Băița Bihor, and, although existence of mineralization is a proven fact, we consider that Romania is not prepared to be prepared for such a challenge, and we did not include this site into the pilot site.

Social

The geothermal heat production has several advantages, such as:

1. Economic opportunity and savings.
2. Improvement of energy security.
3. Reducing greenhouse gas emissions.
4. Harnessing local resources
5. Reducing dependency on fossil fuels for energy use.
6. Local payback in exchange for local support for deep drilling.
7. They complement existing district-heating networks offering an alternative to other fuels.
8. They can be combined with smaller binary cycle (if reservoir and economics allow) electricity generating plants to bring the utilisation of the reservoir to the maximum.
9. May be a useful complement to regional and local economic development programmes with positive effect on employment and the viability of public infrastructure.
10. They raise public awareness for the geothermal energy to a broader section of the public
11. Improving quality of life based on economic and environmental / climate benefits.

The inhabitants of Beiuș are used to benefit for the existance of the GeoDHsys in their city, because they pay less than the rest of Romania's inhabitants, and they have a cleaner air, they do not have to care for making wood provisions for the winter, etc.
Regarding a CHPM system installation, information sessions are needed in order to explain which are the risks for the population. The whole range of activity connected to SLO have to be provided into a future project.

Political

1. Authorities and Regulatory Factors

- Simplify the administrative procedures to create market conditions that facilitate development;
- Separate law regarding geothermal resources and other fossil fuels resources.
- Improve access to geothermal data - to improve development of geothermal utilization.
- Publicise the characteristics and benefits of geothermal energy for regional development

- Design regulation specific to the promotion of direct uses of geothermal energy.
- Promote cooperation with international organisations.

2. Geothermal Resources

- Improvement of geothermal regulation.
- Separate law on geothermal and fossil fuels – to speed up access to geothermal data and avoid hindering geothermal development, and problems due to secrecy of oil and gas information.
- Improvements for data analysis of reservoirs in regions.

3. Scientific and Technical Factors

- Promote relationships with industry.
- Promote alliances with research centres and educational institutions for the formation of specialised human resources.

4. Companies, Management, Expertise – Industry Clusters

- Promote alliances with research centres and educational institutions for the formation of specialised human resources.
- Promote cooperation with IFI for financing, donor support and consulting.
- Organize workshops and conferences to improve knowledge on geothermal energy.
- Identify geothermal energy-related productive chains.

5. Educational and Human Factors

- Support for the generation of the human resources needed for the geothermal industry**.**
- Creating seminars and specialized courses on the different stages of a geothermal project and adding them to the existing engineering degrees.
- Give the personnel technical training to participate in the different stages of a project.
- Implement programs for scientific and technical development.

6. Access to finance, and Cost of Capital

- Promote additional access to financing geothermal projects – domestic and international.
- Increase access to capital by providing capital to exploration and test drilling and DH networks e.g. soft loans or donor grants, to lower the risks at the beginning of projects.

7. Infrastructure, Access to Markets, Sectors and Clusters

- Promote training in the banking system for the development of financial mechanisms specific to geothermal energy.
- Awareness; organize workshops & conferences to improve knowledge of geothermal energy.
- Increase the available knowledge about opportunities and benefits of geothermal resources.

8. Access to International Markets and Services

- Support international cooperation in area of geothermal knowledge, training and service.
- Promote international cooperation with IFI and donors on finance, grants and funding.
- Support international consulting cooperation on various fields of geothermal expertise.

10. Financial aspects

District Heating Costs

The Beiuș city council has contracted SC Transgex S.A., which holds the local geothermal utilisation licence, to operate and expand the GeoDH system. The tariffs for the delivery of central geothermal district heating in Beius are regulated by the state authorities reflecting the real cost of its operation. The way to evaluate the economic advantages of the GeoDH operation is to look at it from the consumer perspective and compare it with the cost and user friendliness of other heating alternatives, being mainly wood burning in Beius.

The geothermal energy is delivered and consequently charged in two different ways at the Beius consumers. Those who receive the heat from a secondary distribution loop from a substation are charged per used energy, which is metered in Gcal.

Those who receive the heat directly from the GeoDH system are charged per used amount of geothermal water metered in m3. The existing two production wells, 3001 and 3002, have different water temperature, hence two different prices/m3, depending on wherefrom the geothermal water comes, see Table 15.

Selling prices for the GeoDH system are regulated by the state organization, National Authority of Regulatory for Community Services (NARCS), according to the Romanian law no. 325/2006.

Table 15 GeoDH consumer heat tariffs for Beius in 2017

Secondary deliv. PT-substations	Price	Direct delivery to houses	Price	Price w/ 19% VAT	Price w/ 19% VAT	Utilisation	Energy content
Energy metering	RON/Gcal	Volume metering	RON/m3	€/m3	€/GJ	DT [°C]	MJ/m3
Production	40.92	From Well 3001	3.30	0.86	5.31	80-40	163
Transport	19.79	From Well 3003	2.75	0.72	5.86	70-40	123
Distribution	19.57		NARCS-price regulation 2017				
Total w/ 19% VAT	**95.53**	Exchange rate RON/€ = 4.55			Based on information from Transgex/ANRM		
€/Gcal incl. VAT	21.00						
€/GJ incl. VAT	5.01						

In the last years there was a market price escalation for wood, see Table 16.

Year	2013	2014	2015	2016	2017
€/m^3	26	33	33	38	63

The effect was that inhabitants became more and more interested in using geothermal energy because with current market prices for wood for heating and GeoDH state regulated heating tariffs the citizens of Beius enjoy between 30% - 50% reduction in annual heating cost, when connected to the GeoDH system, a tremendous advantage for the citizens in addition to better air quality, clean, safer and almost zero manpower operation of their house heating.

For new investments the financial tools developed in WP5 will be used in order evaluate all the economical elements that are needed for a new project.

As potential investors that expressed their intent to be partners in such a project we can mention:

- Local public authority – City hall of Beiuș
- Transgex S.A.
- Geological Institute of Romania

Given the fact that the costs for such a project are high, we think that the best solution is to use EU funding for different stages of project development that follow in the future.

11. Conclusions

The data from several domains converge to the conclusion that there are prerequisites that allow considering part of the study area as a pilot area. Thus, the data analysed in the CHPM2030 project led to the delineation of a perimeter in the Budureasa area that is situated at the border between Beiuş Basin and Bihor Mountains. This perimeter has the following features that encourage the design of new research:

- High geothermal potential characteristic to the eastern border of the Pannonain Basin;
- Existence of granite – granodiorite batholith in the depth that can be intercepted on a width of more than 10 km in Beiuș Basin;
- Mineralization well documented and delineated by detailed magnetometric measurements;
- Based on laboratory experiments that have been performed during the project at least an enrichment of the fluid with magnesium and strontium is to be expected.
- In the future, by using mild leaching substances it is expcted that Co, Sr, Mo, Sb, Mn, Zn, and W to be found in the fluid that is extracted.
- Existence of the geothermal aquifer that, having a regional extension in Beiuș Basin, can provide geothermal energy to an increased number of localities;
- The expertise of the private company in geothermal water exploitation in Beiuș, and other places in Romania;
- Both public local authority and private company expressed their interest to be partners into a project that envisages energy production (and metals) from dry hot rock.
- Existence of surface waters that can be used for a CHPM installation;
- A lower cost of geothermal energy for the population as compared to the energy resulted from burning wood;
- High energy demand for heating and for electricity at local and national level;

Acknowledgements

I would like to express my deep gratitude to Professor Gheorghe Popescu, and Dr. Peter Luffi, for their patient guidance, encouragement and useful critiques of this research work.

References

Andrei, J., Cristescu, T., Calotă, C., Proca, A., Românescu, D., Russo-Săndulescu, A., et al. (1989). Spatial distribution and structural images of banatites from Romania deduced from gravity and magnetic data. *Rev. Roum. Geol., Geophys. et Geogr.- GEOPHYSIQUE, Vol. 33*, 79-85.

Antal, C., Setel, A., & Gavrilescu, O. (2009). Exploitability of geothermal resources in Pannonian Depression. *Analele Universității Oradea, Fascicula de Energetică, Vol. 15*.

Bada, G., Cloetingh, S., Gerner, P., & Horváth, F. (1998). Sources of recent tectonic stress in the Pannonian region: inferences from finite element modelling. *Geophys. J. Int., Vol. 134*.

Bala, A., & Răileanu, V. (2017). Assessing of the crustal models and active faults systems in western part of Romania with applications in seismic hazard. *Romanian Reports in Physics, Vol. 69*.

Bala, A., & Toma-Dănilă, (2017). Crustal models assessment in western part of Romania employing active seismic and seismologic methods: http://www.rrp.infim.ro/IP/A362.pdf.

Balázs, A. (2017). Dynamic model for the formation and evolution of the Pannonian Basin : The link between tectonics and sedimentation. *Utrecht Studies in Earth Sciences, Vol. 132*.

Balázs, A., Magyar, I., Matenco, L., Sztanó, O., Tokés, L., & Horváth, F. (2018). Morphology of a large paleo-lake: Analysis of compaction in the Miocene-Quaternary Pannonian Basin. *Global and Planetary Change, Vol. 171*.

Balázs, A., Matenco, L., Magyar, I., Horváth, F., & Cloetingh, S. (2016). The link between tectonics and sedimentation in back-arc basins: New genetic constraints from the analysis of the Pannonian Basin. *Tectonics, Vol. 35*.

Balázs, A., Matenco, L., Vogt, K., Cloetingh, S., & Gerya, T. (2018). Extensional Polarity Change in Continental Rifts: Inferences From 3-D Numerical Modeling and Observations. *Journal of Geophysics Research: Solid Earth, Vol. 123*.

Balázs, A., Maţenco, L., Magyar, I., Horváth, F., & Cloeting, S. (2016). The link between tectonics and sedimentation in back-arc basins: New genetic constraints from the analysis of the Pannonian Basin. *Tectonics, Vol.35*.

Balintoni, I., & Puşte, A. (2001). Probleme tectonice în partea de vest a Masivului Pădurea Craiului (Munţii Apuseni). *Studia Universitatis Babes-Bolyai Geologia, XLVI,1*.

Békési, E., Lenkey, L., Limberger, J., Porkoláb, K., Balázs, A., Bonté, D., et al. (2017). Subsurface temperature model of the Hungarian part of the Pannonian Basin. *Global and Planetary Change, Vol. 171*.

Bordea, S., & Mantea, G. (1999). The main structural elements of Beiuş Basin and of the adjacent zones (Apuseni Mountains), . *Rev. Roum Geologie, Tome 43*, 101-108.

Bordea, S., & Mantea, G. (1999). The main structural elements of Beiuş Basin and the adjacent zones, Apuseni Mountains. *Rev. Roum. Geol., Geophys., Vol. 43*, 101-108.

Cermak, V., & Rybach, L. (1991). *Terrestrial Heat Flow and the Lithosphere Structure.* Springer-Verlag Berlin Heidelberg.

Cermak, V., Rybach, L., & =. (1991). *Terrestrial Heat Flow in Europe - Heat Flow and itospheric Structure in Romania.* Berlin: Springer Verlag.

Daoxian, Y., & Zaihua, L. (1998). *Global Karst Correlation .* Science Press.

Demetrescu, C. (1982). Thermal structure of the crust and upper mantle of Romania. *Tectonophysics, Vol. 90*.

Demetrescu, C., & Andreescu, M. (1994). On the thermal regime of some tectonic units in a continental collision environment in Romania. *Tectonophysics, Vol. 230*.

Demetrescu, C., & Polonic, G. (1989). The evolution of the Pannonian Depression (Romanian sector) as derived from subsidence and heat flow data. *Tectonophysics, Vol.164*.

Dererova, J., Zeyen, H., Bielik, M., & Salman, K. (2006). Application of integrated geophysical modeling for determination of the continental lithospheric thermal structure in the eastern Carpathians. *Tectonics, Vol. 25*.

Dominguez, X., et al, (2018). CHPM2030 DELIVERABLE D3.2. Report on performance, mass and energy balances and design criteria for gas-diffusion electroprecipitation and electrocrystallization. https://www.chpm2030.eu/wp-content/uploads/2019/03/CHPM2030_D3.3.pdf

Gallhofer, D., Quadt, A. v., Peytcheva, I., Schmid, S. F., & Heinrich, C. A. (2015). Tectonic, magmatic, and metallogenic evolution of the Late Cretaceous arc in the Carpathian-Balkan orogen. *Tectonics, Vol. 34*.

Gavat, I., Airinei, Ș., Botezatu, R., Socolescu, M., Stoenescu, S., & Vencov, I. (1963). The deep geological structure of the territory of the Romanian people's republic according to the present geophysical data (gravimetric and magnetic data). *Tomul 1, Vol.1*, ISSN 1220 - 5265.

Genter, A., Guillou-Frottier, L., Feybess, J., Nicol, N., Dezayes, C., & Schwartz, S. (2003). Typology of potential Hot Fractured Rock resources in Europe. *Geothermics, Vol. 32*, 701-710.

Gunnarsson, A., et al, (2017). Pre-Feasibility Study Geothermal District Heating Beius, Romania. National Energy Authority, ISBN 978-9979-68-426-8.

Horváth, F., Bada, G., Szafián, P., Tari, G., Ádám, A., & Cloetingh, S. (2006). Formation and deformation of the Pannonian Basin: constraints from observational data. *Geological Society, London, Memoirs, Vol. 32*.

Horváth, F., Dulić, I., Vranković, A., Koroknai, B., Tóth, T., Wórum, G., et al. (2018). Overview of geologic evolution and hydrocarbon generation of the Pannonian Basin. *Interpretation*.

Horváth, F., Musitz, B., Balázs, A., Végh, A., Uhrin, A., Nádor, A., et al. (2015). Evolution of the Pannonian basin and its geothermal resources. *Geothermics, Vol. 53*.

Horváth, F., Musitz, B., Balázs, A., Végh, A., Uhrin, A., Nádor, A., et al. (2018). Evolution of the Pannonian basin and its geothermal resources. *Geothermics, Vol. 53*.

Iancu, V. (2011). Field Trip Guidebook. The Late Cretaceous magmatic and Metallogenic Belt and Alpine structures of the western South Carpathians. *Conference: 3rd International Symposium on the Geology of the Black Sea Region, At Bucharest, Volume: Field Trip Guidebook.*

Ivanovici, V. (1976). *Geologia Munților Apuseni.* Editura Academiei Republicii Socialiste România.

Jarosinski, M., Beekman, F., Mețenco, L., & Cloetingh, S. (2011). Mechanics of basin inversion: Finite element modelling of the Pannonian Basin System. *Tectonophysics, Vol. 502*.

Lankreijer, A., Mocanu, V., & Cloetingh, S. (1997). Lateral variations in lithosphere strength in the Romanian Carpathians: constrains on basin evolution. *Tectonophysics, Vol. 272*, 269-290.

Lenkey, L., Dovenyi, P., Horvath, F., & Cloetingh, S. (2002). Geothermics of the Pannonian basin and its bearing on the neotectonics. *Stephan Mueller Special Publication Series, Vol. 3*.

Matenco, L., Munteanu, I., ter Borgh, M., Stănica, A., Tilita, M., Lericolais, G., et al. (2015). he interplay between tectonics, sediment dynamics and gateways evolution in the Danube system from the Pannonian Basin to the western Black Sea. *Science of The Total Environment, Vol. 543*.

Matenco, L., Vogt, K., Cloetingh, S., & Gerya, T. (2018). Extensional Polarity Change in Continental Rifts: Inferences From 3-D Numerical Modeling and Observations. *Journal of Geophysical Research: Solid, Vol. 123*.

Mațenco, L. (2016). Tectonics and Exhumation of Romanian Carpathians: Inferences from Kinematic and Thermochronological Studies. In M. Radoane, & V. A. Stroe, *Landform Dynamics and Evolution in Romania.* Springer Geography.

Mațenco, L., & Radivojević, D. (2012). On the formation and evolution of the Pannonian Basin: Constraints derived from the structure of the junction area between the Carpathians and Dinarides. *Tectonics, Vol. 31*.

Merten, S., Mațenco, L., Foeken, J., & Andriessen, P. (2011). Toward understanding the post-collisional evolution of an orogen influenced by convergence at adjacent plate margins: Late Cretaceous–Tertiary thermotectonic history of the Apuseni Mountains. *Tectonics, Vol. 30*.

Michal, G. (2013). Détermination d'un modèle lithosphérique en Europe centrale: modélisation géophysique intégrée. *University of Paris-Sud, Vol. XI*.

Nemcok, M., Pospisil, L., Lexa, J., & Donelick, R. (1998). Tertiary subduction and slab break-off model of the Carpathian-Pannonian region. *Tectonophysics, Vol. 295*, 307-340.

Neubauer, F., Lips, A., Kouzmano, K., Lexa, J., & Ivăşcanu, P. (2005). 1: Subduction, slab detachment and mineralization: The Neogene in the Apuseni Mountains and Carpathians. *Ore Geology Reviews, Vol. 27*.

Orășeanu, I. (2015). Groundwater dynamics of Beiuş Basin basement and its surrounding mountain areas. *Groundwater dynamics of Beiuș Basin basement*.

Orășeanu, I. (2015). Groundwater dynamics of Beiuș Basin basement and its surrounding mountain areas. *Nymphaea Folia naturae Bihariae, Vol. XLII*, 5-18.

Pătrașcu, Ș., Bleahu, M., & Panaiotu, C. (1990). Tectonic imiplications of paleomagnetic research into Upper Cretaceous magmatic rocks in the Apuseni Mountains, Romania. *Tectonophysics, Vol. 180*, 309-322.

Pătrașcu, Ș., Panaiotu, C., Șeclăman, M., & Panaiotu, C. E. (1994). Timing of rotational motion of Apuseni Mountains (Romania): paleomagnetic data from Tertiary magmatic rocks. *Tectonophysics, Vol. 233*, 163-176.

Proca, A., Albaiu, M., (1979). Contribuții gravimetrice la cunoașterea structurilor eruptive din Munții Bihor – Gilău. Institutul Geologic al României - Studii tehnice și economice, Seria D, nr.13, 1979.

Rădulescu, F., Biter, M., Diaconescu, C., & Nacu, V. (1994). Geological structure and seismicity of Romania. *Mitteilungen aus den Geodatischen Instituten der Rheinschen Friedrich-Wilhems Universitat Bonn, Nr. 82*.

Ren, Y., Stuart, G. W., Houseman, G. A., Dando, B., Ionescu, C., Hegedűs, E., et al. (2012). Upper mantle structures beneath the Carpathian–Pannonian region: Implications for the geodynamics of continental collision. *Earth and Planetary Science Letters*.

Rochelle, C., (2017). CHPM2030 DELIVERABLE D2.2. Report on metal content mobilisation using mild leaching. https://www.chpm2030.eu/wp-content/uploads/2018/03/CHPM2030_D2.2.pdf

Roșu, E., Seghedi, I., Downes, H., Alderton, D., Szakacs, A., Pecskay, Z., et al. (2004). Extension-related Miocene calc-alkaline magmatism in the Apuseni Mountains, Romania: Origin of magmas. *SCHWEIZERISCHE MINERALOGISCHE UND PETROGRAPHISCHE MITTEILUNGEN, Vol. 84*.

Schwarz, G. (2016). *Report on data availability - CHPM2030 Deliverable 1.2.* Hungary: Published by CHPM 2030 project.

Seghedi, I. (2018). 2. GEOLOGICAL EVOLUTION OF THE APUSENI MOUNTAINS WITH EMPHASIS ON THE NEOGENE MAGMATISM – A REVIEW.

Seghedi, I., & Downes, H. (2011). Geochemistry and tectonic development of Cenozoic magmatism in the Carpathian–Pannonian region. *Gondwana Research, Vol. 20*.

Sferle, M. (2018). Transgex. Power Point presentation.

Ștefan, A., Lazăr, C., Berbeleac, I., & Udubașa, G. (1988). Evolution of Banatitic Magmatism in the Apuseni Mts. and Associated Metallogenesis. *D.S. Inst. Geol. Geofiz., Vol. 72-73*.

Ștefan, A., Roșu, E., Andar, A., Robu, N., Bratosin, I., Grabari, G., et al. (1992). Petrological and geochemical features of banatitic magmatites in northern Apuseni Mountains. Rom. J. Petrology, Vol. 75, 97-115.

Ștefan, A., Roșu, E., Audăr, A., Robu, L., Robu, N., Bratosin, et al. (1992). Petrological and Geochemical Features of Banatitic Magmatites in Northern Apuseni Mountains. Rom. J. Petrology, Vol. 75.

Stoicovici, E. & Stoici S. (1970).Contribuții la cunoașterea mineralizației de bor din bazinul superior al Crișului Negru (Băița Bihorului). Studia Universitatis Babes Bolyai, XV nr.2,-15.

Tari, G., Dövényi, P., Dunkl, I., Horváth, F., Lenkey, L., Stefanescu, M., et al. (1999). Lithospheric structure of the Pannonian basin derived from seismic, gravity and geothermal data. Geological Society London Special Publications*, Vol. 156*.

Tiliță, M. (2018). Heat flow modelling in the Transylvanian basin: Implications for the evolution of the intra-Carpathians area. *Global and Planetary Change*.

Tiliță, M. S. (2015). Evolution of the Transylvanian Basin: inferences from seismic interpretation and numerical modelling. *Utrecht Studies in Earth Sciences, Vol. 89*.

Visarion, M., Veliciu, Ș., Constantinescu, P., & Ștefănescu, M. (1978). Crustal temperature - depth profile across Romania derived from heat flow amd other geophysical data. *Rev. Roum. Geol. Geophys. et Geogr. - GEOPHYSIQUE, Vol. 22*, 33-38.

CHPM2030 DELIVERABLE D 6.2 APPENDIX 6.2.4

REPORT ON PILOTS:
THE KRISTINEBERG AND NAUTANEN MINING AREAS
IN NORTHERN SWEDEN

Summary:
This report provides a brief overview of two study areas in northern Sweden around the Kristineberg and the abandoned Nautanen mine, where the CHPM technique can be suitable to be applied. It includes description of the geological settings, and on-going efforts in geophysics increasing resolution for detecting mineralised zones at even larger depth. The report also is attempting to estimate the low enthalpy geothermal potential of these areas.

Authors:
Gerhard Schwarz, Geological Survey of Sweden, Geophysicist
Benno Kathol, Geological Survey of Sweden, Geologist
Magnus Ripa, Geological Survey of Sweden, Geologist
Bo Thunholm, Geological Survey of Sweden, Hydrogeologist
Edward P. Lynch, Geological Survey of Sweden, Geologist
Johan Jönberger, Geological Survey of Sweden, Geophysicist

This project has received funding from the European Union's Horizon 2020 research and innovation programme under grant agreement nº 654100.

TABLE OF CONTENTS

LIST OF FIGURES

LIST OF TABLES

EXECUTIVE SUMMARY

There are four major ore provinces in Sweden, i.e., Bergslagen, the Skellefte district, the Northern Norrbotten ore province and the Caledonian orogen. In these, we have chosen the areas around the Kristineberg mine in the Skellefte district and the abandoned Nautanen mine in Northern Norrbotten for further screening the applicability of the CHPM technology there.

The Kristineberg area in the southwestern part of the Skellefte district is known for its volcanogenic massive sulphide deposits (VMS). Based on their age and geological history of rock sequences, the bedrock in the Skellefte district and surrounding areas in northern Västerbotten and southern Norrbotten counties can be divided and assigned to three major lithotectonic units. These are the Svecokarelian orogen, the Ediacaran to Cambrian sedimentary cover sequence and the Caledonian orogen. The Skellefte district *sensu stricto* belongs entirely to the Svecokarelian orogen.

The bedrock in the Skellefte district was formed or reworked by Svecokarelian orogenic processes, which lasted from about 1.96 to 1.75 Ga. This time interval includes subduction-related processes, collision, and extension-related collapse of the thickened crust. The peak of Svecokarelian deformation and metamorphism occurred between 1.85 and 1.80 Ga, but earlier phases of deformation at 1.89 – 1.87 Ga have been reported under the last decade. The Svecokarelian orogen comprises Svecokarelian intrusive rocks, formed by orogenic processes and Svecofennian supracrustal rocks, i.e. early orogenic sedimentary and volcanic rocks, the latter hosting the VMS deposits of the Skellefte district and thus the Kristineberg mine.

The Kristineberg mine is the oldest and largest massive sulphide mine in the Skellefte district and in continuous operation until today. Mining began in the year 1940 at the ore body outcropping at surface. Since then, production has reached down to around 1 200 m making Kristineberg to one of the deepest mines in Sweden. The ore is a complex massive sulphide with zinc being the main metal, although in some areas copper-gold ores are mined. Until year 2017, 31 million tons have been mined, reserves are 5 million tons and resources about 13 million tons. The combined grades of mined ore, reserves and resources are 3.9 % zinc, 0.7 g/t gold, 44 g/t silver, 0.9 % copper and 0.4 % lead.

The rocks surrounding the Kristineberg deposit have been strongly hydrothermally altered and are multiphase folded and strongly sheared. The schistose rocks are now dominated by quartz–muscovite–chlorite–pyrite in varying proportions, and exhibit marked sodium depletion and co-enrichment of magnesium and potassium. Cordierite, phlogopite and andalusite occur in considerable amounts. Kyanite has rarely been observed, mainly associated with quartz veins. In general, the iron–magnesium alteration minerals are magnesium-rich, and the modal chlorite content increases towards the Kristineberg ore horizon, which is surrounded by a halo of more muscovite-rich rocks.

The Geological Survey of Sweden has a long-standing tradition in geological mapping of the country with the support from airborne geophysics, motivated by the low degree of bedrock exposures. Magnetic properties, electrical resistivity and gamma radiation of shallow crustal rocks were thus studied in the Skellefte district and the Nautanen area, complemed by ground surveys on these rock properties and on gravity.

During the last two decades, reflection seismic investigations were introduced in Sweden in larger extent by academia in cooperation with the mining industry for prospecting after minerals and ores in the Earth's uppermost crust. The Kristineberg area in the western Skellefte district was studied at depth down to 12 km by seismic methods, complimented by drillhole data down to ca 1400 m below surface. High resolution reflection seismic data provided detailed images of an VMS ore body and associated structures. But, the seismic experiments have also shown that considerable efforts need to be undertaken in geologically complex areas to properly acquire data, i.e., preferably by 3D instead of 2D surveys.

The Nautanen deposit is situated in the Northern Norrbotten ore province in northernmost Sweden. At this historical mining location, intermittent exploration has been carried out for over 100 years. Approximately 72 000 tonnes of copper and iron ore were extracted between 1902 and 1907. Further exploration in the 1970s and 80s produced a pre-regulatory total resource estimate for the "old" Nautanen deposit of approximately 2.94 Mt grading 0.78% Cu and 0.52 ppm Au. Present-day exploration by Boliden Mines ral AB has resulted in the discovery of an additional copper-gold mineralisation approximately 1.6 km north-northwest of the old Nautanen mine along the trend of the Nautanen deformation zone (NDZ). This "Nautanen North" deposit has an indicated resource of 9.6 Mt grading 1.7% Cu, 0.8 ppm Au, 5.5 ppm Ag and 73 ppm Mo, with an additional inferred resource of 6.4 Mt grading 1.0% Cu, 0.4 ppm Au, 4.6 ppm Ag and 41 ppm Mo.

The bedrock in Northern Norrbotten is part of the 2.0–1.8 Ga old Svecokarelian orogen. The orogen comprises both pre-orogenic rocks formed in the Archaean and early Palaeoproterozoic, as well as rocks formed during the orogeny itself. The bedrock in the Nautanen area consists of a partly conformable succession of syn-orogenic, Palaeoproterozoic volcano-sedimentary rocks. This supracrustal sequence is generally of calc-alkaline, basaltic andesite to andesite composition and has undergone extensive deformation, metamorphism, recrystallisation and hydrothermal alteration. Intrusive rocks, including deformed gabbroic, syenitic and dioritic bodies and younger, deformed to massive granitic and gabbroic-doleritic plutons and dykes, occur in the area.

The mineralisations at Nautanen are part of several hydrothermal copper-gold occurrences assigned to the iron oxide-copper-gold (IOCG) mineral deposit class which occur within the regional approximately north-northwest-trending Nautanen deformation zone (NDZ). The NDZ represents the most conspicuous structural feature in the area and is clearly delineated on magnetic anomaly maps as a somewhat dilational, linear zone of sub-parallel and tightly banded magnetic susceptibility anomalies. The coupling of high-strain deformation and magnetic banding reflects episodic metasomatic-hydrothermal fluid flow, probably enhanced by increased permeability associated with protracted and focused deformation. Two general styles of mineralisation are recognised in the area: (1) an inferred older phase of disseminated to semi-massive (replacement-style) sulphide mineralisation forming sub-vertical lenses and linear zones mainly within the NDZ; and (2) mineralisation associated with quartz ± tourmaline ± amphibole veins occurring mainly east of the NDZ or as a late-stage brittle overprint within the high-strain zone.

Geophysical surveys, mostly using potential field and electrical methods in the Nautanen area were concentrated on the shallow sub-surface down to some hundred metres depth, being of economic interest. No investigations are known in the surroundings of Nautanen that are covering deeper seated structures and formations.

Our understanding of deep-seated fluids in the crystalline bedrock is still rudimentary. Hydraulic conductivity decreases with depth at a high degree of variability. Investigations in boreholes indicate that hydraulic conductivity below 650 m depth varies between 10^{-7} and 10^{-12} m/s. Data on the composition of fluids indicate that brines (> 5 % TDS/l) occur far inland at several 1000 metres depth. Their residence time was estimated at the order of some hundred million of years by the analysis of He-isotopes. Corrected geothermal heat flow density is about 50 mW/m^2. Data on heat production do not show large differences between rock types related to their content in radioactive elements.

The generally low geothermal gradient of less than 20 °C/km in the crystalline basement of the Fennoscandian Shield was verified by sensing temperature in deep boreholes in the Skellefte district and adjacent to the Nautanen mine. The temperature gradient measured here to about 16 °C/km should allow for low- to mid-enthalpy geothermal systems as part of a possible CHPM unit.

1. INTRODUCTION AND OUTLINE OF WORK

1.1. Country and site specific issues

Available data on the bedrock geology of Sweden (Fig. 1) derive mainly from observations at the Earth's surface. The overall low degree of bedrock exposure (on average < 10 % due to Quaternary till and sediment cover) in the country means that bedrock maps in unexposed areas are based on results from geophysical investigations, e.g., airborne geophysical measurements. At best, the maps should therefore be considered as probable two-dimensional (2D) models of possible rock configuration and structures. Site specific investigations need further geophysical studies as well as results from drilling. Generally, there is a lack of studies related to upper and mid crustal levels of the Earth.

Large volumes of the bedrock in Sweden have been subject to intense tectonic deformation and subsequent erosion, and rocks, including mineralisations, and structures originally formed at considerable depths in the crust are locally accessible for study at or close to the present surface. In contrast, several mineralisations in Sweden that presently are being mined at and evaluated to some depths were however originally formed at or close to the Earth's surface.

1.2. Goals

In a previous report of the CHPM2030 project (D1.2) we were providing an inventory of three major ore districts in Sweden, namely, Bergslagen in central Sweden, and further north the Skellefte district and the Northern Norrbotten ore province. The present report now informs about two of these areas in more detail, i.e., the area around the Kristineberg mine in the Skellefte district and Nautanen, an abandoned mine in Northern Norrbotten. We have identified both mining areas as being suitable for the challenging future technology, *Combined Heat, Power and Metal extraction from ultra-deep ore formations* (CHPM). The CHPM concept proposes establishing an *Enhanced Geothermal System* (EGS) in a metal-bearing geological formation, that will allow to produce both energy and metals.

Based on geological and geophysical data and borehole records, the work presented here includes subsurface information aiming on the occurrence, composition and location of potential deep mineralised formations in the target districts named above. We also shed some light on spatial variations in crustal heat production, heat flow and temperature and discuss to which extent these parameters may be affected by convection related to groundwater flow. Still, the big challenge is to predict fracture geometry and permeability at depth in crystalline bedrock. Though sub-surface information in the Kristineberg and Nautanen mining fields has increased during the last years, the study of deeper formations still is a tough task as large data gaps exist and some of the information is based on few data points of regional character.

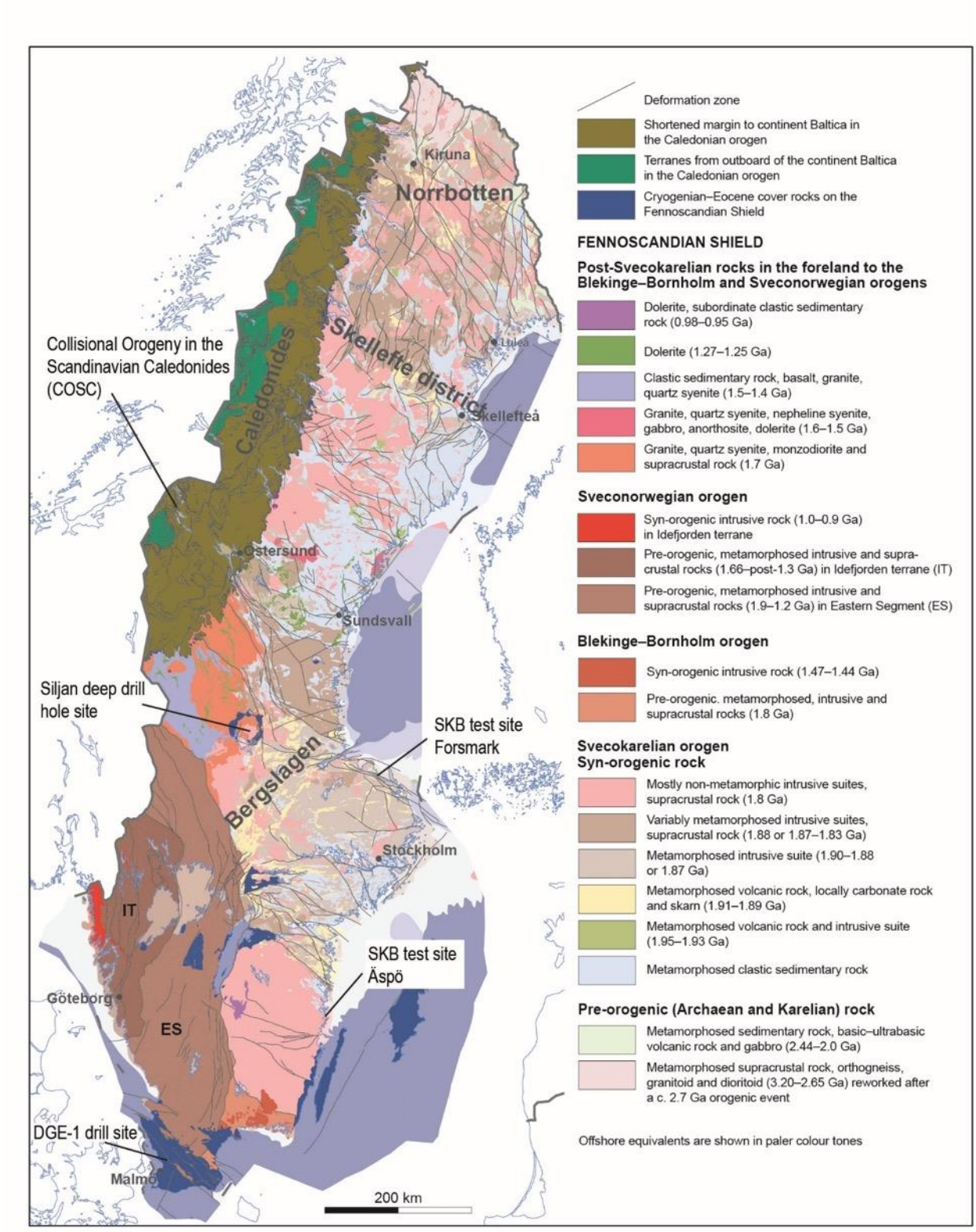

Figure 1: Bedrock geology of Sweden (SGU data), where major ore districts, potential sites for nuclear waste disposal (*SKB test site*) and sites of deep drill holes (*COSC, Siljan, DGE-1*) are noted.

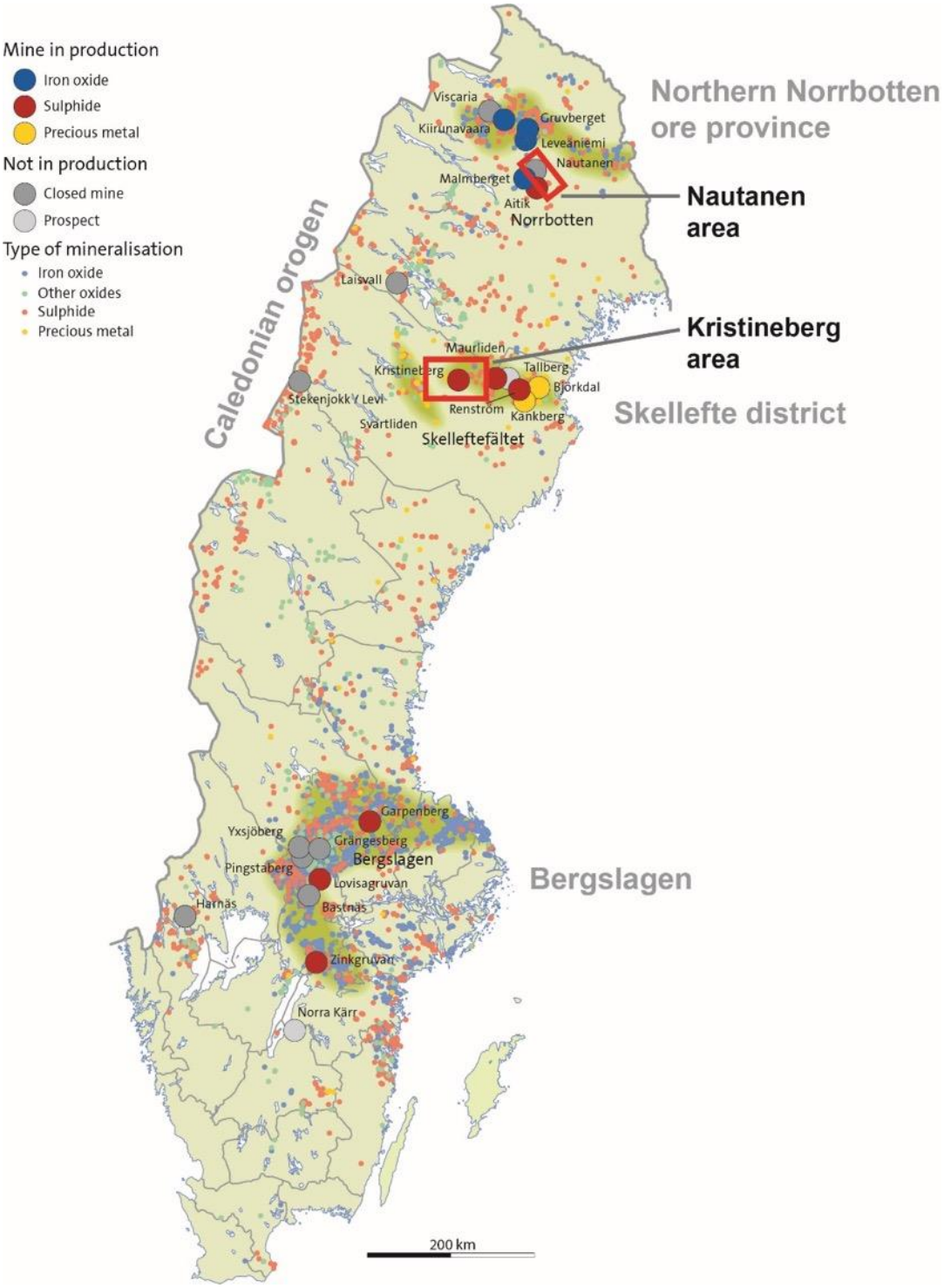

Figure 2. Mines and mineralisations in Sweden, state of activity from 2017. The currently active, major ore provinces of Northern Norrbotten, Skellefte district and Bergslagen are marked with dark green shading. The Nautanen and the Kristineberg mining areas are marked by red boxes.

2. GEOLOGY AND GEOPHYSICS OF THE PROSPECTIVE AREAS

2.1. The Kristineberg mine in the Skellefte district

2.1.1. Skellefte district

The Kristineberg area with the volcanic hosted massive sulphide (VMS) deposit of the Kristineberg mine and other VMS deposits at different stratigraphic levels is situated in the southwestern part of the Skellefte district (Allen et al. 1996; Kathol & Weihed 2005). It is one of four major ore-provinces, of which three are currently ore-producing in Sweden (Fig. 2). The other regions are Bergslagen (Stephens et al. 2009), the Northern Norrbotten ore province (Bergman et al. 2001, Bergman 2018) and the Caledonian orogen. The Skellefte district with surrounding areas is situated in northern Västerbotten and southern Norrbotten counties.

2.1.2. Regional geology

The bedrock in northern Västerbotten and southern Norrbotten counties can, based on the age and geological history of rock sequences be divided and assigned to three major lithotectonic units. These are the Svecokarelian orogen, the Ediacaran to Cambrian sedimentary cover sequence and the Caledonian orogen. Rocks of these three units occur to differing extends in the Skellefte district and surrounding areas (Fig. 3). The Skellefte district *sensu stricto* belongs entirely to the Svecokarelian orogen.

Most of the bedrock in northern Sweden, and thus the Skellefte district, was formed or reworked by Svecokarelian orogenic processes, which lasted from c. 1.96 to 1.75 Ga. This time interval includes subduction-related processes, collision, and extension-related collapse of the thickened crust. The peak of Svecokarelian deformation and metamorphism occurred between 1.85 and 1.80 Ga (Stephens et al. 1997), but earlier phases of deformation at 1.89 – 1.87 Ga have under the last decade been reported by Skyttä et al. (2012).

The Svecokarelian orogen comprises Svecokarelian intrusive rocks, formed by orogenic processes and Svecofennian supracrustal rocks, i.e. early orogenic sedimentary and volcanic rocks, the latter hosting the VMS deposits of the Skellefte district.

The Skellefte district in a wide sense is situated in the transition area between the Bothnian Basin (Hietanen 1975) in the south, and areas consisting mainly of subaqueous marine and subaerial volcanic arc assemblages in the north. Marine, mainly epiclastic supracrustal rocks of the basin are grouped under the name Bothnian supergroup, whereas the volcanic arc assemblages are divided into the subaqueous Skellefte and Vargfors groups and the subaerial Arvidsjaur group. Within the volcanic arc–Bothnian Basin transition zone, epiclastic, commonly turbiditic sedimentary rocks are interpreted to interfinger with subaqueous volcanic rocks of the Skellefte group and sedimentary rocks of the Vargfors group.

Upwards and laterally to the north, the Skellefte group rocks pass into mainly subaerial volcanic sequences of the Arvidsjaur group. The marine equivalent of the Arvidsjaur group is the Vargfors group, which consists mainly of coarse clastic and turbiditic sedimentary rocks and mafic volcanic rocks, deposited on the rocks of the Skellefte and Bothnian groups or the lower parts of the Arvidsjaur group. Differences between the Skellefte, Vargfors, and Bothnian groups are indicated by different geochemical affinities of basic volcanic rocks. However, as these rocks occur only sparsely, especially within the Bothnian supergroup, the boundary between the Skellefte and Vargfors groups on the one hand and the Bothnian supergroup on the other is drawn somewhat arbitrarily on the map (Fig. 3).

This artificial line is generally interpreted as a lateral transition from one group to the other. Rocks of the Skellefte and Vargfors groups have their coeval counterparts within the Bothnian supergroup. In places, the Skellefte/Bothnian groups or Vargfors/Bothnian groups contain laterally equivalent rock associations. In terms of sequence stratigraphy these associations should be considered as one unit, which probably consists of several, individual sequences.

At different stages and at different levels throughout the sedimentary and volcanic evolution within the map area, the supracrustal rocks have been intruded by voluminous amounts of intrusive rocks. On the one hand, these intrusions enable dating of the sedimentary record; on the other hand, they obscure primary relationships between different supracrustal units.

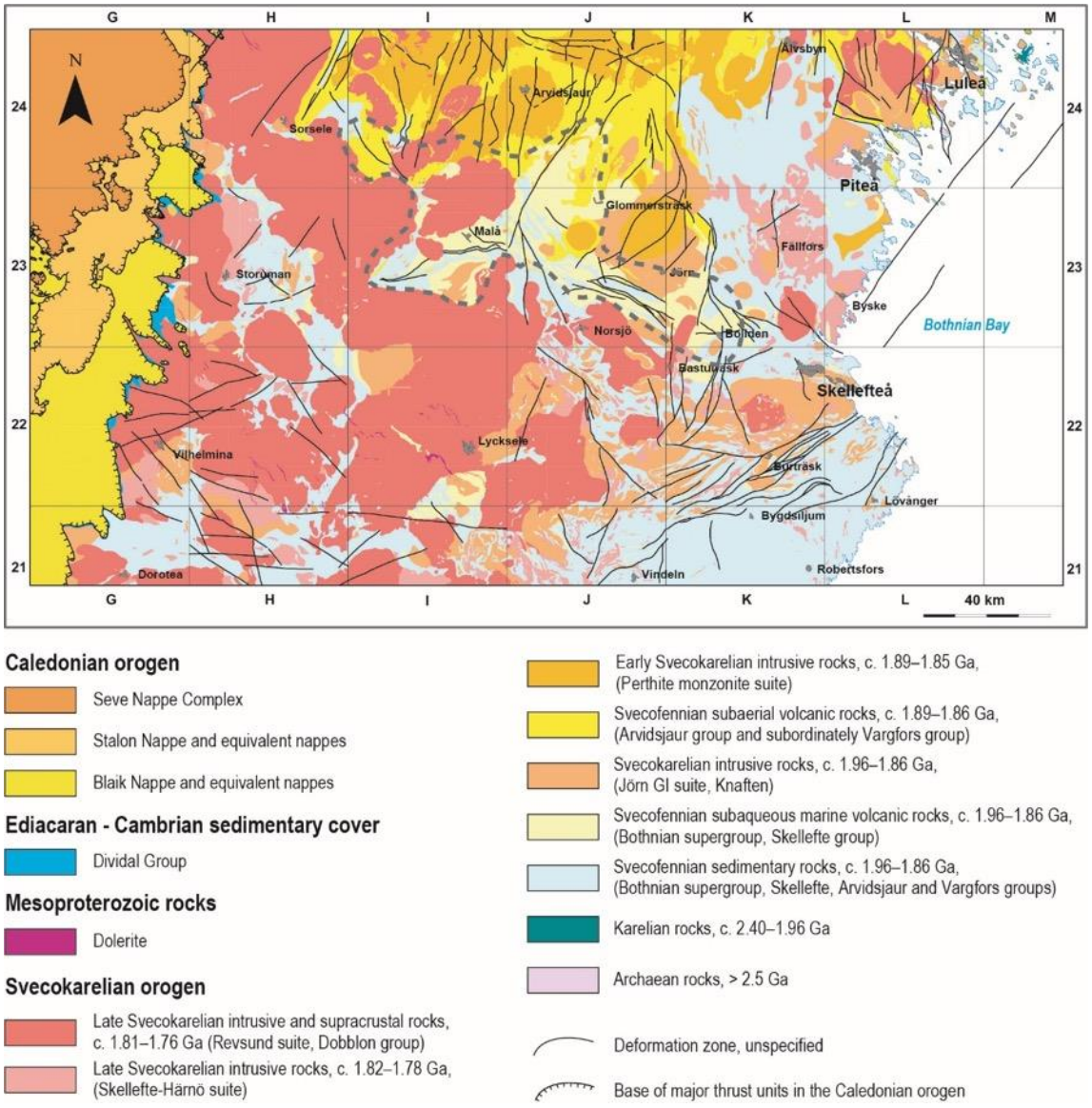

Figure 3. Simplified bedrock map of the Skellefte district and surrounding areas, modified from Kathol & Weihed (2005). The metallogenetic area of the Skellefte district is roughly outlined by a grey, dashed line. Reference grid is the former Swedish National Grid RT90, numbering refers to map sheets of the Swedish land survey.

2.1.3. The Kristineberg area

The Kristineberg area constitutes the southwestern part of the Skellefte district, situated in northern Västerbotten County (Fig. 4). Here, Svecofennian supracrustal rocks form two regional scale, southwest–northeast striking antiforms. The larger, southeastern antiform is cored by a tonalite–granodiorite–granite intrusion, belonging to the early Svecokarelian calc–alkaline granitoids (Jörn GI suite). The northwestern antiform is cored by felsic volcanic rocks (dacites–rhyolite) of the Skellefte group. The antiforms are separated by either a synform (Årebäck et al. 2005) or a large-scale shear zone (Malehmir et al. 2007, Dehghannejad et al. 2010) occurring in the sedimentary rocks of the Vargfors group.

The intrusion, coring the southeastern antiform has been called 'Kristineberg massive' and dated with U–Pb method on zircon (TIMS) to 1907 ± 13 Ma by Bergström et al. (1999). The authors interpreted the Kristineberg massive as either a basement to the rocks of the Skellefte group, or stated, when both rock units are taken as coeval, that the volcanic rocks of the Kristineberg area are older than the volcanic rocks in the eastern and central part of the Skellefte district. Bergström & Sträng (1999) considered the Kristineberg massive to be the result of deeply situated magma-chamber, probably related to the Skellefte group volcanism in the area.

The southeastern antiform enclose two individual second-order west-plunging antiforms, both core by tonalitic (Skyttä et al. 2011) or granitic to tonalitic (Bergström & Sträng 1999) intrusive rocks. The Kristineberg and Rävliden mines and mineralisations are hosted by felsic volcanic rocks of the Skellefte group at the southern limb of the northern second-order antiform.

The intrusion of the 'Kristineberg massive' has in the last decade been reinvestigated by Skyttä et al. (2010, 2011, 2013), who also presented new and more reliable age data by the U–Pb method on zircon (SIMS) for intrusive rocks of what they call the 'Viterliden intrusion' and adjacent volcanic rocks. Skyttä et al. (2011) dated two samples from a hornblende tonalite and a plagioclase porphyritic tonalite each in the southern part of the intrusion. The obtained ages of 1892 ± 3 Ma and 1891 ± 3 Ma imply that the magmatism in the Kristineberg area was synchronous with the 1.89–1.88 Ga early Svecokarelian intrusions of the Jörn GI-suite (Kathol & Weihed 2005) in the eastern part of the Skellefte district which yielded ages in the interval 1.89–1.88 Ga (Bergström et al. 2003, Gonzàles Roldán 2010).

A quartz-plagioclase porphyritic tonalite is considered as the youngest phase of the Viterliden intrusion and has been dated to 1889 ± 3 Ma by Skyttä et al. (2011). A tentative correlation of this tonalite with the Kristineberg 'mine porphyry' suggests that these units are coeval at about 1.89 Ga (Skyttä et al. 2011). According to Kathol & Weihed (2005), a fine-grained, late intrusive facies of the Kristineberg tonalite ('Viterliden porphyry' or 'mine porphyry') has intruded the ore-bearing rocks close to the ore in the Kristineberg mine. Due to the intrusive nature of this 'mine porphyry', the obtained age from the quartz-plagioclase porphyritic tonalite, correlated with the 'mine porphyry' gives a minimum age for the Kristineberg ore deposit. Another minimum is constrained by the age of 1883 ± 6 Ma obtained in a felsic volcanic rock in the hanging-wall of the Kristineberg deposit (Skyttä et al. 2011). Finally, based on these relative tight age intervals, the authors conclude that the Viterliden intrusion may equally have intruded into or locally acted as a basement for the ore-hosting volcanic rocks of the Skellefte group.

The age interval of 1.89–1.88 Ga for the intrusive and supracrustal rocks in the Kristineberg area supports also that the Skellefte group defines a laterally continuous volcanic belt throughout the entire Skellefte district (Skyttä et al. 2011).

In the model of Skyttä et al. (2011), the mineralisation in the Kristineberg area was formed at two main horizons in the volcanic pile by syn-extensional volcanism, mineralisation sedimentation and intrusive activity at c. 1.89–1.97 Ga. Subsequent crustal shortening lead to basin inversion and transposition of the mineralised horizons to the present positions.

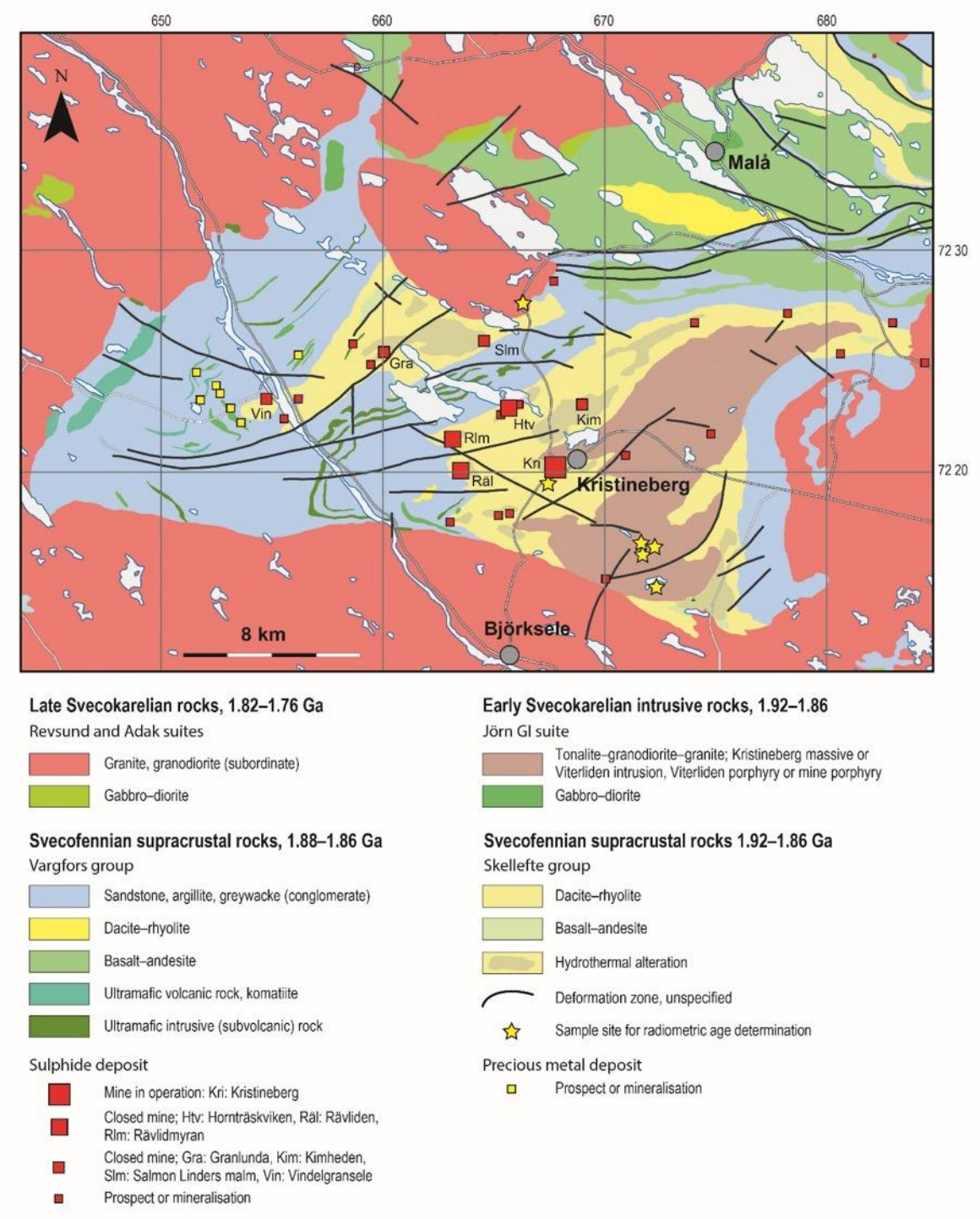

Figure 4. Geological map of the Kristineberg area. Compiled from the SGU databases of maps, mineral resources and bedrock ages. Reference grid SWEREF 99 TM.

Deformation of different intensity has affected the volcanic rocks of the Skellefte group and the sedimentary rocks of the Vargfors group. The deformation intensity is partly a product of the original mica-rich rock, formed by large-scale alteration processes, depending partly on the distance to the important deformation zones separating the bedrock of the Kristineberg area from less deformed rocks to the northwest and north (Kathol & Weihed 2005). These deformation zones are assigned to a major high strain zone which separates deep and shallow crustal domains in the Skellefte district by Skyttä et al. (2012).

The Skellefte group volcanic rocks are mainly rhyolitic subvolcanic intrusions or lava domes and fragment-bearing, locally banded volcaniclastic rocks. Willdén (1986) suggested that the volcaniclastic rocks occupied longitudinal synvolcanic depressions or rifts, formed during extensional phases of the Skellefte group volcanism. The depressions also focused later mafic volcanism, mainly emplaced as subvolcanic sills, and hydrothermal activity. The sericite and chlorite alteration processes affected large volumes of rocks, where original textures can only very rarely be observed. To the south, higher grade metamorphism formed andalusite–cordierite-bearing assemblages in analogous rocks. Magnetite is another important alteration mineral and alteration zones are generally outlined by their magnetic patterns (Fig. 5).

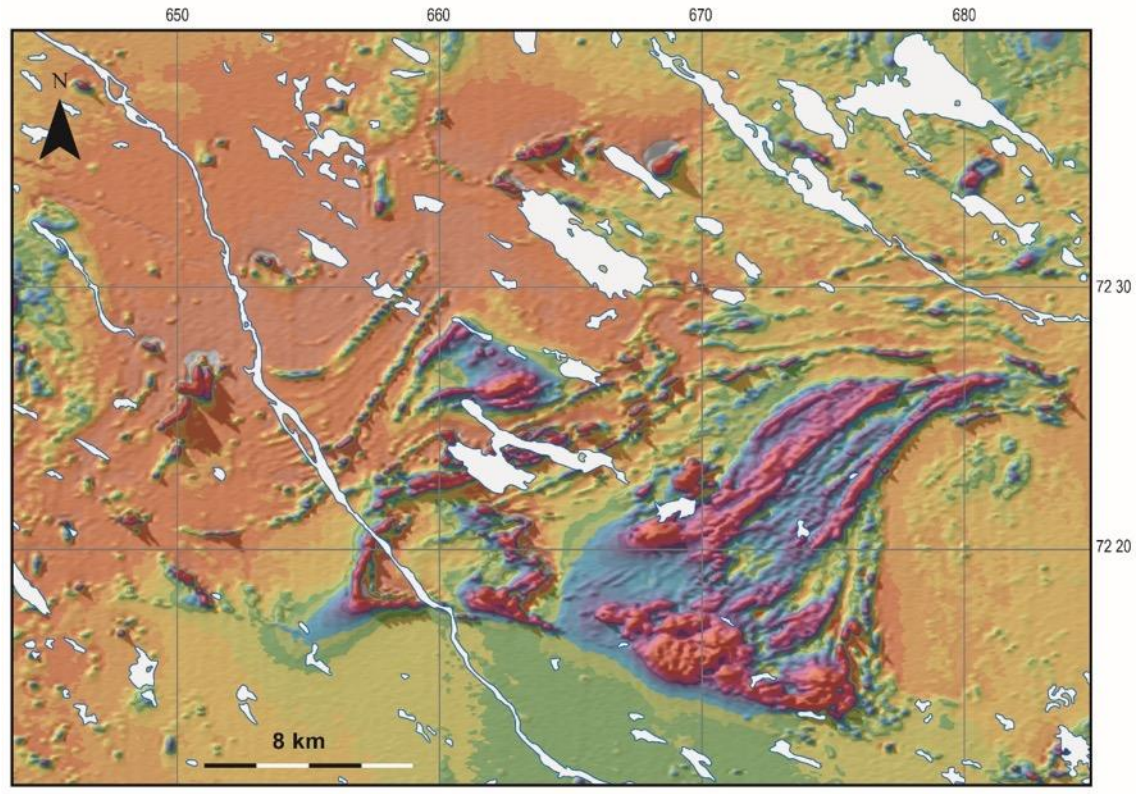

Figure 5. Total magnetic field anomaly map (no field values assigned) of the Kristineberg area. Reference grid is SWEREF 99 TM.

Several ore types are present in the Kristineberg area. The large Kristineberg deposit was a massive pyrite ore body with zinc–copper–gold–silver, which has been deformed into several ore lenses. The Kristineberg deposit was described by Du Rietz (1953), Edelman (1963), Willdén (1986), Vivallo & Willdén (1988) and Årebäck et al. (2005). Further to the north, the massive–disseminated Kimheden pyrite–chalcopyrite deposit occurs at the same structural level as the Kristineberg deposit. Kimheden deposit is hosted by strongly deformed and chlorite-altered volcanic rocks.

In contrast to Kristineberg and Kimheden, the stratigraphic position of the VMS deposits of the Rävliden area further to the west is somewhat different. There, the ores are strongly stratigraphically controlled and occur along the contact between the volcanic rocks and the overlying Vargfors group sedimentary rocks. The favourable ore horizon in the Rävliden area is characterized by small sedimentary intercalations hosted by felsic volcaniclastic rocks. The Rävlidmyran deposit consists of one large pyrite–chalcopyrite ore body and several smaller, zinc–lead-bearing lenses, often associated with strongly deformed argillitic intercalations. In the Hornträskviken deposit, lenses of zinc–lead ore are restricted mainly to small carbonate occurrences. The Rävliden deposit includes one copper-rich ore lens and one zinc-rich lens, situated adjacent to each other.

Further to the south, the small low-grade Mörkliden ore bodies occur along the same stratigraphic horizon. They are mainly sphalerite–chalcopyrite disseminations with very little ferric oxide. The Nyborg deposit to the north is another example of the similar sphalerite disseminated type. The Vindelgransele area hosts only small VMS mineralisations, for example the high-grade Vindelgransele deposit.

The Kristineberg deposit is one of the largest polymetallic volcanogenic massive sulphide (VMS) occurrences in the Skellefte district. It was discovered in 1918 using electromagnetic survey techniques. Due to logistical issues, related to transportation of the ore through swampy areas and forests, production was only initiated once a 96 km long cable way ("Linbana") was constructed in 1941. This cable way connected Kristineberg mine to the concentrator plant set up in Boliden after the discovery of the Boliden ore body in 1927. Up until 1987 the cable way was in use but then was replaced by trucks which are still used today for transporting ore to Boliden (Bauer et al. 2013).

Figure 6. Kristineberg mine with the head frames. Photo: Benno Kathol.

2.1.4. The Kristineberg mine

The Kristineberg mine (65° 03' 48'' N, 18° 34' 00'' E) is the oldest and largest massive sulphide mine in the Skellefte district which has been in continuous operation until today. Mining began in the year 1940 at the orebody which outcrops at surface. Since then production has reached down to around 1 200 m making it one of the deepest mines in Sweden. Some 26.5 million tons of ore were mined at an average grade of 3.56 % zinc, 1.31 g/t gold, 38 g/t silver, 1.05 % copper, 0.24 % lead and 25.6 % sulphur (Bauer et al. 2013). According to the Fennoscandian ore deposit database (see also Eilu et al. 2013), 31 million tons were mined until 2017, reserves are 5 million tons and resources about 13 million tons. The combined grades of mined ore, reserves and resources are 3.9 % zinc, 0.7 g/t gold, 44 g/t silver, 0.9 % copper and 0.4 % lead. The ore is a complex massive sulphide with zinc being the main metal, although in some areas copper-gold ores are mined. The predominant mining method is cut-and-fill with some rill mining. (Bauer et al. 2013).

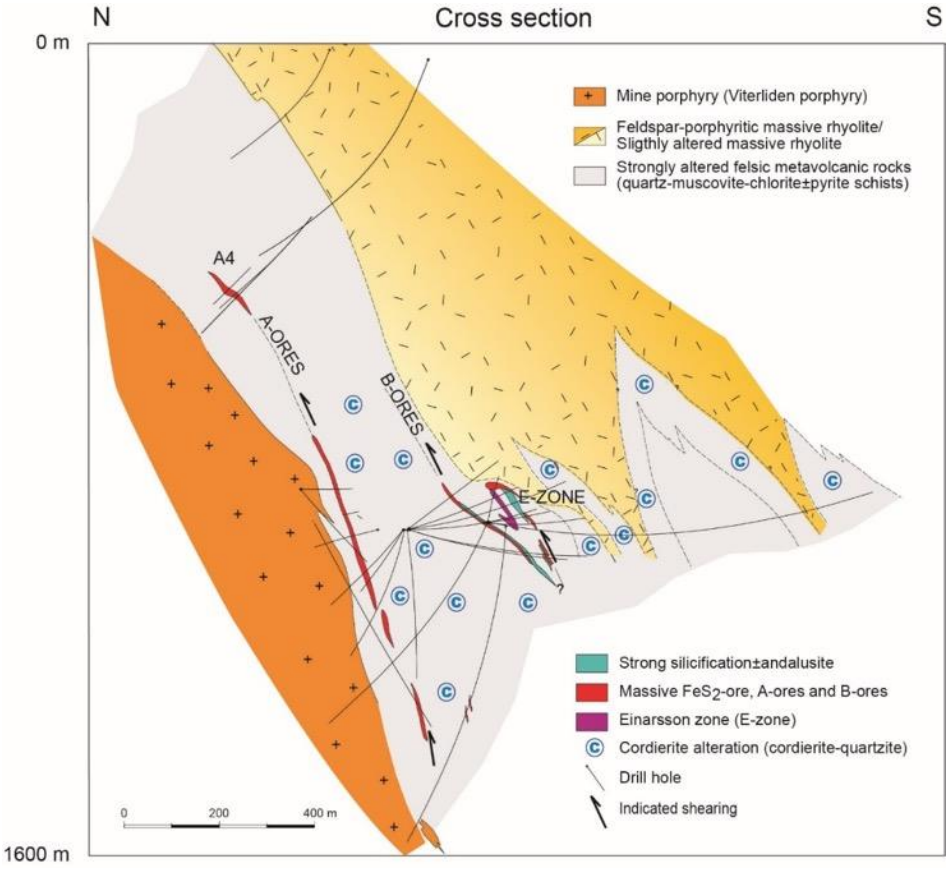

Figure 7. Cross section through the Kristineberg deposit. From Årebäck et al. (2005).

Both, the Kristineberg- and the nearby Kimheden deposit to the north represent an ore horizon which seems to be developed rather deep in the volcanic stratigraphy, compared with many other similar deposits in the Skellefte district. The Rävliden horizon is developed in the upper part of the volcanic pile and occurs about 3 km west of Kristineberg (Fig. 4). In the latter, abundant calc-silicate assemblages and some marble associations occur which are only locally observed at the Kristineberg–Kimheden horizon. Tonnages and grades in the mined deposits in the Kristineberg area are shown in Table 1.

The rocks surrounding the Kristineberg deposit have been strongly hydrothermally altered and are multiphase folded and strongly sheared. The schistose rocks are now dominated by quartz–muscovite–chlorite–pyrite in varying proportions, and exhibit marked sodium depletion and co-enrichment of magnesium and potassium. Cordierite, phlogopite and andalusite occur in considerable amounts. Kyanite has rarely been observed, mainly associated with quartz veins. In general, the iron–magnesium alteration minerals are magnesium-rich, and the modal chlorite content increases towards the Kristineberg ore horizon, which is surrounded by a halo of more muscovite-rich rocks. Due to the strong alteration, the rocks near the Kristineberg mine are connoted as ‘schists and quartzites’ (see Fig. 10), as it is hard to recognise the nature of the volcanic protoliths.

The bedrock of the Kristineberg deposit is shown in cross-section (Fig. 6). The mine porphyry (Viterliden porphyry) occurs in the footwall of the Kristineberg deposit, and a massive, feldspar-porphyritic rhyolite

Table 1. Production tonnage and grades of the VMS deposits in the Kristineberg area. From Kathol & Weihed (2005).

Mine	**In operation** (year)	**Tonnage** (Mt)	**Gold** g/t	**Silver** g/t	**Copper** %	**Zinc** %	**Lead** %	**Sulphur** %
Kristineberg*	1940-	21.1	1.05	36	1.04	3.64	0.24	25.9
Kimheden	1968-1970 1974-1975	0.13	0.44	7	0.95	0.27	-	18.4
Rävlidmyran	1950-1991	7.18	0.79	51	0.95	3.96	0.54	17.8
Rävliden	1941-1950 1966-1988	1.56	0.45	90	1.00	4.23	0.79	16.9
Hornträskviken M.	1981-1991	0.64	0.71	72	1.01	4.90	0.67	11.1
Total	1941-2001	30.3						

* To year end 2001, excluding Einarsson Au-Cu lenses

Table 2. Increased metal content in surrounding formations being of crucial importance for a CHPM system: Chemical data from rock volumes, (a) 500 m and (b) 1000 m away from the modelled ore bodies at Kristineberg. Data by courtesy of Boliden Mines.

a) Metal content 500 m away from ore body
532 samples

Metal	**Ag** ppb	**Au** ppb	**Co** ppm	**Cu** ppm	**Mo** ppm	**Ni** ppm	**Pb** ppm	**Sn** ppm	**W** ppm	**Zn** ppm
Min	0	0,05	0,1	0,05	0,05	0,05	0,3	0,4	0,2	0,5
Max	5500	472	379	1081	122	326	1857	14	2386	4386
Average	317,2	13,1	10,1	44,4	3,3	9,0	17,0	1,8	10,1	124,6

b) Metal content 1000 m away from ore body
350 samples

Metal	**Ag** ppb	**Au** ppb	**Co** ppm	**Cu** ppm	**Mo** ppm	**Ni** ppm	**Pb** ppm	**Sn** ppm	**W** ppm	**Zn** ppm
Min	50	0,05	0,1	0,05	0,05	0,05	0,3	0,5	0,2	0,5
Max	5100	472	379	1081	122	326	162	14	2386	1805
Average	261,3	15,4	11,7	45,4	3,2	10,8	9,3	1,9	13,7	80,4

forms the hanging wall. Close to the deposit, this rhyolite gradually becomes slightly to moderately muscovite±chlorite-altered. The intervening ore hosting sequence consists of strongly altered and schistose volcanic rocks. The dominating mineral assemblage of this unit is quartz–muscovite–chlorite–phlogopite–pyrite±andalusite±cordierite.

2.1.5. Geochemical analyses

The ore grades of the Kristineberg ore bodies have been described in the chapter “The Kristineberg mine”. Increased metal contents occur also in zoned rock volumes around the ore bodies. These alteration and compositional envelopes interfinger with each other, resulting in larger rock volumes with increased metal contents, which are therefore of interest for a CHPM system.

Figure 8 shows a three-dimensional model over the bedrock hosting the Kristineberg deposit and the sample sites for chemical analyses more than 500 m (a) and 1000 m (b) away from the ore bodies. In the model, the analysed rocks of the ore bearing Skellefte group, mainly dacite–rhyolite and a transition zone, have been omitted to make the sample sites visible. These sites are indicated by light yellow or light grey spheres which represent analyses of dacite–rhyolite and the transition zone, respectively. Most of the samples were taken from drill cores, but some samples stem from surface outcrops or from drill cuttings. Analyses of other rock types were omitted also both from the models in Figure 8 and from Table 2, as they are not relevant for this project. Table 2 shows maximum, average and minimum contents of several metals found in the host rocks.

Similar zonations in metal contents or envelopes have been found at the other VMS-deposits in the Kristineberg area (Kimheden, Rävliden, Rävlidmyran and Hornträskviken) and can also be expected around deeper situated, at present unknown mineralisations or deposits in the felsic volcanic rocks (dacites–rhyolite) of the area. This means that an increased metal content can be expected in larger rock volumes of the Skellefte group dacites–rhyolites, which occur at levels deeper than the at present known mineralisations. Three-dimensional models and descriptions of volcanic-hosted massive sulphide (VMS) deposits and associated host rocks are found (summarised) in Bauer et al. (2015).

2.1.6. Drill holes

The pattern of drill holes in and around the Kristineberg mine is shown in Figure 9a. Many of the drillings were carried out as diamond drilling. Drill cores are stored in the Boliden archives. By courtesy of Boliden Mines, photos of two entire cores from drill holes KRC4407 and KRC4317 were available for this project (Fig. 9b, c and Fig. 10).

Bore hole KRC4407 was drilled from the southwestern part of the mine at a depth of approximately 1200 m. The direction of this bore hole was almost horizontally to the south (Fig. 9b), which makes it more likely that vertical and subvertical fractures or brittle deformation zones are recorded by the received drill core. Drill hole KRC4317 was drilled from a depth of c. 1000 m with a steeply dipping direction to the north (Fig. 9c). Thus, the drill core from this hole more likely reports the occurrence of flat lying fractures or brittle deformation zones. In Figure 10a-d, a section of crushed drill cores, probably representing a brittle deformation zone and relatively unbroken cores from more massive rock volumes are shown for both drill holes each.

In both drill holes, and so in the Kristineberg area, the degree of alteration of rocks is more critical for the fracture density than differences in the original rock types, as, e.g., coherent volcanic rock or volcaniclastic rock (pers. com. Lena Albrecht, Boliden Mines).

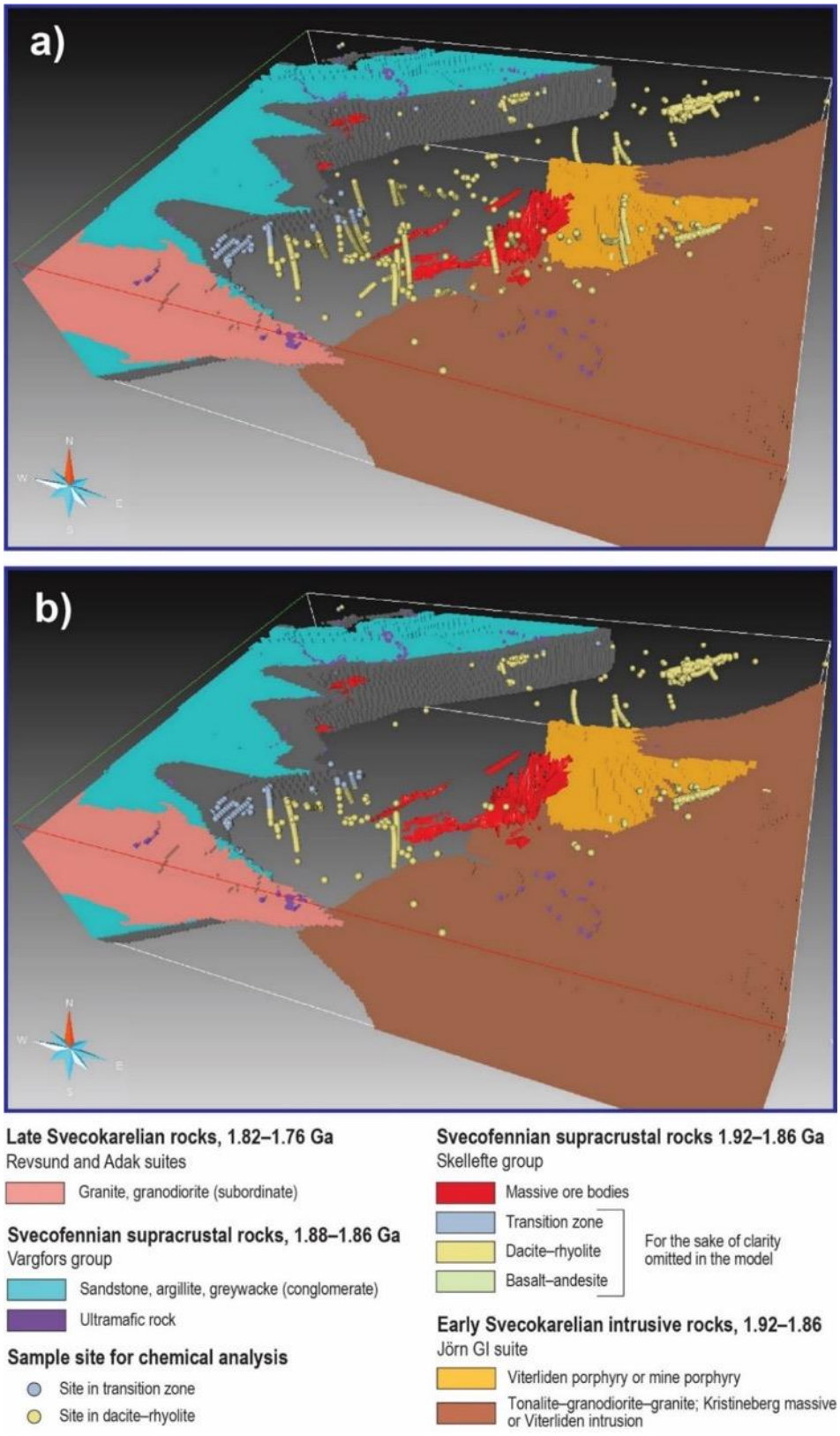

Figure 8. Three-dimensional model (unscaled) of the bedrock around the Kristineberg mine, showing sample sites for chemical analyses at distance of more than 500 m (a) and 1000 m (b) from the ore bodies. View towards the north-northwest. By courtesy of Boliden Mines.

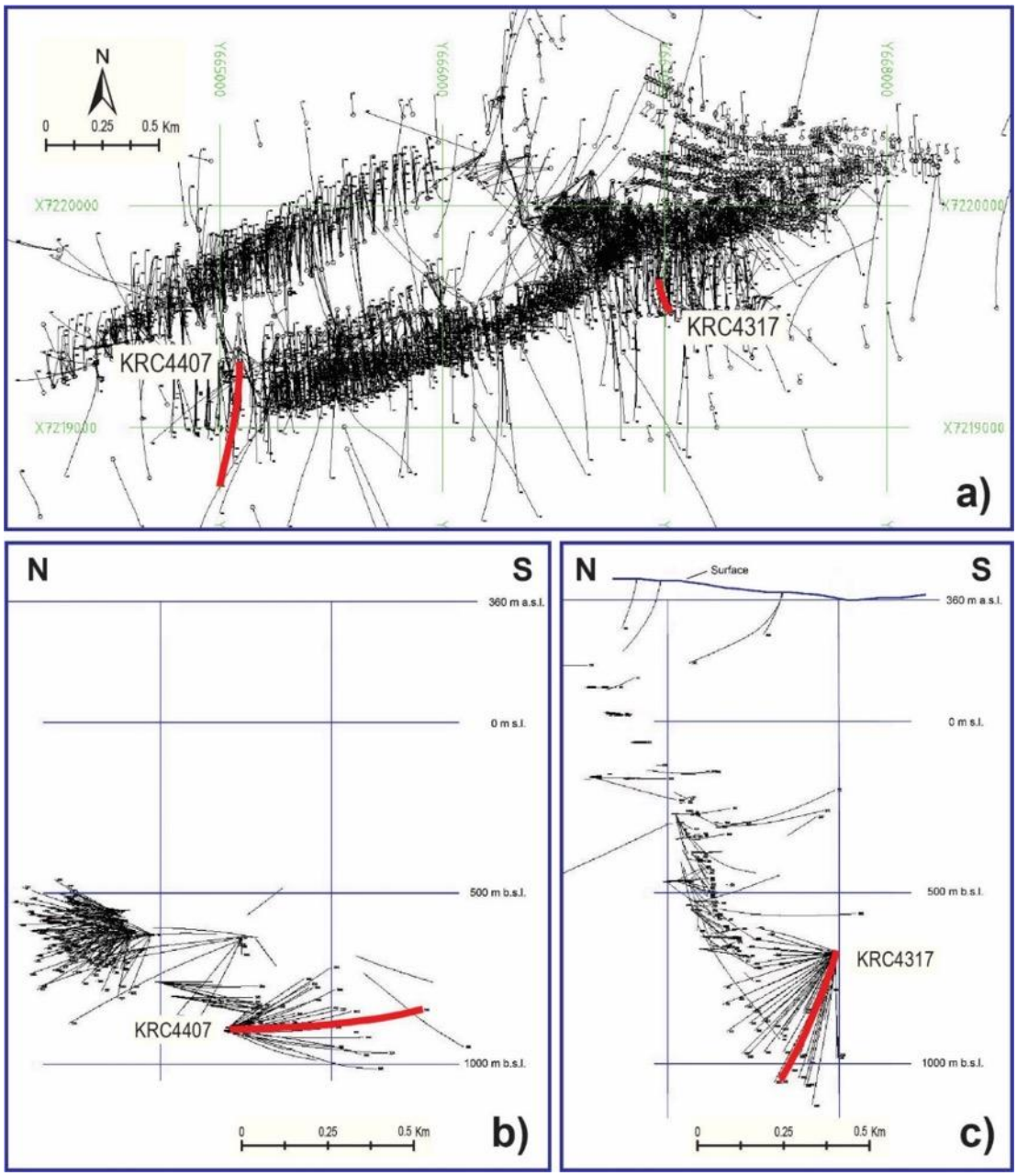

Figure 9. Drill hole maps from the area of the Kristineberg deposit. **A**. Horizontal projection of almost all drill holes around the Kristineberg deposit, view from above. The positions of drill holes KRC 4317 and KRC4407 are marked with red lines. **B**. Vertical projection of drill holes in a narrow, roughly north-south striking section around drill hole KRC4407, the latter marked with a red line. **C**. Vertical projection of drill holes in a 100 m wide north–south striking section around drill hole KRC4317, the latter marked with a red line. By courtesy of Boliden Mines.

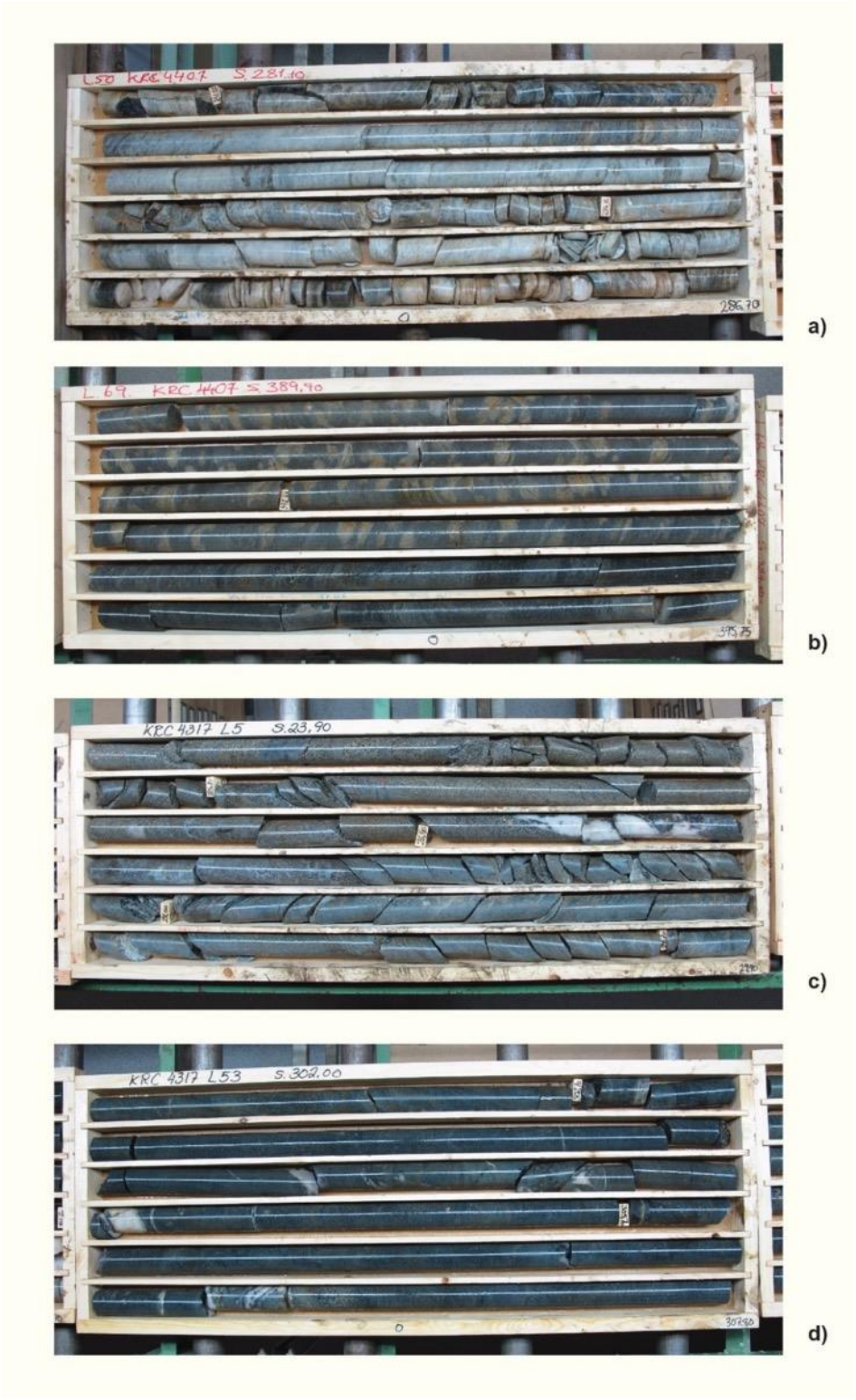

Figure 10. Photos of drill core sections from drill cores KRC4317 and KRC4407. Fractured cores are giving indications of the present and past stress regime in the crust. **A**. Crushed drill core of cordierite quartzite and sericite quartzite, 281,10–286,70 m, drill core KRC4407. **B**. Massive drill core of cordierite quartzite, 389,90–395,75 m, drill core KRC4407. **C**. Crushed drill core of chlorite schist, 23,90–29,90 m, drill core KRC4317. **D**. Massive drill core of chlorite quartzite, 302,00–307,80 m, drill core KRC4317. Photos by courtesy from Boliden Mines.

2.1.7. Geophysics in the Kristineberg area

The Geological Survey of Sweden has a long-standing tradition in geological mapping of the country, especially with the support from airborne geophysics, which is necessary due to the low degree of bedrock exposures. These surveys have acquired data on the Earth magnetic field (e.g., in the Skellefte district, Fig. 5), gamma radiation and the VLF electromagnetic field. In addition to these surveys the gravity field of the Earth was measured using ground-based techniques (see also CHPM2030, D 1.2, Schwarz et al. 2016).

Exploring mineral deposits in more detail by geophysical methods was conducted by the mining industry and partly with the help from academia. Potential field and electrical investigations were in the forefront of these studies. In the last two decades, reflection seismic studies became more attractive even in hard rock imaging for prospecting after minerals and ores in the Earth's uppermost crust, owing to their ability in better resolving geological structures (e.g., Malehmir et al. 2012). Tryggvason et al. (2006) and Rodriguez-Tablante et al. (2007) studied the Kristineberg area in the western Skellefte district while Malehmir et al. (2006) extended these investigations further to the east. The western part of the Skellefte district is well documented by boreholes reaching depths greater than 1000 m, high resolution potential field data, i.e., magnetic and gravity, as well as by petrophysical data. Investigations in the Kristineberg area were followed up by employing magnetotellurics (MT) on one of the seismic lines allowing for the joint interpretation of velocity and electrical resistivity data (Hübert et al. 2009). Malehmir (2007) has summarized the outcome of this pilot study: A strong north-dipping reflection in conjunction with higher electrical conductivity is interpreted as the structural basement for the rocks of the Skellefte group (for a map see Fig. 11), though debated. Late Svecokarelian granites were modeled down to various depths between one and five kilometres.

The Kristineberg area was further investigated by using electromagnetic and seismic methods. Between 2002 and 2012, four reflection seismic lines were acquired around the Kristineberg mine (Fig. 11) and further three in the central and eastern Skellefte district, revealing numerous reflections from the top 12 km of the crust. The data also show a series of steeply dipping to sub-horizontal reflections. Some of these reach the surface and allow correlation with geological structures (Dehghannejad 2014).

Figure 12 visualizes seismic reflection data on profiles 1, 2, and HR from the Kristineberg area, where the ore deposits can directly be associated with reflected and diffracted signals. A deeper cluster of reflections describes a high contrast in impedance, but it is unclear whether this is related to some increase in ore content. Dehghannejad (2014) has further analysed the data concluding the mineralisation and associated structures dipping to the south down to at least 2 km in depth. Further re-processing of the seismic data allowed identifying reflections not recognized before. Dehghannejad et al. (2012) suggest this finding to be a target for further mineral exploration in the Kristineberg area, including the contact between the metasedimentary and metavolcanic rocks at depth.

2.1.8. Electrical resistivity studies

Electrical resistivity was studied at larger scales by, e.g., Jones et al. (1983) and Rasmussen et al. (1987). Magnetotelluric investigations within the Fennolora project (Rasmussen et al. 1987) have revealed a crustal zone of higher electrical conductivity. It is extending laterally more than 150 km, centered on the Skellefte district and considered having at least a thickness of 15 km. New magnetotelluric data acquired on a larger scale in north-west Fennoscandia by Cherevatova et al. (2014, 2015a, b) and Korja et al. (2008) confirm the highly conductive belt in the Skellefte district, assigning it a total conductance of more than 1000 Siemens. The anomalous structure is now interpreted as representing shallow graphitic shales of low thickness, embedded in the otherwise resistive crust.

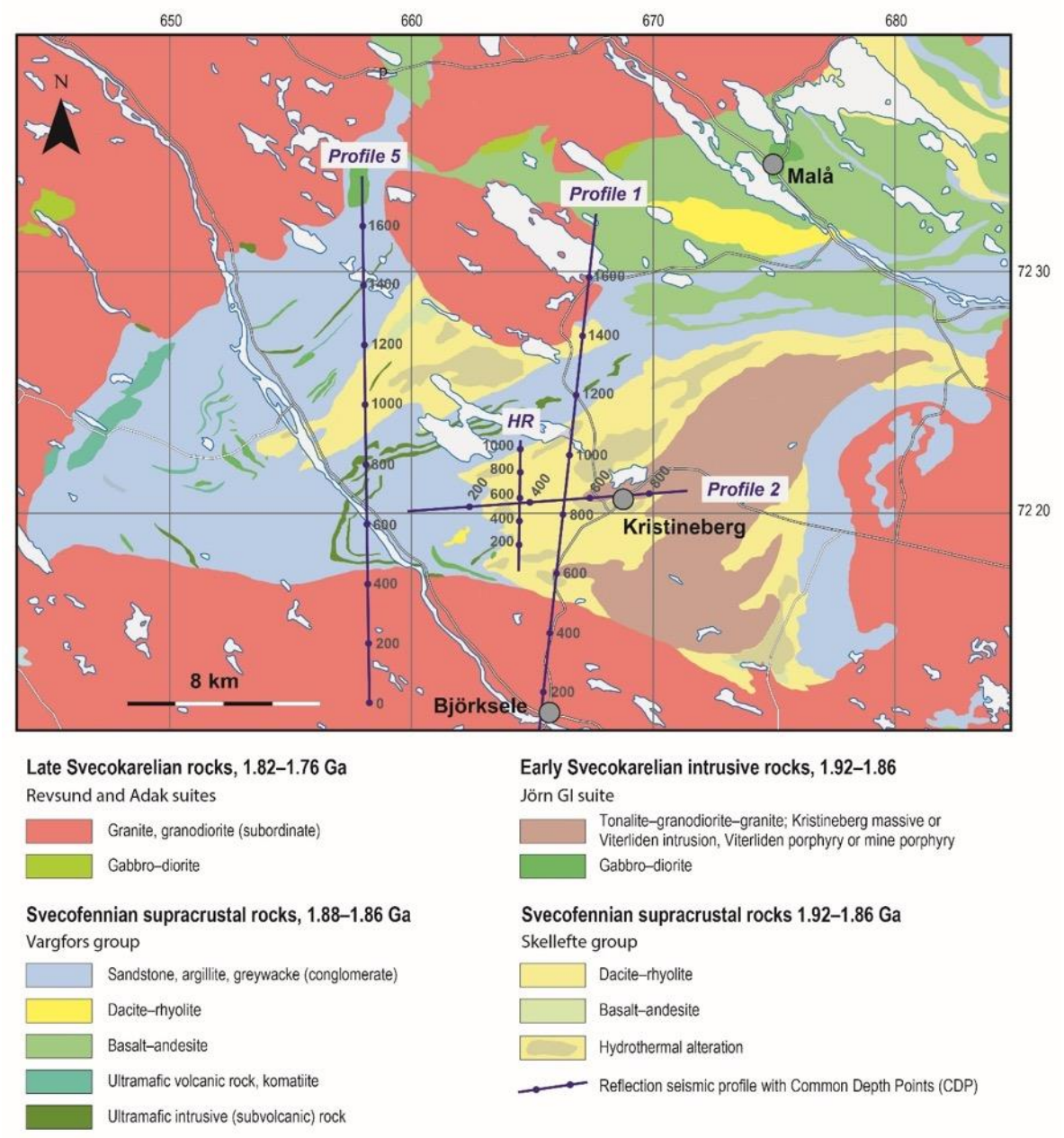

Figure 11. Geological map of the Kristineberg area where, e.g., reflection seismic and magnetotelluric investigations of the upper crust were done. Profiles 1, 2, 5 and HR are shown as black lines with common depth points indicated (Dehgannejad et al. 2012a).

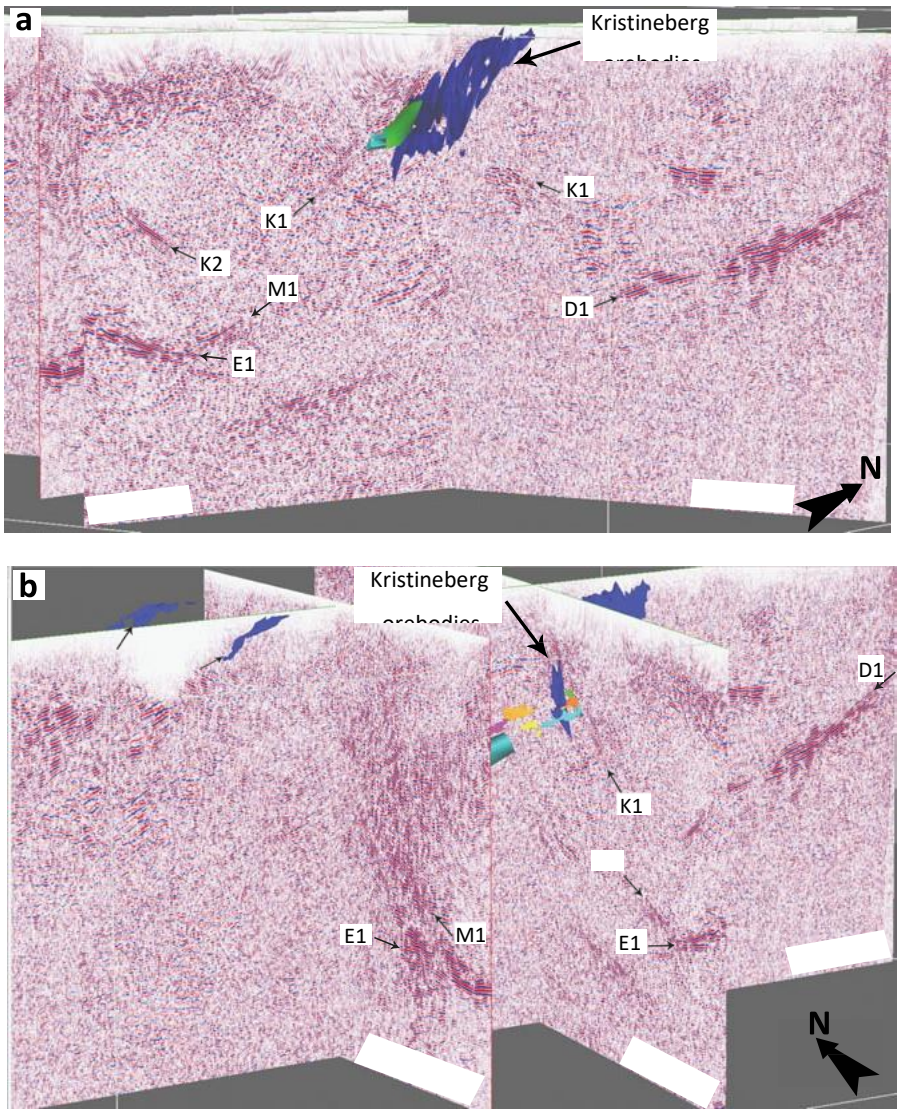

Figure 12. Seismic cross sections with migrated profiles 1, 2 and the HR profile, and mineralisation surfaces from borehole data in the Kristineberg mine (after Ehsan et al. 2012). Reflection K1 correlates with the mineralization horizon (dark blue, green, light blue), belonging to the Rävliden massive sulphide deposits. Section depth is 3800 m, no exaggeration. a) View towards the northwest. B) View towards the northeast.

Among others, e.g., Hübert (2012), Garcia Juanatey (2012), Bauer et al. (2014) and Tavakoli et al. (2012a, 2012b, 2016a, 2016b) further studied the central Skellefte district, to delineate the structures related to VMS ore deposits and to model lithological contacts down to depths of some hundreds to some thousands of metres. The complexity of data necessitated 3D-modelling, where data of geomagnetic deep soundings (GDS), reflection seismics and geological observations were considered, too.

The model developed by Hübert (2012) and Garcia Juanatey (2012) shows distinct contrasts in electrical resistivity with values from several 1000 Ωm to less than 1 Ωm (Fig. 13). Beside some very shallow good conductors, those ones at larger depths are much more prominent, named CI and CIII in Figure 13. CI is said to correspond with the crustal zone of higher electrical conductivity in the Skellefte district, earlier identified by Rasmussen et al. (1987). It is located at about 4 km depth, a value that is well determined. But,

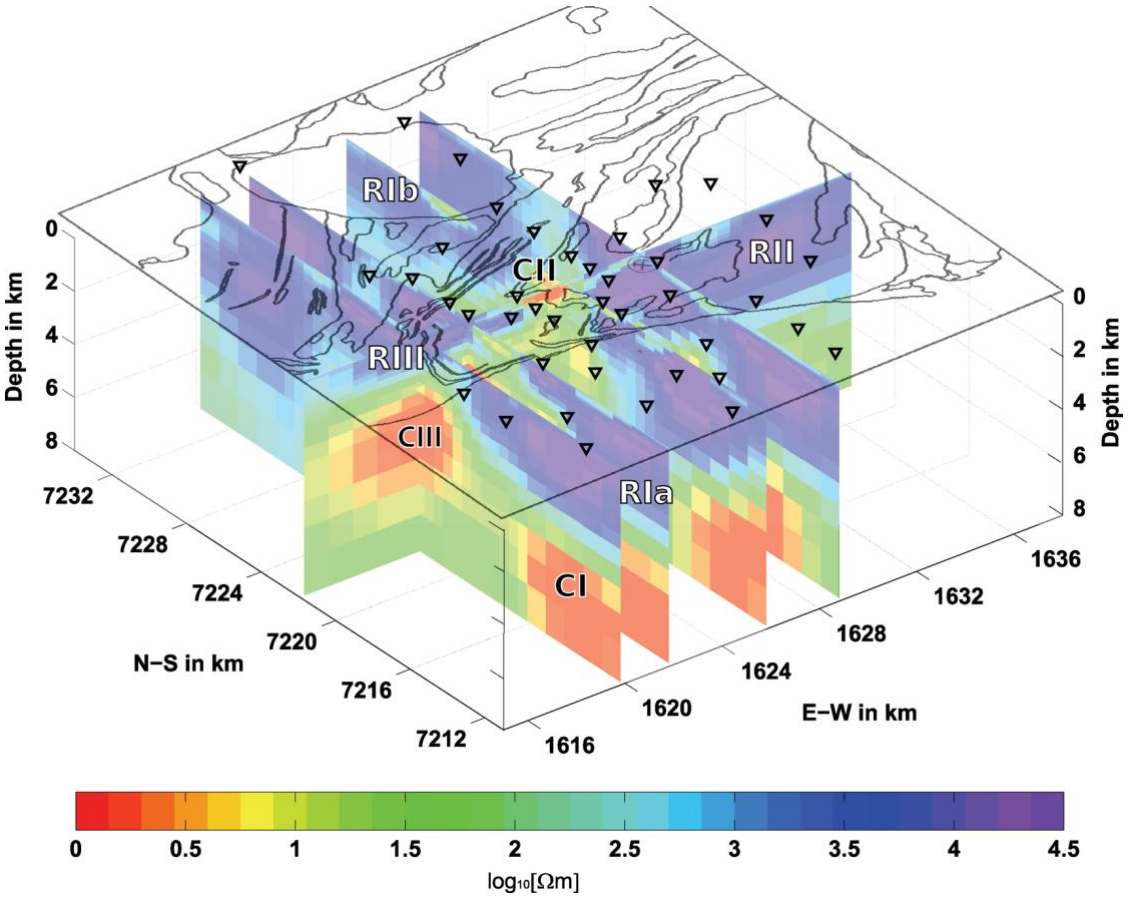

Figure 13. 3D electrical resistivity model of the Kristineberg area, cut into slices (Hübert et al. 2013). On surface, outline of geological structures and position of MT measuring sites (triangles). Coordinate system *Swedish Grid RT90* (in km). Resistors associated with, RIa, RIb: Revsund granite; RII: Viterliden intrusion; RIII: Mafic dykes within the metasedimentary rocks; Conductors related to CI: Skellefte crustal conductivity anomaly; CII: black shales at the base of the metasedimentary rocks; CIII: alteration or mineralised zones (?) in metavolcanic rocks.

because of limited data extend, thickness constraints are unsecure. CI vanishes towards the north, and likely even towards the east which can be inferred from GDS data. Conductors at intermediate depth, downward from about 2 km, are of unknown origin. Hübert et al. (2013) explain them by alteration zones of increased ore content in the volcanic rocks. The very shallow conductors named CII around Kristinberg are only about 200 m thick. They can be explained with black shales rich in graphite, encountered at the base of the sedimentary rocks of the Vargfors group and confirmed by shallow borehole data (T. Hermansson, pers. comm.). The sedimentary rocks show medium resitivities of 30 to 300 Ωm, while the volcanic rocks of the Skellefte group have no unique resistivity values. Depending partly on their degree of alteration, these rocks are not easily to differentiate from the sedimentary rocks and the Viterliden intrusion.

Apart from the superficial conductors CII, uppermost crustal structures have high electrical resistivity. Most obvious are resistors RIa, RIb that have several 1000 Ωm (see Figure 13) with maximum thickness in the south of 3 to 4 km, and more than 5 km in the north. Geologically, they can be associated with the Revsund granites. Resistor RII appears sheet-like and in its northern extend it matches with the contact zone of sdimentary and volcanic rocks of the Vargfors and the Skellefte groups, respectively. Well conducting black shales as reported about above, seem to be absent at this contact. The resistive feature RIII extents less than 2 km in depth and might be linked to mafic dykes within the sedimentary rocks and having a distinct magnetic foot print (Malehmir et al. 2007).

2.1.9. Modelling

In geophysical modelling the strategy behind is essential, e.g., 3D modelling is to prefer 2D modelling, independent of the method. The interpretation of structural settings of individual mineralisations or areas of interest is normally based on combinations of surface data, drill core analyses, geophysical data and 3D- and 4D-modelling, the latter including bedrock evolution in geological times. For deeper structures and mineralisations, geophysical data are often the only available means for 3D evaluation unless drilling has been performed. Examples of 3D- (and 4D-) modelling that relate to Swedish bedrock conditions are Bauer (2013), Bauer et al. (2009, 2010, 2011, 2012, 2014), Malehmir et al. (2009), Carranza and Sadeghi (2010), Kampmann (2015), Skyttä et al. (2009, 2012, 2013), Wareing (2011) and Weihed (2014).

The 3D model inversion of electrical resistivity data from Kristineberg compared with 2D modelling, for computational reasons is using a wider grid and less data as input (Hübert 2012, Garcia Juanatey et al. 2011). Therefore, the 3D model is showing less resolution though the depth of conductors CI and CIII is comparable with that one obtained in 2D modelling. But, it indicates differences in extent and values of high conductivity zones. In 2D models, especially the intermediate and deep conductors (CI, CIII) have much larger depth extent. This is regarded as being due to 3D effects, i.e., lateral effects in data observed.

2.1.10. Combining seismic and magnetotelluric results

Hübert et al. (2012) have compared surface geology and seismic reflectors in the upper crust identified on profiles 1 and 5 with slices of their 3D resistivity model, as shown in Figure 14. Profile 1 displays the lower boundary of resistor RIa associated with the southern Revsund granites and coinciding with an increase of reflectivity, while the uppermost crust is much less reflective. The deep conductor below, CI, in its extent does not resemble seismic reflectors, beside its lower bound in south-southwest. Conductor CIII is positioned in a zone of less distinct reflections. The anticline where the Kristineberg mine is established (marked E in Fig. 14) is not specially resolved in the model.

The section along profile 5 (Fig. 14, lower) evinces lateral boundaries of electrical resistivity where even seismic reflectivity is changing. In the southern part, the top of the deep conductors seems to be bound by seismic reflectors dipping to the north. Resistors RIII and RIb are separated from each other by a zone of higher reflectivity which might be related to many mafic dykes within the sedimentary rocks (Hübert et al. 2012).

Malehmir et al. (2009) have composed 2.5- and 3D-models of the Kristineberg area, compiled from potential field-, seismic reflection-, borehole- and geological data (Fig. 15). A transparent seismic reflection zone observed above the zone of north-dipping reflectivity (Fig. 15a) is explained to belong to volcanic rocks of the Skellefte group (Tryggvason et al. 2006). The role of structures below, interpreted by Malehmir et al. (2009) as representing the basement, is debated (e.g., T. Hermansson, pers. comm.). The inversion of gravity data was most effective owing to the high density contrast in lithology, though structures, e.g., dykes, faults and folded and deformed units are rather complex in the area. In the modelling process, seismic data were a key component for providing constraints for geological units. Modelling of magnetic data could have been improved if magnetic properties of rocks should have been available. This should have required rock magnetic measurements on a larger number of samples in the laboratory.

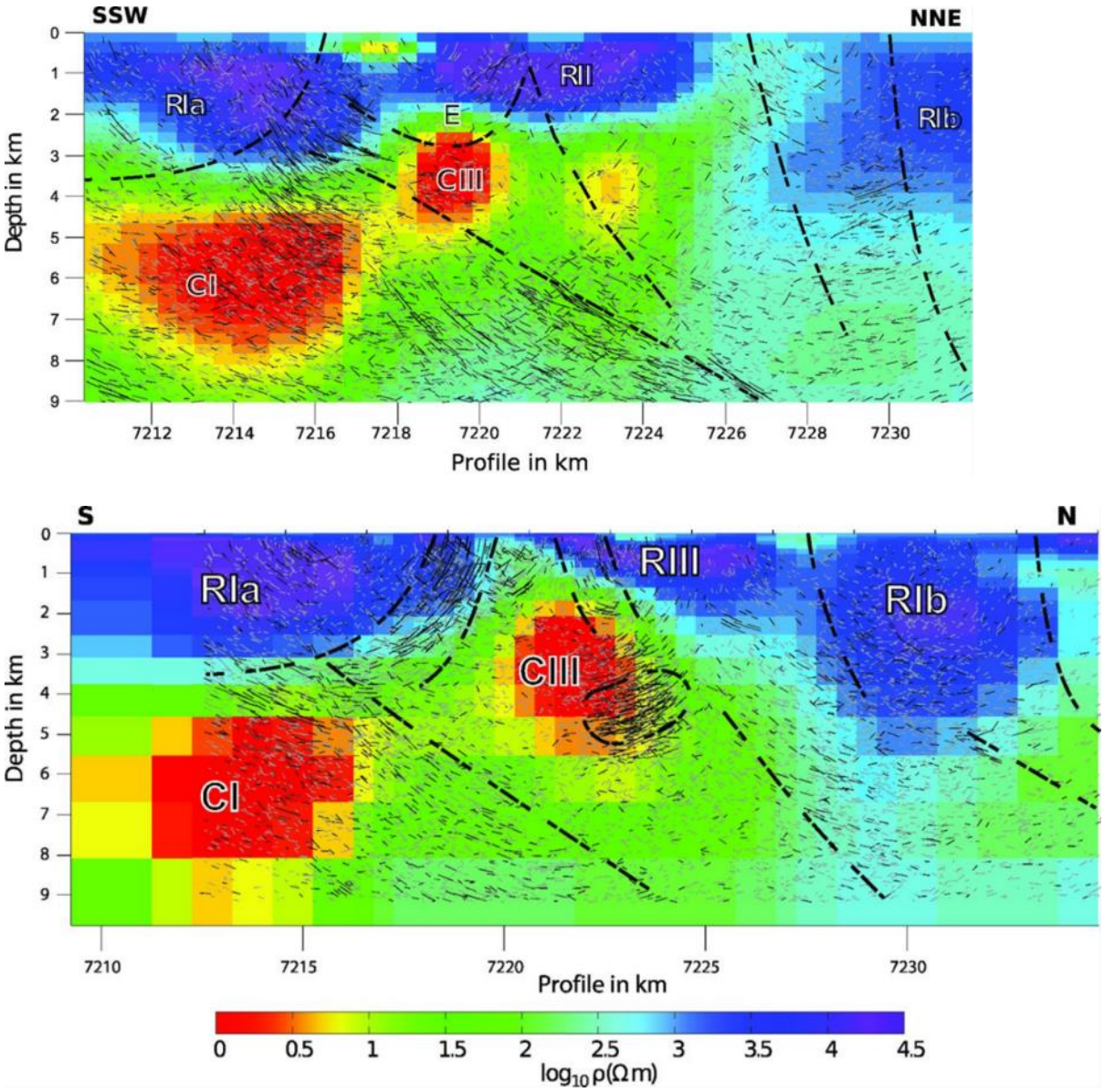

Figure 14. Sections through 3D resistivity model (Hübert et al. 2013), together with seismic reflections along profiles 1 (top) and 5 (bottom) (Malehmir et al. 2007). See Figure 11 for locations of the profiles. Thick dashed lines mark interpreted seismic structures. E in section of profile1 (top) section marks the assumed anticline, hosting Kristineberg mine. RIa, RIb: Revsund granite; RII: Viterliden intrusion; RIII: Mafic dykes within the metasedimentary rocks; Conductors related to CI: Skellefte crustal conductivity anomaly; CII: black shales at the base of the metasedimentary rocks; CII: alteration or mineralised zones (?) in metavolcanic rocks.

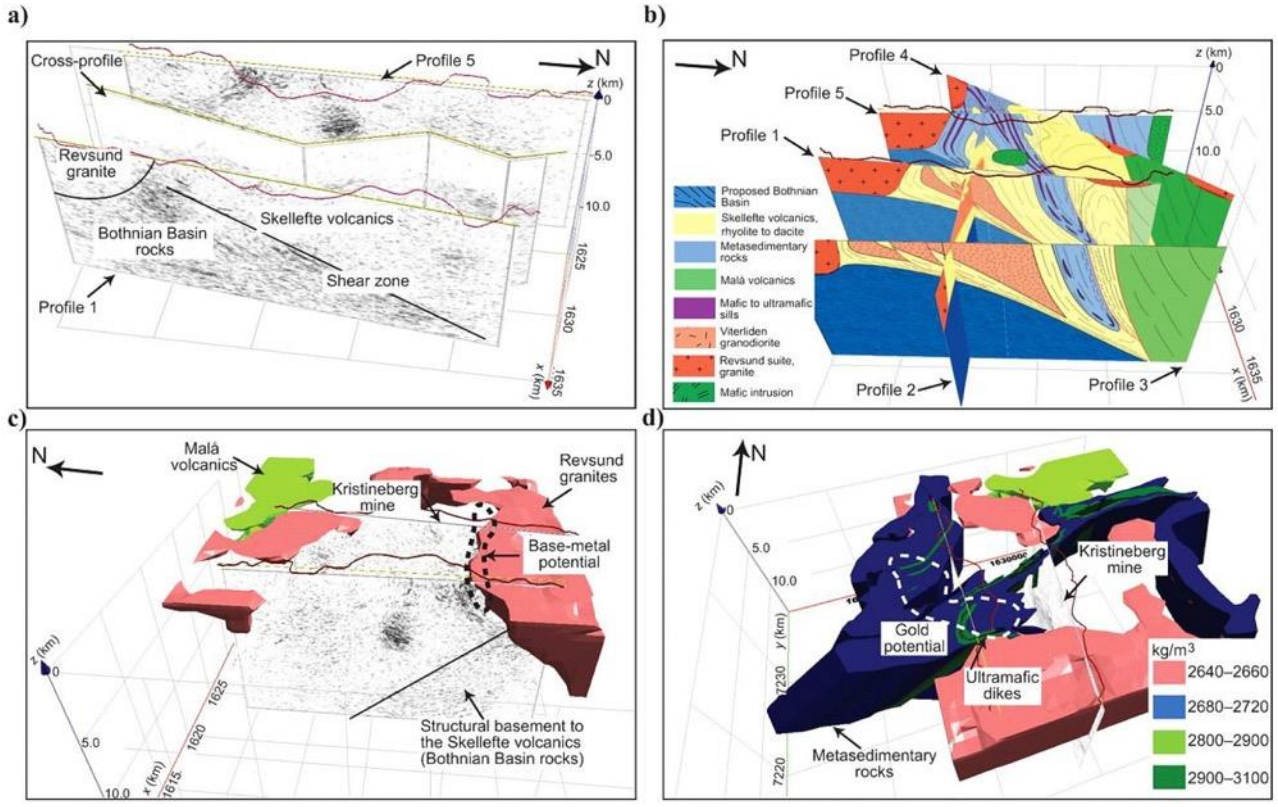

Figure 15. Kristineberg mining area - 3D views showing stages of the geological interpretation (Malehmir et al. 2009b). a) Early interpretation of seismic reflection data (Rodriguez-Tablante et al. 2007); b) Predicted 3D model for major structures obtained from five 2D geologic cross sections (see Malehmir et al. 2007); c, d) Final geological model for metal potential from 3D inverse and forward gravity modelling, all data available combined for targeting new prospecting areas. Horizontal to vertical scale 1:1.

2.1.11. Natural seismicity

The Swedish National Seismic Network (SNSN) started monitoring earthquakes with the installation of a Wiechert seismograph in Uppsala in 1904. The SNSN operates the only permanent, earthquake focused seismic network, consisting of 65 permanent stations in Sweden. The seismic sensors have unusually high gain to facilitate detection of microearthquakes in the regional size network. With an average station spacing of 66 km, the SNSN is complete to magnitude 0.5 (Richter scale) within the network.

Natural seismicity in the Kristineberg area seems to be very low. No local earthquakes were observed in the last two decades, with the observation threshold in magnitude being at about 1.9 on the Richter scale (B. Lund priv.com., SNSN 2019). Thus, seismology does not help to resolve the regional stress regime, and quantitative predictions cannot be done.

2.2. The Nautanen deposit in the Northern Norrbotten ore province

The Nautanen deposit is situated in Northern Norrbotten, the northernmost ore province in Sweden (Figs. 2, 16). The other provinces are Bergslagen, the Skellefte district and the Caledonian orogen. The following description of the regional geology of northernmost Sweden and local geology at Nautanen is modified from Bergman (2018) and Lynch et al. (2018a), respectively. The parts left out are those considered irrelevant to the present CHPM task. The complete reference lists of Bergman (2018) and Lynch et al. (2018a) are however kept.

2.2.1. Regional geology

The Precambrian bedrock in northernmost Sweden is part of the 2.0–1.8 Ga old Svecokarelian orogen. The orogen comprises both pre-orogenic rocks formed in the Archaean and early Palaeoproterozoic, as well as rocks formed during the orogeny itself. All the rocks were deformed and metamorphosed to variable degrees at different stages during the orogenic evolution (Fig. 16).

The oldest rocks were formed in the Archaean (Fig. 16). The main component is gneissic granitoid of mainly tonalitic to granodioritic composition, which shows intrusive relationships with paragneiss, amphibolite and, locally, banded orthogneiss interpreted as metaandesitic to dacitic tuff. Bodies consisting of non-migmatitic metamorphosed granite are locally common. Age determinations suggest crystallisation of granitoids at 2.8–2.7 Ga, and a regional metamorphic event is constrained at 2.7 Ga (Skiöld 1979, Skiöld & Page 1998, cf. Martinsson et al. 1999).

Layered mafic-ultramafic intrusions with an age of 2.5–2.4 Ga occur locally (Fig. 16); more common are mafic dykes and felsic–mafic intrusions related to later events. A metamorphosed volcano-sedimentary sequence, deposited before 2.0 Ga and unconformably overlying the Archaean basement is commonly referred to as Karelian supracrustal rocks (see also Gaál & Gorbatschev 1987). The lowermost Karelian unit in the Kiruna area is the Kovo group, which is composed of a basal clastic sequence of metamorphosed conglomerate and quartzite, overlain by tholeiitic metabasalt and metamorphosed calc-alkaline volcaniclastic rocks of andesitic composition. In the east, the Archean rocks are overlain by quartzite, along with subordinate metamorphosed conglomerate and phyllite. Locally, metavolcanic rocks of andesitic to dacitic composition occur below the quartzite. Metasandstone, quartzite and quartzo-feldspathic gneiss in the Pajala area and to the south are spatially associated with both Karelian and younger metavolcanic rocks.

In the Kiruna area (Fig. 16), the Kovo group is overlain by the Kiruna greenstone group, which predominantly comprises metamorphosed, tholeiitic basalt lava flows, including pillow lava, less important komatiitic lava, tholeiitic tuff and andesitic to dacitic tuffaceous rocks, and minor conglomerate, black schist and carbonate rock (Martinsson 1997). The Viscaria Cu-rich sulphide deposit is hosted by metamorphosed volcaniclastic and associated sedimentary rocks belonging to the Kiruna greenstone group. The stratigraphic sequence is similar but less complete in the area between Kiruna and Pajala. Mafic pyroclastic deposits are overlain by volcaniclastic rocks interlayered with carbonate rock, graphite schist, skarn-related iron oxide deposits, banded iron formation and chert (Martinsson 1993, Martinsson et al. 2018b, Lynch et al. 2018b). Most of these rocks were deposited before 2.14 Ga.

Svecofennian supracrustal rocks, recording the onset of the Svecokarelian orogeny, unconformably to disconformably overlie the Kiruna greenstone group and related units. The lower part of the sequence is characterised by calc-alkaline metavolcanic rocks of andesitic composition. On a regional scale, these rocks show extensive interlayering, with metamorphosed, siliciclastic sedimentary rocks. Metavolcanic and metasedimentary rocks are traditionally included in the Porphyrite group, defined in the low-grade rocks

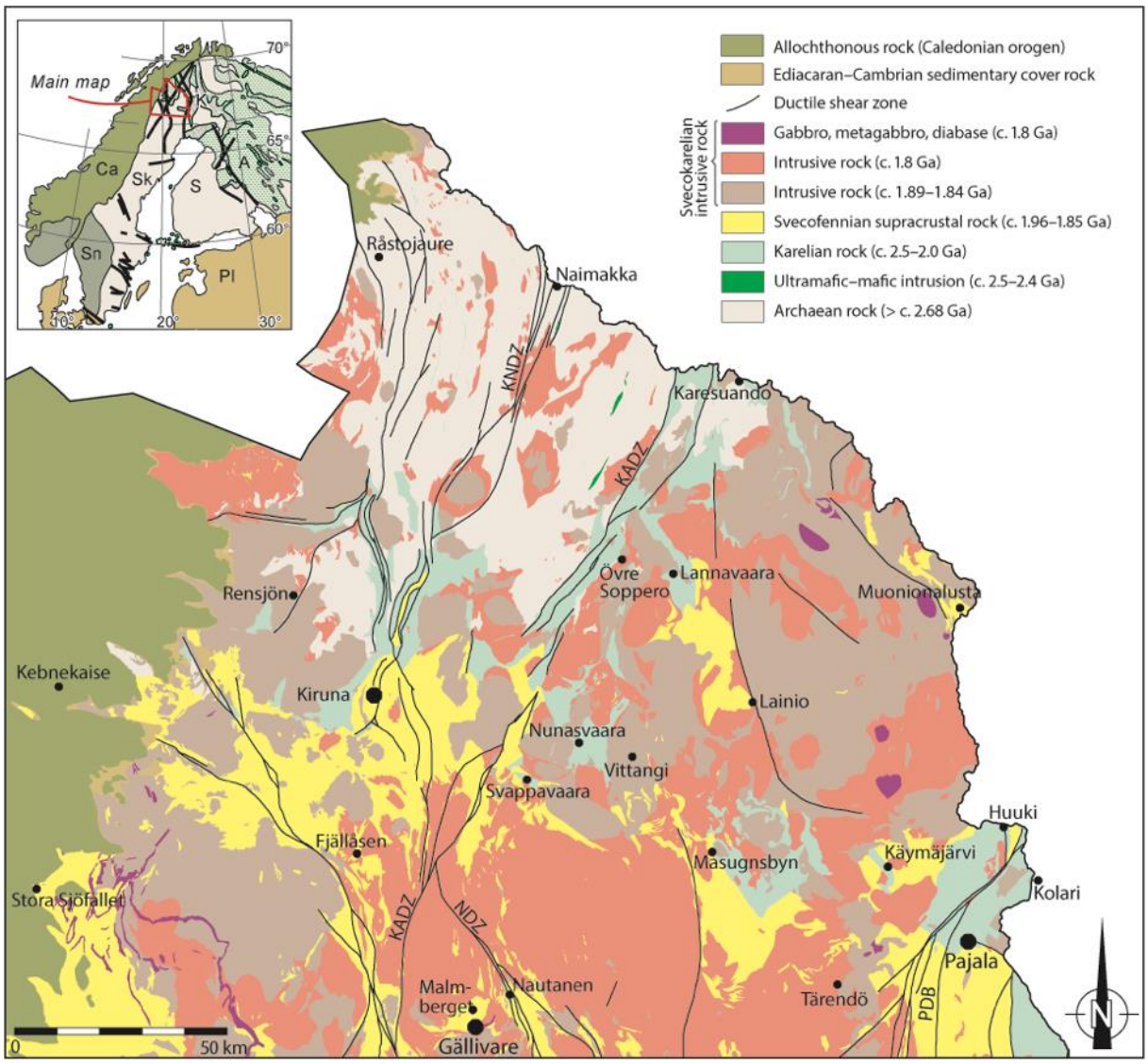

Figure 16. Simplified bedrock map of northern Norrbotten County, modified from Bergman et al. (2001). KNDZ = Kiruna–Naimakka deformation zone, KADZ = Karesuando–Arjeplog deformation zone, NDZ = Nautanen deformation zone, PDB = Pajala deformation belt. Inset map: Sk = Svecokarelian orogen, Sn = Sveconorwegian orogen, Ca = Caledonian orogen, Pl = Platformal sedimentary cover rocks, A (green ornament) = Archaean rocks in part reworked in the Palaeoproterozoic, K (grey ornament) = Karelian rocks, S (without ornament) = Svecofennian supracrustal rocks and Svecokarelian intrusive rocks; thick lines are major deformation zones. The abandoned Nautanen mine (67° 11' 30" N, 20° 52' 49" E) is close to Gällivare at the lower edge of map.

southwest of Kiruna. Equivalent units occur in other areas. Available age determinations show crystallisation ages of 1.89–1.88 Ga (Edfelt et al. 2006, Martinsson et al. 2018b, Hellström et al. 2018, Lynch et al. 2018a).

The Kiirunavaara group stratigraphically overlies the Kurravaara conglomerate in the Kiruna area and the Porphyrite group to the southwest of Kiruna (Fig. 16). In Kiruna, metamorphosed andesitic to trachyandesitic lava flows comprise the footwall of the Kiruna apatite iron oxide ore deposit. This deposit is overlain by porphyritic metadacite of pyroclastic origin (Martinsson 2004). The age of the host rocks is 1.89–1.87 Ga, and the ore has been dated at 1.88–1.87 Ga (Westhues et al. 2016). The uppermost unit in the Kiirunavaara group mainly consists of metamorphosed ignimbritic tuff, basalt and siliciclastic sedimentary rock. Southwest of Kiruna a thick sequence of metamorphosed, high-Ti and high-Zr tholeiitic basaltic lava is overlain by a unit

predominantly comprising pyroclastic metadacite. There are subordinate intercalations of metamorphosed andesite, locally ignimbritic rhyolite, conglomerate, sandstone and siltstone (Offerberg 1967, Perdahl & Martinsson 1995, Martinsson 2004).

The youngest supracrustal unit consists of sandstone with subordinate conglomerate and mudstone, and in some areas of basaltic intercalations (Witschard & Zachrisson 1995). Although the contacts are tectonic in most other areas, there is a locality northwest of Vittangi where a metaconglomerate rests unconformably on a metadiorite (Ödman 1939). The metadiorite is 1.88 Ga old, representing the maximum age of the clastic deposition in this area.

The more or less gneissic intrusive rocks in the Haparanda suite are commonly grey and medium-grained, but fine-grained types are also present; porphyritic varieties are uncommon. Magma mingling textures are common in some areas. There is a wide spectrum of rock types, from predominantly gabbroid and dioritoid, through quartz monzonite, tonalite and granodiorite, to subordinate granite (Ödman 1957, Bergman et al. 2001).

The intrusive rocks in the Perthite monzonite suite, formed between 1.88 and 1.86 Ga, mainly occur in the westernmost part of the area (Fig. 16). Quartz-poor rocks, including monzonite, quartz monzonite and quartz monzodiorite, predominate over granite. Many large intrusions of gabbro and diorite, inferred to belong to this suite, are also present. Magmatic layering has been observed in some of these bodies, and several show a concentric, banded magnetic pattern. Ultramafic rocks such as pyroxenite and serpentinite are present in some areas. Perthite-bearing granite is commonly red and medium- to coarse-grained. Enclaves and hybridisation phenomena show that magma mingling and mixing processes were prevalent. The rocks in the Perthite monzonite suite are typically isotropic but there are also areas where a tectonic fabric is prominent. There are geochemical similarities between the Perthite monzonite suite and the Kiirunavaara group (Witschard 1975, 1984), suggesting that the former was emplaced under sub-volcanic conditions. The rock types in the Perthite monzonite suite are similar to those in the Haparanda suite, but have traditionally been considered separate on the basis of several lines of evidence, including field relationships and lithogeochemical characteristics.

A suite of granite and granodiorite has yielded an age of about 1.85 Ga (Fig. 16; Bergman et al. 2006, Hellström & Bergman 2016). The granitoids are spatially associated with pegmatite, and in many places contain biotite-rich seams and partly assimilated remnants of older rocks. The granitoids are porphyritic, have an unequigranular matrix and are weakly foliated.

Large bodies of intrusive rocks belonging to the Lina suite, which formed around 1.8 Ga (Skiöld 1988, Bergman et al. 2002b), are common throughout the area (Fig. 16), and dykes or veins of rocks belonging to this suite commonly cut older rocks. The Lina suite is mainly composed of greyish-red, medium-grained and weakly porphyritic granite; red, fine-grained and equigranular varieties are also common. The granite is usually weakly foliated, associated with pegmatite, and fragments of assimilated country rock are common. Dykes or veins in older rocks consist of granite, pegmatite or aplite. A suite of intrusive rocks consisting of gabbro to granite, with quartz monzonite, monzonite, syenite, quartz monzodiorite and monzodiorite as intermediate members is found in the east of the area (Fig. 16). They have ages close to 1.8 Ga (Romer et al. 1994, Martinsson et al. 2018a).

The Nabrenjarka diabase, west of Gällivare (Fig. 16), is a conspicuous, flat-lying, bowl-shaped and sill-like intrusion with an exposed length of more than 50 km. It intrudes the Lina suite and is 1.8 Ga in age or younger.

Ductile deformation includes several phases of folding and the formation of major crustal-scale shear zones (Fig. 16). The metamorphic grade within the region is variable from greenschist to upper amphibolite facies,

and the intensity of deformation varies from strong penetrative foliation to texturally and structurally well-preserved rocks, both on a regional and local scale. Up to four separate phases of deformation have been identified in the east (Grigull et al. 2018, Lynch et al. 2018b).

An early event of deformation and metamorphism at c. 1.88 Ga, was followed by one at 1.86–1.85 Ga (e.g. Skiöld & Öhlander 1989, Bergman et al. 2001, Hellström 2018, Bergman et al. 2006). From a protracted event or several separate events during the time interval 1.83–1.78 Ga, including movements along the Pajala deformation belt, Bergman et al. 2001, 2006, Lahtinen et al. 2015, Hellström & Bergman 2016 concluded a regime of ductile deformation in the region.

The most important types of mineralisation are stratiform copper deposits, iron formations, Kiruna-type apatite iron ores and epigenetic copper-gold deposits. Age determinations show that major mineralisation events occurred at 1.88–1.86 Ga and 1.79–1.74 Ga, i.e., close in time to major phases of magmatism, deformation and metamorphism.

Hydrothermal alterations are both of regional character and spatially associated with mineralisations. The most characteristic alteration products are scapolite and albite, but skarn, biotite, carbonate, K-feldspar, sericite, tourmaline, epidote and chlorite are also common (e.g. Bergman et al. 2001, Martinsson et al. 2016, Lynch et al. 2018a). The geochemical composition of till overlying the bedrock reflects these alterations as enrichment in e.g. Ba, Ca, Cl, K, Na, Sr, La, Rb and P (Ladenberger et al. 2018). Age determinations show that major mineralisation events occurred at 1.88–1.86 Ga and 1.79–1.74 Ga (Martinsson et al. 2016), i.e., close in time to major phases of magmatism, deformation and metamorphism.

2.2.2. Local geology

The rocks of the Nautanen area form a partly conformable succession of syn-orogenic, Palaeoproterozoic volcanosedimentary rocks (Fig. 17; Witschard 1996). This supracrustal sequence is generally of calc-alkaline, basaltic andesite to andesite composition and has undergone extensive deformation, metamorphism, recrystallisation and hydrothermal alteration (McGimpsey 2010, Waara 2015, Lynch et al. 2015).

A variety of intrusive rocks occur across the area, including deformed gabbroic, syenitic and dioritic bodies and younger, deformed to massive granitic and gabbroic-doleritic plutons and dykes (e.g. Wanhainen et al. 2006, Sarlus 2016). Two large, sub-rounded, mafic-ultramafic intrusions (named the Dundret and Vasaravaara complexes) occur near Gällivare. These rocks exhibit distinct cumulate zones defining a primary magmatic layering consisting of olivine, pyroxene and plagioclase in varying proportions (Sarlus 2016).

Metasupracrustal rocks in the general Gällivare area host the Malmberget iron mine, Sweden's second largest iron resource after the Kiirunavaara deposit in Kiruna, and the Aitik copper-gold-silver deposit, one of Europe's largest copper mines (Fig. 17; e.g., Lund 2009, Wanhainen et al. 2012). Additionally, several hydrothermal copper-gold occurrences assigned to the iron oxide-copper-gold (IOCG) mineral deposit class occur within a regional approximately north-northwest-trending deformation zone termed the Nautanen deformation zone (NDZ; cf. Smith et al. 2013, Drejing-Carroll et al. 2015). Episodic deformation along this zone probably enhanced permeability and hydrothermal fluid flow, resulting in a relatively focused, linear zone of alteration and mineralisation (cf. Witschard 1996).

Metamorphic mineral assemblages and pressure-temperature (*PT*) estimates suggest the area reached middle amphibolite facies conditions during peak regional metamorphism. Bergman et al. (2001) noted a major metamorphic grade boundary in the area, with rocks east of the NDZ having a lower grade than those within the zone and to the west. Pressure-temperature estimates for regional metamorphism range from approximately 550 to 660°C and 2 to 5 kbar (i.e. lower to middle amphibolite facies), for contact metamorphism adjacent to Lina-type granite (forming a sillimanite-biotite-muscovite assemblage) between

approximately 630 and 710°C and 2.0 to 4.4 kbar, and for retrograde conditions between approximately 430 and 570°C, and 3.0 to 3.5 kbar (Tollefsen (2014). Additionally, *PT* estimates of approximately 630–680°C and 6.5 kbars (equivalent to middle amphibolite facies conditions) for metasomatic garnet growth associated with potassic-ferroan alteration and copper-gold mineralisation at the Nautanen deposit have been made by Waara (2015).

2.2.3. Stratigraphy and correlations with regional successions

The supracrustal rocks in the Nautanen area belong to the so-called Muorjevaara group (see Lynch et al. 2015 and references therein) which represents a basal, mainly calc-alkaline volcanosedimentary sequence. This is overlain by the Kiirunavaara group, comprising alkalic (trachyitic) intermediate to acidic metavolcanic rocks (Martinsson & Wanhainen 2004). This unit hosts the iron oxide-apatite deposit at Malmberget (e.g. Lund 2009). Local quartzite outliers represent an uppermost stratigraphic unit. In the absence of outcropping transitional contacts, the major stratigraphic units are inferred to be separated by unconformities. The Muorjevaara and Kiirunavaara groups partly correspond to regional *Porphyrite* and *Porphyry groups* (Bergman et al. 2001), respectively. Traditionally, these regional stratigraphic units have been considered broadly coeval and have mainly been divided on the basis of petrographic and geochemical considerations (cf. Perdahl 1995).

2.2.4. The Nautanen deformation zone and related iron oxide-copper-gold mineralisation

The Nautanen deformation zone (NDZ; Witschard 1996) represents the most conspicuous structural feature in the area. It is clearly delineated on magnetic anomaly maps as a somewhat dilational, linear zone of sub-parallel and tightly banded magnetic susceptibility anomalies (see *Geophysical modelling* section). The coupling of high-strain deformation and magnetic banding reflects episodic metasomatic-hydrothermal fluid flow, probably enhanced by increased permeability associated with protracted and focused deformation (e.g. Pitkänen 1997, Smith et al. 2013).

Based on regional structural and magnetic lineament geometries, a dextral-oblique shear sense, with a southwest-side up reverse component has been interpreted (Bergman et al. 2001). Geological mapping and geophysical measurements within the shear zone have also identified several sub-parallel, north-northwest-orientated, moderately plunging folds (e.g. Gustafsson 1986, Pitkänen 1997). Internally, the deformation zone is characterised by moderate to intense shearing, mylonitisation, structural transposition and pervasive metasomatic-hydrothermal alteration.

The supracrustal rocks within and adjacent to the NDZ host several replacement- and vein-related (epigenetic-style) copper and gold deposits and prospects (see reviews by Martinsson & Wanhainen 2004, Martinsson & Wanhainen 2013). Important examples include the Nautanen, Liikavaara and Ferrum prospects (Fig. 17). Two general styles of mineralisation are recognised (e.g. Gustafsson 1985, Martinsson & Wanhainen 2004): (1) an inferred older phase of disseminated to semi-massive (replacement-style) sulphide mineralisation forming sub-vertical, lenses and linear zones mainly within the NDZ; and (2) mineralisation associated with quartz ± tourmaline ± amphibole veins occurring mainly east of the NDZ (e.g. the Ferrum prospect, Gustafsson & Johnsson 1984), or as a late-stage brittle overprint within the high-strain zone.

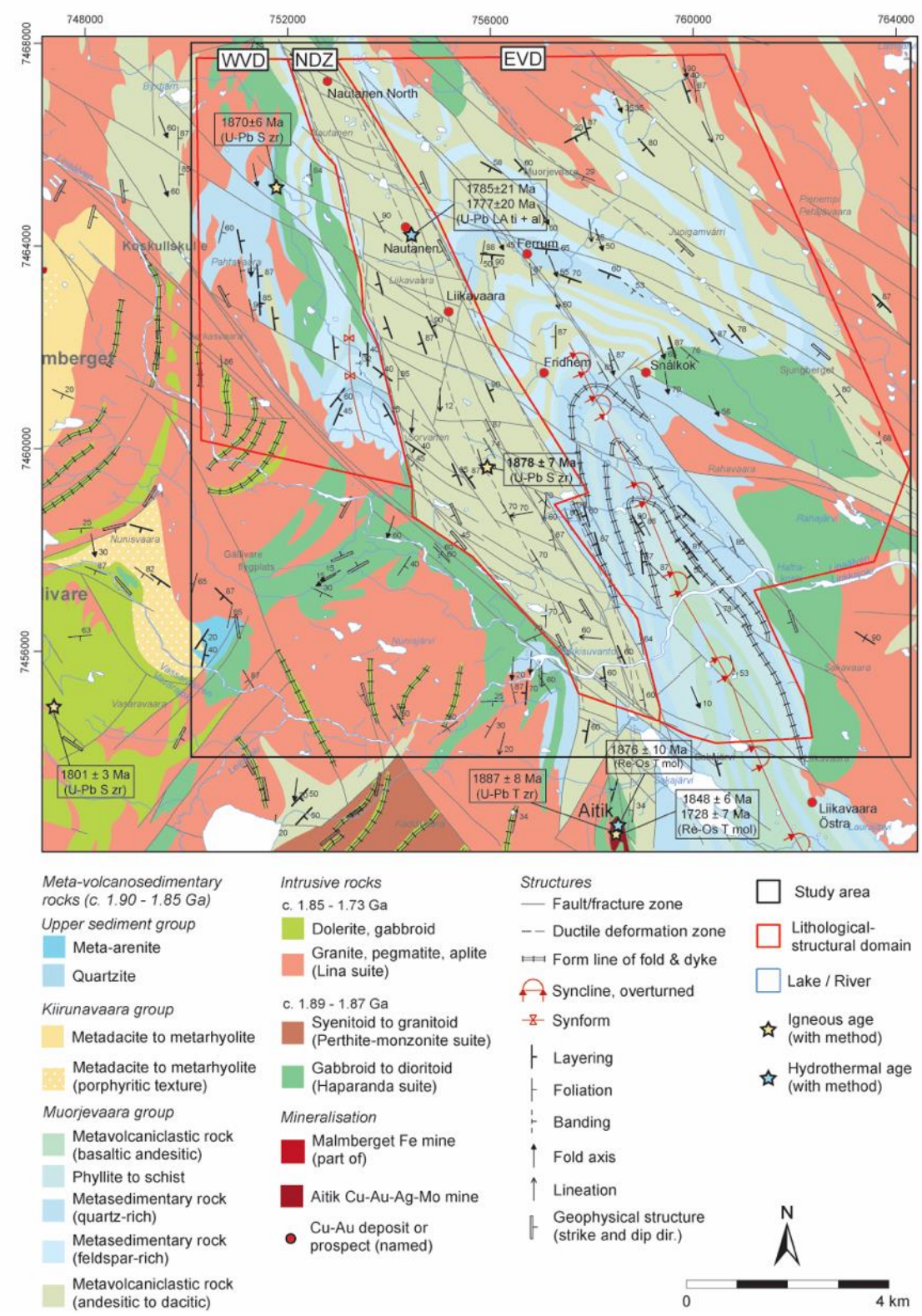

Figure 17. Geology of the Nautanen area (Lynch et al. 2018a). Abbreviations: EVD = eastern volcanosedi-mentary domain; NDZ = Nautanen deformation zone (domain); WVD = western volcanosedimentary domain. Geochronology abbreviations and sources: U-Pb S zr = U-Pb SIMS zircon dating (Sarlus 2016, and this study = highlighted bold text in

NDZ), U-Pb T zr = U-Pb TIMS zircon dating (Wanhainen et al. 2006), Re-Os T mol = Re-Os TIMS molybdenite dating (Wanhainen et al. 2005), U-Pb T ti = U-Pb TIMS titanite dating (Wanhainen et al. 2005), U-Pb LA ti + al = U-Pb laser ablation-inductively coupled-mass spectrometry titanite and allanite dating (Smith et al. 2009). Nautanen is situated in the upper third of the map. Coordinate system is SWEREF 99 TM.

The area around the Nautanen deposit (67° 11' 30" N, 20° 52' 49" E) in the northern NDZ domain is a historical mining location that has experienced intermittent exploration for over 100 years. Copper mineralisation was first discovered in 1898, and approximately 72 000 tonnes of copper and iron ore were extracted between 1902 and 1907 (Geijer 1918). Further exploration in the 1970s and 80s produced a pre-regulatory total resource estimate for the "old" Nautanen deposit of approximately 2.94 Mt grading 0.78% Cu and 0.52 ppm Au (values derived from Danielson 1985). Present-day exploration by Boliden Mineral AB has resulted in the discovery of an additional copper-gold mineralisation approximately 1.6 km north-northwest of the old Nautanen mine along the trend of the NDZ (Fig. 17). This "Nautanen North" deposit has an indicated resource of 9.6 Mt grading 1.7% Cu, 0.8 ppm Au, 5.5 ppm Ag and 73 ppm Mo, with an additional inferred resource of 6.4 Mt grading 1.0% Cu, 0.4 ppm Au, 4.6 ppm Ag and 41 ppm Mo (New Boliden 2016).

The bedrock in the area, largely enclosed by the red line around Nautanen North, "old" Nautanen, Liikavaara and further about 10 km south-southeast in Figure 17, has been systematically sampled and chemically analysed (n = 836) by Boliden Mines (T. Hermansson, pers. com. 2019). Discarding samples with more than 1,000 ppm Cu, background values for several elements were calculated, and some of these are shown in Table 1. The average values reported in Table 1 are comparable to continental crustal abundances (Taylor 1964) except for silver, tungsten and gold, which are enriched. However, the wide compositional range with high upper values suggest heterogeneity and varying degrees of mineralisation.

Table 3. Metal content in surrounding formations being of crucial importance for a CHPM system: Chemical background values of the bedrock in the Nautanen area (see text). Data courtesy of Boliden Mines.

	Ag	Au	Co	Cu	Li	Mo	Ni	Sn	W	Zn
	ppm	ppb	ppm	ppm	ppm	ppm	ppm	ppm	ppm	ppm
Average	1	7	24,5	71,8	12,9	2	15,0	1,3	3,4	90,0
Max	349	523	92	921,2	160	65	97	12	69	698
Min	0	0	0,5	0	0	0	0	0	0	0

According to criteria presented by Grooves et al. (2010), the geological characteristics of the Nautanen copper-gold deposit are consistent with the restricted definition of a *bona fide* iron oxide-copper-gold (IOCG) system. These include (1) enrichment of copper and gold, with both elements representing potential economic commodities; (2) a spatial and genetic association between the mineralisation and iron silicate and iron oxide gangue minerals (i.e. *not* an iron oxide or iron oxide-apatite deposit with anomalous copper and gold; cf. Williams 2010); (3) hydrothermal mineralisation style (i.e. replacement lenses, zones and veins); (4) sulphur mainly present in the S^{2-} oxidation state; (5) clear structural controls on the mineralisation; and (6) a temporal association with magmatism and deformation, but no obvious causative intrusion.

Pervasive and vein-related potassic-ferroan ± calcic alteration occurs variably in the NDZ domain and adjacent areas and is associated with IOCG and related mineralisation (cf. McGimpsey 2010, Lynch et al.

2015). At the "old" Nautanen deposit (Fig. 17), characteristic almandine porphyroblasts are associated with amphibole + biotite + magnetite + sericite ± K-feldspar ± sulphide and tourmaline ± quartz ± sulphide banding, patches and veins. Textural relationships suggest garnet growth slightly predated the main-stage alteration and mineralisation event (cf. Waara 2015). Late-stage epidote ± quartz ± carbonate alteration also occurs. Chalcopyrite with lesser bornite and chalcocite are the main copper-bearing minerals and are typically associated with pyrite, pyrrhotite, magnetite and tourmaline. Quartz-amphibole ± tourmaline veins containing pyrite and minor chalcopyrite post-date the main-stage disseminated and micro-fracture type sulphide mineralisation. Gold generally occurs as inclusions and segregations in pyrite, chalcopyrite, bismuth-bearing phases and locally galena (e.g. Sammelin 2011, Bark et al. 2013).

Comparison of "least altered" metavolcanosedimentary rocks from the eastern volcanosedimentary domain with NDZ-hosted, pervasively altered, mylonitic rocks shows that the latter are relatively enriched in copper, silver, gold, iron, molybdenum, barium, manganese and tungstenCu, Ag, Au, Fe, Mo, Ba, Mn and W. Likewise, the tendency for K/Na ratios to increase when stepping into the NDZ domain reflects the association between potassic alteration and copper-gold-iron enrichment (cf. Lynch et al. 2015). These features are diagnostic of typical geochemical affinities and metal abundance correlations associated with IOCG-style mineralisation, particularly deposits hosted by intermediate to felsic igneous rocks in continental settings (cf. Barton 2014).

Uranium-lead LA-ICP-MS titanite and allanite ages ranging from c. 1.79 to 1.78 Ga for hydrothermal alteration at the Nautanen copper-gold deposit have been reported (Smith et al. 2009). These dates provide a temporal and inferred genetic link between the mineralisation and deformation, fluid mobilisation and late-orogenic granitic magmatism.

2.2.5. Lithologies in the Muorjevaara group

The following petrographic descriptions complement previous accounts by Zweifel (1976), Ros (1980), Monro (1988) and Lynch et al. (2015).

In general, four lithological units are identified in the rocks of the Muorjevaara groups (cf. Fig. 17). They are (1) predominantly intermediate metavolcaniclastic rocks; (2) volcanogenic (epiclastic) metasedimentary rocks; (3) mica schist horizons; and (4) amphibolitic schist (mafic metavolcaniclastic rocks). Units 1 and 2 are the most common units across the Nautanen area.

Units 1, 2 and 3 represent compositionally similar lithologies (mainly basaltic andesitic to andesitic) and are primarily distinguished based on textural, structural and deformation intensity criteria. In the NDZ domain, deformed and altered feldspar-biotite-amphibole schist (locally gneiss) is inferred to represent a composite intermediate metavolcaniclastic unit, probably consisting of a combination of units 1 to 3.

The bedrock in the NDZ domain is affected by relatively intense shearing, transposition and metasomatic-hydrothermal alteration. Thus, primary lithological characteristics are commonly obscured or masked by overprinting processes and remain somewhat equivocal. Nevertheless, local low-strain and "least altered" zones provide some petrographic insights into the primary nature of the rocks in this area and facilitate comparisons with the rocks in the other two lithological-structural domains.

The predominant lithology is a medium to dark grey, fine-to medium-grained, well-sorted and internally laminated, feldspar-biotite ± amphibole schist to gneiss. Locally, more weakly laminated varieties have a recrystallised, granoblastic appearance and appear more feldspar-rich. Inferred bed forms (although rarely preserved) are approximately 0.1–0.5 m thick and are generally laterally continuous, sub-parallel and planar. In general, anhedral and platy biotite and lesser amphibole grains are aligned parallel to the dominant penetrative cleavage and intergrown with feldspar. Local horizons containing coarser (felsic) clasts (approximately 5–15 mm), elongate and stretched lensoidal patches (remnant clasts?), and composite,

aggregated fragments (lithic clasts?) occur throughout the area. These features are consistent with a possible volcaniclastic derivation. Locally, the schist grades into more quartz-rich sections consisting of fine-grained, granular and anhedral quartz, forming banded zones and aggregated, irregular to sub-rounded, lithic (?) clasts.

Throughout the NDZ domain, the bedrock displays moderate to intense penetrative foliation and shows variable degrees of metasomatic-hydrothermal alteration. Dark to pinkish-red, medium-to coarse-grained garnet porphyroblasts occur locally. These appear to pre-date the main alteration assemblage and copper mineralisation event. Locally, the garnets form quite large crystals up to 10 cm in diameter or aggregated clusters. They are typically of the spessartine-almandine variety, appear to be mainly syn-kinematic, and form disseminated grains or clusters associated with amphibole + biotite + magnetite veins and patches.

The most important belt- to deposit-scale alteration assemblage affecting NDZ rocks is a moderate to intense amphibole + biotite + K-feldspar + magnetite ± garnet ± sericite ± pyrite ± chalcopyrite assemblage. Typically, it has developed along seams, linear zones and irregular veins trending parallel to the transposed foliation. This inferred “syn-mineralisation” assemblage overprinted an earlier pervasive scapolite ± albite assemblage. Zones and bands of tourmaline ± quartz alteration represent a paragenetically later assemblage.

Syn-mineralisation magnetite typically occurs as fine-to medium-grained, anhedral tabular and elongate platy grains within foliation planes. It also forms fracture-filling inclusions and patchy rims around garnet porphyroblasts. Consequently, the bedrock throughout the domain is magnetically anomalous. Locally, feldspar-rich metavolcaniclastic rocks display reddish-pink patches and irregular zones indicative of “red rock”-type hematite staining and iron exsolution affecting alkali feldspar. A late-stage epidote ± quartz ± carbonate alteration assemblage is also present and more typically overprints red rock (K-feldspar-altered) zones. Secondary hematite-goethite commonly replaces magnetite, while chlorite replaces biotite and is associated with epidote.

2.2.6. Structures in the eastern volcanosedimentary domain

The eastern volcanosedimentary domain (EVD, cf. Fig. 17) contains a variety of superimposed ductile and brittle structures recording a protracted, multiphase deformation history. The most commonly observed fabric is a variably intense, planar penetrative foliation, here designated S1. This foliation is generally roughly northwest to north-northwest-aligned, moderate to steeply southwest to west-southwest-dipping, and tends to parallel primary bedding, laminae and compositional banding. S1 has a similar orientation to planar foliations in EVD-hosted dioritic intrusions. The intensity of S1 varies between outcrop and lithology, and where it forms a schistose to gneissic texture, S1 may represent a composite transposed foliation. Locally, S1 is axial planar to tight to isoclinal, asymmetric, intrafolial F1 folds.

The EVD is also characterised by tight to isoclinal folding of primary bedding, compositional banding, alteration banding and foliations. To the immediate east of the NDZ, the predominant structure is a distinct, large-scale, asymmetrical and overturned syncline (cf. Fig. 17). The western limb appears to be truncated roughly north-northwest-trending, shear zones and faults related to the NDZ. Fold vergence is typically eastward, with axial surfaces roughly north to north-northwest-aligned and generally dips steeply towards the west. The fold shapes are non-cylindrical and fold axes are locally curvilinear. The larger-scale fold structures are accompanied by parasitic, asymmetric small-scale folding. In the southern part of the EVD, parasitic fold axes commonly plunge at moderate angles towards the south-southwest, whereas in the north, fold axes have doubly plunging geometries (typically roughly northwest and southeast). Mineral lineations are gently plunging and have variable orientations.

A crenulation cleavage, here designated S2, also occurs in the EVD. It is generally roughly north to north-northeast-aligned, sub-vertical, with axial planar to gentle, upright F2 folds, plunging moderately roughly

south to south-southeast. The S2 cleavage is associated with L2 intersection lineations that typically have a moderate plunge to the south and south-southeast, similar to F2 fold axes. Locally, near the hinge zones of larger-scale folds, fairly intense S2–L2 deformation has developed elongated and stretched L-tectonites, which form mullion-like features along bedding surfaces. In eastern limb areas, local bedding plane surfaces with L2 lineations contain slicken-side notches, indicating top-block reverse movement towards the north and north-northwest.

Brittle deformation in the EVD consists of (1) locally developed spaced cleavage and fracture sets that tend to follow earlier planar structures; (2) numerous roughly north-northwest-and east-aligned, generally sub-vertical, amphibole and quartz vein sets, of which the latter are locally sulphide-bearing; and (3) joint sets developed in intrusive rocks. Additionally, discordant roughly north to north-northeast-aligned brittle deformation zones are inferred from aeromagnetic data (cf. Figs. 17, 18). These crosscutting, locally NDZ-related high-strain zones segment the EVD into several localised blocks.

2.2.7. Structures in the Nautanen deformation zone

The Nautanen deformation zone (NDZ) is characterised by a conspicuous roughly north-northwest to northwest- aligned, steep to locally moderate roughly west-dipping, penetrative foliation (S1), with varying but generally strong intensity. Locally, inferred primary bedding, compositional banding and alteration banding are typically transposed into steep orientations parallel to the dominant foliation, and locally produce a composite fabric that may represent several generations of ductile deformation. The dominant shearing direction strikes roughly north-northwest and shows mainly western-block up reverse kinematics and most commonly oblique dextral and less common sinistral components, recorded by asymmetric foliation deflections around garnet porphyroblasts and local asymmetric kink bands.

The predominant north-northwest-trending reverse shear zones within the NDZ are interconnected by roughly north-trending, sub-vertical high-strain zones with mainly dextral kinematics. In general, these secondary zones are interpreted as Riedel shears that formed in the oblique, dextral-reverse shear zone. Additionally, local tensional features such as quartz-filled tension gashes and en-echelon quartz veins occur along the western margin of the NDZ and are mainly orientated north to north-northeast.

Minor asymmetric folding related to shearing is mainly evident from asymmetrically folded hornblende-, magnetite-and epidote-filled veinlets. To the south of the study area, at the Aitik deposit, the reverse shear zones are more north-south orientated and dip moderately towards the west, with distinct roughly west-plunging mineral lineations. Additionally, a set of sub-vertical, north-northeast-trending high-strain zones is observed.

Mineral lineations in the NDZ are defined by stretching of minerals, and their orientations are variable. In general, lineations plunge moderately towards the south and southwest. Local variations, with gentle to horizontal plunges, were also observed.

2.2.8. Structures in the western volcanosedimentary domain

The western volcanosedimentary domain (WVD) is characterised by alternating layers of metasedimentary and metavolcanosedimentary rocks, with a distinct bedding (S0) and parallel foliation (S1) forming a composite S0-1 fabric. Both bedding and the S1 foliation are folded into inclined to overturned asymmetric folds, with open to close interlimb angles. The predominant large-scale structure in the WVD is a repetition of anticlines and synclines, with non-cylindrical, curvilinear fold axis (see Fig. 17). The overall orientation of fold axes is southward with gentle to moderate plunges. Fold axes in the northwest of the WVD appear to be doubly-plunging.

Typically, an axial planar parallel fabric is not observed across the WVD. Nevertheless, a weak foliation or weak-spaced cleavage, here designated S2, could be observed in several outcrops, especially near the NDZ. This S2 fabric clearly overprints the S0-1 foliation obliquely.

Local crenulation lineations, small-scale fold axes and mineral-stretching lineations are orientated sub-parallel to the larger-scale fold axes.

Brittle deformation in the WVD is dominated by a large-scale, northwest-striking fault zone that divides the foliated and folded metavolcanic and metasedimentary rocks to the north from mainly undeformed granites to the south (Fig. 17). The fault zone is characterised by intense fracturing forming distinct topographic depressions.

2.2.9. Geophysics in the Nautanen area

Since the 1960:ties until today, geophysical investigations were done in the Nautanen region, mostly in the Nautanen deformation zone (NDZ). They comprise airborne magnetic, electromagnetic and radiometric studies, and the data helped to clarify geological units of the NDZ. In addition, detailed ground measurements were done, like, e.g., magnetic- and regional gravity surveys, radiometric and electromagnetic (slingram and VLF) exploration and petrophysical sampling (cf. Lynch & Jönberger 2014, Lynch et al. 2015, 2018a, and references therein). Other geophysical data, like, e.g., data from seismic reflection surveys that should give structural information at larger depth down to several kilometres, are not known of the area.

The NDZ is a wide deformation zone, characteristically delineated on the magnetic anomaly map (Fig. 18), compiled from airborne and integrated ground magnetic survey data. The map clearly shows the power of denser ground surveys in their much better resolution of magnetic signatures. The western volcanosedimentary domain (WVD) of the Nautanen area is in its magnetical features relatively heterogeneous, showing tight, sub-parallel magnetic bands. Magnetic lows mainly reflect metasedimentary or felsic metavolcaniclastic rocks, while banded highs in the magnetic field are due to mafic to intermediate metavolcaniclastic rocks. Even mafic intrusive rocks are highly magnetised (see Table 4). Gravity data of the area, lowering in value towards the west indicate that granitic intrusions may extent to larger depth (Fig. 19). The NDZ correlates with a broad positive gravity anomaly, implying that more mafic rocks (of higher density) are underlying the NDZ. The positive gravity anomaly extends eastwards from the central NDZ towards Snålkok (cf. Fig. 17) where gabbroic rocks are found.

In the eastern volcanosedimentary domain (EVD), magnetic anomalies resemble the pattern found in the WVD, where high-magnetic bands alternate with lower ones. A synformal fold in the southern part of the EVD is imaged in the magnetic anomaly map (Fig. 18). High-magnetic bands can be associated with mafic metavolcaniclastics, whereas areas of lower magnetisation reflect metasedimentary rocks. North of the EVD, a granitic intrusion correlates well with a zone of low gravity. Further south, alternating metasedimentary and metavolcaniclastic rocks cannot be distinguished in their density, but give a surplus in gravity (Table 4).

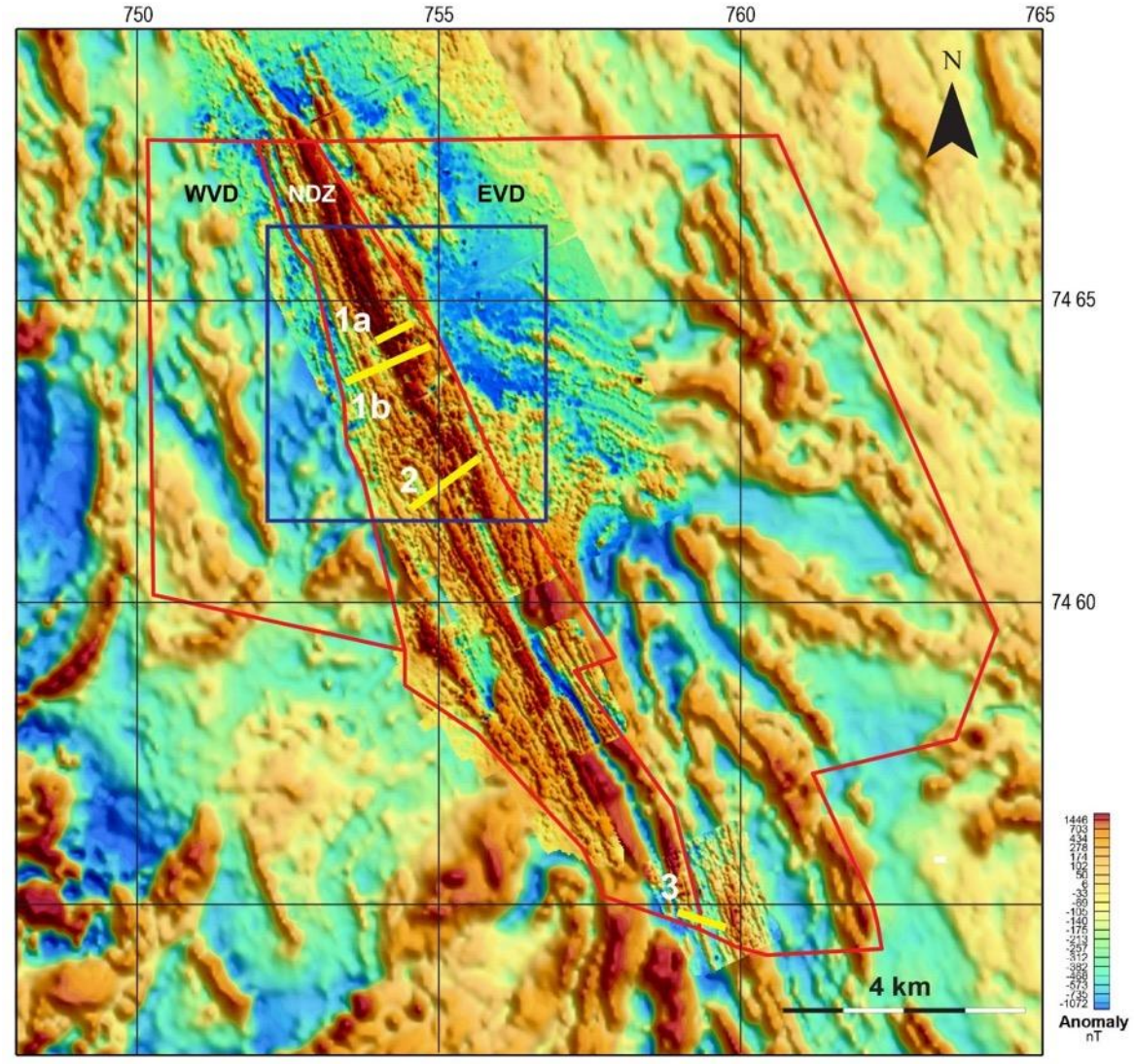

Figure 18. Magnetic anomaly map of the Nautanen area, combined of airborne and ground magnetic total field data (after Lynch et al. 2018a). Coordinate system SWEREF 99 TM in km. Red polygons represent study areas where ground magnetic and VLF data were acquired in recent years, divided into three domains, the western- (WVD) and eastern (EVD) volcanosedimentary domain, and the Nautanen deformation zone (NDZ). Numbers 1a, 1b, 2 and 3 mark profiles discussed in text, relating to Figs. 20, 21. Box in dark blue shows the horizontal extent of the 3D magnetic model presented in Figure 22.

2.2.10. Nautanen – three-dimensional modelling of shallow structures

Three dimensional models of the NDZ were constructed on a smaller scale by inverting ground magnetic data (Lynch et al. 2015, 2018a). The aim was to visualise highly magnetised structures in the sub-surface. Owing to the limited extend of the areas investigated, the magnetic models extend down to a depth of some hundred metres only, which is not the target depth of a CHPM system. But, we present some examples of the modelling attempts here.

The most northerly 3D inversion magnetic model (Fig. 20) was conceived of the Nautanen copper-gold deposit and surrounding area close to profile 1a in Figure 18. Due to the banded highly magnetised structures of the area, susceptibility was constraint to values between 0 and 2 SI units. The cross-section of profile 1b (Fig. 20) shows an overturned, synformal structure in the western part of the profile, with a

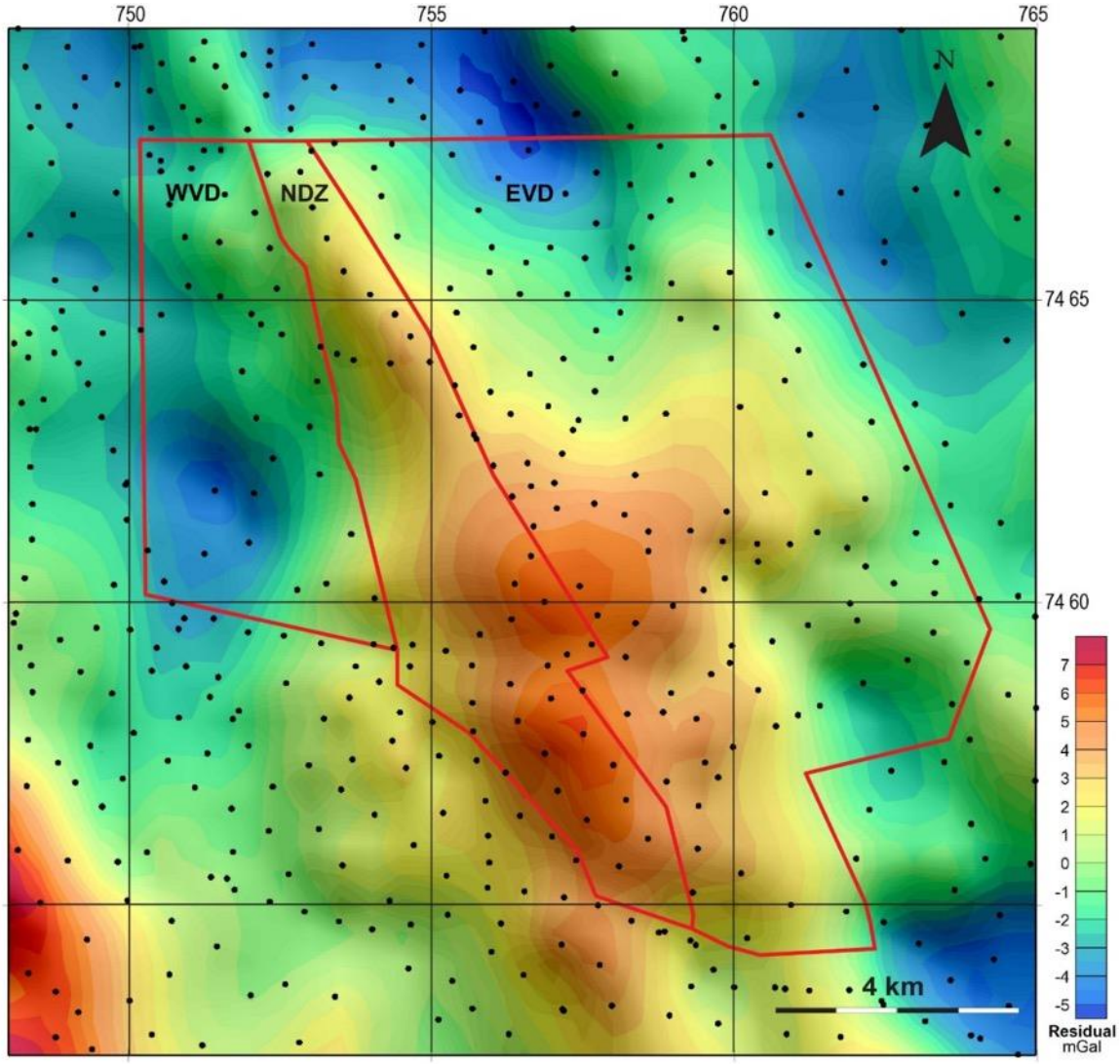

Figure 19. Residual gravity field in the Nautanen area. Black dots show the location of measuring points.

southwesterly dipping axial plane, whereas the magnetic formations on the eastern side dip to the northeast.

Several models were constructed across the NDZ to the south, based on ground magnetic and electrical resistivity (VLF) data. Modelling aimed on visualising the NDZ and bedrock structures (Fig. 20, profiles 1b and 2). However, due to the characteristics of the VLF method, the resolution of resistivity models is limited. Figure 20 shows a cross section (profile 2) through the 3D magnetic susceptibility model, perpendicular to the magnetised structures of the NDZ. Laboratory measurements of rock samples of the area gave a magnetic susceptibility of 0.6 SI units at maximum, but susceptibility of rocks *in-situ* may be higher. Model susceptibility in the inversion was constraint to 0.0001 to 1 SI units. The cross section reveals a magnetic structure in the Southwest, dipping moderately to the southwest. A sudden break in the pattern occurs in the centre of the profile. East of this break, the highest magnetised part of the NDZ can be identified as a synformal pattern continuing towards northeast. From this area, minor magnetite rich structures are likely to extend linearly upwards towards the surface.

Further 8 km south-southeast along the NDZ and predominantly on its eastern side, a broad conductive zone can be seen in the western part of the profile section shown in Figure 21, corresponding to a low in the

magnetic field. In the east, a resistive feature with a relatively shallow south-easterly dip correlates with bands of higher magnetisation as identified in the map of Figure 18.

2.2.11. Three-dimensional geophysical modelling of magnetite-banded rocks in the NDZ

Airborne magnetic data were inverted to a larger 3D model of the deformed and altered bedrock in the NDZ, allowing magnetic susceptibility of the rock to vary (Fig. 22). The model is represented by two surfaces of equal magnetic susceptibility (isosurfaces), highlighting their general 3D form and orientation. Geologically, the isosurfaces can be viewed as proxies for magnetite-alteration and effects of deformation enhanced fluid flow within the NDZ.

In the southern part of the model, the isosurface of lower susceptibility (0.18 SI units, cyan colour) dips to the west-southwest. North of northing grid line 7464000, both the lower and the higher (0.3 SI units, grey colour) isosurfaces tend to have an opposing dip towards the east-northeast. In the aeromagnetic data (Fig. 20, profile 1b), a possible northwest striking deformation zone transects the 7464000 northing grid line. Thus, the lateral change in dip of the isosurface may reflect the primary structural character of the Nautanen deformation zone or later deformational effects that caused a degree of structural re-orientation. Geologically, it cannot be excluded that even deeper levels of the bedrock have a magnetic signature, i.e., magnetic susceptibility is increased.

Table 4. Petrophysical properties, i.e., density, magnetic susceptibility and Königsberger ratio Q of different rocks in the Nautanen area. Total number of samples is 267.

Rock type	No. of samples	Density (SI) Mean	Density (SI) Std. dev.	Susceptibility x 10^{-5} (SI) min	Susceptibility x 10^{-5} (SI) max	Susceptibility x 10^{-5} (SI) median	Q-value min	Q-value max	Q-value median
Granite	13	2 612	17	0	3 691	1 544	0.00	0.87	0.07
Metasedimentary rock	16	2 836	98	18	67 510	784	0.00	89.53	0.16
Gabbro-diorite	22	2 903	50	27	19 781	70	0.00	6.81	0.01
Sandstone	24	2 768	74	12	18 660	1 850	0.00	8.37	0.45
Basalt-andesite	56	2 847	76	44	53 060	5 339	0.00	16.00	0.45
Mica schist	22	2 814	100	44	41 430	1 699	0.00	161.80	0.30
Rhyolite-dacite	18	2 708	34	21	10 933	1 801	0.01	1.76	0.26
Amphibolite	23	2 966	79	60	19 031	7 217	0.00	9.27	1.35
Greywacke	28	2 819	92	39	14 740	2 157	0.00	7.18	0.65
Granodiorite	5	2 714	53	21	3 169	1 975	0.00	1.56	0.16
Argillite	40	2 754	112	234	32 378	2 338	0.03	79.69	0.37

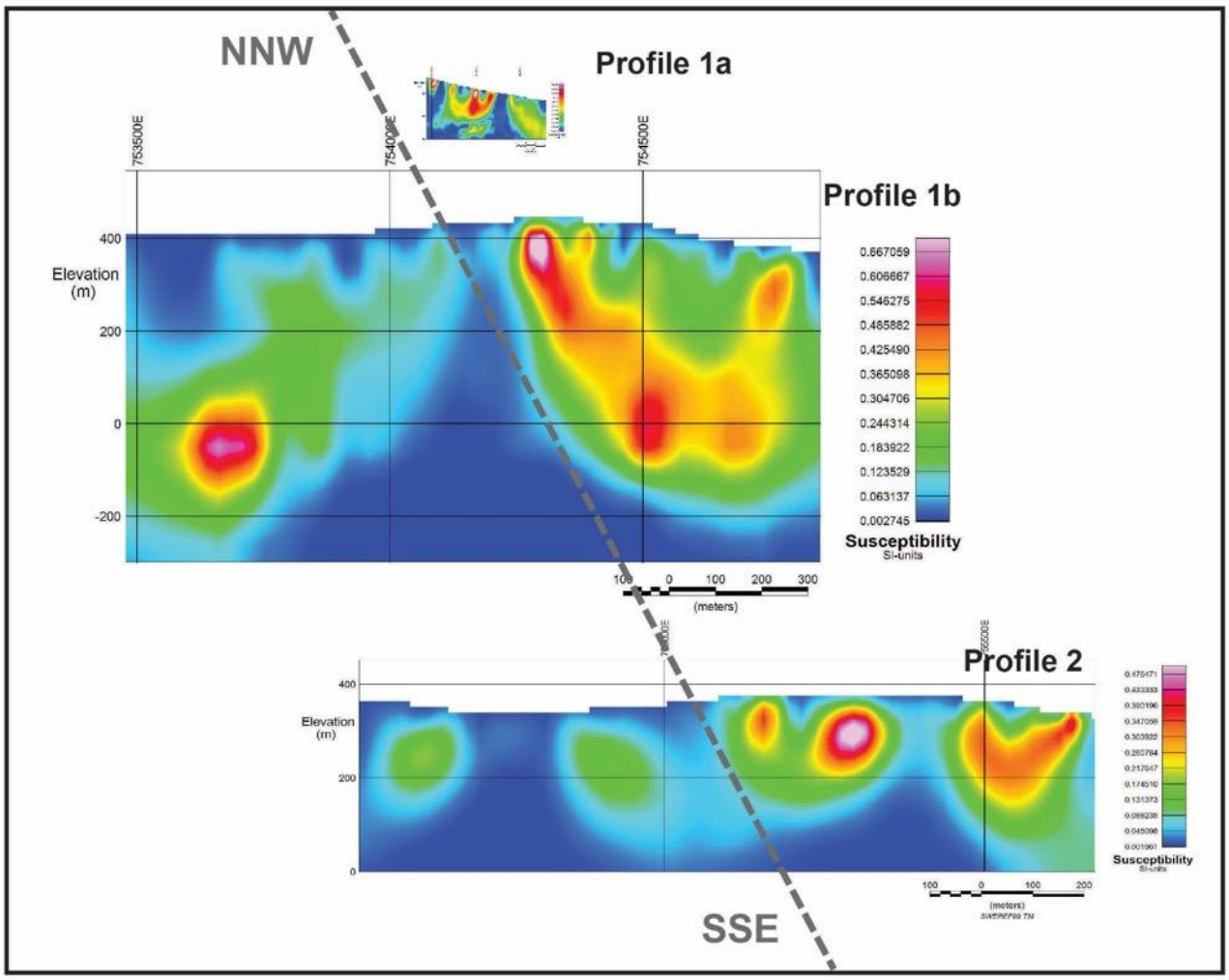

Figure 20. Three cross-sections of magnetic susceptibility of shallow sub-surface structures, taken from 3D inversion models based on ground magnetic data for profiles 1a, 1b and 2 (see fig. 18). The profiles are disposed along the north-northwest–south-southeastern strike of the Nautanen deformation zone, here indicated by the dashed grey line. Profile length in metre, vertical extend in m above sea level. For better orientation, eastern longitude in m according to SWEREF 99 TM annotated.

2.2.12. Natural seismicity

Above, we have introduced the Swedish National Seismic Network (SNSN) and its capabilities. In the last two decades, no local earthquakes were recorded by the network originating from the Nautanen area. But, many blastings from the Malmberget and Aitik mines are found in their archives. As for the Kristineberg area in the Skellefte district, no conclusions can be drawn for the regional stress regime, neither qualitatively nor quantitatively. At the time of writing, owing to an on-going process of legal permitting, we were not able to obtain actual stress data around Nautanen neither from other sources.

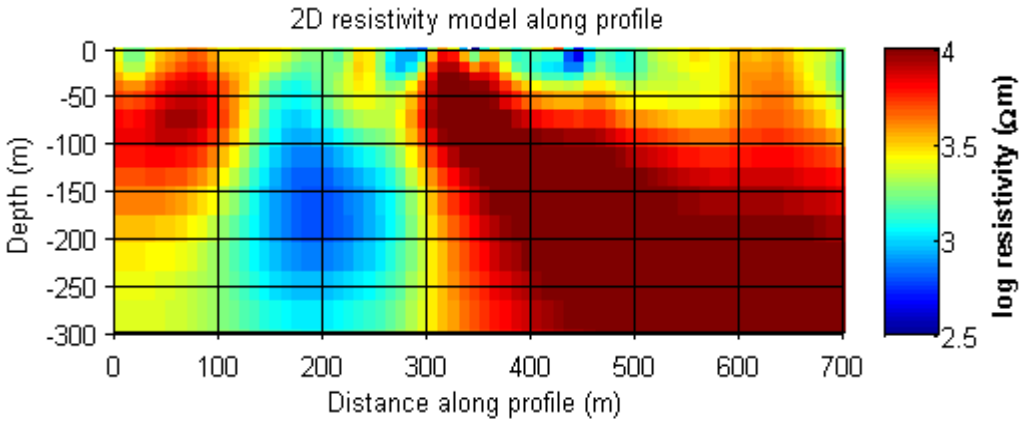

Figure 21. Resistivity cross-section derived by inverting electromagnetic data from VLF measurements along profile 3 in Figure 18. View to the northeast.

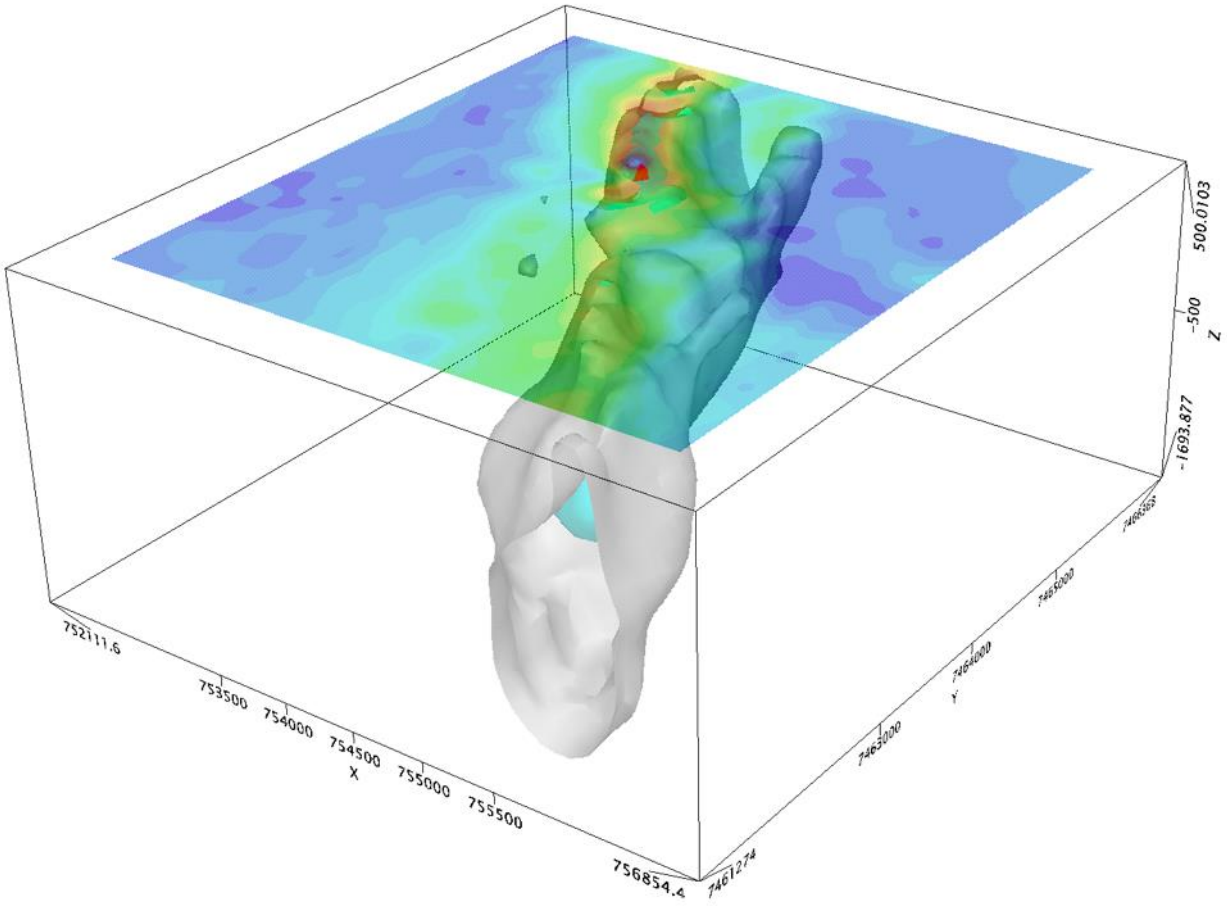

Figure 22. Three-dimensional magnetic susceptibility model for the Nautanen deformation zone (outline marked by dark blue rectangle in Fig. 18). Two isosurfaces coloured in cyan and grey are shown. Total magnetic anomaly field is indicated at the surface (no scale given). View from southeast to northwest. XY-coordinates refer to SWEREF 99 TM, Z is height a.s.l., all in metres.

3. EGS GEOTHERMAL POTENTIAL

3.1. Temperature gradient and heat flow density

Based on temperature measurements in a borehole within the Kristineberg area (Fig. 23, left), the heat flow density was estimated to range between 35 and 50 mW/m^2. The estimation was based on measured gradients of 0.011 – 0.013 ^{o}C/m between 200 and 700 m depth. Parasnis (1975) has estimated corrected heat flow in the Skellefte district at 49 mW/m^2, based on temperature measurements in boreholes ranging in depth between 365 and 780 m.

Temperature measurements were also made in two boreholes close to the iron ore mine at Kiruna (Fig. 23, right), located about 60 km north of Nautanen. Heat flow density was estimated to range between 35 and 55 mW/m^2. The estimation was based on measured gradients of 0.013 – 0.014 ^{o}C/m for a 500-metre interval. Previous measurements in the iron ore district of Malmberget and Kiruna, with depth ranging from 287 to 1 100 m below ground level, have yielded corrected heat flow density of 51 mW/m^2 (Parasnis 1981). In addition, measurements have been made in three boreholes inside the iron ore mine at Kiruna (Fig. 23, right). Measurements were made from a level at about 1 200 m below ground surface. The temperature gradients estimated in these boreholes were almost constant at 0.016 – 0.017 ^{o}C/m. Heat flow density was calculated to range between 51 and 65 mW/m^2. Obviously, this estimate indicates a higher geothermal flow compared to the other measurements.

Heat flow density was calculated by using thermal conductivity values between 3.2 and 3.8 W/m K. This interval was assumed to be representative for the bedrock types in the areas. There was no information available to support any correction of the temperature profile.

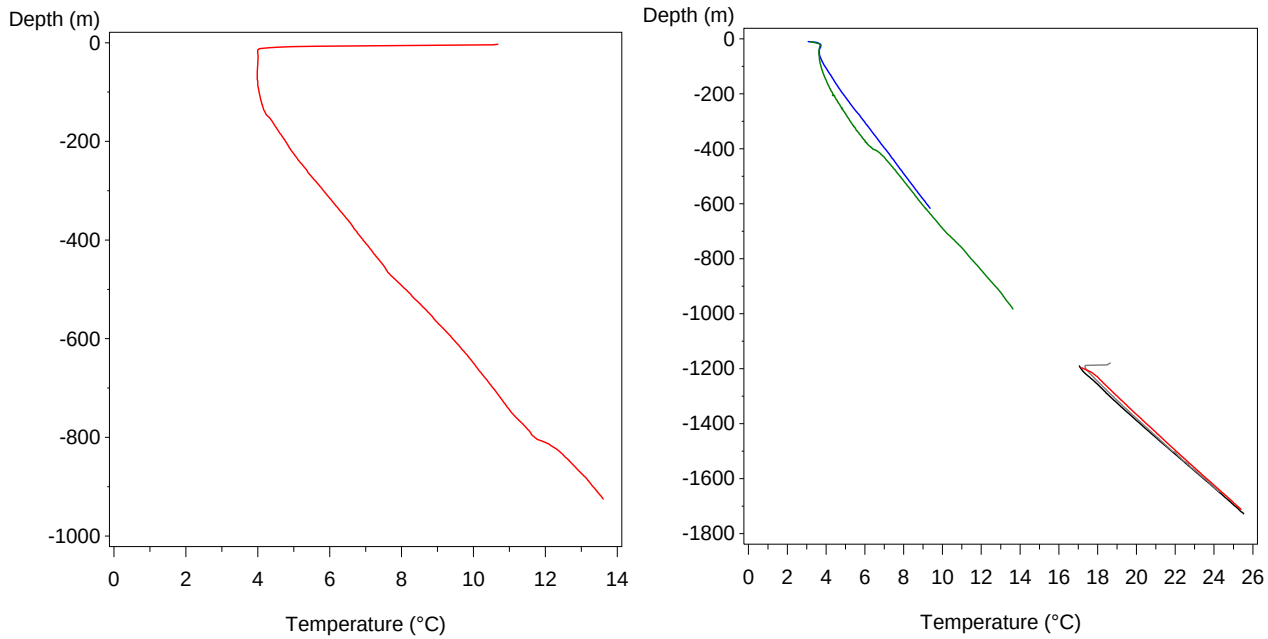

Figure 23. Measured temperature (^{o}C) as a function of borehole depth (in m below ground surface) in the Kristineberg area (left) and in five drill holes located in the Kiruna mining district (right), at about 60 km north of the Nautanen area. Three of the boreholes were measured in the Kiruna iron ore mine at about 1200 m depth. Note different depth and temperature scales in both figures.

When compared with the normal pattern of heat flow density in northern Sweden (Hurter & Haenel 2002), no significant deviation could be found. Estimations of the heat flow, based on the measurement of temperature gradients in the bore holes at Kristineberg and Kiruna could be compared to the map with corrected heat flow density in Scandinavia (Fig. 24, Balling 2013). The map indicates a regional heat flow density of 50 - 60 mW/m^2.

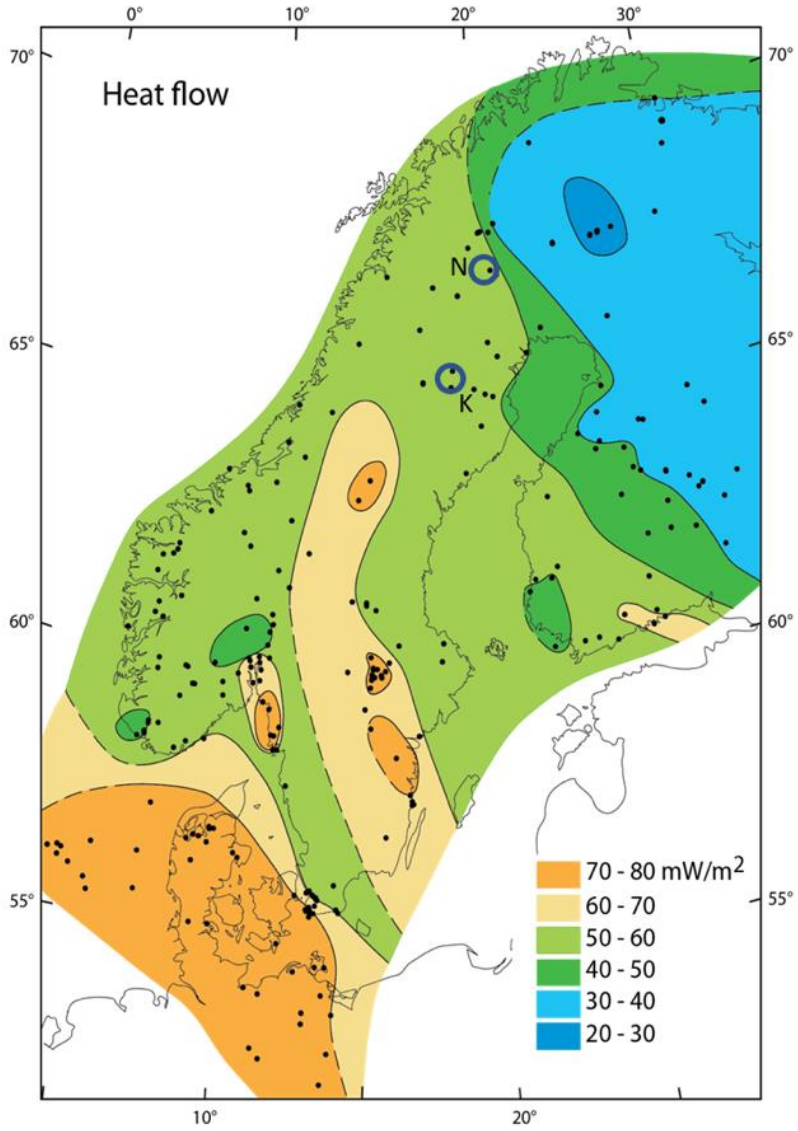

Figure 24. Map with corrected surface heat flow density in Fennoscandia (Balling 2013), based on measurements at more than 250 sites, marked by black dots. K : Kristineberg area, N : Nautanen area.

3.2. Heat production

Heat production of outcrops all over Sweden was estimated using airborne as well as ground based radiometric measurements provided from the gamma radiation database of the Geological Survey of Sweden (Fig. 25, Schwarz et al. 2010). The data from outcrops and site-specific rock types do not indicate any anomalous values in the suggested study areas, Kristineberg and Nautanen. However, in lack of structural

geological data, extrapolation of heat production to deeper levels has not yet been tested. Consequently, heat production at deeper levels could differ considerably when compared to the data from outcrops.

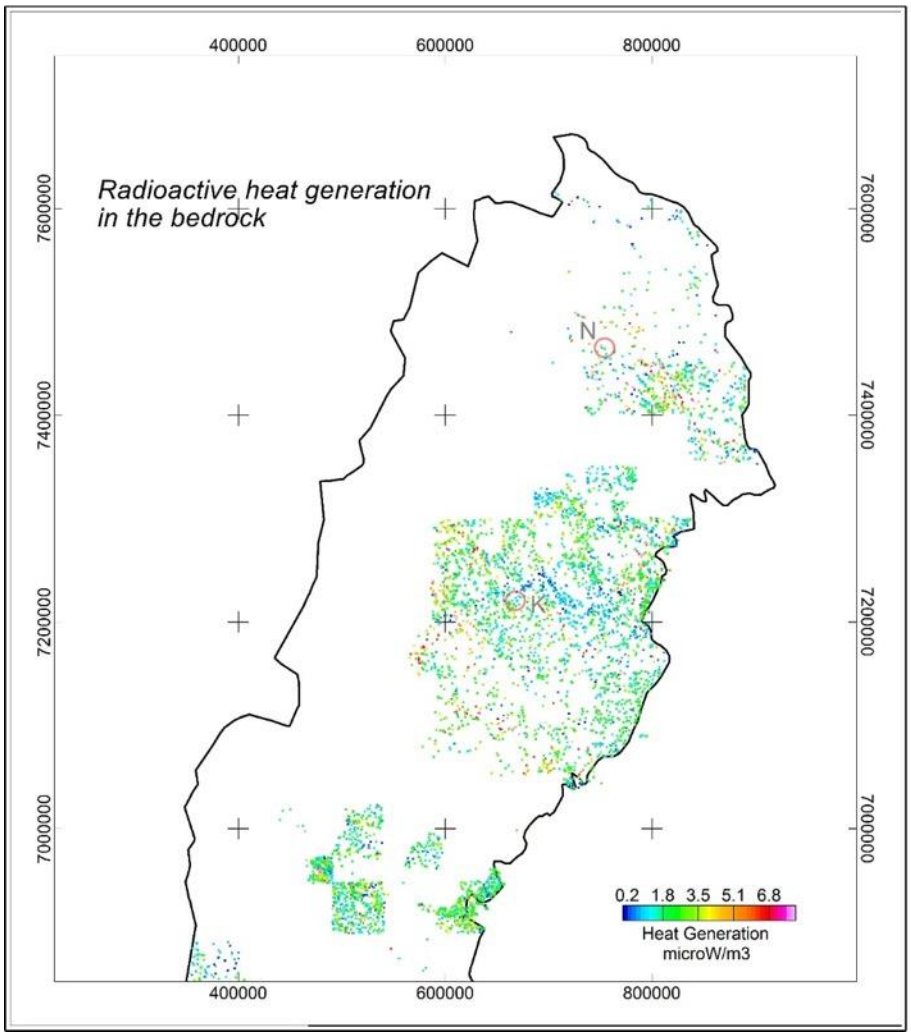

Figure 25. Heat production calculated from airborne radiometric data related to outcrops over northern Sweden (except of the mountain areas), in µW/m^3 (after Schwarz et al. 2010). K : Kristineberg area, N : Nautanen area. Coordinate system is SWEREF 99 TM in m.

3.3. Hydraulic properties, deep fluid flow

There are several reports indicating generally low hydraulic conductivity at deep levels of the Precambrian crystalline bedrock in Sweden. Extensive hydraulic tests were made in several boreholes by the Swedish Nuclear Fuel and Waste Management Company (SKB). In the Äspö area (see Fig. 1), in southern Sweden, the hydraulic conductivity below 650 m depth varies between 10^{-12} and 10^{-7} m/s Sweden (Réhn et al 2008). At deeper levels, about 5 – 10 km, the hydraulic conductivity should be lower, possibly lower than 10^{-8} m/s. These values could probably be used to approximate the hydraulic conductivity at deep levels in the bedrock in Sweden. Trends in hydraulic conductivity down to 2 500 m in the crystalline bedrock have been interpreted by Ericsson et al (2006). At 2 500 m depth the hydraulic conductivity was estimated to about $2 \cdot 10^{-11}$ m/s (Fig. 26). This assessment has been used as a reference for the Kristineberg area (Golder Associates 2017).

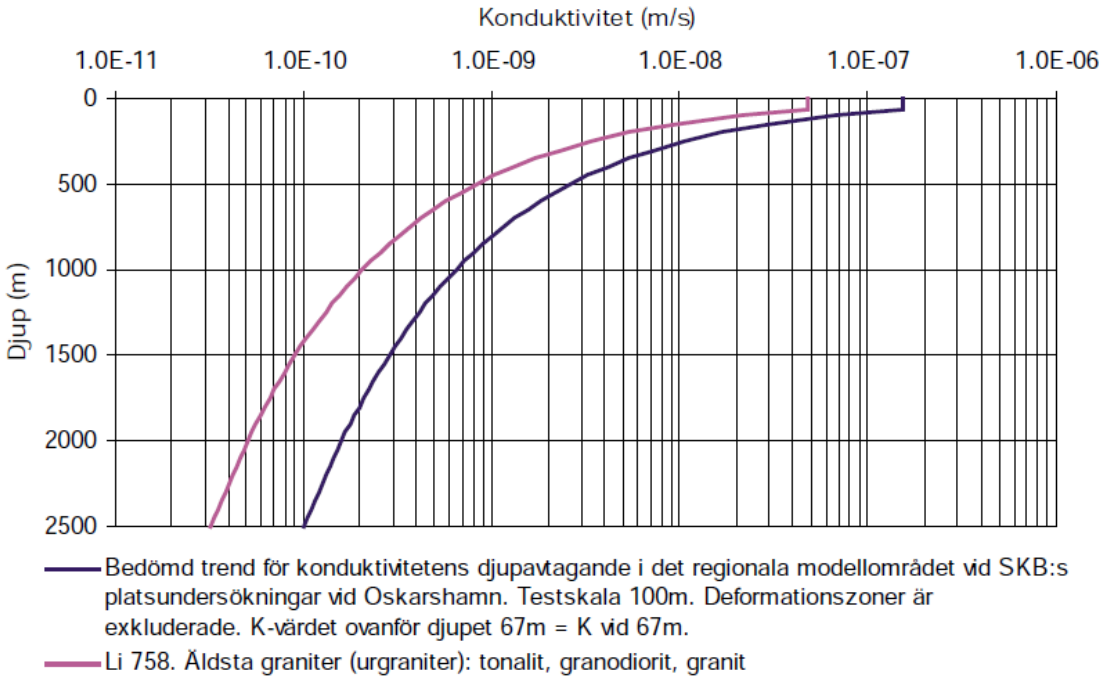

Figure 26. Estimated trends in hydraulic conductivity vs depth in a borehole, meant to represent the Kristineberg area (purple line). The dark blue line indicates hydraulic conductivity at depth close to Oskarshamn in southern Sweden (Ericsson et al. 2006).

About 4 km west of the Kristineberg mine, hydraulic conductivity was measured in 17 boreholes (Golder Associates 2017). A median value of $6.8 \cdot 10^{-8}$ m/s was estimated between the bedrock at surface and an average depth of about 600 m. Extrapolation to depths between 5 and 10 km suggests hydraulic conductivity to decrease to 10^{-10} – 10^{-12} m/s. Data from drill core samples from the Kristineberg area indicate a brittle deformation zone which could be important for the interpretation of hydraulic properties.

The fluid flow from deep boreholes could be roughly estimated by using the following assumptions: Considering a hydraulic conductivity between 10^{-12} and 10^{-8}, an estimated open section of 1000 m and a drawdown of the water pile of 300 m, the flow could range from $3 \cdot 10^{-7}$ to $3 \cdot 10^{-3}$ m^3/s (Fig. 27). Here, we assume a temperature difference of 100 °C being exploited but considered to be at the very upper limit. With the heat capacity of water of 4.186 MJ/m^3, the corresponding extraction of heat from the fluid could be calculated to a minimum value of $1.26 \cdot 10^{-4}$ MW and a maximum of 1.26 MW. This example clearly indicates that the hydraulic conductivity of Precambrian crystalline bedrock at deep levels is a limiting factor for the use of geothermal energy. Moreover, it clearly shows the exigency of hydraulic stimulation of the bedrock to increase fluid flow and to make a CHPM sytem feasible.

3.4. Fluid composition

Data on fluids, brines and meteoric waters from deep boreholes are generally uncommon, and no available data were found from the Kristineberg and Nautanen areas. For reference purposes, data from the borehole at the Siljan deep drilling site Gravberg (see Fig. 1) could be used to provide an indication of total dissolved solids (TDS) at very large depths. Down to 4 000 m below ground surface, the TDS amount to less than 500 mg/l. Below 4000 m, TDS increase and at about 6000 m a brine with about 150 000 mg/l was found (Juhlin and Sandstedt 1989).

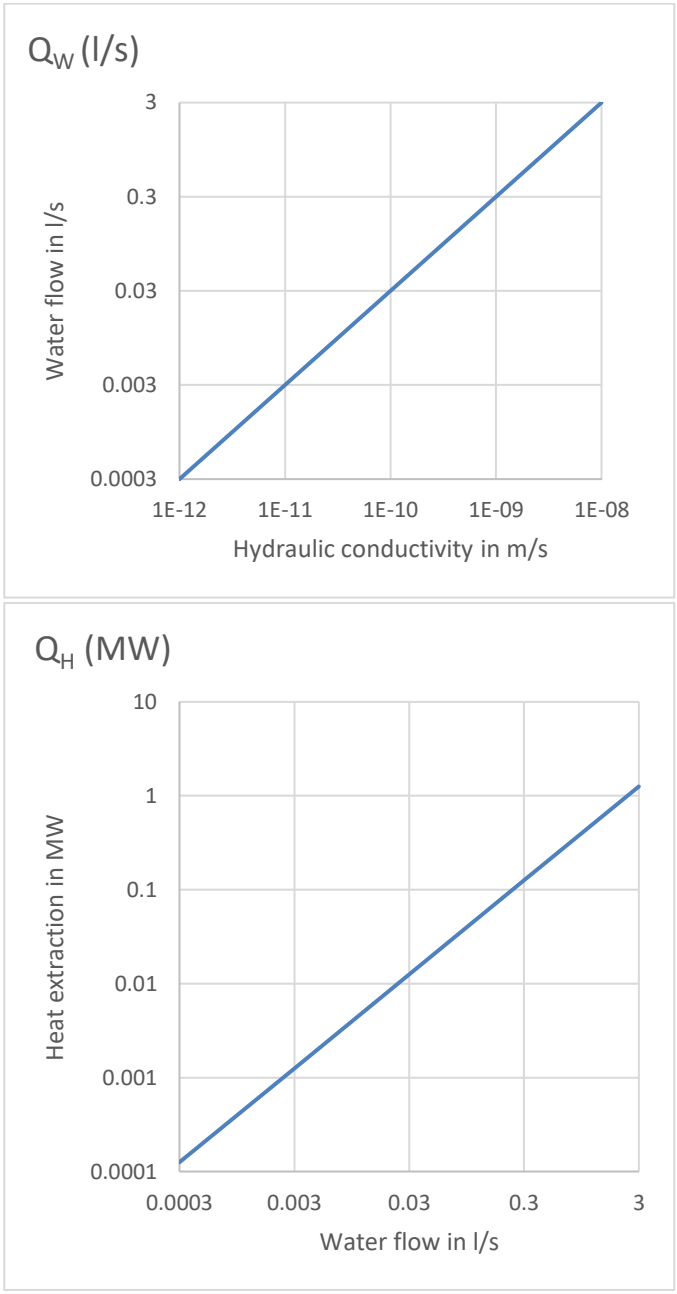

Figure 27. Estimated water flow Q_W (in l/s) as a function of hydraulic conductivity (in m/s) (top) and heat extraction Q_H (in MW) as function of water flow (in l/s) (lower).

Water samples were chemically analysed from nine boreholes nearby the Kristineberg area, representing depths from the ground surface down to about 600 m (Golder associates, 2017). The analysed elements had no exceptional concentrations when compared to regional data of groundwater chemistry in the crystalline bedrock (Geological Survey of Sweden 2013).

3.5. Mineral stability

In this study, we have identified mining areas as being suitable for the challenging future technology, *Combined Heat, Power and Metal extraction from ultra-deep ore formations* (CHPM). The CHPM concept proposes establishing an Enhanced Geothermal System in a metal-bearing geological formation, that will allow the production of energy and metals. The technique under development is meant to be applicable in any crustal environment, given that temperature at depth is not less than 140 ^{o}C, metals exist in some form, and the mobility of fluids is enough or can be enhanced.

For the Earth's crust in northern Sweden, temperatures of about 140 ^{o}C imply a depth of at least 7 km. Lithostatic pressure at these depths can be assumed to be about 2 kbar. Considering leaching of metals from such depths, one must consider that minerals, as for example copper sulphides, silver sulphides, sulpho salts, antimon phases like stibnite, tellurides and selenites can be altered, replaced or transformed (phase transition).

3.6. A case study in short: The st1 project

In our simple calculations above we have shown, that extracting heat from deeper crystalline rocks by establishing an *Enhanced Geothermal System* (EGS) could be of interest. However, it requires hydraulic conductivity to be improved. Finland, the eastern neighbor country of Sweden, and geologically also part of the Svecokarelian orogen, at the time of writing, is preparing for its first deep EGS in Espoo, close to Helsinki (Saarno 2019, St1, project website). The investigations and drillings there can help to shed some light on the physical properties and the state of the bedrock, which is comparable to the bedrock in the Kristineberg and Nautanen areas. The deep st1 project aims on establishing an EGS only, with the rock volume and temperatures encountered less than those needed for establishing a CHPM system. But, the knowledge already gained and coming lessons to be learned from this project can give valuable information for the further development of the CHPM technique.

The planned geothermal plant for urban district heating will use two boreholes with a maximum (measured) depth of 6 400 m. The deeper one of these holes was drilled already, having a true depth of 6100 m, where bottom hole temperature reaches 120 ^{o}C. This wellbore is meant to be the production hole. According to project targets, when completed, the heating plant is estimated to produce about 40 MW_h by extracting hot fluids at a temperature of about 115 ^{o}C (Saarno 2019).

During summer of 2018, the first hole was used for stimulation experiments. Water at high pressure of 60 to 90 MPa was injected at an interval of true depth of 5500 to 6100 m, split up into five sections (S1 – S5, see Fig. 28), to increase hydraulic conductivity of the bedrock. The stimulation was injection rate–controlled, with flow rates varying at discrete levels to keep microseismicity at a low level (Leary 2018, Kwiatek et al. 2019). For 49 days, 400 – 800 l/min of water, a total of 18160 m^3 was fed into the basement rocks.

As experienced elsewhere (e.g., Diehl et al. 2017), controlling injection-induced seismicity is of utmost importance for public acceptance of energy projects using EGS. Therefore, a year ahead of starting drilling operations, a network of geophones was installed in the area at surface and in boreholes to monitor natural seismicity. When stimulating the bedrock hydraulically, seismic monitoring was performed with a 24-station borehole seismometer network: Additionally, 14 strong-motion seismometers were installed at critical infrastructure sites nearby (Kwiatek et al. 2019). The instruments were recording micro-seismic events due to the influx of water into the bedrock, when opening fissures and fractures. Thus, seismic events recorded during stimulation should allow to monitor connectivity pathways due to the flow of water. The maximum strength of seismic events during stimulation was 1.9 in magnitude on the Richter scale. For security reasons, set by local authorities, the limit for an immediate stop of all operations was set to a magnitude of 2.5 (Saarno 2019). A total of 43882 earthquakes induced were measured during a period covering the time of stimulation

and 1 week after. When the analysis of seismic events recorded will be completed, presumably in late 2019, the second borehole will be drilled down to about 5500 m in depth. Directed into the zone where water flow should be increased, this wellbore will be used for reinjecting the thermal water after heat extraction.

The Espoo on-site experiments can be summarised as follows (Leary 2018): The fluid stimulation of the crystalline rock at 5500 to 6100 m depth did not produce pipe-like flow structures, as implied by spatially-uncorrelated crustal flow properties. Rather, water injection was reactivating fossilised spatially-correlated flow structures, attested by a distribution of low magnitude seismic slip events independent of fluid injection points. An EGS programme of wellbore-centric fluid stimulation appears to be feasible for deep crystalline rock. Leary (2018) analysed the thermal energy to be extracted from a 1000 m wellbore, where crustal temperature is about 100 °C and well- to wellbore distance is about 50 m. The thermal energy output of such a system is determined to about 10 MW_h for a period of about 30 years. This amount of heat extractable is four times less than the value of the official project target (Saarno 2019).

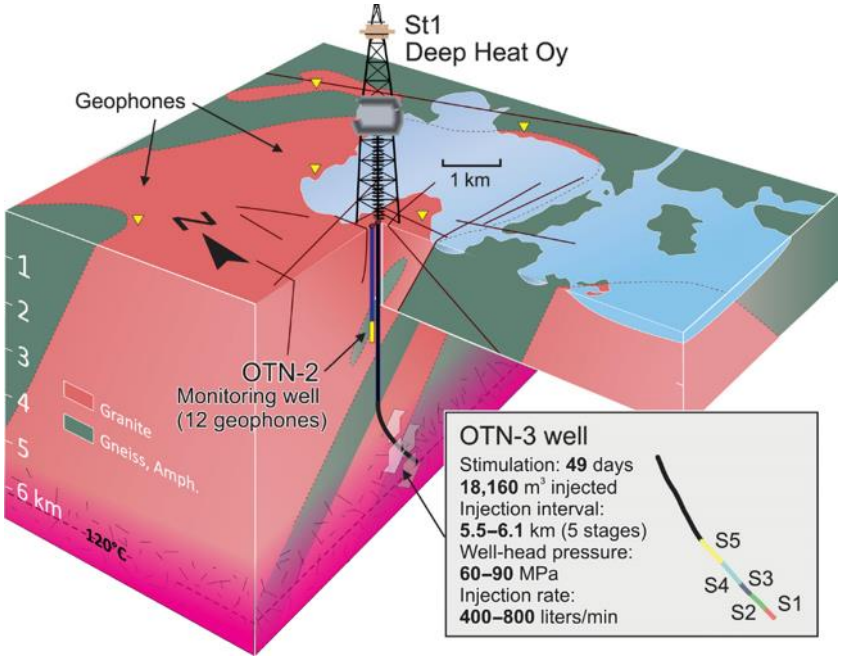

Figure 28. Sketch of the first deep Enhanced Geothermal System (EGS) under construction in southern Finland, at Espoo, close to Helsinki, planned for urban heating (Kwiatek et al. 2019). Drilling of the production borehole was finished in 2018. The bedrock was hydraulically stimulated at depth between 5500 to 6100 m. Induced seismicity was surveyed by a network of 38 geophones installed either in boreholes or on surface (Saarno 2019). The insert shows the location of stimulation stages S1 to S5 into the bottom open hole section and basic stimulation parameters. Note: Geologically, southern Finland and most of northern Sweden belong to the Svecokarelian orogen, i.e., crustal structures and conditions are comparable, and analogies may be drawn for the bedrock in the Kristineberg and Nautanen areas.

4. CONCLUDING REMARKS

The CHPM2030 project requires envisaging structures and lithologies in complex environments at depth down to 7 km. Predicting fracture geometry and permeability at depth in the crystalline bedrock is a crucial point as well and highly challenging. Further intensive multi-disciplinary studies must be considered, e.g., three-dimensional electromagnetic and seismic surveys, as well as better predictions of temperature, heat flow and permeability at depth. The 3D integration of geological and geophysical results will then better allow for planning and conducting of exploration and possibly later-on production drillings.

The ore deposits of Kristineberg and Nautanen originally formed at the Earth's surface or at some depth in the crust have a complex structure. We have identified the mineralised bedrock volumes around these deposits as possible candidates for the challenging future technology, *Combined Heat, Power and Metal extraction from ultra-deep ore formations* (CHPM). The generally low geothermal gradient being of about 16 ^{o}C/km in the investigated ore districts will allow for low- to mid-enthalpy enhanced geothermal systems as part of a possible CHPM unit.

ACKNOWLEDGEMENTS

We thank our colleagues at Uppsala and Luleå universities, Boliden Mines and the Geological Survey of Sweden for valuable input to this report. Tobias B. Weisenberger is thanked for reviewing this report.

REFERENCES[1]

Aastrup, M., Thunholm, B., Johnson, J., Berntell, A. & Bertills, U., 1995: Groundwater Chemistry in Sweden. *Swedish EnvironmentAal Protection Agency, Report 4416*, 52 pp.

Abtahi, S.M., Pedersen, L.B., Kamm, J. & Kalscheuer, T., 2016: Extracting geoelectrical maps from vintage very-low-frequency airborne data, tipper inversion, and interpretation: A case study from northern Sweden. *Geophysics 81*, B135–B147

Ahl, M., Bergman, S., Bergström, U., Eliasson, T., Ripa, M. & Weihed, P., 2001. Geochemical classification of plutonic rocks in central and northern Sweden. *Sveriges geologiska undersökning, Rapporter och meddelanden 106*, 82 pp.

Ahlbom, A., Olsson, O. & Sehlstedt, S., 1995: Temperature Conditions in the SKB Study Sites. *SKB Technical report TR-95-16*. 19 pp.

Ahmadi, O., Juhlin, C., Malehmir, A. & Munck, M., 2013: High-resolution 2D seismic imaging and forward modeling of a polymetallic sulfide deposit at Garpenberg, central Sweden. *Geophysics 78*: B339–B350.

Albino, B. & Weihed. P., 1997: Au-deposits. *In* P. Weihed & T. Mäki (eds.): Volcanic hosted massive sulphide deposits and gold deposits in the Skellefte district, Sweden and western Finland. Research and exploration - where do they meet? 4th Biennial SGA meeting, august 11–13, 1997, Turku Finland, excursion guidebook A2. Geologian tutkimuskeskus, Opas - *Geological survey of Finland Guide 41*, 36–42.

Allen, R. L., Weihed, P. & Svenson, S.-Å., 1996: Setting of Zn-Cu-Au-Ag Massive Sulfide Deposits in the Evolution and Facies Architecture of a 1.9 Ga Marine Volcanic Arc, Skellefte District, Sweden. *Economic Geology 91*, 1022–1053.

Alm, P.-G. & Bjelm, L., 2006: Proceedings, Thirty-first Workshop on Geothermal Reservoir Engineering, Stanford University, Stanford, CA, 30 January – 1 February 2006. *SGP-TR-179*, 6 pp.

Årebäck, H., Einarsson, H., Fagerström, P. & Sandström, B., 2000: Nature of recent Cu-Au and Zn discoveries at the Kristineberg Cu-Zn sulfide deposit, Skellefte district, Sweden. Abstract – *The 24th Nordic Geological Winter meeting 2000, Trondheim, Norway*, 182.

Årebäck, H., Barrett, T.J., Abrahamsson, S. & Fagerström, P., 2005: The Paleoproterozoic Kristineberg VMS deposit, Skellefte district, northern Sweden, part I: Geology. *Mineralium Deposita 40*, 351–367.

Babel Working Group 1990. Evidence for early Proterozoic plate tectonics from seismic reflection profiles in the Baltic shield. *Nature 348*, 34–38.

BABEL Working Group, 1993: Integrated seismic studies of the Baltic shield using data in the Gulf of Bothnia region. *Geophys. J. Int. 112*, 305–324.

Balling, N., 2013: *The Lithosphere Beneath Northern Europe: Structure and Evolution Over Three Billion Years: Contributions from Geophysical Studies.* Doctoral Dissertation, Aarhus University, 191 pp.

Bark, G., Wanhainen, C. & Pålsson, B.I., 2013: Textural setting of gold and its implications on mineral processing: preliminary results from three gold deposits in northern Sweden. *Proceedings of the 12th SGA Biennial Meeting, Uppsala 1*, 302–305.

Barton, M.D., 2014: Iron oxide (-Cu-Au-REE-P-Ag-U-Co) systems. *In* H. Holland & K. Turekian (eds.): *Treatise on Geochemistry*. Elsevier, 2nd edition, volume 13, 515–541.

Barrett, T.J. & MacLean, W.H., 1999: Volcanic sequences, lithogeochemistry, and hydrothermal alteration in some bimodal volcanic-associated massive sulfide systems. *In* C.T. Barrie & M.D. Hannington (eds.): Volcanic-associated massive sulfide deposits: processes and examples in modern and ancient environments. *Reviews in Economic Geology 8*, 101–131.

Bastani, M., Antal Lundin, I., Wang, S. & Bergman, S., 2018: Imaging deeper crustal structures by 2D and 3D modelling of geophysical data. Examples from northern Norrbotten. *In* S. Bergman (ed.): Geology of the Northern Norrbotten ore province, northern Sweden. *Rapporter och Meddelanden 141,* Sveriges geologiska undersökning, 341–359.

Båth, M. & Tryggvason, E., 1962: Deep seismic reflection experiments at Kiruna. *Geofisica Pura e Applicata 51*.

[1] *With additional literature, not cited in text.*

Bauer, T. 2013: *The crustal architecture of the central Skellefte District, Sweden – structural analysis, setting of VMS deposits and 3D-modelling*. PhD thesis, Luleå University of Technology, Sweden, 142 pp.

Bauer, T., Skyttä, P., Allen, R.L. & Weihed, P., 2009: 3-D modelling of the Central Skellefte District, Sweden. Smart science for exploration and mining: *Proceedings of the 10th biennial SGA meeting*, Townsville, Australia, 394–396.

Bauer, T., Tavakoli, S., Dehghannejad, M., Garcia, M. & Weihed, P., 2010: 4-dimensional geological modelling of the Skellefte district, Sweden. *The international archives of the photogrammetry, remote sensing and spatial information sciences. XXXVIII-4.*, 93–96.

Bauer, T.E., Skyttä, P., Tavakoli, S., Dehghannejad, M. & Weihed, P., 2011: *From deposit to regional scale: 4-dimensional geological modeling in the Skellefte Mining District, Sweden*. 3D@GEUS.DK, International workshop on 3D Geological Modeling, Copenhagen, Denmark.

Bauer, T.E., Skyttä, P., Hermansson, T. & Weihed, P., 2012: *The comparison of ore body shapes and regional deformation patterns as a base for prospectivity mapping in the Skellefte Mining District, Sweden*. Mineral resources potential maps workshop, Nancy, France.

Bauer, T.E., Paulik, H., Kathol, B. & Pitcairn, I. (eds.), 2013: The Skellefte district, volcanostratigraphy and structures related to Palaeproterozoic base metal deposits. *Excursion guidebook SWE1, 12th Biennial SGA Meeting, Uppsala*, Sveriges geologiska undersökning, 68 pp.

Bauer, T.E., Skyttä, P., Hermansson, T., Allen, R.L. & Weihed, P., 2014: Comparison of provenance, ore body shape and regional deformation patterns of VMS deposits for mapping the prospectivity in the Skellefte district, Sweden. *Mineralium Deposita 19*, 555–573.

Bauer, T.E., Skyttä, P., Hermansson, T., Dehghannejad, M. & Tavakoli, S., 2015: The Skellefte District. *In* P. Weihed (ed.): *3D, 4D and Predictive Modelling of Major Mineral Belts in Europe.* Mineral Resource Reviews, Springer International Publishing Switzterland, 93–121.

Berggren, M., 1998: *Hydraulic conductivity in Swedish bedrock estimated by means of geostatistics. A study based on data recorded in the Archive on Wells at the Geological Survey of Sweden*. Royal Institute of Technology, Dept. Civil & Environmental Engineering. Thesis Report, Series 1998:9, 48 pp.

Bergman Weihed, J., 1997: Regional deformation zones in the Skellefte and Arvidsjaur areas. *Sveriges geologiska undersökning. Final research report of SGU-project 03-862/93*, 39 pp.

Bergman Weihed, J., 2001. Palaeoproterozoic deformation zones in the Skellefte and Arvidsjaur areas, northern Sweden. *In* P. Weihed (ed.): Economic Geology Research 1. *Sveriges geologiska undersökning C 833*, 46–68.

Bergman, S., 2018: Regional geology of northern Norrbotten County. *In* S. Bergman (ed.): Geology of the Northern Norrbotten ore province, northern Sweden. *Rapporter och Meddelanden 141,* Sveriges geologiska undersökning, 9–17.

Bergman, S., Kübler, L. & Martinsson, O., 2001: Description of regional geological and geophysical maps of northern Norrbotten County (east of the Caledonian orogen). *Sveriges geologiska undersökning Ba 56*, 110 pp.

Bergman, S., Martinsson, O. & Persson, P.-O., 2002a: U-Pb zircon age of a metadiorite of the Haparanda suite, northern Sweden. *In* S. Bergman (ed.): *Radiometric dating results 5. Sveriges geologiska undersökning C 834*, 6–11.

Bergman, S., Persson, P.-O. & Kübler, L., 2002b: U-Pb titanite and zircon ages of the Lina granite at the type locality NW of Gällivare, northern Sweden. *In* S. Bergman (ed.): *Radiometric dating results 5. Sveriges geologiska undersökning C 834*, 12–17.

Bergman, S., Billström, K., Persson, P.-O., Skiöld, T. & Evins, P., 2006: U-Pb age evidence for repeated Palaeoproterozoic metamorphism and deformation near the Pajala shear zone in the northern Fennoscandian Shield. *GFF 128*, 7–20.

Bergman, S., Weihed, P., Martinsson, O., Eilu, P. & Iljina, M., 2007: Geological and tectonic evolution of the northern part of the Fennoscandian Shield. *In* V.J. Ojala, P. Weihed, P. Eilu & M. Iljina (eds.): Metallogeny and tectonic evolution of the Northern Fennoscandian Shield: Field trip guidebook. *Geological Survey of Finland, Guide 54*, 6–15.

Bergman, S., & Stephens, M.B., Anderson, J., Kathol, B. & Bergman T., 2012: Bedrock map of Sweden, scale 1:1 million. *Sveriges geologiska undersökning K 423*.

Bergström, U., 2001. Geochemistry and tectonic setting of volcanic units in the northern Västerbotten county, northern Sweden. *In* Weihed P. (ed.). Economic Geology Research 1. *Sveriges geologiska undersökning C 833*, 69–92.

Bergström, U. & Sträng, T., 1999: Bedrock map 23I Malå NV, NO, SV, SO, scale 1:50 000. *Sveriges geologiska undersökning Ai 114–117*.

Bergström, U., Billström, K. & Sträng, T., 1999: Age of the Kristineberg pluton, western Skellefte District, northern Sweden. *In* S. Bergman, (ed.): Radiometric dating results 4. *Sveriges geologiska undersökning C 831*, 7–19.

Bergström, U., Antal Lundin, I., Winnes, K. & Weihed, P., 2003: Bedrock map 23J Norsjö NV, NO, SV, SO, scale 1:50 000. *Sveriges geologiska undersökning Ai 174–177*.

Carlon, C.J., 2000: Iron oxide systems and base metal mineralisation in northern Sweden. *In* T.M. Porter (ed.): *Hydrothermal iron oxide copper–gold and related deposits: a global perspective*. Australian Mining Foundation, Glenside, Australia, 283–296.

Carranza, E.J.M. & Sadeghi, M., 2010: Predictive mapping of prospectivity and quantitative estimation of undiscovered VMS deposits in Skellefte district (Sweden). *Ore Geology Reviews 38*, 219–241.

Cassard, D., Bertrand, G., Billa, M., Serrano, J.J., Tourlière, B., Angel, J.M. & Gaál, G., 2015: ProMine Mineral Databases: New Tools to Assess Primary and Secondary Mineral Resources in Europe. *In*: Weihed, P. (ed.). *3D, 4D and predictive modelling of major mineral belts in Europe*. Springer Int. publishing, 9–59.

Cherevatova, M., Smirnov, M., Korja, T., Kaikkonen, P., Pedersen, L., Hübert, J., Kamm, J. & Kalscheuer, T., 2014: Crustal structure beneath southern Norway imaged by magnetotellurics. *Tectonophysics 628*, 55–70.

Cherevatova, M., Smirnov, M.Yu., Jones, A.G., Pedersen, L.B. & MaSca Working Group, 2015a: Magnetotelluric array data analysis from north-west Fennoscandia. *Tectonophysics 653*, 1–19

Cherevatova, M., Smirnov, M.Yu., Korja, T., Pedersen, L.B., Ebbing, J., Gradmann, S., Becken, M. & MaSca Working Group, 2015b: Electrical conductivity structure of north-west Fennoscandia from three-dimensional inversion of magnetotelluric data. *Tectonophysics 653*, 20-32

Danielsson, S., 1985: Nautanen. Borrhålsprotokoll och analysintyg från 1985-årsarbeten. *Sveriges geologiska undersökning Prap 85090*, 241 pp.

Dehghannejad, M., 2014: *Reflection seismic investigation in the Skellefte ore district: A basis for 3D/4D geological modeling*. Diss., Uppsala Univ., 68 pp.

Dehghannejad, M., Juhlin, C., Malehmir, A., Skyttä, P. & Weihed, P., 2010: Reflection seismic imaging of the upper crust in the Kristineberg mining area, northern Sweden. *Journal of Applied Geophysics 71*, 125–136.

Dehghannejad, M., Bauer, T., Malehmir, A., Juhlin, C. & Weihed, P., 2012a: Crustal geometry of the central Skellefte district, northern Sweden – constraints from reflection seismic investigations. *Tectonophysics 524*, 87–99.

Dehghannejad, M., Malehmir, A., Juhlin, C. & Skytta, P., 2012b: 3D constraints and finite-difference modeling of massive sulfide deposits: The Kristineberg seismic lines revisited, northern Sweden. *Geophysics 77*, WC69–WC79.

Diehl, T., Kraft, T., Kissling, S. & Wiemer, S., 2017: The induced earthquake sequence related to the St. Gallen deep geothermal project (Switzerland): Fault reactivation and fluid interactions imaged by microseismicity. *J. Geophys. Res. 122*, 7272–7290.

Drejing-Carroll, D, Bauer, T., Karlsson, P., Coller, D., Nordin, R., Hitzman, M. & Allen, R., 2015: New Insight into the links between major porphyry copper, IOCG, and magnetite-apatite deposits from the Gällivare area, Northern Sweden. Society of Economic Geologists, Annual Conference 2015, Hobart, Tasmania. Program and abstracts.

Du Rietz, T., 1953: Geology and ores of the Kristineberg deposit, Vesterbotten, Sweden. *Sveriges geologiska undersökning C 524*, 1–89.

Edelman, N., 1963: Structural studies in the western part of the Skellefte district, northern Sweden. *Geologiska Föreningens i Stockholm Förhandlingar 85*, 185–211.

Edfelt, Å., Sandrin, A., Evins, P., Jeffries, T., Storey, C., Elming S.-Å. & Martinsson O., 2006: Stratigraphy and tectonic setting of the host rocks to the Tjårrojåkka Fe-oxide Cu-Au deposits, Kiruna area, northern Sweden. *GFF 128*, 221–232.

Ehsan, S., Malehmir, A. & Dehghannejad, M., 2012: Re-processing and interpretation of 2D seismic data from the Kristineberg mining area, northern Sweden. *Journal of Applied Geophysics 80*, 43–55.

Eilu, P. (ed.), 2012: Mineral deposits and metallogeny of Fennoscandia. Geological Survey of Finland, *Special Paper 53*, 401 pp.

Eilu, P., Bergman, T., Bjerkgård, T., Feoktistov, V., Hallberg, A., Korsakova, M., Krasotkin, S., Litvinenko, V., Nurmi, P.A., Often, M., Philippov, N., Sandstad, J.S. and Voytekhovsky, Y.L. (comp.) 2013. *Metallic Mineral Deposit Map of the Fennoscandian Shield 1:2 000 000. Revised edition.* Geological Survey of Finland, Geological Survey of Norway, Geological Survey of Sweden, The Federal Agency of Use of Mineral Resources of the Ministry of Natural Resources of the Russian Federation.

Eliasson, T., Eriksson, K.G., Lindquist, G., Malmquist, D. & Parasnis, D., 1991: Sweden. *In* Hurtig, E., Cermák, V., Haenel, R. & Zui, V. (eds.), *Geothermal Atlas of Europe*, Herman Haack Verlagsgesellschaft, Gotha, p. 78.

Elming, S.-Å., Thunehed, H., 1991. A seismic reflection investigation in the Skellefte District, northern Sweden. *Geologiska Föreningens i Stockholm Förhandlingar 113*, 258–259.

Ericsson, L.-O., Holmén, J., Rhén, I. & Blomquist, N., 2008: Storregional grundvattenmodellering –fördjupad analys av flödesförhållanden i östra Småland. Jämförelse av olika konceptuella beskrivningar. *SKB Rapport R-06-64*.

Eriksson, B. & Hallgren, U., 1975: Beskrivning till berggrundskartbladen Vittangi NV, NO, SV, SO. *Sveriges geologiska undersökning Af 13–16*, 203 pp.

Eriksson, T., 1954: Pre-Cambrian geology of the Pajala district, northern Sweden. *Sveriges geologiska undersökning C 522*, 38 pp.

Fennoscandian ore deposit Database: http://en.gtk.fi/informationservices/databases/fodd/index.html.

Fredholm, K.A., 1886: Öfversigt af Norrbottens geologi inom Pajala, Muonionalusta och Tärändö socknar. *Sveriges geologiska undersökning C 83*, 39 pp.

Frietsch, R., 1975: Alkali metasomatism in the ore-bearing metavolcanics of central Sweden. *Sveriges geologiska undersökning C 791*, 54 pp.

Frietsch, R., Tuisku, P., Martinsson, O. & Perdahl, J.-A., 1997: Cu-(Au) and Fe ore deposits associated with Na-Cl metasomatism in early Proterozoic rocks of northern Fennoscandia: A new metallogenic province. *Ore Geology Review 12*, 1–34.

Gaál, G., & Gorbatschev, R., 1987: An outline of the Precambrian evolution of the Baltic shield. *Precambrian Research 35*, 15–52.

García Juanatey, M., 2012: *Seismics, 2D and 3D Inversion of Magnetotellurics. Jigsaw pieces in understanding the Skellefte Ore District*. Diss., Uppsala Univ. 55 pp.

García Juanatey, M., Hübert, J., Tryggvason, A. & Pedersen, L., 2013: Imaging the Kristineberg mining area with two perpendicular magnetotelluric profiles in the Skellefte Ore District, northern Sweden. *Geophysical Prospecting 61*, 200–219.

Gee, D., Juhlin, C., Pascal, C. & Robinson, P., 2010: Collisional Orogeny in the Scandinavian Caledonides (COSC). *GFF 132*, 29–44.

Geijer, P., 1918: Nautanenområdet. En malmgeologisk undersökning. *Sveriges geologiska undersökning C 283*, 103 pp.

Geijer, P., 1931: Berggrunden inom malmtrakten Kiruna–Gällivare–Pajala. *Sveriges geologiska undersökning C 366*, 225 pp.

Geological Survey of Sweden, 2013: Bedömningsgrunder för grundvatten. *SGU-rapport 2013:01*, Sveriges geologiska undersökning, 125 pp.

Gharibi, M., 2000: *Electromagnetic Studies of the Continental Crust in Sweden*. Diss., Uppsala Univ., 24 pp.

Gold, T., 1992: The deep, hot biosphere. *Proc. Natl. Acad Sci. USA. Vol 89*, 6045–6049.

Golder Associates, 2017: *Ansökan om bearbetningskoncession. Hydrogeologisk förstudie Rävliden*. Rapport, unpubl.

Gonzàlez-Roldán, M. J. 2010: *Mineralogia, petrologia y geocuimica de intrusions sin-volcanicas en el distrito minero de Skellefte, norte Suecia*, unpublished Ph.D. thesis (in Spanish with English summary), University of Huelva, Spain, 273 pp., 2010.

Grigull, S., Berggren, R., Jönberger, J., Jönsson, C., Hellström, F.A. & Luth, S., 2018: Folding observed in Palaeoproterozoic supracrustal rocks in northern Sweden. *In* S. Bergman (ed.): Geology of the Northern Norrbotten ore province, northern Sweden. *Rapporter och Meddelanden 141,* Sveriges geologiska undersökning, 205–257.

Grip, E., 1973: Skelleftefältets sulfidmalmer. *In* E. Grip & R. Frietsch (eds.): *Malm i Sverige 2, Norra Sverige*. Almqvist & Wiksell, 194–273.

Grooves, D.I., Bierlein, F.P., Meinert, L.D. & Hitzman, M.W., 2010: Iron oxide copper-gold (IOCG) deposits through Earth history: Implications for origin, lithospheric setting, and distinction from other epigenetic iron oxide deposits. *Economic Geology 105*, 641–654.

Guggisberg, B., Kaminski, W. & Prodehl, C., 1991: Crustal structure of the Fennoscandian Shield: a traveltime interpretation of the long-range FENNOLORA seismic refraction profile. *Tectonophysics 195*, 105–137.

Gustafsson, B., 1985: Fältarbeten 1984 inom delprojektområde Gällivare J Gällivare SV och SO. Slutrapport. *Sveriges geologiska undersökning Prap 85005*, 125 pp.

Gustafsson, B., 1986: Projekt 5515 Malmberget. Prospekteringsarbeten 1985. Rekommendationer för 1986. Lägesrapport 1986-01-15. *Sveriges geologiska undersökning Prap 86004*, 220 pp.

Gustafsson, B. & Johansson, L., 1984: Ferrum kopparfyndighet geofysik och geologi 1984. *Sveriges geologiska undersökning Prap 84158*, 18 pp.

Hanski, E.J., 2012: Evolution of the Palaeoproterozoic (2.50–1.95) non-orogenic magmatism in the eastern part of the Fennoscandian Shield. *In* V.A. Melezhik, A.R. Prave, E.J. Hanski, A.E. Fallick, A. Lepland, L.R. Kump & H. Strauss (eds.): *Reading the archive of Earth's oxygenation*, Volume 1, Springer, Berlin, 179–245.

Hanski, E.J. & Huhma, H., 2005: Central Lapland greenstone belt. *In* R. Lehtinen, P.A. Nurmi, O.T. Rämö (eds.) *Precambrian Geology of Finland – key to the evolution of the Fennoscandian Shield*. Elsevier, Amsterdam, 139–194.

Heidbach, O., Tingay, M., Barth, A., Reinecker, J., Kurfeß, D. & Müller, B., 2008: The World Stress Map database release 2008.

Hellström, F.A., 2018: Early Svecokarelian migmatisation west of the Pajala Deformation Belt, northeastern Norrbotten Province, northern Sweden. *In* S. Bergman (ed.): Geology of the Northern Norrbotten ore province, northern Sweden. *Rapporter och Meddelanden 141,* Sveriges geologiska undersökning, 361–379.

Hellström, F. & Bergman, S., 2016: Is there a 1.85 Ga magmatic event in northern Norrbotten? − U-Pb SIMS zircon dating of the Pingisvaara metagranodiorite and the Jyryjoki granite, northern Sweden, *GFF, DOI: 10.1080/11035897.2016.1171254.*

Hellström, F.A., Kumpulainen, R., Jönsson, C., Thomsen, T.B., Huhma, H. & Martinsson, O., 2018: Age and lithostratigraphy of Svecofennian volcanosedimentary rocks at Masugnsbyn, northernmost Sweden – host rocks to Zn-Pb-Cu-and Cu ±Au sulphide mineralisations. *In* S. Bergman (ed.): Geology of the Northern Norrbotten ore province, northern Sweden. *Rapporter och Meddelanden 141,* Sveriges geologiska undersökning, 151–203.

Hietanen, A. 1975. Generation of potassium-poor magmas in the northern Sierra Nevada and the Svecofennian of Finland. *U.S. Geological Survey Journal of Research 3*, 631−645.

Högbom, A.G., 1899: Skelleftefältets geologi och bergarter. *Geologiska Föreningens i Stockholm Förhandlingar 21*, 636–638.

Högdahl, K., Andersson, U.B. & Eklund, O. (eds.), 2004: The Transscandinavian Igneous Belt (TIB) in Sweden: a review of its character and evolution. *Geological Survey of Finland, special paper 37*, 125 pp.

Holmgren, J. 2013. *Seismic modeling of reflection survey near Kiruna*. BSc thesis, Luleå university, 41 pp.

Holmqvist, P.J., 1906: Studien über die Granite von Schweden: *Bulletin of the Geological Institution of the University of Upsala VII*, 77–269.

Hübert J., Malehmir A., Smirnow M., Tryggvason A. & Pedersen L.B., 2009: MT measurements in the western part of the Paleoproterozoic Skellefte Ore District, Northern Sweden: A contribution to an integrated geophysical study. *Tectonophysics 475,* 493–502.

Hübert, J., 2012: *From 2D to 3D Models of Electrical Conductivity based upon Magnetotelluric Data. Experiences from two Case Studies*. Diss., Uppsala Univ., 55 pp.

Hübert, J., García Juanatey, M., Malehmir, A., Tryggvason, A. & Pedersen, L., 2013: The upper crustal 3-D resistivity structure of the Kristineberg area, Skellefte district, northern Sweden revealed by magnetotelluric data. *Geophysical Journal International 192*, 500–513

Hurter, S., & Haenel, R. (eds.), 2002: *Atlas of Geothermal Resources in Europe*, Office for Official Publications of the European Communities, Luxemburg, 91 pp., 89 plates.

Hurtig, E., Cermak, V., Haenel, R. & Zui, V. (eds.), 1991. *Geothermal Atlas of Europe*. Herman Haack Verlagsgesellschaft, Gotha, 156 pp.

Isaksson, H., Johansson, R. & Triumf, C.-A., 1994: Förstudie Malå. Geofysisk dokumentation och tolkning. *SKB Djupförvar Projekt Rapport PR 44-94-029*, 1–23.

Jensen, M., Kashubin, A., Juhlin, C. & Elming, S., 2012: Multidisciplinary study of the hanging wall of the Kiirunavaara iron ore deposit, northern Sweden. *Geophysics 77*, B269-B285.

Jönberger, J., Jönsson, C. & Luth, S., 2018: Geophysical 2D and 3D modeling in the areas around Nunasvaara and Masugnsbyn, northern Sweden. *In* S. Bergman (ed.): Geology of the Northern Norrbotten ore province, northern Sweden. *Rapporter och Meddelanden 141,* Sveriges geologiska undersökning, 311–339.

Jones, A.G., Olafsdottir, B. & Tiikkainen, J., 1983: Geomagnetic induction studies in Scandinavia. Ill. Magnetotelluric observations. *Journal of Geophysics 54*, 35–50.

Juhlin, C. & Sandstedt, H., 1989: Storage of nuclear waste in very deep boreholes: Feasibility study and assessment of economic potential. *SKB Technical Report TR-89-39*, 92 pp.

Juhlin, C., A. A. Aldahan, J. Castano, B. Collini, T. Gorody, & H. Sandstedt, 1991: *Scientific Summary Report for the Deep Gas Drilling Project in the Siljan Ring Impact Structure*. Naturgas. Älvkarleby, Sweden: Vattenfall Research & Development.

Juhlin C., Wallroth T., Smellie J., Eliasson T., Ljunggren C., Leijon B. & Beswick J., 1998: The Very Deep Hole Concept: Geoscientific appraisal of conditions at great depth. *SKB Technical Report TR 98-05*, 124 pp.

Juhojuntti, N., Olsson, S., Bergman, S. & Antal Lundin, I., 2014: Reflexionsseismiska mätningar vid Kiruna – preliminär tolkning, *SGU-rapport 2014:05*, Sveriges geologiska undersökning, 26 pp.

Kathol, B. & Weihed, P. (eds.), 2005: Description of regional geological and geophysical maps of the Skellefte District and surrounding areas. *Sveriges geologiska undersökning Ba 57*, 197 pp.

Kathol, B., Weihed, P., Antal Lundin, I., Bark, G., Bergman Weihed, J., Bergström, U., Billström, K., Björk, L., Claesson, L., Daniels, J., Eliasson, T., Frumerie, M., Kero, L., Kumpulainen, R.A., Lundström, H., Lundström, I., Mellqvist, C., Petersson, J., Skiöld, T., Sträng, T., Stølen, L.-K., Söderman, J., Triumf, C.-A., Wikström, A., Wikström, T. & Årebäck, H., 2005: Regional geological and geophysical maps of the Skellefte District and surrounding areas. Bedrock map. *Sveriges geologiska undersökning Ba 57:1.*

Kautsky, G., 1957: Ein Beitrag zur Stratigraphie und dem Bau des Skelleftefeldes, Nordschweden. *Sveriges geologiska undersökning C 543*, 1–65.

Koistinen, T., Stephens, M.B., Bogatchev, V., Nordgulen, Ø., Wennerström, M. & Korhonen, J., 2001: Geological map of the Fennoscandian Shield, scale 1 : 2 000 000. *Geological Surveys of Finland, Norway and Sweden and the North-West Department of Natural Resources of Russia.*

Korja, A., Lahtinen, R. & Nironen, M., 2006: The Svecofennian orogen: a collage of microcontinents and island arcs. *In* D.G. Gee & R.A. Stephenson (eds.): European lithosphere dynamics. *Geological Society, London, Memoirs 32*, 561–578.

Kousa, J. & Lundqvist, T., 2000: Svecofennian domain. *In* Th. Lundqvist & S. Autio (eds): Description to the Bedrock Map of Central Fennoscandia (Mid-Norden). *Geological Survey of Finland, Special Paper 28*, 47–75.

Kukkonen, I. T., 2007: Outokumpu Deep Drilling Project. Second International Workshop. Geological Survey of Finland, *Report Q10.2/2007/29*, Espoo, 86 pp.

Kwiatek, G. and 16 others, 2019: Controlling fluid-induced seismicity during a 6.1-km-deep geothermal stimulation in Finland. *SCIENCE ADVANCES*, 01 May 2019, EAAV7224.

Ladenberger, A., Andersson, M., Smith, C. & Carlsson, M., 2018: Till geochemistry in northern Norrbotten – regional trends and local signature in the key areas. *In* S. Bergman (ed.): Geology of the Northern Norrbotten ore province, northern Sweden. *Rapporter och Meddelanden 141,* Sveriges geologiska undersökning, 401–428.

Lagerblad, B. & Gorbatschev, R., 1985: Hydrothermal alteration as a control of regional geochemistry and ore formation in the central Baltic Shield. *Geologische Rundschau 74*, 33–49.

Lahtinen, R., Korja, A. & Nironen, M., 2005: Paleoproterozoic tectonic evolution. *In:* M. Lehtinen, P.A. Nurmi & O.T. Rämö (eds.): *Precambrian geology of Finland – key to the evolution of the Fennoscandian Shield*. Elsevier, Amsterdam, 481–532.

Lahtinen, R., Garde, A.A. & Melezhik, V.A., 2008: Paleoproterozoic evolution of Fennoscandia and Greenland. *Episodes 31*, 1–9.

Lahtinen, R., Huhma, H., Lahaye, Y, Jonsson, E., Manninen, T., Lauri, L.S., Bergman, S., Hellström, F., Niiranen, T. & Nironen, M., 2015: New geochronological and Sm-Nd constraints across the Pajala shear zone of northern Fennoscandia: Reactivation of a Paleoproterozoic suture. *Precambrian Research 256*, 102–119.

Lahtinen, R., Korja, A., Nironen, M. & Heikkinen, P., 2009: Paleoproterozoic accretionary processes in Fennoscandia. *Geological Society, London, Special Publications 318*, 237–259.

Lauri, L.S., Hellström, F., Bergman, S., Huhma, H. & Lepistö, S., 2016: New insights into the geological evolution of the Archean Norrbotten province, Fennoscandian Shield. *Bulletin of the Geological Society of Finland Special Volume 1*, p. 151.

Leary, P., 2018. Enhanced/Engineered Geothermal Systems (EGS). Uppsala university, Geophysics div., Invited lecture, Uppsala, November 8, 2018.

Lehnert, O., Meinhold, G., Bergström, S.M., Calner, M., Ebbestad, J.O., Egenhoff, S., Frisk, Å.M., Hannah, J.L., Högström, A.E.S., Huff, W.D., Juhlin, C., Maletz, J., Stein, H.J., Sturkell, E. & Vandenbroucke, T.R.A., 2012: New Ordovician-Silurian drill cores from the Siljan impact structure in central Sweden: an integral part of the Swedish Deep Drilling Program. *GFF 134*, 87–98.

Le Maitre, R.W., 1976: The chemical variability of some common igneous rocks. *Journal of Petrology 17*, 589–637.

Lorenz, H. 2010. The Swedish deep drilling program: for science and society. *GFF 132*, 25–27.

Louvat, D., J. L. Michelot, & J. F. Aranyossy, 1999: Origin and residence time of salinity in the Äspö groundwater system. *Applied Geochemistry 14*, 917–925.

Ludwig, K.R., 2012: User's manual for Isoplot 3.75. A geochronological toolkit for Microsoft Excel. *Berkeley Geochronology Center Special Publication No. 5,* 75 pp.

Lund, C., 2009: *Mineralogical, chemical and textural properties of the Malmberget iron deposit. A process mineralogically characterisation.* M.Sc. thesis, Luleå University of Technology, Luleå, Sweden, 98 p.

Lund, C.E., Heikkinen, P. 1987. Reflection measurements along the EGT POLAR-profile, northern Baltic Shield. *Geophys. J. R. Astron. Soc. 89*, 361–364.

Lundberg, B., 1980: Aspects of the geology of the Skellefte field, northern Sweden. *Geologiska Föreningens i Stockholm Förhandlingar 102*, 156–166.

Lundberg, E., 2014: 2D and 3D Reflection Seismic Studies over Scandinavian Deformation Zones. Diss., Uppsala Univ., 57 pp.

Lundbohm, H., 1898: Kirunavara-traktens geologi. *Geologiska Föreningens i Stockholm Förhandlingar 20*, 68–78.

Lundbohm, H., 1910: Sketch of the geology of the Kiruna district. *Geologiska Föreningens i Stockholm Förhandlingar 32*, 751–788.

Lundqvist, T., Bøe, R., Kousa, J., Lukkarinen, H., Lutro, O., Roberts, D., Solli, A., Stephens, M. & Weihed, P., 1996a: *Bedrock map of Central Fennoscandia. Scale 1:1 000 000*. Geological Surveys of Finland (Espoo), Norway (Trondheim) and Sweden (Uppsala).

Lundqvist, T., Bøe, R., Kousa, J., Lukkarinen, H., Lutro, O., Luukas, J., Roberts, D., Solli, A., Stephens, M. & Weihed, P., 1997: *Metamorphic, structural and isotope age map of Central Fennoscandia. Scale 1:1 000 000*. Geological Surveys of Finland (Espoo), Norway (Trondheim) and Sweden (Uppsala).

Luth, S., Jönberger, J. & Grigull, S., 2018a: The Vakko and Kovo greenstone belts north of Kiruna: Integrating structural geological mapping and geophysical modelling. *In* S. Bergman (ed.): Geology of the Northern Norrbotten ore province, northern Sweden. *Rapporter och Meddelanden 141,* Sveriges geologiska undersökning, 287–309.

Luth, S., Jönsson, C., Jönberger, J., Grigull, S., Berggren, R., van Assema, B., Smoor, W. & Djuly, T., 2018b: The Pajala Deformation Belt in northeast Sweden: Structural geological mapping and 3D modelling around Pajala. *In* S. Bergman (ed.): Geology of the Northern Norrbotten ore province, northern Sweden. *Rapporter och Meddelanden 141,* Sveriges geologiska undersökning, 259–285.

Luth, S., Jönsson C., Hellström, F., Jönberger J., Djuly, T., van Assema, B. & Smoor, W., 2016: Structural and geochronological studies on the crustal-scale Pajala deformation zone, northern Sweden. *Bulletin of the Geological Society of Finland Special Volume 1*, p. 263.

Lynch, E.P., Bauer, T.E., Jönberger, J., Sarlus, Z., Morris, G.A. & Persson, P.-O., 2018a: Petrology and deformation of c. 1.88 Ga meta-volcanosedimentary rocks hosting iron oxide-copper-gold and related mineralisation in the Nautanen-Gällivare area, northern Sweden. *In* S. Bergman (ed.): Geology of the Northern Norrbotten ore province, northern Sweden. *Rapporter och Meddelanden 141,* Sveriges geologiska undersökning, 107–149.

Lynch, E.P. & Jönberger, J., 2014: Summary report on available geological, geochemical and geophysical information for the Nautanen key area, Norrbotten. *Sveriges geologiska undersökning report 2014:34,* 40 pp.

Lynch, E.P., Jönberger, J., Bauer, T.E., Sarlus, Z. & Martinsson, O., 2015: Meta-volcanosedimentary rocks in the Nautanen area, Norrbotten: Preliminary lithological and deformation characteristics. *Sveriges geologiska undersökning report 2015:30,* 51 pp.

Lynch, E.P., Bauer, T.E., Huhma, H., Drejling-Caroll, D., 2018c: Petrogenesis of c. 1.9 Ga meta-volcanosedimentary rocks in the Nautanen-Aitik area, northern Sweden: Geological, lithogeochemical and Sm-Nd isotopic constraints. Proceedings of the 33rd Nordic Geological Winter Meeting, Copenhagen. Program and abstracts.

Lynch, E.P., Hellström, F.A., Huhma, H., Jönberger, J., Persson, P.-O. & Morris, G.A., 2018b: Geology, lithostratigraphy and petrogenesis of c. 2.14 Ga greenstones in the Nunasvaara and Masugnsbyn areas, northernmost Sweden. *In* S. Bergman (ed.): Geology of the Northern Norrbotten ore province, northern Sweden. *Rapporter och Meddelanden 141,* Sveriges geologiska undersökning, 19–77.

Magnusson, N.H., 1970: *Malm i Sverige 1. Mellersta och södra Sverige*. Almqvist & Wiksell, Stockholm, 320 pp.

Malehmir, A., 2007: *3D Geophysical and Geological Modeling in the Skellefte Ore District: Implications for Targeting Ore Deposits*. Diss., Uppsala Univ., 84 pp.

Malehmir, A., Tryggvason, A., Juhlin, C., Rodriguez-Tablante, J. & Weihed, P., 2006: Seismic imaging and potential field modeling to delineate structures hosting VHMS deposits in the Skellefte Ore District, northern Sweden. *Tectonophysics 426*, 319–334.

Malehmir, A., Tryggvason, A., Lickorish, H. & Weihed, P., 2007: Regional structural profiles in the western part of the Palaeoproterozoic Skellefte ore district, northern Sweden. *Precambrian Research 159*, 1−18.

Malehmir, A., Schmelzbach, C., Bongajum, E., Bellefleur, G., Juhlin, C. & Tryggvason, A., 2009a: 3D constraints on a possible deep > 2.5 km massive sulphide mineralization from 2D crooked-line seismic reflection data in the Kristineberg mining area, northern Sweden. *Tectonophysics 479*, 223–240.

Malehmir, A., Thunehed, H. & Tryggvason, A., 2009b: The Paleoproterozoic Kristineberg mining area, northern Sweden: Results from integrated 3D geophysical and geologic modeling, and implications for targeting ore deposits. *Geophysics 74*, B9–B22.

Malehmir, A., Durrheim, R., Bellefleur, G., Urosevic, M., Juhlin, C., White, D.J., Milkereit, B. & Campbell, G., 2012a: Seismic methods in mineral exploration and mine planning: A general overview of past and present case histories and a look into the future. *Geophysics 77*, WC173–WC190.

Malehmir, A., Urosevic, M., Bellefleur, G., Juhlin, C. & Milkereit, B., 2012b: Seismic methods in mineral exploration and mine planning - Introduction. *Geophysics 77*, WC1–WC2.

Malehmir, A., Andersson, M., Lebedev, M., Urosevic, M. & Mikhaltsevitch, V., 2013: Experimental estimation of velocities and anisotropy of a series of Swedish crystalline rocks and ores. *Geophysical Prospecting 61*, 153–167.

Malehmir, A., Wang, S., Lamminen, J., Brodic, B. & Bastani, M. et al., 2015: Delineating structures controlling sandstone-hosted base-metal deposits using high-resolution multicomponent seismic and radio-magnetotelluric methods: a case study from Northern Sweden. *Geophysical Prospecting 63*, 774–797.

Malin, P.E., 2016: Drilling 5 km to Boiling: The St1 Helsinki District-Heating Gamble. Presentation at the SMU Power Plays Conf.,26 April 2016. https://www.smu.edu/-/media/Site/Dedman/Academics/Programs/Geothermal-Lab/Conference/PastPresentations/2016/Malin_SMUPowerPlays_2016.pdf?la=en

Marsic, N. & Grundfelt, B., 2013: Review of geoscientific data of relevance to disposal of spent nuclear fuel in deep boreholes in crystalline rock. *SKB report P-13-12*, 31 pp.

Martinsson, O., 1993: Stratigraphy of greenstones in the eastern part of northern Norrbotten. *In* O. Martinsson, J.-A. Perdahl & J. Bergman: Greenstone and porphyry hosted ore deposits in northern Norrbotten, *NUTEK Project nr 92-00752P*, 1–5.

Martinsson, O., 1995: Greenstone and porphyry hosted ore deposits in northern Norrbotten. *PIM/NUTEK report #3*, 58 pp.

Martinsson, O., 1997a: *Tectonic Setting and Metallogeny of the Kiruna Greenstones*. Ph.D. thesis, Luleå University of Technology, Luleå, Sweden.

Martinsson, O., 1997b: Paleoproterozoic greenstones at Kiruna in northern Sweden: a product of continental rifting and associated mafic-ultramafic volcanism. *In* O. Martinsson: *Tectonic setting and metallogeny of the Kiruna greenstones. Doctoral thesis 1997:19, Paper I,* 1–49. Luleå University of Technology.

Martinsson, O., 1999a: Berggrundskartan 30J Rensjön SO, skala 1:50 000. *Sveriges geologiska undersökning Ai 13*3.

Martinsson, O., 1999b: Berggrundskartan 31J Råstojaure SV/SO, skala 1:50 000. *Sveriges geologiska undersökning Ai 135*.

Martinsson, O., 2004: Geology and Metallogeny of the Northern Norrbotten Fe-Cu-Au Province. *In* R.L. Allen, O. Martinsson & P. Weihed (eds.): Svecofennian Ore-Forming Environments: Volcanic-Associated Zn-Cu-Au-Ag, Intrusion-Associated Cu-Au, Sediment-Hosted Pb-Zn, and Magnetite-Apatite Deposits of Northern Sweden. *Society of Economic Geologists, Guidebook Series 33*, 131–148.

Martinsson, O. & Wanhainen, C., 2004: Character of Cu-Au mineralisation and related hydrothermal alteration along the Nautanen deformation zone, Gällivare area, northern Sweden. *In* R.L. Allen, O. Martinsson & P. Weihed (eds.): Svecofennian ore-forming environments of northern Sweden – volcanic-associated Zn-Cu-Au-Ag, intrusion-associated Cu-Au, sediment-hosted Pb-Zn, and magnetite-apatite deposits in northern Sweden. *Society of Economic Geologists, guidebook series 33*, 149–160.

Martinsson, O. & Wanhainen, C. (eds.), 2013a: Fe oxide and Cu-Au deposits in the northern Norrbotten ore district. *Excursion guidebook SWE5, 12th Biennial SGA Meeting, Uppsala*, Sveriges geologiska undersökning, 70 pp.

Martinsson, O. & Wanhainen, C., 2013b: The Northern Norrbotten ore district. *In* O. Martinsson & C. Wanhainen (eds.): Fe oxide and Cu-Au deposits in the northern Norrbotten ore district. Excursion guidebook SWE5, 12th Biennial SGA Meeting, Uppsala, Sweden, 19–28.

Martinsson, O., Vaasjoki, M. & Persson, P.-O., 1999: U-Pb ages of Archaean to Palaeoproterozoic granitoids in the Torneträsk-Råstojaure area, northern Sweden. *In* S. Bergman (ed.): Radiometric dating results 4. *Sveriges geologiska undersökning C 831*, 70–90

Martinsson, O., Billström, K., Broman, C., Weihed, P. & Wanhainen, C., 2016: Metallogeny of the Northern Norrbotten Ore Province, northern Fennoscandian Shield with emphasis on IOCG and apatite-iron ore deposits. *Ore Geology Reviews 78*, 447–492.

Martinsson, O., Bergman, S., Persson, P.-O. & Hellström, F.A., 2018a: Age and character of late-Svecokarelian monzonitic intrusions in north-eastern Norrbotten, northern Sweden. *In* S. Bergman (ed.): Geology of the Northern Norrbotten ore province, northern Sweden. *Rapporter och Meddelanden 141,* Sveriges geologiska undersökning, 381–399.

Martinsson, O., Bergman, S., Persson, P.-O., Schöberg, H., Billström, K. & Shumlyanskyy, L., 2018b: Stratigraphy and ages of Palaeoproterozoic metavolcanic and metasedimentary rocks at Käymäjärvi, northern Sweden. *In* S. Bergman (ed.): Geology of the Northern Norrbotten ore province, northern Sweden. *Rapporter och Meddelanden 141,* Sveriges geologiska undersökning, 79–105.

Martinsson, O., Billström, K., Broman C., Weihed, P. & Wanhainen C., 2016: Metallogeny of the Northern Norrbotten ore province, northern Fennoscandian Shield with emphasis on IOCG and apatite-iron ore deposits. *Ore Geology Reviews 78*, 447–492.

McGimpsey, I., 2010: *Petrology and lithogeochemistry of the host rocks to the Nautanen Cu-Au deposit, Gällivare area, northern Sweden*. M.Sc. thesis, Lund University, Lund, Sweden, 82 pp.

McPhie, J., Doyle, M. & Allen, R., 1993: *Volcanic textures: A guide to the interpretation of volcanic textures in volcanic rocks*. CODES Key Centre, University of Tasmania, 198 pp.

Melezhik, V.A. & Fallick, A.E., 2010: On the Lomagundi-Jatuli carbon isotopic event: The evidence from the Kalix Greenstone Belt, Sweden. *Precambrian Research 179*, 165–190.

Melezhik, V.A. & Hanski, E.J., 2012: The early Paleoproterozoic of Fennoscandia: Geological and tectonic settings. *In* V.A. Melezhik, A.R. Prave, E.J. Hanski, A.E. Fallick, A. Lepland, L.R. Kump & H. Strauss (eds.): *Reading the archive of Earth's oxygenation*, Volume 1, Springer, Berlin. 33–38.

Melezhik, V.A., Kump, L.R., Hanski, E.J., Fallick, A.E. & Prave, A.R., 2012. Tectonic evolution and major global Earth-surface palaeoenvironmental events in the Palaeoproterozoic. *In* V.A. Melezhik, A.R. Prave, E.J. Hanski, A.E. Fallick, A. Lepland, L.R. Kump & H. Strauss (eds.): *Reading the archive of Earth's oxygenation*, Volume 1, Springer, Berlin, 3–21.

Mellqvist, C., Öhlander, B., Skiöld, T. & Wickström, A., 1999: The Archean-Proterozoic paleoboundary in the Luleå area, northern Sweden: field and isotope geochemical evidence for a sharp terrane boundary. *Precambrian Research 96*, 225–243.

Monro, D., 1988: *The geology and genesis of the Aitik Cu-Au deposit, arctic Sweden*. Ph.D. thesis, University College Cardiff, UK, 386 pp.

Muhamad, H., Juhlin, C., Lehnert, O., Meinhold, G. & Andersson, M., et al. 2015: Analysis of borehole geophysical data from the Mora area of the Siljan Ring impact structure, central Sweden. Journal of Applied *Geophysics 115*, 183–196.

New Boliden, 2016. *Nautanen copper-mineralization in northern Sweden*. Company press release, 05-02-2016. <www.boliden.com>

Nironen, M., 1997: The Svecofennian orogen: a tectonic model. *Precambrian Research 86*, 21–44.

Ödman, O. H., 1939: Urbergsgeologiska undersökningar inom Norrbottens län. *Sveriges geologiska undersökning C 426,* 100 pp.

Ödman, O. H., 1957: Beskrivning till berggrundskarta över urberget i Norrbottens län. *Sveriges geologiska undersökning Ca 41*, 151 pp.

Ödman, O. H., Härme, M., Mikkola, A. & Simonen, A., 1949: Den svensk-finska geologiska exkursionen i Tornedalen sommaren 1948. *Geologiska Föreningens i Stockholm Förhandlingar 71*, 113–126.

Offerberg, J., 1967: Beskrivning till berggrundskartbladen Kiruna NV, NO, SV, SO. *Sveriges geologiska undersökning Af 1–4*, 147 pp.

Öhlander, B. & Skiöld, T., 1994: Diversity of 1.8 Ga potassic granitoids along the edge of the Archaean craton in northern Scandinavia: a result of melt formation at various depths and from various sources. *Lithos 33*, 265–283.

Öhlander, B., Skiöld, T., Hamilton, P.J. & Claesson, L.-Å., 1987: The western border of the Archaean province of the Baltic Shield evidence from northern Sweden. *Contributions to Mineralogy & Petrology 95*, 437–450.

Padget, P., 1970: Beskrivning till berggrundskartbladen Tärendö NV, NO, SV, SO. *Sveriges geologiska undersökning Af 5–8*, 95 pp.

Parasnis, D.S., 1975: Temperature Phenomena and Heat Flow Estimates in Two Precambrian Ore-bearing Areas in North Sweden. *Geophysical Journal of the Royal Astronomical Society 43*, 531–554.

Parasnis, D.S., 1981: Geothermal flow and phenomena in two Swedish localities north of the Arctic circle. *Geophysical Journal of the Royal Astronomical Society 71*, 545–554.

Perdahl, J.A., 1995: *Svecofennian volcanism in northernmost Sweden*. Ph.D. thesis, Luleå University of Technology, Luleå, Sweden.

Perdahl, J.-A. & Einarsson, Ö., 1994: The marine-continental transition of the Early Proterozoic Skellefte–Arvidsjaur volcanic arc in the Bure area, northern Sweden. *GFF 116*, 133–138.

Perdahl, J.-A., & Frietsch, R., 1993: Petrochemical and petrological characteristics of 1.9 Ga old volcanics in northern Sweden. *In* R. Gorbatschev (ed.): The Baltic Shield. *Precambrian Research 64*, 239–252.

Perdahl, J.-A. & Martinsson, O., 1995: Paleoproterozoic flood basalt magmatism in the Kiruna area, northern Sweden. *In* J.-A. Perdahl: *Svecofennian volcanism in northern Sweden, Doctoral thesis 1995:169D, Paper V,* 1–10. Luleå University of Technology.

Pitcairn, I. (ed.), 2013: The gold line and gold deposits in the Skellefte district. *Excursion guidebook SWE2, 12th Biennial SGA Meeting, Uppsala*, Sveriges geologiska undersökning, 46 pp.

Pitkänen, T., 1997: *Anisotropy of magnetic susceptibility of mylonites from the Kolkonjoki and Nautanen deformation zones in Norrbotten, Sweden*. M.Sc. thesis, Luleå University of Technology, Luleå, Sweden, 64 pp.

Pousette, J., 1988: Groundwater documentation in Sweden. *Water Quality Bulletin 13 (4)*, 138–147.

Reddy, S.M. & Evans, D.A.D., 2009: Palaeoproterozoic supercontinents and global evolution: correlations from core to atmosphere. *In* S.M. Reddy, R. Mazumdr, D.A.D. Evans, A.S. Collins (eds): *Paleoproterozoic supercontinents and global evolution*. *Geological Society, London, Special Publication 323*, 1–26.

Rhén, I., Forsmark, T., Jackson, P., Roberts, D., Swan, D. & Gylling, B., 2008: Hydrogeological conceptualization and parameterization. Site descriptive modeling SDM-Site Laxemar. *SKB Report R-08-78*, 306 pp.

Rodriguez-Tablante, J., Tryggvason, A., Malehmir, A., Juhlin, C. & Palm, H., 2007: Cross-profile acquisition and cross-dip analysis for extracting 3D information from 2D surveys, a case study from the western Skellefte District, northern Sweden. Journal of Applied Geophysics 63, 1–12.

Romer, R.L., Martinsson, O. & Perdahl, J.-A., 1994: Geochronology of the Kiruna iron ores and hydrothermal alterations. *Economic Geology 89*, 1249–1261.

Ros, F., 1980: Nautanenområdet. Rapport över SGU:s arbeten utförda under 1966–1979. *Sveriges geologiska undersökning Brap 81530*, 33 pp.

Rosberg J.-E., 2006: Flow test of a perforated deep dual cased well. Proceedings, Thirty-first Workshop on Geothermal Reservoir Engineering, Stanford University, Stanford, CA, 30 January – 1 February 2006. *SGB-TR-179*, 8 pp.

Rosberg, J.-E., 2010: *Well testing, methods and applicability*. Doctoral Thesis, Department of Engineering Geology, Lund University, 78 pp.

Rutland, R.W.R., Kero, L., Nilsson, G. & Stølen, L.K., 2001a: Nature of a major tectonic discontinuity in the Svecofennian province of northern Sweden. *Precambrian Research 112*, 211–237.

Rutland, R.W.R., Skiöld, T. & Page R.W., 2001b. Age of deformation episodes in the Palaeoproterozoic domain of northern Sweden, and evidence for a pre-1.9 Ga crustal layer. *Precambrian Research 112*, 239–259.

Saarno, T., 2019. St1 Deep Heat Oy, First deep geothermal project in Scandinavia, Achievements today. IEA – Geothermal Baltic Sea Symposium, GeoTHERM, Offenburg, 13 February 2019.

Sammelin, M., 2011. *The Nature of Gold in the Aitik Cu-Au Deposit. Implications for Mineral Processing and Mine Planning*. Licentiate thesis, Luleå University of Technology, Luleå, Sweden, 67 pp.

Sarlus, Z., 2013: *Geology of the Salmijärvi Cu-Au deposit*. M.Sc. thesis, Luleå University of Technology, Luleå, Sweden, 75 pp.

Sarlus, Z., 2016: *Geochemical and geochronological constraints on 1.88 and 1.80 Ga magmatic events in the Gällivare area, northern Sweden*. Licentiate thesis, Luleå University of Technology, Luleå, Sweden, 106 pp.

Sarlus, Z., Andersson, U.B., Bauer T.E., Wanhainen, C., Martinsson, O., Nordin, R., Andersson, J.B.H., 2017: Timing of plutonism in the Gällivare area: implications for Proterozoic crustal development in the northern Norrbotten ore district, Sweden. *Geological Magazine 154,* 1–26. 148

Schellschmidt, R. & Hurter, S., 2002: *Atlas of Geothermal Resources in Europe*, Office for Official Publications of the European Communities, Luxemburg.

Schmelzbach, C., H. Horstmeyer, & Juhlin, C., 2007: Shallow 3D seismic reflection imaging of fracture zones in crystalline rock. *Geophysics 72*, B149–B160.

Schwarz, G., Göransson, M., Thunholm, B. & Förster, A., 2010: Mapping thermal conductivity of the Swedish bedrock. 29th Nordic Geological Winter Meeting, Oslo. *NGF abstracts and proceedings 1*, p. 177.

Schwarz, G. and 18 others, 2016. CHPM2030 Deliverable D 1.2, report on data availability. Publ. by the CHPM2030 project, 18 p. with 5 app.

Skiöld, T., 1979: Zircon ages from an Archean gneiss province in northern Sweden. *Geologiska Föreningens i Stockholm Förhandlingar 101*, 169–171.

Skiöld, T., 1986: On the age of the Kiruna Greenstones, northern Sweden. *Precambrian Research 32*, 3544.

Skiöld, T., 1988: Implications of new U-Pb zircon chronology to early Proterozoic crustal accretion in northern Sweden. *Precambrian Research 38*, 147–164.

Skiöld, T. & Cliff, R.A., 1984: Sm–Nd and U–Pb dating of Early Proterozoic mafic–felsic volcanism in northernmost Sweden. *Precambrian Research 26*, 1–13.

Skiöld, T. & Öhlander, B., 1989: Chronology and geochemistry of late Svecofennian processes in northern Sweden. *Geologiska Föreningens i Stockholm Förhandlingar 111*, 347–354.

Skiöld, T. & Page, R., 1998: SHRIMP and isotope dilution zircon ages on Archaean basement–cover rocks in northern Sweden. 23. *Nordiske geologiske vintermøde, Aarhus 13–16 January 1998,* Abstracts, 273.

Skiöld, T. & Rutland, R.W.R., 2006: Successive ~1.94 Ga plutonism and ~1.92 Ga deformation and metamorphism south of the Skellefte district, northern Sweden: Substantiation of the marginal basin accretion hypothesis of Svecofennian evolution. *Precambrian Research 148*, 181–204.

Skyttä, P., Hermansson, T. & Bauer, T., 2009: Three-Dimensional Structure of the VMS-hosting Palaeoproterozoic Kristineberg Area, Northern Sweden. Smart science for exploration and mining: *Proceedings of the 10th biennial SGA meeting*, Townsville, Australia, 909–911.

Skyttä, P., Hermansson, T., Elming, S-A. & Bauer, T., 2010: Magnetic fabrics as constraints on the kinematic history of a pretectonic granitoid intrusion, Kristineberg, northern Sweden. *Journal of Structural Geology 32*, 1125–1136.

Skyttä, P., Hermansson, T., Andersson, J. & Weihed, P., 2011: New zircon data supporting models of short-lived igneous activity at 1.89 Ga in the western Skellefte District, central Fennoscandian Shield. *Solid Earth 2*, 205–217.

Skyttä, P., Bauer, T., Tavakoli, S., Hermansson, T., Andersson, J. & Weihed, P., 2012a: Evolution of early-orogenic deformation zones and their significance for the development of contrasting structural domains within the Palaeoproterozoic Skellefte District, Sweden. *Geophysical Research Abstracts 14*, EGU2012–14180, EGU General Assembly 2012.

Skyttä, P., Bauer, T.E., Tavakoli, S., Hermansson, T., Andersson, J. & Weihed, P., 2012b: Pre-1.87 Ga development of crustal domains overprinted by 1.87 Ga transpression in the Palaeoproterozoic Skellefte district, Sweden. *Precambrian Research 206–207*, 109–136.

Skyttä, P., Bauer, T., Hermansson, T., Dehghannejad, M., Juhlin, C., Garcia Juanatey, M., Hübert, J. & Weihed, P., 2013: Crustal 3-D deometry of the Kristineberg area (Sweden) with implications on VMS deposits. *Solid Earth 4*, 387–404.

Smith, M., Coppard J., Herrington R. & Stein H., 2007: The geology of the Rakkurijärvi Cu– (Au) prospect, Norrbotten: A new iron-oxide–copper–gold deposit in northern Sweden. *Economic Geology 102*, 393–414.

Smith, M.P., Storey, C.D., Jefferies, T.E. & Ryan, C., 2009: In situ U–Pb and trace element analysis of accessory minerals in the Kiruna district, Norrbotten, Sweden: New constraints on the timing and origin of mineralisation. *Journal of Petrology 50*, 2063–2094.

Smith, M.P., Gleeson S. A. & Yardley B. W. D., 2013: Hydrothermal fluid evolution and metal transport in the Kiruna District, Sweden: Contrasting metal behaviour in aqueous and aqueous–carbonic brines. *Geochimica et Cosmochimica Acta 102*, 89–112.

Spitz, G. & Darling, R., 1978: Major and minor element lithogeochemical anomalies surrounding the Louvem copper deposit, Val d'Or, Quebec. *Canadian Journal of Earth Sciences 15*, 1161–1169.

St1, project website: https://www.st1.eu/geothermal-heat

Stacey, J.S. & Kramers, J.D., 1975: Approximation of terrestrial lead isotope evolution by a two-stage model. *Earth and Planetary Science Letters 26*, 207–221.

Steiger, R.H. & Jäger, E., 1977: Convention on the use of decay constants in geo-and cosmochronology. *Earth and Planetary Science Letters 36*, 359–362.

Stephens, M.B., Wahlgren, C.-H. & Weihed, P., 1997: Sweden. *In* E.M. Moores & R.W. Fairbridge (eds.) *Encyclopedia of European and Asian Regional Geology,* Chapman & Hall, 690–704.

Stephens, M.B., Ripa, M., Lundström, I., Persson, L., Bergman, T., Ahl, M., Wahlgren, C.-H., Persson, P.-O. & Wickström, L., 2009: Synthesis of the bedrock geology in the Bergslagen region, Fennoscandian Shield, south-central Sweden. *Sveriges geologiska undersökning Ba 58*, 259 pp.

Storey, C.D., Smith M.P. & Jefferies T.E., 2007: In situ LA-ICP-MS U–Pb dating of metavolcanics of Norrbotten, Sweden: Records of extended geological histories in complex titanite grains. *Chemical Geology 240*, 163–181.

Sundius, N., 1912: Pebbles of magnetite-syenite-porphyry in the Kurravaara conglomerate. *Geologiska Föreningens i Stockholm Förhandlingar 34*, 703–726.

Sundius, N., 1915: *Beiträge zur Geologie des südlichen Teils des Kirunagebiets.* Vetenskapliga och praktiska undersökningar i Lappland, arrangerade av Luossavaara–Kiirunavaara Aktiebolag, Uppsala, 237 pp.

Svenonius, F., 1900. Öfversikt af Stora Sjöfallets och angränsande fjälltrakters geologi. *Geologiska Föreningens i Stockholm Förhandlingar 22*, 273–322.

Tavakoli, S., Bauer, T. E., Rasmussen, T. M., Weihed, P. & Elming, S.-Å., 2016: Deep massive sulphide exploration using 2D and 3D geoelectrical and induced polarization data in Skellefte mining district, northern Sweden. *Geophysical Prospecting 64*, 1602-1619.

Taylor, S.R., 1964: Abundance of chemical elements in the continental crust: a new table. *Geochimica et Cosmochimica Acta 28*, 1273–1285.

Tegengren, F.R. et al. 1924: Sveriges ädlare malmer och bergverk. *Sveriges geologiska undersökning Ca 17*, 408 pp.

Thomas, M.D., Ford, K.L. & Keating, P., 2016: Review paper: Exploration geophysics for intrusion-hosted rare metals. *Geophysical Prospecting 64*, 1275–1304

Tollefsen, E., 2014: *Thermal and chemical variations in metamorphic rocks in Nautanen, Gällivare, Sweden*. M.Sc. thesis, Stockholm University, Stockholm, Sweden, 50 pp.

Tryggvason, A., Malehmir, A., Rodriguez-Tablante, J., Juhlin, C. & Weihed, P., 2006: Reflection seismic investigations in the western part of the paleoproterozoic VHMS-bearing Skellefte district, northern Sweden. *Economic geology and the bulletin of the Society of Economic Geologists 101*, 1039–1054.

Tucker, M.E., 1991: *Sedimentary petrology: An introduction to the origin of sedimentary rocks*. Blackwell Science, Oxford, 260 pp.

Vivallo, W. & Willdén, M., 1988. Geology and geochemistry of an early Proterozoic volcanic arc sequence at Kristineberg, Skellefte district, Sweden. *Geologiska Föreningens i Stockholm Förhandlingar 110*, 1–12.

Waara, S., 2016: *Garnet occurrence and its relationship to mineralization at the Nautanen deposit, northern Sweden.* M.Sc. thesis, Luleå University of Technology, Luleå, Sweden.

Wanhainen, C., 2005: *On the origin and evolution of the Palaeoproterozoic Aitik Cu-Au-Ag deposit, northern Sweden*. PhD thesis, Luleå University of Technology 2005:36, 38 pp.

Wanhainen, C., Billström, K., Stein, H., Martinsson, O. & Nordin, R., 2005: 160 Ma of magmatic/hydrothermal and metamorphic activity in the Gällivare area: Re-Os dating of molybdenite and U–Pb dating of titanite from the Aitik Cu-Au-Ag deposit, northern Sweden. *Mineralium Deposita 40*, 435–447.

Wanhainen, C., Billström, K. & Martinsson, O., 2006: Age, petrology and geochemistry of the porphyritic Aitik intrusion, and its relation to the disseminated Aitik Cu-Au-Ag deposit, northern Sweden. *GFF 128*, 273–286.

Wanhainen, C., Broman, C., Martinsson, O. & Magnor, B., 2012: Modification of a Palaeoproterozoic porphyry-like system: Integration of structural, geochemical, petrographic, and fluid inclusion data from the Aitik Cu–Au–Ag deposit, northern Sweden. *Ore Geology Reviews 48*, 306–331.

Weihed, P., 2001a: A review of Palaeoproterozoic intrusive hosted Cu-Au-Fe-oxide deposits in northern Sweden. *In* P. Weihed (ed.): Economic geology research, volume 1, 1999-2000. *Sveriges geologiska undersökning C 833*, 4–32.

Weihed, P., 2001b: Economic geology research, volume 1, 1999-2000. *Sveriges geologiska undersökning C 833*, 136 pp.

Weihed, P., 2010: Palaeoproterozoic mineralised volcanic arc systems: the Skellefte district (PaMVAS). *In* Lorenz et al. 2010: *The Swedish Deep Drilling Program. Science and Technology Plan*. Dept. of Earth Sciences, Uppsala University, 47–50 (unpublished).

Weihed, P.; (ed.), 2015: *3D, 4D and predictive modelling of major mineral belts in Europe*. Springer Int. publishing. 331 pp.

Weihed, P., Isaksson, I. & Svensson, S.-Å., 1987: The Tallberg porphyry copper deposit in northern Sweden: a preliminary report. *Geologiska Föreningens i Stockholm Förhandlingar 109*, 47-53.

Weihed, P., Bergman, J. & Bergström, U., 1992: Metallogeny and tectonic evolution of the early Proterozoic Skellefte District, northern Sweden. *Precambrian Research 58*, 143–167.

Weihed, P., Arndt, N., Billström, K., Duchesne, J.-C., Eilu, P., Martinsson, O., Papunen, H. & Lahtinen, R., 2005: Precambrian geodynamics and ore formation: The Fennoscandian Shield. *Ore Geology Reviews 27*, 273–322.

Westhues, A., Hanchar, J.M., Whitehouse, M.J. & Martinsson, O., 2016: New constraints on the timing of host-rock emplacement, hydrothermal alteration, and iron oxide-apatite mineralization in the Kiruna district, Norrbotten, Sweden. *Economic Geology, 111*, 1595–1618.

White, J.D.L. & Houghton, B.F., 2006: Primary volcaniclastic rocks. *Geology 34*, 677–680.

Whitehouse, M.J. & Kamber, B.S., 2005: Assigning dates to thin gneissic veins in high-grade metamorphic terranes: a cautionary tale from Akilia, southwest Greenland. *Journal of Petrology 46*, 291–318.

Whitehouse, M.J., Claesson, S., Sunde, T. & Vestin, J., 1997: Ion-microprobe U–Pb zircon geochronology and correlation of Archaean gneisses from the Lewisian Complex of Gruinard Bay, north-west Scotland. *Geochimica et Cosmochimica Acta 61*, 4429–4438.

Whitehouse, M.J., Kamber, B.S. & Moorbath, S., 1999: Age significance of U–Th–Pb zircon data from Early Archaean rocks of west Greenland: a reassessment based on combined ion-microprobe and imaging studies. *Chemical Geology 160*, 201–224.

Wiedenbeck, M., Alle, P., Corfu, F., Griffin, W.L., Meier, M., Oberli, F., Quadt, A.V., Roddick, J.C. & Spiegel, W., 1995: Three natural zircon standards for U–Th–Pb, Lu–Hf, trace element and REE analysis. *Geostandards Newsletter 19*, 1–23.

Wiedenbeck, M., Hanchar, J.M., Peck, W.H., Sylvester, P., Valley, J., Whitehouse, M., Kronz, A., Morishita, Y., Nasdala, L., Fiebig, J., Franchi, I., Girard, J.P., Greenwood, R.C., Hinton, R., Kita, N., Mason, P.R.D., Norman, M., Ogasawara, M.,

Piccoli, P.M., Rhede, D., Satoh, H., Schulz-Dobrick, B., Skår, O., Spicuzza, M.J., Terada, K., Tindle, A., Togashi, S., Vennemann, T., Xie, Q. & Zheng, Y.F., 2004: Further characterisation of the 91500 zircon crystal. *Geostandards and Geoanalytical Research 28*, 9–39.

Willdén, M., 1986: Geology of the western part of the Skellefte field and the Kristineberg and Horntrask sulphide deposits: *In* D. Rickard (ed.): The Skellefte field. *Sveriges geologiska undersökning Ca 62*, 46–52.

Williams, P.J., 2010: ”Magnetite-group” IOCGs with special reference to Cloncurry (NW Queensland) and northern Sweden: settings, alteration, deposit characteristics, fluid sources, and their relationship to apatite-rich iron ores. *In* L. Corriveau & H. Mumin (eds.): *Exploring for iron oxide copper-gold deposits: Canada and global analogues*. Geological Association of Canada Short Course 20, 23–38.

Winchester, J.A. & Floyd, P.A., 1977: Geochemical discrimination of different magma series and their differentiation products using immobile elements. *Chemical Geology 20*, 325–343.

Witschard, F., 1970: Description of the geological maps Lainio NV, NO, SV, SO. *Sveriges geologiska undersökning Af 9–12*, 116 pp.

Witschard, F., 1975: Description of the geological maps Fjällåsen NV, NO, SV, SO. *Sveriges geologiska undersökning Af 17–20*, 125 pp.

Witschard, F., 1984: The geological and tectonic evolution of the Precambrian of northern Sweden a case for basement reactivation? *Precambrian Research 23*, 273–315.

Witschard, F., 1996: Berggrundskartan 28K Gällivare NO, NV, SO, SV. 1:50 000-scale maps. *Sveriges geologiska undersökning Ai 98–101*. (With a description in English).

Witschard, F., & Zachrisson, E., 1995: Berggrundskartan 28I Stora Sjöfallet SO, 1:50 000, *Sveriges geologiska undersökning Ai 91*.

Zweifel, H., 1976: Aitik, geological documentation of a disseminated copper deposit – A preliminary Investigation: *Sveriges geologiska undersökning C 720*, 80 pp.

APPENDIX

Abbreviations

EGS	Enhanced geothermal system
EVD	Eastern volcanosedimentary domain
GDS	Geomagnetic deep soundings
IOCG	Iron oxide-copper-gold mineral deposit
LA-ICP-MS	Laser Ablation Inductively Coupled Mass Spectrometry
MT	Magnetotellurics
NDZ	Nautanen deformation zone
VLF	Very low frequency
VMS	Volcanogenic massive sulphides
WVD	Western volcanosedimentary domain

List of databases

Table A.1. Summary of databases held by SGU and relevant for the CHPM2030 project, i.e., the two study areas in northern Sweden around the Kristineberg and the abandoned Nautanen mine.

Table A.2. Summary of data in web map services (WMS) – as from the Map Viewer (Swedish: kartvisaren), held by SGU and relevant for the two Swedish study areas of the CHPM2030 project, presented in tthis report. In accordance with INSPIRE access is free of charge.

Table A1: Databases at SGU	**Kristineberg comments (scale, coverage, number)**	**Nautanen comments (scale, coverage, number)**
Map area - this report	*1172 km²*	*202 km²*
Bedrock, ores and minerals		
Bedrock observations	Data from the outcrop database, 1779 observation points	Data from the outcrop database, 288 observation points
Bedrock samples	Numerous but not registered	128
Outcrop map	Included in Bedrock map 1:50 000 – 1:250 000	Included in Bedrock map 1:50 000 – 1:250 000
Bedrock map	1:1 000 000, entire area 1:50 000 – 1:250 000, entire area	1:1 000 000, entire area 1:50 000 – 1:250 000, entire area
Dating, isotope analysis	6 analyses	4 analyses
Drill cores	1103 cores, partly scanned	236 cores, partly scanned
Ores and minerals	Entire area	Entire area
Mineral resources	Data from 41 objects (mine to prospect)	Data from 71 objects (mine to prospect)
Mineral permits	254 km²	119 km²
Mineral deposits of national interest	51 km²	21 km²
Geophysics		
Ground geophysics, different methods, prospecting areas	Almost entire area	Almost entire area
Airborne geophysics, total magnetic field	Line spacing mostly 200 m, data points every 18 m, entire area	Line spacing mostly 200 m, data points every 18 m, entire area
Airborne geophysics, gamma radiation (K -Th - U)	One dataset each for potassium, thorium, uranium, entire area	One dataset each for potassium, thorium, uranium, entire area
Ground geophysics, gamma radiation (K - Th - U)	63 measuring sites	56 measuring sites
Ground geophysics, gravity	Bouguer anomaly field, 2512 regional and 12021 local measuring points	Bouguer anomaly field, 328 regional measuring points
Petrophysical observations	90	103
Petrophysical laboratory measurements	96	191
Magnetic susceptibility measured in laboratory	0	351
Magnetic susceptibility measured on outcrop	2020	696
VLF-profiles	0	570 measuring points
MP-profiles	0	75054 measuring points
Geochemistry		
Ground geochemistry, copper	x measuring points	x measuring points
Lithogeochemistry	Measuring points with analysed data, 511 analyses	Measuring points with analysed data, 152 analyses
Ground geochemistry, physical samples	632	157
Groundwater, well and groundwater monitoring		
Wells	137	13
Groundwater	1:1 000 000, entire area	1:1 000 000, entire area
Springs	2	2
Quaternary deposits		
Soil map	1:1 000 000, entire area 1:50 000 – 1:250 000, entire area	1:1 000 000, entire area 1:50 000 – 1:250 000, entire area
Soil map	Midnorden, 1: 750 000, entire area	Northernmost Sweden, 1:250 000, entire area
Soil thickness	Map and measuring points, entire area	Map and measuring points, entire area
Glacial striation	114 measuring points	23 measuring points
Ground stability properties	> 1:100 000, entire area	> 1:100 000, entire area
Ground permeability	> 1:100 000, entire area	> 1:100 000, entire area
Landslides and gullies	Some observation points	No observations

Table A2: Datasets in Mapviewer	Language	Kristineberg comments (scale, coverage, number)	Nautanen comments (scale, coverage, number)
Access of data	https://apps.sgu.se/kartvisare/index-en.html Remark: Data covered by INSPIRE or for scientific research are free of charge		
Map area this report		*1172 km²*	*202 km²*
Bedrock, ores and minerals			
Bedrock map	Swedish, English	1:1 000 000, entire area	1:1 000 000, entire area
Bedrock map	Swedish	1:50 000 – 1:250 000, entire area	1:50 000 – 1:250 000, entire area
Dating, isotope analysis	Swedish	6	4
Drill cores	Swedish, English	1103	236
Drill cores, hyperspectral scanning, IR data	Swedish, English	Yes	Yes
Ores and minerals	Swedish, English	Entire area	Entire area
Mineral resources, included in Mapviewer for ores and minerals	Swedish, English	41	71
Mineral permits	Swedish, English	254 km²	119 km²
Mineral deposits of national interest	Swedish, English	51 km²	21 km²
Geophysics			
Ground geophysics, different methods, prospecting areas	Swedish	Almost entire area	Almost entire area
Airborne geophysics, Total magnetic field	Swedish	Line spacing mostly 200 m, data points every 18 m, entire area	Line spacing mostly 200 m, data points every 18 m, entire area
Airborne geophysics, gamma radiation (uranium, potassium, thorium)	Swedish	One dataset each for uranium, potassium and thorium, entire area	One dataset each for uranium, potassium and thorium, entire area
Ground geophysics, gravity	Swedish	Bouguer anomaly field, 2512 regional and 12021 local measuring points	Bouguer anomay field, 328 regional measuring points
Geochemistry			
Ground geochemistry, copper	Swedish, English	Measuring points with copper content	Measuring points with copper content
Lithogeochemistry	Swedish, under construction	Measuring points with analyse data	Measuring points with analyse data
Groundwater, well and groundwater monitoring			
Wells	Swedish, English	137	13
Groundwater	Swedish, English	1:1 000 000, entire area	1:1 000 000, entire area
Springs	Swedish, English	2	2
Quaternary deposits			
Soil map	Swedish	1:1 000 000, entire area	1:1 000 000, entire area
Soil map	Swedish	1:50 000 – 1:250 000, entire area	1:50 000 – 1:250 000, entire area
Soil map	Swedish	Midnorden, 1: 750 000,m entire area	Northernmost Sweden, 1:250 000, entire area
Soil thickness	Swedish	Map and measuring points, entire area	Map and measuring points, entire area
Ground stability properties	Swedish	> 1:100 000, entire area	> 1:100 000, entire area
Ground permeability	Swedish	> 1:100 000, entire area	> 1:100 000, entire area
Landslides and gullies	Swedish, English	Some observation points	No observations

CHPM2030 DELIVERABLE D6.2.5

EUROPEAN OUTLOOK

Summary:
This report summarises the studies provided by the Linked Third Parties, about the potential areas of CHPM development in Europe. The data was collected based on guidelines provided by the European Federation of Geologists.
The geological data related to mineral deposit and geothermal projects, were collected in WP1 and WP6. It has been grouped and presented on an online ESRI© application based on OpenStreetMap, as the European perspective areas for the future development of CHPM technology.
This activity, whose outputs is accessible to the public, is interest for technology developers, the external research groups and policy makers at national and EU level, informing them about areas where CHPM could be developed in the future. The application is available from the following link: http://bit.ly/CHPMinfoplatform

Authors:
Domenico Marchese, Project Officer, European Federation of Geologist
Anita Demény, Project Officer, European Federation of Geologist
Isabel Fernandez, Executive Director, European Federation of Geologist

TABLE OF CONTENT

LIST OF TABLES

LIST OF *FIGURES*

LIST OF ABBREVIATIONS

CHM	Combined Heat and Metal extraction
CHPM	Combined Heat, Power and Metal extraction
EFG	European Federation of Geologists
EGS	Enhanced Geothermal System
LTP	Linked Third Parties
OSM	OpenStreetMap

1 Executive summary

This report is part of the Deliverable D6.2 "Report on Pilot – compiled from 5 reports" within WP6 - "Roadmapping and Preparation for Pilots" aimed at preparing the ground for the pilot implementation which represents the step forward towards the realization of the novel technological solution (Combined Heat, Power and Metal extraction from ultra-deep ore bodies). This work has put together the data collected with the results of the most recent predictive metallogenic models. The report provides a "European perspective" on the potential areas of CHPM development.

The Linked Third Parties, following the guidelines and indications provided by the European Federation of Geologists, have evaluated the existing geological data relating to mineral deposits and geothermal projects, previously collected in Work Package 1, according to the potential application of CHPM technology. This work has put together the data collected with the results of the most recent predictive metallogenic models.

The task of the LTPs were three-fold:

1. Area selection: this task was concerning with the selection of a limited number of sites where drill holes showed the entry characteristics to define an area most likely to be a future CHPM candidate (temperature, metal enrichments, fluids and so on).
2. Basic area evaluation: the task continued with the evaluation of the basic characteristics of the selected areas by taking into account geological and geophysical data with a CHPM relevance, mineralisation, integrated 3D models, EGS potential info and so on.
3. CHPM characteristics: this task considered a deeper investigation and data comprehension of the most likely CHPM sites where some operational characteristics were taken into account as well as the related environmental and social impacts that may arise from such CHPM systems.

The area selection was a screening process, looking for areas for future CHPM application, that is intended to be further investigated in the future, as interest for CHPM technology arise. Areas selected as type B, has the potential for metal extraction and direct heating systems (“CHM”), while areas type A has the potential for heat, power and metal extraction (”CHPM”). In either case the next step is further geophysical/geological exploration at the identified areas.

16 of the LTPs have been involved in the task, investigating CHPM potential in the following countries: Belgium, Czech Republic, Finland, France (investigation conducted by EFG), Germany, Greece, Hungary, Ireland, Italy, Netherlands, Poland, Portugal, Serbia, Slovenia, Spain, Switzerland, Ukraine.

Besides, the "Institut Royal des Sciences Naturelles de Belgique" (IRSBN), collected and evaluated the data provided by 8 countries, that were not directly involved in the project (e.g. Austria, Croatia, Cyprus, Luxembourg, Slovakia, Sweden the United Kingdom).

As a summary, 37 over 70 places have been identified with “Type A: T > 100°C” and 20 with "Type B: T > 40-50°C" that have future potential for applying CHPM technology.

In the selected areas several kinds of mineralisation have been identified: hydrothermal (incl. epithermal) and porphyry are those most commonly reported. The depth of mineralisation, as well as the correspondence temperature, vary considerably site by site. Exhaustive reports

of each selected site have been collected in Annexes below, including a list of commodities and the degree of mineralisation expressed in % or ppm when provided by the LTPs.
The study has been supported by a concise visual map of all the CHPM prospective areas selected within the participant Linked Third Parties countries (see Paragraph 5), and openly available from the following link: http://bit.ly/CHPMinfoplatform

2 Introduction and scope of the work

The work this report is concerning with, is based on the previous study[1] performed by the Linked Third Parties (LTPs) in which 24 European Countries, under the guide and supervision of the European Federation of Geologists (EFG), collected publicly available data at national level on deep drilling programs, geophysical and geochemical explorations and any kind of geo-scientific data related to the potential deep metal enrichments[2] as well as real ore bodies[3].
The WP1 allowed to draw up a "European outlook" on data availability in order to identify data gaps.
The study performed by the LTPs has taken into account, in particular, the occurrence of the following metals, such as Cu, Zn, Pb, Fe, As, Sb, Ag, Au, Li, Co, Cr, Ni, U, Sn, W and Mo, even though they could report about any other metal enrichment they found important and relevant in their countries.
The study other than providing a European outlook on data availability, aimed at identifying data gaps, represented a first step to prepare the conceptual framework for a novel enhanced geothermal system (EGS) by gathering information on deep metal enrichments that could be converted into an orebody EGS as well as to investigate the characteristics of these bodies.
The scope of the present work is to the develop a study and a spatial database on European scale of prospective CHPM areas by assessing the geological data on suitable ore-bearing formations and geothermal projects collected in the WP1 in relation with the potential application of the CHPM technology.

3 Objectives and Methodology

Taking into account the main objective of Task 6.2, which is to support the development of technology and economic feasibility for pilot implementation of a CHPM system, the Task 6.2.5 focuses the attention on the selection and basic evaluation of European potential areas.
The EFG LTPs, in particular, were called to evaluate the geological data on suitable ore-bearing formations and geothermal projects collected in WP1 "Methodology framework definition" that aimed at the preparation of the conceptual framework for a novel EGS system.
To train the LTPs on how to reach the goals of the Task 6.2.5, and to harmonise the work in order to obtain from all the LTPs the same level of quality for the data acquired, the EFG

[1] See CHPM2030 Deliverable D1.2 APPENDIX 1.2.5;
[2] Geological formations in which the metal content is at least five times higher than the average in the given formation type;
[3] Ore bodies which have economic value on their own;

organised an “orientation workshop” for the National Associations (Linked Third Parties), involved in CHPM2030 project.

EFG LTPs involved in CHPM2030 (16+1)			Data collected by RBINS (7)
• Belgium	• Hungary	• Serbia	• Austria
• Czech Republic	• Ireland	• Slovenia	• Croatia
• Finland	• Italy	• Spain	• Cyprus
• France (by EFG)	• The Netherlands	• Switzerland	• Luxemburg
• Germany	• Poland	• Ukraine	• Slovakia
• Greece	• Portugal		• Sweden
			• United Kingdom

Table 1: Countries included in the European outlook for prospective locations

The aim of the workshop, held in Brussels on 12th of April 2018 and managed by “La Palma Research Centre” leader of the Task 6.2 “Preparation for Pilots”, was to update the LTPs about the recent development of the project and to create guidelines and instructions for CHPM prospective areas selection & evaluation.

The LTPs were introduced to the scope of their involvement through presentations from Éva Hartai, CHPM2030 Project’s Coordinator (UNIM), who delivered a general project presentation. Details of the CHPM technology building blocks, such as underground heat exchanger, production pump, metal recovery at high pressure/temperature, surface heat exchanger in the geothermal power plant, gas diffusion electro-precipitation metal recovery, salt gradient power generation, injection well, were explained by Tamas Madarász (UNIM).

Gerhard Schwarz (SGU) presented the Data Availability, Summary of the Country Reports as collected in WP1.

Tamas Miklovicz (LPRC), introduced the overall picture at WP6 level, and explained objectives for the study area evaluation. Followed the contribution of Anita Demény, from EFG, who detailed the objective of the LTP efforts.

During the workshop, LTPs, based on different geological cases that could have been encountered in several countries, decided to develop and to elaborate a harmonised framework to adopt a shareable guide towards a possible study area evaluation for CHPM potential. Finally, guidelines and the framework to study a possible area were both defined and approved.

After the workshop the template was finalised and the three LTP main tasks were outlined:

Area selection of prospective CHPM areas

EFG LTPs were asked to define at minimum one, but maximum 6 prospective CHPM areas in their country, and have to indicate the requested information on these areas in the Prospective CHPM areas table (Table 3).

If more than 6 areas were identified in one country, all of them could be indicated into the prospective CHPM areas table, but the area assessment, which was the upcoming task, had been done only for the 6 most suitable areas. The main parameters that had to be taken into consideration during the prospective CHPM area(s) selection were 1) the existence of deep

metal enrichment(s): degree of the mineralization, and type of mineralization; 2) the temperature: considering the possibility of heat and power production (type A: T > 100 °C) or only heat production (type B: T > 40-50 °C).

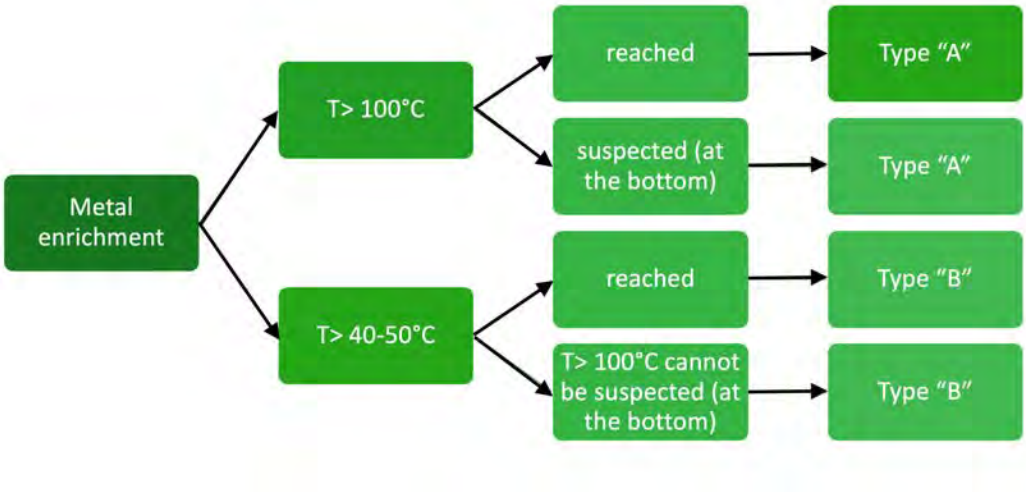

Figure 1: Decisional scheme for selecting the prospective areas

LTPs were recommended to collect the relevant information for the area selection by considering the following sources: 1) results of Work Package 1 (focusing on the publicly available data sets on deep drilling programmes); 2) Geological maps and heat flow maps; 3) Geological archives; 4) drilling data; 5) Open access geo-data sources; 6) Publications;

Name of the National Association (LTP)							
No.	Type of the selected area(s) (type "A" or type "B")	Depth(s) of the metal enrichment(s) (m)	Temperature /at these depths/ (°C)	Description of the metal enrichment(s)			
				degree of the mineralization(s) (% or ppm)	*type of the mineralization(s)[1]*	*element(s)*	*area delineation(s)[2]*

Table 2: Template to be filled in with data for Prospective CHPM areas selection

A. Evaluation of basic characteristics of prospective CHPM areas

The second task was to define prospective CHPM areas in their country and filled out the Prospective CHPM areas table (see Table 2) to list the selected prospective CHPM areas. As "Type of mineralisation" (note 1 in Table 2) LTPs could choose several options (e.g. Skarn, Porphy, etc.), whereas for "Area delineation" (note 2 in Table 2) they could refer to coordinates of one significant point, including the buffer zone around the point, or even more points.

For the six most suitable chosen areas, LTPs were also asked to evaluate the basic characteristics of each of them by filling a template form containing the information reported in Table 3 (a).

Evaluation of basic characteristics	Evaluation of CHPM characteristics
CHPM geology → local geology (in regional context) → target formation → available cross sections, geological maps, geochemical results, lithological information	**Operational characteristics: expected design parameters** → **Expected design parameters of the CHPM technological building blocks** • underground heat exchanger • production + injection wells • electrolytic metal recovery • gas diffusion electro-precipitation • power plant (heat exchanger) • local heat and electricity demand • salt gradient power generation → **Environmental, social and political background** • gaseous and solids emissions • water and noise pollution • land and water use • induced seismicity/landslides, subsidence • public acceptance • political support • legislation, regulatory framework → **Financial aspects** • local demand for heat and electricity
CHPM geophysics → previous geophysical measurement (in CHPM relevance) → what measurements can be used and how to locate/define the ultradeep orebody/heat exchanger → available geophysical maps, cross sections, logs, other measurements	
Deep metal enrichment → (expected) metal enrichment based on available geophysical, geological, drill data, samples information, geochemistry	
Integrated 3D-4D model → existing 3D models of the target area and of the deep metal enrichment	
EGS geothermal potential → EGS potential (heat & energy) of the area → geothermal characteristics (temperature gradient, heat flux, stress field, water availability, EGS geology) → presence of deep fluids/brines, fracture system, crustal permeability	
(a)	(b)

Table 3: (a) requested information for the evaluation of basic characteristics; (b) Evaluation of CHPM characteristics

B. Evaluation of CHPM characteristics of prospective CHPM areas

For the six most suitable areas (from the selected ones), EFG Linked Third Parties had to report on the evaluation of the basic characteristics of the areas by 31 August 2018 followed by the report on the evaluation of the CHPM characteristics of the same areas.

A suitable template form containing the information reported in Table 3 (b) was filled in by the LTPs.

However, it is important to mention that this area selection for prospective areas, was a rough screening for areas that may be further investigated in the future. Areas selected as “type B”, has the potential for use “CHM” technology and use the delivered metal extraction technological couples with direct heating application. Areas selected as “type A” may be actual areas for a full scale CHPM application, after a thorough geophysical exploration that can show the ultra-deep mineral enrichment. On the other hand, if the requirements were set too high (T > 170 °C + indicated metal enrichment), many potential areas would have been ruled out due to the lack of information or direct evidence at such depths.

4 Linked Third Parties data report

Data collected from the 23 European countries revealed the potential of some countries for CHPM EGS application providing the European overview on data availability, during the first half of the project. The 19 countries, out of 23, which participated in this survey reported that 6
drillholes with temperatures exceeding 100°C exists in their country. The number of such entries varies from 1 (Ireland) to 2809 (Germany).
Among them, eight countries mentioned the identification of metal enrichment, such as Austria, Belgium, Cyprus, Hungary, Poland, Serbia, Slovak Republic and UK, while five of those (Belgium, Hungary, Poland, Serbia and Slovak Republic) provided more detailed information about these metal enrichments including some data on geographical, geological, geochemical and geophysical data. These latter countries could be of further interest of the CHPM technology.
In the second part of the project, the focus was on data evaluation and selection of prospective areas for CHPM technology. The areas are summaries in a table at each country. In the summary tables, each row in the column “Temperature” is an individual site/well.
Since the relevant information for the project is not fully available, or sometimes are partially available, it is necessary to set up further cooperation with Nation experts and/or Organisation that own and manage the required data in order to fill the gap.
The following section of this document summaries the data availability (deep drillholes with metal enrichment), and data evaluation (summary tables of the CHPM areas).
The original country reports, provided by the National Associations, annexed to this document.

4.1 CHPM Area selection per country

4.1.1 Austria

Data Provided by: Institut royal des Sciences naturelles de Belgique (IRSBN)

According to the available data, Austria could have a large geothermal potential throughout its deep (alkali) metal enrichment zones. The Geological Survey of Austria reported that around 100 drilling programmes reached the +100°C isotherm of which some with known Ni-enriched reservoir(s). Nevertheless, most of the data requested is not or only partly publicly available since most of the hydro chemical datasets related to deep aquifers are obtained by the hydrocarbon industry. Interesting to note is an ongoing research on scaling and erosion

at thermal wells in Austria with focus on geochemical components in deep reservoirs. One area has been identified as potential future CHPM site (Table 4.). Read the full country report from Austria here (link).

Geographical name	Type of selected area(s)	Depth(s) of the metal enrichment(s), m	Temperature, °C (and depth in m, if provided)	Type of mineralisation	Elements
Furstenfeld (Frutura dublet)	A	3188 (final well depth)	115	Hydrothermal	As, F, Fe, Li, Sr, S, Cu, Zn, Ni, Mn

Table 4: Summary of the CHPM areas selected in Austria

4.1.2 Belgium

Data Provided by: Institut royal des Sciences naturelles de Belgique (IRSBN)

In Belgium, according to the data collected, there might be 5 wells that reach the 100°C isotherm depth and, hence, they could be of CHPM interest. Among those, only 4 sites have been selected. Among those, only 4 sites have been selected (Table 5). Read the full country report from Belgium here (link).

Geographical name	Type of selected area(s)	Depth(s) of the metal enrichment(s), m	Temperature, °C (and depth in m, if provided)	Type of mineralisation	Elements
Havelange	A	I) 5370, II) 5449, III) 5532	I) 118, II) 120, III) 123	Hydrothermal	I) LREE, Allanite II) Th Co Au Pb, Te Bi, III) idem as II)
Grand Halleux	B	2850 --> 2886	61	Hydrothermal vein-associated	REE, P, As, Cu, Pb, Co, Ni
Saint-Ghislain	A	I) 1841 --> 2150, II) 4320	I) 64 --> 165 (@4830), II) 120	Evaporite	I) Anhydrite Ba F Sr, II) Fe
Mol, Balmatt	A	3200 --> 3800	139 --> 142	SEDEX (Sedimentary Exhalative)	Fe, Mn, Zn

Table 5: Summary of the CHPM areas selected in Belgium

4.1.3 Croatia

Data Provided by: Institut royal des Sciences naturelles de Belgique (IRSBN)

Poor drilling data were found in publication as the boreholes datasets belongs to the Ministry of Economy and are until now unavailable. Data on deep metal enrichments may exist but are not listed in databases, nor examined or have not been made publicly available. A comparison between the geological map and the scarce information on the metallogenic map brought to no results. Several areas can be selected, but only for geothermal potential. Read the full country report from Croatia here (link).

4.1.4 Cyprus

Data Provided by: Institut Royal des Sciences Naturelles de Belgique (IRSBN)

In Cyprus, no borehole that reaches the depths where the temperature exceeds 100 ° C, neither any metal enrichment has been identified below the depths where the temperature exceeds 100 ° C. However, some general information has been gathered about metal enrichment and the summary is reported here (Table 6). Read the full country report from Cyprus here (link).

Geographical name	Type of selected area(s)	Depth(s) of the metal enrichment(s), m	Temperature, °C (and depth in m, if provided)	Type of mineralisation	Elements
Kokkinoiyia	B	>300	30 (@300)	VMS (Volcanogenic Massive Sulfide)	S, Cu, Zn
Agrokipia B	B	>530	40 (@530)	VMS (Volcanogenic Massive Sulfide)	Fe, Zn, Cu, Si, As, Ba, K
Skouriotissa - Apliki	B	>200	28 (@200)	VMS (Volcanogenic Massive Sulfide)	Cu, Zn, Fe
Mathiatis	B	>400	35 (@400)	VMS (Volcanogenic Massive Sulfide)	Cu, Zn, Ni, Co

Table 6: Summary of the CHPM areas selected in Cyprus

4.1.5 Finland

Data Provided by: Finnish Union of Environmental Professionals YKL (LOIMU)

Finland did not report the existence of the drillholes with temperatures exceeding 100°C. However, in T6.2 two areas have been selected for CHPM potential (Table 7). Read the full country report from Finland here (link).

Geographical name	Type of selected area(s)	Depth(s) of the metal enrichment(s), m	Temperature, °C (and depth in m, if provided)	Type of mineralisation	Elements
Outokumpu Deep Hole	B	2500	40	Pegmatite	Li
Not provided	A/B	6400	90 - 100	No mineralisation reported. Not likely to be any metal enrichments.	Not provided

Table 7: Summary of the CHPM areas selected in Finland

4.1.6 France

Data Provided by: European Federation of Geologists EFG

In French territories, only two sites have been identified: one is in continental Europe and the other one is located in the French overseas region, Guadeloupe, in the Lesser Antilles (Table 8). Read the full country report from France here (link).

Geographical name	Type of selected area(s)	Depth(s) of the metal enrichment(s), m	Temperature, °C (and depth in m, if provided)	Type of mineralisation	Elements
Bouillante (Guadalupe Island)	A	I) 500 II) 1 000	I) 200 II) 250 – 260	Epithermal	A sodium chloride (NaCl) brine + traces of As, Zn, Fe, Cs the geothermal fluid is enriched in K, Ca, Si, B, F, Sr, Li, Rb, Cs and most metals Fe, Al, Mn, Cu, Ni, Pb, Zn, Co, Cd
Soultz-sous-Forêts	A	I) 1440 II) 3500 III) 5000 IV) Deep Reservoir	I) 124 II) 160 III) 203 IV) 230-240	Hydrothermal	Fluids are NaCl type, enriched in calcium and lithium. The hottest brines are very enriched in K, Ca, SiO2, Li, Rb, Cs, As, Sr, Ba, Mn, Nd, U and in metals such as Zn, Pb, Cu, Co, Cd, Sb.

Table 8: Summary of the CHPM areas selected in France

4.1.7 Greece

Data Provided by: Association of Greek Geologists (A.G.G.)

Greece reported the existence of 6 site (Table 9) located in two islands: Lesvos and Xanthi with unknown occurrence of metal enrichments (each cell in the fourth column represents exploration and/or productive wells). Read the full country report from Greece here (link).

Geographical name	Type of selected area(s)	Depth(s) of the metal enrichment(s), m	Temperature, °C (and depth in m, if provided)	Type of mineralisation	Elements
Northern Lesvos (Stypsi Area)	A	Unknown	100 (250) 98 (400) 91.4 (1015) 83 (1400)	Porphyry	Cu, Mo, Re, Bi, Pb, Se, Ag, Au
Northern Lesvos Argenos Area)		Unknown	85-87 (50-120) 74 (140) 79-81 (140-200) 72 (220-230) 65-70 (50-100) 52.6 (150) 49.4 (200)	Porphyry	
Wester Milos	A	Unknown	44 (65) 39 (70) 41 (65) 40 (70) 43 (70) 41.5 (75)	Epithermal	Pb, Zn, Ag, Au, Cu, Sb, Te
Central Milos			310-320 (837-1080) 323 (1150) 318 (1150-1200)		Ag, Au, As, Bi, W, Mo

			270 (827) 310 ? (1000)		
Aristino Alexandroupolis	A	Unknown	72.3 (360) 51.8 (216) 86.8 (340) 89 (360) 60.1 (370) 64 (440) 79 (120) 89 (235)	Ephitermal	Cu, Au, Ag, Pb, Zn, Bi, Sn, Ge, Ga, In, Mo, V, As, Hg, Te, Se
Aristino Evros Delta area			136 (3975) 146 (4229) 100 (3000) 104 (2650) 108 (2860)		
Sappea	B	Unknown	40.6 (440) 38.9 (360)	Epithermal	Cu, Fe, Mo, Au, Pb, Zn, Sb, As
Xanthi - Nestos Delta area (Eratino)	A	Unknown	75 (650) 60.9 (430) 52.6 (400) 62.8 (470) 61.4 (400) 69.7 (530) 65 (510) 122 (1377)		Fe, Cu, Zn, W, Bi, Au, Mo
Xanthi - Nestos Delta area (Neo Erasmio)			64.3 (170) 68 (380) 66.7 (350)		
Xanthi - Nestos Delta area (Nea Kessani)			83 (460) 80 (120) 79 (350) 77.6 (340) 74.5 (170) 73.7 (350) 71.9 (420) 71.7 (340) 70.4 (226) 70 (272) 65.9 (470) 65 (60) 76.8 (430) 72.7 (463) 72.3 (512) 71 (473)		Fe, Cu, Pb, Zn, Mn, Cd, As, Sb, Bi, Te, Ag, Au
Thermes Xanthi	B	Unknown	41 (200)	Carbonate Replacement, Vein	Pb, Zn, Fe, Cu, Mn, As, Sb, Cd, Te, Ag, Au

Table 9: Summary of the CHPM areas selected in Greece

4.1.8 Hungary

Data provided by: Hungarian Geological Society (UGS)

Around 100 drillholes, which reached the depths where the temperature exceeds 100°C, were identified in Hungary. For more than 10 of them the data, which could be useful for the future actions of the project, are publicly available via database of National Office of Mining and Geology, in concession database of Oil researches. Unfortunately, not any metal enrichment relevant for the scope of the project was identified below the depths where the temperature

exceeds 100°C. The only one site that, currently, has been selected (Table 10). Read the full country report from Hungary here (link).

Geographical name	Type of selected area(s)	Depth(s) of the metal enrichment(s), m	Temperature, °C (and depth in m, if provided)	Type of mineralisation	Elements
Recsk	B	1100 . 1200	62	Skarn + vein associated	Cu, Zn, Fe

Table 10: Summary of the CHPM areas selected in Hungary

4.1.9 Germany

Data Provided by: BDG – Berufsverband Deutscher Geowissenschaftler e.V.

Among 2809 drillholes that reached the depths where the temperature exceeds 100°C (data not publicly available), only 4 have been selected and considered as potential interest of the CHPM (Table 11). Read the full country report from Germany here (link).

Geographical name	Type of selected area(s)	Depth(s) of the metal enrichment(s), m	Temperature, °C (and depth in m, if provided)	Type of mineralisation	Elements
Grube Anna-Elisabeth	A	Not enough data available	25-30 (300) 30°-35 (500) 55-60 (1000) 70-75 (1500) 90-95 (2000) 115-120 (2500) 140 (>3000)	Porphyry	Pb, Cu, Ag
Silberbergwerk Suggental	A	idem	20-25 (300) 20-25 (500) 50-55 (1000) 60-65 (1500) 70-75 (2000) 115-120 (2500) 140-150 (>3000)	Hydrothermal	Pb, Cu, Ag, Au
Schwarzenberg	B	idem	100 - 130	Skarn + vein-associated	U, W, Ag, Fe, Cu, Sn, Zn
Revier Halsbrücke	B	idem	100 - 130	Hydrothermal vein-associated	Ag, Pb, Zn, Cu, Bi, Co, W, Ni, U, (Au)

Table 11: Summary of the CHPM areas selected in Germany

4.1.10 Ireland

Data Provided by: Irish Geological Institue (IGI)

One drillhole which reached the depths where the temperature exceeds 100°C was identified in Ireland. It was drilled in 1965 for hydrocarbon exploration with no mineral enrichment noted. The data from the drillhole is only partly publicly available. Additionally, there is regional geophysical data (magnetics, radiometrics and EM) for approximately one third of the country available on www.tellus.ie. One site has been selected under T6.1 for potential CHPM application (Figure 12). Read the full country report from Ireland here (link).

Geographical name	Type of selected area(s)	Depth(s) of the metal enrichment(s), m	Temperature, °C (and depth in m, if provided)	Type of mineralisation	Elements
Mourne Mountains	A	Not provided	100	--	Th, As, Sn, Y, Nb, Mn, Ce

Table 12: Summary of the CHPM areas selected in Ireland

4.1.11 Italy

Data Provided by: Consiglio Nazionale dei geologi (CNG)

Exactly 694 drillholes, which reached the depths where the temperature exceeds 100°C, were identified in Italy managed by the Ministry of Economic Development in the frame of "Geothermal Resources National Inventory". The inventory comprises data for 948 geothermal wells (the first one was drilled in 1900, the last one is being drilled yet). At the moment the 268 are free for consultation. Among all the geothermal wells included in the inventory, 694 of them can be distinguished as those with T > 100°C. Unfortunately, none of the geothermal wells provide any metal enrichment information. The existing geothermal wells are fully devoted to the production of electricity. All the information related to possible metal enrichments might be held by the drilling companies with no obligation to deliver such specific data to the Ministry of Economic Development who is the Authority that manages the data. Currently, the inventory of the geothermal wells and areas is under deep revision and an exhaustive WebGis Database might be consulted at this web address http://bit.ly/2UqFZqI *"Banca Dati Nazionale Geotermica a cura di: CNR - Istituto di Geoscienze e Georisorse In collaborazione con ENI S.P.A. - Div. R&M"*. The database, which incorporates the subsurface stratigraphic data, indicate the characteristic of hot springs, gas and events with relevant data of geothermal wells, the isotherms at 1000, 2000 and 3000 meters from ground level and the heat flow to the surface, and the positions of the aquifers, all over the country.

4.1.12 Luxembourg

Data Provided by: Institut Royal des Sciences Naturelles de Belgique (IRSBN)

For Luxembourg there is no area eligible for the CHPM project. No deep metal enrichment has been identified in the country: only shallow metal enrichments are located in south Luxembourg in the mining region of Esch sur Alzette. No metal enrichments were identified below the depths where the temperature exceeds 100°C. Read the full country report from Luxembourg here (link).

4.1.13 Netherlands

Data Provided by: Royal Geological and Mining Society of the Netherlands, the Netherlands (KNGMG)

More than 800 drillholes, mostly drilled for the purposes of oil/gas industry, which reached the depths where the temperature exceeds 100°C have been identified in Netherlands. There are data publicly available for each drillhole (www.nlog.nl). No metal enrichment has been

identified below the depths where the temperature exceeds 100°C during the first part of the project. Most of the data about the subsurface is freely available via various web portals with regards to subsurface models, drillhole descriptions and geothermal potential like www.thermogis.nl, www.nlog.nl and www.dinoloket.nl. For the scope of the Task, only 5 sites have been selected (Figure 12). Read the full country report from The Netherlands here (link).

Geographical name	Type of selected area(s)	Depth(s) of the metal enrichment(s), m	Temperature, °C (and depth in m, if provided)	Type of mineralisation	Elements
Bergermeer, BGM-03	A	2904/5	105	SSC (Stratiform Sediment-hosted Copper)	Cu
Ameland Westgat, AWG-106	A	4012/3	130	Idem	Cu
Borgsweer, BRW-04	B	2955	95	Idem	Cu
Koekoekspolder, KGP-GT-02	B	2017	70	Idem	Cu (pyrite present between 2105 and 2108)
Venio, CAL-GT-01	B	1802.00	60	MVT (Mississipi Valley Type)	Pb, Zn

Table 13: Summary of the CHPM areas selected in Netherlands

4.1.14 Poland

Data Provided by: Polish Association of Minerals Asset Valuators, Poland (PAMAV)

A few dozen of drillholes which reached the depths where the temperature exceeds 100°C were identified in Poland with publicly available data and metal enrichment identified. The selected areas are summarised in Table 14. Read the full country report from Poland here (link).

Geographical name	Type of selected area(s)	Depth(s) of the metal enrichment(s), m	Temperature, °C (and depth in m, if provided)	Type of mineralisation	Elements
Mozów	B	2530	80 - 85	SSC (Stratiform Sediment-hosted Copper)	Cu, Ag, (Au, Pt, Pb, Co, Ni)
Kaleje	A/B	3130	100 - 105	Idem	Cu, Ag, (Au, Pt, Pb, Co, Ni)
Żerków	A	3540	115 - 120	Idem	Cu, Ag, (Au, Pt, Pb, Co, Ni)
Florentyna	A	3860.00	125 -130	Idem	Cu, Ag, (Au, Pt, Pb, Co, Ni)

Table 14: Summary of the CHPM areas selected in Poland

4.1.15 Portugal

Data Provided by: Portuguese Association of Geologists (APG)

A set of drillholes has been identified and selected for the scope of the Task, within the Iberian Pyrite Belt (IPB) which is a metallogenetic province about 250-km long and 20–70 km wide

located in the SW part of the Iberian Peninsula, between Seville (Andalusia, Spain) and Marateca (Alentejo, Portugal). The concrete site selected is in Table 15.
More detailed data are included in the Deliverable 6.2.2: Report on Pilots: Portugal, Iberian Pyrite Belt, by the Portuguese Geological Survey. The full country report from, provided by the National Association, is available here (link).

Geographical name	Type of selected area(s)	Depth(s) of the metal enrichment(s), m	Temperature, °C (and depth in m, if provided)	Type of mineralisation	Elements
Minas de Neves-Corvo	B	250 to 1200	22° (@250), 42°(@1200)	VMS (Volcanic Massive Sulphide)	Minas de Neves-Corvo

Table 15: Summary of the CHPM areas selected in Portugal

4.1.16 Serbia

Data Provided by: Serbian Geological Society (SGS)

Only 3 drillholes which reached the depths where the temperature exceeds 100°C were identified in Serbia. A few more (5) are close to this temperature, and it will be probably reached if drilling will proceed deeper. The data of 4 of these drillholes are publicly available and metal enrichment identified in 2 drillholes (Table 16). Read the full country report from Serbia here (link).

Geographical name	Type of selected area(s)	Depth(s) of the metal enrichment(s), m	Temperature, °C (and depth in m, if provided)	Type of mineralisation	Elements
Borska reka	Not defined	from 449 to 879	70 (@bottom)	Porphyry	Cu, Au
Chukaru Peki (Bor District)	Not defined	2068 (from 200 to 2268)	57.00	Porphyry	Cu, Au

Table 16: Summary of the CHPM areas selected in Serbia

4.1.17 Slovakia

Data Provided by: Institut royal des Sciences naturelles de Belgique (IRSBN)

Two metal enrichment sites were identified below the depths where the temperature exceeds 100°C in Slovak Republic. For the scope of the Task only one site has been selected (Table 17). Read the full country report from Slovakia here (link).

Geographical name	Type of selected area(s)	Depth(s) of the metal enrichment(s), m	Temperature, °C (and depth in m, if provided)	Type of mineralisation	Elements
Košice Basin / Ďurkov Depression	A	1600-2000, 2600-4000	87, 180	Epithermal	As

Table 17: Summary of the CHPM areas selected in Slovakia

4.1.18 Slovenia

Data Provided by: Slovenian Geological Society, Slovenia (SGD)

In Slovenia exists 41 drillholes that have reached the depths where the temperature exceeds 100°C (+additional 24 drillholes where 100°C would be reached certainly if measured). All these drillholes are managed by O&G Companies, hence most of data are not publicly available. Some of them were published in the scope of EU funded projects T-JAM and TRANSENERGY and can be found at the following links, respectively: http://bit.ly/2UloacF and http://bit.ly/2YL1lOH (Log in requested). Only one site was selected for data evaluation (Table 18). Read the full country report from Slovenia here (link).

Geographical name	Type of selected area(s)	Depth(s) of the metal enrichment(s), m	Temperature, °C (and depth in m, if provided)	Type of mineralisation	Elements
Mala Kopa	B (Hypothetical)	Hypothetical 2,000 Hypothetical 3,000	Not provided	Hydrothermal	Fe, Pb, Zn +/- minor Cu, Ag?

Table 18: Summary of the CHPM areas selected in Slovenia

4.1.19 Spain

Data Provided by: Ilustre Colegio Oficial de Geologos (ICOG)

The 33 drillholes which reached the depths where the temperature exceeds 100°C were identified in Spain. For 8 of them the data are publicly available. The metal enrichment below the depths where the temperature exceeds 100°C were not identified. Only 1 site has been selected (Table 19). Read the full country report from Spain here (link).

Geographical name	Type of selected area(s)	Depth(s) of the metal enrichment(s), m	Temperature, °C (and depth in m, if provided)	Type of mineralisation	Elements
Mazarrón, Murcia	B	100	50	Epithermal	Pb, Zn, Cu, Fe-sulphides, Pb-SbCu-sulphosalts, Native Silver
Tenerife	A	no mineralization	no mineralization	no mineralization	no mineralization

Table 19: Summary of the CHPM areas selected in Slovenia

4.1.20 Sweden

Data Provided by: Institut royal des Sciences Naturelles de Belgique (IRSBN)

The generally low geothermal gradient being less than 20°C/km in the crystalline basement of the Fennoscandian Shield in Sweden (Eliasson et al. 1991) will allow for low-to-mid-enthalpy geothermal systems as part of a potential CHPM unit. For the scope of the Task, 4 sites were identified and selected (Table 20). The full country report, provided by the National Association, is available here (link). Deliverable 6.2.4 Report on Pilots: Sweden, contains more detailed information provided by the Swedish Geological Survey.

Geographical name	Type of selected area(s)	Depth(s) of the metal enrichment(s), m	Temperature, °C (and depth in m, if provided)	Type of mineralisation	Elements
Zinkgruvan	B	1125	20-25 (calculated from average geothermal gradient)	Skarn + SEDEX	Cu, Zn, Pb, Ag
Yxsjober	B	600	15-20 (calculated from average geothermal gradient)	Skarn	Cu, W
Renstrom	B	1450	30 (calculated from average geothermal gradient)	VMS (Volcanic Massive Sulphide)	Zn, Cu, Pb, Au, Ag
Kirunavaara	B	1540	25 (calculated from average geothermal gradient)	Volcanogenic stratiform	Not provided

Table 20: Summary of the CHPM areas selected in Sweden

4.1.21 Switzerland

Data Provided by: Swiss Association of Geologists (CHGEOL)

Although in Switzerland have been identified some mineralisation, their concentration was never considered sufficient for industrial exploration.

It is still unclear if such mineralised rock volume could ever be exploited economically using leaching techniques. There is no metallogenic province in Switzerland and the potential is low. Historically, this is confirmed by the fact that Switzerland has never had any metallic industry in the past. Read the full country report from Switzerland here (link).

4.1.22 Ukraine

Data Provided by: Ukrainian Association of Geologists (UAG)

Only 1 site has been selected by UAG for the scope of the Task (Table 21). Read the full country report from Ukraine here (link).

Geographical name	Type of selected area(s)	Depth(s) of the metal enrichment(s), m	Temperature, °C (and depth in m, if provided)	Type of mineralisation	Elements
Transcarpathian	A	Floating	100 – 150 (3000)	Hydrothermal	Pb, Zn, Ag, Au, Hg

Table 21: Summary of the CHPM areas selected in Sweden

4.1.23 United Kingdom

Data Provided by: Institut royal des Sciences Naturelles de Belgique (IRSBN)

The Cornubian orefield, or other orebodies in SW England (Cornwall, Devon & part of Somerset), are related to high heat productivity and stress history of these granite batholiths. The whole region is enriched with a variety of metals, the primary ones of which occur in zones around bodies of granite. The Deliverable 6.2.1 Report on Pilots: South West England, contains more detailed information provided by the British Geological Survey. The Table 22

reports data summary provided by the LTP IRSBN. Read the full country report from the United Kingdom here (link).

Geographical name	Type of selected area(s)	Depth(s) of the metal enrichment(s), m	Temperature, °C (and depth in m, if provided)	Type of mineralisation	Elements
Dartmoor	A	Few Hundreds ms to 1000m	185 (@5000)	Hydrothermal	Co, Sb, Mn, Cu, Zn, As, Pb, Fe, Ce, Mg, Al, Si, S, K
Bodmin	A	Few Hundreds ms to 1000m	200 (@5000)	Hydrothermal	Co, Sb, Mn, Cu, Zn, As, Pb, Fe, Ce, Mg, Al, Si, S, K
St Austell	A	Few Hundreds ms to 1000m	221 (@5000)	Greisen	Co, Sb, Mn, Cu, Zn, As, Pb, Fe, Ce, Mg, Al, Si, S, K
Land's End	A	FHms-1000m	206 (5000)	Hydrothermal	Co, Sb, Mn, Cu, Zn, As, Pb, Fe, Ce, Mg, Al, Si, S, K

Table 22: Summary of the CHPM areas selected in Sweden

5 Online mapping of the selected CHPM sites

The entire set of selected CHPM sites have been concisely mapped on a publicly available web-based application named "Story Map" by ESRI© based on OpenStreetMap (OSM) data. The application consists of 5 thematic tabs: the first is a general introduction to the CHPM project; the second tab, as well as the third and the fourth tabs, contain the CHPM selected sites based on the location (Figure 2), temperature (Figure 3) and type of mineralisation (Figure 4). The last tab shows the map of the Linked Third parties and the Partners of the project.

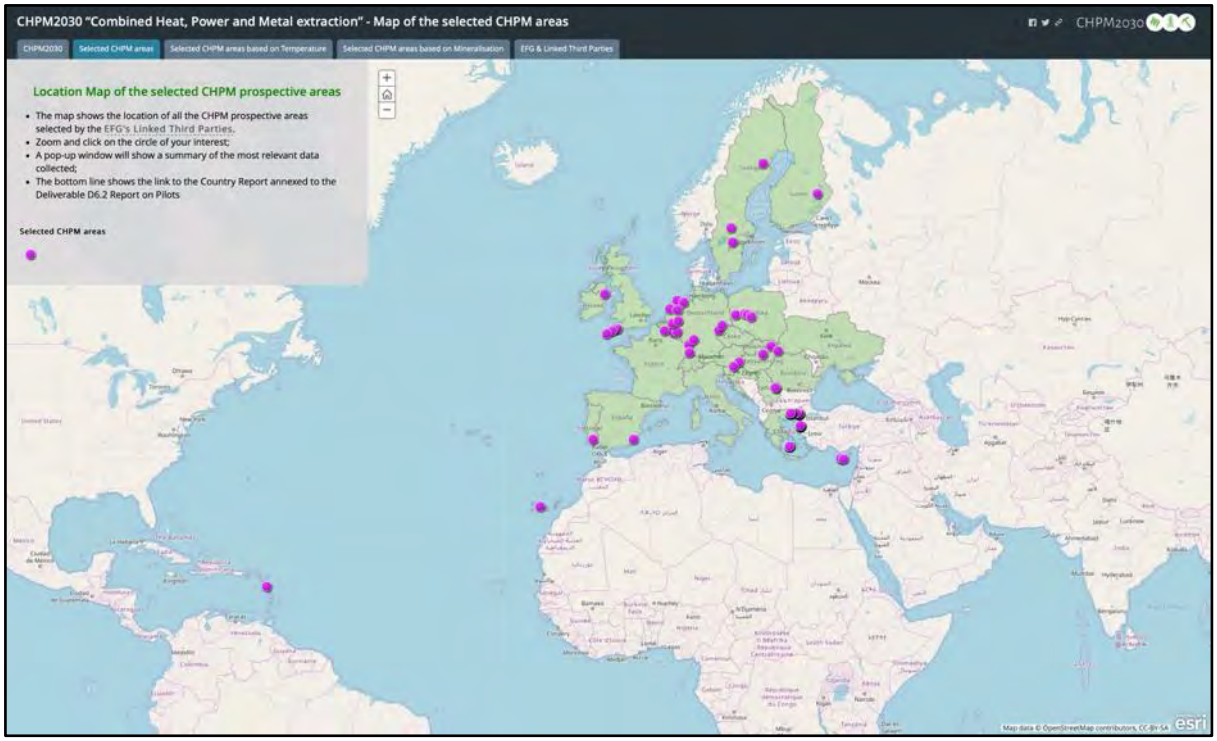

Figure 2: Location of all the selected CHPM areas as provided by LTPs

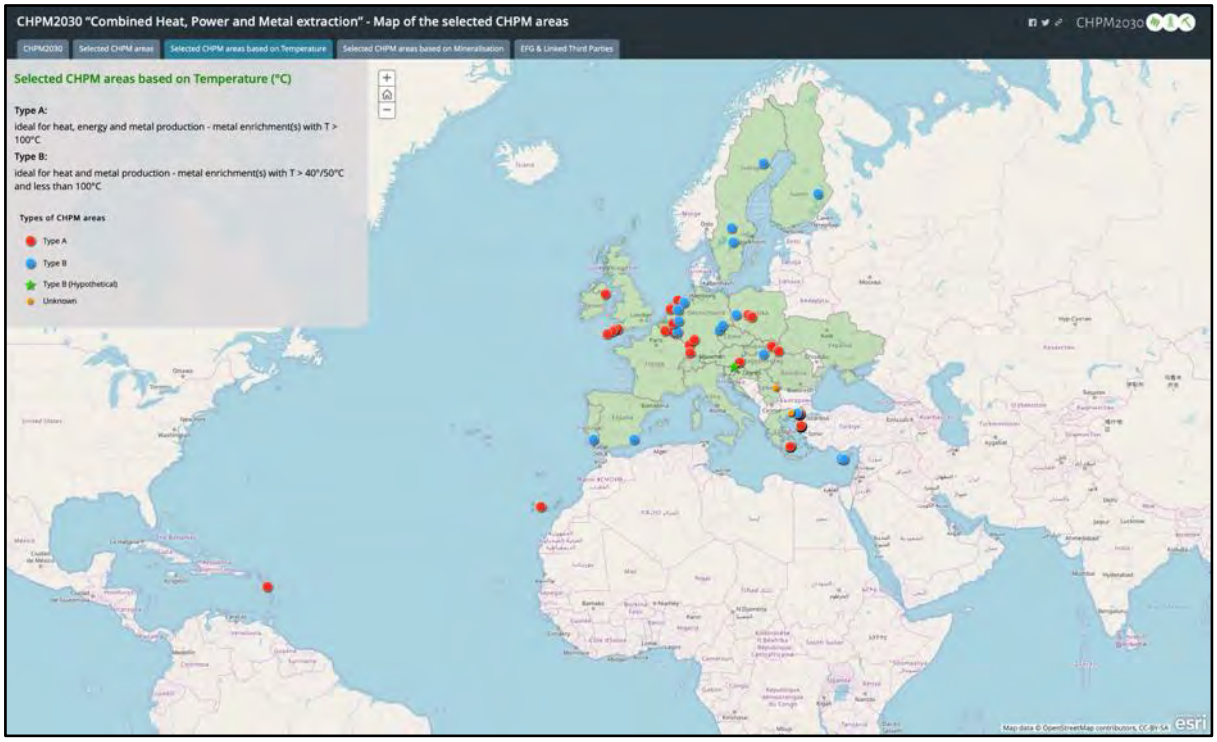

Figure 3: Selected CHPM areas based on the temperature as provided by LTPs

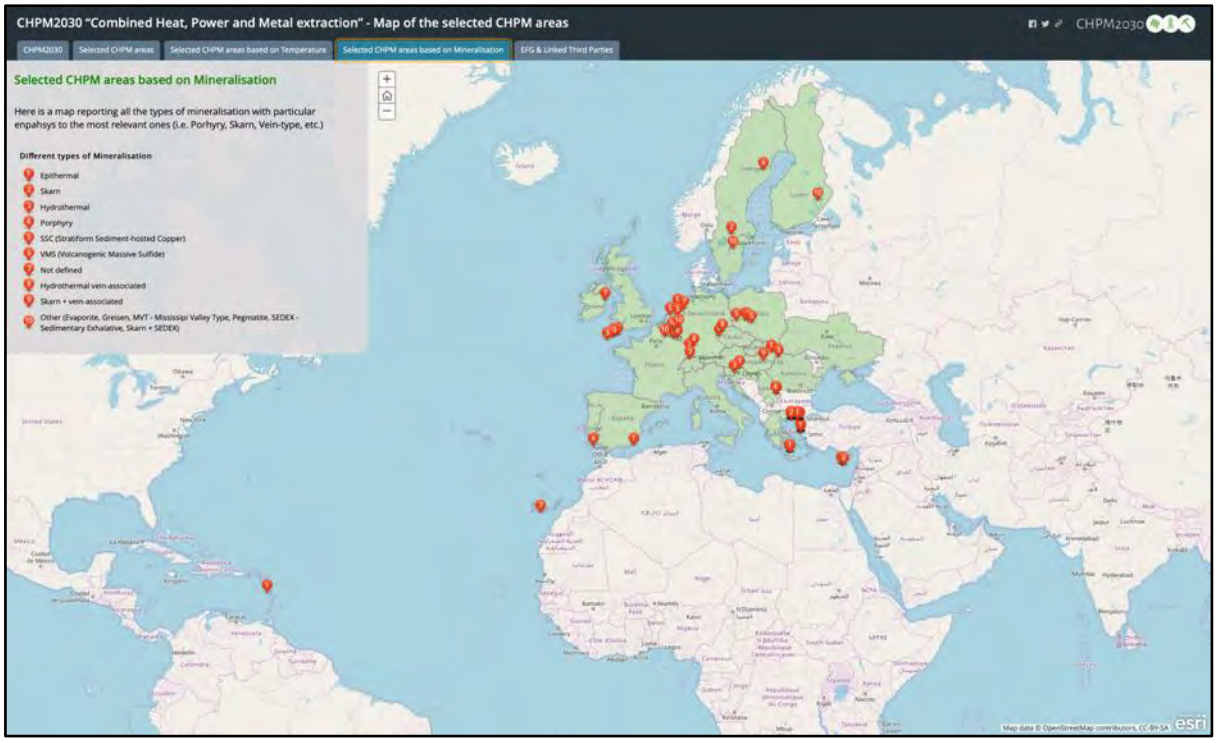

Figure 4: Selected CHPM areas based on the type of mineralisation as provided by LTPs

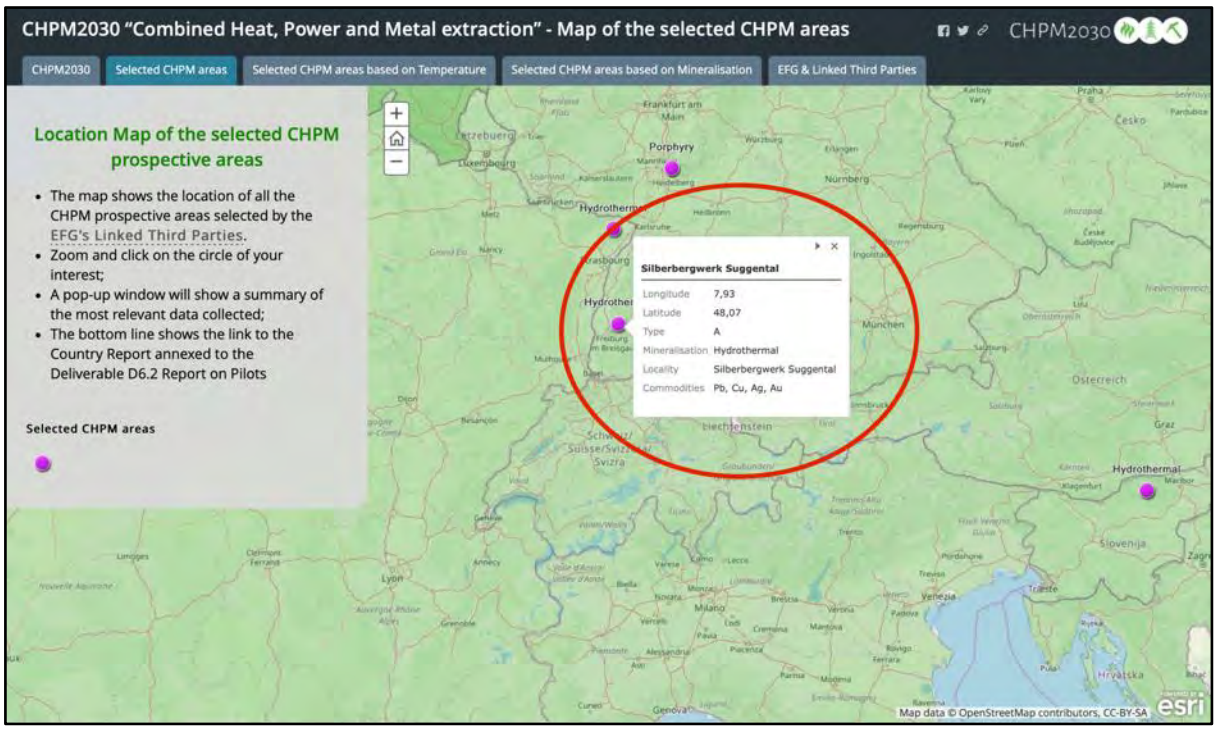

Figure 5: Large scale screenshot with a pop-up window, reporting the main information of the selected CHPM site

In any tabs, the user may click on each selected site and a pop-up window will display (Figure 5) a summary of the main features of the site itself, such as:

1) Locality (reported on the top line of the window)
2) Coordinates
3) Type of the site (according to the scheme reported in Figure 2)

CHPM information platform on prospective is available here: http://bit.ly/CHPMinfoplatform

6 Conclusion

This report has summarised the results provided by the study of potential areas of CHPM development in Europe performed by the Linked Third Parties following the guidelines provided by the European federation of Geologists.

The database of prospective CHPM areas created so far on the European scale, is a first screening for potential areas for future CHPM application.

This work has shown a number of areas that has potential to develop a CHPM site, but the lack of publicly available data may still represent a bottleneck to improve the knowledge needed implement CHPM technology at any of the selected sites. Furthermore, as no new surveys have been carried out and only existing datasets were employed, it is recommended that more data publicly available by the national data repositories.

7 Annexes

The Annex collects the original reports provided by the LTPs which are merely divided into a general summary of the selected areas (see Table 3) and two other sections, when provided, with the evaluation o "Basic characteristics" (e.g. CHPM geology, geophysics, mineralisation, integrated 3D model and EGS geothermal system) and a more deep "Evaluation of CHPM characteristics" (see Table 4a, 4b).
A list of the reports provided by the LTPs, divided per sections, is placed below.

Country	Prospective CHPM areas selection	Evaluation basic characteristics of prospective CHPM areas	Evaluation of the CHPM characteristics
Austria (IRSBN)	✓		
Belgium (IRSBN)	✓		
Croatia (IRSBN)	✓		
Cyprus (IRSBN)	✓		
Czech Republic (CAEG)	✓		
Finland (LOIMU)	✓	✓	✓
France (EFG)	✓	✓	✓
Germany (BDG)	✓	✓	✓
Greece (AGG)	✓	✓	✓
Ireland (IGI)	✓	✓	✓
Italy (CNG)			
Luxembourg (IRSBN)	✓		
Netherlands (KNGMG)	✓	✓	
Poland (PAMAV)	✓	✓	
Portugal (APG)	✓	✓	✓
Serbia (SGS)	✓		
Slovakia (IRSBN)	✓		
Slovenia (SGD)	✓	✓	
Spain (ICOG)	✓	✓	
Sweden (IRSBN)	✓		
Switzerland (CHGEOL)	✓		
Ukraine (UAG)	✓	✓	
United Kingdom (IRSBN)	✓		
Hungary (UGS)	✓	✓	

Table 23: Summary of the reports provided by the Linked Third Parties

Table 1

Prospective CHPM areas

RBINS Austria							
Number	**Type of the selected area(s) (type "A" or type "B")**	**Depth(s) of the metal enrichment(s) (m)**	**Temperature /at these depths/ (°C)**	**Description of the metal enrichment(s)**			
				degree of the mineralization(s) (% or ppm)	***type of the mineralization(s)[1]***	***element(s)***	***area delineation(s)[2]***
1 Furstenfeld (Frutura dublet)	A	Final well depth 3188 m	115°C	Cu up to 1250 ppm Mn up to 350 ppm Zn up to 180 ppm Sn up to 90 ppm Ni up to 60 ppm Cr up to 35 ppm	Data not available (Lead zinc ores low content of silver common in paleozoic rocks (paleozoic of graz and gurktal nappe))	As, F, Fe, Li, Sr, S, (Cu, Zn, Ni, MnO)	Lat: 47.0061 Long: 16.1204

[1] Like skarn, porphy, etc.

[2] There are 3 options for the indication of the area delineation: a. coordinates (latitude, longitude) of 1 point; b. coordinates (latitude, longitude) of 1 points and radius (m); c. coordinates (latitude, longitude) of more points.

Table 1

Prospective CHPM areas

RBINS Belgium							
Number	**Type of the selected area(s) (type "A" or type "B")**	**Depth(s) of the metal enrichment(s) (m)**	**Temperature /at these depths/ (°C)**	**Description of the metal enrichment(s)**			
				degree of the mineralization(s) (% or ppm)	***type of the mineralization(s)[1]***	***element(s)***	***area delineation(s)[2]***
1 (Havelange)	A	i) 5370 m ii) 5449 m iii) 5532 m	i) 118 ii) 120 iii) 123	Mainly unknown but possibility to restudy the logging, core and cuttings	i) Probably hydrothermal and mineral crystallization in conglomerate or veins ii) Idem iii) Idem	i) LREE (Allanite) ii) Th, Co, Au, Pb, Te, Bi iii) Idem as ii)	Lat: 50.3002° N; Long: 5.2471° E, Alt: 284 m
2 (Grand Halleux)	B	2850->2886 m	61	Unknown, need a re-interpretation of logs and samples	Different vein generations (from syn-tectonic to post-tectonic)	REE, P, As, Cu, Pb, Co, Ni	Lat: 50.3108° N, Long: 5.9052° E, Alt: 321 m

[1] Like skarn, porphy, etc.

[2] There are 3 options for the indication of the area delineation: a. coordinates (latitude, longitude) of 1 point; b. coordinates (latitude, longitude) of 1 points and radius (m); c. coordinates (latitude, longitude) of more points.

3 (Saint-Ghislain)	A	i) 1841->2150 m ii) 4320 m	i) 64 (165°C @4830 m) ii) 120	i) Thick sequence of evaporates ii) Unknown, need to be restudied	i) Evaporite ii) Iron oolithes	i) Anhydrite, Ba, F, Sr ii) Fe	Lat: 50.4459° N, Long: 3.8283° E, Alt: 22 m
4 Mol	A	3200->3800 m	139-142	NaCl-brine (160 – 165 g/l) with elevated levels off iron (divalent, 1000 mg/l).	Sulphides associated with black shales on top of the limestone (reservoir).	Fe, Mn, Zn	Lat: 51.2241° N, Long: 5.1099° E.

Table 1

Prospective CHPM areas

RBINS Croatia							
Number	**Type of the selected area(s) (type "A" or type "B")**	**Depth(s) of the metal enrichment(s) (m)**	**Temperature /at these depths/ (°C)**	**Description of the metal enrichment(s)**			
				degree of the mineralization(s) (% or ppm)	***type of the mineralization(s)[1]***	***element(s)***	***area delineation(s)[2]***
1	There are no prospective areas in Croatia						

CHPM2030 – Summary of Croatia

In the procedure of selection of the area scientific publication and existing data (WP1) have been considered. Unfortunately, as the Croatian Geological Survey do not currently have resources to help preparing the data required by the project, the geological information and the previous data from WP1 could not be enhanced.

The research was focused on the comparison of the geological map with heat flow map, but no area has been selected for Croatia.

[1] Like skarn, porphy, etc.

[2] There are 3 options for the indication of the area delineation: a. coordinates (latitude, longitude) of 1 point; b. coordinates (latitude, longitude) of 1 points and radius (m); c. coordinates (latitude, longitude) of more points.

Poor drilling data were found in publication as the boreholes datasets belongs to the Ministry of Economy and are until now unavailable. Data on deep metal enrichments may exist but are not listed in databases, not examined or have not been made publicly available. A comparison between the geological map and the scarce information on the metallogenic map brought to no results.

Several areas can be selected only for geothermal potential.

Bibliography

Kurevija and Vulin (2011) High Enthalpy Geothermal Potential of the Deep Gas Fields in Central Drava Basin, Croatia. Water Resour Manage (2011) 25:3041–3052

Geothermal Energy Utilisation Potential in Croatia – Field and study visits' report June 2017

Croatian Geological Survey http://www.hgi-cgs.hr/eng/

Minister of Mining https://www.mingo.hr/

Table 1

Prospective CHPM areas

RBINS Cyprus							
Number	**Type of the selected area(s) (type "A" or type "B")**	**Depth(s) of the metal enrichment(s) (m)**	**Temperature /at these depths/ (°C)**	**Description of the metal enrichment(s)**			
				degree of the mineralization(s) (% or ppm)	***type of the mineralization(s)[1]***	***element(s)***	***area delineation(s)[2]***
1 Kokkinoiyia	B	> 300 m	At 300m ~ 30°C	2% S, 2% Cu, 1% Zn (surface mine value)	VMS	S, Cu, Zn	Lat: 35.042 Long: 33.108 Radius: 5 km
2 Agrokipia B	B	> 530 m	At 530m ~40°C	25% S (surface mine value)	VMS	Fe, Zn, Cu, Si, As, Ba, K.	Lat: 35.0438 Long: 33.1463 Radius: 7 km
3 Skouriotissa - Apliki	B	> 200 m	At 200 m ~28°C	2.3% Cu, 42% S (surface mine value)	VHMS	Cu, Zn, Fe	Lat: 35.099 Long: 32.883 Radius: 10 km
4 Mathiatis	B	> 400 m	At 400 m ~35°C	33% S, 0.24% Cu, 0.92% Zn (surface mine value)	VMS	Cu, Zn, Ni, Co	Lat: 34.966 Long: 33.333 Area: 6 km²

[1] Like skarn, porphy, etc.

[2] There are 3 options for the indication of the area delineation: a. coordinates (latitude, longitude) of 1 point; b. coordinates (latitude, longitude) of 1 points and radius (m); c. coordinates (latitude, longitude) of more points.

Table 1

Prospective CHPM areas

CAEG Czech Republic							
Number	**Type of the selected area(s) (type "A" or type "B")**	**Depth(s) of the metal enrichment(s) (m)**	**Temperature /at these depths/ (°C)**	**Description of the metal enrichment(s)**			
				degree of the mineralization(s) (% or ppm)	***type of the mineralization(s)[1]***	***element(s)***	***area delineation(s)[2]***
1	There are no prospective areas in the Czech Republic						

CHPM2030 – Summary of the Czech Republic data

CAEG find out following information:

There is database of boreholes of the Czech Republic created by the Czech Geological Survey, Prague. The boreholes inventory (http://www.geology.cz/app/gdo/?l=e) includes geological, hydrogeological and geophysical data. The database provides key information on geological investigations carried out in the Czech Republic and helps to provide a detailed view of the geological structure of the country. Currently, the information stored in the databases is provided to users in the form of individual outputs, or via the geologically documented objects and Geological Map Server applications. In the end of 2017, there are 693 806 objects (boreholes mainly). There are 185 boreholes with depth more than ca 100 m and with measurement of temperature. In boreholes with depth more than 1000 m: temperature 40-49,9 ° C was reached in 38 boreholes, temperature 50-59,9 ° C was reached in

[1] Like skarn, porphy, etc.

[2] There are 3 options for the indication of the area delineation: a. coordinates (latitude, longitude) of 1 point; b. coordinates (latitude, longitude) of 1 points and radius (m); c. coordinates (latitude, longitude) of more points.

37 boreholes, temperature 60-69,9 ° C was reached in 9 boreholes, temperature 70-79,9 ° C was reached in 12 boreholes, temperature 80-89,9 ° C was reached in 13 boreholes, temperature 90-99,0 ° C was reached in 6 boreholes. No one measurement of borehole temperature reached more than 100 ° C. **All those boreholes are situated outside of known ore bodies (this information was consulted with ore exploration experts).**

The most frequent geothermal gradient of the Czech Republic area is 20–30 °C/km. Isotherms at the depth of 500 m below surface is in Fig. 1.

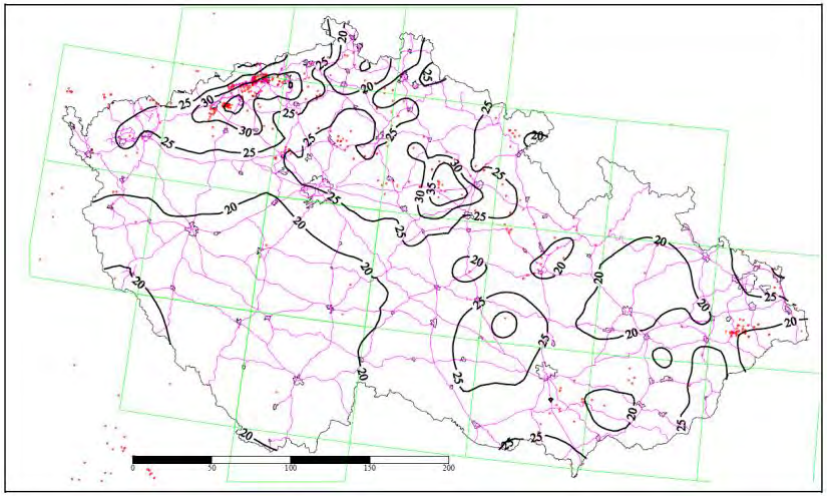

Fig. 1. Isotherms at the depth of 500 m b.s.

Temperature at the depth of 1000 m is 25–40 °C. Temperature 60–80 °C is almost everywhere at the depth of 3 km, in some places at the depth of 2 km. Temperature 130 °C is common at the depth of 6 km, 180 °C is common at the depth of more than 8–9 km. Temperature 130 (180) °C is estimated at the depth of 5 (7) km in Sub-Erzgebirge Region, Erzgebirge, Bohemian Cretaceous Basin, Upper-Silesian Basin and some others areas.

Literature:

(1) https://www.geothermal-energy.org/pdf/IGAstandard/WGC/2000/R0823.PDF :
Myslil V., Stibitz M. (2000): Geothermal resources of the Czech Republic – general overview. Proceedings World Geothermal Congress 2000, Kyushu – Tohoku, Japan, May 28 – June 10, 2000.

(2) https://vesmir.cz/cz/casopis/archiv-casopisu/2008/cislo-9/teplo-z-nitra-zeme.html

Table 1

Prospective CHPM areas

LOIMU Finland							
Number	**Type of the selected area(s) (type "A" or type "B")**	**Depth(s) of the metal enrichment(s) (m)**	**Temperature /at these depths/ (°C)**	**Description of the metal enrichment(s)**			
				degree of the mineralization(s) (% or ppm)	***type of the mineralization(s)[1]***	***element(s)***	***area delineation(s)[2]***
1 Outokumpu Deep Hole	B	2500	40	In waters at the bottom of hole 15-17 mg/l lithium, in some water samples 30-50 mg/l. No lithium mineralisation reported in bedrock.	Granite pegmatite	Li	Granite pegmatites intruding Outokumpu ophiolite formation. Outokumpu formation 2*30 km^2. Coordinates of the drill hole: N=62.718 E=29.059

[1] Like skarn, porphy, etc.

[2] There are 3 options for the indication of the area delineation: a. coordinates (latitude, longitude) of 1 point; b. coordinates (latitude, longitude) of 1 points and radius (m); c. coordinates (latitude, longitude) of more points.

2	A/B	6400	90-100	This drill holes is the first of the two intended drill holes. The goal of project is to build Finland's first industrial scale heat plant running on geothermal energy. The project is run by private energy company St1.	No mineralisation reported. Not likely to be any metal enrichments.		Granite, Southern Finland granite suite

Evaluation of the basic characteristics of prospective CHPM areas

LOIMU
Finland

AREA 1 - Outokumpu Deep Hole

1. **Geology of the prospective area**

Requested information on:

- ✓ local geology (in regional context)
- ✓ CHPM target formation
- ✓ list of available cross sections, geological maps, geochemical results, lithological information

Notes: briefly summarized, referenced to more detailed studies.

The drill hole intersects Outokumpu ophiolite rock association with some sediments and cross-cutting granite pegmatites.

2. **Geophysics of the prospective area**

Requested information:

- ✓ previous geophysical measurements (in CHPM relevance)
- ✓ geophysical results that can be used for locating/defining the deep metal enrichment
- ✓ list of available geophysical maps, cross sections, logs, other measurements

The Figure below interpretation of reflection seismic study in the area of the deep drill hole.

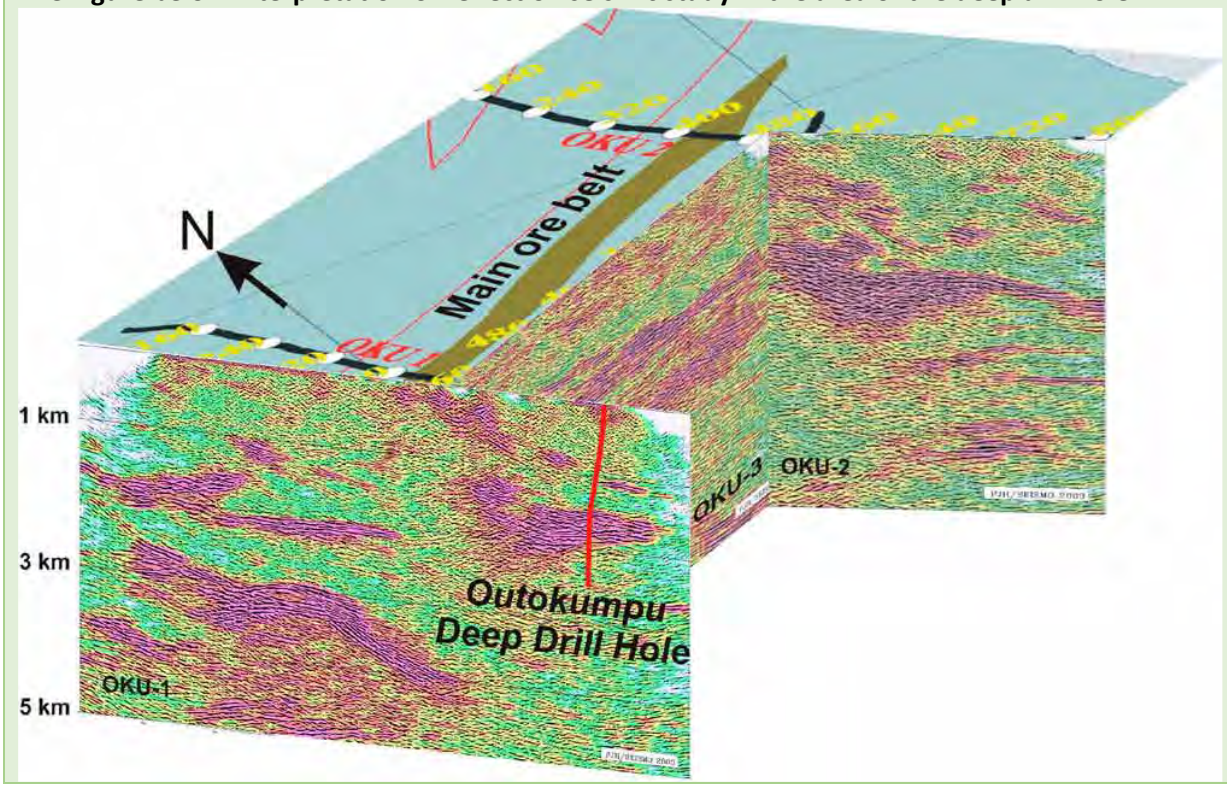

3. **Deep metal enrichment**

Requested information:

- ✓ **(**expected) metal enrichment based on available geophysical, geological and drill data, samples information, geochemistry

Outokumpu association rocks host several sulphide ore deposits, mainly copper deposits. The region has been of the copper producer in the Europe. One copper mine in operation, and one Ni-Co-Cu in advanced stage development.

However, the waters in the deep hole are not particularly enriched in base metals but lithium instead. In waters at the bottom of hole 15-17 mg/l lithium, in some water samples 30-50 mg/l. No lithium mineralisation reported in bedrock.

4. **Integrated 3D- 4D model**

Requested information:

- ✓ existing 3D-4D models of the target area and the deep metal enrichment
- ✓ if no 3D-4D models exist, collect the following necessary data: geological setting, mineralization, fluid flow models, stress field determination

Notes: e.g. openly available datasets, models.

5. **EGS potential**

Requested information:

- ✓ EGS potential (heat & energy) of the area
- ✓ geothermal characteristics (temperature gradient, heat flux, stress field, water availability, EGS geology)
- ✓ presence/indication of deep fluids/brines, fracture system, crustal permeability

Marginally potential for metal extraction.

List of references

Kukkonen, I. T. (ed.) 2011. Outokumpu Deep Drilling Project 2003–2010. Geological Survey of Finland, Special Paper 51, 252 pages, 127 figures, 40 tables and 2 appendices.

Kietäväinen, R. 2017. Deep Groundwater Evolution at Outokumpu, Eastern Finland: From Meteoric Water to Saline Gas-Rich Fluid. Geological Survey of Finland, Espoo. 37 pages, 9 figures, 2 tables and 1 appendix, with original articles (I-IV).

Annexes

Evaluation of the CHPM characteristics of prospective CHPM areas

LOIMU
Finland

AREA 1 - Outokumpu Deep Hole

1. **CHPM operational characteristics - Information for CHPM technological elements**
   Requested information:
✓ please fill in the table below with the requested data for the CHPM technology elements

Underground heat exchanger (deep metal enrichment + potential geothermal reservoir)	
Extension of the metal enrichments *(volumetric interpretation)*	**Unknown**
Expected type of the reservoir and porosity/permeability *(fractured, porous, etc)*	**Unknown.**
Mineralization *(type and enriched metals)*	**In waters at the bottom of hole 15-17 mg/l lithium, in some water samples 30-50 mg/l. No lithium mineralisation reported in bedrock.** **In general the hosting Outokumpu ophiolite is well known for its copper deposits. One mine in operation close to hole.**

Production and injection wells	
Depth of potential wells (m)	**The present hole 2,500 m, can be extended.**

Electrolytic metal recovery and gas diffusion electro- precipitation	
Potential target metals to be recovered	**Lithium, copper, nickel, zinc.**

Power plant (heat exchanger)	
Local heat and electricity demand *(industrial, municipal, agricultural, etc.)*	**Close to regional town of Outokumpu, 10,000 people. Outokumpu is an industrial town. 40 km to town of Joensuu with 80,000 people.**

Salt gradient power generation	
Salinity of expected geothermal brine	**70-80 g/l, mainly $CaCl_2$, but also NaCl.**
Fresh water supply from the surface *(water sources)*	**Close by.**

2. CHPM operational characteristics - Environmental, social and political background

Requested information:

- ✓ toleration to gaseous and solids emissions, water and noise pollution,
- ✓ local competition to land and water availability
- ✓ public acceptance
- ✓ political support
- ✓ presence of supporting legislation, regulatory framework

Notes: all of above refers to the selected area and its surroundings.

The area is old mining district, still mines in operations and in plans. Public acceptance expected to be good. The drill hole in the possession of the Geological Survey of Finland.

3. Financial aspects

Requested information:

- ✓ list of potential local stakeholders (community, political, companies)

List of references

Kukkonen, I. T. (ed.) 2011. Outokumpu Deep Drilling Project 2003–2010. Geological Survey of Finland, Special Paper 51, 252 pages, 127 figures, 40 tables and 2 appendices.

Kietäväinen, R. 2017. Deep Groundwater Evolution at Outokumpu, Eastern Finland: From Meteoric Water to Saline Gas-Rich Fluid. Geological Survey of Finland, Espoo. 37 pages, 9 figures, 2 tables and 1 appendix, with original articles (I-IV).

Annexes

Table 1

Prospective CHPM areas

France							
Number	**Type of the selected area(s) (type "A" or type "B")**	**Depth(s) of the metal enrichment(s) (m)**	**Temperature /at these depths/ (°C)**	**Description of the metal enrichment(s)**			
				degree of the mineralization(s) (% or ppm)	***type of the mineralization(s)[1]***	***element(s)***	***area delineation(s)[2]***
1	Type A • Bouillante geothermal field western coast of Basse-Terre of the island of Guadeloupe Lesser Antilles • Well BO-1 to Well BO-7	500 – 1000	250 – 260	• TDS 20 g/l • pH 5.3 ± 0.3 at 250-260 °C • Steam condensate acidic pH 4,3 / 4,5 20-30 mg/l sulphide • pyrite + Zn + Cu + Ni • sulphide 0.1-0.7 mg/l • Cu 15 mg/l • Si 600 mg/l • Li As B	• active volcanic island arc of the Lesser Antilles • Peri volcanic geothermal sodium- chloride reservoir • Epithermal type Au Ag Hg • Potential Cu	Cl 12 g/l Na 5 g/l Ca 1,8 g/l K 750 mg/l HCO3 110 mg/l Mg 12 mg/l SO4 13 mg/l H2S 34 mg/l SiO2 500 mg/l Al 100 µg/l Br 42 mg/l B 12 mg/l Li 6 mg/l Sr 20 mg/l) Cs 260 µg/l Cu 15 mg/l Zn 650 µg/l As 450 µg/l	Latitude 16°07'49"Nord Longitude 61°46'09"Ouest

[1] Like skarn, porphy, etc.

[2] There are 3 options for the indication of the area delineation: a. coordinates (latitude, longitude) of 1 point; b. coordinates (latitude, longitude) of 1 points and radius (m); c. coordinates (latitude, longitude) of more points.

						Co 13 µg/l	
2	Type A • Northern Alsace • Soultz-sous-Forêts	2 000 to 5 000	• 1400 m 124° C 83°C/km • Then 28°C/km 5000 m 203 °C • The reservoir temperature was set to 230-240°C	Na, Ca, Cl and K dominant geothermal brine show TDS values ranging from 96 to 107 g/l with pH values close to 5 and d : 1,065 g/cm3	The Upper Rhine Graben (URG) is characterized by several local thermal anomalies associated to hydrothermal convective cells circulating inside a nearly vertical fracture network in the granite basement and in the Triassic fractured sediments above it	Na 27,5 g/l K 3,25 g/l Ca 6,9 g/l Mg 125 mg/l Cl 59 g/l SO4 59 mg/l SiO2 427mg/l NH423,5mg/l Br 220 mg/l B 35 mg/l F 4,5 mg/l Sr 450mg/l Li 140 mg/l Fe 100 mg/l Rb 22 mg/l Cs 14 mg/l Ge 53 µg/l Be 30 µg/l Ni 100 µg/l Zn 3000 µg/l Ti 200 µg/l Pb 300 µg/l	○
	Well GPK-1	3590m	160°C -165°C				
	Production Well GPK-2 (is on the same site as GPK- 3 and 4)	5084m	• 26 L/s @ 157 °C • 19 bar	Li content 150 – 200 mg/l As 12 mg/l SiO2 427 mg/l	fluids are NaCl type, enriched in calcium and lithium and depleted in magnesium, with a pH value around 5.0		GPK-2 • WGS 84 : • Lat : 48,93084 m, • Lon = 7,86657 m Lambert I Nord – • X :

							1004814.0 m • Y : 151574.0 m Lambert 93 – • X : 1056342.000 m • Y : 6881078.000 • Alt 167,9 m
	Injection Wells GPK-3 & GPK-4 (are on the same site as GPK- 2, their locations are centralized to GKP-2)	5100m 5270m	>150°C		Part of the geothermal resources is underlying the Pechelbronn oil deposits and can be described as oilfield brine.		
	Well EPS-1	2227m					

Bibliography

Web

https://hal-brgm.archives-ouvertes.fr/hal-00773163v1/html_references

https://umap.openstreetmap.fr/fr/map/perimetres-des-titres-miniers-de-gitesgeothermiqu_158171#6/46.973/4.922

www.ademe.fr/sites/.../files/.../4fiche_instruct_geothermie_fds_chal_2018_01-03-18.doc...

https://www.geothermal-energy.org/explore/our-databases/conference-paper-database/

http://geodeep.fr

http://unt.unice.fr/uved/bouillante/cours/ii.-etude-de-cas-la-centrale-geothermique-de-bouillante-en-guadeloupe/1.-contexte-geologique-particulier-du-site-de-bouillante/1.2-quelle-est-lorigine-de-ces-manifestations-geothermiques/b.-les-failles-permettent-la-circulation-des-fluides.html

http://www.brgm.fr/brgm/le-groupe-brgm/geothermie-bouillante

http://www.geothermie-perspectives.fr/article/centrale-egs-soultz-forets-alsace

http://labex-geothermie.unistra.fr/article200.html

http://alsace.edf.com/wp-content/uploads/2016/07/2016-LIVRET-A5-GEOTHERMIE_BAT.compressed.pdf

http://www.geopotenziale.org

BRGM reports http://infoterre.brgm.fr/

RP-57252-FR, 2009

RR-36203-FR 1992

RP 39880

RP 40646

RP-52587-FR

RP 52643

RP 52667

RP 52311

RP 50883

RP-54776

Publications

Fouillac Ch., Michard G. (1981) - Sodium/lithium ratio in water applied to geochemistry of geothermal reservoir. Geothermics, 10, 55-70.

Baujard, C., Genter, A., Graff, J.-J., Maurer, V., Dalmais, E., 2015. ECOGI, a New Deep EGS Project in Alsace, Rhine Graben, France, in: Proceedings of World Geothermal Congress 2015. Melbourne, Australia.

Genter, A., Evans, K., Cuenot, N., Fritsch, D., Sanjuan, B., 2010. Contribution of the exploration of deep crystalline fractured reservoir of Soultz to the knowledge of enhanced geothermal systems (EGS). Comptes Rendus Geoscience 342, 502–516.

Gérard, A., Genter, A., Kohl, Th., Lutz, Ph., Rose, P., Rummel, F., 2006. The deep EGS (Enhanced Geothermal System) project at Soultz-sous- Forêts (Alsace, France). Geothermics, Vol. 35, No. 5-6, 473-483.

Maurer, V., Cuenot, N., Gaucher, E., Grunberg, M., Vergne, J., Wodling, H., Lehujeur, M., Schmittbuhl, J., 2015. Seismic monitoring of the Rittershoffen EGS project (France), Proceedings of World Geothermal Congress, Melbourne, Australia.

Pribnow, D., Clauser, C., 2000. Heat and fluid flow at the Soultz Hot Dry Rock system in the Rhine Graben, in: Proceedings of World Geothermal Congress 2000. Kyushu - Tohoku, Japan.

Sanjuan, B., Millot, R., Dezayes, Ch., Brach, M., 2010. Main characteristics of the deep geothermal brine (5 km) at Soultz (France) determined using geochemical and tracer test data. C. R. Geoscience, 342, 546-559.

Sanjuan, B., Millot, R., Innocent, Ch., Dezayes, Ch.,Scheiber, J., Brach, M., 2016. Major geochemical characteristics of geothermal brines from the Upper Rhine Graben granitic basement with constraints on temperature and circulation. Chemical Geology, Volume 428, 27-47.

Scheiber, J., Ravier, G., Cuenot, N., Genter, A., 2015. Situ material and corrosion studies at the Soultz-sous-Forêts (France) EGS Site. Proceedings World Geothermal Congress 2015, Melbourne, Australia, 19-25 April 2015.

Scheiber, J., Seibt, A., Birner, J., Genter, A., Cuenot, N., Moeckes, W., 2015.. Scale inhibition at the Soultz-sous-Forêts (France) EGS site: laboratory and on-site studies. Proceedings World Geothermal Congress 2015, Melbourne, Australia, 19-25 April 2015

Schellschmidt, R., Clauser, C., 1996. The thermal regime of the Upper Rhine Graben and the anomaly at Soultz. Zeitschrift für Angewandte Geologie 42, 40–44.

Schindler, M., Baumgärtner, J., Gandy, T., Hauffe, P., Hettkamp, Th., Menzel, H., Penzkofer, P., Teza, D., Tischner, T., Wahl, G., 2010. Successful hydraulic stimulation techniques for electric power production in the Upper Rhine Graben, central Europe. Proceedings World Geothermal Congress 2010, Bali, Indonesia, April 2010.

Vidal, J., Genter, A., Schmittbuhl, J., 2015. How permeable fractures in the Triassic sediments of Northern Alsace characterize the top of hydrothermal convective cells? Evidences

Vidal, J., Genter, A., Schmittbuhl, J., 2016. Pre- and post-stimulations of the geothermal well GRT-1 (Rittershoffen, France): insights from acoustic image logs on hard fractured rock investigations, Geophysical Journal International. 206, 845-860.

Sanjuan B., Millot R., Dezayes C., Brach M., (2010). Main characteristics of the deep geothermal brine (5 km) at Soultz-sous-Forêts (France) determined using geochemical and tracer test data. C. R. Geoscience, 342, 546-559.

New stratigraphic interpretation of the Soultz-sous-Forêts 30-year-old geothermal wells calibrated on the recent one from Rittershoffen (Upper Rhine Graben, France)

Geochemical and mineralogical monitoring of the geothermal power plant in soultz-sous-forêts (france) Laboratory and In-Situ Corrosion Studies in Geothermal Environments N. Mundhenk1, P. Huttenloch2, T. Kohl1, H. Steger1, and R. Zorn21Institute of Applied Geosciences/KIT 2European Institute for Energy Research (EIFER), Karlsruhe

ADEMA – BRGM : Étude physico-chimique des fluides produits par la centrale géothermique de Bouillante (Guadeloupe) et des dépôts susceptibles de se former pendant leur exploitation et leur réinjection dans le sous-sol Christelle DIXIT

France – Other potential areas

In addition to the selection of prospective CHPM areas, for CHPM2030 6.2.3 report, several areas with medium / high temperature geothermal resources and located in a geological environment known for their mineralizations do exist in France (Bertrand et al. 2013), but not enough documented specially in depth. See in annexes *Map of geothermal resources in France* and *permit map of prospective geothermal* sites (Boissavy et al. 2016).

Massif Central, limagne. The French Massif Central, and more particularly the Auvergne district, displays several surficial expressions that would indicate potentially favourable conditions for the development of high-enthalpy geothermal energy. These include hydrothermal springs with geothermometers revealing reservoir conditions above 150 °C and up to 200 °C, (Bouchot et al., 2010), which could relate to recent volcanic activity. Volcanism is characterized by differentiated products, evidence of the possible existence of a shallow magma chamber as a heat source. (Sanciaut et al. 2012). BRGM has produced a bibliographic synthesis (Serra et al. 2003) of the geochemistry of thermal waters of Limagne. The sedimentary basins close to Clermont-Ferrand (Puy de Dôme) outcropping in the northern part of the French Massif Central, (Allier, Loire, Ambert, constitute the *Limagne system*. Geologically, those basins correspond to a large-scale graben system belonging to the Western European Rift System with a rather shallow Moho (<30 km depth) promising geothermal gradient as well as highly fractured zones in the deep underlying basement (Genter et al., 2003a, 2010). Locally, they are NNE to NS oriented basins bounded by regional normal faults. They are filled by tertiary sediments up to 2 km thick which overlain Palaeozoic basement. Tertiary and Quaternary volcanism occurred inside and outside the Limagne system.

There are a lot of thermal springs distributed along the graben border faults indicating potential hydrothermal circulation (Millot et al., 2007). Recent volcanic activity could represent an additional heat source. This area was explored for oil purposes until 80's. The Limagne basin has been studied for its geothermal potential for several years (Gable, 1978; Genter et al., 2003 and 2005; Bouchot et al., 2008.; Calcagno et al. 2009)

Fluids are CO_2 rich and Na is the major dissolved cation. The maximal TDS (Total Dissolved Solids) is 10g/l on the western part of the basin. The ubiquitous presence of CO_2 in the fluid is interpreted as a crustal contribution.

Calculations of the reservoir temperature based on cation geothermometers (Na, Li) gave values ranging between 170 and 200°C for the western part of the basin (Montpensier, Aigueperse, Royat, Chatelguyon). For the northeastern part (Vichy), calculated temperatures are lower with about 130°C. For the southern part (Margeride, Chaudes Aigues), the calculated temperatures are higher than 150°C. Based on the geochemical data, fluid flow paths could be related to large-scale fluid percolations through deep crystalline or volcanic fractured rocks. After reaching 130 to 200°C, fluids migrated upward to the detritic reservoirs connected to the fault system, (Genter et al. 2005). The Limagne basin actually is probably hotter than previously assumed, with temperatures possibly exceeding 240 ◦ C at 5 km depth.

Noticed the drilling of Croix-de-Neyrat (63), Limagne border, 4 km north of Clermont-Ferrand, 107°C at 1880 m, Li : 81,2mg/l – Na : 10920 mg/l – SiO_2 : 75 mg/l – Ca : 1,8 mg/l (Pauwels et al. 1991).

Alsace. Others industrial geothermal project in Alsace driven by oil and gas industry are under studies, see map of extrapolate temperatures of the URG with major geothermal projects (Aichholzer et al., 2016).

Cronenbourg in the suburbs of Strasbourg, is a geothermal drilling done in 1980 targeted deep porous Permo-Triassic sandstones to 3000 m deep. Drilling results were not successful as expected due to the absence of natural permeability, even though some fractures and faults were cross-cut by this geothermal well, chemical treatment or hydraulic stimulation was not tried.

Cronenbourg : T:160°C, Li 220 mg/l – Na : 32186 mg/l – SiO2 : 235 mg/l – Ca : 4600 mg/l (Pauwels et al.1991).

More recently, a deep geothermal project located at *Rittershoffen* 6 km east of Soultz-sous-Forêts was initiated in 2011 by the company ECOGI. This project is based on a geothermal doublet that produces geothermal heat from the reservoir at the sediment basement interface (Baujard et al., 2015). A doublet of deep geothermal wells has been drilled to a depth of approximately 2.6 km between 2012 and 2014. However the deepest bottom-hole temperature measurements shows 140°C at 1600 m in the Muschelkalk (Middle Trias) and 158°C at 1780 m in the Buntsandstein (lower Trias). Hydraulic tests demonstrated that an industrial flowrate of 70kg/s and a surface temperature higher than 160°C could be achieved (Baujard et al., 2015). Only the injection well was thermally, chemically and hydraulically stimulated. The natural initial permeability of the production well was so good that the second well was not stimulated. The ECOGI project is operating from summer 2016 and produces 24MWth to industry.

Studies relative to the Bühl and Bruchsal geothermal wells only give interesting information on fluids discharged from the Buntsandstein and Permian aquifers close to the granite basement.

Geochemical data were also found for the Riehen geothermal water, in the Upper Muschelkalk formation (He et al., 1999), and other publications (e.g. Griesshaber et al., 1992, Clauser et al., 2002) provide data concerning the escape of deep gases in the graben. The geochemical data in the literature (especially German studies) concern shallow aquifers of the Upper Rhine Graben. Chemical and isotopic compositions of fluids from several saline thermal springs (Niederbronn-les-bains, Morsbronn-les-bains, Hélions, Baden-Baden, etc.) and shallow wells for the exploration and production of thermal water (spas) and mineral water (bottled drinking water) within the Rhine Graben (Friedrichsen, 1981, Pauwels et al., 1993, Aquilina et al., 1997, Aquilina et al., 2000, Stober and Bucher, 1999, Sanner, 2000, Stober and Jodocy, 2011, Loges et al., 2012, Göb et al., 2013) indicate a predominant contribution of surface water.

Pyrénées **:** Numerous alkaline thermal springs are known and mostly used for bathing on the north side of the Eastern and Central Pyrenees Range. (Vuataz, et al. 1985)These surface manifestations of deep thermal circulations are encountered along the axial zone of the Pyrenees, which is essentially formed by Precambrian basement overlain by a Paleozoic cover. These two formations are intersected by Hercynian granites and were folded and metamorphosed through the Hercynian orogenesis. The thermal springs usually occur from faults within *Luchon* is a typical example of the Pyrenean alkaline sulphureted thermal waters, installed in granitic environments, (Auqué et al. 1997).

Luchon : 80 to 120°C at depths of 2 to 3 km.

Cauteret : 60°C emerging temperature, sulphide H_2S content 6,8 mg/l, 90°C at 2 km depht probably with gradien 25°C / km (Jean et al. 1990).

Fonroche Géothermie develope several high-enthalpy pilot project on Pau-Tarbes and Arzacq permits as well as in Massif central and Alsace.

Carribbean islands*:* Geothermal energy development in a active volcanism of insular arc context.

The *Roseau Valley* in Dominica (West Indies) is characterized by recent volcanic activity (less than 50,000 years BP) with several eruptive centres and abundant surface manifestations, which are observed in two main spots distant of 4 kilometers: *Wotten Waven* in the Roseau Valley and the adjacent *Boiling Lake* –Valley of Desolation area.

It is characterized by recent volcanic activity (less than 50,000 years BP) with several eruptive centres and abundant surface manifestations. Several types of thermal manifestations have been recorded, including warm springs, hot springs, fumaroles and steam vents, cold gas discharges, solfatares, fossil alteration areas and phreatic craters.

Some of the hot springs discharge Na-Cl and Ca-rich Na-Cl waters, which point out the existence of a high temperature geothermal reservoir. These waters might have a common origin, but would have evolved separately during their ascent to the surface. They have experienced water-rock interactions at high temperature as indicated by their oxygen-18 shift.

The Na-Cl waters discharged in the *Roseau Valley* area have deep equilibrium temperature around 200-225°C. Ca-rich Na-Cl waters are discharged in the Valley of Desolation and the vicinity of the Boiling Lake. Their higher contents of calcium and chloride could be indicative of a strong degassing before they reach the surface. Na-K geothermometers indicate higher deep equilibrium temperatures (up to 300°C).

Despite limited depth of penetration, the MT survey provided a clear resistivity pattern for some soundings which points out a highly conductive, argillic cap-rock and an underlying less conductive reservoir. (Traineau et al., 2015)

In Guadeloupe, there are areas other than Bouillante with geological characteristics and surface indices (thermo-mineral sources) favorable to the existence of hydrothermal systems:
the hydrothermal system of the volcanic massif of the *soufrière* ;
the hydrothermal system of the *sans-filiers* ;
the hydrothermal system of *Ravine Chaude, Lamentin* ;
the *Sofaïa* hydrothermal system located in the northern part of the island, within the ancient volcanic formations of the northern chain. *(Bourdon et al., 2008)*

Références bibliographiques

Aquilina L., Pauwels H., Genter A., Fouillac C. (1997), Water-rock interaction processes in the Triassic sandstone and the granitic basement of the Rhine Graben: geochemical investigation of a geothermal reservoir Geochim. Cosmochim. Acta, 60, pp. 4281-4295

Aichholzer C., Duringer Ph. , Orciani S. and Genter A., 2016, New stratigraphic interpretation of the Soultz-sous-Forêts 30-year-old geothermal wells calibrated on the recent one from Rittershoffen (Upper Rhine Graben, France) *Geothermal Energy* https://doi.org/10.1186/s40517-016-0055-7

Auqué L-F., Mandado, J., Lopez P-L., Gimeno, M-J., (1997). Los sistemas geotermales del Pirineo Central.

Baujard, C., Genter, A., Graff, J-J., Maurer, V., Dalmais, E., 2015, Ecogi, a New Deep EGS Project in Alsace, Rhine Graben, France

Bertrand G., Dupuy J.-J., Melleton J., Tourlière B., Cassard D., Audion A.-S., Angel J.-M., Gloaguen E., Husson Y. et Berthier H. (2013) – Réévaluation du potentiel français en ressources minérales : retraitement des données géochimiques de l'Inventaire et établissement de fiches de cibles minières. Rapport final. BRGM/RP-62960-FR, 150 p., 34 fig., 4 tabl., 3 ann..

Boissavy C., Rocher P., Laplaige P., Brange C., 2016. European Geothermal Congress Strasbourg, France. Geothermal Energy Use, Country Update for France

Bouchot V., Calcagno P., Genter A. (2010) – Les atouts énergétiques du bassin de la Loire, Géosciences n° 12, dec. 2010, pp. 88-99

Bourdon E., Bès de Berc S., Traineau H., Sanjuan B., Chauvet M., Hervé J.-Y, Miehe J.-M., Bézèlgues-Courtade S. 2008. Inventaire des ressources géothermiques potentielles de la Guadeloupe. Rapport BRGM/RP-56631-FR, pages, 50 illustrations, 2 annexes.

Calcagno, P.; Baujard, C.; Dagallier, A.; Guillou-Frottier, L.; Genter, A. 2009. Three-Dimensional Estimation of Geothermal Potential from Geological Field Data: The Limagne Geothermal Reservoir Case Study (France)

Calcagno, P., et al., Estimation of the deep geothermal potential within the Tertiary Limagne basin (French Massif Central), 2014: An integrated 3D geological and thermal approach. Geothermics (2014), http://dx.doi.org/10.1016/j.geothermics.2014.02.002

COPGEN, 2003a. Méthodologie de l'inventaire du potentiel géothermique des Limagne: projet COPGEN, Compilation des données, BRGM Open File report, RP-52644-FR.

COPGEN, 2003b. Méthodologie de l'inventaire du potentiel géothermique des Limagne: projet COPGEN, Compilation des données géophysiques, BRGM Open File report, RP-52667-FR.

De Gramont, X., feybesse j-l., lambert a. Mars 1990. Synthèse du district de Briouude-massiaac et des Confins nord de la Margeride (Massif Central). R 30695 DL/C DAM 90

Dezayes C., Thinon I., Genter A. Courrioux G. 2007 Clastic Reservoirs in the Rhine Graben: Geothermal Potential of the Triassic Sandstones Based on Seismic Profiles and Deep Boreholes

Gable, R., 1978. Acquisition et rassemblement de données géothermiques disponibles en France. BRGM Open File report, SGN 284 GTH

Gama S., 2000 Evénements métallogéniques à W-Bi (Au) à 305 Ma en Châtaigneraie du Cantal : apport d'une analyse multi-spectrométrique (micro PIXE-PIGE et Raman) des minéraux et des fluides occlus à l'identification des sources de fluides hydrothermaux. Minéralogie. Université d'Orléans. tel-00002404

Genter A., Giot D., Lieutenant N., Nehlig P., Rocher Ph., Roig J.Y ., Chevremont Ph., Guillou-Frottier L., Martelet G., Bitri A., Perrin J., Serrano O., Courtois N., Vigouroux Ph., Négrel Ph., Serra H., Petelet- Giraud E. 2003. Méthodologie de l'inventaire géothermique des Limagnes. Compilation des données. *BRGM Open File report*, R52644, 122 p.

Genter A., Giot D., Guillou-Frottier L., Bertin C., Bitri A., Calcagno P., Courrioux G., Courtois N., Giraud-Petellet E., Goyeneche O., Martelet G., Negrel P., Nehlig P., Perrin J., Rocher P., Serra H., Serrano O., Laplaige Ph. 2005. Low to Medium Temperature Geothermal Resources in the Limagne Basins (France)

Jean, Ph., Soulé, J-C. 1990. Programme de recherche finalisée thermalisme : eaux sulfurées des Pyrénées rapport de synthèse final R30881

Labbé J.F. et Daw G., 2012 – Panorama 2011 du marché du lithium. Rapport public. BRGM/RP-61340-FR. 154 p., 51 fig., 29 tab.

Laplaige, P., Durimel, H., Mompelat, J-M., 2013. Développement de la géothermie dans la Caraïbe. Geosciences, pp.26-35. hal-01060522

Millot R., Négrel Ph., 2007. Multi-isotopic tracing (δ7Li, δ11B, 87Sr/86Sr) and chemical geothermometry: evidence from hydro-geothermal systems in France. Chemical Geology, 244: 664-678.

Pauwels H., Lambert M., Genter A., 1991. Valorisation des fluides géothermaux contenant du lithium en vue d'une production industrielle. BRGM R 33547

Sanciaut, M., Bouchet, L., Bouttes, O., Bouchot, V., 2013. Des projets géothermiques in-dustriels en Auvergne ... innover ensemble, agir local. Geosciences, pp.36-43. <hal-01061098>

Serra H., Petelet-Giraud E., Négrel Ph., 2003. Inventaire du potentiel géothermique de la Limagne (COPGEN) Synthèse bibliographique de la géochimie des eaux thermales. BRGM/RP-52587-FR

Traineau H., Lasne E., Coppo N., Baltassat J-M., 2015.Recent Geological, Geochemical and Geophysical Surveys of the Roseau Valley, High Temperature Geothermal Field in Dominica, West Indies

Vigouroux P, Blanchard L., 2004. Ressources en eau thermale de la station de Vals-les-bains. Rapport final – BRGM RP-53190 – FR 113p.

Vuataz, F-D., Criaud, A., Foui11ac, C., 1985. Detailed geochemical study of alkaline thermal waters : a geothermal evaluation i n the pyrenees range, southern France.

Sites internet

www.geothermal-energy.org/explore/our-databases/conference-paper-database/

www.geothermie-perspectives.fr/: general geothermal website for France created by ADEME (French Agency for Energy and Environment) and BRGM (French Geological Survey).

www.developpement-durable.gouv.fr/Les-titres-miniers-en-cours-de.html: list of valid high temperature geothermal permits.

www.geothermie-caraibes.org website of Interreg IV project “Caribbean Geothermal” gathers information about the whole Caribbean region. INTERREG IV project “Carribean Geothermal”,

www.geothermie-soultz.fr

www.brgm.fr/brgm/le-groupe-brgm/geothermie-bouillante

DReAL Alsace

www.fonroche.fr FoNRoChe énergie

Annexes

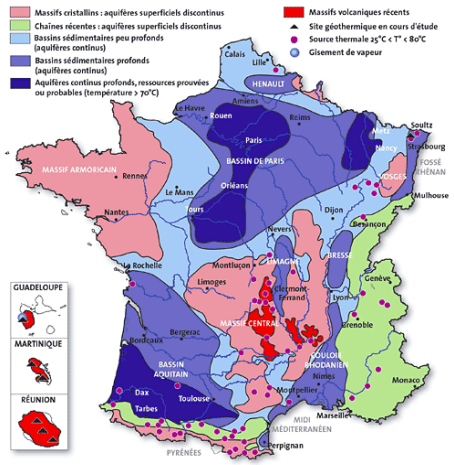

Permits map Ministry of environment January 2016 (ADEME)

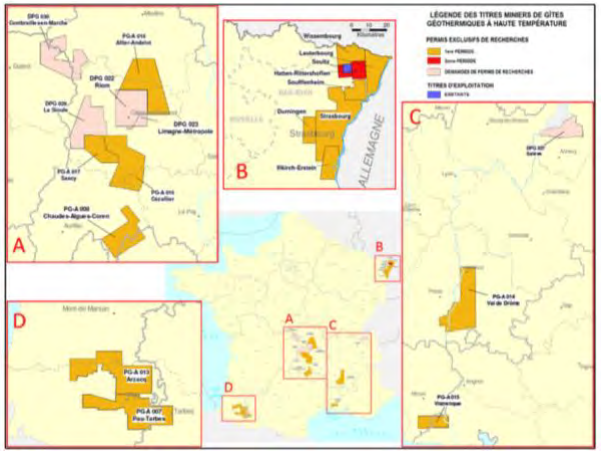

Map of geothermal resources in France (Boissavy et al. 2016).

A :Massif Central and Limagne, B:Alsace, C:Rhone et Haute Savoie, D:Sud-Ouest. (Boissavy et al 2016)

DEMANDE	PÉTITIONNAIRE	DATE DE PÉTITION
Salève	GEOFORON	22.04.2013
La Sioule	TLS GEOTHERMICS	22.06.2015
Combrailles en Marche	TLS GEOTHERMICS	24.08.2015
PERMIS	TITULAIRE	EXPIRATION
Soultz	GEIE EXPLOITATION MINIÈRE DE LA CHALEUR	05.10.2017
Hatten-Rittershoffen	ROQUETTES FRÈRES, ÉLÉCTRICITÉ DE STRASBOURG	22.03.2018
Lauterbourg	ÉLÉCTRICITÉ DE STRASBOURG	03.12.2016*
Wissembourg	ÉLÉCTRICITÉ DE STRASBOURG	03.12.2016*
Pau-Tarbes	FONROCHE GÉOTHERMIE	30.03.2018
Chaudes-Aigues-Coren	ELECTERRE	30.03.2018
Strasbourg	FONROCHE GÉOTHERMIE	23.06.2018
Illkirch-Erstein	ÉLÉCTRICITÉ DE STRASBOURG	23.06.2018
Arzacq	FONROCHE GÉOTHERMIE	14.02.2019
Val-de-Drôme	FONROCHE GÉOTHERMIE	27.03.2019

Vistrenque	FONROCHE GÉOTHERMIE	02.04.2019
Cézallier	FONROCHE GÉOTHERMIE	24.07.2019
Sancy	ELECTERRE	24.07.2019
Allier-Andelot	FONROCHE GÉOTHERMIE	27.08.2019
Riom-Clermont-Métropole	FONROCHE GÉOTHERMIE, ELECTERRE	02.02.2021
Vieux-Habitants	GÉOTHERMIE DE GUADELOUPE	20.05.2021
Salazie-Cilaos	VOLCANERGIE	28.10.2021

* Prolongation sollicitée High temperature geothermal permits, situation on 1 july 2017.

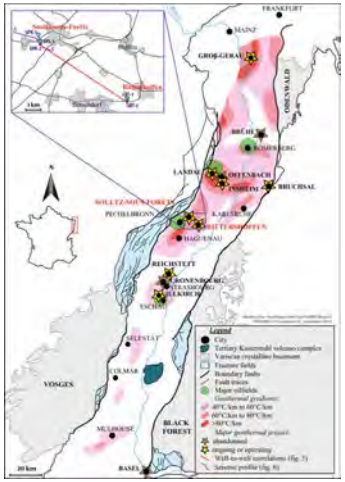

Map of extrapolate temperatures of the URG with major geothermal projects (Aichholzer et al., 2016)

Evaluation of the basic characteristics of prospective CHPM areas

France

AREA 1 - Bouillante Guadeloupe (971)

1. **Geology of the prospective area**

Requested information on:

- ✓ local geology (in regional context)
- ✓ CHPM target formation
- ✓ list of available cross sections, geological maps, geochemical results, lithological information

Notes: briefly summarized, referenced to more detailed studies.

Location and geological context

The Bouillante geothermal field is located in the French West Indies in the Guadeloupe archipelago. This archipelago forms part of the 850-km-long N-S- trending Lesser Antilles volcanic arc located at the northeastern edge of the Caribbean plate where the Atlantic lithosphere subducts beneath the Caribbean plate (Feuillet et al., 2002). The geothermal field is on the west coast of Basse-Terre Island, which is the westernmost and highest island (1467 m). It is contained within a volcanic substratum largely attributed to sub-product of the axial Pitons de Bouillante volcanic chain cropping out along the N-S axis of Basse-Terre Island and lies near two recent units: the 'axial Chain complex' (1.023 to 0.445 Ma; Samper et al., 2007) and the 'Bouillante Chain complex' (1.1 to 0.2 Ma; Gadalia et al.,1988).

The persistence of volcanic activity in the area for almost 1 Ma and the associated magmatic differentiation argue in favor of a deep magma reservoir below the Bouillante Chain complex. The magma is thought to come from the partial melting of the subducted oceanic crust and would be blocked at an undetermined depth to form a common magma reservoir. This deep magma reservoir is the most likely heat source of the Bouillante geothermal system, (Bouchot et al. 2010).

CHPM target formation

Surface expressions of the geothermal field are characterized by direct discharges of geothermal fluid along the coast and offshore hot springs and hot soils, with gas emissions (e.g. He, CO2, CH4, Rn). The density of surface indicators is the highest in the Bouillante Bay where submarine springs and gas emissions can reach ~120 °C. These manifestations are also located along a 6 km long N-S alignment within the volcanic chain that reflects spatial fluid leakage from a high-temperature geothermal reservoir (Bouchot et al. 2010). These geothermal surface indicators vanish southward though the local toponymy may still reflect their former presence.

List of data

Geological maps (Bourdon et al., 2008)

Regional structural sketch of the Montserrat-Bouillante-Les Saintes and Marie-Galante tectonic systems. (Bouchot et al. 2010)

Location of the Bouillante geothermal field (western Basse-Terre)

Preliminary conceptual model along a N-S section of the Bouillante geothermal system based on multidisciplinary borehole and surface data. (Bouchot et al. 2010)

Location of the Bouillante geothermal wells. Projection at surface of the wells BO-5, BO-6 and BO-7 (from CFG Services, Sanjuan et al., 2010)

From south (B07) to north (B02), well data (modified from on hydrothermal alteration, temperatures and/or resistivities Bourgeois and Debeglia, 2008) (Bouchot et al. 2010).

Bouillante lease are assigned from 2009 to 2050, to the titulaire Geothermie Bouillante.

2. Geophysics of the prospective area

Requested information:

- ✓ previous geophysical measurements (in CHPM relevance)
- ✓ geophysical results that can be used for locating/defining the deep metal enrichment
- ✓ list of available geophysical maps, cross sections, logs, other measurements

Different geophysical methods have been applied in 2001, 2003 and 2004 in order to constrain the conceptual model of the known geothermal field and to locate this hypothetical reservoir:
2-D electrical imaging survey, bathymetry mapping, off shore high resolution seismics, off shore and on shore magnetic survey.
Geological, thermal and production data from existing wells have been used to constrain geophysical interpretation.
Electric imaging has been performed using a dipole-dipole array along an 6-km long profile, parallel to the coast. The interpretation outlines faults and conductive zones which are interpreted as either productive or intensely hydrothermally altered zones.
High resolution marine seismic data have been acquired along the shore with a 6-channel streamer and a 1000 J sparker source. Faults are pointed out and related to faults mapped inland.
The offshore magnetic survey detects anomalies which correlates, from one part, with those faults and, on the other part, with volcanic cones that appear on the bathymetric map of the bay.
Magnetic measurements inland help to link the structures detected offshore to the geological structures inland. (Fabriol et al. 2005)

List of data

Champ géothermique de Bouillante : synthèse des études géophysiques BRGM RP 50259 (Fabriol, 2001).
Champ géothermique de Bouillante: synthèse des travaux réalisés avant 1999. Report BRGM/RC-51673-FR 2001; 46 p. (Sanjuan, 2001)
Regional and local tectonic settings of the Bouillante field, and associated volcanism (Thinon et al.).
Structural pattern of the Bouillante geothermal field (network of E-W faults) with position of the main superficial geothermal expressions (modified from Mas et al., 2006).
Resistivity model for the NS dipole-dipole profile. (Fabriol et al. 2005)

3. Deep metal enrichment

Requested information:

✓ (expected) metal enrichment based on available geophysical, geological and drill data, samples information, geochemistry

Bouchot et al., 2009 compared parameters of Bouillante, active high-enthalpy geothermal systems in island-arc environments and low-sulfidation (L-S) Au-Ag epithermal paleosystems.
«... At Bouillante under the natural P-T conditions, the fluids occur as hot saline water (no boiling). Boiling is, however, active in the production well where it provokes the precipitation of silica, calcite, Mn, Fe oxides and traces of sphalerite, galena ± pyrite, chalcopyrite, argentite (Ag_2S); i.e. the same metallic paragenesis as found in L-S epithermal orebodies."
The presence explosion breccia pipes is assumed from evidence of adularia-bearing hydrothermal breccia identified at the surface (Sanjuan et Traineau, 2000; Bouchot et al., 2009). Although the cap rock is highly developed, there are some evidences on surface of reservoir leakages through local fracture zone due to the presence of Illite/Smectite minerals (Patrier et al., 2003). Thus hydrothermal alteration study from surface samples can give access to deep information about the hydrothermal mineralogy within the reservoir.

The geothermal fluid in the reservoir corresponds to a sodium chloride (NaCl) brine (+ traces of As, Zn, Fe, Cs) with a salinity approaching 20 g/l and a pH of around 5.3 ± 0.3 at 250-260 °C. The chemical and isotopic compositions indicate that the fluid derives from a mixture of sea water (58%) and meteoric water (42%) at chemical equilibrium with the host rock at reservoir temperature (Sanjuan et al., 2001).
Compared to seawater diluted with freshwater, the geothermal fluid is enriched in K, Ca, Si, B, F, Sr, Li, Rb, Cs and most metals Fe, Al, Mn, Cu, Ni, Pb, Zn, Co, Cd, etc....Compared to seawater diluted with freshwater, the geothermal fluid is enriched in K, Ca, Si, B, F, Sr, Li, Rb, Cs, Co, Cd, etc.. ; a combined magmatic, marine and meteoric origin for the fluid.

Considering that the heat source of the Bouillante geothermal field is the 20-km-long Bouillante Chain complex, and that this alignment of small volcanic centers is in a low-relief environment along the coast of the island, then it is probable that a magmatic intrusion is partly located just below the active Bouillante field and its upflow area.
The reservoir of the Bouillante field can be defined by two units:

- a heat reservoir corresponding to the total rock volume affected by intense pervasive hydrothermal alteration (mainly illite and chlorite zone) with a homogenized temperature of 250-260 °C;
- a hydraulic network made up of permeable faults and porous aquifers along which the geothermal fluids circulate within the confines of the heat reservoir.

4. Integrated 3D- 4D model

Requested information:

- ✓ existing 3D-4D models of the target area and the deep metal enrichment
- ✓ if no 3D-4D models exist, collect the following necessary data: geological setting, mineralization, fluid flow models, stress field determination

Notes: e.g. openly available datasets, models.

3D fault interpretation combines onshore and offshore knowledge (Calcagno et al., 2012)

2D conceptual model of Bouillante geothermal field (From Bouchot et al., 2010).

3D-model of the Bouillante geothermal field using the EARTHVISION code (area of the production wells) (Traineau et al., 2008)

5. EGS potential

Requested information:

- ✓ EGS potential (heat & energy) of the area
- ✓ geothermal characteristics (temperature gradient, heat flux, stress field, water availability, EGS geology)
- ✓ presence/indication of deep fluids/brines, fracture system, crustal permeability

The maximum discharge of geothermal fluid is close to 600 tons/h, among which 120 tons/h of steam for 15 MWe electricity production. *(Sanjuan et al., 2015)*

Temperature gradient: 120 to 150°C/Km
Fractured system: a main E-W oriented normal fault network and a secondary N-S fault network.
Geothermal reservoir fluid: NaCl fluid, with a TDS of about 20 g/l and pH close to 5.3. Origin: mixing of 58% seawater and 42% freshwater which reacts with volcanic rocks at 250- 260°C in the reservoir.
The Gas-Steam Ratio is about 0.4-0.5% (4-4.5 kg CO2/ton steam because CO2 is predominant (95% in volume) in the associated gases; H2S content is about 2.5% in volume).
Stress field: not found
Estimated porosity: 10-15%
Intrinsic Transmissivity Kh: 24-34 D.m
Hydrogeological storage capacity S: 0.04-0.16
Wells characteristics:
BO-2: 150 tons/h fluid (30 tons/h steam); Production level depth: 300-330 m TVD
BO-4: 130 tons/h fluid (26 tons/h steam; maximum production), relative Transmissivity: 0.5-0.7 10-8 m3/Pa s; Storage capacity: 1-5 10-8 m/Pa; Production level depth: 560-1050 m TVD
Stimulation by thermal cracking carried out in the well BO-4 in 1998 using about 8,000 m3 of cold seawater with IDOS-130 as an inhibitor of anhydrite scale deposit. Improvement of the permeability and productivity of this well
BO-5: > 220 tons/h fluid (44 tons/h steam); relative Transmissivity: 5-10 10-8 m3/Pa s; Storage capacity: 4-5 10-8 m/Pa; Production level depth: 900-1150 m TVD
BO-6: 300-320 tons/h fluid (60 tons/h steam); relative Transmissivity: 2 10-8 m3/Pa s; Storage capacity: 4-10 10-8 m/Pa; Production level depth: 900-1150 m TVD
BO-7: very low production; relative Transmissivity: 1-2 10-8 m3/Pa s; Storage capacity: 2-10 10-8 m/Pa; Production level depths: 600-700; 900-1000 m TVD
Connectivity between wells: pressure interferences but complex hydraulic connections between wells (an organic tracer injected in the well BO-4 was observed in the wells BO-5 and BO-6 16 months later)
Estimated reservoir fluid volume using tracer test results (Na-benzoate and 1,6-nds): > 30 millions tons (Traineau et al., 2008).

List of references

Abouakar A., Matray J.-M., Brach M., 1992, étude géochimique du fluide géothermal du puits B02 (centrale EDF) et des sources thermales de la région de Bouillante (Guadeloupe) BRGM/R36 203

Bouchot, V., Traineau, H., Guillou-Frottier, L., Thinon, I., Baltassat, J-M., 2010. Assessment of the Bouillante Geothermal Field (Guadeloupe, French West Indies): Toward a Conceptual Model of the High Temperature Geothermal System. International Geothermal Association. World Geothermal Congress Bali, Indonesia. hal-00493695

Bouchot, Vincent & Genter, Albert. 2009. Exploration guides for active high temperature geothermal systems, as modern analogs for paleo-epithermal systems. Transactions - Geothermal Resources Council. 33.

Bouchot, V., 2009. Modèle conceptuel du champ géothermique haute température de Bouillante, Guadeloupe, Antilles françaises. Report n° BRGM/RP-57252-FR, BRGM

Bourdon E., Bès de Berc S., Traineau H., Sanjuan B., Chauvet M., Hervé J.-Y, Miehe J.-M., Bézèlgues-Courtade S. 2008. Inventaire des ressources géothermiques potentielles de la Guadeloupe. Rapport BRGM/RP-56631-FR, 145 pages, 50 illustrations, 2 annexes.

Calcagno P., Bouchot V., Thinon I., Bourgine B., 2012. A new 3D fault model of the Bouillante geothermal province combining onshore and offshorestructuralknowledge (French West Indies). Tectonophysics. http://dx.doi.org/10.1016/j.tecto.2011.08.012

Dixit, C., 2014, Étude physico-chimique des fluides produits par la centrale géothermique de Bouillante (Guadeloupe) et des dépôts susceptibles de se former pendant leur exploitation et leur réinjection dans le sous-sol. Thèses ADEME – BRGM

Fabriol H. 2001. Champ géothermique de Bouillante : synthèse des études géophysiquesBRGM RP 50259

Fabriol, H., Bitri, A., Bourgeois, B., Debeglia, N., Genter, A., et al.. 2005. Geophysical Methods Applied to the Assessment of the Bouillante Geothermal Field (Guadeloupe, French West Indies). World Geothermal Congress 2005, Antalaya, Turkey. <hal-00768756>

Feuillet, N., I. Manighetti, P. Tapponnier, E. Jacques, 2002. Arc parallel extension and localization of volcanic complexes in Guadeloupe, Lesser Antilles, Journal of Geophysical Research, 107, B12, doi:10.1029/2001JB000308.

Feuillet N., Manighetti I., Tapponnier P. 2002 - Arc parallel extension and localization of volcanic complexes in Guadeloupe, Lesser Antilles. Journal of Geophysical Research, 107, B12, 2331-2359.

Gadalia A., Gstalter N., Westercamp D. 1988 - La chaîne volcanique de Bouillante, Basse-Terre de Guadeloupe, (Petites Antilles).Identité pétrographique, volcanologique et géodynamique, Géologie de la France, vol. 2–3, 101–130.

Genter A., Traineau H. (2004) - Synthèse méthodologique sur l'exploration géothermique haute énergie dans les DOM : approche géologique. Projet GHEDOM. BRGM/RP-53130-FR, 85 p., 37 fig., 4 tabl.

Lopez S., Bouchot V., Lakhssassi M., Calcagno P., Grappe B., 2010 Modeling of bouillante geothermal field (guadeloupe, french lesser antilles)

Patrier, P., Beaufort, D., Mas, A., Traineau, H. 2003. Surficial clay assemblage associated
with the hydrothermal activity of Bouillante (Guadeloupe, FWI). J. Volc. Geotherm. Res.,
126: 143-156.

Patrier, P., Beaufort, D., Mas, A., Traineau, H. 2003. Surficial clay assemblage associated with the hydrothermal activity of Bouillante (Guadeloupe, FWI). J. Volc. Geotherm. Res., 126: 143-156.

Samper, A., 2007. Etude géochronologique, aspects géomorphologiques et géochimiques du volcanisme de l'île de Basse Terre (Guadeloupe), et datation des structures d'effondrement de l'Arc des Petites Antilles. Géologie appliquée. Université Paris Sud - Paris XI, 2007. tel-00398601

Sanjuan B. Champ géothermique de Bouillante: synthèse des travaux réalisés avant 1999, 2001. Report BRGM/RC-51673-FR 2001; 46

Sanjuan, B. Abou Akar, A. Brach, M. Crouzet C. 2005. Valorisation des eaux chaudes de la centrale géothermique de Bouillante (Guadeloupe): étude géochimique BRGM/RP-54554-FR Final

Sanjuan, B. Traineau H. 2008 Development of the Bouillante geothermal field (Guadeloupe, French West Indies) IGA News, Newsletter of the International Geothermal Association, Quaterly No. 73,

Sanjuan, B., Bouchot, V., Mathieu F., Jousset P., Delatre M., De Michele M., Millot R., Innocent C., 2009–2012. Travaux de recherche sur le champ géothermique haute température de Bouillante en Guadeloupe. BRGM/ RP-61715-FR Final Report

Sanjuan, B., Jousset, P., Pajot, G., Debeglia, N., Marcello De Michele, et al. 2010. Monitoring of the Bouillante Geothermal Exploitation (Guadeloupe, French West Indies) and the Impact on Its Immediate Environment. International Geothermal Association. World Geothermal Congress, Bali, Indonesia. hal-00496141

Serra, H. Sanjuan, B. Azaroual M. 2004. Modélisation géochimique des risques de dépôts minéraux au cours de l'exploitation des forages géothermiques de Bouillante (Guadeloupe) BRGM/RP-53154-FR

Traineau, H., Tournaye, D., Sanjuan, B., Genter, A., 2008 Engine, Geothermal lighthouse project in Europe-engine.brgm.fr Update of Bouillante. http://engine.brgm.fr/mediapages/lighthouseProjects/LH-Quest_HydroTherm_1_Bouillante.pdf

Annexes

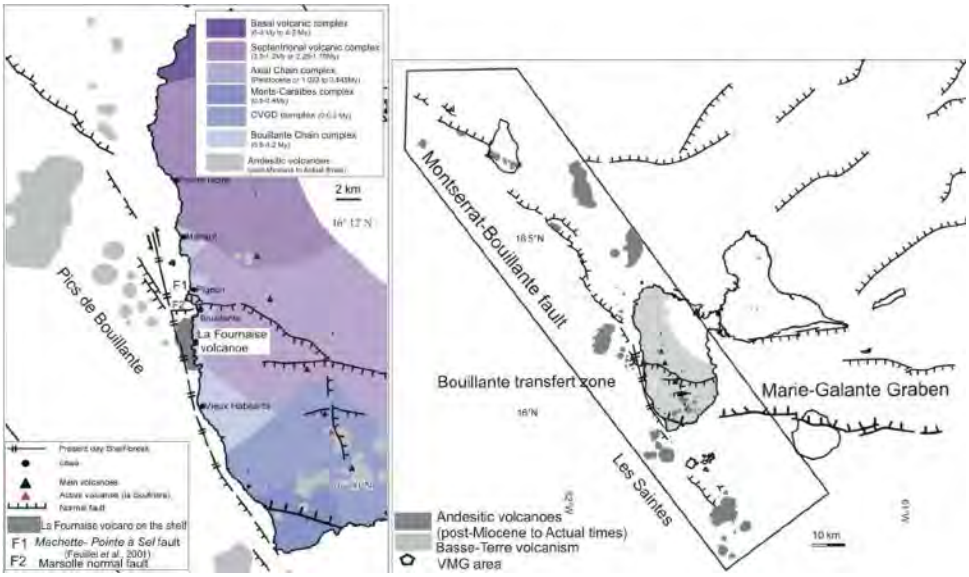

The Bouillante geothermal field (Guadeloupe, France) in its structural context at two scales. (Bouchot et al. 2009)
A) Structural synthesis of the western shelf of Basse-Terre;
B) Regional synthesis of the Guadeloupe archipelago. The Bouillante Chain complex (probably heat source) is structurally controlled by the Bouillante NNE-SSW-trending strike slip fault, as a transfer zone of the Montserrat-Bouillante-fault system (Thinon et al., 2009).

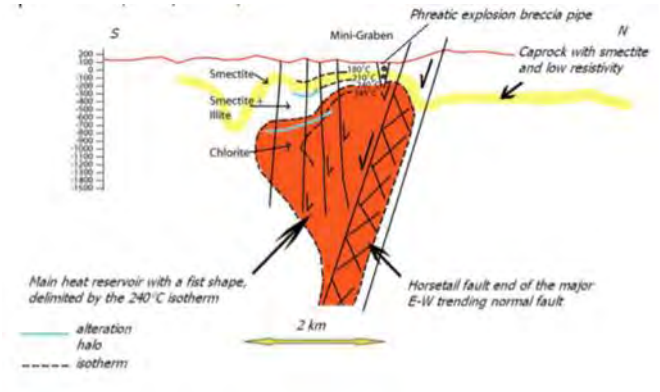

Preliminary conceptual model along a N-S section of the Bouillante geothermal system based on multidisciplinary borehole and surface data (Bouchot et al. 2010)

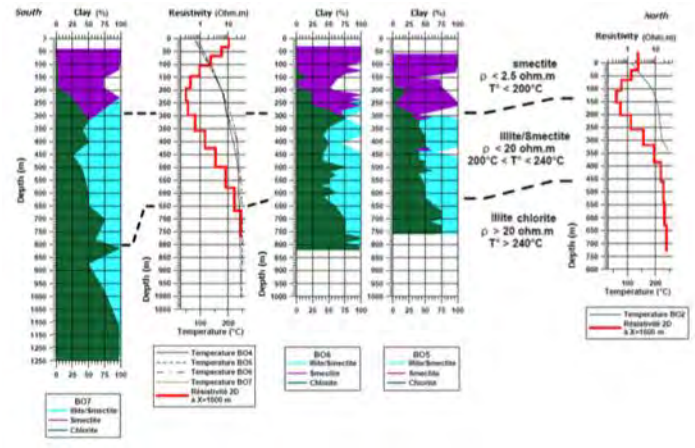

From south (B07) to north (B02), well data (modified from on hydrothermal alteration, temperatures and/or resistivities (Bouchot et al. 2010)

AREA 2 - Soultz-sous-forêt Bas-Rhin (67)

1. **Geology of the prospective area**

Requested information on:

- ✓ local geology (in regional context)
- ✓ CHPM target formation
- ✓ list of available cross sections, geological maps, geochemical results, lithological information

Notes: briefly summarized, referenced to more detailed studies.

Target

The Buntsandstein sandstone of the Alsace trias and the Palaeozoic granite basement. Brines with Li=220 mg. 5 hight temperature exploration permits (>150°C) : Soultz, Rittershoffen, Illkirch, Wissembourg, Lauterbourg. Soultz is the most and the best documented.

Local geology

The Soultz geothermal area is located in the Upper Rhine Graben (URG) which is part of the European Cenozoic rift system (Ziegler, 1992). The French part in Alsace of the URG extends from the Jura Mountains (south) to the Rhenish Massif (north). The rift basin was explored for oil and potash (Haas and Hoffmann 1929; Clapp 1932; Schnaebele et al. 1948; Blumenroeder 1962; Blanc-Valleron 1990; Wannesson 1998) and is now mainly exploited for geothermal energy (Munck et al. 1979; Genter et al. 2003; Gérard and Kappelmeyer 1987; Gérard et al. 2006a; Genter et al. 2015); (Aichholzer et al., 2016).
The graben itself forms a complex evaporite setting in which the rifting process played a major role by providing space for sedimentation basins, and facilitating a network of faults that promoted fluid circulation. The general tectonic structure of the Rhine Graben is represented by a series of N10°E-striking faults.
The URG's deep thermal structure, which is likely to be related to mantle uplift, was investigated by deep seismic surveys (Brun and Wenzel, 1991).
The graben's Paleozoic crystalline basement comprises massive granite (334 ± 3.8 Ma; Cocherie et al., 2004), the top of which, where unaltered, is a porphyritic granite with quartz, K-feldspar megacrysts, plagioclase, biotite, hornblende and accessory titanite and magnetite.
The overlying sedimentary sequencesconsist of Cenozoic evaporites and claystone underlain by Mesozoic limestone and sandstone, (Le Masne and Lambert, 1993). The most important aquifer is the Triassic Buntsandstein composed of continental conglomerate to siltstone with interbeds of claystone and dolomite (Aquilina et al., 1997).
In the region of Soultz, the faulted granitic basement is overlain by 1400 m of sediments. Deep drilling has shown that the granite is intensively fractured by faults extending down into the basement (Genter and Traineau, 1992), and that deep fluids circulate along these fractures. The amount of alteration (biotite and plagioclase dissolution, and illite, quartz and carbonate precipitation) is locally intense, with open fractures being partially filled by quartz (Aquilina et al., 1997).

List of available informations

Carte géologique harmonisée du département du Bas- Rhin (67). Notice géologique. BRGM/RP-56028-FR, 319 p., 4 fig., 3 tab., 8 ann., 3 pl. hors- texte. http://infoterre.brgm.fr/rapports/RP-56028-FR.pdf
1/50 000 N° 198 Haguenau http://ficheinfoterre.brgm.fr/Notices/0198N.pdf
http://sigesar.brgm.fr/?page=carto&mapid=19&bbox=1042394.5,6884684,1054103,6894764
Detailed geological map of superficial formations (regolith) covering the Haguenau regular map at 1/50 000 scale
Digital document supplementing the 2nd edition of this map published in 2015 (Ménillet, 2015a-b)
http://geolfrance.brgm.fr/sites/default/files/upload/documents/haguenau_carte_regolithe.pdf
1/50 000 N° 168 Lembach http://ficheinfoterre.brgm.fr/Notices/0168N.pdf
1/50 000 N° 199 Seltz http://ficheinfoterre.brgm.fr/Notices/0199N.pdf
Upper Rhine Geopotentials of the deep Upper Rhine Graben, INTERREG IV mapviewer GeORG metadata http://maps.geopotenziale.eu
Schematic NW-SE cross-section of the Upper Rhine Graben (from Le Carlier et al., 1994, and Sanjuan et al., 2010) in which several deep wells (Bruchsal, Cronenbourg, Landau, Insheim, Soultz) drilled to depths of 2540 to 5000 m have been reported.
Thermal gradient values ranging from 40 to 60 °C/km (Vernoux and Lambert, 1993), (Sanjuan et al., 2016).
Geological profile section according to Cautru, 1989.

Location of the EGS Soultz site and geology of the Upper Rhine Graben,(Dezayes et al, 2010)
Étude pétrographique des altérations hydrothermales du granite de Soultz-sous-Forêts. (Girard Berthet 2015)
Geological cross-section trouht the GPK1 well.
Complete chrono-lithostratigraphic logs showing all the limits and geological formations encountered in GPK-1 and GPK-2, wells located at Soultz-sous-Forêts, (Aichholzer, 2016)

2. Geophysics of the prospective area

Requested information:

- ✓ previous geophysical measurements (in CHPM relevance)
- ✓ geophysical results that can be used for locating/defining the deep metal enrichment
- ✓ list of available geophysical maps, cross sections, logs, other measurements

Previous geophysical measurements

Deep boreholes closely spaced at approximately 500 m (EPS-1, GPK-1, GPK-2, GPK-3 and GPK-4), provide abundant geological and geophysical data for the Soultz-sous-Forêts site:
Conventional geophysical measurements; clipper log, spectral gamma ray log and ultrasonic borhol image logs (UBI), carried out in the whole granite section (1420-5100m).
Seismic reflection profile interpreted (Cautru 1988 redrawn by Koelbel et al. 2011).
Geophysics Gamma-ray well-logging. (Howell et al. 1939)
Geological study of GPK3 HFR borehole (Dzayes et al.2003)
Bulk density of the rock formation (recorded in g/cm3) and neutron porosity (measured in percent).
In GPK1, a standard Schlumberger log, calls Compensated Neutron Litho density tool (CND) has been run for measuring, gamma ray, neutron porosity and bulk density in the Triassic layers from 900 to 1400 m depth (Genter et al. 1999). In GPK2, only caliper and gamma ray logs were collected in the sedimentary parts of the well.
Composite logs for fracture zones in GPK1 (A) and GPK3 (B);
UBI: acoustic borehole image;
HAC: Hierarchical Ascendant Classification.

List of available data

GPK-1 (Soultz) complete chronolithostratigraphic log with the gamma ray log showing all the limits and geological formations encountered
GPK-2 (Soultz) complete chrono-lithostratigraphic log with the gamma ray log showing all the limits and geological formations encountered
Seismic reflection profile (Cautru 1988, redrawn by Koelbel et al. 2011)

3. **Deep metal enrichment**
Requested information:

✓ (expected) metal enrichment based on available geophysical, geological and drill data, samples information, geochemistry

This region is known for its metallogenic potential. The granites of the Erzgebirge region are associated with Tin(Sn),Tungsten (W), Lead (Pb), Zinc (Zn), Fluorine (F), Barium (Ba) and U mineralisation, with the high U and Th contents and crustal heat flow values.

The BRGM has conducted geochemical surveys in the Vosges-Alsace-Moselle region (lougnon, 1985) whose results, among others, show Cu, Pb, Zn, Ag anomalies, in the sector of Lembach, the closest to Soult. Katzenthal had been exploited for silver-lead. Multi-element analyzes revealed Pb and Cu, Pb, Zn anomalies at Durrenberg, Mattstal, Landersberg, Erlenkeopf, Sturzelbre, Kochen, Muhlenberg, Philippsbourg. The multielements geochemical survey concern 694 samples and 189 pans, (Lougnon, 1985).

Studies concerning Soultz-sous-Forêts provide geochemical data on the fluids present within the granite basement.

The high salinities of the geothermal brines, their similar chemical compositions, their Li, B and Sr isotopic signatures and the geothermometer results all suggest that these fluids have reacted with sedimentary rock at temperatures close to 225 ± 25 °C, main reservoirs could be located further east, towards the graben's centre where the sedimentary Triassic Buntsandstein is deepest and hottest (Sanjuan et al., 2010).

Very few analyses representative of the deep geothermal fluids are available but a most representative chemical composition of the deep native geothermal brine is given in Suanjan et al. 2010 from 1999 to 2005 samplings (µg/l) : Ni: 100, Cu: 45, Co: 50, Cr: 40, Cd : 10, Zn: 3000, Ag: <5, Ti: 200, Pb: 300

The hottest brines are very enriched in K, Ca, SiO2, Li, Rb, Cs, As, Sr, Ba, Mn, Nd, U and in metals such as Zn, Pb, Cu, Co, Cd, Sb, they are depleted mainly in Mg, SO4 and B.(Sanjuan et al., 2016)

Geochemical data of the geothermal fluids of the Upper Rhine Graben, relative to the deepest fluids circulating in the area, and within the granite basement are in the publications of Pauwels et al. (1991 et 1993), Aquilina et al., 1997, Aquilina et al., 2000, Sanjuan et al., 2006, Sanjuan et al., 2010, Bucher and Stober (2010), Stober and Jodocy (2011) and Sanjuan (2014).

4. **Integrated 3D- 4D model *Requested information:***

✓ existing 3D-4D models of the target area and the deep metal enrichment

✓ if no 3D-4D models exist, collect the following necessary data: geological setting, mineralization, fluid flow models, stress field determination

Notes: e.g. openly available datasets, models.

3D structural regional model of the EGS soultz site (northern upper rhine graben, france) (Baillieux et al., 2011)

3D views of the whole modelled faults cross-cut by the wells or derived from VSP and microseismicity interpretation.

3D model of fracture zones at Soultz-sous-Forêts based on geological data, image logs, induced microseismicity and vertical seismic profiles (Sausse, at al., 2010)

Convection model and numerical 3D modelling (Bächler, 2003).

Basin-scale numerical models (Guillou-Frottier et al. 2013)

5. **EGS potential**

Requested information:

- ✓ EGS potential (heat & energy) of the area
- ✓ geothermal characteristics (temperature gradient, heat flux, stress field, water availability, EGS geology)
- ✓ presence/indication of deep fluids/brines, fracture system, crustal permeability

The Soultz power plant : a 1.5 MWe geothermal power plant using an Organic Rankine Cycle (ORC) system that used a low boiling-point working fluid (isobutane) in the heat-power conversion scheme. The turbine radial operates at around 13000 rpm. The generator asynchronous, operates at around 1500 rpm, and has an 11 kV output, which is transformed up to feed into the 20 kV local power network. The geothermal fluid is cooled down to 80–90 °C in the heat exchangers of the binary unit before reinjection. either or both of the two wells is used to feed the power production loop. The expected production flow rate from both wells together is about 35 l/s for a production temperature of 175 °C. (Genter et al.2012)

EGS Targeted Granites	Age (Ma)	Lithology	Sio2 (Wt%)	K2o (Wt%)	U (Ppm)	Th
Soultz-sous- Forêts Upper Rhine Graben, France	334-319	Porphyritic monzogranite	67-69	3.8-4	6.2-14.1	23-37

Temperature gradient : The shallow geothermal gradient in the graben ranges between 60 and 120 °C/km which corresponds to very high heat flow: up to 360 mW/m2 assuming a typical thermal conductivity of 3 W/K/m and a purely conductive regime in the shallow crust (Pribnow and Schellschmidt, 2000).
At Soultz, GPK-2, temperatures of 200 °C are reached at 5 km depth with a profile divided into three sections with different geothermal gradients : The upper section lies entirely in the sediments from the surface to 1 km depth and has a very high gradient of about 110 °C/km, indicating heat transport is predominantly conductive; The intermediate depth section from 1 km to about 3.3 km depth is characterized by a very low gradient of about 5 °C/km, which suggests heat transport is dominated by advection, probably in the up-flowing limb of a convective system that is active in the granite and Triassic sandstones (Le Carlier et al., 1994). This implies significant natural fluid movement is occurring within faults and fracture zones, at least between 1.0 and 3.3 km. Below 3.3 km, the geothermal gradient increases again to 30 °C/km and becomes linear with depth, indicating a return to a conduction-dominated heat flow regime.
Geothermal gradient in the Soultz wells (data from LIAG, Hannover)
Geothermal characteristics (Sanjuan et al., 2016) (Genter et al., 2010)

Heat flux : A natural flux value of 1–1.2 m^3/h was estimated for the deep native geothermal brine (Sanjuan et al., 2004; Sanjuan et al., 2006a; Sanjuan et al., 2006b)

Stress field : The stress state at Soultz is consistent with a graben setting, with a minimum principal stress that is horizontal and about 53% of the vertical stress. The maximum horizontal principal stress, SHmax, is oriented N169°E ± 14°. The alignment of the wells at Soultz was chosen to coincide approximately with SHmax. The principal stress magnitudes are given as a function of depth z, by (Valley and Evans, 2007):
Sv [MPa] = 0.3 + 25.60z [km] Shmin [MPa] = –1.8 + 14.09z [km] –1.2 + 22.95z [km] ≤ SHmax [MPa] < –1.4 + 26.775z [km] (Valley et al.,2007)

Fluid geochemistry : A tracer test conducted between 2000 and 2002 in the GPK-2 open-hole section below 4.5 km indicated a natural flow rate of native geothermal brine of 1.0–1.2 m3/h (Sanjuan et al., 2006a, Sanjuan et al., 2006b)

Deep fluids/brines : Analytical data of fluids discharged from the wells GPK-1 (Pauwels et al., 1993; Aquilina et al., 1997; Sanjuan et al., 2001), GPK-2, GPK-3 and GPK-4 (Vaute, 1998; Sanjuan et al., 2001; Sanjuan et al., 2004; Sanjuan et al., 2006b) used in order to determine the most representative chemical and isotopic composition of the deep Soultz geothermal brine (3500–5000 m). The most relevant geochemical data on the nature, origin, circulation and deep temperature of these fluids were obtained from GPK-1 and GPK-2 (Aquilina et al., 1997, Pauwels et al., 1993, Sanjuan et al., 2006a, Sanjuan et al., 2010).

Fracture system Desayes et al., 2010
Fracture orientation in the Soultz wells based in cores and various borehole image logs. For the GPK3 and GPK4 wells, data are grouped in relation with the major petrographical sections (from Hooijkaas et al., 2006).

List of references

Aichholzer C., Duringer Ph. , Orciani S. and Genter A., 2016, New stratigraphic interpretation of the Soultz-sous-Forêts 30-year-old geothermal wells calibrated on the recent one from Rittershoffen (Upper Rhine Graben, France) *Geothermal Energy* https://doi.org/10.1186/s40517-016-0055-7

Aquilina L., Pauwels H., Genter A., Fouillac C. (1997), Water-rock interaction processes in the Triassic sandstone and the granitic basement of the Rhine Graben: geochemical investigation of a geothermal reservoir Geochim. Cosmochim. Acta, 60, pp. 4281-4295

Bächler, D., 2003. Coupled thermal-hydraulic-chemical modeling at the Soultz-sous-Forêts HDR reservoir (France), Thesis Doctor of Natural Sciences, Swiss Federal Institute of Technology, Zürich, 151 p.

Baillieux P., Schill E., Dezayes C. 2011, 3D structural regional model of the egs soultz site (northern upper rhine graben, france): insights and perspectives. PROCEEDINGS, Thirty-Sixth Workshop on Geothermal Reservoir Engineering Stanford University, Stanford, California, SGP-TR-191

Bauer JF, Meier S, Philipp SL. Architecture, fracture system, mechanical properties and permeability structure of a fault zone in Lower Triassic sandstone, Upper Rhine Graben. Tectonophysics. 2015;647–648:132–45. doi:10.1016/j. tecto.2015.02.014.

Boissavy, C., Rocher, P., Laplaige, P., Brange, C., European Geothermal Congress 2016 Strasbourg, France, 19-24 Sept 2016 Geothermal Energy Use, Country Update for France

Cautru J.P., (1988), Coupe géologique passant par le forage GPK-1 calée sur la sismique réflexion, document BRGM. Institut Mixte de Recherches Géothermiques, Rapport interne

Dezayes C., Genter A., Valley B., (2010), Structure of the low permeable naturally fractured geothermal reservoir at Soultz C.R. Geosci., 342 pp. 517-530

Dezayes Ch., Genter A., Homeier G., Degouy M., Stein G. (2003) - Geological study of GPK-3 HFR borehole (Soultz-sous-Forêts, France). BRGM/RP-52311-FR, 128 p.

Dezayes C., Villemin, T., Genter, A., Traineau, H., Angelier, J., 1995. Analysis of fractures in boreholes of the Hot Dry Rock project at Soultz-sous-Foreˆts (Rhine Graben, France). Sci. Drilling 5, 31–41.

Genter A., Evans K. , Cuenot N. , Fritsch D. , Sanjuan B., Contribution of the exploration of deep crystalline fractured reservoir of Soultz to the knowledge of Enhanced Geothermal Systems (EGS) C.R. Geosci., 342 (2010), pp. 502-516

Genter, A., Cuenot, N., Goerke, X., Bernd, M., Sanjuan, B., et al.. Status of the Soultz geothermal project during exploitation between 2010 and 2012. 37th Workshop on Geothermal Reservoir Engineering, Stanford University, California, USA, Jan 2012, Stanford, United States. SGP-TR-194, 12 p., 2012. <hal-00697602>

Gentier S., with the collaboration of Genter A., Sanjuan B., Bourgine B., Dezayes C., Hosni A., Breton J.P., Nicol N., Quinquis J.P., Crouzet C., Braibant G., Brach M., Moussay A., Foucher J.C., Jouin F. (2003) – « Hot Dry Rock Energy » Project (Soultz-sous-Forêts) – BRGM contribution (progress report). BRGM/RP-52730-FR, 51 p., 24 Fig., 15 Tables.

Girard Berthet Violaine, Master 2, 2014/2015 Étude pétrographique des altérations hydrothermales du granite de Soultz-sous-Forêts à l'interface socle- couverture en contexte géothermique.

Guillou-Frottier, L., Carré, C., Bourgine, B., Bouchot, V., Genter, A., 2013, Structure of hydrothermal convection in the Upper Rhine Graben as inferred from corrected temperature data and basin-scale numerical models. Journal of Volcanology and Geothermal Research, Elsevier, 256, pp.29-49. <10.1016/j.jvolgeores.2013.02.008>. <hal-00801798>

Howell LG, Frosh A. Gamma-ray well-logging. Geophysics. 1939;4(2):106–14.

Kölbel, T., Genter, A., 2017 Enhanced Geothermal Systems: The Soultz-sous-Forêts Project 243-248. 10.1007/978-3-319-45659-1_25.

Le Carlier C., Royer J.-J., Flores E.L. (1994), Convective heat transfer at the Soultz-sous-Forêts geothermal site: implication for oil potential First Break, 12 pp. 553-560

Lougnon, J., 1985 Contribution à la connaissance de la Gîtologie de la région Vosges-Alsace-Moselle
Après 14 années de Prospection B.R.G.M. 85 Dam038 0p4

Ménillet F., Benecke E.W., Schumacher E., Van Werveke L., LepPia A., ThüRach H., Konrad H.J., Illies H., Rinck G., Schwoerer P. (1989) - Carte GéOl. France (1/50 000), Feuille Lembach (168) - Orléans : Bureau de

recherches géologiques et minières. Notice explicative Par Ménillet F. et coll. (1989), 91 p.

Ménillet F., Avec La Collaboration De C. Coulombeau, F. Geissert, H. J. Konrad, P. Schwœrer (1989) - Notice Explicative, Carte GéOl. France, Feuille Lembach (168) - OrléAns : Bureau De Recherches GéOlogiques Et MinièRes, 91 P. Carte GéOlogique Par MéNillet F., Benecke E.W., Schumacher E., Van Werveke L., Leppia A., ThüRach H., Konrad H.J., Illies H., Rinck G., Schwoerer P. (1989).

Pauwels H., Lambert M., Genter A., 1991, Valorisation des fluides géothermaux contenant du lithium en vue d'une production Industrielle. BRGM/R 33547 les reserves en lithium des aquiferes du trias de la zone nord Alsace pp 33-67

Place J. , Diraison M. , Naville C. , Géraud Y. , Schaming M. , C. Dezayes, (2010), Decoupling of deformation in the Upper Rhine Graben sediments. Seismic reflection and coupled analysis of diffraction on 3-component Vertical Seismic Profiling (Soultz-sous-Forêts area), Geoscience, 342 pp. 575-586.

Sanjuan B., Millot R., Innocent Ch., Dezayes Ch., Scheiber J., Brach M., june 2016, Major geochemical characteristics of geothermal brines from the Upper Rhine Graben granitic basement with constraints on temperature and circulation. Chemical geology, vol. 428, 27-47 https://doi.org/10.1016/j.chemgeo.2016.02.021

Sanjuan B, Millot R, Dezayes C, Brach M. 2010. Main characteristics of the deep geothermal brine (5 km) at Soultz-sous-Forêts (France) determined using geochemical and tracer test data. CR Geosci. 2010, 342:546–59.

Sausse, J., Dezayes, C., Dorbath, L., Genter, A., Place, J., 2010, 3D model of fracture zones at Soultz-sous-Forêts based on geological data, image logs, induced microseismicity and vertical seismic profiles Comptes Rendus Geoscience, Volume 342, Issues 7–8, pp. 531-545 doi:10.1016/j.crte.2010.01.011.

Sausse J. , Dezayes C. , Genter A. (2007) From geological interpretation and 3D modelling to the characterization of the deep seated EGS reservoir of Soultz (France) Proceedings, European Geothermal Congress 2007, Unterhäching, Germany

Sausse J. , Dezayes C. , Genter A. Characterization of fracture connectivity and fluid flow pathways derived from geological interpretation and 3D modelling of the deep seated EGS reservoir of Soultz (France)

Skrzypek E., Cruz Mermy D., Chèvremont P. et Ménillet F., (2007) - Carte géologique harmonisée du département du Bas- Rhin (67). Notice géologique. BRGM/RP-56028-FR, 319 p., 4 fig., 3 tab., 8 ann., 3 pl. hors-texte.

Valley B., Evans K.F. (2007), Stress state at Soultz-sous-Forêts to 5 km depth from wellbore failure and hydraulic observations, 32nd Workshop on Geothermal Reservoir Engineering, Stanford University, California, USA.

Ziegler P.A. (1992), European Cenozoic rift system, Tectonophysics, 208 pp. 91-111

Web resources

INTERREG IV Upper Rhine Geopotentials of the deep Upper Rhine Graben GeORG mapviewer GeORG metadata http://maps.geopotenziale.eu

BRGM reports http://infoterre.brgm.fr/

https://umap.openstreetmap.fr/fr/map/perimetres-des-titres-miniers-de-gitesgeothermiqu_158171#6/46.973/4.922

Cartes geologiques http://sigesar.brgm.fr

Annexes

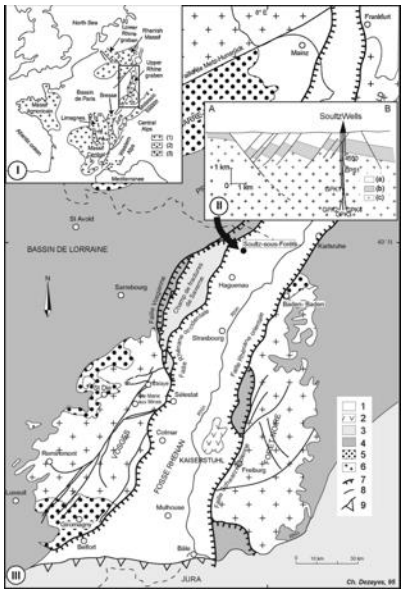

Location map

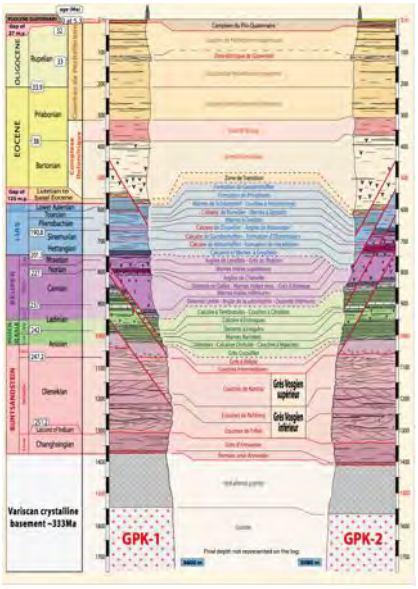

Chrono-lithostratigraphic log (Aichholzer, 2016)

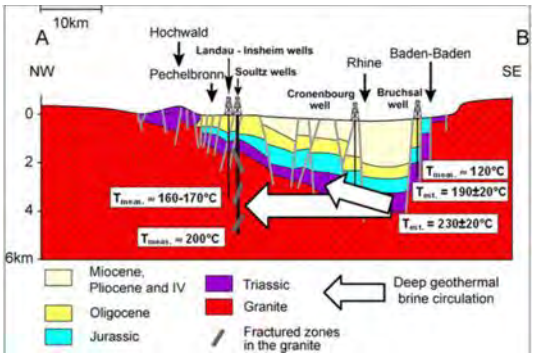

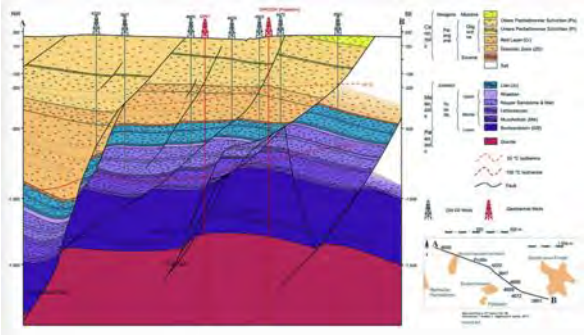

Seismic reflection profile (Aichholzer, 2016)

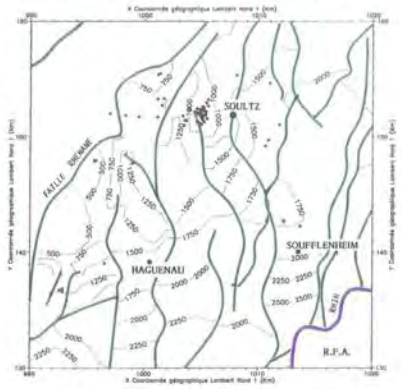

Figure 5 - Cote (m NGF) du toit du Buntsandstein

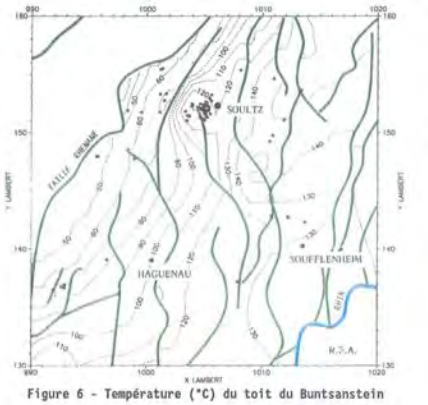

Figure 6 - Température (°C) du toit du Buntsanstein

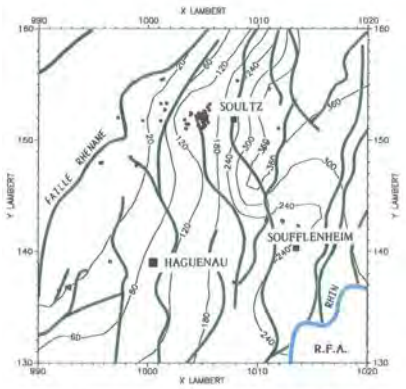

Figure 8 - Répartition du lithium dans la zone Alsace Nord

Buntsandstein top elevation (m) temperature (°C) lithium distribution
Pauwel et al. 1991

Evaluation of CHPM characteristics of prospective CHPM areas

France

Area 1 Bouillante Guadeloupe (971)

1. CHPM operational characteristics - Information for CHPM technological elements

Requested information:

✓ please fill in the table below with the requested data for the CHPM technology elements

Underground heat exchanger (deep metal enrichment + potential geothermal reservoir)	
Extension of the metal enrichments *(volumetric interpretation)*	Lopez et al., 2010 summarized volumetric interpretation of the reservoir from previous studies: The top of the reservoir is located at the base of an illite smectite alteration zone. It deepens from north (~300 m) to south (~600 m) of the geothermal field, moving away from the apical zone of the reservoir centred on Bouillante Bay. In a N-S section the envelope of the heat reservoir is in the shape of a fist, and it is about 2 km wide between Descoudes and Pointe Lézard. Its extension is controlled by the geometry of the Bouillante Bay mini-graben that is likely to drive fluid circulation through a hydraulic network made up of permeable faults zones and fractures and a few relatively shallow porous aquifers. The envelope of the heat reservoir could be rooted at about 2500-3000 m deep in the Marsolle – Pointe Lézard corridor at the depth where mixing of the geothermal fluid is thought to occur. Based on ^{7}Li isotopic arguments, this mixing zone would be at the transition between the ocean floor and the overlying andesitic lavas (Sanjuan et al., 2008). Yet, the location of this interface is not precisely constrained. It is estimated to be about 3 km deep but could even be deeper. Then, the reservoir would be at least 2.5 km thick. On the 3D view from S-E of the regional scale geological model (South part) integrating both onshore and offshore structural data. The domain size is 15km from W to E, 16km from S to N and 12km along vertical. There are many geothermal fluid discharges along the E-W axis of the Bouillante Bay graben. This gives indications about the offshore extension of the reservoir. The width of the reservoir could then be of the order of 1 km onshore and 2 km offshore eastward up to a major N160°E fault.
Expected type of the reservoir and porosity/permeability *(fractured, porous, etc)*	Type A, with a water temperature of about 260°C, no vapor in the aquifer and an enthalpy of about 1100 kJ/kg, the Bouillante geothermal field is considered as a high energy, high temperature, high enthalpy geothermal field (Zarrouk et al., 2006). **Estimated reservoir fluid volume** using tracer test results (Na-benzoate and 1,6-nds): > 30 millions tons (Traineau et al., 2008). **Estimated porosity:** 10-15% (Bouchot, et al., 2010). **Fractured system:** a main E-W oriented normal fault network and a secondary N-S fault network. In terms of permeability, the most productive conduits are the high-angle E-W faults and, to a lesser extent, certain lithological facies such as the discontinuous sandy layers, located at 400 m depth in two wells. The Cocagne fault is the zone of highest permeability intersected by two wells, providing a fracture zone several tens of metres wide (Bouchot, et al. 2010).

Mineralization *(type and enriched metals)*	Peri volcanic geothermal sodium- chloride reservoir. Epithermal type Au Ag Hg and Cu potentiel, same metallic paragenesis as found in low-sulfidation epithermal orebodies, (Bouchot et al., 2009). But the question concerning the thermal source responsible for the geothermal field remains open (unconstrained magma intrusion in the vicinity of Bouillante or thermal anomaly generated by the bulk magmatic activity of the arc). Recently, numerous samples of highly silicified breccias containing high temperature minerals have been identified in the Bouillante Bay (Anse Marsolle). Their petrographic study reveals several hydrothermal parageneses typical of distinctive alteration facies. These results highlight assemblages and mineral textures characteristic of high temperature hydrothermal alterations in epithermal context. Such breccias are the first surficial evidences of high temperature hydrothermal activity in this area. They can be considered as indicators of a deeper hindered hydrothermal system, the origin of which needs to be elucidated, particularly regarding its relationships with the present geothermal system. (Patrier et al., 2013)

Production and injection wells	
Depth of potential wells (m)	Wells characteristics (TVD true vertical depth): BO-1 vertical no HP production: total length 850m BO-2 vertical injection well: 150 tons/h fluid (30 tons/h steam); Production level depth: 300-330 m TVD. Total length 350m. BO-3 vertical no HP production. Total length 850m BO-4 vertical, observation well: 130 tons/h fluid (26 tons/h steam; maximum production); relative Transmissivity: 0.5-0.7 10-8 m3/Pa s; Storage capacity: 1-5 10-8 m/Pa; Production level depth: 560-1050 m TVD. Total length 2500m. BO-5 producer well: > 220 tons/h fluid (44 tons/h steam); relative Transmissivity: 5-10 10-8 m3/Pa; Storage capacity: 4-5 10-8 m/Pa; Production level depth: 900-1150 m TVD. Total length 1197m BO-6 deviated, producer well: 300-320 tons/h fluid (60 tons/h steam); relative Transmissivity: 2 10-8 m3/Pa s; Storage capacity: 4-10 10-8 m/Pa; Production level depth: 900-1150 m TVD. Total length 1248m. BO-7 deviated, observation well: very low production; relative Transmissivity: 1-2 10-8 m3/Pa s; Storage capacity: 2-10 10-8 m/Pa; Production level depths: 600-700 m & 900-1000 m TVD production. Total length 1400m. (Entrepose, 2018 - http://www.lowbin.eu/public/BRGM-GTH%20fields-France.pdf - http://engine.brgm.fr/mediapages/lighthouseProjects/LHQuest_HydroTherm_1_Bouillante.pdf) Bouillante 1: This unit has a capacity of 4.5 MWe and can produce 30GWh annually. The commissioning was done in 1985 and was completely restored in 2013. Bouillante 2: In operation since 2005, with an installed capacity of 11MWe.

Electrolytic metal recovery and gas diffusion electro- precipitation	
Potential target metals to be recovered	An epithermal Au-Ag orebody (white et al., 1995) forms relatively close to the surface (<1-2 km). The circulating hydrothermal fluids at these shallow levels are typically dilute and therefore relatively low in base metals, but enhanced in precious metals (Ag, Au, As, Hg [± Pb, Zn, Sb, Se] [rare Cu]). (Bouchot et al., 2009, Patrier et al., 2013)

Power plant (heat exchanger)	
Local heat and electricity demand *(industrial, municipal, agricultural, etc.)*	Guadeloupe key figures: 1628 km2, 397 390 inhabitants (source INSEE). Guadeloupe is very dependent on imported fossil fuels and coal. In 2017, the total final energy consumption in Guadeloupe is equal to 6,835 GWh. The final annual electricity consumption is on average 1752 GWh, fuel consumption is 4727 GWh, butane 158 GWh, heat 192 GWh. Distributed according to: fuels transport 67% - electricity 26% - heat 3% - fuels 2% - butane 2% The gross electricity consumption is by the domestic sector 48% and professional sector 37.7%, communities 7.7%, street lighting 2.5%, agriculture 0.1%. The consumption of heat in domestic hot water is 62 GWh, in candy 129 GWh (mainly steam), in distillery (12 GWh in 2016), (OREC, 2017 – EDF, 2017).

Salt gradient power generation	
Salinity of expected geothermal brine	**Exploited fluid:** NaCl fluid (TDS about 20 g/l; 25 g/l after steam separation) (BRGM, 2008) The geothermal fluid in the reservoir corresponds to a sodium chloride (NaCl) brine (+ traces of As, Zn, Fe, Cs) with a salinity approaching 20 g/l and a pH of around 5.3 ± 0.3 at 250-260 °C. (Bouchot et al., 2009)
Fresh water supply from the surface *(water sources)*	Local fresh water supply could not assure sufficient flow rate for the stimulation, it was decided to use sea water which was pumped from the Power Plant pumping station, located in the BO-3 drill pad. Maximum flow rate was 25 l/s with an initial well-head injection pressure of 25 bar-g. Taking into account the risk of anhydrite scaling due to the mixing of cold sea water/geothermal fluid and predicted by geochemical modelling (Sanjuan, 1998), it was decided to inject an anhydrite scale inhibitor (IDOS 130) at a continuous concentration of 30 ppm in the sea water. (Sanjuan et al., 2000) The climate of Guadeloupe is humid tropical type, characterized by a dry season from December to May and a wet season from June to November. Precipitation is very important, always greater than evapotranspiration over a large part of Basse-Terre, where the Soufriere massif is considered as the water tower of Guadeloupe. In Basse-Terre, the rivers have a permanent flow fed by rainfall runoff and supported by the resurgences of groundwater of altitude. The rivers of Basse-Terre are characterized by small watersheds (10 to 30 km²). As result of heavy rainfall, flows can go from 1 m3 / s to 300 or 400 m3 /s.

2. CHPM operational characteristics - Environmental, social and political background

Requested information:

- ✓ toleration to gaseous and solids emissions, water and noise pollution,
- ✓ local competition to land and water availability
- ✓ public acceptance
- ✓ political support
- ✓ presence of supporting legislation, regulatory framework

Notes: all of above refers to the selected area and its surro undings.

Legislation: the Bouillante geothermal power station is an ICPE (Installations Classées pour la Protection de l'Environnement) subject to authorization as a mine, with DEAL survey.

In general, residents complain of the nuisance caused by the operation of the power plant (noises, odors, vibrations, aesthetics). Some of these nuisances are real and directly related to the operation of the power plant (noise, vibrations, aesthetics), but there are solutions to mitigate or avoid these nuisances (insulation of future installations, decrease in turbine speed, adjustment of operating hours). Other nuisances such as smells are more questionable in the sense that they exist independently of the plant. In particular, emissions of gases such as hydrogen sulphide (H2S), which has a nauseating odor, exist naturally in volcanic environments.
In addition to the hazard of induced seismicity, no earthquakes could be related to the exploitation of the Bouillante geothermal field (Sanjuan et al., 2010), (Zang et al.,2014)

3. Financial aspects

Requested information:

- ✓ list of potential local stakeholders (community, political, companies)

Since March 2016, the American company ORMAT Technologies, Inc., (www.ormat.com) based in Reno, Nevada, USA, has signed an Investment and Equity Agreement with the holding company SAGEOS, a wholly-owned subsidiary of the BRGM, to acquire progressively 85% stake in SA Geothermie Bouillante.

ADEME Agence de l'environnement et de la maitrise de l'énergie https://guadeloupe.ademe.fr
BRGM : Bureau of Geological and Mining Research: public establishment of an industrial and commercial character www.brgm.fr SAGEOS is a BRGM holding.
CDC caisse des dépôts et consignation www.caissedesdepots.fr
DEA Guadeloupe : Direction de l'environnement, de l'aménagement et de logement www.guadeloupe.developpement-durable.gouv.fr/
EDF www.edf.gp/edf-en-archipel-guadeloupe/
Geodenergie GIS (Groupement d'interet scinetifique) (www.geodenergies.com) Partner companies: Actys-Bee, (http://actys-bee.com), CFG Services, (www.cfgservices.fr), Drillscan,(www.drillscan.com), Electerre de France,(www.electerre.fr/), Enertime, (www.enertime.com), Entrepose Group,(www.entrepose.com), ÉS Géothermie, (https://geothermie.es.fr/), Fonroche Géothermie, (www.fonroche-geothermie.com/), KAPPA, (www.kappaeng.com), Total (www.total.fr) and Solexperts (www.solexpert.fr). Through the ROSTOCK H project, Géodénergies is working with Air liquide and INERIS.
Public institutions supervising research laboratories: BRGM, CNRS, MINES ParisTech - Armines, University of Orléans, University of Lorraine, University of Pau and Pays de l'Adour, and the University of Antilles.
Competitiveness cluster : S2E2 Smart electricity cluster (www.s2e2.fr) and AVENIA (www.pole-avenia.com)
Pole synergiles www.synergile.fr
OREC (Observatoire national energie climat) gather public and private partners and patrons AFD Agence Française de développemnt (www.afd.com) and Albioma (www.albioma.com)

List of references

Bibliography

Bouchot, Vincent & Genter, Albert. 2009. Exploration guides for active high temperature geothermal systems, as modern analogs for paleo-epithermal systems. Transactions - Geothermal Resources Council. 33.

Bouchot, V., Traineau, H., Guillou-Frottier, L., Thinon, I., Baltassat, J-M., 2010. Assessment of the Bouillante Geothermal Field (Guadeloupe, French West Indies): Toward a Conceptual Model of the High Temperature Geothermal System. International Geothermal Association. World Geothermal Congress Bali, Indonesia. hal-00493695

Bouchot V., Sanjuan B., Calcagno P., Gloaguen E., Thinon I., Gailler L., Baltassat J.-M., Bourgeois B., Lerouge C., Gadalia A., Bourdon E., Traineau H., Patrier-Mas P., Beaufort D. & Verati C., 2011. The high-temperature geothermal system of Bouillante (Guadeloupe, French West Indies). – 19ème Conférence géologique de la Caraïbe 2011, Le Gosier, Guadeloupe, France, p.26.

Lopez S., Bouchot V., Lakhssassi M., Calcagno P., Grappe B., 2010. Modeling of bouillante geothermal field (guadeloupe, french lesser antilles)

OREC 180703-orec-chiffres-cles-de-lenergie-2017.pdf https://www.guadeloupe-energie/chiffres-cles-de-lenergie/

Patrier, P., Bruzac, S., Pays, R., Beaufort, D., Bouchot, V., Verati, C., Gadalia, A., 2013 Occurrence of K-feldspar-bearing hydrothermal breccias in the Bouillante geothermal field (Basse Terre – Guadeloupe), Bull. Soc. géol. France, t. 184, no 1-2, pp. 119-128

Sanjuan, B. 1998, "Champ géothermique de Bouillante. Rapport d'état d'avancement des travaux en géochimie", BRGM report N2592, 29 p.

Sanjuan, B., Lasne, E. and Brach, M., 2000. Bouillante geothermal field (Guadeloupe, West Indies): Geochemical monitoring during a thermal stimulation operation, *Proceedings, 25th Workshop on Geothermal Reservoir Engineering, Stanford University, California, January 24-26*, 215-222.

Sanjuan, B. Traineau H. 2008. Development of the Bouillante geothermal field (Guadeloupe, French West Indies) IGA News, Newsletter of the International Geothermal Association, Quaterly No. 73,

Sanjuan, B., Jousset, P., Pajot, G., Debeglia, N., Marcello De Michele, et al. 2010. Monitoring of the Bouillante Geothermal Exploitation (Guadeloupe, French West Indies) and the Impact on Its Immediate Environment. International Geothermal Association. World Geothermal Congress, Bali, Indonesia. hal-00496141

Traineau, H., Tournaye, D., Sanjuan, B., Genter, A., 2008 Engine, Geothermal lighthouse project in Europe- engine.brgm.fr Update of Bouillante. http://engine.brgm.fr/mediapages/lighthouseProjects/LH-Quest_HydroTherm_1_Bouillante.pdf

White N.C., Hedenquist J.W. 1995. – Epithermal gold deposits: styles, characteristics and exploration. – *SEG newsletter*, 23, 1, 9-13.

Zang, A., Oye, V., Jousset, P., Deichmann, N., Gritto, R., McGarr, A., Majer, E., Bruhn, D., 2014. Analysis of induced seismicity in geothermal reservoirs – An overview. - Geothermics, 52, p. 6-21. DOI: http://doi.org/10.1016/j.geothermics.2014.06.005

Zarrouk S., Kaya E. et O'Sullivan M., 2006 - A review of woridwide experience of rêinjection in geothermal fields. 28th New Zealand Geothermal Workshop, Auckland, New Zealand.

Annexes

Evaluation of CHPM characteristics of prospective CHPM areas

France

Area 2 : Soultz-sous-forêts, Bas-Rhin (67)

1. CHPM operational characteristics - Information for CHPM technological elements

Requested information:

✓ please fill in the table below with the requested data for the CHPM technology elements

Underground heat exchanger (deep metal enrichment + potential geothermal reservoir)	
Extension of the metal enrichments *(volumetric interpretation)*	The Upper Rhine Graben (URG) is part of the European Cenozoic rift system. It extends about 300 km from the Rhine massif in the north to the Jura mountains in the south on an average width of 35 to 40 km. The URG is characterized by several thermal anomalies with temperatures above 140°C at 2-km depth, mainly concentrated on the western side, associated with hydrothermal convective cells circulating within an almost vertical fracture network in the granitic basement and in the fractured sediments of the Triassic above (Baillieux et al., 2013). There are two reservoir lithologies in the URG: the crystalline basement, the granite, used as an improved geothermal reservoir at Soultz-sous-Forêts and the upper porous and conductive sedimentary formations, Buntsandstein or Muschelkalk, as a hydrothermal reservoir. (Aichholzer et al., 2016) At Soultz-sous-Forêts, thermal anomalies are interpreted as natural hydrothermal systems (Kohl et al., 2000). Natural hot water circulates very slowly in large convection loops, (Guillou-frottier,et al., 2013). They move and are channeled into fracture / fault networks created by the successive fragile tectonic events of the Graben du Rhin. At Soultz-sous-Forêts, EGS developments consist of crystalline basement rock and extend over three reservoir levels: 2000 m TVD (upper reservoir), 3500 m TVD (intermediate reservoir), and 5000 m TVD (deep reservoir). In the intermediate and deep reservoirs, long-term productivity was demonstrated during nine periods in 1997, 2005 and between 2008 and 2013. The deepest reservoir was developed to ensure electricity production. Potential shallow reservoirs (sedimentary reservoir) from 900m to 1400 m TVD in the Triassic sediments and the altered top of the granitic basement have shown some occurrences of partial or total mud losses related to fracture zones in the sediments during drilling operations. (Meller, 2014; Vidal et al., 2015; Vidal et al., 2018; Genter et al. 2016; Heap et al., 2017).

Expected type of the reservoir and porosity/permeability *(fractured, porous, etc)*	Type A, with expected production flow rate from both wells together about 35 l/s for production temperature of 175 °C. (Genter et al.2012) Soultz-sous-Forêts reservoirs, located in altered fractures and in deep fracture granitic system, required enhanced geothermal system (EGS) technology. The granite reservoir rock has been characterized in terms of fracture density, structure, alteration, thermal conductivity, and permeability (e.g. Rummel 1992; Ledésert et al. 1993, 1999, 2010; Genter and Traineau 1996; Dezayes et al. 2000, 2010; Surma and Géraud 2003; Sausse et al. 2006, 2010; Bartier et al. 2008; Géraud et al. 2010; Vidal et al. 2017, 2018; Meller and Ledésert 2017). The in-situ rock mass strength and rock mass elastic modulus, estimates are provided in Villeneuve et al., 2018. Thermo-hydro-mechanical (THM) model of the Soultz-sous-Forêts geothermal reservoir (Magnenet et al., 2014). **Permeability** at the bore-hole scale is estimated from anomalies on temperature logs, flow logs, mud losses and gas occurrences (Sausse et al., 2006; Dezayes et al., 2010b; Genter et al., 2010; Magnenet et al., 2014,; Vidal et al., 2018). The statistical characterization of the fractures and faults was realized with the re-interpretation of the whole ultra-sonic borehall images (U.B.I.) database available at Soultz-sous-Forêts. 1800 fractures are determined along the three deep Soultz-sous-Forêts well paths, grouped into main conjugates fractures sets, showing a mean N-S orientation and a mean dip of 70°, consistent with the Oligocene N-S extension responsible of the formation of the French Rhine graben. (Massart, et al., 2010). Permeability is strongly related to natural fracture zones which present complex cluster indication with major permeable drains surrounded by damage zone. The dominating orientations of the nearly-vertical fractures in the granite are between N20W and N20E. In the well, the geometry of the fracture system is derived from borehole image logs (Dezayes et al., 2010). **Stress field:** The maximum horizontal principal stress, SHmax, is oriented N169°E ± 14°, (Valley and Evans, 2007; Evans 2005) **Fracture system** Fracture orientation in the Soultz-sous-Forêts wells based in cores and various borehole image logs. (Desayes et al., 2010). For the GPK3 and GPK4 wells, data are grouped in relation with the major petrographical sections (from Hooijkaas et al., 2006). **Porosity:** An analysis of the tracers indicates a connected porous volume in the range of 0.5 to 2.5 × 10^6 m^3, with a connected porosity of the order of 0.9 to 2.3% (Aquilina et al., 2004; Kushnir et al., 2018).
Mineralization *(type and enriched metals)*	Geochemical data of the geothermal fluids of the Upper Rhine Graben, relative to the deepest fluids circulating in the area, and within the granite basement are in the publications of Pauwels et al.1991 et 1993; Aquilina et al. 1997; Aquilina et al., 2000; Sanjuan et al., 2006; Sanjuan et al., 2010; Bucher et Stober, 2010; Stober, 2017; Sanjuan, 2014; Nitschke et al., 2014. Soultz-sous-Forêts host a high salinity Na-Cl brine (Sanjuan et al., 2010). The hottest brines are very enriched in K, Ca, SiO2, Li, Rb, Cs, As, Sr, Ba, Mn, Nd, U and in metals such as Zn, Pb, Cu, Co, Cd, Sb, they are depleted mainly in Mg, SO4 and B.(Sanjuan et al., 2016), (Boiron et al.2010). Deep native geothermal brine chemical composition from 1999 to 2005 samplings (µg/l) : Ni: 100, Cu: 45, Co: 50, Cr: 40, Cd : 10, Zn: 3000, Ag: <5, Ti: 200, Pb: 300 (Sanjuan et al. 2010) We noticed the studies regarding abiotic H2 generation from felsic rocks like the biotite-rich granite of the Upper Rhine Graben basement (Murray et al., 2018). Previous measurements of gases in the Soultz-sous-Forêts boreholes have reported values in a range of 0.25 – 46.3% vol. of H2 (Sanjuan et al., 2010; Sanjuan et al.,

	2016).

Production and injection wells	
Depth of potential wells (m)	The Soultz-sous-Forêts pilot project includes five deep wells intersecting the Triassic sediments and reaching the deep crystalline basement. Drilling of GK4 and GK3 at a depth of 5,000 m are spaced 650 m, GK3 and GK2 at 5,000 m are spaced 600 m, and GK2 and GK1 drilling at 3500 m depth are spaced 450 m. Well EPS1: 2200m Well GPK-1: 3590m, sub-vertical, top of the open-hole 2850 m in hydrothermally altered granite of the upper / intermediate reservoir injection well GPK-3: 5110 m, sub-vertical and highly deviated to the south, top of open-hole 4592 m deep granitic reservoir production wells GPK-2: 5060m, subvertical deviated to the NW, top of open-hole 4440m deep granitic reservoir and GPK-4: 5270m, sub-vertical and highly deviated to the south, top of open-hole 4767 m deep granitic reservoir (Vidal et al., 2018)

Electrolytic metal recovery and gas diffusion electro- precipitation	
Potential target metals to be recovered	Lithium :160 mg/l On an area of 15 km by 15 km centered on the Merkwiller-Pechelbronn field, the two reservoirs of the Muschelkalk and Buntsandstein should contain around 300 000 t of lithium metal (Pauwels et al., 1991). 85 -90% recovery is assumed in test for lithium carbonate battery grade, (Lebouil, 2018)

Power plant (heat exchanger)	
Local heat and electricity demand *(industrial, municipal, agricultural, etc.)*	Soultz-sous-Forêts is a rural French commune in the department of Bas-Rhin. It is located about 40 km north of Strasbourg. Population: 3100 inhabitants – Gaz consumption 6457MWh and electricity 10653MWh (https://www.fournisseur-energie.com/edf-gdf/bas-rhin/autres/) Bas-Rhin is a department of the historic Alsace region with a population of 1.12 million inhabitants Total energy consumption (in GWh, 2014 figure) 29633 GWh by sector: electricity 8142 GWh-natural gas 7095 GWh -petroleum products 10880 GWh -CMS17,4 GWh EnR 3000 GWh networks 399 GWh . The transport, manufacturing and residential sectors are the three main sectors

	consumers up to +/- 8000GWh. (http://www.atmo-grandest.eu/sites/prod/files/2017-12/ACC-EN-168_V20171127.pdf)

Salt gradient power generation	
Salinity of expected geothermal brine	The main geochemical characteristics of the native brines collected from all the geothermal wells penetrating the granite basement underlying the sedimentary cover in the Upper Rhine Graben shows that the salinity is very high (100g/l). The geothermal fluids have a multiple origin with mixing between primary brine formed by advanced evaporation of seawater and dilute meteoric water, plus contributions from halite dissolution following successive marine transgression-regression cycles from the Triassic to the Oligocene (Sanjuan et al., 2016). Fluid is of the Na-Cl type with high salinity values, TDS values ranging from 99 to 107 g/l with pH values close to 5 (Sanjuan et al., 2016, Sanjuan et al., 2014).
Fresh water supply from the surface *(water sources)*	The drinking water of Bas-Rhin is taken mainly from the alluvium of the Rhine and from the Vosges sandstone, where water is easily accessible and generally of good quality. Approximately 90 million m^3 are collected each year by communities including: 5% distributed to large consumers (consumption greater than 6,000 m3 / year), or about 4 million m^3 / year. 95% for domestic use, ie 224 liters / day / inhabitant. In order to meet this demand, communities exploit: 178 boreholes and 492 springs that draw water into the natural environment 217 treatment stations (disinfection, neutralization, ...) to distribute quality drinking water 376 tanks for storing water 6,400 km of network to distribute drinking water (13 meters of pipe per inhabitant) Regarding Soultz-sous-Forêts, the geothermal fluid pomped is fully reinjected through two injection drills.

2. CHPM operational characteristics - Environmental, social and political background

Requested information:

- ✓ toleration to gaseous and solids emissions, water and noise pollution,
- ✓ local competition to land and water availability
- ✓ public acceptance
- ✓ political support
- ✓ presence of supporting legislation, regulatory framework

Notes: all of above refers to the selected area and its surroundings.

Political support / legislation / regulatory framework/

National level: BRESS Bureau Ressources Énergétiques du Sous-Sol is part of the General Directorate for Energy and Climate (DGEC) which depend on the Minister of Ecological and Solidarity Transition. The main missions of the BRESS are to manage, develop and promote the exploitation of deep geothermal and French hydrocarbons. The BRESS validates (or not) the deep geothermal research permit and then can deliver a mining concession for a deep geothermal production if the resource is proven.
Regional level: DREAL Regional Directorate for Environment, Planning and Housing sets up public policies for the Ministry of Ecological and Solidarity Transition and the Ministry of Housing and Sustainable Housing. The DREAL validates the compliance of the drilling authorization and then performs monitoring and control of the drilling and testing operations.
Department level ("county"): Prefecture is a territorial administrative division that authorizes and regulates the work related to the deep geothermal project. The prefecture asks the local population its opinion on the project during a public inquiry.
City level: the mayor and city council, is a very important level since the project aims at responding to the energetic needs of the city. Its territorial integration is a key issue. The mayor can facilitate the social acceptability of the project by helping in its geographical location and by communicating with the concerned population.
The CODERST is the Departmental Council for Environment and Health and Technological Risks, and is composed of Representatives of the state services, local authorities, local associations, geothermal and drilling experts, sanitary experts and doctor. These members are appointed by the prefect.

Public acceptance
In general, people agree with the use of deep geothermal resources to generate electric power in all countries. However, the population may have questions or doubts about the production of electricity from geothermal resources. (Lopez-Sanchez et al., 2018).

Five kinds of impacts are identified and monitored from large to local scale influence: induced seismicity and surface deformation, surface water and shallow groundwater resources protection, neighborhood disturbance, such as vibrations or noise emissions, and evolution of the natural radioactivity resulting from the scaling. For example, slow deformation based on GPS measurements, ground leveling or satellite radar interferometry (InSar) are under development in the URG (Heimlich et al., 2015). Ground motion monitoring is also investigated with a permanent or temporary seismological network of sensors which measures induced seismic activity before drilling operations or during the operational phase of a geothermal plant. (Genter et al., 2016).

Soultz's operations generated 50,000 seismic shocks, including a dizain of level 2 on the Richter scale. Only one was close to level 3, but the subject is taken very seriously. Especially since the experience of Bâle stopped under the pressure of the public. European Commission has funded a project on controlling seismicity of deep geothermal energy.

Soultz-sous-Forêts has become one of the best-known geothermal sites and representative of the global geothermal industry with close collaboration with local elected officials, visits (around 1800 visitors per year between 2007 and 2014), conferences on scientific research conducted on the site, setting up an Internet site, very close collaboration with the global scientific community and numerous publications in international scientific journals (250 publications, more than 50 doctorates, 800 conferences) (Kempf, B., 2015; Lacirignola et al. 2013; Ravier et al., 2016)
But fears are still expressed regarding induced seismicity, radon emission, ground-table water pollution, guarantees of pipes sealing (Réponses du Groupe ES concernant certaines des observations consignées www.bas-rhin.gouv.fr)

3. Financial aspects

Requested information:

- ✓ list of potential local stakeholders (community, political, companies)

www.geothermie-soultz.fr
Joint venture: Groupe ES (40%), Roquette Frères (40%), Caisse des dépôts (20%) http://www.caissedesdepots.fr
Projet ECOGI (Exploitation de la Chaleur d'Origine Géothermale pour l'Industrie)
Groupe ES-Géothermie, (www.es-goupe.fr), a subsidiary of Électricité de Strasbourg (ÉS), assumes the role of an expert consultancy firm in deep geothermal energy. https://geothermie.es.fr
Électricité de Strasbourg Géothermie (ESG)
Fonroche Géothermie (www.fonroche-geothermie.com/),
Geolith, start-up, GeoLith is developing selective lithium extraction technology jpgibaud@geolith.fr
Geoforage www.geoforage.fr
CFG Services www.cfgservices.fr
Cryostar www.cryostar.com

EOST Université de Strasbourg www.eost.unistras.fr Labex G-eau-thermie profonde
IUT Robert Schuman iutrs.unistra.fr

DREAL alsace www.grand-est.developpement-durable.gouv.fr
National Research agency ANR www.agence-nationale-recherche.fr http://labex-geothermie.unistra.fr/
Regional and departmental council, Agency for the Environment and Energy Management (ADEME), www.ademe.fr/
AFPG (Association Française des Professionnels de la Géothermie) Afgp.asso.fr Correpondant régional Alsace jean-jacques.graff@es-groupe.fr
IGA www.geothermal-energy.org/explore/our-databases/conference-paper-database/
Pole Avenia (www.pole-avenia.com)
Eramet research Lithium extraction www.eramet.com
GEODEEP: http://geodeep.fr multi-disciplinary Cluster gathering large worldwide corporations and specialized companies in geothermal engineering and power plant EPC
BRGM Geothermie perspectives www.geothermie-perspectives.fr/article/acteurs-publics-professionnels

Europe (H2020) www.horizon2020.gouv.fr/ https://geothermie.es.fr/references/projet-h2020-meet/
GEIE EMC Exploitation minière de la chaleur
EGEC (European Geothermal Council), www.egec.org
IGA (International Geothermal Association) https://www.geothermal-energy.org
EGW 2018 : 6th European Geothermal Workshop : http://labex-geothermie.unistra.fr/spip.php?article16

List of references

Bibliography

Aichholzer C, Duringer P, Orciani S, Genter A., 2016; New stratigraphic interpretation of the Soultz-sous-Forêts 30-year-old geothermal wells calibrated on the recent one from Rittershoffen (Upper Rhine Graben, France). Geotherm Energy. 4:13.CrossRefGoogle Scholar

Aquilina L., Pauwels H., Genter A., Fouillac C., 1997, Water-rock interaction processes in the Triassic sandstone and the granitic basement of the Rhine Graben: geochemical investigation of a geothermal reservoir Geochim. Cosmochim. Acta, 60, pp. 4281-4295

Aquilina, L., de Dreuzy, J.R., Bour, O., Davy, P., 2004. Porosity and fluid velocities in the upper continental crust (2 to 4km) inferred from the injection tests at the Soultz-sous-Forêts geothermal site. Geochim. Cosmochim. Acta 68, 2405.

Baillieux, P., Schill, E., Edel, J., Mauri, G., 2013. Localization of temperature anomalies in the Upper Rhine Graben: Insights from geophysics and neotectonic activity. International Geology Review. 55. 1-19. 10.1080/00206814.2013.794914.

Bartier D., Ledésert B., Clauer N., Meunier A., Liewig N., Morvan G., Addad A.. 2008. Hydrothermal alteration of the Soultz-sous-Forêts granite (Hot Fractured Rock geothermal exchanger) into a tosudite and illite assemblage. Eur J Mineral. 20(1):131–42.CrossRefGoogle Scholar

Boiron, M-C., Cathelineau, M., Richard, A., 2010. Fluid Flows and Metal Deposition near Basement/Cover Unconformity: Lessons and Analogies from Pb-Zn-F-Ba Systems for the Understanding of Proterozoic U Deposits. Geofluids. 10. 270 - 292. 10.1111/j.1468-8123.2010.00289. x.

Bucher, k., Stober, I. (2010): Fluids in the upper continental crust. – Geofluids, 10, 241-253 (DOI 10.1111/j.1468-8123.2010.00279.x).

Dezayes C, Villemin T, Genter A, Traineau H, Angelier J. 1995; Analysis of fractures in boreholes of hot dry rock project at Soultz-sous-Forêts (Rhine Graben, France). J Sci Drill. 5(1):31–41.Google Scholar

Dezayes C, Villemin T, Pêcher A. 2000; Microfracture pattern compared to core-scale fractures in the borehole of Soultz-sous-Forêts granite, Rhine graben, France. J Struct Geol. 22(6):723–33.CrossRefGoogle Scholar

Dezayes C, Genter A, Valley B. 2010; Structure of the low permeable naturally fractured geothermal reservoir at Soultz. C R Geosci. 342(7):517–30.CrossRefGoogle Scholar

Evans K., 2005. Permeability creation and damage due to massive fluid injections into granite at 3.5 km at Soultz: Critical stress and fracture strength. J Geophys Res SolidEarth. https://doi.org/10.1029/2004JB003168.Google Scholar

Genter A, Traineau H. 1992; Borehole EPS-1, Alsace, France: preliminary geological results from granite core analyses for Hot Dry Rock research. Sci Drill. 3(5):205–14.Google Scholar

Genter A, Traineau H. 1996; Analysis of macroscopic fractures in granite in the HDR geothermal well EPS-1, Soultz-sous-Forêts, France. J Volcanol Geotherm Res. 72(1–2):121–41.CrossRefGoogle Scholar

Genter A, Castaing C, Dezayes C. 1997; Comparative analysis of direct (core) and indirect (borehole imaging tools) collection of fracture data in the Hot Dry Rock Soultz reservoir (France). J Geophys Res Solid Earth. 102(B7):15419–31.CrossRefGoogle Scholar

Genter,a., Baujard, C., Cuenot, N., Dezayes, C., Kohl, T., Masson, F., Sanjuan, B., Scheiber, J., Schill, E., Schmittbuhl, J., Vidal, J., 2016. Geology, Geophysics and Geochemistry in the Upper Rhine Graben: the frame for geothermal energy use European Geothermal Congress 2016 Strasbourg, France,

Géraud Y, Rosener M, Surma F, Place J, Le Garzic É, Diraison M. 2010; Physical properties of fault zones within a granite body: example of the Soultz-sous-Forêts geothermal site. C R Geosci. 342(7):566–74.CrossRefGoogle Scholar

Guillou-Frottier L, Carré C, Bourgine B, Bouchot V, Genter A. 2013; Structure of hydrothermal convection in the Upper Rhine Graben as inferred from corrected temperature data and basin-scale numerical models. J Volcanol Geotherm Res. 256:29–49.CrossRefGoogle Scholar

Heap MJ, Kushnir ARL, Gilg HA, Wadsworth FB, Reuschlé T, Baud P. 2017; Microstructural and petrophysical properties of the Permo-Triassic sandstones (Buntsandstein) from the Soultz-sous-Forêts geothermal site (France). Geotherm Energy. 5(1):26.CrossRefGoogle Scholar

Hooijkaas GR, Genter A, Dezayes C., 2006. Deep-seated geology of the granite intrusions at the Soultz EGS site based on data from 5 km-deep boreholes. Geothermics. 2006;35(5):484–506.

Kempf, B., 2015 Le retour d'expérience du projet de géothermie de SOULTZ dans le projet ECOGI pour l'acceptabilité publique , 4ème forum pour la géothermie dans le Rhin supérieur, Offenburg, www.trion-climate.net/html/seiten/output_adb_file.php?id=2500

Kushnir, A., Heap, M. J., Baud, P., Gilg, H., Reuschlé, T., Lerouge, C., Dezayes, C., Duringer, P., 2018. Characterizing the physical properties of rocks from the Paleozoic to Permo-Triassic transition in the Upper Rhine Graben. Geothermal Energy. 6. 10.1186/s40517-018-0103-6.

Kushnir ARL, Heap MJ, Baud P. 2018; Assessing the role of fractures on the permeability of the Permo-Triassic sandstones at the Soultz-sous-Forêts (France) geothermal site. Geothermics. 74:181–9.CrossRefGoogle Scholar

Lacirignola M., Blanc I., 2013 Environmental analysis of practical design options for enhanced geothermal systems (EGS) through life-cycle assessment Renew. Energy, 50, pp. 901-914,

Lebouil, S., 2018 PhD. ERAMET IDeas European Geothermal brines Lithium, Pole Avenia.

Ledésert B, Dubois J, Genter A, Meunier A. Fractal analysis of fractures applied to Soultz-sous-Forêts hot dry rock geothermal program. J Volcanol Geotherm Res. 1993;57(1–2):1–17.CrossRefGoogle Scholar

Ledésert B, Hebert R, Genter A, Bartier D, Clauer N, Grall C. Fractures, hydrothermal alterations and permeability in the Soultz enhanced geothermal system. C R Geosci. 2010;342(7):607–15.CrossRefGoogle Scholar

Lopez-Sanchez J., Blessent, D., Malo M., Raymond J., Dezayes C. , Goderniaux P., Daniele L., Le Borgne T., Ramirez E., Portela J.P., Hernandez J.E., 2018 Social acceptability of deep geothermal energy: overview of an

online survey from five European and American countries. EGW 2018 6° European Geothermal Workshop.
Magnenet V, Fond C, Genter A, Schmittbuhl J. 2014. Two-dimensional THM modelling of the large scale natural hydrothermal circulation at Soultz-sous-Forêts. Geotherm Energy. 2014;2(1):17.CrossRefGoogle Scholar
Massart, B., Paillet, M., Henrion, V., Sausse, J., Dezayes, C., 2010.Fracture Characterization and Stochastic Modeling of the Granitic Basement in the HDR Soultz Project (France). International Geothermal Association. World Geothermal Congress 2010, Bali, Indonesia. 7 p., 2010. <hal-00496923>
Meller C, 2014. Localization and characterization of hydrothermal alteration zones in a geothermal reservoir and their significance for rock mechanics. Dissetation Doktors Der Naturwissenschaften von der Fakultät für Bauingenieur-, Geo- und Umweltwissenschaften des Karlsruher Instituts für Technologie (KIT) genehmigte
Meller C, Ledésert B. Is there a link between mineralogy, petrophysics, and the hydraulic and seismic behaviours of the Soultz-sous-Forêts granite during stimulation? A review and reinterpretation of petro-hydromechanical data toward a better understanding of induced seismicity and fluid flow. J Geophys Res Solid Earth. 2017; 122:9755–74. https://doi.org/10.1002/2017JB014648.CrossRefGoogle Scholar
Murray, J., Clément, A., Fritz, B., Schmittbuhl, J., Bordmann, V., Fleury, J-M., 2018 Applying geochemical and reactive transport modeling for abiotic H2 generation in the Soultz-sous-Forêts geothermal system, Rhine graben, France, EGW 2018 6° European Geothermal Workshop
Nitschke F., Scheiber J., Kramar U. & Neumann T. 2014: Formation of alternating layered Ba-Sr-sulfate and Pb-sulfide scaling in the geothermal plant of Soultz-sous-Forêts. Neu. Jb. Mineral. Abh. 191, 2, 145—156.
Pauwels H., Lambert M., Genter A., 1991, Valorisation des fluides géothermaux contenant du lithium en vue d'une production Industrielle. BRGM/R 33547 les reserves en lithium des aquiferes du trias de la zone nord Alsace pp 33-67
Pauwels H, Fouillac C, Fouillac AM (1993) Chemistry and isotopes of deep geothermal saline fluids in the upper Rhine Graben: origin of compounds and water–rock interactions.Geochimica Cosmochimica Acta,57, 2737–49.
Ravier, G., Baujard, C., Dalmais, E., Maurer, V., Cuenot, N., 2016. Towards a comprehensive environmental monitoring of a geothermal power plant in the Rhine graben. *European Geothermal Congress*, Strasbourg, 19-23 September, Strasbourg, France.
Rummel F. Physical properties of the rock in the granitic section of borehole GPK1, Soultz-sous-Forêts. Geothermal Energy in Europe: the Soultz Hot Dry Rock Project; 1992. p. 199–216.Google Scholar
Rummel F, König E. Physical properties of core samples, borehole EPS1, Soultz-sous-Forêts: velocity, density- and magnetic susceptibility-logs, depth interval 933–2227 m, Yellow report 6, Ruhr-Universität, Bochum, unpublished report; 1991. p. 58.Google Scholar
Sanjuan B, Millot R, Dezayes C, Brach M. 2010. Main characteristics of the deep geothermal brine (5 km) at Soultz-sous-Forêts (France) determined using geochemical and tracer test data. CR Geosci. 2010, 342:546–59.
Sanjuan, B., Millot, R., Innocent, Ch., Dezayes, Ch., Scheiber, J., Brach, M., 2016. Major geochemical characteristics of geothermal brines from the Upper Rhine Graben granitic basement with constraints on temperature and circulation. *Chemical Geology*, Volume 428, 27-47.
Sausse J, Fourar M, Genter A. Permeability and alteration within the Soultz granite inferred from geophysical and flow log analysis. Geothermics. 2006;35(5):544–60.CrossRefGoogle Scholar
Sausse J, Dezayes C, Dorbath L, Genter A, Place J. 2010. 3D model of fracture zones at Soultz-sous-Forêts based on geological data, image logs, induced microseismicity and vertical seismic profiles. C R Geosci.;342(7):531–45.CrossRefGoogle Scholar
Stober et al., 2017 Deep Geothermal energy. Leibniz Institute for Applied Geophysics (LIAG)
Surma F, Geraud Y. 2003Porosity and thermal conductivity of the Soultz-sous-Forêts granite. In: Thermo-hydro-mechanical coupling in fractured rock. Basel: Birkhäuser;; p. 1125–36.Google Scholar
Traineau H, Genter A, Cautru JP, Fabriol H, Chevremont P. 1991Petrography of the granite massif from drill cutting analysis and well log interpretation in the geothermal HDR borehole GPK1 (Soultz, Alsace, France). Geotherm Sci Technol.;3(1–4):1–29.Google Scholar
Valley B, Evans KF. 2006. Strength and elastic properties of the Soultz granite. In: EHDRA scientific conference, Soultz-sous-Forêts, France; p. 15–6.Google Scholar
Valley B, Evans KF. 2010. Stress heterogeneity in the granite of the Soultz EGS reservoir inferred from analysis of wellbore failure. In: Proceedings of world geothermal congress 2010;.Google Scholar
Vidal J, Genter A, Schmittbuhl J. How, 2015. How permeable fractures in the Triassic sediments of Northern Alsace characterize the top of hydrothermal convective cells? Evidence from Soultz geothermal boreholes (France). Geotherm Energy.;3(1):8.CrossRefGoogle Scholar
Vidal, J., Genter, A., 2018 Overview of naturally permeable fractured reservoirs in the central and southern Upper Rhine Graben: Insights from geothermal wells
Villeneuve, M.C., Heap, M.J., Kushnir, A.R.L. et al. Geotherm Energy (2018) Estimating in situ rock mass strength and elastic modulus of granite from the Soultz-sous-Forêts geothermal reservoir (France)

https://doi.org/10.1186/s40517-018-0096-1

Annexes

Prospective CHPM areas

BDG – Berufsverband Deutscher Geowissenschaftler e.V. Germany							
Number	**Type of the selected area(s) (type "A" or type "B")**	**Depth(s) of the metal enrichment(s) (m)**	**Temperature /at these depths/ (°C)**	**Description of the metal enrichment(s)**			
				degree of the mineralization(s) (% or ppm)	***type of the mineralization(s)[1]***	***element(s)***	***area delineation(s)[2]***
1. Schriesheimer Gruben ***Grube Anna-Elisabeth***	A	*No high-quality information found during first survey on site selection. In-depth investigations required. These would include, e.g. inquiries to the geological service of the federal state.*	**100-130 (-160 °C)** [A)] 300 m: 25-30 [B)] 500 m: 30-35 [C)] 1.000 m: 55-60 [D)] 1.500 m: 70-75 [E)] **2.000 m: 90-95** [F)] **2.500 m: 115-120** [G)] **3.000 m: > 140** [I)]	Ag_{PbS}: > 1 %	porphyry	Pb, Cu, Ag	a: 49.47780 / 8.6736
2. Bleibach-Glottertaler Gruben ***Silberbergwerk Suggental***	A	*No high-quality information found during first survey on site selection. In-depth investigations required. These would include, e.g. inquiries to the geological service of the federal state.*	**100-130°C** [A)] 300 m: 20-25 [B)] 500 m: 20-25 [C)] 1.000 m: 50-55 [D)] 1.500 m: 60-65 [E)] 2.000 m: 70-75 [F)] **2.500 m: 115-120** [G)] **3.000 m: 140-150** [I)]	Ag_{PbS}: 0,02 % $Ag_{tennantite}$: 0,57 %	hydrothermal	Pb, Cu, Ag, (Au)	a: 48.0668 / 7.9347

[1] Like skarn, porphy, etc.

[2] There are 3 options for the indication of the area delineation: a. coordinates (latitude, longitude) of 1 point; b. coordinates (latitude, longitude) of 1 points and radius (m); c. coordinates (latitude, longitude) of more points.

3. Schwarzenberg	B	*No high-quality information found during first survey on site selection. In-depth investigations required. These would include, e.g. inquiries to the geological service of the federal state.*	**100-130** [A)]	Indicated resources: 28.000 t Sn, 23.000 t W, 95.000 t Zn & other	skarn / vein	U, W, Ag, Fe, Cu, Sn, Zn	a: 50.5069 / 12.7875
4. Revier Halsbrücke	B	*No high-quality information found during first survey on site selection. In-depth investigations required. These would include, e.g. inquiries to the geological service of the federal state.*	**100-130** [A)] 130 m: 57,5-60,0 W/m [H)]	Pb_{Ore}: 18,9 kg/t Zn_{Ore}: 8,9 kg/t	vein deposit (polymetallic)	Ag, Pb, Zn, Cu, Bi, Co, W, Ni, U, (Au)	b: 50.9602 / 13.2808 r = 10.000 m

[A)] Source: WMS LIAG GeotIS / KarteC („areas with petrothermal potential“)
[B)] Source: WMS LGRB-BW GEOTH / erd_z300 („underground temperature 300 m depth“)
[C)] Source: WMS LGRB-BW GEOTH / erd_z500 („underground temperature 500 m depth“)
[D)] Source: WMS LGRB-BW GEOTH / erd_z1000 („underground temperature 1.000 m depth“)
[E)] Source: WMS LGRB-BW GEOTH / erd_z1500 („underground temperature 1.500 m depth“)
[F)] Source: WMS LGRB-BW GEOTH / erd_z2000 („underground temperature 2.000 m depth“)
[G)] Source: WMS LGRB-BW GEOTH / erd_z2500 („underground temperature 2.500 m depth“)
[H)] Source: WMS LfULG-SA / 4 („Heat extraction capacity in W/m for 1.800 h - up to 130 m depth”)
[I)] Source: LIAG/Schellschmidt, 2003 (“Underground temperatures in Germany at 3.000 m depth”)

Outline of the methodical approach:

WP1 (“European data integration and evaluation”) ended on 31 October 2016. In this early phase of the project, the basis for the investigations now performed were created. It consisted mainly of information on geothermal sites and deep drilling in Germany.

At the beginning of WP 6 ("European Outlook"), the project status was evaluated and updated. All previous results have been **restructured, sorted and inventoried**. After that and after participation in the project workshop of the LTPs in April 2018, the **database from WP1 was expanded**. For this purpose, intensive research took place, which on the one hand concerned scientific publications and other publicly accessible specialist literature.

At the same time, the previous data basis was significantly expanded by **creating a project in the geoinformation system (GIS)**. The research of web map services, raster files (e.g. maps) and shapefiles formed a central part of the work done so far.

As a result, the GIS project consists of **405 different information sources/layers**, which are allocated to the EU, whole Germany, northern Germany and the individual federal states of Germany. The topics of the information are geology, (ore-) deposits and especially geothermal energy. The corresponding WMS servers are generally publicly accessible information. For a better overview and structuring, all layers in the GIS have been grouped into groups and categories and named according to an easy-to-understand scheme.

Overall, both geothermal potential maps and information on the deposits were now available. On that basis, the selection of possible CHPM locations was started in WP6. This was done by **graphically combining the aspects "geothermal energy" and "ore deposits"**, so that the amount of data was increasingly limited to relevant areas. Based on the criteria defined in advance (e.g. with regard to temperature and the desired metals and ore deposit types), only a few possible CHPM locations were finally found. On the one hand, for example, there is a lack of suitable deposits in northern Germany, although very good petrothermal conditions are to be expected there. On the other hand, there are areas in Germany with well-known, large ore deposits (e.g. Sauerland, Siegerland, Lahn-area), at which however the petrothermal conditions for a CHPM site are hopeless. From the remaining areas, the most suitable and probable were finally selected.

Subsequently, it is planned to conduct **further intensive research** within WP6. Not all information could yet be provided with sufficiently secure sources, so that no reliable statements were possible. The table on the first page still contains some open points which need clarification. Information regarding the metal content and the possible depth expansion of ore deposits is to be obtained via extended drilling data sets. For this step inquiries to the corresponding geological services of the federal states (Baden-Württemberg and Saxony) are possible.

Geothermal overwiew (Source: GeotIS[A)])

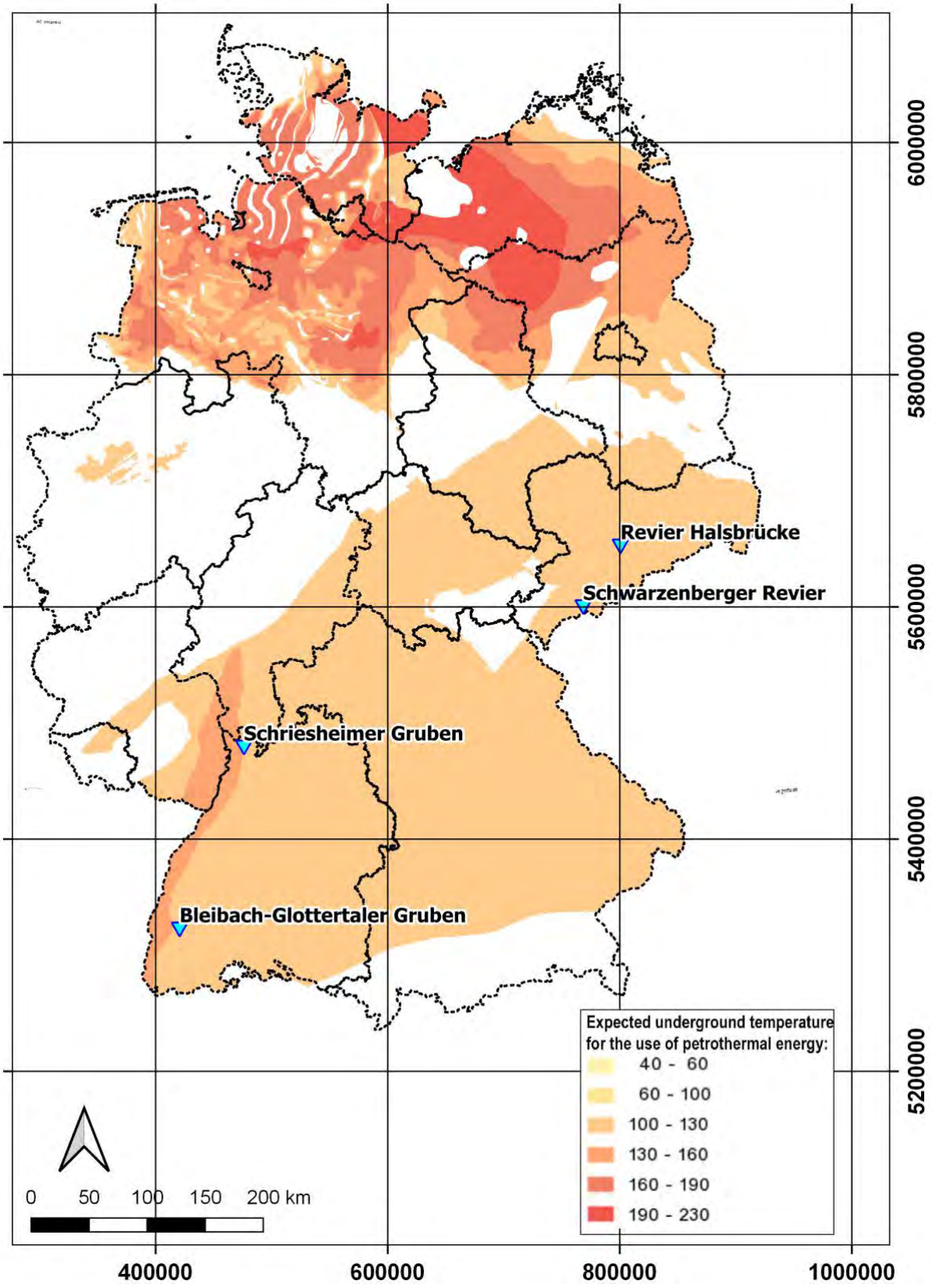

Evaluation of the basic characteristics of prospective CHPM areas

BDG

Germany

AREA 1 – Schriesheimer Gruben, Grube Anna-Elisabeth

1. **Geology of the prospective area**

Requested information on:

- ✓ local geology (in regional context)
- ✓ CHPM target formation
- ✓ list of available cross sections, geological maps, geochemical results, lithological information

Notes: briefly summarized, referenced to more detailed studies.

The Anna-Elisabeth mine is located near Schriesheim in the Rhine-Neckar metropolitan region, about 10 km north of the city of Heidelberg and about 20 km east of Mannheim. The associated deposit is located at the border of the Upper Rhine Graben to the Odenwald. The Odenwald is a predominantly crystalline low mountain range that produced gneisses, granitoids and migmatides through metamorphosis about 570 million years ago. The Odenwald belongs to the Variscan mountains. About 520 to 320 million years ago, several phases with intrusions and sedimentary deposits took place, so that greywacken, pelites, quartzites, limestones, gabbros, diorites, granites, gneiss and marble were formed. Another phase in the Triassic was marked by subsidence, in which the Germanic Basin was formed with mainly sedimentary rocks. These layers were later removed by erosion due to subsequent lifts down to the basement. About 60 to 50 million years ago, volcanoes formed along a fault zone that produced basalts. The origin of the Upper Rhine Graben is also to be assigned to the Eocene.

During the tectonic processes of Variscan orogenesis, fissures were repeatedly formed in the rock masses, into which partially metal-containing fluids could penetrate, crystallizing into matrix rocks. Furthermore, during the formation of the Upper Rhine Graben, barium-bearing ascending hydrothermal fluids arose, with partly metal-bearing and produced barite deposits throughout the Odenwald.

Mining on silver as well as iron and copper vitriol took place in the Schriesheim mine from 1473 at the latest (first mention). From 1894 onwards, the mining of lead, copper and sulphur ores continued, but after closure most of the mine openings and shafts were filled. The Anna-Elisabeth mine is now a visitor mine.
An overview of the mining history on site is given on the following page: https://www.bergwerk-schriesheim.de/Html_DE/Geschichte_alt.htm (Last access: 29.08.2018).

The following media can be obtained as WMS servers from „Landesamt für Geologie, Rohstoffe und Bergbau (LGRB) im Regierungspräsidium Freiburg“ (federal geological survey):
Mining:
http://services.lgrb-bw.de/index.phtml?SERVICE=WMS&REQUEST=GetCapabilities&VERSION=1.1.1&SERVICE_NAME=lgrb_bergbau(Last access: 29.08.2018).

Geological overview map 1:300.000:
http://services.lgrb-bw.de/index.phtml?SERVICE=WMS&REQUEST=GetCapabilities&VERSION=1.1.1&SERVICE_NAME=lgrb_uek350_geologie (Last access: 29.08.2018).
Geogenous basic concentrations (background values) in petrochemical units in Baden-Württemberg, 1:300.000
http://services.lgrb-bw.de/index.phtml?SERVICE=WMS&REQUEST=GetCapabilities&VERSION=1.1.1&SERVICE_NAME=lgrb_hw_geo (Last access: 29.08.2018).

2. Geophysics of the prospective area

Requested information:

- ✓ previous geophysical measurements (in CHPM relevance)
- ✓ geophysical results that can be used for locating/defining the deep metal enrichment
- ✓ list of available geophysical maps, cross sections, logs, other measurements

The Upper Rhine Graben has a lower gravity due to large fillings with light sediments of the Tertiary.

Heavy anomalies in the area of the Upper Rhine Graben were investigated by Plaumann:

1. Plaumann, S., 1991: Die Schwerekarte 1:500 000 der Bundesrepublik Deutschland (Bouguer-Anomalien), Blatt Mitte.- Geol. Jahrbuch, Reihe E Geophysik, 46: 3-16, 5 Abb, 1 Tab., 1 Taf.; Hannover
2. SPlaumann, S., 1995: Die Schwerekarte 1:500 000 der Bundesrepublik Deutschland (Bouguer-Anomalien), Blatt Süd.- Geol. Jahrbuch, Reihe E Geophysik, 53: 13 S., 4 Abb, 1 Taf.; Hannover

Further geophysical data sets or information could not be found in detail, but various non-public data sets are used in the 3D models of the Upper Rhine Graben described in the chapter below.

3. **Deep metal enrichment**

Requested information:

✓ (expected) metal enrichment based on available geophysical, geological and drill data, samples information, geochemistry

It is a barytspar mine in which various metal ores are associated with the surrounding barytes. The deposit is formed by a barite fluorite vein containing pyrite, lead and silver ores. It should be noted that the ore is sometimes found in a mixture of large gypsum crystals, limonite, melanterite, arsenate-rich ferrous sinter. Later veins of fluorite with a pitchblende and silver-cobalt ores are also found in the host rock, a granite. Iron and copper sulphides come from a four metre wide tectonically brecciated zone of granite.

Listing of some minerals:
Arsenopyrite, Barite, Chalcedony (Var.: Quartz, Mogánite), Chalcopyrite, Emplectite, Fluorite, Galenite, Gypsum, Hematite, Limonite, Markasite, Melanterite, Uraninite, Pyrite, Pyrolusite, Quartz, Safflorite, Solid Silver, Sphalerite

List of the most important rocks:
Biotite-Granite, Breccia, Mylonite

In the area of the deposit exists a mining licence for hydrocarbons owned by Rhein Petroleum GmbH Heidelberg. Northeast of the location an open-ended mining licence for tungsten has been granted to Bergbau Goslar GmbH, the field name is "Kirsten".

A drill location map of Germany is available from the Federal Insititute for Geosciences and Natural Resources: https://boreholemap.bgr.de/mapapps/resources/apps/boreholemap/index.html?lang=de (Last access: 29.08.2018).

The following media can be obtained as WMS servers from „Landesamt für Geologie, Rohstoffe und Bergbau (LGRB) im Regierungspräsidium Freiburg“ (federal geological survey):

1. exploratory database / drilling database:
http://services.lgrb-bw.de/index.phtml?SERVICE=WMS&REQUEST=GetCapabilities&VERSION=1.1.1&SERVICE_NAME=lgrb_adb (Last access: 29.08.2018)
2. Drill core storage:
http://services.lgrb-bw.de/index.phtml?SERVICE=WMS&REQUEST=GetCapabilities&VERSION=1.1.1&SERVICE_NAME=lgrb_bkl (Last access: 29.08.2018)
3. Commodity geological overviews, 1:350.000
http://services.lgrb-bw.de/index.phtml?SERVICE=WMS&REQUEST=GetCapabilities&VERSION=1.1.1&SERVICE_NAME=lgrb_uek350_rohstoffe (Last access: 29.08.2018)
4. Authorisation map: Concessions for mineral resources, 1:5.000 (last access on 29. August 2018)
http://services.lgrb-bw.de/index.phtml?SERVICE=WMS&REQUEST=GetCapabilities&VERSION=1.1.1&SERVICE_NAME=lgrb_berechtsamskarte (Last access: 29.08.2018)

4. **Integrated 3D- 4D model**

Requested information:

- ✓ existing 3D-4D models of the target area and the deep metal enrichment
- ✓ if no 3D-4D models exist, collect the following necessary data: geological setting, mineralization, fluid flow models, stress field determination

Notes: e.g. openly available datasets, models.

A large project of the GFZ Potsdam included a sedimentation basin modeling of the Upper Rhine Graben under geothermal aspects. It shows temperature distributions with their influencing heat transport processes (including groundwater movements) in the underground. As part of the EU-funded "IMAGE" project (Integrated Methods for Advanced Geothermal Exploration), a 3D structural model of the most important geological units of the entire lithosphere in the Upper Rhine Graben area is produced. All existing geophysical and geological information is taken into account.

An important publication in this context is:
Freymark, J. Sippel, M. Scheck-Wenderoth, K. Bär, M. Stiller, J.-H. Fritsche, M. Kracht, 2017: The deep thermal field of the Upper Rhine Graben. Tectonophysics 694, 114-129.

Neighboring 3D models are the 3D model of Hesse developed by the TU Darmstadt in cooperation with the Hessischen Landesamt für Umwelt und Geologie (HLUG) (federal geological survey), which shows the geometries of the most important sedimentary units in the subsoil of the northern part of the Upper Rhine Graben as well as the 3D model GeORG of the Landesamtes für Geologie, Rohstoffe und Bergbau (LGRB).

In addition, seismic reflection profiles (DEKORP projects) are integrated into the GFZ Potsdam project. However, the corresponding data records are not freely available.

Furthermore, the Landesamt für Geologie, Rohstoffe und Bergbau (LGRB) im Regierungspräsidium Freiburg (federal geological survey) offers a geological 3D state model 1:500,000 as WMS server. All relevant data, such as stratification of the individual horizons, thickness data, and also tectonic regions are indicated there: http://services.lgrb-bw.de/index.phtml?SERVICE=WMS&REQUEST=GetCapabilities&VERSION=1.1.1&SERVICE_NAME=lgrb_gu500 (Last access: 29.08.2018)

The ISONG-System of the Landesamts für Geologie, Rohstoffe und Bergbau (LGRB) im Regierungspräsidium Freiburg (federal geological survey) also contains information on faults. It is available as a WMS server at the following address:
http://services.lgrb-bw.de/index.phtml?SERVICE_NAME=lgrb_isong&REQUEST=GetCapabilities&SERVICE=WMS (Last access: 29.08.2018)

5. **EGS potential**

Requested information:

- ✓ EGS potential (heat & energy) of the area
- ✓ geothermal characteristics (temperature gradient, heat flux, stress field, water availability, EGS geology)
- ✓ presence/indication of deep fluids/brines, fracture system, crustal permeability

The Upper Rhine Graben has a special geothermal significance. Besides the Bavarian Molasse Basin and the North German Basin (in which no suitable mineralizations could be found), it offers high potential for deep hydrothermal geothermal energy. The geothermal anomaly results from the circulation of groundwater coming from the adjacent mountains and rising again in the center of the trench. As a result, convection and conduction overlap. The filling of the trench with tertiary sediments ensures good permeability of the rocks.

According to geothermie.de A technical geothermal potential of 186 TWh/a is stated for the entire Upper Rhine Graben. Temperatures between 80 °C and 160 °C can be reached at a depth of 2,000 m to 7,000 m. A known usable part of the aquifer, which is suitable for geothermal use, covers an area of 4,000 km².

Existing geothermal plants in the German part of the Upper Rhine Graben are located in Landau, Insheim and Rittershoffen.

A valid mining licence for geothermal energy exists for the nearby town of Weinheim. It contains as mineral resources: "geothermal energy and other energies arising in connection with its extraction (with restrictions regarding near-surface exploration)" and brine (registered as a mining licence for salt). A nearby indoor swimming pool (Miramar Freizeitzentrum Weinheim GmbH) also has a licence for the same mineral resources.

In the context of a research project, the Landesamt für Geologie, Rohstoffe und Bergbau (LGRB) im Regierungspräsidium Freiburg (federal geological survey) also investigated storage rocks for the climate-friendly geotechnical and energetic use of the deeper underground. The result was a general overview of the storage and barrier potential of geological horizons. Some of the results are freely accessible as WMS servers (see below).

The following media can be obtained as WMS servers from „Landesamt für Geologie, Rohstoffe und Bergbau (LGRB) im Regierungspräsidium Freiburg“:

1. Geothermal overview map, 1:1.000.000

http://services.lgrb-bw.de/index.phtml?SERVICE=WMS&REQUEST=GetCapabilities&VERSION=1.1.1&SERVICE_NAME=lgrb_uek350_geothermie (Last access: 29.08.2018)

2. Hydrogeological structure and aquifer properties of the unconsolidated rocks in the Upper Rhine Graben 1:50.000

http://services.lgrb-bw.de/index.phtml?SERVICE=WMS&REQUEST=GetCapabilities&VERSION=1.1.1&SERVICE_NAME=lgrb_p203 (Last access: 29.08.2018)

3. project storage inventory - part Upper Rhine Graben

http://services.lgrb-bw.de/index.phtml?SERVICE=WMS&REQUEST=GetCapabilities&VERSION=1.1.1&SERVICE_NAME=lgrb_p203 (Last access: 29.08.2018)

4. Surface-oriented Geothermal Energy Information System for Baden-Württemberg (ISONG)

http://services.lgrb-bw.de/index.phtml?SERVICE_NAME=lgrb_isong&REQUEST=GetCapabilities&SERVICE=WMS (Last access: 29.08.2018)

List of references

Amstutz, G.C., Meisl S., Nickel, E.,1975 Mineralien und Gesteine im Odenwald. Aufschluss, Sonderh. Nr.27, 344 pp.

Blömeke, C., 1893: Erzlagerstätten im Odenwald. Z. prakt. Geol.: 1, 346 – 347.

Boigk, H., Schöneich, H., 1970: Die Tiefenlage der Permbasis im nördlichen Teil des Oberrheingrabens. In: Illies, J. H. & Müller, S. (Hrsg.): Graben Problems: 45 - 55. Aufl. Suttgart, Schweizerbart.

Ditter, R., 2006: Die wirtschaftliche Entwicklung des Odenwaldes, insbesondere Kap. 3.3.1 Bergbau, Diplomica Verlag.

Fettel, M., 1975: Bergbaugeschichte des Odenwaldes. Der Aufschluss – Sonderb. 27 (Odenwald), 267–280.

Freymark, J., Sippel, J., Scheck-Wenderoth, M., Bär, K., Stiller, M., Fritsche, J.-H., Kracht, M., 2017: The deep thermal field of the Upper Rhine Graben. Tectonophysics 694, 114-129.

Geyer, M., 1999: Schaubergwerke in Baden-Württemberg (D). Schw. Strahler, Nr.9, 393-401.

Henningsen, D., Katzung, G., 2006: Einführung in die Geologie Deutschlands, 7. Aufl., Springer.

Köbrich, C., 1936: Hessische Erzvorkommen, Teil I: Die Nichteisenerze, Handbuch der hessischen Bodenschätze, Heft 3, Darmstadt.

Landesamt für Geologie, Rohstoffe und Bergbau (LGBR) Im Regierungspräsidium Freiburg, 2005: Geothermische Synthese/Bestandsaufnahme des Oberrheingrabens (1979/1981), Freiburg.

Levin, P., 1975: Über eine gangförmige Vererzung bei Schriesheim im südwestlichen Odenwald, in: Sonderband 27, 255–262, Der Aufschluss, Zeitschrift der Vereinigung der Mineralogie und Geologie.

Mößinger, F., 1955: Aus der Geschichte des Odenwälder Bergbaus, in: Der Aufschluss, Zeitschrift der Vereinigung der Mineralogie und Geologie, Sonderband 2, 75–81.

Münch, W., Sistenich, P., Bücker, C., Blanke, T., 2005: Möglichkeiten der geothermischen Stromerzeugung im Oberrheingraben, 10. Aufl., VGB PowerTech.

Neuhauser A., 2005: Exkursionsbericht Odenwald.

Nickel, E., Fettel, M.,1985: Odenwald. Sammlung geologischer Führer, 65, 2, 231 pp.

Plein, E., 1993: Voraussetzungen und Grenzen der Bildung von Kohlenwasserstoff-Lagerstätten im Oberrheingraben. Jber. Mitt. oberrhein. geol. Ver., N.F., Stuttgart.

Sauer, K., Munck, E. (ed.), Maget, P., Neeb, I., Tietze, R., 1979: Geothermische Synthese des Oberrheingrabens (Bestandsaufnahme). Veröff. des geologischen Landesamtes Baden-Württemberg, Strasbourg/Freiburg.

Slotta, R., 1986: Technische Denkmäler in der Bundesrepublik Deutschland. Hrsg.: Deutsches Bergbau Museum Bochum, 5, 1, 1108 pp.

Stein, E. 1985: Die magmatischen Gesteine des Bergsträßer Odenwaldes und ihre Platznahme-Geschichte.- Jber. Mitt. Oberrhein. Geol. Ver. N.F., 83, Stuttgart, 267-283.

Stober, I., Jodocy, M., 2009: Eigenschaften geothermischer Nutzhorizonte im baden-württembergischen und französischen Teil des Oberrheingrabens. In: Grundwasser, 14, 127–137.

Stober, I., Jodocy, M., Hintersberger, B., 2012: Vergleich von Durchlässigkeiten aus unterschiedlichen Verfahren - Am Beispiel des tief liegenden Oberen Muschelkalk-Aquifers im Oberrheingraben und westlichen Molassebecken. In: Z. geol. Wiss., 40, 1, 1-18.

Stober, I., Jodocy, M., Burisch, M., Person, P., 2013: Tiefenwässer im Oberen Muschelkalk-Aquifer des Oberrheingrabens und des Südwestdeutschen Molassebeckens. In: Grundwasser, 18, 2, 117-127.

Weiß, S., 1990: Mineralfundstellen Atlas, Deutschland West, Weise Verlag, München.

Annexes

Additional images can be generated using the specified WMS servers

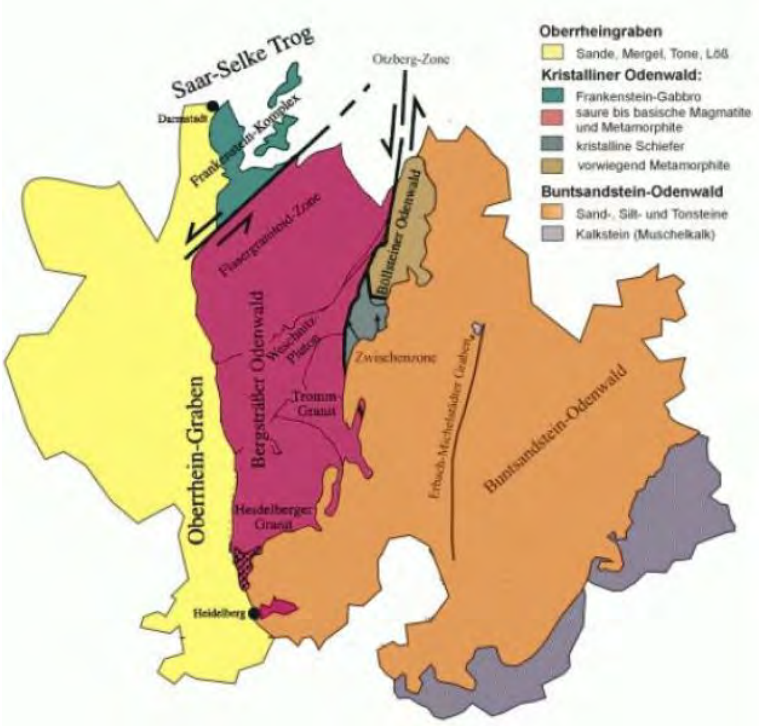

Fig. 1: Geological sketch of the Odenwald with an adjoining Upper Rhine Graben to the west. Source: www.geo-naturpark.de (Last access: 29.08.2018).

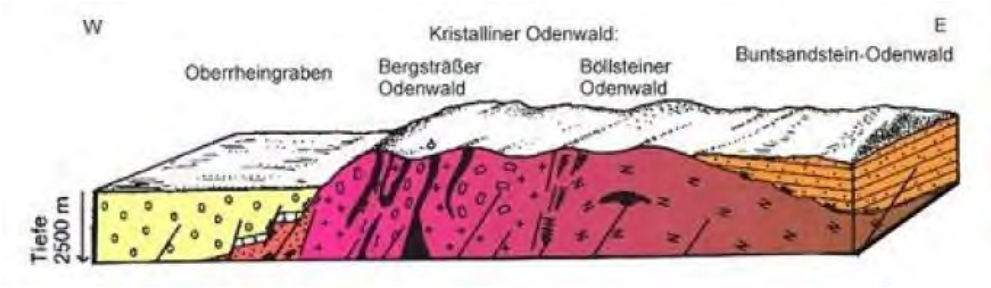

Fig. 2: Sketch of a geological profile through the Odenwald and the Upper Rhine Graben in a west-east direction. Source: www.geo-naturpark.de (Last access: 29.08.2018).

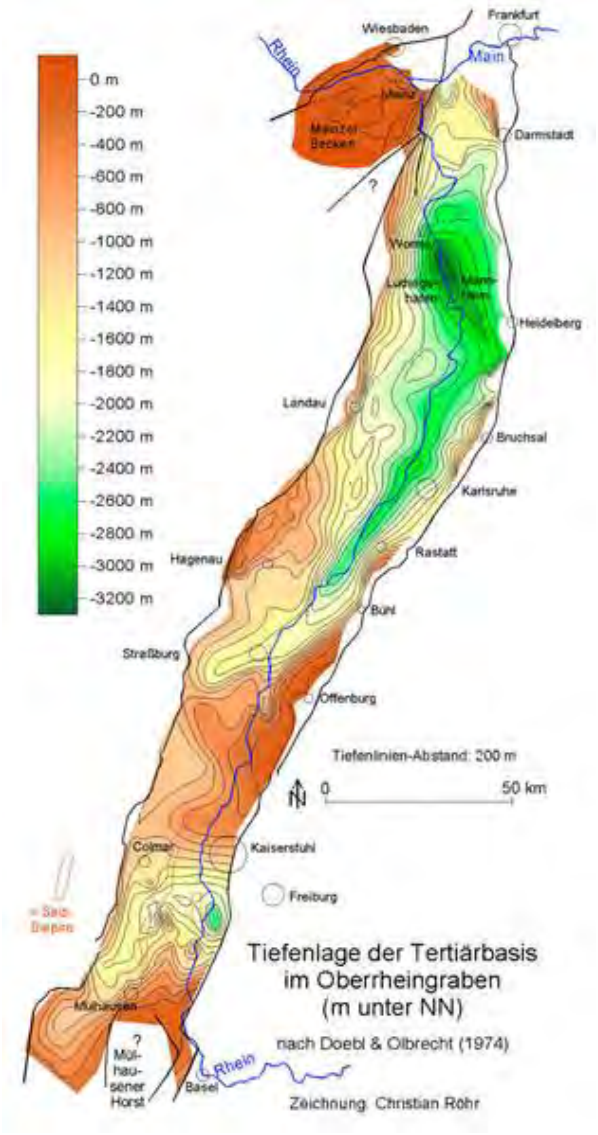

Fig. 3: Depth of the tertiary base in the Upper Rhine Graben (m below sea level). Source: geothermie.de

AREA 2 – Bleibach-Glottertaler Gruben – Silberbergwerk Suggental

1. **Geology of the prospective area**

Requested information on:

- ✓ local geology (in regional context)
- ✓ CHPM target formation
- ✓ list of available cross sections, geological maps, geochemical results, lithological information

Notes: briefly summarized, referenced to more detailed studies.

The Suggental ore deposit is located near the town of Waldkirch near Freiburg im Breisgau in the German federal state Baden-Württemberg. There, in the middle Black Forest, several silver deposits are known. The site is located on the western edge of the southern part of the Upper Rhine Graben, which is the main reason for the geothermal potential.

As the counterpart of the Vosges Mountains, the Black Forest is a trench shoulder of the Upper Rhine Graben. The active lifting of the mountains almost completely removed the Mesozoic cover strata. Below, the crystalline variscan bedrock is exposed. It consists of gneisses in which additional granites are embedded. The Black Forest is divided into numerous individual nappes by a complicated fault system. The thicknesses of the uplifted layers reach values of up to 1.5 km.

The western Upper Rhine Graben was formed by the Black Forest since the Eocene. It is widened by passive rifting, with two phases representing an expansion regime 50 to 20 million years ago and a strike-slip regime from 20 million years ago.

The Suggental deposit is located in the so-called Zentralschwarzwälder Gneismasse, with the parent rock being a hornblende paragneiss with an intermediate orthogneiss unit. The age of the rocks is estimated to be 325 million years. High tectonics have formed slabs, including the Kandel-Scholle to which the Suggental (Suggen valley) is connected. The valley itself follows a fault that is associated to the faultsystem of the Upper Rhine Graben. The southern boundary of the block is a fault that extends NW-SE and in which the ores of the deposit are embedded. It is of tertiary origin.

The Silberbergwerk Suggental (Suggental silver mine) is an exhibition mine nowadays. The information about the visitor mine provides some background information on the geology and mining history of the site: https://www.silberbergwerk-suggental.com/silberbergwerk-suggental/silberbergwerk-geologie/ (Last access: 29.08.2018)

Further information on geology can be found in the media of the Landesamt für Geologie, Rohstoffe und Bergbau (LGRB) im Regierungspräsidium Freiburg (federal geological survey), whose addresses are already given in the first report (Schriesheimer Gruben, Grube Anna-Elisabeth).

2. Geophysics of the prospective area

Requested information:

- ✓ previous geophysical measurements (in CHPM relevance)
- ✓ geophysical results that can be used for locating/defining the deep metal enrichment
- ✓ list of available geophysical maps, cross sections, logs, other measurements

According to the visitor mine operator, various geophysical measurements were carried out for the Silberbergwerk Suggental by EG Geosciences of Einstein-Gymnasium Kehl. The following methods were used: geomagnetics, geoelectrics, hammer strike seismics and gamma spectroscopy. Useable data were generated in the context of geoelectrics. However, the original data could not be retrieved. Further information can be found on the following website: http://kartan.de/index.php?id=geophysik (Last access: 29.08.2018).

Within the 3D models of the Upper Rhine Graben, geophysical data sets are available, but they are not publicly accessible and therefore not part of the investigation. The 3D models themselves are described in the respective chapter (see below) and contain, for example, seismic reflection profiles (from DEKORP projects).

Furthermore, the Upper Rhine Graben has recently been the subject of various investigations into gravity anomalies published by Plaumann:

3. Plaumann, S., 1991: Die Schwerekarte 1:500 000 der Bundesrepublik Deutschland (Bouguer-Anomalien), Blatt Mitte.- Geol. Jahrbuch, Reihe E Geophysik, 46: 3-16, 5 Abb, 1 Tab., 1 Taf.; Hannover
4. Plaumann, S., 1995: Die Schwerekarte 1:500 000 der Bundesrepublik Deutschland (Bouguer-Anomalien), Blatt Süd.- Geol. Jahrbuch, Reihe E Geophysik, 53: 13 S., 4 Abb, 1 Taf.; Hannover

3. Deep metal enrichment

Requested information:

✓ (expected) metal enrichment based on available geophysical, geological and drill data, samples information, geochemistry

As a hydrothermal deposit, Suggental contains several corridors. Remarkable is the formerly worth-mining St. Josephi-Gang, which is composed of quartz, baryte and sulfide ores. The baryte forms the much larger parts of the veins.

The ores were deposited following five tectonic phases during which they were exposed to strong cataclasic stress (formation of fault bursts). In a first stage hematite was deposited together with pyrite, marcasite, chalcopyrite, tetrahedrite and galenite. This was followed by fillings of the fault zones with barite, which were accompanied by deposits of mainly galena. Especially galena and pale ores such as tetrahedrite and tennantite characterized the economic mining viability by stored silver.

The hydrothermal formation produced a vein group with three different areas. They are called "Suggental A", "Suggental B" and "Suggental C" and show slightly different mineralizations. All in all, the three subgroups show a simultaneous strike. The focus of old mining activities was in the Suggental B area, where the St. Josephi Gang is also found.

Listing of some minerals: Solid silver, solid sulphur, arsenopyrite, bournonite, chalcopyrite, free mountainite, galenite, marcasite, polybasite, pyrargyrite, pyrite, sphalerite, tennantite, tetrahedrite, cuprite, goethtite, hematite, limonite, quartz, anchorite, dolomite, siderite, barytite

Silver-containing minerals of the deposit are pale ore and galena, but no real silver ores are present.

Listing of the most important rocks: Hornblende-Paragneis, Hornblende-Orthogneis

A distinction must be made between different vein types in the vicinity of the deposit:

Firstly, there are quartz antimony gravel veins, which partly carry gold and can also be found in the Suggental area. Pyrite, marcasite, and arsenopyrite can be found, on the one hand bound to chertlike quartz. In the Suggental area, massive barytes with various non-ferrous metal sulfides (e.g. spahlerite and galenite) are present. In the surroundings, Sb-Ag ores and rarely solid gold also appeared in this vein type.

The second mineralization type is also located around the Suggental mine. It essentially contains limonite and $FeCO_3$ with attached galenite and sphalerite. Further details can be found in Bliedtner & Martin (1986).

The thicknesses of the corridors are up to six meters.

For further information on possible drilling information, please refer to the database of the Federal Insititute for Geosciences and Natural Resources and the WMS servers of the Landesamt für Geologie, Rohstoffe und Bergbau (LGRB) im Regierungspräsidium Freiburg (federal geological survey). The addresses are given in the report for the first location (Schriesheimer Gruben, Grube Anna-Elisabeth).

4. **Integrated 3D- 4D model**

Requested information:

- ✓ existing 3D-4D models of the target area and the deep metal enrichment
- ✓ if no 3D-4D models exist, collect the following necessary data: geological setting, mineralization, fluid flow models, stress field determination

Notes: e.g. openly available datasets, models.

A connection of the deposit to the eastern main fault of the Upper Rhine Graben is assumed. The strike direction of most faults in the Suggen valley is 130°. Apart from the quartz veins, the average dip is 80° to the southwest. The quartz veins line orthogonally to the southeast. Movement indicators indicate oblique shifts, which are also directed dextrally. However, the vertical component clearly dominates.

For this deposit, the 3D model "GeORG" of the Landesamts für Geologie, Rohstoffe und Bergbau (federal geological survey), which is offered as a WMS server at a scale of 1:500,000, can be helpful. There you can find thickness specifications, tectonic information as well as position statements for individual horizons:
http://services.lgrb-bw.de/index.phtml?SERVICE=WMS&REQUEST=GetCapabilities&VERSION=1.1.1&SERVICE_NAME=lgrb_gu500 (Last access: 29.08.2018).

More detailed information on tectonics can also be found for this location in the ISONG system, which also provides data on faults in addition to information on the near-surface geothermal yield of the areas. As a WMS server, the service can be reached at the following address:
http://services.lgrb-bw.de/index.phtml?SERVICE_NAME=lgrb_isong&REQUEST=GetCapabilities&SERVICE=WMS (Last access: 29.08.2018).

For this location it is also referred to the 3D model of the GFZ Potsdam, which includes a sedimentation basin model of the Upper Rhine Graben. A three-dimensional structural model is provided for the investigation of the geothermal potential, including all geophysical and geological information. The results are data on temperature distributions and the associated heat transfer processes and groundwater movements.
Link to the research program of the GFZ: https://www.gfz-potsdam.de/en/section/basin-modeling/projects/thermal-modelling-upper-rhine-graben/ (Last access: 29.08.2018).

5. **EGS potential**

Requested information:

- ✓ EGS potential (heat & energy) of the area
- ✓ geothermal characteristics (temperature gradient, heat flux, stress field, water availability, EGS geology)
- ✓ presence/indication of deep fluids/brines, fracture system, crustal permeability

The geothermal overview map of Landesamts für Geologie, Rohstoffe und Bergbau (federal geological survey) contains temperature data for different depths from 300 m below ground to 2500 m below ground. Temperatures of up to 120 °C are expected in the Bleibach-Glottertaler mining area.
The corresponding geothermal overview map can be reached at the following address:
http://services.lgrb-bw.de/index.phtml?SERVICE=WMS&REQUEST=GetCapabilities&VERSION=1.1.1&SERVICE_NAME=lgrb_uek350_geothermie (Last access: 29.08.2018).

Near the deposit, a thermal well was drilled between 1964 and 1966. The examination of the drill cores showed that the drill was penetrating a mineralization containing pyrite and sphalerite.
In contrast to the Schriesheim mines (Anna-Elisabeth mine), no geothermal activities are known in the area around this site.

Nevertheless, this deposit is also located close to the Upper Rhine Graben, which offers enormous potential for geothermal use, as already described for the first site. Groundwater streams also run from the adjacent Black Forest into the centre of the trench, penetrating deep layers through the highly permeable sediments. There, the water is heated, and circulation cells are created. According to the ISONG system, some artesian groundwater conditions exist in the Suggental area.
The ISONG system can be accessed at the following WMS address:
http://services.lgrb-bw.de/index.phtml?SERVICE_NAME=lgrb_isong&REQUEST=GetCapabilities&SERVICE=WMS (Last access: 29.08.2018).

The technical geothermal potential of the Upper Rhine Graben of 186 TWh/a was already mentioned in the description of the first location. The size of the geothermally usable aquifer section accordingly covers an area of 4,000 km².

Ultimately, the site is close to the investigation area "Teilgebiet Süd", for which the hydrogeological construction and the aquifer properties of the unconsolidated rocks in the Upper Rhine Graben were investigated in more detail. The various hydrogeological thematic maps are available at the following address:
http://services.lgrb-bw.de/index.phtml?SERVICE=WMS&REQUEST=GetCapabilities&VERSION=1.1.1&SERVICE_NAME=lgrb_p203 (Last access: 29.08.2018).

List of references

Bliedtner, M., Martin, M., 1986: Erz- und Minerallagerstätten des Mittleren Schwarzwaldes. Geol. LA Baden-Württemb., Freiburg.

Goldenberg, G., 1993: Frühe Blei-, Silber- und Kupfergewinnung im Südschwarzwald. Hüttenplätze und Bergschmieden. In: H.Steuer/U.Zimmermann (eds.), Montanarchäologie in Europa. Archäologie und Geschichte.

Groschopf, R., Schreiner, A., 1996: Erläuterungen zum Blatt 7913 Freiburg i. Br.-NO, 2., ergänzte Aufl.- Geol. Kt. Baden-Württ. 1:25 000: 130 S., 6 Abb., 8 Tab., 4 Taf., 5 Beil.; Freiburg i. Br. (Geol. L.-Amt Baden-Württ.).

Haasis-Berner, A., 1999: Der Bergbau nördlich von Freiburg und die montane Wasserwirtschaft. Archäologische Informationen aus Baden-Württemberg, 41, 97-101.

Haasis-Berner, A., 2012: Besiedlung und Bergbau im Glottertal. In: Arbeitskreis Glottertäler Ortsgeschichte (eds.): Bergbau im Glottertal. Beiträge zur 900-Jahr-Feier der Gemeinde Glottertal, Freiburg, 9–102.

Henglein, M., 1924: Erz- und Minerallagerstätten des Schwarzwalds. Stuttgart, Schweizerbart, 196 pp.

Homann, W., 2000: Das Gold in der Sage des Suggentales bei Waldkirch (Südschwarzwald). Der Erzgräber, 14: 62-70, 5 Abb.; Oberwolfach.

Hoppe, A., Foellmer, A., Noeltner, T., 1993: Historischer Erzbergbau im Schwarzwald und Schwermetalle in Böden der Staufener Bucht. In: H.Steuer, Zimmermann U. (eds.), Montanarchäologie in Europa. Archäologie und Geschichte, 4, Sigmaringen, 249-254.

Huth, T., 2002: Erlebnis Geologie. Streifzüge über und unter Tage. Besucherbergwerke, Höhlen, Museen und Lehrpfade in Baden-Württemberg, Freiburg i. Br. (L.-Amt Geol. Rohst. Bergb. Baden-Württ.), 470 pp.

Kirchheimer, F., 1976: Bericht über Spuren römerzeitlichen Bergbaus in Baden-Württemberg, Der Aufschluss, 27, Heidelberg, 361-371.

Lieber, W., Leyerzapf, H., 1986: German silver. An historical persepctive on silver mining in Germany; Min. Rec., 17, 3-18.

Markl, G., Lorenz, S., 2004: Silber Kupfer Kobalt. Bergbau im Schwarzwald, Schriftenr. des Mineralienmuseums Oberwolfach, Bd. I.

Markl, G., Lorenz, S., 2004: Silber, Kupfer, Kobalt-Bergbau im Schwarzwald. Markstein Verlag, Filderstadt.

Metz, R., Richter, M., Schürenberg, H., 1957: Die Blei-Zink-Erzgänge des Schwarzwaldes, Beih. Geol. Jb., 29, Hannover.

Metz, R., 1961: Der frühe Bergbau im Suggental und der Urgraben am Kandel im Schwarzwald. Alemannisches Jahrbuch, 1961: 281–316, Freiburg.

Schneider, K., 1995: Bergbauspuren. In Das Glottertal. Geschichte und Erinnerungen. Beitrag zur 25-Jahr-Feier der Gesamtgemeinde Glottertal, Hoch, B. et al. (eds.), 176-181.

Steen, H., 1995: Bergbau und Mineralien aus dem Suggental bei Waldkirch im mittleren Schwarzwald. Erzgräber, 9 (2), 104-17.

Steen, H., 2004: Geschichte des modernen Bergbaus im Schwarzwald. 485 pp.

Steuer, H., 1991: Erzbergbau im Schwarzwald zur Salierzeit.

Steuer, H., Zettler, A., 1996: Der Bergbau und seine Bedeutung für Freiburg. In Haumann, H., Schadeck, H., Geschichte der Stadt Freiburg im Breisgau, Vol. 1: Von den Anfängen bis zum „Neuen Stadtrecht“ von 1529, Stuttgart.

Walenta, K., Schmeltzer, H., Sachs, P.M., 1989: Erzmikroskopische Untersuchungen an Erzen vom Hornbühl bei Suggental im Schwarzwald. Der Erzgräber, 3: 122-127, 5 Abb.; Oberwolfach.

Walenta, K., 1992: Die Mineralien des Schwarzwaldes, Weise Verlag, München.

Walenta, K., 1996: Neufunde aus dem Schwarzwald (6.F., 2T.). Lapis, 21 (12), 39 pp.

Werner, W., Dennert, V., 2004: mit Beiträgen v. Meyerdirks, U., Tegel, W., Lagerstätten und Bergbau im Schwarzwald. Ein Führer unter besonderer Berücksichtigung der für die Öffentlichkeit zugänglichen Bergwerke, 271 Abb., Freiburg (Landesamt f. Geol. Rohst. Bergb. Baden-Württ.), 334 pp.

Wölker, F., Leser, C., 1993: Bergbaugeschichte im Suggental. In: Bericht Bergbauforschungsgruppe Suggental.

Zimmermann, U., 1993: Untersuchungen zum frühen Bergbau im Südschwarzwald. In: Steuer, H., Zimmermann, U.(eds.): Montanarchäologie in Europa. Archäologie und Geschichte 4. Sigmaringen, 201-230.

Annexes

No annexes. Illustration

AREA 3 – Schwarzenberg

1. **Geology of the prospective area**

Requested information on:

- ✓ local geology (in regional context)
- ✓ CHPM target formation
- ✓ list of available cross sections, geological maps, geochemical results, lithological information

Notes: briefly summarized, referenced to more detailed studies.

The Schwarzenberg site is located 10 km south of the town of Aue in the Western Erzgebirge (engl: Ore Mountains) and 10 km from the Czech border.

The Erzgebirge is part of the Variscan geosynclinale, which existed in the region as an ENE-WSW axis for a maximum of 400 million years. The several kilometers thick marine sediments were unfolded to the Variscan Mountains at the end of the Devonian and in the Carboniferous. Of particular importance for the Erzgebirge are the penetrated plutons and the strong metamorphosis grades (various gneisses). The rocks are located in the saxo-thuringic zone of the Variszikum, the given location more precisely in the so-called "Fichtelgebirgs-Erzgebirgs-Antiklinalzone".

Subsequent erosion of the sediment layer in the Permian exposed some of the structures formed during orogenesis, with most of them being eroded by the end of the Tertiary period. The boundaries of the Erzgebirge were also established in the Tertiary. They represent the Egertalgraben and the Bohemian Basin. They were caused by various faults with NE SW strokes. One of these supraregional faults is the Gera Jáchymov fault zone. The subsequent uplift was accompanied by basaltic volcanism and lasted for about 30 million years.

The most dominant rocks of the Erzgebirge are various shales, such as mica schist and quartzite schist, amphibolites, muscovite gneiss as well as marbles and finally Skarne (important for the occurring deposits).

The Schwarzenberg Kuppel (dome) has a complicated geological history with many tectonic and mineralogic phases and thus also complicated deposit conditions. It is dominated by gneiss, quartzites, crystalline shales, as well as the carbonate rocks with different carnations. The surrounding rocks have been contact-metamorphically overprinted due to the various granite intrusions. The area is known for its intensive mining of various ores. Especially silver, iron, copper, tin and zinc were mined in the past.

A geological overview map can be obtained as a WMS server via the Geoportal Sachsen: https://geoportal.umwelt.sachsen.de/arcgis/services/geologie/geologie/MapServer/WMSServer?request=GetCapabilities&service=WMS&version=1.3.0 (Last access: 29.08.2018)

2. Geophysics of the prospective area

Requested information:

- ✓ previous geophysical measurements (in CHPM relevance)
- ✓ geophysical results that can be used for locating/defining the deep metal enrichment
- ✓ list of available geophysical maps, cross sections, logs, other measurements

For this location, extensive geophysical investigations have been carried out, which were already aiming at its potential utilization for deep geothermal energy. Detailed information can be found in "Tiefengeothermie Sachsen", available at: https://publikationen.sachsen.de/bdb/artikel/15145 (Last access: 29.08.2018)

Summary of the main findings:

- Seismic profiles are not available for the study area.
- SDAG Wismut measured profiles in the course of the former uranium mining around the Schwarzenfeld site. They are NE-SW oriented and showed tectonic units, which are separated from each other by faults.
- The Bouger Heaviness Map shows a minimum of gravity in the granite zone near Schwarzenberg. As a result, granites and superimposed metamorphites characterize gravimetry. Gravimetric field fluctuations due to surface-near granites and regional fault structures can be seen even more clearly in transformation maps according to GRIFFIN (1949).
- Density measurements show values of 2.64 x 10^3 kg/m^3 for granites, 2.76 x 10^3 kg/m^3 for phyllites and 2.80 x 10^3 kg/m^3 for contact metamorphic phyllite/ mica schist.
- Geomagnetics do not show the granite areas. However, geomagnetic measurements in the Schwarzenberg area show magnetite-bearing rocks (magnetite carts, magnetite quartzites).

3. **Deep metal enrichment**

Requested information:

✓ (expected) metal enrichment based on available geophysical, geological and drill data, samples information, geochemistry

The Schwarzenberg site is located in one of many mining areas of the Erzgebirge with different deposits. It is the westernmost district of the mining region Erzgebirge / Krušnohoří.
In the closer surrounding of the site there are shales of crystalline rocks (mica slate) as well as quartzites and amphibolites. The granites, in contrast, have a sub-permian to Upper Carboniferous age. Skarn metacarbonate rock horizons are also present, which dip to SO at approx. 10 - 30° with a NE SW strike.

During the orogenesis process, the Eibenstock granite was also created, bringing siliceous, metal-containing hydrothermal fluids to the described site. These are the existing skarn deposits, although a distinction between pre- and synvariscan is difficult. Through this, iron and non-ferrous metals were injected in the surrounding carbonatic rocks. Former marbles were transformed to areas of magnetite, pyrite, arsenopyrite, chalcopyrite, sphalerite, and galena. Several ore types are available in the area of the site.
The skarn ores appear as ore bodies with lenticular to layer shapes. In contrast, "Greisen-" and "Zersatzerze" are often discordant and irregular. The skarn ores have a complex and very variable mineral composition and are spatially linked to lithological and tectonic features.
Locally, silver, tin and cobalt minerals are enriched. Overall, the intensity of the skarn overmining fluctuates, making it difficult to predict the grades of the deposits in general.
A study by the Landesamts für Umwelt, Landwirtschaft und Geologie (federal geological survey) shows indicated resources of 28,000 t (tin), 23,000 t (bismuth), 95,000 t (zinc) among others.

For reasons of environmental protection, numerous soil samples of the organic layer and of the upper and lower soil were analyzed for a large number of trace elements in the study region. This can be used as an indication of deep underground conditions and is provided by the Sächsische Landesamt für Umwelt, Landwirtschaft und Geologie (federal geological survey) at the following address:
https://www.umwelt.sachsen.de/umwelt/boden/19200.htm (Last access: 29.08.2018)

In addition, the Geoportal Sachsen provides further sources as WMS servers:

1. near-surface commodities

https://geoportal.umwelt.sachsen.de/arcgis/services/geologie/rohstoffe_wms/MapServer/WMSServer?request=GetCapabilities&service=WMS&version=1.3.0 (Last access: 29.08.2018)

2. Geochemical overview map

https://geoportal.umwelt.sachsen.de/arcgis/services/boden/gcbuek400/MapServer/WMSServer?request=GetCapabilities&service=WMS&version=1.3.0 (Last access: 29.08.2018)

3. geological explorations/drilled holes

https://geoportal.umwelt.sachsen.de/arcgis/services/geologie/bohrungen/MapServer/WMSServer?request=GetCapabilities&service=WMS&version=1.3.0 (Last access: 29.08.2018)

4. Integrated 3D- 4D model

Requested information:

- ✓ existing 3D-4D models of the target area and the deep metal enrichment
- ✓ if no 3D-4D models exist, collect the following necessary data: geological setting, mineralization, fluid flow models, stress field determination

Notes: e.g. openly available datasets, models.

Currently, the Sächsische Landesamt für Umwelt, Landwirtschaft und Geologie (federal geological survey) is developing an extensive 3D underground model. The underground is visualized in its full extent and a comprehensive data basis for geoscientific applications is generated. The entire area is divided into different model units, reflecting the geologically highly heterogeneous underground.
Further information on the project and the corresponding contact person can be found at: http://www.geologie.sachsen.de/geologisches-3d-untergrundmodell-fuer-sachsen-13660.html (Last access: 29.08.2018)

There are also 3D models of the federal geological survey that are not publicly available.

In 2009/2010, the Sächsische Landesamt für Umwelt, Landwirtschaft und Geologie (federal geological survey) also investigated three preferential areas for the potential construction of a petrothermal geothermal energy plant in Saxony. 3D models were used, but they are also not publicly available. However, a project description can be found at: http://www.geologie.sachsen.de/tiefe-geothermie-in-sachsen-12832.html (Last access: 29.08.2018)

5. **EGS potential**

Requested information:

- ✓ EGS potential (heat & energy) of the area
- ✓ geothermal characteristics (temperature gradient, heat flux, stress field, water availability, EGS geology)
- ✓ presence/indication of deep fluids/brines, fracture system, crustal permeability

According to Sächsischen Landesamt für Umwelt, Landwirtschaft und Geologie (federal geological survey), there is a potential for petrothermal geothermal energy in Saxony.
An analysis commissioned by the State Office forms the basis for this, which also covered the deep geothermal utilization possibilities of the "Schwarzenberg" site. Thermal, geological and petrophysical data were processed and converted into three-dimensional models. The study was extended by investigations of TU Bergakademie Freiberg and resulted in a framework concept for deep geothermal energy in Saxony.
In the corresponding final report, Schwarzenberg is located in a preferred area for potentially deep geothermal use. It is remarkable that the site Schwarzenberg around the investigation area "Aue-Schneeberg" has the best conditions for the construction of a geothermal power plant, according to the investigations.

Important findings are:

- The temperature measurements show an increase in the geothermal gradient below the 990 m level of a mine near the study area.
- For the range from -540 to -990 m gradients of 3.73 - 3.36 °C/100m are given, for deeper levels the value is 3.29 or 3.15 °C/100m. An underground well (No. 346A) shows a temperature of 81 °C at a depth of 2365 m below ground level. A gradient of 3.1 °C/100m can also be derived from this. An extrapolation in depths of 4.5 km or 5 km ultimately leads to predicted temperatures of 147-162 °C.
- It is concluded that an electricity production is possible with drillings to 5 km depth in the area at Schwarzenberg.

Further information can be found at:
http://www.geologie.sachsen.de/tiefe-geothermie-in-sachsen-12832.html (Last access: 29.08.2018)
The final report with detailed descriptions of the results of the investigation is available at:
https://publikationen.sachsen.de/bdb/artikel/15145 (Last access: 29.08.2018)

As a supplement, the Sächsisches Landesamt für Umwelt, Landwirtschaft und Geologie (federal geological survey) provides the following sources of information as a WMS server:

1. Hydrogeological overview:

https://geoportal.umwelt.sachsen.de/arcgis/services/geologie/huek/MapServer/WMSServer?request=GetCapabilities&service=WMS&version=1.3.0 (Last access: 29.08.2018)

2. Groundwater dynamics

https://geoportal.umwelt.sachsen.de/arcgis/services/wasser/grundwasserdynamik/MapServer/WMSServer?request=GetCapabilities&service=WMS (Last access: 29.08.2018)

3. Geothermal overview:

https://geoportal.umwelt.sachsen.de/arcgis/services/boden/gcbuek400/MapServer/WMSServer?request=GetCapabilities&service=WMS&version=1.3.0 (Last access: 29.08.2018)

4. Geothermal map:
https://geoportal.umwelt.sachsen.de/arcgis/services/geologie/gtk50/MapServer/WMSServer?request=GetCapabilities&service=WMS&version=1.3.0 (Last access: 29.08.2018)

5. Geothermal extraction capacity
https://www.umwelt.sachsen.de/umwelt/infosysteme/wms/services/geologie/gtk50_utm?REQUEST=GetCapabilities&SERVICE=WMS (Last access: 29.08.2018)

List of references

Baumann, L., 1967: Zur Frage der varistischen und postvaristischen Mineralisation im sächsischen Erzgebirge.- FFH C 209, Leipzig, 15-38.

Baumann, L., 1968: Die Mineralparagenesen des Erzgebirges - Charakteristik und Genese.- FFH C 230, Leipzig.

Baumann, L., 1994. Klassische Erzlagerstätten des Erzgebirges. Aufschluss, 45, 2, 56-66.

Baumann, L., Kuschka, E., Seifert, T., 2000: Lagerstätten des Erzgebirges. Enke Stuttgart.

Beck, R., 1903: Über die Erzlager der Umgebung von Schwarzenberg im Erzgebirge, T.I. Jb. für das Berg- und Hüttenwesen im Königreiche Sachsen, Freiberg.

Beck, R., 1904: Über die Erzlager der Umgebung von Schwarzenberg im Erzgebirge, T.II. Jb. für das Berg- und Hüttenwesen im Königreiche Sachsen, Freiberg, A56-A96.

Haake, R., 1972: Zur Altersstellung granitoider Gesteine im Erzgebirge. Geologie, 21, 6, 641-76.

Haake, R., Hofmann, F., 1991: Die Mineralien der Skarn-Lagerstätte von Pöhla im Erzgebirge. Mineralienwelt, 2, 3, 26-41.

Haake, R., 1970: Über die Skarnlager bei Schwarzenberg/Erzgeb. Fundgrube 7 (1/2), 6-11.

Hösel, G., 1968: Die Skarnlager im Raum Schwarzenberg (Erzgebirge). Ber.dtsch.Ges.geol.Wiss., B, 13/4, Berlin, 469-77.

Mädler, F. 1992: Das Bergbaurevier von Breitenbrunn und Antonsthal im oberen Erzgebirge, Lapis, 17, 10, 13-24.

Martin, M., 1990: Zum Emplektit von Schwarzenberg. Fundgrube 26 (1), 17-22.

Massone, H.J., Bautsch, H.J., 2004: Ultrahigh and high pressure rocks of Saxonia. 32.Int. geol. congress. Vol.2, B21. Florence Italy 20.-28.8.2004.

Neese, T., 2015: Relikte Prähistorischer Goldseifen in Sachsen. Aufschluss, 66, 6, 305-19.

Pälchen, W., Walter, H., 2008: Geologie von Sachsen. Schweitzerbart, Stuttgart.

Pitsch, K., 1956: Abriß der Geologie von Sachsen. Berlin.

Reh, H., 1932: Beitrag zur Kenntnis der Erzgebirgischen Erzlager.- N. Jb. Min. etc., 65, A, Stuttgart, 1-86.

Sebastian, U., 1995: Die Strukturentwicklung des spätorogenen Erzgebirgsaufstiegs in der Flöha-Zone – Ein weiterer Beitrag zur postkollisionalen Extension am Nordrand der Böhmischen Masse, Freib. Forsch-H C 461

Sebastian, U., 2013: Geologie des Erzgebirges. Springer-Verlag, Berlin Heidelberg.

Seifert, T., 1985: Beitrag zur Typisierung von Sn-Lagerstätten im Erzgebirge. Bergakademie Freiberg, Sektion Geowissenschaften. 162 pp.

Seifert, T., 1999: Relationship between late Variscan lamprophyres and hydrothermal vein mineralization in the Erzgebirge. In Stanley, C.J. u.a. (eds.), Mineral Deposits: Processes to Processing. Vol.1. Proc. 5th biennial SGA meeting and the 10th quadr. IAGOD symposium. London 22-25 Aug.1999. Balkema, 429-32.

Tetzner, A., Edelmann, F., 1927: Neue sächsische Mineralvorkommen (Erzgänge zu Frenzel's "Mineralogisches Lexicon für das Königreich Sachsen"). Jahrb. Berg- und Hüttenwesen 1926 u. 1927, Freiberg.

Tichomirowa, M., 2003: Die Gneise des Erzgebirges – hochmetamorphe Äquivalente von neoproterozoisch-frühpaläozoischen Grauwacken und Granitoiden der Cadomiden, Freib Forsch-H C495.

Vollstädt, H., Weiß, S., 1991: Mineralfundstellen Sächisches Erzgebirge.- Weise Verlag, München.

Wagenbreth, O., Wächtler, E., 1990: Bergbau im Erzgebirge – Technische Denkmale und Geschichte. Deutscher Verlag für Grundstoffindustrie, Leipzig.
Woidtke, S., 2006: Der Berg ist frei - Bergbau im Erzgebirge, 4, 263-369.

Annexes

Many other figures and tables for the location Schwarzenberg are contained in the publication "Tiefengeothermie Sachsen" of Sächsisches Landesamt für Umwelt, Landwirtschaft und Geologie (federal geological survey). This is attainable under: https://publikationen.sachsen.de/bdb/artikel/1514 (Last access: 29.08.2018)

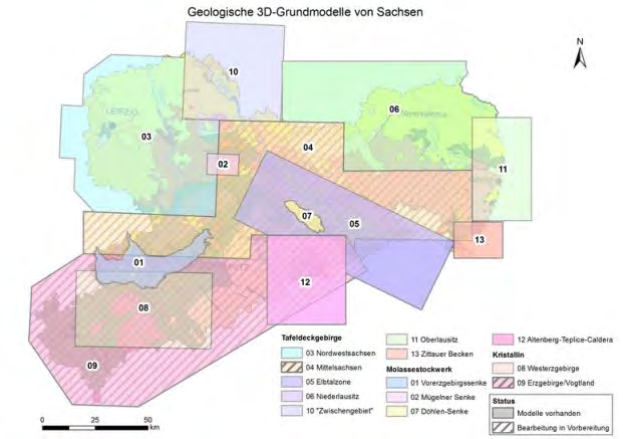

Fig. 4: Areas with 3D models of the state of Saxony. Source: http://www.geologie.sachsen.de/geologisches-3d-untergrundmodell-fuer-sachsen-13660.html (Last access: 29.08.2018).

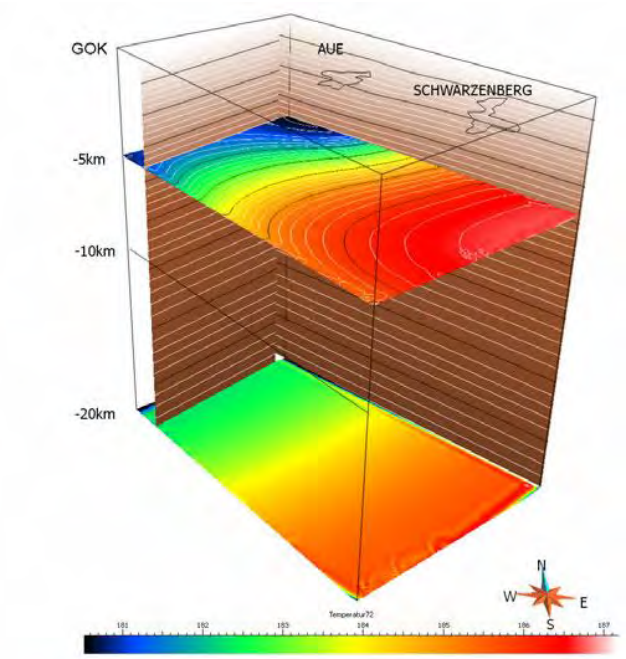

Fig. 5: 3D temperature model for the preferential area of Aue with horizontal sectional plane at a depth of 5 km below ground surface. Source: „Tiefengeothermie Sachsen“, Source: https://publikationen.sachsen.de/bdb/artikel/15145 (Last access: 29.08.2018).

AREA 4 – Revier Halsbrücke

1. **Geology of the prospective area**

Requested information on:

- ✓ local geology (in regional context)
- ✓ CHPM target formation
- ✓ list of available cross sections, geological maps, geochemical results, lithological information

Notes: briefly summarized, referenced to more detailed studies.

As part of the Freiberg Gangerz deposit, the Halsbrücke site in central Saxony is located at an altitude of about 350 to 400 m above sea level. The distance to the nearest district town Freiberg is only a few kilometres south of the deposit. Dresden is located about 30 km northwest of Halsbrücke.
The Freiberger Gangerz deposit has a total extent of 20 km (N-S) and 10 km (E-W). Halsbrücke is one of the core areas of the many-zoned deposit.
It is located in the north of the Erzgebirgsscholle, which merges into the hilly region of Central Saxony at a short distance.

Like the Schwarzenberg site, the investigation area around Halsbrücke is still in the characteristic area of the Erzgebirge. The regional geological conditions are therefore very similar - the terrain is also situated in the saxo-thuringic zone of the Variszikum.
As part of the ENE-WSW extending variscan geosynclinal, marine sediments of several kilometres thickness were folded up from the end of Devonian to the Carboniferous to the Variscan Mountains in the surrounding region. Plutonic intrusions, which together with strong metamorphosis processes often produced gneisses, are significant.
Various supra-regional faults led to a natural confinement of the Erzgebirge, as this has been uplifted as a block and tilted to the northwest.

The area around the site consists mainly of orthoclase biotite gneisses with a grey color. In the northern part of the Freiberg deposit there are also gabbro and serpentinite, while to the west there are mica schist containing coal beds and in the south there is a red gneiss dome.

The hydrothermal ore deposit has three centers with dense veins located in the reservoir area. The Halsbrücke area is one of these centers, where mainly lead and silver ores occur. In addition, lamprophyre and rhyolite are mentioned as secondary rocks, while the veins consist mainly of barite and fluorite.

A geological overview map can be obtained as a WMS server via the Geoportal Sachsen:
https://geoportal.umwelt.sachsen.de/arcgis/services/geologie/geologie/MapServer/WMSServer?request=GetCapabilities&service=WMS&version=1.3.0 (Last access: 29.08.2018)

2. Geophysics of the prospective area

Requested information:

- ✓ previous geophysical measurements (in CHPM relevance)
- ✓ geophysical results that can be used for locating/defining the deep metal enrichment
- ✓ list of available geophysical maps, cross sections, logs, other measurements

As for the Schwarzenberg site, various geophysical investigations were also carried out in the area of Halsbrücke, ultimately focusing on the topic of deep geothermal energy.

Important results of the geophysical data evaluation are:

- Data from the geomagnetic surveys show a stable sensitivity in the area around the site; minor deviations are caused by surrounding porphyry veins, which cause lower values.
- Regarding seismic measurements, deep profiles with the names "FB01V" and "EV05" are located in the area of the Freiberg deposit. They extend from NW to SE and show tectonic structures down to a depth of about 30 km. From these results, different calculations for the underlying pluton depths of six to ten kilometers were derived.
- The gravimetry surveys show the nearby granites with an average density of 2.64 x 10^3 kg/m^3. However, an upper surface of the Freiberg pluton cannot be detected. Grey gneiss from Freiberg has an average density of 2.72 x 10^3 kg/m^3 in the outer area and an average density of 2.69 x 10^3 kg/m^3 in the inner part. Porphyries are the surrounding rocks with the lowest average density (2.60 x 10^3 kg/m^3).

Further, detailed information can be found in "Tiefengeothermie Sachsen", available at: https://publikationen.sachsen.de/bdb/artikel/15145 (Last access: 29.08.2018).

3. **Deep metal enrichment**

Requested information:

- ✓ (expected) metal enrichment based on available geophysical, geological and drill data, samples information, geochemistry

As part of the Freiberger lead-zinc ore deposit, the Halsbrücke area is part of Saxony's most important mineral deposit. This refers to both the expansion and to the old mining activities.
It is a hydrothermal ore deposit of polymetallic character with a late to post-variscan age. Quartz, calcite, barite and fluorite were the primary raw mineral materials mined. The most important ores are galenite, sphalated, pyrite, arsenopyrite, as well as silver-containing minerals.

The veins of the deposit are named differently depending on their contents. At first, there are "Gesteinsgänge" ("rock veins") in which various porphyries (granitic, quartzitic, etc.) are found. The "Mineralgänge" ("mineral veins") with fluorite, barite and quartz also stand out. Furthermore, the metalliferous "Erzgänge" ("ore veins") with mineralizations of among others silver, lead-zinc, copper, iron exist.
A report by Landesamt für Umwelt, Landwirtschaft und Geologie (federal geological survey) assumes metal contents in the ore of 18.9 kg/t for Pb and 8.9 kg/t for Zn.

Two vein systems characterize the deposit structure, consisting of "standing veins", which have an N-S directional strike, and "spade veins", which extend almost vertically to the first. The "Spatgänge" are the relatively older gear system. The vein groups pass parallel with dip values of 70 - 90 degrees and reach lengths of up to 18 km.
The "Halsbrücker Spatgang", which is about seven kilometers long and up to six meters thick, is striking ESE-WNW. It contains in particular barite, fluorite and galenite, which make the site economically interesting not because of its concentrations but because of its masses.

Several deep wells were drilled in the area of the study area. One of the projects is a well in the Beihilfe mine (Halsbrücke), which extends to 590 m below ground level. Further away, wells of up to 747 m and 660 m were drilled near Freiberg and Brand-Erbisdorf. The bore logs and investigation results for the extracted rocks are not open to the public. Finally, the deep wells Großschirma 2/77 in the northwest of the site and Riechberg were drilled to depths of 1,200 and 701 meters.

The Geoportal Sachsen provides further sources as WMS servers at the following addresses:

1. Surface-near commodities

https://geoportal.umwelt.sachsen.de/arcgis/services/geologie/rohstoffe_wms/MapServer/WMSServer?request=GetCapabilities&service=WMS&version=1.3.0 (Last access: 29.08.2018).

2. Geochemical overview

https://geoportal.umwelt.sachsen.de/arcgis/services/boden/gcbuek400/MapServer/WMSServer?request=GetCapabilities&service=WMS&version=1.3.0 (Last access: 29.08.2018).

3. Geological exploration/drillings

https://geoportal.umwelt.sachsen.de/arcgis/services/geologie/bohrungen/MapServer/WMSServer?request=GetCapabilities&service=WMS&version=1.3.0 (Last access: 29.08.2018).

4. **Integrated 3D- 4D model**

Requested information:

- ✓ existing 3D-4D models of the target area and the deep metal enrichment
- ✓ if no 3D-4D models exist, collect the following necessary data: geological setting, mineralization, fluid flow models, stress field determination

Notes: e.g. openly available datasets, models.

At present, Sächsisches Landesamt für Umwelt, Landwirtschaft und Geologie (federal geological survey) is developing an extensive 3D underground model. The underground is visualized in its full extent and a comprehensive data basis for geoscientific applications is generated. The entire area is divided into different model units, which reflects the geologically highly heterogeneous underground.
Further information on the project and the corresponding contact person can be found at: http://www.geologie.sachsen.de/geologisches-3d-untergrundmodell-fuer-sachsen-13660.html (Last access: 29.08.2018)

So far, findings indicate a relatively simple structure for the site's area. The model mainly shows the Freiberg granodiorite gneiss and various gneiss types of the surrounding metamorphic units. In addition, masses of granite and crust units deeper than five kilometers are modeled as magmatites and para/ortho-metamorphites. The granite pluton, which is not yet clearly proven, is not included in the model due to a lack of data.

In 2009/2010, the Sächsisches Landesamt für Umwelt, Landwirtschaft und Geologie (federal geological survey) also investigated three preferred areas for the prospective construction of a petrothermal geothermal power plant in Saxony. 3D models were used, but they are also not publicly available. However, a project description can be found at: http://www.geologie.sachsen.de/tiefe-geothermie-in-sachsen-12832.html (Last access: 29.08.2018)

The basic 3D model of Freiberg is also characterized by a simple structure. It represents the central anticlinal structure, containing granodiorite gneiss in the center and outer grey gneiss. In addition, intruded granite masses and some of the most important ore veins are included. It is important to note that about 300 mining illustrations were also used for investigations, extending to a depth of about 800 m.

5. **EGS potential**

Requested information:

- ✓ EGS potential (heat & energy) of the area
- ✓ geothermal characteristics (temperature gradient, heat flux, stress field, water availability, EGS geology)
- ✓ presence/indication of deep fluids/brines, fracture system, crustal permeability

An analysis commissioned by the State Office, which also included the deep geothermal potential uses of the "Halsbrücke" site, compiled thermal, geological and petrophysical data and transferred them into three-dimensional models. One final product is the framework concept for deep geothermal energy in Saxony, which is available at:
http://www.geologie.sachsen.de/tiefe-geothermie-in-sachsen-12832.html (Last access: 29.08.201)
In the corresponding final report, the Halsbrücke site is located in a preferred area for potential deep geothermal use. The detailed final report with descriptions of the study results is available at:
https://publikationen.sachsen.de/bdb/artikel/15145 (Last access: 29.08.2018)

Summary of the most important findings to date:

- The dominating rock of the surrounding area is the Freiberg metagranodiorite, which is also often called Freiberg core gneiss or Freiberg granodiorite gneiss. It has a strong anisotropy of its thermal conductivity. In addition, biotite and muscovite proportions are highly varying, resulting in a wide range of 2.7 to 4.0 W/m.K. The average value is 3.3 ± 0.6 W/m.K. The surrounding schists, which contain both biotite and muscovite, also exhibit great differences in their thermal conductivity. The values range from 2.1 to 4.5 W/m.K and also have an average value of 3.3 ± 0.6 W/m.K.
- A modelled, two-dimensional temperature field shows temperatures of 130 to 140°C at a depth of five kilometres in the area of the Freiberg granodiorite gneiss.
- A three-dimensional model shows temperatures of 120 to 130 °C at a depth of five kilometres, taking the thermal conductivity values of the Freiberger Granoidiroitgneis of at least 2.7 W/m.K into account.
- Overall, it is concluded that the vicinity of the Halsbrücke site is suitable for petrothermal use, although it does not match the characteristics of the Schwarzenberg site. The tectonic imprints have a favourable effect.

In addition, the Sächsisches Landesamt für Umwelt, Landwirtschaft und Geologie (federal geological survey) provides the following information sources as WMS servers:

1. Hydrogeological overview

https://geoportal.umwelt.sachsen.de/arcgis/services/geologie/huek/MapServer/WMSServer?request=GetCapabilities&service=WMS&version=1.3.0 (Last access: 29.08.2018)

2. Groundwater dynamics

https://geoportal.umwelt.sachsen.de/arcgis/services/wasser/grundwasserdynamik/MapServer/WMSServer?request=GetCapabilities&service=WMS (Last access: 29.08.2018)

3. Geothermal overview

https://geoportal.umwelt.sachsen.de/arcgis/services/boden/gcbuek400/MapServer/WMSServer?request=GetCapabilities&service=WMS&version=1.3.0 (Last access: 29.08.2018)

4. Geothermal map

https://geoportal.umwelt.sachsen.de/arcgis/services/geologie/gtk50/MapServer/WMSServer?request=GetCapabilities&service=WMS&version=1.3.0 (Last access: 29.08.2018)

5. Geothermal extraction capacity

https://www.umwelt.sachsen.de/umwelt/infosysteme/wms/services/geologie/gtk50_utm?REQUEST=GetCapabilities&SERVICE=WMS (Last access: 29.08.2018)

List of references

Baumann, L., 1958: Tektonik und Genese der Erzlagerstätte Freiberg. FFH C 46, Leipzig.

Baumann, L., 1964: Die Erzlagerstätten der Freiberger Randgebiete. FFH C 188, Leipzig.

Baumann, L., 1967: Zur Frage der varistischen und postvaristischen Mineralisation im sächsischen Erzgebirge.- FFH C 209, Leipzig, 15-38.

Baumann, L., 1968: Die Mineralparagenesen des Erzgebirges - Charakteristik und Genese.- FFH C 230, Leipzig.

Baumann, L., 1994: Klassische Erzlagerstätten des Erzgebirges. Aufschluss, 45, 2, 56-66.

Baumann, L., Hofmann, F., Weber, W., 1997: Glückauf Freiberg. Bergbau, Erze, Mineralien. Bode Verlag Haltern, 168 pp.

Baumann L., Kuschka E., Seifert T., 2000: Lagerstätten des Erzgebirges. Enke Stuttgart.

Drechsel, M., Seifert, T., Götze, J., 2003: Comparison of quartz-types from the polymetallic sulfide veins of the Freiberg district based on cathodoluminescence investigations. In: Eliopoulos, D.G., et al. (Hgs.), Mineral Exploration and Sustainable Development. Proceedings of the 7th biennial SGA meeting. Athens 24-28 Aug. 2003. Millpress, Rotterdam, 763-65.

Flach, S., 1986: Mineralien und Bergbaugeschichte von Freiberg, Erzgebirge. Emser Hefte 7, 2/3,

Flach, S., 1986: Über die Mineralien und Bergbaugeschichte der 800 jährigen Bergstadt Freiberg. Bode Verlag. 111 pp.

Haake, R., Flach, S., Bode, R., 1994: Mineralien und Fundstellen Deutschland 2. Bode Verlag.

Hofmann, F., 1986: Die Freiberger Mineralien. Lapis, 11, 7/8, 28-55.

Massanek, A., Sandmann, D., Neumeier, G., 2015: The Freiberg Mining District,Saxony,Germany: The Mineralogical Record 46, 3, 310-381.

Müller, H., 1901: Die Erzgänge des Freiberger Bergreviers. Verl. W. Engelmann, Leipzig.

Pälchen W., Walter H., 2008: Geologie von Sachsen. Schweitzerbart, Stuttgart.

Pitsch, K., 1956: Abriß der Geologie von Sachsen. Berlin.

Reh, H., 1932: Beitrag zur Kenntnis der Erzgebirgischen Erzlager.- N Jb. Min. etc., 65, A, Stuttgart, 1-86.

Seifert, T., Sandmann, D., 2006: Mineralogy and geochemistry of indium-bearing polymetallic vein-type deposits: Implications for host minerals from the Freiberg district, Eastern Erzgebirge, Germany. Ore Geol. Rev., 28, 1-31.

Seifert, Th., Sandmann, D., 2006: Contribution to the Metallogeny of the Silver-base Metal Deposit Freiberg, Eastern Erzgebirge, Germany: Trace elements. 12th Quadr. IAGOD symposium "Understanding the Genesis of Ore Deposits - To Meet The Demands of 21st Century", Moscow, 21-24 Aug. 2006.

Ulrich, S., 2013: Die Geologie des Erzgebirges, Springer-Verlag 2013.

Vollstädt, H., & Weiß, S., 1991: Mineralfundstellen Sächisches Erzgebirge.- Weise Verlag, München.

Wagenbreth, O., Wächtler, E., 1986: Der Freiberger Bergbau. Technische Denkmale und Geschichte. VEB Deutscher Verlag für Grundstoffindustrie Leipzig.

Wagenbreth O., Wächtler E., 1990: Bergbau im Erzgebirge – Technische Denkmale und Geschichte. Deutscher Verlag für Grundstoffindustrie, Leipzig.

Woidtke, S., 2006: Der Berg ist frei - Bergbau im Erzgebirge, 4, 263-369.

Wagenbreth, O., Wächtler, E., 1986: Der Freiberger Bergbau. Technische Denkmale und Geschichte. VED Dt. Verlag für Grundstoffindustrie. Leipzig.

Weber, W., 1986: Der Freiberger Bergbau. Lapis, 11, 7/8, 13-27.

Annexes

Many other figures and tables for the location Halsbrücke can be found in the publication "Tiefengeothermie Sachsen" of Sächsischen Landesamts für Umwelt, Landwirtschaft und Geologie (federal geological survey)This can be accessed at: https://publikationen.sachsen.de/bdb/artikel/1514.

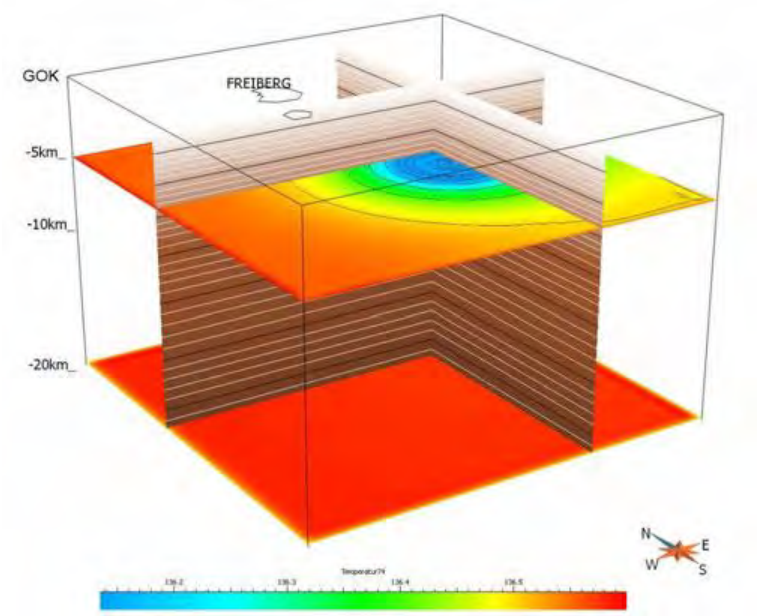

Fig. 6: Geothermal 3D temperature model in the area of the study area. Source: https://publikationen.sachsen.de/bdb/artikel/15145 (Last access: 29.08.2018).

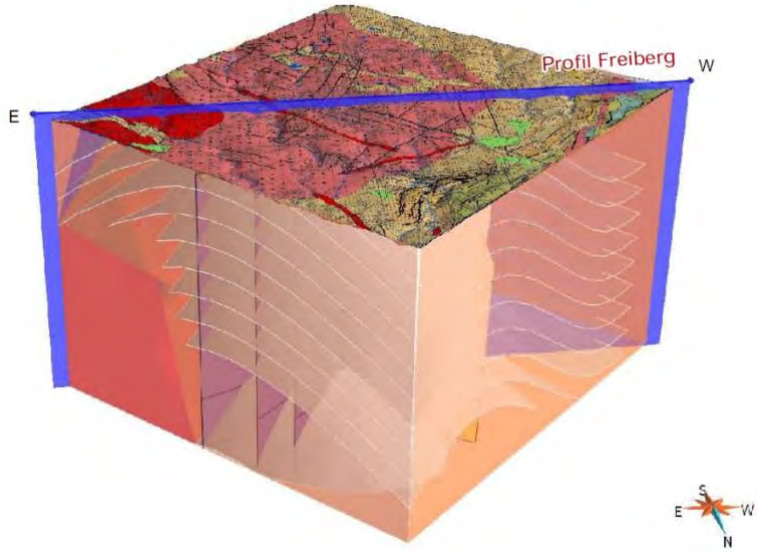

Fig. 7: Geological 3D model in the area of the study area. Source: https://publikationen.sachsen.de/bdb/artikel/15145 (Last access: 29.08.2018).

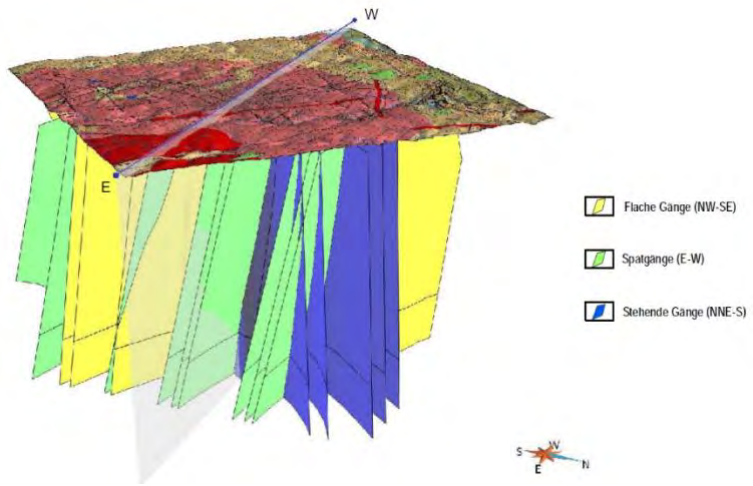

Fig. 8: Structure geological 3D model in the space of the investigation model. Source: https://publikationen.sachsen.de/bdb/artikel/15145 (Last access: 29.08.2018).

Evaluation of CHPM characteristics of prospective CHPM areas

BDG – Berufsverband Deutscher Geowissenschaftler (LTP)

Prospective area No. 1 – Schriesheimer Gruben, Grube Anna-Elisabeth

1. CHPM operational characteristics - Information for CHPM technological elements

Requested information:

✓ please fill in the table below with the requested data for the CHPM technology elements

Underground heat exchanger (deep metal enrichment + potential geothermal reservoir)	
Extension of the metal enrichments *(volumetric interpretation)*	The publicly available information does not offer a reliable interpretation of the extent of the ore deposits. Geophysical data or drilling exploration data which are required for this purpose are not publicly available. The coordinate 49.47780 / 8.6736 describes the location of the Schriesheim Visitors Mine, which was the focus of previous mining activities. Another aspect is that the type of deposit does not permit any prediction about the extent and continuation of the deposit into depth. However, it can be said for the close-to-surface mines that they are economically exhausted in all cases.
Expected type of the reservoir and porosity/permeability *(fractured, porous, etc)*	The immediate vicinity to the Upper Rhine Graben allows for conclusions about increased tectonic activities. The predominant rocks at the edge of the Odenwald are mostly granitoids, gneisses and migmatites. It has been proven that the rocks around the deposit have been strongly tectonically influenced during the Variscian Orogeny. As a result, numerous fissures are present and fissures that do not contain crystallized hydrothermal fluids can be closed. However, it can be concluded that both porosity and permeability at the deposit location will be comparatively low, as the rocks will merely be fissured solid rocks instead of, for example, well-permeable sedimentary rocks. Only in brecciated subzones of the granitic deposit, which have been particularly tectonically stressed, increased permeability and porosity values are to be expected.

Mineralization *(type and enriched metals)*	The present deposit is a vein (barytespar) deposit. It primarily contains a fluorite barite vein. Various iron-, lead- and silver-containing minerals are enriched in this vein. The silver content in galena is up to one percent. The enriched metals are mainly: Iron, lead, copper, arsenic, cobalt, silver, (uranium) These metals can be found, among others, in the following minerals: Arsenopyrite, Chalcopyrite, Emplektite, Galenite, Hematite, Limonite, Markasite, Pitticite, Pyrite, Pyrolusite, Safflorite, Skutterudite, Sphalerite, Uraninite, Uraninite, Limonite

Production and injection wells	
Depth of potential wells (m)	According to the Leibniz Institute for Applied Geophysics (LIAG), temperatures of up to 100-130 °C and a maximum of 160 °C can be achieved at the location "Schriesheimer Gruben, Grube Anna-Elisabeth" suitable for the temperature window required for the economical operation of a CHPM plant. This is the case for the petrothermal range and a depth range of 2,000 m to 7,000 m. In comparison, data from the federal geological survey ("Landesamt für Geologie, Rohstoffe und Bergbau im Regierungspräsidium Freiburg (LGRB)") shows more detailed temperature distributions for different depths. According to this data, temperatures of over 70-75 °C can be reached at depths beyond 1,500 m. The temperature distributions for the different depths are as follows: The range of required temperatures around 100 °C begins at depths >2,000 m (there 90-95°C). Below a depth of 2,500 m temperatures of 115-120 °C can be expected and at >3,000 m more than 140 °C are likely.

Electrolytic metal recovery and gas diffusion electro- precipitation	
Potential target metals to be recovered	As already mentioned in the section "Mineralization", iron, lead, copper, arsenic, and cobalt are to be expected as recoverable metals at the site of the deposit. Silver is only present in very small quantities. The same applies to uranium, which would only be found as traces.

Power plant (heat exchanger)	
Local heat and electricity demand *(industrial, municipal, agricultural, etc.)*	As a production site for electricity and heat, the location "Schriesheimer Gruben - Grube Anna-Elisabeth" is the most suitable in Germany. Situated in the Rhine-Neckar metropolitan region (extension approx. 5,500 km²), it is densely populated and has a correspondingly high demand for heat and electricity. In the closer vicinity are the cities of Heidelberg (centre approx. 10 km distant) with approx. 160,000 inhabitants as well as Mannheim am Rhein and Ludwigshafen am Rhein (centres approx. 20 km distant) with a total of approx. 475,000 inhabitants. Besides the municipal factors, the surrounding area of the deposit is also an important industrial location in Germany. Examples of important local companies are the chemical group BASF, HeidelbergCement, Daimler and SAP, where high energy and heating requirements can be found. According to information from the Rhine-Neckar Regional Association ("Verbands Region Rhein-Neckar"), 41.7 % of the area is agricultural and 17.8 % is residential and transport. Further details on the economic situation can also be found at https://www.m-r-n.com/zahlen-und-fakten (in German).

Salt gradient power generation	
Salinity of expected geothermal brine	The host rocks of the deposit, granitoids, gneisses and migmatites, indicate a rather low salt content of the expected geothermal brine. Nevertheless, in addition to barium, numerous sulphurous minerals as well as gypsum are present in the veins of the deposit. Since this deposit was formed by metalliferous hydrothermal fluids, it cannot be completely excluded that the respective elements will be dissolved, resulting in a brine with an increased salt content.
Fresh water supply from the surface *(water sources)*	Due to the close location to the Neckar and Rhine, no restrictions in water availability are to be expected. Furthermore, enough rainfall is available throughout the year. Finally, there is a river ("Kanzelbach") directly in the deposit area, which also supplies water all year round.

2. **CHPM operational characteristics - Environmental, social and political background**

Requested information:

- ✓ toleration to gaseous and solids emissions, water and noise pollution,
- ✓ local competition to land and water availability
- ✓ public acceptance
- ✓ political support
- ✓ presence of supporting legislation, regulatory framework

Notes: all of above refers to the selected area and its surroundings.

The location "Schriesheim - Grube Anna Elisabeth" is characterized by historical mining activities. Today there is also a visitor mine with a local touristic mining community. Accordingly, the public acceptance of a larger CHPM plant is to be regarded as critical.

The tolerances to emissions of any kind can also be classified as very low, particularly because environmental protection is assigned a high priority. Numerous laws and other regulations are to be expected as restrictions and obstacles to a CHPM plant. Although the demand for cheap energy and heat at the site is high, discharges of waste water into surface waters and noise emissions are subject to strict regulations throughout whole Germany.

Purchasing land can lead to high costs, especially in metropolitan zones such as the Rhine-Neckar metropolitan region.

Regarding political support, no positive effect is to be expected either, since the current (as of 12-2018) government does indeed promote economic interests, but also names environmental issues the core of its work.

3. **Financial aspects**

Requested information:

- ✓ use of economic tools developed in WP5 (more information is going to be provided in September)
- ✓ list of potential local stakeholders (community, political, companies)

The potential stakeholders at the site include the following contacts:

1. Landesamt für Geologie, Rohstoffe und Bergbau (LGRB) im Regierungspräsidium Freiburg
2. Stadt Schriesheim
3. Landratsamt Rhein-Neckar-Kreis
4. Bergwerksverein Schriesheim e.V.
5. Verband Region Rhein-Neckar
6. Zukunft Metropolregion Rhein-Neckar e.V.
7. Metropolregion Rhein-Neckar GmbH
8. Leibniz-Institut für Angewandte Geophysik (LIAG)

List of references

Amstutz, G.C., Meisl S., Nickel, E.,1975 Mineralien und Gesteine im Odenwald. Aufschluss, Sonderh. Nr.27, 344 pp.

Blömeke, C., 1893: Erzlagerstätten im Odenwald. Z. prakt. Geol.: 1, 346 – 347.

Boigk, H., Schöneich, H., 1970: Die Tiefenlage der Permbasis im nördlichen Teil des Oberrheingrabens. In: Illies, J. H. & Müller, S. (Hrsg.): Graben Problems: 45 - 55. Aufl. Suttgart, Schweizerbart.

Ditter, R., 2006: Die wirtschaftliche Entwicklung des Odenwaldes, insbesondere Kap. 3.3.1 Bergbau, Diplomica Verlag.

Fettel, M., 1975: Bergbaugeschichte des Odenwaldes. Der Aufschluss – Sonderb. 27 (Odenwald), 267–280.

Freymark, J., Sippel, J., Scheck-Wenderoth, M., Bär, K., Stiller, M., Fritsche, J.-H., Kracht, M., 2017: The deep thermal field of the Upper Rhine Graben. Tectonophysics 694, 114-129.

Geyer, M., 1999: Schaubergwerke in Baden-Württemberg (D). Schw. Strahler, Nr.9, 393-401.

Henningsen, D., Katzung, G., 2006: Einführung in die Geologie Deutschlands, 7. Aufl., Springer.

Köbrich, C., 1936: Hessische Erzvorkommen, Teil I: Die Nichteisenerze, Handbuch der hessischen Bodenschätze, Heft 3, Darmstadt.

Landesamt für Geologie, Rohstoffe und Bergbau (LGBR) Im Regierungspräsidium Freiburg, 2005: Geothermische Synthese/Bestandsaufnahme des Oberrheingrabens (1979/1981), Freiburg.

Levin, P., 1975: Über eine gangförmige Vererzung bei Schriesheim im südwestlichen Odenwald, in: Sonderband 27, 255–262, Der Aufschluss, Zeitschrift der Vereinigung der Mineralogie und Geologie.

Mößinger, F., 1955: Aus der Geschichte des Odenwälder Bergbaus, in: Der Aufschluss, Zeitschrift der Vereinigung der Mineralogie und Geologie, Sonderband 2, 75–81.

Münch, W., Sistenich, P., Bücker, C., Blanke, T., 2005: Möglichkeiten der geothermischen Stromerzeugung im Oberrheingraben, 10. Aufl., VGB PowerTech.

Neuhauser A., 2005: Exkursionsbericht Odenwald.

Nickel, E., Fettel, M.,1985: Odenwald. Sammlung geologischer Führer, 65, 2, 231 pp.

Plein, E., 1993: Voraussetzungen und Grenzen der Bildung von Kohlenwasserstoff-Lagerstätten im Oberrheingraben. Jber. Mitt. oberrhein. geol. Ver., N.F., Stuttgart.

Sauer, K., Munck, E. (ed.), Maget, P., Neeb, I., Tietze, R., 1979: Geothermische Synthese des Oberrheingrabens (Bestandsaufnahme). Veröff. des geologischen Landesamtes Baden-Württemberg, Strasbourg/Freiburg.

Slotta, R., 1986: Technische Denkmäler in der Bundesrepublik Deutschland. Hrsg.: Deutsches Bergbau Museum Bochum, 5, 1, 1108 pp.

Stein, E. 1985: Die magmatischen Gesteine des Bergsträßer Odenwaldes und ihre Platznahme-Geschichte.- Jber. Mitt. Oberrhein. Geol. Ver. N.F., 83, Stuttgart, 267-283.

Stober, I., Jodocy, M., 2009: Eigenschaften geothermischer Nutzhorizonte im baden-württembergischen und französischen Teil des Oberrheingrabens. In: Grundwasser, 14, 127–137.

Stober, I., Jodocy, M., Hintersberger, B., 2012: Vergleich von Durchlässigkeiten aus unterschiedlichen Verfahren - Am Beispiel des tief liegenden Oberen Muschelkalk-Aquifers im Oberrheingraben und westlichen Molassebecken. In: Z. geol. Wiss., 40, 1, 1-18.

Stober, I., Jodocy, M., Burisch, M., Person, P., 2013: Tiefenwässer im Oberen Muschelkalk-Aquifer des Oberrheingrabens und des Südwestdeutschen Molassebeckens. In: Grundwasser, 18, 2, 117-127.

Weiß, S., 1990: Mineralfundstellen Atlas, Deutschland West, Weise Verlag, München.

Evaluation of CHPM characteristics of prospective CHPM areas

BDG – Berufsverband Deutscher Geowissenschaftler (LTP)

Prospective area No. 2 – Bleibach-Glottertaler Gruben – Silberbergwerk Suggental

1. **CHPM operational characteristics - Information for CHPM technological elements**

Requested information:

✓ please fill in the table below with the requested data for the CHPM technology elements

Underground heat exchanger (deep metal enrichment + potential geothermal reservoir)	
Extension of the metal enrichments *(volumetric interpretation)*	An estimation of the volume of metal enrichments at this location is not possible without high quality data sets due to the type of deposit. The continuation of vein systems to greater depths requires comprehensive geophysical or drilling prospection data. Consequently, the volumetric extent of the deposit cannot be estimated from the open-source data. The extend and quality of the publicly available data is not sufficient for a volume interpretation. The coordinates of the location (48.0668 / 7.9347) indicate the location of the visitor mine located on the deposit. There, the center of historical mining activities is located nearer to the surface.
Expected type of the reservoir and porosity/permeability *(fractured, porous, etc)*	As part of the Central Black Forest gneiss mass ("Zentralschwarzwälder Gneissmasse"), the surrounding and host rocks of the deposit were heavily affected by tectonic activity. These rocks originate from the Variscan Basement and consist of gneisses and granites. A complicated system of faults separates the entire Black Forest into numerous individual slabs. These various factors demonstrate that the rocks of the deposit environment are most likely to have very low porosity and permeability. Pathways may only be controlled by fault systems. In zones with fault breccias, however, an increased permeability is to be assumed.

Mineralization *(type and enriched metals)*	The location "Bleibach-Glottertaler Gruben - Silberbergwerg Suggental" is a silver deposit in the form of a hydrothermal ore deposit. Quartz and barite dominate as veins; in these sulphide ores are embedded. There are five phases of tectonically controlled ore mineralization. The average silver content in galenite is 0.02%, silver content in tennantite up to 0.57%. The following metals are expected to be enriched at this deposit location: Iron, Lead, Arsenic, Copper, Zinc, Silver, (Gold) The metals listed are bound to the following minerals, among others: Arsenopyrite, bournonite, chalcopyrite, freibergite, galenite, marcasite, polybasite, pyrargyrite, pyrite, sphalerite, tennantite, tetrahedite, cuprite, goethite, hematite, limonite, siderite

Production and injection wells	
Depth of potential wells (m)	According to the Leibniz Institute for Applied Geophysics (LIAG), temperatures from 100 °C to a maximum of 130 °C can be reached for petrothermal use at a depth of 2,000 m to 7,000 m at the location "Bleibach-Glottertaler Gruben - Silberbergwerk Suggental" for petrothermal applications. The federal geological survey of the state of Baden-Württemberg ("Landesamt für Geologie, Rohstoffe und Bergbau im Regierungspräsidium Freiburg (LGRB)"), on the other hand, indicates a temperature of over 100 °C (115-120 °C) only from a depth of 2,500 m. Above, in the depth range from 2,000 m to 2,500 m, only temperatures between 70-75 °C can be expected. According to the LGRB, a temperature of 140-150°C can be reached from 3,000 m onwards.

Electrolytic metal recovery and gas diffusion electro- precipitation	
Potential target metals to be recovered	Like the section "Mineralization" the metals iron, lead, arsenic, copper and zinc are present at the location "Bleibach-Glottertaler Gruben - Silberbergwerg Suggental". Silver and gold were found in historical mining activities only as traces.

Power plant (heat exchanger)	
Local heat and electricity demand *(industrial, municipal, agricultural, etc.)*	The municipality of Glottertal, where the site is located, is not characterized by a high population density. In the direct vicinity (distance: 5 km) there is the town Waldkirch with about 22'000 inhabitants. Freiburg im Breisgau is about 10 km away with about 230,000 inhabitants. Thus, there is a municipal demand for inexpensive heat and electrical energy. Freiburg is one of the most populated cities in the state of Baden-Württemberg and counts as an economic center. However, it is not industrial applications that are in the foreground, rather the service sector and tourism. Companies in the fields of solar technology, medical technology and IT are dominant with a nearby university. Furthermore, agriculture and forestry are also an important part of the economic activities in the entire region. Overall, however, it can be concluded that in the vicinity of this location no customers with significant consumption of energy can be found.

Salt gradient power generation	
Salinity of expected geothermal brine	As a hydrothermal ore deposit, the present mineral deposit contains a wide variety of minerals that could dissolve again when metals are recovered. In addition to sulphur-containing sulfides, carbonates and barytes are also present. These constituents could result in a brine with a significantly higher salt content if the CHPM technology is applied. The surrounding host rocks of the deposit are mainly gneiss and partly intercalated granite. From these, on the other hand, no dissolved substances are to be expected.
Fresh water supply from the surface *(water sources)*	In the area of the Black Forest there is enough rainfall throughout the year. There are also numerous small streams and rivers (mainly the "Glotter" flowing through the Glottertal and the "Talbach" flowing through the Suggental) in the area around the mineral deposit. Further away, there is a larger river, the "Elz", with an average runoff of more than 2 m^3/s. The availability of water is therefore completely unproblematic.

2. **CHPM operational characteristics - Environmental, social and political background**

Requested information:

- ✓ toleration to gaseous and solids emissions, water and noise pollution,
- ✓ local competition to land and water availability
- ✓ public acceptance
- ✓ political support
- ✓ presence of supporting legislation, regulatory framework

Notes: all of above refers to the selected area and its surroundings.

Freiburg is known for renewable energy production in the context of solar energy. For this reason, further expansion in this area of renewable energy sources could certainly receive positive feedback. Furthermore, the given site is not located in a densely populated area, so that any difficulties such as noise emissions are rather low. Prices for land also tend to be favorable, as the area is rather rural.

However, no positive effect is to be expected in terms of political support, since the current (12-2018) government, although supporting the economic sector, also sees environmental issues as the core of its work. Especially in the tourism sector, health is an important factor, so that doubts are to be expected. Since a historical mining museum with a visitor mine is located at the site, there could be further competitions for use.

However, other effects that could have an impact on the environment are to be regarded as problematic, as environmental protection is given high priority. Numerous laws and other regulations are to be expected as restrictions and obstructions to a CHPM plant. Although the demand for inexpensive energy and heat at the site is rather high, discharges of waste water into surface waters and noise emissions are strictly regulated for the whole of Germany.

3. **Financial aspects**

Requested information:

- ✓ use of economic tools developed in WP5 (more information is going to be provided in September)
- ✓ list of potential local stakeholders (community, political, companies)

The potential stakeholders at the site include the following contacts:

1. Landesamt für Geologie, Rohstoffe und Bergbau (LGRB) im Regierungspräsidium Freiburg
2. Gemeinde Glottertal
3. Landkreis Breisgau-Hochschwarzwald
4. Silberbergwerk Suggental e.V.
5. Leibniz-Institut für Angewandte Geophysik (LIAG)
6. Universität Freiburg, Institut für Geo- und Umweltnaturwissenschaften

List of references

Bliedtner, M., Martin, M., 1986: Erz- und Minerallagerstätten des Mittleren Schwarzwaldes. Geol. LA Baden-Württemb., Freiburg.

Goldenberg, G., 1993: Frühe Blei-, Silber- und Kupfergewinnung im Südschwarzwald. Hüttenplätze und Bergschmieden. In: H.Steuer/U.Zimmermann (eds.), Montanarchäologie in Europa. Archäologie und Geschichte.

Groschopf, R., Schreiner, A., 1996: Erläuterungen zum Blatt 7913 Freiburg i. Br.-NO, 2., ergänzte Aufl.- Geol. Kt. Baden-Württ. 1:25 000: 130 S., 6 Abb., 8 Tab., 4 Taf., 5 Beil.; Freiburg i. Br. (Geol. L.-Amt Baden-Württ.).

Haasis-Berner, A., 2012: Besiedlung und Bergbau im Glottertal. In: Arbeitskreis Glottertäler Ortsgeschichte (eds.): Bergbau im Glottertal. Beiträge zur 900-Jahr-Feier der Gemeinde Glottertal, Freiburg, 9–102.

Henglein, M., 1924: Erz- und Minerallagerstätten des Schwarzwalds. Stuttgart, Schweizerbart, 196 pp.

Homann, W., 2000: Das Gold in der Sage des Suggentales bei Waldkirch (Südschwarzwald). Der Erzgräber, 14: 62-70, 5 Abb.; Oberwolfach.

Hoppe, A., Foellmer, A., Noeltner, T., 1993: Historischer Erzbergbau im Schwarzwald und Schwermetalle in Böden der Staufener Bucht. In: H.Steuer, Zimmermann U. (eds.), Montanarchäologie in Europa. Archäologie und Geschichte, 4, Sigmaringen, 249-254.

Lieber, W., Leyerzapf, H., 1986: German silver. An historical persepctive on silver mining in Germany; Min. Rec., 17, 3-18.

Markl, G., Lorenz, S., 2004: Silber, Kupfer, Kobalt-Bergbau im Schwarzwald. Markstein Verlag, Filderstadt.

Metz, R., 1961: Der frühe Bergbau im Suggental und der Urgraben am Kandel im Schwarzwald. Alemannisches Jahrbuch, 1961: 281–316, Freiburg.

Schneider, K., 1995: Bergbauspuren. In Das Glottertal. Geschichte und Erinnerungen. Beitrag zur 25-Jahr-Feier der Gesamtgemeinde Glottertal, Hoch, B. et al. (eds.), 176-181.

Steen, H., 1995: Bergbau und Mineralien aus dem Suggental bei Waldkirch im mittleren Schwarzwald. Erzgräber, 9 (2), 104-17.

Steen, H., 2004: Geschichte des modernen Bergbaus im Schwarzwald. 485 pp.

Steuer, H., 1991: Erzbergbau im Schwarzwald zur Salierzeit.

Walenta, K., Schmeltzer, H., Sachs, P.M., 1989: Erzmikroskopische Untersuchungen an Erzen vom Hornbühl bei Suggental im Schwarzwald. Der Erzgräber, 3: 122-127, 5 Abb.; Oberwolfach.

Walenta, K., 1992: Die Mineralien des Schwarzwaldes, Weise Verlag, München.

Walenta, K., 1996: Neufunde aus dem Schwarzwald (6.F., 2T.). Lapis, 21 (12), 39 pp.

Werner, W., Dennert, V., 2004: mit Beiträgen v. Meyerdirks, U., Tegel, W., Lagerstätten und Bergbau im Schwarzwald. Ein Führer unter besonderer Berücksichtigung der für die Öffentlichkeit zugänglichen Bergwerke, 271 Abb., Freiburg (Landesamt f. Geol. Rohst. Bergb. Baden-Württ.), 334 pp.

Wölker, F., Leser, C., 1993: Bergbaugeschichte im Suggental. In: Bericht Bergbauforschungsgruppe Suggental.

Zimmermann, U., 1993: Untersuchungen zum frühen Bergbau im Südschwarzwald. In: Steuer, H., Zimmermann, U.(eds.): Montanarchäologie in Europa. Archäologie und Geschichte 4. Sigmaringen, 201-230.

Evaluation of CHPM characteristics of prospective CHPM areas

BDG – Berufsverband Deutscher Geowissenschaftler (LTP)

Prospective area No. 3 – Schwarzenberg

1. CHPM operational characteristics - Information for CHPM technological elements

Requested information:

✓ please fill in the table below with the requested data for the CHPM technology elements

Underground heat exchanger (deep metal enrichment + potential geothermal reservoir)	
Extension of the metal enrichments *(volumetric interpretation)*	Since only open access resources were used in the course of this investigation, specifications regarding the volume of metal enrichments are not possible. A depth estimation in particular is not possible due to a lack of high-quality geophysical data sets or information on drilled wells. The federal geological survey of Saxony ("Landesamt für Umwelt, Landwirtschaft und Geologie (LULG)") only provides estimates of the masses of indicated resources of the deposit. These include 28,000 tons of tin, 23,000 tons of bismuth and 95,000 tons of zinc. At the same time, however, it is pointed out that the skarn ores that can be found in these areas have a complicated and very variable mineral content, which additionally complicates a volumetric interpretation of the deposit. This already demonstrates that the varying intensity of skarn overprinting makes it difficult to predict the grade of the deposit. The coordinates 50.5069 / 12.7875 indicate the approximate center of the deposit.
Expected type of the reservoir and porosity/permeability *(fractured, porous, etc)*	In the close surrounding of the mineral deposit mainly schists of crystalline rocks as well as quartzites and amphibolites are to be found. For these rocks, rather low porosity and permeability values are to be expected and permeabilities will be mainly controlled by fractures. Moreover, the skarn metacarbonate horizons, which form the deposit rock itself, are also present. For these and for the carbonate rocks in the surrounding areas, higher porosities and permeabilities are to be expected, although the characteristics can still be significantly modified by the processes of metamorphosis.

Mineralization *(type and enriched metals)*	The mineralization type of the deposit corresponds to that of a skarn deposit. The ore bodies are mainly present as lenses and layers. In this context, various silicate and metal-containing fluids were also present. So-called "Greisen-" and " Zersatzerze " are distinguished from each other. Primarily the enrichment of the following metals is considered to be significant: tin, tungsten, zinc, cobalt, silver, arsenic, iron, lead, (uranium) Among others, these metals are embedded in the following minerals: magnetite, pyrite, arsenite, chalcopyrite, sphalerite, galenite

Production and injection wells	
Depth of potential wells (m)	In the area of this deposit, temperatures of up to 130 °C can be achieved according to Leibniz Institute for Applied Geophysics (LIAG). These temperatures refer to depths from 2'000 to 7'000 m and to petrothermal applications. The geothermal gradients given by the Saxon geological survey ("Sächsisches Landesamt für Umwelt, Landwirtschaft und Geologie (LULG)") vary between 3.1 °C / 100 m and 3.7 °C / 100 m. Consequently, the required depth range for a technically and economically feasible application of CHPM technology also varies. In the best case, the limit of 100 °C is exceeded at a depth of about 2,700 m, in the worst case only at a depth of about 3,200 m. The resulting uncertainty range is 500 m. The actual measured temperature value at the end of a 2365 m deep borehole was 81 °C.

Electrolytic metal recovery and gas diffusion electro- precipitation	
Potential target metals to be recovered	In the section "Mineralization" the potential recoverable metals have already been described. These are primarily tin, tungsten and zinc. Indicated resources are even given for these metals (see section "Extension of the metal enrichments"). The metals iron, arsenic, cobalt and lead are further important. As a result of the surrounding granites, uranium may also be a recoverable metal of the mineral deposit. Silver, however, can only be expected in traces.

Power plant (heat exchanger)	
Local heat and electricity demand *(industrial, municipal, agricultural, etc.)*	The surroundings of the "Schwarzenberg" deposit are characterized by a rather low population density. The "Erzgebirge" district itself has a population of only 340,000 inhabitants with a surface area of approx. 1,800 km². The city of Schwarzenberg has about 17,000 inhabitants. The closest major district town to Schwarzenberg is Aue, situated at about 10 km away. There, the population of 16,000 inhabitants goes hand in hand with a twice as high population density. However, no significant municipal demand for electricity and heat is to be identified. On the industrial side, there are predominantly small and medium-sized enterprises operating in the area of the site. Although many companies are in the electrical engineering and mechanical engineering sectors, they are no customers for large quantities of thermal and electrical energy.

Salt gradient power generation	
Salinity of expected geothermal brine	The surrounding rocks consist on the one hand of granite and various shales, from which no larger resulting salinity is to be expected. The same applies to the gneisses, amphibolites and quartzites which are present in the surrounding area of the mineral deposit. On the other side, however, the skarn rocks are present, forming the deposit rock itself. They are dominated by carbonates, which can cause higher concentrations of dissolved solids in the expected geothermal brine. Sulphurous minerals should also be considered in this context.
Fresh water supply from the surface *(water sources)*	Situated in the western part of the Erzgebirge Mountains, the site does not have any restrictions on the availability of fresh water. Not far from the deposit the river "Schwarzwasser" is located, with an average discharge of approx. 6 m³/s and a enough water throughout the year. At the same time, precipitation values of over 800 mm/a are to be expected, which also represents a sufficiently high value for the application of CHPM technology.

2. **CHPM operational characteristics - Environmental, social and political background**

Requested information:

- ✓ toleration to gaseous and solids emissions, water and noise pollution,
- ✓ local competition to land and water availability
- ✓ public acceptance
- ✓ political support
- ✓ presence of supporting legislation, regulatory framework

Notes: all of above refers to the selected area and its surroundings.

Since the intensive uranium mining in the former GDR, the present society has been fundamentally doubtful about further mining activities. Numerous contaminated abandoned sites of the former mining operations reduce the public acceptance of new raw material projects significantly.

And this is also reflected in the state and national laws, with a clear focus on environmental protection. Environmental damage caused by emissions to air, water or noise can be regarded as very critical.

A change towards innovative approaches and the use of renewable energies is indeed welcomed and politically supported. Nevertheless, any technology that can be associated with the hydraulic stimulation of the underground is subject to very negative biases.

However, a positive aspect is that there are no problems to be expected with regard to competition for land or necessary additives such as water.

3. **Financial aspects**

Requested information:

- ✓ use of economic tools developed in WP5 (more information is going to be provided in September)
- ✓ list of potential local stakeholders (community, political, companies)

The following contacts are some of the potential stakeholders at the site:

1. Sächsisches Landesamt für Umwelt, Landwirtschaft und Geologie (LULG)
2. Stadt Schwarzenberg
3. Landkreis Erzgebirgskreis
4. Wismut GmbH
5. Leibniz-Institut für Angewandte Geophysik (LIAG)
6. TU Bergakademie Freiberg

List of references

Baumann, L., 1967: Zur Frage der varistischen und postvaristischen Mineralisation im sächsischen Erzgebirge.- FFH C 209, Leipzig, 15-38.

Baumann, L., 1968: Die Mineralparagenesen des Erzgebirges - Charakteristik und Genese.- FFH C 230, Leipzig.

Baumann, L., Kuschka, E., Seifert, T., 2000: Lagerstätten des Erzgebirges. Enke Stuttgart.

Beck, R., 1903: Über die Erzlager der Umgebung von Schwarzenberg im Erzgebirge, T.I. Jb. für das Berg- und Hüttenwesen im Königreiche Sachsen, Freiberg.

Haake, R., 1972: Zur Altersstellung granitoider Gesteine im Erzgebirge. Geologie, 21, 6, 641-76.

Haake, R., Hofmann, F., 1991: Die Mineralien der Skarn-Lagerstätte von Pöhla im Erzgebirge. Mineralienwelt, 2, 3, 26-41.

Haake, R., 1970: Über die Skarnlager bei Schwarzenberg/Erzgeb. Fundgrube 7 (1/2), 6-11.

Hösel, G., 1968: Die Skarnlager im Raum Schwarzenberg (Erzgebirge). Ber.dtsch.Ges.geol.Wiss., B, 13/4, Berlin, 469-77.

Mädler, F. 1992: Das Bergbaurevier von Breitenbrunn und Antonsthal im oberen Erzgebirge, Lapis, 17, 10, 13-24.

Martin, M., 1990: Zum Emplektit von Schwarzenberg. Fundgrube 26 (1), 17-22.

Massone, H.J., Bautsch, H.J., 2004: Ultrahigh and high pressure rocks of Saxonia. 32.Int. geol. congress. Vol.2, B21. Florence Italy 20.-28.8.2004.

Neese, T., 2015: Relikte Prähistorischer Goldseifen in Sachsen. Aufschluss, 66, 6, 305-19.

Pälchen, W., Walter, H., 2008: Geologie von Sachsen. Schweitzerbart, Stuttgart.

Pitsch, K., 1956: Abriß der Geologie von Sachsen. Berlin.

Reh, H., 1932: Beitrag zur Kenntnis der Erzgebirgischen Erzlager.- N. Jb. Min. etc., 65, A, Stuttgart, 1-86.

Sebastian, U., 1995: Die Strukturentwicklung des spätorogenen Erzgebirgsaufstiegs in der Flöha-Zone – Ein weiterer Beitrag zur postkollisionalen Extension am Nordrand der Böhmischen Masse, Freib. Forsch-H C 461

Sebastian, U., 2013: Geologie des Erzgebirges. Springer-Verlag, Berlin Heidelberg.

Seifert, T., 1985: Beitrag zur Typisierung von Sn-Lagerstätten im Erzgebirge. Bergakademie Freiberg, Sektion Geowissenschaften. 162 pp.

Seifert, T., 1999: Relationship between late Variscan lamprophyres and hydrothermal vein mineralization in the Erzgebirge. In Stanley, C.J. u.a. (eds.), Mineral Deposits: Processes to Processing. Vol.1. Proc. 5th biennial SGA meeting and the 10th quadr. IAGOD symposium. London 22-25 Aug.1999. Balkema, 429-32.

Tetzner, A., Edelmann, F., 1927: Neue sächsische Mineralvorkommen (Erzgänge zu Frenzel's "Mineralogisches Lexicon für das Königreich Sachsen"). Jahrb. Berg- und Hüttenwesen 1926 u. 1927, Freiberg.

Tichomirowa, M., 2003: Die Gneise des Erzgebirges – hochmetamorphe Äquivalente von neoproterozoisch-frühpaläozoischen Grauwacken und Granitoiden der Cadomiden, Freib Forsch-H C495.

Vollstädt, H., Weiß, S., 1991: Mineralfundstellen Sächisches Erzgebirge.- Weise Verlag, München.

Wagenbreth, O., Wächtler, E., 1990: Bergbau im Erzgebirge – Technische Denkmale und Geschichte. Deutscher Verlag für Grundstoffindustrie, Leipzig.

Evaluation of CHPM characteristics of prospective CHPM areas

BDG – Berufsverband Deutscher Geowissenschaftler (LTP)

Prospective area No. 4 – Revier Halsbrücke

1. **CHPM operational characteristics - Information for CHPM technological elements**

Requested information:

✓ please fill in the table below with the requested data for the CHPM technology elements

Underground heat exchanger (deep metal enrichment + potential geothermal reservoir)	
Extension of the metal enrichments *(volumetric interpretation)*	As part of the re-evaluation of spar and ore deposits in the Free State of Saxony by the Saxon geological survey ("Sächsische Landesamt für Umwelt, Landwirtschaft und Geologie (LULG)"), an assessment of the "Halsbrücke" mining area was carried out. (http://www.bergbau.sachsen.de/download/mining/raw_materials_catalog_spat_ore_occurrence.pdf, last access 23/11/2018) While there are no direct volumetric data available, the extension of the district is estimated to be 20 km (N-S) x 10 (E-W) km. The average width of the veins is estimated as 1 m according to this report. In terms fof depth extension, only 700 m were indicated but the degree of exploration is only determined based on underground core drillings and a few exploration crossings in the historical mines. Since the deposit is a hydrothermal lead-silver vein deposit, it is highly unpredictable to estimate enrichments located at greater depths without further high-quality geophysical data or exploration drilling.
Expected type of the reservoir and porosity/permeability *(fractured, porous, etc)*	The area of the mineral deposits is characterized by a high degree of metamorphism and both supra-regional and local fault systems are present. Because of these naturally existing fractures, there may be pathways and (comparatively low) permeabilities. The area of metal enrichment itself is predominantly located in a complex consisting of orthoclase-biotite gneisses, gabbros and serpentinites, whereby rhyolites and lamprophyre are also found as host rocks. The permeability of those rocks tends to be rather low. However, in the vicinity of the "Halsbrücke" site, there are several kilometers of marine sedimentary sequences. They can be traced back to the Saxo-thuringian zone of the Varsicum. Partly porous reservoir conditions may be expected in these sediment formations. Correspondingly, porosity and permeability values are comparatively high in this area.

Mineralization *(type and enriched metals)*	The location of "Halsbrücke", like most other German potential sites for CHPM technology, is a hydrothermal ore deposit. The genesis and several details about the individual characteristics have already been described in the previously submitted document of "Basic CHPM Characteristics". The ore-bearing veins contain quartz as well as barite, calcite and fluorite as host structures. In addition, some veins are filled with porphyries (granite, quartzite, etc.). As one of the most important ore deposits in the surrounding region, this site is well known for its polymetallic character, which mainly includes the following metals: Silver, lead, zinc, copper, iron, arsenic, (nickel, cobalt, tungsten, bismuth) As the most important of the numerous minerals in which the metals are bound, count: Galenite, Sphalerite, Pyrite, Arsenopyrite

Production and injection wells	
Depth of potential wells (m)	At a depth of five kilometres, a two-dimensional temperature modelling of the deposit environment was carried out by the federal geological survey of Saxony ("Sächsisches Landesamt für Umwelt, Landwirtschaft und Geologie (LULG)"). This investigation indicated achievable temperature values in the range of 130 °C to 140 °C in the Freiberg granodiorite gneiss zone, which is in the close vicinity of the site. Nevertheless, the potential petrothermal usability of the deposit was not only confirmed by the LULG, but also by the Leibniz Centre for Applied Geology (LIAG). An overview of the petrothermal utilization possibilities at depths of 2,000 m to 7,000 m of the site also shows that temperatures of at least 100 °C to 130 °C are to be expected in the designated areas of this site.

Electrolytic metal recovery and gas diffusion electro- precipitation	
Potential target metals to be recovered	As described in the chapter "Mineralization", numerous metals are available and potentially recoverable at the location of "Halsbrücke". The most important are iron, lead, zinc, copper and silver. Other metals such as nickel, cobalt, bismuth and tungsten are expected to be only as trace metals. The detected metal contents of the different ores are significant. In ores, the lead content is estimated to be about 18.9 kg/t, while zinc is estimated to be about 8.9 kg/t. However, due to the type of deposit, it should also be noted that the recoverable metal contents can be very variable at local level.

Power plant (heat exchanger)	
Local heat and electricity demand *(industrial, municipal, agricultural, etc.)*	Located in the administrative district "Mittelsachsen" the municipality Halsbrücke itself has only a population of about 5,000 inhabitants. The population density in the direct vicinity of the deposit location is also low. For higher demands of municipal energy consumption, it is therefore necessary to take a further look at the surrounding region. Only a few kilometers to the south, there is the university town of Freiberg with about 41,000 inhabitants. There, the population density is significantly higher, so that there is a municipal need for inexpensive electrical and thermal energy. At about 30 km in the north-west, Dresden is the second largest city in Saxony with about 550'000 inhabitants. With a population of approx. 780,000, the entire agglomeration area of Dresden is a strong area for municipal demand for energy. The municipality "Halsbrücke" itself has only two smaller industrial areas where mainly small and medium-sized companies are located. Nevertheless, there is also a factory in the direct proximity of the potential CHPM location, which could represent an industrial customer for larger amounts of energy in the course of recovering noble metals and manufacturing products. For further industrial energy requirements, Freiberg and above all the economically important metropolitan area of Dresden can also be considered. Various high-tech companies are based in Freiberg, while a wide range of companies from the mechanical engineering, vehicle construction, biotechnology, pharmaceuticals, IT and electronics sectors can be found in Dresden.

Salt gradient power generation	
Salinity of expected geothermal brine	The "Halsbrücke" mineral deposit area lays in an environment with several kilometers of sedimentary rock sequences. These are mainly carbonate rocks which, although not expected to produce excessive salinity, contain numerous substances which could be dissolved by the application of CHPM technology. In addition, the hydrothermal mineralization veins are consisting of carbonate, barite and fluorite. These minerals can also be dissolved under given boundary conditions and provide an increased salinity of the expected geothermal brine. On the other hand, the ore-bearing veins of the deposit are primarily located in gneisses and gabbros as well as serpentinites. These, as well as the other host rocks (lamprophyres and rhyolites) will most likely not cause a high salinity of the expected geothermal brine.
Fresh water supply from the surface *(water sources)*	The annual precipitation in the surrounding region provides sufficient quantities of fresh water for the application of CHPM technology. In addition, the "Freiberger Mulde" river is in the area of the deposit. It is a larger river with an average discharge volume of 35.7 m^3/s. Therefore, critical conditions regarding the availability of fresh water are not to be expected at this location.

2. **CHPM operational characteristics - Environmental, social and political background**

Requested information:

- ✓ toleration to gaseous and solids emissions, water and noise pollution,
- ✓ local competition to land and water availability
- ✓ public acceptance
- ✓ political support
- ✓ presence of supporting legislation, regulatory framework

Notes: all of above refers to the selected area and its surroundings.

Due to its close distance to the other prospective CHPM location in Saxony, "Schwarzenberg", comparable environmental, social and political conditions can be expected for this area.

On the one hand, there are numerous negative biases due to the extensive historical mining activities, particularly because numerous negative environmental impacts have resulted, and their remediation continues in the present time.

The public acceptance of new mining activities is therefore very low. Furthermore, requirements for emissions of gases, wastewater and noise are strongly regulated and restricted by laws and other guidelines.

However, a positive aspect for the location of "Halsbrücke" is the fact that due to the low population density and low competition, no obstacles to the availability of land and water are to be expected.

3. **Financial aspects**

Requested information:

- ✓ use of economic tools developed in WP5 (more information is going to be provided in September)
- ✓ list of potential local stakeholders (community, political, companies)

The following contacts are some of the potential stakeholders at the site:

1. Sächsisches Landesamt für Umwelt, Landwirtschaft und Geologie (LULG)
2. Gemeinde Halsbrücke
3. Landkreis Mittelsachsen
4. Wismut GmbH
5. Leibniz-Institut für Angewandte Geophysik (LIAG)
6. TU Bergakademie Freiberg

List of references

Baumann, L., 1958: Tektonik und Genese der Erzlagerstätte Freiberg. FFH C 46, Leipzig.

Baumann, L., 1964: Die Erzlagerstätten der Freiberger Randgebiete. FFH C 188, Leipzig.

Baumann, L., 1967: Zur Frage der varistischen und postvaristischen Mineralisation im sächsischen Erzgebirge.- FFH C 209, Leipzig, 15-38.

Baumann, L., 1968: Die Mineralparagenesen des Erzgebirges - Charakteristik und Genese.- FFH C 230, Leipzig.

Baumann, L., 1994: Klassische Erzlagerstätten des Erzgebirges. Aufschluss, 45, 2, 56-66.

Baumann, L., Hofmann, F., Weber, W., 1997: Glückauf Freiberg. Bergbau, Erze, Mineralien. Bode Verlag Haltern, 168 pp.

Baumann L., Kuschka E., Seifert T., 2000: Lagerstätten des Erzgebirges. Enke Stuttgart.

Drechsel, M., Seifert, T., Götze, J., 2003: Comparison of quartz-types from the polymetallic sulfide veins of the Freiberg district based on cathodoluminescence investigations. In: Eliopoulos, D.G., et al. (Hgs.), Mineral Exploration and Sustainable Development. Proceedings of the 7th biennial SGA meeting. Athens 24-28 Aug. 2003. Millpress, Rotterdam, 763-65.

Flach, S., 1986: Mineralien und Bergbaugeschichte von Freiberg, Erzgebirge. Emser Hefte 7, 2/3,

Flach, S., 1986: Über die Mineralien und Bergbaugeschichte der 800 jährigen Bergstadt Freiberg. Bode Verlag. 111 pp.

Haake, R., Flach, S., Bode, R., 1994: Mineralien und Fundstellen Deutschland 2. Bode Verlag.

Hofmann, F., 1986: Die Freiberger Mineralien. Lapis, 11, 7/8, 28-55.

Massanek, A., Sandmann, D., Neumeier, G., 2015: The Freiberg Mining District,Saxony,Germany: The Mineralogical Record 46, 3, 310-381.

Müller, H., 1901: Die Erzgänge des Freiberger Bergreviers. Verl. W. Engelmann, Leipzig.

Pälchen W., Walter H., 2008: Geologie von Sachsen. Schweitzerbart, Stuttgart.

Pitsch, K., 1956: Abriß der Geologie von Sachsen. Berlin.

Reh, H., 1932: Beitrag zur Kenntnis der Erzgebirgischen Erzlager.- N Jb. Min. etc., 65, A, Stuttgart, 1-86.

Seifert, T., Sandmann, D., 2006: Mineralogy and geochemistry of indium-bearing polymetallic vein-type deposits: Implications for host minerals from the Freiberg district, Eastern Erzgebirge, Germany. Ore Geol. Rev., 28, 1-31.

Seifert, Th., Sandmann, D., 2006: Contribution to the Metallogeny of the Silver-base Metal Deposit Freiberg, Eastern Erzgebirge, Germany: Trace elements. 12th Quadr. IAGOD symposium "Understanding the Genesis of Ore Deposits - To Meet The Demands of 21st Century", Moscow, 21-24 Aug. 2006.

Ulrich, S., 2013: Die Geologie des Erzgebirges, Springer-Verlag 2013.

Vollstädt, H., & Weiß, S., 1991: Mineralfundstellen Sächisches Erzgebirge.- Weise Verlag, München.

Wagenbreth, O., Wächtler, E., 1986: Der Freiberger Bergbau. Technische Denkmale und Geschichte. VEB Deutscher Verlag für Grundstoffindustrie Leipzig.

Wagenbreth O., Wächtler E., 1990: Bergbau im Erzgebirge – Technische Denkmale und Geschichte. Deutscher Verlag für Grundstoffindustrie, Leipzig.

Woidtke, S., 2006: Der Berg ist frei - Bergbau im Erzgebirge, 4, 263-369.

Wagenbreth, O., Wächtler, E., 1986: Der Freiberger Bergbau. Technische Denkmale und Geschichte. VED Dt. Verlag für Grundstoffindustrie. Leipzig.

Weber, W., 1986: Der Freiberger Bergbau. Lapis, 11, 7/8, 13-27.

Table 1

Prospective CHPM areas

AGG Greece							
Number	**Type of the selected area(s) (type "A" or type "B")**	**Depth(s) of the metal enrichment(s) (m)**	**Temperature / at these depths/ (°C)**	**Description of the metal enrichment(s)**			
				degree of the mineralization(s) (% or ppm)	***type of the mineralization(s)[1]***	***element(s)***	***area delineation(s)[2]***
1. Northern Lesvos ***(Stypsi and Argennos area)***	Type "A" *(The recorded temperature reaches 100°C at shallow depths)*	Unknown *(Data for the metal enrichment are limited only at surface or very shallow depth. It is believed that metal enrichment exists at great depths, but it has not been identified)*	<u>Stypsi geothermal field - Borehole temperature data:</u> • Exploration well STE-1: 250m → 100°C • Exploration well STE-2: 400m → 97.8°C 1015m → 91.4°C • Exploration well S-1: 1400m → 83.1°C (probably 2500m → 140°C)	<u>Stypsi area</u> ▪ 2 ppb Au, 120 ppb (0.120 ppm), up to 0.5 ppm Au, 0.10 g/t Au ▪ 5 ppb (0.005 ppm) - up to 1.7 ppm Ag ▪ 111 pm Cu, 843 ppm Cu, up to1330 ppm Cu ▪ 10 ppm Mo, 76 ppm Mo, 170 ppm Mo (maybe up to 330 ppm Mo) ▪ 142-160 ppm Pb, 339 ppm Pb, up to 1020 ppm Pb ▪ 65 ppm Zn, up to 815 ppm Zn ▪ 3 ppm Se, up to 13 ppm Se ▪ up to 4 ppm Te	<u>Stypsi area</u> • Porphyry type mineralization •Type: Sub-alk Cu-Mo • The porphyry-style mineralization consists of dense quartz stockworks containing molybdenite, bismuthinite, and galena, overprinted by intermediate-sulfidation epithermal quartz-carbonate veins	<u>Stypsi area</u> • Cu, Mo, Re, Bi, Pb, Se, Ag, Au • Main metals: Mo, Bi	<u>Stypsi geothermal area - Coordinates of wells</u> (decimal / WGS84): • Exploration well S-1 ϕ: 39.3238477 (39° 19′25.85″), λ: 26.21269 (26° 12′45.68′′) • Exploration well STE-1 ϕ: 39.28301 (39° 16′58.84″), λ: 26.22726 (26° 13′38.14′′) • Exploration well STE-2 ϕ: 39.2945 (39° 17′40.20″), λ: 26.21319 (26° 12′47.48′′)

[1] Like skarn, porphy, etc.

[2] There are 3 options for the indication of the area delineation: a. coordinates (latitude, longitude) of 1 point; b. coordinates (latitude, longitude) of 1 points and radius (m); c. coordinates (latitude, longitude) of more points.

			<u>Stypsi field - Heat flow density:</u> 200-400 mW/m^2 *(average global heat flow density 70 mW/m^2)*	▪ 4 ppm Bi, up to 36 ppm Bi ▪ up to 23 ppm Sn, 0.009-0.010% Sn ▪ up to 1.92 wt% Re in molybdenite ▪ 0.26-4.74 wt% Fe in sphalerite ▪ up to 8 ppm Sb ▪ up to 1176 ppm Ba ▪ up to 16 ppm As ▪ up to 22 ppm Co ▪ up to 40 ppm Cr ▪ up to 129 ppm Ce ▪ up to 12 ppm Hf ▪ up to 1 ppm Hg ▪ up to 5 ppm Ir ▪ up to 238 ppm Rb ▪ up to 22.2 ppm Sc ▪ up to 1.6 ppm Ta ▪ up to 42.2 ppm Th ▪ up to 12.8 ppm U ▪ up to 17 ppm Cs ▪ up to 3 ppm W ▪ up to 71.4 ppm La ▪ up to 71.4 ppm Nd ▪ up to 128 ppm Mn ▪ up to 5 ppm Be ▪ up to 0.53 wt% Ti ▪ up to 200 ppm V ▪ up to 12 ppm Y • Re in molybdenites: 300-10600 g/t (average: 2460 g/t)	• Critical and precious metal mineralogy: Re-rich molybdenite, bismuthinite		<u>Coordinates of polygon vertices of the Stipsi geothermal area</u> (WGS84): • Vertex A ϕ: 39^o 20′10.43”N, λ: 26^o 11′44.52”E • Vertex B ϕ: 39^o 20′03.86”N, λ: 26^o 14′47.97”E • Vertex C ϕ: 39.2625629 (39^o 15′45.23”), λ: 26.2514137 (26^o 15′05.09”) • Vertex D ϕ: 39^o 15′53.16”N λ: 26^o 12′19.26”E • Vertex E ϕ: 39^o 18′09.21”N λ: 26^o 10′39.72”E <u>Coordinates of polygon vertices of the Stipsi mineralization area</u> (WGS84): • Vertex A ϕ: 39^o 20′48.25”N λ: 26^o 11′19.47”E • Vertex B ϕ: 39^o 20′32.29”N λ: 26^o 19′29.35”E • Vertex C ϕ: 39^o 15′23.02”N λ: 26^o 19′17.91”E • Vertex D ϕ: 39^o 15′22.19”N λ: 26^o 11′35.52”E

			<u>Argenos geothermal field - Borehole temperature data:</u> • Exploration well GA-3 50-120m → 85-87°C 140m → 74°C • Exploration well AR-2 140-200m → 79-81°C 220-230m → 72°C • Exploration well AR-1 50-100m → 65-70°C 150m → 52.6°C 200m → 49.4°C <u>Argenos field - Heat flow density:</u> 200-400 mW/m^2 *(average global heat flow density 70 mW/m^2)*	<u>Megala Therma - Argenos area</u> ▪ 163 ppb Au, up to 21 ppm Au ▪ 5 ppb (0.005 ppm) Ag ▪ 220-1010 pm Cu ▪ 24 ppm Mo, ▪ up to 52 ppm Pb ▪ up to 119 ppm Zn ▪ up to 32 ppm Bi ▪ 0.009-0.010% Sn ▪ up to 3.5 wt% Fe ▪ up to 35.5 ppm Sb ▪ up to 1700 ppm Ba ▪ up to 73 ppm As ▪ up to 11 ppm Co ▪ up to 38 ppm Cr ▪ up to 273 ppm Ce ▪ up to 12 ppm Hf ▪ up to 2 ppm Hg ▪ up to 5 ppm Ir ▪ 70 ppm Rb ▪ up to 28.5 ppm Sc ▪ up to 4 ppm Se ▪ up to 1411 ppm Sr ▪ up to 2 ppm Ta ▪ up to 48.1 ppm Th ▪ up to 8.1 ppm U ▪ up to 3 ppm Cs ▪ up to 2.9 ppm W ▪ up to 140 ppm La ▪ up to 100 ppm Nd ▪ up to 1370 ppm Mn ▪ up to 3 ppm Be ▪ up to 0.73 wt% Ti ▪ up to 163 ppm V ▪ up to 25.9 ppm Y	<u>Megala Therma</u> • Type: Intermediate-sulfidation epithermal deposit • Metal-rich Ag-Au mineralization • Ore bodies: Veinlets, veins, breccia • Main host rocks: andesite, latite	<u>Megala Therma</u> • Au, Ag, Pb, Zn, Fe, Cu, Mo	<u>Argenos geothermal area - Coordinates of wells</u> (decimal / WGS84): • Exploration well GA-3 ϕ: 39.3750585 (39° 22′30.21″), λ: 26.2543881 (26° 15′15.80′′) • Exploration well AR-2 ϕ: 39.3743193 (39° 22′27.55″), λ: 26.2512994 (26° 15′4.68′′) • Exploration well AR-1 ϕ: 39.3761844 (39° 22′34.26″), λ: 26.2489397 (26° 14′56.18′′) <u>Coordinates of polygon vertices of the Argenos geothermal field</u> (decimal / WGS84): • Vertex A ϕ: 39.3772512 (39° 22′38.10″), λ: 26.2675716 (26° 16′03.26′′) • Vertex B ϕ: 39.3696311 (39° 22′10.67″), λ: 26.2621211 (26° 15′43.64′′)

							• Vertex C ϕ: 39.3762283 (39º 22′34.42″), λ: 26.2117963 (26º 12′42.47′′) • Vertex D ϕ: 39.3781011 (39º 22′41.16″), λ: 26.209658 (26º 12′34.77′′) • Vertex D ϕ: 39.3781011 (39º 22′41.16″), λ: 26.209658 (26º 12′34.77′′) • Vertex E ϕ: 39.3834351 (39º 23′0.37″), λ: 26.2246788 (26º 13′28.84′′) • Vertex Z ϕ: 39.3831918 (39º 22′59.49″), λ: 26.2352461 (26º 14′06.89′′) • Vertex L ϕ: 39.3777702 (39º 22′39.97″), λ: 26.2534404 (26º 15′12.39′′) <u>Coordinates of polygon vertices of the Megala Therma - Argenos mineralization area</u> (WGS84): • Vertex A ϕ: 39º 22′36.88″N λ: 26º 12′31.29″E

							• Vertex B ϕ: 39º 23′0.37″ N, λ: 26º 13′28.84′′ E • Vertex C ϕ: 39º 22′59.49″ N λ: 26º 14′06.89″ E • Vertex D ϕ: 39º 22′39.97″ N λ: 26º 15′12.39″ E • Vertex E ϕ: 39º 22′38.10″ N λ: 26º 16′03.26″ E • Vertex F ϕ: 39º 22′35.26″ N λ: 26º 17′14.31″ E • Vertex G ϕ: 39º 22′25.21″ N λ: 26º 18′17.28″ E • Vertex H ϕ: 39º 20′32.29″N λ: 26º 18′17.28″ E • Vertex I ϕ: 39º 20′48.25″N λ: 26º 11′19.47″E <u>Coordinates of polygon vertices of the prospective CHPM area</u> (WGS84): • Vertex A ϕ: 39º 22′36.88″N λ: 26º 12′31.29″E • Vertex B ϕ: 39º 23′00.37″N λ: 26º 13′28.84″E

							• Vertex C ϕ: 39° 22′59.49”N λ: 26° 14′06.89”E • Vertex D ϕ: 39° 22′39.97”N λ: 26° 15′12.39”E • Vertex E ϕ: 39° 22′38.10”N λ: 26° 16′03.26”E • Vertex F ϕ: 39° 22′35.26”N λ: 26° 17′14.31”E • Vertex G ϕ: 39° 22′25.21”N λ: 26° 18′17.28”E • Vertex H ϕ: 39° 20′32.29”N λ: 26° 19′29.35”E • Vertex I ϕ: 39° 15′23.02”N λ: 26° 19′17.91”E • Vertex J ϕ: 39° 15′22.19”N λ: 26° 11′35.52”E • Vertex K ϕ: 39° 18′09.21”N λ: 26° 10′39.72”E • Vertex L ϕ: 39° 20′48.25”N λ: 26° 11′19.47”E

2. Western Milos	Type "A" (*The recorded temperature exceeds 100°C a few km eastward, in the central part of Milos island. The values of geothermal gradient and the heat flow density are really high in Western Milos)*	Unknown *(Data for the metal enrichment are limited only at surface or very shallow depth. It is believed that metal enrichment exists at great depths, but it has not been identified)*	<u>Western Milos - Heat flow density:</u> 300-400 mW/m^2 *(average global heat flow density 70 mW/m^2)* <u>Western Milos geothermal field - Borehole data:</u> • Well in Rivari 65m → 44°C • Well in Emporios 70m → 39°C • Wells in Xylokeratia 65m → 41°C 70m → 40°C 70m → 43°C 75m → 41.5°C	<u>Profitis Ilias</u> ▪ Estimated reserves: 5 Mt (million tonnes) of ore grading at 4.4 g/t Au and 43 ppm Ag or 5.5 Mt at 4.4 g/t Au and 43 g/t Ag ▪ < 0.5 wt.% Fe and 0.2-1.2 wt.% Fe in sphalerite	<u>Profitis Ilias</u> • Type: Epithermal type rich in Au-Ag-Te, Intermediate sulfidation • Ore bodies: Massive to semi-massive ore, veins • Main host rocks: Rhyolite, pyroclastic rocks • Veins widths are up to 3m and extend to depths of at least 300m.	<u>Profitis Ilias</u> • Pb, Zn, Ag, Au, Cu, Sb, Te	<u>Coordinates of polygon vertices of the Western Milos geothermal field</u> (decimal / WGS84): • Vertex R ϕ: 36.6891267 (36° 41′20.86″), λ: 24.4344284 (24° 26′03.94′′) • Vertex S ϕ: 36.7490052 (36° 44′56.42″), λ: 24.3518067 (24° 21′06.50′′) • Vertex T ϕ: 36.6458091 (36° 38′44.91″), λ: 24.3219754 (24° 19′19.11′′) • Vertex Y ϕ: 36.6693392 (36° 40′09.62″), λ: 24.4479295 (24° 26′52.55′′)

			<u>Western Milos geothermal field:</u> <u>Geothermal gradient</u> up to 3.78°C/10m or 37.8°C/100m *(mean geothermal gradient 3°C/00m)*	<u>Chondro Vouno</u> ▪ 3.3 Mt grading 4.2 g/t Au (cut-off grade 2 g/t) or 2.2 Mt grading 5.14 g/t Au (cut-off grade 2.5 g/t) or 1.2 Mt at 1.0 g/t Au and 124 g/t Ag ▪ < 0.5 wt.% Fe and 0.2-1.2 wt.% Fe in sphalerite	<u>Chondro Vouno</u> • Type: Epithermal type - Intermediate sulfidation • Ore bodies: Veins • Main host rocks: Pyroclastic rocks	<u>Chondro Vouno</u> • Pb, Zn, Ag, Au, Cu, Sb, Te	<u>Central Milos high enthalpy geothermal field</u> - <u>Coordinates of geothermal wells</u> (decimal / WGS84): • Exploration well MZ-1 ϕ: 36.7046457 (36° 42′16.72″ N), λ: 24.4872448 (24° 29′14.08″ E) • Exploration well M-1 ϕ: 36.7000996 (36° 42′0.36″ N), λ: 24.498777 (24° 29′55.60″ E) • Exploration well M-2 ϕ: 36.7107506 (36° 42′38.70″ N), λ: 24.5009214 (24° 30′03.32″ E) • Well MA-1 ϕ: 36.735605 (36° 44′08.18″ N), λ: 24.448729 (24° 26′55.42″ E)

			<u>Central Milos geothermal field - Borehole temperature data:</u> • Exploration well MZ-1 837-1080m → 310-320°C • Exploration well M-1 1150m → 323°C • Exploration well M-2 1150-1200m → 318°C • Well MA-1 827m → 270°C 1000m → 310°C (?) • EGS system can be developed in fractured rocks (Western Milos) in the vicinity of the Central Milos active hydrothermal system (proven high temperature geothermal field)	<u>Triades-Galana</u> ▪ Reported estimated reserves: 10 Mt with a mean Ag content: 500 g/t ▪ Resources: 1.2 Mt at 4.2g/t Au or 1.2 Mt at 1 g/t Au and 124 g/t Ag ▪ up to 4.1 ppm Au ▪ up to 855 ppm Ag ▪ up to 265 mg/kg Mo ▪ up to 848 mg/kg W ▪ Tetraedrites/ tennantites contain: up to 15.07 wt.% Ag, 6.3-10.9 wt.% Zn, up to 7.37 wt.% Cd, up to 7.42 wt.% Hg, up to 9.34 wt.% Pb ▪ Enargites contain: up to 2.57 wt.% or 7.1 wt.% Ag ▪ Samples from Triades: up to 265 mg/kg Mo, up to 15 wt.% Zn, up to 3.27 wt.% Pb, up to 3.28% Cu, up to 2370 mg/kg Cd, up to 0.7 wt.% As, up to 2.2 wt.% Sb, up to 89 mg/kg Tl, up to 848 mg/kg W ▪ Samples from Galana: up to 225 mg/kg Cd, up to 305 mg/kg As, up to 78 mg/kg Sb, up to 440 mg/kg W ▪ Oxidized hydrothermal breccias contain up to: 176 ppm Mo, 677 ppm W, 2575 ppm Bi	<u>Triades-Galana</u> • Type: Epithermal type - Intermediate sulfidation • Ore bodies: Veins • Main host rocks: Dacites, andesites, pyroclastic and volcano-sedimentary rocks	<u>Triades-Galana</u> • Ag, Au, As, Bi, W, Mo	<u>The Profitis Ilias deposit - Coordinates of polygon vertices of the area</u> (WGS84): • Vertex A ϕ: 36° 40′53.30″N λ: 24° 22′26.48″E • Vertex B ϕ: 36° 40′52.72″N λ: 24° 23′12.63″E • Vertex C ϕ: 36° 40′12.17″N λ: 24° 23′09.83″E Vertex D ϕ: 36° 40′13.95″N λ: 24° 22′23.90″E <u>The Chondro Vouno deposit - Coordinates of polygon vertices of the area</u> (WGS84): • Vertex A ϕ: 36° 41′03.57″N λ: 24° 21′52.80″E • Vertex B ϕ: 36° 41′08.05″N λ: 24° 22′35.86″E • Vertex C ϕ: 36° 40′40.19″N λ: 24° 22′34.26″E • Vertex D ϕ: 36° 40′41.36″N λ: 24° 21′56.39″E

				<u>Kondaros-Katsimouti-Vani (KKV)</u> • up to 24 mg/kg Mo • up to 439 mg/kg W (Kondaros-Katsimouti) • up to 31.8 wt.% Pb • up to 16.5 wt.% Zn • up to 1 mg/kg Bi • up to 247 mg/kg Cd (in Kondaros) • up to 769 mg/kg Cd (in Katsimouti) • up to 243 mg/kg Sb (in Kondaros) • up to 178 mg/kg Sb (in Katsimouti) • up to 36 mg/kg As (in Kondaros) • up to 42 mg/kg As (in Katsimouti) • Tetrahedrites contain: ▪ 24.3-32.05 wt. % Cu ▪ 26.5-28.5 wt.% Sb ▪ up to 16.2 wt.% Ag or up to 23.06 wt.% Ag ▪ 3-5 wt.% Zn ▪ up to 7.5 wt.% Pb ▪ up to 5.39 wt.% Cd • Sphalerite contains: ▪ 0.8-2.5 wt.% Fe ▪ up to 0.3 wt.% In • Polybasite contains: ▪ up to 70 wt.% Ag ▪ up to 8.3 wt.% Cu ▪ 10.8 wt.% Sb ▪ < 1.5 wt.% Pb • Vani deposit: ▪ fossil stratabound Mn-Ba-Pb-Zn-As-Sb-W-rich hydrothermal deposit	<u>Kondaros-Katsimouti-Vani</u> • Type: Epithermal type - Intermediate sulfidation • Ore bodies: Massive to semi-massive ore, veins, stratabound and stratiform layers • Main host rocks: Dacites, andesites, pyroclastic and volcano-sedimentary rocks	<u>Kondaros-Katsimouti-Vani</u> • Ag, Au, As, Bi, W, Mo	<u>The Triades Galana deposit area- Coordinates of polygon vertices</u> (WGS84): • Vertex A ϕ: 36° 42′50.74”N λ: 24° 20′13.11”E • Vertex B ϕ: 36° 42′50.74”N λ: 24° 20′52.05”E • Vertex C ϕ: 36° 42′08.82”N λ: 24° 20′52.05”E • Vertex D ϕ: 36° 42′08.82”N λ: 24° 20′09.01”E <u>The Kondaros-Katsimouti-Vani deposit area - Coordinates of polygon vertices of the area</u> (WGS84): • Vertex A ϕ: 36° 45′04.37”N λ: 24° 21′15.33”E • Vertex B ϕ: 36° 44′48.33”N λ: 24° 21′12.56”E • Vertex C ϕ: 36° 43′40.05”N λ: 24° 22′34.41”E • Vertex D ϕ: 36° 43′26.24”N λ: 24° 22′07.99”E • Vertex E ϕ: 36° 44′22.13”N λ: 24° 20′15.81”E

				▪ two types of deposits have been recognized: (a) “high-temperature” hydrothermal Mn deposits and (b) bedded hydrothermal Mn deposits ▪ enriched in Mn, Pb, Zn, Cu, Ba, As Sb, Cd, Tl, Co, W, Mo, Sr, Ag, U, Li, i.e. ▪ up to 428-630 ppm *or* up to 2870 mg/kg W ▪ up to 24-27 ppm Mo ▪ up to 69 wt% MnO ▪ up to 6.6 wt% Pb ▪ up to 1.2 wt% Zn ▪ up to 0.8 wt% TiO_2 ▪ up to 3679 ppm Sb ▪ up to 3515 ppm As ▪ up to 2873 ppm W ▪ up to 3499 ppm Sr ▪ up to 114 ppm Ag ▪ up to 7.7 ppm Eu ▪ 7.7-91 ppm Ce ▪ 4.5-54.3 ppm La ▪ 5.6-34.5 ppm Y ▪ 1.7-18.6 ppm Nb ▪ 0.8-6.4 ppm Pr ▪ 3.5-26.3 ppm Nd ▪ 0.8-5.7 ppm Sm ▪ 1.3-6.7 ppm Gd ▪ up to 0.8 ppm Tb ▪ up to 5.3 ppm Dy ▪ up to 1.1 ppm Ho ▪ up to 4.1 ppm Er ▪ up to 0.7 ppm Tm ▪ up to 5.3 ppm Yb ▪ up to 0.9 ppm Lu ▪ up to 8.1 ppm Hf ▪ 3.9-13.1 ppm Ta ▪ 1.0-10.4 ppm Th ▪ 1.2-19.0 ppm U			<u>Coordinates of polygon vertices of the prospective CHPM area</u> (WGS84): • Vertex A ϕ: 36.6891267 (36° 41′20.86”), λ: 24.4344284 (24° 26′03.94′′) • Vertex B ϕ: 36.7490052 (36° 44′56.42”), λ: 24.3518067 (24° 21′06.50′′) • Vertex C ϕ: 36.6458091 (36° 38′44.91”), λ: 24.3219754 (24° 19′19.11′′) • Vertex D ϕ: 36.6693392 (36° 40′09.62”), λ: 24.4479295 (24° 26′52.55′′)

3. Aristino Alexandroupolis - Evros Delta area	Type "A" (*The recorded temperature exceeds 100°C)*	Unknown *(Data for the metal enrichment are limited only at surface or very shallow depth. It is believed that metal enrichment exists at great depths, but it has not been identified)*	<u>Aristino Alexandroupolis geothermal field</u> - <u>Borehole termperature data:</u> • Exploration well AA-1 360m → 72.3°C • Production well AA-1P 216m → 51.8°C • Exploration well AA-3 340m → 86.8°C • Production well AA-3P 360m → 89°C • Exploration well AA-4 370m → 60.1°C • Production well AA-4P 440m → 64°C • Well KO-1 120m → 79°C • Well E-3 235m → 89°C	<u>Evros - Pefka</u> • Past mining operation: 3 Kt ore at 7 wt.% Cu • Au: up to 10 ppm • Mo: up to 23.5 ppm • Bi: up to 105 ppm • Te: up to 468 ppm • In: up to 675 ppm • Ga: up to 17 ppm • Ge: up to 16 ppm • Ag: >100 ppm • Cu: > 1 wt.% • As:> 1 wt.% • Te: >1000 ppm	<u>Evros - Pefka</u> • Type: Epithermal type - High and Intermediate sulfidation • Cu-Au-Ag-Te deposit • Ore bodies: Veins • Main host rocks: andesitic to rhyolitic volcanic rocks, i.e. tuffs, andesite, rhyodacite, latite • The andesites, dacites and rhyodacites occur in agglomerate tuffs, lava flows, domes and ash-flow tuffs • Critical and precious metal mineralogy: tetradymite, hessite, stützite, altaite, native Te, native Au, coloradoite, sylvanite goldfieldite	<u>Evros - Pefka</u> • Cu, Au, Ag, Pb, Zn, Bi, Sn, Ge, Ga, In, Mo, V, As, Hg, Te, Se	<u>Aristino Alexandroupolis geothermal field</u> - <u>Coordinates of wells</u> (decimal / WGS84): • Wells AA-1 & AA-1P ϕ: 40.8758432 (40° 52′33.04″), λ: 26.0088844 (26° 0′31.98′′) • Well AA-3 ϕ: 40.8867651 (40° 53′12.35″), λ: 25.9940676 (25° 59′38.64′′) • Well AA-3P ϕ: 40.8866479 (40° 53′11.93″), λ: 25.9940797 (25° 59′38.69′′) • Well AA-4 ϕ: 40.8760431 (40° 52′33.76″), λ: 25.9973566 (25° 59′50.48′′) • Well AA-4P ϕ: 40.8761064 (40° 52′33.98″), λ: 25.9975442 (25° 59′51.16′′) • Well KO-1 ϕ: 40.8817545 (40° 52′54.32″), λ: 26.0122028 (26° 0′43.93′′) • Well E-3 ϕ: 40.8870732 (40° 53′13.46″), λ: 26.0130177 (26° 0′46.86′′)

			<u>Aristino Alexandroupolis field - Geothermal gradient:</u> 4.5-21°C/100m *(mean geothermal gradient 3°C/100m)* <u>Aristino Alexandroupolis field</u> - <u>Heat flow density:</u> 70-300 mW/m^2	<u>Evros - Loutros</u> • The mineralized barite veins are enriched in: ▪ Mo (up to ≤ 15.6 g/t) ▪ As (up to 1058 g/t) ▪ Ag (up to 31 g/t) • Ag: up to 31 ppm	<u>Evros - Loutros</u> • Type: Epithermal type - Intermediate sulfidation • Ore bodies: Veins • Main host rocks: Rhyolite	<u>Evros - Loutros</u> • Fe, Pb, As, Ag	<u>Coordinates of polygon vertices of the Aristino Alexandroupolis geothermal field</u> (decimal/WGS84): • Vertex A ϕ: 40.8556286 (40° 51′20.26″), λ: 25.9563682 (25° 57′22.93′′) • Vertex B ϕ: 40.9092449 (40° 54′33.28″), λ: 25.9763494 (25° 58′34.86′′) • Vertex C ϕ: 40.898444 (40° 53′54.40″), λ: 26.1053902 (26° 06′19.40′′) • Vertex D ϕ: 40.8472987 (40° 50′50.28″), λ: 26.1079398 (26° 06′28.58′′) <u>Coordinates of deep hydrocarbon exploration wells in the Evros Delta area</u> (WGS84): • Borehole DEV-1 ϕ: 40° 49′50″, λ: 26° 06′15′′ • Borehole DEV-2 ϕ: 40° 48′56.04″, λ: 26° 06′58.42′′ • Borehole DEV-3 ϕ: 40° 49′10.44″, λ: 26° 09′ 14.01′

			<u>Evros Delta area - Borehole temperature data:</u> • Exploration well DEV-1 3975m → 136°C 4229m → 146°C • Exploration well DEV-2 3000m → 100°C • Exploration well DEV-3 2650m → 104°C 2860m → 108°C <u>Evros Delta area - Mean geothermal gradient:</u> 24-37°C/km *(mean geothermal gradient 30°C/km)* <u>Evros Delta area - Heat flow density:</u> 50-70 mW/m^2 *(average global heat flow density 70 mW/m^2)*				<u>Coordinates of polygon vertices of the Pefka - Loutros mineralization area</u> (WGS84): • Vertex A ϕ: 40° 55′20.91″ N λ: 26° 00′15.38″ E • Vertex B ϕ: 40° 55′09.59″ N λ: 26° 06′37.17″ E • Vertex C ϕ: 40° 50′37.44″ N λ: 26° 06′35.04″ E • Vertex D ϕ: 40° 52′14.61″ N λ: 26° 00′16.86″ E <u>Coordinates of polygon vertices of the prospective CHPM area</u> (WGS84): • Vertex A ϕ: 40° 50′41.73″ N λ: 25° 56′08.83″ E • Vertex B ϕ: 40° 56′50.81″ N λ: 25° 56′10.28″ E • Vertex C ϕ: 40° 55′55.32″ N λ: 26° 16′45.93′′E • Vertex D ϕ: 40° 45′03.51″ N λ: 26° 01′50.08″ E

4. Sappes	Type "B" *(The recorded temperature exceeds 40°C. The heat flow density is higher than average, but temperature of >100°C has not been measured yet at great depths)*	Unknown *(Data for the metal enrichment are limited only at surface or very shallow depth. It is believed that metal enrichment exists at great depths, but it has not been identified)*	<u>Sappes geothermal field - Borehole temparature data:</u> • Exploration well GS-4 440m → 40.6°C • Production well GS-3P 360m → 38.9°C <u>Sappes field - Heat flow density:</u> 70-150 mW/m^2 *(average global heat flow density 70 mW/m^2)*	<u>Maronia:</u> • Re: 0.12-4.21 wt.% in molybdenite (2.88 wt.% Re) • Re in molybdenites: 1200-28800 g/t (average: 7600 g/t) • Surface samples: ▪ up to 7600 ppm Mo ▪ up to 5460 ppm Cu ▪ up to 1 ppm Au • Bulk ore analyses from porphyry-style ore: ▪ average grade of 0.1 g/t Au ▪ up to 2763 g/t Cu ▪ up to 3909 g/t Mo • Drilling yielded a 10 m intercept grading: ▪ 12 ppm Au ▪ 17 ppm Ag ▪ 2 wt.% Cu • REE: 133-221 ppm (propylitic alteration) <u>Maronia:</u> ----	<u>Maronia:</u> • Type: Tertiary porphyry Cu-Mo-Re-Au type mineralization • Ore bodies: Stockwork, disseminated, veins • Main host rocks: porphyry microgranite • Surface exposure 0.5 km × 0.5 km • Critical and precious metal mineralogy: Re-rich molybdenite, bismuthinite <u>Maronia:</u> • Type: Skarn • Main host rocks: Pluton of of gabbroic-monzogabbroic-monzonitic composition in	<u>Maronia:</u> • Cu, Fe, Mo, Au, Pb, Zn, Sb, As • Main metals: Cu, Au, Mo • Critical & rare metals: Re <u>Maronia:</u> • The andradites are sometimes Ti-rich and Ti-Cr-Zr-rich	<u>Sappes geothermal field - Coordinates of wells</u> (decimal/WGS84): • Well GS-4 ϕ: 41.01246 (41° 0′44.86″), λ: 25.698292 (25° 41′53.85′′) • Well GS-3P ϕ: 40.9660602 (40° 57′57.82″), λ: 25.6099206 (25° 36′35.71′′)

				<u>Petrota Graben / Perama Hill</u> • Underground reserves: 9.697 Mt at 3.13 g/t Au and 4 g/t Ag, with a total of 0.975 Moz Au and 1.151 Moz Ag • Se: up to 15.9 wt.% in bismuthinite, up to 1.9 wt.% in tetradymite • Content of sylvanite: ▪ Au: 25.7-34.8 wt.%, ▪ Ag: 5.4-13.7 wt.% • Native Au: 98.99 wt.% Au • The upper oxidized part of Perama Hill deposit is free of As, Pb or other heavy metals • Te: up to 45 ppm	contact with calcareous schists and marbles <u>Petrota Graben / Perama Hill</u> • Type: Au-Ag-Te-Se epithermal type - High and Intermediate sulfidation • Ore bodies: (a) upper parts: oxidized (stratabound) (b) deeper parts: disseminated, vein, massive sulfide lodes • Main host rocks: Andesite, conglomerate, sandstone • Critical and precious metal mineralogy: bismuthinite, heyrovskyite, gustavite-lillianite solid solution, hessite, petzite, sylvanite, krennerite, calaverite, coloradoite, native Te, melonite	<u>Petrota Graben / Perama Hill</u> • Au, Ag, Cu, Bi, Pb, Te, Se • Main metals: Cu, As, Au, Bi • Critical & rare metals: Te	<u>Coordinates of polygon vertices of the Sappes geothermal field</u> (decimal/WGS84): • Vertex A ϕ: 40.9535371 (40° 57′12.73″), λ: 25.5690578 (25° 34′08.61′′) • Vertex B ϕ: 40.9512081 (40° 57′04.35″), λ: 25.6404153 (25° 38′25.50′′) • Vertex C ϕ: 40.9766265 (40° 58′35.86″), λ: 25.7132164 (25° 42′47.58′′) • Vertex D ϕ: 41.0266147 (41° 01′35.81″), λ: 25.7252458 (25° 43′30.88′′) • Vertex E ϕ: 41.02727 (41° 01′38.17″), λ: 25.6732355 (25° 40′23.65′′)

				<u>Petrota Graben / Mavrokoryfi</u> • Pb: up to 1.5 wt.% • Surface grab samples: ▪ up to 1.5 ppm Au ▪ up to 162 ppm Ag <u>Sappes-Kassiteres-Kirki-Esimi/ Pagoni Rachi</u> • Re-enriched molybdenite mineralization • Re in molybdenites: 379-46900 g/t (average: 16318 g/t) • Surface samples: ▪ up to 5.1 ppm (g/t) Au (average: 0.57 g/t Au) ▪ up to 0.5 wt.% Cu or 1 wt.% Cu ▪ up to 40 ppm Te ▪ up to 2000 ppm (2000 g/t) Mo ▪ up to 20 ppm (20 g/t) Re	<u>Petrota Graben / Mavrokoryfi</u> • Type: Cu-Ag-Au-Te epithermal type - High sulfidation • Ore bodies: vein, massive sulfide lodes, breccia • Main host rocks: Andesite, hyaloclastite <u>Sappes-Kassiteres-Kirki-Esimi / Pagoni Rachi</u> • Type: Tertiary porphyry type mineralization • porphyry-epithermal system • Ore bodies: stockwork, disseminated, veins • Main host rocks: Granodiorite - tonalite porphyry	<u>Petrota Graben / Mavrokoryfi</u> • Ag, Au, Cu, Te • Main metals: Cu, Sb, Ag, Au • Critical & rare metals: Te <u>Sappes-Kassiteres-Kirki-Esimi/ Pagoni Rachi</u> • Cu, Mo, Fe, Re • Main metals: Cu, Au, Mo • Critical & rare metals: Te, Re	<u>Coordinates of polygon vertices of the Sappes – Kassiteres - Esimi mineralization area</u> (WGS84): • Vertex A ϕ: 41° 02′26.99″ N λ: 25° 41′31.87″ E • Vertex B ϕ: 41° 02′26.99″ N λ: 26° 02′57.29″ E • Vertex C ϕ: 40° 58′0.71″ N λ: 26° 02′21.27″ E • Vertex D ϕ: 40° 57′43.99″ N λ: 25° 43′18.79″ E

				(up to 4.69 wt.% Re in molybdenite) ▪ up to 0.03 ppd Pd • up to 6 wt.% Mo in rheniite • The Pagoni Rachi prospect is highly anomalous in Au <u>Sappes-Kassiteres-Kirki-Esimi/ Konos Hill</u> • Re-enriched molybdenite mineralization • Re in molybdenites: 750-31100 g/t (average: 15621 g/t) • Au: 0.04 g/t • up to 6 wt.% Mo in rheniite	• Surface exposure of quartz stockworks: 1 km × 1 km • Critical and precious metal mineralogy: bornite, Re-rich molybdenite, native Au, rheniite, tetradymite, hessite, petzite, stützite, altaite, aikinite, Ag-Au, hammarite, berryite, lindströmite, gustavite-lillianite solid solution, Se-Bi sulfosalts, wittichenite <u>Sappes-Kassiteres-Kirki-Esimi/ Konos Hill</u> • Type: Tertiary porphyry type mineralization • Ore bodies: stockwork, disseminated • Main host rocks: Granodiorite porphyry	<u>Sappes-Kassiteres-Kirki-Esimi/ Konos Hill</u> • Cu, Mo, Fe, Re • Main metals: Cu, Au, Mo • Critical & rare metals: Te, Re	<u>Coordinates of polygon vertices of the Petrota - Maronia mineralization area</u> (WGS84): • Vertex A ϕ: 40° 53′46.37″ N λ: 25° 27′31.14″ E • Vertex B ϕ: 40° 55 20.72″ N λ: 25° 27′41.74″ E • Vertex C ϕ: 40° 56′36.21″ N λ: 25° 32′37.70″ E • Vertex D ϕ: 40° 56′13.14″ N λ: 25° 42′30.39″ E • Vertex E ϕ: 40° 51′29.24″ N λ: 25° 39′42.11″ E • Vertex F ϕ: 40° 52′07.95″ N λ: 25° 35′19.65″ E • Vertex G ϕ: 40° 51′25.86″ N λ: 25° 33′41.00″ E • Vertex H ϕ: 40° 52′23.89″ N λ: 25° 30′29.49″ E

					• Surface exposure: 3 km × 2 km • Critical and precious metal mineralogy: Re-rich molybdenite, rheniite		
				<u>Sappes-Kassiteres-Kirki-Esimi/ Kassiteres-Koryfes</u> • Surface samples: ▪ up to 700 ppm Cu ▪ up to 0.5 ppm Au • The highest Ag-content (up to 9.6 wt% Ag) occurs in Sb-rich members of tetrahedrite-group minerals • High-grade veins contain up to ▪ 0.43 wt% Cu, ▪ 0.7 wt% Pb, ▪ 1.23 wt% Zn and ▪ 190 ppm Mo	<u>Sappes-Kassiteres-Kirki-Esimi/ Kassiteres-Koryfes</u> • Type: Tertiary porphyry type mineralization • Ore bodies: Disseminated, vein, stockwork • Main host rocks: microdiorite porphyry • Critical and precious metal mineralogy: Tetradymite	<u>Sappes-Kassiteres-Kirki-Esimi / Kassiteres-Koryfes</u> • Cu, Au, Mo, Pb, Zn, Ag, Bi, Te	<u>Coordinates of polygon vertices of the Xylagani mineralization area</u> (WGS84): • Vertex A ϕ: 40° 59′40.32″ N λ: 25° 26′38.32″ E • Vertex B ϕ: 40° 59′40.32″ N λ: 25° 29′26.73″ E • Vertex C ϕ: 40° 58′34.97″ N λ: 25° 29′15.42″ E • Vertex D ϕ: 40° 58′28.20″ N λ: 25° 26′49.52″ E
				<u>Sappes-Kassiteres-Kirki-Esimi/ Myli</u> • Re-enriched	<u>Sappes-Kassiteres-Kirki-Esimi/ Myli</u>	<u>Sappes-Kassiteres-Kirki-Esimi/ Myli</u>	

				molybdenite mineralization • Re in molybdenites: 440-19200 g/t (average: 2733 g/t) • Au: 0.09 g/t • Grades: ▪ up to 2100 g/t Cu, ▪ up to 210 g/t Mo, ▪ up to 0.2 g/t Au	• Type: telescoped porphyry - epithermal system • Ore bodies: stockwork, disseminated, vein • Main host rocks: Granodiorite porphyry • Surface exposure: 0.5 km × 1 km • Critical and precious metal mineralogy: Re-rich molybdenite, native Au	• Cu, Mo, Au, Re, Pb, Zn, Ag, As • Main metals: Cu, Au, Mo	<u>Coordinates of polygon vertices of the prospective CHPM area</u> (WGS84): • Vertex A ϕ: 40° 53′46.37″ N λ: 25° 27′31.14″ E • Vertex B ϕ: 40° 59′40.32″ N λ: 25° 26′38.32″ E • Vertex C ϕ: 41° 04′05.21″ N λ: 25° 45′04.01′′E • Vertex D ϕ: 40° 50′42.99″ N λ: 25° 43′52.18″ E • Vertex E ϕ: 40° 51′29.24″ N λ: 25° 39′42.11″ E • Vertex F ϕ: 40° 52′07.95″ N λ: 25° 35′19.65″ E • Vertex G ϕ: 40° 51′25.86″ N λ: 25° 33′41.00″ E • Vertex H ϕ: 40° 52′23.89″ N λ: 25° 30′29.49″ E
				<u>Sappes-Kassiteres-Kirki-Esimi / Viper</u> • High-grade gold-sulfide zone (Au-Cu-Ag deposit) • Reserves of 1.2 million tons at 18.4 g/t Au • Resources of 0.28 Mt at ▪ 19.5 g/t Au, ▪ 9 g/t Ag, and	<u>Sappes-Kassiteres-Kirki-Esimi/ Viper</u> • Type: epithermal type - High and intermediate sulfidation • Ore bodies: Breccia, disseminated, veinlets, vugs fillings	<u>Sappes-Kassiteres-Kirki-Esimi/ Viper</u> Cu, Au, As, Sb, Ag, Pb, Zn, Bi, Te, Se	

				▪ 0.4% Cu • Measured resources of 710 kt at ▪ 22.2 g/t Au, ▪ 11.5 g/t Ag, ▪ 0.4% Cu • Inferred resources of 1109 kt at ▪ 17.2 g/t Au, ▪ 8.8 g/t Ag, ▪ 0.3% Cu • cut-off grades of 4 g/t Au • native Au at 200-250m depth (53.3 g/t Au in 40m drill core) • native Au may contain up to 9 wt.% Ag <u>Sappes-Kassiteres-Kirki -Esimi/ Scarp</u> • Resources: 0.87 Mt at ▪ 2.2 g/t Au, and ▪ 1.5 g/t Ag • cut-off grades of 1 g/t Au	• Dimensions of economic mineralization: 550 x 1310m, ~60m thick, at depth of 200-240m • Main host rocks: Granodiorite-tonalite porphyry, tuff, rhyodacite <u>Sappes-Kassiteres-Kirki-Esimi / Scarp</u> • Type: epithermal type - High sulfidation • Ore bodies: Breccia, disseminated • Main host rocks: Granodiorite-	<u>Sappes-Kassiteres-Kirki-Esimi/ Scarp</u> • Cu, Au	

				<u>Sappes-Kassiteres-Kirki Esimi/ St. Demetrios</u> • Reserves of 0.21 Mt at ▪ 3.5 g/t Au, and ▪ 5.2 g/t Ag • Reserves of 260000 t at 3.5 g/t Au • cut-off grades of 1 g/t Au • Au content: ▪ 2 g/t Au at surface (oxidized mineralization), and ▪ grades up to 22 g/t Au at depth (pyrite-chalcopyrite-enargite mineralization) • Native Au: 97.98 wt.% Au 0.4-1.6 wt% Ag	tonalite porphyry, tuff, rhyodacite <u>Sappes-Kassiteres-Kirki-Esimi/ St. Demetrios</u> • Type: epithermal type - High and intermediate sulfidation • Ore bodies: Breccia, disseminated, veinlets, vugs fillings • Main host rocks: Granodiorite-tonalite porphyry, tuff, rhyodacite • Critical and precious metal mineralogy: Calaverite, sylvanite, hessite, stützite, altaite, native Au, goldfieldite	<u>Sappes-Kassiteres- -Kirki-Esimi/ St. Demetrios</u> • Cu, Au, As, Sb, Ag, Pb, Zn, Bi, Te, Se • Main metals: Cu, As, Au, Ag • Critical & rare metals: Te	

				<u>Sappes-Kassiteres-Kirki Esimi/ St. Barbara</u> • Three (3) stages are recognized in the vein-type mineralization at St Barbara. • Oxidized alunitic breccia rock samples (stage I) contain: ▪ Pb (up to 950 ppm), ▪ Bi (up to 640 ppm), ▪ Au (800 ppb), ▪ Te (up to 13 ppm), ▪ Se (up to 12 ppm). • Stage II material: 11 g/t Au • Oxidized hydrothermal breccia (stage II) matrix material contain up to: ▪ 370 ppm Cu, ▪ 820 ppm As, ▪ 72 ppm Mo, ▪ 23 ppm Se, ▪ 2 ppm Te, ▪ 7 ppm Ag, ▪ 2 ppm Au. • Stage II material: ▪ Pyrite: up to 0.23 wt.% As, and <0.07 wt.% Au ▪ Tetrahedrite-group minerals: < 0.7 wt.% Ag ▪ Altaite: 1.2 wt.% Se, 0.1 wt.% Ag	<u>Sappes-Kassiteres-Kirki-Esimi/ St. Barbara</u> • Type: epithermal type - High and intermediate sulfidation • Ore bodies: veins, breccia • Main host rocks: Andesite, tuff, monzodiorite • Critical and precious metal mineralogy: bornite, hessite, petzite, sylvanite, altaite, native Te, native Au	<u>Sappes-Kassiteres-Kirki-Esimi/ St. Barbara</u> • Cu, Au, As, Sb, Ag, Pb, Zn, Bi, Te, Se • Main metals: Cu, Au, Ag • Critical & rare metals: Te	

				▪ Hessite: 61.2-63.6 wt.% Ag, up to 0.3 wt% Au ▪ Sylvanite: 12 wt.% Ag • Stage III material (quartz veins): ▪ Pyrite: up to 0.85 wt% As ▪ Bulk rock sample analyses: up to 0.4 ppm Au 21 ppm Ag <u>Sappes-Kassiteres-Kirki-Esimi/ St. Philippos</u> • Past mining produced 0.2 Mt at 7.5 % Pb + Zn (4-10% Pb+Zn) ▪ Concentrates at 60-70% Pb, 3-7% Cu, 500 g/t Au, 48-54% Zn, 0.4-0.5% Cd were produced • In: up to 3.5 wt.% (in wurtzite & sphalerite) • Ga: up to 1.6 wt.% (in wurtzite & sphalerite) • Ge: up to 0.3 wt.% (in wurtzite & sphalerite)	<u>Sappes-Kassiteres-Kirki-Esimi / St. Philippos</u> • Type: epithermal type - High and intermediate sulfidation • Pb-Zn-Ag-Bi-Sn-In deposit • Ore bodies: vein, breccia, disseminated • Main host rocks: sandstone, conglomerate,	<u>Sappes-Kassiteres-Kirki-Esimi/ St. Philippos</u> • Pb, Zn, Ag, As, Cu, Bi, Sn, Cd, In, Ga, Ge, Au • Main metals: Pb, As, Cu, Ag, Bi • Critical & rare metals: In, Ga, Ge	

				<u>Sappes/ Xylagani</u> • Fe: 18.94 wt.% • Cu: 2.0 wt.% • Zn: 367 ppm • Pb: 458 ppm • Au: 3.5 ppm (0.1-6.4 ppm)	marl, tuff, microgranite porphyry • Critical and precious metal mineralogy: bismuthinite, hessite, altaite, tellurobismuthite <u>Sappes/ Xylagani</u> • Mineralization type: VMS (Cyprus- and Kuroko-type) • Au-bearing Fe-Cu-(Zn-Pb) stratabound deposit • Ore bodies: thin layered, disseminated, massive sulphide, veins • Main host rocks: volcanic rocks (lavas and tuffs) metamorphosed to very low to low grade stage	<u>Sappes/ Xylagani</u> • Main metals: Cu, Fe, Au	

5. Xanthi - Nestos Delta area	Type "A" *(The recorded*	Unknown *(Data for the metal*	<u>Eratino geothermal field -</u>				<u>Eratino geothermal field</u> - <u>Coordinates</u>

	temperature exceeds 100°C at depths > 1 km)	*enrichment are limited only at surface or very shallow depth. It is believed that metal enrichment exists at great depths, but it has not been identified)*	<u>Borehole temperature data:</u> Production wells N-1P & N-2P 650m → 75°C Exploration well N2 430m → 60.9°C Exploration well N6 400m → 52.6°C Exploration well N14 470m → 62.8°C Exploration well N10 500m → 61.4°C Exploration well N11 530m → 69.7°C Exploration well N12 510m → 65°C Deep Exploration borehole N1-G 1377m → 122°C <u>Eratino field - Geothermal gradient:</u> 3.6-10°C/100m *(mean geothermal gradient 3°C/100m)* <u>Eratino field - Heat flow density:</u> 70-200 mW/m^2 *(average global heat flow density 70 mW/m^2)*	<u>Xanthi – Kimmeria</u> • Resource of ≈ 2 Mt: Cu: 1.98 % Ag: 20 g/t <u>Xanthi - Kimmeria</u> • Cu: >1 wt.% • Mo: > 0.2 wt.% • Au: up to 2.7 g/t • W: up to 79.5 g/t • Bi: up to 456.6 g/t • Te: up to 4 g/t	<u>Xanthi - Kimmeria</u> • Type: Skarn • Ore bodies: Massive, disseminated • Main host rocks: marble, gneiss, amphibolite) • Massive Cu-W-Mo-Au-bearing skarn-type mineralization <u>Xanthi - Kimmeria</u> • Type: vein • Ore bodies: veins • Main host rocks: granodiorite • Mo-Cu-Bi-W quartz vein mineralization <u>Palea Kavala</u>	<u>Xanthi - Kimmeria</u> • Fe, Cu, Zn, W, Bi, Au, Mo <u>Xanthi - Kimmeria</u> • Cu, Mo, W, Bi <u>Palea Kavala</u>	<u>of wells</u> (decimal / WGS84): • Production well N-1P ϕ: 40.9557687 (40° 57′20.77″), λ: 24.6236073 (24° 37′24.99′′) • Production well N-2P ϕ: 40.9474538 (40° 56′50.83″), λ: 24.6416845 (24° 38′30.06′′) • Exploration well N2 ϕ: 40.9622834 (40° 57′44.22″), λ: 24.62472 (24° 37′28.99′′) • Exploration well N6 ϕ: 40.9752193 (40° 58′30.79″), λ: 24.6227716 (24° 37′21.98′′) • Exploration well N14 ϕ: 40.9594971 (40° 57′34.19″), λ: 24.6243598 (24° 37′27.70′′) • Exploration well N10 ϕ: 40.9644468 (40° 57′52.01″), λ: 24.6405753 (24° 38′26.07′′) • Exploration well N11

			<u>Neo Erasmio field - Borehole temperature data:</u> Exploration well M6 170m → 64.3°C Exploration well M15 380m → 68°C Exploration well M13 350m → 66.6°C <u>Neo Erasmio field - Geothermal gradient:</u> 4.8-28.3°C/100m *(mean geothermal gradient 3°C/100m)* <u>Neo Erasmio field - Heat flow density:</u> 70-300 mW/m^2 *(average global heat flow density 70 mW/m^2)* <u>Nea Kessani field -</u>	<u>Palea Kavala</u> • 1.5 Mt containing: up to 34.5 g/t Au, up to 180 g/t Ag, up to 13% Pb + Zn, up to 40% Fe & up to 42% Mn	• Type: intrusion hosted veins, carbonate replacement, vein • Ore bodies: veins, disseminated, massive fissures (pods), mantos, breccia • Main host rocks: granodiorite, marble, schist • Oxidized Fe-Mn-Au and Fe-Mn (Pb ± Zn ± Ag) bodies • Fe-As-Au, Fe-Cu-Au, and Bi-Te-Au deposits • Bi-Te-Pb-Sb ± Au mineralization • Bi-Te-Au mineralization • Critical and precious metal mineralogy: bismuthinite, tetradymite, Bi-sulfosalts, cosalite, native Au	• Fe, Cu, Pb, Zn, Mn, Cd, As, Sb, Bi, Te, Ag, Au • Main metals: Au, Bi • Critical & rare metals: Te	ϕ: 40.9558396 (40° 57′21.02″), λ: 24.6250704 (24° 37′30.25′′) • Exploration well N12 ϕ: 40.9390418 (40° 56′20.55″), λ: 24.6476367 (24° 38′51.49′′) • Deep exploration well N1-G ϕ: 40.9553721 (40° 57′19.34″), λ: 24.622717 (24° 37′21.78′′) <u>Coordinates of polygon vertices of the Eratino geothermal field</u> (decimal / WGS84): • Vertex A ϕ: 40.9837717 (40° 59′1.58″), λ: 24.6276192 (24° 37′39.43′′) • Vertex B ϕ: 40.9935653 (40° 59′36.84″), λ: 24.7117969 (24° 42′42.47′′) • Vertex C ϕ: 40.8799348 (40° 52′47.77″), λ: 24.7069594 (24° 42′25.05′′) • Vertex D ϕ: 40.8719317 (40° 52′18.95″),

			<u>Borehole temperature data:</u> • Exploration well G3 Depth: 473m 460m → 83.0°C Mean geothermal gradient: 14°C/100m (0-460m) Heat flow: 393 $mW.m^{-2}$ • Exploration well G16 Depth: 201m 120m → 80°C Mean geothermal gradient: 45°C/100m (0-140m) • Exploration well G13 Depth: 450m 350m → 79°C Mean geothermal gradient: 17.5°C/100m 17.3°C/100m (0-360m) • Exploration well G22 Depth: 505m 340m → 77.6°C Mean geothermal gradient: 15.7°C/100m 13.6°C/100m (0-440m) • Exploration well G17 Depth: 200m 170m → 74.5°C Mean geothermal gradient: 36.8°C/100m 33.7°C/100m (0-170m) • Exploration well G12 Depth: 491m 350m → 73.7°C Mean geothermal gradient: 17.8°C/100m (0-300m) 11.8°C/100m (0-470m) • Exploration well G24 Depth: 470m 420m → 71.9°C				λ: 24.6333499 (24° 38′0.06′′) • Vertex E ϕ: 40.9459457 (40° 56′45.40″), λ: 24.5837807 (24° 35′01.61′′) <u>Neo Erasmio geothermal field</u> - <u>Coordinates of wells</u> (decimal / WGS84): • Exploration well M-6 ϕ: 40.9271368 (40° 55′37.69″), λ: 24.8411491 (24° 50′28.14′′) • Exploration well M-15 ϕ: 40.922303 (40° 55′20.29″), λ: 24.8277524 (24° 49′39.91′′) • Exploration well M-13 ϕ: 40.9230492 (40° 55′22.98″), λ: 24.8355497 (24° 50′07.98′′) <u>Coordinates of polygon vertices of the Neo</u>

			Mean geothermal gradient: 13.5°C/100m 12.4°C/100m (0-445m) • Exploration well G21 Depth: 390m 340m → 71.7°C Mean geothermal gradient: 15.6°C/100m 15.2°C/100m (0-360m) • Exploration well G8 Depth: 255m 226m → 70.4°C Mean geothermal gradient: 24.8°C/100m 24.7°C/100m (0-220m) Heat flow: 360 $mW.m^{-2}$ • Exploration well G9 Depth: 325m 272m → 70.0°C Mean geothermal gradient: 19.5°C/100m 19°C/100m (0-260m) Heat flow: 297 $mW.m^{-2}$ • Exploration well G14 Depth: 485m 470m → 65.9°C Mean geothermal gradient: 10.1°C/100m 10.5°C/100m (0-470m) • Exploration well G4 Depth: 60m 60m → 65.0°C Mean geothermal gradient: 80.5°C/100m (0-60m) • Production well GP13 Depth: 430m Depth temperature: 76.8°C • Production well GP12 Depth: 463m Depth temperature: 72.7°C			<u>Erasmio geothermal field</u> (decimal / WGS84): • Vertex A ϕ: 40.934747 (40° 56′5.09″), λ: 24.7742894 (24° 46′27.44′′) • Vertex B ϕ: 40.9539001 (40° 57′14.04″), λ: 24.8745905 (24° 52′28.53′′) • Vertex C ϕ: 40.9140198 (40° 54′50.47″), λ: 24.8884148 (24° 53′18.29′′) • Vertex D ϕ: 40.8927304 (40° 53′33.83″), λ: 24.7982979 (24° 47′53.87′′) <u>Nea Kessani geothermal field</u> -

			• Production well GP22 Depth: 512m Depth temperature: 72.3°C • Production well GP21 Depth: 473m Depth temperature: 71.0°C <u>Nea Kessani field - Geothermal gradient:</u> From 5 to higher than 20°C/100m *(mean geothermal gradient 3°C/100m)* <u>Nea Kessani field - Heat flow density:</u> From 70 to higher than 300 mW/m^2 *(average global heat flow density 70 mW/m^2)*				<u>Coordinates of wells</u> (decimal / WGS84): • Production well GP-13 ϕ: 41.0317463 (41° 01′54.29″), λ: 25.0546579 (25° 03′16.77′′) • Production well GP-12 ϕ: 41.0362076 (41° 02′10.35″), λ: 25.0602047 (25° 03′36.74′′) • Production well GP-22 ϕ: 41.0389237 (41° 02′20.13″), λ: 25.0540957 (25° 03′14.74′′) • Production well GP-21 ϕ: 41.0296628 (41° 01′46.79″), λ: 25.0490762 (25° 02′56.67′′) • Exploration well G3 ϕ: 41° 01′34″ λ: 25° 03′00′′ • Exploration well G8 ϕ: 41° 01′50″ λ: 25° 03′00′ • Exploration well G9 ϕ: 41° 02′24″

							λ: 25° 03′51′ <u>Coordinates of polygon vertices of the Nea Kessani geothermal field</u> (decimal / WGS84): • Vertex A ϕ: 41.0494442 (41° 02′58.00″), λ: 25.0220615 (25° 01′19.42′′) • Vertex B ϕ: 41.0557006 (41° 03′20.52″), λ: 25.0795065 (25° 04′46.22′′) • Vertex C ϕ: 41.0130837 (41° 00′47.10″), λ: 25.0902928 (25° 05′25.05′′) • Vertex D ϕ: 41.0018184 (41° 00′06.55″), λ: 25.0308637 (25° 01′51.11″)

			<u>Nestos Delta area - Borehole temperature data:</u> Exploration borehole NESTOS-1 2400m → 85°C 2970m → 115°C 3156m → 126.4°C Exploration borehole NESTOS-2 3104m → 127°C 3960m → 164°C Exploration borehole NESTOS-3 3601m → 138°C 3851m → 160°C <u>Nestos Delta area - Mean geothermal gradient:</u> 31-40°C/km *(mean geothermal gradient 30°C/km)* <u>Delta Nestos area - Heat flow density:</u> 50-70 mW/m^2 *(average global heat flow density 70 mW/m^2)*				<u>Coordinates of deep hydrocarbon exploration boreholes in the Nestos Delta area</u> (decimal / WGS84): • Exploration well NESTOS-1 ϕ: 40.8959099 (ϕ: 40° 53′45.28″), λ: 24.6594634 (λ: 24° 39′34.07′′) or ϕ: 40° 53′48″ λ: 24° 39′30′′ • Exploration well NESTOS-2 ϕ: 40.8902876 (ϕ: 40° 53′25.04″), λ: 24.6253817 (λ: 24° 37′31.37′′) or ϕ: 40° 53′36″ λ: 26° 37′42′′ • Exploration well NESTOS-3 ϕ: 40.8762674 (ϕ: 40° 52′34.56″) λ: 24.6493074 (λ: 24° 38′57.51′′) or ϕ: 40° 52′37″, λ: 26° 38′ 56′′

							<u>Coordinates of polygon vertices of the Kimmeria Xanthi pluton area</u> (scarn occurrences & mineralized vein system) (WGS84): • Vertex A ϕ: 41° 08′23.77″ N λ: 24° 52′05.96′′ E • Vertex B ϕ: 41° 08′17.34″ N λ: 24° 58′21.30′′ E • Vertex C ϕ: 41° 08′38.51″ N λ: 25° 01′22.51′′ E • Vertex D ϕ: 41° 10′08.31″ N λ: 25° 01′37.74′′ E • Vertex E ϕ: 41° 11′28.95″ N λ: 24° 58′07.71′′ E • Vertex F ϕ: 41° 09′36.02″ N λ: 24° 52′11.90′′ E <u>Coordinates of polygon vertices of the Palea Kavala ore deposit area</u> (WGS84): • Vertex A ϕ: 41° 03′36.48″ N λ: 24° 21′44.11′′ E • Vertex B ϕ: 40° 55′54.81″ N λ: 24° 21′54.94′′ E

							• Vertex C ϕ: 40° 57′50.73″ N λ: 24° 29′16.56′′ E • Vertex D ϕ: 41° 03′26.32″ N λ: 24° 29′33.53′′ E <u>Coordinates of polygon vertices of the prospective CHPM area</u> (WGS84/decimal): • Vertex A ϕ: 40° 57′15.30″ (40.9542512) λ: 24° 32′55.87″ (24.5488517) • Vertex B ϕ: 41° 09′26.34″ (41.157317) λ: 24° 53′26.95″ (24.8908192) • Vertex C ϕ: 41° 09′26.34″ λ: 25° 04′32.41″ • Vertex D ϕ: 41° 00′22.55″ (41.006263) λ: 25° 04′58.12″ (25.0828102)

6. Thermes Xanthi	Type "B" *(The recorded temperature exceeds 50°C. The heat flow density is higher than average, but temperature of >100°C has not been measured yet at great depths)*	Unknown *(Data for the metal enrichment are limited only at surface or very shallow depth. It is believed that metal enrichment exists at great depths, but it has not been identified)*	<u>Thermes Xanthi - Spirings' Temperature data:</u> 43-53°C <u>Thermes Xanthi: Borehole Temperature data:</u> 200m → 41°C <u>hermes Xanthi: Heat flow density:</u> 70-200 mW/m^2 *(average global heat flow density 70 mW/m^2)*	<u>Thermes Xanthi</u> Resource of ≈ 1 Mt: Au: <4 g/t Ag: 10-340 g/t Pb: 1.2-14.5% Zn: 2.1-16.7% Cu: 0.06-0.10%	<u>Thermes Xanthi</u> • Type : Carbonate Replacement, Vein • Ore bodies: Veins, manto • Main host rocks : marble, amphibolite, orthogneiss • Polymetallic Zn-Pb-Fe-Cu-As-Ag-Au-Te carbonate-replacement deposit • Veins and breccias containing Pb-Zn-(Fe-Cu) mineralization • Critical and precious metal mineralogy: gersdorffite, hessite, altaite, native Au	<u>Thermes Xanthi</u> • Pb, Zn, Fe, Cu, Mn, As, Sb, Cd, Te, Ag, Au • Main metals: Pb, Zn, Ag • Critical & rare metals: In, Ge, Ga	<u>Thermes Xanthi - Coordinates of springs</u> (decimal / WGS84): • Spring 1 ϕ: 41.3484596 (ϕ: 41° 20′54.45″), λ: 25.012383 (λ: 25° 0′44.58′′) • Spring 2 ϕ: 41.3484407 (ϕ: 41° 20′54.39″), λ: 25.0122751 (λ: 25° 0′44.19′′) • Spring 3 ϕ: 41.3482695 (ϕ: 41° 20′53.77″), λ: 25.0097579 (λ: 25° 0′35.13′′) • Spring 4 ϕ: 41.348297 (ϕ: 41° 20′53.87″), λ: 25.0096985 (λ: 25° 0′34.91′′) • Spring 5 ϕ: 41.3484318 (ϕ: 41° 20′54.35″), λ: 25.0157626 (λ: 25° 0′56.75′′) <u>Coordinates of polygon vertices of the Thermes ore field</u> (WGS84): • Vertex A ϕ: 41° 24′07.61″ N λ: 24° 55′15.09′′ E

							• Vertex B ϕ: 41° 22′42.31” N λ: 24° 55′16.06’’ E • Vertex C ϕ: 41° 20′46.04” N λ: 24° 58′41.82’’ E • Vertex D ϕ: 41° 20′17.34” N λ: 25° 01′59.77’’ E • Vertex E ϕ: 41° 22′03.09” N λ: 25° 02′29.30’’ E <u>Coordinates of polygon vertices of the prospective CHPM area</u> (WGS84): • Vertex A ϕ: 41° 24′07.61” N λ: 24° 55′15.09’’ E • Vertex B ϕ: 41° 22′42.31” N λ: 24° 55′16.06’’ E • Vertex C ϕ: 41° 20′46.04” N λ: 24° 58′41.82’’ E • Vertex D ϕ: 41° 20′17.34” N λ: 25° 01′59.77’’ E • Vertex E ϕ: 41° 22′03.09” N λ: 25° 02′29.30’’ E

Important notes regarding the selection of the prospective CHPM areas in Greece:

In all cases of the above table:

- *The temperature exceeds the 50°C at shallow depths.*
- *The temperature exceeds or is surely expected to exceed the 100°C at greater depths.*
- *Data for the metal enrichment(s) are limited only at surface or very shallow depths.*
- *There are no data for the metal enrichment(s) at great depths.*
- *It is believed that metal enrichment exists at great depths, but it has not been identified.*

Evaluation of the basic characteristics of prospective CHPM areas

Name of the National Association: AGG
Number of the prospective area 1 Northern Lesvos
(Stypsi and Argennos area)

1. **Geology of the prospective area**

Requested information on:

- ✓ local geology (in regional context)
- ✓ CHPM target formation
- ✓ list of available cross sections, geological maps, geochemical results, lithological information

Notes: briefly summarized, referenced to more detailed studies.

LOCAL GEOLOGY

The following tectonic units, in order of decreasing age, constitute the structure of Lesbos (Katsikatsos et al., 1982): Autochthonous series (basement); volcanosedimentary series (tectonic cover}; tectonic cover of ophiolites; meta-alpine formation.

1. The epimetamorphic series (crystalline sequence) forming the stratigraphic "basement" of the island, is locally and tectonically associated with peridotitic bodies. It consists of metamorphic rocks, mainly schists. This series is characterized by low-grade metamorphism, the presence of intercalations of limestones and marbles, and the absence of greenschists. The age of the rocks is Neo-Palaeozoic to Triassic. The basement outcrops mainly in the southeastern part of the island, along with peridotite massif outcrops in the central-eastern part.
2. The overlying sequence of volcanic rocks of calc-alkaline affinity mainly occurs in the west. The volcano-sedimentary series is in tectonic contact with the autochthonous series. It consists of different types of low-grade metabasites and sedimentary rocks (crystalline limestones and some schists).
3. The ophiolites which are overthrust on the Triassic rocks (basement), include two rock types: (a) the upper group which consists of pyroxene peridotite, dunite and serpentinised peridotite; and (b) the lower group, consisting of metamorphosed ophiolitic rocks.
4. The meta-alpine formations are subdivided into Neogene and Quaternary. The Neogene includes pyroclastic materials, various lava types, and sedimentary deposits of marine or lacustrine origin.

According to Pe-Piper and Piper Pc-Piper, (1980b; Pc-Piper and Piper, 1980) and Hecht (1971- 1974), the volcanic sequence is as follows: (a) lower lava unit: andesites, basalts, dacites, zones of intense hydrothermal alteration; (b) acidic volcanics: pyroclastics, ignimbrites, and rhyolites; (c) upper lava unit: basalts, andesites and dacites; and (d) intrusions: dacite plugs.

Three major fault systems have been recognized: NW-, NNE- and E-trending. The most important trend is the NW-SE, which corresponds to normal faulting during the Neocene episode that continued during the Pleocene (Simeakis and Someritis, 1982). A series of tectonic features of the basement such as lows, highs and normal faults trending NNE-SSW and NW-SE, some of which are still active at present, have facilitated the ascent of hot fluids from depth. The Stypsi prospect is bounded on the north and west by a caldera structure, and to the east by a northeast-trending fault zone (Rokos et al. 2000).

CHPM TARGET FORMATION

The Stypsi prospect in the north-central part of the island is hosted by shoshonitic subvolcanic and volcanic rocks (Fig. 1,2). Especially the brittle and relatively unreactive andesites which host the mineralization, created an environment suited to veins as well as for breccia ore bodies and stockwork mineralization. The quartz veins have been formed mainly by the filling of faults systems with NNE-SSW and NW-SE directions (Fig. 3). Some of the quartz veins are up to 10 m wide, whereas tectonic breccia is often present at the edge of the quartz veins as a result of intense postmineralizing tectonic movements. The breccia ore bodies are characterized by the presence of quartz breccia disseminated within kaolinite (for example at the sample position D).

The Megala Therma Pb-Zn-Cu-Ag-Au intermediate-sulfidation epithermal deposit on Lesvos Island, is related to NNE–SSW- and NW–SE-trending quartz veins hosted in 21–18 Ma old andesite-latite lavas (Fig. 1,2,3; Kontis et al., 1994). Silicic, propylitic, argillic, and adularia-sericite are the main alteration types. The breccia, veinlets and veins are enriched in Au, Ag, Pb, Zn, Cu and Mo (Kontis et al., 1994).

2. Geophysics of the prospective area

Requested information:

- ✓ previous geophysical measurements (in CHPM relevance)
- ✓ geophysical results that can be used for locating/defining the deep metal enrichment
- ✓ list of available geophysical maps, cross sections, logs, other measurements

3. Deep metal enrichment

Requested information:

- ✓ (expected) metal enrichment based on available geophysical, geological and drill data, samples information, geochemistry

Post-collisional orogenic magmatism occured in northern Greece during the Oligocene to Miocene and this resulted in the formation of porphyry type mineralization of Stipsi area. The Stipsi porphyry Sub-alk Cu-Mo prospect in the north-central part of Lesvos Island is hosted by a high-K calc-alkaline granodiorite porphyry and the surrounding volcanic rocks. It is characterized by intense propylitic, sericite-carbonate, argillic, and at the upper levels, advanced argillic and silicic alteration (Fig. 5d; Voudouris and Alfieris, 2005). The porphyry-style mineralization consists of dense quartz stockworks containing molybdenite, bismuthinite, and galena (Fig. 5e), overprinted by intermediate-sulfidation epithermal quartz-carbonate veins (Voudouris and Alfieris, 2005), which extend northwards to Megala Therma, where they host economic precious metal mineralization (Kontis et al. 1994).

More analytically, a dacitic andesite porphyry body in the western part of the island has been altered to kaolinite, illite and smectite. Mapping has delineated a target area that consists of a stockwork of grey to black silica veinlets crosscutting a dacite porphyry body. Early veinlets that contain grey quartz + actinolite + minor magnetite, chalcopyrite and pyrite are related to K-Na-silicate alteration of the porphyry. These are cut by black quartz ± calcite veins associated with sericite-carbonate alteration. The black quartz veinlets contain early magnetite, which is overgrown by pyrite, chalcopyrite, bismuthinite, molybdenite and then by galena and sphalerite (Fig. 3c and d). Late-stage milky to amethystine quartz and platy calcite veins with pyrite and galena were formed along the major NNE-SSW trending fault zone, and have overprinted earlier-formed alteration and mineralization. Barren jasperoidal silicic

alteration, which overlies kaolinitized ± minor alunite volcanics is well exposed at higher elevations to the north of the prospect area.

Stypsi area analyses showed compositions of 2 ppb Au, 120 ppb (0.120 ppm) - up to 0.5 ppm Au, up to 0.10 g/t Au, 5 ppb (0.005 ppm) - up to 1.7 ppm Ag, 111 pm Cu up to1330 ppm Cu, 10 ppm Mo up to 170 ppm Mo (maybe up to 330 ppm Mo according to Kelepertsis and Esson (1987)), 142-160 ppm Pb up to 1020 ppm Pb, 65 ppm Zn up to 815 ppm Zn, 3 ppm Se up to 13 ppm Se, up to 4 ppm Te, 4 ppm Bi up to 36 ppm Bi, up to 23 ppm Sn, 0.009-0.010% Sn, up to 1.92 wt% Re in molybdenite, 0.26-4.74 wt% Fe in sphalerite, up to 8 ppm Sb, up to 1176 ppm Ba, up to 16 ppm As, up to 22 ppm Co, up to 40 ppm Cr, up to 129 ppm Ce, up to 12 ppm Hf, up to 1 ppm Hg, up to 5 ppm Ir, up to 238 ppm Rb, up to 22.2 ppm Sc, up to 1.6 ppm Ta, up to 42.2 ppm Th, up to 12.8 ppm U, up to 17 ppm Cs, up to 3 ppm W, up to 71.4 ppm La, up to 71.4 ppm Nd, up to 128 ppm Mn, up to 5 ppm Be, up to 0.53 wt% Ti, up to 200 ppm V and up to 12 ppm Y. Also contain Re in molybdenites: 300-10600 g/t (average: 2460 g/t).

The Megala Therma Pb-Zn-Cu-Ag-Au intermediate-sulfidation epithermal deposit on Lesvos Island, is related to NNE–SSW- and NW–SE-trending quartz veins hosted in 21–18 Ma old andesite-latite lavas (Fig. 3; Kontis et al., 1994). Silicic, propylitic, argillic, and adularia-sericite are the main alteration types. The breccia, veinlets and veins are enriched in Au, Ag, Pb, Zn, Cu and Mo (Kontis et al., 1994). The Megala Therma epithermal system extends further to the south, where similar intermediate-sulfidation quartzcarbonate veins with platy calcite (Fig. 6b) overprint the porphyry Cu-Mo mineralization at Stipsi (Voudouris and Alfieris, 2005).

The mineralization includes the following gangue minerals: quartz, adularia, chlorite, kaolinite, illite, sericite, baryte, alunite and jarosite. Quartz, which is the predominant nonmetallic mineral, appears in a fine-grained form. In addition, secondary copper minerals, such as malachite and azurite, have been found to occur as supergene impregnations within clay minerals. The metallic assemblage consists of pyrite, galena, sphalerite, chalcopyrite, bornite, chalcocite, covellite, goethite and native gold. Gold has been observed commonly in polished sections under the ore microscope and appears to be as allotriomorphic isolated grains up to 25-30 gm in diameter, or rarely as intergrowths with pyrite (on grain boundaries). Microprobe analyses showed that it is pure native gold (100% Au). The base metal sulfides occur as disseminations or in the form of veinlets and are often altered. Covellite and pseudomorphic goethite are the main alteration products of chalcopyrite and pyrite respectively.

The principal types of alteration which occur in the Megala Therma-Argenos area are: silicification, propylitization, argillic alteration and potassic, phyllic alteration. Si is strongly enriched during the ore-forming processes as a result of the intense silicification, whereas most of the other elements decrease with the increasing degree of silicification and are characterized by relatively low concentrations. Some of the elements, such as Ca, Na, Ni and Cr have low values. A typical suite of elements in anomalous concentrations related to the mineralization includes Au, Ag, Mo, Pb, Zn, Cu and Ba. Lead is more abundant than other base metals (Cu, Zn). It is obvious that the gold and silver distributions, even in the same sampling profile, are not uniform. The distribution is controlled by complicated fracture systems, silicification, diverse alteration assemblages and the grain size of gold. About 45% of the analysed samples reveal Au concentrations up to 3 ppm, while the Au/Ag ratio varies from 1.157 to 0.007.

Megala Therma - Argenos area analyses showed compositions of 163 ppb Au, up to 21 ppm Au, 5 ppb (0.005 ppm) Ag, 220-1010 pm Cu, 24 ppm Mo, up to 52 ppm Pb, up to 119 ppm Zn, up to 32 ppm Bi, 0.009-0.010% Sn, up to 3.5 wt% Fe, up to 35.5 ppm Sb, up to 1700 ppm Ba, up to 73 ppm As, up to 11 ppm Co, up to 38 ppm Cr, up to 273 ppm Ce, up to 12 ppm Hf, up to 2 ppm Hg, up to 5 ppm Ir, 70 ppm Rb, up to 28.5 ppm Sc, up to 4 ppm Se, up to 1411 ppm Sr, up to 2 ppm Ta, up to 48.1 ppm Th, up to 8.1 ppm U, up to 3 ppm Cs, up to 2.9 ppm W, up to 140 ppm La, up to 100 ppm Nd, up to 1370 ppm Mn, up to 3 ppm Be, up to 0.73 wt% Ti, up to 163 ppm V and up to 225.9 ppm Y.

The spatial coordinates (in WGS84 format) of the polygon vertices of the Megala Therma - Argenos mineralization area are defined as follows:

• Vertex A
ϕ: 39o 22′36.88”N, λ: 26o 12′31.29”E
• Vertex B
ϕ: 39o 23′0.37” N,, λ: 26o 13′28.84’’ E
• Vertex C
ϕ: 39o 22′59.49” N, λ: 26o 14′06.89” E
• Vertex D
ϕ: 39o 22′39.97” N, λ: 26o 15′12.39” E
• Vertex E
ϕ: 39o 22′38.10” N, λ: 26o 16′03.26” E
• Vertex F
ϕ: 39o 22′35.26” N, λ: 26o 17′14.31” E
• Vertex G
ϕ: 39o 22′25.21” N, λ: 26o 18′17.28” E
• Vertex H
ϕ: 39o 20′32.29”N, λ: 26o 18′17.28” E
• Vertex I
ϕ: 39o 20′48.25”N, λ: 26o 11′19.47”E

The spatial coordinates (in WGS84 format) of the polygon vertices of the Stypsi mineralization area are defined as follows:

• Vertex A
ϕ: 39o 20′48.25”N, λ: 26o 11′19.47”E
• Vertex B
ϕ: 39o 20′32.29”N, λ: 26o 19′29.35”E
• Vertex C
ϕ: 39o 15′23.02”N, λ: 26o 19′17.91”E
• Vertex D
ϕ: 39o 15′22.19”N, λ: 26° 11′35.52”E

The polygon of the Stipsi and Megala Therma - Argenos mineralization area on Google Earth is depicted in Figure 7.

4. Integrated 3D- 4D model

Requested information:

- ✓ existing 3D-4D models of the target area and the deep metal enrichment
- ✓ if no 3D-4D models exist, collect the following necessary data: geological setting, mineralization, fluid flow models, stress field determination

Notes: e.g. openly available datasets, models.

5. **EGS potential**

Requested information:

- ✓ EGS potential (heat & energy) of the area
- ✓ geothermal characteristics (temperature gradient, heat flux, stress field, water availability, EGS geology)
- ✓ presence/indication of deep fluids/brines, fracture system, crustal permeability

GEOPHYSICAL SURVEYS ABOUT GEOTHERMAL CHARACTERISTICS

Previous geophysical surveys on Lesvos island have focussed on local geothermal and hydrogeological problems. The first geophysical project (VES) was carried out by Oikonomou (1971) to study Polyhnitos geothermal field. Nathanael (1979) applied the geoelectrical method (VES) in the Kalloni area, while Thanassoulas (1982) carried out 10 deep VES (AB/2 = 4 km) in a reconnaissance study of the deep regional geological and tectonic features of Lesvos island. The gravity map of the island was compiled by Hamburg University (Professor Makris) in cooperation with the IGME (1982). A small-scale geophysical study was performed by Xanthopoulos et al. (1988), for the evaluation of the geothermal potential of Argenos area. Taktikos (1985) compiled a temperature map of Lesvos island (-250 m below ground surface) that is presented in Fig. 5.

The heat flow density is about 200-400 mW/m^2 (average global heat flow density 70 mW/m^2).

There are hot (50–85 ◦C) springs near the seashore in the northern and southeastern parts of Lesvos and inland of the Gulf of Kalloni . Geothermal exploration of the surveys, geochemical investigations, drilling of and temperature measurements in shallow wells (Fytikas et al., 1989b). In Argenos and Polichnitos the salinity of most hot springs with T>50◦C is about 12 g/kg. In Argenos, the K–Na–Mg geothermometer suggests the existence of a deep source of NaCl-type water with K–Mg and K–Na equilibrium temperatures of 127 ◦C and 217 ◦C, respectively. The hot spring waters of Thermi have a salinity of 36 g/kg; the K–Na–Mg geothermometer indicates K–Mg and K–Na equilibrium temperatures of 110 ◦C and 175 ◦C, respectively.

There are many other low-temperature bicarbonate type springs on Lesvos with a TDS typically less than 2 g/kg; these derive from shallow aquifers. Recently, PPC has drilled a 1.4km deep exploration well approximately 1.5km NWW of Stipsi, which encountered a maximum temperature of 82 ◦C at well bottom (Michalis Fytikas, personal communication, July 2009). Specifically for the Stypsi geothermal field the geothermal survey carried out by the PPCR-Greece revealed that the exploration well STE-1 at 250m showed temperatures that reached 100°C, the exploration well STE-2 at 400m measured temperatures of 97.8°C and at 1015m reached 91.4°C. The exploration well S-1 at 1400m showed temperature of 83.1°C and it is estimated that at the depth of 2500m temperature will reach 140°C. For the Argenos geothermal field the geothermal survey carried out by the PPCR-Greece revealed that the exploration well GA-350 at 120m showed temperatures that reached 85-87°C and at 140m measured 74°C, the exploration well AR-2140 at 200m reached temperatures of 79-81°C and at 220-230m measured 72°C. The exploration well AR-150 at 100m showed temperature of 65-70°C, at 150m temperature 52.6 °C and at 200m temperature of 49.4 °C.

At present, geothermal utilization on Lesvos involves thermal spas and heating of greenhouses, i.e. hot waters of about 40 ◦C around the Gulf of Geras, of about 60 ◦C at Thermie, of 65–80 ◦C at Polichnitos and Lisvori (south of the Gulf of Kalloni), and of 80–90 ◦C at Argenos.

The coordinates (decimal/WGS84) of significant wells (T: 83-100°C) in Stypsi are as follows:

- Exploration well S-1

ϕ: 39.3238477 (39° 19′25.85”), λ: 26.21269 (26° 12′45.68’’)

- Exploration well STE-1

ϕ: 39.28301 (39° 16′58.84”), λ: 26.22726 (26° 13′38.14’’)

• Exploration well STE-2
ϕ: 39.2945 (39° 17′40.20”), λ: 26.21319 (26° 12′47.48′′)

The coordinates (decimal/WGS84) of significant wells (T: 50-90°C) in Argenos are as follows:

• Exploration well GA-3
ϕ: 39.3750585 (39° 22′30.21”), λ: 26.2543881 (26° 15′15.80′′)

• Exploration well AR-2
ϕ: 39.3743193 (39° 22′27.55”), λ: 26.2512994 (26° 15′4.68′′)

• Exploration well AR-1
ϕ: 39.3761844 (39° 22′34.26”), λ: 26.2489397 (26° 14′56.18′′)

The locations of these wells on Google Earth are depicted in Figure 7.

Three major fault systems have been recognized: NW-, NNE- and E-trending. The most important trend is the NW-SE, which corresponds to normal faulting during the Neocene episode that continued during the Pleocene (Simeakis and Someritis, 1982). A series of tectonic features of the basement such as lows, highs and normal faults trending NNE-SSW and NW-SE, some of which are still active at present, have facilitated the ascent of hot fluids from depth. (Rokos et al. 2000).

CONCLUSIONS AND

JUSTIFICATION FOR THE CHOICE OF THE THERMES AREA AS A PROSPECTIVE CHPM AREA

Taking into account that

- the Stipsi porphyry Sub-alk Cu-Mo mineralization is hosted in dense stockworks containing molybdenite, bismuthinite, and galena, overprinted by intermediate-sulfidation epithermal quartz-carbonate veins and the Megala Therma Pb-Zn-Cu-Ag-Au intermediate-sulfidation epithermal mineralization is hosted in veins and breccia in andesites and latites
-both Stipsi and Megala Therma mineralization are connected to faults systems with NNE-SSW and NW-SE directions
- exploration wells at 400m-1400 m measured temperatures that reached 100°C, and it is estimated that at the depth of 2500m temperature will reach 140°C

the choice of the Northern Lesvos area as a CHPM target for further exploration can be justified.

The spatial coordinates (in WGS84 format) of the polygon vertices of the prospective CHPM area of Stipsi and Megala Therma-Argenos are defined as follows:

• Vertex A
ϕ: 39o 22′36.88”N, λ: 26o 12′31.29”E
• Vertex B
ϕ: 39o 23′00.37”N, λ: 26o 13′28.84”E
• Vertex C
ϕ: 39o 22′59.49”N, λ: 26o 14′06.89”E
• Vertex D
ϕ: 39o 22′39.97”N, λ: 26o 15′12.39”E
• Vertex E
ϕ: 39o 22′38.10”N, λ: 26o 16′03.26”E
• Vertex F
ϕ: 39o 22′35.26”N, λ: 26o 17′14.31”E
• Vertex G
ϕ: 39o 22′25.21”N, λ: 26o 18′17.28”E
• Vertex H
ϕ: 39o 20′32.29”N, λ: 26o 19′29.35”E

• Vertex I
ϕ: 39o 15′23.02″N, λ: 26o 19′17.91″E
• Vertex J
ϕ: 39o 15′22.19″N, λ: 26o 11′35.52″E
• Vertex K
ϕ: 39o 18′09.21″N, λ: 26o 10′39.72″E
• Vertex L
ϕ: 39o 20′48.25″N, λ: 26o 11′19.47″E
The polygon of this prospective CHPM area on Google Earth is depicted in Figure 7.

List of references

Fytikas M., Innocenti F., Manetti P., Mazzuoli R., Peccerillo A., Villari L., 1984. Tertiary to Quaternary evolution of volcanism in the Aegean region. Geol. Soc., London, Spec. Publ. 17, 687–699.

Hecht, J., 1971--1974. Geological Map of Lesbos Island (scale 1:50.000). I.G.M.E.

Katsikatsos, G., et al., 1982. Geological Study of Lesbos Island. I.G.M.E. Internal report.

Kelepertsis A.E. and Esson J., 1987. Major- and Trace-Element Mobility in Altered Volcanic Rocks Near Stypsi, Lesbos, Greece and Genesis of a Kaolin Deposit. Applied Clay cience, 2: 11-28.

Kilias S. P., Naden J., Cheliotis I., Shepherd T. J., Constandinidou H., Crossing J. And Simos I., 2001. Epithernal gold minineralisation in the active Aegean Volcanic Arc: the Proitis llias deposit, Milos lsland, Greece. Mineralium Deposita 36: 32-44.

Kontis E., Kelepertsis A. E. and Skounakis S., 1994. Geochemistry and alteration facies associated with epithermal precious metal mineralization in an active geothermal system, northern Lesbos, Greece. Mineral Deposita 2: 430- 433.

Oikonomou, P. (1971) Geoelectrical investigations of the Polyhnitos, Lesvos island area. IGME 1914, 1-12.

Pe-Piper, G., 1980. Geochemistry of Miocene shoshonites, Lesbos, Greece. Contrib. Mineral. Petrol., 72: 387--396.

Pe-Piper, G., 1980b. The Cenozoic volcanic sequence of Lesbos, Greece. S-Dtsch. Geol. Ges., 131: 889--901.

Pe-Piper G. and Piperb D.J.W., 1992. Geochemical variation with time in the Cenozoic high-K volcanic rocks of the island of Lesbos, Greece: significance for shoshonite petrogenesis. Journal of Volcanology and Geothermal Research, 53: 371-387.

Rokos D., Argialas D., Mavrantza R., Seymour K.St., Vamvoukakis C., Kouli M., Lamera S., Paraskevas H., Karfakis I., Denes G., (2000). Structural analysis for gold mineralization using remote sensing and geochemical techniques in a GIS environment: island of Lesvos, Hellas, Nat Res Research 9(4): 277-293.

Simeakis, C. and Someritis, Y. (1982) Etude n6otectonique-mikrotectonique, Etude de fracturation, Etude geologique et perspectives g6othermique de l'fle de Lesvos. IGME.

Taktikos, S. (1985). Temperature distribution on Lesvos island at -250 m from ground surface. (Unpublished map of IGME.)

Thanassoulas, C. (1982). Deep geoelectrical soundings (VES) on Lesvos island. IGME 3562, 1-10.

Thanassoulas C. and Xanthopoulos N., 1991. Location of possibly productive geothermal fracture zones/faults using integrated geophysical methods over lesvos island geothermal field, Greece. Geothermics, Vol. 20, No. 516, pp. 355-368.

Voudouris P. and Alfieris D., 2005. New porphyry - Cu ± Mo occurrences in the north-eastern Aegean, Greece. Ore mineralogy and epithermal relationships. Chapter 4-31.

Xanthopoulos, N., Karmis, P. and Thanassoulas, C. (1988). Geophysical study of the Argenos geothermal field, northern Lesvos island. IGME E5683, 1-15.

Annexes

Contact projects@eurogeologists.eu for the full list of Annexes, or open it at the CHPM Information Platform on Prospective Locations (http://bit.ly/CHPMinfoplatform)

Evaluation of the basic characteristics of prospective CHPM areas

Name of the National Association AGG

Number of the prospective area 2. Western Milos

1. **Geology of the prospective area**

Requested information on:

- ✓ local geology (in regional context)
- ✓ CHPM target formation
- ✓ list of available cross sections, geological maps, geochemical results, lithological information

Notes: briefly summarized, referenced to more detailed studies.

LOCAL GEOLOGY

The geology, geochronology, geothermal activity and structure of Milos Island are described in detail by Fytikas (1977), Fytikas et al. (1976, 1984, 1986, 1989), Briqueu et al. (1986), Fytikas (1989), Papanikolaou et al. (1990), Liakopoulos et al. (1991) and Tsokas (1996), and only a summary is given here. The rocks, which make up the island, can be divided into four main lithological units (Fig. 1).

1. The oldest rocks on the island consist of Alpine metasedimentary rocks. They include micaschists, calcareous schists with intercalated lavas and calcareous rocks, chloritic schists, and quartzites, which were metamorphosed to blueschist (64.2 ± 6.5 Ma) and greenschist facies (35.2 ± 1.0 Ma).

2. Unconformably overlying the metamorphic basement is a sequence of Upper Miocene-Lower Pliocene transgressive marine sediments consisting mainly of limestones, marls and conglomerates. These rocks form the platform sediments on which the volcanic island is built. It is important to note that there are no known evaporite sequences within the marine sedi- ments.

3. Volcanism, on the western part of Milos, commenced 3.5 Ma. The oldest volcanic rocks comprise felsic pumice flows, tuffs, ignimbrites and tuffites, which make up the Basal Pyroclastic Series (3.5-2.5 Ma). This lower sequence is overlain by dome complexes and lava flows (2.5-2.0 Ma), which are accompanied by andesitic to dacitic pyroclastic material.

4. The eastern and central parts of the island are made up of a younger volcanic suite (the Pyroclastic Series), consisting of rhyolitic complexes (1.9-0.1 Ma) com- prising lahars and tuffs accompanied by rhyolitic torhyodacitic domes and flows.The island of Milos is located in the central part of the early Pliocene to Recent South Aegean Active Volcanic Arc, and belongs to the Cycladic Blueschist Unit of the Cyclades (Fytikas et al., 1986). Calc-alkaline volcanic activity in western Milos spans a period from 3.5 to 0.9 Ma and originated from several emergent eruptive centers that produced submarine felsic pyroclastic deposits, pumice flows, dacitic-andesitic flow domes, lava flows, and felsic subvolcanic rocks (Fytikas et al., 1986; Stewart and McPhie, 2006; Alfieris et al., 2013).

In NW Milos, there are three fault systems which define the geometry of the region. These are the Vromolimni-Kondaros (e.g. Kondaros-Katsimouti-VAD) fault which trends NW-SE and marks the western margin of the Gulf of Milos, the NE-trending faults which is orthogonal to the Vromolimni-Kondaros-VAD fault (e.g. the AG fault on the west coast of Milos, the Triades-Galana-Katsimoutis fault) and finally the E-trending fault inside the VA deposit, which also crosscut the AG area. As mentioned by Liakopoulos (1987), Liakopoulos et al. (2001), Alfieris (2006) and Alfieris et al. (2013), this strong tectonic control is believed to have played a critical role in the deposition of the VA (and AG) manganese deposit, as well as the base metal-rich Kondaros- Katsimouti mineralization. The NE-trending vein systems at AG can be followed further to the northeast up to the VAD area . NE-trending Mn-rich barite veins crosscut the

Mn-bearing conglomerates about 150–200 m SE of the VAD (Cape Vani), indicating that the structural system which fed the AG deposit, may controlled the formation of the VA deposit. The NE family of faults at the NW part of Milos Island is also sulfide-mineralized (e.g. the Triades-Galana- Katsimoutis fault). However, this mineralization is characterized by strong silicification and also comprises barite and carbonates. Nevertheless, manganese oxides occur as micro veins and manganese is also present in the mineralized hydrothermal fluid as carbonate minerals (Liakopoulos, 1987; Liakopoulos et al., 2001; Alfieris et al., 2013). On the other hand, Liakopoulos et al. (2001), Alfieris and Voudouris (2005), Alfieris (2006) and Alfieris et al. (2013) suggested that the VA deposit seems to be also controlled by the major NW-trending Kondaros- Katsimouti-VAD fault system, which crosscuts the NE-trending veins at VAD and Katsimouti. According to the above authors, this NW–trending tectonic system was a principal conduit along which hydrothermal solutions partly recharged in a shallow submarine environment forming the Pb–Zn–Ag–Sb–Mn Kondaros–Katsimouti–VAD mineralization, partly in a subaerial setting where they created the sinters at Kondaros. Alfieris and Voudouris (2005) and Alfieris (2006) suggested that formation of the VA manganese deposit marks the final stage of activity along the Kondaros–Katsimouti–VAD fault.

Based on the above statements, it is considered that this tectonic setting was the key to the mineralization in the AG, VA and VAD area, as all field evidences clearly show a spatial and temporal relation to NE-, E-, and NW-trending fault systems. Due to the Kontaros – Katsimoutis fault, the Vani area is open to the sea at NE and part of the Vani Mn deposit is actually under the sea. Similarly, at Aspro Gialoudi, the NE trending fault seems to produce the same results.
(Fig.1,2,8,9,10)

CHPM TARGET FORMATION

The Profitis Ilias prospect in the central-western part of the island is hosted by rhyolites and pyroclastic rocks (rhyolitic lapilli tuffs and ignimbrites) which created an environment suited to veins as well as massive to semi-massive ore bodies mineralization. These ore bodies are enriched in Pb, Zn, Ag, Au, Cu, Sb and Te. Vein widths are up to 3 m across and extend to depths of at least 300 m below the resent-day surface.

The Chondro Vouno epithermal deposit, also located in the central-western part of Milos island, is formed mainly in veins in pyroclastic rocks. The veins are enriched in Pb, Zn, Ag, Au, Cu, Sb and Te.

The Triades-Galana prospect located in the northern-western part of the island is related to veins hosted in dacites, andesites, pyroclastic and volcanosedimentary rocks. These veins are enriched in Ag, Au, As, Bi, W and Mo.

The Kondaros-Katsimouti epithermal Pb-Zn-Ag deposit located along the NW-trending Kondaros-Katsimouti-Vani fault, NW Milos island, is hosted within propylitically and argillically altered dacites, andesites, pyroclastic and volcanosedimentary rocks which created an environment suited to stratabound and stratiform layers, to veins, as well as massive to semi-massive ore bodies mineralization. All these ore bodies are enriched in Ag, Au, As, Bi, W and Mo. The Kondaros-Katsimouti epithermal Pb-Zn-Ag system evolves at higher elevation into the Vani Ag-Pb mineralization, which occurs proximal to the Vani manganese deposit. This VA deposit is a fossil stratabound hydrothermal Mn deposit, enriched in Ba, Pb, Zn, As, Sb and W. At Vani two types of deposits have been recognized: (a) “high-temperature” hydrothermal Mn deposits and (b) bedded hydrothermal Mn, deposits enriched in Mn, Pb, Zn, Cu, Ba, As Sb, Cd, Tl, Co, W, Mo, Sr, Ag, U, Li, i.e.

At Aspro Gialoudi, mineralization is characterized by a stratabound Mn-barite-rich deposit mainly within a package of propylitized intrusive hyaloclastites and within the overlying sandstones. Banded epithermal veins trending NE-SW and composed of chalcedonic silica/quartz + barite + Mn-oxide ±

sulfides crosscut the dacitic lavas, the hyaloclastites and the overlying volcaniclastic sequence at Aspro Gialoudi and are considered to represent the feeder zones of the manganese-barite mineralization. Within the veins, early sulfide (galena-sphalerite) barite and quartz deposition is followed by manganese oxides and aragonite, thus resembling the epithermal-style Pb-Zn-Ag-Mn mineralization across the NW-trending Katsimoutis-Kondaros-Vani fault. Mineralization in Aspro Gialoudi and Vani deposits seems to be controlled by alternating cycles of deposition of sulfides and hydrothermal manganese oxides within the faults.

2. **Geophysics of the prospective area**

Requested information:

- ✓ previous geophysical measurements (in CHPM relevance)
- ✓ geophysical results that can be used for locating/defining the deep metal enrichment
- ✓ list of available geophysical maps, cross sections, logs, other measurements

3. **Deep metal enrichment**

Requested information:

- ✓ **(**expected) metal enrichment based on available geophysical, geological and drill data, samples information, geochemistry

Milos Island is one of the most densely mineralized areas in Greece, characterized by intermediate sulfidation epithermal Au-Ag-Te and base metal deposits (Fig. 6c) under transitional shallow submarine to subaerial conditions (Vavelidis and Melfos, 1998; Kilias et al., 2001; Naden et al., 2005; Alfieris et al., 2013; Papavassiliou et al., 2017). Epithermal type mineralization rich in Au-Ag-Te occurs at **Profitis Ilias** (reserves: 5 Mt at 4.4 g/t Au, 43g/t Ag, and < 0.5 wt.% Fe and 0.2-1.2 wt.% Fe in sphalerite) and **Chondro Vouno** (reserves: to 2.2 Mt grading 5.14 g/tonne Au (cut-off grade 2.5 g/ tonne) or 3.3 Mt grading 4.2 g/tonne (cut-off grade 2 g/ tonne) or 1.2 Mt at1.0 g/t Au and 124 g/t Ag, and < 0.5 wt.% Fe and 0.2-1.2 wt.% Fe in sphalerite), whereas Pb-Zn-Cu-Ag-Mn-Ba-rich mineralization occurs at in the **Triades-Galana** (reported estimated reserves: 10 Mt with a mean Ag content: 500 g/t, resources: 1.2 Mt at 4.2g/t Au or 1.2 Mt at 1 g/t Au and 124 g/t Ag,) and **Kondaros-Katsimouti-Vani** districts (Fig. 4). (Naden et al., 2005; Alfieris et al., 2013; Papavassiliou et al., 2017, RoyalGold news release; www.royalgold.com/news/990615.htm).

This VA deposit lies proximal to the sea between 35 m above sea level and an unknown depth below sea level. The VA deposit is estimated to cover an area between 100,000 and 176,000 m^2 (Liakopoulos et al., 2001)

A far as Profitis Ilias deposit is concerned, in order of decreasing abundance, the main sulphide phases comprise sphalerite, pyrite, galena, chalcopyrite, bornite, marcasite, tetrahedrite and Sb-Ag-Cu

sulphosalts. Post-ore mineralisation comprises barite intergrown with fine-grained quartz and more rarely with galena, sphalerite, pyrite and chalcopyrite. Lastly, the supergene mineralisation consists of native gold, electrum, silver halides, copper sulphides and carbonates, iron oxides, lepidocrocite, tenorite, cerussite, Pb and Zn carbonates, Fe-Al hydroxides, alunite and Mn-oxides.

The metallic mineralogical assemblage at Kondaros-Katsimouti includes mainly galena and sphalerite and minor pyrite. Silver is present in the form of Ag-(Cd)-rich tetrahedrite (up to 23.1 wt. % Ag) and polybasite included in galena. Bulk ore analyses indicate enrichment in W (up to 439 mg/kg) and Mo (up to 24 mg/kg), similarly to the other neighboring mineralizations in western Milos (e.g. Vani, Triades-Galana). Ore samples are also highly enriched in Pb and Zn with concentrations of up to 31.8 wt % and 16.5 wt % respectively. This enrichment suggests a magmatic-hydrothermal contribution to the ore fluids, probably from a buried granitoid at depth. Boiling, in addition to mixing processes between magmatic- and seawater, resulted in pH increase, oxidation and temperature decrease, and resulted into ore deposition.

The Cd concentrations in bulk ore analyses is up to 247 mg/kg Cd for Kondaros area and up to 769 mg/kg Cd for Katsimouti area, which can be explained by the presence of Cd in the structural formula of low-Fe sphalerite and Cd-Ag-rich tetrahedrite. Similarly, the presence of Sb-bearing sulfosalts with minor As-content are responsible for the relevant concentrations in the bulk geochemical analyses (Kondaros: up to 243 mg/kg Sb and up to 36 mg/kg As; Katsimouti: up to 178 mg/kg Sb and up to 42 mg/kg As). Bi, up to 1 mg/kg, may indicate the presence of minor Bi-sulfosalts in the mineralization.

At Aspro Gialoudi, within the veins, early sulfide (galena-sphalerite) barite and quartz deposition is followed by manganese oxides and aragonite, thus resembling the epithermal-style Pb-Zn-Ag-Mn mineralization across the NW-trending Katsimoutis-Kondaros-Vani fault. Mineralization in Aspro Gialoudi and Vani deposits seems to be controlled by alternating cycles of deposition of sulfides and hydrothermal manganese oxides within the faults.

All the ore-forming elements (Mn, Pb, Zn, Cu, As, Sb, Cd, Tl, Co, W and Mo) and elements such as U and Li are enriched in both AG and VA area formations in relation to the mean concentration for the same elements of the continental crust. This indicates an additional source (e.g. the Mn hydro-oxides-bearing feeder zones and the bedded hydrothermal Mn deposit), which can scavenge large quantities of elements like Pb, Zn, Cu, As, U, Mo, Cd and REE (Glasby et al., 2005; Liakopoulos et al., 2001). The metallic mineralization at both AG and VA-VAD is highly enriched in W (up to 428 and 630 ppm respectively) and in lesser amounts of Mo (24 and 27 ppm respectively), in common to other mineralization in northwestern Milos. Glasby et al. (2005) reported extremely high-enrichment (up to 2870 ppm W) for the Vani manganese deposit, Alfieris et al. (2013) reported on a tungsten anomaly (up to 677 ppm) related to Mo anomaly along the NE-trending Triades–Katsimoutis lineament and Papavasiliou et al. (2016) enrichment in W (up to 424 ppm) and Mo (up to 24 ppm) along the Kondaros-Katsimouti epithermal Pb-Zn-Ag mineralization.

Molybdenum is enriched (up to 176 ppm) along two major NE trending lineaments, which also control the surface distribution of silicic- and advanced argillic alteration in northwestern Milos Island: the first one going from Agathia Bay to the Fourkovouni Fyropotamos area (eastern Milos), and the second one along the Triades–Katsimoutis area. Bismuth (up to 2575 ppm in oxidized material) correlates to the molybdenum and tungsten anomalies, and is enriched along the Triades–Katsimoutis lineament in the Triades–Galana area. A Cd enrichment (between Triades–Galana area) is related to the presence of sphalerite in the mineralization. Gold is mostly enriched in the southern sector (around Profitis Ilias–Chondro Vouno) with minor anomalies in the northern sector (e.g., Triades–Galana area). The Au anomalies in the southern sector (up to 32 ppm) are related to NE- (and subordinate NW-) trending patterns, which correspond to the auriferous quartz–chalcedony–base metals–Au–Ag veins in the area. The Au anomalies are disposed in an arcuate manner around a postulated volcanic edifice, which is subjected to a partial caldera collapse. At the northern sector (Triades– Galana) the contours are tightly

spaced and related to the breccia pipes present in the area . Silver shows elevated content (up to 377 ppm) along NW- and NE-trending faults in both the northern and southern sectors and especially in the Triades–Galana and Katsimouti–Vani areas. Vavelidis and Melfos (1998) suggested up to 855 ppm Ag in the Triades mineralization. The similar geochemical pattern between silver and copper (northern sector) and silver and gold (southern sector) is related to the incorporation of these elements in the structure of silver-bearing sulfosalts (e.g., polybasite, pyrargyrite, perceite) and electrum respectively. The base metals Cu, Pb and Zn show a similar distribution in both sectors. In the southern sector, the copper and lead anomalies mostly occur along NW-trending structures around the Chondro Vouno and Profitis Ilias deposits. In the northern sector the lead, zinc and copper anomalies are well pronounced at Vani, Agathia, and Triades–Galana and related to the NE-trending Triades–Katsimouti and Kalogries–Vani faults around the Vani and the Galana areas, respectively.

Enrichment of Cu, Pb and Zn also occurs at the junction of NE and NW–trending faults around Vani. The arcuate-shaped Zn anomalies at Triades–Galana may be related to a caldera structure. Arsenic is almost absent in the southern sector (Profitis Ilias– Chondro Vouno deposits) and is highly enriched (more than 0.4 wt.%) at the northern sector (e.g., Vani, Kondaros, Galana and Triades), where it is related to NE-trending faults. This can explained by the presence of As-bearing sulfosalts (e.g., tennantite, enargite, perceite) in the northern sector compared to their absence in the Profitis Ilias–Chondro Vouno area. The Sb pattern reflects the presence of Sb-bearing sulfosalts (e.g. tetrahedrite, polybasite, pyrargyrite) throughout all mineralization in western Milos. The Sb distribution is related to NE- and N trending faults in both the northern (Vani, Triades, Galana) and southern (Profitis Ilias) sectors. Anomalous mercury (up to 24 ppm) is present at Vani, and Triades–Galana along N-, E- and NE-trending faults. Since no tellurides have been observed in the northern sector, this anomaly may indicate the presence of cinnabar in the mineralization. The presence of coloradoite at Profitis Ilias deposit also suggests anomalous Hg in the southern sector.

Triades-Galana deposit analyses showed up to 4.1 ppm Au, up to 855 ppm Ag, up to 265 mg/kg Mo, up to 848 mg/kg W. Tetraedrites/ tennantites contain up to 15.07 wt.% Ag, 6.3-10.9 wt.% Zn, up to 7.37 wt.% Cd, up to 7.42 wt.% Hg, up to 9.34 wt.% Pb, while enargites contain up to 2.57 wt.% or 7.1 wt.% Ag. Sample analyses from Triades revealed up to 265 mg/kg Mo, up to 15 wt.% Zn, up to 3.27 wt.% Pb, up to 3.28% Cu, up to 2370 mg/kg Cd, up to 0.7 wt.% As, up to 2.2 wt.% Sb, up to 89 mg/kg Tl, up to 848 mg/kg W. Sample analyses from Galana showed up to 225 mg/kg Cd, up to 305 mg/kg As, up to 78 mg/kg Sb, up to 440 mg/kg W. Oxidized hydrothermal breccias contain up to 176 ppm Mo, up to 677 ppm W and up to 2575 ppm Bi.

Kondaros-Katsimouti-Vani (KKV) ore deposit contains up to 24 mg/kg Mo, up to 439 mg/kg W (Kondaros-Katsimouti), up to 31.8 wt.% Pb, up to 16.5 wt.% Zn, up to 1 mg/kg Bi, up to 247 mg/kg Cd (in Kondaros), up to 769 mg/kg Cd (in Katsimouti), up to 243 mg/kg Sb (in Kondaros), up to 178 mg/kg Sb (in Katsimouti), up to 36 mg/kg As (in Kondaros) and up to 42 mg/kg As (in Katsimouti).Tetrahedrites contain around 24.3-32.05 wt. % Cu, 26.5-28.5 wt.% Sb, up to 16.2 wt.% Ag or up to 23.06 wt.% Ag, 3-5 wt.% Zn, up to 7.5 wt.% Pb and up to 5.39 wt.% Cd. Sphalerites contain around 0.8-2.5 wt.% Fe, up to 0.3 wt.% In. Polybasite samples contain up to 70 wt.% Ag, up to 8.3 wt.% Cu, 10.8 wt.% Sb and < 1.5 wt.% Pb.

Vani deposit analyses showed up to 428-630 ppm or up to 2870 mg/kg W, up to 24-27 ppm Mo, up to 69 wt% MnO, up to 6.6 wt% Pb, up to 1.2 wt% Zn, up to 0.8 wt% TiO_2, up to 3679 ppm Sb, up to 3515 ppm As, up to 2873 ppm W, up to 3499 ppm Sr, up to 114 ppm Ag, up to 7.7 ppm Eu, 7.7-91 ppm Ce, 4.5-54.3 ppm La, 5.6-34.5 ppm Y, 1.7-18.6 ppm Nb, 0.8-6.4 ppm Pr, 3.5-26.3 ppm Nd, 0.8-5.7 ppm Sm, 1.3-6.7 ppm Gd, up to 0.8 ppm Tb, up to 5.3 ppm Dy, up to 1.1 ppm Ho, up to 4.1 ppm Er, up to 0.7 ppm Tm, up to 5.3 ppm Yb, up to 0.9 ppm Lu, up to 8.1 ppm Hf, 3.9-13.1 ppm Ta, 1.0-10.4 ppm Th and 1.2-19.0 ppm U.

The spatial coordinates (in WGS84 format) of the polygon vertices of the Profitis Ilias mineralization area are defined as follows:
• Vertex A
ϕ: 36o 40′53.30”N, λ: 24o 22′26.48”E
• Vertex B
ϕ: 36o 40′52.72”N, λ: 24o 23′12.63”E
• Vertex C
ϕ: 36o 40′12.17”N, λ: 24o 23′09.83”E
Vertex D
ϕ: 36o 40′13.95”N, λ: 24o 22′23.90”E

The spatial coordinates (in WGS84 format) of the polygon vertices of the Chondro Vouno mineralization area are defined as follows:
• Vertex A
ϕ: 36o 41′03.57”N, λ: 24o 21′52.80”E
• Vertex B
ϕ: 36o 41′08.05”N, λ: 24o 22′35.86”E
• Vertex C
ϕ: 36o 40′40.19”N, λ: 24o 22′34.26”E
• Vertex D
ϕ: 36o 40′41.36”N, λ: 24o 21′56.39”E

The spatial coordinates (in WGS84 format) of the polygon vertices of the Triades-Galana mineralization area are defined as follows:
• Vertex A
ϕ: 36o 42′50.74”N, λ: 24o 20′13.11”E
• Vertex B
ϕ: 36o 42′50.74”N, λ: 24o 20′52.05”E
• Vertex C
ϕ: 36o 42′08.82”N, λ: 24o 20′52.05”E
• Vertex D
ϕ: 36o 42′08.82”N, λ: 24o 20′09.01”E

The spatial coordinates (in WGS84 format) of the polygon vertices of the Triades-Galana mineralization area are defined as follows:
• Vertex A
ϕ: 36o 45′04.37”N, λ: 24o 21′15.33”E
• Vertex B
ϕ: 36o 44′48.33”N, λ: 24o 21′12.56”E
• Vertex C
ϕ: 36o 43′40.05”N, λ: 24o 22′34.41”E
• Vertex D
ϕ: 36o 43′26.24”N, λ: 24o 22′07.99”E
• Vertex E
ϕ: 36o 44′22.13”N, λ: 24o 20′15.81”E

The polygons of the above mineralization areas on Google Earth are depicted in Figure 7.

4. **Integrated 3D- 4D model**

Requested information:

- ✓ existing 3D-4D models of the target area and the deep metal enrichment
- ✓ if no 3D-4D models exist, collect the following necessary data: geological setting, mineralization, fluid flow models, stress field determination

Notes: e.g. openly available datasets, models.

5. **EGS potential**

Requested information:

- ✓ EGS potential (heat & energy) of the area
- ✓ geothermal characteristics (temperature gradient, heat flux, stress field, water availability, EGS geology)
- ✓ presence/indication of deep fluids/brines, fracture system, crustal permeability

GEOPHYSICAL SURVEYS

Milos Island is characterized by a high-enthalpy geothermal field and is one of the few places in the world where submarine hydrothermal vents occur at shallow depths (Fitzsimons et al., 1997; Dando et al., 1999, 2000; Liakopoulos, 1987; Liakopoulos et al., 1991, 2001; Pflumio et al., 1991; Wu et al., 2016). All Milos deposits are closely associated with active geothermal systems that are characterized by mixing of seawater, meteoric and, minor magmatic water (Naden et al., 2005; Alfieris et al., 2013; Papavassiliou et al., 2017, RoyalGold news release; www.royalgold.com/news/990615.htm).

The heat flow density of Western Milos is about 300-400 mW/m^2 (average global heat flow density 70 mW/m^2) and the geothermal gradient up to 3.78^{o}C/10m or 37.8^{o}C/100m.

Geothermal exploration on Milos was started in 1971 by IGME with geological mapping, thermal manifestation surveys, soil and water sampling and geochemical analyses. Also a thermal gradient survey in shallow boreholes (50–80m depth; Fig. 4) was done. IGME and Compagnie Gınırale de Gıophysique (CGG) carried out Schlumberger resistivity surveys in the eastern half of the island in 1972–1973. The first two exploration wells MA1 and MZ1 (Fig. 6,7) were drilled in 1975, reaching depths of 1163mand 1101 m, respectively. These initial geothermal exploration efforts were complemented by an Ente Nazionale per l'Energia Elettrica (ENEL) study in 1977 that included: mapping of volcanic, hydrogeologic, thermal, stratigraphic and structural features; geochemical investigations with fluid sampling of hot springs, shallow and deep wells, and logging and testing of wells MA1 and MZ1. In 1981, deep wells M1, M2 and M3(1180 m, 1381mand 1017 m, respectively) were drilled by the PPC (Fig. 7); the project was supported by the EC. As part of another Milos EC project a gravity survey and some additional DC-Schlumberger resistivity surveys were carried out by IGME between 1982 and 1984. The project also included volcanologic, petrologic, mineralogical, tectonic and geomorphologic studies of Milos and nearby islands. Between 1985 and 1987, the EC supported a series of geophysical explorations of the island that included magneto-telluric (MT) soundings by teams from the Technische Universitat Braunschweig (Drews et al., 1989), the Bureau de Recherches Gıologiques et Minieres (Beauce et al., 1989), the University of Edinburgh (Hutton et al., 1989), and the University of Frankfurt and the Freie University of Berlin (Haak et al., 1989), monitoring of micro earthquakes by the Rheinisch-Westfaelische Technische Hochschule-Aachen (Ochmann et al., 1989) and the Physique du Globe Institute, Paris (Hirn et al., 1989), as well as self-potential and magnetic surveys by IGME (Thanassoulas, 1989). The MT surveys identified a zone of coherent low resistivity at depth (see Fig. 2). Since then, other reservoir and chemical studies have been performed. These include modelling of heat and mass transfer in the Milos hydrothermal system (Mendrinos, 1988), which estimated the potential of the high-enthalpy geothermal resources of Milos as 150MWe, an estimation of the conductive heat loss (77MWt) over the island of Milos (Mendrinos, 1991), as well as sampling and analysis of submarine springs near the coast of the island during the summers of 1996–1999 by a team of scientists from the Natural History Museum of London, the National University of Athens, the University of Nottingham, the Scottish Universities Environmental Research Centre, the College of Staten Island, the University of London and the University of Bristol (Valsami-Jones et al., 2005).

On the eastern part of the island there are phreatomagmatic craters, hot water and steam discharge sites (up to 115 °C) both on-land and off-shore, indicative of intense active geothermal activity (Cronan and Varnavas, 1999; Dando et al., 1995; Fytikas, 1989; Fytikas and Marinelli, 1976; Fytikas et al., 1986, 1989; Stüben and Glasby, 1999; Valsami-Jones et al., 2005; Wu et al., 2012). The active submarine hydrothermal system at Palaeochori Bay (offshore of the southeastern coast of Milos) discharges gas and brines from the sea bottom at a depth of 10 m and temperatures higher than 90 °C similar to Lihir (60 to 96 °C; Pichler et al., 1999a), Papua New Guinea (89 to 98 °C; Pichler et al., 1999b), and Bahia Concepcion, Mexico (62 to 87 °C; Canet et al., 2005). Geothermal drilling carried out during the 70's and 80's by the Greek Public Power Corporation (PPC) demonstrated the presence of a high-enthalpy geothermal field characterized by two-cell circulation (Fitzsimons et al., 1997; Fytikas and Marinelli,

1976; Liakopoulos, 1987; Liakopoulos et al., 1991; Naden et al., 2003, 2005; Pflumio et al., 1991; Wu et al., 2012): (a) a high-temperature (300–325 °C), saline reservoir at 1–2 km depth with chlorinity >2.5 times seawater (average 9 wt.% equiv. NaCl) and (b) a low temperature (b248 °C), shallow reservoir inferred at 500 m below seafloor (Naden et al., 2005; Wu et al., 2012). Subcritical phase separation (boiling) close to the top of the deep reservoir forms low-Cl vapor-like fluids and residual high-Cl brines. Both reservoirs are contributing to the hydrothermal vent fluids, which were recovered from the shallow submerged system at Palaeochori Bay (Valsami-Jones et al., 2005; Wu et al., 2011, 2012). The vapor-like fluids rise directly to form near sea-level low pH and chlorinity discharges, whereas the saline fluids transport in different pathways and are influenced by seawater mixing to form the variable submarine-brine fluids (Wu et al., 2011, 2012). A third type of hydrothermal vent fluid at Paleochori Bay, the seawater-like fluids, probably resulted from heating of down-flow seawater and may have experienced boiling in the shallow reservoir without pre-existing brines (Wu et al., 2011, 2012). Metalliferous sediments and chimney-like structures in the immediate vicinity of areas of active discharge at shallow depths (0–15 m water depth) at Palaeohori Bay consist of arsenian pyrite, marcasite, orpiment, native sulfur, barite, gypsumand calcite (Cronan and Varnavas, 1999; Kati et al., 2003; Price et al., 2012; Stüben and Glasby, 1999). According to Price et al. (2012), the hydrothermal fluids discharging in Paleochori Bay (both the vapor and brine) contain the highest concentration of arsenic reported for any hydrothermal system, including mid-ocean ridge and back-arc basin vent fluids. The deposition of sulfide-bearing scales at temperatures of about 200–230 °C and upon boiling in the geothermal plant facilities (Andritsos and Karabelas, 1991)

For the Western Milos geothermal field borehole data from well in Rivari at 65 m showed temperature of 44^{o}C, from well in Emporios at 70 m showed temperature of 39^{o}C, while in Xylokeratia 1 well at 65m, 2 wells at 70m and 1 well at 75m showed temperatures of 41^{o}C, 40^{o}C, 43^{o}C and 41.5^{o}C respectively.

For the Central Milos geothermal field the geothermal survey carried out by the PPCR-Greece revealed that the exploration well MZ-1837 at 1080 m showed temperatures that reached 310-320^{o}C, the exploration well M-21150 at 1200 m showed temperatures that reached 318^{o}C and the exploration well MA at 1827 m showed temperatures that reached 270^{O}c and at 1000m reached 310^{o}C.

The coordinates (decimal/WGS84) of significant wells (T: 270-323^{o}C) in central Milos are as follows

• Exploration well MZ-1
ϕ: 36.7046457 (36o 42′16.72” N), λ: 24.4872448 (24o 29′14.08” E)
• Exploration well M-1
ϕ: 36.7000996 (36o 42′0.36” N), , λ: 24.498777 (24o 29′55.60” E)
• Exploration well M-2
ϕ: 36.7107506 (36o 42′38.70” N), λ: 24.5009214 (24o 30′03.32” E)
• Well MA-1
ϕ: 36.735605 (36o 44′08.18” N), λ: 24.448729 (24o 26′55.42” E)

The locations of these wells on Google Earth are depicted in Figure 11.

CONCLUSIONS AND

JUSTIFICATION FOR THE CHOICE OF THE THERMES AREA AS A PROSPECTIVE CHPM AREA

Taking into account that

- the Profitis Ilias prospect rich in Pb, Zn, Ag, Au, Cu, Sb, Te is hosted in rhyolites and pyroclastic rocks forming massive to semi-massive ore bodies

- the Chondro Vouno prospect rich in Pb, Zn, Ag, Au, Cu, Sb, Te is hosted in veins in pyroclastic rocks

- the Triades-Galana prospect rich in Ag, Au, As, Bi, W, Mo is hosted in veins in dacites, andesites, pyroclastic and volcanosedimentary rocks

- the Kondaros-Katsimouti-Vani prospect rich in Ag, Au, As, Bi, W, Mo is hosted in dacites, andesites, pyroclastic and volcanosedimentary rocks forming stratabound and stratiform layers, veins, as well as massive to semi-massive ore bodies.

- as it is stated at section tables of the report 1 and 3, three fault systems define the geometry of the region and it is considered that this tectonic setting was the key to the mineralization.

- exploration wells at 800-1200m measured temperatures between 270- 320^{o}C
- EGS system can be developed in fractured rocks (Western Milos) in the vicinity of the Central Milos active hydrothermal system (proven high temperature geothermal field)

the choice of the Western Milos island area as a CHPM target for further exploration can be justified.

The spatial coordinates (in WGS84 format) of the polygon vertices of the prospective CHPM area of Western Milos are defined as follows:

• Vertex A
ϕ: 36.6891267 (36o 41′20.86”), λ: 24.4344284 (24o 26′03.94′′)
• Vertex B
ϕ: 36.7490052 (36o 44′56.42”), λ: 24.3518067 (24o 21′06.50′′)
• Vertex C
ϕ: 36.6458091 (36o 38′44.91”), λ: 24.3219754 (24o 19′19.11′′)
• Vertex D
ϕ: 36.6693392 (36o 40′09.62”), λ: 24.4479295 (24o 26′52.55′′)

The polygon of this prospective CHPM area on Google Earth is depicted in Figure 11.

List of references

Alfieris, D. and Voudouris, P., 2005. Ore mineralogy of transitional submarine to subaerial magmatic-hydrothermal deposits in W. Milos, Greece. In: Cook, N.G., Bonev, I., eds., Au-Ag-Te–Se deposits, Geochemistry, Mineralogy and Petrology, 43. Sofia, 1–6.

Alfieris, D., 2006. Geological, geochemical and mineralogical studies of shallow submarine epithermal mineralization in an emergent volcanic edifice, at western Milos island, Greece. PhD thesis, University of Hamburg, Germany, 211 pp.

Alfieris D., Voudouris P. and Spry P.G., 2013. Shallow submarine epithermal Pb–Zn–Cu–Au–Ag–Te mineralization on western Milos Island, Aegean Volcanic Arc, Greece: Mineralogical, geological and geochemical constraints. Ore Geology Reviews 53: 159–180.

Andritsos, N.and Karabelas, A.J., 1991. Sulfide scale formation and control: the case of lead sulfide. Geothermics 20, 343–353.

Canet C., Prol-Ledesma R.-M., Proenza J.A., Rubio-Ramos M.A., Forrest M.J., Torres Vera M.A. and Rodriguez-Diaz A.A., 2005. Mn–Ba–Hg mineralization at shallow submarine hydrothermal vents in Bahia Concepcion, Baja California Sur, Mexico. Chem. Geol. 224, 96–112.

Christanis K. and Seymour K., 1995. A study of scale deposition: an analogue of meso- to epithermal ore formation in the volcano of Milos, Aegean arc, Greece. Geothermics Vol. 24, No. 4, pp. 541-552.

Cronan, D.S. and Varnavas, S.P., 1999. Metalliferous sediments off Milos, Hellenic Volcanic Arc. Explor. Min. Geol. 8, 289–297.

Dando P.R., Stuben D. and Varnavas S.P., 1999. Hydrothermalism in the Mediterranean Sea. Proc. Oceanogr. 44, 333–367.

Dando P.R., Alian, S., Arab H., Bianchi C.N., Brehmer M., Cocito S., Fowler S.W., Gundersen J., Hooper L.E., Kolbl R., Kuever J., Linke P., Makropoulos K.C., Meloni R., Miquel J.C., Morri C., Muller S., Robinson C., Schlesner H., Sievert S., Stohr R., Stuben D., Thomm M., Varnavas S.P. and Ziebis, W., 2000. Hydrothermal studies in the Aegean Sea. Phys. Chem. Earth 25, 1–8.

Fitzsimons M.F., Dando P.R., Hughes J.A., Thierman, F., Akoumianaki I., Pratt, S.M. and 1997. Submarine hydrothermal brine seeps offMilos, Greece: observations and geochemistry. Mar. Chem. 57, 325–340.

Fu Wu S., Feng You C., Po Lin Y., Valsami-Jones E and Baltatzis E., 2016. New boron isotopic evidence for sedimentary and magmatic fluid influence in the shallow hydrothermal vent system of Milos Island (Aegean Sea, Greece). Journal of Volcanology and Geothermal Research 310: 58–71.

Fytikas M., Giuliani 0., Innocenti F., Marinelli G. and Mazzuoli R., 1976. Geochronological data on recent magmatism of the Aegean Sea. Tectonophysics 31: 29-34.

Fytikas M. And Marinelli G., 1976. Geology and geothermics of the island of Milos (Greece). International Congress on Thermal Waters, Geothermal Energy and Volcanism of the Mediterranean Area. Institute of Geology and Mineral Exploration (58 pp.).

Fytikas M., 1977. Geological and geothermal study of Milos island (in Greek with English abstract). Unpublished report, IGME Athens, Greece, XVII No 1.

Fytikas M., Innocenti F., Manetti P., Mazzuoli R., Peccerillo A. and Villari L., 1984. Tertiary to Quaternary evolution of volcanism in the Aegean region. In: Dixon JE, Robertson AHF (eds) The geological evolution of the eastern Mediterranean. Geol Soc Lond Spec Publ 17: 687-699.

Fytikas M., Innocenti F., Kolios N., Manetti P., Mazzuoli R., Poli G., Rita F. and Villari L., 1986. Volcanology and petrology of volcanic products from the island of Milos and neighbouring islets. J Volcanol Geotherm Res 28: 297-317.

Fytikas M., 1989. Updating of the geological and geothermal re- search on Milos island. Geothermics 18: 485-496.

Fytikas M., Garnish .JD., Hutton V.R.S., Staroste E. and Wohlenberg J., 1989. An integrated model for the geothermal field of Milos from geophysical experiments. Geothermics 18: 611-628

Glasby, G.P., Papavassiliou, C.T., Mitsis, J., Valsami-Jones, E., Liakopoulos, A., Renner, R.M., 2005. The Vani manganese deposit, Milos island, Greece: a fossil stratabound Mn– Ba–Pb–Zn–As–Sb–W-rich hydrothermal deposit. In: Fytikas, M., Vougioukalakis, G.E. (Eds.), The South Aegean Active Volcanic Arc: Present Knowledge and Future Perspectives. Developments in Volcanology, 7. Elsevier, pp. 255–291.

Kati, M., Valsami-Jones, E., Baltatzis, E. and Magganas, A., 2003. Hydrothermal precipitates from the active submarine vents in Paleochori Bay, Milos Island, Greece. The South Aegean Active Volcanic Arc, International Conference, Milos Island, Greece, Book of Abstracts, p. 71.

Kilias S. P., Naden J., Cheliotis I., Shepherd T. J., Constandinidou H., Crossing J. and Simos I., 2001. Epithernal gold minineralisation in the active Aegean Volcanic Arc: the Profitis Ilias deposit, Milos Island, Greece. Mineralium Deposita 36: 32-44.

Liakopoulos A. and Boulegue J.,(1987. A geochemical model for the origin of geothermal fluids and the genesis of mineral deposits on Milos Island. Terra Cognita 7: 228.

Liakopoulos A., Katerinopoulos A., Markopoulos T. and Boulegue J., 1991. A mineralogical petrographic and geochemical study of samples from wells in the geothermal field of milos island (Greece). Jeorhermics. VoL 20. No. 4, pp. 237-256.

Liakopoulos, A., Glasby, G.P., Papavassiliou, C.T. and Boulegue, J., 2001. Nature and origin of the Vani manganese deposit, Milos, Greece: an overview. Ore Geol. Rev. 18, 181–209.

Naden J., Kilias S. P. and Darbyshire F., 2005. Active geothermal systems with entrained seawater as analogues for low-sulphidation epithermal Mineralization. Geology Manuscript.

Papavasiliou, K., Voudouris, P., Kanellopoulos, C., Alfieris, D. and Xydous, S., 2016. The Kondaros-Katsimouti Intermediate-Sulfidation Epithermal Pb-Zn-Ag-Mn Mineralization, Western Milos, Greece: New Mineralogical and Geochemical Data. Bull. Geol. Soc, Greece in press.

Papavassiliou K., Voudouris P., Kanellopoulos C., Glasby G., Alfieris D. and Mitsis I., 2017. New geochemical and mineralogical constraints on the genesis of the Vani hydrothermal manganese deposit at NW Milos island, Greece: Comparison with the Aspro Gialoudi deposit and implications for the formation of the Milos manganese mineralization. Ore Geology Reviews 80: 594–611.

Pflumio C., Boulegue J., Liakopoulos A. and Brique L., 1991. Oxygen, hydrogen, strontium isotopes and metals in the present-date and past geothermal systems of Milos Island (Aegean arc). In: Pagel, M., Leroy, J.L. (Eds.), Source. Transport and Deposition of Metals. Balkema, Rotterdam, pp. 107–112.
Price R.E., Savov I., Planer-Friedrich B., Bühring S.I., Amend J. And Pichler, T., 2012. Processes influencing extreme As enrichment in shallow-sea hydrothermal fluids of Milos Island, Greece. Chem. Geol. http://dx.doi.org/10.1016/j.chemgeo.2012.06.007.

Pichler T., Giggenbach W.F., McInnes B.I.A. and Duck B., 1999a. Fe–sulfide formation due to seawater–gas–sediment interaction in a shallow-water hydrothermal system, Lihir Island, Papua New Guinea. Econ. Geol. 94, 281–288.

Pichler T., Veizer J. and Hall G.E.M., 1999b. The origin and chemical composition of shallow-water hydrothermal fluids in Tutum Bay, Ambitle Island, Papua New Guinea and their effect on ambient seawater. Mar. Chem. 64, 229–252.

Price R. E., Savov I., Planer-Friedrich B., Bühring S. I., Amend J. and Pichler T., 2013. Processes influencing extreme As enrichment in shallow-sea hydrothermal fluids of Milos Island, Greece. Chemical Geology 348: 15–26.

Stewart A. L. and McPhie J., 2006. Facies architecture and Late Pliocene – Pleistocene evolution of a felsic volcanic island, Milos, Greece. Bull Volcanol 68: 703–726 DOI 10.1007/s00445-005-0045-2.

Stüben D. and Glasby, G.P., 1999. Geochemistry of shallow submarine hydrothermal fluids from Paleohori Bay, Milos, Aegean Sea. Explor. Min. Geol. 8, 273–287.

Tsokas G.N., 1996. Interpretation of the Bouguer anomaly of Milos island (Greece). J Volcanol Geotherm Res 72: 163-181.

Valsami-Jones E., Baltatzis E., Bailey E.H., Boyce A.J., Alexander J.L., Magganas A., Anderson L., Waldron S. and Ragnarsdottir, K.V., 2005. The geochemistry of fluids from an active shallow submarine hydrothermal system: Milos island, Hellenic Volcanic Arc. J. Volcanol. Geotherm. Res. 148, 130–151.

Vavelidis, M., Melfos, V., 1998. Fluid inclusion evidence for the origin of the barite silver– gold-bearing Pb–Zn mineralization of the Triades area, Milos Island, Greece. Bull. Geol. Soc. Greece 32, 137–144.

Wu S.F., You C.F., Wang B.S., Valsami-Jones E. and Baltatzis, E., 2011. Two-cells phase separation in shallow submarine hydrothermal system at Milos Island, Greece: Boron isotopic evidence. Geophys. Res. Lett. 38 http://dx.doi.org/10.1029/2011 GL047409.

Wu S.F., You C.F., Valsami-Jones E., Baltatzis E. and Shen M.L., 2012. Br/Cl and I/Cl systematic in the shallow-water hydrothermal system at Milos Island, Hellenic Arc. Mar. Chem. 140–141, 33–43.

Wu S.F., You C.F., Lin Y.P. Valsami-Jones and E., Baltatzis, E., 2016. New boron isotopic evidence for sedimentary and magmatic fluid influence in the shallow hydrothermal vent system of Milos Island (Aegean Sea, Greece). J. Volcanol. Geoth. Res. 310, 58–71.

Annexes

Contact projects@eurogeologists.eu for the full list of Annexes, or open it at the CHPM Information Platform on Prospective Locations (http://bit.ly/CHPMinfoplatform)

Evaluation of the basic characteristics of prospective CHPM areas

Name of the National Association AGG
Number of the prospective area 3 **Evros Area**

1. Geology of the prospective area
Requested information on:
- ✓ local geology (in regional context)
- ✓ CHPM target formation
- ✓ list of available cross sections, geological maps, geochemical results, lithological information

Notes: briefly summarized, referenced to more detailed studies.

- ✓ **Local geology**

The area of Evros that includes the Pefka and Loutros ore districts have the following geological formations

1. Quaternary Alluvial Sediments
2. Tertiary Sedimentary and Volcanosedimentary series
3. Oligocene- Miocene Volcanic Rocks

- ✓ The basin occasionally reaches depths of 3,500 to 4,000 m and it is bounded by major faults. The Paleogene – Eocene sediments have been deposited unconformably upon the Mesozoic formations or to the west upon the gneisses, amphibolites and ophiolites of the Rhodope massif. The marine Paleogene sediments (average thickness of about 2,000 m) consist of sandstones, marls, limestones, polygenic volcanic breccia, tuffs and siltstones. The Neogene and Quaternary sediments (maximum thickness of 1,500 m) consist of clays, siltstones, sandstones, lignitic layers and in the upper section of the sedimentary sequence sands, sandstones and clays exist. The beginning of the marine Tertiary invasion in the Evros basin is suggested during the Middle Eocene (Lutetian). **Fig 1.1** features a geological map of the area

2. Geophysics of the prospective area
Requested information:
- ✓ previous geophysical measurements (in CHPM relevance)
- ✓ geophysical results that can be used for locating/defining the deep metal enrichment
- ✓ list of available geophysical maps, cross sections, logs, other measurements

3. Deep metal enrichment

Requested information:

- ✓ **(**expected) metal enrichment based on available geophysical, geological and drill data, samples information, geochemistry

At **Pefka** mine, precious metal mineralization occurs in a quartz-enargite-rich vein and in a quartz-carbonate vein of high- and intermediate sulfidation affinity respectively (Dimou et al. 1994; Voudouris 2006; Repstock 2011; Repstock et al. 2015). The latter resembles the carbonate veins at Kassiteres-Sapes area. High-to-intermediate sulfidation epithermal Cu-Au- Ag-Te deposit located in the Evros mineralization district is hosted in andesitic to rhyolitic volcanic rocks. A whole rock KAr age of 30.7 ± 1.2 Ma was reported for a trachyandesite (Christofides et al., 2004). The main alteration styles are silicification, sericitization, and advanced argillic alteration, which are crosscut by late carbonate-bearing veins related to E- and NNW-trending faults. Two distinct mineralization styles are observed in Pefka (Voudouris, 2006; Repstock et al., 2015):

(1) Early high-sulfidation veins with enargite, Bi-sulfosalts, and gold; and (2) late intermediate-sulfidation veins with tennantite/tetrahedrite and Au-Ag tellurides. Bulk analyses of mineralized samples from both epithermal mineralization styles contain up to 10 ppm Au, up to 23.5 ppm Mo, up to 105 ppm Bi, up to 468 ppm Te, up to 675 ppm In, 17 ppm Ga, 6 ppm Ge, >100 ppm Ag, >1 wt.% Cu and >1 wt.% As (Melfos and Voudouris, 2012; this study). Past mining operations produced 3 Kt ore at 7% Cu.

The **Loutros** area, close to the Greek-Turkish border, hosts an intermediate-sulfidation epithermal deposit associated with a zeolite-altered rhyolitic lava dome, which yielded which yielded a whole rock K-Ar age of 19.53 ± 0.75 Ma (Christofides et al., 2004). The mineralization consists mainly of early NWtrending massive pyrite and marcasite veins and breccias, and late-stage barite-galena veins with sphalerite and minor chalcopyrite.The barite-galena veins contain up to 31 ppm Ag. See **Fig 3.1** for the chemical analysis tables.

4. Integrated 3D- 4D model

Requested information:

- ✓ existing 3D-4D models of the target area and the deep metal enrichment
- ✓ if no 3D-4D models exist, collect the following necessary data: geological setting, mineralization, fluid flow models, stress field determination

Notes: e.g. openly available datasets, models.

5. EGS potential

Requested information:

- ✓ EGS potential (heat & energy) of the area
- ✓ geothermal characteristics (temperature gradient, heat flux, stress field, water availability, EGS geology)
- ✓ presence/indication of deep fluids/brines, fracture system, crustal permeability

- ✓ The thermal springs of Traianoupolis with water temperature at 50°C indicate initially the geothermal interest in the Evros Delta basin. The geothermal interest in the area is associated with the favorable stratigraphy, the active tectonics with faults in the N70o and N160o directions, the uprising of the isothermal curves towards to the surface, the alternations of the volcanics with the pyroclastites, the volcanic activity and the magmatic bodies related to heat production.
- ✓ The geothermal anomaly is located at the places where the magmatic bodies and the active faults occur (Figure 3) and it seems to be developed gradually northwards. The hydrothermal aquifers are located in the altered volcanic formations and pyroclastites of high secondary permeability. One geothermal reservoir with water temperatures T>86°C are located at about 360 m depth within the volcanic products (pyroclastites). Another hydraulic system with water temperature of 50°C is developed at depths of 200 m in the area of the primary geothermal interest. This is a case of superficial hydraulic system with local geothermal interest located NE of the Aristino village and heated by conduction. The recharge area of the hydrothermal system in the Aristino field is likely placed in the Rhodope Mounts northwards and the Aegean Sea southwards. Possibly this hydrothermal aquifer is supplied through faults by the underlying deeper reservoir containing higher temperature waters. Southwards and at the deeper levels of the basin, geothermal reservoirs containing waters with temperatures up to 32°C are developed in the base of the Neogene sediments at depths >350 m. The geothermal waters in the Aristino field are of the Na-Cl type in chemical composition. Their TDS values range from 4.3 to 10.5 g/l and their Ca2+ and SO4 2- content are relatively high. The thermal waters from the springs of Traianoupolis belong to the same type.
- ✓ Deep oil exploration boreholes EVROS-1, DELTA-1, DEV-1, DEV-2, and DEV-3 were drilled in the Evros Delta basin. Borehole EVROS-1 of 2658 m was drilled during 1956-57 for defining the Neogene sediments of the area. In order to study the sedimentary sequence another exploration well, DELTA-1, was constructed during 1962- 63 at depth of 3548 m. Oil exploration boreholes DEV-1, DEV-2 and DEV-3 were drilled in the Evros Delta basin during 1981-1982. Borehole DEV-1 has a depth of 4229 m. The stratigraphic column of this well is: 0-650 m Plio-Quaternary deposits (alternations of sands, clays and sandstones), 650-1153 m Miocene sediments (clays, siltstones, sandstones, dolomites with layers of lignites), 1153-3270 m Oligocene – Eocene formations (limestones, alternations of marls, sandstones and siltstones, tuffs, polygenic conglomerates, polygenic and volcanic breccias) and 3270-4229 m basement (quartzitic, dioritic porphyres) (S.P.E.G., 1982a,b; Lalechos, 1986). The temperatures of 68, 96, 136 and 146°C were measured at 1600, 2740, 3975 and 4229 m respectively (S.P.E.G., 1982a,b). The stratigraphy of borehole DEV-2 drilled to a total depth of 3213 m was: 0-600 m Plio-Quaternary deposits (sandstones, clays, gravels), 600-1650 m Miocene sediments (alternations of clays, clayey-sandstones and conglomerates with layers of lignite), 1650-2980 m. See **Fig 5.1** and **Fig 5.2** for the isothermal curves distribution and the hydrothermal model of the geothermal field respectively.
- ✓ <u>Aristino Alexandroupolis geothermal field - Coordinates of wells (decimal / WGS84):</u>

  · Wells AA-1 & AA-1P
    - ϕ: 40.8758432 (40° 52′33.04″), λ: 26.0088844 (26° 0′31.98′′)

  · Well AA-3
    - ϕ: 40.8867651 (40° 53′12.35″), λ: 25.9940676 (25° 59′38.64′′)

  · Well AA-3P
    - ϕ: 40.8866479 (40° 53′11.93″), λ: 25.9940797 (25° 59′38.69′′)

  · Well AA-4

    ϕ: 40.8760431 (40° 52′33.76″), λ: 25.9973566 (25° 59′50.48′′)

  · Well AA-4P
    - ϕ: 40.8761064 (40° 52′33.98″), λ: 25.9975442 (25° 59′51.16′′)

  · Well KO-1

- ϕ: 40.8817545 (40° 52′54.32”), λ: 26.0122028 (26° 0′43.93’’)

· Well E-3

- ϕ: 40.8870732 (40° 53′13.46”), λ: 26.0130177 (26° 0′46.86’’)

➢ Coordinates of polygon vertices of the Aristino Alexandroupolis geothermal field (decimal/WGS84):

· Vertex A

- ϕ: 40.8556286 (40° 51′20.26”), λ: 25.9563682 (25° 57′22.93’’)

· Vertex B

- ϕ: 40.9092449 (40° 54′33.28”), λ: 25.9763494 (25° 58′34.86’’)

· Vertex C

- ϕ: 40.898444 (40° 53′54.40”), λ: 26.1053902 (26° 06′19.40’’)

· Vertex D

- ϕ: 40.8472987 (40° 50′50.28”), λ: 26.1079398 (26° 06′28.58’’)

➢ Coordinates of deep hydrocarbon exploration wells in the Evros Delta area (WGS84):

· Borehole DEV-1

ϕ: 40o 49′50”, λ: 26o 06′15’’

· Borehole DEV-2

ϕ: 40o 48′56.04”, λ: 26o 06′58.42’’

· Borehole DEV-3

ϕ: 40o 49′10.44”, λ: 26o 09′ 14.01’

➢ Coordinates of polygon vertices of the Pefka - Loutros mineralization area (WGS84):

· Vertex A

ϕ: 40o 55′20.91” N λ: 26o 00′15.38” E

· Vertex B

ϕ: 40o 55′09.59” N λ: 26o 06′37.17” E

· Vertex C

ϕ: 40o 50′37.44” N λ: 26o 06′35.04” E

· Vertex D

ϕ: 40o 52′14.61” N λ: 26o 00′16.86” E

➢ Coordinates of polygon vertices of the prospective CHPM area (WGS84):

· Vertex A

ϕ: 40o 50′41.73” N λ: 25o 56′08.83” E

· Vertex B

ϕ: 40o 56′50.81” N λ: 25o 56′10.28” E

· Vertex C

ϕ: 40° 55′55.32” N λ: 26° 16′45.93’’E

· Vertex D

ϕ: 40° 45′03.51” N λ: 26° 01′50.08” E

List of references

Melfos V., Voudouris P., 2017. Cenozoic metallogeny of Greece and potential for precious, critical and rare metals exploration, *Ore Geology Reviews 89, p.1030-1057*

Mendrinos D., Choropanitis I., Polyzou O., Karytsas C., 2010. Exploring for geothermal resources in Greece , *Geothermics 39, p. 124-137*

Kolios N., Koutsinos S., Arvanitis A., Karydakis G., 2005. Geothermal situation in Northeastern Greece. *Proceedings World Geothermal Congress*

Kolios N., Fytikas M., Arvanitis A., Andritsos N., Koutsinos S., 2007. Prospective Medium Enthalpy Geothermal Resources in Sedimentary Basins of Northern Greece*, Proceedings European Geothermal Congress*

Repstock A., Voudouris P., Zeug M., Melfos V., Zhai M., Li H., Kartal T., Matuszczak J., 2016. Chemical composition and varieties of fahlore-group minerals from Oligocene mineralization in the Rhodope area, Southern Bulgaria and Northern Greece.

Christofides G., Pecskay Z., Eleftheriadis G., Soldatos T., Koroneos A., 2004. The Tertiary Evros Volcanic Rocks (Thrace, Northeastern Greece): Petrology and K/Ar Geochronology, *Geologica CArpathica, 55, 5, Bratislava, p. 397-409*

Annexes

Contact projects@eurogeologists.eu for the full list of Annexes, or open it at the CHPM Information Platform on Prospective Locations (http://bit.ly/CHPMinfoplatform)

Evaluation of the basic characteristics of prospective CHPM areas

Name of the National Association AGG
Number of the prospective area
***4* Sapes – Kirki - Kassiteres**

1. **Geology of the prospective area**

Requested information on:

- ✓ local geology (in regional context)
- ✓ CHPM target formation
- ✓ list of available cross sections, geological maps, geochemical results, lithological information

Notes: briefly summarized, referenced to more detailed studies.

- ✓ **Local Geology**

The Sapes-kirki-Kassiteres ore district is mostly comprised of **(Fig 1.1)**:

1. Quaternary Alluvial Sediments,
2. Tertiary Sedimentary and Volcanosedimentary series,
3. Oligocene- Miocene Volcanic Rocks,
4. Eocene –Miocene Plutonic Rocks ,
5. Metavolcanosedimentary Rocks and Metasedimentary series of the Circum Rhodope Belt Unit
6. Metamorphic Core Complex of the Rhodope Massif Unit.

- ✓ **CHPM target formation**

A more detailed map of the area of interest, shows the different kinds of volcanic sediments **(Fig 1.2)** Five types of intrusive rocks have been recognized in the area, which are from oldest to youngest based on crosscutting relationships:

(a) hornblende-biotite granodiorite-tonalite porphyry,
b) pyroxene-hornblende diorite porphyry'
(c) pyroxene-biotite microdiorite,
(d)quartz monzodiorite,
(e) microgranite porphyry (Voudouris et al., 2006, 2016c; Ortelli et al., 2009; Voudouris, 2014).

At least three of them (phases a, b and e) are related to Porphyry-style mineralization. The granodiorite-tonalite porphyry is the earliest intrusive phase in the study area and hosts the Konos Hill Cu-Mo-Re porphyry prospect (Voudouris et al., 2006; Ortelli et al., 2009) **(Fig 1.3)**

2. **Geophysics of the prospective area**

Requested information:

- ✓ previous geophysical measurements (in CHPM relevance)
- ✓ geophysical results that can be used for locating/defining the deep metal enrichment
- ✓ list of available geophysical maps, cross sections, logs, other measurements

3. **Deep metal enrichment**

Requested information:

- ✓ **(**expected) metal enrichment based on available geophysical, geological and drill data, samples information, geochemistry

Post-collisional magmatism gave rise to a broad variety of styles of hydrothermal mineralization, formed during the final stage of the Tertiary orogenic collapse which led to the formation of widespread Oligocene-Miocene silicic to intermediate magmatism). The Kassiteres-Sapes area represents a deeply eroded Tertiary volcanic center built upon a sedimentary sequence of Middle to Upper Eocene age. Strongly controlled by a NS- and E-W trending fault system, this area shows a close spatial association of Cu-Mo porphyry with LS/IS and HS epithermal overprinting evidenced by Au-Ag-rich polymetalllic veins(**fig3.1**)(**fig3.2**).Past exploration activities by Greenwich and Glory Resources in the area delineated over twenty individual prospects mainly of the epithermal type(**fig 3.3**)(**fig3.4**). The chemical commodities we encounter are **Cu, Fe, Mo, Au, Pb, Zn, Sb, As, Re, Bi, Te, Ag, Se** in various different sites of this ore district and in various concentrations. There are several hydrothermal features suggesting that the Kassiteres-Sappes is a multi-centered porphyry/epithermal system:(a) porphyry-related advanced argillic alteration zones (Sillitoe, 1999) that include high-temperature minerals like diaspore, corundum and topaz at both Koryfes Hill and St Demetrios, (b) K–Na-silicate alteration of the microdiorite exposed at the Koryfes Hill prospect, (c) dacite-hosted porphyry-type stockworks about 800m ESE of St Demetrios. The dacite has been altered to quartz, illite and pyrite, (d) alteration typical of high-sulfidation epithermal deposits best developed west of Koryfes Hill and in the northern part of the district, (e) adularization of volcanic rocks in the
St Barbara prospect and also in isolated outcrops throughout the district. See **Fig 3.3** to **Fig 3.11** for the chemical analysis tables and **Fig. 3.12** to Fig. 3.15 for Glory Resources data for the underground distribution of the ore.

4. **Integrated 3D- 4D model**

Requested information:

- ✓ existing 3D-4D models of the target area and the deep metal enrichment
- ✓ if no 3D-4D models exist, collect the following necessary data: geological setting, mineralization, fluid flow models, stress field determination

Notes: e.g. openly available datasets, models.

5. **EGS potential**

Requested information:

- ✓ EGS potential (heat & energy) of the area
- ✓ geothermal characteristics (temperature gradient, heat flux, stress field, water availability, EGS geology)
- ✓ presence/indication of deep fluids/brines, fracture system, crustal permeability

- ✓ The high heat flow in the area **(locally > 100 mW/m2)** because of magmatism, the favourable stratigraphy and the active tectonics contribute to the formation of the geothermal fields.(fig. 5). In some places the sedimentary column is up to 3.5km thick; it is made up (from top to bottom) of Upper Plio-Pleistocene sands, clays, gravels and micro-conglomerates; Miocene clays, marls and siltstones; and Eocene-Oligocene sediments. In this basin the Rhodope Massif metamorphic basement consists of gneisses, mica-schists, amphibolites and marbles. Deep oil exploration well (KOM-1; Table 2) was drilled in the central part of the Xanthi-Komotini basin in 1977. Temperatures of 60 ◦C at 1300mand 72 ◦C at 1736mdepth were measured, indicating the possibility of finding intermediate-temperature geothermal fluids in that area (Karytsas, 1990). The development of these resources would require additional geophysical surveys and deep exploratory drilling. The characteristics of the shallow aquifers encountered in the upper section of the basin are listed in Table 1. K–Na–Mg geothermometer data for the Nea Kessani and Sappes springs and wells did not yield reliable results due to the low maturity indices (MI < 2.0) of the waters.
- ✓ Sappes geothermal field - Coordinates of wells (decimal/WGS84):

· Well GS-4

ϕ: 41.01246 (41° 0′44.86”), λ: 25.698292 (25° 41′53.85’’)

· Well GS-3P

ϕ: 40.9660602 (40° 57′57.82”), λ: 25.6099206 (25° 36′35.71’’)

- ➢ Coordinates of polygon vertices of the Sappes geothermal field (decimal/WGS84):

Vertex A

ϕ: 40.9535371 (40° 57′12.73”), λ: 25.5690578 (25° 34′08.61′′)
· Vertex B
ϕ: 40.9512081 (40° 57′04.35”), λ: 25.6404153 (25° 38′25.50′′)
· Vertex C
ϕ: 40.9766265 (40° 58′35.86”), λ: 25.7132164 (25° 42′47.58′′)
· Vertex D
ϕ: 41.0266147 (41° 01′35.81”), λ: 25.7252458 (25° 43′30.88′′)
· Vertex E
ϕ: 41.02727 (41° 01′38.17”), λ: 25.6732355 (25° 40′23.65′′)

- Coordinates of polygon vertices of the Sappes – Kassiteres - Esimi mineralization area (WGS84):

· Vertex A
ϕ: 41° 02′26.99” N λ: 25° 41′31.87” E
· Vertex B
ϕ: 41° 02′26.99” N λ: 26° 02′57.29” E
· Vertex C
ϕ: 40° 58′0.71” N λ: 26° 02′21.27” E
· Vertex D
ϕ: 40° 57′43.99” N λ: 25° 43′18.79” E

- Coordinates of polygon vertices of the Petrota - Maronia mineralization area (WGS84):

· Vertex A
ϕ: 40° 53′46.37” N λ: 25° 27′31.14” E
· Vertex B
ϕ: 40° 55 20.72” N λ: 25° 27′41.74” E
· Vertex C
ϕ: 40° 56′36.21” N λ: 25° 32′37.70” E
· Vertex D
ϕ: 40° 56′13.14” N λ: 25° 42′30.39” E
· Vertex E
ϕ: 40° 51′29.24” N λ: 25° 39′42.11” E
· Vertex F
ϕ: 40° 52′07.95” N λ: 25° 35′19.65” E
· Vertex G
ϕ: 40° 51′25.86” N λ: 25° 33′41.00” E
· Vertex H
ϕ: 40° 52′23.89” N λ: 25° 30′29.49” E

- Coordinates of polygon vertices of the Xylagani mineralization area (WGS84):

· Vertex A
ϕ: 40° 59′40.32” N λ: 25° 26′38.32” E
· Vertex B
ϕ: 40° 59′40.32” N λ: 25° 29′26.73” E
· Vertex C
ϕ: 40° 58′34.97” N λ: 25° 29′15.42” E
· Vertex D
ϕ: 40° 58′28.20” N λ: 25° 26′49.52” E

- Coordinates of polygon vertices of the prospective CHPM area (WGS84):

· Vertex A
ϕ: 40º 53′46.37″ N λ: 25º 27′31.14″ E
· Vertex B
ϕ: 40º 59′40.32″ N λ: 25º 26′38.32″ E
· Vertex C
ϕ: 41º 04′05.21″ N λ: 25º 45′04.01′′E
· Vertex D
ϕ: 40º 50′42.99″ N λ: 25º 43′52.18″ E
· Vertex E
ϕ: 40º 51′29.24″ N λ: 25º 39′42.11″ E
· Vertex F
ϕ: 40º 52′07.95″ N λ: 25º 35′19.65″ E
· Vertex G
ϕ: 40º 51′25.86″ N λ: 25º 33′41.00″ E
· Vertex H
ϕ: 40º 52′23.89″ N λ: 25º 30′29.49″ E

List of references

Repstock A., Voudouris P., Zeug M., Melfos V., Zhai M., Li H., Kartal T., Matuszczak J**., 2016. Chemical composition and varieties of fahlore-group minerals from Oligocene mineralization in the Rhodope area, Southern Bulgaria and Northern Greece.**

Kolios N., Fytikas M., Arvanitis A., Andritsos N., Koutsinos S., **2007. Prospective Medium Enthalpy Geothermal Resources in Sedimentary Basins of Northern Greece**, *Proceedings European Geothermal Congress*

Melfos V., Voudouris P**., 2017. Cenozoic metallogeny of Greece and potential for precious, critical and rare metals exploration,** *Ore Geology Reviews 89, p.1030-1057*

Voudouris P., Tarantola A., Melfos V**., 2017. A Field Guide to the Tertiary Hydrothermal ore Deposits of Northern Greece**

Mendrinos D., Choropanitis I., Polyzou O., Karytsas C**., 2010. Exploring for geothermal resources in Greece ,** *Geothermics 39, p. 124-137*

Melfos V., Bogdanov K**., 2013. A Field Guide to the Ore Deposits of NE Greece**

Kolios N., Koutsinos S., Arvanitis A., Karydakis G**., 2005. Geothermal situation in Northeastern Greece.** *Proceedings World Geothermal Congress*

Christofides G., Pecskay Z., Eleftheriadis G., Soldatos T., Koroneos A**., 2004. The Tertiary Evros Volcanic Rocks (Thrace, Northeastern Greece): Petrology and K/Ar Geochronology,** *Geologica CArpathica, 55, 5, Bratislava, p. 397-409*

Voudouris P., Tarkian M., Arikas K**., 2006. Mineralogy of telluride-bearing epithermal ores in the Kassiteres-Sappes area, Western Thrace, Greece,** *Mineralogy and Petrology 87, p.31-52*

Voudouris P., Melfos V., Spry P., Bindi L., Moritz R., Ortelli M., Kartal T**., 2013. Extremely Re-Rich Molybdenite from Porphyry Cu-Mo-Au Prospects in Northeastern Greece: Mode of Occurence, Causes of Enrichment, and Implications for Gold Exploration,** *Minerals, 3, p.165-191*

Annexes

Contact projects@eurogeologists.eu for the full list of Annexes, or open it at the CHPM Information Platform on Prospective Locations (http://bit.ly/CHPMinfoplatform)

Evaluation of the basic characteristics of prospective CHPM areas

Name of the National Association AGG
Number of the prospective area
5 **Nestos -Kimmeria**

1. **Geology of the prospective area**

Requested information on:

- ✓ local geology (in regional context)
- ✓ CHPM target formation
- ✓ list of available cross sections, geological maps, geochemical results, lithological information

Notes: briefly summarized, referenced to more detailed studies.

- ✓ **Local geology**

The Delta of Nestos river area and Kimmeria of Xanthi are comprised of (Fig 1.1):

4. Quaternary Alluvial Sediments
5. Tertiary Sedimentary and Volcanosedimentary series
6. Oligocene- Miocene Plutonic Rocks
7. Metamorphic rocks of the Rhodope Massif
8. Metamorphic Core Complexes of the Rhodope Massif

- ✓ **CHPM target formation**

The Nestos sedimentary basin started its formation at the end of the Lower Miocene (Serravalian), after the main compressive phase of Eocene age. Sedimentation began With clastic – deltaic continental deposits alternating generally with fine-grained sandstones, mudstones and argillites. These were followed by conglomerates with intercalation of lignite (Middle – Upper Miocene). During the Upper Miocene the sedimentation continued with an Evaporitic sequence consisting of anhydrites alternating with thin layers of sandstones, clays and marls (Proedrou, 1979). The Plio-Quaternary sediments are characterized by deltaic deposits lying unconformably over the previous series. These formations are composed of loose sandstones and clays at the basin margins and marine and lacustrine sediments in the central part of the basin. The total thickness of this sedimentary sequence is about 4,000 m (Lalechos and Savoyat, 1977).

The Kimmeria intrusion-related Mo-Cu-W-Bi-Au deposit is associated with the Oligocene Xanthi I-type pluton (Fig. 14), which consists predominantly of granodiorite and minor outcrops of tonalite, quartz-diorite, monzonite and gabbroic rocks (Koukouvelas and Pe-Piper, 1991; Christofides et al., 2010). Kyriakopoulos (1987) determined a whole-rock Rb-Sr age between 28.8 ± 0.7 Ma and 26.3 ± 0.1 Ma for the granodiorite, whereas Liati (1986) determined a K-Ar age for hornblende of 30.4 ± 0.6 Ma. The pluton intruded gneiss, mica schist, amphibolite and marble of the Rhodope Massif. The emplacement of the pluton was controlled by the Kavala-Xanthi-Komotini normal fault, which marks the boundary with Tertiary and Quaternary sediments of the Xanthi-Komotini supra-detachment basin. This intrusion has created an extensive metamorphic aureole within the surrounding marbles, gneisses and amphibolites. Two different ore types are genetically connected with this granodioritic intrusion: 1. Massive Au-bearing skarn-type mineralization and 2. Mo-Cu-Bi-W quartz vein mineralization .

2. Geophysics of the prospective area

Requested information:

- ✓ previous geophysical measurements (in CHPM relevance)
- ✓ geophysical results that can be used for locating/defining the deep metal enrichment
- ✓ list of available geophysical maps, cross sections, logs, other measurements

- ✓ Two sizable anomalies dominate the low pass map (**fig.2.3**). The northern one coincides with the granite outcrop near the city of Xanthi. It suggests that the body which causes the anomaly should be much wider than the exposed part. It also suggests that the shape of that body somehow should be like a truncated pyramid with the top surface coinciding with the outcrop. The southern anomaly leaves space for varied speculation since the data are incomplete, but it also should be caused by a wide body. The uplifting of the basement occurs in that region. The .gravity interpretation of THANASSOULAS *et al.* (1987) and KIRIAKIDIS *et al.* (1988) suggested that uplifted dense rocks occur at this part of the basin. Furthermore, the gravity pattern in this area suggests that a major fault might be present, which would be equivalent to the large Kavala-Xanthi-Komotini fault. The interpretation of the magnetic data also suggests a major fault. The concealed feature in that particular location has strong magnetic properties. This is not likely solely a variation in magnetic basement, because it is not manifested so pronounced on the magnetic maps on the northern flank of the basin. Scarce strong anomalies of relatively much smaller wavelength than those mentioned previously are present in the high pass map. The magnetic bodies which should cause them could be small concealed granitic intrusions. Such a hypothesis is supported by the fact that small scarce granitic bodies are exposed at the surface
- ✓ Fig.(**2.4**), Fig(**2.5**) show the pseudogravity transformation of the low passed magnetic total field data, using again the computer program given by HILDENBRAND (1983).
  That particular software employs the operator

  [WGp /2rcl] / [(iul' + ivm' + wm')(iul + ivm + wn)]

  where, l', m' and n' are the direction cosines of the earth's ambient field relative to x, y, x coordinate respectively, and l, m and n the direction cosines of the magnetization vector. G, is the gravitational constant, I, the intensity of magnetization
  and p, the density contrast (LouR~Nco, 1973). The wavenumbers are presented
  by u, v for the horizontal dimensions and w for the vertical.
  The transformation is by definition a long wavelength enhancing operation
  which rectifies the magnetic anomalies. Therefore, the aim of its application is
  two-fold: to exactly locate the big bodies and to obtain the requisite symmetries for
  the application of "terracing." Because of the dipolar signature of the magnetic
  anomalies, "terracing" cannot be applied to magnetic data unless they have been
  reduced to a monopolar (rectified) form. An alternative procedure to achieve that
  could have been reduction to the magnetic pole or inverse filtering (TSOKAS and
  PAPAZACHOS, 1992).
- ✓ The anomalies marked with B, D, and E display a rather elongated character. Thus, 2-D depth estimation methods were employed to gain information regarding the bodies which cause them. **Fig (2.7) fig (2.8) Fig (2.9).** The estimates for profile B have picked up only one corner of the lower surface of the disturbing body, which is the central one in Figure 7. It lies at about 500 m depth below sea level. The other small discrepancies of the field possibly reflect much smaller features or errors. The estimates for profile D demonstrate that one surface of the sources which cause the anomaly lies approximately at the depth of the sea level, i.e., 1 km beneath the flight altitude. The lower surface of the body crossed by profile E seems to be at an average depth of 300 m below sea level, and two corners of this surface have been picked
  up.

- ✓ Profiles A and B shown in **Fig (2.10), Fig (2.11) Fig (2.12)** were not drawn on the magnetic but on the Bouguer anomaly map of Greece (LAGIOS et al., 1988). The depth estimates along them reveal the undulations of the basement of the basin, which has no strong magnetic properties.

3. <u>Deep metal enrichment</u>

<u>Requested information:</u>

- ✓ **(**expected) metal enrichment based on available geophysical, geological and drill data, samples information, geochemistry

- ✓ At Kimmeria **(fig 3.1)(fig 3.2)** a massive Cu-W-Mo-Au-bearing **<u>skarn-type</u>** mineralization consisting of chalcopyrite, magnetite, pyrrhotite, scheelite, and minor molybdenite and gold, is genetically related to the Xanthi I-type pluton (Walenta and Pantzartzis, 1969; Vavelidis et al., 1990; Voudouris et al., 2010). The Xanthi pluton ranges in composition from gabbro through monzonite to granodiorite, and has an Oligocene age (28.8 ± 0.7 and 26.3 ± 0.1 Ma; Rb-Sr in whole rock and biotite; Kyriakopoulos, 1987). The emplacement of the pluton is controlled by two major regional structures: the Kavala-Xanthi-Komotini normal fault and the Nestos thrust fault. The pluton intrudes gneisses, mica schists, amphibolites and marbles of the Northern Rhodope Domain. Mining operations in the 1930s, including underground galleries as well as surface excavations, extracted the magnetite-pyrrhotite-rich skarn mineralization and the Cu-Mo ore. The remaining resource is estimated to be ~2 Mt with 20 g/t Ag and 1.98% Cu (Gialoglou and Drymniotis, 1983).
- ✓ The Oligocene Kimmeria **<u>intrusion-hosted</u>** Mo-Cu-W-Bi-Au deposit is located close to the Nestos thrust in the Rhodopes and is associated with the Oligocene Xanthi pluton (Figs. 2 and 3), described above in terms of its skarn mineralization. The Kimmeria ore district includes sheeted quartz veins crosscutting sericite carbonate- altered granodiorite and contains pyrite, molybdenite, scheelite, wolframite, and chalcopyrite (Fig. 6f; Walenta and Pantzartzis, 1969; Voudouris et al., 2010; Theodoridou et al., 2016). Vein hosted mineralization contains >1 wt.% Cu, >0.2 wt.% Mo, up to 2.7 g/t Au, up to 79.5 g/t W, up to 456.6 g/t Bi, and traces of Te (up to 4 g/t) (Theodoridou et al., 2016). Primary fluid inclusion studies indicate CO2 in the sheeted veins
- ✓ In the Palea Kavala area **(Fig. 3.3)**, metamorphic rocks of the lower tectonic unit of the Southern Rhodope Core Complex were intruded by the _22–19 Ma Kavala (or Symvolon) pluton (Christofides et al., 1998) along the trend of the Kavala-Komotini fault zone. The Kavala pluton is an I-type intrusion and is dominantly composed of amphibole-biotite granodiorite with subordinate amounts of diorite, tonalite, monzogranite, and monzodiorite. The Palea Kavala region contains _150 base- and precious-metal occurrences within the Kavala pluton and the surrounding metamorphic rocks. These occurrences **(Fig 3.4)(Fig 3.5)** have variable metal contents and are mostly weathered and oxidized (particularly those that contain Mn). The

estimated total resources are 1.5 Mt containing up to34.5 g/t Au, up to 180 g/t Ag, up to 13% Pb + Zn, up to 40% Fe, and up to 42% Mn (Chatzipanagis and Dimitroula, 1996). Oxidized Fe-Mn-Au and Fe-Mn (Pb ± Zn ± Ag) bodies are localized in marbles, whereas Fe-As-Au, Fe-Cu-Au, and Bi-Te-Au deposits occur in gneisses and granitoids, as well as along the gneiss-marble contact of the lower tectonic unit in milky quartz veins. The Miocene Kavala pluton is crosscut by an approximately 4 km-long sheeted-quartz vein system (Kavala vein) that contains Bi-Te-Pb-Sb ± Au mineralization (Melfos et al., 2008; Fornadel et al., 2011) and the 30 m-long Chalkero quartz vein (Chalkero vein). The Kavala quartz vein system is characterized by several parallel to subparallel quartz veins _1 m thick and tens of meters apart.

4. Integrated 3D- 4D model

Requested information:

- ✓ existing 3D-4D models of the target area and the deep metal enrichment
- ✓ if no 3D-4D models exist, collect the following necessary data: geological setting, mineralization, fluid flow models, stress field determination

Notes: e.g. openly available datasets, models.

The concluded plane view of the 3-D models, which simulates the intrusion along the effect which they produce, is shown in **Fig (4.1)**. The method of HANSEN and WANG (1988) has also been employed for these calculations. All models are irregular trapezoids with parallel top and bottom surfaces. The susceptibility contrast was set to the same value as for the Xanthi pluton. The obtained depth parameters of the bodies are given in **Fig (4.2).** Anomaly C is caused by two bodies called northern and southern**.**

5. EGS potential

Requested information:

- ✓ EGS potential (heat & energy) of the area
- ✓ geothermal characteristics (temperature gradient, heat flux, stress field, water availability, EGS geology)
- ✓ presence/indication of deep fluids/brines, fracture system, crustal permeability

✓ Two significant low enthalpy geothermal fields are located in the Nestos Delta basin:
(a) the geothermal field of Neo Erasmio – Magana lies at the eastern edge of the Nestos basin and west of the Avdira horst with water temperatures ranging from 40 to 65 degrees C and
(b) The field of Eratino -Chrysoupolis on the western side of the Nestos River .
The geothermal field of Neo Erasmio – Magana is a characteristic example of low enthalpy field where the stratified aquifers are supplied by an active fault system that affects the substratum of the migmatitic gneisses. The geothermal reservoir is situated at depths between 200 and 400 m within the basal part of the post-alpine sedimentary sequence and mainly at the top of the metamorphic basement. The values of the geothermal gradient are very high (up to 25oC/100 m). The thermal fluids rise through NNW-SSE trending major fault system in the area of the Neo Erasmio village from a deeper reservoir within the metamorphic basement
The water temperatures range from 40 to 65oC. The waters with T.D.S. values between 0.57 and 10.1 g/l are classified into two main categories: Na-CI and Na-HCO3CI waters (Kolios et al., 2005).
Three deep oil exploration boreholes (N-1, N-2 and N-3 at depths of 3159, 3970 and 3851 m respectively) were drilled during the period 1976-1978 west of the Nestos River Delta and out of the main geothermally anomalous area.
Fig. 5.1 to **Fig 5.9** show various attributes of the geothermal field of the area

- Eratino geothermal field - Coordinates of wells (decimal / WGS84):

Production well N-1P

ϕ: 40.9557687 (40° 57′20.77″), λ: 24.6236073 (24° 37′24.99′′)
· Production well N-2P
ϕ: 40.9474538 (40° 56′50.83″), λ: 24.6416845 (24° 38′30.06′′)
· Exploration well N2
ϕ: 40.9622834 (40° 57′44.22″) λ: 24.62472

(24° 37′28.99′′)
· Exploration well N6
ϕ: 40.9752193 (40° 58′30.79″), λ: 24.6227716 (24° 37′21.98′′)
· Exploration well N14
ϕ: 40.9594971 (40° 57′34.19″), λ: 24.6243598 (24° 37′27.70′′)
· Exploration well N10
ϕ: 40.9644468 (40° 57′52.01″), λ: 24.6405753 (24° 38′26.07′′)
· Exploration well N11
ϕ: 40.9558396 (40° 57′21.02″), λ: 24.6250704 (24° 37′30.25′′)
· Exploration well N12
ϕ: 40.9390418 (40° 56′20.55″), λ: 24.6476367 (24° 38′51.49′′)
· Deep exploration well N1-G
ϕ: 40.9553721 (40° 57′19.34″), λ: 24.622717 (24° 37′21.78′′

Coordinates of polygon vertices of the Eratino geothermal field (decimal / WGS84):

· Vertex A
ϕ: 40.9837717 (40° 59′1.58″), λ: 24.6276192 (24° 37′39.43′′)
· Vertex B
ϕ: 40.9935653 (40° 59′36.84″), λ: 24.7117969 (24° 42′42.47′′)
· Vertex C
ϕ: 40.8799348 (40° 52′47.77″), λ: 24.7069594 (24° 42′25.05′′)
· Vertex D
ϕ: 40.8719317 (40° 52′18.95″), λ: 24.6333499 (24° 38′0.06′′)
· Vertex E
ϕ: 40.9459457 (40° 56′45.40″), λ: 24.5837807 (24° 35′01.61′′)

Neo Erasmio geothermal field - Coordinates of wells (decimal / WGS84):
· Exploration well M-6
ϕ: 40.9271368 (40° 55′37.69″), λ: 24.8411491 (24° 50′28.14′′)
· Exploration well M-15
ϕ: 40.922303 (40° 55′20.29″), λ: 24.8277524 (24° 49′39.91′′)
· Exploration well M-13
ϕ: 40.9230492 (40° 55′22.98″), λ: 24.8355497 (24° 50′07.98′′)

Coordinates of polygon vertices of the Neo Erasmio geothermal field (decimal / WGS84):
· Vertex A
ϕ: 40.934747 (40° 56′5.09″), λ: 24.7742894 (24° 46′27.44′′)
· Vertex B
ϕ: 40.9539001 (40° 57′14.04″), λ: 24.8745905 (24° 52′28.53′′)
· Vertex C
ϕ: 40.9140198 (40° 54′50.47″), λ: 24.8884148 (24° 53′18.29′′)
· Vertex D
ϕ: 40.8927304 (40° 53′33.83″), λ: 24.7982979 (24° 47′53.87′′)

Nea Kessani geothermal field - Coordinates of wells
(decimal / WGS84):
· Production well GP-13
ϕ: 41.0317463 (41° 01′54.29″), λ: 25.0546579 (25° 03′16.77′′)
· Production well GP-12
ϕ: 41.0362076 (41° 02′10.35″), λ: 25.0602047 (25° 03′36.74′′)
· Production well GP-22
ϕ: 41.0389237 (41° 02′20.13″), λ: 25.0540957 (25° 03′14.74′′)
· Production well GP-21
ϕ: 41.0296628 (41° 01′46.79″), λ: 25.0490762 (25° 02′56.67′′)

· Exploration well G3
ϕ: 41° 01′34″ λ: 25° 03′00′′
· Exploration well G8
ϕ: 41° 01′50″ λ: 25° 03′00′
· Exploration well G9
ϕ: 41° 02′24″ λ: 25° 03′51′

Coordinates of polygon vertices of the Nea Kessani geothermal field

(decimal / WGS84):

Vertex A
ϕ: 41.0494442 (41° 02′58.00”), λ: 25.0220615 (25° 01′19.42′′)
· Vertex B
ϕ: 41.0557006 (41° 03′20.52”), λ: 25.0795065 (25° 04′46.22′′)
· Vertex C
ϕ: 41.0130837 (41° 00′47.10”), λ: 25.0902928 (25° 05′25.05′′)
· Vertex D
ϕ: 41.0018184 (41° 00′06.55”), λ: 25.0308637 (25° 01′51.11”)

Coordinates of deep hydrocarbon exploration boreholes in the Nestos Delta area (decimal / WGS84):
· Exploration well NESTOS-1
ϕ: 40.8959099 (ϕ: 40° 53′45.28”), λ: 24.6594634 (λ: 24° 39′34.07′′)
or
ϕ: 40° 53′48” λ: 24° 39′30′′
· Exploration well NESTOS-2
ϕ: 40.8902876 (ϕ: 40° 53′25.04”), λ: 24.6253817 (λ: 24° 37′31.37′′)
or
ϕ: 40° 53′36” λ: 26° 37′42′′
· Exploration well NESTOS-3
ϕ: 40.8762674 (ϕ: 40° 52′34.56”) λ: 24.6493074 (λ: 24° 38′57.51′′)
or
ϕ: 40° 52′37”, λ: 26° 38′ 56′′
Coordinates of polygon vertices of the Kimmeria Xanthi pluton area (scarn occurrences & mineralized vein system)
(WGS84):
· Vertex A
ϕ: 41° 08′23.77” N λ: 24° 52′05.96′′ E
· Vertex B
ϕ: 41° 08′17.34” N λ: 24° 58′21.30′′ E
· Vertex C
ϕ: 41° 08′38.51” N λ: 25° 01′22.51′′ E
· Vertex D
ϕ: 41° 10′08.31” N λ: 25° 01′37.74′′ E
· Vertex E
ϕ: 41° 11′28.95” N λ: 24° 58′07.71′′ E
· Vertex F
ϕ: 41° 09′36.02” N λ: 24° 52′11.90′′ E

Coordinates of polygon vertices of the Palea Kavala ore deposit area
(WGS84):
· Vertex A
ϕ: 41° 03′36.48” N λ: 24° 21′44.11′′ E
· Vertex B
ϕ: 40° 55′54.81” N λ: 24° 21′54.94′′ E
· Vertex C
ϕ: 40° 57′50.73” N λ: 24° 29′16.56′′ E
· Vertex D
ϕ: 41° 03′26.32” N λ: 24° 29′33.53′′ E

Coordinates of polygon vertices of the prospective CHPM area
(WGS84/decimal):
· Vertex A
ϕ: 40° 57′15.30″ (40.9542512) λ: 24° 32′55.87″ (24.5488517)
· Vertex B
ϕ: 41° 09′26.34″ (41.157317) λ: 24° 53′26.95″ (24.8908192)
· Vertex C
ϕ: 41° 09′26.34″ λ: 25° 04′32.41″
· Vertex D
ϕ: 41° 00′22.55″ (41.006263) λ: 25° 04′58.12″ (25.0828102)

List of references

Melfos V., Voudouris P., 2017. Cenozoic metallogeny of Greece and potential for precious, critical and rare metals exploration, *Ore Geology Reviews 89, p.1030-1057*

Voudouris P., Tarantola A., Melfos V., 2017. A Field Guide to the Tertiary Hydrothermal ore Deposits of Northern Greece

Mendrinos D., Choropanitis I., Polyzou O., Karytsas C., 2010. Exploring for geothermal resources in Greece , *Geothermics 39, p. 124-137*

Melfos V., Bogdanov K., 2013. A Field Guide to the Ore Deposits of NE Greece

Kolios N., Koutsinos S., Arvanitis A., Karydakis G., 2005. Geothermal situation in Northeastern Greece. *Proceedings World Geothermal Congress*

Fornadel A., Spry P., Melfos V., Vavelidis M., Voudouris P. 2011. Is the Palea Kavala Bi-Te-Pb-Sb+/-Au district, Northeastern Greece an intrusion-related system*?, Ore geology Reviews 39, p.119-133*

Kolios N., Fytikas M., Arvanitis A., Andritsos N., Koutsinos S., 2007. Prospective Medium Enthalpy Geothermal Resources in Sedimentary Basins of Northern Greece*, Proceedings European Geothermal Congress*

Tsokas G., Christofides G., Papakonstantinou C. 1996. A Geophysical Study of the Granites and the Sedimentary Basins of the Xanthi Area (N. Greece)*, Pageoph, vol. 146, no. 2*

Repstock A., Voudouris P., Zeug M., Melfos V., Zhai M., Li H., Kartal T., Matuszczak J., 2016. Chemical composition and varieties of fahlore-group minerals from Oligocene mineralization in the Rhodope area, Southern Bulgaria and Northern Greece.

Annexes

Contact projects@eurogeologists.eu for the full list of Annexes, or open it at the CHPM Information Platform on Prospective Locations (http://bit.ly/CHPMinfoplatform)

Evaluation of the basic characteristics of prospective CHPM areas

Name of the National Association: AGG

Number of the prospective area: 6. Thermes Xanthi

1. **Geology of the prospective area**

Requested information on:

- ✓ local geology (in regional context)
- ✓ CHPM target formation
- ✓ list of available cross sections, geological maps, geochemical results, lithological information

Notes: briefly summarized, referenced to more detailed studies.

GEOLOGY OF THE THERMES AREA

The Thermes area is located at a distance of about 50 km North of Xanthi (Thrace, Northeastern Greece), adjacent to the Greek-Bulgarian borders (Figure 1).

The regional geology of the Thermes area is composed of metamorphic rocks belonging to the Rhodope Massif (RM). The Rhodope Massif includes Pre-Devonian to Mesozoic rocks and occupies most of northeastern Greece and southern Bulgaria (Figure 2). To the west, the Rhodope Massif is separated from the Servo-Macedonian Massif (SMM) by the Strimon River fracture zone, whereas the Rhodope Massif is bounded to the S and SE by the Triassic-Jurassic Circum-Rhodope Belt (CRB) (Fig. 2 and 3).

The Rhodope Massif is a heterogenous crustal body composed of two main sub-domains: (a) the Northern Rhodope Domain and (b) the Southern Rhodope Core Complex (Figure 2A). The Northern Rhodope Domain consists of the following main metamorphic units (Melfos and Voudouris, 2017): (i) a lower unit of high-grade basement including orthogneisses derived from Permo-Carboniferous protoliths; this unit includes four metamorphic core complexes (the Arda, Biala Reka, Kechros, Kesebir-Kardamos migmatic domes); (ii) an intermediate unit of high-grade basement rocks that have both continental and oceanic affinities, and with protoliths; and (iii) an overlying uppermost Mesozoic low-grade unit of the Circum-Rhodope Belt and Evros ophiolite (Turpaud and Reischmann, 2010; Kirchenbaur et al., 2012; Meinhold and Kostopoulos, 2013; Bonev et al., 2015). The rocks of the intermediate unit experienced high to ultra-high pressure metamorphism with subsequent high grade amphibolite-facies overprint (Mposkos and Kostopoulos, 2001). The Southern Rhodope Core Complex (SRCC), which is tectonically juxtaposed against the Vertiskos Unit, is composed of Permo-Carboniferous orthogneiss and massive Triassic marble intercalated with amphibolitic and metapelitic rocks (Dinter et al., 1995; Brun and Sokoutis, 2007; Turpaud and Reischmann, 2010). The SRCC displays intense, penetrative, top-to-the-southwest shearing under amphibolite and greenschist facies conditions (Burg et al., 1996). In the central and eastern Rhodope area (e.g., the Northern Rhodope Domain core complexes), the Arda, Biala Reka-Kechros, and Kesebir-Kardamos migmatitic domes (Fig. 2 and 3) were progressively exhumed along several ductile to brittle shear zones, all active from 42-35 Ma (Melfos and Voudouris, 2017; Bonev et al., 2006a,b, 2010; 2013; Wüthrich, 2009; Márton et al., 2010; Moritz et al., 2010; Kaiser-Rohrmeier et al., 2013). In the Rhodope Massif the exhumation of metamorphic core complexes along detachment faults resulted in the formation of Palaeocene to early Eocene, late Eocene-Oligocene, and Miocene supra-detachment sedimentary basins (Bonev et al., 2006a,b; Márton et al., 2010; Kilias et al., 2013). Sediments transgressively or tectonically overlie the metamorphic units of the domes in fault bounded half-grabens located along the hanging wall of the low angle detachment

faults (Melfos and Voudouris, 2017). Late Eocene-Oligocene igneous rocks cover large areas in the Rhodope Massif (Figure 4) and have calc-alkaline, shoshonitic, to ultra potassic affinity and mafic-intermediate and felsic composition (Melfos and Voudouris, 2017; Innocenti et al., 1984; Jones et al., 1992; Pe-Piper and Piper,2002; Christofides et al., 2004; Perugini et al., 2004; Marchev et al., 2005, 2013; Ersoy and Palmer, 2013). Within the Rhodope area, major Oligocene intrusive and volcanic areas occur in Borovitsa, Lozen, Madzharovo, Iran Tepe, Zvezdel, Kotyli-Vitinia, Kalotycho-Zlatograd, and Xanthi (Innocenti et al., 1984; Marchev et al., 2005). Other volcanic areas belong to the so-called Evros volcanic rocks, which include the Tertiary basins in Rhodopi and Evros counties (Arikas and Voudouris, 1998; Christofides et al., 2004). Several plutons (e.g., Vrondou, Xanthi, Maronia-Kirki-Leptokarya) intruded contemporaneously with detachment faulting (e.g., in the footwall of detachments) and are partly mylonitized. The late Eocene-Oligocene magmatism shows a decreasing influence of crustal contamination with time and an increasing input from the mantle, until the eruption of purely asthenospheric magmas (Melfos and Voudouris, 2017). It is suggested that the late Eocene-Oligocene (35-25 Ma) magmatism in the Rhodope Massif was caused by convective removal of the lithospheric mantle (lithospheric delamination) and subsequent upwelling of the asthenosphere (Christofides et al., 2004; Marchev et al., 2005; Pe-Piper and Piper, 2006; Melfos and Voudouris, 2017).

The Thermes area belongs to the Northern Rhodope Domain (Figure 2A). The predominantly felsic supracrustal series hosting the mineralizations is a structurally complex, E-W-trending zone consisting of felsic gneisses (Figure 5) alternating with amphibolites, amphibolites-biotite and biotite gneisses and marbles (Kalogeropoulos et al., 1996). This zone comprises a lower “autochthon” and an upper “allochthon” part (unit). These two units are separated by a major Tertiary, low-angle (10-30^{o}) thrust fault Marbles occur both in the lower "autochthon" unit (>700m thick) comprised of felsic gneisses with minor amphibolites, biotite-gneisses, and locally migmatites, and the upper "allocthon" unit (400-600 m thick) consisting of alternations of marbles and amphibole-gneisses, which are infrequently invaded by pegmatites. (Kalogeropoulos et al., 1996). Strongly serpentinized pyroxene peridotite appears conformably associated with amphibolites. Jasperoidal rocks are extensively exposed and represent silicification products of marbles at the overthrust plane of the two units (Arvanitidis et al., 1989b; Arvanitidis and Dimou, 1990). Some migmatites being present in the lower felsic gneisses are part of a general granite forming event (Arvanitidis and Dimou, 1990). Based on geochemical studies of protoliths, it is suggested that the gneisses have been derived mainly from igneous rocks of calc-alkaline affinity (Mposkos et al., 1990; Arvanitidis et al., 1989a) whereas most of the amphibolites were interpreted as tholeiites, bearing both island arc and MORB (Mid-Ocean Ridge Basalts) signatures (Mposkos et al. 1990). The precursor to the “lower” units were volcanic rocks of calc-alkaline affinity with some pelagic sediments, cut by tholeiitic basalts, while the “upper”, overthrust units were originally shallow water limestones, marls and sediments with intercalations of felsic to intermediate volcanics (Arvanitidis and Dimou, 1990). The rocks in the Thermes area have been deformed and metamorphosed regionally to the amphibolite facies (pressures 5-7 kbar, temperatures 580-620^{o}C) (Arvanitidis et at. 1989a) in Upper Cretaceous-Eocene times (45-50 Ma) (Yordaniv et al., 1962; Liati, 1986) and were subsequently retrograded to greenschist facies metamorphism of Miocene age (Kalogeropoulos et al., 1996), i.e. 13.9-15.9 Ma (Kyriakopoulos, 1987) and 15.5-17.8 Ma (Kokkinakis, 1980). Granitoids of Oligocene age, and volcanic rocks of Eocene-Oligocene age, crosscut the metamorphic rocks (Kalogeropoulos et al., 1996). In particular, metamorphic rocks in the vicinity of Thermes were intruded by Oligocene granitoids of calc-alkaline affinity in Xanthi [26.3-28.8 Ma (Kyriakopoulos, 1987) or 27.1-27.9 Ma (Meyer, 1968)] and Paranesti [29.1-38.5 Ma (Sklavounos, 1981) or 38.3 Ma (Meyer, 1968)]. Volcanic rocks occur both in Eocene to Oligocene (37-25 Ma) basins (Fytikas et al., 1985; Eleftheriadis et al., 1989) and along linear structures in the metamorphic terrane (Alfieris et al., 1989).

The Thermes ore-field is hosted by a structurally complex E-W trending zone within the Rhodope Massif (Kalogeropoulos et al., 1996). A major NW-SE fault system crosses the region and is related to the ore field. A second set of WNW-ESE trending faults intersects the first set (Arvanitidis and Dimou, 1990). The metal sulfide mineralization of the Thermes ore field is hosted in marbles, amphibolites and orthogneisses (Melfos and Voudouris, 2017). In an earlier study of the mineralization, Arvanitidis et al.

(1986) observed a lateral variation in sulfide mineral associations from high-T skarn ores, near the Oligocene volcanics, to low-T vein/replacement ores (Kalogeropoulos et al., 1996). The Thermes prospect is a polymetallic Zn-Pb-Fe-Cu-As-Ag-Au-Te carbonate-replacement deposit (Arvanitidis and Dimou, 1990; Kalogeropoulos et al., 1996; Melfos and Voudouris, 2017) located at the southernmost part of the Arda dome (Figure 2A). Veins and breccias containing Pb-Zn-(Fe-Cu) mineralization also occur, associated with NNW- and NNE-trending faults (Melfos and Voudouris, 2017). Consequently, based on the mode of occurrence and morphology, chemical character, ore mineralogy and alteration features, two major base metal sulfide ore varieties have been recognized in the Thermes ore field (Arvanitidis et al., 1986; 1989b): (1) a brecciated vein Pb-Zn(Fe-Cu) mineralization related to NNW- and NNE-trending faults and (2) stratabound (manto), replacing marbles with extension to mineralized veins in faults. The second variety is subdivided into (a) polymetallic (Zn-Pb-Fe-Cu-As-Ag-Au-Cd-Sb) and (b) Pb-Zn(Cu-Mn-Ag-Cd) types (Figure 6). On the basis of the ore geochemistry, as well as field and textual evidence, these two ore form part of a vein associated skarn-replacement base metal sulfide ore system (Kalogeropoulos et al., 1996). As the granitic stocks in the Thermes area are of Oligocene age, this may also be considered as the most likely age for the formation of the Thermes ores (Kalogeropoulos et al., 1996).

Uniform sulfur isotope systematics and sulfur isotopic temperatures, compositional data for ore-fluids and deposition conditions for Thermes and Madan deposits, coupled with geological and mineralogical similarities (Manev et al., 1990), indicate a common source of ore-forming fluids for the Madan-Thermes ore district (Figure 7) driven by the Tertiary igneous activity for the entire Thermes-Madan ore-field (Kalogeropoulos et al., 1996). The comparative study between the Madan (MOF) and Thermes ore fields (TOF) showed that these ore fields have common features and belong to the same metallogenic province. They are hosted in the same metamorphic lithologies exposed in two superimposed antiforms. Pb-Zn mineralizations are represented by vein type ore bodies associated with NW-SE and less common NE-SW and WNW-ESE faults, and metasomatic ore bodies hosted in marbles near the mineralized faults. The two ore field territories are independent deformational domains but faulting and the related ore deposition occurred in the same regional tectonic stress field. Mineral compositions, geochemical and thermobaric conditions and Pb isotopic characteristics of the Madan and Thermes mineralizations indicate a common metal source and restricted formation time of the ore-forming hydrothermal solutions (Manev et al., 1990). For more details, see section “4. Integrated 3D-4D model”.

Therefore, Thermes represents the southern extension of the Madan ore field in Bulgaria (Kaiser-Rohrmeier et al., 2013). The suggestion that Thermes and Mantan ore-fields constitute a single ore district and Thermes represents the southern extension of the Madan ore-field reinforces the choice of the Thermes ore system as a CHPM target.

2. Geophysics of the prospective area

Requested information:

- ✓ previous geophysical measurements (in CHPM relevance)
- ✓ geophysical results that can be used for locating/defining the deep metal enrichment
- ✓ list of available geophysical maps, cross sections, logs, other measurements

GEOPHYSICAL METHODS, MEASUREMENTS AND RESULTS IN THE THERMES AREA

Two geophysical logging techniques were applied in three (3) boreholes (GTH-8, GTH-12 and GTH-13) in the Kato Thermes area aiming at defining the lithological units and determining the depth and thickness of ore deposits. These techniques were as follows: (a) total count gamma ray intensity logs and (b) bulk density logs. The interpretation of the geophysical measurements resulted in the following conclusions: (a) In borehole GTH-8, three (3) distinct mineralized zones have been identified at depths of 278-282m, 292-294m and 305-310m. In the 278-282m depth zone, massive mineralization occurs. (b) In borehole GTh-12, disseminated mineralization has been found at depths of 337-343m. (c) In borehole GTH-13, disseminated mineralization of minor importance (Sideris and Papakonstantinou, 1990). 3D schemes based on the pre-mentioned geophysical methods are shown in Figures 9 and 10 .

Except for the above-mentioned borehole log techniques, the Transient EM (TEM) method was applied by I.G.M.E. in the Diaspaston-Thermes area in 1991 (Figure 11) aiming to delineate the underground extension (depth, thickness, subhorizontal dip, geometry) of the graphite and contribute to the evaluation of its mining potential. High quality information has been obtained by the 2D interpreted sections (Figure 11). The graphite subsurface extent is structurally controlled by NW bearing faults and continues at a minimum distance of 180m to the NW of the outcrop position. The graphitic body dips to the NW (Figure 11). Its NW continuation is interrupted due to fault with a throw of about 60m. A number of 10 drillholes were sited and intersected a graphitic horizon of varying thickness between 1.5 and 10m. Boreholes sited on geophysical evidence have found the graphitic horizon, 5-12m thick, at depths of 60-120m (Karmis and Tsourlos, 2004).

Unfortunately, there are no any ultra deep geophysical results for locating/defining the deep metal enrichment.

3. Deep metal enrichment

Requested information:

✓ **(**expected) metal enrichment based on available geophysical, geological and drill data, samples information, geochemistry

As above-mentioned, two major ore varieties occur in the Thermes ore-field (Kalogeropoulos et al., 1996): (a) a fault-related, breccia Pb-Zn-(Fe-Cu) mineralization, and (b) stratabound (manto) polymetallic [Zn-Pb-Fe-Cu-As-Ag-Au-Cd-Sb (Kalogeropoulos et al., 1996); Pb-Zn-Fe-Cu-Mn-As-Sb-Cd-Te-Ag-Au (Melvos and Voudouris, 2017)] and Pb-Zn-(Cu-Mn-Ag-Cd) replacement ores with associated veins (Kalogeropoulos et al., 1996).

The polymetallic type of mineralization, though proportionally subordinate, may be of economic interest due to relatively high concentrations of Au and Ag. Electrum (Au=77.7 wt%, Ag=22.2 wt%), the Pb-bearing silver telluride Hessite (Ag_2Te; Ag=61.3-63.1 wt%) and the Ag-bearing lead telluride Altaite (PbTe; Ag=1,0 wt%) were identified in a mineral assemblage of galena, sphalerite, arsenopyrite, pyrite, chalcopyrite, neodigenite, covallite and graphite. Electrum occurs as very fine veins transecting hessite, which together with altaite forms inclusions in galena. Au occurs in a mineral assemblage of sphalerite, galena, pyrite, arsenopyrite, chalcopyrite, tennantite, Ag-bearing tetrahedrite, gersdorffite and graphite as indicated measured Au concentrations and up to now no Au-minerals or tellurides have been found (Arvanitidis and Dimou, 1990). Three major occurrences, namely Kato Thermes, Kasli and Milos, of the polymetallic type have been referred (Arvanitidis and Dimou, 1990):

(a) The Kato Thermes polymetallic mineralization has a complex ore mineralogy consisting of arsenopyrite, pyrite, sphalerite, galena, chalcopyrite, neodigenite, graphite, hessite and electrum. Bulk chemical AAS-analyses from such mineralized core-samples, around 130m depth, gave the following results: Au=1.7-3.1 ppm, Ag=46-210 ppm and As=2.8-17.8wt%. At the same time, an INAA-analysis of the sample where Au was microscopically identified gave the following concentrations: Au=13.6 ppm and As=2.9wt%. Au participation (with an electrum composition) is related to the formation of hessite. The paragenetic features and the chemical compositions of the gold (Au) particles suggest a close relationship of gold and silver fractionation in the Kato Thermes polymetallic mineralization. The Kato Thermes polymetallic constitutes a subordinate part of a major base metal (Pb-Zn) predominant prospect (Arvanitidis and Dimou, 1990).

(b) The Kasli polymetallic mineralization consists of pyrite, sphalerite, galena, chalcopyrite, altaite, hessite and graphite. It is characterized by the presence of altaite (Pb telluride) and the absence of arsenopyrite. AAS-analyses of bulk ore samples showed: Au=0,4-3.4 ppm and Ag=65-104 ppm. Although any Au minerals were not visible in the microscope, the overall ore mineralogy indicates that, even in this case, Au has a close relationship to the telluride crystallization (Arvanitidis and Dimou, 1990).

(c) The Milos polymetallic mineralization consists of sphalerite, galena, pyrite, arsenopyrite, chalcopyrite, tennantite, tetrahedrite, gersdorffite and graphite and indicates a distinct trend an As- and Cu- enriched affiliation. It is characterized by the absence of any tellurides. The presence of the Ni-bearing gersdorffite is consistent to the bulk transition element (Ni, Cr. Co) rich character of the mineralization. Au concentrations have been confirmed by analyses of five mineralized sampled and not by the microscope (for more details, see below). It is certain that Au in the Milos mineralization is related to sulphide mineral formation, as any tellurides were not identified (Arvanitidis and Dimou, 1990).

Main mineral assemblages of both major mineralization types (i.e. breccia Pb-Zn-(Fe-Cu) as well as stratabound (manto) polymetallic and Pb-Zn-(Cu-Mn-Ag-Cd) mineralizations) consist of coexisting sphalerite, galena, pyrite with quartz, sericite and carbonates gangue; chalcopyrite also occurs in subordinate amounts. Table 1 presents the sphalerite chemistry for the Thermes ore varieties (Kalogeropoulos et al., 1996). Arsenopyrite is present in the polymetallic ore variety only (Kalogeropoulos et al., 1996), that is clearly indicated by the bulk ore chemistry (As=2.3-17.8%). In the Milos polymetallic occurrence, located 4.84 km NW of the Kato Thermes occurrence, arsenopyrite is accompanied by idiomorphic gersdorffite (Grf). Table 2 present the characteristic gersdorffite compositions (wt%) from the Milos polymetallic occurence (Arvanitidis and Dimou, 1990). Chalcopyrite is a characteristic mineral of the polymetallic mineralization. Galena and chalcopyrite from the polymetallic mineralization show Te and Bi contents of 0.34 and 0.29 wt% respectively. Tetrahedrite has been found in drillcore specimen from the Kato Thermes polymetallic occurrence and tetrahedrite and tennantite constitute chararacteristics components of the Milos polymetallic ore-mineral assemblage. Tennantite compositions showed trace elements of Te (0.1 wt%) and Sn (0.1 wt%), where as in a tetrahedrite grain the Ag maximum of about 3.5 wt% coincides with a high Pb content of 2.5 wt%. Table 3 presents the characteristics composition (wt%) of tetrahedrite and tennantite from the Milos and Kato Thermes polymetallic occurrences (Arvanitidis and Dimou, 1990).

Pb, Zn and Ag constitute the main metals of the Thermes ore-field (Melfos et al., 2012). The critical and precious metal mineralogy includes gersdorffite (Grf), hessite (Hs), altaite (Alt), electrum and native Au (Arvanitidis and Dimou, 1990; Voudouris et al., 2018), as well as the critical and rare metals of In, Ge and Ga (Melfos et al., 2012). Hessite (Ag_2Te) and altaite (PbTe) are typical telluride minerals of the polymetallic mineralization, although altaite was once found in a base-metal representative of the Thermes ore field. Among the three above-mentioned polymetallic occurrences (Kato Thermes, Milos, Kasli), Kasli comprises both hessite and altaite, Kato Thermes exclusively hessite and Milos lacks any presence of tellurides. Table 4 presents characteristic hessite and altaite compositions (wt%) from the Kato Thermes and Kasli polymetallic occurrences (Arvanitidis and Dimou, 1990). Hessite, altaite and electrum were identified as inclusions in galena (Arvanitidis and Dimou, 1990; Voudouris et al., 2007). Gold grains of 5-30 μm were identified only in core specimens from the Kato Thermes polymetallic mineralization. Hessite is the only host-mineral of gold grains that show compositional characteristics

of electrum (Arvanitidis and Dimou, 1990): Au=77.72%wt, Ag=22.15%wt and Cu=0.15%wt (Tot=100.02). Free gold (Au), occurring as electrum, in the Kato Thermes and probably the Kasli polymetallic occurrences, show a clear connection with the crystallization of silver telluride, hessite, and therefore a common evolutionary course with silver. Five (5) mineralized samples from the Milos polymetallic mineralization gave the following results: Au=4.5-12.5 ppm, Ag=73-240 ppm and As=2.3-5.5 wt%, but gold (Au) is invisible in the microscope, as well as the presence of any tellurides. However, the high analytical gold concentrations are related to the sulphide minerals of the tetrahedrite-tennantite series and a Ni-bearing arsenic character (e.g. gersdorffite); coincides with the overall geochemical enrichment of Ni in mineralized rocks, in accordance to the predominantly mafic composition of the host- and associated rocks. This lithology may be the gold contributing source as well and the Milos polymetallic mineralization is of high priority for further gold mineralogical studies (Arvanitidis and Dimou, 1990).
The Thermes deposit should be also evaluated for their In, Ge and Ga potential (Tsirambides and Filippidis, 2012; Melfos et al., 2012).
The Thermes ore deposit contains a resource of about 1 Mt with grades of <4 g/t Au, 10-340 g/t Ag, 1.2-14.5% Pb, 2.1-16.7% Zn and 0.06-0.10% Cu (Gialoglou and Drymniotis, 1983; Melvos and Voudouris, 2017).
Based on mineral exploration work carried out by I.G.M.E. (Institute of Geology and Mineral Exploration of Greece), the marginally unexploitable reserves are estimated to be 352 Kt Pb+Zn and 143 t Ag (Arvanitidis, 2010).
Garnets and graphite horizon have also been found in Thermes (Tsirambides and Filippidis, 2012).
The spatial coordinates (in WGS84 format) of the polygon vertices of the Thermes mineralization area are defined as follows:

- Vertex A: ϕ: 41° 24′07.61″ N, λ: 24° 55′15.09″ E
- Vertex B: ϕ: 41° 22′42.31″ N, λ: 24° 55′16.06″ E
- Vertex C: ϕ: 41° 20′46.04″ N, λ: 24° 58′41.82″ E
- Vertex D: ϕ: 41° 20′17.34″ N, λ: 25° 01′59.77″ E
- Vertex E: ϕ: 41° 22′03.09″ N, λ: 25° 02′29.30″ E

The polygon of the Thermes mineralization area on Google Earth is depicted in Figure 12.

4. Integrated 3D- 4D model

Requested information:

- ✓ existing 3D-4D models of the target area and the deep metal enrichment
- ✓ if no 3D-4D models exist, collect the following necessary data: geological setting, mineralization, fluid flow models, stress field determination

Notes: e.g. openly available datasets, models.

3D-4D models of the Thermes ore-field illustrating the ultra-deep metal enrichment have not been found in the literature.

- Thermes Ore Field

The metal sulfide mineralization of the Thermes ore-field is hosted in marbles, amphibolites and orthogneisses (Melfos and Voudouris, 2017). Ore concentrations in the Thermes ore field are controlled mainly by NW-SE faults and the tectonostratigraphic position of marbles (Arvanitidis et al., 1989a; Arvanitidis and Dimou, 1990). WNW-ESE trending faults are also locally mineralized, particularly where they intersect the NW-SE faults (Arvanitidis and Dimou, 1990).
Two major base metal sulfide ore varieties have been recognized in the Thermes ore field (Arvanitidis et al., 1986; 1989b): (1) a brecciated vein Pb-Zn(Fe-Cu) mineralization related to NNW- and NNE-trending faults and (2) stratabound (manto), replacing marbles with extension to mineralized veins in faults. The second variety is subdivided into (a) polymetallic (Zn-Pb-Fe-Cu-As-Ag-Au-Cd-Sb) and (b) Pb-Zn(Cu-Mn-Ag-Cd) types (Figure 6).
Pb-Zn replacement deposits, (sub)horizontal, are controlled by the intersection of N30-45° faults, intersecting with WNW-ESE faults, with marbles and overthrust plane. These mineralization generally occur in the lower part of the upper marble-amphibolitic gneiss tectonic unit. Pb-Zn(Fe) breccias mineralization occurs in open system sub-parallel fracture zones, found in relation to large scale

silification of the surrounding wall rocks. Vein type Pb-Zn(Fe-Cu) mineralization occurs as fractures and cracks hosted by zones of silicification (Arvanitidis and Dimou, 1990).
Polymetallic mineralization associated is associated with the top sequence lithologies of the upper amphibolitic gneiss-marble unit. The Kato Therma polymetallic mineralization is controlled by the intersection of a NW-SE trending ore-bearing fault and a graphite-bearing marble-two-mica gneiss intebedded sequence, leading to silicification, brecciation and mineralization of the reactive carbonate bed and the formation of mineralized jasperoidal breccias. The Kasli polymetallic mineralization shows in many ways similar characteristics with the previous one, particularly regarding the tectonostratigraphic position and subordinate presence of marbles (thin carbonate beds) in relation to interbedded gneisses (thick silicate beds of variable lithology). The Milos polymetallic mineralization is controlled by a NNE-SSW trending ore-bearing fault intersecting a stratigraphic top-section of the upper unit, comprising an alternation of marbles and amphibolites associated with pegmatite sills; the amphibolitic rocks being the predominant lithology (Arvanitidis and Dimou, 1990).
In the Thermes ore field, there is an E-W variation in ore type and metal ratios. In addition to this variation, a vertical variation relative to the position of a mineralization in the stratigraphic sequence has been observed, and a variation from lower Zn>Pb>>Cu to upper Zn>Pb≈Cu in an individual mineralization is common (Arvanitidis and Dimou, 1990).
Hydrothermal alteration of the wall rocks is an important part of the ore forming system, with silicification and related oxidation being the most common. Sericitization, chloritization and carbonitization are also wide spread. Silicification is widely developed in the upper tectonic unit above the thrust fault, which clearly has served as a fluid pathway. The hydrothermal reactions are often controlled by the precursor mineralogy of the wall rock, certain types of alternation being found only in certain rock units (Arvanitidis and Dimou, 1990).

- Madan Ore Field

Considering that Thermes represents the southern extension of the Madan ore field (MOF) in Bulgaria (Kaiser-Rohrmeier et al., 2013), some useful data can be obtained from this ore field: The Pb-Zn ores constitute hydrothermal Pb-An-Ag deposits. Three morphogenetic types of ore bodies have been recognized: (i) steep simple veins (1-3m wide; up to 7 km length), (ii) complex disseminated stockworks and (iii) replacement ore bodies (skarn-ore bodies). Their formation is structurally controlled by the ore-controlling fault systems and lithological variety of the host Rhodope metamorphic complex. These types often co-exist in one and the same deposit, showing close connections and transitions from one type to another. The veins and stockworks are controlled by 6 large NNW-SSE (320-340^{o}) striking faults, whereas gently dipping bed-like and irregular manganoan skarn-ore bodies are formed at the intersections of the faults with the three major marble horizons (Vassileva et al., 2005; 2009). The richest vein and replacement mineralizations of economic importance in the Madan area occur at the intersections of the NNW-SSE and WNW-ESE fault systems. Veins comprise regularly-shaped, simple, single, steeply-dipping mineralized bodies, as parts of the ore-bearing NNW fault zones and their contacts with the embedding gneisses are sharp. Ore textures in the veins are massive, breccias, crustifications, druses. Stockwork zones are genetically and spatially connected to the veins and they are 1-2 to 10-20 m wide and up to 1-2 km long. This morphogenetic type is characteristic for the relatively deeper levels of the deposits. The mineralized stockwork zones are represented by disseminated ores in thin, irregularly-shaped, discordant sulphide veins and veinlets, impregnations and breccias. Replacement ore bodies (width: 30-60m or even more, thickness: 4-5m and rarely up to 20-25m) are the most interesting ones from genetic and economic aspect and variable from morphological point of view. The replacement ore bodies reveal complex morphology according to the number, thickness and position of the host marble layers, shifts along the fault structures and local physicochemical parameters. They are always embedded in the marble horizons of the Rhodopean metamorphic complex and host rich ores of economic importance. The ore textures are indicative for crystallization in open space or metasomatic growth in solid state. Ore textures in the replacement ore bodies are radial, rhythmic-banded, impregnations, massive, nests and druses. The massive, coarse-grained metasomatic sulphide ores are characterized by high porosity. A system of open space cavities

are often developed within the skarn bodies as a result of selective dissolution mainly of the retrograde carbonates. According to their geological position and morphology, the following subtypes of replacement bodies can be distinguished in the Madan Pb-Zn deposits: (a) single beds, (b) multilayered beds, (c) multi-layered sheet-like bodies in the thick Ist marble horizon (they are deep seated and therefore detected only by drilling), (c) massive, bed-like skarn-ore ledges developed around the ore vein in the IInd marble layer, (d) complex multilayered ledges, replacing several thick marble layers along several large ore veins. (e) vein-like, columnar or mushroom-like and irregular in cross section ore bodies within thick marble horizons along a thin steep non-mineralized fault, (f) bed-like replacement bodies in the IIIrd marble horizon, developed around the intersection of NNW-SSE and WNW-ESE fault systems, (g) irregular metasomatic bodies with complex shape in cross section embedded in the IIIrd graphite-bearing marble horizon (the replacement ores are associating with and screened by pegmatites). Main factors controlling the morphology of ore bodies are the features of ore-controlling faults and lithology. The six steeply-dipping NNW-SSE striking faults in the area are the main ore-conducting and ore-bearing structure and the deposits are genetically connected to this fault system.The economically important mineralizations occur at the intersections with the WNW-striking fault system. Since the NNW-SSE striking fault system provides pathways for the movement of the ascending hydrothermal fluids, the number, size and position of these faults in certain location controls the scale of the resulting ore deposition. Dense systems of adjacent, large faults control the deposition of large and rich vein and replacement ore bodies. Movements along the ore-bearing and non-mineralized fault structures complicate the morphology of the vein and replacement ore bodies. The three marble horizons in the Madan area are favourable medium for development of metasomatic processes: formation of manganoan skarns and subsequent deposition of rich sulphide ores therein. The tectonic fragmentariness and permeability of the ore-hosting rocks increase the reactive surface, interacting with the upcoming fluids. The simple sulphide veins are perspective above the critical level, where rich ores (~10 % metals) are deposited, but in depth, these ore bodies do not contain economically important ores. The stockworks contain ores with low metal content (2-3%) and are currently unprofitable. The metasomatic bodies concentrate an important part of the ore resources of the Madan area and they can be considered as a potential future resource for base metals (Vassileva et al., 2009; Vassileva et al., 2010). Three main mineralization stages have been divided on the basis of temporal and spatial mineral relationships and microthermometry study on fluid inclusions (Vassileva et al., 2010): (a) Skarn stage, (b) Main ore stage and (c) Late post-ore stage.

Figure 13 illustrates a simplified geological map of the Central Rhodopean Dome (Southern Bulgaria) and main ore districts focused on the Madan area, in the vicinity of the Thermes ore-field. By deep structural drillholes in the south part of the Madan Ore Field, the carbonate rocks have been revealed. In the carbonate rocks, considerable metasomatic ore bodies have beem formed (Dragiev and Danchev, 1990). Figure 14

Figure 15 illustrates very well the generalized results of the study of metasomatic ore bodies in the Erma Reka area of the Madan Ore Field. The presence of carbonate rocks favours the formation of metasomatic ore bodies.

- <u>Comparison between Madan and Thermes Ore Fields – Common features</u>

  Geology:

As mentioned above (section "1. Geology of the prospective area") a comparative study between the Madan (MOF) and Thermes (TOF) ore fields showed that these ore fields have many common features and they belong to the same metallogenic province. They are hosted in the same metamorphic lithologies. The rocks, which comprise the two ore fields may group into the following suites (Manev et al., 1990): (i) variegated gneiss-marble suite (gneisses, gneiss-schists of diverse mineral composition, marbles) in the interval 820-2020m from surface in the Erma village area, (ii) carbonate suite (mainly marbles; minor constituents: gneisses, calc-schists, skarnoids), (iii) leucocratic gneiss suite (muscovite gneisses, gneiss-schists, aplitoid muscovite gneisses, two-mica gneisses, quartz-muscovite gneisses), 20-750m thick, (iv) fine-grained hornblende-biotite gneiss and amphibolite suite, 1,500m thick, (v) granitized biotite gneiss suite, 100-600m thick, (vi) variegated marble-amphibolite suite, 100-700m

thick, and (vii) injected gneiss suite with parallel-bedding and cross-cutting pegmatoid veins, 1,200m thick. The "lower" unit includes the first five suites (Manev et al., 1990).

Tectonic setting

There are four (4) distinct group of faults in the area NNW-SSE, ENE-WSW, NW-SE and NE-SW. (a) The main mineralized faults in MOF (Madan Ore Field) are those of NW(320-340^{o})-SE direction. They form a fault swarm about 5 km wide and 20 km long. Their density increases in the southern periphery of the ore field. In TOF (Thermes Ore Field), there are similar ore-hosting structures. The NW-SE faults are of larger dimensions in its western part (e.g. Ano Thermes in Greece). (b) The WNW-ESE faults are widely developed in both ore fields. These faults may be traced in a distance up to 10km and there are marked by intensely deformed and hydrothermally altered rocks. In MOF (Madan Ore Field) they don't host economic mineralizations but they control their distribution within the faults in the other two groups. A fault of this group hosts the mineralization in the Kato Thermes area. (b) NE-SW faults occur mainly in the southern and eastern parts of MOF and in the eastern part of TOF and contain Pb-Zn mineralization. Their dimensions are small. Cleavage and jointing are very well developed and their average statistical strike is usually parallel to that of the main fault groups (Manev et al., 1990).

Ore Mineralization

Pb-Zn mineralization is related to vein and stratabound (of irregular form) ore bodies and its mineral composition is highly variable. In MOF (Madan Ore Field), the vein ore bodies occur mainly in NW-SE faults and far less common in NE-SW faults. In TOF (Thermes Ore Field), Pb-Zn mineralization is related to these faults and to a WNW-ESE fault in Kato Thermes. The morphology of the vein ore bodies depends mainly on the structure of the mineralized faults and the type of ore deposition. Faults, in which there was free space before ore deposition, enclose ore bodies of massive, brecciated and/or ore banded structure. Faults, which were infilled with deformed and hydrothermally altered pre-ore material, enclose ore bodies of vein-impregnated type, common of large dimensions but with lower metal content. The morphology of the vein ore bodies is complicated by many apophyses. The vein ore bodies show strong varying thickness (from a few cm to ~20m). The distribution of metals is also irregular and the highest metal concentrations usually outline vertical or steeply dipping ore columns. The direction of ore-hosting faults played an important role in the localization of vein mineralization (Manev et al., 1990).

The bed-like ore bodies and those of irregular form are located in the marbles. There are products of metasomatic replacement of the marbles around the ore-hosting faults and were formed contemporaneously with the vein ore bodies. They contain Pb-Zn rich ores and their form and dimensions are widely varying. Three types of ore deposition may be distinguished: (a) infilling of cavities in faults and karstified marbles; (b) impregnation of pore spaces in the pre-ore fillings of faults; (c) metasomatic replacement of carbonate ore-hosting rocks. The formation of metasomatic ore bodies was controlled by the presence of carbonate horizons (Manev et al., 1990).

The formation and the economic significance of vein ore bodies were most essentially influenced by the elements of tectonic stress field during the ore deposition and the resulting movements of tectonic blocks. The domination of N-S tangential active stresses during the ore deposition stage in both MOF and TOF (Manev et al., 1990).

The established vertical distribution of the economic mineralization in the individual MOF (Madan Ore Field) deposits varies from 200 to 1,500m and for the whole ore field exceeds 2,000m (Manev et al., 1990).

Mineralization in both ore fields belong to identical morphogenetic types. Ore depositional mechanism, mineral composition and mineral paragenesis are essentially the same. Pb isotopic characterestics suggest a common crustal source of the metals and restricted formation time. Most likely both ore fields were fed from a single regional hydrothermal flow which, with minor exceptions, retained its hydrodynamic unity also at the level of the mineralized rock complexes and structures (Manev et al., 1990).

Taking into account that mineralization is controlled mainly by deep faults, the existence of mineral deposits at great depths is considered highly probable.

5. EGS potential

Requested information:

- ✓ EGS potential (heat & energy) of the area
- ✓ geothermal characteristics (temperature gradient, heat flux, stress field, water availability, EGS geology)
- ✓ presence/indication of deep fluids/brines, fracture system, crustal permeability

GEOTHERMAL CHARACTERISTICS OF THE THERMES AREA AND ITS SURROUNDINS

Hydrothermal alterations are scattered in the Thermes area. These alterations include sericitization, silicification and pyrite alteration (Kolios and Sarandeas, 1990).

The heat flow density of the area is about 70-200 mW/m^2 (average global heat flow density 70 mW/m^2), as it is shown on the Figure 16.

At the Thermes (Xanthi) area, 29 thermal springs have been identified (25 of therm are located in Loutra Thermes area and other 4 springs in the Kato Thermes area) as Figure 17 shows.

The coordinates (decimal/WGS84) of some significant springs (T: 39-53^{o}C) in Loutra Thermes are as follows:

- Spring 1: ϕ: 41.3484596 / 41^{o}20΄54.45”, λ: 25.012383 / 25^{o}0΄44.58”
- Spring 2: ϕ: 41.3484407 / 41^{o}20΄54.39”, λ: 25.0122751 / 25^{o}0΄44.19”
- Spring 3: ϕ: 41.3482695 / 41^{o}20΄53.77”, λ: 25.0097579 / 25^{o}0΄35.13”
- Spring 4: ϕ: 41.348297 / 41^o 20΄53.87”, λ: 25.0096985 / 25^o 0΄34.91”
- Spring 5: ϕ: 41.3484318 / 41^o 20΄54.35”, λ: 25.0157626 / 25^o 0΄56.75”

The locations of these springs on Google Earth are depicted in Figure 18. A simplified geological map of the area with the position of hot springs is shown in Figure 19, while a more detailed geological map is shown in Figure 20.

The total flow rate of the springs from the Loutra Thermes area is estimated to exceed 100 m^3/h, and the measured temperatures range from 29 to 53^{o}C (Kolios and Sarandeas, 1990). At the Kato Thermes area, the temperatures of 18-23^{o}C have been recorded and the total flow rate doesn’t exceed the 8 m^3/h. However, two (2) wells were drilled by I.G.M.E. at a distance of about 500m NW of the village of Kato Thermes (Figure 17). One of them was artesian and tapped a hot aquifer of 41^{o}C at depth of about 200m in fractured gneisses (Kolios and Sarandeas, 1990).

The thermal waters of the area belong to the Na-HCO_3 type having electrical conductivity of 900-1600 μS/cm and pH 6.1-6.9 (Kolios and Sarandeas, 1990; Minissale et al., 1989; Athanassoulis et al., 2009). The chemical composition of gas discharges is: 531.1 m.mol.mol^{-1} CO_2 and 455.7 m.mol.mol^{-1} N_2 (Kolios

and Sarandeas, 1990; Minissale et al., 1989). High N_2 percentages point to relatively long residence times (Minissale et al., 1989) and the marked presence of air in most of the hydrologic circuits (Kolios and Sarandeas, 1990; Minissale et al., 1989). With the aid of chemical geothermometers, the temperatures of 80-150^{o}C have been calculated for geothermal fluids at great depths (Minissale et al., 1989). The most likely deeper temperatures range from 100 to 120^{o}C (Kolios and Sarandeas, 1990).
Figure 21 illustrates the probable geothermal conditions and a conceptual model for the Thermes area. It constitutes a fault-hosted geothermal system. The circulation of geothermal fluids seems to be controlled by deep faults and take place within the intensely fractured metamorphic basement rocks. Three fault systems occur in the Thermes area. The observed orientations of these faults are: WNW (270-315^o), NE (10-30^o) and NW (330^o). The dominant and oldest fault system is WNW-oriented (Kolios and Sarandeas, 1990). The presence of granitic gneisses and granitoids in the area favors the increased regional heat flow. Under these geological, tectonic and geothermal conditions, the development of an EGS system is considered to be very probable.
It is very important to underline the presence of the Erma Reka geothermal system very close to the Thermes hot springs, in the territory of Bulgaria (Figure 22). The Erma Reka geothermal system and constitutes a combination with a polymetallic Pb-Zn mineralization (Benderev et al., 2015) because it is situated within the southern part of the Madan ore-field (Teneva-Georgieva and Andreev, 2005). Numerous mining galleries, exploitation horizons, mine and ventilation shafts, including the main shaft to a depth of 650m (the deepest in the Rhodopes massif) were built. Their construction was done under extreme high temperatures up to 70^{o}C, hazardous geological, mining and hydrogeological conditions. Before ore exploitation a lowering of water level in the heated marble body was done (Benderev et al., 2015). The Erma Reka system constitutes a complicated tectonic structure and is made up of (Teneva-Georgieva and Andreev, 2005; Benderev et al., 2015) gneisses, granitic gneisses, amphibolites, amphibolite gneisses, schists, marbles and volcanites (Figure 23). There are no marble outcrops in the territory of Bulgaria, but marbles, more than 1,000m thick, with silicitizated cavernous zone formed the upper part, are underlain by gneisses at depths greater than 450m. Marbles are karstified and cavernous and a thick quartz cavernous zone is formed on the boundary between marbles and gneisses. The structure is crossed by many faults and fractures, which are essential for the hydrothermal system. The faults are oriented in three main directions: NW(275-305^o), SE(60-80°), NE(40-70^o) and E(90-100^o). The high-angle faults form the complicated block structure of the area. The geological and tectonic settings favour the formation of two water-bearing systems: (a) fissure waters in the fractured silicate metamorphic and igneous rocks and (b) karst waters in the fractured and karstified marbles. The thermal water is mainly accumulated in karst and cavernous marble body and ascends through the numerous faults and fractures to the gneisses (Fig. 23 and 24). The faults create also conditions for cold waters penetration in depth. A hydraulic link exists between cold and warmed fractured unconfined waters formed in gneisses (zone of regional fracturing) and confined waters containing in the upper zone of the marble body (Teneva-Georgieva and Andreev, 2005). The results obtained from pumping-tests performed in 78 wells indicate that hydrogeological parameters vary widely. Transmissivity (T) values range from 60 to more than 2000 m^2/d and hydraulic conductivity varies between 5 and more than 100 m/d (Benderev et al., 2015). These results confirm the heterogeneous hydrogeological properties of the permeable rocks in horizontal and vertical direction (Teneva-Georgieva and Andreev, 2005). Water temperature within Erma Reka reservoir reaches 94^{o}C (Teneva-Georgieva and Andreev, 2005; Benderev et al., 2015). TDS measured for thermal water samples taken from wells vary between 700 and 1646 mg/l depending on the depth and special deposition of the reservoir (Benderev et al., 2015). Na-HCO_3 waters are connected to the marble hydrothermal zone, while Na-SO_4 and Ca-SO_4 waters are mainly accumulated into the gneisses (Teneva-Georgieva and Andreev, 2005). Some ions, like HCO_3^-, Ca^{2+}, Na^+ are typical for cold waters, while HCO_3^-, SO_4^{2+}, Na^+ for thermal waters. Similar results are obtained for the Thermes thermal springs. Some trace elements such as Ga, Ge, Li, Ti, Mo, V increase their concentration in hot water, which is associated with ascending water from the deeper part of the reservoir. Other elements such as Mn, Ni, Pb, Sr, Zn, Cr, Zr, Cd exhibit higher concentrations in cold, mixed and cooled thermal waters. They are probably coming as a result of interaction with the host

rocks or from waters passed through ore mineralization. No significant change in Ag, Al, As, Ba, Cu, Fe, Co concentrations in terms of water temperature is established. Elevated F concentration (up to 8 mg/l) is observed in hot waters (Benderev et al., 2015). Based on the results of chemical geothermometers, it can be concluded that the equilibrium temperature is 120-150°C and even higher at great depths. In the most west part of the area, the temperature of 128°C has been measured at depth 1,345m. Assuming that the source temperature is 100-120°C at depth of 3,000m, the geothermal gradient of 3.3-4°C/100m is calculated. This almost normal gradient means that the water is heated due to its deeper circulation along deep faults (Teneva-Georgieva and Andreev, 2005).

As mentioned above, there are no surface thermal manifestations in the Erma Reka geothermal field, in the territory of Bulgaria (Teneva-Georgieva and Andreev, 2005; Benderev et al., 2015). The geothermal system has distinct surface manifestations only in the Greek territory (Teneva-Georgieva and Andreev, 2005). Thermal water from Erma Reka reservoir discharges through several springs located in the Thermes area (Benderev et al., 2015). Therefore, it is considered that Erma Reka field and Thermes springs constitute a single geothermal system. A proof of this consideration is as follows:

Before mineral exploitation in the Madan ore-field (territory of Bulgaria), a lowering of water level in the heated marble body of the Erma Reka geothermal system was done. This process reflected on the decreasing of water quantity of the Thermos springs (Benderev et al., 2015).

The varying hydraulic conductivity of the tectonic zones and irregularities, and the network of criss-crossing irregularities create very complex routes for the circulation of the thermal waters and hydraulic connection between the fissure systems (Teneva-Georgieva and Andreev, 2005).

CONCLUSIONS AND
JUSTIFICATION FOR THE CHOICE OF THE THERMES AREA AS A PROSPECTIVE CHPM AREA

Taking into account that

- the Thermes base metal sulfide ore-field includes Pb-Zn (Fe-Cu)/Pb-Zn(Cu-Mn-Ag-Cd) and polymetallic Zn-Pb-Fe-Cu-As-Ag-Au-Cd-Sb/Pb-Zn-Fe-Cu-Mn-As-Sb-Cd-Te-Ag-Au mineralization types and is hosted in marbles
- the Thermes and Madan-ore fields constitute a single ore district and the Thermes area represents the southern extension of the Madan ore field
- the Thermes ore-field is controlled regionally by deep faults and the tectono-stratigraphic position of marble units
- the mineralization probably continues to greater depths
- thermal springs of 39-53°C manifest themselves in the Thermes area
- the Thermes springs constitutes the surface manifestations of the adjacent Erma-Reka geothermal system (in the territory of Bulgaria) where the water temperature reaches 94°C and the temperature of 128°C has been measured at depth of 1,345m
- the metamorphic rocks of the area are intensely fractured

the choice of the Thermes area as a CHPM target for further exploration can be justified.

The spatial coordinates (in WGS84 format) of the polygon vertices of the prospective CHPM area of Thermes are defined as follows:

- Vertex A: ϕ: 41° 24′07.61″ N, λ: 24° 55′15.09″ E
- Vertex B: ϕ: 41° 22′42.31″ N, λ: 24° 55′16.06″ E
- Vertex C: ϕ: 41° 20′46.04″ N, λ: 24° 58′41.82″ E
- Vertex D: ϕ: 41° 20′17.34″ N, λ: 25° 01′59.77″ E
- Vertex E: ϕ: 41° 22′03.09″ N, λ: 25° 02′29.30″ E

The polygon of this prospective CHPM area on Google Earth is depicted in Figure 25.

List of References

Alfieris D., Arvanitidis N.D., Katirtzoglou K., 1989, "Petrology and geochemistry of acid dyke-rocks in the East Rhodope, Esimi area", Geol. Rhodopica, 1, 268-279

Arikas, K. and Voudouris, P., 1998, Hydrothermal alterations and mineralizations of magmatic rocks in the southern Rhodope Massif", Acta Vulcanol., 10, 353-365.

Arvanitidis N.D., Favas N., Dimadis E., Zanas I. and Kalogeropoulos S.I., 1986, "Zn-Pb-Cu sulfide mineralizations in the area of Thermes, Central Rhodope massif", Summary of preliminary geologic, petrologic and geochemical considerations", Final Rep., EEC-Rhodope R&D project, IGME, Athens, Greece, 47 p.

Arvanitidis N.D., Dimadis E., Favas N. and Zanas I., 1989a, "The geology, mineralogy, and petrogenesis of metamorphic rocks from the area of Thermes, Central Rhodope massif", 1st Hellenic-Bulgarian Symposium on the Geology and Physical Geography of the Rhodope Massif, Univ. Sofia. Geol. Rhodopica, 1, 169-185

Arvanitidis N.D., Kalogeropoulos S.I. and Favas N., 1989b, "Zn-Pb-Cu sulfide mineralization in the area of Thermes, Central Rhodope Massif", Geol. Rhodopica, 1, 306-321

Arvanitidis N. and Dimou E., 1990, "Electrum and silver telluride occurrences in the polymetallic sulfide mineralization of the Thermes ore-field, N. Greece", Geol. Rhodopica, 2nd Hellenic-Bulgarian Symposium (Thessaloniki, 1989), 2, 309-325.

Arvanitidis N., 2010, "Economically viable mineral deposits in Macedonia and Thrace", Presentation, Workshop "The treasures of Northern Greece", Thessaloniki, 29 May 2010

Athanassoulis C., Vakalopoulos P., Xenakis M., Persianis D. and Taktikos S., 2009, "Periodical monitoring of the curative springs of Greece", Technical Report, I.G.M.E., Athens, 57-61 (in Greek)

Benderev A., Atanassova R., Andreev A., Hristov V., Bojadgieva K. and Kolev S., 2015, "Hydrochemical Characteristics of Erma Reka Geothermal Reservoir (S. Bulgaria)", Proceedings, World Geothermal Congress 2015, Melbourne, Australia, 19-25 April 2015, 9 p.

Bonev N., Burg J.P. and Ivanov Z., 2006a, "Mesozoic-Tertiary structural evolution of an extensional gneiss dome - the Kesebir-Kardamos dome, E. Rhodopes, Bulgaria", Int. J. Earth Sci. 95, 318-340

Bonev N., Marchev P. and Singer B., 2006b, "40Ar/39Ar geochronology constraints on the Middle Tertiary basement extensional exhumation, and its relation to oreforming and magmatic processes in the Eastern Rhodope (Bulgaria)", Geodin. Acta, 19, 265-280

Bonev N., Moritz R., Márton I., Chiaradia M., Marchev P., 2010, "Geochemistry,tectonics, and crustal evolution of basement rocks in the Eastern Rhodope Massif, Bulgaria", Int. Geol. Rev., 52, 269-297

Bonev N., Spikings R., Moriz R. and Marchev, P., 2013, "$^{40}Ar/^{39}Ar$ age constraints on the timing of Tertiary crustal extension and its temporal relation to ore-forming and magmatic processes in the Eastern Rhodope Massif, Bulgaria", Lithos, 180-181, 264–278.

Bonev N., Marchev, P., Moritz R. and Collings D., 2015, "Jurassic subduction zone tectonics of the Rhodope Massif in the Thrace region (NE Greece) as revealed by new U-Pb and $^{40}Ar/^{39}Ar$ geochronology of the Evros ophiolite and high-grade basement rocks", Gondwana Res., 27, 760-775

Brun J.-P. and Sokoutis D., 2007, "Kinematics of the Southern Rhodope core complex (Northern Greece)", Int. J. Earth Sci. 96, 1079-1099

Burg J.P., Ricou L.E., Ivano Z., Godfriaux I., Dimov D. and Klain, L., 1996, "Synmetamorphic nappe complex in the Rhodope Massif", Structure and kinematics, Terra Nova, 8, 6-15

Christofides G., Pecskay Z., Eleftheriadis G., Soldatos T. and Koroneos A., 2004, "The Tertiary Evros volcanic rocks (Thrace, northeastern Greece): petrology and K-Ar geochronology", Geol. Carpath., 55, 397-410

Dinter D.A., Macfarlane A., Hames W., Isachsen C., Bowring S. and Royden L., 1995, "U-Pb and $^{40}Ar/^{39}Ar$ geochronology of the Symvolon granodiorite: implications for the thermal and structural evolution of the Rhodope metamorphic core complex, northeastern Greece. Tectonics 14, 886-908.

Dragiev H. and Danchev J., 1990, "Morphological-structural specialities of metasomatic deposits in the Erma Reka area in the Madan's ore field", Geologica Rhodopica, 2, 352-361

Eleftheriadis G., Christofides G., Mavroudchiev B., Nedyalkov R., Andreev A. and Hristov L., 1989, "Tertiary volcanics from the East Rhodope in Greece and Bulgaria", Geol. Rhodopica, l, 202-217

Ersoy E.Y. and Palmer M.R., 2013, "Eocene-Quaternary magmatic activity in the Aegean: implications for mantle metasomatism and magma genesis in an evolving orogeny", Lithos 180-181, 5-24

Institute of Geology and Mineral Exploration, (I.G.M.E.), 2001, Map of Heat Flow Density in Greece, Scale 1:1,000,000, Athens

Fytikas M., Innocenti F., Manneti P., Mazzuoli R., Pesserillo G. and Villari L., 1985, "Tertiary to Quaternary evolution of the volcanism in the Aegean region", In: Dixon, J.E., Robertson, A.H.F. (eds.) The geological evolution of the Eastern Mediterranean, Spec. Publ. Geol. Soc., 17. Blackwells, Oxford, 687-699

Gialoglou G. and Drymniotis D., 1983, "Northeastern Greece: mining activities, mineral exploration and future developments", Trans. Inst. Min. Metall., Sect. A 92, A180-183

Innocenti F., Kolios N., Manetti O., Mazzuoli R., Peccerilo G., Rita F. and Villari L., 1984, "Evolution and geodynamic significance of the Tertiary orogenic volcanism in northeastern Greece", Bull. Volcanol., 47, 25–37

I.G.M.E. (Institute of Geology and Mineral Exploration), 2009, "Geological Map of Greece, Scale: 1:50,000, Sheets: "Echinos" and "Medousa"

Jones C.E., Tarney J., Baker J.H. and Gerouki, F., 1992, "Tertiary granitoids of Rhodope, northern Greece: magmatism related to extensional collapse of the Hellenic Orogen", Tectonophysics, 210, 295-314

Kaiser-Rohrmeier M., von Quadt A., Driesner T., Heinrich C.A., Handler R., Ovtcharova M., Ivanov Z., Petrov P., Sarov S. and Peytcheva I., 2013, "Post-orogenic extension and hydrothermal ore formation: high precision geochronology of the Central Rhodopian metamorphic core complex (Bulgaria-Greece)", Econ. Geol., 108, 691-718

Kalogeropoulos S.I., Kilias S.P. and Arvanitidis N.D., 1996, "Physicochemical conditions of deposition and origin of carbonate-hosted base metal sulfide mineralization, Thermes ore-field, Rhodope Massif, northeastern Greece", Mineralium Deposita, 31, 407-418

Karmis P. and Tsourlos P.I., 2004, "Transient electromagnetic surveys in mineral exploration", Proceedings, 1st International Conference on Advances in Mineral Resources Management and Environmental Geotechnology, Hania 2004, Greece, 95-100

Kilias A., Falalakis G., Sfeikos A., Papadimitriou E., Vamvaka A. and Gkarlaouni C., 2013, "The Thrace basin in the Rhodope province of NE Greece - a Tertiary supradetachment basin and its geodynamic implications", Tectonophysics, 595-596, 90-105

Kirchenbaur M., Pleuger J., Jahn-Awe S., Nagel T.J., Froitzheim N., Fonseca R.O.C. and Münker C., 2012, "Timing of high-pressure metamorphic events in the Bulgarian Rhodopes from Lu–Hf garnet geochronology", Contrib. Miner. Petrol. 163, 897-921

Kokkinakis A., 1980, "Altersbeziehungen swischen Metamorphosen, mechanismen, deformationen and intrusionen and Sudrand, des Rhodope-Massives (Makedonicn, Griechenland)", Geol. Rundsch., 69.3, 726-744

Kolios N. and Sarandeas A., 1990, "Thermal manifestations in the Rhodope Masif (Thermes Xanthi area)", Proceedings, 2nd Conference of Thermal Mineral Waters, Thessaloniki 7-9 October 1988, 103-108 (in Greek)

Kojonen, Kari, K., Cook, Nigel, J. & Ojala, V. Juhani (ed.) 2007: Au-Ag telluride-selenide deposits. Geological Survey of Finland, Guide 53. 94 pages, 62 figures and 14 tables.

Kyriakopoulos K., 1987, "A geochronological, geochemical and mineralogical study of some Tertiary plutonic rocks of the Rhodope Massif and their isotopic characteristics", Ph.D. Thesis, University of Athens, 343 p. (in Greek)

Manev D., Katzkov N., Miler V., Malinov D., Arvanitidis N.D., Constantinides D.C., Dimadis E., Romaidis N. and Favas N., 1990, "Comparison between Madan (Bulgaria) and Thermes (Greece) ore fields. Geology and metallogenesis", 2nd Hellenic-Bulgarian Symp. Geology and Physical Geography of the Rhodope Massif, University of Thessaloniki, Geol. Rhodopica, 2, 399-408

Marchev P., Downes H., Thirlwall M. F. and Moritz R., 2002, "Small-scale variations of $^{87}Sr/^{86}Sr$ isotope composition of barite in the Madjarovo low-sulphidation epithermal system, SE Bulgaria: Implications for sources of Sr, fluid fluxes and pathways of the ore-forming fluids", Mineralium Deposita, 37, 669-677

Marchev P., Kaiser-Rohrmeier B., Heinrich C., Ovtcharova M., von Quadt A. and Raicheva R., 2005, "Hydrothermal ore deposits related to post-orogenic extensional magmatism and core complex formation: the Rhodope Massif of Bulgaria and Greece", Ore Geol. Rev., 27, 53-89

Marchev P., Georgiev S., Raicheva R., Peytcheva, I., von Quadt, A., Ovtcharova, M. and Bonev, N., 2013, "Adakitic magmatism in post-collisional setting: an example from the early-middle Eocene Magmatic Belt in Southern Bulgaria and Northern Greece", Lithos, 180-181, 159-180

Márton I., Moritz R. and Spikings R., 2010, "Application of low-temperature thermochronology to hydrothermal ore deposits: formation, preservation and exhumation of epithermal gold systems from the Eastern Rhodope, Bulgaria", Tectonophysics, 483, 240-254

Meinhold G. and Kostopoulos D.K., 2013, "The Circum-Rhodope Belt, northern Greece: age, provenance, and tectonic setting", Tectonophysics, 595-596, 55-68

Melfos V., Vavelidis M., Christofides G. and Seidel E., 2002, "Origin and evolution of the Tertiary Maronia porphyry copper-molybdenum deposit, Thrace, Greece", Mineral Deposita, 37, 648-668

Melfos V. and Voudouris P., 2012, "Geological, Mineralogical and Geochemical Aspects for Critical and Rare Metals in Greece", Minerals, 2, 300-317, doi: 10.3390/min2040300

Melfos V. and Bogdanov K., 2012, "A field guide to the ore deposits of NE Greece", 19th-22nd October 2012, In the frame of the cooperation between the Aristotle University of Thessaloniki, the Sofia University "St. Kliment Ohridski", the Sofia University SEG Student Chapter, 19 p.

Melfos V. and Voudouris P., 2017, "Cenozoic metallogeny of Greece and potential for precious, critical and rare metals exploration", Ore Geology Reviews, 89, 1030–1057

Meyer W., 1968, "Zur alterstellumg des plutonismus im Sudteil der Rila-Rhodope masse (Nordgrienchenland)", Geol. Palaeontologica, 2, 173-192

Minissale A., Duchi V., Kolios N. and Totaro G., 1989, "Geochemical characteristics of Greek thermal springs", Journal of Volcanology and Geothermal Research, 39, 1-16

Moritz R., Márton I., Ortelli M., Marchev P., Voudouris P., Bonev N., Spikings R. and Cosca M., 2010, "A review of age constraints of epithermal precious and base metal deposits of the Tertiary Eastern Rhodopes: coincidence with Late Eocene-Early Oligocene tectonic plate reorganization along the Tethys", In: Christofides, G., et al. (Eds.), Proceedings of the XIX Congress of the Carpathian-Balkan Geological Association, Thessaloniki. Scientific Annals of the School of Geology A.U.Th., 100, 351-358

Mposkos E., Liati A., Katagas, C. and Arvanitidis, N.D., 1990, "Petrology of the metamorphic rocks of West Rhodope, Drama area, N. Greece", 2nd Hellenic-Bulgarian Symp. Geology and Physical Geography of the Rhodope Massif, University Thessaloniki, Geol. Rhodopica, 2, 127-142

Mposkos E.D. and Kostopoulos D.K., 2001, "Diamond, former coesite and supersilicic garnet in metasedimentary rocks from the Greek Rhodope: a new ultrahighpressure metamorphic province established", Earth Planet. Sci. Lett., 192, 497-506

Pe-Piper G. and Piper D.J.W, 2002, "The igneous rocks of Greece. The anatomy of an orogen", Beiträge der regionalen Geologie der Erde 30. Berlin-Stuttgart. 573 p.

Pe-Piper G. andPiper, D.J.W., 2006, "Unique features of the Cenozoic igneous rocks of Greece", Geol. Soc. Am., Spec. Pap., 409, 259-281.

Perugini D., Poli G., Christofides G., Eleftheriadis G., Koroneos A. and Soldatos T., 2004, "Mantle-derived and crustal melts dichotomy in northern Greece: spatiotemporal and geodynamic implications", Geol. J., 39, 63–80

Sideris G.N. and Papakonstantinou C. N., 1990, "Application of geophysical borehole logging in the Kato Thermes area", Technical Report, I.G.M.E., Athens, 28 p. (in Greek)

Sklavounos S., 1981, "The Paranesti granite (Mineralogy-Petrography)", Ph.D. Thesis, Univ. of Thessaloniki, Greece, 175 p. (in Greek)

Soldatos T., Koroneos A., Christofides G. and Del Moro A., 2001, "Geochronology and origin of the Elatia plutonite (Hellenic Rhodope Massif, N Greece) constrained by new Sr data", N. Jb. Miner. Abh., 176, 179-209

Teneva-Georgieva S.I. and Andreev A., 2005, "The Erma Reka Low-Enthalpy System (S-Bulgaria) - Geothermal Characteristics", Proceedings, World Geothermal Congress 2005, Antalya, Turkey, 24-29 April 2005, 7 p.

Tsirambides A. and Filippidis A, 2012, "Exploration key to growing Greek industry", Industrial Minerals, 44-47.

Turpaud P. and Reischmann T., 2010, "Characterisation of igneous terranes by zircon dating: implications for UHP occurrences and suture identification in the Central Rhodope, northern Greece", Int. J. Earth Sci. 99, 567-591

Vassileva R.D., Bonev I.K., Marchev P. & Atanassova R., 2005, "2-1: Pb-Zn deposits in the Madan ore field, South Bulgaria", In: "Geodynamics and Ore Deposit Evolution in Europe", Eds: D. Blundell, N. Arndt, P.R. Cobbold and C. Heinrich, Box 2-1, 90-91

Vassileva R.D., Atanassova R. and Bonev I.K., 2009, "A review of the morphological varieties of ore bodies in the Madan Pb-Zn deposits, Central Rhodopes, Bulgaria", Geochemistry, Mineralogy and Petrology, 47, 31-49

Vassileva R.D., Atanassova R. and Bonev I.K., 2010, "Morphogenetic types of ore bodies, ore textures and crystallization mechanisms in the hydrothermal Madan deposits, Central Rhdopes", Scientific Annals, Special Volume 99, Proceedings of the XIX CBGA Congress, Thessaloniki, Greece, 355-361

Voudouris P., Spry P.G., Melfos V. and Alfieris D., 2007, "Tellurides and bismuth sulfosalts in gold occurrences of Greece: mineralogical and genetic considerations", Geologian tutkimuskeskus, Opas 53 - Geological Survey of Finland, Guide 53, 85-94

Voudouris P., Spry P.G., Melfos V., Haase K., Reiner K., Mavrogonatos C., Repstock A. and Alfieris D., 2018, "Gold deposits in Greece: Hypogene ore mineralogy as a guide for precious and critical metal exploration", Conference Proceedings Paper, International Electronic Conference on Mineral Science 2018 - IECMS 2018, 13 p., DOI: 10.3390/IECMS2018-05452

Wüthrich E., 2009, "Low temperature thermochronology of the Northern Aegean Rhodope Massif", Unpublished Doctoral thesis, Zürich, Switzerland, ETH Zürich, 216 p.

Annexes

Contact projects@eurogeologists.eu for the full list of Annexes, or open it at the CHPM Information Platform on Prospective Locations (http://bit.ly/CHPMinfoplatform)

Evaluation of CHPM characteristics of prospective CHPM areas

Name of the National Association AGG
Number of the prospective area 1
Northern Lesvos
(Stypsi and Argennos area)

1. **CHPM operational characteristics - Information for CHPM technological elements**
Requested information:

✓ please fill in the table below with the requested data for the CHPM technology elements

Underground heat exchanger (deep metal enrichment + potential geothermal reservoir)	
Extension of the metal enrichments *(volumetric interpretation)*	Stypsi area analyses showed compositions of 2 ppb Au, 120 ppb (0.120 ppm) - up to 0.5 ppm Au, up to 0.10 g/t Au, 5 ppb (0.005 ppm) - up to 1.7 ppm Ag, 111 pm Cu up to1330 ppm Cu, 10 ppm Mo up to 170 ppm Mo (maybe up to 330 ppm Mo according to Kelepertsis and Esson (1987)), 142-160 ppm Pb up to 1020 ppm Pb, 65 ppm Zn up to 815 ppm Zn, 3 ppm Se up to 13 ppm Se, up to 4 ppm Te, 4 ppm Bi up to 36 ppm Bi, up to 23 ppm Sn, 0.009-0.010% Sn, up to 1.92 wt% Re in molybdenite, 0.26-4.74 wt% Fe in sphalerite, up to 8 ppm Sb, up to 1176 ppm Ba, up to 16 ppm As, up to 22 ppm Co, up to 40 ppm Cr, up to 129 ppm Ce, up to 12 ppm Hf, up to 1 ppm Hg, up to 5 ppm Ir, up to 238 ppm Rb, up to 22.2 ppm Sc, up to 1.6 ppm Ta, up to 42.2 ppm Th, up to 12.8 ppm U, up to 17 ppm Cs, up to 3 ppm W, up to 71.4 ppm La, up to 71.4 ppm Nd, up to 128 ppm Mn, up to 5 ppm Be, up to 0.53 wt% Ti, up to 200 ppm V and up to 12 ppm Y. Also contain Re in molybdenites: 300-10600 g/t (average: 2460 g/t). Megala Therma - Argenos area analyses showed compositions of 163 ppb Au, up to 21 ppm Au, 5 ppb (0.005 ppm) Ag, 220-1010 pm Cu, 24 ppm Mo, up to 52 ppm Pb, up to 119 ppm Zn, up to 32 ppm Bi, 0.009-0.010% Sn, up to 3.5 wt% Fe, up to 35.5 ppm Sb, up to 1700 ppm Ba, up to 73 ppm As, up to 11 ppm Co, up to 38 ppm Cr, up to 273 ppm Ce, up to 12 ppm Hf, up to 2 ppm Hg, up to 5 ppm Ir, 70 ppm Rb, up to 28.5 ppm Sc, up to 4 ppm Se, up to 1411 ppm Sr, up to 2 ppm Ta, up to 48.1 ppm Th, up to 8.1 ppm U, up to 3 ppm Cs, up to 2.9 ppm W, up to 140 ppm La, up to 100 ppm Nd, up to 1370 ppm Mn, up to 3 ppm Be, up to 0.73 wt% Ti, up to 163 ppm V and up to 225.9 ppm Y.
Expected type of the reservoir and porosity/permeability *(fractured, porous, etc)*	Depth of the geothermal reservoir is estimated from 150m-1000 m for Stipsi area and 1000 m for Argenos area. Based on the above and the fact that the entire area is fault controlled the type of the reservoir is expected to be fractured.

Mineralization *(type and enriched metals)*	The Stipsi porphyry Sub-alk Cu-Mo mineralization is hosted in dense stockworks containing molybdenite, bismuthinite, and galena, overprinted by intermediate-sulfidation epithermal quartz-carbonate veins and it is enriched in Cu, Mo, Re, Bi, Pb, Se, Ag, Au. Appearance of critical and precious metal mineralogy: Re-rich molybdenite, bismuthinite. (Re in molybdenites: 300-10600 g/t (average: 2460 g/t)). The Megala Therma Pb-Zn-Cu-Ag-Au intermediate-sulfidation epithermal deposit on Lesvos Island, is related to NNE–SSW- and NW–SE-trending quartz veins hosted in 21–18 Ma old andesite-latite lavas (Fig. 3; Kontis et al., 1994). Silicic, propylitic, argillic, and adularia-sericite are the main alteration types. The breccia, veinlets and veins are enriched in Au, Ag, Pb, Zn, Cu and Mo (Kontis et al., 1994). The Megala Therma epithermal system extends further to the south, where similar intermediate-sulfidation quartzcarbonate veins with platy calcite (Fig. 6b) overprint the porphyry Cu-Mo mineralization at Stipsi (Voudouris and Alfieris, 2005).

Production and injection wells	
Depth of potential wells (m)	Recently, PPC has drilled a 1.4km deep exploration well approximately 1.5km NWW of Stipsi, which encountered a maximum temperature of 82 ◦C at well bottom (Michalis Fytikas, personal communication, July 2009). Specifically for the Stypsi geothermal field the geothermal survey carried out by the PPCR-Greece revealed that the exploration well STE-1 at 250m showed temperatures that reached 100°C, the exploration well STE-2 at 400m measured temperatures of 97.8°C and at 1015m reached 91.4°C. The exploration well S-1 at 1400m showed temperature of 83.1°C and it is estimated that at the depth of 2500m temperature will reach 140°C. For the Argenos geothermal field the geothermal survey carried out by the PPCR-Greece revealed that the exploration well GA-350 at 120m showed temperatures that reached 85-87°C and at 140m measured 74°C, the exploration well AR-2140 at 200m reached temperatures of 79-81°C and at 220-230m measured 72°C. The exploration well AR-150 at 100m showed temperature of 65-70°C, at 150m temperature 52.6°C and at 200m temperature of 49.4°C. Based on all the above, depth of the potential wells will be around 1000-2000 m.

Electrolytic metal recovery and gas diffusion electro- precipitation	
Potential target metals to be recovered	We are interested in recovering metals commonly found or mined, metals 'At Risk' (BGS Risk List 2015) and Rare Earth Elements. Apart from the main metal that characterize the deposits like Cu, Ag, Au, Mo, Pb, Zn and As the appearance of Re-rich molybdenite and bismuthinite (Re in molybdenites: 300-10600 g/t (average: 2460 g/t), constitutes Re the main target metal to be recovered. Other potential metals that present great interest to be recovered are Bi, Se, Rb, Ce, Nd, La, V, Y , but further analyses should be made though to determine their content at the geothermal fluids.

Power plant (heat exchanger)	
Local heat and electricity demand *(industrial, municipal, agricultural, etc.)*	As it is shown on the figure from the Hellenic Statistic Agency, the total electric energy consumption of the Lesvos island in 2012 was 334.999.000 kWh. 160.184.000 kwh were consumed for domestic use, 101.006 kWh were consumed for commercial use, 12.733.000 kWh were consumed for industrial use, 12.932.000 kWh were consumed for agricultural use, 38.408.000 kWh for Public and Municipal Authorities use and 9.737.000 kWh were consumed for Street Lightening use. Apparently, the domestic sector dominates the electrical consumption in Lesvos as at the rest of the Greece. According to a survey on energy consumption in households conducted by ELSTAT for the period 2011-2012, 38.4 % of the annual total electricity consumed in a household is used for cooking, 14.7 % for the fridge, 10.6 % for the washing machine, 6.6 % for lighting and 4.9 % for space cooling. Moreover there has been a plan of interconnection of the Cycladic Islands, and specifically Lesvos with Chios island. Therefore, a CHPM plant can fulfil part of energy demands of nearby islands too.

Salt gradient power generation	
Salinity of expected geothermal brine	Waters from thermal springs tested so far showed that most of the samples are of the NaCl type. Only two waters (LES 7 and LES 9), less mineralized and cooler, are of the Ca-HCO_3 type. Chloride and bromide are considered to be conservative ions, even in geothermal environments (see, e.g. Henley and Ellis, 1983). Their behaviour is thus particularly interesting in studies of the origin of salinity. The Br-/Cl- ratio in the samples is homogeneous and very close to that of mean sea water (i.e. ~3.4 10 -3, Herrmann et al., 1973). The

	Na+/CI - ratio in the samples also equals that of sea water, as do the SO]-/CI - ratios of most samples . This suggests that Na +, Br-, CI-, and most SO]- in the springs derive from sea water, which is more (LES 7 and 9) or less (LES 8) diluted by fresh, bicarbonate water, and that supply of these ions by rock leaching is negligible. On the contrary, the Ca 2+, Mg 2+, and K + contents are controlled not only by this dilution process but also by water-rock interactions. Ionic ratios (Br-/CI-, Na+/C1 -, SO42-/C1 -) of the samples taken from thermal springs sited at Argenos-Eftalou, Polichnitos-Lisvori, and near Mytilini, on Lesbos Island, are typical of marine solutions. Stable isotope contents of these waters show that they may result from mixing between meteoric and sea water. Virtually no CI- is supplied by rock leaching. Balance equations based on oxygen-18, deuterium, and CI- contents indicate that marine sources contribute approximately one-third of the water at Argenos area. Megala Therma area is expected to have the same results of salinity since it is located very close to marine area too.
Fresh water supply from the surface *(water sources)*	Precipitation follows the Mediterranean pattern, so it's concentrated from October to March, and it amounts to about 700-750 millimetres per year. In summer it practically never rains as it seems from figure. Other water sources of the area are small rivers, like Tsiknias river. The Monthly average flow graph associated with precipitation, shows high values (20 to 120 m^3 /sec) during winter season (December, January, February and March) and low values (0 to 1 m^3 /sec) during summer season, as it is shown at the monthly flow diagram.

2. **CHPM operational characteristics - Environmental, social and political background**

Requested information:

- ✓ toleration to gaseous and solids emissions, water and noise pollution,
- ✓ local competition to land and water availability
- ✓ public acceptance
- ✓ political support
- ✓ presence of supporting legislation, regulatory framework

Notes: all of above refers to the selected area and its surroundings.

Beyond the technical-economical obstacles, the policy and the legislation, the penetration of RES and energy saving techniques in a society is determined to a great degree by their social acceptance.

The general attitude of residents and local authorities of islands towards RES and energy savings, with regard to small scale applications, is rather positive, without however some reactions, objections, disagreements and skepticism. As far as large scale constructions is concerned like wind turbines for example, one of their main reasons of opposition of residents is the aesthetics, which is subjective, and makes them afraid of loosing their tourism rates. The other causes for objection of societies are owed in their ignorance and lack of briefing and familiarization with RES.

Nevertheless, some local societies and local authorities of islands tend to be more positive towards RES applications. Such societies are those that have been informed adequately, or have been familiarized with geothermal energy, or are not based mainly on the tourism for their growth, therefore are less afraid of any repercussions in this sector. Another important reason for which local societies of islands, but also of mainland, react in the RES investments, is their suspiciousness against private investors. However, a method for changing this negative attitude, is to include the residents of a region or municipality that hosts RES investments as shareholders. From the above, results the necessity of a national strategic approach on public briefing and awareness via the media and the press. Moreover, briefing of local authorities is required in order that these will advance not only in the briefing of citizens, but also in pilot projects and RES installations. Informing of public, dissemination activities and action to the sensitization of local societies are required. This can be strengthened from the interest of private institutions and stakeholders of local market, from the action of not governmental organisations and policy makers and from the informing of local authorities.

With regard to potential large scale RES installations, such as wind parks or geothermic plants the attitude of societies is almost always opposite. Specifically, in the case of small islands the reactions against large scale RES applications are very intense. Inevitably, those create negative attitude and suspiciousness in the local societies, because these societies are immature to accept such large RES penetration, while in certain cases, these projects are excessive and exceed the scale of such small and sensitive islands. The controversial question of size of potential RES applications can be approached with various scientific and effective ways, as is the landscape architecture, combined with study of various likely scenarios of investment.

Current situation:

Specifically in Lesvos island, there was the district heating project “Thermopolis” in Polichnitos (Lesvos Island) which would use geothermal waters of 88°C for the heating of 5 public and municipal buildings.

- A new production well, 150m deep, was drilled in the Polichnitos area in 2008 in order to replace an old well and provides waters at 88oC.
- Unfortunately, the system is still out of operation due to the failure of the submersible pump.

At present, geothermal utilization on Lesvos involves thermal spas and heating of greenhouses, i.e. hot waters of about 4^0C around the Gulf of Geras, of about 60 ^{0}C at Thermie, of 65–80 ◦C at Polichnitos

and Lisvori (south of the Gulf of Kalloni), and of 80–90 ^{0}C at Argenos. Exploration for deeper geothermal resources would require drilling 2–3km deep wells. This indicates that the residents of the island are becoming more familiar with geothermal energy and willing to endorse it to their way of living.

Moreover, PPC holds the exclusive rights to explore, exploit and manage the geothermal potential in the following areas :
(a) Milos - Kimolos - Polyaigos
(b) Nisyros
(c) Lesvos
(d) Methana
PPC intends to produce electricity from the geothermal potential that exists in these areas and aims to find suitable partners who will cooperate with PPC in the company that will develop and manage the Geothermal Power Plants that are going to be installed in the aforementioned areas (of 8MW geothermal power station in Lesvos and of 5MW geothermal power stations in each of the other areas).

In the first phase of the procedure (expression of interest of partnership with PPC), seven companies were present, six of whom qualified for the second phase:

1.Enel Green Power Hellas S.A. (Greece)
2.Helector S.A. (Hellas)
3.Storengy (France)
4.KS Orka Renewables Pte Ltd. (Singapore)
5.Zorlu Enerji Elektrik Uterim A. S. - Turboden S.p.A. (Turkey - Italy)
6.Terna Energy S.A. - Terna Aioliki Xerovouniou S.A. (Hellas)

The objective of PPC is to speed up the selection process of the strategic partner and to sign the cooperation agreement soon.

Based on all the above, Lesvos island has the political support, the local community acceptance and the interest of local and foreign investors that is needed to proceed at exploiting the geothermal field of the area for energy production, part of the operation of the CHPM facility.

Regulatory framework in Greece:
The current geothermal legislation (Law 3175/2003 "Exploitation of geothermic capacity, district heating and other provisions" and relative Ministerial Decrees) classifies the geothermal fields as “high” (T>90°C) or “low” (T<90°C) temperature fields. The geothermal fields are also classified as “proven” or “probable”, depending on their preceding exploration. By the end of 2015, a total number of 32 areas had been officially characterized as “geothermal”, corresponding to more than 40 ‘proven/probable’ and ‘high/low’ temperature geothermal fields. The terms, procedures and regulations for the concession of the geothermal exploration and management rights are determined in the Ministerial Decree “Geothermal Regulations” (Gazette B’ 635/12.05.2005 and 1530/7.11.2005). The procedures for the exploitation of shallow geothermal energy are provided for by the L3175/2003 and the Ministerial Decree published in the Gazette B’ 1249/24.6.2006. The national energy policy in Greece is regulated by the Law 3851/2010 and the National Action Plan 20-20-20.
Licenses for exploration, exploitation and management of a geothermal field (or parts of this, according to article 37 of the Law 3734/2009) are provided by

- the Decentralized Administrations (for low temperature fields) or
- directly from the Ministry of Environment and Energy (for high temperature fields).

"Operating aid" for electricity production from geothermal energy according to the Law 4414/2016:

- The operating aid can be granted as sliding "premium" (sliding "Feed-in-Premium") or Feed-in-Tariff (in a few particular cases) when the geothermal electricity generation becomes competitive and therefore, it is not expected in the near future.
- The operating aid can be granted to power plants in both mainland and non-interconnected islands for a period of 20 years.
- The operating aid is calculated on the basis of a "Reference Value", which is fixed at (without investment aid):

(a) 139 €/MWh for geothermal power plants with an installed capacity of up to 5 MWe.
(b) 108 €/MWh for geothermal power plants with an installed capacity of more than 5 MWe.

Law 4001/2011 ("Operation of Electricity and Gas Energy Markets, for Exploration, Production and Transmission Networks of Hydrocarbons and other provisions") transposes into national legislation EU Directives concerning common rules for the internal market in electricity and common rules for the internal market in gas.

A Ministerial Decree (Government Gazette, Issue 1249/B/24 June 2009) determines the terms, conditions, restrictions, required documentation and licensing procedures for installing the energy systems. Except for this main Ministerial Decree, some other Laws and Ministerial Decrees can be involved, such as:

- Law 3661/2008 on "Measures for the reduction of energy consumption in buildings and other provisions" and Ministerial Decree on "Approval of regulations of energy performance of buildings"
- Presidential Decree 7/2011 (Government Gazette, Issue 14/A)
- Law 4062/2012 on "Promotion of the use of energy from RES"
- Law 4122/2013 on "Energy performance of buildings"

In 2010 Greece endorsed its National Renewable Energy Action Plan (NREAP) aiming to reform the country's energy sector in order to achieve the above mentioned targets. The Law 3851/2010 (Accelerating the development of RES to deal with climate change and other regulations addressing issues under the authority of the Ministry of Environment Energy and Climate Change) establishes a supportive legislative framework to achieve these ambitious goals. Both the NREAP and the L3851/2010 set specific targets regarding the share of RES in final energy consumption, electricity generation and contribution in heating, cooling and transport.

As for the geothermal energy contribution in the electricity sector, the plan of the NREAP includes power production from medium/small scale geothermal plants in the interconnected system and local plants in the non-interconnected islands. For the year 2020 the expected installed capacity from the geothermal power plants is 120 MW.

The Feed-in-Tariffs set by L3851/2010, valid from June 2010 and for 20 years, is €150/MWh for the electricity production from low temperature fluids (T<90°C) and €99.45/MWh for electricity from high temperature fluids. These FITs stand for both mainland and non-interconnected islands. (Arvanitis A,2017, Kolios et al ,2007, Caralis G. et Emmanouilidis G. ,2009)

To conclude, the introduction of complementary and cohesive legal and regulatory system is an essential condition to create a long-term and stable system for CHPM technology development. This geothermal-specific legislative framework, includes all important aspects that need to be covered so as to install a CHPM facility, from indicating the type of geothermal field to defining the state committee responsible for all the licensing procedures. By keeping the transparency and simplifying the licensing procedures for the investors we remove any remaining barriers for the full-scale commercial implementation of the CHPM systems.

3. **Financial aspects**

Requested information:

- ✓ use of economic tools developed in WP5 (more information is going to be provided in September)
- ✓ list of potential local stakeholders (community, political, companies)

In a perfectly competitive environment, prices are assumed to reflect the production costs, while being directed by the overall balance between demand and supply. Therefore, RES electricity producers who are not able to reduce production costs, are vulnerable to free competition. In fact, the progress of the liberalization process is quite dissimilar in each EU country, while energy prices do also greatly differ according to the adopted policies regarding:

Total charges on production costs

Environmental taxes

Subsidies

A key-factor for CHPM development is the availability of the necessary funds. Funding is combined with the transferring of the risk associated with CHPM investments. This is the case with Third Party Financing (TPF) which is widely applied for implementing innovative and/or high capital intensive technologies.

The deterioration of the environmental quality and the growing environmental awareness of the last two decades has generally assisted in the development of RES, which are practically exempt from major environmental burdens. The most important environmental issues connected with RES exploitation are global warming and atmospheric pollution. The development of RES can positively affect environmental quality, which are affected by conventional systems, principally at the local level. Nevertheless, RES are often accused to cause also environmental repercussions, such as noise and visual intrusion, which do not have a detrimental effect on human health or on natural ecosystems, but sometimes cause a negative attitude of public against RES. Environmental effects of RES which should be taken into account in the design and implementation of local plans.

Greek islands possess a high degree of biodiversity at all levels-genetic, species, habitat and landscape. Many of the habitats have been identified as important to nature and are statutorily protected (NATURA 2000 network). Accordingly to the recent ministerial decision, 49828/2008 (ΦΕΚ 2464 Β' / 03.12.08), RES installations are generally prohibited in these areas. The minimum allowed distance of potential RES installations from them is determined at case and depends mainly on the RES technology and the potential installed power.

The overall legislation regarding the operation of the energy sector may directly or indirectly affect the deployment of CHPM technology. Relevant legislative measures can be classified in two broad categories:

Measures enhancing the development of RES. The greatest effect have regulations concerning the encouragement of RES projects and minimization of financial risks through incentives, such as subsidies, tax exemptions, pay-back tariffs and long-term contracts. Furthermore, the establishment targets and programs at the national or regional level related with the development of RES may also considerably motivate market forces.

Measures removing barriers hindering the development of RES Pollution charges or taxes on fossil fuels constitute the opposite side of incentives for RES and have both the same objective. Implementation of RES projects in Greece is usually retarded or hindered due to malfunctions created

by administrative procedures and legal gaps. Among the most crucial obstacless is the very complicated and time consuming process of issuing installation and operation licenses, a simplification of which is necessary. (Caralis G. et Emmanouilidis G. ,2009). The setting of a legislation framework was the first step though, and as it is mentioned above, by keeping the transparency and simplifying the licensing procedures for the investors we remove any remaining barriers for the full-scale commercial implementation of the CHPM systems.
For the moment PPC only is active in the area. In the first phase of the expression of interest of partnership with PPC, seven companies were present, six of whom qualified for the second phase:

1.Enel Green Power Hellas S.A. (Greece)
2.Helector S.A. (Hellas)
3.Storengy (France)
4.KS Orka Renewables Pte Ltd. (Singapore)
5.Zorlu Enerji Elektrik Uterim A. S. - Turboden S.p.A. (Turkey - Italy)
6.Terna Energy S.A. - Terna Aioliki Xerovouniou S.A. (Hellas)

The results of which company will be the partner of PPC in developing and managing the Geothermal Power Plants are not yet available.

List of references

Andritsos N., Arvanitis A., Papachristou M. & Fytikas M. (2011), "Status of Geothermal Energy in Greece – 2011", Presentation, GEOFAR European Conference "Innovative Solutions for Geothermal Energy Financing", Athens, 17 - 18 March 2011

Andritsos N., Dalabakis P., Karydakis G., Kolios N. & Fytikas M. (2011), "Characteristics of low-enthalpy geothermal applications in Greece", Renewable Energy, 36, 1298-1305

Andritsos N., Arvanitis A. Dalabakis P., Karytsas C., Mendrinos D. & Papachristou M. (2013), "Geothermal Energy Use, Country Update for Greece", Proceedings European Geothermal Congress 2013, Pisa, Italy, 3-7 June 2013, Paper Number CUR-14, 10 p.

Andritsos N., Dalambakis P., Arvanitis A., Papachristou M. & Fytikas M. (2015), "Geothermal Developments in Greece - Country update 2010-2014", Proceedings World Geothermal Congress 2015, Melbourne, Australia, 19-25 April 2015, Paper Number 01048, 11 p.

Andritsos N., Arvanitis A., Papachristou M., Fytikas M. & Dalambakis P. (2010), "Geothermal Activities in Greece During 2005- 2009", Proceedings World Geothermal Congress 2010, Bali, Indonesia, 25-29 April 2010, Paper Number 0138, 10 p.

Andritsos N., Dalampakis P. & Kolios N. (2003), "Use of Geothermal Energy for Tomato Drying", GeoHeat Center Quarterly Bul., 24(1), March 2003, 9-13.

Arvanitis A., Geothermal Energy in Greece-Exploration-Fields-Exploitation-Legal Framework EuroWorkshop: Geothermal - The Energy of the Future Fira, Santorini, Greece, 18-19 May 2017

Arvanitis A., Sotiroudis T., Nerantzis E., Fournadzhieva S. & Koultsiakis E. (2004), "Mass culture of the microalga Spirulina using geothermal fluids in Greece - Antioxidant activities of Spirulina powder extracts", Proceedings, International Conference on Geothermal Energy Applications in Agriculture, May 2004, Athens, Greece, 6 p. https://www.scribd.com/document/349817008/Mass-culture-of-the-microalga-Spirulina-using-geothermal-fluids-in-Greece- Antioxidant-activities-of-Spirulina-powder-extracts.

Avarikiotis C. (2012), "Geothermal energy technology and installations of geothermal systems", Presentation, GEO.POWER local forum on geothermal energy and energy efficiency strategies in domestic and industrial sectors, Athens, 16 January 2012 (in Greek), http://www.cres.gr/kape/publications/pdf/Geopower/2.pdf (accessed 16 May 2017)

Benou A. (2008), "Geothermal Heat Pumps - CRES Applications in Greece", Presentation, GROUNREACH Workshop "GroundReach Heating and Cooling with Ground Source Heat Pumps", Athens, 24 January 2008 (in Greek), http://www.cres.gr/kape/publications/pdf/GROUND_REACH/6 ABenou.pdf (accessed 16 May 2017)

Caralis G and Emmanouilidis G, 2009. Executive summary of the work done on Energy planning (Work package 3), IOS_Aegean Energy Agency.

Dalabakis P., Papachristou M., Kolios P., Arvanitis A. & Kolios N. (2015), "Geothermal exploitation in Neo Erasmio (Xanthi)", Proceedings of the 9th Panhellenic Congress of the

Hellenic Society of Agricultural Engineers (Thessaloniki 8-9 October 2015), 711-718 (in Greek), https://www.scribd.com/document/350138510/Αξιοποίηση-γεωθερμικών-ρευστών-στο-Νέο-Εράσμιο-Ξάνθης

Dalabakis P., Ilias A. & Ladas P. (2014), "Use of shallow geothermal energy by means of heat pumps for early growing of asparagus fields under low tunnel", Proceedings, 10th National Conference on Renewable Energy Sources (Thessaloniki 26-28 November 2014), Institute of Solar Technology, Thessaloniki, A, 409-418 (full text in Greek, abstract in English), http://solarinstitute.gr/wp-content/uploads/pdf/IHT 10o Synedrio C Tomos.pdf (accessed 16 May 2017)

Evrytanika News (2016), "The heated sidewalks melt ice in Karpenisi - How geothermal energy works on urban renewal project", evrytanika.gr, 31 January 2016, http://www.evrytanika.gr/index.php?option=com_content&view=article&id=1092971:2016-01-20-19-27-27&catid=43:2011-11- 19-19-46-40&Itemid=124 (accessed 16 May 2017)

Electric energy consumption by great geographic area, region and department and by category of use (Κατανάλωση ηλεκτρικής ενέργειας, κατά μεγάλη γεωγραφική περιοχή, περιφέρεια, νομό και κατά κατηγορία χρήσης),2012, ELSTAT.

Fournadzhieva S., Pilarsky P., Arvanitis A., Fytikas M. & Koultsiakis E. (2002), "Use of Geothermal Fluids for Cultivation of the Microalga Spirulina in Nigrita - Serres", Proceedings, 7th National Conference on the Renewable Energy Sources, Institute of Solar Technology, Patras 6-8 November 2002, University of Patras, Vol. B, 97-104, http://solarinstitute.gr/wp-content/uploads/pdf//IHT 7o Synedrio B Tomos.pdf (accessed 16 May 2017)

Fytikas M., Andritsos N., Dalabakis P. & Kolios N. (2005), "Greek Geothermal Update 2000-2004", Proceedings World Geothermal Congress 2005, Antalya, Turkey, 24-29 April 2005, Paper Number 0172, 8 p.

Fytikas M. & Arvanitis A. (2011), "The Cultivation of Spirulina: An Innovative Geothermal Application in Greece", Presentation, GEOFAR European Conference "Innovative Solutions for Geothermal Energy Financing", Athens, 17 - 18 March 2011, https://www.slideshare.net/ApostolosArvanitis2/the-cultivation-of-spirulina-an-innovative-geothermal-application-in-greece (accessed 16 May 2017)

Fytikas M., Innocenti F., Manetti P., Mazzuoli R., Peccerillo A., Villari L., 1984. Tertiary to Quaternary evolution of volcanism in the Aegean region. Geol. Soc., London, Spec. Publ. 17, 687–699.

Hecht, J., 1971--1974. Geological Map of Lesbos Island (scale 1:50.000). I.G.M.E.

Karagiorgas M., Mendrinos D. & Karytsas C. (2003), "Solar and geothermal heating and cooling of the European Centre for Public Law building in Greece", Renewable Energy, 29, 461–470, http://www.bonair.gr/data/24_1.pdf

Karytsas C. & Choropanitis I. (2013), "Alternative heating and cooling solutions in public buildings using geothermal systems", Presentation, REGEOCITIES, National Validation Workshop, Athens, 22 May 2013 (in Greek), http://regeocities.eu/wp-content/uploads/2013/06/3.C.-KARYTSAS-PRESENTATION-22-05-2013.pdf (accessed 16 May 2017)

Karytsas C. & Choropanitis I. (2013), "Geothermal systems for public buildings and swimming pools", Presentation, GROUND- MED Workshop "Ground Source Heat Pump Systems for Heating and Cooling in a Mediterranean Climate", Athens, 27 November 2013 (in Greek), http://www.cres.gr/kape/publications/pdf/Ground-Med/4. Karytsas C - GSHP studies.pdf (accessed 16 May 2017)

Katsikatsos, G., et al., 1982. Geological Study of Lesbos Island. I.G.M.E. Internal report.

Kelepertsis A.E. and Esson J., 1987. Major- and Trace-Element Mobility in Altered Volcanic Rocks Near Stypsi, Lesbos, Greece and Genesis of a Kaolin Deposit. Applied Clay cience, 2: 11-28.

Kilias S. P., Naden J., Cheliotis I., Shepherd T. J., Constandinidou H., Crossing J. And Simos I., 2001. Epithernal gold minineralisation in the active Aegean Volcanic Arc: the Proitis llias deposit, Milos lsland, Greece. Mineralium Deposita 36: 32-44.

Kolios N., Dalabakis P. & Arvanitis A. (2011), "Agricultural applications in the Neo Erasmio geothermal field (Thrace, Northeastern Greece)", Presentation, GEOFAR European Conference "Innovative Solutions for Geothermal Energy Financing", Athens, 17 - 18 March 2011, https://www.slideshare.net/ApostolosArvanitis2/agricultural-applications-in-the-neo-erasmio-geothermal-field- thrace-northeastern-greece (accessed 16 May 2017)

Kontis E., Kelepertsis A. E. and Skounakis S., 1994. Geochemistry and alteration facies associated with epithermal precious metal mineralization in an active geothermal system, northern Lesbos, Greece. Mineral Deposita 2: 430- 433.

Mavroudis V. (2014), "Practical applications of geothermal energy in buildings in Greece", BSc Thesis, School of Production Engineering and Management, Technical University of Crete, Chania, 123 p. (in Greek), dias.library.tuc.gr/view/manf/22889 (accessed 16 May 2017)

Mendrinos D. & Karytsas C. (2005), "Geothermal Energy, Geothermal Heat Pumps, CRES Experience", Mining & Metallurgical Annals, 15, July - December 2005, 29 p, (in Greek) http://www.cres.gr/kape/pdf/geotherm/22.pdf (accessed 16 May 2017)

Mendrinos D., Karagiorgas M. & Karytsas K., "Use of geothermal heat pumps for heating of buildings in Greece", http://www.lowex.net/guidebook/additional_information/lowexx/3_lowexx_paper_gr.pdf (accessed 16 May 2017)

Mendrinos D. & Karytsas C., "Geothermal heat pumps", EnergyReS, http://library.tee.gr/digital/books_notee/book_60568/book_60568_mendrinos.pdf (accessed 16 May 2017)

Michelot J., Dotsika E. and Fytikas M., 1993. A Hydrochemical and isotopic study of Thermal waters of Lesbos Island (GREECE). Geothermics, Vol. 22, No. 2, pp. 91-99.

Nabih S., 2016. Assessment of the Climate Change Impacts on the hydrologic regime of an insular Mediterranean watershed (Tsiknias river, Greece) with SWAT. Msc. University of Aegean school of Environmental Studies. Department of Marine Sciences.

Oikonomou, P. (1971) Geoelectrical investigations of the Polyhnitos, Lesvos island area.

IGME 1914, 1-12.

Petrakopoulou F., 2015. Energy Statistics and Renewable Energy Potential of Greece. GENESIS-Green Energy for Islands. 2012-IEF-332028. Deliverable II.

Pe-Piper, G., 1980. Geochemistry of Miocene shoshonites, Lesbos, Greece. Contrib. Mineral. Petrol., 72: 387--396.

Pe-Piper, G., 1980b. The Cenozoic volcanic sequence of Lesbos, Greece. S-Dtsch. Geol. Ges., 131: 889--901.

Pe-Piper G. and Piperb D.J.W., 1992. Geochemical variation with time in the Cenozoic high-K volcanic rocks of the island of Lesbos, Greece: significance for shoshonite petrogenesis. Journal of Volcanology and Geothermal Research, 53: 371-387.

Rokos D., Argialas D., Mavrantza R., Seymour K.St., Vamvoukakis C., Kouli M., Lamera S., Paraskevas H., Karfakis I., Denes G., (2000). Structural analysis for gold mineralization using remote sensing and geochemical techniques in a GIS environment: island of Lesvos, Hellas, Nat Res Research 9(4): 277-293.

Savvanis P., "Municipality of Karpenisi: Pavement snow melting and deicing using geothermal energy", https://web.facebook.com/pg/energyautomation/photos/?tab=album&album_id=1692981290916253 (accessed 16 May 2017)

Stylianou G. (2007), "Heating of Traianoupolis Spa facilities (Evros area) with geothermal water", Presentation, Workshop "Development of geothermal applications for heating-cooling and energy saving", Thessaloniki, 11 December 2007 (in Greek)

Simeakis, C. and Someritis, Y. (1982) Etude n6otectonique-mikrotectonique, Etude de fracturation, Etude geologique et perspectives g6othermique de l'fle de Lesvos. IGME.

Taktikos, S. (1985). Temperature distribution on Lesvos island at -250 m from ground surface. (Unpublished map of IGME.)

Terzis K, 2016. Geothermic stations for the production of electric energy applications in island Greece.Bsc.

Thanassoulas, C. (1982). Deep geoelectrical soundings (VES) on Lesvos island. IGME 3562, 1-10.

Thanassoulas C. and Xanthopoulos N., 1991. Location of possibly productive geothermal fracture zones/faults using integrated geophysical methods over lesvos island geothermal field, Greece. Geothermics, Vol. 20, No. 516, pp. 355-368.

Vrachopoulos M., Fytrolakis N., Kyrousis N. & Kravvaritis E. (2005), "Energy saving by exploiting normal geothermal energy at the NTUA Campus, Zografos" , 5o RENES Conf. , Athens, 7 p., http://poseidonenergy.gr/content%5CEMP_anak_22-02-05f.doc (accessed 16 May 2017)

Voudouris P. and Alfieris D., 2005. New porphyry - Cu ± Mo occurrences in the north-eastern Aegean, Greece. Ore mineralogy and epithermal relationships. Chapter 4-31.

Xanthopoulos, N., Karmis, P. and Thanassoulas, C. (1988). Geophysical study of the Argenos geothermal field, northern Lesvos island. IGME E5683, 1-15.

http://www.rae.gr/old/sub3/3B/3b3.htm

ENERGYPRESS(2016),https://energypress.gr/news/xekinise-i-kataskeyi-paragogikis-geothermikis-geotrisis-stin-traianoypoli (accessed 16 May 2017)

e-evros.gr (2016), http://www.e-evros.gr/gr/eidhseis/3/ner http://adesmeuti-thrakis.blogspot.gr/2017/04/blog-post_469.html (accessed 16 May 2017)

http://www.thessnews.gr/article/33498/ependysi-7-ek-eyro-apo-ton-omilo-eythymiadi-gia-thermokipia-me-geothermia-stin- kessani (accessed 16 May 2017)

http://www.agrotika-nea.gr/a/ston-omilo-eythymiadh-h-diaxeirish-toy-gewthermiko/22803764 (accessed 16 May 2017)

ethnos.gr (2016), http://www.ethnos.gr/koinonia/arthro/thermokipia_me_xorigo_ti_fysi-64389658 (accessed 16 May 2017)

Selecta Klemm (2016), "New Production location Selecta Hellas", http://www.selecta-one.com/en/posts/New_Production_location_Selecta_Hellas/latest_news/08203125843/ (accessed 16 May 2017)

Annexes

Contact projects@eurogeologists.eu for the full list of Annexes, or open it at the CHPM Information Platform on Prospective Locations (http://bit.ly/CHPMinfoplatform)

Evaluation of CHPM characteristics of prospective CHPM areas

Name of the National Association AGG
Number of the prospective area 2
Western Milos

1. CHPM operational characteristics - Information for CHPM technological elements
Requested information:
✓ please fill in the table below with the requested data for the CHPM technology elements

Underground heat exchanger (deep metal enrichment + potential geothermal reservoir)	
Extension of the metal enrichments *(volumetric interpretation)*	Epithermal type mineralization rich in Au-Ag-Te occurs at **Profitis Ilias** (reserves: 5 Mt at 4.4 g/t Au, 43g/t Ag, and < 0.5 wt.% Fe and 0.2-1.2 wt.% Fe in sphalerite) and **Chondro Vouno** (reserves: to 2.2 Mt grading 5.14 g/tonne Au (cut-off grade 2.5 g/ tonne) or 3.3 Mt grading 4.2 g/tonne (cut-off grade 2 g/ tonne) or 1.2 Mt at1.0 g/t Au and 124 g/t Ag, and < 0.5 wt.% Fe and 0.2-1.2 wt.% Fe in sphalerite), whereas Pb-Zn-Cu-Ag-Mn-Ba-rich mineralization occurs at in the **Triades-Galana** (reported estimated reserves: 10 Mt with a mean Ag content: 500 g/t, resources: 1.2 Mt at 4.2g/t Au or 1.2 Mt at 1 g/t Au and 124 g/t Ag,) and **Kondaros-Katsimouti-Vani** districts (Fig. 4). (Naden et al., 2005; Alfieris et al., 2013; Papavassiliou et al., 2017, RoyalGold news release; www.royalgold.com/news/990615.htm). Kondaros-Katsimouti-Vani (KKV) ore deposit contains up to 24 mg/kg Mo, up to 439 mg/kg W (Kondaros-Katsimouti), up to 31.8 wt.% Pb, up to 16.5 wt.% Zn, up to 1 mg/kg Bi, up to 247 mg/kg Cd (in Kondaros), up to 769 mg/kg Cd (in Katsimouti), up to 243 mg/kg Sb (in Kondaros), up to 178 mg/kg Sb (in Katsimouti), up to 36 mg/kg As (in Kondaros) and up to 42 mg/kg As (in Katsimouti).Tetrahedrites contain around 24.3-32.05 wt. % Cu, 26.5-28.5 wt.% Sb, up to 16.2 wt.% Ag or up to 23.06 wt.% Ag, 3-5 wt.% Zn, up to 7.5 wt.% Pb and up to 5.39 wt.% Cd. Sphalerites contain around 0.8-2.5 wt.% Fe, up to 0.3 wt.% In. Polybasite samples contain up to 70 wt.% Ag, up to 8.3 wt.% Cu, 10.8 wt.% Sb and < 1.5 wt.% Pb. Vani deposit analyses showed up to 428-630 ppm or up to 2870 mg/kg W, up to 24-27 ppm Mo, up to 69 wt% MnO, up to 6.6 wt% Pb, up to 1.2 wt% Zn, up to 0.8 wt% TiO_2, up to 3679 ppm Sb, up to 3515 ppm As, up to 2873 ppm W, up to 3499 ppm Sr, up to 114 ppm Ag, up to 7.7 ppm Eu, 7.7-91 ppm Ce, 4.5-54.3 ppm La, 5.6-34.5 ppm Y, 1.7-18.6 ppm Nb, 0.8-6.4 ppm Pr, 3.5-26.3 ppm Nd, 0.8-5.7 ppm Sm, 1.3-6.7 ppm Gd, up to 0.8 ppm Tb, up to 5.3 ppm Dy, up to 1.1 ppm Ho, up to 4.1 ppm Er, up to 0.7 ppm Tm, up to 5.3 ppm Yb, up to 0.9 ppm Lu, up to 8.1 ppm Hf, 3.9-13.1 ppm Ta, 1.0-10.4 ppm Th and 1.2-19.0 ppm U.

Expected type of the reservoir and porosity/permeability *(fractured, porous, etc)*	Passive seismic surveys showed that the hydrothermal system extends down to 5 km through a system of active faults and fracture zones. The five deep wells drilled on Milos yield two-phase fluids from a liquid-dominated reservoir encountered in the Neogene sediments (250◦C measured in well MA1 only) and within the fractures of the metamorphic basement (310–325 ◦C measured in all five wells). The **transmissivities** estimated on the basis of pressure drawdown test data are in the **3.2–8.4 darcy-meter** range in wells MA1, MZ1, M1 and M3, and between 0.14 and 2.3 darcy-meter in well M2 (Mendrinos, 1988). Drilling of many shallow and deep wells proved the existence of three main types of groundwater: (a) low-temperature (up to 100 ◦C) shallow water in areas with high-temperature gradient at shallow depths, (b) 100–250 ◦C water within the Neogene sediments at intermediate depth (100–200m for 100◦C, and 400–600m for 250◦C) in areas with adequate sediment thickness (>100 m), and (c) pressurized 300–325◦C brine with total dissolved solids (TDS) of up to 80 g/kg (Table 1) within faults and fracture zones in the basement, at 1–5km depth.
Mineralization *(type and enriched metals)*	The Profitis Ilias epithermal type (Intermediate sulfidation) mineralization is hosted by rhyolites and pyroclastic rocks (rhyolitic lapilli tuffs and ignimbrites) which created an environment suited to veins as well as massive to semi-massive ore bodies mineralization. These ore bodies are enriched in Pb, Zn, Ag, Au, Cu, Sb and Te. Vein widths are up to 3 m across and extend to depths of at least 300 m below the resent-day surface. The Chondro Vouno epithermal (Intermediate sulfidation) deposit, also located in the central-western part of Milos island, is formed mainly in veins in pyroclastic rocks. The veins are enriched in Pb, Zn, Ag, Au, Cu, Sb and Te. The Triades-Galana epithermal type (Intermediatesulfidation) mineralization is located in the northern-western part of the island is related to veins hosted in dacites, andesites, pyroclastic and volcanosedimentary rocks. These veins are enriched in Ag, Au, As, Bi, W and Mo. The Kondaros-Katsimouti epithermal (Intermediate sulfidation) Pb-Zn-Ag deposit located along the NW-trending Kondaros-Katsimouti-Vani fault, NW Milos island, is hosted within propylitically and argillically altered dacites, andesites, pyroclastic and volcanosedimentary rocks which created an environment suited to stratabound and stratiform layers, to veins, as well as massive to semi-massive ore bodies mineralization. All these ore bodies are enriched in Ag, Au, As, Bi, W and Mo. The Kondaros-Katsimouti epithermal Pb-Zn-Ag system evolves at higher elevation into the Vani Ag-Pb mineralization, which occurs proximal to the Vani manganese deposit. This VA deposit is a fossil stratabound hydrothermal Mn deposit, enriched in Ba, Pb, Zn, As, Sb and W. At Vani two types of deposits have been recognized: (a) “high-temperature” hydrothermal Mn deposits and (b) bedded hydrothermal Mn, deposits enriched in Mn, Pb, Zn, Cu, Ba, As Sb, Cd, Tl, Co, W, Mo, Sr, Ag, U, Li, i.e.

Production and injection wells	
Depth of potential wells (m)	For the Western Milos geothermal field borehole data from well in Rivari at 65 m showed temperature of 44°C, from well in Emporios at 70 m showed temperature of 39°C, while in Xylokeratia 1 well at 65m, 2 wells at 70m and 1 well at 75m showed temperatures of 41°C, 40°C, 43°C and 41.5°C respectively. For the Central Milos geothermal field the geothermal survey carried out by the PPCR-Greece revealed that the exploration well MZ-1837 at 1080 m showed temperatures that reached 310-320°C, the exploration well M-21150 at 1200 m showed temperatures that reached 318°C and the exploration well MA at 1827 m showed temperatures that reached 270°C and at 1000m reached 310°C. Based on all the above depth of the potential wells will be around 1000- 1500 m.

Electrolytic metal recovery and gas diffusion electro- precipitation	
Potential target metals to be recovered	We are interested in recovering metals commonly found or mined, metals 'At Risk' (BGS Risk List 2015) and Rare Earth Elements. According to the enrichments of metals that was mentioned above potential target metals to be recovered apart from the Cu, Mo, Pb, Zn, Ag, Au, great interest will present the recovery of Sb, Te, Bi, W, Mo, Se, Ba, Co, Sb, Li etc. Further analyses should be made though to determine their content at the geothermal fluids.

Power plant (heat exchanger)	
Local heat and electricity demand *(industrial, municipal, agricultural, etc.)*	As it is shown on the figure from the Hellenic Statistic Agency, the total electric energy consumption of cycladic islands in 2012 was 585.885.000 kWh. 214.892.000 kwh were consumed for domestic use, 270.221.000 kWh were consumed for commercial use, 54.398.000 kWh were consumed for industrial use, 10.327.000 kWh were consumed for agricultural use, 29.285.000 kWh for Public and Municipal Authorities use and 6.762.000 kWh were consumed for Street Lightening use. At this case we realise the extent of tourism activities on the Cycladic islands as the consumption for commercial use is higher than the consumption for domestic use.

	From PPC collected data of 2001, Milos and connected island Kimolos annual energy demand was 23.912.000 kWh. It is expected (from the total raise of the islands demand) that this annual energy consumption will have risen to 38.187.000 kWh.

Salt gradient power generation	
Salinity of expected geothermal brine	Geothermal drilling carried out during the 70's and 80's by the Greek Public Power Corporation (PPC) demonstrated the presence of a high-enthalpy geothermal field characterized by two-cell circulation (Fitzsimons et al., 1997; Fytikas and Marinelli, 1976; Liakopoulos, 1987; Liakopoulos et al., 1991; Naden et al., 2003, 2005; Pflumio et al., 1991; Wu et al., 2012): (a) a high-temperature (300–325°C), saline reservoir at 1–2 km depth with chlorinity >2.5 times seawater (average 9 wt.% equiv. NaCl) and (b) a low temperature (b248°C), shallow reservoir inferred at 500 m below seafloor (Naden et al., 2005; Wu et al., 2012). Subcritical phase separation (boiling) close to the top of the deep reservoir forms low-Cl vapor-like fluids and residual high-Cl brines. It overlies the high-enthalpy system and it is recharged by meteoric water and seawater intrusion, is commonly saline (up to 5 wt % salts) and heated by gas escapes from the underlying deep reservoir. Seawater, as a major component of both the deep and shallow reservoirs, is documented on the basis of 87Sr/86Sr and δD–δ18O–Cl systematics (Pflumio et al., 1991).
Fresh water supply from the surface *(water sources)*	Precipitation follows the Mediterranean pattern, so it's concentrated from October to March, and it amounts to about 410 millimetres per year. In summer it practically never rains, as it seems from figure. Milos has no forests, no rich vegetation, running waters and rivers, so no other fresh water supplies.

2. **CHPM operational characteristics - Environmental, social and political background**

Requested information:

- ✓ toleration to gaseous and solids emissions, water and noise pollution,
- ✓ local competition to land and water availability
- ✓ public acceptance
- ✓ political support
- ✓ presence of supporting legislation, regulatory framework

Notes: all of above refers to the selected area and its surroundings.

The general attitude of residents and local authorities of islands towards RES and energy savings, with regard to small scale applications, is rather positive, without however some reactions, objections, disagreements and skepticism. With regard to potential large scale RES installations, such as wind parks or geothermic plants the attitude of societies is almost always opposite. Specifically, in the case of small islands the reactions against large scale RES applications are very intense. Inevitably, those create negative attitude and suspiciousness in the local societies, because these societies are immature to accept such large RES penetration, while in certain cases, these projects are excessive and exceed the scale of such small and sensitive islands.

Another important reason for which local societies of islands, but also of mainland, react in the RES investments, is their suspiciousness against private investors. However, a method for changing this negative attitude, is to include the residents of a region or municipality that hosts RES investments as shareholders.

From the above, results the necessity of a national strategic approach on public briefing and awareness via the media and the press. Moreover, briefing of local authorities is required in order that these will advance not only in the briefing of citizens, but also in pilot projects and RES installations. Informing of public, dissemination activities and action to the sensitization of local societies are required. This can be strengthened from the interest of private institutions and stakeholders of local market, from the action of not governmental organisations and policy makers and from the informing of local authorities.

Current situation:

In 1987 a 2MWe pilot plant was commissioned; it delivered 10GWhe in 1988. The plant was retired due to public opposition directed against excess steam venting to the atmosphere, silica in the steam, H2S odour and loud noise. A few years later, following a blow out of well M2, all deep wells on the island were plugged. However, modern technology and improved plant design/operation practices would now allow the elimination of all these environmental impacts.

At present, a few houses and one hotel use shallow, low (45–60 ◦C) temperature ground water for space heating and in a swimming pool. The development of the high-enthalpy geothermal reservoir at Milos for heat (16MWt) and power (16MWe) production would cover the needs of the local population and the mining industry. Further exploitation would require the construction of a submarine cable for transporting electricity to the nearby Cyclades Islands. Development of the reservoir to its full potential (inferred 150MWe) would require a power cable connection to mainland Greece. However, it would present a major environmental challenge due to the flora and fauna protection zones extending over large parts of Milos Island. Apparently PPC is going to take on this challenge. PPC holds the exclusive rights to explore, exploit and manage the geothermal potential in the following areas :

(a) Milos - Kimolos - Polyaigos
(b) Nisyros
(c) Lesvos
(d) Methana

PPC intends to produce electricity from the geothermal potential that exists in these areas and aims to find suitable partners who will cooperate with PPC in the company that will develop and manage the Geothermal Power Plants that are going to be installed in the aforementioned areas (of 8MW geothermal power station in Lesvos and of 5MW geothermal power stations in each of the other areas).

In the first phase of the procedure (expression of interest of partnership with PPC), seven companies were present, six of whom qualified for the second phase:

1.Enel Green Power Hellas S.A. (Greece)
2.Helector S.A. (Hellas)
3.Storengy (France)
4.KS Orka Renewables Pte Ltd. (Singapore)
5.Zorlu Enerji Elektrik Uterim A. S. - Turboden S.p.A. (Turkey - Italy)
6.Terna Energy S.A. - Terna Aioliki Xerovouniou S.A. (Hellas)

The objective of PPC is to speed up the selection process of the strategic partner and to sign the cooperation agreement soon.

Conclusively, Milos island doesn't have local community acceptance especially in large scale projects. The fact that Lesvos island is more positive in geothermal exploitation and that PPC is going to be involved in this large project provides a more optimistic view on winning residents acceptance too.

The regulatory framework in Greece is mentioned in details in Northern Lesvos area.
The implementation of a cohesive legal and regulatory system is an essential condition to create a long-term and stable system for CHPM technology development. The geothermal-specific legislative framework that already exists, includes all important aspects that need to be covered so as to install a CHPM facility, from indicating the type of geothermal field to defining the state committee responsible for all the licensing procedures. By keeping the transparency and simplifying the licensing procedures for the investors we remove any remaining barriers for the full-scale commercial implementation of the CHPM systems.

3. **Financial aspects**

Requested information:

- ✓ use of economic tools developed in WP5 (more information is going to be provided in September)
- ✓ list of potential local stakeholders (community, political, companies)

In a perfectly competitive environment, prices are assumed to reflect the production costs, while being directed by the overall balance between demand and supply. Therefore, RES electricity producers who are not able to reduce production costs, are vulnerable to free competition. In fact, the progress of the liberalization process is quite dissimilar in each EU country, while energy prices do also greatly differ according to the adopted policies regarding:

- Total charges on production costs
- Environmental taxes
- Subsidies

A key-factor for CHPM development is the availability of the necessary funds. Funding is combined with the transferring of the risk associated with CHPM investments. This is the case with Third Party Financing (TPF) which is widely applied for implementing innovative and/or high capital intensive technologies.

The deterioration of the environmental quality and the growing environmental awareness of the last two decades has generally assisted in the development of RES, which are practically exempt from major environmental burdens. The most important environmental issues connected with RES exploitation are global warming and atmospheric pollution. The development of RES can positively affect environmental quality, which are affected by conventional systems, principally at the local level. Nevertheless, RES are often accused to cause also environmental repercussions, such as noise and visual intrusion, which do not have a detrimental effect on human health or on natural ecosystems, but sometimes cause a negative attitude of public against RES. Environmental effects of RES which should be taken into account in the design and implementation of local plans.

Greek islands possess a high degree of biodiversity at all levels-genetic, species, habitat and landscape. Many of the habitats have been identified as important to nature and are statutorily protected (NATURA 2000 network). Accordingly to the recent ministerial decision, 49828/2008 (ΦΕΚ 2464 Β' / 03.12.08), RES installations are generally prohibited in these areas. The minimum allowed distance of potential RES installations from them is determined at case and depends mainly on the RES technology and the potential installed power.

The overall legislation regarding the operation of the energy sector may directly or indirectly affect the deployment of CHPM technology. Relevant legislative measures can be classified in two broad categories:

Measures enhancing the development of RES. The greatest effect have regulations concerning the encouragement of RES projects and minimization of financial risks through incentives, such as subsidies, tax exemptions, pay-back tariffs and long-term contracts. Furthermore, the establishment targets and programs at the national or regional level related with the development of RES may also considerably motivate market forces.

Measures removing barriers hindering the development of RES. Pollution charges or taxes on fossil fuels constitute the opposite side of incentives for RES and have both the same objective.

Implementation of RES projects in Greece is usually retarded or hindered due to malfunctions created

by administrative procedures and legal gaps. Among the most crucial obstacles is the very complicated and time consuming process of issuing installation and operation licenses, a simplification of which is necessary. (Caralis G. et Emmanouilidis G. ,2009). The setting of a legislation framework was the first step though, and as it is mentioned above, by keeping the transparency and simplifying the licensing procedures for the investors, we remove any remaining barriers for the full-scale commercial implementation of the CHPM systems.

Companies already active in the area:
1) IMERYS INDUSTRIAL MINERALS GREECE S.A.
2) LAVA Mining & Quarrying SA
3) ZID CHEMI KE SIA ELLAS EPE
4) PPC. In the first phase of the expression of interest of partnership with PPC, seven companies were present, six of whom qualified for the second phase:

1.Enel Green Power Hellas S.A. (Greece)
2.Helector S.A. (Hellas)
3.Storengy (France)
4.KS Orka Renewables Pte Ltd. (Singapore)
5.Zorlu Enerji Elektrik Uterim A. S. - Turboden S.p.A. (Turkey - Italy)
6.Terna Energy S.A. - Terna Aioliki Xerovouniou S.A. (Hellas)

The selection process of the strategic partner will end soon.

List of references

Alfieris, D. and Voudouris, P., 2005. Ore mineralogy of transitional submarine to subaerial magmatic-hydrothermal deposits in W. Milos, Greece. In: Cook, N.G., Bonev, I., eds., Au-Ag-Te–Se deposits, Geochemistry, Mineralogy and Petrology, 43. Sofia, 1–6.

Alfieris, D., 2006. Geological, geochemical and mineralogical studies of shallow submarine epithermal mineralization in an emergent volcanic edifice, at western Milos island, Greece. PhD thesis, University of Hamburg, Germany, 211 pp.

Alfieris D., Voudouris P. and Spry P.G., 2013. Shallow submarine epithermal Pb–Zn–Cu–Au–Ag–Te mineralization on western Milos Island, Aegean Volcanic Arc, Greece: Mineralogical, geological and geochemical constraints. Ore Geology Reviews 53: 159–180.

Andritsos N., Arvanitis A., Papachristou M. & Fytikas M. (2011), "Status of Geothermal Energy in Greece – 2011", Presentation, GEOFAR European Conference "Innovative Solutions for Geothermal Energy Financing", Athens, 17 - 18 March 2011

Andritsos N., Dalabakis P., Karydakis G., Kolios N. & Fytikas M. (2011), "Characteristics of low-enthalpy geothermal applications in Greece", Renewable Energy, 36, 1298-1305

Andritsos N., Arvanitis A. Dalabakis P., Karytsas C., Mendrinos D. & Papachristou M. (2013), "Geothermal Energy Use, Country Update for Greece", Proceedings European Geothermal Congress 2013, Pisa, Italy, 3-7 June 2013, Paper Number CUR-14, 10 p.

Andritsos N., Dalambakis P., Arvanitis A., Papachristou M. & Fytikas M. (2015), "Geothermal Developments in Greece - Country update 2010-2014", Proceedings World Geothermal Congress 2015, Melbourne, Australia, 19-25 April 2015, Paper Number 01048, 11 p.

Andritsos N., Arvanitis A., Papachristou M., Fytikas M. & Dalambakis P. (2010), "Geothermal Activities in Greece During 2005- 2009", Proceedings World Geothermal Congress 2010, Bali, Indonesia, 25-29 April 2010, Paper Number 0138, 10 p.

Andritsos N., Dalampakis P. & Kolios N. (2003), "Use of Geothermal Energy for Tomato Drying", GeoHeat Center Quarterly Bul., 24(1), March 2003, 9-13.

Arvanitis A., Geothermal Energy in Greece-Exploration-Fields-Exploitation-Legal Framework EuroWorkshop: Geothermal - The Energy of the Future Fira, Santorini, Greece, 18-19 May 2017

Arvanitis A., Sotiroudis T., Nerantzis E., Fournadzhieva S. & Koultsiakis E. (2004), "Mass culture of the microalga Spirulina using geothermal fluids in Greece - Antioxidant activities of Spirulina powder extracts", Proceedings, International Conference on Geothermal Energy Applications in Agriculture, May 2004, Athens, Greece, 6 p. https://www.scribd.com/document/349817008/Mass-culture-of-the-microalga-Spirulina-using-geothermal-fluids-in-Greece- Antioxidant-activities-of-Spirulina-powder-extracts.

Avarikiotis C. (2012), "Geothermal energy technology and installations of geothermal systems", Presentation, GEO.POWER local forum on geothermal energy and energy efficiency strategies in domestic and industrial sectors, Athens, 16 January 2012 (in Greek),

http://www.cres.gr/kape/publications/pdf/Geopower/2.pdf (accessed 16 May 2017)

Andritsos, N.and Karabelas, A.J., 1991. Sulfide scale formation and control: the case of lead sulfide. Geothermics 20, 343–353.

Benou A. (2008), "Geothermal Heat Pumps - CRES Applications in Greece", Presentation, GROUNREACH Workshop "GroundReach Heating and Cooling with Ground Source Heat Pumps", Athens, 24 January 2008 (in Greek), http://www.cres.gr/kape/publications/pdf/GROUND_REACH/6 ABenou.pdf (accessed 16 May 2017)

Canet C., Prol-Ledesma R.-M., Proenza J.A., Rubio-Ramos M.A., Forrest M.J., Torres Vera M.A. and Rodriguez-Diaz A.A., 2005. Mn–Ba–Hg mineralization at shallow submarine hydrothermal vents in Bahia Concepcion, Baja California Sur, Mexico. Chem. Geol. 224, 96–112.

Christanis K. and Seymour K., 1995. A study of scale deposition: an analogue of meso- to epithermal ore formation in the volcano of Milos, Aegean arc, Greece. Geothermics Vol. 24, No. 4, pp. 541-552.

Cronan, D.S. and Varnavas, S.P., 1999. Metalliferous sediments off Milos, Hellenic Volcanic Arc. Explor. Min. Geol. 8, 289–297.

**Dando P.R., Stuben D. and Varnavas S.P., 1999. Hydrothermalism in the Mediterranean Sea.
Proc. Oceanogr. 44, 333–367.**

Dando P.R., Alian, S., Arab H., Bianchi C.N., Brehmer M., Cocito S., Fowler S.W., Gundersen J., Hooper L.E., Kolbl R., Kuever J., Linke P., Makropoulos K.C., Meloni R., Miquel J.C., Morri C., Muller S., Robinson C., Schlesner H., Sievert S., Stohr R., Stuben D., Thomm M., Varnavas S.P. and Ziebis, W., 2000. Hydrothermal studies in the Aegean Sea. Phys. Chem. Earth 25, 1–8.

Dalabakis P., Papachristou M., Kolios P., Arvanitis A. & Kolios N. (2015), "Geothermal exploitation in Neo Erasmio (Xanthi)", Proceedings of the 9th Panhellenic Congress of the Hellenic Society of Agricultural Engineers (Thessaloniki 8-9 October 2015), 711-718 (in Greek), https://www.scribd.com/document/350138510/Αξιοποίηση-γεωθερμικών-ρευστών-στο-Νέο-Εράσμιο-Ξάνθης

Dalabakis P., Ilias A. & Ladas P. (2014), "Use of shallow geothermal energy by means of heat pumps for early growing of asparagus fields under low tunnel", Proceedings, 10th National Conference on Renewable Energy Sources (Thessaloniki 26-28 November 2014), Institute of Solar Technology, Thessaloniki, A, 409-418 (full text in Greek, abstract in English), http://solarinstitute.gr/wp-content/uploads/pdf/IHT 10o Synedrio C Tomos.pdf (accessed 16 May 2017)

Evrytanika News (2016), "The heated sidewalks melt ice in Karpenisi - How geothermal

energy works on urban renewal project", evrytanika.gr, 31 January 2016, http://www.evrytanika.gr/index.php?option=com_content&view=article&id=1092971:2016-01-20-19-27-27&catid=43:2011-11- 19-19-46-40&Itemid=124 (accessed 16 May 2017)

Electric energy consumption by great geographic area, region and department and by category of use (Κατανάλωση ηλεκτρικής ενέργειας, κατά μεγάλη γεωγραφική περιοχή, περιφέρεια, νομό και κατά κατηγορία χρήσης),2012, ELSTAT.

Fitzsimons M.F., Dando P.R., Hughes J.A., Thierman, F., Akoumianaki I., Pratt, S.M. and 1997. Submarine hydrothermal brine seeps offMilos, Greece: observations and geochemistry. Mar. Chem. 57, 325–340.

Fournadzhieva S., Pilarsky P., Arvanitis A., Fytikas M. & Koultsiakis E. (2002), "Use of Geothermal Fluids for Cultivation of the Microalga Spirulina in Nigrita - Serres", Proceedings, 7th National Conference on the Renewable Energy Sources, Institute of Solar Technology, Patras 6-8 November 2002, University of Patras, Vol. B, 97-104, http://solarinstitute.gr/wp-content/uploads/pdf//IHT 7o Synedrio B Tomos.pdf (accessed 16 May 2017)

Fu Wu S., Feng You C., Po Lin Y., Valsami-Jones E and Baltatzis E., 2016. New boron isotopic evidence for sedimentary and magmatic fluid influence in the shallow hydrothermal vent system of Milos Island (Aegean Sea, Greece). Journal of Volcanology and Geothermal Research 310: 58–71.

Fytikas M., Andritsos N., Dalabakis P. & Kolios N. (2005), "Greek Geothermal Update 2000-2004", Proceedings World Geothermal Congress 2005, Antalya, Turkey, 24-29 April 2005, Paper Number 0172, 8 p.

Fytikas M. & Arvanitis A. (2011), "The Cultivation of Spirulina: An Innovative Geothermal Application in Greece", Presentation, GEOFAR European Conference "Innovative Solutions for Geothermal Energy Financing", Athens, 17 - 18 March 2011, https://www.slideshare.net/ApostolosArvanitis2/the-cultivation-of-spirulina-an-innovative-geothermal-application-in-greece (accessed 16 May 2017)

Fytikas M., Giuliani 0., Innocenti F., Marinelli G. and Mazzuoli R., 1976. Geochronological data on recent magmatism of the Aegean Sea. Tectonophysics 31: 29-34.

Fytikas M. And Marinelli G., 1976. Geology and geothermics of the island of Milos (Greece). International Congress on Thermal Waters, Geothermal Energy and Volcanism of the Mediterranean Area. Institute of Geology and Mineral Exploration (58 pp.).

Fytikas M., 1977. Geological and geothermal study of Milos island (in Greek with English abstract). Unpublished report, IGME Athens, Greece, XVII No 1.

Fytikas M., Innocenti F., Manetti P., Mazzuoli R., Peccerillo A. and Villari L., 1984. Tertiary to Quaternary evolution of volcanism in the Aegean region. In: Dixon JE, Robertson AHF (eds) The geological evolution of the eastern Mediterranean. Geol Soc Lond Spec Publ 17:

687-699.

Fytikas M., Innocenti F., Kolios N., Manetti P., Mazzuoli R., Poli G., Rita F. and Villari L., 1986. Volcanology and petrology of volcanic products from the island of Milos and neighbouring islets. J Volcanol Geotherm Res 28: 297-317.

Fytikas M., 1989. Updating of the geological and geothermal re- search on Milos island. Geothermics 18: 485-496.

Fytikas M., Garnish .JD., Hutton V.R.S., Staroste E. and Wohlenberg J., 1989. An integrated model for the geothermal field of Milos from geophysical experiments. Geothermics 18: 611-628

Glasby, G.P., Papavassiliou, C.T., Mitsis, J., Valsami-Jones, E., Liakopoulos, A., Renner, R.M., 2005. The Vani manganese deposit, Milos island, Greece: a fossil stratabound Mn–Ba–Pb–Zn–As–Sb–W-rich hydrothermal deposit. In: Fytikas, M., Vougioukalakis, G.E. (Eds.), The South Aegean Active Volcanic Arc: Present Knowledge and Future Perspectives. Developments in Volcanology, 7. Elsevier, pp. 255–291.

Gelegenis J., Dalabakis P. & Ilias A. (2006), "Heating of wintering ponds by means of low enthalpy geothermal energy. The case of Porto Lagos", Geothermics, 35, 87-103

Kati, M., Valsami-Jones, E., Baltatzis, E. and Magganas, A., 2003. Hydrothermal precipitates from the active submarine vents in Paleochori Bay, Milos Island, Greece. The South Aegean Active Volcanic Arc, International Conference, Milos Island, Greece, Book of Abstracts, p. 71.

Karytsas C. & Choropanitis I. (2013), "Alternative heating and cooling solutions in public buildings using geothermal systems", Presentation, REGEOCITIES, National Validation Workshop, Athens, 22 May 2013 (in Greek), http://regeocities.eu/wp-content/uploads/2013/06/3.C.-KARYTSAS-PRESENTATION-22-05-2013.pdf (accessed 16 May 2017)

Karytsas C. & Choropanitis I. (2013), "Geothermal systems for public buildings and swimming pools", Presentation, GROUND- MED Workshop "Ground Source Heat Pump Systems for Heating and Cooling in a Mediterranean Climate", Athens, 27 November 2013 (in Greek), http://www.cres.gr/kape/publications/pdf/Ground-Med/4. Karytsas C - GSHP studies.pdf (accessed 16 May 2017)

Kilias S. P., Naden J., Cheliotis I., Shepherd T. J., Constandinidou H., Crossing J. and Simos I., 2001. Epithernal gold minineralisation in the active Aegean Volcanic Arc: the Profitis Ilias deposit, Milos Island, Greece. Mineralium Deposita 36: 32-44.

Kolios N., Fytikas M., Arvanitis A.,Andritsos N. and Koutsinos S., 2007. Prospective Medium Enthalpy Geothermal Resources in Sedimentary Basins of Northern Greece, Proceedings European Geothermal Congress 2007 Unterhaching, Germany, 30 May-1 June 2007.

Kolios N., Dalabakis P. & Arvanitis A. (2011), "Agricultural applications in the Neo Erasmio geothermal field (Thrace, Northeastern Greece)", Presentation, GEOFAR European

Conference "Innovative Solutions for Geothermal Energy Financing", Athens, 17 - 18 March 2011, https://www.slideshare.net/ApostolosArvanitis2/agricultural-applications-in-the-neo-erasmio-geothermal-field- thrace-northeastern-greece (accessed 16 May 2017)

Liakopoulos A. and Boulegue J., 1987. A geochemical model for the origin of geothermal fluids and the genesis of mineral deposits on Milos Island. Terra Cognita 7: 228.

Liakopoulos A., Katerinopoulos A., Markopoulos T. and Boulegue J., 1991. A mineralogical petrographic and geochemical study of samples from wells in the geothermal field of milos island (Greece). Jeorhermics. VoL 20. No. 4, pp. 237-256.

Liakopoulos, A., Glasby, G.P., Papavassiliou, C.T. and Boulegue, J., 2001. Nature and origin of the Vani manganese deposit, Milos, Greece: an overview. Ore Geol. Rev. 18, 181–209.

Mavroudis V. (2014), "Practical applications of geothermal energy in buildings in Greece", BSc Thesis, School of Production Engineering and Management, Technical University of Crete, Chania, 123 p. (in Greek), dias.library.tuc.gr/view/manf/22889 (accessed 16 May 2017).

Mendrinos D. and O'Sullivan M., 1987. Modelling of the Milos geothermal field, Proceedings 9th NZ Geothermal Workshop 1987.

Mendrinos D. & Karytsas C. (2005), "Geothermal Energy, Geothermal Heat Pumps, CRES Experience", Mining & Metallurgical Annals, 15, July - December 2005, 29 p, (in Greek) http://www.cres.gr/kape/pdf/geotherm/22.pdf (accessed 16 May 2017)

Mendrinos D., Karagiorgas M. & Karytsas K., "Use of geothermal heat pumps for heating of buildings in Greece", http://www.lowex.net/guidebook/additional_information/lowexx/3_lowexx_paper_gr.pdf (accessed 16 May 2017)

Mendrinos D. & Karytsas C., "Geothermal heat pumps", EnergyReS, http://library.tee.gr/digital/books_notee/book_60568/book_60568_mendrinos.pdf (accessed 16 May 2017)

Naden J., Kilias S. P. and Darbyshire F., 2005. Active geothermal systems with entrained seawater as analogues for low-sulphidation epithermal Mineralization. Geology Manuscript.

Papavasiliou, K., Voudouris, P., Kanellopoulos, C., Alfieris, D. and Xydous, S., 2016. The Kondaros-Katsimouti Intermediate-Sulfidation Epithermal Pb-Zn-Ag-Mn Mineralization, Western Milos, Greece: New Mineralogical and Geochemical Data. Bull. Geol. Soc, Greece in press.

Papavassiliou K., Voudouris P., Kanellopoulos C., Glasby G., Alfieris D. and Mitsis I., 2017. New geochemical and mineralogical constraints on the genesis of the Vani hydrothermal manganese deposit at NW Milos island, Greece: Comparison with the Aspro Gialoudi deposit and implications for the formation of the Milos manganese mineralization. Ore Geology Reviews 80: 594–611.

Petrakopoulou F., 2015. Energy Statistics and Renewable Energy Potential of Greece. GENESIS-Green Energy for Islands. 2012-IEF-332028. Deliverable II.

Pflumio C., Boulegue J., Liakopoulos A. and Brique L., 1991. Oxygen, hydrogen, strontium isotopes and metals in the present-date and past geothermal systems of Milos Island (Aegean arc). In: Pagel, M., Leroy, J.L. (Eds.), Source. Transport and Deposition of Metals. Balkema, Rotterdam, pp. 107–112.
Price R.E., Savov I., Planer-Friedrich B., Bühring S.I., Amend J. And Pichler, T., 2012. Processes influencing extreme As enrichment in shallow-sea hydrothermal fluids of Milos Island, Greece. Chem. Geol. http://dx.doi.org/10.1016/j.chemgeo.2012.06.007.

Pichler T., Giggenbach W.F., McInnes B.I.A. and Duck B., 1999a. Fe–sulfide formation due to seawater–gas–sediment interaction in a shallow-water hydrothermal system, Lihir Island, Papua New Guinea. Econ. Geol. 94, 281–288.

Pichler T., Veizer J. and Hall G.E.M., 1999b. The origin and chemical composition of shallow-water hydrothermal fluids in Tutum Bay, Ambitle Island, Papua New Guinea and their effect on ambient seawater. Mar. Chem. 64, 229–252.

Price R. E., Savov I., Planer-Friedrich B., Bühring S. I., Amend J. and Pichler T., 2013. Processes influencing extreme As enrichment in shallow-sea hydrothermal fluids of Milos Island, Greece. Chemical Geology 348: 15–26.

Savvanis P., "Municipality of Karpenisi: Pavement snow melting and deicing using geothermal energy", https://web.facebook.com/pg/energyautomation/photos/?tab=album&album_id=1692981290916253 (accessed 16 May 2017)

Stewart A. L. and McPhie J., 2006. Facies architecture and Late Pliocene – Pleistocene evolution of a felsic volcanic island, Milos, Greece. Bull Volcanol 68: 703–726 DOI 10.1007/s00445-005-0045-2.

Stylianou G. (2007), "Heating of Traianoupolis Spa facilities (Evros area) with geothermal water", Presentation, Workshop "Development of geothermal applications for heating-cooling and energy saving", Thessaloniki, 11 December 2007 (in Greek)

Stüben D. and Glasby, G.P., 1999. Geochemistry of shallow submarine hydrothermal fluids from Paleohori Bay, Milos, Aegean Sea. Explor. Min. Geol. 8, 273–287.

Terzis K, 2016. Geothermic stations for the production of electric energy applications in island Greece.Bsc.

Tsokas G.N., 1996. Interpretation of the Bouguer anomaly of Milos island (Greece). J Volcanol Geotherm Res 72: 163-181.

Valsami-Jones E., Baltatzis E., Bailey E.H., Boyce A.J., Alexander J.L., Magganas A., Anderson L., Waldron S. and Ragnarsdottir, K.V., 2005. The geochemistry of fluids from an

active shallow submarine hydrothermal system: Milos island, Hellenic Volcanic Arc. J. Volcanol. Geotherm. Res. 148, 130–151.

Vavelidis, M., Melfos, V., 1998. Fluid inclusion evidence for the origin of the barite silver–gold-bearing Pb–Zn mineralization of the Triades area, Milos Island, Greece. Bull. Geol. Soc. Greece 32, 137–144.

Vrachopoulos M., Fytrolakis N., Kyrousis N. & Kravvaritis E. (2005), "Energy saving by exploiting normal geothermal energy at the NTUA Campus, Zografos" , 5o RENES Conf. , Athens, 7 p., http://poseidonenergy.gr/content%5CEMP_anak_22-02-05f.doc (accessed 16 May 2017)

Wu S.F., You C.F., Wang B.S., Valsami-Jones E. and Baltatzis, E., 2011. Two-cells phase separation in shallow submarine hydrothermal system at Milos Island, Greece: Boron isotopic evidence. Geophys. Res. Lett. 38 http://dx.doi.org/10.1029/2011 GL047409.

Wu S.F., You C.F., Valsami-Jones E., Baltatzis E. and Shen M.L., 2012. Br/Cl and I/Cl systematic in the shallow-water hydrothermal system at Milos Island, Hellenic Arc. Mar. Chem. 140–141, 33–43.

Wu S.F., You C.F., Lin Y.P. Valsami-Jones and E., Baltatzis, E., 2016. New boron isotopic evidence for sedimentary and magmatic fluid influence in the shallow hydrothermal vent system of Milos Island (Aegean Sea, Greece). J. Volcanol. Geoth. Res. 310, 58–71.

http://www.rae.gr/old/sub3/3B/3b3.htm

ENERGYPRESS(2016),https://energypress.gr/news/xekinise-i-kataskeyi-paragogikis-geothermikis-geotrisis-stin-traianoypoli (accessed 16 May 2017)

e-evros.gr (2016), http://www.e-evros.gr/gr/eidhseis/3/ner http://adesmeuti-thrakis.blogspot.gr/2017/04/blog-post_469.html (accessed 16 May 2017)

http://www.thessnews.gr/article/33498/ependysi-7-ek-eyro-apo-ton-omilo-eythymiadi-gia-thermokipia-me-geothermia-stin- kessani (accessed 16 May 2017)

http://www.agrotika-nea.gr/a/ston-omilo-eythymiadh-h-diaxeirish-toy-gewthermiko/22803764 (accessed 16 May 2017)

ethnos.gr (2016), http://www.ethnos.gr/koinonia/arthro/thermokipia_me_xorigo_ti_fysi-64389658 (accessed 16 May 2017)

Selecta Klemm (2016), "New Production location Selecta Hellas", http://www.selecta-one.com/en/posts/New_Production_location_Selecta_Hellas/latest_news/08203125843/ (accessed 16 May 2017).

Annexes

Contact projects@eurogeologists.eu for the full list of Annexes, or open it at the CHPM Information Platform on Prospective Locations (http://bit.ly/CHPMinfoplatform)

Evaluation of CHPM characteristics of prospective CHPM areas

Name of the National Association AGG
Number of the prospective area 3
Aristino Alexandroupolis - Evros Delta area

1. **CHPM operational characteristics - Information for CHPM technological elements**
   Requested information:
   ✓ please fill in the table below with the requested data for the CHPM technology elements

Underground heat exchanger (deep metal enrichment + potential geothermal reservoir)	
Extension of the metal enrichments *(volumetric interpretation)*	**Evros Pefka** Evros Pefka past mining operation showed 3 Kt ore at 7% wt. Cu Deposit analyses measured Au 10 ppm, Mo 23.5 ppm, Bi 105 ppm, Te up to 468 ppm, In 675 ppm, Ga up to 17 ppm , Ge up to 16 ppm, Ag >100 ppm , Cu > 1 wt.% and As> 1 wt.%. **Evros Loutros** At Evros Loutros area the mineralized barite veins are enriched in up to ≤ 15.6 g/t Mo, up to 1058 g/t As, up to 31 g/t Ag, and Ag up to 31 ppm.
Expected type of the reservoir and porosity/permeability *(fractured, porous, etc)*	Deep oil exploration boreholes EVROS-1, DELTA-1, DEV-1, DEV-2, and DEV-3 were drilled in the Evros Delta basin. Borehole EVROS-1 of 2658 m was drilled during 1956-57 for defining the Neogene sediments of the area. In order to study the sedimentary sequence another exploration well, DELTA-1, was constructed during 1962-63 at depth of 3548 m. Oil exploration boreholes DEV-1, DEV-2 and DEV-3 were drilled in the Evros Delta basin during 1981-1982. Borehole DEV-1 has a depth of 4229 m. The stratigraphic column of this well is: 0-650 m Plio-Quaternary deposits (alternations of sands, clays and sandstones), 650-1153 m Miocene sediments (clays, siltstones, sandstones, dolomites with layers of lignites), 1153-3270 m Oligocene - Eocene formations (limestones, alternations of marls, sandstones and siltstones, tuffs, polygenic conglomerates, polygenic and volcanic breccias) and 3270-4229 m basement (quartzitic, dioritic porphyres) (S.P.E.G., 1982a,b; Lalechos, 1986). The temperatures of 68, 96, 136 and 146oC were measured at 1600, 2740, 3975 and 4229 m respectively (S.P.E.G., 1982a,b). The stratigraphy of borehole DEV-2 drilled to a total depth of 3213 m was: 0-600 m Plio-Quaternary deposits (sandstones, clays, gravels), 600-1650 m Miocene sediments (alternations of clays, clayey-sandstones and conglomerates with layers of lignite), 1650-2980 m, Oligocene formations (alternations of clays, sandstones, conglomerates and siltstones), 2980-3148 m Eocene formations (alternations of limestones, conglomerates, siltstones and marls) and 3148-

	3213 m Substratum (diabases). The temperatures of 81, 90 and 100oC were registered at 2000, 2500 and 3000 m correspondingly. Exploration oil borehole DEV-3 has a depth of 2860 m. The temperatures of 62.7, 104 and 108°C (Horner corrected) were recorded at depths of 1520, 2650 and 2860 m respectively. The values of geothermal gradient were calculated to be 2.9°C/100 m for depth <1500 m, 2.8°C/100 m at 1520 m, 3.2°C/100 m at 2620 m and 3.1°C/100 m at 2860 m. In this borehole for the upper 1000 m the **porosity** of the interesting horizons was found to vary **between 17 and 31%** (P.P.C., 1988). North of the Evros River Delta, exploration wells ARDANION-1 (ARD-1) and BOUGIONOU-1 (BOUG-1) were drilled during 1955-56 and 1961 at depths of 2323 and 1745 m correspondingly. In ARD-1 the temperature of 98°C was measured at 2322 m (S.P.E.G., 1982b).
Mineralization *(type and enriched metals)*	**Evros Pefka** The Evros Pefka epithermal, high and intermediate sulfidation Cu-Ag-Au-Te deposit is enriched in metals: Cu, Au, Ag, Pb, Zn, Bi, Sn, Ge, Ga, In, Mo, V, As, Hg, Te, Se. Apart from the main metal that characterize the deposits like Cu-Ag-Au-Te, of high importance is the mineralogy of the deposit like tetradymite, hessite, stützite, altaite, native Te, native Au, coloradoite, sylvanite, goldfieldite. **Evros Loutros** The Evros Loutros epithermal, intermediate sulfidation deposit is enriched in metals: Fe, Pb, As, Ag.

Production and injection wells	
Depth of potential wells (m)	**Evros Pefka** Exploration and production wells from 120m to 440 m showed temperatures of 60-89°C, as below: Exploration well AA-1: 360m 72.3°C Production well AA-1P: 216m 51.8°C Exploration well AA-3: 340m 86.8°C Production well AA-3P: 360m 89°C Exploration well AA-4: 370m 60.1°C Production well AA-4P: 440m 64°C Well KO-1: 120m 79°C Well E-3 : 235m 89°C

	Evros Delta Exploration and production wells from 2650m to 4229 m showed temperatures of 100-146°C. Exploration well DEV-1: 3975m → 136°C 4229m → 146° Exploration well DEV-2: 3000m → 100°C Exploration well DEV-3: 2650m → 104°C 2860m → 108°C The water temperature of geothermal field of Aristino is about 30-900°C and the depth of reservoir is about 150 – 450m. Based on all the above the depth of potential wells should be relative to the exact area we will refer to. Especially when we are locating near to the Delta of Evros river, depth can reach over 3000m.

Electrolytic metal recovery and gas diffusion electro- precipitation	
Potential target metals to be recovered	We are interested in recovering metals commonly found or mined, metals 'At Risk' (BGS Risk List 2015) and Rare Earth Elements. According to the enrichments of metals that was mentioned above potential target metals to be recovered apart from the Cu, Au, Ag, Pb, Zn, great interest will present the recovery of Zn, Bi, Sn, Ge, Ga, In, Mo, V, As, Hg, Te, Se. Further analyses should be made though to determine their content at the geothermal fluids.

Power plant (heat exchanger)	
Local heat and electricity demand *(industrial, municipal, agricultural, etc.)*	As it is shown on the figure from the Hellenic Statistic Agency, the total electric energy consumption of Evros area in 2012 was 518.528.000 kWh. 199.360.000 kwh were consumed for domestic use, 133.417.000 kWh were consumed for commercial use, 81.535.000 kWh were consumed for industrial use, 39.722.000 kWh were consumed for agricultural use, 53.889.000 kWh for Public and Municipal Authorities use and 10.605.000 kWh were consumed for Street Lightening use. Apparently, the domestic sector dominates the electrical consumption in Evros areas as at the rest of the Greece. According to a survey on energy consumption in households conducted by ELSTAT for the period 2011-2012, 38.4 % of the annual total electricity consumed in a household is used for cooking, 14.7 % for the fridge, 10.6 % for the washing machine, 6.6 % for lighting and 4.9 % for space cooling.

Salt gradient power generation	
Salinity of expected geothermal brine	The geothermal waters in the Aristino field are of the Na-Cl type in chemical composition. Their TDS values range from 4.3 to 10.5 g/l and their Ca2+ and SO_4 2- content are relatively high. The thermal waters from the springs of Traianoupolis belong to the same type.
Fresh water supply from the surface *(water sources)*	Precipitation of the Alexandroupolis area is concentrated from October to April, and it amounts to about 577 millimetres per year and of Evros area is about 508 millimetres per year. Other water sources is from Evros River that crosses the area. It has a total length of 528 km, 310 km of which belong to Bulgaria and the remaining 218 km comprise the boundary between Greece and Turkey. The area of Evros catchment is 53,000 km^2 . The minimum flow of the river is estimated to be about 8 m^3 /s, while the average flow ranges between 50 and 100 m^3 /s (National Park of Evros Delta Management Authority 2010; Konstantinou et al. 2006; Hellenic Ministry of Development 2006). The maximum flow is observed between March and May and the minimum between July and September. Evros Delta, one of the most important wetland on a national and European level, covers an area of 9,500 ha (8,000 ha of land and 1,500 ha of water) and is included in the list of wetlands designated as internationally important under the Ramsar Convention (1971), due to the numerous species hosted.

2. CHPM operational characteristics - Environmental, social and political background

Requested information:

- ✓ toleration to gaseous and solids emissions, water and noise pollution,
- ✓ local competition to land and water availability
- ✓ public acceptance
- ✓ political support
- ✓ presence of supporting legislation, regulatory framework

Notes: all of above refers to the selected area and its surroundings.

Beyond the technical-economical obstacles, the policy and the legislation, the penetration of RES and energy saving techniques in a society is determined to a great degree by their social acceptance.

The general attitude of residents and local authorities of islands towards RES and energy savings, with regard to small scale applications, is rather positive, without however some reactions, objections, disagreements and skepticism. As far as large scale constructions is concerned like wind turbines for example, one of their main reasons of opposition of residents is the aesthetics, which is subjective, and makes them afraid of loosing their tourism rates. The other causes for objection of societies are owed in their ignorance and lack of briefing and familiarization with RES.

Another important reason for which local societies react in the RES investments, is their suspiciousness against private investors. However, a method for changing this negative attitude, is to include the residents of a region or municipality that hosts RES investments as shareholders.

From the above, results the necessity of a national strategic approach on public briefing and awareness via the media and the press. Moreover, briefing of local authorities is required in order that these will advance not only in the briefing of citizens, but also in pilot projects and RES installations. Informing of public, dissemination activities and action to the sensitization of local societies are required. This can be strengthened from the interest of private institutions and stakeholders of local market, from the action of not governmental organisations and policy makers and from the informing of local authorities.

In case of Alexandroupolis-Evros area all these were turned from ideas into action. Especially the political support was the the key factor that led everything to the current significant result.

Current Situation:

In March 2011, international open tenders took place for the leasing of the right to explore the geothermal potential of four promising areas: Evros River Delta (1,307 km²) in Thrace and in Nestos River Delta(803km²) in Eastern Macedonia.

The interest was focused on probable medium enthalpy geothermal resources suitable for binary cycle power generation. A consortium of two Greek private companies (Terna Energy S.A. and ITA Group S.A.) awarded all the tenders. Unfortunately, the lease contracts were never signed, the consortium withdrew from the exploration projects and the tenders have been officially declared void.

Today, Alexandroupolis is the first European municipality that will be crossed by the Trans Adriatic Pipeline (TAP), which has been selected as a PCI for its role in opening up the Southern Gas Corridor, one of 12 so-called energy corridors identified by the EU as priorities for the achievement of European energy policy objectives. Moreover, the developed and updated SEAP for Alexandroupolis includes plans for the promotion of RES and energy savings some of which are listed below:

- Two autonomous PV stations of 5kWp and one of 12,5kWp and two heat pumps (180kW and 200kW) installed in public buildings. Two (2) solar thermal systems of 40m2 (selective collectors) for DHW production and two (2) geothermal heat pumps of 100kW each in public buildings. Monitoring equipment will also be installed to measure the hourly electric and thermal consumption (EEA-Grants (Iceland, Liechtenstein, Norway) ~0.75 m€

- Plan for DH geothermal network: ALEX has a long-term (30 years) lease for the exploitation and development of the low-enthalpy geothermal field of Aristino-Traianoupoli area (~90 oC, 9.8 MWt) and aims to build a geothermal DHN, which constitutes the keystone of its SEAP. The DH network will supply heat to public buildings, greenhouse cultivations, breeding farms, municipal -pellet production plant etc.(~4.5 m€). Basic design data, according to the study: power of 10MWth, 18km pipelines, two (2) drillings of 500m depth, 450.000 m3 volume flow rate of geothermal fluids in the primary network (20.000 ha) and 500.000 m3 in the secondary network (30.000 ha). The exploitation of the Aristino geothermal field, with a total budget of 6,262,868.17 €, is included as a new action in the Eastern Macedonia and Thrace Operational Programme (OP) 2014-2020.
Alexandroupolis was awarded this September in NIngbo, China from Euro-China Green & Smart City Awards comitee for the activities at the field of RES.

Apart from this great importance project, in Traianoupoli (Alexandroupoli area) there is a heating of a 1,300-m^2 spa building using geothermal water at 52°C. Also in Alexandroupolis already public buildings, school building and senior citizens health centers benefit from geothermal energy for their free heating and cooling.

Apparently of great importance, it is not only informing the local residents about the general consequences that new investments will have at the area, but also the benefits they will have from welcoming geothermal energy in their everyday life.

Based on all the above, geothermal exploitation in this target CHPM area has both public acceptance and political support too.

The regulatory framework in Greece is mentioned in details in Northern Lesvos area.
The introduction of complementary and cohesive legal and regulatory system is an essential condition to create a long-term and stable system for CHPM technology development. This geothermal-specific legislative framework, includes all important aspects that need to be covered so as to install a CHPM facility, from indicating the type of geothermal field to defining the state committee responsible for all the licensing procedures. By keeping the transparency and simplifying the licensing procedures for the investors we remove any remaining barriers for the full-scale commercial implementation of the CHPM systems.

3. **Financial aspects**

Requested information:

- ✓ use of economic tools developed in WP5 (more information is going to be provided in September)
- ✓ list of potential local stakeholders (community, political, companies)

In a perfectly competitive environment, prices are assumed to reflect the production costs, while being directed by the overall balance between demand and supply. Therefore, RES electricity producers who are not able to reduce production costs, are vulnerable to free competition. In fact, the progress of the liberalization process is quite dissimilar in each EU country, while energy prices do also greatly differ according to the adopted policies regarding:

- Total charges on production costs
- Environmental taxes
- Subsidies

A key-factor for CHPM development is the availability of the necessary funds. Funding is combined with the transferring of the risk associated with CHPM investments. This is the case with Third Party Financing (TPF) which is widely applied for implementing innovative and/or high capital intensive technologies.

The deterioration of the environmental quality and the growing environmental awareness of the last two decades has generally assisted in the development of RES, which are practically exempt from major environmental burdens. The most important environmental issues connected with RES exploitation are global warming and atmospheric pollution. The development of RES can positively affect environmental quality, which are affected by conventional systems, principally at the local level. Nevertheless, RES are often accused to cause also environmental repercussions, such as noise and visual intrusion, which do not have a detrimental effect on human health or on natural ecosystems, but sometimes cause a negative attitude of public against RES. Environmental effects of RES which should be taken into account in the design and implementation of local plans.

Greek islands and mainland possess a high degree of biodiversity at all levels-genetic, species, habitat and landscape. Many of the habitats have been identified as important to nature and are statutorily protected (NATURA 2000 network). Accordingly to the recent ministerial decision, 49828/2008 (ΦΕΚ 2464 B' / 03.12.08), RES installations are generally prohibited in these areas. The minimum allowed distance of potential RES installations from them is determined at case and depends mainly on the RES technology and the potential installed power.

The overall legislation regarding the operation of the energy sector may directly or indirectly affect the deployment of CHPM technology. Relevant legislative measures can be classified in two broad categories:

Measures enhancing the development of RES. The greatest effect have regulations concerning the encouragement of RES projects and minimization of financial risks through incentives, such as subsidies, tax exemptions, pay-back tariffs and long-term contracts. Furthermore, the establishment targets and programs at the national or regional level related with the development of RES may also considerably motivate market forces.

Measures removing barriers hindering the development of RES. Pollution charges or taxes on fossil fuels constitute the opposite side of incentives for RES and have both the same objective.

Implementation of RES projects in Greece is usually retarded or hindered due to malfunctions created by administrative procedures and legal gaps. Among the most crucial obstacles is the very complicated and time consuming process of issuing installation and operation licenses, a simplification of which is

necessary. (Caralis G. et Emmanouilidis G. ,2009). The setting of a legislation framework was the first step though, and as it is mentioned above, by keeping the transparency and simplifying the licensing procedures for the investors, we remove any remaining barriers for the full-scale commercial implementation of the CHPM systems.

Companies already active in the area:
1) Selecta Hellas as the result of the unification of the German company “Selecta one” and the Greek companies “Agrohoum S.A.” and “Agroflora S.A”. (Eratino - Chrysoupoli Area)
2) AGRITEX Energy S.A. (Nea Kessani Area)
3) Thrace Greenhouses which is member of Thrace Group Co S.A. (Neo Erasmio, Xanthi)

List of references

Andritsos N., Arvanitis A., Papachristou M. & Fytikas M. (2011), "Status of Geothermal Energy in Greece – 2011", Presentation, GEOFAR European Conference "Innovative Solutions for Geothermal Energy Financing", Athens, 17 - 18 March 2011

Andritsos N., Dalabakis P., Karydakis G., Kolios N. & Fytikas M. (2011), "Characteristics of low-enthalpy geothermal applications in Greece", Renewable Energy, 36, 1298-1305

Andritsos N., Arvanitis A. Dalabakis P., Karytsas C., Mendrinos D. & Papachristou M. (2013), "Geothermal Energy Use, Country Update for Greece", Proceedings European Geothermal Congress 2013, Pisa, Italy, 3-7 June 2013, Paper Number CUR-14, 10 p.

Andritsos N., Dalambakis P., Arvanitis A., Papachristou M. & Fytikas M. (2015), "Geothermal Developments in Greece - Country update 2010-2014", Proceedings World Geothermal Congress 2015, Melbourne, Australia, 19-25 April 2015, Paper Number 01048, 11 p.

Andritsos N., Arvanitis A., Papachristou M., Fytikas M. & Dalambakis P. (2010), "Geothermal Activities in Greece During 2005- 2009", Proceedings World Geothermal Congress 2010, Bali, Indonesia, 25-29 April 2010, Paper Number 0138, 10 p.

Andritsos N., Dalampakis P. & Kolios N. (2003), "Use of Geothermal Energy for Tomato Drying", GeoHeat Center Quarterly Bul., 24(1), March 2003, 9-13.

Arvanitis A., Geothermal Energy in Greece-Exploration-Fields-Exploitation-Legal Framework EuroWorkshop: Geothermal - The Energy of the Future Fira, Santorini, Greece, 18-19 May 2017

Arvanitis A., Sotiroudis T., Nerantzis E., Fournadzhieva S. & Koultsiakis E. (2004), "Mass culture of the microalga Spirulina using geothermal fluids in Greece - Antioxidant activities of Spirulina powder extracts", Proceedings, International Conference on Geothermal Energy Applications in Agriculture, May 2004, Athens, Greece, 6 p. https://www.scribd.com/document/349817008/Mass-culture-of-the-microalga-Spirulina-using-geothermal-fluids-in-Greece- Antioxidant-activities-of-Spirulina-powder-extracts.

Avarikiotis C. (2012), "Geothermal energy technology and installations of geothermal systems", Presentation, GEO.POWER local forum on geothermal energy and energy efficiency strategies in domestic and industrial sectors, Athens, 16 January 2012 (in Greek), http://www.cres.gr/kape/publications/pdf/Geopower/2.pdf (accessed 16 May 2017)

Benou A. (2008), "Geothermal Heat Pumps - CRES Applications in Greece", Presentation, GROUNREACH Workshop "GroundReach Heating and Cooling with Ground Source Heat Pumps", Athens, 24 January 2008 (in Greek), http://www.cres.gr/kape/publications/pdf/GROUND_REACH/6 ABenou.pdf (accessed 16 May 2017)

Caralis G and Emmanouilidis G, 2009. Executive summary of the work done on Energy planning (Work package 3), IOS_Aegean Energy Agency.

Christofides G., Pecskay Z., Eleftheriadis G., Soldatos T., Koroneos A., 2004. The

Tertiary Evros Volcanic Rocks (Thrace, Northeastern Greece): Petrology and K/Ar Geochronology, *Geologica CArpathica, 55, 5, Bratislava, p. 397-409*

Dalabakis P., Papachristou M., Kolios P., Arvanitis A. & Kolios N. (2015), "Geothermal exploitation in Neo Erasmio (Xanthi)", Proceedings of the 9th Panhellenic Congress of the Hellenic Society of Agricultural Engineers (Thessaloniki 8-9 October 2015), 711-718 (in Greek), https://www.scribd.com/document/350138510/Αξιοποίηση-γεωθερμικών-ρευστών-στο-Νέο-Εράσμιο-Ξάνθης

Dalabakis P., Ilias A. & Ladas P. (2014), "Use of shallow geothermal energy by means of heat pumps for early growing of asparagus fields under low tunnel", Proceedings, 10th National Conference on Renewable Energy Sources (Thessaloniki 26-28 November 2014), Institute of Solar Technology, Thessaloniki, A, 409-418 (full text in Greek, abstract in English), http://solarinstitute.gr/wp-content/uploads/pdf/IHT 10o Synedrio C Tomos.pdf (accessed 16 May 2017)

Evrytanika News (2016), "The heated sidewalks melt ice in Karpenisi - How geothermal energy works on urban renewal project", evrytanika.gr, 31 January 2016, http://www.evrytanika.gr/index.php?option=com_content&view=article&id=1092971:2016-01-20-19-27-27&catid=43:2011-11- 19-19-46-40&Itemid=124 (accessed 16 May 2017)

Electric energy consumption by great geographic area, region and department and by category of use (Κατανάλωση ηλεκτρικής ενέργειας, κατά μεγάλη γεωγραφική περιοχή, περιφέρεια, νομό και κατά κατηγορία χρήσης),2012, ELSTAT.

Fournadzhieva S., Pilarsky P., Arvanitis A., Fytikas M. & Koultsiakis E. (2002), "Use of Geothermal Fluids for Cultivation of the Microalga Spirulina in Nigrita - Serres", Proceedings, 7th National Conference on the Renewable Energy Sources, Institute of Solar Technology, Patras 6-8 November 2002, University of Patras, Vol. B, 97-104, http://solarinstitute.gr/wp-content/uploads/pdf//IHT 7o Synedrio B Tomos.pdf (accessed 16 May 2017)

Fytikas M., Andritsos N., Dalabakis P. & Kolios N. (2005), "Greek Geothermal Update 2000-2004", Proceedings World Geothermal Congress 2005, Antalya, Turkey, 24-29 April 2005, Paper Number 0172, 8 p.

Fytikas M. & Arvanitis A. (2011), "The Cultivation of Spirulina: An Innovative Geothermal Application in Greece", Presentation, GEOFAR European Conference "Innovative Solutions for Geothermal Energy Financing", Athens, 17 - 18 March 2011, https://www.slideshare.net/ApostolosArvanitis2/the-cultivation-of-spirulina-an-innovative-geothermal-application-in-greece (accessed 16 May 2017)

Gelegenis J., Dalabakis P. & Ilias A. (2006), "Heating of wintering ponds by means of low enthalpy geothermal energy. The case of Porto Lagos", Geothermics, 35, 87-103

Karagiorgas M., Mendrinos D. & Karytsas C. (2003), "Solar and geothermal heating and cooling of the European Centre for Public Law building in Greece", Renewable Energy, 29, 461–470, http://www.bonair.gr/data/24_1.pdf

Karytsas C. & Choropanitis I. (2013), "Alternative heating and cooling solutions in public buildings using geothermal systems", Presentation, REGEOCITIES, National

Validation Workshop, Athens, 22 May 2013 (in Greek), http://regeocities.eu/wp-content/uploads/2013/06/3.C.-KARYTSAS-PRESENTATION-22-05-2013.pdf (accessed 16 May 2017)

Karytsas C. & Choropanitis I. (2013), "Geothermal systems for public buildings and swimming pools", Presentation, GROUND- MED Workshop "Ground Source Heat Pump Systems for Heating and Cooling in a Mediterranean Climate", Athens, 27 November 2013 (in Greek), http://www.cres.gr/kape/publications/pdf/Ground-Med/4. Karytsas C - GSHP studies.pdf (accessed 16 May 2017)

Kolios N., Dalabakis P. & Arvanitis A. (2011), "Agricultural applications in the Neo Erasmio geothermal field (Thrace, Northeastern Greece)", Presentation, GEOFAR European Conference "Innovative Solutions for Geothermal Energy Financing", Athens, 17 - 18 March 2011, https://www.slideshare.net/ApostolosArvanitis2/agricultural-applications-in-the-neo-erasmio-geothermal-field- thrace-northeastern-greece (accessed 16 May 2017)

Kolios N., Koutsinos S., Arvanitis A., Karydakis G., 2005. Geothermal situation in Northeastern Greece. *Proceedings World Geothermal Congress*

Kolios N., Fytikas M., Arvanitis A., Andritsos N., Koutsinos S., 2007. Prospective Medium Enthalpy Geothermal Resources in Sedimentary Basins of Northern Greece*, Proceedings European Geothermal Congress*

Mavroudis V. (2014), "Practical applications of geothermal energy in buildings in Greece", BSc Thesis, School of Production Engineering and Management, Technical University of Crete, Chania, 123 p. (in Greek), dias.library.tuc.gr/view/manf/22889 (accessed 16 May 2017)

Mendrinos D. & Karytsas C. (2005), "Geothermal Energy, Geothermal Heat Pumps, CRES Experience", Mining & Metallurgical Annals, 15, July - December 2005, 29 p, (in Greek) http://www.cres.gr/kape/pdf/geotherm/22.pdf (accessed 16 May 2017)

Mendrinos D., Karagiorgas M. & Karytsas K., "Use of geothermal heat pumps for heating of buildings in Greece", http://www.lowex.net/guidebook/additional_information/lowexx/3_lowexx_paper_gr.pdf (accessed 16 May 2017)

Mendrinos D. & Karytsas C., "Geothermal heat pumps", EnergyReS, http://library.tee.gr/digital/books_notee/book_60568/book_60568_mendrinos.pdf (accessed 16 May 2017)

Melfos V., Voudouris P., 2017. Cenozoic metallogeny of Greece and potential for precious, critical and rare metals exploration, *Ore Geology Reviews 89, p.1030-1057*

Mendrinos D., Choropanitis I., Polyzou O., Karytsas C., 2010. Exploring for geothermal resources in Greece, *Geothermics 39, p. 124-137*

Repstock A., Voudouris P., Zeug M., Melfos V., Zhai M., Li H., Kartal T., Matuszczak J., 2016. Chemical composition and varieties of fahlore-group minerals from Oligocene mineralization in the Rhodope area, Southern Bulgaria and Northern Greece.

Savvanis P., "Municipality of Karpenisi: Pavement snow melting and deicing using

geothermal energy", https://web.facebook.com/pg/energyautomation/photos/?tab=album&album_id=1692981290916253 (accessed 16 May 2017)

Stylianou G. (2007), "Heating of Traianoupolis Spa facilities (Evros area) with geothermal water", Presentation, Workshop "Development of geothermal applications for heating-cooling and energy saving", Thessaloniki, 11 December 2007 (in Greek)

Vrachopoulos M., Fytrolakis N., Kyrousis N. & Kravvaritis E. (2005), "Energy saving by exploiting normal geothermal energy at the NTUA Campus, Zografos", 5o RENES Conf. , Athens, 7 p., http://poseidonenergy.gr/content%5CEMP_anak_22-02-05f.doc (accessed 16 May 2017)

http://www.rae.gr/old/sub3/3B/3b3.htm

ENERGYPRESS(2016),https://energypress.gr/news/xekinise-i-kataskeyi-paragogikis-geothermikis-geotrisis-stin-traianoypoli (accessed 16 May 2017)

e-evros.gr (2016), http://www.e-evros.gr/gr/eidhseis/3/ner http://adesmeuti-thrakis.blogspot.gr/2017/04/blog-post_469.html (accessed 16 May 2017)

http://www.thessnews.gr/article/33498/ependysi-7-ek-eyro-apo-ton-omilo-eythymiadi-gia-thermokipia-me-geothermia-stin- kessani (accessed 16 May 2017)

http://www.agrotika-nea.gr/a/ston-omilo-eythymiadh-h-diaxeirish-toy-gewthermiko/22803764 (accessed 16 May 2017)

ethnos.gr (2016), http://www.ethnos.gr/koinonia/arthro/thermokipia_me_xorigo_ti_fysi-64389658 (accessed 16 May 2017)

Selecta Klemm (2016), "New Production location Selecta Hellas", http://www.selecta-one.com/en/posts/New_Production_location_Selecta_Hellas/latest_news/08203125843/ (accessed 16 May 2017)

Annexes

Contact projects@eurogeologists.eu for the full list of Annexes, or open it at the CHPM Information Platform on Prospective Locations (http://bit.ly/CHPMinfoplatform)

Evaluation of CHPM characteristics of prospective CHPM areas

Name of the National Association AGG
Number of the prospective area 4
Sappes

1. **CHPM operational characteristics - Information for CHPM technological elements**
   Requested information:
   ✓ please fill in the table below with the requested data for the CHPM technology elements

Underground heat exchanger (deep metal enrichment + potential geothermal reservoir)	
Extension of the metal enrichments *(volumetric interpretation)*	**Maronia** Maronia area deposit analyses showed compositions of Re: 0.12-4.21 wt.% in molybdenite (2.88 wt.% Re), and around 1200-28800 g/t (average: 7600 g/t) Re in molybdenites. Surface samples tested measured up to 7600 ppm Mo, up to 5460 ppm Cu and up to 1 ppm Au. Bulk ore analyses from porphyry-style ore showed average grade of 0.1 g/t Au, up to 2763 g/t Cu and up to 3909 g/t Mo. Drilling yielded a 10 m intercept grading of 12 ppm Au, of 17 ppm Ag and 2wt% Cu. In propylitic alteration REE analyses reached up to 133-221 ppm. **Petrota Graben/ Perama hill** Petrota Graben/ Perama hill area with underground reserves 9.697 Mt showed up to 3.13 g/t Au and 4 g/t Ag, with a total of 0.975 Moz Au and 1.151 Moz Ag. Specifically Se content reaches up to 15.9 wt.% in bismuthinite and up to 1.9 wt.% in tetradymite, while in sylvanite Au measured is about 25.7-34.8 wt.% and Ag measured is about 5.4-13.7 wt.%. The native Au is characterised by mean composition of 98.99 wt.% Au. Te measured reaches up to 45 ppm. The upper oxidized part of Perama Hill deposit is free of As, Pb or other heavy metals. **Petrota Graben/ Mavrokoryfi** Petrota Graben/Mavrokoryfi deposit analyses showed up to 1.5 wt.% Pb, while surface grab samples analyses showed up to1.5 ppm Au and up to 162 ppm Ag. **Sappes-kassiteres-Kirki-Esimi/Pagoni Rachi** The Sappes-kassiteres-Kirki-Esimi/Pagoni Rachi Re-enriched molybdenite mineralization analyses showed 379-46900 g/t (average: 16318 g/t) Re in molybdenites. Surface samples tested measured up to up to 5.1 ppm (g/t) Au (average: 0.57 g/t Au), up to 0.5 wt.% Cu or1 wt.% Cu, up to 40 ppm Te, up to 2000 ppm (2000 g/t) Mo, up to 20 ppm (20 g/t)Re(up to 4.69 wt.% Rein molybdenite), up to 0.03 ppd Pd and up to 6 wt.% Mo in rheniite.

The Pagoni Rachi prospect is also highly anomalous in Au.

Sappes-kassiteres-Kirki-Esimi/Konos hill

The Sappes-kassiteres-Kirki-Esimi/Konos hill Re-enriched molybdenite mineralization analyses showed 750-31100 g/t (average: 15621 g/t) Re in molybdenites and up to 6 wt.% Mo in rheniite. Also Au detected at 0.04 g/t.

Sappes-kassiteres-Kirki-Esimi/Kassiteres - Koryfes

Sappes-kassiteres-Kirki-Esimi/Kassiteres – Koryfes area surface samples analyses showed up to 700 ppm Cu and up to 0.5 ppm Au, while high-grade veins contain up to 0.43 wt% Cu, 0.7 wt% Pb, 1.23 wt% Zn and 190 ppm Mo.

The highest Ag-content (up to 9.6 wt% Ag) occurs in Sb-rich members of tetrahedrite-group minerals.

Sappes-kassiteres-Kirki-Esimi/Myli

The Sappes-kassiteres-Kirki-Esimi/Myli hill Re-enriched molybdenite mineralization analyses showed 440-19200 g/t (average: 2733 g/t) Re in molybdenites and Au at 0.09 g/t. Also grade samples analysed showed up to up to 2100 g/t Cu, up to 210 g/t Mo, up to 0.2 g/t Au.

Sappes-kassiteres-Kirki-Esimi/Viper

The Sappes-kassiteres-Kirki-Esimi/Viper high-grade gold-sulfide zone (Au-Cu-Ag deposit) has reserves of 1.2 million tons at 18.4 g/t Au and resources of 0.28 Mt at 19.5 g/t Au, 9 g/t Ag, and 0.4% Cu.

Deposit's measured resources of 710 kt at 22.2 g/t Au, 11.5 g/t Ag, 0.4% Cu and inferred resources of 1109 kt at 17.2 g/t Au, at 8.8 g/t Ag and at 0.3% Cu.

Deposit's cut-off grades of 4 g/t Au, while native Au detected at 200-250m depth (53.3 g/t Au in 40m drill core) may contain up to 9 wt.% Ag.

Sappes-kassiteres-Kirki-Esimi/Scarp

Sappes-kassiteres-Kirki-Esimi/Scarp area resources are 0.87 Mt at 2.2 g/t Au, and 1.5 g/t Ag.
Deposit's cut-off grades of 1 g/t Au.

Sappes-kassiteres-Kirki-Esimi/St Demetrios

Sappes-kassiteres-Kirki-Esimi/St Demetrios area has reserves of 0.21 Mt at 3.5 g/t Au, and 5.2 g/t Ag.

Also it has reserves of 260000 t at 3.5 g/t Au, and deposit's cut-off grades of 1 g/t Au.

Au content is 2 g/t Au at surface (oxidized mineralization), and grades up to 22 g/t Au at depth (pyrite-chalcopyrite-enargite mineralization)

The native Au is characterised by mean composition of 97.98 wt.% Au and contain up to 0.4-1.6 wt% Ag.

Sappes-kassiteres-Kirki-Esimi/St Barbara

	Three (3) stages are recognized in the vein-type mineralization at St Barbara. Oxidized alunitic breccia rock samples (stage I) contains Pb up to 950 ppm, Bi up to 640 ppm, Au 800 ppb, Te up to 13 ppm, Se up to 12 ppm. Stage II material analyses showed 11 g/t Au. Oxidized hydrothermal breccia (stage II) matrix material contains up to 370 ppm Cu, 820 ppm As, 72 ppm Mo, 23 ppm Se, 2 ppm Te, 7 ppm Ag, 2 ppm Au. Stage II material analyses showed at pyrite: up to 0.23 wt.% As and <0.07 wt.% Au , at tetrahedrite-group minerals:< 0.7 wt.% Ag, at altaite:1.2 wt.% Se, and 0.1 wt.% Ag, at hessite: 61.2-63.6 wt.% Ag and up to 0.3 wt% Au, at sylvanite:12 wt.% Ag. Stage III material (quartz veins) analyses showed at pyrite up to 0.85 wt% As. Bulk rock sample analyses measured up to 0.4 ppm Au and 21 ppm Ag. **<u>Sappes-kassiteres-Kirki-Esimi/St Philippos</u>** Past mining in St Philippos area produced 0.2 Mt at 7.5 % Pb and Zn (4-10% Pb+Zn). Also concentrates at 60-70% Pb, 3-7% Cu, 500 g/t Au, 48-54% Zn, 0.4-0.5% Cd were produced. In wurtzite & sphalerite In measured up to 3.5 wt.%, Ga up to 1.6 wt.% and Ge up to 0.3 wt.%. **<u>Sappes/ Xylagani</u>** Xylagani area analyses showed Fe 18.94 wt.%, Cu:2.0 wt.%, Zn 367 ppm, Pb 458 ppm, and Au 3.5 ppm (0.1-6.4 ppm).
Expected type of the reservoir and porosity/permeability *(fractured, porous, etc)*	In some places the sedimentary column is up to 3.5km thick; it is made up (from top to bottom) of Upper Plio-Pleistocene sands, clays, gravels and micro-conglomerates; Miocene clays, marls and siltstones; and Eocene-Oligocene sediments. In this basin the Rhodope Massif metamorphic basement consists of gneisses, mica-schists, amphibolites and marbles. Deep oil exploration well (KOM-1; Table 2) was drilled in the central part of the Xanthi-Komotini basin in 1977. Temperatures of 60 ◦C at 1300m and 72 ◦C at 1736 m depth were measured, indicating the possibility of finding intermediate-temperature geothermal fluids in that area (Karytsas, 1990). The reservoir is located mainly at the Tertiary volcanics interbedded in the sediments.
Mineralization *(type and enriched metals)*	**<u>Maronia</u>** The Maronia porphyry Cu-Mo-Re-Au type mineralization is hosted in skarns and it is enriched in metals: Cu, Fe, Mo, Au, Pb, Zn, Sb, As. Apart from the main metal that characterize the deposits like Cu, Au, Mo high importance is the appearance of Re-rich molybdenite and bismuthinite. Also andradites are sometimes Ti-rich and Ti-Cr-Zr-rich. **<u>Petrota Graben/ Perama hill</u>** The Petrota Graben/Perama hill Au-Ag-Te-Se epithermal type - High and Intermediate sulfidation mineralization is enriched in metals: Au, Ag, Cu, Bi, Pb,

Te, Se.
Apart from the main metal that characterize the deposits like Cu, As, Au, Bi of high importance is the Critical and precious metal mineralogy of the deposit like bismuthinite, heyrovskyite, gustavite-lillianite solid solution, hessite, petzite, sylvanite, krennerite, calaverite, coloradoite, native Te, melonite.

Petrota Graben/ Mavrokoryfi

The Petrota Graben/Mavrokoryfi Cu-Ag-Au-Te epithermal type - High sulfidation mineralization is enriched in metals: Ag, Au, Cu, Te.
Apart from the main metal that characterize the deposits like Cu, Sb, Ag, Au is enriched in Te.

Sappes-kassiteres-Kirki-Esimi/Pagoni Rachi

The Sappes-kassiteres-Kirki-Esimi/Pagoni Rachi porphyry type mineralization – epithermal system mineralization is enriched in metals: Cu, Mo, Fe, Re.
Apart from the main metal that characterize the deposits like Cu, Au, Mo of high importance is the critical and precious metal mineralogy of the deposit like bornite, Re-rich molybdenite, native Au, rheniite, tetradymite, hessite, petzite, stützite, altaite, aikinite, Ag-Au, hammarite, berryite, lindströmite, gustavite-lillianite solid solution, Se-Bi sulfosalts, wittichenite.

Sappes-kassiteres-Kirki-Esimi/Konos hill

The Sappes-kassiteres-Kirki-Esimi/Konos hill porphyry type mineralization – epithermal mineralization is enriched in metals: Cu, Mo, Fe, Re.
Apart from the main metal that characterize the deposits like Cu, Au, Mo, it is enriched in Te and Re. Of high importance is the critical and precious metal mineralogy of the deposit like Re-rich molybdenite and rheniite.

Sappes-kassiteres-Kirki-Esimi/Kassiteres - Koryfes

The Sappes-kassiteres-Kirki-Esimi/Kassiteres – Koryfes porphyry type - epithermal mineralization is enriched in metals: Cu, Au, Mo, Pb, Zn, Ag, Bi, Te.
Apart from the main metal that characterize the deposits like Cu, Au, Mo, of high importance is the critical and precious metal mineralogy of the deposit like tetradymite.

Sappes-kassiteres-Kirki-Esimi/Myli

The Sappes-kassiteres-Kirki-Esimi/Myli telescoped porphyry – epithermal system mineralization is enriched in metals: Cu, Mo, Au, Re, Pb, Zn, Ag, As.
Apart from the main metal that characterize the deposits like Cu, Au, Mo, of high importance is the critical and precious metal mineralogy of the deposit like Re-rich molybdenite and native Au.

Sappes-kassiteres-Kirki-Esimi/Viper

The Sappes-kassiteres-Kirki-Esimi/Viper High and intermediate sulfidation epithermal type mineralization is enriched in metals: Cu, Au, As, Sb, Ag, Pb, Zn, Bi, Te, Se. The economic mineralization is at depth of 200-240m, ~60m thick, and has dimensions 550*1310 m.

Sappes-kassiteres-Kirki-Esimi/Scarp

The Sappes-kassiteres-Kirki-Esimi/Scarp epithermal type - High sulfidation mineralization is enriched in metals: Cu, Au.

	Sappes-kassiteres-Kirki-Esimi/St Demetrios The Sappes-kassiteres-Kirki-Esimi/St Demetrios epithermal type - High and intermediate sulfidation mineralization is enriched in metals: Cu, Au, As, Sb, Ag, Pb, Zn, Bi, Te, Se. Apart from the main metal that characterize the deposits like Cu, As, Au, Ag, it is enriched in critical metals like Te. Of high importance is the critical and precious metal mineralogy of the deposit like Calaverite, sylvanite, hessite, stützite, altaite, native Au, goldfieldite. **Sappes-kassiteres-Kirki-Esimi/St Barbara** The Sappes-kassiteres-Kirki-Esimi/St Barbara epithermal type - High and intermediate sulfidation mineralization is enriched in metals: Cu, Au, As, Sb, Ag, Pb, Zn, Bi, Te, Se. Apart from the main metal that characterize the deposits like Cu, Au, Ag, it is enriched in critical metals like Te. Of high importance is the critical and precious metal mineralogy of the deposit like bornite, hessite, petzite, sylvanite, altaite, native Te, native Au. **Sappes-kassiteres-Kirki-Esimi/St Philippos** The Sappes-kassiteres-Kirki-Esimi/St Philippos epithermal type - High and intermediate sulfidation mineralization is enriched in metals: Pb, Zn, Ag, As, Cu, Bi, Sn, Cd, In, Ga, Ge, Au. Apart from the main metal that characterize the deposits like Cu, Au, Ag, it is enriched in critical metals like In, Ga, Ge. Of high importance is the critical and precious metal mineralogy of the deposit like bismuthinite, hessite, altaite, tellurobismuthite. **Sappes/ Xylagani** type: VMS (Cyprus- and Kuroko-type) Enriched metals: Cu, Fe, Au The Sappes/ Xylagani VMS (Cyprus- and Kuroko-type) type mineralization is enriched in metals: Cu, Fe, Au.

Production and injection wells	
Depth of potential wells (m)	**Sappes** Exploration well at 440 m showed temperature of 40.6^{o}C and production well at 440 m showed temperature of 38.9^{o}C. The depth of potential exploration wells is estimated at 1000m, but further investigation is needed.

Electrolytic metal recovery and gas diffusion electro- precipitation	
Potential target metals to be recovered	According to the enrichments of metals that was mentioned above potential target metals to be recovered apart from the Cu, Au, Mo, As, Sb, Ag, Pb, Zn, great interest will present the recovery of Bi, Se, Te, Re, In, Ga, Ge. Further analyses should be made though to determine their content at the geothermal fluids.

Power plant (heat exchanger)	
Local heat and electricity demand *(industrial, municipal, agricultural, etc.)*	As it is shown on the figure from the Hellenic Statistic Agency, the total electric energy consumption of Rodopi regional area, where Sappes belong to, in 2012 was 545.735.000 kWh. 136.135.000 kwh were consumed for domestic use, 96.131.000 kWh were consumed for commercial use, 135.089.000 kWh were consumed for industrial use, 60.417.000 kWh were consumed for agricultural use, 22.707.000 kWh for Public and Municipal Authorities use and 4.257.000 kWh were consumed for Street Lightening use. Apparently, the domestic sector dominates the electrical consumption in Rodopi area as at the rest of the Greece. According to a survey on energy consumption in households conducted by ELSTAT for the period 2011-2012, 38.4 % of the annual total electricity consumed in a household is used for cooking, 14.7 % for the fridge, 10.6 % for the washing machine, 6.6 % for lighting and 4.9 % for space cooling.

Salt gradient power generation	
Salinity of expected geothermal brine	Reservoir depth at Sappes is around 400 m with water total flow 500t/h. Temperature measured was about 40 ^{o}C. Geothermal water at Sappers are HCO3 type, with TDS 2kg/kg.
Fresh water supply from the surface *(water sources)*	Precipitation of the Xanthi area amounts to about 573 millimetres per year. As it seems from the figure, it rains even in summer period. Next to the potential CHPM area only one major river is close, Fyliris river. In the potential CHPM area, next to the Sapes village there are Saporema and Skylorema small rivers, coming from Fyliris river. Rivers water flow depends on precipitation.

2. CHPM operational characteristics - Environmental, social and political background

Requested information:

- ✓ toleration to gaseous and solids emissions, water and noise pollution,
- ✓ local competition to land and water availability
- ✓ public acceptance
- ✓ political support
- ✓ presence of supporting legislation, regulatory framework

Notes: all of above refers to the selected area and its surroundings.

The general attitude of residents and local authorities of islands towards RES and energy savings, with regard to small scale applications, is rather positive, without however some reactions, objections, disagreements and skepticism. With regard to potential large scale RES installations, such as wind parks or geothermic plants the attitude of societies is almost always opposite. Inevitably, those create negative attitude and suspiciousness in the local societies, because these societies are immature to accept such large RES penetration. The controversial question of size of potential RES applications can be approached with various scientific and effective ways, as is the landscape architecture, combined with study of various likely scenarios of investment.

Another important reason for which local societies of islands, but also of mainland, react in the RES investments, is their suspiciousness against private investors. However, a method for changing this negative attitude, is to include the residents of a region or municipality that hosts RES investments as shareholders.

From the above, results the necessity of a national strategic approach on public briefing and awareness via the media and the press. Moreover, briefing of local authorities is required in order that these will advance not only in the briefing of citizens, but also in pilot projects and RES installations. Informing of public, dissemination activities and action to the sensitization of local societies are required. This can be strengthened from the interest of private institutions and stakeholders of local market, from the action of not governmental organisations and policy makers and from the informing of local authorities.

Current situation:

In Sappes there are no recorded implementations of geothermal energy. However, it is located in Northern Greece where there has been a great step in August 2017, when the governor of the Region of Eastern Macedonia and Thrace decided that the exploitation of the Aristino geothermal field, with a total budget of 6,262,868.17 €, is included as a new action in the Eastern Macedonia and Thrace Operational Programme (OP) 2014-2020. Conclusively, relative actions should be dealt positively in Sappes area too.

The regulatory framework in Greece is mentioned in details in Northern Lesvos area.

The implementation of a cohesive legal and regulatory system is an essential condition to create a long-term and stable system for CHPM technology development. The geothermal-specific legislative framework that already exists, includes all important aspects that need to be covered so as to install a CHPM facility, from indicating the type of geothermal field to defining the state committee responsible for all the licensing procedures. By keeping the transparency and simplifying the licensing procedures for the investors we remove any remaining barriers for the full-scale commercial implementation of the CHPM systems.

3. **Financial aspects**

Requested information:

- ✓ use of economic tools developed in WP5 (more information is going to be provided in September)
- ✓ list of potential local stakeholders (community, political, companies)

In a perfectly competitive environment, prices are assumed to reflect the production costs, while being directed by the overall balance between demand and supply. Therefore, RES electricity producers who are not able to reduce production costs, are vulnerable to free competition. In fact, the progress of the liberalization process is quite dissimilar in each EU country, while energy prices do also greatly differ according to the adopted policies regarding:

- Total charges on production costs
- Environmental taxes
- Subsidies

A key-factor for CHPM development is the availability of the necessary funds. Funding is combined with the transferring of the risk associated with CHPM investments. This is the case with Third Party Financing (TPF) which is widely applied for implementing innovative and/or high capital intensive technologies.

The deterioration of the environmental quality and the growing environmental awareness of the last two decades has generally assisted in the development of RES, which are practically exempt from major environmental burdens. The most important environmental issues connected with RES exploitation are global warming and atmospheric pollution. The development of RES can positively affect environmental quality, which are affected by conventional systems, principally at the local level. Nevertheless, RES are often accused to cause also environmental repercussions, such as noise and visual intrusion, which do not have a detrimental effect on human health or on natural ecosystems, but sometimes cause a negative attitude of public against RES. Environmental effects of RES which should be taken into account in the design and implementation of local plans.

Greek islands and mainland possess a high degree of biodiversity at all levels-genetic, species, habitat and landscape. Many of the habitats have been identified as important to nature and are statutorily protected (NATURA 2000 network). Accordingly to the recent ministerial decision, 49828/2008 (ΦΕΚ 2464 B' / 03.12.08), RES installations are generally prohibited in these areas. The minimum allowed distance of potential RES installations from them is determined at case and depends mainly on the RES technology and the potential installed power.

The overall legislation regarding the operation of the energy sector may directly or indirectly affect the deployment of CHPM technology. Relevant legislative measures can be classified in two broad categories:

Measures enhancing the development of RES. The greatest effect have regulations concerning the encouragement of RES projects and minimization of financial risks through incentives, such as subsidies, tax exemptions, pay-back tariffs and long-term contracts. Furthermore, the establishment targets and programs at the national or regional level related with the development of RES may also considerably motivate market forces.

Measures removing barriers hindering the development of RES. Pollution charges or taxes on fossil fuels constitute the opposite side of incentives for RES and have both the same objective.

Implementation of RES projects in Greece is usually retarded or hindered due to malfunctions created by administrative procedures and legal gaps. Among the most crucial obstacles is the very complicated and time consuming process of issuing installation and operation licenses, a simplification of which is

necessary**. (Caralis G. et Emmanouilidis G. ,2009).** The setting of a legislation framework was the first step though, and as it is mentioned above, by keeping the transparency and simplifying the licensing procedures for the investors, we remove any remaining barriers for the full-scale commercial implementation of the CHPM systems.

List of references

Andritsos N., Arvanitis A., Papachristou M. & Fytikas M. (2011), "Status of Geothermal Energy in Greece – 2011", Presentation, GEOFAR European Conference "Innovative Solutions for Geothermal Energy Financing", Athens, 17 - 18 March 2011

Andritsos N., Dalabakis P., Karydakis G., Kolios N. & Fytikas M. (2011), "Characteristics of low-enthalpy geothermal applications in Greece", Renewable Energy, 36, 1298-1305

Andritsos N., Arvanitis A. Dalabakis P., Karytsas C., Mendrinos D. & Papachristou M. (2013), "Geothermal Energy Use, Country Update for Greece", Proceedings European Geothermal Congress 2013, Pisa, Italy, 3-7 June 2013, Paper Number CUR-14, 10 p.

Andritsos N., Dalambakis P., Arvanitis A., Papachristou M. & Fytikas M. (2015), "Geothermal Developments in Greece - Country update 2010-2014", Proceedings World Geothermal Congress 2015, Melbourne, Australia, 19-25 April 2015, Paper Number 01048, 11 p.

Andritsos N., Arvanitis A., Papachristou M., Fytikas M. & Dalambakis P. (2010), "Geothermal Activities in Greece During 2005- 2009", Proceedings World Geothermal Congress 2010, Bali, Indonesia, 25-29 April 2010, Paper Number 0138, 10 p.

Andritsos N., Dalampakis P. & Kolios N. (2003), "Use of Geothermal Energy for Tomato Drying", GeoHeat Center Quarterly Bul., 24(1), March 2003, 9-13.

Arvanitis A., Geothermal Energy in Greece-Exploration-Fields-Exploitation-Legal Framework EuroWorkshop: Geothermal - The Energy of the Future Fira, Santorini, Greece, 18-19 May 2017

Arvanitis A., Sotiroudis T., Nerantzis E., Fournadzhieva S. & Koultsiakis E. (2004), "Mass culture of the microalga Spirulina using geothermal fluids in Greece - Antioxidant activities of Spirulina powder extracts", Proceedings, International Conference on Geothermal Energy Applications in Agriculture, May 2004, Athens, Greece, 6 p. https://www.scribd.com/document/349817008/Mass-culture-of-the-microalga-Spirulina-using-geothermal-fluids-in-Greece- Antioxidant-activities-of-Spirulina-powder-extracts.

Avarikiotis C. (2012), "Geothermal energy technology and installations of geothermal systems", Presentation, GEO.POWER local forum on geothermal energy and energy efficiency strategies in domestic and industrial sectors, Athens, 16 January 2012 (in Greek), http://www.cres.gr/kape/publications/pdf/Geopower/2.pdf (accessed 16 May 2017)

Benou A. (2008), "Geothermal Heat Pumps - CRES Applications in Greece", Presentation, GROUNREACH Workshop "GroundReach Heating and Cooling with

Ground Source Heat Pumps", Athens, 24 January 2008 (in Greek), http://www.cres.gr/kape/publications/pdf/GROUND_REACH/6 ABenou.pdf (accessed 16 May 2017)

Caralis G and Emmanouilidis G, 2009. Executive summary of the work done on Energy planning (Work package 3), IOS_Aegean Energy Agency.

Christofides G., Pecskay Z., Eleftheriadis G., Soldatos T., Koroneos A., 2004. The Tertiary Evros Volcanic Rocks (Thrace, Northeastern Greece): Petrology and K/Ar Geochronology, Geologica CArpathica, 55, 5, Bratislava, p. 397-409

Dalabakis P., Papachristou M., Kolios P., Arvanitis A. & Kolios N. (2015), "Geothermal exploitation in Neo Erasmio (Xanthi)", Proceedings of the 9th Panhellenic Congress of the Hellenic Society of Agricultural Engineers (Thessaloniki 8-9 October 2015), 711-718 (in Greek), https://www.scribd.com/document/350138510/Αξιοποίηση-γεωθερμικών-ρευστών-στο-Νέο-Εράσμιο-Ξάνθης

Dalabakis P., Ilias A. & Ladas P. (2014), "Use of shallow geothermal energy by means of heat pumps for early growing of asparagus fields under low tunnel", Proceedings, 10th National Conference on Renewable Energy Sources (Thessaloniki 26-28 November 2014), Institute of Solar Technology, Thessaloniki, A, 409-418 (full text in Greek, abstract in English), http://solarinstitute.gr/wp-content/uploads/pdf/IHT 10o Synedrio C Tomos.pdf (accessed 16 May 2017)

Evrytanika News (2016), "The heated sidewalks melt ice in Karpenisi - How geothermal energy works on urban renewal project", evrytanika.gr, 31 January 2016, http://www.evrytanika.gr/index.php?option=com_content&view=article&id=1092971:2016-01-20-19-27-27&catid=43:2011-11- 19-19-46-40&Itemid=124 (accessed 16 May 2017)

Electric energy consumption by great geographic area, region and department and by category of use (Κατανάλωση ηλεκτρικής ενέργειας, κατά μεγάλη γεωγραφική περιοχή, περιφέρεια, νομό και κατά κατηγορία χρήσης),2012, ELSTAT.

Fournadzhieva S., Pilarsky P., Arvanitis A., Fytikas M. & Koultsiakis E. (2002), "Use of Geothermal Fluids for Cultivation of the Microalga Spirulina in Nigrita - Serres", Proceedings, 7th National Conference on the Renewable Energy Sources, Institute of Solar Technology, Patras 6-8 November 2002, University of Patras, Vol. B, 97-104, http://solarinstitute.gr/wp-content/uploads/pdf//IHT 7o Synedrio B Tomos.pdf (accessed 16 May 2017)

Fytikas M., Andritsos N., Dalabakis P. & Kolios N. (2005), "Greek Geothermal Update 2000-2004", Proceedings World Geothermal Congress 2005, Antalya, Turkey, 24-29 April 2005, Paper Number 0172, 8 p.

Fytikas M. & Arvanitis A. (2011), "The Cultivation of Spirulina: An Innovative Geothermal Application in Greece", Presentation, GEOFAR European Conference "Innovative Solutions for Geothermal Energy Financing", Athens, 17 - 18 March 2011, https://www.slideshare.net/ApostolosArvanitis2/the-cultivation-of-spirulina-an-innovative-geothermal-application-in-greece (accessed 16 May 2017)

Gelegenis J., Dalabakis P. & Ilias A. (2006), "Heating of wintering ponds by means of

low enthalpy geothermal energy. The case of Porto Lagos", Geothermics, 35, 87-103

Karagiorgas M., Mendrinos D. & Karytsas C. (2003), "Solar and geothermal heating and cooling of the European Centre for Public Law building in Greece", Renewable Energy, 29, 461–470, http://www.bonair.gr/data/24_1.pdf

Karytsas C. & Choropanitis I. (2013), "Alternative heating and cooling solutions in public buildings using geothermal systems", Presentation, REGEOCITIES, National Validation Workshop, Athens, 22 May 2013 (in Greek), http://regeocities.eu/wp-content/uploads/2013/06/3.C.-KARYTSAS-PRESENTATION-22-05-2013.pdf (accessed 16 May 2017)

Karytsas C. & Choropanitis I. (2013), "Geothermal systems for public buildings and swimming pools", Presentation, GROUND- MED Workshop "Ground Source Heat Pump Systems for Heating and Cooling in a Mediterranean Climate", Athens, 27 November 2013 (in Greek), http://www.cres.gr/kape/publications/pdf/Ground-Med/4. Karytsas C - GSHP studies.pdf (accessed 16 May 2017)

Kolios N., Dalabakis P. & Arvanitis A. (2011), "Agricultural applications in the Neo Erasmio geothermal field (Thrace, Northeastern Greece)", Presentation, GEOFAR European Conference "Innovative Solutions for Geothermal Energy Financing", Athens, 17 - 18 March 2011, https://www.slideshare.net/ApostolosArvanitis2/agricultural-applications-in-the-neo-erasmio-geothermal-field- thrace-northeastern-greece (accessed 16 May 2017)

Kolios N., Fytikas M., Arvanitis A., Andritsos N., Koutsinos S., 2007. Prospective Medium Enthalpy Geothermal Resources in Sedimentary Basins of Northern Greece, Proceedings European Geothermal Congress

Kolios N., Koutsinos S., Arvanitis A., Karydakis G., 2005. Geothermal situation in Northeastern Greece. Proceedings World Geothermal Congress

Mavroudis V. (2014), "Practical applications of geothermal energy in buildings in Greece", BSc Thesis, School of Production Engineering and Management, Technical University of Crete, Chania, 123 p. (in Greek), dias.library.tuc.gr/view/manf/22889 (accessed 16 May 2017)

Mendrinos D. & Karytsas C. (2005), "Geothermal Energy, Geothermal Heat Pumps, CRES Experience", Mining & Metallurgical Annals, 15, July - December 2005, 29 p, (in Greek) http://www.cres.gr/kape/pdf/geotherm/22.pdf (accessed 16 May 2017)

Mendrinos D., Karagiorgas M. & Karytsas K., "Use of geothermal heat pumps for heating of buildings in Greece", http://www.lowex.net/guidebook/additional_information/lowexx/3_lowexx_paper_gr.pdf (accessed 16 May 2017)

Mendrinos D. & Karytsas C., "Geothermal heat pumps", EnergyReS, http://library.tee.gr/digital/books_notee/book_60568/book_60568_mendrinos.pdf (accessed 16 May 2017)

Mendrinos D., Choropanitis I., Polyzou O., Karytsas C., 2010. Exploring for geothermal resources in Greece , Geothermics 39, p. 124-137

Mendrinos D., Choropanitis I., Polyzou O., Karytsas C., 2010. Exploring for geothermal resources in Greece , Geothermics 39, p. 124-137.

Melfos V., Voudouris P., 2017. Cenozoic metallogeny of Greece and potential for precious, critical and rare metals exploration, Ore Geology Reviews 89, p.1030-1057

Melfos V. and Voudouris P., 2012. Geological, Mineralogical and Geochemical Aspects for Critical and Rare Metals in Greece, Minerals 2012, 2, 300-317.

Melfos V., Bogdanov K., 2013. A Field Guide to the Ore Deposits of NE Greece

Repstock A., Voudouris P., Zeug M., Melfos V., Zhai M., Li H., Kartal T., Matuszczak J., 2016. Chemical composition and varieties of fahlore-group minerals from Oligocene mineralization in the Rhodope area, Southern Bulgaria and Northern Greece.

Savvanis P. , "Municipality of Karpenisi: Pavement snow melting and deicing using geothermal energy", https://web.facebook.com/pg/energyautomation/photos/?tab=album&album_id=1692981290916253 (accessed 16 May 2017)

Stylianou G. (2007), "Heating of Traianoupolis Spa facilities (Evros area) with geothermal water", Presentation, Workshop "Development of geothermal applications for heating-cooling and energy saving", Thessaloniki, 11 December 2007 (in Greek)

Vrachopoulos M., Fytrolakis N., Kyrousis N. & Kravvaritis E. (2005), "Energy saving by exploiting normal geothermal energy at the NTUA Campus, Zografos" , 5o RENES Conf. , Athens, 7 p., http://poseidonenergy.gr/content%5CEMP_anak_22-02-05f.doc (accessed 16 May 2017)

Voudouris P., Tarkian M., Arikas K., 2006. Mineralogy of telluride-bearing epithermal ores in the Kassiteres-Sappes area, Western Thrace, Greece, Mineralogy and Petrology 87, p.31-52

Voudouris P., Melfos V., Spry P., Bindi L., Moritz R., Ortelli M., Kartal T., 2013. Extremely Re-Rich Molybdenite from Porphyry Cu-Mo-Au Prospects in Northeastern Greece: Mode of Occurence, Causes of Enrichment, and Implications for Gold Exploration, Minerals, 3, p.165-191

Voudouris P., Tarantola A., Melfos V., 2017. A Field Guide to the Tertiary Hydrothermal ore Deposits of Northern Greece

http://www.rae.gr/old/sub3/3B/3b3.htm

Annexes

Contact projects@eurogeologists.eu for the full list of Annexes, or open it at the CHPM Information Platform on Prospective Locations (http://bit.ly/CHPMinfoplatform)

Evaluation of CHPM characteristics of prospective CHPM areas

Name of the National Association AGG
Number of the prospective area 5
Xanthi - Nestos Delta area

1. **CHPM operational characteristics - Information for CHPM technological elements**
Requested information:

✓ please fill in the table below with the requested data for the CHPM technology elements

Underground heat exchanger (deep metal enrichment + potential geothermal reservoir)	
Extension of the metal enrichments *(volumetric interpretation)*	**Xanthi – Kimmeria** Xanthi – Kimmeria area analyses showed that resource of 2 Mt contains up to Cu 1.98% and Ag: 20 g/t. Xanthi – Kimmeria area deposit analyses showed compositions of Cu: >1 wt.% , Mo: > 0.2 wt.%, Au: up to 2.7 g/t , W: up to 79.5 g/t , Bi: up to 456.6 g/t, Te: up to 4 g/t. **Palea Kavala** Palea Kavala area analyses showed that resource of 1.5 Mt contains up to 34.5 g/t Au, up to 180 g/t Ag, up to 13% Pb + Zn, up to 40% Fe and up to 42% Mn.
Expected type of the reservoir and porosity/permeability *(fractured, porous, etc)*	Two significant low enthalpy geothermal fields are located in the Nestos Delta basin: (a) the geothermal field of Neo Erasmio – Magana lies at the eastern edge of the Nestos basin and west of the Avdira horst with water temperatures ranging from 40 to 65oC and (b) the field of Eratino - Chrysoupolis on the western side of the Nestos River. Three deep oil exploration boreholes (N-1, N-2 and N-3 at depths of 3159, 3970 and 3851 m respectively) were drilled during the period 1976-1978 west of the Nestos River Delta and out of the main geothermally anomalous area. In borehole N-1, with a depth of 3159 m, the temperatures of 55oC, 85oC and 115^{o}C were measured at 1096, 2400 and 2970 m correspondingly (S.P.E.G., 1982b; P.P.C., 1988). This well has drilled Plio-Quaternary sediments (0-779 m) and Miocene formations (779-3120 m). The Upper Miocene (779-1194 m) is characterized by the “evaporitic zone”. The basement (marbles, chlorite schists, quartzites) is found at 3120 m. The maximum temperature is 126.4oC and it was registered at depth of 3156 m. The average value of the geothermal gradient for this borehole is estimated to be 3.48^{o}C/100 m. By the temperature profile of this well it has proved that the geothermal gradient is higher into the Lower Miocene continental sediments and one interesting aquifer is located at 2374-2400 m with **porosity reaching 20%.** In N-1 the values of **9-15% porosity and 7-15 mD permeability** were measured between 1781 and 1786 m depth. Low values of these physical characteristics and especially **4-7% porosity and 0.03-0.05 mD permeability** were recorded

between 1940 and 1949 m (S.P.E.G., 1982a).

Borehole N-2 of 3970 m depth has drilled Plio-Quaternary (0-953 m) and Miocene (953-3958 m) sediments (953-1545 m: "evaporitic zone"). The Lower-Middle Miocene formations (1545-3958 m) consisting of alternations of sandstones, siltstones and clays indicate continental – deltaic palaoenvironment. The crystalline basement (at 3958 m) is mainly composed of amphibolitic and chlorite schists with a few intercalations of quartzites and marbles. The temperatures of 93, 102, 127 and 164°C were registered at 2370, 2774, 3104 and 3960 m respectively in well N-2 (S.P.E.G., 1982b; P.P.C., 1988). The downhole temperature logging has showed normal increase up to 2400 m. In the deeper Lower Miocene formations the geothermal gradient is significant indicating a crystalline substratum with temperature of 180oC and relatively low thermal conductivity into the overlying Lower Miocene sediments. Therefore, the temperature of 178°C at 4000 m depth might be registered within exploration borehole N-2. The average geothermal gradient is estimated to be 41°C/km. In N-2 the values of **8-9% porosity and 0.3-1.9 mD permeability** were measured between 3080 and 3088 m (S.P.E.G., 1982a).

The only geothermal exploration well of intermediate depth (N-1G) was drilled in the zone of the highest thermal gradient at the center of the Eratino geothermal field (in the vicinity of the Eratino village, West of the Nestos River). The temperature of 122°C was measured at 1377 m (Sotiropoulos, 1989), which corresponds to an average gradient of 78oC/km. It showed that: (a) the upper sedimentary sequence consists of 550 m of clays, marls, sands and conglomerates constituting the impermeable cover of a geothermal reservoir located just below, at 550 – 650 m depths. In this part, the thermal gradient is high (up to 120oC/km). (b) The reservoir formation consists mainly of sandstones, oolitic limestones, micro-conglomerates and cemented gravels (calcarenitic formation) alternating with thin impermeable clay intercalations. The total thickness of these aquifers is estimated to be approximately 40 m containing geothermal fluids at 70°C heated probably by conduction. (c) The deepest Neogene sediments (650-760 m) consist mainly of basal conglomerates, which are impermeable due to their argillaceous matrix. (d) The crystalline basement (below 760 m) is intensively fractured and it is composed of gneisses and amphibolites with minor quartzites and mica schists. The **permeability** is low due to hydrothermal alteration and fillings of calcite and clay Kolios et al. 7 minerals. The Miocene sediments are absent in this area of the main geothermal interest.

On the western side of the sedimentary basin of the Nestos River two main hydrothermal targets exist (Figure 2): (a) the permeable zone in the lowest part of the sedimentary sequence (formation No.3) and (b) the fractured and permeable (carbonate?) parts of the metamorphic basement (formation No.5). Low enthalpy (70°C) geothermal fluids occur at 600 m depth

(formation No.3) and medium enthalpy ones probably exist into the basement (formation No.5). These fluids have an equilibrium temperature of 150-180°C and probably constitute an important and extensive reservoir within the substratum. The existence of such a reservoir is necessary to justify the extended thermal anomaly covering an area of about 40 km^2 in a region without active but only fossil magmatism. The geology and lithology of the basement together with the high values of the geothermal gradient indicate that: (a) the crystalline series acts initially as a cap for the hot hydrothermal system and (b) this reservoir is located at a depth of 1500-1800 m with a temperature in order of 150-180°C and should be the source, which heats the overlying formations and the secondary reservoir by conduction. No well-defined fracture zone was encountered by borehole N-1G, at the center of the area of high thermal gradient, except for some small fractures in the altered lower marble – amphibolitic series (formation No.4) which are favorable for heat transfer (both conductive and convective) towards the sedimentary (secondary) reservoir (formation No.3).

The Nea Kessani geothermal field is a very important low enthalpy system in Greece. The maximum temperature registered within the wells is 82°C. The main hot reservoir is located at shallow depth (150-400 m) with temperatures ranging from 75 to 80°C. It is made up of Eocene – Oligocene clastic sediments overlain by a cap-rock of Oligocene flysch formations, Pliocene lacustrine sediments and Quaternary alluvial deposits. Sometimes, the alluvial deposits host aquifers with cold superficial waters. The geothermal anomaly occurs mainly due to fault systems trending WSW-ENE and NNW-SSE. The waters are of the Na-Cl/HCO_3 and Na-HCO_3 types. The hydrothermal system is characterized by rise of thermal fluids from depth. The fluids rise through a major fault system or along the intersection of the SSE-NNW and ENE-WSW fault systems from a deep reservoir. This deeper reservoir is probably made up of marbles of the Rhodope metamorphic basement. During their ascent, the thermal fluids enter the arkosic aquifer, which acts as a secondary shallow confined reservoir. There is little or no interconnection between the thermal reservoir and either the deep or shallow aquifers of the cap-rock. Most of the hot water is cooled conductively as it flows through the arkosic reservoir towards the marginal parts of the field. The temperature distribution is homogeneous vertically within the reservoir. The water rising from depth probably undergoes significant chemical modifications during its ascent towards the surface because of its high CO_2 content. Some changes in the pressure could be due to the changes in the viscosity and the density of the fluids associated with their temperature (Kolios, 1993; Grassi et al., 1996; Kolios et al., 2005).

Mineralization *(type and enriched metals)*	**Xanthi – Kimmeria** The Xanthi – Kimmeria has 2 types: The massive Cu-W-Mo-Au-bearing skarn-type mineralization which is enriched in metals: Fe, Cu, Zn, W, Bi, Au, Mo and the Mo-Cu-Bi-W quartz vein mineralization is enriched in metals: Cu, Mo, W, Bi. **Palea Kavala** The Palea Kavala mineralization also is appeared in different types like intrusion hosted veins, carbonate replacement and veins. The main appearences are • Oxidized Fe-Mn-Au and Fe-Mn (Pb ± Zn ± Ag) bodies • Fe-As-Au, Fe-Cu-Au, and Bi-Te-Au deposits • Bi-Te-Pb-Sb ± Au mineralization • Bi-Te-Au mineralization The deposits are enriched in metals: Fe, Cu, Pb, Zn, Mn, Cd, As, Sb, Bi, Te, Ag, Au. Apart from the main metal that characterize the deposits like Au, Bi, it is enriched in Te. Of high importance is the critical and precious metal mineralogy of the deposit like bismuthinite, tetradymite, Bi-sulfosalts, cosalite, native Au.

Production and injection wells	
Depth of potential wells (m)	**Eratino** Exploration and production wells from 400m to 1377 m showed temperatures of 52.6 - 122°C, as below: Production wells N-1P & N-2P 650m → 75°C Exploration well N2 430m → 60.9°C Exploration well N6 400m → 52.6°C Exploration well N14 470m → 62.8°C Exploration well N10 500m → 61.4°C Exploration well N11 530m → 69.7°C Exploration well N12 510m → 65°C Deep Exploration borehole N1-G 1377m → 122°C The water temperature within the reservoir of geothermal field of Eratino - Chrysoupolis is about 750C and the depth of reservoir is about 550 - 650m. The discharge from existing wells is measured at 300m^3/h.

Nea Kessani

Exploration and production wells from 60m to 512 m showed temperatures of 65- 83°C, as below:

Exploration well G3 Depth:473m 460m → 83.0°C

Exploration well G16 Depth: 201m 120m → 80°C

Exploration well G13 Depth: 450m 350m → 79°C

Exploration well G22 Depth: 505m 340m → 77.6°C

Exploration well G17 Depth: 200m 170m → 74.5°C

Exploration well G12 Depth: 491m 350m → 73.7°C

Exploration well G24 Depth: 470m 420m → 71.9°C

Exploration well G21 Depth: 390m 340m → 71.7°C

Exploration well G8 Depth: 255m 226m → 70.4°C

Exploration well G9 Depth: 325m 272m → 70.0°C

Exploration well G14 Depth: 485m 470m → 65.9°C

Exploration well G4 Depth: 60m 60m → 65.0°C

Production well GP13 Depth: 430m Depth temperature: 76.8°C

Production well GP12 Depth: 463m Depth temperature: 72.7°C

Production well GP22 Depth: 512m Depth temperature: 72.3°C

Production well GP21 Depth: 473m Depth temperature: 71.0°C

The water temperature of geothermal field of Nea kassani is about 40 - 83^{0}C and the depth of reservoir is about 120 - 500m. The discharge from existing wells is measured at >300m^3/h.

Nestos Delta area

Exploration and production wells from 2400m to 3960 m showed temperatures of 85- 164°C, as below:

Exploration borehole NESTOS-1
2400m → 85°C 2970m → 115°C 3156m → 126.4°C

Exploration borehole NESTOS-2
3104m → 127°C 3960m → 164°C

Exploration borehole NESTOS-3
3601m → 138°C 3851m → 160°C

The water temperature of geothermal field of Neo Erasmio - Magana is about 27 - 68^{0}C and the depth of reservoir is about 200 - 500m. The discharge from existing wells is measured at 250m^3/h.

Based on all the above the depth of potential wells will be from 1300-3800 m so as to retrieve the highest temperature fluids.

Electrolytic metal recovery and gas diffusion electro- precipitation	
Potential target metals to be recovered	We are interested in recovering metals commonly found or mined, metals 'At Risk' (BGS Risk List 2015) and Rare Earth Elements. According to the enrichments of metals that was mentioned above potential target metals to be recovered apart from the Fe, Cu, Pb, Zn, Mn, Cd, As, Ag, Au and Mo great interest will present the recovery of Sb, Bi, Te, W. Further analyses should be made though to determine their content at the geothermal fluids.

Power plant (heat exchanger)	
Local heat and electricity demand *(industrial, municipal, agricultural, etc.)*	As it is shown on the figure from the Hellenic Statistic Agency, the total electric energy consumption of Xanthi regional area, where Xanthi - Nestos Delta area belong to, in 2012 was 438.476.000 kWh. 143.359.000 kwh were consumed for domestic use, 103.116.000 kWh were consumed for commercial use, 122.926.000 kWh were consumed for industrial use, 39.357.000 kWh were consumed for agricultural use, 21.399.000 kWh for Public and Municipal Authorities use and 8.320.000 kWh were consumed for Street Lightening use. Apparently, the domestic sector dominates the electrical consumption in Xanthi area as at the rest of the Greece. According to a survey on energy consumption in households conducted by ELSTAT for the period 2011-2012, 38.4 % of the annual total electricity consumed in a household is used for cooking, 14.7 % for the fridge, 10.6 % for the washing machine, 6.6 % for lighting and 4.9 % for space cooling.

Salt gradient power generation	
Salinity of expected geothermal brine	The water temperatures range from 40 to 65°C. The waters with T.D.S. values between 0.57 and 10.1 g/l are classified into two main categories: Na-Cl and Na-HCO_3Cl waters (Kolios et al., 2005). **Eratino** The chemical composition of waters showed that they are Na-Cl type with TDS of 12.6 – 15.2g/l. **Nea Kessani** The chemical composition of waters showed that they are Na-Cl/HCO_3 type with TDS of 0.4 – 5.5g/l. **Nestos Delta area** The chemical composition of waters showed that they are Na-Cl and Na-HCO_3Cl type with TDS of 0.57 – 10.1g/l.
Fresh water supply from the surface *(water sources)*	Precipitation of the Xanthi area amounts to about 469 millimetres per year. As it seems from the figure, it rains even in summer period. Other water sources is from Nestos River that crosses the area. It is one of the most important rivers in Greece. It has its sources in Mt Rila (S.Bulgaria) between the mountain ranges of Aimos and Rodope. The total length of Nestos is 234 km, 140 km of which are within Greece. The delta of Nestos River lies in the south boundaries of Kavala district and Xanthi district. The delta begins at the point where the river exits the massifs of Rodope in Toxotes and spreads to the south covering quite a large area (125,000 acres) from Nea Karvali to Avdera (coastline length: 50 km). The average annual rainfall in the delta area is 546.5 mm.

2. **CHPM operational characteristics - Environmental, social and political background**

Requested information:

- ✓ toleration to gaseous and solids emissions, water and noise pollution,
- ✓ local competition to land and water availability
- ✓ public acceptance
- ✓ political support
- ✓ presence of supporting legislation, regulatory framework

Notes: all of above refers to the selected area and its surroundings.

Beyond the technical-economical obstacles, the policy and the legislation, the penetration of RES and energy saving techniques in a society is determined to a great degree by their social acceptance.

The general attitude of residents and local authorities of islands towards RES and energy savings, with regard to small scale applications, is rather positive, without however some reactions, objections, disagreements and skepticism. The other causes for objection of societies are owed in their ignorance and lack of briefing and familiarization with RES.

An important reason for which local societies of islands, but also of mainland, react in the RES investments, is their suspiciousness against private investors. However, a method for changing this negative attitude, is to include the residents of a region or municipality that hosts RES investments as shareholders.

From the above, results the necessity of a national strategic approach on public briefing and awareness via the media and the press. Moreover, briefing of local authorities is required in order that these will advance not only in the briefing of citizens, but also in pilot projects and RES installations. Informing of public, dissemination activities and action to the sensitization of local societies are required. This can be strengthened from the interest of private institutions and stakeholders of local market, from the action of not governmental organisations and policy makers and from the informing of local authorities.

Current situation:

In March 2011, international open tenders took place for the leasing of the right to explore the geothermal potential of four promising areas: Evros River Delta (1,307 km²) in Thrace and in Nestos River Delta (803km²) in Eastern Macedonia.

The interest was focused on probable medium enthalpy geothermal resources suitable for binary cycle power generation. A consortium of two Greek private companies (Terna Energy S.A. and ITA Group S.A.) awarded all the tenders. Unfortunately, the lease contracts were never signed, the consortium withdrew from the exploration projects and the tenders have been officially declared void.

However other projects considering benefiting from geothermal energy moved on.

Already geothermal energy has been used at a hydroponics greenhouse at Neo Erasmio,(east of Nestos River), at floriculture greenhouse at Erasmio-Chrysoupolis for greenhouse heating, at intensive non-covered cultivations for soil heating in Neo Erasmio and in Myrodato (Xanthi, Northern Greece), at a novel tomato dehydration plant in Neo Erasmio (South of Xanthi) for dehydration of agricultural products, at aquaculture ponds in Porto Lagos and Neo Erasmio (both in Thrace) for anti-frost protection/heating and at a 2,000 m^2 area of offices and process facilities in the Neo Erasmio greenhouse unit for space heating.

Moreover, there are other projects ongoing for the development and exploitation of the proven low temperature geothermal field of Nea Kessani (Thrace, NE Greece) in greenhouse heating. The exploitation rights for a part of this field have been awarded to AGRITEX Energy S.A. since 25 April

2017. AGRITEX's investment will reach 7 million € and a greenhouse complex of 5 ha (50 stremmas) will be built.
Another projects are ongoing too for the development and exploitation of the proven low temperature geothermal field of Eratino - Chrysoupolis (Kavala, Northern Greece) in agricultural uses. The exploitation rights have been awarded to the Municipal Authority of Nestos since 2007. Except for the German Company "Selecta One", which has already invested in this field, investment interest has also been expressed by other companies.

The regulatory framework in Greece is mentioned in details in Northern Lesvos area.
The implementation of a cohesive legal and regulatory system is an essential condition to create a long-term and stable system for CHPM technology development. The geothermal-specific legislative framework that already exists, includes all important aspects that need to be covered so as to install a CHPM facility, from indicating the type of geothermal field to defining the state committee responsible for all the licensing procedures. By keeping the transparency and simplifying the licensing procedures for the investors we remove any remaining barriers for the full-scale commercial implementation of the CHPM systems.

To conclude, the public acceptance step by step, the investors interest, along with the more favorable legal framework that is set, are leading to the positive scenario that more projects exploiting geothermal field like CHPM technology will follow.

3. Financial aspects

Requested information:

- ✓ use of economic tools developed in WP5 (more information is going to be provided in September)
- ✓ list of potential local stakeholders (community, political, companies)

In a perfectly competitive environment, prices are assumed to reflect the production costs, while being directed by the overall balance between demand and supply. Therefore, RES electricity producers who are not able to reduce production costs, are vulnerable to free competition. In fact, the progress of the liberalization process is quite dissimilar in each EU country, while energy prices do also greatly differ according to the adopted policies regarding:

- Total charges on production costs
- Environmental taxes
- Subsidies

A key-factor for CHPM development is the availability of the necessary funds. Funding is combined with the transferring of the risk associated with CHPM investments. This is the case with Third Party Financing (TPF) which is widely applied for implementing innovative and/or high capital intensive technologies.

The deterioration of the environmental quality and the growing environmental awareness of the last two decades has generally assisted in the development of RES, which are practically exempt from major environmental burdens. The most important environmental issues connected with RES exploitation are global warming and atmospheric pollution. The development of RES can positively affect environmental quality, which are affected by conventional systems, principally at the local level. Nevertheless, RES are often accused to cause also environmental repercussions, such as noise and visual intrusion, which do not have a detrimental effect on human health or on natural ecosystems, but sometimes cause a negative attitude of public against RES. Environmental effects of RES which

should be taken into account in the design and implementation of local plans.

Greek islands and mainland possess a high degree of biodiversity at all levels-genetic, species, habitat and landscape. Many of the habitats have been identified as important to nature and are statutorily protected (NATURA 2000 network). Accordingly to the recent ministerial decision, 49828/2008 (ΦΕΚ 2464 B' / 03.12.08), RES installations are generally prohibited in these areas. The minimum allowed distance of potential RES installations from them is determined at case and depends mainly on the RES technology and the potential installed power.

The overall legislation regarding the operation of the energy sector may directly or indirectly affect the deployment of CHPM technology. Relevant legislative measures can be classified in two broad categories:
Measures enhancing the development of RES. The greatest effect have regulations concerning the encouragement of RES projects and minimization of financial risks through incentives, such as subsidies, tax exemptions, pay-back tariffs and long-term contracts. Furthermore, the establishment targets and programs at the national or regional level related with the development of RES may also considerably motivate market forces.
Measures removing barriers hindering the development of RES. Pollution charges or taxes on fossil fuels constitute the opposite side of incentives for RES and have both the same objective.
Implementation of RES projects in Greece is usually retarded or hindered due to malfunctions created by administrative procedures and legal gaps. Among the most crucial obstacles is the very complicated and time consuming process of issuing installation and operation licenses, a simplification of which is necessary. (Caralis G. et Emmanouilidis G. ,2009). The setting of a legislation framework was the first step though, and as it is mentioned above, by keeping the transparency and simplifying the licensing procedures for the investors, we remove any remaining barriers for the full-scale commercial implementation of the CHPM systems.

Companies already active in the area:

- AGRITEX Energy S.A investment of 7 million € in greenhouse heating

Expressed interest from the German Company "Selecta One" and other companies for the exploitation of geothermal field of Eratino - Chrysoupolis.

List of references

Andritsos N., Arvanitis A., Papachristou M. & Fytikas M. (2011), "Status of Geothermal Energy in Greece – 2011", Presentation, GEOFAR European Conference "Innovative Solutions for Geothermal Energy Financing", Athens, 17 - 18 March 2011

Andritsos N., Dalabakis P., Karydakis G., Kolios N. & Fytikas M. (2011), "Characteristics of low-enthalpy geothermal applications in Greece", Renewable Energy, 36, 1298-1305

Andritsos N., Arvanitis A. Dalabakis P., Karytsas C., Mendrinos D. & Papachristou M. (2013), "Geothermal Energy Use, Country Update for Greece", Proceedings European Geothermal Congress 2013, Pisa, Italy, 3-7 June 2013, Paper Number CUR-14, 10 p.

Andritsos N., Dalambakis P., Arvanitis A., Papachristou M. & Fytikas M. (2015), "Geothermal Developments in Greece - Country update 2010-2014", Proceedings World Geothermal Congress 2015, Melbourne, Australia, 19-25 April 2015, Paper Number 01048, 11 p.

Andritsos N., Arvanitis A., Papachristou M., Fytikas M. & Dalambakis P. (2010), "Geothermal Activities in Greece During 2005- 2009", Proceedings World Geothermal Congress 2010, Bali, Indonesia, 25-29 April 2010, Paper Number 0138, 10 p.

Andritsos N., Dalampakis P. & Kolios N. (2003), "Use of Geothermal Energy for Tomato Drying", GeoHeat Center Quarterly Bul., 24(1), March 2003, 9-13.

Arvanitis A., Geothermal Energy in Greece-Exploration-Fields-Exploitation-Legal Framework EuroWorkshop: Geothermal - The Energy of the Future Fira, Santorini, Greece, 18-19 May 2017

Arvanitis A., Sotiroudis T., Nerantzis E., Fournadzhieva S. & Koultsiakis E. (2004), "Mass culture of the microalga Spirulina using geothermal fluids in Greece - Antioxidant activities of Spirulina powder extracts", Proceedings, International Conference on Geothermal Energy Applications in Agriculture, May 2004, Athens, Greece, 6 p. https://www.scribd.com/document/349817008/Mass-culture-of-the-microalga-Spirulina-using-geothermal-fluids-in-Greece- Antioxidant-activities-of-Spirulina-powder-extracts.

Avarikiotis C. (2012), "Geothermal energy technology and installations of geothermal systems", Presentation, GEO.POWER local forum on geothermal energy and energy efficiency strategies in domestic and industrial sectors, Athens, 16 January 2012 (in Greek), http://www.cres.gr/kape/publications/pdf/Geopower/2.pdf (accessed 16 May 2017)

Benou A. (2008), "Geothermal Heat Pumps - CRES Applications in Greece",

Presentation, GROUNREACH Workshop "GroundReach Heating and Cooling with Ground Source Heat Pumps", Athens, 24 January 2008 (in Greek), http://www.cres.gr/kape/publications/pdf/GROUND_REACH/6 ABenou.pdf (accessed 16 May 2017)

Caralis G and Emmanouilidis G, 2009. Executive summary of the work done on Energy planning (Work package 3), IOS_Aegean Energy Agency.

Dalabakis P., Papachristou M., Kolios P., Arvanitis A. & Kolios N. (2015), "Geothermal exploitation in Neo Erasmio (Xanthi)", Proceedings of the 9th Panhellenic Congress of the Hellenic Society of Agricultural Engineers (Thessaloniki 8-9 October 2015), 711-718 (in Greek), https://www.scribd.com/document/350138510/Αξιοποίηση-γεωθερμικών-ρευστών-στο-Νέο-Εράσμιο-Ξάνθης

Dalabakis P., Ilias A. & Ladas P. (2014), "Use of shallow geothermal energy by means of heat pumps for early growing of asparagus fields under low tunnel", Proceedings, 10th National Conference on Renewable Energy Sources (Thessaloniki 26-28 November 2014), Institute of Solar Technology, Thessaloniki, A, 409-418 (full text in Greek, abstract in English), http://solarinstitute.gr/wp-content/uploads/pdf/IHT 10o Synedrio C Tomos.pdf (accessed 16 May 2017)

Evrytanika News (2016), "The heated sidewalks melt ice in Karpenisi - How geothermal energy works on urban renewal project", evrytanika.gr, 31 January 2016, http://www.evrytanika.gr/index.php?option=com_content&view=article&id=1092971:2016-01-20-19-27-27&catid=43:2011-11- 19-19-46-40&Itemid=124 (accessed 16 May 2017)

Electric energy consumption by great geographic area, region and department and by category of use (Κατανάλωση ηλεκτρικής ενέργειας, κατά μεγάλη γεωγραφική περιοχή, περιφέρεια, νομό και κατά κατηγορία χρήσης),2012, ELSTAT.

Fornadel A., Spry P., Melfos V., Vavelidis M., Voudouris P. 2011. Is the Palea Kavala Bi-Te-Pb-Sb+/- Au district, Northeastern Greece an intrusion-related system?, Ore geology Reviews 39, p.119-133.

Fournadzhieva S., Pilarsky P., Arvanitis A., Fytikas M. & Koultsiakis E. (2002), "Use of Geothermal Fluids for Cultivation of the Microalga Spirulina in Nigrita - Serres", Proceedings, 7th National Conference on the Renewable Energy Sources, Institute of Solar Technology, Patras 6-8 November 2002, University of Patras, Vol. B, 97-104, http://solarinstitute.gr/wp-content/uploads/pdf//IHT 7o Synedrio B Tomos.pdf (accessed 16 May 2017)

Fytikas M., Andritsos N., Dalabakis P. & Kolios N. (2005), "Greek Geothermal Update 2000-2004", Proceedings World Geothermal Congress 2005, Antalya, Turkey, 24-29 April 2005, Paper Number 0172, 8 p.

Fytikas M. & Arvanitis A. (2011), "The Cultivation of Spirulina: An Innovative

Geothermal Application in Greece", Presentation, GEOFAR European Conference "Innovative Solutions for Geothermal Energy Financing", Athens, 17 - 18 March 2011, https://www.slideshare.net/ApostolosArvanitis2/the-cultivation-of-spirulina-an-innovative-geothermal-application-in-greece (accessed 16 May 2017)

Gelegenis J., Dalabakis P. & Ilias A. (2006), "Heating of wintering ponds by means of low enthalpy geothermal energy. The case of Porto Lagos", Geothermics, 35, 87-103

Gkiougkis I., Kallioras A., Pliakas F., Pechtelidis A., Diamantis V., Diamantis I., Ziogas A. and Dafnis I., 2014. Assessment of soil salinization at the eastern Nestos River Delta, N.E. Greece, CATENA-02244; No of Pages 14.

Karagiorgas M., Mendrinos D. & Karytsas C. (2003), "Solar and geothermal heating and cooling of the European Centre for Public Law building in Greece", Renewable Energy, 29, 461–470, http://www.bonair.gr/data/24_1.pdf

Karytsas C. & Choropanitis I. (2013), "Alternative heating and cooling solutions in public buildings using geothermal systems", Presentation, REGEOCITIES, National Validation Workshop, Athens, 22 May 2013 (in Greek), http://regeocities.eu/wp-content/uploads/2013/06/3.C.-KARYTSAS-PRESENTATION-22-05-2013.pdf (accessed 16 May 2017)

Karytsas C. & Choropanitis I. (2013), "Geothermal systems for public buildings and swimming pools", Presentation, GROUND- MED Workshop "Ground Source Heat Pump Systems for Heating and Cooling in a Mediterranean Climate", Athens, 27 November 2013 (in Greek), http://www.cres.gr/kape/publications/pdf/Ground-Med/4. Karytsas C - GSHP studies.pdf (accessed 16 May 2017)

Kolios N., Dalabakis P. & Arvanitis A. (2011), "Agricultural applications in the Neo Erasmio geothermal field (Thrace, Northeastern Greece)", Presentation, GEOFAR European Conference "Innovative Solutions for Geothermal Energy Financing", Athens,17-18March2011, https://www.slideshare.net/ApostolosArvanitis2/agricultural-applications-in-the-neo-erasmio-geothermal-field- thrace-northeastern-greece (accessed 16 May 2017)

Kolios N., Koutsinos S., Arvanitis A., Karydakis G., 2005. Geothermal situation in Northeastern Greece. Proceedings World Geothermal Congress.

Kolios N., Fytikas M., Arvanitis A., Andritsos N., Koutsinos S., 2007. Prospective Medium Enthalpy Geothermal Resources in Sedimentary Basins of Northern Greece, Proceedings European Geothermal Congress.

Melfos V., Voudouris P., 2017. Cenozoic metallogeny of Greece and potential for precious, critical and rare metals exploration, Ore Geology Reviews 89, p.1030-1057.

Melfos V. and Voudouris P., 2012. Geological, Mineralogical and Geochemical

Aspects for Critical and Rare Metals in Greece, Minerals 2012, 2, 300-317.

Melfos V., Bogdanov K., 2013. A Field Guide to the Ore Deposits of NE Greece.

Mendrinos D., Choropanitis I., Polyzou O., Karytsas C., 2010. Exploring for geothermal resources in Greece , Geothermics 39, p. 124-137.

Mendrinos D., Polyzou O. and Karytsas C.,2014. Geothermal exploration in Greece.

Mavroudis V. (2014), "Practical applications of geothermal energy in buildings in Greece", BSc Thesis, School of Production Engineering and Management, Technical University of Crete, Chania, 123 p. (in Greek), dias.library.tuc.gr/view/manf/22889 (accessed 16 May 2017)

Mendrinos D. & Karytsas C. (2005), "Geothermal Energy, Geothermal Heat Pumps, CRES Experience", Mining & Metallurgical Annals, 15, July - December 2005, 29 p, (in Greek) http://www.cres.gr/kape/pdf/geotherm/22.pdf (accessed 16 May 2017)

Mendrinos D., Karagiorgas M. & Karytsas K., "Use of geothermal heat pumps for heating of buildings in Greece", http://www.lowex.net/guidebook/additional_information/lowexx/3_lowexx_paper_gr.pdf (accessed 16 May 2017)

Mendrinos D. & Karytsas C., "Geothermal heat pumps", EnergyReS, http://library.tee.gr/digital/books_notee/book_60568/book_60568_mendrinos.pdf (accessed 16 May 2017)

Repstock A., Voudouris P., Zeug M., Melfos V., Zhai M., Li H., Kartal T., Matuszczak J., 2016. Chemical composition and varieties of fahlore-group minerals from Oligocene mineralization in the Rhodope area, Southern Bulgaria and Northern Greece.

Savvanis P., "Municipality of Karpenisi: Pavement snow melting and deicing using geothermal energy", https://web.facebook.com/pg/energyautomation/photos/?tab=album&album_id=1692981290916253 (accessed 16 May 2017)

Stylianou G. (2007), "Heating of Traianoupolis Spa facilities (Evros area) with geothermal water", Presentation, Workshop "Development of geothermal applications for heating-cooling and energy saving", Thessaloniki, 11 December 2007 (in Greek)

Tsokas G., Christofides G., Papakonstantinou C. 1996. A Geophysical Study of the Granites and the Sedimentary Basins of the Xanthi Area (N. Greece), Pageoph, vol. 146, no. 2.

Voudouris P., Tarantola A., Melfos V., 2017. A Field Guide to the Tertiary Hydrothermal ore Deposits of Northern Greece.

Vrachopoulos M., Fytrolakis N., Kyrousis N. & Kravvaritis E. (2005), "Energy saving

by exploiting normal geothermal energy at the NTUA Campus, Zografos", 5o RENES Conf., Athens, 7 p., http://poseidonenergy.gr/content%5CEMP_anak_22-02-05f.doc (accessed 16 May 2017)

http://www.rae.gr/old/sub3/3B/3b3.htm

ENERGYPRESS (2016), https://energypress.gr/news/xekinise-i-kataskeyi-paragogikis-geothermikis-geotrisis-stin-traianoypoli (accessed 16 May 2017)

e-evros.gr (2016), http://www.e-evros.gr/gr/eidhseis/3/ner http://adesmeuti-thrakis.blogspot.gr/2017/04/blog-post_469.html (accessed 16 May 2017)

http://www.thessnews.gr/article/33498/ependysi-7-ek-eyro-apo-ton-omilo-eythymiadi-gia-thermokipia-me-geothermia-stin- kessani (accessed 16 May 2017)

http://www.agrotika-nea.gr/a/ston-omilo-eythymiadh-h-diaxeirish-toy-gewthermiko/22803764 (accessed 16 May 2017)

ethnos.gr (2016), http://www.ethnos.gr/koinonia/arthro/thermokipia_me_xorigo_ti_fysi-64389658 (accessed 16 May 2017)

Selecta Klemm (2016), "New Production location Selecta Hellas",

http://www.selecta-one.com/en/posts/New_Production_location_Selecta_Hellas/latest_news/08203125843/ (accessed 16 May 2017)

Annexes

Contact projects@eurogeologists.eu for the full list of Annexes, or open it at the CHPM Information Platform on Prospective Locations (http://bit.ly/CHPMinfoplatform)

Evaluation of CHPM characteristics of prospective CHPM areas

Name of the National Association AGG
Number of the prospective area 6
Thermes

1. **CHPM operational characteristics - Information for CHPM technological elements**
Requested information:
✓ please fill in the table below with the requested data for the CHPM technology elements

Underground heat exchanger (deep metal enrichment + potential geothermal reservoir)	
Extension of the metal enrichments *(volumetric interpretation)*	The Thermes ore deposit contains a resource of about 1 Mt with grades of <4 g/t Au, 10-340 g/t Ag, 1.2-14.5% Pb, 2.1-16.7% Zn and 0.06-0.10% Cu (Gialoglou and Drymniotis, 1983; Melvos and Voudouris, 2017).
Expected type of the reservoir and porosity/permeability *(fractured, porous, etc)*	Thermal water from Erma Reka reservoir discharges through several springs located in the Thermes area (Benderev et al., 2015). Therefore, it is considered that Erma Reka field and Thermes springs constitute a single geothermal system. The Erma Reka system constitutes a complicated tectonic structure and is made up of (Teneva-Georgieva and Andreev, 2005; Benderev et al., 2015) gneisses, granitic gneisses, amphibolites, amphibolite gneisses, schists, marbles and volcanites. There are no marble outcrops in the territory of Bulgaria, but marbles, more than 1,000m thick, with silicitizated cavernous zone formed the upper part, are underlain by gneisses at depths greater than 450m. Marbles are karstified and cavernous and a thick quartz cavernous zone is formed on the boundary between marbles and gneisses. The structure is crossed by many faults and fractures, which are essential for the hydrothermal system. The thermal water is mainly accumulated in karst and cavernous marble body and ascends through the numerous faults and fractures to the gneisses (Fig. 23 and 24). The faults create also conditions for cold waters penetration in depth. A hydraulic link exists between cold and warmed fractured unconfined waters formed in gneisses (zone of regional fracturing) and confined waters containing in the upper zone of the marble body (Teneva-Georgieva and Andreev, 2005). The results obtained from pumping-tests performed in 78 wells indicate that hydrogeological parameters vary widely. **Transmissivity** (T) values range from 60 to more than 2000 m^2/d and **hydraulic conductivity** varies between 5 and more than 100 m/d (Benderev et al., 2015). These results confirm the heterogeneous hydrogeological properties of the permeable rocks in horizontal and vertical direction (Teneva-Georgieva and Andreev, 2005).

Mineralization *(type and enriched metals)*	Two major base metal sulfide ore varieties have been recognized in the Thermes ore field (Arvanitidis et al., 1986; 1989b): (1) a brecciated vein Pb-Zn (Fe-Cu) mineralization related to NNW- and NNE-trending faults and (2) stratabound (manto), Zn-Pb-Fe-Cu-As-Ag-Au-Te carbonate-replacement type with extension to mineralized veins in faults. The second variety is subdivided into (a) polymetallic (Zn-Pb-Fe-Cu-As-Ag-Au-Cd-Sb) and (b) Pb-Zn (Cu-Mn-Ag-Cd) types. Of high importance is the critical and precious metal mineralogy of the deposit like gersdorffite, hessite, altaite, native Au, In, Ge, Ga.

Production and injection wells	
Depth of potential wells (m)	Thermal spring in Thermes Xanthi area showed temperature of 43-53^{o}C, while borehole well at 200m showed temperature of 41^{o}C. Since the Thermes springs constitutes though the surface manifestations of the adjacent Erma-Reka geothermal system (in the territory of Bulgaria) where the water temperature reaches 94^{o}C and the temperature of 128^{o}C has been measured at depth of 1,345m, we can estimate that depth of potential wells can be 1000m.

Electrolytic metal recovery and gas diffusion electro- precipitation	
Potential target metals to be recovered	We are interested in recovering metals commonly found or mined, metals 'At Risk' (BGS Risk List 2015) and Rare Earth Elements. According to the enrichments of metals that was mentioned above potential target metals to be recovered apart from the Zn, Pb, Cu, As, Ag, Au, Cd and Mn, great interest will present the recovery of Sb, Te, In, Ge, Ga. Further analyses should be made though to determine their content at the geothermal fluids.

Power plant (heat exchanger)	
Local heat and electricity demand *(industrial, municipal, agricultural, etc.)*	As it is shown on the figure from the Hellenic Statistic Agency, the total electric energy consumption of Xanthi regional area, where Sappes belong to, in 2012 was 438.476.000 kWh. 143.359.000 kwh were consumed for domestic use, 103.116.000 kWh were consumed for commercial use, 122.926.000 kWh were consumed for industrial use, 39.357.000 kWh were consumed for agricultural use, 21.399.000 kWh for Public and Municipal Authorities use and 8.320.000 kWh were consumed for Street Lightening use.

Salt gradient power generation	
Salinity of expected geothermal brine	The thermal waters of the area belong to the Na-HCO3 type having electrical conductivity of 900-1600 μS/cm and pH 6.1-6.9 (Kolios and Sarandeas, 1990; Minissale et al., 1989; Athanassoulis et al., 2009). The chemical composition of gas discharges is: 531.1 m.mol.mol-1 CO_2 and 455.7 m.mol.mol-1 N2 (Kolios and Sarandeas, 1990; Minissale et al., 1989). High N2 percentages point to relatively long residence times (Minissale et al., 1989) and the marked presence of air in most of the hydrologic circuits (Kolios and Sarandeas, 1990; Minissale et al., 1989).
Fresh water supply from the surface *(water sources)*	Precipitation of the Thermes Xanthi area amounts to about 469 millimetres per year. As it seems from the figure, it rains even in summer period. No significant rivers cross the area.

2. CHPM operational characteristics - Environmental, social and political background

Requested information:

- ✓ toleration to gaseous and solids emissions, water and noise pollution,
- ✓ local competition to land and water availability
- ✓ public acceptance
- ✓ political support
- ✓ presence of supporting legislation, regulatory framework

Notes: all of above refers to the selected area and its surroundings.

Beyond the technical-economical obstacles, the policy and the legislation, the penetration of RES and energy saving techniques in a society is determined to a great degree by their social acceptance.

The general attitude of residents and local authorities towards RES and energy savings, with regard to small scale applications, is rather positive, without however some reactions, objections, disagreements and skepticism.

With regard to potential large scale RES installations, such as wind parks or geothermic plants the attitude of societies is almost always opposite. The causes for objection of societies are owed in their ignorance and lack of briefing and familiarization with RES.

Another important reason for which local societies of islands, but also of mainland, react in the RES investments, is their suspiciousness against private investors. However, a method for changing this negative attitude, is to include the residents of a region or municipality that hosts RES investments as shareholders.

From the above, results the necessity of a national strategic approach on public briefing and awareness via the media and the press. Moreover, briefing of local authorities is required in order that these will advance not only in the briefing of citizens, but also in pilot projects and RES installations. Informing of public, dissemination activities and action to the sensitization of local societies are required. This can be strengthened from the interest of private institutions and stakeholders of local market, from the action of not governmental organisations and policy makers and from the informing of local authorities.

Current situation:

Specifically, in Thermes, Xanthi, geothermal energy is applied for space heating in a high school having a total area of 60 m^2. At this heating system, geothermal waters (at 51.5^oC) coming from hot springs are used (discharge of springs: 5 m^3/h). The heating system yields 7,680 kcal/h (0.009 MWt or around 0.01 MWt) (considering $\Delta T=2^oC$).

It has been fully operational since 3 March 2003 and tested at various outdoor temperatures. Specifically, it covers (a) 80% of the designed peak load at an outdoor temperature of -9oC and (b) 100% of this at an outdoor temperature of 0^oC.

The design and installation of this heating system constitutes a pilot project performed by NAGREF - National Agricultural Research Foundation (now Greek Agricultural Organization “DEMETER”).

The regulatory framework is mentioned in details in Northern Lesvos area.

The introduction of complementary and cohesive legal and regulatory system is an essential condition to create a long-term and stable system for CHPM technology development. This geothermal-specific legislative framework, includes all important aspects that need to be covered so as to install a CHPM facility, from indicating the type of geothermal field to defining the state committee responsible for all the licensing procedures. By keeping the transparency and simplifying the licensing procedures for the investors we remove any remaining barriers for the full-scale commercial implementation of the CHPM systems.

3. **Financial aspects**

Requested information:

- ✓ use of economic tools developed in WP5 (more information is going to be provided in September)
- ✓ list of potential local stakeholders (community, political, companies)

In a perfectly competitive environment, prices are assumed to reflect the production costs, while being directed by the overall balance between demand and supply. Therefore, RES electricity producers who are not able to reduce production costs, are vulnerable to free competition. In fact, the progress of the liberalization process is quite dissimilar in each EU country, while energy prices do also greatly differ according to the adopted policies regarding:

- Total charges on production costs
- Environmental taxes
- Subsidies

A key-factor for CHPM development is the availability of the necessary funds. Funding is combined with the transferring of the risk associated with CHPM investments. This is the case with Third Party Financing (TPF) which is widely applied for implementing innovative and/or high capital intensive technologies.

The deterioration of the environmental quality and the growing environmental awareness of the last two decades has generally assisted in the development of RES, which are practically exempt from major environmental burdens. The most important environmental issues connected with RES exploitation are global warming and atmospheric pollution. The development of RES can positively affect environmental quality, which are affected by conventional systems, principally at the local level. Nevertheless, RES are often accused to cause also environmental repercussions, such as noise and visual intrusion, which do not have a detrimental effect on human health or on natural ecosystems, but sometimes cause a negative attitude of public against RES. Environmental effects of RES which should be taken into account in the design and implementation of local plans.

Greek islands possess a high degree of biodiversity at all levels-genetic, species, habitat and landscape. Many of the habitats have been identified as important to nature and are statutorily protected (NATURA 2000 network). Accordingly to the recent ministerial decision, 49828/2008 (ΦΕΚ 2464 Β' / 03.12.08), RES installations are generally prohibited in these areas. The minimum allowed distance of potential RES installations from them is determined at case and depends mainly on the RES technology and the potential installed power.

The overall legislation regarding the operation of the energy sector may directly or indirectly affect the deployment of CHPM technology. Relevant legislative measures can be classified in two broad categories:

Measures enhancing the development of RES. The greatest effect have regulations concerning the encouragement of RES projects and minimization of financial risks through incentives, such as subsidies, tax exemptions, pay-back tariffs and long-term contracts. Furthermore, the establishment targets and programs at the national or regional level related with the development of RES may also considerably motivate market forces.

Measures removing barriers hindering the development of RES. Pollution charges or taxes on fossil fuels constitute the opposite side of incentives for RES and have both the same objective. Implementation of RES projects in Greece is usually retarded or hindered due to malfunctions created by administrative procedures and legal gaps. Among the most crucial obstacles is the very complicated and time consuming process of issuing installation and operation licenses, a simplification of which is

necessary. (Caralis G. et Emmanouilidis G. ,2009). The setting of a legislation framework was the first step though, and as it is mentioned above, by keeping the transparency and simplifying the licensing procedures for the investors, we remove any remaining barriers for the full-scale commercial implementation of the CHPM systems.

Companies/Foundations active at the area:
NAGREF - National Agricultural Research Foundation (now Greek Agricultural Organization "DEMETER").

List of references

Alfieris D., Arvanitidis N.D., Katirtzoglou K., 1989, "Petrology and geochemistry of acid dyke-rocks in the East Rhodope, Esimi area", Geol. Rhodopica, 1, 268-279

Andritsos N., Arvanitis A., Papachristou M. & Fytikas M. (2011), "Status of Geothermal Energy in Greece – 2011", Presentation, GEOFAR European Conference "Innovative Solutions for Geothermal Energy Financing", Athens, 17 - 18 March 2011

Andritsos N., Dalabakis P., Karydakis G., Kolios N. & Fytikas M. (2011), "Characteristics of low-enthalpy geothermal applications in Greece", Renewable Energy, 36, 1298-1305

Andritsos N., Arvanitis A. Dalabakis P., Karytsas C., Mendrinos D. & Papachristou M. (2013), "Geothermal Energy Use, Country Update for Greece", Proceedings European Geothermal Congress 2013, Pisa, Italy, 3-7 June 2013, Paper Number CUR-14, 10 p.

Andritsos N., Dalambakis P., Arvanitis A., Papachristou M. & Fytikas M. (2015), "Geothermal Developments in Greece - Country update 2010-2014", Proceedings World Geothermal Congress 2015, Melbourne, Australia, 19-25 April 2015, Paper Number 01048, 11 p.

Andritsos N., Arvanitis A., Papachristou M., Fytikas M. & Dalambakis P. (2010), "Geothermal Activities in Greece During 2005- 2009", Proceedings World Geothermal Congress 2010, Bali, Indonesia, 25-29 April 2010, Paper Number 0138, 10 p.

Andritsos N., Dalampakis P. & Kolios N. (2003), "Use of Geothermal Energy for Tomato Drying", GeoHeat Center Quarterly Bul., 24(1), March 2003, 9-13.

Arikas, K. and Voudouris, P., 1998, Hydrothermal alterations and mineralizations of magmatic rocks in the southern Rhodope Massif", Acta Vulcanol., 10, 353-365.

Arvanitidis N.D., Favas N., Dimadis E., Zanas I. and Kalogeropoulos S.I., 1986, "Zn-Pb-Cu sulfide mineralizations in the area of Thermes, Central Rhodope massif", Summary of preliminary geologic, petrologic and geochemical considerations", Final Rep., EEC-Rhodope R&D project, IGME, Athens, Greece, 47 p.

Arvanitis A., Geothermal Energy in Greece-Exploration-Fields-Exploitation-Legal Framework EuroWorkshop: Geothermal - The Energy of the Future Fira, Santorini, Greece, 18-19 May 2017

Arvanitidis N.D., Dimadis E., Favas N. and Zanas I., 1989a, "The geology, mineralogy, and petrogenesis of metamorphic rocks from the area of Thermes, Central Rhodope massif", 1st Hellenic-Bulgarian Symposium on the Geology and Physical Geography of the Rhodope Massif, Univ. Sofia. Geol. Rhodopica, 1, 169-185

Arvanitidis N.D., Kalogeropoulos S.I. and Favas N., 1989b, "Zn-Pb-Cu sulfide mineralization in the area of Thermes, Central Rhodope Massif", Geol. Rhodopica, 1, 306-321

Arvanitidis N. and Dimou E., 1990, "Electrum and silver telluride occurrences in the polymetallic sulfide mineralization of the Thermes ore-field, N. Greece", Geol. Rhodopica, 2nd Hellenic-Bulgarian Symposium (Thessaloniki, 1989), 2, 309-325.

Arvanitidis N., 2010, "Economically viable mineral deposits in Macedonia and Thrace", Presentation, Workshop "The treasures of Northern Greece", Thessaloniki, 29 May 2010

Arvanitis A., Sotiroudis T., Nerantzis E., Fournadzhieva S. & Koultsiakis E. (2004), "Mass culture of the microalga Spirulina using geothermal fluids in Greece - Antioxidant activities of Spirulina powder extracts", Proceedings, International Conference on Geothermal Energy Applications in Agriculture, May 2004, Athens, Greece, 6 p. https://www.scribd.com/document/349817008/Mass-culture-of-the-microalga-Spirulina-using-geothermal-fluids-in-Greece- Antioxidant-activities-of-Spirulina-powder-extracts.

Athanassoulis C., Vakalopoulos P., Xenakis M., Persianis D. and Taktikos S., 2009, "Periodical monitoring of the curative springs of Greece", Technical Report, I.G.M.E., Athens, 57-61 (in Greek)

Benderev A., Atanassova R., Andreev A., Hristov V., Bojadgieva K. and Kolev S., 2015, "Hydrochemical Characteristics of Erma Reka Geothermal Reservoir (S. Bulgaria)", Proceedings, World Geothermal Congress 2015, Melbourne, Australia, 19-25 April 2015, 9 p.

Benou A. (2008), "Geothermal Heat Pumps - CRES Applications in Greece", Presentation, GROUNREACH Workshop "GroundReach Heating and Cooling with Ground Source Heat Pumps", Athens, 24 January 2008 (in Greek), http://www.cres.gr/kape/publications/pdf/GROUND_REACH/6 ABenou.pdf (accessed 16 May 2017)

Bonev N., Burg J.P. and Ivanov Z., 2006a, "Mesozoic-Tertiary structural evolution of an extensional gneiss dome - the Kesebir-Kardamos dome, E. Rhodopes, Bulgaria", Int. J. Earth Sci. 95, 318-340

Bonev N., Marchev P. and Singer B., 2006b, "40Ar/39Ar geochronology constraints on the Middle Tertiary basement extensional exhumation, and its relation to oreforming and magmatic processes in the Eastern Rhodope (Bulgaria)", Geodin. Acta, 19, 265-280

Bonev N., Moritz R., Márton I., Chiaradia M., Marchev P., 2010, "Geochemistry,tectonics, and crustal evolution of basement rocks in the Eastern Rhodope Massif, Bulgaria", Int. Geol. Rev., 52, 269-297

Bonev N., Spikings R., Moriz R. and Marchev, P., 2013, "40Ar/39Ar age constraints on the timing of Tertiary crustal extension and its temporal relation to ore-forming and magmatic processes in the Eastern Rhodope Massif, Bulgaria", Lithos, 180-181, 264–278.

Bonev N., Marchev, P., Moritz R. and Collings D., 2015, "Jurassic subduction zone tectonics of the Rhodope Massif in the Thrace region (NE Greece) as revealed by new U-Pb and 40Ar/39Ar geochronology of the Evros ophiolite and high-grade

basement rocks", Gondwana Res., 27, 760-775

Brun J.-P. and Sokoutis D., 2007, "Kinematics of the Southern Rhodope core complex (Northern Greece)", Int. J. Earth Sci. 96, 1079-1099

Burg J.P., Ricou L.E., Ivano Z., Godfriaux I., Dimov D. and Klain, L., 1996, "Synmetamorphic nappe complex in the Rhodope Massif", Structure and kinematics, Terra Nova, 8, 6-15

Caralis G and Emmanouilidis G, 2009. Executive summary of the work done on Energy planning (Work package 3), IOS_Aegean Energy Agency.

Christofides G., Pecskay Z., Eleftheriadis G., Soldatos T. and Koroneos A., 2004, "The Tertiary Evros volcanic rocks (Thrace, northeastern Greece): petrology and K-Ar geochronology", Geol. Carpath., 55, 397-410

Dalabakis P., Papachristou M., Kolios P., Arvanitis A. & Kolios N. (2015), "Geothermal exploitation in Neo Erasmio (Xanthi)", Proceedings of the 9th Panhellenic Congress of the Hellenic Society of Agricultural Engineers (Thessaloniki 8-9 October 2015), 711-718 (in Greek), https://www.scribd.com/document/350138510/Αξιοποίηση-γεωθερμικών-ρευστών-στο-Νέο-Εράσμιο-Ξάνθης

Dalabakis P., Ilias A. & Ladas P. (2014), "Use of shallow geothermal energy by means of heat pumps for early growing of asparagus fields under low tunnel", Proceedings, 10th National Conference on Renewable Energy Sources (Thessaloniki 26-28 November 2014), Institute of Solar Technology, Thessaloniki, A, 409-418 (full text in Greek, abstract in English), http://solarinstitute.gr/wp-content/uploads/pdf/IHT 10o Synedrio C Tomos.pdf (accessed 16 May 2017)

Dinter D.A., Macfarlane A., Hames W., Isachsen C., Bowring S. and Royden L., 1995, "U-Pb and 40Ar/39Ar geochronology of the Symvolon granodiorite: implications for the thermal and structural evolution of the Rhodope metamorphic core complex, northeastern Greece. Tectonics 14, 886-908.

Dragiev H. and Danchev J., 1990, "Morphological-structural specialities of metasomatic deposits in the Erma Reka area in the Madan's ore field", Geologica Rhodopica, 2, 352-361

Electric energy consumption by great geographic area, region and department and by category of use (Κατανάλωση ηλεκτρικής ενέργειας, κατά μεγάλη γεωγραφική περιοχή, περιφέρεια, νομό και κατά κατηγορία χρήσης),2012, ELSTAT.

Eleftheriadis G., Christofides G., Mavroudchiev B., Nedyalkov R., Andreev A. and Hristov L., 1989, "Tertiary volcanics from the East Rhodope in Greece and Bulgaria", Geol. Rhodopica, l, 202-217

Ersoy E.Y. and Palmer M.R., 2013, "Eocene-Quaternary magmatic activity in the Aegean: implications for mantle metasomatism and magma genesis in an evolving orogeny", Lithos 180-181, 5-24

Evrytanika News (2016), "The heated sidewalks melt ice in Karpenisi - How geothermal energy works on urban renewal project", evrytanika.gr, 31 January

2016, http://www.evrytanika.gr/index.php?option=com_content&view=article&id=1092971:2016-01-20-19-27-27&catid=43:2011-11- 19-19-46-40&Itemid=124 (accessed 16 May 2017)

Institute of Geology and Mineral Exploration, (I.G.M.E.), 2001, Map of Heat Flow Density in Greece, Scale 1:1,000,000, Athens

Fournadzhieva S., Pilarsky P., Arvanitis A., Fytikas M. & Koultsiakis E. (2002), "Use of Geothermal Fluids for Cultivation of the Microalga Spirulina in Nigrita - Serres", Proceedings, 7th National Conference on the Renewable Energy Sources, Institute of Solar Technology, Patras 6-8 November 2002, University of Patras, Vol. B, 97-104, http://solarinstitute.gr/wp-content/uploads/pdf//IHT 7o Synedrio B Tomos.pdf (accessed 16 May 2017)

Fytikas M., Andritsos N., Dalabakis P. & Kolios N. (2005), "Greek Geothermal Update 2000-2004", Proceedings World Geothermal Congress 2005, Antalya, Turkey, 24-29 April 2005, Paper Number 0172, 8 p.

Fytikas M. & Arvanitis A. (2011), "The Cultivation of Spirulina: An Innovative Geothermal Application in Greece", Presentation, GEOFAR European Conference "Innovative Solutions for Geothermal Energy Financing", Athens, 17 - 18 March 2011, https://www.slideshare.net/ApostolosArvanitis2/the-cultivation-of-spirulina-an-innovative-geothermal-application-in-greece (accessed 16 May 2017)

Fytikas M., Innocenti F., Manneti P., Mazzuoli R., Pesserillo G. and Villari L., 1985, "Tertiary to Quaternary evolution of the volcanism in the Aegean region", In: Dixon, J.E., Robertson, A.H.F. (eds.) The geological evolution of the Eastern Mediterranean, Spec. Publ. Geol. Soc., 17. Blackwells, Oxford, 687-699

Gelegenis J., Dalabakis P. & Ilias A. (2006), "Heating of wintering ponds by means of low enthalpy geothermal energy. The case of Porto Lagos", Geothermics, 35, 87-103

Gialoglou G. and Drymniotis D., 1983, "Northeastern Greece: mining activities, mineral exploration and future developments", Trans. Inst. Min. Metall., Sect. A 92, A180-183

Innocenti F., Kolios N., Manetti O., Mazzuoli R., Peccerilo G., Rita F. and Villari L., 1984, "Evolution and geodynamic significance of the Tertiary orogenic volcanism in northeastern Greece", Bull. Volcanol., 47, 25–37

I.G.M.E. (Institute of Geology and Mineral Exploration), 2009, "Geological Map of Greece, Scale: 1:50,000, Sheets: "Echinos" and "Medousa"

Jones C.E., Tarney J., Baker J.H. and Gerouki, F., 1992, "Tertiary granitoids of Rhodope, northern Greece: magmatism related to extensional collapse of the Hellenic Orogen", Tectonophysics, 210, 295-314

Kaiser-Rohrmeier M., von Quadt A., Driesner T., Heinrich C.A., Handler R., Ovtcharova M., Ivanov Z., Petrov P., Sarov S. and Peytcheva I., 2013, "Post-orogenic extension and hydrothermal ore formation: high precision geochronology of the Central Rhodopian metamorphic core complex (Bulgaria-Greece)", Econ.

Geol., 108, 691-718

Kalogeropoulos S.I., Kilias S.P. and Arvanitidis N.D., 1996, "Physicochemical conditions of deposition and origin of carbonate-hosted base metal sulfide mineralization, Thermes ore-field, Rhodope Massif, northeastern Greece", Mineralium Deposita, 31, 407-418

Karmis P. and Tsourlos P.I., 2004, "Transient electromagnetic surveys in mineral exploration", Proceedings, 1st International Conference on Advances in Mineral Resources Management and Environmental Geotechnology, Hania 2004, Greece, 95-100

Karagiorgas M., Mendrinos D. & Karytsas C. (2003), "Solar and geothermal heating and cooling of the European Centre for Public Law building in Greece", Renewable Energy, 29, 461–470, http://www.bonair.gr/data/24_1.pdf

Karytsas C. & Choropanitis I. (2013), "Alternative heating and cooling solutions in public buildings using geothermal systems", Presentation, REGEOCITIES, National Validation Workshop, Athens, 22 May 2013 (in Greek), http://regeocities.eu/wp-content/uploads/2013/06/3.C.-KARYTSAS-PRESENTATION-22-05-2013.pdf (accessed 16 May 2017)

Karytsas C. & Choropanitis I. (2013), "Geothermal systems for public buildings and swimming pools", Presentation, GROUND- MED Workshop "Ground Source Heat Pump Systems for Heating and Cooling in a Mediterranean Climate", Athens, 27 November 2013 (in Greek), http://www.cres.gr/kape/publications/pdf/Ground-Med/4. Karytsas C - GSHP studies.pdf (accessed 16 May 2017)

Kilias A., Falalakis G., Sfeikos A., Papadimitriou E., Vamvaka A. and Gkarlaouni C., 2013, "The Thrace basin in the Rhodope province of NE Greece - a Tertiary supradetachment basin and its geodynamic implications", Tectonophysics, 595-596, 90-105

Kirchenbaur M., Pleuger J., Jahn-Awe S., Nagel T.J., Froitzheim N., Fonseca R.O.C. and Münker C., 2012, "Timing of high-pressure metamorphic events in the Bulgarian Rhodopes from Lu–Hf garnet geochronology", Contrib. Miner. Petrol. 163, 897-921

Kokkinakis A., 1980, "Altersbeziehungen swischen Metamorphosen, mechanismen, deformationen and intrusionen and Sudrand, des Rhodope-Massives (Makedonicn, Griechenland)", Geol. Rundsch., 69.3, 726-744

Kolios N., Dalabakis P. & Arvanitis A. (2011), "Agricultural applications in the Neo Erasmio geothermal field (Thrace, Northeastern Greece)", Presentation, GEOFAR European Conference "Innovative Solutions for Geothermal Energy Financing", Athens, 17 - 18 March 2011, https://www.slideshare.net/ApostolosArvanitis2/agricultural-applications-in-the-neo-erasmio-geothermal-field- thrace-northeastern-greece (accessed 16 May 2017)

Kolios N. and Sarandeas A., 1990, "Thermal manifestations in the Rhodope Masif (Thermes Xanthi area)", Proceedings, 2nd Conference of Thermal Mineral Waters,

Thessaloniki 7-9 October 1988, 103-108 (in Greek)

Kojonen, Kari, K., Cook, Nigel, J. & Ojala, V. Juhani (ed.) 2007: Au-Ag telluride-selenide deposits. Geological Survey of Finland, Guide 53. 94 pages, 62 figures and 14 tables.

Kyriakopoulos K., 1987, "A geochronological, geochemical and mineralogical study of some Tertiary plutonic rocks of the Rhodope Massif and their isotopic characteristics", Ph.D. Thesis, University of Athens, 343 p. (in Greek)

Manev D., Katzkov N., Miler V., Malinov D., Arvanitidis N.D., Constantinides D.C., Dimadis E., Romaidis N. and Favas N., 1990, "Comparison between Madan (Bulgaria) and Thermes (Greece) ore fields. Geology and metallogenesis", 2nd Hellenic-Bulgarian Symp. Geology and Physical Geography of the Rhodope Massif, University of Thessaloniki, Geol. Rhodopica, 2, 399-408

Mavroudis V. (2014), "Practical applications of geothermal energy in buildings in Greece", BSc Thesis, School of Production Engineering and Management, Technical University of Crete, Chania, 123 p. (in Greek), dias.library.tuc.gr/view/manf/22889 (accessed 16 May 2017)

Marchev P., Downes H., Thirlwall M. F. and Moritz R., 2002, "Small-scale variations of 87Sr/86Sr isotope composition of barite in the Madjarovo low-sulphidation epithermal system, SE Bulgaria: Implications for sources of Sr, fluid fluxes and pathways of the ore-forming fluids", Mineralium Deposita, 37, 669-677

Marchev P., Kaiser-Rohrmeier B., Heinrich C., Ovtcharova M., von Quadt A. and Raicheva R., 2005, "Hydrothermal ore deposits related to post-orogenic extensional magmatism and core complex formation: the Rhodope Massif of Bulgaria and Greece", Ore Geol. Rev., 27, 53-89

Marchev P., Georgiev S., Raicheva R., Peytcheva, I., von Quadt, A., Ovtcharova, M. and Bonev, N., 2013, "Adakitic magmatism in post-collisional setting: an example from the early-middle Eocene Magmatic Belt in Southern Bulgaria and Northern Greece", Lithos, 180-181, 159-180

Márton I., Moritz R. and Spikings R., 2010, "Application of low-temperature thermochronology to hydrothermal ore deposits: formation, preservation and exhumation of epithermal gold systems from the Eastern Rhodope, Bulgaria", Tectonophysics, 483, 240-254

Meinhold G. and Kostopoulos D.K., 2013, "The Circum-Rhodope Belt, northern Greece: age, provenance, and tectonic setting", Tectonophysics, 595-596, 55-68

Melfos V., Vavelidis M., Christofides G. and Seidel E., 2002, "Origin and evolution of the Tertiary Maronia porphyry copper-molybdenum deposit, Thrace, Greece", Mineral Deposita, 37, 648-668

Melfos V. and Voudouris P., 2012, "Geological, Mineralogical and Geochemical Aspects for Critical and Rare Metals in Greece", Minerals, 2, 300-317, doi: 10.3390/min2040300

Melfos V. and Bogdanov K., 2012, "A field guide to the ore deposits of NE Greece",

19th-22nd October 2012, In the frame of the cooperation between the Aristotle University of Thessaloniki, the Sofia University "St. Kliment Ohridski", the Sofia University SEG Student Chapter, 19 p.

Melfos V. and Voudouris P., 2017, "Cenozoic metallogeny of Greece and potential for precious, critical and rare metals exploration", Ore Geology Reviews, 89, 1030–1057

Mendrinos D. & Karytsas C. (2005), "Geothermal Energy, Geothermal Heat Pumps, CRES Experience", Mining & Metallurgical Annals, 15, July - December 2005, 29 p, (in Greek) http://www.cres.gr/kape/pdf/geotherm/22.pdf (accessed 16 May 2017)

Mendrinos D., Karagiorgas M. & Karytsas K., "Use of geothermal heat pumps for heating of buildings in Greece", http://www.lowex.net/guidebook/additional_information/lowexx/3_lowexx_paper_gr.pdf (accessed 16 May 2017)

Mendrinos D. & Karytsas C., "Geothermal heat pumps", EnergyReS, http://library.tee.gr/digital/books_notee/book_60568/book_60568_mendrinos.pdf (accessed 16 May 2017)

Meyer W., 1968, "Zur alterstellumg des plutonismus im Sudteil der Rila-Rhodope masse (Nordgrienchenland)", Geol. Palaeontologica, 2, 173-192

Minissale A., Duchi V., Kolios N. and Totaro G., 1989, "Geochemical characteristics of Greek thermal springs", Journal of Volcanology and Geothermal Research, 39, 1-16

Moritz R., Márton I., Ortelli M., Marchev P., Voudouris P., Bonev N., Spikings R. and Cosca M., 2010, "A review of age constraints of epithermal precious and base metal deposits of the Tertiary Eastern Rhodopes: coincidence with Late Eocene-Early Oligocene tectonic plate reorganization along the Tethys", In: Christofides, G., et al. (Eds.), Proceedings of the XIX Congress of the Carpathian-Balkan Geological Association, Thessaloniki. Scientific Annals of the School of Geology A.U.Th., 100, 351-358

Mposkos E., Liati A., Katagas, C. and Arvanitidis, N.D., 1990, "Petrology of the metamorphic rocks of West Rhodope, Drama area, N. Greece", 2nd Hellenic-Bulgarian Symp. Geology and Physical Geography of the Rhodope Massif, University Thessaloniki, Geol. Rhodopica, 2, 127-142

Mposkos E.D. and Kostopoulos D.K., 2001, "Diamond, former coesite and supersilicic garnet in metasedimentary rocks from the Greek Rhodope: a new ultrahighpressure metamorphic province established", Earth Planet. Sci. Lett., 192, 497-506

Pe-Piper G. and Piper D.J.W, 2002, "The igneous rocks of Greece. The anatomy of an orogen", Beiträge der regionalen Geologie der Erde 30. Berlin-Stuttgart. 573 p.

Pe-Piper G. andPiper, D.J.W., 2006, "Unique features of the Cenozoic igneous rocks of Greece", Geol. Soc. Am., Spec. Pap., 409, 259-281.

Perugini D., Poli G., Christofides G., Eleftheriadis G., Koroneos A. and Soldatos T.,

2004, "Mantle-derived and crustal melts dichotomy in northern Greece: spatiotemporal and geodynamic implications", Geol. J., 39, 63–80

Savvanis P. , "Municipality of Karpenisi: Pavement snow melting and deicing using geothermal energy", https://web.facebook.com/pg/energyautomation/photos/?tab=album&album_id=1692981290916253 (accessed 16 May 2017)

Sideris G.N. and Papakonstantinou C. N., 1990, "Application of geophysical borehole logging in the Kato Thermes area", Technical Report, I.G.M.E., Athens, 28 p. (in Greek)

Sklavounos S., 1981, "The Paranesti granite (Mineralogy-Petrography)", Ph.D. Thesis, Univ. of Thessaloniki, Greece, 175 p. (in Greek)

Soldatos T., Koroneos A., Christofides G. and Del Moro A., 2001, "Geochronology and origin of the Elatia plutonite (Hellenic Rhodope Massif, N Greece) constrained by new Sr data", N. Jb. Miner. Abh., 176, 179-209

Stylianou G. (2007), "Heating of Traianoupolis Spa facilities (Evros area) with geothermal water", Presentation, Workshop "Development of geothermal applications for heating-cooling and energy saving", Thessaloniki, 11 December 2007 (in Greek)

Teneva-Georgieva S.I. and Andreev A., 2005, "The Erma Reka Low-Enthalpy System (S-Bulgaria) -Geothermal Characteristics", Proceedings, World Geothermal Congress 2005, Antalya, Turkey, 24-29 April 2005, 7 p.

Tsirambides A. and Filippidis A, 2012, "Exploration key to growing Greek industry", Industrial Minerals, 44-47.

Turpaud P. and Reischmann T., 2010, "Characterisation of igneous terranes by zircon dating: implications for UHP occurrences and suture identification in the Central Rhodope, northern Greece", Int. J. Earth Sci. 99, 567-591

Vassileva R.D., Bonev I.K., Marchev P. & Atanassova R., 2005, "2-1: Pb-Zn deposits in the Madan ore field, South Bulgaria", In: "Geodynamics and Ore Deposit Evolution in Europe", Eds: D. Blundell, N. Arndt, P.R. Cobbold and C. Heinrich, Box 2-1, 90-91

Vassileva R.D., Atanassova R. and Bonev I.K., 2009, "A review of the morphological varieties of ore bodies in the Madan Pb-Zn deposits, Central Rhodopes, Bulgaria", Geochemistry, Mineralogy and Petrology, 47, 31-49

Vassileva R.D., Atanassova R. and Bonev I.K., 2010, "Morphogenetic types of ore bodies, ore textures and crystallization mechanisms in the hydrothermal Madan deposits, Central Rhdopes", Scientific Annals, Special Volume 99, Proceedings of the XIX CBGA Congress, Thessaloniki, Greece, 355-361

Voudouris P., Spry P.G., Melfos V. and Alfieris D., 2007, "Tellurides and bismuth sulfosalts in gold occurrences of Greece: mineralogical and genetic considerations", Geologian tutkimuskeskus, Opas 53 - Geological Survey of

Finland, Guide 53, 85-94

Voudouris P., Spry P.G., Melfos V., Haase K., Reiner K., Mavrogonatos C., Repstock A. and Alfieris D., 2018, "Gold deposits in Greece: Hypogene ore mineralogy as a guide for precious and critical metal exploration", Conference Proceedings Paper, International Electronic Conference on Mineral Science 2018 - IECMS 2018, 13 p., DOI: 10.3390/IECMS2018-05452

Vrachopoulos M., Fytrolakis N., Kyrousis N. & Kravvaritis E. (2005), "Energy saving by exploiting normal geothermal energy at the NTUA Campus, Zografos" , 5o RENES Conf. , Athens, 7 p., http://poseidonenergy.gr/content%5CEMP_anak_22-02-05f.doc (accessed 16 May 2017)

Wüthrich E., 2009, "Low temperature thermochronology of the Northern Aegean Rhodope Massif", Unpublished Doctoral thesis, Zürich, Switzerland, ETH Zürich, 216 p.

http://www.rae.gr/old/sub3/3B/3b3.htm

ENERGYPRESS(2016),https://energypress.gr/news/xekinise-i-kataskeyi-paragogikis-geothermikis-geotrisis-stin-traianoypoli (accessed 16 May 2017)

e-evros.gr (2016), http://www.e-evros.gr/gr/eidhseis/3/ner http://adesmeuti-thrakis.blogspot.gr/2017/04/blog-post_469.html (accessed 16 May 2017)

http://www.thessnews.gr/article/33498/ependysi-7-ek-eyro-apo-ton-omilo-eythymiadi-gia-thermokipia-me-geothermia-stin- kessani (accessed 16 May 2017)

http://www.agrotika-nea.gr/a/ston-omilo-eythymiadh-h-diaxeirish-toy-gewthermiko/22803764 (accessed 16 May 2017)

ethnos.gr (2016), http://www.ethnos.gr/koinonia/arthro/thermokipia_me_xorigo_ti_fysi-64389658 (accessed 16 May 2017)

Selecta Klemm (2016), "New Production location Selecta Hellas", http://www.selecta-one.com/en/posts/New_Production_location_Selecta_Hellas/latest_news/08203125843/ (accessed 16 May 2017)

Annexes

Contact projects@eurogeologists.eu for the full list of Annexes, or open it at the CHPM Information Platform on Prospective Locations (http://bit.ly/CHPMinfoplatform)

Table 1

Prospective CHPM area

MFT Hungary							
Number	**Type of the selected area(s) (type "A" or type "B")**	**Depth(s) of the metal enrichment(s) (m)**	**Temperature /at these depths/ (°C)**	**Description of the metal enrichment(s)**			
				degree of the mineralization(s) (% or ppm)	***type of the mineralization(s)[1]***	***element(s)***	***area delineation(s) (WGS84)[2]***
1	B	1100-1200	62	0,09-1,25% Cu	Skarn and veins	Cu	Latitude 47.92303 N Longitude 20.07241 E
				1,65-11,1% Zn	Skarn and veins	Zn	
				13,8-27,0% Fe	Skarn and veins	Fe	

Name: Recsk, Deeper polimetalic ore

Coordinates: Recsk RM-90 borehole x=-48994,64 y=-76606,26 z=+217,465 m above sea level (Hungarian Stereo system)

[1] Like skarn, porphy, etc.

[2] There are 3 options for the indication of the area delineation: a. coordinates (latitude, longitude) of 1 point; b. coordinates (latitude, longitude) of 1 points and radius (m); c. coordinates (latitude, longitude) of more points.

Evaluation of the basic characteristics of prospective CHPM areas

MFT

Hungary

AREA 1 – Recsk

1. **Geology of the prospective area**

Requested information on:

- ✓ local geology (in regional context)
- ✓ CHPM target formation
- ✓ list of available cross sections, geological maps, geochemical results, lithological information

Notes: briefly summarized, referenced to more detailed studies.

The most geological and geophysical information come from 3 large exploration campaign: 1) 1960-1968 Deep Drilling project from surface and underground drillings)Gagyi-Pálffy et al. 1971, Cseh-Németh et al. 1984). 2) 1970-1976 Exploration of Lejtakna ore mineralization (Baksa 1984). 3) 1993-1997 Re-examination of Lahóca and Veresagyagbérc zone (Földessy et al. 1997).

The ore deposit of Recsk (NE-Hungary) located in the Mátra Mts, which belongs to the Paleogene igneous complex. The Paleogene volcanic outcrops can be found along the Darno Zone. The Paleogene magmatism (diorite, quartz-diorite) penetrated to Mesozoic rocks (limestone, sandstone, shale). The Cu porphyry ore was formed inside the magmatic intrusion. The skarn mineralisation occurs along the contact between the magmatic intrusion and the Mesozoic limestone.

https://map.mbfsz.gov.hu/furas/ : You can find here the archive boreholes in Hungary (name of the borehole, coordinates and other data)

Important studies and monographs:
Földessy & Hartai (ed) (2008)
Supplementum (1975)

2. **Geophysics of the prospective area**

Requested information:

- ✓ previous geophysical measurements (in CHPM relevance)
- ✓ geophysical results that can be used for locating/defining the deep metal enrichment
- ✓ list of available geophysical maps, cross sections, logs, other measurements

The position of the magmatic bodies of Recsk is well determined by some geophysical measurements: airborne magnetic, radioactive spectrometry and EM geophysical surveys have been carried out. Attached maps in annexes.

Important studies:
Morvai & Viola (1975)
Szalay (1975)
Zelenka & Kiss (2008)

3. **Deep metal enrichment**

Requested information:

- ✓ **(**expected) metal enrichment based on available geophysical, geological and drill data, samples information, geochemistry

Cu-Au porphyry ore: The main ore mineralisation was identified between 700-900 m below the surface within diorite porphyry. The main ore minerals are chalcopyrite, pyrite, molybdenite and few magnetite. Top of the ore zone is at ~500 m below the surface. The average copper grade is 0.4%, in the high grade zones (cut-off 0.8%) the average Cu grade can be 1.1%, which is located in the transition zone to the skarn deposit. The grade of the gold occurrence is between 0.2-1.5 g/t.

Cu-Au skarn: There is two skarn ore bodies: 500-700 m (unexplored) and 900-1100 m below the surface. The skarn mineralisation occurs along the contact of the magmatic and sedimentary rocks, but the richest ore zone could be found by the contact of the limestone (dolomite), siltstones and the diorite porphyry. The copper enrichment can reach the 2.3% but the average grade is between 1-2%. . The grade of the gold occurrence can reach the 1.1 g/t.

Important studies
Földessy & Hartai (ed) (2008)
Supplementum (1975)

4. **Integrated 3D- 4D model**

Requested information:

- ✓ existing 3D-4D models of the target area and the deep metal enrichment
- ✓ if no 3D-4D models exist, collect the following necessary data: geological setting, mineralization, fluid flow models, stress field determination

Notes: e.g. openly available datasets, models.

There are no available public 3D-4D models but the archive drilling descriptions, manuscripts of the exploration reports are available (in Hungarian) in the Mining and Geological Survey of Hungary.

5. **EGS potential**

Requested information:

- ✓ EGS potential (heat & energy) of the area
- ✓ geothermal characteristics (temperature gradient, heat flux, stress field, water availability, EGS geology)
- ✓ presence/indication of deep fluids/brines, fracture system, crustal permeability

The average temperature gradient is between 3°C - 4°C/100 m within the magmatic intrusion. The Mesozoic rocks have ~ 5°C/100 m temperature gradient. The temperature is at the 800 m below the surface (main Cu porphyry zone) is ca. 45-50°C and at 1000 m below the surface (Cu skarn) is ca. 55-60°C.

Important studies:
Földessy & Hartai (ed) (2008)
Supplementum (1975)

List of references

Baksa, Cs. (1984): The genetic framework of the Recsk ore genesis, C

Cseh-Németh, J. (1984): Final report of the Recsk surface drilling exploration (Manuscript in Hungarian)

Gagyi-Pálffy, A. (1971): Final report of the Recsk deep ore exploation (Manuscript in Hungarian)

Földessy, J. (1997): Gold exploration of Recsk-Lahóca area, Földtani Kutatás, Vol. 34, pp. 12-15

Földessy, J., Hartai, É. (ed) (2008): Recsk and Lahóca, Geology of the Paleogene Complex, Miskolc University Press, Series A, Mining, Vol. 73., 226 p.

Morvai, L., Viola, B. (1975): Results of well-logging at Recsk, Bulletin of Hungarian Geological Society, Vol. 105, pp. 733-739 (in Hungarian with English abstract and figures)

Supplementum: Special edition of Bulletin of Hungarian Geological Society, 1975, Vol. 105, pp. 559-754 (Publications of the Recsk ore deposit Conference 1974) (in Hungarian with English abstracts and figures)

Szalay I. (1975): Geophysical measurements for structural-geological purposes in the esploration area of Recsk and their results, Bulletin of Hungarian Geological Society, Vol. 105, pp. 724-732 (in Hungarian with English abstract and figures)

Zelenka, T. (1975): Bulletin of Hungarian Geological Society, Vol. 105, pp. 582-597 (in Hungarian with English abstract and figures)

Zelenka T., Kiss J. (2008): The structure of the Recsk paleogene magmatites from the aspects of geophysical and geological data in Földessy, J., Hartai, É. (ed), Recsk and Lahóca, Geology of the Paleogene Complex, Miskolc University Press, Series A, Mining, Vol. 73., pp. 21-32

Annexes

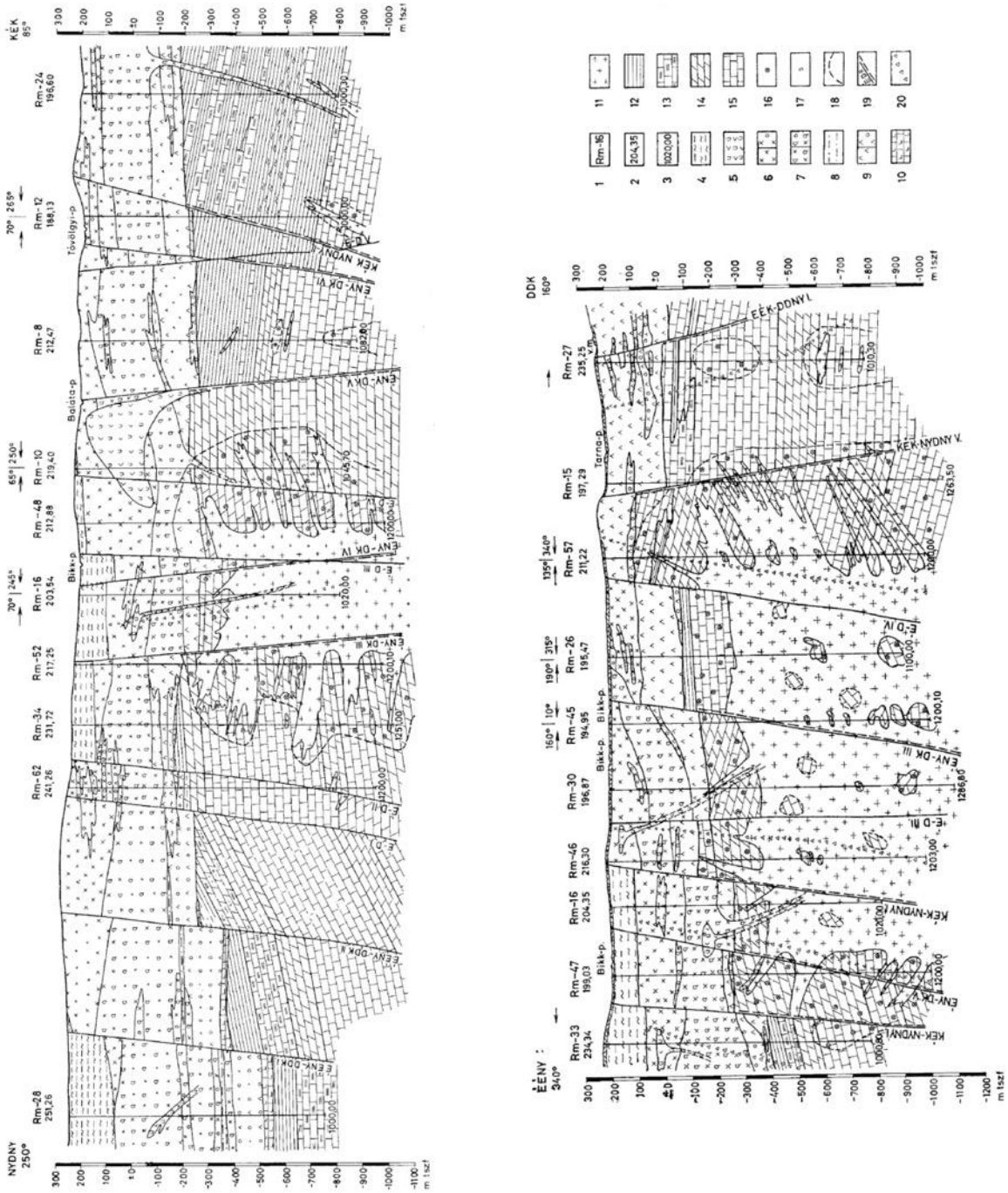

1. Figure: Geological section of the subvolcanic ore prospecting area of Recsk in transversal and strike direction. Legend: 1) Site, symbol and number of exploratory borehole. 2) Altitude (above Baltic ea level) of exploratory borehole. 3) Final bottom hole depth of exploratory borehole. 4) Clayey Marl (Middle Oligocene). 5) Pyroxene-hornblende andesite. 6) Biotite-hornblende andesite and its agglomerates. 7) Quartzbiotite-hornblende andesite. 8) Glauconite-tuffitic marl. 9) Hornblende-biotite andesite. 10) Bizuminous limestone. 11) Subvolcanic biotite-hornblende andesite. 12) Shale. 13) Limestone with shale bands. 14) Quartzite, siliceous schist. 15) Limestone. 16) Limestone injected by andesite. 17) Skarnified rock. 18) Track, direction and number of plotted tectonic plane. 20) Breccious tectonic zone (Zelenka, 1975)

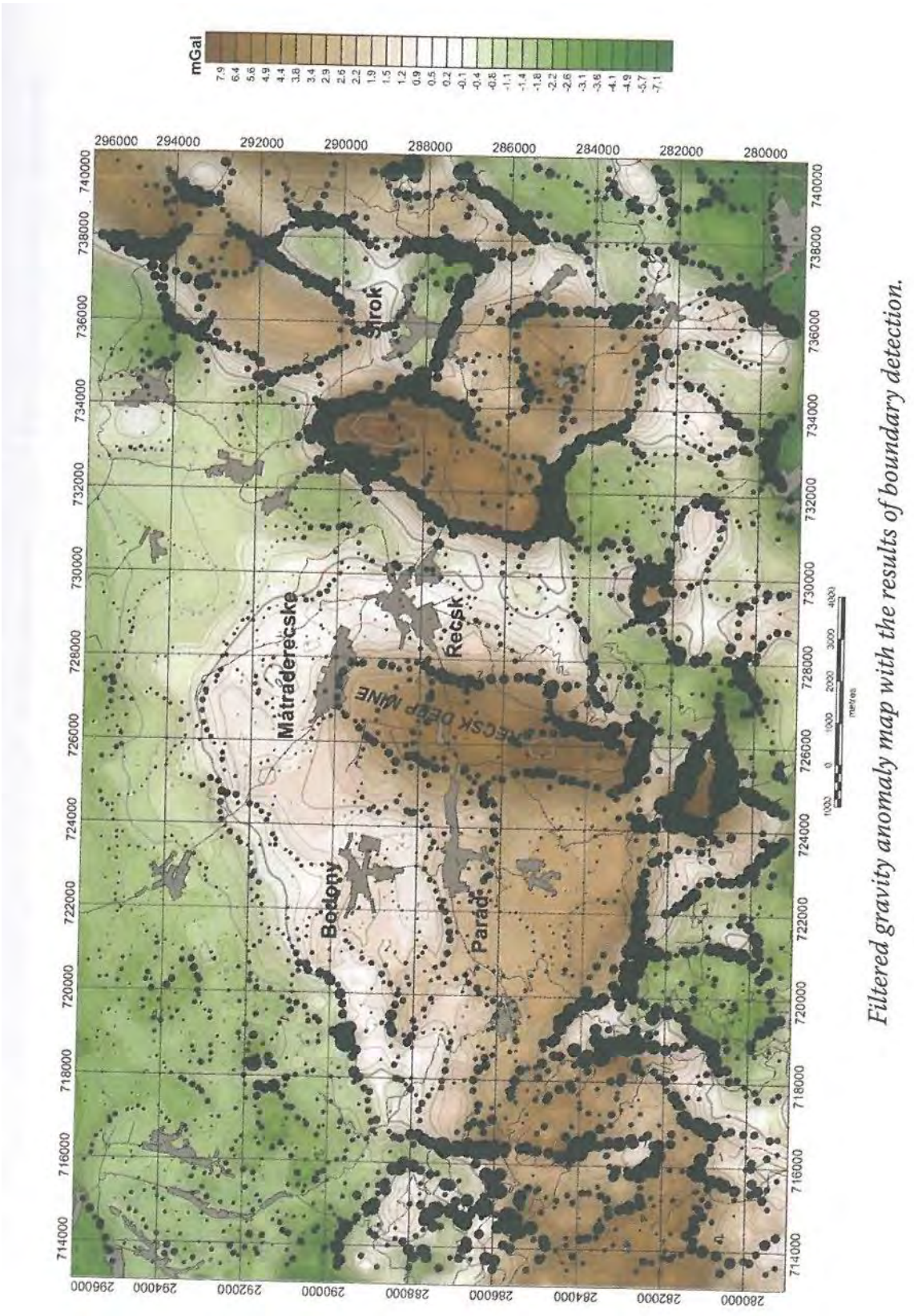

Filtered gravity anomaly map with the results of boundary detection.

2. Figur:e (Zelenka & Kiss, 2008)

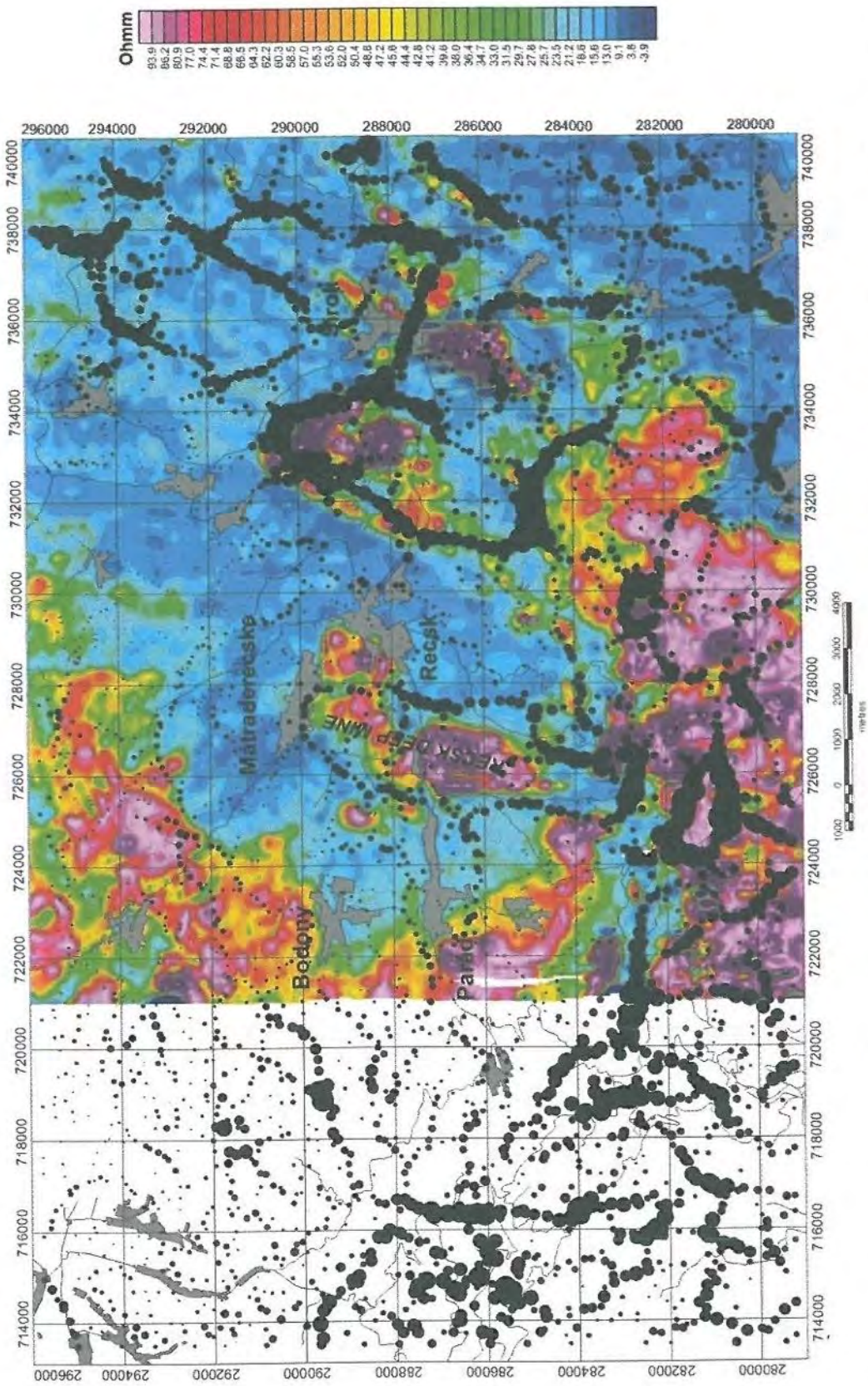

Apparent resistivity map from the airborne measurements with the results of gravity boundary detection.

3. Figure: (Zelenka & Kiss, 2008)

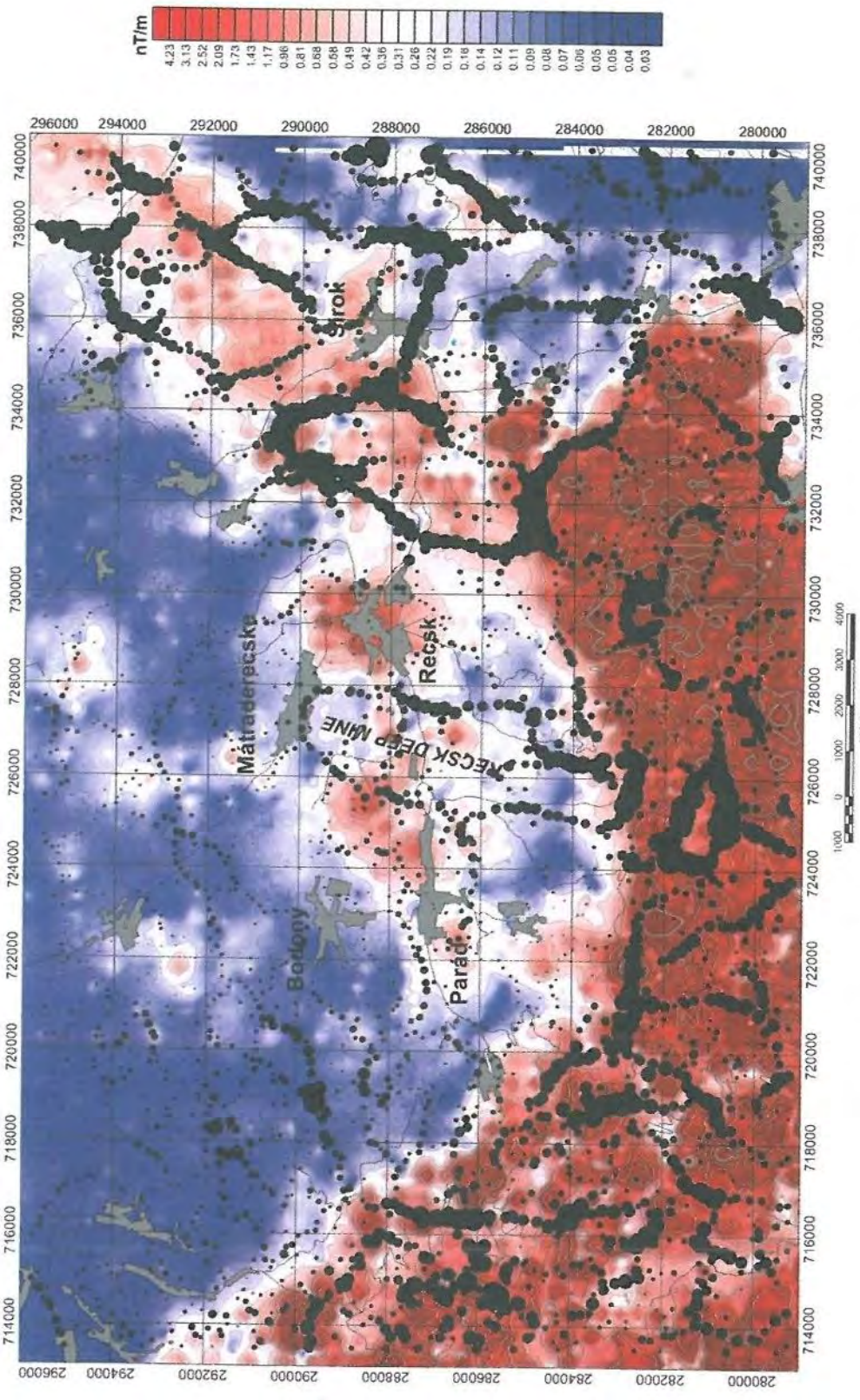

Analytical signal map from airborne magnetic measurements with the results of gravity boundary detection (Kiss, 1995).

4. Figure: (Zelenka & Kiss, 2008)

Table 1

Prospective CHPM areas

Ireland							
Number	**Type of the selected area(s) (type "A" or type "B")**	**Depth(s) of the metal enrichment(s) (m)**	**Temperature /at these depths/ (°C)**	**Description of the metal enrichment(s)**			
				degree of the mineralization(s) (% or ppm)	***type of the mineralization(s)[1]***	***element(s)***	***area delineation(s)[2]***
1. Mourne Mountains	Type A	Not available	~100	Not available	Not available	Thorium, Arsenic, Tin, Yttrium, Niobium, Manganese and Cerium.	54.1533N, 6.0663W
2							
3							
4							
5							
6							

[1] Like skarn, porphy, etc.

[2] There are 3 options for the indication of the area delineation: a. coordinates (latitude, longitude) of 1 point; b. coordinates (latitude, longitude) of 1 points and radius (m); c. coordinates (latitude, longitude) of more points.

Evaluation of the basic characteristics of prospective CHPM areas

Name of the National Association (LTP)
Number of the prospective area (1-6)

1. **Geology of the prospective area**

Requested information on:

- ✓ local geology (in regional context)
- ✓ CHPM target formation
- ✓ list of available cross sections, geological maps, geochemical results, lithological information

Notes: briefly summarized, referenced to more detailed studies.

The CHPM target formation is the Mourne Mountain Granite Complex which is composed of granites ranging from G1 (oldest) to G5 (youngest) as presented in Figure 1. These rocks are formed in the Palaeogene Period approximately 23-66 Million years ago.

Figure 1. Geological map of Mourne Mountains (Moore et al, 2013)

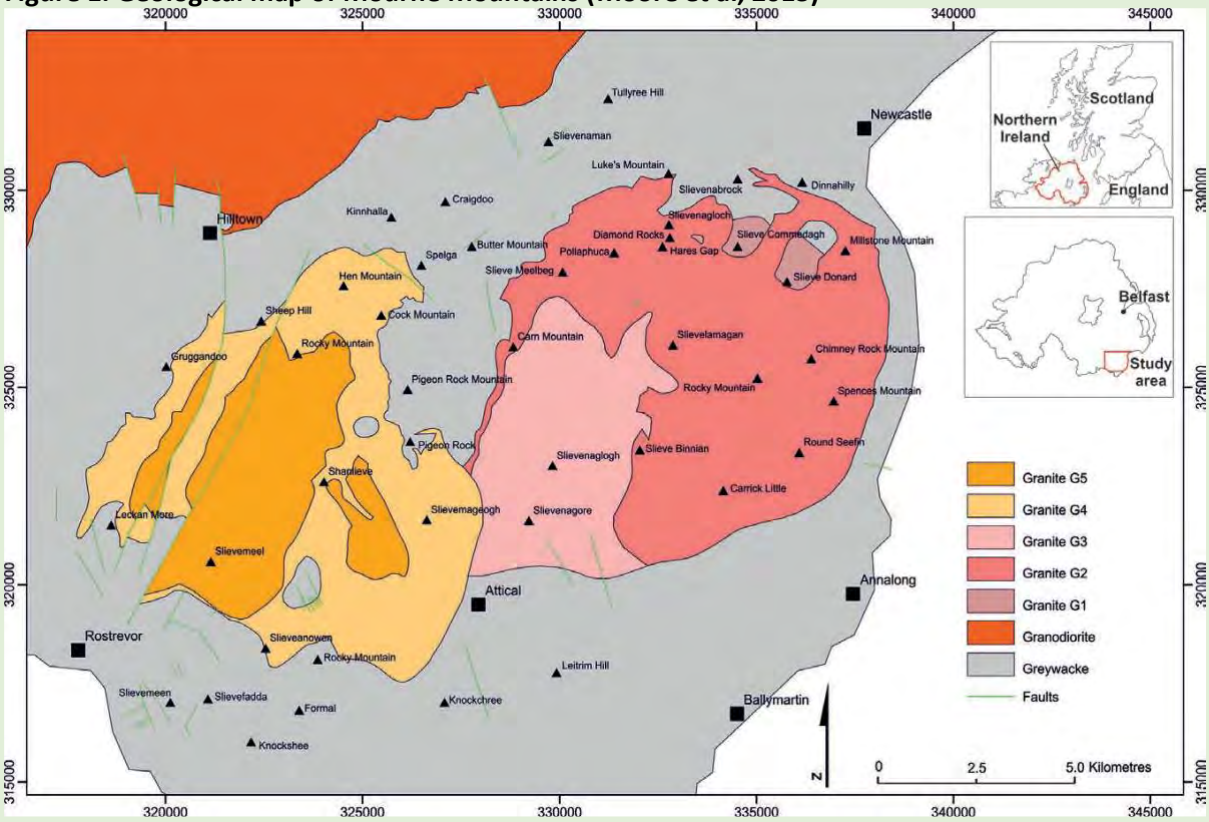

Geological mapping in the region has identified a number of faults which are shown in Figure 2.

Figure 2. Fault mapping in Mourne granite Complex (UCD Fault Analysis Group)

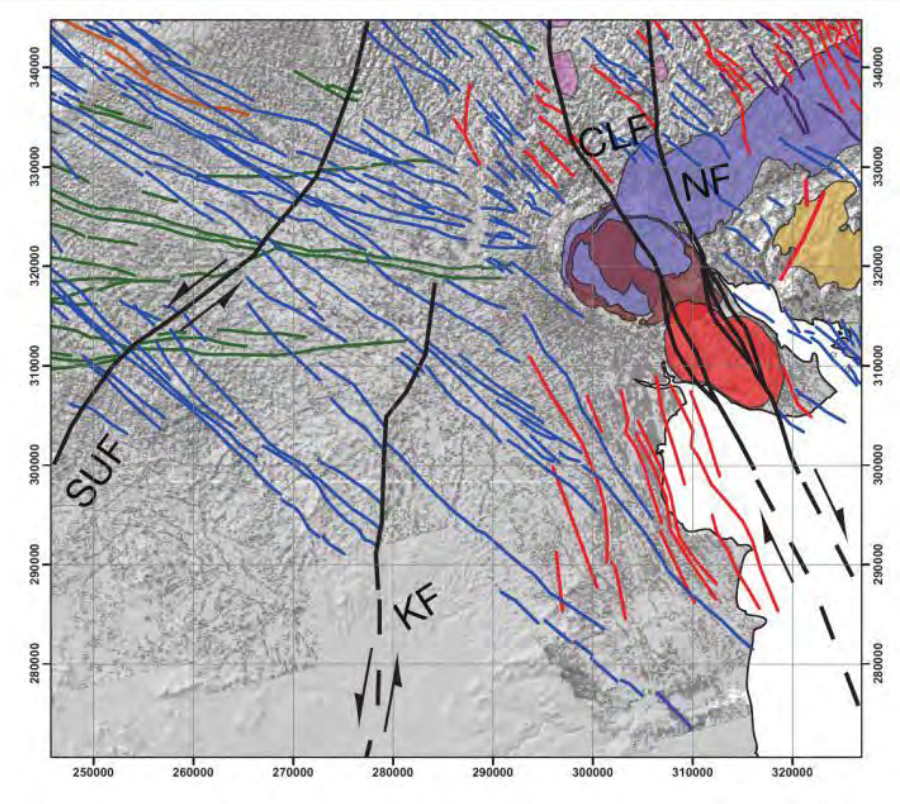

No borehole data is available to allow deep geochemical data to be analysed, however as part of the Tellus Border project, samples were collected from stream sediment. Geochemical data is available for these and the sampling locations are shown in Figure 3.

Figure 3. Tellus sample locations (Moore et al, 2013)

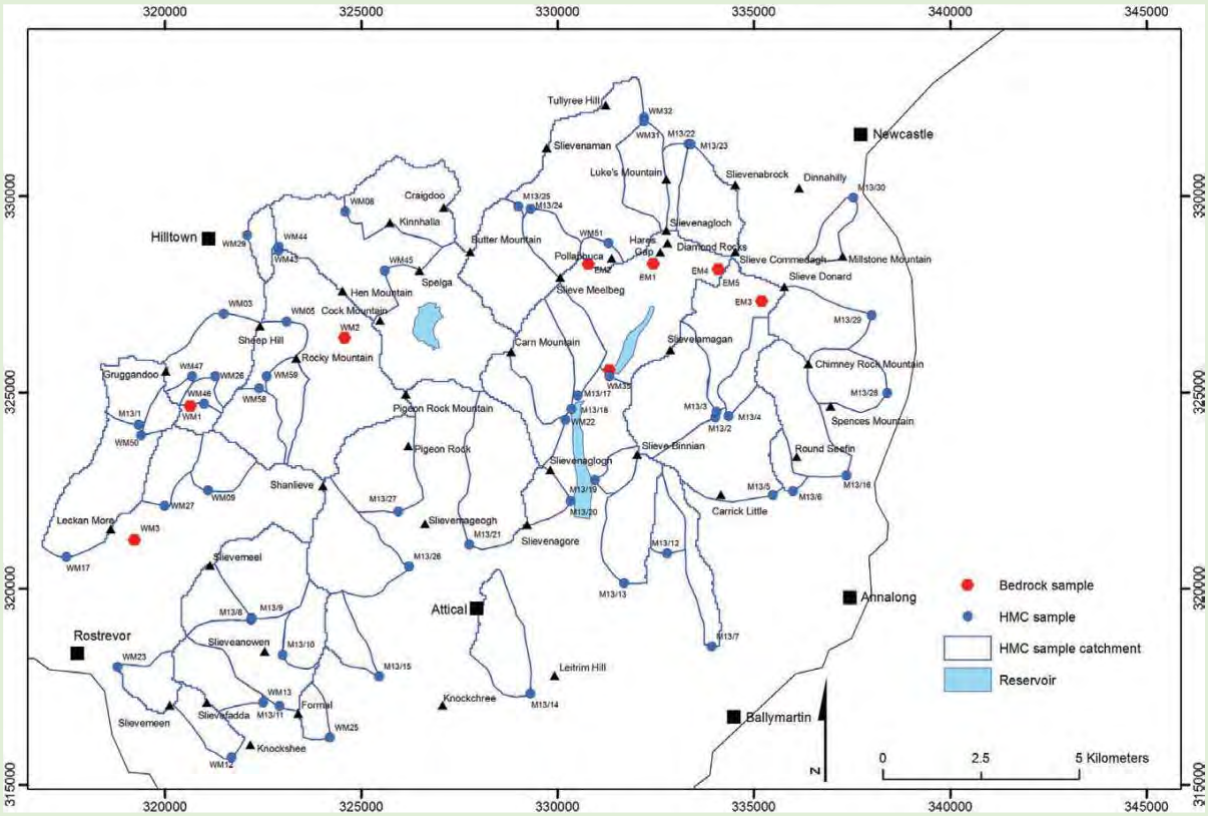

2. Geophysics of the prospective area

Requested information:

- ✓ previous geophysical measurements (in CHPM relevance)
- ✓ geophysical results that can be used for locating/defining the deep metal enrichment
- ✓ list of available geophysical maps, cross sections, logs, other measurements

Tellus geophysics data is available for download at https://www.bgs.ac.uk/gsni/tellus/data_licensing/index.html

Figure 4 shows radiometric data from Tellus and three magnetotelluric survey lines across the Mourne Mountains complex. The Mourne Mountains complex contains High Heat Production granites because they contain anomalously high concentrations of radiogenic elements, confirmed by geochemical analyses and the Tellus airborne radiometric data (Reay & Raine 2015, Figure 5)

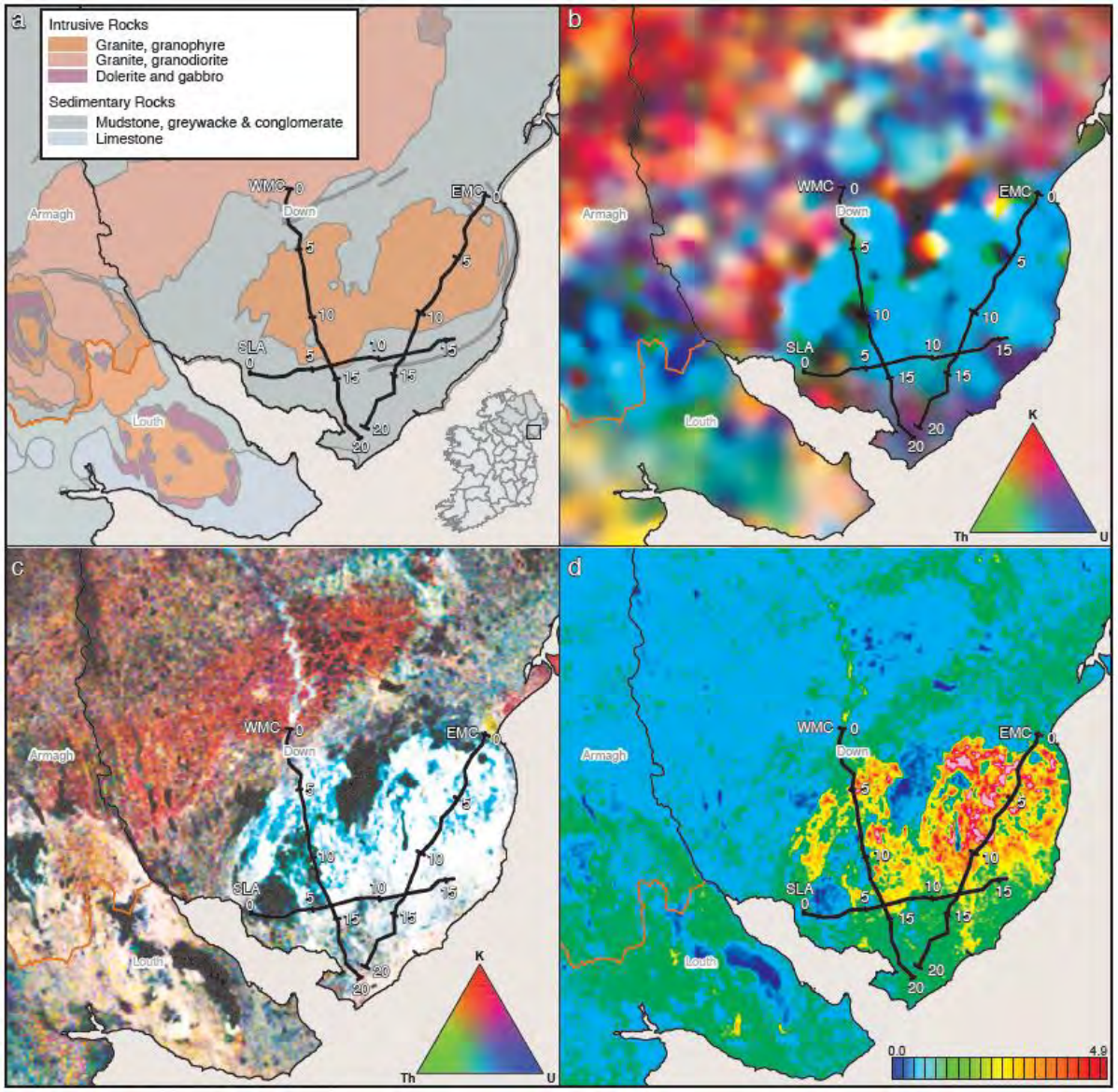

Figure 4. The Mourne Mountains Complex: (a) geology; (b) ternary image of soil U, Th and K; (c) ternary image of AGRS eU, eTh and K; (d) radiogenic heat production. EMC, Eastern Magmatic Centre; WMC, Western Magmatic Centre. Black lines are three MT survey lines, numbered with distances (km). From Ture et al. (2016)

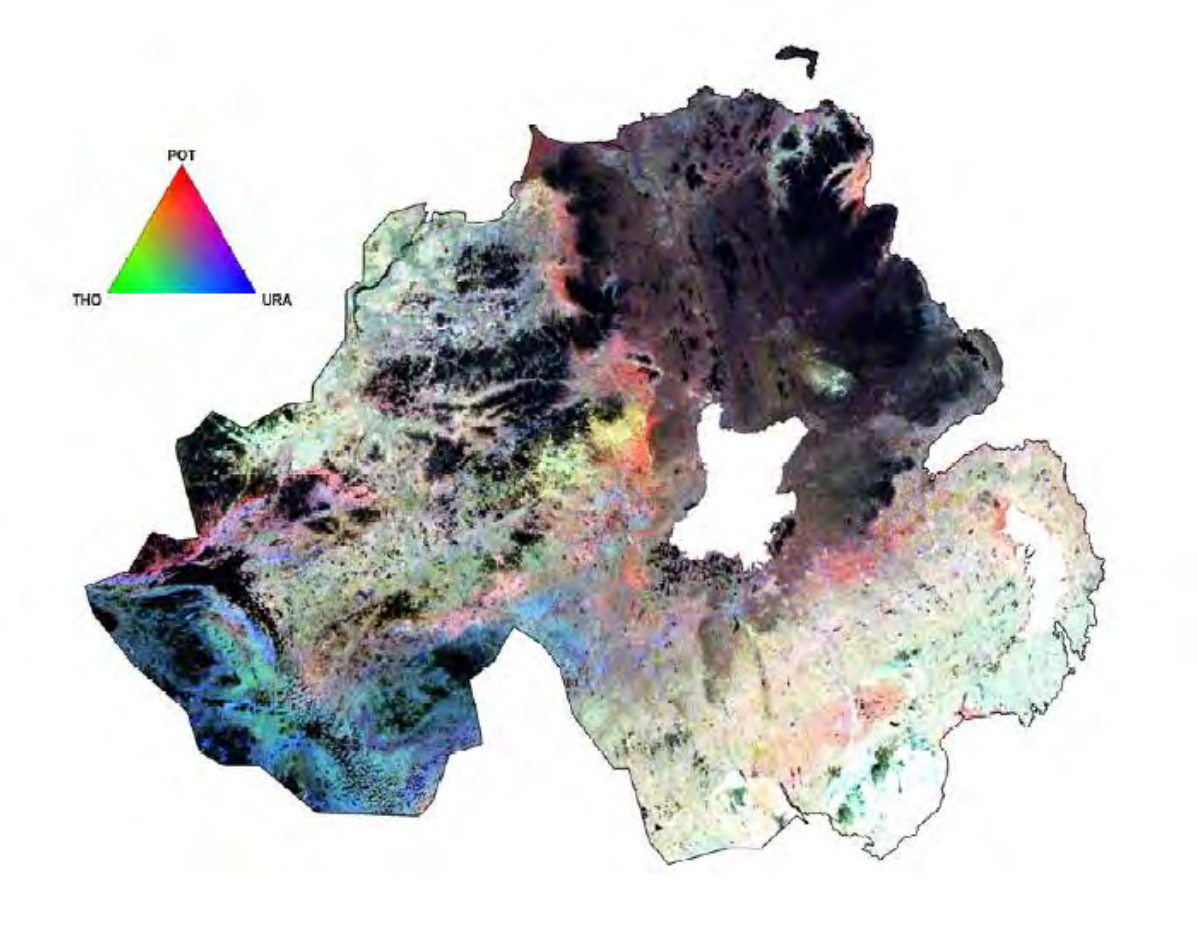

Figure 5. Ternary colour image of radiometric data (Red = Potassium=POT, Green = Thorium=THO and Blue=Uranium=URA). The granitic Mourne Mountains Complex stands out in white (where all three elements are high) and turquoise (where Uranium and Thorium are high relative to Potassium)

3. **Deep metal enrichment**

Requested information:

✓ **(**expected) metal enrichment based on available geophysical, geological and drill data, samples information, geochemistry

No deep geochemical data is available for the area, however geochemical analysis of the stream sediment has indicated that there are critical metals present in the Mourne granites as indicated in Figure 6.

Figure 6. Example analysis for concentrations of Sn in stream sediment in Mourne Mountains (Moore et al, 2013)

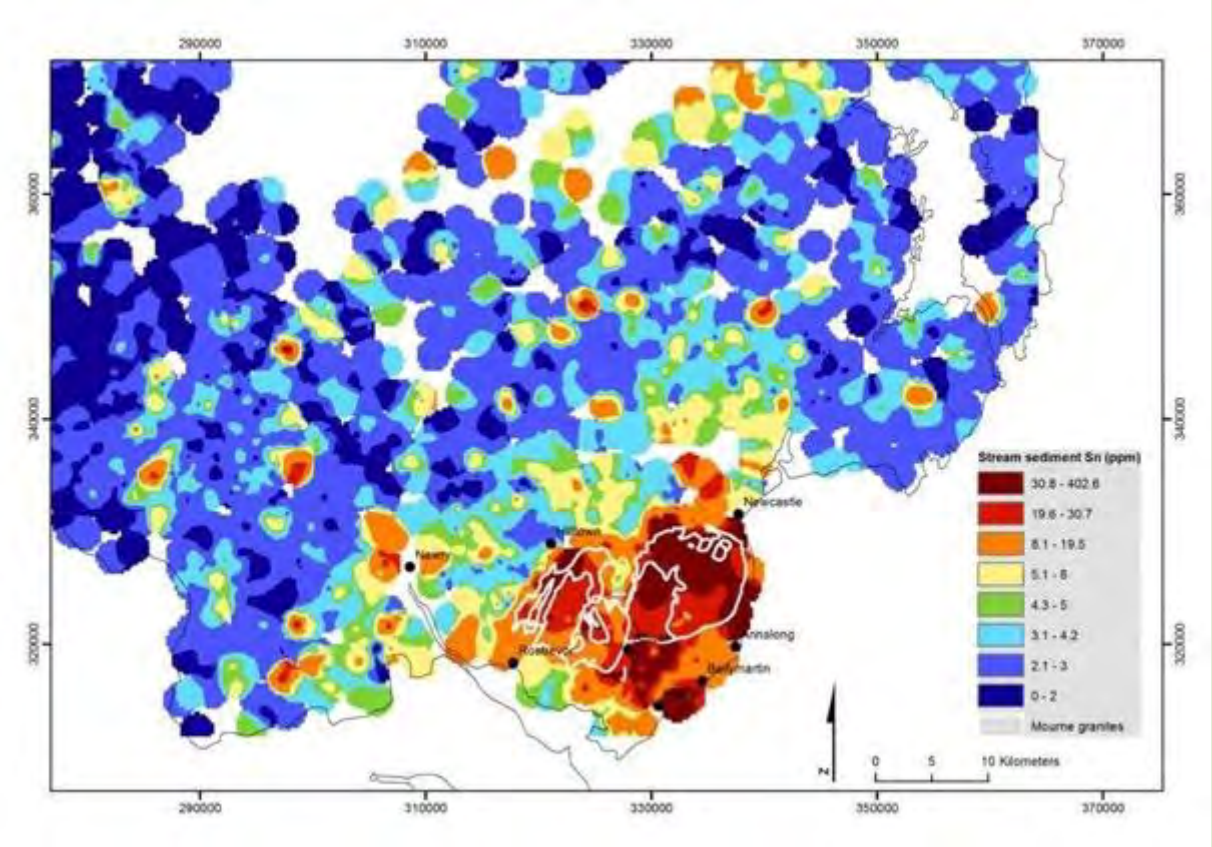

4. **Integrated 3D- 4D model**

Requested information:

- ✓ existing 3D-4D models of the target area and the deep metal enrichment
- ✓ if no 3D-4D models exist, collect the following necessary data: geological setting, mineralization, fluid flow models, stress field determination

Notes: e.g. openly available datasets, models.

No 3D-4D models available

5. EGS potential

Requested information:

- ✓ EGS potential (heat & energy) of the area
- ✓ geothermal characteristics (temperature gradient, heat flux, stress field, water availability, EGS geology)
- ✓ presence/indication of deep fluids/brines, fracture system, crustal permeability

In 2009 a borehole was drilled at Silent Valley in the central Mourne Mountains to a depth of 601.5m, and a suite of geophysics logs run. The temperature log showed a geothermal gradient of 21.07°C/km, although granite core samples sent for thermal conductivity analysis showed typical values. Existing regional gravity data is confined to the roads and sparse over the mountainous granite complex so the granite bodies cannot be modelled accurately. Infill gravity data was acquired by Terradat as part of the project and this additional data should help to improve the 3D modelling.
Potential as an Enhanced Geothermal System (EGS) is reduced by the fact that the granite forms the surface outcrop rather than being covered by a blanket of low thermal conductivity insulating sedimentary rocks. The calculated radiogenic heat maximum is 4.8 µW/m³, similar to calculations of heat generated at other Hot Dry Rock locations in the UK (Reay & Kelly, 2010).

Core and data is available from Geological Survey of Northern Ireland.

No data on the presence of deep fluids/brines, fracture system, or crustal permeability are available.

Geothermal modelling indicates that the temperatures in the Mourne Mountains area are likely to be in the order of 100°C as shown on Figure 7.

Figure 7. Deep geothermal resource map (Goodman et al, 2004)

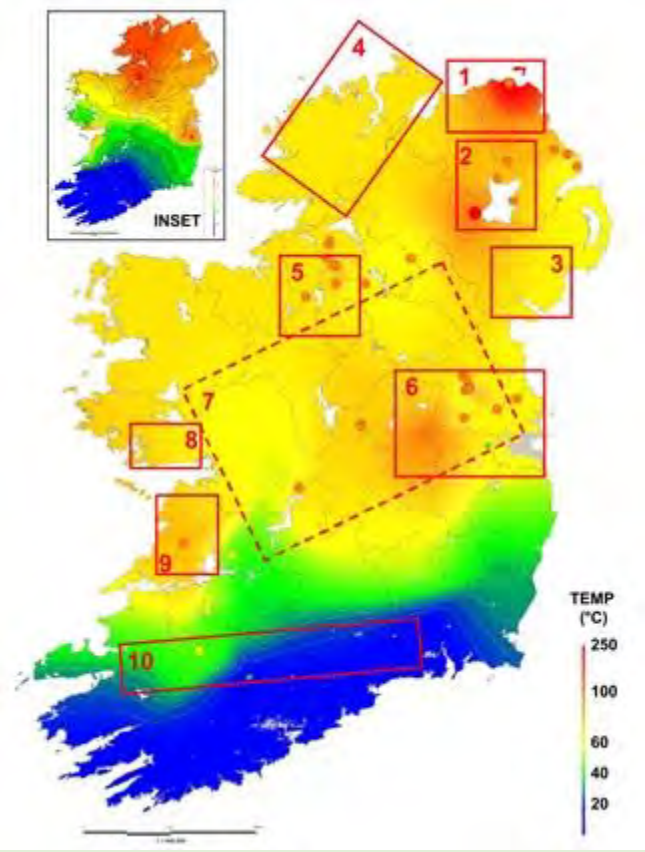

List of references

Beamish, D., and Young, M., (2009) The Geophysics of Northern Ireland: the Tellus Effect. First Break. Vol.27, No 8

Goodman, R., Jones, G.L., Kelly, J., Slowey, E. and O'Neill, N. (2004). Geothermal Resource Map of Ireland. Prepared for Sustainable Energy Ireland.

Jones, G.L., Goodman, R., Pasquali, P., Kelly, J.G., O'Neill, N. and Slowey, E. (2007). The status of Geothermal Resource Development in Ireland. Proceedings European Geothermal Congress 2007, pp. 3, Unterhaching, Germany, 30-May – 1 June 2007.

Moore, K., Lusty, P. and Moles, N (2013). Tracing the mineralogical source of Tellus geochemical anomalies in the Mourne Mountains to investigate processes that concentrate critical metals. The Tellus Border Results and Research Conference 2013.

Moore, K. (2013). Critical Metal potential of the Mourne Mountains: the geological source of Rare Earth Elements, Nb, Ta, W and U anomalies - insights from Tellus data. University of Exeter.

Reay, D. and Kelly, J., (2010). Deep geothermal energy resource potential in Northern Ireland, European Geologist, 29, 14–18.

Ture, M.D., Reay, D.M., Muller, M.R., Yeomans, C.M. and Ayres, L.A., 2016. 'Geothermal potential of granitic rocks of the Mourne Mountains' in M.E. Young (ed.), Unearthed: impacts of the Tellus surveys of the north of Ireland. Dublin. Royal Irish Academy.

Yeomans, C. (2011). Geothermal implications of the Mourne Mountains: constraints from magnetotelluric modelling. Thesis for MSci at University of Exeter

Yeomans, C., Muller, M.R., Daly, S. and Jones, A.G. (2012). The IRETHERM Project: Geothermal energy potential of the Greater Dublin area, Ireland and the Mourne Mountains Granite Complex, Northern Ireland. 21st EletroMagnetic Induction Workshop (EMIW), Darwin, Australia

Annexes

Evaluation of CHPM characteristics of prospective CHPM areas

Ireland

1. **CHPM operational characteristics - Information for CHPM technological elements**

Requested information:

✓ please fill in the table below with the requested data for the CHPM technology elements

Underground heat exchanger (deep metal enrichment + potential geothermal reservoir)	
Extension of the metal enrichments *(volumetric interpretation)*	None identified
Expected type of the reservoir and porosity/permeability *(fractured, porous, etc)*	No information available (Pasquali 2010) There is no information on the reservoir properties
Mineralization *(type and enriched metals)*	None identified at depth.

Production and injection wells	
Depth of potential wells (m)	Unknown

Electrolytic metal recovery and gas diffusion electro- precipitation	
Potential target metals to be recovered	Prospective for Rare Earth Elements associated with Sn and U. (https://www.bgs.ac.uk/gsni/minerals/prospectivity/rees/) Tin and REE geochemical anomalies found throughout the Mourne Granites (Moore et al. 2016) Some of the most extensive Nb, Ta, and Yb anomalies in Northern Ireland occur in the soils of the Mourne Mountains. (https://www.bgs.ac.uk/gsni/minerals/downloads/GSNIFlyers.pdf)

Power plant (heat exchanger)	
Local heat and electricity demand *(industrial, municipal, agricultural, etc.)*	Municipal and industrial (Belfast, regional capital, 1m people), agricultural

Salt gradient power generation	
Salinity of expected geothermal brine	Unknown Deep drilling (> 1000m) would be required to determine this parameter.
Fresh water supply from the surface *(water sources)*	The Mourne Mountains host several lakes and rivers, as well as the Spelga (2.7 million m^3), Ben Crom (1.7 million m^3) and Silent Valley reservoirs.

2. **CHPM operational characteristics - Environmental, social and political background**
Requested information:

- ✓ toleration to gaseous and solids emissions, water and noise pollution,
- ✓ local competition to land and water availability
- ✓ public acceptance
- ✓ political support
- ✓ presence of supporting legislation, regulatory framework

Notes: all of above refers to the selected area and its surroundings.

The Mourne Mountains are designated as an Area of Outstanding Natural Beauty (AONB) by the Department of Agriculture, Environment and Rural Affairs (NI).

Eastern Mournes is a Natura 2000 Special Area of Conservation (SAC) and Area of Special Scientific Interest (ASSI 95) (Figure 1) (https://appsd.daera-ni.gov.uk/nedmapviewer/)

The sources of the Rivers Lagan and Bann are within the Mourne Mountains.

A range of economic activities are supported including farming, forestry, fishing, mineral extraction, water supply, tourism and recreation (www.mournelive.com)

Permissions from the Northern Ireland Environment Agency (NIEA) may be required to undertake investigations in the Mourne AONB (Figure 2).

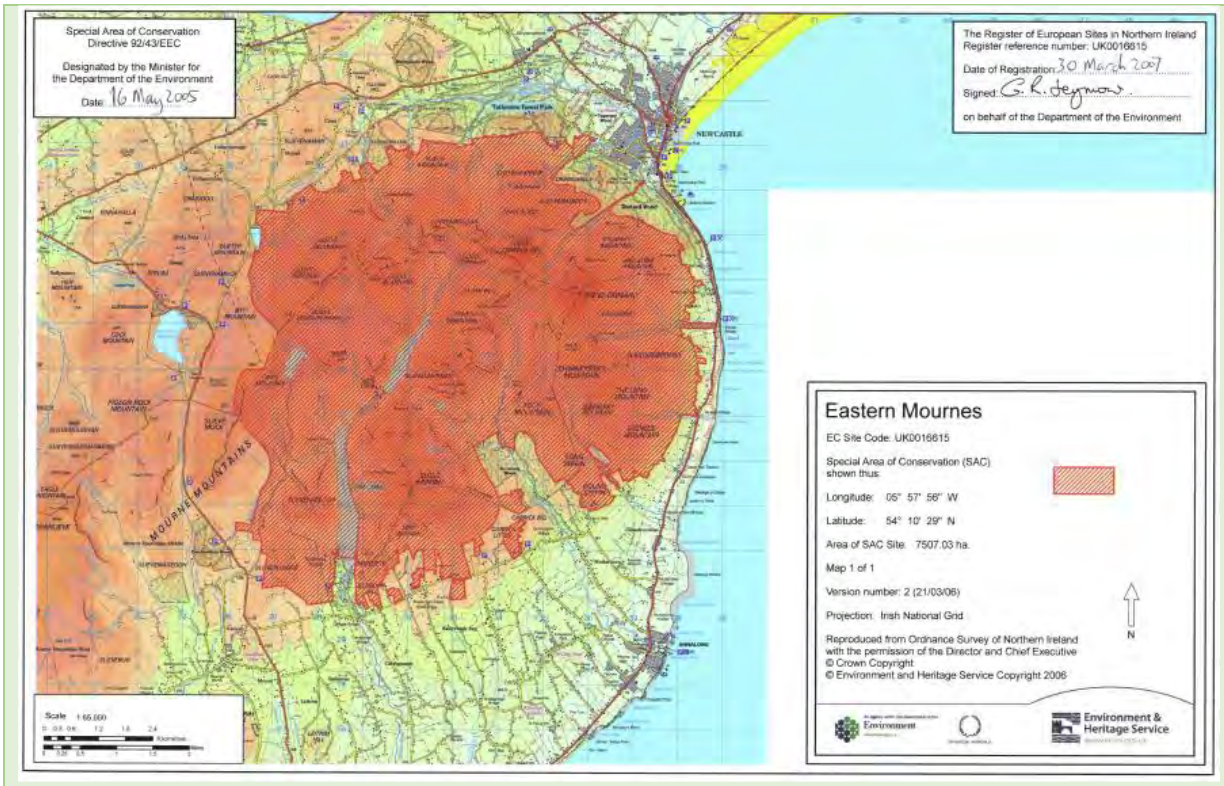

Figure 1 Eastern Mournes SAC Map (https://www.daera-ni.gov.uk/publications/reasons-designation-special-area-conservation-eastern-mournes)

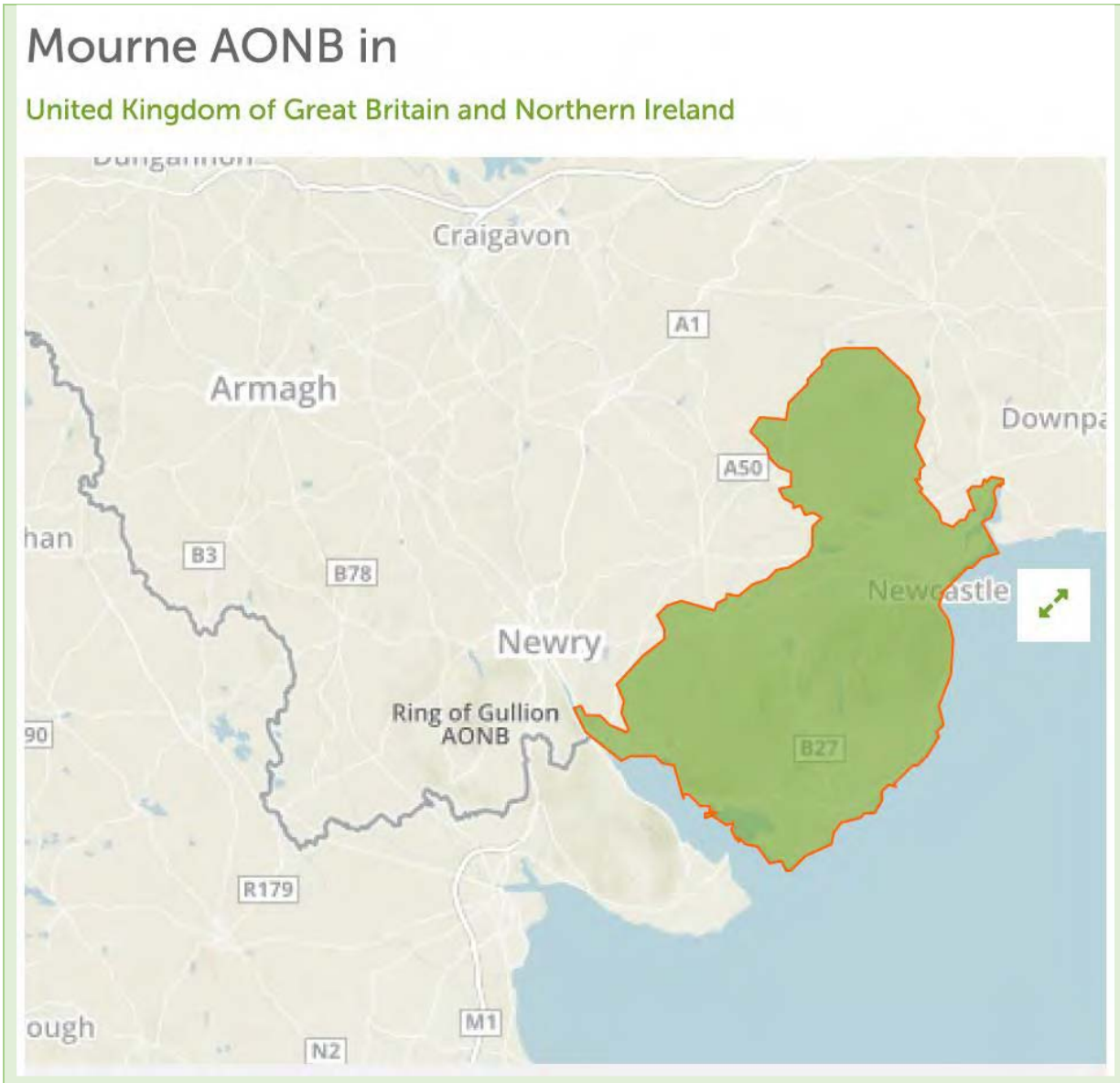

Figure 2. Location map of Mourne AONB (source: European Environment Agency (EEA) www.protectedplanet.net)

3. Financial aspects

Requested information:

✓ list of potential local stakeholders (community, political, companies)

Department for the Economy NI

Geological Survey of Northern Ireland

Northern Ireland Environment Agency

British Geological Survey

Geological Survey of Ireland

Department of Communications, Climate Action and Environment (Republic of Ireland)

Geothermal Association of Ireland

International Association of Hydrogeologists - Irish Group

Heat Pump Association of Ireland

National Trust Northern Ireland

Mourne Heritage Trust

County Down Rural Community Network

Ulster Farmers Union

Mountaineering Ireland

Local Walking Clubs

List of references

Moore, K.R., Moles, N.R. and Lusty, P.A.J., 2016 'A natural laboratory for critical metals investigations in the Mourne Mountains granites' in M.E. Young (ed.), *Unearthed: impacts of the Tellus surveys of the north of Ireland*. Dublin. Royal Irish Academy.

Pasquali, R., O'Neill, N., Reay, D., Waugh, T., The Geothermal Potential of Northern Ireland, Proceedings World Geothermal Congress, Bali, Indonesia, 25-29 April 2010

https://appsd.daera-ni.gov.uk/nedmapviewer/

www.mournelive.com

www.protectedplanet.net

https://www.bgs.ac.uk/gsni/minerals/prospectivity/rees/

https://www.bgs.ac.uk/gsni/minerals/downloads/GSNIFlyers.pdf

Annexes

Table 1

Prospective CHPM areas

RBINS Luxembourg							
Number	**Type of the selected area(s) (type "A" or type "B")**	**Depth(s) of the metal enrichment(s) (m)**	**Temperature /at these depths/ (°C)**	**Description of the metal enrichment(s)**			
				degree of the mineralization(s) (% or ppm)	***type of the mineralization(s)[1]***	***element(s)***	***area delineation(s)[2]***
1	There are no prospective areas in Luxembourg						

CHPM2030 – Summary of Luxembourg

In the procedure of selection of the area scientific publication, existing data (WP1), and answer from the Geological Survey of Luxembourg have been considered.

The research was focused on the comparison of the geological map with heat flow map and drilling data.

For Luxembourg there is no area eligible for the CHPM project. No deep metal enrichment has been identified in the country: only shallow metal enrichments are located in south Luxembourg in the mining region of Esch sur Alzette. No metal enrichments were identified below the depths where the temperature exceeds 100°C.

In the Eifel region there are some quartzite-rich Lochkovian deposits that could be eligible for combined geothermal heat production and power generation.

[1] Like skarn, porphy, etc.

[2] There are 3 options for the indication of the area delineation: a. coordinates (latitude, longitude) of 1 point; b. coordinates (latitude, longitude) of 1 points and radius (m); c. coordinates (latitude, longitude) of more points.

Bibliography

Schintgen T. (2015) *Exploration for deep geothermal reservoirs in Luxembourg and the surroundings – perspectives of geothermal energy use.* Geothermal Energy 3:9

Service géologique du Luxembourg: http://www.geology.lu

Soil Atlas of Europe: https://esdac.jrc.ec.europa.eu/content/soil-atlas-europe

Table 1

Prospective CHPM areas

KNGMG the Netherlands							
Number	**Type of the selected area(s) (type "A" or type "B")**	**Depth(s) of the metal enrichment(s) (m)**	**Temperature /at these depths/ (°C)**	**Description of the metal enrichment(s)**			
				degree of the mineralization(s) (% or ppm)	***type of the mineralization(s)[1]***	***element(s)***	***area delineation(s)[2]***
1	A	2904-2905	~ 105°C	exist, but the exact degree is unknown	Copper shale	Cu	***Bergermeer, BGM-03,*** 52.65128397 4.71881713
2	A	4012-4013	~130°C	exist, but the exact degree is unknown	Copper shale	Cu	***Ameland Westgat, AWG-106,*** 53.49275185 5.94174898
3	**B**	2954-2955	~95°C	exist, but the exact degree is unknown	Copper shale	Cu	***Borgsweer,*** BRW-04, 53.29108611 7.01795771
4	B	2104-2017	~70°C	exist, but the exact degree is unknown	Copper shale	Cu; pyrite, also present between	***Koekoekspolder,*** KKP-GT-02, 52.58083974 5.95045108

[1] Like skarn, porphy, etc.

[2] There are 3 options for the indication of the area delineation: a. coordinates (latitude, longitude) of 1 point; b. coordinates (latitude, longitude) of 1 points and radius (m); c. coordinates (latitude, longitude) of more points.

						2105-2108)	
5	B	1802	~60°C	exist, but the exact degree is unknown	Possible enrichment in silicified karst carbonate (top Dinantian)	Pb, Zn	Venlo, CAL-GT-01 side track, 51.42218805 6.09139302

Detailed description of the areas

The CHPM2030 project aims to investigate a combines geothermal energy and mineral resources production. In search of adequate pilot areas, in the Netherlands two main mineral deposits could be of interest; 1) the Coppershale (Permian) and 2) lead-and zinc mineralization related to silicified limestones (Dinantian).

In order to assess possible pilot area information on current geothermal wells in combination with the depth of each of these mineral deposits are used. However, in the Netherlands some of these wells are relatively shallow, tens of metres, and may not have been examined in detail. More extensive studies are present from (former) oil- and gas exploration wells and documented by the Dutch Geological Survey, (www.nlog.nl). Figure 1 depicts the geothermal potential and the potential power per doublet in the Netherlands (Kramers et al. 2012a). Further information on geothermal power in the Netherlands is available on the website www.geothermie.nl.

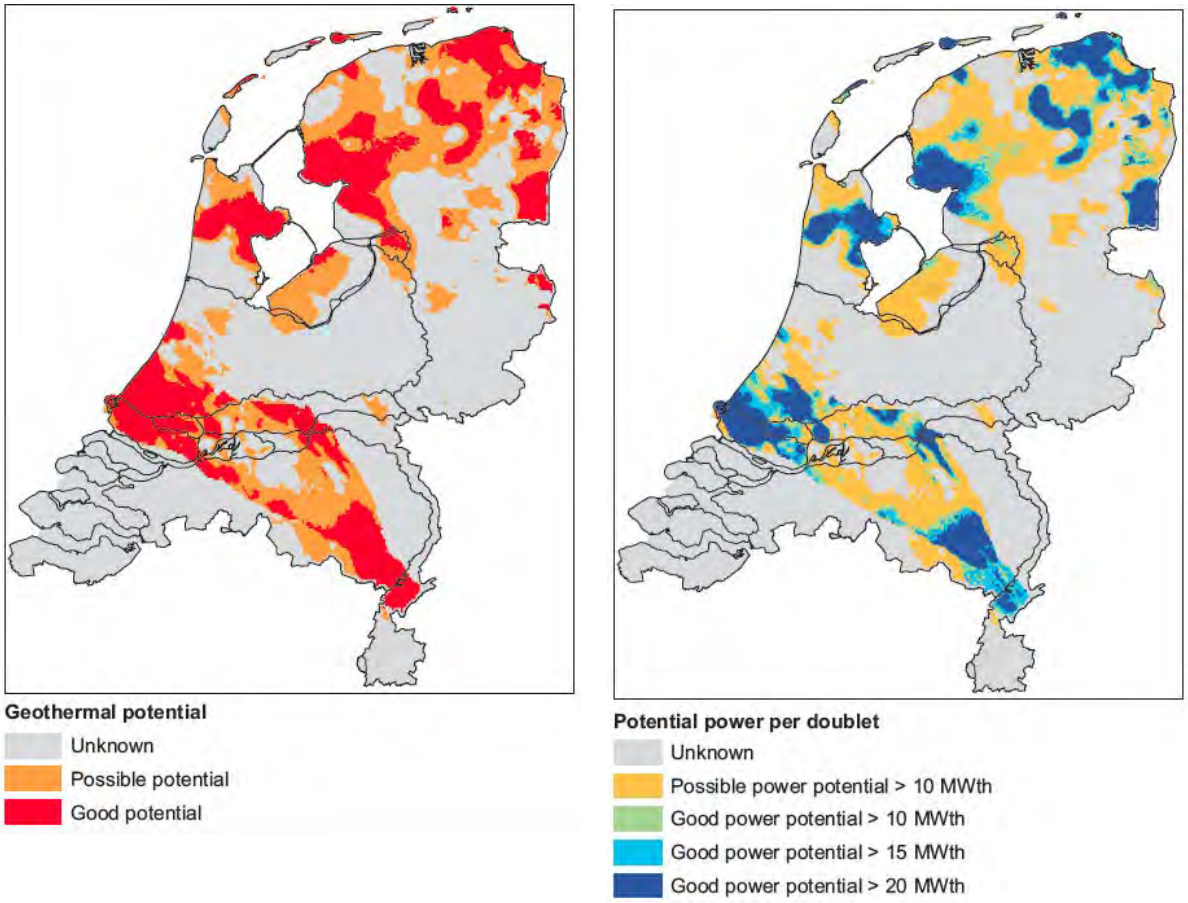

Figure 1

Geothermal potential map and the potential power per doublet (Figure 3b,d in Kramers et al. 2012a).

In the Netherlands extensive studies on subsurface temperature were performed by Bonté and others (2012). Their results are shown in Figure 2. In combination with well- and lithostratigraphic data (www.nlog.nl) the water temperature at a certain mineralisation depth can be estimated whenever not provided.

In this report only prospect areas primarily based on their relation to two mineralisation levels, the Coppershale and top of the Dinantian limestone, are discussed.

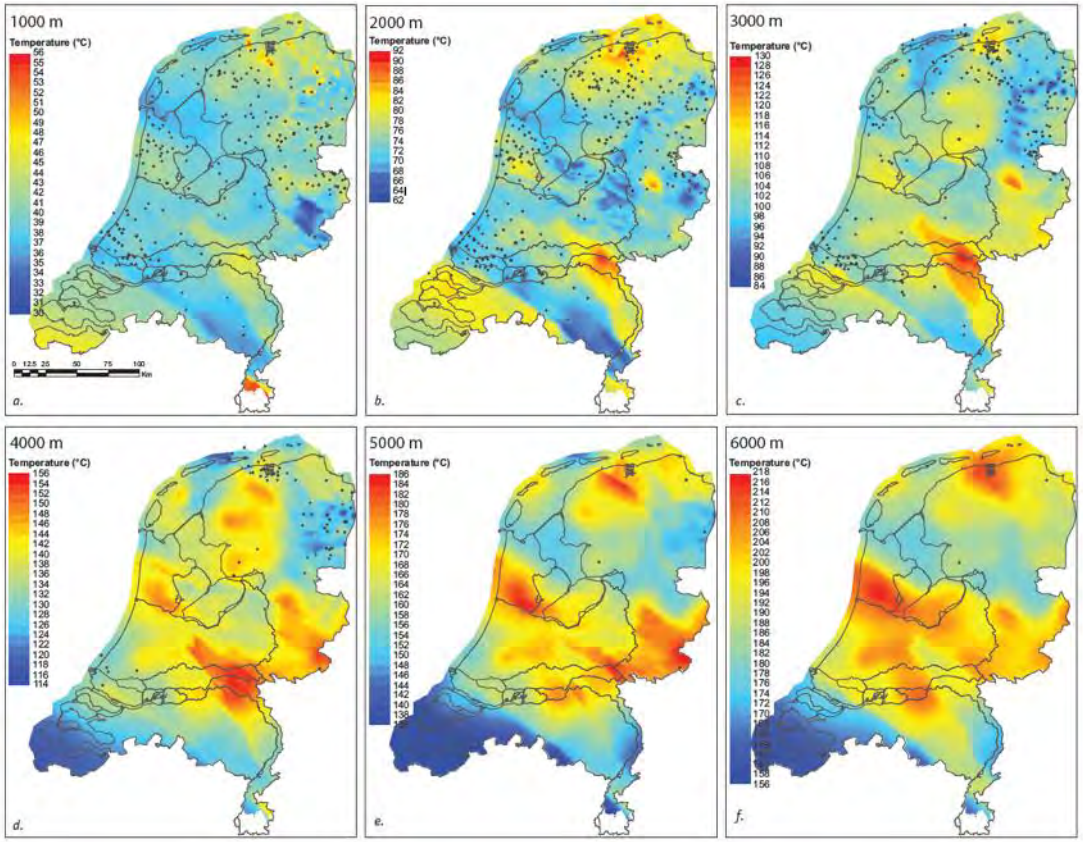

Figure 2

Modelled isodepth temperature map from 1000 to 6000m (Figure 6 in Bonté et al., 2012).

The Coppershale

Deposits of the Coppershale also known as Kupferschiefer, are recovered at the base of the Upper Permian Zechstein Group. Coppershale deposits can be encountered in the northern half of the Netherlands as part of the Southern Permian Basin. Their Southern boundary is depicted in Figure 3 and is roughly located along the line Venlo-Oss-Utrecht-Leiden (Geluk, 2007).

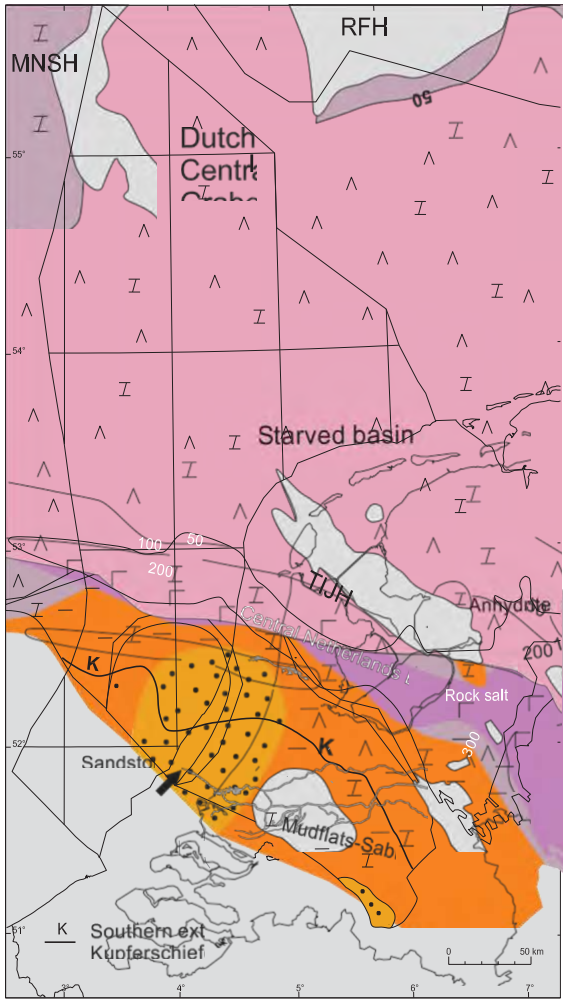

Figure 3

Distribution map of the base of the Zechstein group and therefore the Coppershale marked by a black line indicated by K (Figure 12 in Geluk, 2007). Please note, that the Zechstein deposits are absent in the Texel-IJssel High (TIJH) region.

In general, the Coppershale consists of a 0.5 meter thick finely laminated claystone with an organic carbon content up to 5% enriched with zinc, lead and copper sulphides (Geluk, 2007; Wedepohl, 1994) as well as rare elements as vanadium, molybdenum and uranium. Studies by Wedepohl (1994) and (Paul, 2006) reveal that areas high concentrations of these metals are restricted to small regions at the margins of the Southern Permian Basin; Lower Silesia in Poland, east of the Harz Mountains, Richelsdorf and Mansfeld-Sangerhaus areas. Northwestern Germany and northeastern Netherlands do not reveal any major copper, lead and zinc mineralisation in their study (Figure 4).

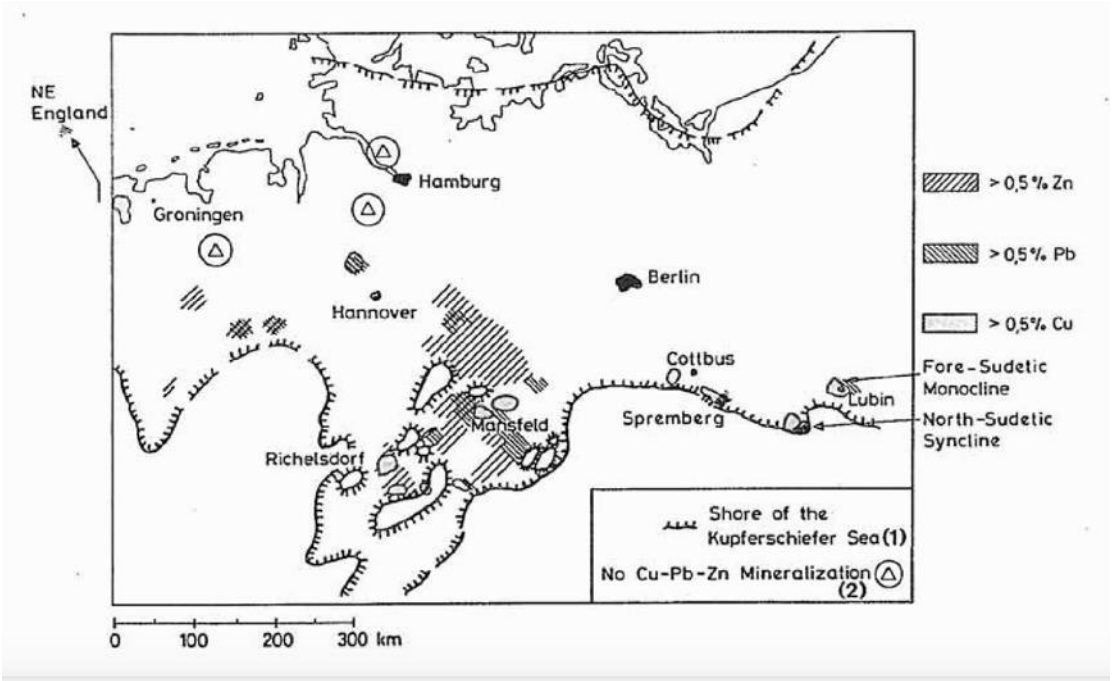

Figure 4

Map of Coppershale deposition in Central Europe and areal distribution of Coppershale mineralization exceeding 0.5% copper, lead or zinc (Figure 4 in Wedepohl, 1994)

The subsurface temperature at depth of the Coppershale can be inferred from combining isodepth temperature maps (Figure 2) and well data. Bonté and others (2012) provided two parallel cross sections roughly from the southwest towards the northeast correlating the main geological layers and their subsurface temperatures (Figure 5). The subsurface temperature at depth of the Coppershale varies from about 130°C in the North of Netherlands, e.g. Ameland Westgat, to about 70°C in the southern part of the Coppershale distribution in the Netherlands, Koekoekspolder.

No accurate data on metal concentrations in the Netherlands are retrieved (yet). Provided sufficient metal concentrations the region near the island of Ameland, in the North of the Netherlands, as well as Bergermeer near Alkmaar in the western part of the Netherlands could be targeted as an pilot area based on the subsurface temperatures at the base of the Coppershale.

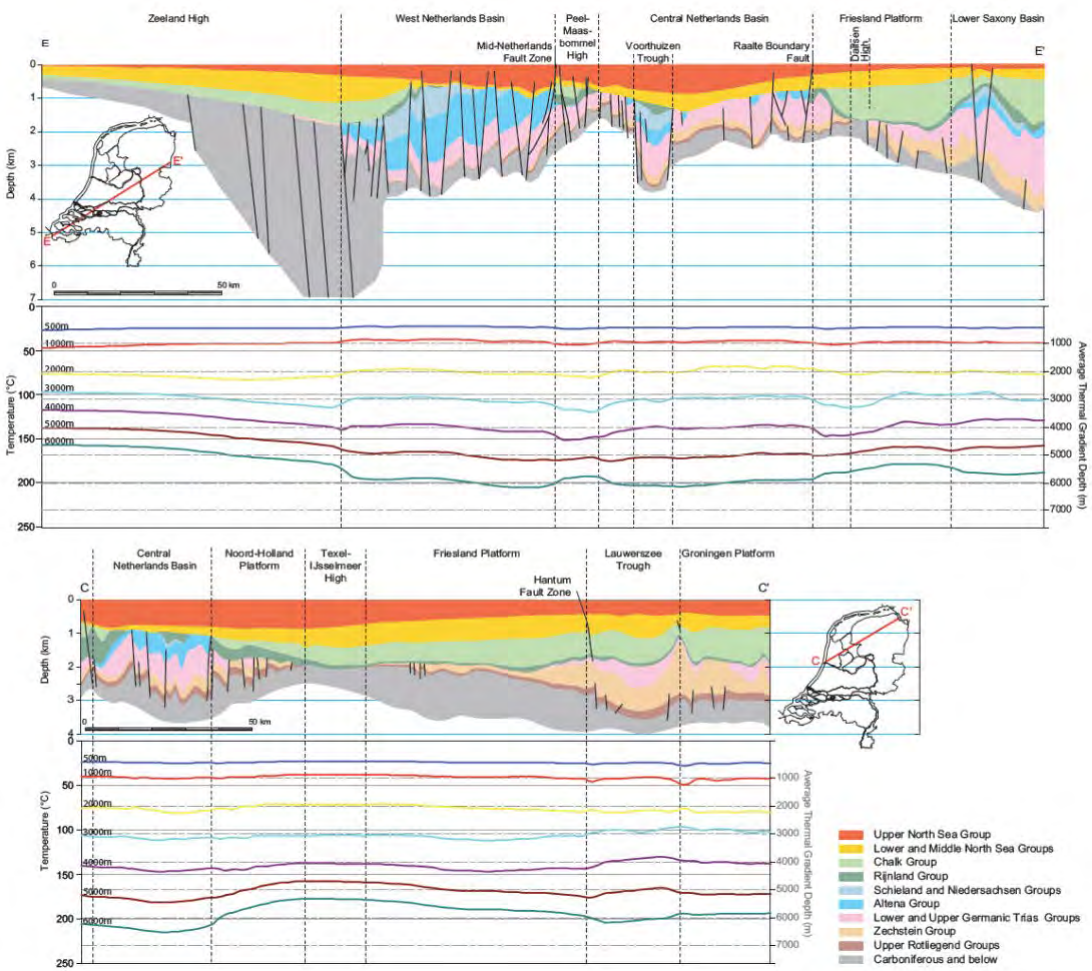

Figure 5

Cross-sections correlating the main geological layers and modelled subsurface temperatures (Figure 14 in Bonté et al., 2012). The profile in the lower panel, from the southwest to the northeast, approximately crosses Bergermeer (situated in the Central Netherlands Basin), Koekoekspolder and Ameland (situated on the Groningen Platform). Please note, that the Zechstein deposits are absent in the Texel-IJssel High (TIJH) region – see also Figure 3.

Top of the Dinantian limestone

In the province of Limburg the top of the Dinantian limestones are often characterized by silicified carbonates (Bless, 1987; Friedrich et al., 1987; Reijmer et al., 2017). Leaching and subsequent silicification took place at those locations where the overlying Namurian and Westphalian strata had been eroded completely before deposition of Upper Cretaceous sediments; meteoric water played an important role in these surface-controlled processes (Friedrich et al., 1987).

In the southernmost part of Limburg, borehole studies of Thermae 2000 and Thermae 2002 display two different mineralized zones; a well-developed "Schalenblende" in upper zone and a less important mineralization lower zone (Figure 6). In the upper zone sphalerite, iron sulphides, galena and quartz are found at a depth of 242-248m and 238-248m, respectively. The concentration of sulphide minerals varies strongly with a borehole as well as between the Thermae boreholes located at a short distance from each other. Friedrich and others (1987) report in Thermae 2000 that the sulphide zone contains up to 12% sulphide minerals, whereas in Thermae 2002 this zone is marked by two horizons, one at 242.5m with 83% sulphide minerals and another at 248m with 36% separated by a minimum of only 8 % at 244m. In the lower zone sulphides are rare. In Thermae 2000 maximum sulphide values up to 3% are recorded between 309 and 321m. In Thermae 2002 two intervals are noticed; one between 333 and 343m with a maximum of 15% sulphide minerals and another one between 374 and 376m with up to 2%.

Friedrich and others (1987) also report lead and zinc enrichments for silicified Dinantian rocks near Maastricht, borehole Heugem-1 and Site Kastanjelaan-2 (Figure 6).

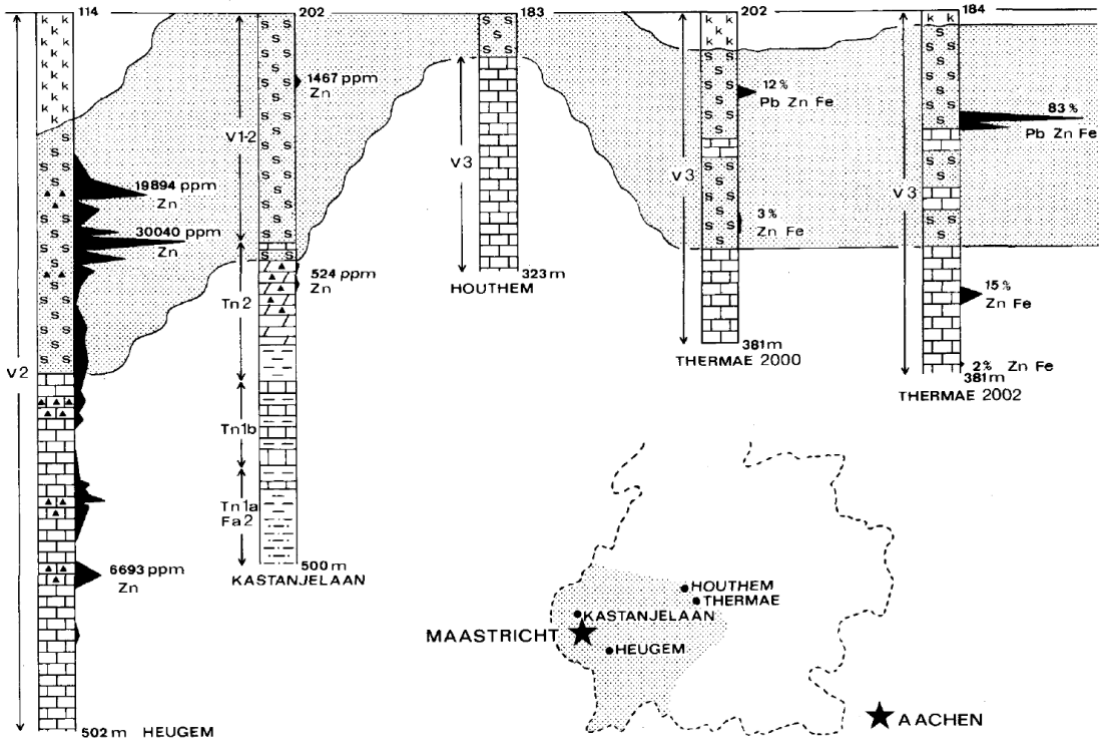

Figure 6

Comparison between main silicification (punctated) and occurrence of sulphide minerals (in %) or Zinc (in ppm) in the Dinantian rocks of some selected boreholes in South Limburg. Datum line represents top Dinantian below Cretaceous overburden (Figure 2 in Friedrich et al., 1987).

Figure 7 shows that in the southernmost part of Limburg the subsurface at these horizons is however relatively ‘cold’, below 30°C (Kramers et al., 2012b) and therefore unsuitable as a target or pilot area in the CHPM 2030 project.

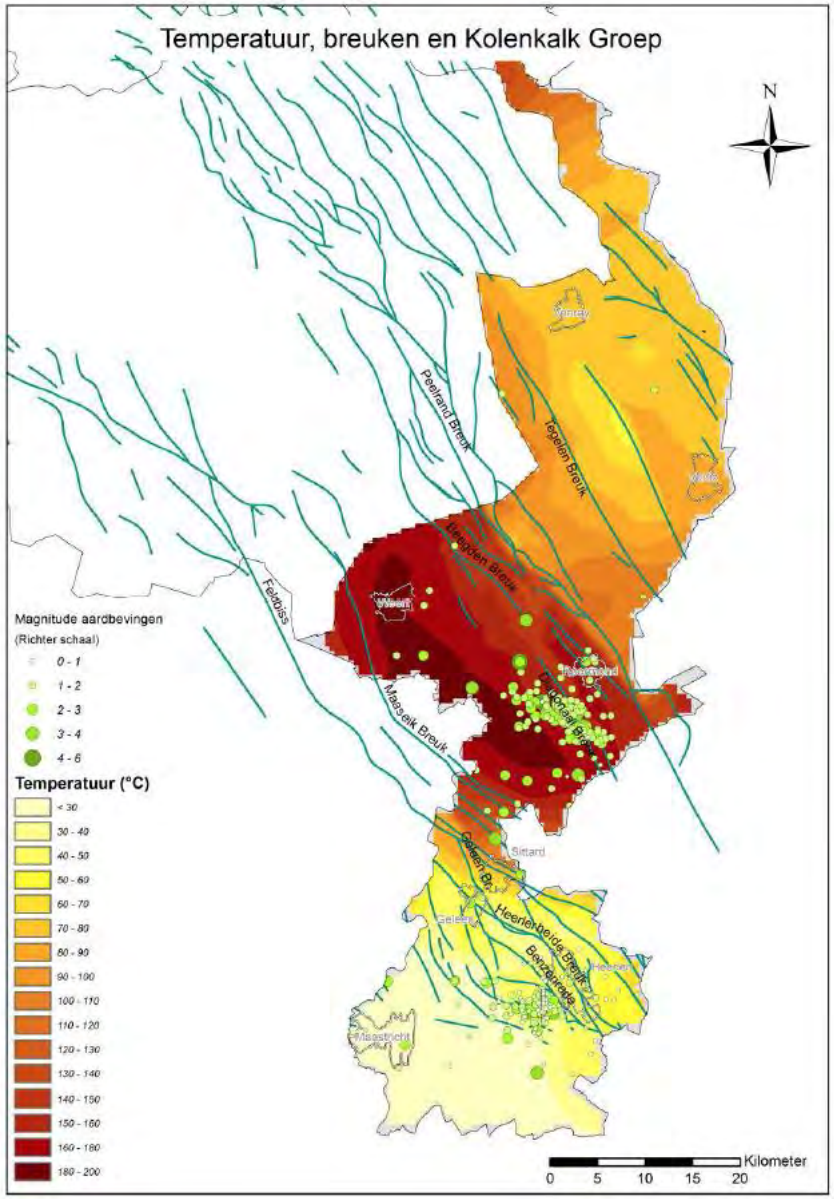
Temperatuur, breuken en Kolenkalk Groep
N
Peelrand Breuk
Tegelen Breuk
Feldbiss
Magnitude aardbevingen
(Richter schaal)
0 - 1
1 - 2
2 - 3
3 - 4
4 - 6
Temperatuur (°C)
< 30
30 - 40
40 - 50
50 - 60
60 - 70
70 - 80
80 - 90
90 - 100
100 - 110
110 - 120
120 - 130
130 - 140
140 - 150
150 - 160
160 - 180
180 - 200
Sittard
Geleen
Maastricht
Kilometer
0 5 10 15 20

Figure 7

Overview of faults, temperature and registered natural earthquakes within the Dinantian limestones or “Kolenkalk” in Limburg (Figure 57 in Kramers et al., 2012b).

Further North in the province of Limburg, near Venlo, successful geothermal projects have been preformed in borehole CAL-GT-1 (Kramers et al., 2012b; www.californie.nu). Here silicified carbonates from the top of the Dinantian have been encountered at a depth of 1636 m (www.nlog.nl; Reijmer et al., 2017) producing a subsurface water temperature of about 60°C (Figure 7; Kramer et al., 2012b). Reports of cutting samples however, did not report on mineral concentration in borehole CAL-GT-01 (Poty, 2014). Recently, on 28 May 2018, geothermal activity was ceased in borehole CAL-GT-01 due to exploration risks in combination with natural earthquakes related to the vicinity of the Tegelen fault zone (https://www.limburger.nl/cnt/dmf20180529_00062856/winning-aardwarmte-in-grubbenvorst-stilgelegd).

In general, in Mid- and North Limburg the silicified carbonates at the top of Dinantian limestones (or “Kolenkalk”) could serve as a target area combing the information in Figures 7 and 8. In regions where the top of the Dinantian is recorded below 300m depth, subsurface water temperatures of about 100°C are met (Kramer et al., 2012b). Here, however, the largest uncertainty is the distribution of sulphide minerals.

As such, Limburg in general, may have suitable minerals and subsurface water temperatures, however unfortunately not likely recovered at the same location. Awareness of the presence of numerous faults and natural earthquakes should be incorporated any pilot project.

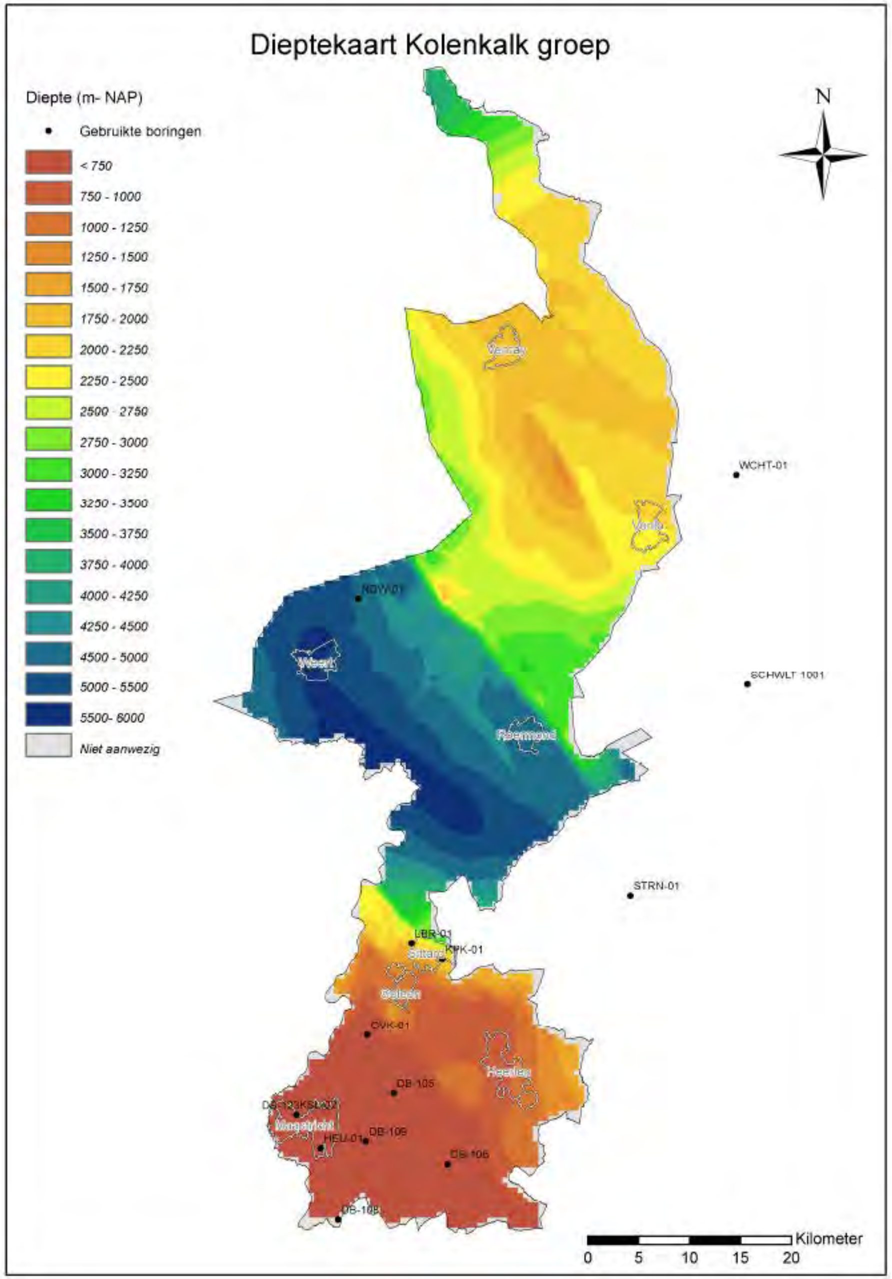
Dieptekaart Kolenkalk groep
Diepte (m- NAP)
Gebruikte boringen
< 750
750 - 1000
1000 - 1250
1250 - 1500
1500 - 1750
1750 - 2000
2000 - 2250
2250 - 2500
2500 - 2750
2750 - 3000
3000 - 3250
3250 - 3500
3500 - 3750
3750 - 4000
4000 - 4250
4250 - 4500
4500 - 5000
5000 - 5500
5500- 6000
Niet aanwezig
N
WCHT-01
SCHWLT 1001
STRN-01
Roermond
LBR-01
KPK-01
OVK-01
DB-105
DB-109
HEU-01
DB-106
DB-108
Kilometer
0
5
10
15
20

Figure 8

Distribution map of the top of the Dinantian limestones or “Kolenkalk” in Limburg (Figure 55 in Kramers et al., 2012b).

References

Bonté, D., van Wees, J. D., and Verweij, J. M., 2012, Subsurface temperature of the onshore Netherlands: new temperature dataset and modelling: Netherlands Journal of Geosciences - Geologie en Mijnbouw, v. 91, no. 4, p. 491-515.

Friedrich, G., Bless, M. J. M., Vogtmann, J., and Wiechowski, A., 1987, Lead-zinc mineralization in Dinantian rocks of boreholes Thermae 2000 and Thermae 2002 (Valkenburg a/d Geul, the Netherlands): Annales de la Société Géologique de Belgique, v. 110, p. 59–75.

Geluk, M. C., 2007, Permian, Amsterdam, Royal Netherlands Academy of Arts and Sciences (KNAW), Geology of the Netherlands.

Kramers, L., van Wees, J. D., Pluymaekers, M. P. D., Kronimus, A., and Boxem, T., 2012a, Direct heat resource assessment and subsurface information systems for geothermal aquifers; the Dutch perspective: Netherlands Journal of Geosciences - Geologie en Mijnbouw, v. 91, no. 4, p. 637-649.

Kramers, L., Vis, G. J., den Dulk, M., Duin, E. J. T., Witmans, N., Pluymaekers, M. P. D., and Doornenbal, J. C., 2012b, Regionale studie aardwarmte potentie provincie Limburg.: TNO.

Paul, J., 2006, Der Kupferschiefer: Lithologie, Stratigraphie, Fazies und Metallogenese eines Schwarzschiefers [The Kupferschiefer: Lithology, stratigraphy, facies and metallogeny of a black-shale]: Zeitschrift der Deutschen Gesellschaft für Geowissenschaften, v. 157, p. 57-76.

Poty, E., 2014, Report on cuttings from the CAL (California)-GT-01 borehole. Unpublished report, NLOG_GS_Pub_1073.

Reijmer, J. J. G., ten Veen, J. H., Jaarsma, B., and Boots, R., 2017, Seismic stratigraphy of Dinantian carbonates in the southern Netherlands and northern Belgium: Netherlands Journal of Geosciences, v. 96, no. 4, p. 353-379.

Wedepohl, K. H., 1994, Composition and origin of the Kupferschiefer bed: Geological Quarterly, v. 38, no. 4, p. 623-638.

Websites

www.geothermie.nl

www.nlog.nl

Evaluation of the basic characteristics of prospective CHPM

KNGMG

Netherland

AREA 1- NL1-BGM

1. **Geology of the prospective area**

Requested information on:

- ✓ local geology (in regional context)
- ✓ CHPM target formation
- ✓ list of available cross sections, geological maps, geochemical results, lithological information

Notes: briefly summarized, referenced to more detailed studies.

Bergermeer, BGM-03, type A

Lithostratigraphy:

Depth Coppershale : 2904-2905 m (well depth)

Location: 52.65128397 4.71881713

https://www.nlog.nl/nlog/requestData/nlogp/allBor/metaData.jsp?tableName=BorLocation&id=106504878

A study on the effects of Underground Gas Storage in the Bergermeer gas field revealed a detailed subsurface analysis (Muntendam-Bos et. al., 2008). Detailed information on all strata recovered in this well is further provided by nlog.nl; see also appendix NL1-BGM-1.

The lowermost unit, the Slochteren sandstone, is of Permian age and consists of well-sorted, fine-grained eolian sandstone. Porosity is in general high, ranging form 15 to 30%. However, a number of thin low-porosity streaks occur throughout the reservoir. The reservoir is sealed by the Zechstein evaporites including a meter thick Coppershale (Kupferschiefer) at its base.

The Bergermeer Field is situated on a narrow NW-SE trending horst block subdivided by internal faults.

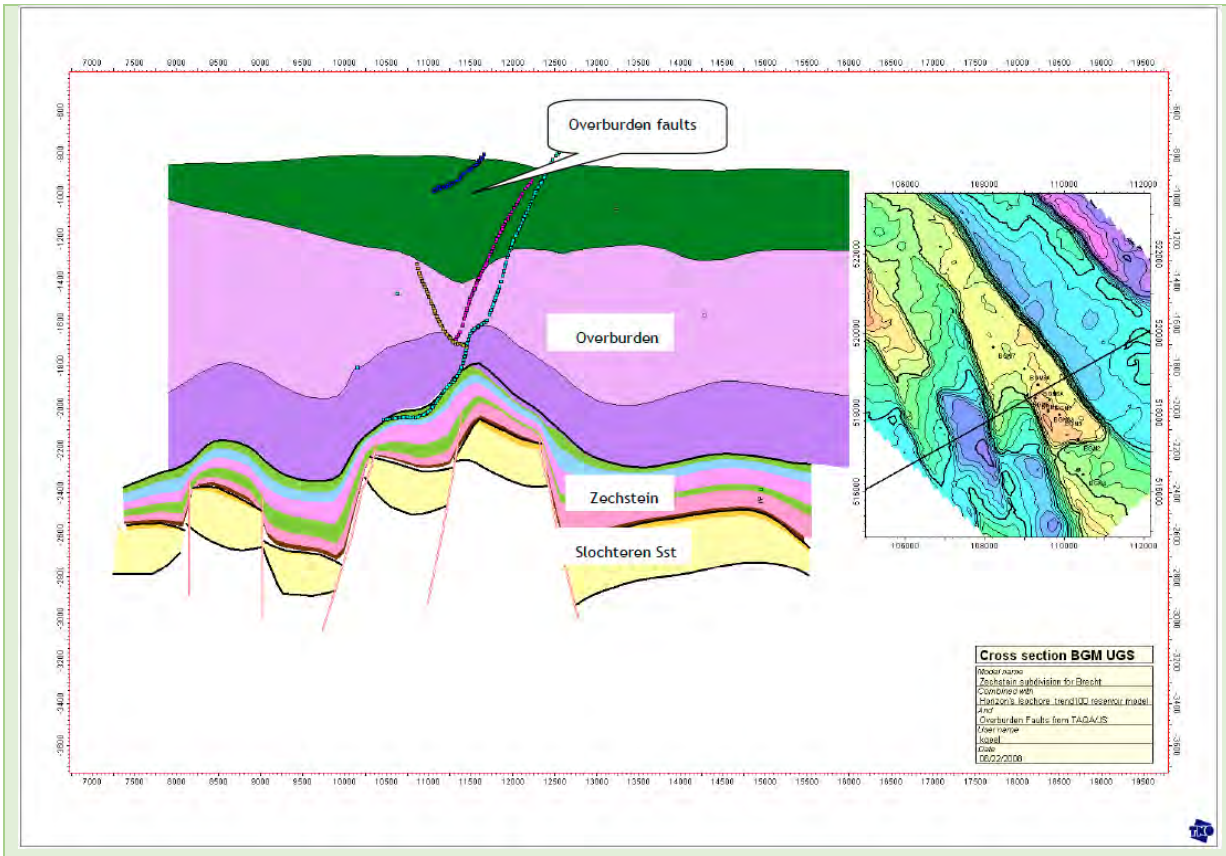

Cross-section through BGM field composed of a Petrel model of the Slochteren Sandstone (by Horizon Energy Partners, 2006), a separated model for the Zechstein, and TAQA's overburden surfaces and faults (after figure 3.6 in Muntendam-Bos et. al., 2008).

2. Geophysics of the prospective area

Requested information:

- ✓ previous geophysical measurements (in CHPM relevance)
- ✓ geophysical results that can be used for locating/defining the deep metal enrichment
- ✓ list of available geophysical maps, cross sections, logs, other measurements

All borehole documents and logs can be found on:
https://www.nlog.nl/nlog/requestData/nlogp/allBor/metaData.jsp?tableName=BorLocation&id=106504878

Detailed section of the gamma-ray and interval transit time (2912 m to 2849 m depth). Very high gamma-ray units at 2905 m depth reveal the stratigraphic position of the Coppershale.

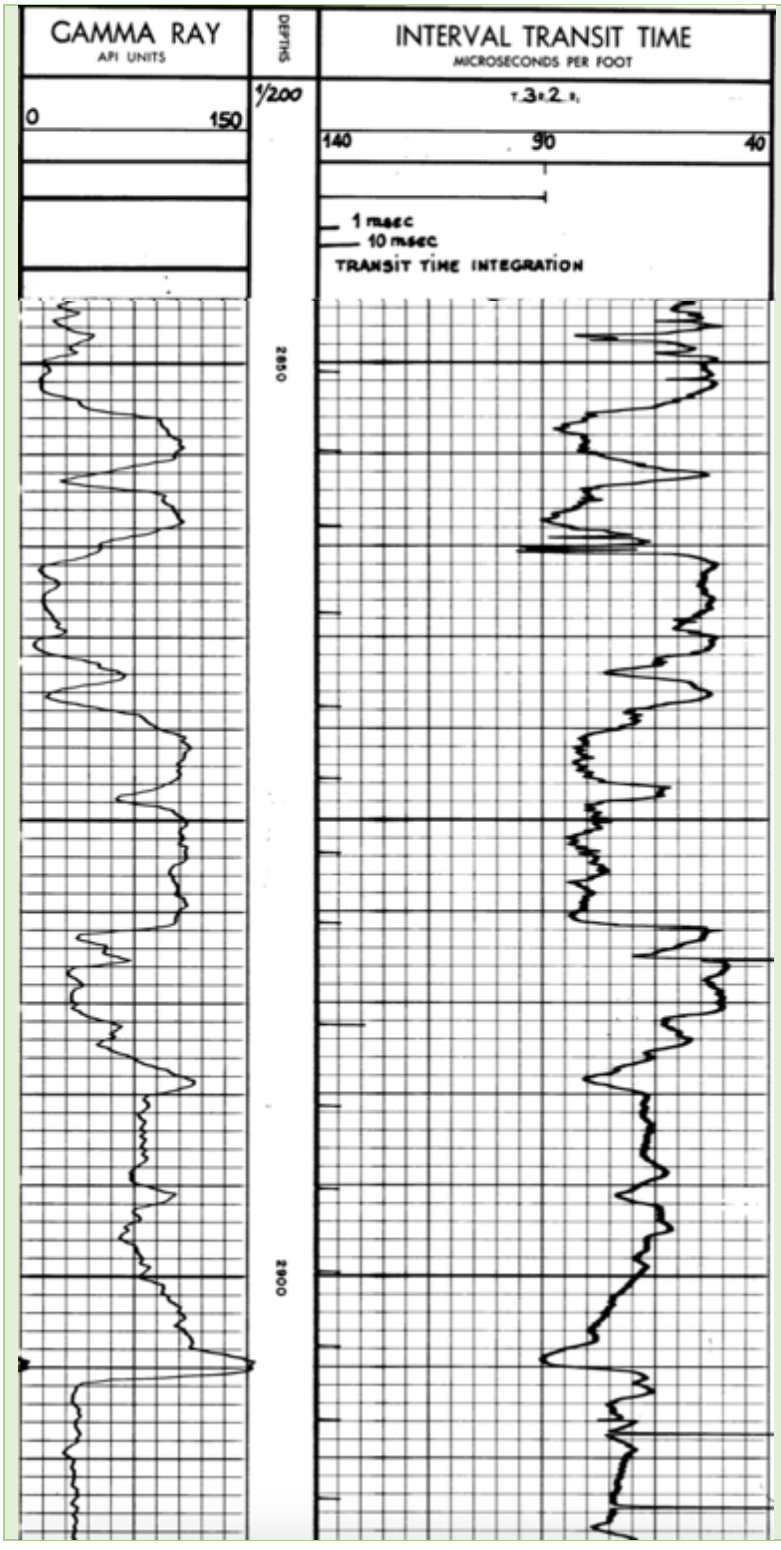
GAMMA RAY
API UNITS
DEPTHS
INTERVAL TRANSIT TIME
MICROSECONDS PER FOOT
1/200
0
150
140
90
40
1 msec
10 msec
TRANSIT TIME INTEGRATION
2900
2800

3. Deep metal enrichment

Requested information:

✓ (expected) metal enrichment based on available geophysical, geological and drill data, samples information, geochemistry

No further specific data are available on the Coppershale. There is no mining history in this region. However, a study by Schmidt (2000) reveals the mineral composition of the Coppershale in NW Drenthe, at a distance of about 130 km of the Bergermeer site. The tables below may serve as a coarse indication of elemental composition (Table 2.3 and 2.4 in Schmidt, 2000). Core C1 and C2 are located a short distance from each other. The exact location of these cores is confidential.

Table 2.3 - Major elements (wt%)

Core	Sample no. and type	SiO_2	TiO_2	Al_2O_3	Fe_2O_3	MgO	MnO	CaO	K_2O	Na_2O	P_2O_5	LOI*	Total
C1	1 Grey sandstone	82.79	0.20	7.01	1.89	0.49	0.04	0.39	2.35	0.74	0.08	2.91	98.89
C1	2 Bituminous sst.	87.38	0.09	4.76	0.45	0.12	0.01	0.70	1.82	0.66	0.07	3.37	99.43
C1	3 Bituminous sst.	82.22	0.08	4.16	0.40	0.10	0.01	2.98	1.61	0.56	0.07	6.17	98.36
C1	4 Bituminous sst.	86.55	0.08	5.09	0.35	0.19	0.01	0.46	1.95	0.65	0.07	4.14	99.54
C2	5 Kupferschiefer	42.71	0.68	13.84	3.65	3.52	0.15	9.53	3.61	0.77	0.17	25.13	103.75
C2	6 Bituminous sst.	84.35	0.10	5.20	5.12	0.69	0.09	0.29	1.91	0.66	0.07	4.22	102.69
C2	7 Bituminous sst.	86.00	0.12	2.92	2.01	1.36	0.12	4.04	0.97	0.37	0.07	5.52	103.50
C2	8 Bituminous sst.	87.29	0.08	5.16	2.22	0.29	0.03	0.73	1.87	1.01	0.07	2.98	101.74
C2	9 Conglomerate	80.33	0.12	3.30	6.53	2.14	0.09	3.90	0.71	0.22	0.11	5.71	103.17
C2	10 Grey shale	59.38	1.05	23.58	3.79	0.67	0.01	0.00	4.35	0.55	0.05	5.37	98.78

* : loss on ignition

Table 2.4 - Trace elements (ppm) and carbon contents (wt%)

Core	Sample no. and type	As	Co	Cu	Ni	Pb	V	S	Ba	Th	U	C_{total}	$C_{organic}$	$C_{carbonate}$
C1	1 Grey sandstone	4	221	10	16	9	28	0	441	11	0	0.55	0.27	0.28
C1	2 Bituminous sandstone	296	323	26	46	34	45	1882	555	6	36	1.42	0.77	0.65
C1	3 Bituminous sandstone	29	237	75	12	11	31	12478	322	10	327	4.19	2.77	1.42
C1	4 Bituminous sandstone	240	268	42	43	30	84	485	1034	9	139	2.51	1.65	0.86
C2	5 Kupferschiefer	140	334	14390	218	714	2243	12806	311	3	52	12.08	9.87	2.21
C2	6 Bituminous sandstone	2	319	10	26	15	14	588	709	8	0	1.25	0.55	0.70
C2	7 Bituminous sandstone	4	195	8	12	12	18	4675	1000	8	5	1.45	0.27	1.18
C2	8 Bituminous sandstone	5	204	6	15	9	15	1745	1340	9	0	0.81	0.50	0.31
C2	9 Conglomerate	8	258	10	13	10	46	670	2081	7	2	1.39	0.17	1.22
C2	10 Grey shale	5	65	13	67	13	130	0	524	20	5	0.04	0.02	0.02

4. **Integrated 3D- 4D model**

Requested information:

- ✓ existing 3D-4D models of the target area and the deep metal enrichment
- ✓ if no 3D-4D models exist, collect the following necessary data: geological setting, mineralization, fluid flow models, stress field determination

Notes: e.g. openly available datasets, models.

Geothermal data on the Rotliegend of the Bergermeer
Source: thermogis.nl (beta version)

Depth (m)	2081.15
Thickness (m)	172.77
Permeability (mD)	1499.08
Transmissivity (Dm)	257.9
Net to Gross	1
Temperature (°C)	77.73
Pump pressure (bar)	18.22
Flow rate (m3/h)	499.97
Power indication (MW)	25.62
Heat in place (GJ/m2)	39.28
Potential recoverable heat (GJ/m2)	0.31
Potential	unknown

Further information on http://thermogis.nl/thermogis_en.html (updated version available from October 2018).

5. **EGS potential**

Requested information:

- ✓ EGS potential (heat & energy) of the area
- ✓ geothermal characteristics (temperature gradient, heat flux, stress field, water availability, EGS geology)
- ✓ presence/indication of deep fluids/brines, fracture system, crustal permeability

Initial temperatures and rock thermal properties (after table 5.3 in Muntendam-Bos et. al., 2008).

	Initial temperature (°C)	Thermal conductivity (kJ/m/day/K)	Heat Capacity (kJ/m3/K)
Cap rock (Zechstein)	82	600	3200
Reservoir rock - Sandstone	89	250	2200
Reservoir rock - Shale	89	150	3000
Base rock (Carboniferous)	90	350	2200

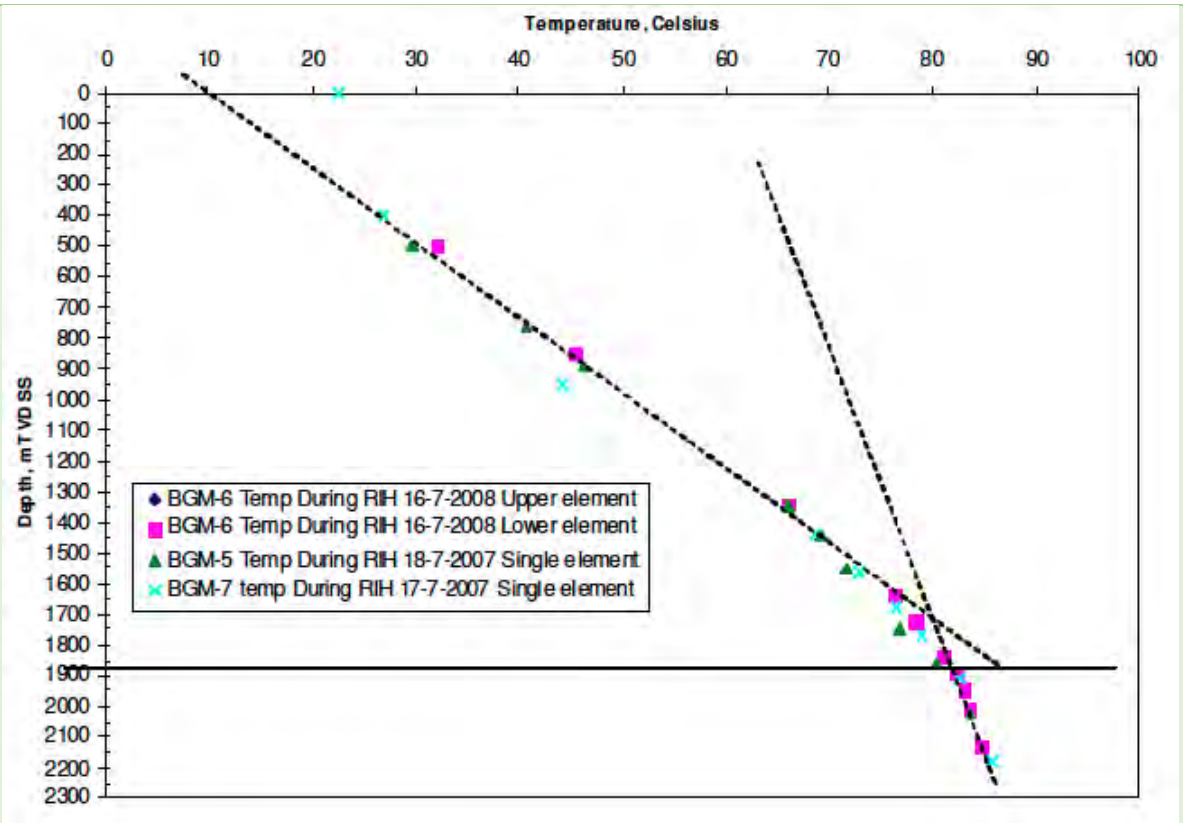

Temperature at some well locations of the Bergermeer field (after figure 5.1 in Muntendam-Bos et. al., 2008).

A study on the effects of Underground Gas Storage in the Bergermeer gas field revealed a history of induced seismicity (Muntendam-Bos et al., 2008). The geomechanical behaviour of the reservoir to gas injection and production depends significantly on the pressure and temperature changes. Especially lateral extension of the temperature response of the reservoir to cold gas injection, and therefore likely to cold-water injection, is crucial for the seismic behaviour of the reservoir. However, reconstructed temperature changes due to UGS and production do not affect the stability of actual faults provided injection points are located at a distance (well) over 200 m of these faults.

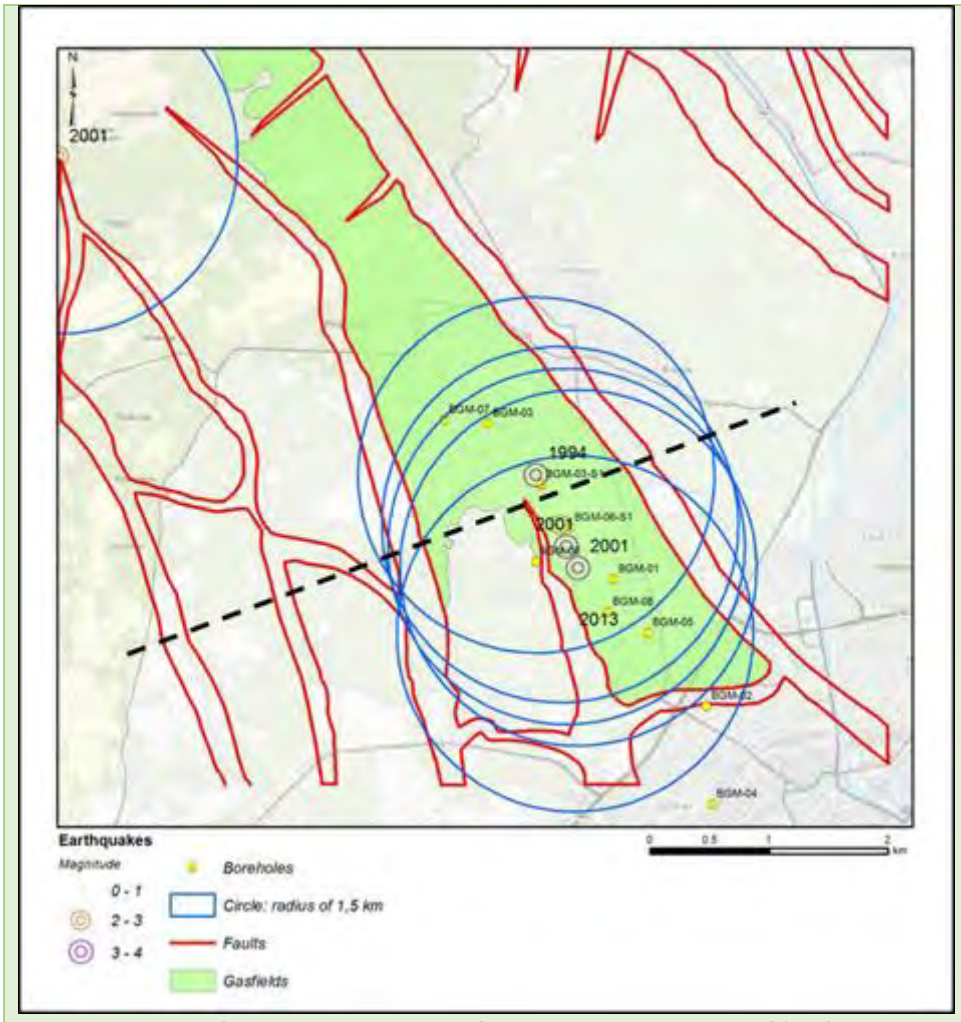

Structural map of the Bergermeer gas field, showing location of 'old' production wells at reservoir level, faults and recorded seismicity in the vicinity of the gas field (TNO, 2015).

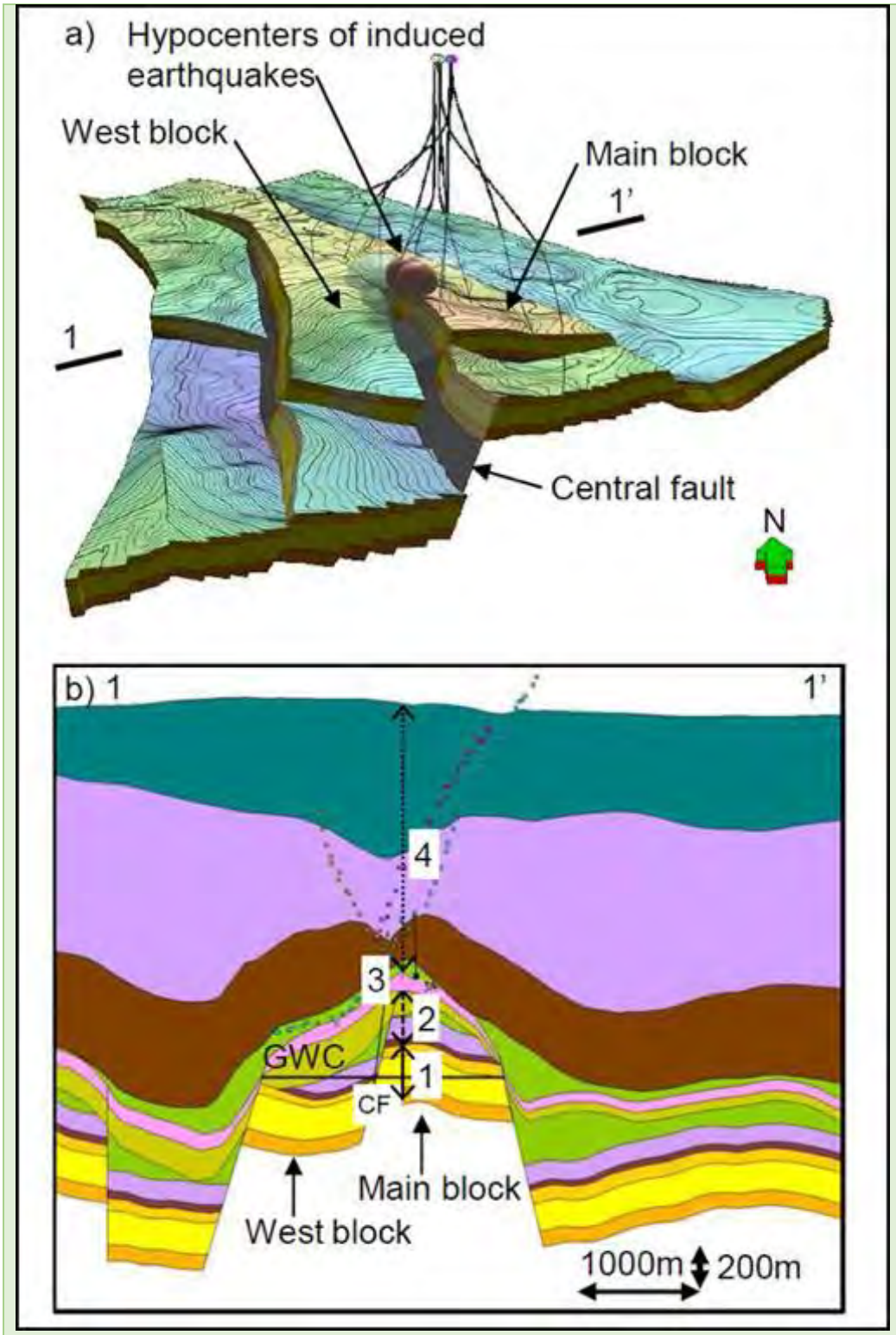

Reservoir structure of the Bergermeer field, a) showing the Main reservoir block, western reservoir block and the Central fault (CF) intersecting the gas reservoir. Four seismic events during primary production have been localized at the Central fault and spheres at the tip of the Central fault are interpreted locations of these seismic events. b) Cross section through the reservoir (location of this cross section is shown in Figure 17): 1) Slochteren Sandstone reservoir, 2) Zechstein Formation (mixed lithology caprock), 3) Zechstein halite caprock, 4) Overburden (Orlic et al., 2013 in TNO, 2015).

The Bergermeer gas field is currently is use as an Underground Gas Storage facility (http://www.taqainnederland.nl/).

List of references

Muntendam-Bos, A.G., Wassing, B.B.T., Geel, C.R., Louh, M. and van Thienen-Visser, K., 2008, Bergermeer seismicity study. TNO report 2008-U-R1071/B.

Schmidt, A.P., 2000. Naturally Occurring Radioactive Materials in the gas and oil industry. Origin, transport and deposition of stable lead and 210Pb from Dutch gas reservoirs. PhD Thesis Universiteit Utrecht, 144 p.

TNO, 2015. Injection-Related Induced Seismicity and its relevance to Nitrogen Injection: Description of Dutch field cases. TNO report 2015 R10906. 34 p.

Websites:

https://www.nlog.nl/nlog/requestData/nlogp/allBor/metaData.jsp?tableName=BorLocation&id=106504878

http://www.tagainnederland.nl/

http://thermogis.nl/thermogis_en.html

Annexes

NL1-BGM-1 Stratigraphic information – **Find them in the folder: Additional information on basic and CHPM characteristics evaluation**

AREA 2- NL2-AWG

1. **Geology of the prospective area**

Requested information on:

- ✓ local geology (in regional context)
- ✓ CHPM target formation
- ✓ list of available cross sections, geological maps, geochemical results, lithological information

Notes: briefly summarized, referenced to more detailed studies.

Ameland Westgat, AWG-106, type A

Lithostratigraphy:

Depth Coppershale : 4009-4010 m; Sidetrack1 4012-4013 m

See also appendix NL2-AWG-1

Location: 53.49275185 5.94174898

https://www.nlog.nl/nlog/requestData/nlogp/allBor/metaData.jsp?tableName=BorLocation&id=106518416

The Ameland Westgat well is located offshore as shown in the figure below; NE of the island of Ameland (source NAM, 2011) and at the northern end of the Groningen gas field.
The dominant gasreservoir formations are part of the Permian Rotliegend Group are eolian and fluvial siliciclastics with a thickness of approximately 100 m. in the south becoming thicker towards the north. On top of the reservoirs, Permian Zechstein evaporites and carbonates form an effective seal that is locally up to 800m thick but that has undergone severe halokinesis (Grötsch et al., 2011 in Clerx, 2014).
During reservoir rock deposition the Greater Ameland Area was situated in the distal part of the Southern Permian Basin, an elongate E-W trending land-locked basin extending from Poland to the UK. Gas is currently produced from distal Rotliegend aeolian-fluvial sandstones that exhibit relatively poor porosity and permeability properties (Clerx, 2014).

The schematic geological cross section is generated on the website of dinoloket (https://www.dinoloket.nl/ondergrondmodellen; RO = Rotliegend, ZE = Zechstein). In the SSW-NNE profile Ameland Westgat is located halfway.

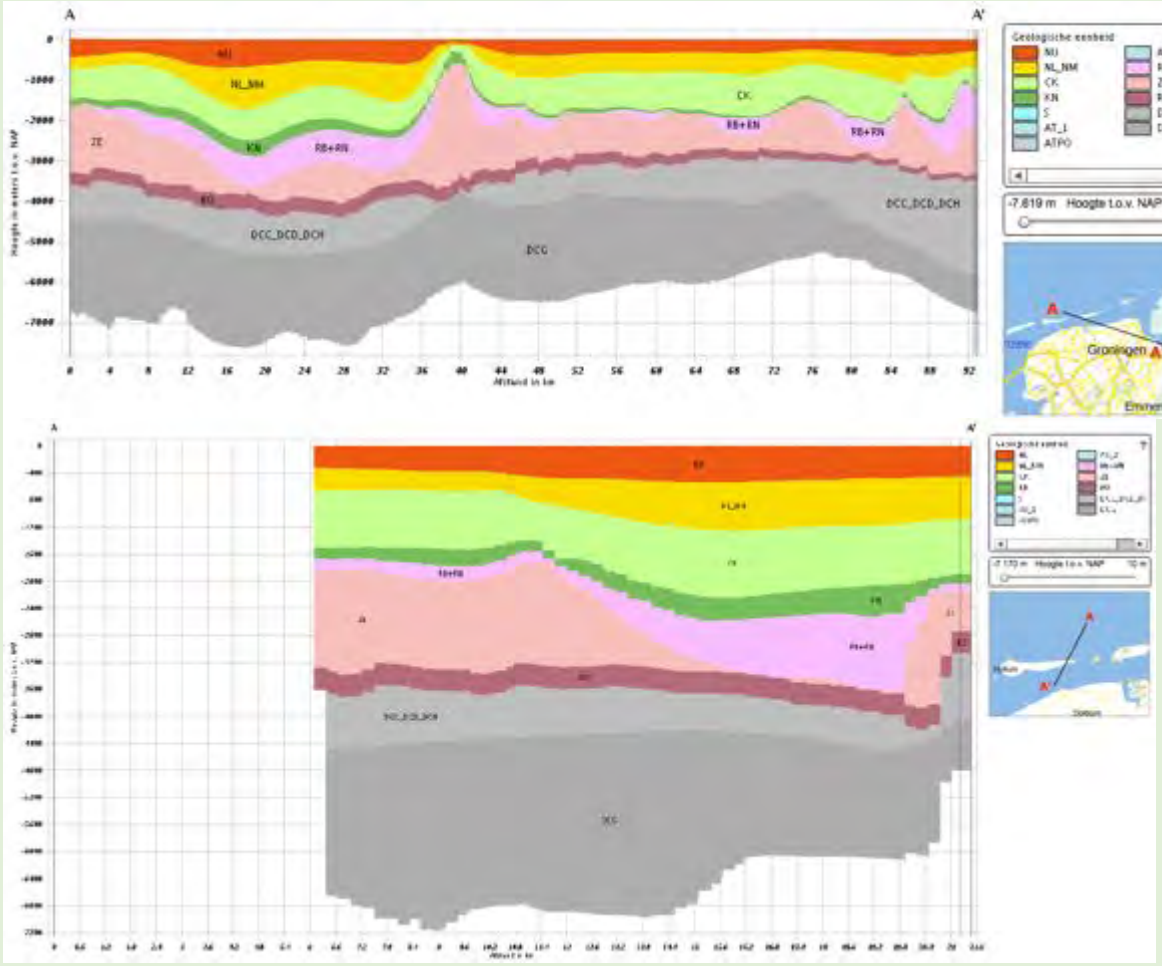

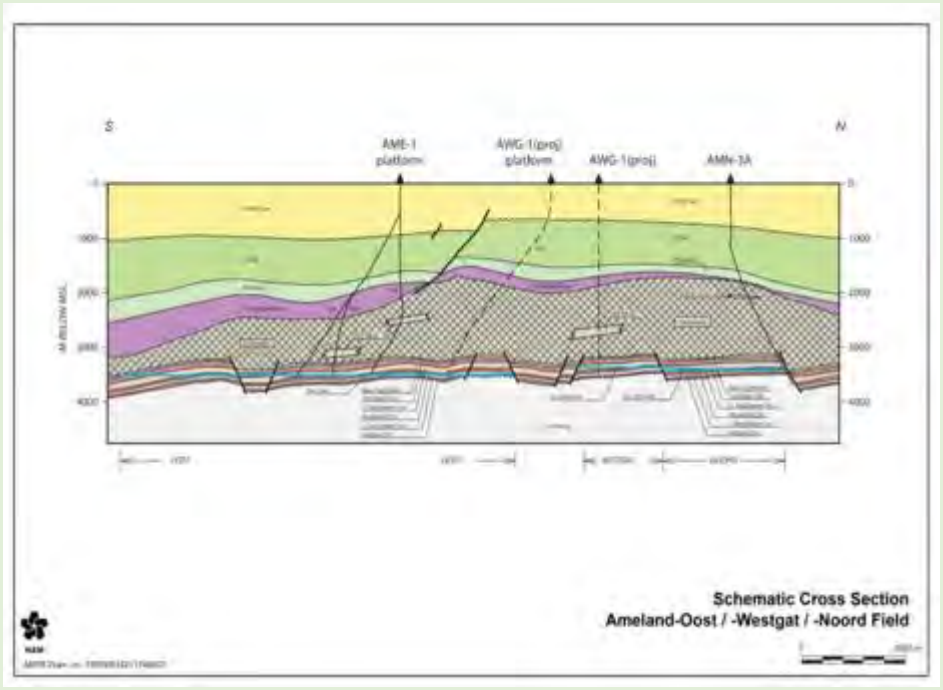

A more detailed cross-section of the Ameland Westgast region (NAM, 2011). The hatched area denotes the Zechstein deposits.

2. **Geophysics of the prospective area**

Requested information:

- ✓ previous geophysical measurements (in CHPM relevance)
- ✓ geophysical results that can be used for locating/defining the deep metal enrichment
- ✓ list of available geophysical maps, cross sections, logs, other measurements

Ameland Westgat, AWG-106,
All borehole documents and logs can be found on:
https://www.nlog.nl/nlog/requestData/nlogp/allBor/metaData.jsp?tableName=BorLocation&id=106518416
Detailed section of the gamma-ray and interval transit time (3950 m to 4150 m depth). The brief peak in gamma-ray units at 4010 m depth reveals the stratigraphic position of the Coppershale.

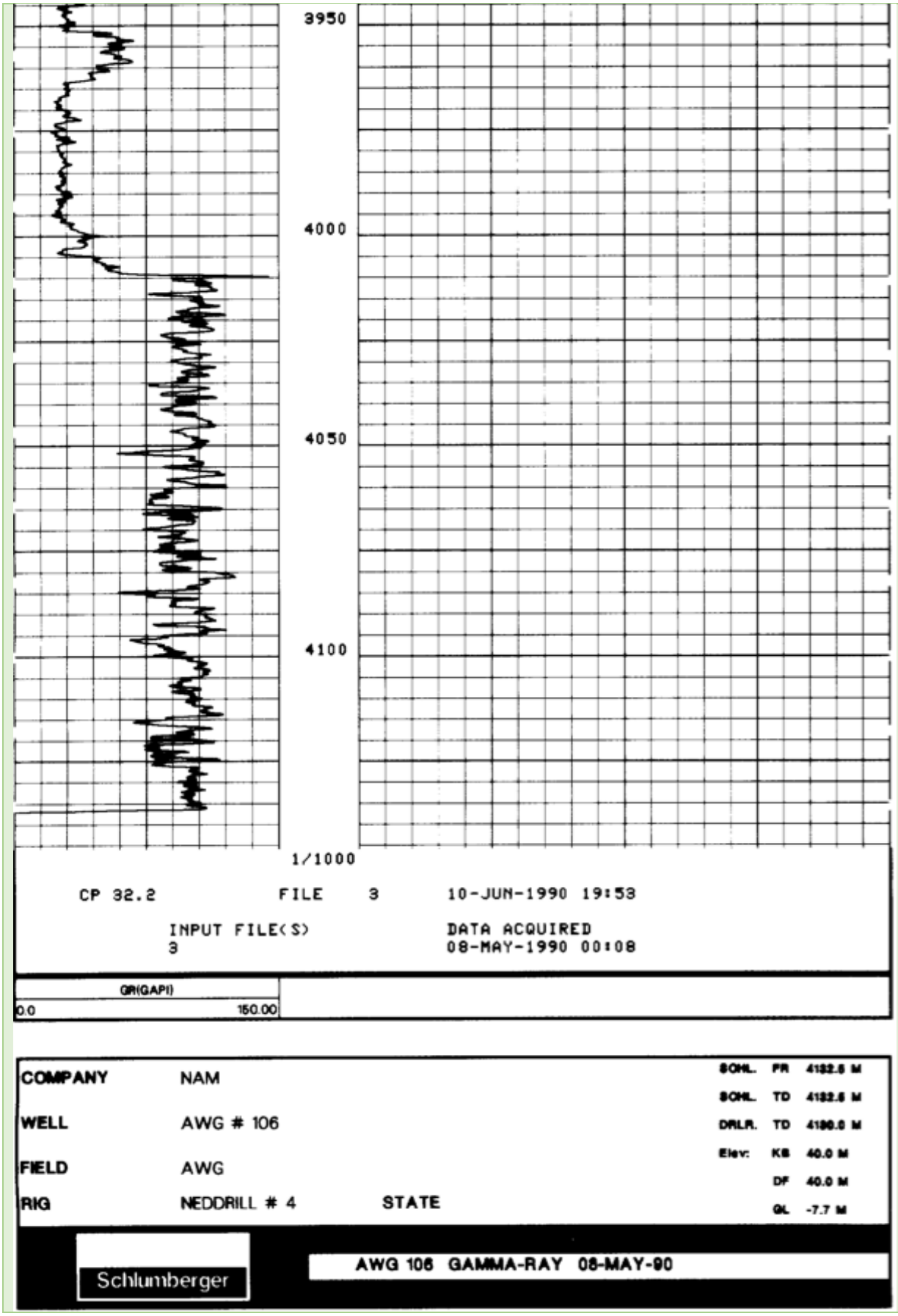
3950
4000
4050
4100
1/1000
CP 32.2
FILE 3
10-JUN-1990 19:53
INPUT FILE(S)
3
DATA ACQUIRED
08-MAY-1990 00:08
GR(GAPI)
0.0
150.00
COMPANY
NAM
WELL
AWG # 106
FIELD
AWG
RIG
NEDDRILL # 4
STATE
SONL. FR 4132.5 M
SONL. TD 4132.5 M
DRLR. TD 4130.0 M
Elev: KB 40.0 M
DF 40.0 M
GL -7.7 M
Schlumberger
AWG 106 GAMMA-RAY 08-MAY-90

3. Deep metal enrichment

Requested information:

✓ (expected) metal enrichment based on available geophysical, geological and drill data, samples information, geochemistry

No further specific data are available on the Coppershale.
However, a study by Schmidt (2000) reveals the mineral composition of the Coppershale in NW Drenthe, at a distance of about 50 km of the Ameland Westgat site. The tables below may serve as a coarse indication of elemental composition (Table 2.3 and 2.4 in Schmidt, 2000). Core C1 and C2 are located a short distance from each other. The exact location of these cores is confidential.

Table 2.3 - Major elements (wt%)

Core	Sample no. and type	SiO_2	TiO_2	Al_2O_3	Fe_2O_3	MgO	MnO	CaO	K_2O	Na_2O	P_2O_5	LOI*	Total
C1	1 Grey sandstone	82.79	0.20	7.01	1.89	0.49	0.04	0.39	2.35	0.74	0.08	2.91	98.89
C1	2 Bituminous sst.	87.38	0.09	4.76	0.45	0.12	0.01	0.70	1.82	0.66	0.07	3.37	99.43
C1	3 Bituminous sst.	82.22	0.08	4.16	0.40	0.10	0.01	2.98	1.61	0.56	0.07	6.17	98.36
C1	4 Bituminous sst.	86.55	0.08	5.09	0.35	0.19	0.01	0.46	1.95	0.65	0.07	4.14	99.54
C2	5 Kupferschiefer	42.71	0.68	13.84	3.65	3.52	0.15	9.53	3.61	0.77	0.17	25.13	103.75
C2	6 Bituminous sst.	84.35	0.10	5.20	5.12	0.69	0.09	0.29	1.91	0.66	0.07	4.22	102.69
C2	7 Bituminous sst.	86.00	0.12	2.92	2.01	1.36	0.12	4.04	0.97	0.37	0.07	5.52	103.50
C2	8 Bituminous sst.	87.29	0.08	5.16	2.22	0.29	0.03	0.73	1.87	1.01	0.07	2.98	101.74
C2	9 Conglomerate	80.33	0.12	3.30	6.53	2.14	0.09	3.90	0.71	0.22	0.11	5.71	103.17
C2	10 Grey shale	59.38	1.05	23.58	3.79	0.67	0.01	0.00	4.35	0.55	0.05	5.37	98.78

* : loss on ignition

Table 2.4 - Trace elements (ppm) and carbon contents (wt%)

Core	Sample no. and type	As	Co	Cu	Ni	Pb	V	S	Ba	Th	U	C_{total}	$C_{organic}$	$C_{carbonate}$
C1	1 Grey sandstone	4	221	10	16	9	28	0	441	11	0	0.55	0.27	0.28
C1	2 Bituminous sandstone	296	323	26	46	34	45	1882	555	6	36	1.42	0.77	0.65
C1	3 Bituminous sandstone	29	237	75	12	11	31	12478	322	10	327	4.19	2.77	1.42
C1	4 Bituminous sandstone	240	268	42	43	30	84	485	1034	9	139	2.51	1.65	0.86
C2	5 Kupferschiefer	140	334	14390	218	714	2243	12806	311	3	52	12.08	9.87	2.21
C2	6 Bituminous sandstone	2	319	10	26	15	14	588	709	8	0	1.25	0.55	0.70
C2	7 Bituminous sandstone	4	195	8	12	12	18	4675	1000	8	5	1.45	0.27	1.18
C2	8 Bituminous sandstone	5	204	6	15	9	15	1745	1340	9	0	0.81	0.50	0.31
C2	9 Conglomerate	8	258	10	13	10	46	670	2081	7	2	1.39	0.17	1.22
C2	10 Grey shale	5	65	13	67	13	130	0	524	20	5	0.04	0.02	0.02

4. **Integrated 3D- 4D model**

Requested information:

- ✓ existing 3D-4D models of the target area and the deep metal enrichment
- ✓ if no 3D-4D models exist, collect the following necessary data: geological setting, mineralization, fluid flow models, stress field determination

Notes: e.g. openly available datasets, models.

Geothermal data on the Rotliegend of the Ameland Westgat
Source: thermogis.nl (beta version)

Depth (m)	3478.28
Thickness (m)	167.46
Permeability (mD)	1.28
Transmissivity (Dm)	0.21
Net to Gross	1
Temperature (°C)	110.93
Pump pressure (bar)	0
Flow rate (m3/h)	0
Power indication (MW)	0
Heat in place (GJ/m2)	56.84
Potential recoverable heat (GJ/m2)	0.51
Potential	unknown

Further information on http://thermogis.nl/thermogis_en.html (updated version available from October 2018).

5. EGS potential

Requested information:

- ✓ EGS potential (heat & energy) of the area
- ✓ geothermal characteristics (temperature gradient, heat flux, stress field, water availability, EGS geology)
- ✓ presence/indication of deep fluids/brines, fracture system, crustal permeability

See also point 4.

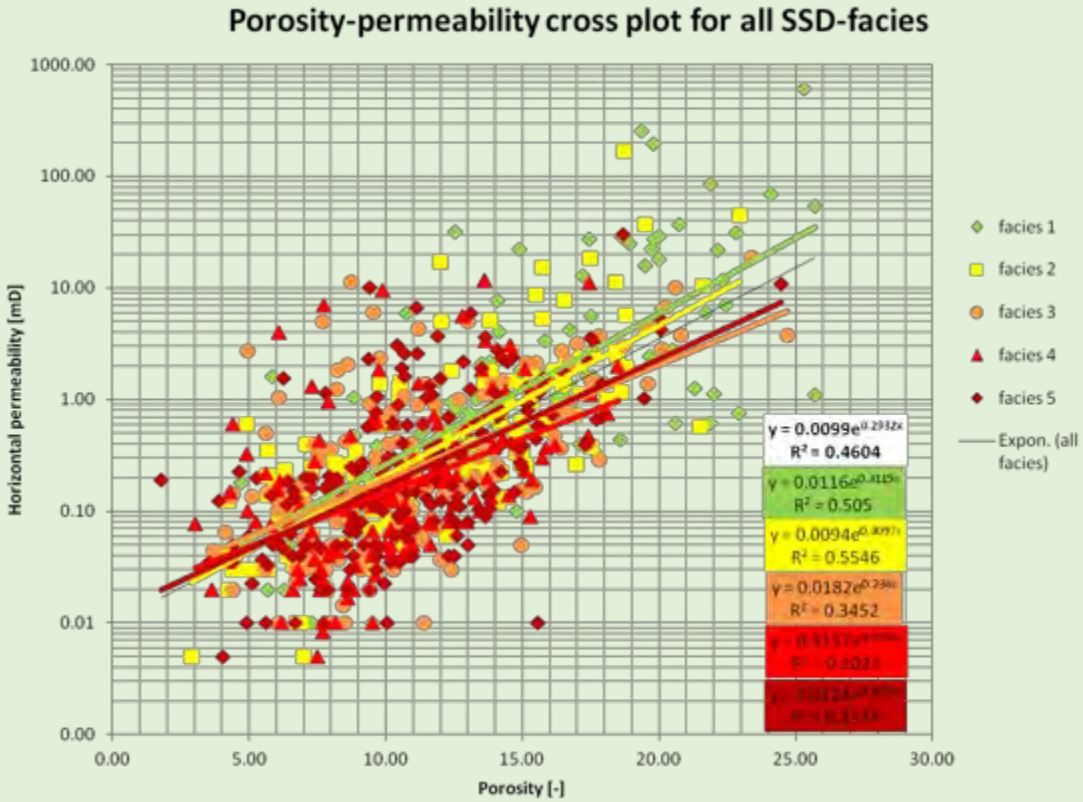

Porosity- Permeability plot for the Greater Ameland area (Clerx, 2014); various facies are no further specified.

List of references

Clerx, N.E., 2014. An integrated study of Permian Rotliegend reservoir rocks in the Greater Ameland Area. MSc thesis TU Delft. 98 p.

NAM, 2011. Winningsplan Ameland 2011. https://nam-feitenencijfers.data-app.nl/download/rapport/53af1b78-9253-4663-a93a-586d3fb7e392?open=true

Schmidt, A.P., 2000. Naturally Occurring Radioactive Materials in the gas and oil industry. Origin, transport and deposition of stable lead and 210Pb from Dutch gas reservoirs. PhD Thesis Universiteit Utrecht, 144 p.

Websites

https://www.dinoloket.nl/ondergrondmodellen

https://nam-feitenencijfers.data-app.nl/download/rapport/53af1b78-9253-4663-a93a-586d3fb7e392?open=true

https://www.nlog.nl/nlog/requestData/nlogp/allBor/metaData.jsp?tableName=BorLocation&id=106518416

http://thermogis.nl/thermogis_en.html

Annexes

NL2-AWG-1 Stratigraphic information– **Find them in the folder: Additional information on basic and CHPM characteristics evaluation**

AREA 3- NL3-BRW

1. **Geology of the prospective area**
   Requested information on:
- ✓ local geology (in regional context)
- ✓ CHPM target formation
- ✓ list of available cross sections, geological maps, geochemical results, lithological information

Notes: briefly summarized, referenced to more detailed studies.

Borgsweer, BRW-04, ***type B***
Lithostratigraphy:
Depth Coppershale : 2954-2955 m
Location: 53.29108611 7.01795771
See also appendix NL3-BRW-1
https://www.nlog.nl/nlog/requestData/nlogp/allBor/metaData.jsp?tableName=BorLocation&id=106522064

Well BRW-4 is located in the eastern part of the Groningen gas field. The gasreservoir consists of eolian and fluvial sandstone and conglomerates of the Rotliegend. The reservoir is sealed by the Zechstein salts. The Coppershale marks the base of the Zechstein.

Until recently, (production waste) water injection took place via the BRW-04 well, with BRW-2A as a back-up well for injection. In 2013 a new injection well BRW-5 was drilled, which is now used as replacement for the BRW-4 injection well. No gas production takes place from the Borgsweer location; the nearest production cluster to the Borgsweer location is Amsweer (TNO, 2015).

The geological profile is generated on the website of dinoloket (https://www.dinoloket.nl/ondergrondmodellen; RO = Rotliegend, ZE = Zechstein). In the SSW-NNE profile Borgsweer is located halfway.

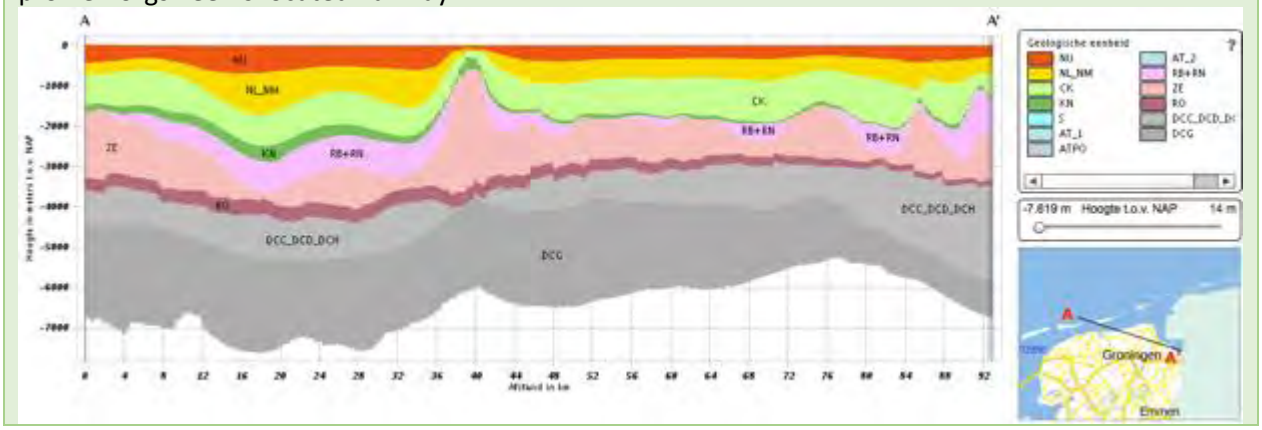

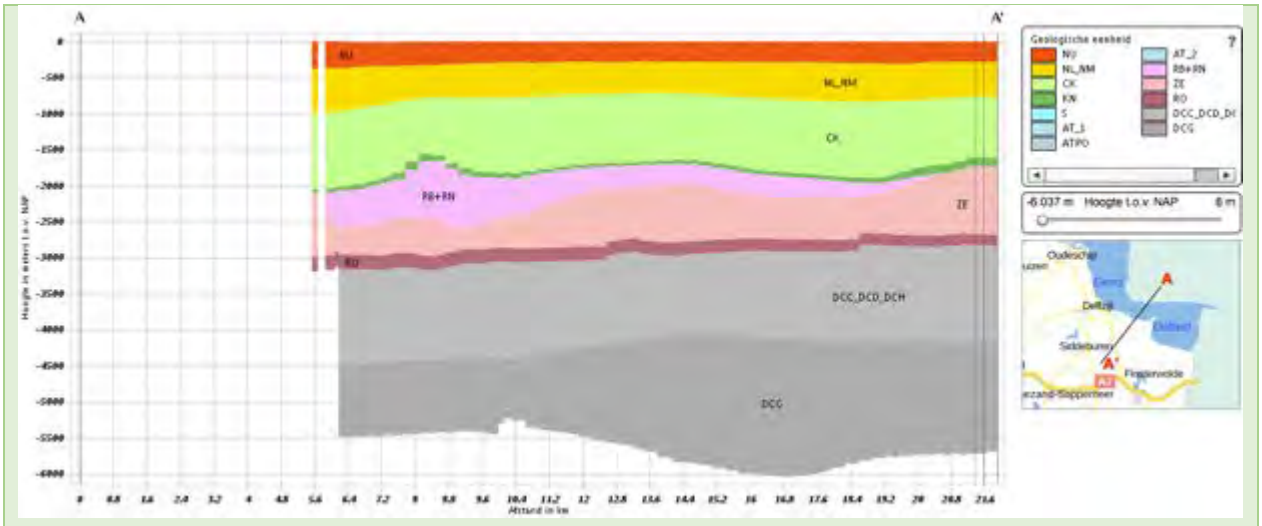

2. Geophysics of the prospective area

Requested information:

- ✓ previous geophysical measurements (in CHPM relevance)
- ✓ geophysical results that can be used for locating/defining the deep metal enrichment
- ✓ list of available geophysical maps, cross sections, logs, other measurements

All borehole documents and logs can be found on:
https://www.nlog.nl/nlog/requestData/nlogp/allBor/metaData.jsp?tableName=BorLocation&id=106522064

Detailed section of the gamma-ray and interval transit time (2850 m to 2960 m depth). The brief peak in gamma-ray units at 2954 m depth reveals the stratigraphic position of the Coppershale.

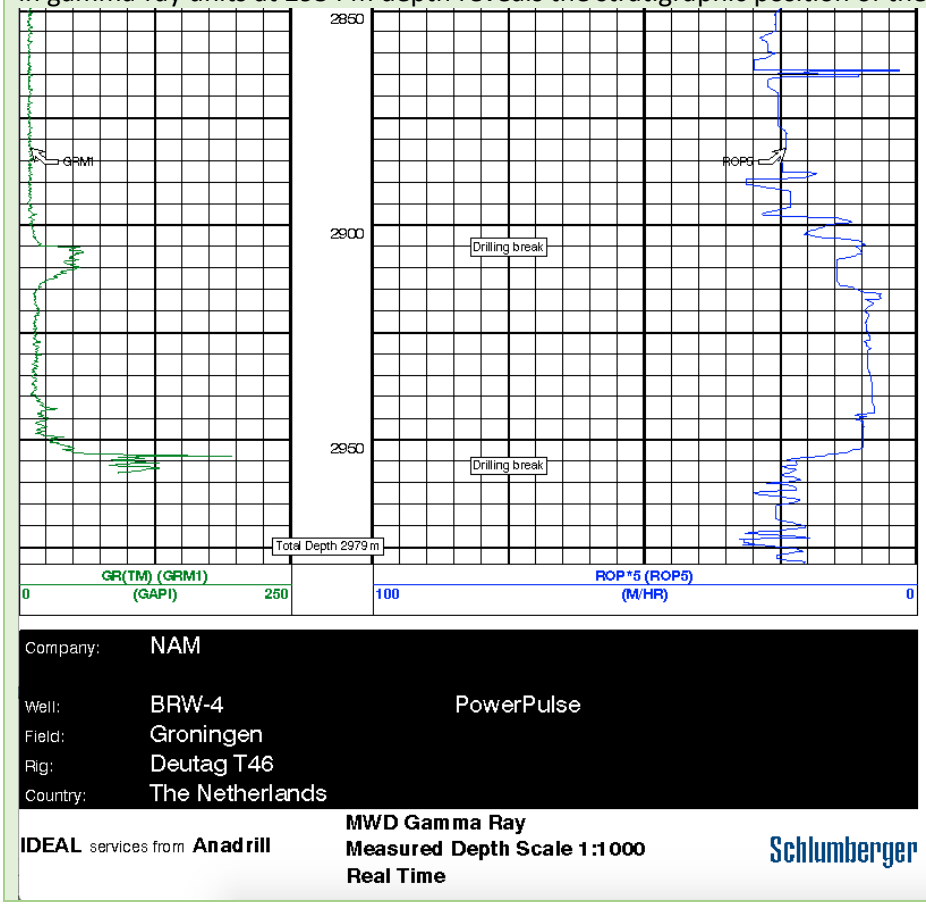

3. Deep metal enrichment

Requested information:

✓ (expected) metal enrichment based on available geophysical, geological and drill data, samples information, geochemistry

No further specific data are available on the Coppershale.
However, a study by Schmidt (2000) reveals the mineral composition of the Coppershale in NW Drenthe, at a distance of about 45 km of the Borgsweer site. The tables below may serve as a coarse indication of elemental composition (Table 2.3 and 2.4 in Schmidt, 2000). Core C1 and C2 are located a short distance from each other. The exact location of these cores is confidential.

Table 2.3 - Major elements (wt%)

Core	Sample no. and type	SiO_2	TiO_2	Al_2O_3	Fe_2O_3	MgO	MnO	CaO	K_2O	Na_2O	P_2O_5	LOI*	Total
C1	1 Grey sandstone	82.79	0.20	7.01	1.89	0.49	0.04	0.39	2.35	0.74	0.08	2.91	98.89
C1	2 Bituminous sst.	87.38	0.09	4.76	0.45	0.12	0.01	0.70	1.82	0.66	0.07	3.37	99.43
C1	3 Bituminous sst.	82.22	0.08	4.16	0.40	0.10	0.01	2.98	1.61	0.56	0.07	6.17	98.36
C1	4 Bituminous sst.	86.55	0.08	5.09	0.35	0.19	0.01	0.46	1.95	0.65	0.07	4.14	99.54
C2	5 Kupferschiefer	42.71	0.68	13.84	3.65	3.52	0.15	9.53	3.61	0.77	0.17	25.13	103.75
C2	6 Bituminous sst.	84.35	0.10	5.20	5.12	0.69	0.09	0.29	1.91	0.66	0.07	4.22	102.69
C2	7 Bituminous sst.	86.00	0.12	2.92	2.01	1.36	0.12	4.04	0.97	0.37	0.07	5.52	103.50
C2	8 Bituminous sst.	87.29	0.08	5.16	2.22	0.29	0.03	0.73	1.87	1.01	0.07	2.98	101.74
C2	9 Conglomerate	80.33	0.12	3.30	6.53	2.14	0.09	3.90	0.71	0.22	0.11	5.71	103.17
C2	10 Grey shale	59.38	1.05	23.58	3.79	0.67	0.01	0.00	4.35	0.55	0.05	5.37	98.78

* : loss on ignition

Table 2.4 - Trace elements (ppm) and carbon contents (wt%)

Core	Sample no. and type	As	Co	Cu	Ni	Pb	V	S	Ba	Th	U	C_{total}	$C_{organic}$	$C_{carbonate}$
C1	1 Grey sandstone	4	221	10	16	9	28	0	441	11	0	0.55	0.27	0.28
C1	2 Bituminous sandstone	296	323	26	46	34	45	1882	555	6	36	1.42	0.77	0.65
C1	3 Bituminous sandstone	29	237	75	12	11	31	12478	322	10	327	4.19	2.77	1.42
C1	4 Bituminous sandstone	240	268	42	43	30	84	485	1034	9	139	2.51	1.65	0.86
C2	5 Kupferschiefer	140	334	14390	218	714	2243	12806	311	3	52	12.08	9.87	2.21
C2	6 Bituminous sandstone	2	319	10	26	15	14	588	709	8	0	1.25	0.55	0.70
C2	7 Bituminous sandstone	4	195	8	12	12	18	4675	1000	8	5	1.45	0.27	1.18
C2	8 Bituminous sandstone	5	204	6	15	9	15	1745	1340	9	0	0.81	0.50	0.31
C2	9 Conglomerate	8	258	10	13	10	46	670	2081	7	2	1.39	0.17	1.22
C2	10 Grey shale	5	65	13	67	13	130	0	524	20	5	0.04	0.02	0.02

4. **Integrated 3D- 4D model**

Requested information:

- ✓ existing 3D-4D models of the target area and the deep metal enrichment
- ✓ if no 3D-4D models exist, collect the following necessary data: geological setting, mineralization, fluid flow models, stress field determination

Notes: e.g. openly available datasets, models.

Geothermal data on the Rotliegend of Borgsweer
Source: thermogis.nl (beta version)

	Rotliegend
Depth (m)	2944.85
Thickness (m)	137.11
Permeability (mD)	154.01
Transmissivity (Dm)	20.84
Net to Gross	1
Temperature (°C)	99.74
Pump pressure (bar)	88.35
Flow rate (m3/h)	354.04
Power indication (MW)	25.6
Heat in place (GJ/m2)	41.28
Potential recoverable heat (GJ/m2)	0.36
Potential	unknown

Further information on http://thermogis.nl/thermogis_en.html (updated version available from October 2018).

The Slochteren reservoir at the Borgsweer area consists of sandstones with porosities between 15 and 20% and permeabilities between 10 and 100 mD. The lower part of the sandstone reservoir is of a slightly less quality. Initial reservoir temperatures in the Slochteren sandstone are around 105 ^{o}C (adapted from TNO, 2015).

5. **EGS potential**

Requested information:

- ✓ EGS potential (heat & energy) of the area
- ✓ geothermal characteristics (temperature gradient, heat flux, stress field, water availability, EGS geology)
- ✓ presence/indication of deep fluids/brines, fracture system, crustal permeability

As shown in figure above, both injection wells BRW-4 and BRW-5 are located close to an N-S striking fault intersecting the reservoir. Here, BRW-4 is located to the west of the N-S fault, at a distance of approximately 250 m, and BRW-5 intersects the reservoir to the east of the fault at a distance of around 150 m. The offset of the N-S striking normal fault is limited; close to the injection well the fault offset is around 15-25 m. A further 400 m to the north a second NNW-SSE striking normal fault with an offset between 25-30 m is encountered (adapted from TNO, 2015).

Induced seismicity is recorded in the Groningen gasfield production area. Seismicity near Borgsweer is likely due to water injection (TNO, 2015).

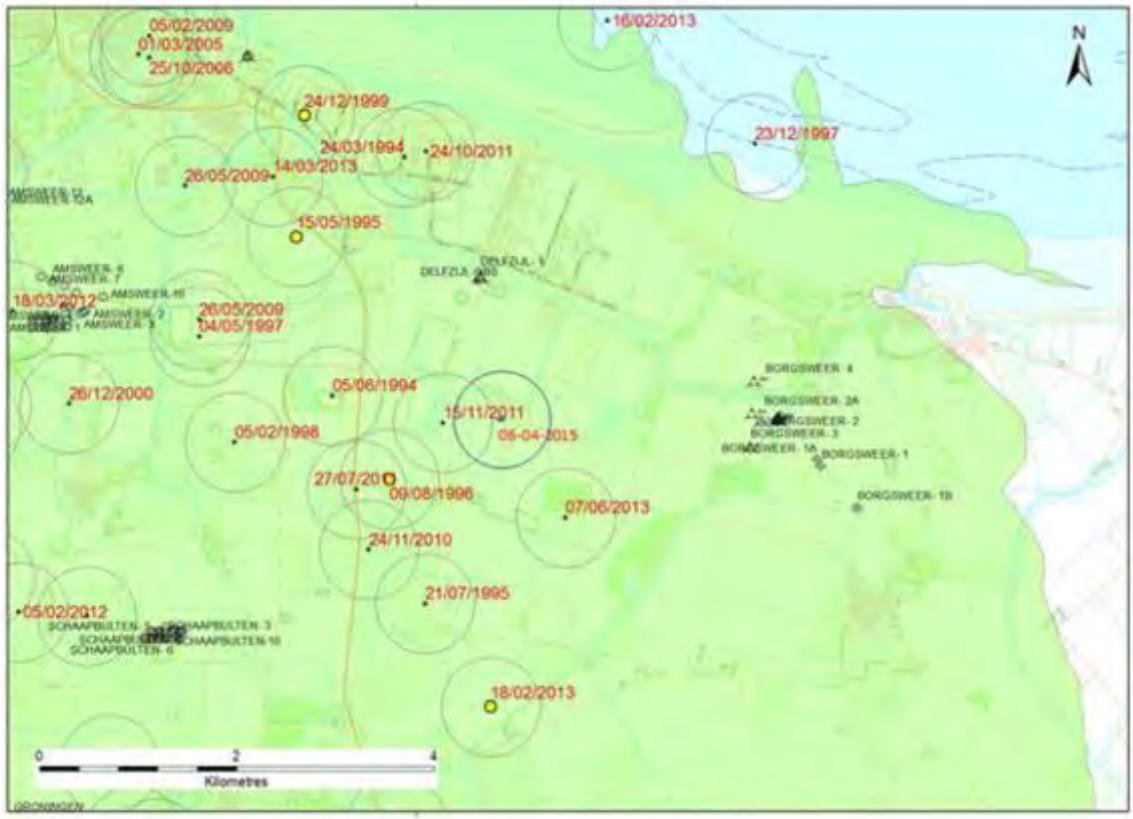

Figure 16. Seismic events recorded in the region to the west of the Borgsweer injection wells. Locations of the wells are presented at reservoir level. All events are shown till end June 2013 (Source: NAM-report EP201306210959, 2013). In addition the recent M=1.3 seismic event (April 2015) is shown.

Various recordings of earthquakes near Borgsweer
(http://www.oosterwijtwerd.net/geschiedenis/aardbevingen-in-de-regio/aardbevingen-overzicht/)
2014-03-30 20:58:47 Borgsweer 1.4
2015-04-06 13:10:26 Borgsweer 1.3
2017-07-14 07:55:29 Borgsweer 53.282 6.994 3.0 0.6

Currently an approximately 4 km long tunnel is being produced to the west of the town of Emden (Germany), which will cross the River Ems in the direction of the Netherlands. The aim of the tunnel is to carry a 48 inch gas pipeline. The tunnel will be exactly 4,016 m long. It crosses below the Ems from the German centre of Knock finishing up at the Dutch town of Borgsweer (http://www.tunnel-online.info/en/artikel/tunnel_Crossing_the_Ems_near_Emden_D_101706.html) .

List of references

Schmidt, A.P., 2000. Naturally Occurring Radioactive Materials in the gas and oil industry. Origin, transport and deposition of stable lead and 210Pb from Dutch gas reservoirs. PhD Thesis Universiteit Utrecht, 144 p.

TNO, 2015. Injection-Related Induced Seismicity and its relevance to Nitrogen Injection: Description of Dutch field cases. TNO report 2015 R10906. 34 p.

Websites

https://www.nlog.nl/nlog/requestData/nlogp/allBor/metaData.jsp?tableName=BorLocation&id=106522064

http://thermogis.nl/thermogis_en.html

https://www.dinoloket.nl/ondergrondmodellen

http://www.tunnel-online.info/en/artikel/tunnel_Crossing_the_Ems_near_Emden_D_101706.html

http://www.oosterwijtwerd.net/geschiedenis/aardbevingen-in-de-regio/aardbevingen-overzicht/)

Annexes

NL3-BRW-1 Stratigraphic information– **Find them in the folder: Additional information on basic and CHPM characteristics evaluation**

AREA 4- NL4-KKP

1. **Geology of the prospective area**

Requested information on:

- ✓ local geology (in regional context)
- ✓ CHPM target formation
- ✓ list of available cross sections, geological maps, geochemical results, lithological information

Notes: briefly summarized, referenced to more detailed studies.

Koekoekspolder, KKP-GT-02, ***type B***

Lithostratigraphy:

Depth Coppershale : 2104-2107 m

Location: 52.58083974 5.95045108

See also appendix NL4-KKP-1

https://www.nlog.nl/nlog/requestData/nlogp/allBor/metaData.jsp?tableName=BorLocation&id=872287025

The geothermal target reservoir in which the doublet is situated is the sandstone of the Slochteren Formation. The reservoir is bounded at the top by the Coppershale Member (Kupferschiefer), Z1 Carbonate Member and Z1 Anhydrite Member which are all members of the Zechstein Group. At the bottom the reservoir is bounded by the Ruurlo Formation of the Limburg Group.
The thickness of the Slochteren sandstone Formation is about 75 m (Aardwarmtecluster, 2013).

Stratigraphic profile based on sample description and rate of penetration. GeoService GmbH started monitoring the well at 60 m and sampling at 100 m (MD).

Period	Epoch	Stage	Group	Formation	Member	Top Depth [m] (TVD)	Top Depth [m] (MD)
Quaternary	Holocene - Pleistocene	"Diverse"	Upper North Sea NU	"Diverse"	"Diverse"	0	0
	Early Pleistocene			Maassluis NUMS		200	200
Tertiary	Pliocene			Oosterhout NUOT		250	250
	Miocene			Breda NUBA		290	290
	Oligocene	Chattian	Middle North Sea NM	Veldhoven NMVF	Veldhoven Clay NMVFO	500	500
		Rupelian- Early Chattian		Rupel NMRF	Rupel Clay NMRFC	545	545
	Eocene	Priabolian - Rupelian			Vessem NMRFV	595	595
		Lutetian to Bartonian	Lower North Sea NL	Dongen NLFF	Asse NLFFB	635.9	636
		Ypresian to Lutetian			Brussels Sand NLFFS	727.9	729
		Ypresian			Ieper NLFF	796.6	800
					Basal Dongen Tuffite NLFFT	990.7	1024
	Paleocene	Thabetian		Landen NLLF	Landen Clay	1015.9	1055
Cretaceous	Upper Cretaceous	Turonian - Maastrichtian	Chalk CK	Ommelanden CKGR		1033.5	1077
		Cenomanian		Texel CKTX		1422.6	1567.5
	Lower Cretaceous	Late Albian	Rijnland KN	Holland KNGL	Upper Holland Marl KNGLU	1501.2	1665
		Early Albian			Middle Holland Claystone KNGLM	1554.4	1730
		Early Aptian			Lower Holland Marl KNGLL	1566.8	1745
Permian	Upper Permian	Thurigian	Zechstein ZE	Zechstein 2 (Staßfurt)	Z2 Carbonate ZEZ2C	1591.9	1776
				Zechstein 1 (Werra)	Z1 Anhydrite ZEZ1W	1617.3	1808
					Z1 Carbonate ZEZ1C	1818.7	2070
					Coppershale ZEZ1K	1844.9	2104
	Lower Permian	Saxonian	Upper Rotliegend RO	Slochteren ROSL	Slochteren	1847.2	2107
MD = Measured depth; TVD = Total vertical depth						1923.9 m Final Depth	2205.3 m Final Depth

Stratigraphic Profile by GeoService GmbH (2011)

2. Geophysics of the prospective area

Requested information:

- ✓ previous geophysical measurements (in CHPM relevance)
- ✓ geophysical results that can be used for locating/defining the deep metal enrichment
- ✓ list of available geophysical maps, cross sections, logs, other measurements

Koekoekspolder, KKP-GT-02

All borehole documents and logs can be found on:

https://www.nlog.nl/nlog/requestData/nlogp/allBor/metaData.jsp?tableName=BorLocation&id=872287025

Detailed section of the gamma-ray (in green) and other logs (2100 m to 2150 m depth). The peak in gamma-ray units at 2109 m depth reveals the stratigraphic position of the Coppershale.

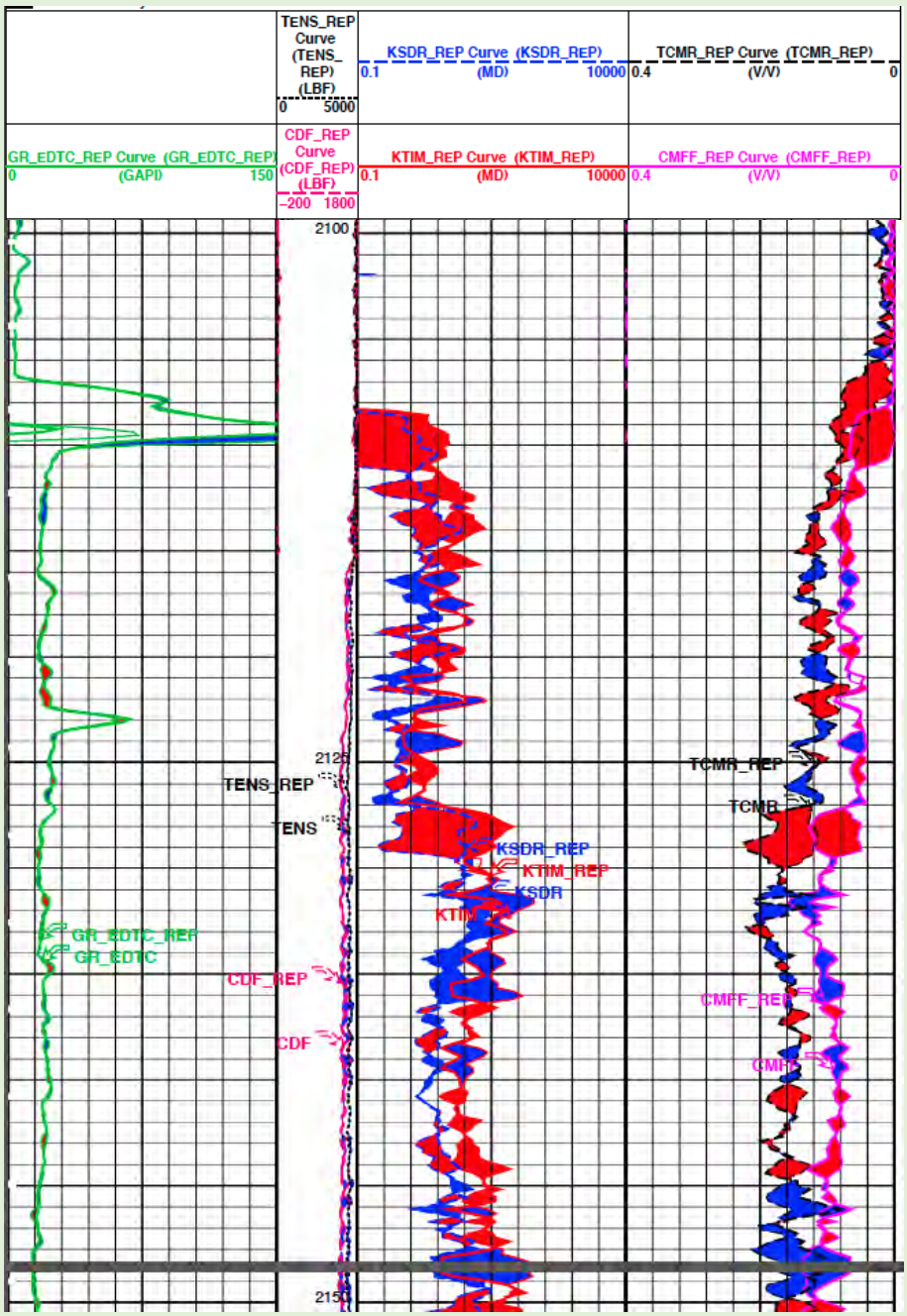

In the graph below show a combined lithostratigraphy as well as logging results at a well depth of 2070 to 2225 m (Aardwarmtecluster, 2013). Please mark the peak in gamma ray at the level of the dark grey claystone at a depth of about 2105 m representing the Coppershale.

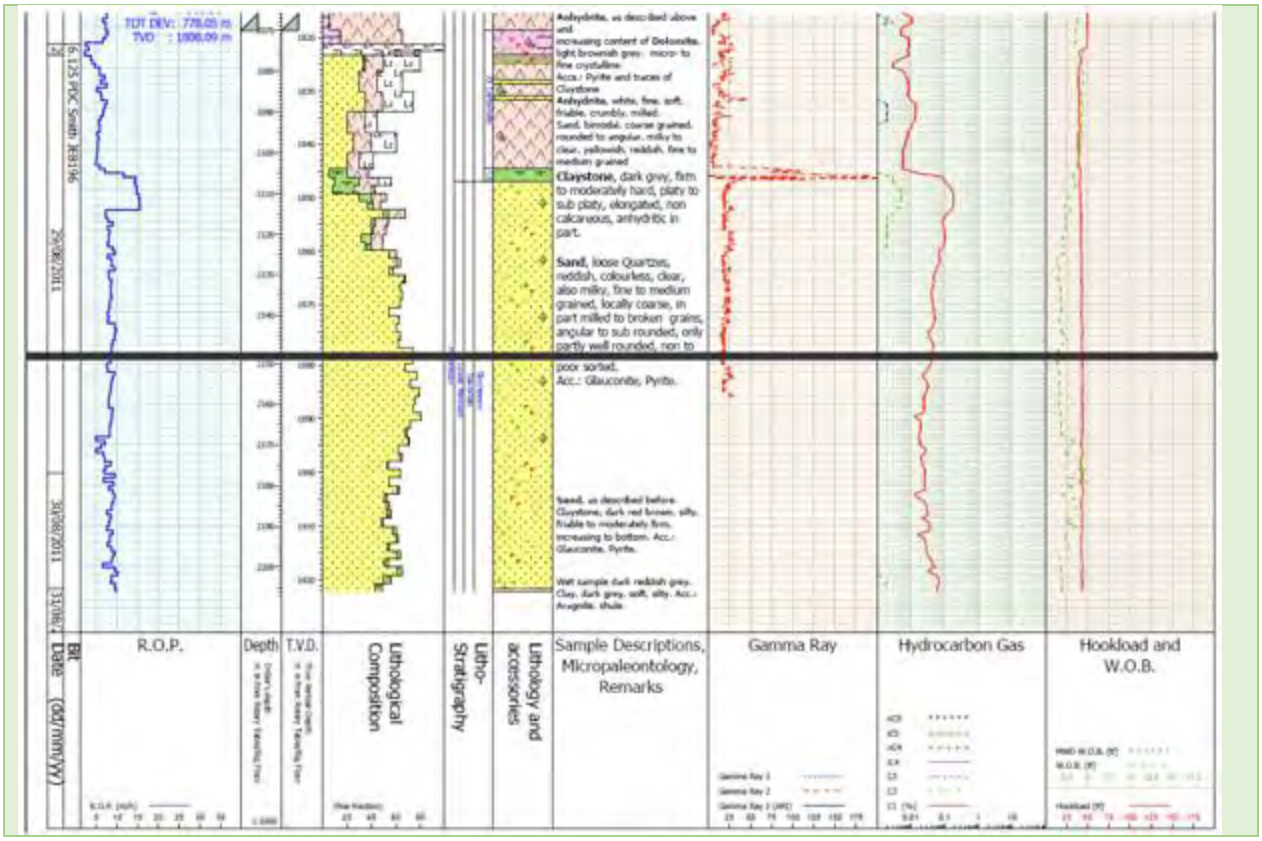

3. <u>Deep metal enrichment</u>

<u>Requested information:</u>

✓ (expected) metal enrichment based on available geophysical, geological and drill data, samples information, geochemistry

IF Technology (2011) reports on low metal concentrations in water samples:

METALS	
aluminium	<2500 µg/l (production well formation water)
barium	3100 µg/l
cadmium	83 µg/l
calcium	16000000 µg/l
potassium	1300000 µg/l
copper	<250 µg/l (production well formation water)
lead	2700 µg/l
magnesium	1200000 µg/l
manganese	6400 µg/l
sodium	68000000 µg/l
nickel	<500 µg/l (production well formation water)
strontium	400000 µg/l
iron	85000 µg/l
zinc	34000 µg/l

The depth interval comprising the base of the Zechstein (and below) reports on the presence of pyrite (GeoService GmbH, 2011). Description of other depth intervals can be found in the final report by GeoService GmbH (2011).

1840 - 1915	**Anhydrite**, white to off-white, soft, friable, crumbly, milled by bit, calcareous in part. Acc.: Dolomite, light brownish grey to light grey, as previously described, Claystone as cavings and Pyrite.

No further specific data are available on the Coppershale. region.However, a study by Schmidt (2000) reveals the mineral composition of the Coppershale in NW Drenthe, at a distance of about 65 km of the Koekoekspolder site. The tables below may serve as a coarse indication of elemental composition (Table 2.3 and 2.4 in Schmidt, 2000). Core C1 and C2 are located a short distance from each other. The exact location of these cores is confidential.

Table 2.3 - Major elements (wt%)

Core	Sample no. and type	SiO_2	TiO_2	Al_2O_3	Fe_2O_3	MgO	MnO	CaO	K_2O	Na_2O	P_2O_5	LOI*	Total
C1	1 Grey sandstone	82.79	0.20	7.01	1.89	0.49	0.04	0.39	2.35	0.74	0.08	2.91	98.89
C1	2 Bituminous sst.	87.38	0.09	4.76	0.45	0.12	0.01	0.70	1.82	0.66	0.07	3.37	99.43
C1	3 Bituminous sst.	82.22	0.08	4.16	0.40	0.10	0.01	2.98	1.61	0.56	0.07	6.17	98.36
C1	4 Bituminous sst.	86.55	0.08	5.09	0.35	0.19	0.01	0.46	1.95	0.65	0.07	4.14	99.54
C2	5 Kupferschiefer	42.71	0.68	13.84	3.65	3.52	0.15	9.53	3.61	0.77	0.17	25.13	103.75
C2	6 Bituminous sst.	84.35	0.10	5.20	5.12	0.69	0.09	0.29	1.91	0.66	0.07	4.22	102.69
C2	7 Bituminous sst.	86.00	0.12	2.92	2.01	1.36	0.12	4.04	0.97	0.37	0.07	5.52	103.50
C2	8 Bituminous sst.	87.29	0.08	5.16	2.22	0.29	0.03	0.73	1.87	1.01	0.07	2.98	101.74
C2	9 Conglomerate	80.33	0.12	3.30	6.53	2.14	0.09	3.90	0.71	0.22	0.11	5.71	103.17
C2	10 Grey shale	59.38	1.05	23.58	3.79	0.67	0.01	0.00	4.35	0.55	0.05	5.37	98.78

* : loss on ignition

Table 2.4 - Trace elements (ppm) and carbon contents (wt%)

Core	Sample no. and type	As	Co	Cu	Ni	Pb	V	S	Ba	Th	U	C_{total}	$C_{organic}$	$C_{carbonate}$
C1	1 Grey sandstone	4	221	10	16	9	28	0	441	11	0	0.55	0.27	0.28
C1	2 Bituminous sandstone	296	323	26	46	34	45	1882	555	6	36	1.42	0.77	0.65
C1	3 Bituminous sandstone	29	237	75	12	11	31	12478	322	10	327	4.19	2.77	1.42
C1	4 Bituminous sandstone	240	268	42	43	30	84	485	1034	9	139	2.51	1.65	0.86
C2	5 Kupferschiefer	140	334	14390	218	714	2243	12806	311	3	52	12.08	9.87	2.21
C2	6 Bituminous sandstone	2	319	10	26	15	14	588	709	8	0	1.25	0.55	0.70
C2	7 Bituminous sandstone	4	195	8	12	12	18	4675	1000	8	5	1.45	0.27	1.18
C2	8 Bituminous sandstone	5	204	6	15	9	15	1745	1340	9	0	0.81	0.50	0.31
C2	9 Conglomerate	8	258	10	13	10	46	670	2081	7	2	1.39	0.17	1.22
C2	10 Grey shale	5	65	13	67	13	130	0	524	20	5	0.04	0.02	0.02

4. **Integrated 3D- 4D model**

Requested information:

- ✓ existing 3D-4D models of the target area and the deep metal enrichment
- ✓ if no 3D-4D models exist, collect the following necessary data: geological setting, mineralization, fluid flow models, stress field determination

Notes: e.g. openly available datasets, models.

IF Technology (2011) observed temperatures up to 74°C.

Geothermal data on the Rotliegend of the Koekoekspolder Geothermal Facility
Source: thermogis.nl (beta version)

Depth (m)	1756.97
Thickness (m)	113.27
Permeability (mD)	127.25
Transmissivity (Dm)	13.94
Net to Gross	1
Temperature (°C)	66.69
Pump pressure (bar)	52.71
Flow rate (m3/h)	141.2
Power indication (MW)	5.46
Heat in place (GJ/m2)	21.54
Potential recoverable heat (GJ/m2)	0.17
Potential	good

Further information on http://thermogis.nl/thermogis_en.html (updated version available from October 2018).

5. EGS potential

Requested information:

- ✓ EGS potential (heat & energy) of the area
- ✓ geothermal characteristics (temperature gradient, heat flux, stress field, water availability, EGS geology)
- ✓ presence/indication of deep fluids/brines, fracture system, crustal permeability

See also point 4.

Well tests at the end of the construction phase performed by IF-Technology (2011) yielded various geothermal characteristics of the well.

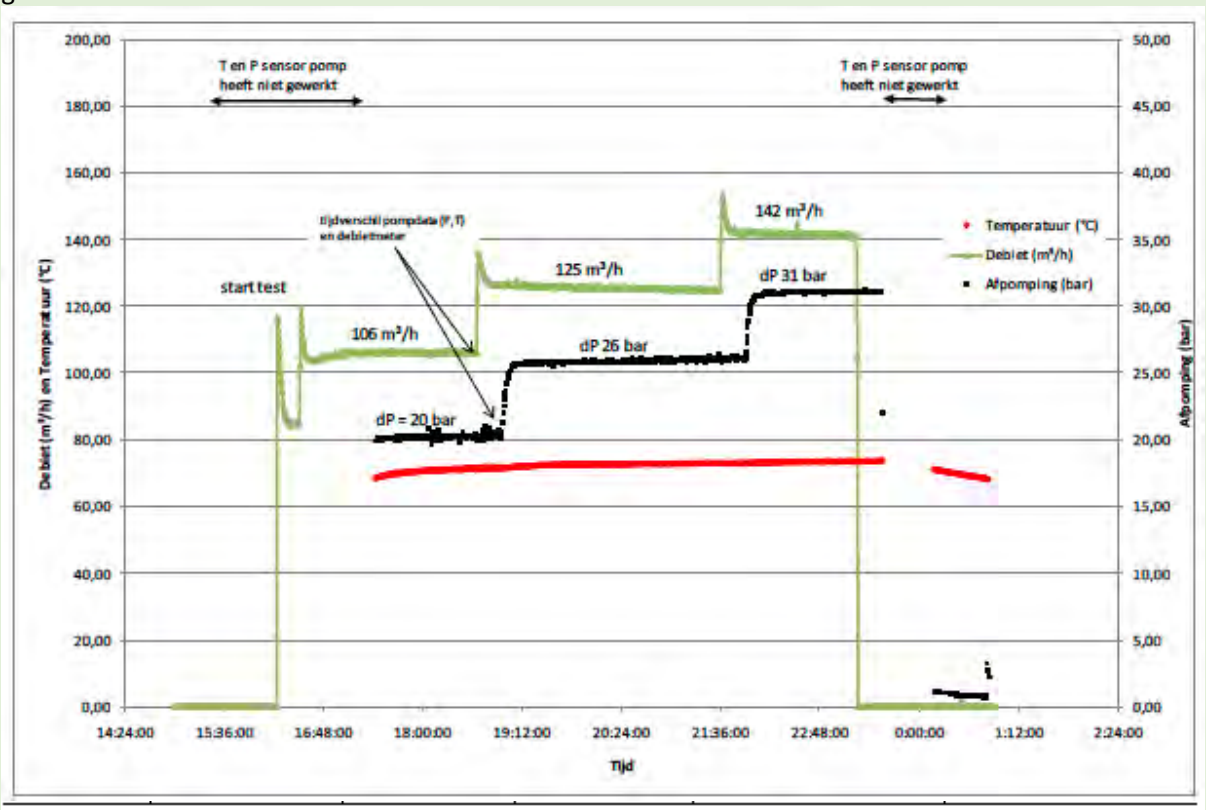

Stap	Frequentie Pomp	Debiet	Afpomping	Reservoir druk	Weerstand Liner/casings
1	40 Hz	106 m³/h	20 bar	16,6 bar	3,4 bar
2	45 Hz	126 m³/h	26 bar	21,2 bar	4,8 bar
3	50 Hz	142 m³/h	31 bar	24,8 bar	6,2 bar

In three steps the drawdown (afpompen) frequency was increased from 40 to 50 Hz resulting in a fluid flow (debiet) of 106 to 142 m^3/h. At a depth of 500 m temperatures of about 74*C were reached.

The measured gas flow was about 140 Nm^3/h at a water flow of 125 m^3/h. The measured gas-water ratio is 0,8 - 0,9 N m^3/ m^3.

During the course of 2013 the production was stopped as the injection well was clogged. Camera inspection revealed a precipitation in the well at a vertical depth of 1750 m. Analysed samples yielded a composition of salt and lead including small amounts of Pb210, a Naturally Occurring Radioactive Material. The well is in production again since the end of 2013 and running stable ever since (Besselink, 2015).

The average porosity of the Slochteren sandstone formation is 17 %, ranging from 8.2 to 24.3%. The resultant permeability is about 120 mD (Aardwarmtecluster, 2013).

The seismic interpretations show several faults in the vicinity of the geothermal doublet (see figure below). The influence of nearby faults has not yet been visible during the well tests - probably due to short pumping times (Aardwarmtecluster, 2013).

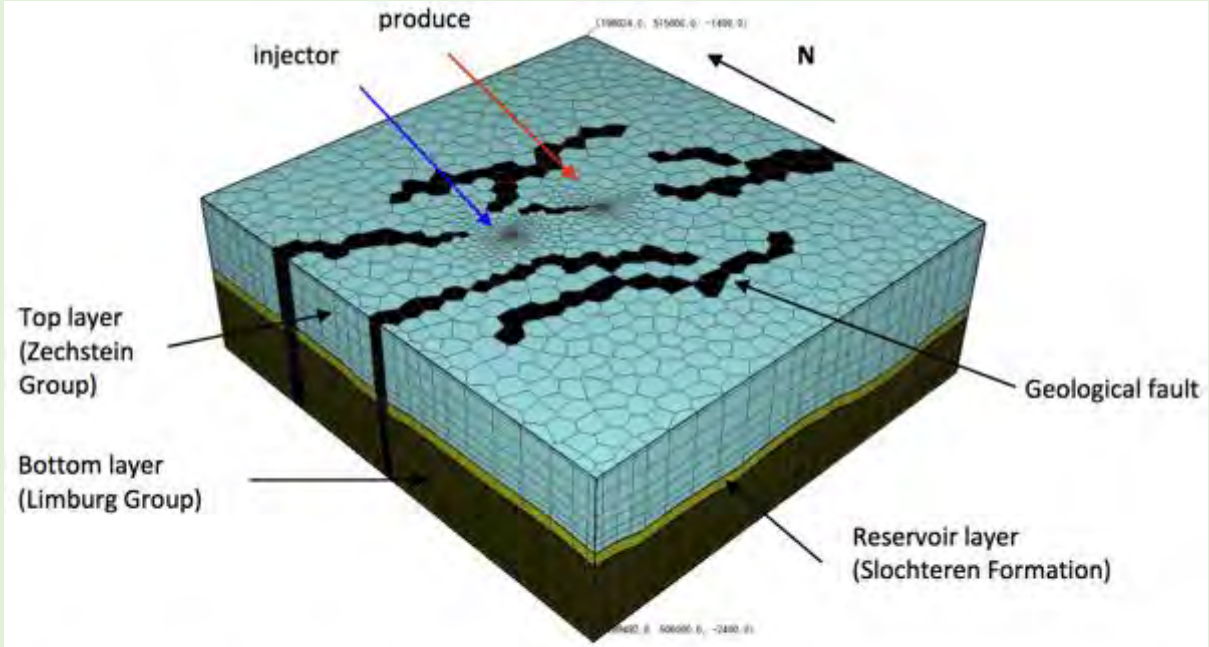

Figure 1 Model grid showing the geological layers and the location of the producer and injector. The geological faults - shown in black - are only included in that particular scenario.

List of references

Aardwarmtecluster 1 KKP BV, 2013. Bodemenergie in de glastuinbouw-pilot Koekoekspolder - Geologische 'logging' voor aardwarmte. Project in het kader van het programma Kas als Energiebron. Projectnummer 1400008471. 31p.

Besselink, 2015. SKB-showcase Gebiedsontwikkeling IJssel-Vechtdelta. Eindrapportage deelproject 7: Verkenning mogelijkheden uitbreiding en toepassing van geothermie in de Koekoekspolder. Report Provincie Overijssel. 15p. **https://soilpedia.nl …**

GeoService GmbH, 2011. Geothermal exploration / development well Koekoekspolder – GT-02. Final Well Report. NLOG_GS_PUB_3786_Final_Well_Report_KKP-GT-02.pdf

IF Technology, 2011. Puttest Productieput Koekoekspolder. NLOG_GS_PUB_5596_Rapportage_puttest_producer.pdf

Schmidt, A.P., 2000. Naturally Occurring Radioactive Materials in the gas and oil industry. Origin, transport and deposition of stable lead and 210Pb from Dutch gas reservoirs. PhD Thesis Universiteit Utrecht, 144 p.

Websites

https://www.nlog.nl/nlog/requestData/nlogp/allBor/metaData.jsp?tableName=BorLocation&id=872287025

http://thermogis.nl/thermogis_en.html

https://soilpedia.nl/Bikiwiki%20documenten/SKB%20Projecten/XX4027%20Gebiedsontwikkeling%20IJssel-Vechtdelta/150120%20%20Eindrapport%20deelproject%207%20Geothermie%20Koekoekspolder.pdf

Annexes

NL4-KKP-1 Stratigraphic information– **Find them in the folder: Additional information on basic and CHPM characteristics evaluation**

AREA 5- NL5-CAL

1. **Geology of the prospective area**

Requested information on:

- ✓ local geology (in regional context)
- ✓ CHPM target formation
- ✓ list of available cross sections, geological maps, geochemical results, lithological information

Notes: briefly summarized, referenced to more detailed studies.

Venlo, CAL-GT-01, ***type B***

Lithostratigraphy:

See also appendix NL5-CAL-1

Depth top Dinantian: 1596 in the main well to 1802 m in the sidetrack

Location: 51.42218805 6.09139302

All borehole documents and logs can be found on:

https://www.nlog.nl/nlog/requestData/nlogp/allBor/metaData.jsp?tableName=BorLocation&id=949495773

In the province of Limburg the top of the Dinantian limestones are often characterized by silicified carbonates (Bless, 1987; Friedrich et al., 1987; Reijmer et al., 2017). Leaching and subsequent silicification took place at those locations where the overlying Namurian and Westphalian strata had been eroded completely before deposition of Upper Cretaceous sediments; meteoric water played an important role in these surface-controlled processes (Friedrich et al., 1987). In the South of Limburg the silicification is accompanied by the occurrence of sulphide minerals (Friedrich et al., 1987).

Near Venlo, successful geothermal projects have been preformed in borehole CAL-GT-1 (Kramers et al., 2012b; www.californie.nu). Here silicified carbonates from the top of the Dinantian have been encountered at a depth of about 1600 m (www.nlog.nl) producing a subsurface water temperature of about 60°C (Figure 7; Kramer et al., 2012). Reports of cutting samples however, did not report on mineral concentration in borehole CAL-GT-01 (Poty, 2014). Recently, on 28 May 2018, geothermal activity was ceased in borehole CAL-GT-01 due to exploration risks in combination with natural earthquakes related to the vicinity of the Tegelen fault zone (https://www.limburger.nl/cnt/dmf20180529_00062856/winning-aardwarmte-in-grubbenvorst-stilgelegd).

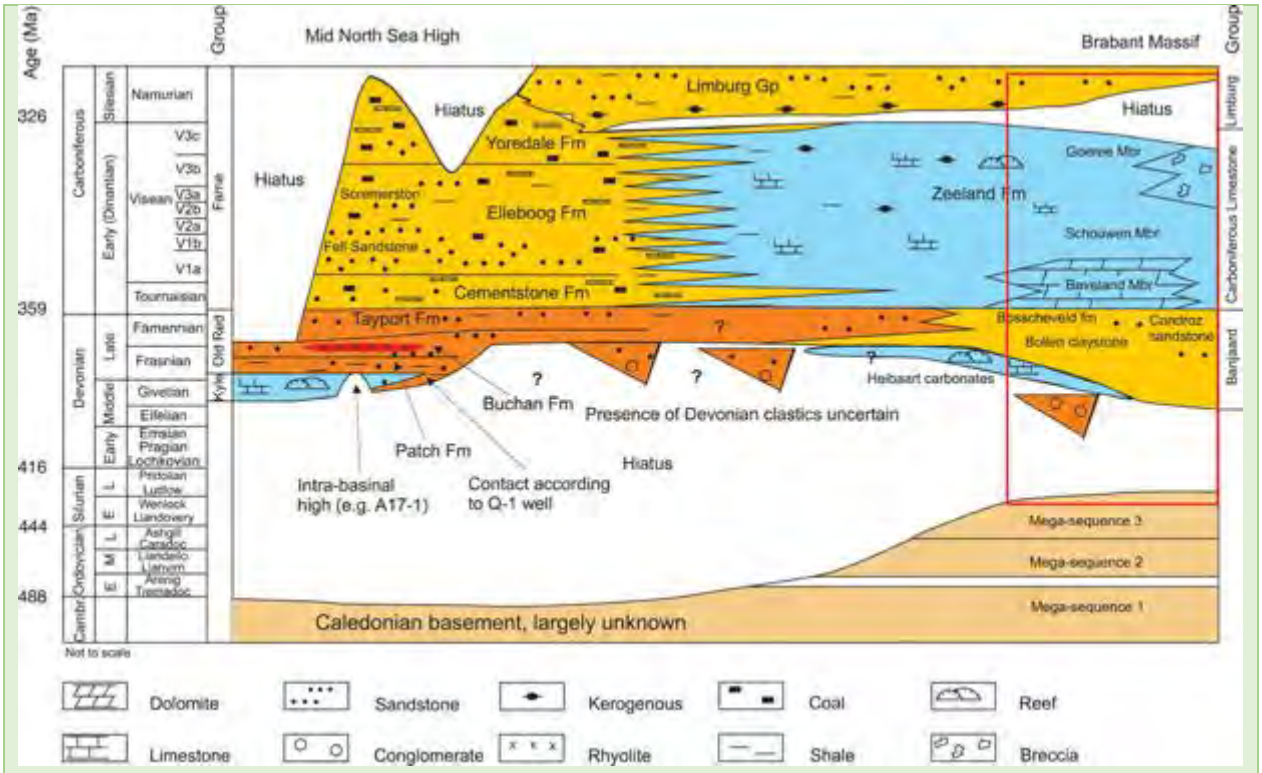

The graph above (after Reijmer et al., 2017) reveals schematic distribution of Pre-Silesian strata along a west-east transect in the Dutch subsurface. Here, the top of the Zeeland formation represents the top of the Dinantian.

2. Geophysics of the prospective area

Requested information:

- ✓ previous geophysical measurements (in CHPM relevance)
- ✓ geophysical results that can be used for locating/defining the deep metal enrichment
- ✓ list of available geophysical maps, cross sections, logs, other measurements

Venlo, CAL-GT-01

All borehole documents and logs can be found on:
https://www.nlog.nl/nlog/requestData/nlogp/allBor/metaData.jsp?tableName=BorLocation&id=949495773

Detailed section of the gamma-ray and other parameters (1589 m to 1621 m depth). The top of the Dinantian is e.g. marked by an increase in gamma-ray at about 1599 m.

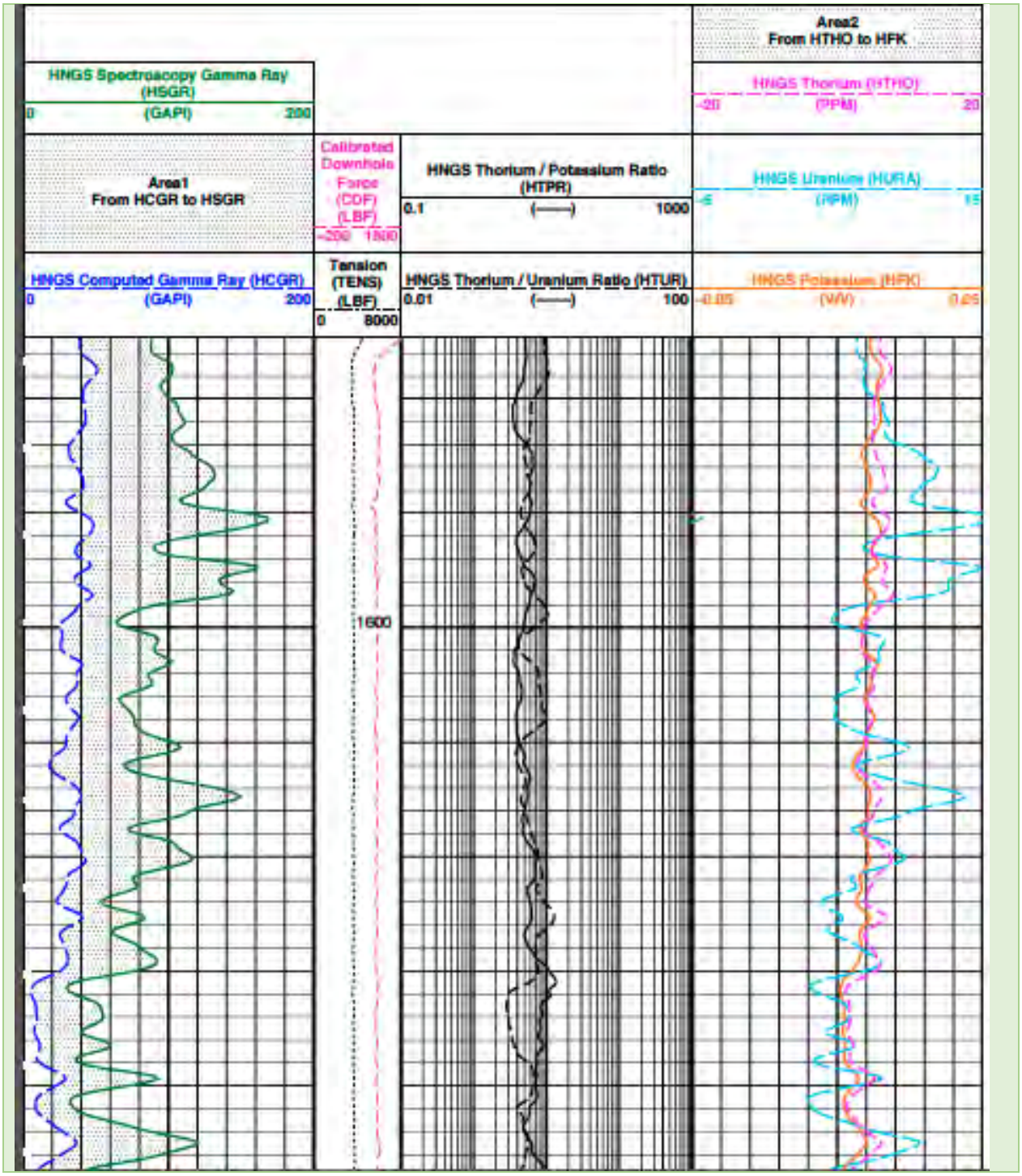
Area2
From HTHO to HFK
HNGS Spectroscopy Gamma Ray
(HSGR)
0
(GAPI)
200
HNGS Thorium (HTHO)
-20
(PPM)
20
Area1
From HCGR to HSGR
Calibrated
Downhole
Force
(CDF)
(LBF)
-200
1600
HNGS Thorium / Potassium Ratio
(HTPR)
0.1
(——)
1000
HNGS Uranium (HURA)
-5
(PPM)
15
HNGS Computed Gamma Ray (HCGR)
0
(GAPI)
200
Tension
(TENS)
(LBF)
0
8000
HNGS Thorium / Uranium Ratio (HTUR)
0.01
(——)
100
HNGS Potassium (HFK)
-0.05
(W/W)
0.25
1600

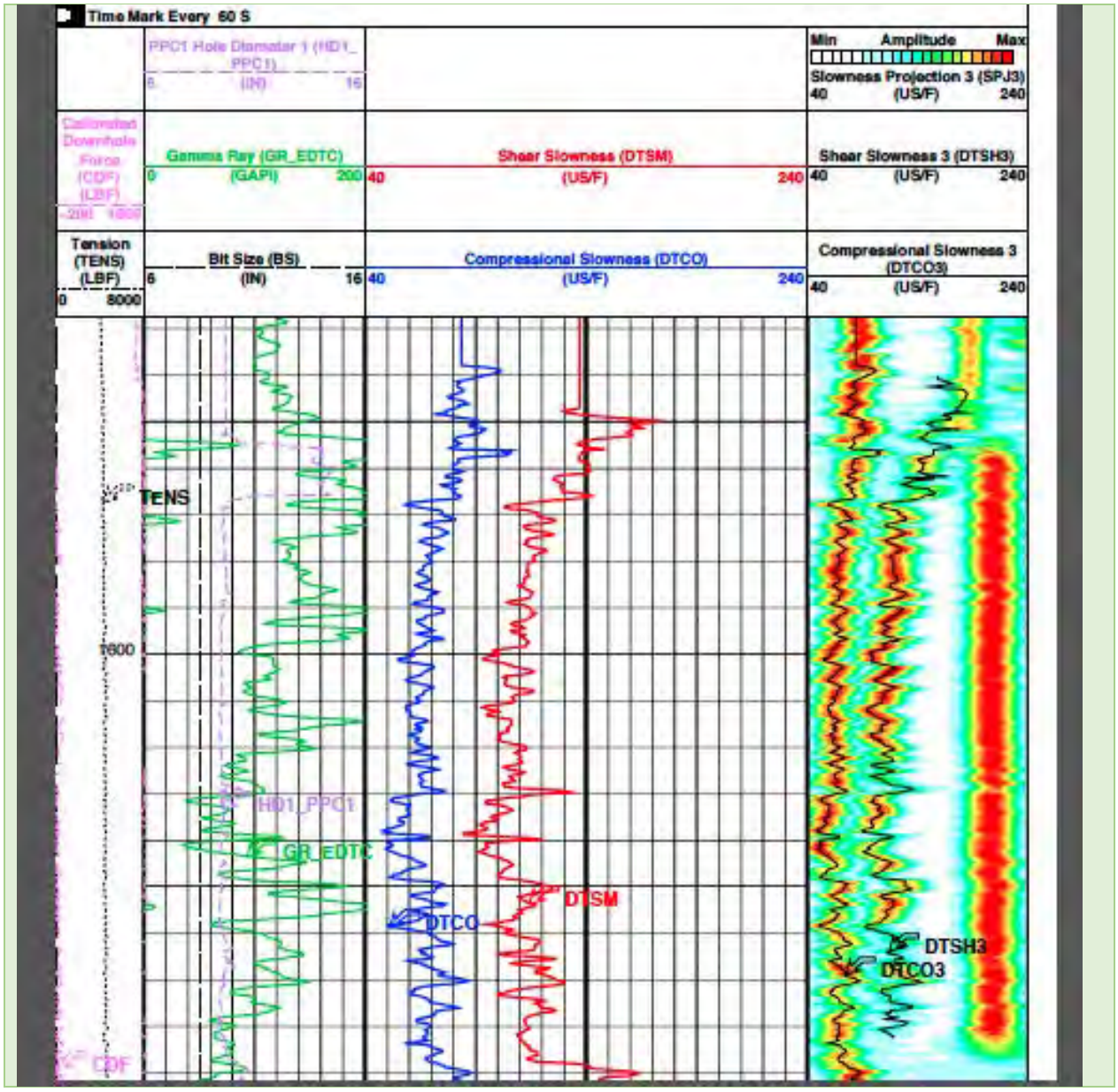
Time Mark Every 60 S
PPC1 Hole Diameter 1 (HD1_PPC1)
6 (IN) 16
Min Amplitude Max
Slowness Projection 3 (SPJ3)
40 (US/F) 240
Calibrated Downhole Force (CDF) (LBF)
-200 1000
Gamma Ray (GR_EDTC)
0 (GAPI) 200
Shear Slowness (DTSM)
40 (US/F) 240
Shear Slowness 3 (DTSH3)
40 (US/F) 240
Tension (TENS) (LBF)
0 8000
Bit Size (BS)
6 (IN) 16
Compressional Slowness (DTCO)
40 (US/F) 240
Compressional Slowness 3 (DTCO3)
40 (US/F) 240
TENS
7600
HD1_PPC1
GR_EDTC
DTCO
DTSM
DTSH3
DTCO3
CDF

3. **Deep metal enrichment**

Requested information:

✓ (expected) metal enrichment based on available geophysical, geological and drill data, samples information, geochemistry

Water analysis of well CAL-GT-01 by Panterra (2012) showed the following composition.

Anions

Table 6 – Water Composition

Chloride (Cl^-)	48000 mg/l
Bicarbonate(HCO_3^-)	360 mg/l
Carbonate ($CO_3^=$)	< 10 mg/l
Sulphate(SO4=)	15 mg/l

Cations

Sodium(Na^+)	23800 mg/l
Calcium(Ca^{+2})	3580 mg/l
Magnesium (Mg^{+2})	533 mg/l
Potasium (K^+)	1600 mg/l
Iron (Fe^{+2})	29.2 mg/l
Barium (Ba^{+2})	6.7 mg/l
Aluminium (Al^{+3})	133 mg/l
Strontium (Sr^{+2})	163 mg/l

pH(at 20.°C)	6.7
Total Dissolved solids (TDS)	78101 mg/l
Ca/Mg Hardness as CaCO3	11140 mg/l
Specific gravity	1.054 g/cm3 at 20.°C
Resistivity	0.11 Ohms/meter

Reports of cutting samples however, did not report other mineral concentration in borehole CAL-GT-01 (Poty, 2014).

4. **Integrated 3D- 4D model**

Requested information:

- ✓ existing 3D-4D models of the target area and the deep metal enrichment
- ✓ if no 3D-4D models exist, collect the following necessary data: geological setting, mineralization, fluid flow models, stress field determination

Notes: e.g. openly available datasets, models.

The well is situated in the Peel-Venlo block, North of the Roerdal graben. The region is marked by NW-SE oriented faulting.

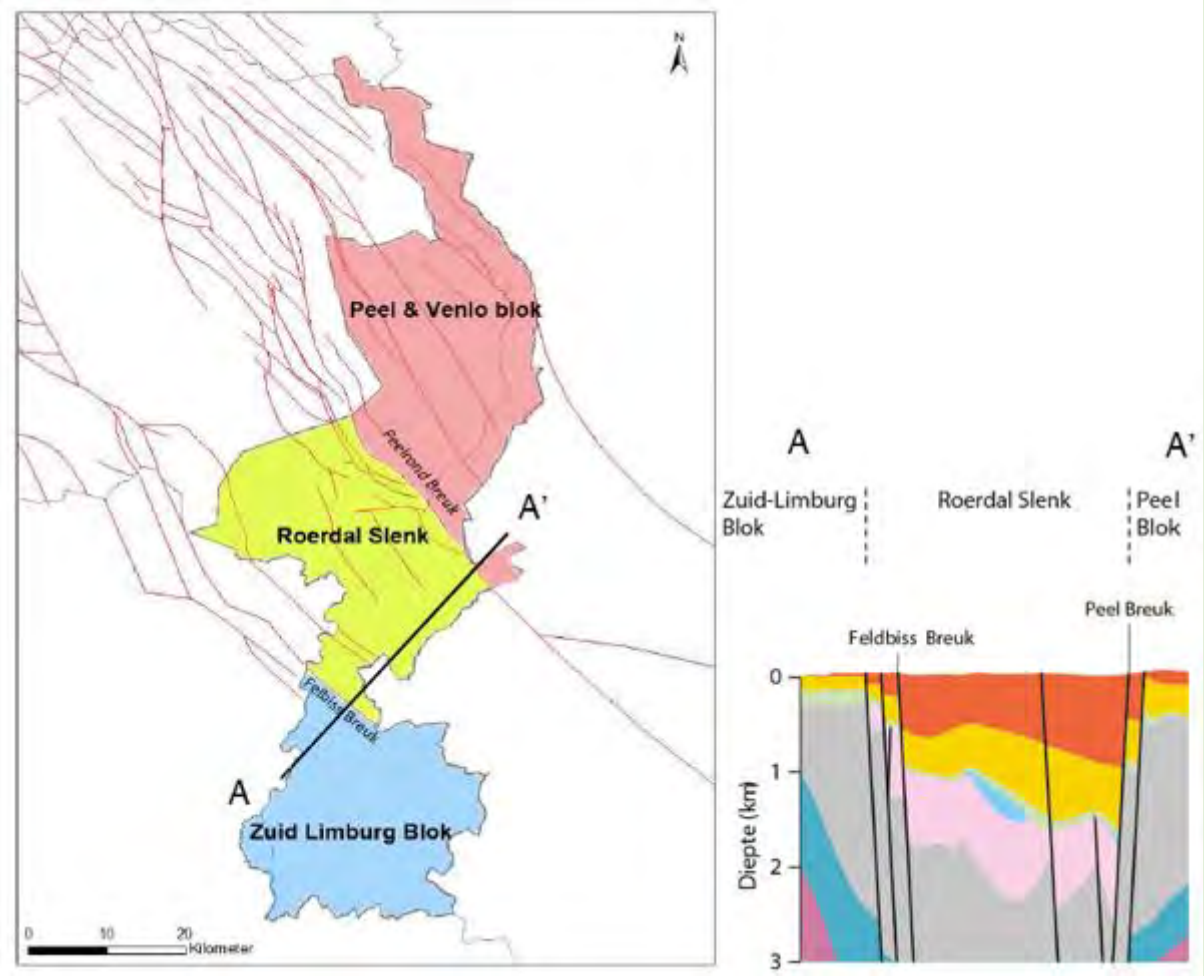

The subsurface of Limburg can be divided into three blocks. The cross section reveals the tectonic setting and strong subsidence of the Roerdal graben (Kramers et al., 2012).

5. **EGS potential**

Requested information:

- ✓ EGS potential (heat & energy) of the area
- ✓ geothermal characteristics (temperature gradient, heat flux, stress field, water availability, EGS geology)
- ✓ presence/indication of deep fluids/brines, fracture system, crustal permeability

Tabel 8. Ruwe indicatie van vermogen bij wisselende debieten. Voor de berekeningen is de temperatuur aan de top van de Kolenkalk genomen.

	Vermogen (MW_{th})			
Debiet (m^3/u)	**50**	**100**	**150**	**200**
Peel-Venlo Blok	1,5-5	3-10	4-18	4-20
Roerdal Slenk	5,5-7,5	10-15	16-24	20-30
Zuid-Limburg Blok	1-3,5	2-7	2-10	4-12

Coarse power indication at various flow rates as only few data on permeability are available. Regionale studie aardwarmte potentie provincie Limburg (Kramers et al., 2012).

Production tests revealed a high flow rate of 300 m^3/u with a water temperature of 60°C (geothermie.nl; Kramers et al., 2012).

No further EGS data available yet. A new version of http://thermogis.nl/thermogis_en.html will be available from October 2018.

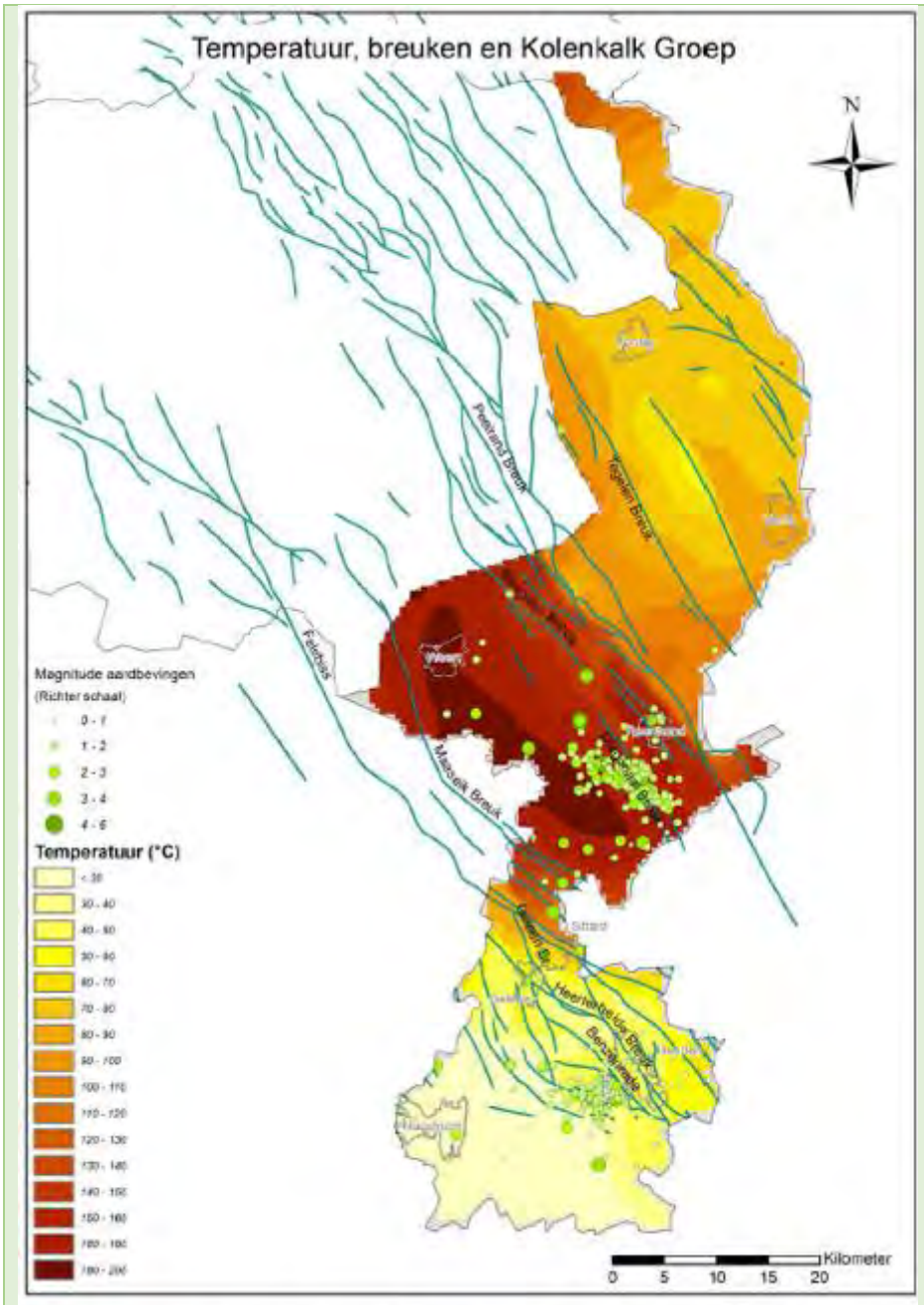

Figuur 57. Overzicht van breuken, temperatuur en geregistreerde natuurlijke bevingen (KNMI.nl) in Limburg.

Overview of faults, temperature and registered earthquakes in Limburg at the top of the Dinantian (Kramers et al., 2012).

List of references

Bless, M. J. M., 1987, Summary of geology and hydrogeology of Thermae boreholes (South Limburg, the Netherlands): Annales de la Société Géologique de Belgique, v. 110, p. 97-99.

Bonté, D., van Wees, J. D., and Verweij, J. M., 2012, Subsurface temperature of the onshore Betherlands: new temperature dataset and modelling: Netherlands Journal of Geosciences - Geologie en Mijnbouw, v. 91, no. 4, p. 491-515.

Friedrich, G., Bless, M. J. M., Vogtmann, J., and Wiechowski, A., 1987, Lead- zinc mineralization in Dinantian rocks of boreholes Thermae 2000 and Thermea 2002 (Valkenburg a/d Geul, the Netherlands): Annales de la Société Géologique de Belgique, v. 110, p. 59-75.

Kramers, L., Vis, G. J., den Dulk, M., Duin, E. J. T., Witmans, N., Pluymaekers, M. P. D., and Doornrnbal, J. C., 2012, Regionale studie aardwarmte potentie provincie Limburg. TNO rapport 056.01872. https://www.onderzoeksbanklimburg.nl/dowload_rapport.php?id=1035

PanTerra Geoconsultants, 2012, Analysis Report. Water/Gas Samples CAL-GT-01 – Grubbenvorst Californie Wijnen. 17p; NLOG_GS_PUB_7269_CWG_CAL_01_Panterra_report_CAL_GT01_-_rev1-_Aug20

Poty, E., 2014, Report on cuttings from the CAL (California)- GT-01 borehole. Unpublished report, NLOG_GS_Pub_1073.

Rejimer, J. J. G., ten Veen, J. H., Jaarsma, B., and Boots, R., 2017, Seismic stratigrapgy of Dinantian carbonates in the southern Netherlands and northern Belgium: Netherlands Journal of Geosciences, v. 96, no. 4, p. 353-379.

Websites

www.californie.nu
https://www.limburger.nl/cnt/dmf20180529_00062856/winning-aardwarmte-in-grubbenvorst-stilgelegd
https://www.nlog.nl/nlog/requestData/nlogp/allBor/metaData.jsp?tableName=BorLocation&id=949495773
http://thermogis.nl/thermogis_en.html

Annexes

NL5-CAL-1 Stratigraphic information– **Find them in the folder: Additional information on basic and CHPM characteristics evaluation**

Evaluation of CHPM characteristics of prospective CHPM areas
KNGMG Netherlands
NL1-BGM

1. **CHPM operational characteristics - Information for CHPM technological elements**
Requested information:
✓ please fill in the table below with the requested data for the CHPM technology elements

Underground heat exchanger (deep metal enrichment + potential geothermal reservoir)	
Extension of the metal enrichments *(volumetric interpretation)*	The thickness of the Coppershale (Kupferschiefer) is in general about half a meter (in accordance with well log) - *https://www.nlog.nl/nlog/requestData/nlogp/allBor/metaData.jsp?tableName=BorLocation&id=106504878*
Expected type of the reservoir and porosity/permeability *(fractured, porous, etc)*	Target reservoir – Rotliegend – Slochteren Sst Permeability - ~ 1500 mD (thermogis.nl) The sandstone is variably cemented (2 - 17%; average 11 %), mainly by carbonate cement. Well BGM 1 revealed porosities of 15 – 26% (accompanying permeability is 41 to 1880 mD) – see below NAM, 1996.

Well	Depth	Formation	Texture						Core Analysis		Porosity				Classification
			Grain Size	Grain size range	Sorting	Roundness	Compaction	Structure	Permeability	Porosity	Total porosity	Intergranular	Dissolution	Partial dissolution	
Bergermeer-1	2084.45	ROSLN	SS2l	SS1l-SS3l	Ts7	Tr4	Tc5	l	*	*	14	10	1	3	Gaa
Bergermeer-1	2087.45	ROSLN	SS2u	SJ-SS2u	Ts5	Tr4	Tc5	l	*	*	9	7	tr	2	Gag
Bergermeer-1	2105.10	ROSLN	SS2l	SJ-SS3l	Ts7	Tr4	Tc5	m	41.00	15.40	13	10	1	2	Gal
Bergermeer-1	2114.04	ROSLN	SS1l/2u	SS1l-SS2u	Tsb	Tr5	Tc5	l	*	*	6	5	0	1	Gal
Bergermeer-1	2116.98	ROSLN	SS1u	SS1l-SS2u	Ts7	Tr4	Tc3	l	*	*	18	15	1	2	Gaa
Bergermeer-1	2211.00	ROSLN	SS2u	SJ-SS3u	Ts7	Tr4	Tc5	Df	1145.00	24.60	14	10	3	1	Gal
Bergermeer-1	2211.70	ROSLN	SS2l	SJ-SS3l	Ts7	Tr4	Tc7	Df	1880.00	28.30	9	9	0	tr	Gal
Bergermeer-1	2264.30	ROSLN	SS2l/4l	SJ-SS4l	Tsb	Tr4	Tc5	m	*	*	9	8	tr	1	Gal
Bergermeer-1	2264.40	ROSLN	SS2u	SJ-SS4l	Ts3	Tr4	Tc5	m	247.00	16.90	12	12	tr	tr	Gal
Bergermeer-1	2287.60	ROSLN	SS3l	SJ-SS3u	Ts7	Tr4	Tc5	l	*	*	15	15	tr	tr	Gal

The detrital mineralogy of the sandstone samples is generally with quartz the dominant grain type (average 47% monocrystalline quartz and 19% polycrystalline quartz). Rock fragments (average 10%) and feldspar (average 9%) are also major detrital components throughout.

Indeterminate authigenic clays (trace - 6%, average 3%) are present.

Throughout, both grain coating and intergranular. Kaolinite (0% - 3%, average 2%) - most commonly present as pore-filling aggragates.

	NAM, 1996. End of well report: Net pay: 24 m. Top Rotliegendes 2209 TVD Gas/Water Contact 2233 TVD In the neighbouring well BGM1, 8 meters below the Coppershale (Kupferschiefer) horizon, the density of the Rotliegend is 2.650 g/cm^3. https://www.nlog.nl/nlog/requestData/nlogp/allBor/metaData.jsp?tableName=BorLocation&id=106504868
Mineralization *(type and enriched metals)*	Copper sulfides in organic-rich shales of the Coppershale (Kupferschiefer) The nearest water samples available, at a distance of about 20 km, are from Heemskerk (HEK-GT1-S2; https://www.nlog.nl/nlog/requestData/nlogp/allBor/metaData.jsp?tableName=BorLocation&id=1174054851). Average values from 9 samples are presented below. Metals (Conform NEN 6961/NEN 6966/C1) - Aluminium as A,l µg/l 5643 - Barium, µg/l 5967 - Cadmium, µg/l 45 - Calcium, µg/l 7700000 - Copper, µg/l 128 - Iron, µg/l 248889 - Lead, µg/l 2678 - Magnesium, µg/l 1211111 - Manganese, µg/l 12933 - Nickel, µg/l 194 - Total phosphor, µg/l 647 - Kalium, µg/l 2166667 - Sodium, µg/l 81555556 - Strontium, µg/l 306667 - Zinc, µg/l 18778

Production and injection wells	
Depth of potential wells (m)	Top Rotliegend – 2081.5 m (thermogis.nl)

Electrolytic metal recovery and gas diffusion electro- precipitation	
Potential target metals to be recovered	Copper sulfides in organic-rich shales of the Coppershale (Kupferschiefer) + vanadium, lead, cobalt, barium, nickel, arsenic and uranium (in decreasing order) (based on samples from NW Drenthe in Schmidt, 2000)
Power plant (heat exchanger)	
Local heat and electricity demand *(industrial, municipal, agricultural, etc.)*	Municipal – heating of houses, sports facilities (ice skating-ring, football stadium) Agricultural - greenhouses

Salt gradient power generation	
Salinity of expected geothermal brine	No data. The average density of the Heemskerk water samples is 1.158 kg/l. https://www.nlog.nl/nlog/requestData/nlogp/allBor/metaData.jsp?tableName=BorLocation&id=1174054851 Dissolution of the overlying Zechstein evaporates may have an impact on the salinity of the expected geothermal brine.
Fresh water supply from the surface *(water sources)*	Noord-Holland Kanaal - ~ 1.8 km to the east The drill site is surrounded by small canals (www.thermogis.nl/mapviewer)

2. **CHPM operational characteristics - Environmental, social and political background**

Requested information:

- ✓ toleration to gaseous and solids emissions, water and noise pollution,
- ✓ local competition to land and water availability
- ✓ public acceptance
- ✓ political support
- ✓ presence of supporting legislation, regulatory framework

Notes: all of above refers to the selected area and its surroundings.

HVC will explore the geothermal potential of the Alkmaar, Langedijk and Heerhugowaard subsurface for heating houses as well as greenhouses. An exploration licence has been issued by the Mining authoroties. (https://www.fluxenergie.nl/bij-alkmaar-begint-de-geothermische-victorie/)

HVC is involved in a (non-geothermal) heat-network supplying 12 000 households. (https://www.fluxenergie.nl/bij-alkmaar-begint-de-geothermische-victorie/)

The site location is licensed for gas storage.

3. **Financial aspects**

Requested information:

- ✓ list of potential local stakeholders (community, political, companies)

Main stakeholder at this site: TAQA - gas storage
The region is licensed for gas storage.

A wider region towards the NE is licensed for geothermal exploration.

HVC will explore the geothermal potential of the Alkmaar, Langedijk and Heerhugowaard subsurface for heating houses as well as greenhouses. An exploration licence has been issued by the Mining authoroties. (https://www.fluxenergie.nl/bij-alkmaar-begint-de-geothermische-victorie/)

List of references

NAM, 1996. Petrography of Selected Samples From the Slochteren Sandstone Member from 6 wells located in the Northwestern Dutch Onshore. NAM report. Report Number: D-779. 76p. NLOG_GS_PUB_6038_Petrography.pdf

Websites:

https://www.nlog.nl/nlog/requestData/nlogp/allBor/metaData.jsp?tableName=BorLocation&id=106504868

https://www.nlog.nl/nlog/requestData/nlogp/allBor/metaData.jsp?tableName=BorLocation&id=106504878

https://www.fluxenergie.nl/bij-alkmaar-begint-de-geothermische-victorie/

www.thermogis.nl/mapviewer

https://www.nlog.nl/nlog/requestData/nlogp/allBor/metaData.jsp?tableName=BorLocation&id=1174054851

Annexes

Evaluation of CHPM characteristics of prospective CHPM areas
KNGMG Netherlands
NL2-AWG

1. **CHPM operational characteristics - Information for CHPM technological elements**
   Requested information:
   ✓ please fill in the table below with the requested data for the CHPM technology elements

Underground heat exchanger (deep metal enrichment + potential geothermal reservoir)	
Extension of the metal enrichments *(volumetric interpretation)*	The thickness of the Coppershale (Kupferschiefer) is in general about half a meter. (https://www.nlog.nl/nlog/requestData/nlogp/allBor/metaData.jsp?tableName=BorLocation&id=106505196)
Expected type of the reservoir and porosity/permeability *(fractured, porous, etc)*	Target reservoir – Rotliegend – Slochteren Sst Thickness Slochteren Sst – 113 m Core analysis well AWG106 - Slochteren fm (https://www.nlog.nl/nlog/requestData/nlogp/allBor/metaData.jsp?tableName=BorLocation&id=106505196) Porosity: 5.6 – 25.3 %; average 12.9 % Horizontal Permeability: 0.01 – 12.1 mD; average 1 mD Vertical Permeability: 0.02 –16.87 mD; average 2.6 mD Density: 2.5655 – 2.746 g/cm^3; 2.695 g/cm^3

	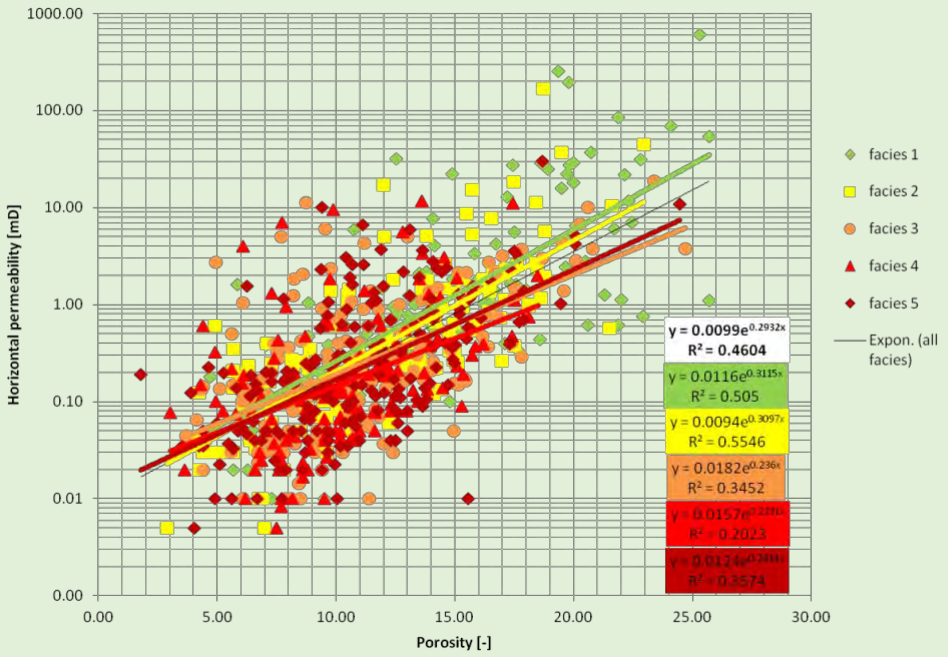 Porosity- Permeability plot for the Greater Ameland area (Clerx, 2014); various facies are no further specified.
Mineralization *(type and enriched metals)*	Copper sulfides in organic-rich shales of the Coppershale (Kupferschiefer) + vanadium, lead, cobalt, barium, nickel, arsenic and uranium (in decreasing order) (based on samples from NW Drenthe in Schmidt, 2000)

Production and injection wells	
Depth of potential wells (m)	Top Rotliegend – 3273 (t=top Ten Boer fm) Top Slochteren fm – 3370 m https://www.nlog.nl/nlog/requestData/nlogp/allBor/metaData.jsp?tableName=BorLocation&id=106518416

Electrolytic metal recovery and gas diffusion electro- precipitation	
Potential target metals to be recovered	Copper sulfides in organic-rich shales of the Coppershale (Kupferschiefer) + vanadium, lead, cobalt, barium, nickel, arsenic and uranium (in decreasing order) (based on samples from NW Drenthe in Schmidt, 2000)

Power plant (heat exchanger)	
Local heat and electricity demand *(industrial, municipal, agricultural, etc.)*	Island (municipality) of Ameland. ~ 1700 houses

Salt gradient power generation	
Salinity of expected geothermal brine	No data. Dissolution of the overlying Zechstein evaporates may have an impact on the salinity of the expected geothermal brine.
Fresh water supply from the surface *(water sources)*	Rain water Salt Water – North Sea

2. CHPM operational characteristics - Environmental, social and political background

Requested information:

- ✓ toleration to gaseous and solids emissions, water and noise pollution,
- ✓ local competition to land and water availability
- ✓ public acceptance
- ✓ political support
- ✓ presence of supporting legislation, regulatory framework

Notes: all of above refers to the selected area and its surroundings.

The island of Ameland aims to largely energy self sufficient as well as a CO_2-neutral energy supply. Ameland aims to become in leader in energy transition (from fossil fuel towards electricity and greengas') over a period of 15 to 20 years.
https://www.ameland.nl/ameland-actueel/nieuws_42176/item/innovatief-energienet-voor-verdere-verduurzaming-ameland_37354.html

Ameland Westgat is located closely to the Waddenzee – UNESCO world heritage site.

3. Financial aspects

Requested information:

✓ list of potential local stakeholders (community, political, companies)

Tourism related businesses
Municipality of Ameland

List of references

Clerx, N.E., 2014. An integrated study of Permian Rotliegend reservoir rocks in the Greater Ameland Area. MSc thesis TU Delft. 98 p.

Schmidt, A.P., 2000. Naturally Occurring Radioactive Materials in the gas and oil industry. Origin, transport and deposition of stable lead and 210Pb from Dutch gas reservoirs. PhD Thesis Universiteit Utrecht, 144 p.

Websites:

https://www.nlog.nl/nlog/requestData/nlogp/allBor/metaData.jsp?tableName=BorLocation&id=106518416

https://www.ameland.nl/ameland-actueel/nieuws_42176/item/innovatief-energienet-voor-verdere-verduurzaming-ameland_37354.html

Annexes

Evaluation of CHPM characteristics of prospective CHPM areas
KNGMG Netherlands
NL3-BRW

1. **CHPM operational characteristics - Information for CHPM technological elements**
   Requested information:
   ✓ please fill in the table below with the requested data for the CHPM technology elements

Underground heat exchanger (deep metal enrichment + potential geothermal reservoir)	
Extension of the metal enrichments *(volumetric interpretation)*	The thickness of the Coppershale (Kupferschiefer) is in general about half a meter. https://www.nlog.nl/nlog/requestData/nlogp/allBor/metaData.jsp?tableName=BorLocation&id=106522064
Expected type of the reservoir and porosity/permeability *(fractured, porous, etc)*	Target reservoir – Rotliegend – Slochteren Sst, Thickness Slochteren Sst – 152 m Core analysis neighbouring well BRW2 Slochteren fm (https://www.nlog.nl/nlog/requestData/nlogp/allBor/metaData.jsp?tableName=BorLocation&id=106505196 Porosity: 9.1 – 26.9 %; average 19.7 % Horizontal Permeability: 2.1 – 812 mD; average 265.3 mD Vertical Permeability: 0.6 –993 mD; average 109.1 mD Density: 2.534 – 2.754 g/cm^3; 2.654 g/cm^3
Mineralization *(type and enriched metals)*	Copper sulfides in organic-rich shales of the Coppershale (Kupferschiefer)

Production and injection wells	
Depth of potential wells (m)	Top Rotliegend – 2897.5 m (stratigraphic information; https://www.nlog.nl/nlog/requestData/nlogp/allBor/metaData.jsp?tableName=BorLocation&id=106522064) Top Slochteren formation – 2943.5 m

Electrolytic metal recovery and gas diffusion electro- precipitation

Potential target metals to be recovered	Copper sulfides in organic-rich shales of the Coppershale (Kupferschiefer) + vanadium, lead, cobalt, barium, nickel, arsenic and uranium (in decreasing order) (based on samples from NW Drenthe in Schmidt, 2000)

Power plant (heat exchanger)	
Local heat and electricity demand *(industrial, municipal, agricultural, etc.)*	Chemical industry, the port and energy facility in the Eemshaven region Municipality Delfzijl: 12:000 houses

Salt gradient power generation	
Salinity of expected geothermal brine	No data. Dissolution of the overlying Zechstein evaporates may have an impact on the salinity of the expected geothermal brine.
Fresh water supply from the surface *(water sources)*	Wells are located next to a canal, Termunterzijldiep Waddenzee, Eems-Dollard region (UNESCO-site) - https://www.unesco.nl/erfgoed/waddenzee#zoom=3&lat=53.3598&lon=5.659&layers=BT

2. CHPM operational characteristics - Environmental, social and political background

Requested information:

- ✓ toleration to gaseous and solids emissions, water and noise pollution,
- ✓ local competition to land and water availability
- ✓ public acceptance
- ✓ political support

✓ presence of supporting legislation, regulatory framework

Notes: all of above refers to the selected area and its surroundings.

The public acceptance I expect to be low in view of the current earthquakes in response to gas extraction. Extraction of any kind from the subsurface is sensitive matter and should be communicated with the utmost prudence.

Policy: change in energy source from (hydro)carbons to renewable sources.

The vicinity of the Waddenzee (Unesco- world heritage-site)

The policy of region is to have a sustainable balance between economy and ecology (agriculture). The region Eemsdelta is characterised by e.g. chemical industry, the port and energy facility in the Eemshaven (Provincie Groningen, 2011).

The Borgsweer well is currently in use as a water disposal injection site (TNO, 2015).
Initial reservoir temperatures in the Slochteren sandstone are around 105 ^{o}C. Local cooling up to 30 ^{o}C around the injection well is expected due to the injection of the cold water.

3. Financial aspects

Requested information:

✓ list of potential local stakeholders (community, political, companies)

Region Eemsdelta municipality of Delfzijl
Chemical industry, the port and energy facilities in the Eemshaven

List of references

Provincie Groningen, 2011. Ecologie & Economie in balans in de Eemsdelta. 34 p. https://www.waddenzee.nl/fileadmin/content/Dossiers/Energie/pdf/Ecologie_en_Economie_in_balans.pdf

Schmidt, A.P., 2000. Naturally Occurring Radioactive Materials in the gas and oil industry. Origin, transport and deposition of stable lead and 210Pb from Dutch gas reservoirs. PhD Thesis Universiteit Utrecht, 144 p.

TNO, 2015. Injection-Related Induced Seismicity and its relevance to Nitrogen Injection: Description of Dutch field cases. TNO report 2015 R10906. 34 p.

Websites:

https://www.nlog.nl/nlog/requestData/nlogp/allBor/metaData.jsp?tableName=BorLocation&id=106522064

https://www.unesco.nl/erfgoed/waddenzee#zoom=3&lat=53.3598&lon=5.6594&layers=BT

https://www.waddenzee.nl/fileadmin/content/Dossiers/Energie/pdf/Ecologie_en_Economie_in_balans.pdf

thermogis.nl

https://www.nlog.nl/nlog/requestData/nlogp/allBor/metaData.jsp?tableName=BorLocation&id=106505196

Annexes

Evaluation of CHPM characteristics of prospective CHPM areas
KNGMG Netherlands
NL4-KKP

1. **CHPM operational characteristics - Information for CHPM technological elements**
   Requested information:
   ✓ please fill in the table below with the requested data for the CHPM technology elements

Underground heat exchanger (deep metal enrichment + potential geothermal reservoir)	
Extension of the metal enrichments *(volumetric interpretation)*	The thickness of the Coppershale (Kupferschiefer) is in general about half a meter. https://www.nlog.nl/nlog/requestData/nlogp/allBor/metaData.jsp?tableName=BorLocation&id=803909123
Expected type of the reservoir and porosity/permeability *(fractured, porous, etc)*	Target reservoir – Rotliegend – Slochteren Sst Properties of the target reservoir (Aardwarmtecluster 1 KKP BV, 2013): *Parameter* / *Unit* / *Value* Reservoir / - / Slochteren Forma Top / [m] / Top Slochteren Fr Bottom / [m] / 75 m below top S Average permeability / [mD] / 190 Porosity / [%] / 18 Salinity (NaCl) / [g/l] / 185 *Layer* / *Bulk thermal conductivity (W/m K)* / *Density (kg/m³* Zechstein / 4.0 / 2,200 Slochteren / 3.0 / 2,500 Limburg / 2.1 / 2,600 The Slochteren sandstone formation is 99 m thick (along borehole between 2106 and 2205m). The true vertical thickness is 76 m. The porosity varies between 8,2 % and 24,3 %. Based on porosity-permeability comparison studies by PanTerra (2010) the average aritmetic permeabilityvan is about 120 milliDarcy (Aardwarmtecluster 1 KKP BV, 2013).

Mineralization *(type and enriched metals)*	Copper sulfides in organic-rich shales of the Coppershale (Kupferschiefer)

Production and injection wells	
Depth of potential wells (m)	Top Rotliegend – 2081.5 m (thermogis.nl)

Electrolytic metal recovery and gas diffusion electro- precipitation

Potential target metals to be recovered

Copper sulfides in organic-rich shales of the Coppershale (Kupferschiefer)

+ vanadium, lead, cobalt, barium, nickel, arsenic and uranium (in decreasing order) (based on samples from NW Drenthe in Schmidt, 2000).

At a flow rate of about 140 m3/h (thermogis.nl) and reported metal concentrations (IF Technology, 2011) a metal recovery as stated below could be expected.

		mg/m3 µg/l	flow rate 140 m3/h g/h	 kg/h	
aluminium	<	2500	350	0.35	(prod. well fm water)
barium		3100	434	0.434	
cadmium		83	11.62	0.0116	
calcium		16000000	2240000	2240	
potassium		1300000	182000	182	
copper	<	250	35	0.035	(prod. well fm water)
lead		2700	378	0.378	
magnesium		1200000	168000	168	
manganese		6401	896.14	0.8961	
sodium		68000000	9520000	9520	
nickel	<	500	70	0.07	(prod. well fm water)
strontium		400000	56000	56	
iron		85000	11900	11.9	
zinc		34000	4760	4.76	

prod. well fm water=production well formation water

During the summer of 2013 the injection well got clogged diminishing the volume of water to be injected. Upon inspection, at a depth of 1750 m salts (salinity about 6 times seawater) and dissolved lead amongst which lead 210, a Naturally Occurring Radioactive Materials with a Low Specific Activity (Besselink, 2015).

Power plant (heat exchanger)	
Local heat and electricity demand *(industrial, municipal, agricultural, etc.)*	The site is currently in use as a geothermal facility for heating greenhouses.

Salt gradient power generation	
Salinity of expected geothermal brine	The NaCl concentration of the geothermal fluid of the target reservoir, Slochteren formation, was determined from water analyses to be approx. 185 g/l. Aardwarmtecluster 1 KKP BV, 2013 Dissolution of the overlying Zechstein evaporates may have an impact on the salinity of the expected geothermal brine.
Fresh water supply from the surface *(water sources)*	River IJssel

2. CHPM operational characteristics - Environmental, social and political background

Requested information:

- ✓ toleration to gaseous and solids emissions, water and noise pollution,
- ✓ local competition to land and water availability
- ✓ public acceptance
- ✓ political support
- ✓ presence of supporting legislation, regulatory framework

Notes: all of above refers to the selected area and its surroundings.

Provinciale Staten van Overijssel, de Gemeenteraad van Kampen (regional and local authorities) and farmers are involved in this project.
The site is licensed as an geothermal facility.
The authorites focus on (Besselink, 2015):

- Sustainable water management
- Use of renewable energy
- Increase of rural identity – production of local crops
- Green regional spatial layout

3. Financial aspects

Requested information:

- ✓ list of potential local stakeholders (community, political, companies)

Provinciale Staten van Overijssel, de Gemeenteraad van Kampen (regional and local authorities) and farmers are involved in this project.

List of references

Aardwarmtecluster 1 KKP BV, 2013. Bodemenergie in de glastuinbouw-pilot Koekoekspolder - Geologische 'logging' voor aardwarmte. Project in het kader van het programma Kas als Energiebron. Projectnummer 1400008471. 31p.

Besselink, 2015. SKB-showcase Gebiedsontwikkeling IJssel-Vechtdelta. Eindrapportage deelproject 7: Verkenning mogelijkheden uitbreiding en toepassing van geothermie in de Koekoekspolder. Report Provincie Overijssel. 15p. **https://soilpedia.nl …**

IF Technology, 2011. Puttest Productieput Koekoekspolder. NLOG_GS_PUB_5596_Rapportage_puttest_producer.pdf

Schmidt, A.P., 2000. Naturally Occurring Radioactive Materials in the gas and oil industry. Origin, transport and deposition of stable lead and 210Pb from Dutch gas reservoirs. PhD Thesis Universiteit Utrecht, 144 p.

Websites

https://www.nlog.nl/nlog/requestData/nlogp/allBor/metaData.jsp?tableName=BorLocation&id=803909123

Annexes

Evaluation of CHPM characteristics of prospective CHPM areas
KNGMG Netherlands
NL5 - CAL

1. **CHPM operational characteristics - Information for CHPM technological elements**
   Requested information:

✓ please fill in the table below with the requested data for the CHPM technology elements

Underground heat exchanger (deep metal enrichment + potential geothermal reservoir)	
Extension of the metal enrichments *(volumetric interpretation)*	Lead, zinc and iron sulphides in analogues to S. Limburg stratigraphy (Friedrich et al., 1987) The organic-rich claystone at the base of the Epen Formation (Geverik Member) overlaying the Zeeland Formation contains locally pyrite. Panterra Geoconsultants, 2012a).
Expected type of the reservoir and porosity/permeability *(fractured, porous, etc)*	Dolomitic limestone / dolomite (nlog – composite log; https://www.nlog.nl/nlog/requestData/nlogp/allBor/metaData.jsp?tableName=BorLocation&id=949495773) Thickness: 402 – 441 m Porosity and permeability unknown / hard to assess (Kramers et al., 2012). Analysis of core cutting from CAL-GT-01 by Panterra Geoconsultants (2012a) reveal the following results on porosity and fractures: • The carbonate fragments are mostly tight; some intercrystalline porosity in partly dolomitized carbonate. • Dissolution porosity (in chert cuttings) is probably related to the chertification process in Carboniferous carbonates. • Thin section studies on top Dinantian limestones reveal that interparticle pores and pores within the fossil fragments are completely filled with calcite cement. Intrafossil porosity is partially preserved. Pyrite and calcite act as fracture filling in the claystone.
Mineralization *(type and enriched metals)*	unknown

Production and injection wells	
Depth of potential wells (m)	Within the range of the Zeeland formation (Dinantian); ~ 1421 to 1823 (or 1863) m NAP. https://www.nlog.nl/nlog/requestData/nlogp/allBor/metaData.jsp?tableName=BorLocation&

Electrolytic metal recovery and gas diffusion electro- precipitation	
Potential target metals to be recovered	Based on water analysis by Panterra Geoconsultants (2012b) and an average (assumed) flow rate of e.g. 150 m^3/h (Kramers et al., 2012) the following elements might be retrieved (Recovery in kg/h).

Cations	Concentration (mg/l)	Recovery (kg/h)
Potasium (K)	1600	240
Iron (Fe2+)	29.2	4.38
Aluminium (Al)	133	19.95
Strontium (Sr)	163	24.45

Power plant (heat exchanger)	
Local heat and electricity demand *(industrial, municipal, agricultural, etc.)*	May 2018, geothermal activity was ceased in borehole CAL-GT-01 due to exploration risks in combination with natural earthquakes related to the vicinity of the Tegelen fault zone (https://www.limburger.nl/cnt/dmf20180529_00062856/winning-aardwarmte-in-grubbenvorst-stilgelegd). However over a period of 4 years water from a 2100 m deep layers and a water temperature of 75°C heated a 32 hectare large greenhouse complex. (https://www.wijlimburg.nl/nieuws-overzicht/californie-wijnen-geothermie-stopt-met-winnen-aardwarmte-in-grubbenvorst/)

Salt gradient power generation	
Salinity of expected geothermal brine	Water analysis of well CAL-GT-01 by Panterra Geoconsultants (2012b) showed the following composition. No specific salinity data have been provided.

Anions

Table 6 – Water Composition

Chloride (Cl^-)	48000 mg/l
Bicarbonate(HCO_3^-)	360 mg/l
Carbonate ($CO_3^=$)	< 10 mg/l
Sulphate(SO4=)	15 mg/l

Cations

Sodium(Na^+)	23800 mg/l
Calcium(Ca^{+2})	3580 mg/l
Magnesium (Mg^{+2})	533 mg/l
Potasium (K^+)	1600 mg/l
Iron (Fe^{+2})	29.2 mg/l
Barium (Ba^{+2})	6.7 mg/l
Aluminium (Al^{+3})	133 mg/l
Strontium (Sr^{+2})	163 mg/l

pH(at 20.°C)	6.7
Total Dissolved solids (TDS)	78101 mg/l
Ca/Mg Hardness as CaCO3	11140 mg/l
Specific gravity	1.054 g/cm3 at 20.°C
Resistivity	0.11 Ohms/meter

Fresh water supply from the surface *(water sources)*	River Maas – located about 3 km to the East

2. **CHPM operational characteristics - Environmental, social and political background**

Requested information:

- ✓ toleration to gaseous and solids emissions, water and noise pollution,
- ✓ local competition to land and water availability
- ✓ public acceptance
- ✓ political support
- ✓ presence of supporting legislation, regulatory framework

Notes: all of above refers to the selected area and its surroundings.

In May 2018, geothermal activity was ceased in borehole CAL-GT-01 due to exploration risks in combination with natural earthquakes related to the vicinity of the Tegelen fault zone. Closure was issued by the Staatstoezicht op de Mijnen. (https://www.limburger.nl/cnt/dmf20180529_00062856/winning-aardwarmte-in-grubbenvorst-stilgelegd).

3. **Financial aspects**

Requested information:

- ✓ list of potential local stakeholders (community, political, companies)

Currently the greenhouse complex (Wijnen Square Crops.) is the main stakeholder.

Other potential stakeholders:
-In general town counsels in order to change from gas to electrical supply.
-Neighbouring villages (Horst aan de Maas): ~ 18 000 houses

List of references

Articles:

Friedrich, G., Bless, M. J. M., Vogtmann, J., and Wiechowski, A., 1987, Lead-zinc mineralization in Dinantian rocks of boreholes Thermae 2000 and Thermae 2002 (Valkenburg a/d Geul, the Netherlands): Annales de la Société Géologique de Belgique, v. 110, p. 59–75.

Kramers, L., Vis, G. J., den Dulk, M., Duin, E. J. T., Witmans, N., Pluymaekers, M. P. D., and Doornenbal, J. C., 2012, Regionale studie aardwarmte potentie provincie Limburg. TNO rapport 056.01872. https://www.rvo.nl / http://www.onderzoeksbanklimburg.nl/download_rapport.php?id=1035

PanTerra Geoconsultants, 2012a, Description and microscopic analysis of 2 cuttings samples, Well CAL-GT-01. Project G984.

PanTerra Geoconsultants, 2012b, Analysis Report. Water/Gas Samples CAL-GT-01 - Grubbenvorst Californie Wijnen. 17p. NLOG_GS_PUB_7269_CWG_CAL_01_Panterra_report_CAL_GT01_-_rev1-_Aug20

Websites:

https://www.nlog.nl/nlog/requestData/nlogp/allBor/metaData.jsp?tableName=BorLocation&id=949495773

(https://www.limburger.nl/cnt/dmf20180529_00062856/winning-aardwarmte-in-grubbenvorst-stilgelegd).

https://www.wijlimburg.nl/nieuws-overzicht/californie-wijnen-geothermie-stopt-met-winnen-aardwarmte-in-grubbenvorst/

Annexes

Table 1

Prospective CHPM areas

PAMAV Poland							
Number	**Type of the selected area(s) (type "A" or type "B")**	**Depth(s) of the metal enrichment(s) (m)**	**Temperature /at these depths/ (°C)**	**Description of the metal enrichment(s)**			
				degree of the mineralization(s) (% or ppm)	***type of the mineralization(s)[1]***	***element(s)***	***area delineation(s)[2]***
1. Mozów	B	Ca. 2530	80-85	3.7% Cu, 63 ppm Ag	Kupferschiefer stratiform	Cu, Ag, (Au, Pt, Pb, Co, Ni)	N52°05' E15°34' (a)
2. Kaleje	A/B	Ca. 3130	100-105	7.0% Cu	Kupferschiefer stratiform	Cu, Ag, (Au, Pt, Pb, Co, Ni)	N52°10' E17°06' (a)
3. Żerków	A	Ca. 3540	115-120	1.4% Cu, 22 ppm Ag	Kupferschiefer stratiform	Cu, Ag, (Au, Pt, Pb, Co, Ni)	N52°04' E17°33' (a)
4. Florentyna	A	Ca. 3860	125-130	3.0% Cu, 33 ppm Ag	Kupferschiefer stratiform	Cu, Ag, (Au, Pt, Pb, Co, Ni)	N51°50' E18°10' (a)

[1] Like skarn, porphy, etc.

[2] There are 3 options for the indication of the area delineation: a. coordinates (latitude, longitude) of 1 point; b. coordinates (latitude, longitude) of 1 points and radius (m); c. coordinates (latitude, longitude) of more points.

Evaluation of the basic characteristics of prospective CHPM areas

PAMAV

Poland

AREAS 1-4 in one questionnaire[1]

1. Geology of the prospective area

Requested information on:

- ✓ local geology (in regional context)
- ✓ CHPM target formation
- ✓ list of available cross sections, geological maps, geochemical results, lithological information

Notes: briefly summarized, referenced to more detailed studies.

4 areas were proposed:

1. Mozów – on the basis of Mozów 1 borehole, borehole depth: 2414 m, depth of metals enrichment: ca. 2365 m, drilling year: 1990, borehole No. in database: 25946, Drilled for: hydrocarbons, Location: N52°03'48,73", E15°31'38,40", Locality: Mozów
2. Kaleje – on the basis of Kaleje 5 borehole, borehole depth 3500 m, depth of metals enrichment: ca. 3135 m, drilling year: 1975, borehole No. in database: 29666, Drilled for: hydrocarbons, Location: N52°09'28,83", E17°09'21,41", Locality: Zaniemyśl
3. Żerków – on the basis of Żerków 1 borehole, borehole depth: 3602 m, depth of metals enrichment: ca. 3545 m, drilling year: 1990, borehole No. in database: 31009, Drilled for: hydrocarbons, Location: N52°05'07,85", E17°32'57,43", Locality: Bieździadów
4. Florentyna – on the basis of Florentyna IG-2 borehole, borehole depth: 3882 m, depth of metals enrichment: ca. 3865 m, drilling year: 1982, borehole No. in database: 18156, Drilled for: hydrocarbons, Location: N51°50'48,87", E18°11'23,47", Locality: Zborów

All of these boreholes were drilled for hydrocarbons prospection. Cu-Ag mineralization was studied on drilling cores many years later (after 2005).

All of these boreholes occur at the so-called Fore-Sudetic Monocline, declining (in general) to NE. It is Kupferschiefer stratiform type of mineralization (CHPM target formation). Mineralization is located in so-called Red Floor Sandstone (*Czerwony Spągowiec*) formation of Permian age, just below 4 Zechstein saline cyclotems.

More detailed information on regional geology in context of prospective areas, with lithological information and some maps – see attached papers: Oszczepalski et al. 2016; Oszczepalski, Speczik 2011.

Mineralization occurs in Kupferschiefer black shale, in underlying white sandstone and sometimes also in overlying carbonate rock (mostly limestone). It is mostly copper and silver mineralization, with minor importance of other metals (Au, PGE, Pb, Zn, Co, Ni and others). It is mainly sulfide mineralization, with some areas of oxidized mineralization (examples – see attached paper: Oszczepalski et al 2017).

2. Geophysics of the prospective area

Requested information:

- ✓ previous geophysical measurements (in CHPM relevance)
- ✓ geophysical results that can be used for locating/defining the deep metal enrichment
- ✓ list of available geophysical maps, cross sections, logs, other measurements

[1] All four proposed area have common genesis, type of mineralization and other main features (though they are located in various locations, even over 100 km one form another, and at different depths), so for all 4 areas one common questionnaire was prepared. Information common for all 4 areas is given, and in some cases also detailed infromation on each area

Geophysical survey of the majority of proposed areas was made forty or more years ago. It was 2D seismic with use of outdated measuring apparatus. For convenient knowledge, mostly on regional geological setting, faults etc., modern 3D seismic techniques should be applied. Other geophysical methods are not useful in this case.
Moreover, geophysical measurements in boreholes were made. They are not openly available, as the majority of geological information from boreholes.

3. Deep metal enrichment

Requested information:

- ✓ (expected) metal enrichment based on available geophysical, geological and drill data, samples information, geochemistry

Information on metals content from Cu & Ag on the basis of studied samples from boreholes cores:

1. Mozów 1 - average content 3.22% Cu and 63 ppm Ag with average thickness 2.14 m; hypothetical resources of Mozów area ca. 83.3 million t on area 484 km^2.
2. Kaleje 5 - average content 7.07% Cu with average thickness 1.0 m; hypothetical resources of Kaleje area 47.4 milllion t on area 268 km^2.
3. Żerków 1 - average content 1.38% Cu and 22 ppm Ag with average thickness 2.80 m; hypothetical resources of Żerków area 15,6 million t on area 162 km^2.
4. Florentyna IG-2 - average content 2.99% Cu and 33 ppm Ag with average thickness 1.0 m; hypothetical resources of Florentyna area 8,6 million t on area 115 km^2.

In all of these boreholes copper and silver mineralization occur on the border of Kupferschiefer black shale, underlying white sandstone and overlying limestone.
Genetic characteristics of orebodies and ore forming processes – see e.g.: Kucha, Pawlikowski 2010; Oszczepalski 1999; Oszczepalski, Speczik 2010.

4. Integrated 3D- 4D model

Requested information:

- ✓ existing 3D-4D models of the target area and the deep metal enrichment
- ✓ if no 3D-4D models exist, collect the following necessary data: geological setting, mineralization, fluid flow models, stress field determination

Notes: e.g. openly available datasets, models.

3D-4D models of all 4 target areas of deep metal enrichment do not exist.
Basic data on geological setting and type of mineralization – in attached papers.
Fluid flow models – some information could be in borehole information cards, but they are not openly available.
Stress field determination – unclear term (rock mechanics?), but such detailed information is not available for these areas.
Remark on openly available datasets: the whole information on geological information from boreholes in Poland is available in the Central Geological Database of the Polish Geological Institute: http://otworywiertnicze.pgi.gov.pl/ but only very basic information on boreholes is openly available there (more detailed information is paid).

5. EGS potential

Requested information:

- ✓ EGS potential (heat & energy) of the area
- ✓ geothermal characteristics (temperature gradient, heat flux, stress field, water availability, EGS geology)
- ✓ presence/indication of deep fluids/brines, fracture system, crustal permeability

EGS potential of proposed 4 areas was not assessed. Some EGS potential studies of larger areas covering some of proposed 4 areas were done (e.g. attached paper: Sowizdrzal et al. 2013), but they usually are related to some overlying formations (Triassic, Jurassic, Cretaceous).
Information on temperature gradient:

1. Mozów – depth of metals enrichment: ca. 2365 m, rock temperature: 80-85°C
2. Kaleje – depth of metals enrichment: ca. 3135 m, rock temperature: 100-105°C
3. Żerków – depth of metals enrichment: ca. 3545 m, rock temperature: 115-120°C
4. Florentyna – depth of metals enrichment: ca. 3865 m, rock temperature: 125-130°C

Information on heat flux, stress field, fracture system – not available.
Information on deep fluids/brines: their presence is likely, but openly available information on that is not available (see point 4).
Information on crustal permeability – possible, but openly available information on that is not available.
Water availability – meaning of the term unclear.

List of references

- Oszczepalski S., Speczik S., 2010 – Copper and silver ores. In: Prospective resources of Poland. S. Wołkowicz, T. Smakowski , S. Speczik (Eds.), Polish Geological Institute – PRI, Warsaw, 2011 (in Polish).
- Oszczepalski S., Speczik S., Małecka K., Chmielewski A., 2016 – Prospective copper resources in Poland. Gospodarska Surowcami Mineralnymi – Mineral Resources Management, 32, 2, 5-30 (in English).
- Oszczepalski S., Chmielewski A., 2017 – Variability of ore mineralization in the north-west-trending extension of the Lubin-Sieroszowice deposit. Biuletyn Państwowego Instytutu Geologicznego 468, 109-142 (in Polish with English abstract).
- Oszczepalski S., 1999 – Origin of the Kupferschiefer polymetallic mineralization in Poland. Mineralium Deposita, 34, 599-613 (in English).
- Kucha H., Pawlikowski M., 2010 – Genetic investigations of copper Zechstein deposits, Poland. Geologia, 36, 4, 513-538 (in Polish with English abstract).
- Asael D., Matthews A., Oszczepalski S., Bar-Matthews M., Halicz L., 2009 – Fluid speciation controls of low temperature copper isotope fractionation applied to the Kupferschiefer and Timna ore deposits. Chemical Geology, 262, 147-158.
- Sowizdrzal A., Papiernik B., Machowksi G., Hajto M., 2013 - Characterization of petrophysical parameters of the Lower Triassic deposits in a prospective location for Enhanced Geothermal System (central Poland). Geological Quarterly, 57 (4), 729–744.

Annexes

Table 1

Prospective CHPM areas

APG Portugal							
Number	**Type of the selected area(s) (type "A" or type "B")**	**Depth(s) of the metal enrichment(s) (m)**	**Temperature /at these depths/ (°C)**	**Description of the metal enrichment(s)**			
				degree of the mineralization(s) (% or ppm)	***type of the mineralization(s)[1]***	***element(s)***	***area delineation(s)[2]***
1	B	250 m to 1200 m (Geophysical studies point out the possibility of existing mineralizations at greater depths; Inverno, C. *et al*, 2015b; Carvalho J. *et al*. 2016).	250m – 22°C 1200 m – ≈42°C (Temperatures at greater depths: 2000 m – 64 °C 3500 m – 100-150 °C 5000 m – 130 °C 5 500 m – 150-200 °C)	(average grade of VHMS deposits in the Iberian Pyrite Belt; Inverno, C. *et al*, 2015a) 45% S, 40% Fe, 1,3% Cu, 2,0% Zn, 0,7% Pb, 26 ppm Ag, 0,5 ppm Au **Neves Corvo Deposit** (Sas, J. *et al* 2018): *Copper-rich ore body* – 2.7% Cu; 0.8% Zn; 0.2% Pb and 37 ppm Ag *Zinc-rich ore body* – 0.4% Cu; 7.1% Zn; 1.7% Pb and 66 ppm Ag	Polymetallic massive sulphide deposits (VHMS deposits)	S, Fe, Cu, Zn, Pb, Ag, Au	Neves Corvo Area: (considering Inverno, C. *et al*, 2015a and Inverno, C. *et al*, 2015b) **Point 1:** 37°37'43.22''N; 8°01'26.36''W **Point 2:** 37°36'06.78''N; 8°03'42.87''W **Point 3:**

[1] Like skarn, porphy, etc.

[2] There are 3 options for the indication of the area delineation: a. coordinates (latitude, longitude) of 1 point; b. coordinates (latitude, longitude) of 1 points and radius (m); c. coordinates (latitude, longitude) of more points.

							37°32’02.06’’N; 7°59’37.18’’W **Point 4:** 37°25’58.29’’W; 7°43’33.00’W **Point 5:** 37°31’03.57’’N; 7°45’02.49’’W **Point 6:** 37°33’43.62’’N; 7°54’02.99’’W

Evaluation of the basic characteristics of prospective CHPM areas

Portuguese Association of Geologists (LTP)

AREA 1- Iberian Pyrite Belt (Neves Corvo Area)

1. **Geology of the prospective area**

Requested information on:

- ✓ local geology (in regional context)
- ✓ CHPM target formation
- ✓ list of available cross sections, geological maps, geochemical results, lithological information

Notes: briefly summarized, referenced to more detailed studies.

Prospective Area: Iberian Pyrite Belt (Neves Corvo Area) – 1

The Iberian Pyrite Belt (IPB) is a metallogenetic province about 250-km long and 20–70 km wide (Oliveira *et al.* 2013), located in the SW part of the Iberian Peninsula, between Seville (Andalusia, Spain) and Marateca (Alentejo, Portugal). The IPB contains a total of 1,850 Mt of sulphide deposits (1,600 Mt massive sulphide and 250 Mt stock work) represented by 11 deposits in Portugal and 80 deposits in Spain (Oliveira *et al.* 2013). This is one of the largest crustal sulphur anomalies and hosts many of the largest concentration of massive volcanic sulphide deposits worldwide (Inverno *et al.* 2015a). The Neves-Corvo deposit exploited by Somincor/Lundin Mining is the main IPB mining area, with seven massive ore lenses identified Neves, Corvo, Graça, Zambujal Lombador, Semblana, and Monte Branco, the last two still in exploration phase (Oliveira *et al.* 2013; Owen and Meyer 2013). The Neves-Corvo underground mining is being developed down to 900-m depth. Geologically, the IPB belongs to the South Portuguese Zone (SPZ) main Variscan domain (Oliveira *et al.* 2013). It was formed during the Variscan orogeny with the SPZ terrain and the Ossa-Morena terrain oblique collision. The result of this tensional tectonics was the pull-apart basins, which triggered submarine volcanism in the area. This volcanism was episodic, it has three felsic and two mafic cycles between them (Oliveira *et al.* 2004), which are intercalated with sediments. The deformation of the IPB during the Variscan orogeny is characterized by south to southwest-verging folds. In the region, there are several main antiform structures, with the axis of the antiforms located along the distinct volcanic axis. The Rosário–Neves-Corvo is one of them, with a complex antiform area characterized by several thrusts faults with southwest vergency. The IPB consists of two branches; the northern part built up by autochthonous and parautochthonous successions, whereas the southern part comprises rooted anticline structures (Pereira *et al.* 2008; Oliveira *et al.* 2013).

The sequence of the area is built up by three major units, from bottom to top the Phyllite–Quartzite Group (PQG), the volcano-sedimentary complex (VSC), and the Baixo Alentejo Flysch Group (BAFG, where the Mértola Formation is included). The PQG is dominated by black and grey shales in which are interbedded quartzites, quartz wacke siltstones, rarely conglomerates, and limestones. It is from Middle to Late Devonian in age and represents a shallow marine depositional environment, indicating a stable epicontinental platform. It is the IPB siliciclastic basement. On the other hand, the VSC is dominated by shales, thin-bedded siltstones, and minor volcanic sediments and later felsic (rhyolite, rhyodacites, and dacites) and mafic (basalt and dolerites) volcanic rocks with minor andesite. The occurrence of the felsic volcanic rocks, dominantly lava/dome complexes, is associated with minor pyroclastic flows and intrusions. The felsic volcanic units and/or black shales host the massive sulphide deposits. The volcanic sequence can reach the 1,300-m thickness and is from Late Devonian–Early Carboniferous age. It was formed in an extensional graben-type basin on a disrupted siliciclastic platform (Oliveira *et al.* 2013; Inverno *et al.* 2015b). The BAFG is a turbiditic sequence of shales, graywackes, and rare conglomerates.

It is from Carboniferous age and represents the synorogenic foreland flysch associated with Variscan collision and tectonic inversion (Oliveira *et al.* 2013; Inverno *et al.* 2015b).
The sulphide mineralization genesis is related to hydrothermal fluid circulation, in the volcanic and sedimentary host rocks (Barriga *et al.* 1997). The IPB deposits were formed by the bimodal submarine volcanism and the convective cells of the hydrothermal system related to it (Inverno *et al.* 2015a), and the deformational shear corridor of the Neves-Corvo main thrust controls the mineralization and the concentration of the copper-rich ore (Inverno *et al.* 2015b). The main metal is the copper, and the zinc is additional; other elements that appear in the Neves-Corvo ore body are tin, lead, silver, gold, and indium. Primary mineralization includes pyrite, chalcopyrite, sphalerite, and cassiterite; secondary minerals are arsenopyrite, galena, gold, silver, and tennantite (Sas, J. *et al.* 2018).

As it would be very extensive to list all the available requested data, the relevant references containing these information will be listed in the References section.

2. Geophysics of the prospective area

Requested information:

- ✓ previous geophysical measurements (in CHPM relevance)
- ✓ geophysical results that can be used for locating/defining the deep metal enrichment
- ✓ list of available geophysical maps, cross sections, logs, other measurements

Several seismic profiles were acquired by CGG in 1991 and 1996 (Carvalho *et al.* 1996). Carvalho *et al*. 2016 developed six 2D seismic profiles for the area between the Neves-Corvo mine and the Portuguese/Spanish border. The location of the seismic profiles was chosen to investigate the crust below the flysch cover for the possible extension of the Neves-Corvo volcanic axis to the Alcoutim area (close to the Spanish border), where the VSC outcrops again, and its southern region; along this extension, the VSC rocks were intersected by exploration drill-holes at 400–810 m depth (Billinton exploration project developed in the 1980s). The interpretation of the seismic profiles was complemented with available land gravimetric and aeromagnetic data. The VSC units deepen from the region of the Neves- Corvo mine (where they outcrop) and in profile 1 to profile 4, located further SE. East of profile 4, along profiles 5 and 6, the VSC rises and is located at depths of 400–500 m. Drill-hole data very close to profile 6, located south of Alcoutim and near the Spanish border, show the presence of VSC basic and acid volcanic rocks. The extension of the volcanic axis and of its structural framework from the Neves-Corvo mine to Alcoutim, together with the depth of VSC units in the SE part of the studied area, shows the existence within the IPB of new promising exploration areas. This may lead to the discovery of polymetallic massive sulphide deposits of the Neves-Corvo type.

Relevant references containing these information will be listed in the References section.

3. **Deep metal enrichment**

Requested information:

- ✓ **(**expected) metal enrichment based on available geophysical, geological and drill data, samples information, geochemistry

There are still no detailed information regarding deep metal enrichment, although the available data are promissing. LNEG is developing a more detailed study on this area that will be will discussed in their CHPM final report.

4. **Integrated 3D- 4D model**

Requested information:

- ✓ existing 3D-4D models of the target area and the deep metal enrichment
- ✓ if no 3D-4D models exist, collect the following necessary data: geological setting, mineralization, fluid flow models, stress field determination

Notes: e.g. openly available datasets, models.

Carvalho *et al.* (2017) developed a 3D structural stratigraphic model based on the interpretation of the geophysical, drill-hole and geological data. The 3D structural models were obtained by the creation of the transition surfaces between the following main groups: flysch (Mértola and Mira Formations), VSC and PQG.

Inverno *et al.* (2015) developed 3D, 4D and predictive geological modelling for the Neves Corvo project area. These models enabled to correlate its geological, stratigraphical, geochronological, structural, mineral deposit, geophysical, geochemical and other characteristics.

5. EGS potential

Requested information:

- ✓ EGS potential (heat & energy) of the area
- ✓ geothermal characteristics (temperature gradient, heat flux, stress field, water availability, EGS geology)
- ✓ presence/indication of deep fluids/brines, fracture system, crustal permeability

There is a theoretical potential estimation for an enhanced geothermal system (EGS; Chamorro *et al*. 2014) for the entire Iberian Peninsula also covering the IPB. Temperature estimations reached different depths (up to 9,500 m), based on the heat-flow density and the heat production (Chamorro *et al.* 2014). However, the Portuguese National Geothermal Atlas (PNGA; Ramalho 2014) does not reach such depths. As seen in the PNGA, surface heat flow density shows relatively high variation in small distances near the IPB, but the small-scale variations are more likely to be correlated with crustal composition than changes in the underlying heat flow (Sas *et al*. 2018). The surface heat-flow density of the South Portuguese Zone [mainly measured in mining wells, water wells, hydrocarbon wells, geothermal wells, and in thermometric wells in the area] varies between 60 and 100 mW/m^2 (Fernández *et al*. 1998; Correia and Ramalho 1999), and the mean value of the Peninsula is 73.3 mW/m2 (Chamorro *et al.* 2014). In the case of Neves-Corvo, the mean value is 80 mW/m^2, which belongs to the suitable areas in the mainland of Portugal. The mean radiogenic heat production value of the area is 2.93–3 $\mu W/m^3$ (Fernández *et al.* 1998; Correia and Ramalho 1999; Chamorro *et al.* 2014), but it decreases with the depth (Correia and Ramalho 1999). This increase in depth indicates that for the study area, temperatures at 2 and 5 km depths are 64 and 130 °C, respectively. The available energy for an EGS power plant is stored in the range of 3–10 km depth (Chamorro *et al*. 2014). The estimated temperature in Neves-Corvo is 100–150 °C at 3,500-m depth and 150–200 °C at 5,500-m depth (Chamorro *et al*. 2014), which is suitable for an EGS project (Sas *et al*. 2018). According to LNEG database, the temperature at 2,000 m is 63–65 °C and at 5,000 m is 131–134 °C (LNEG 2015).

The area is built up by low-permeability Paleozoic and Mesozoic volcanic rocks. During the Variscan orogeny faults, thrusts and folds developed significant permeability in these rocks (Fernández-Rubio *et al.* 1988). Infiltrating rainwater and the water of the Oeiras River are the main water sources through faults and fractures (Fernández-Rubio and Carvalho 1993). Fernández-Rubio *et al*. (1988) distinguished the following three main hydrological units:

- Cutaneous complex, which includes the alluvial terrace and weathered zone. In this case, permeability decreases with the depth.
- Intermediate complex, including the Flysch Group above the orebody. This unit has secondary permeability due to faults and fractures.
- The third zone is the Ore System, which includes the deposits and the footwall formation. The permeability of the zone is characterized by microfissures in the orebodies.

A particularly relevant feature of the area is the NW-SE (dipping to NE) Neves Corvo main thrust bringing VSC rocks on top of the Mértola Fm., extremely close to Neves Corvo VHMS ores. Late Variscan faults displaced all former geological units and Variscan structures, including thrusts, as shown by the 3D models. They are strike-slip oblique faults, mostly striking NE-SW to ENE-WSW (sinistral) and N-S to NNW-SSE (dextral). In some cases the seismic sections show deep development (>5 km depth) of these fault zones. Also in late Variscan time, small vein-type Cu (and other metals) deposits and occurrences, abundant in the eastern part of the area, were emplaced along these faults, also used during the Middle Jurassic to locally accommodate intrusions of dolerite dykes, particularly along the prominent NW-SE sinistral Messejana fault in the northwesternmost end of the area (Inverno *et al.* 2015).

List of references

Geology of the prospective area
(includes cross sections, geological maps, geochemical results and lithological information)

Barriga, F., Carvalho, Ribeiro, A. 1997: Introduction to the Iberian Pyrite Belt. In Barriga, F. & Carvalho, D. Eds. Geology and VMS Deposits of the Iberian Pyrite Belt. SEG Neves Corvo Field Conference. Guidebook Series, V. 27. Society of Economic Geologists

Inverno, C., A. Diez-Montes, C. Rosa, J. García-Crespo, J.X. Matos, J.L. García-Lobón, J. Carvalho, F. Bellido, J.M. Castello-Branco, C. Ayala, M.J. Batista, F. Rubio, I. Granado, F. Tornos, J.T. Oliveira, C. Rey,V. Araújo, T. Sánchez-García, Z. Pereira, P. Represas, A.R. Solá, P. Sousa 2015a: Chapter 9 – Introduction and geological setting of the Iberian Pyrite Belt. – In: Weihed, P. (Ed): 3D, 4D and Predictive Modelling of Major Mineral Belts in Europe. Springer, Cham, pp. 191–208.

Inverno, C., C. Rosa, J.X. Matos, J. Carvalho, J.M. Castello-Branco, M.J. Batista, I. Granado, J.T. Oliveira, V. Araújo, Z. Pereira, P. Represas, A.R. Solá, P. Sousa 2015b: Chapter 11 – Modelling of the Neves- Corvo Area. – In: Weihed, P. (Ed): 3D, 4D and Predictive Modelling of Major Mineral Belts in Europe. Springer, Cham, pp. 231–261.

Oliveira, J.T., Z. Pereira, P. Carvalho, N. Pacheco, D. Korn 2004: Stratigraphy of the tectonically imbricated lithological succession of the Neves-Corvo mine area, Iberian Pyrite Belt, Portugal. – Mineralium Deposita, 39, pp. 422–436

Oliveira, J.T., C.J.P. Rosa, Z. Pereira, D.R.N. Rosa, J.X. Matos, C. Inverno, T. Andersen 2013: Geology of the Rosário-Neves-Corvo antiform, Iberian Pyrite Belt, Portugal: New insights from physical volcanology, palynostratigraphy and isotope geochronology studies. – Mineralium Deposita, 48, pp. 749–766.

Owen and Meyer 2013. Lundin Mining. NI 43-101 Technical Report for Neves-Corvo Mine and Semblana Deposit, Portugal. – Wardell Armstrong, London, 224 p.

Pereira, Z., J.X. Matos, P. Fernandes, J.T. Oliveira 2008: Devonian and Carboniferous palynostratigraphy of the South Portuguese Zone, Portugal – An overview. – Comunicações Geológicas, 94, pp. 53–79.

Sas, J., Osvald, M., Ramalho, E., Matos, J.X. 2018: Combined study of mineral deposits and deep geothermal for energy production or urban heating – Comparison between the Portuguese (Neves-Corvo) and the Hungarian (Recsk) case studies. – Central European Geology, 61/2, pp. 118–135

Other references concerning Geology of the prospective area

Barriga, F.J.A.S. 1990: Metallogenesis in the Iberian Pyrite Belt. In Dallmeyer, R.D., Martinez Garcia, E. (Eds.). Pre-Mesozoic Geology of Iberia. Springer-Verlag Berlin Heidelberg. ISBN-13 :978-3-642-83982-5, e-ISBN-13 :978-3-642-83980-1, 001: 10.1007/978-3-642-83980-1, pp. 369–378

Carvalho, J.R.S, Relvas, J.M.R.S., Pinto, A.M.M., Frenzel, M., Krause, J., Gutzmer, J., Pacheco, N., Fonseca, R., Santos, S., Caetano, P., Reis, T., Gonçalves, M. 2018: Indium and selenium distribution in the Neves-Corvo deposit, Iberian Pyrite Belt, Portugal. Mineralogical Magazine, May 2018, Vol. 82(S1), pp. S5–S41

Carvalho, P., Ferreira, A. (?): Geologia de Neves Corvo: Estado actual do conhecimento. SOMINCOR, pp. 30

Fernandez-Rubio, R., Carvalho, P., Real, F. 1988: Mining-Hydrological Characteristics of Underground Copper Mine of Neves-Corvo, Portugal. IMWA Proceedings, pp. 49–63

Gaspar, O. 2002: Mineralogy and Sulfide Mineral Chemistry of the Neves-Corvo Ores, Portugal: Insight into their Genesis. The Canadian Mineralogist, Vol. 40, pp. 611–636

Leistel, J.M., Marcoux, E., Thiéblemont, D., Quesada, C., Sánchez, A., Almodóvar, G.R., Pascual, E., Sáez, R. 1998: The volcanic-hosted massive sulphide deposits of the Iberian Pyrite Belt – Review and preface to the Thematic Issue. Mineralium Deposita, 33: 2 – 30

Oliveira, J.T. 1990: Stratigraphy and Synsedimentary Tectonism. In Dallmeyer, R.D., Martinez Garcia, E. (Eds.). Pre-Mesozoic Geology of Iberia. Springer-Verlag Berlin Heidelberg. ISBN-13 :978-3-642-83982-5, e-ISBN-13 :978-3-642-83980-1, 001: 10.1007/978-3-642-83980-1, pp. 334–347

Owen and Meyer 2017. Lundin Mining. NI 43-101 Technical Report for Neves-Corvo Mine, Portugal. – Wardell Armstrong, London, 236 p.

Silva, J.B., Oliveira, J.T., Ribeiro, A. 1990: Structural Outline. In Dallmeyer, R.D., Martinez Garcia, E. (Eds.). Pre-Mesozoic Geology of Iberia. Springer-Verlag Berlin Heidelberg. ISBN-13 :978-3-642-83982-5, e-ISBN-13 :978-3-642-83980-1, 001: 10.1007/978-3-642-83980-1, pp. 348–362

Technical Report: Hole (ALFP001) completed at Alcoutim Cu-Zn Project in Portugal. Auroch Minerals Ltd. 5 p.

Geophysics of the prospective area
(includes geophysical maps, cross sections, logs, other measurements)

Carvalho P, Pacheco N, Beliz A, Ferreira A (1996) Últimos desenvolvimentos em prospeção realizados pela Somincor. Bol. Geologico y Minero ITGE, vol 107 (5–6), Madrid, 39–54

Carvalho, J., Inverno, C., Matos, J.X., Rosa, C., Granado, I., Branch, T., Represas, P., Carabaneanu, L., Matias, L., Sousa, P. 2017: Subsurface mapping in the Iberian Pyrite Belt using seismic reflection profiling and potential field data. Int J Earth Sci (Geol Rundsch), Vol. 106, 3, pp. pp 899–915, DOI 10.1007/s00531-016-1340-1

Other references concerning Geophysics of the prospective area

Carvalho J., Sousa P., Matos J., Pinto C. 2011: Ore prospecting in the Iberian Pyrite Belt using seismic and potential-field data. J Geophys Eng 8(2), pp. 142–153

Integrated 3D- 4D model

Carvalho, J., Inverno, C., Matos, J.X., Rosa, C., Granado, I., Branch, T., Represas, P., Carabaneanu, L., Matias, L., Sousa, P. 2017: Subsurface mapping in the Iberian Pyrite Belt using seismic reflection profiling and potential field data. Int J Earth Sci (Geol Rundsch), Vol. 106, 3, pp. pp 899–915, DOI 10.1007/s00531-016-1340-1

Inverno C., Rosa C., Matos J., Carvalho J., Castello-Branco J.M., Batista, M.J., Granado I., Oliveira J.T., Araújo V., Pereira Z., Represas, P., Solá A.R., Sousa P. 2015: Modelling of the Neves Corvo area. In: Weihed P (ed) 3D, 4D and predictive modelling of major mineral belts in Europe, chapter 11. Springer, Berlin, pp. 231–261

EGS potential

Chamorro, C.R., J.L. García-Cuesta, M.E. Mondéjar, M.M. Linares 2014: An estimation of the enhanced geothermal systems potential for the Iberian Peninsula. Renewable Energy, 66, pp. 1–14.

Correia, A., E.C. Ramalho 1999: One-dimensional thermal models constrained by seismic velocities and surface radiogenic heat production for two main geotectonic units in southern Portugal. Tectonophysics, 306, pp. 261–268.

Fernández, M., I. Marzán, A. Correia, E. Ramalho 1998: Heat flow, heat production, and lithospheric thermal regime in the Iberian Peninsula. Tectonophysics, 291, pp. 29–53.

Fernández-Rubio, R., P. Carvalho 1993: Surface water inflow reduction at the underground Neves-Corvo mine, Portugal. Mine Water and the Environment, 12/1, pp. 11–20.

Fernández-Rubio, R., P. Carvalho, F. Real 1988: Mining hydrogeological characteristics of the underground copper mine of Neves-Corvo, Portugal. Third International Mine Water Congress, Melbourne, 15 p.

Inverno C., Rosa C., Matos J., Carvalho J., Castello-Branco J.M., Batista, M.J., Granado I., Oliveira J.T., Araújo V., Pereira Z., Represas, P., Solá A.R., Sousa P. 2015: Modelling of the Neves Corvo area. In: Weihed P (ed) 3D, 4D and predictive modelling of major mineral belts in Europe, chapter 11. Springer, Berlin, pp. 231–261

LNEG 2015: Geothermal Maps – http://geoportal.lneg.pt/geoportal/mapas/index.html

Ramalho, E.C. 2014: Geothermal Energy. State of the Art in Portugal. Geothermal Energy Workshop, Salta, 25 p.

Sas, J., Osvald, M., Ramalho, E., Matos, J.X. 2018: Combined study of mineral deposits and deep geothermal for energy production or urban heating – Comparison between the Portuguese (Neves-Corvo) and the Hungarian (Recsk) case studies. – Central European Geology, 61/2, pp. 118–135

Annexes

Evaluation of CHPM characteristics of prospective CHPM areas

Portugal

1. **CHPM operational characteristics - Information for CHPM technological elements**

Requested information:

✓ please fill in the table below with the requested data for the CHPM technology elements

Underground heat exchanger (deep metal enrichment + potential geothermal reservoir)	
Extension of the metal enrichments *(volumetric interpretation)*	Until the end of 2017: Copper ore: hoisted 54.116 Mt, in situ resources 71.800 Mt Zinc ore: hoisted 6.203 Mt, in situ resources120.680 Mt
Expected type of the reservoir and porosity/permeability *(fractured, porous, etc)*	The deep reservoir is below 0 m (m a.s.l.). The circulation of groundwater has essentially preferred paths conditioned by the structure: circulates through faults, thrusts, fractures, lithologic discontinuities and is much smaller through rock fissures. The low hydraulic conductivity of rocks is about 0.001 m/day.
Mineralization *(type and enriched metals)*	Copper ore: MC, MF (fissural) and MH with penalizes – mercury) Zinc ore: MZ, MCZ (copper and zinc), MZP (with zinc and lead), MCZP (high content of Copper and lead)

Production and injection wells	
Depth of potential wells (m)	The mining prospecting boreholes, currently carried out at Neves-Corvo mine, reach 1600 m depth and intersect the water levels of the deep aquifer.

Electrolytic metal recovery and gas diffusion electro- precipitation	
Potential target metals to be recovered	Not in application in Neves Corvo Currently Neves Corvo produce Cu, Zn and Pb concentrates, by using traditional floating technics,

Power plant (heat exchanger)		
Local heat and electricity demand *(industrial, municipal, agricultural, etc.)*	Data from 2017. **Diesel:** **Month** / **Consumption (litre)** Jan 541.950,61 Fev 523.224,26 Mar 581.281,41 Apr 530.352,65 May 540.585,15 Jun 572.471,10 Jul 555.348,11 Aug 536.176,90 Sep 586.700,68 Oct 604.907,75 Nov 576.475,89 Dec 499.531,52 TOTAL **6.649.006,03**	**Energy:** **Neves Corvo** **Year** / **Amount** / **Unit** Jan 21.338,62 MWh Fev 20.590,97 MWh Mar 22.130,37 MWh Apr 20.256,94 MWh May 20.130,57 MWh Jun 21.162,33 MWh Jul 20.035,21 MWh Aug 21.269,92 MWh Sep 20.299,66 MWh Oct 19.342,26 MWh Nov 19.662,42 MWh Dec 17.622,92 MWh

Salt gradient power generation	
Salinity of expected geothermal brine	For depths reaching 1000 m (m.a.s.l.), the fluid temperature ranges from 30 to 39°C with dissolved solids dried at 105 °C ranging from 800 to 23200 mg/L.

Fresh water supply from the surface *(water sources)*	645.000 m3 in 2017. 784.160 until November 2018 From Santa Clara National Dam

2. CHPM operational characteristics - Environmental, social and political background

Requested information:

- ✓ toleration to gaseous and solids emissions, water and noise pollution,
- ✓ local competition to land and water availability
- ✓ public acceptance
- ✓ political support
- ✓ presence of supporting legislation, regulatory framework

Notes: all of above refers to the selected area and its surroundings.

No available information.

There is no specific legislation regarding a CHPM system.

3. Financial aspects

Requested information:

- ✓ list of potential local stakeholders (community, political, companies)

The potential local stakeholders might be the Counties of Almodôvar, Castro Verde, Aljustrel, Ourique and Mértola and neighbours and owners of homestead.

Table 1

Prospective CHPM areas

SGD Serbia							
Number	**Type of the selected area(s) (type ''A'' od type ''B'')**	**Depth(s) of the metal enrichment(s) (m)**	**Temperature /at these depths/ (°C)**	**Description of tge metal enrichment(s)**			
				degree of the mineralization(s) (% or ppm)	***type of the mineralization(s)***	***element(s)***	***area delineation(s)***
1	B	430 m (from -449 m to -879 m)1	70 (at the bottom)	0.707 % 0.24 g/t	porphyry	Cu Au	7.587.362 4.983.689
2	B	2068 m (from -200 m to -2,268 m)	57	0.74 % 0.16 g/t	porphyry	Cu Au	7.590.975 4.876.305

Number 1 – Metal enrichment 1: Borska reka porphyry copper deposit

Present surface: 398 m. The mineralization continues in depth

No published data – no data available. Exploitation field (permition) of RTB Bor (Mining and Smelting Basin Bor).

Source: Janković S., Jelenković R., Koželj D., 2002: The Bor cooper and gold deposit, Mining and Smelting Basin Bor (RTB Bor) – Copper Institute (CIB), 298 p.

Number 2 – Metal enrichment 2: Chukaru Peki porphyry copper deposit

Present surface: 404 m. The mineralization continues in depth.

No published data – no data available. Exploratation right (permition) of Rakita Exploration d.o.o, Bor.

Source: Jelenković R., 2018: Istraživanje metaličnih mineralnih sirovina u Srbiji, zaštita životne sredine i prostorno planranje. XVII Kongres geologa Srbije, Vrnjačka banja, 1-17 str.

Table 1

Prospective CHPM areas

RBINS Slovakia							
Number	**Type of the selected area(s) (type "A" or type "B")**	**Depth(s) of the metal enrichment(s) (m)**	**Temperature /at these depths/ (°C)**	**Description of the metal enrichment(s)**			
				degree of the mineralization(s) (% or ppm)	***type of the mineralization(s)[1]***	***element(s)***	***area delineation(s)[2]***
***1* KOŠICE BASIN / ĎURKOV DEPRESSION**	A	1600 – 2000 m (geothermal reservoir top), 2600-4000 m (geothermal reservoir bottom)	87-180°C	Unknown	Hg-As-Pb mineralization associated with Neogene volcanism (a result of NEP subduction beneath ALCAPA microplate)	As	34 km²

[1] Like skarn, porphy, etc.

[2] There are 3 options for the indication of the area delineation: a. coordinates (latitude, longitude) of 1 point; b. coordinates (latitude, longitude) of 1 points and radius (m); c. coordinates (latitude, longitude) of more points.

Table 1

Prospective CHPM areas

SGD Slovenia							
Number	**Type of the selected area(s) (type "A" or type "B")**	**Depth(s) of the metal enrichment(s) (m)**	**Temperature /at these depths/ (°C)**	**Description of the metal enrichment(s)**			
				degree of the mineralization(s) (% or ppm)	***type of the mineralization(s)[1]***	***element(s)***	***area delineation(s)[2]***
1	Hypothetical ''B''	Hypothetical 2,000 m Hypothetical 3,000 m	60 +/- 6 °C 84 +/- 8 °C	na	Hypothetical mineralized HORNFELSES	Fe, Pb, Zn +/- minor Cu, Ag?	46°30'49,67'' 15°11'56,05''

Explanation:

In Slovenia, we didn't discover any metal enrichment with deep research drilling yet in the depth > 1,000 m. Because we wished to fulfil at least one row in the Table 1, we propose Hypothetical type ''B'' mineralization NE from the outcrops of hornfelses with ore occurrences at **Mala Kopa on the Pohorje Mountains** (in the contact aureole of the granodiorite intrusion with the low grade metamorphic rocks). We assume that the ore body there is developed to the depth of very roughly about 2,000 m, considering the new model of the Pohorje tectonic block. The temperature at that depth is believed to be between 54 and 66 °C. The mineralisation comprises magnetite, hematite, chalcopyrite, galena, sphalerite, pyrrhotite…. Main metal element is Fe, minor are Pb and Zn, while Ag and some trace elements have been detected in the near-surface explorations. The expert knowledge of the mineralization is provided by dr. Mirka Trajanova who is studying Pohorje magmatic body and origin of the Pohorje tectonic block (GeoZS, member of SGD).

[1] Like skarn, porphy, etc.

[2] There are 3 options for the indication of the area delineation: a. coordinates (latitude, longitude) of 1 point; b. coordinates (latitude, longitude) of 1 points and radius (m); c. coordinates (latitude, longitude) of more points.

Evaluation of the basic characteristics of prospective CHPM areas

SGD

Slovenia

AREA 1- Mala Kopa on the Pohorje Mountains

1. **Geology of the prospective area**

Requested information on:

- ✓ local geology (in regional context)
- ✓ CHPM target formation
- ✓ list of available cross sections, geological maps, geochemical results, lithological information

Notes: briefly summarized, referenced to more detailed studies.

- ✓ Local geology (in regional context)

The Pohorje region of the northern Slovenia represents south-easternmost exposed parts of the Precambrian Austroalpine (Saualpe and Koralpe) polymetamorphic units at the southwestern margin of the Pannonian Basin. It extends between the towns Dravograd at the northwest, Slovenjske Konjice at the south, Slovenska Bistrica at the southeast and Maribor at the northeast. Its lithology consists mainly of metamorphic rocks, which continue north-westward to the Košenjak region and further to the Koralpe in Austrija. Below the Ribnica-Selnica Miocene clastic rocks, metamorphic suite extends northward to the Kobansko hilly area.

Granitoid magma intruded into the central part of the Pohorje massif. In the eastern part, it intruded medium to high grade metamorphic rocks of the Pohorje Formation (called Pohorje Series by Mioč, 1978; Mioč & Žnidarčič, 1977), which show no considerable contact metamorphic alteration (Hinterlechner-Ravnik, 1971). Gneisses and mica schists prevail, containing numerous lenses of amphibolite, eclogite, marble, quartzite and pegmatite gneiss. Their mineral paragenesis shows polyphase metamorphism as a consequence of Variscan and Alpine events (Hinterlechner-Ravnik, 1971, 1973, 1982). Pohorje tectonic block has nappe structure on its north-western part, consisting of Ordovician to Carboniferous low-metamorphic rocks (slates with infrequent lenses of recrystallized carbonate rocks, quartzite, and altered basalts, formerly called diabases) of the Magdalensberg Formation, comprised in the Remschnig thrust (Mioč, 1978). The Magdalensberg Formation is discordantly overlain by Permo-Triassic clastic rocks, some patches of Triassic dolomite and relics of Gossau Cretaceous.

The igneous body intruded the entire rock sequence, except the Karpatian (Jelen et al. 2008) sandy-gravely conglomerates to the northwest at the apical part of the succession, which determine intrusion's upper age limit (Trajanova, 2013). The intrusion is represented by granodiorite and subvolcanic dacite of Lower Miocene age (Trajanova et al., 2008; Fodor et al. 2008). Miocene sedimentary rocks in the surrounding of the pluton are of the Upper Ottnangian/Karpatian to Lower Badenian age (Čorić et al., 2011; Ivančič et al., 2017).

- ✓ Ore mineralization target formations

Discussion on the prospectivity of the Pohorje for a deep seated ore mineralization is based entirely on the model of the Pohorje tectonic block origin proposed by Trajanova (2013). The model is made on the basis of structural, petrological, geochemical, radiometric, and paleomagnetic data. The wider belt bordered within the rectangle Slovenj Gradec, Šmartno pri Slovenj Gradcu, and Primoški vrh and Ribnica na Pohorju covers broadly the target area. There, several small abandoned mine pits exist, where iron ore was exploited mostly in the 19th century. The shallow ore occurrences are known as

the Zoiss mines. Ore mineralization is restricted to the thrust zone of the Remschnig nappe (Trajanova, 2013) consisting of the Magdalensberg Formation and the retrogressed bedrock schists of the Pohorje Formation. The zone comprises slates of the Magdalensberg formation around the main granodiorite intrusion above the thrust plane and to some extent the retrogressed schists below. Mineralized relic patches of the latter can be found in the area of Volovica and Rakovec. The slates and weakly metamorphosed limestone lenses in them were altered to epidote and garnet hornfelses, and subordinate skarns, which carry Fe, and some Pb, Zn (± Mn, traces of Cu, Ag, Bi and W) mineralization at the contact with subvolcanic dacite/porphyric granodiorite. This polymetallic mineralization occurs close to the surface in the area of Velika and Mala Kopa, and in the direction of Sv. Primož. Drovenik et al. (1980) treated all mentioned deposits as Paleozoic in origin. According to the Štrucl and Kluge (1991) presumption, it could originate from primary old-Paleozoic syngenetic magmato-sedimentary mineralization, similar as the one in the Magdalensberg Formation at Lom north of Mežica.

Due to the lack of any geophysical proofs on the correctness of the proposed model of Trajanova (2013), it is not possible to deduce a univocal characterization of the Pohorje ore occurrences. Nevertheless, several data support direct connection of the ore mineralization with the Pohorje magmatism (Trajanova, 2013). No detailed study of the mineralization in the Remšnik thrust zone has been made. Investigations of the surface did not give economically interesting occurrences of the ore minerals.

- ✓ Available geological maps and cross-sections

Only in the Basic geol. map of Mioč & Žnidarčič, 1977 and appertained Explanatory notes;

Some data on ore mineralization are stored in the Mežica Pb-Zn abandoned mine archive.

No spatial data on the mineralization are available.

2. <u>Geophysics of the prospective area</u>

<u>Requested information:</u>

- ✓ previous geophysical measurements (in CHPM relevance)
- ✓ geophysical results that can be used for locating/defining the deep metal enrichment
- ✓ list of available geophysical maps, cross sections, logs, other measurements

No geophysical investigations have been made in the area of Pohorje

3. Deep metal enrichment

Requested information:

- ✓ **(**expected) metal enrichment based on available geophysical, geological and drill data, samples information, geochemistry

It should be noted here that considerable part of the Pohorje tectonic block is sub-horizontally sheared/detached and unroofed toward the east due to the Late Miocene tectonics (Trajanova, 2013). Hence, the near-surface ore mineralization is lost. We expect it on both sides and especially below the granodiorite body. The depth depends on the thickness of the intrusion and on the tilt degree, for which we have no data, just a model. If the intrusion is dipping steeply, then the predicted depth could be a few thousands of meters, but if it is gently inclined then we expect depths of just some hundreds of meters.

4. Integrated 3D- 4D model

Requested information:

- ✓ existing 3D-4D models of the target area and the deep metal enrichment
- ✓ if no 3D-4D models exist, collect the following necessary data: geological setting, mineralization, fluid flow models, stress field determination

Notes: e.g. openly available datasets, models.

No data on the requested information.

5. **EGS potential**

Requested information:

- ✓ EGS potential (heat & energy) of the area
- ✓ geothermal characteristics (temperature gradient, heat flux, stress field, water availability, EGS geology)
- ✓ presence/indication of deep fluids/brines, fracture system, crustal permeability

✓ geothermal characteristics (temperature gradient, heat flux, stress field, water availability, EGS geology)

Forecast for geothermal characteristics of Mala Kopa location
Lat 46°30'49,67''
Lon 15°11'56,05''
Z = 1257 m
T_0= 5,44°

Geothermal gradient, gradT (to the depth 500 m): 28 +/- 5°C/km

Temp. in depth 1000m = 34 +/- 5 °C

Temp. in depth 2000m = 60 +/- 6 °C

Temp. in depth. 3000m = 84 +/- 8 °C

Heat flow density q = 0,070 +/- 0,010 W/m^2

Rajver & Ravnik, 2002; Rajver et al., 2012a, Rajver et al., 2012b, Rajver et al., 2013a, Rajver et al 2013b.

✓ presence/indication of deep fluids/brines, fracture system, crustal permeability

There is no available data on deep fuids/brines, fracture system and crustal permeability in the location

List of references

BERCE, B. 1963. The formation of ore-deposits in Slovenia. *Rendiconti della Società Mineralogica Italiana*, vol. 19, 1-16.

DROVENIK, M., DUHOVNIK, J. and PEZDIČ, J. 1976. Izotopska sestava žvepla v sulfidnih rudnih nahajališčih v Sloveniji. Rud. met. zbornik, 2-3, 193-246.

DROVENIK, M., PLENIČAR, M. and DROVENIK, F. 1980. Nastanek rudišč v SR Sloveniji. Geologija, let. 23/1, 1-157.

DUHOVNIK, J. 1956. Über die metallogenetischen Epochen und Provinzen Jugoslawiens. *Berg- und Hüttenmännische Monatsh* 101/2, 30-32.

FODOR, L., GERDES, A., DUNKL, I., KOROKNAI, B., PÉCSKAY, Z., TRAJANOVA, M., HORVÁTH, P., VRABEC, M., JELEN, B., BALOGH, K. & FRISCH, W. 2008: Miocene emplacement and rapid cooling of the Pohorje pluton at the Alpine-Pannonian-Dinaridic junction, Slovenia. Swiss J. Geosci., Birkhäuser Verlag, 255-271.

Geological service of the Mežica mine: Metalogenetska problematika kovinskih nahajališč v metamorfnih kameninah na Kobanskem in Pohorju, ECM Inštitut za gospodarski in socialni razvoj Ravne na Kor. Arhivska poročila o delu od 1984 do 1989 (Metalogenetic problems of metal deposits in metamorphic rocks in Kobansko-Pohorje, ECM Institute for Economic and Social Development Ravne na Kor. Archive work reports for the years from 1984 to 1989).

GRAFENAUER, S. 1965. Genetska razčlenitev svinčevih in cinkovih nahajališč v Sloveniji. *Rud. Met. Zbornik,* let. 2, str. 165-171.

GRAFENAUER, S. 1966: Metalogenija i mineraloške karakteristike bakrovih pojava u Sloveniji. Referati VI. savetovanja geologa SFRJ II, Ohrid, 377-396.

HINTERLECHNER-RAVNIK, A. 1971. Metamorfne kamnine Pohorja. *Geologija* 14, 187-226.

HINTERLECHNER-RAVNIK, A. 1973. Pohorske metamorfne kamenine II. *Geologija* 16, 245-270.

HINTERLECHNER-RAVNIK, A. 1982. Pohorski eklogit. Geologija, 25/2, 251-288.

JELEN, B., RIFELJ, H., SKABERNE, D., POLJAK, M. & KRALJ, P. 2008. Palaeogene and Neogene, Slovenian Paratethys basins. In McCann, T. (Ed.). The geology of central Europe, Mesozoic and Cenozoic, vol. 2. Geol. Soc. London, 1098-1102.

MIOČ, P. and ŽNIDARČIČ, M. 1977. Osnovna geološka karta SFRJ 1:100.000. L 33-55, Slovenj Gradec. Zvezni geološki zavod, Beograd.

MIOČ, P. 1978. Tolmač za list Slovenj Gradec Osnovne geološke karte SFRJ 1:100.000. Beograd: Zvezni geološki zavod, 74 pp.

RAJVER, D., RAVNIK, D., 2002. Geotermična slika Slovenije - razširjena baza podatkov in izboljšane geotermične karte. Geothermal pattern of Slovenia-enlarged data base and improved geothermal maps. Geologija 45/2, 519-524. doi:10.5474/geologija.2002.058

RAJVER D., PRESTOR J., LAPANJE A., PESTOTNIK S., JANŽA M., 2012a. GEOTERMALNI VIRI SLOVENIJE – prikaz treh tem: osnutek podatkovne baze geotermalnih vrtin in njihove izrabe, geotermične karte za globine od 100 do 5000 m, razdelitev Slovenije glede virov geotermične energije po dosegljivosti in geološkem zagotovilu. V: Senegačnik, A. (ur.): Bilten mineralne surovine v letu 2011. Ljubljana, Geološki zavod Slovenije: 136-145.

RAJVER, D., LAPANJE, A., RMAN, N., 2012b. Možnosti proizvodnje elektrike iz geotermalne energije v Sloveniji v naslednjem desetletju. Geologija 55/1, 117-140.

RAJVER D., PESTOTNIK S., PRESTOR J., LAPANJE A., RMAN N., JANŽA M., 2013a: Geotermalni viri Slovenije: Bilanca rabe geotermalne energije v Sloveniji v letu 2012, Možnosti uporabe sistemov geotermalnih toplotnih črpalk v Sloveniji, geotermične karte Slovenije – pričakovane globine do izoterm 90 °C in 150 °C. V: Senegačnik, A. (ur.): Bilten mineralne surovine v letu 2012. Ljubljana, Geološki zavod Slovenije: 165-175.

RAJVER D., RMAN N., LAPANJE A., PRESTOR J., 2013b: Geotermalni viri Slovenije: Bilanca rabe geotermalne energije v Sloveniji v letu 2015. V: Senegačnik, A. (ur.): Bilten mineralne surovine v letu 2012. Ljubljana, Geološki zavod Slovenije: 137-147.

REČNIK, A. 2007. *Nahajališča mineralov v Sloveniji*. Ljubljana: Institut »Jožef Stefan«, Odsek za nanostrukture in materiale, 384 pp.

ŠTRUCL, I. 1984-1989. *Metalogenetska problematika kovinskih nahajališč v metamorfnih kameninah na Kobanskem in Pohorju.* Ravne na Koroškem: ECM Inštitut za gospodarski in socialni razvoj. Archieve reports from 1984 to 1989.

ŠTRUCL, I. and KLUGE, R.1991. Zur metallogenetischen Problematik der Erzvorkommen in den altpaläozoischen metamorphen Gesteinsserien. = Metalogenetska problematika železovih nahajališč v staropaleozojskih metamorfnih kameninah. *Geologija*, let. 34, 305-335.

TRAJANOVA, M. 2013: Starost pohorskega magmatizma; nov pogled na nastanek pohorskega tektonskega bloka (Age of the Pohorje magmatism; new view on the origin of the Pohorje tectonic block). PhD thesis, 183 pp., Univ. Ljubljana.

TRAJANOVA, M. and ŽORŽ, Z. 2013. Opuščeni rudnik Remšnik z ramsbeckitom in namuwitom(?). *Geologija,* let. 56, št.1, 57-72, doi:10.5474/geologija.2013.005.

ZUPANČIČ, N. 1994a. Petrološke in geokemične značilnosti pohorskih magmatskih kamnin: doktorska disertacija. Ljubljana, 197 pp.

ZUPANČIČ, N. 1994b. Petrografske značilnosti in klasifikacija pohorskih magmatskih kamnin. *Rud. met. zb*. 41, 101-112.

ZUPANČIČ, N. 1994c. Geokemične značilnosti in nastanek pohorskih magmatskih kamnin. *Rud. met. zb*. 41, 113-128.

ZUPANČIČ, N. 1996a. Minerali pohorskega magmatskega masiva. *Geologija*, let. 37, 271-295.

ZUPANČIČ, N. 1996b. Uporaba statističnih metod pri interpretaciji podatkov o geokemični sestavi pohorskih magmatskih kamnin. Rud. met. zb., let. 43, 171-177.

ŽORŽ, Z., PODGORŠEK, V., REČNIK, A. and MIOČ, P. 1999. Minerali Pohorja in Kobanskega. Published by the author, Radlje ob Dravi.

Annexes

Table 1

Prospective CHPM areas

Spain ICOG							
Number	**Type of the selected area(s) (type "A" or type "B")**	**Depth(s) of the metal enrichment(s) (m)**	**Temperature /at these depths/ (°C)**	**Description of the metal enrichment(s)**			
				degree of the mineralization(s) (% or ppm)	***type of the mineralization(s)[1]***	***element(s)***	***area delineation(s)[2]***
***1*- Mazarrón, Murcia (South-East of Spain)**	B	100	50	300 ppm Pb, 309 ppm Zn, 70 ppm Cu, 4547 ppm Ba.	Ephi-thermal	Pb-Zn-Cu-Fe sulphides. Pb-SbCu sulphosalts. native silver,	X 48510.02 Y4162340.78
***2*- Tenerife**	A	No mineralization	No mineralization	No mineralization	No mineralization	No mineralization	No mineralization

[1] Like skarn, porphy, etc.

[2] There are 3 options for the indication of the area delineation: a. coordinates (latitude, longitude) of 1 point; b. coordinates (latitude, longitude) of 1 points and radius (m); c. coordinates (latitude, longitude) of more points.

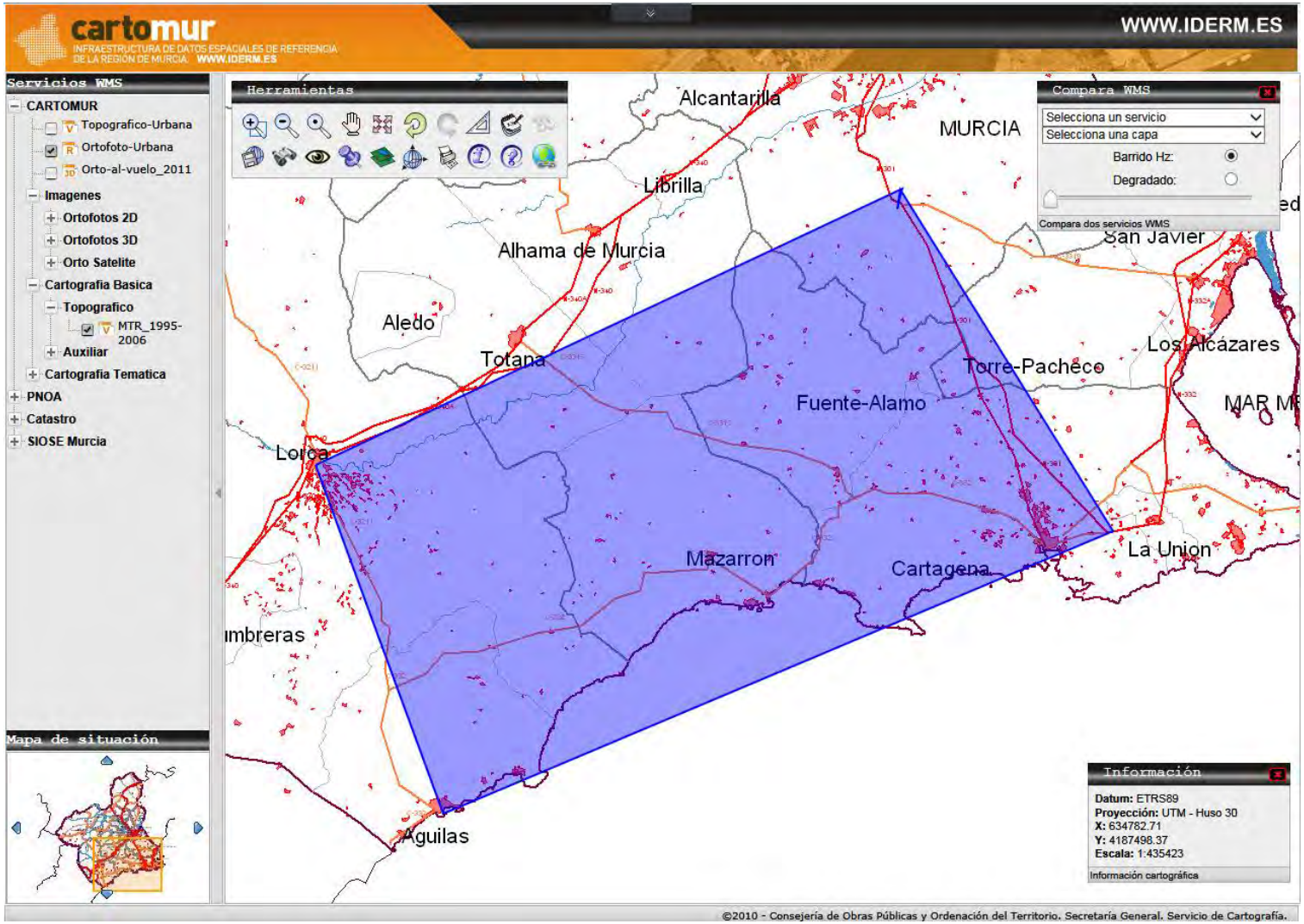
cartomur
INFRAESTRUCTURA DE DATOS ESPACIALES DE REFERENCIA DE LA REGIÓN DE MURCIA. WWW.IDERM.ES
WWW.IDERM.ES
Servicios WMS
CARTOMUR
Topografico-Urbana
Ortofoto-Urbana
Orto-al-vuelo_2011
Imagenes
Ortofotos 2D
Ortofotos 3D
Orto Satelite
Cartografia Basica
Topografico
MTR_1995-2006
Auxiliar
Cartografia Tematica
PNOA
Catastro
SIOSE Murcia
Mapa de situación
Herramientas
Compara WMS
Selecciona un servicio
Selecciona una capa
Barrido Hz:
Degradado:
Compara dos servicios WMS
Información
Datum: ETRS89
Proyección: UTM - Huso 30
X: 634782.71
Y: 4187498.37
Escala: 1:435423
Información cartográfica
Alcantarilla
MURCIA
Librilla
Alhama de Murcia
San Javier
Aledo
Totana
Los Alcázares
Torre-Pacheco
Fuente-Alamo
Lorca
Mazarron
Cartagena
La Union
Águilas
©2010 - Consejería de Obras Públicas y Ordenación del Territorio. Secretaría General. Servicio de Cartografía.

Evaluation of the basic characteristics of prospective CHPM areas

ICOG

Spain

AREA 1 – Mazarrón, Murcia (South-East of Spain)

AREA 2 - Tenerife, Canary Island

1. **Geology of the prospective area**

Requested information on:

- ✓ local geology (in regional context)
- ✓ CHPM target formation
- ✓ list of available cross sections, geological maps, geochemical results, lithological information

Notes: briefly summarized, referenced to more detailed studies.

AREA 1) Mazarrón, Murcia (South-East of Spain): Local geology is part of the Eastern area of Baetic Range that was generated during Alpine Orogenic. The CHPM target formation is included into the inner zones that during the Mesozoic and Cenozoic belonged to the Mesomediterranean microplate. The territory is composed of three different complexes: the lower, called Nevado-Filábride complex is composed only of metamorphic rocks like gneiss, schists, quarzites…dated between Precambric and lower Triasic. Next rocks from Alpujárride Complex, belonging to the Paleozoic-Triasic period, are mainly metamorphic as well but it has purple phillites and sedimentary rocks, like dolomites and limestones at the end of the period. Finally, the Maláguide complex is composed by sedimentary rocks belonging to Paleozoic to Eocene period. The materials of inner zones were affected by pre-alpine strains while the first post- Variscan structures were formed in lower Cretaceus period. During lower and mid Miocene overthrusting and folded stages were insensitive. Finally during Quaternary, started a compressive tectonic that it continues in our period and it responsible of several earthquakes.

AREA 2- Tenerife, Canary Island: The island is a volcanic building that rises up from the bottom of the ocean, more than 3000 metres deeper. It started to build 10-15 millions of years ago for the accumulation of lavic materials. The rise of the magma is produced by several tectonic activity periods through faults and fractures that exists in the oceanic bottom, during the Alpine Orogeny due to the African plate movement. In the first formation stage, during those years, we can find basaltic rocks, pillow, the second stage is a calm period with no eruptions during one million of years, where the erosion transform all the previous structures. Finally, the volcanic activity started again, the third stage was coming and basaltic rocks of fisure type were deposit in the stratigrafic sequence.

List of cross sections, geological maps, geochemical results are in the list of references.

2. Geophysics of the prospective area

Requested information:

- ✓ previous geophysical measurements (in CHPM relevance)
- ✓ geophysical results that can be used for locating/defining the deep metal enrichment
- ✓ list of available geophysical maps, cross sections, logs, other measurements

There is no public geophysical measurements in these areas.

3. Deep metal enrichment

Requested information:

- ✓ (expected) metal enrichment based on available geophysical, geological and drill data, samples information, geochemistry

There is no metal enrichment in Tenerife area. In Mazarrón exists the Zn-Pb-(Ag) epithermal Mineralization. Neogene volcanism in Mazarron basin is linked to the metallic mineral deposits. The fractures have allowed the circulation of hydrothermal solutions and empty spaces for the mineral deposits. Those deposits are in limestones and dolomite rocks.

There no public information about geophysical or drill data.

4. Integrated 3D- 4D model

Requested information:

- ✓ existing 3D-4D models of the target area and the deep metal enrichment
- ✓ if no 3D-4D models exist, collect the following necessary data: geological setting, mineralization, fluid flow models, stress field determination

Notes: e.g. openly available datasets, models.

No any public integrated 3D- 4D models available in two areas.

5. **EGS potential**

Requested information:

- ✓ EGS potential (heat & energy) of the area
- ✓ geothermal characteristics (temperature gradient, heat flux, stress field, water availability, EGS geology)
- ✓ presence/indication of deep fluids/brines, fracture system, crustal permeability

There is no public data about the potential EGS in Mazarrón and Canary Islands. Neither about the geothermal characteristics.

List of references

http://info.igme.es/cartografiadigital/geologica/mapa.aspx?parent=../geologica/geologiaregional.aspx&Id=7&language=es
http://www.igme.es/geotermia/Ficheros%20PDF/conclusiones.pdf
http://www.igme.es/geotermia/presentacion2.htm
https://www.researchgate.net/publication/274409946_The_Zn-Pb-Ag_epithermal_mineralization_of_Mazarron_Spain_A_preliminary_isotope_study
http://info.igme.es/cartografia/regionales/pdf/MapaGeoMurcia_200.pdf
http://www.atlasdemurcia.com/index.php/secciones/3/la-geologia/1/
http://info.igme.es/cartografiadigital/datos/Regionales/pdfs/MapaGeoMurcia_200.pdf
http://info.igme.es/cartografiadigital/datos/mgd50/memorias/Memoria955.pdf
http://info.igme.es/cartografiadigital/datos/mgd50/memorias/Memoria976.pdf
http://www.igme.es/actividadesIGME/lineas/CartoGeo/geoquimica/geoquimicaEsp.htm#resul
http://www.igme.es/actividadesIGME/lineas/CartoGeo/geoquimica/MapaMuestras/Default.aspx
http://www.igme.es/geotermia/Ficheros%20PDF/Manual_Geotermia_2,5.pdf
http://www.igme.es/geotermia/IGMEEstudiosgenerales.htm
http://www.igme.es/geotermia/Ficheros%20PDF/3%20Bajamedia%20entalp%EDa.pdf
http://www.igme.es/geotermia/potencial%20geot%E9rmic.htm
http://www.igme.es/geotermia/desarrollo%20geot%E9rmico.htm
http://diposit.ub.edu/dspace/bitstream/2445/61175/4/IIR_3de10.pdf
http://www.gobiernodecanarias.org/geotecnia/Canarias_clasif_roc_Rguez-Losada.pdf
http://info.igme.es/cartografiadigital/geologica/Magna50Hoja.aspx?Id=1105A
http://info.igme.es/cartografia/geotecnico200.asp?hoja=91
http://diposit.ub.edu/dspace/bitstream/2445/61175/4/IIR_3de10.pdf
http://info.igme.es/cartografiadigital/datos/mgd50/memorias/Memoria976.pdf
https://www.researchgate.net/publication/265244355_Estudio_de_estabilidad_en_depositos_de_lodos_del_Distrito_Minero_de_Mazarron_SE_Espana_Riesgos_potenciales_sobre_la_Rambla_de_Las_Moreras
https://www.researchgate.net/publication/36720723_Los_yacimientos_Zn_Pb_Ag-Fe_del_distrito_minero_de_la_La_Union-Cartagena_Betica_Oriental

Annexes

Evaluation of CHPM characteristics of prospective CHPM areas

Name of the National Association (ICOG)- TENERIFE AREA

1. **CHPM operational characteristics - Information for CHPM technological elements**

Requested information:

✓ please fill in the table below with the requested data for the CHPM technology elements

Underground heat exchanger (deep metal enrichment + potential geothermal reservoir)	
Extension of the metal enrichments *(volumetric interpretation)*	No data.
Expected type of the reservoir and porosity/permeability *(fractured, porous, etc)*	No data.
Mineralization *(type and enriched metals)*	There are no mineralization.

Production and injection wells	
Depth of potential wells (m)	No data.

Electrolytic metal recovery and gas diffusion electro- precipitation	
Potential target metals to be recovered	No data.

Power plant (heat exchanger)	
Local heat and electricity demand *(industrial, municipal, agricultural, etc.)*	No data.

Salt gradient power generation	
Salinity of expected geothermal brine	No data
Fresh water supply from the surface *(water sources)*	There are no representative water surfaces in the island, but groundwater is available in the island. 500 galleries has been opened until 1500 km. For that reason phreatic surface has retreated 2500 m.

2. **CHPM operational characteristics - Environmental, social and political background**

Requested information:

- ✓ toleration to gaseous and solids emissions, water and noise pollution,
- ✓ local competition to land and water availability
- ✓ public acceptance
- ✓ political support
- ✓ presence of supporting legislation, regulatory framework

Notes: all of above refers to the selected area and its surroundings.

We do not have any notes about.

3. **Financial aspects**

Requested information:

- ✓ list of potential local stakeholders (community, political, companies)

IGME
consejo insular de aguas de Tenerife
Aguas de Murcia
Empresa Mixta de Aguas de Santa Cruz de Tenerife
Agencia Insular de energía de Tenerife

List of references

https://www.aguastenerife.org/index.php?option=com_content&view=article&id=115&Itemid=280
https://ciatf.maps.arcgis.com/apps/webappviewer/index.html?id=31e713a5f7024cb3b8d3581b0e49cdc3
https://www.adaptecca.es/sites/default/files/documentos/braojos_etal.pdf
http://aguas.igme.es/igme/publica/libro44/pdf/lib44/12_1.pdf
http://oa.upm.es/19965/1/Libro_digital_AGUAS.pdf

Annexes

Evaluation of CHPM characteristics of prospective CHPM areas

Name of the National Association (ICOG)- MAZARRON AREA

1. **CHPM operational characteristics - Information for CHPM technological elements**

Requested information:

✓ please fill in the table below with the requested data for the CHPM technology elements

Underground heat exchanger (deep metal enrichment + potential geothermal reservoir)	
Extension of the metal enrichments *(volumetric interpretation)*	No data.
Expected type of the reservoir and porosity/permeability *(fractured, porous, etc)*	No data.
Mineralization *(type and enriched metals)*	In Mazarrón exists the Zn-Pb-(Ag) epithermal Mineralization. Neogene volcanism in Mazarron basin is linked to the metallic mineral deposits. The fractures have allowed the circulation of hydrothermal solutions and empty spaces for the mineral deposits. Those deposits are in limestones and dolomite rocks.

Production and injection wells	
Depth of potential wells (m)	50m.

Electrolytic metal recovery and gas diffusion electro- precipitation	
Potential target metals to be recovered	No data.

Power plant (heat exchanger)	
Local heat and electricity demand *(industrial, municipal, agricultural, etc.)*	No data.

Salt gradient power generation	
Salinity of expected geothermal brine	No data
Fresh water supply from the surface *(water sources)*	There are several aquifers (20) belonging to Segura basin in Mazarron Area. (nº3 list references).

2. **CHPM operational characteristics - Environmental, social and political background**

Requested information:

- ✓ toleration to gaseous and solids emissions, water and noise pollution,
- ✓ local competition to land and water availability
- ✓ public acceptance
- ✓ political support
- ✓ presence of supporting legislation, regulatory framework

Notes: all of above refers to the selected area and its surroundings.

We do not have any notes about.

3. **Financial aspects**

Requested information:

- ✓ list of potential local stakeholders (community, political, companies)

IGME
Confederación Hidrográfica del Segura
Aguas de Murcia
Concejalía de medio ambiente de Murcia
Agencia Local de Energía de Murcia
Dirección General de Energía y Actividad Industrial y Minera

List of references

1-http://info.igme.es/SidPDF/148000/4/148004_0000003.pdf
2-http://aguas.igme.es/igme/publica/lib112/pdf/lib112/in_02.pdf
3-ftp://ftp.chsegura.es/oph/phcsegura/borrador/anejo12docs/FichaSub_070_058_Mazarron.pdf
4- https://www.chsegura.es/export/descargas/cuenca/sequias/pes/docsdescarga/LAMINA_5.pdf

Annexes

Table 1

Prospective CHPM areas

RBINS Sweden							
Number	**Type of the selected area(s) (type "A" or type "B")**	**Depth(s) of the metal enrichment(s) (m)**	**Temperature /at these depths/ (°C)**	**Description of the metal enrichment(s)**			
				degree of the mineralization(s) (% or ppm)	***type of the mineralization(s)[1]***	***element(s)***	***area delineation(s)[2]***
1 Zinkgruvan	B	i) 1125m	i) Supposed 20-25 from normal geothermal gradient. Further studies are necessary	Skarn : Cu 3 %, Zn 0.4 %, Ag 30 g/t. SEDEX: Zn 9 %, Pb 3.5 %, Ag 75 g/t	Skarn (Cu) i) SEDEX (Zn)	i) Copper, zinc, lead, silver	Lat: N8.81528 Long: E15.10250 Radius 10km
2 Yxsjoberg	B	600 m	Supposed 15-20 from normal geothermal gradient. Further studies are necessary	Cu 0.4 %, WO3 0.4 %, CaF2 <5 %	Skarn	Copper, tungsten	Lat: N60.05 Long: E14.76667 Radius 5 km

[1] Like skarn, porphy, etc.

[2] There are 3 options for the indication of the area delineation: a. coordinates (latitude, longitude) of 1 point; b. coordinates (latitude, longitude) of 1 points and radius (m); c. coordinates (latitude, longitude) of more points.

3 Renstrom	B	i) 1450 m	i) Supposed 30 from normal geothermal gradient. Further studies are necessary	i) Not available	i) VMS	i) zinc, copper, lead, gold and silver	Lat: N64.92321 Long: E20.09288 Radius 6 km
4 Kirunavaara	B	1540 m	Supposed 25 from normal geothermal gradient. Further studies are necessary	Fe 60-68 %, P 0.04-0.32 %	Orthomagmatic-hydrothermal		Lat: N67.83743 Long: E20.18597 Radius 5 km

Table 1

Prospective CHPM areas

CHGEOL Switzerland							
Number	**Type of the selected area(s) (type "A" or type "B")**	**Depth(s) of the metal enrichment(s) (m)**	**Temperature /at these depths/ (°C)**	**Description of the metal enrichment(s)**			
				degree of the mineralization(s) (% or ppm)	***type of the mineralization(s)[1]***	***element(s)***	***area delineation(s)[2]***
1	There are no prospective areas in Switzerland						

CHPM2030 – Summary of the Switzerland data

Generally speaking the situation in Switzerland is the following:

- Switzerland is a country "rich in poor mines", i.e. mineralizations have been identified, but there were never in sufficient concentration and quantity for large scale industrial exploitation. It is unclear if such mineralized rock volume could ever be exploited economically using leaching techniques.
- The deep underground in Switzerland is poorly explored. Not so many deep borehole are available. Very few in the alps where most of the signs of mineralization are located. This makes site selection very difficult.

[1] Like skarn, porphy, etc.

[2] There are 3 options for the indication of the area delineation: a. coordinates (latitude, longitude) of 1 point; b. coordinates (latitude, longitude) of 1 points and radius (m); c. coordinates (latitude, longitude) of more points.

A compilation from swisstopo (map.geo.admin.ch) is presented in the attached file. This map presents an overlap of the location of deep geothermal project, mineralizations, deep wells and heat flux. One cannot exclude possible opportunities for CHPM as for example targeting basement rock in the Rhone valley area. There is for example a geothermal project in Lavey currently targeting geothermal resources at 3 km depth. More in-depth study would be required for assessing properly the CHPM potential of such project.

Additional information are available from the following compilations:

- ProMine Mineral Databases: New Tools to Assess Primary and Secondary Mineral Resources in Europe https://www.springer.com/cda/content/document/cda_downloaddocument/9783319174273-c2.pdf?SGWID=0-0-45-1519226-p177326553

As stated above, it shows that there is no metallogenic province in Switzerland and the potential is low. Historically, this is confirmed by the fact that Switzerland has never had any metallic industry in the past. We have all sorts of occurrences but none has ever been commercially sustainable.

- Properties of geothermal fluids in Switzerland: A new interactive database http://doc.rero.ch/record/13041/files/Sonney_Romain_-_Properties_of_geothermal_fluids_in_Switzerland_20091125.pdf https://www.researchgate.net/publication/228835496_BDFGeotherm_the_Database_of_Geothermal_Fluids_in_Switzerland

There are a few drillholes with water reaching 40°C but there is no indication of a metallic enrichment.

Based on these data, this is not possible to propose any prospective area.

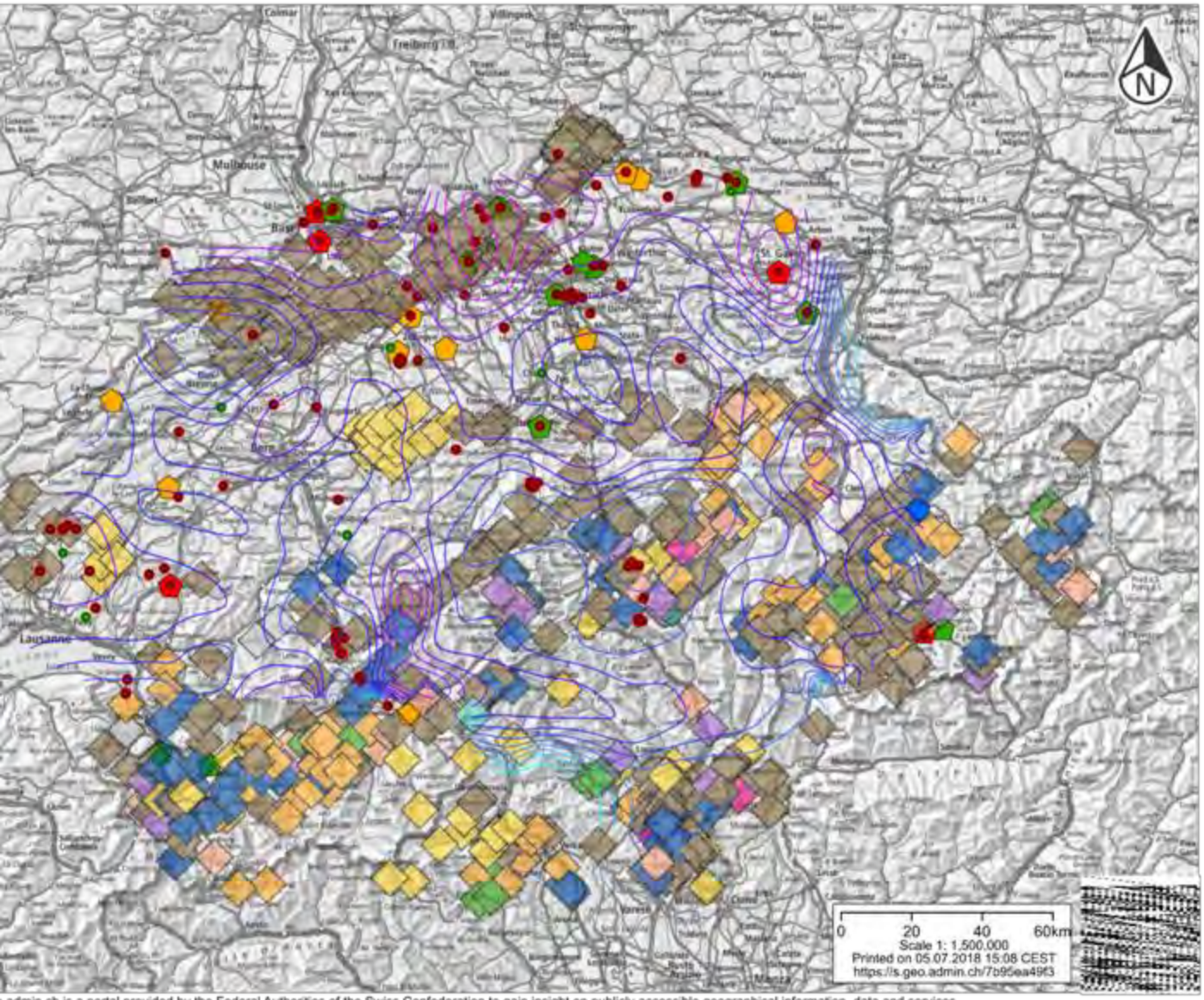

Table 1

Prospective CHPM areas

RBINS UK							
Number	**Type of the selected area(s) (type "A" or type "B")**	**Depth(s) of the metal enrichment(s) (m)**	**Temperature /at these depths/ (°C)**	**Description of the metal enrichment(s)**			
				degree of the mineralization(s) (% or ppm)	***type of the mineralization(s)[1]***	***element(s)***	***area delineation(s)[2]***
1 Dartmoor	A	i) Few hundred meters-1000m	i) At 5 Km 185°C	Not available	i) Granite-related	i) Co, Sb, Mn, Cu, Zn, As, Pb, Fe, Ce, Mg, Al, Si, S, K	Lat: N50.57 Long: -3.90 Radius 25km
2 Bodmin	A	Few hundred meters-1000m	At 5 Km 200°C	Not available	Granite-related	Co, Sb, Mn, Cu, Zn, As, Pb, Fe, Ce, Mg, Al, Si, S, K	Lat: N50.55 Long: -4.57 Radius 15km
3 St Austell	A	Few hundred meters-1000m	At 5 Km 221°C	Not available	Greisen (spaced quartz-tourmaline veins up to 0.1 m wide that host wolframite, cassiterite,	Co, Sb, Mn, Cu, Zn, As, Pb, Fe, Ce, Mg, Al, Si, S, K	Lat: N50.37 Long: -4.83 Radius 5km

[1] Like skarn, porphy, etc.

[2] There are 3 options for the indication of the area delineation: a. coordinates (latitude, longitude) of 1 point; b. coordinates (latitude, longitude) of 1 points and radius (m); c. coordinates (latitude, longitude) of more points.

					stannite, arsenopyrite and other sulphides)		
4 Land's End	A	Few hundred meters-1000m	At 5 Km 206°C	Not available	Granite-related	Co, Sb, Mn, Cu, Zn, As, Pb, Fe, Ce, Mg, Al, Si, S, K	Lat: N50.10 Long: -5.68 Radius 20km

Prospective CHPM areas

EA UAG Ukraine							
Number	**Type of the selected area(s) (type "A" or type "B")**	**Depth(s) of the metal enrichment(s) (m)**	**Temperature /at these depths/ (°C)**	**Description of the metal enrichment(s)**			
				degree of the mineralization(s) (% or ppm)	***type of the mineralization(s)[1]***	***element(s)***	***area delineation(s)[2]***
1 Transcarpathian	A	floating	100-150°C at depth 3000 m	not determined	hydrothermal (non-partitioned), hydrothermal-metasomatic, endogenous	Pb, Zn, Ag, Au, Hg	Lot - 48° 20', long – 22° 30', average radius radius – 30 000 m

[1] Like skarn, porphy, etc.

[2] There are 3 options for the indication of the area delineation: a. coordinates (latitude, longitude) of 1 point; b. coordinates (latitude, longitude) of 1 points and radius (m); c. coordinates (latitude, longitude) of more points.

Evaluation of the basic characteristics of prospective CHPM areas

UAG

Ukraine

AREA 1 – Transcarpathian

1. Geology of the prospective area

Requested information on:

- ✓ local geology (in regional context)
- ✓ CHPM target formation
- ✓ list of available cross sections, geological maps, geochemical results, lithological information

Notes: briefly summarized, referenced to more detailed studies.

Local geology in regional context is due to geotectonic position within Transcarpathian trough of Carpathian folded structures. The territory of the area is composed of the rocks of two tectonic floors. The lower one comprises basement of Trans-Carpathian Trough and Folded Carpathians. In the Trough basement there are mainly developed extensively dislocated sedimentary, volcanogenic and metamorphic rocks of Paleozoic and Meso-Cenozoic (up to Oligocene inclusively). The Folded Carpathians are composed of Meso-Cenozoic carbonateterrigenous and terrigenous formations (flysch mainly) which constitute some tectonic-facial zones. These ones are extensively dislocated and do form the batch of nappe structures. Coeval sediments of these structures often display diverse facial appearance and by these reasons are subdivided into the individual stratigraphic units (suites, sequences – see stratigraphic columns). The upper tectonic floor sediments fill up the Trans-Carpathian Internal Trough. These are Neogene-Quaternary sedimentary, volcanogenic and volcano-mictic, coaliferous in places, molassa rocks of mainly horizontal laying.

The CHPM target formation in included into Carpathian and Trans-Carpathian zones of Carpathian metallogenic province.

Cross sections, geological maps, geochemical results, lithological information are available.

2. Geophysics of the prospective area

Requested information:

- ✓ previous geophysical measurements (in CHPM relevance)
- ✓ geophysical results that can be used for locating/defining the deep metal enrichment
- ✓ list of available geophysical maps, cross sections, logs, other measurements

All complex of geophysical data by area is available in the corresponding survey and search reports. This includes gravimetric, magnetometric maps, geophysical studies of wells, etc. in various scales and detail. The list of reports is given below.

3. **Deep metal enrichment**

Requested information:

- ✓ **(**expected) metal enrichment based on available geophysical, geological and drill data, samples information, geochemistry

Deep metal enrichment by drill data, in the main, is 500-650 m for Pb, Zn, 20-220 m for Hg, 90-800 m for Au, 300-700 m for Ag

4. **Integrated 3D- 4D model**

Requested information:

- ✓ existing 3D-4D models of the target area and the deep metal enrichment
- ✓ if no 3D-4D models exist, collect the following necessary data: geological setting, mineralization, fluid flow models, stress field determination

Notes: e.g. openly available datasets, models.

No any integrated 3D- 4D models available. Mineralization of ores is associated with hydrothermal fluid vein bodies involved morphology associated with Miocene volcanism.

5. **EGS potential**

Requested information:

- ✓ EGS potential (heat & energy) of the area
- ✓ geothermal characteristics (temperature gradient, heat flux, stress field, water availability, EGS geology)
- ✓ presence/indication of deep fluids/brines, fracture system, crustal permeability

Temperature according to maps of geothermal resources within 100-150°C at depth 3000 m. Hydrothermal mineralization always corresponds with fracture system & crustal permeability.

List of references

1. MINISTRY OF ECOLOGY AND NATURAL RESOURCES OF UKRAINE, DEPARTMENT OF GEOLOGY AND SUBSURFACE USE, SGE “ZAKHIDUKRGEOLOGIYA”, STATE GEOLOGICAL MAP OF UKRAINE, Scale 1:200 000, CARPATHIAN SERIES, MAP SHEETS, M-34-XXIX (Snina), M-34-XXXV (Uzhgorod), L-34-V (Satu Mare), Kyiv – 2003
2. Temperature distribution maps and the density of the heat flow subsoil at a depth of 3000 m in Ukraine
3. АСПЕКТИ ОЦІНКИ ТА ОСВОЄННЯ ГЕОТЕРМАЛЬНИХ РЕСУРСІВ УКРАЇНИ, Ю.П. Стародуб, В.М. Карпенко, В.М. Стасенко, М.С. Нікорюк, О.В. Карпенко, В.Л. Рибчак, Геодинаміка 2(13)/2012, Lviv Polytechnic National University Institutional Repository
4. СУЧАСНІ НАПРЯМИ РОЗВИТКУ ГЕОТЕРМАЛЬНОЇ ЕНЕРГЕТИКИ, Ю. П. Морозов, д-р техн. наук, завідувач відділу (Інститут відновлюваної енергетики НАН України), Київ, Україна,
5. Пошуково-оціночні роботи на Берегівському золото-поліметалічному родовищі, 1992-1994 р.р.ДРАЧУК В.П. 1994
6. Разработка новых методик крупномасштабного и локального прогноза эндогенных месторождений путем выделения основных рудоконтролирующих факторов, изучения их пространственных, генетических и возрастных связей с промышленным оруденением, 1991-93 г.г.ШИРКУНОВ В.В.1993
7. Отчет о научно-исследовательской работе: Накопление и систематизация геологической информации для технологического обоснования ускоренного освоения месторождений руд цветных и редких металлов на Украине.Римарчук Б.И.1993
8. Закономірності розміщення зруденіння та прогнозна оцінка рудоносності Берегівського рудного поля.Пеньковська Б.В.1993
9. Обобщение и прогнозная разбраковка литохимических аномалий Закарпатья, 1987-1993 г.г.Галахов І.Н.1993
10. Звіт про результати пошуків та оцінка рудоносності навколожерлових частин вулканічних апаратів в межах Берегівського рудного поля за 1988-1993 рр.Верхогляд В.М.1993
11. Магматизм Закарпатского внутреннего прогиба и связанная с магматизмом рудоносность.Зайцева В.Н.1991
12. Комплексная металлогеническая карта Закарпатской области масштаба 1:100000.Галахов И.Н.1988
13. Отчет о поисках золотых и серебряных руд на Квасовском и Беганьском участках, проведенных в 1985-1988 гг. (Закарпатская обл.).Роздобудько М.В.1988
14. Отчет по крупномасштабному глубинному геологическому картированию в пределах листов М-34-141-Б; М-34-142-А,В; М-34-142-Б-в,г (Береговский рудный район) за 1981-1985 гг.Приходько М.Г.1985
15. Отчет о результатах поисково-оценочных работ на свинец и цинк на северном фланге и глубоких горизонтах 6-рудной зоны, 41-й, 43-й рудных зон Западного участка Береговского месторождения Закарпатской области УССР за 1980-1983 гг.ШКЛЯНКА В.М.1983

Annexes

-

Evaluation of CHPM characteristics of prospective CHPM areas

EA UAG (LTP) Ukraine

1. **CHPM operational characteristics - Information for CHPM technological elements**
   Requested information:

✓ please fill in the table below with the requested data for the CHPM technology elements

Underground heat exchanger (deep metal enrichment + potential geothermal reservoir)	
Extension of the metal enrichments *(volumetric interpretation)*	Deep metal enrichment by drill data, in the main, is 500-650 m for Pb, Zn, 20-220 m for Hg, 90-800 m for Au, 300-700 m for Ag
Expected type of the reservoir and porosity/permeability *(fractured, porous, etc)*	Local inhomogeneous volcanic-plutonium ore-control structure, control of radial and ring faults complicated by increased fracturing.
Mineralization *(type and enriched metals)*	Alunite-kaolin-gold-polymetallic mineralization, enriched metals – Pb, Zn, Hg, Au, Ag

Production and injection wells	
Depth of potential wells (m)	500-650 m for Pb, Zn, 20-220 m for Hg, 90-800 m for Au, 300-700 m for Ag

Electrolytic metal recovery and gas diffusion electro- precipitation	
Potential target metals to be recovered	Al, Fe, Na, K

Power plant (heat exchanger)	
Local heat and electricity demand *(industrial, municipal, agricultural, etc.)*	Industrial, municipal, agricultural, recreational etc.

Salt gradient power generation	
Salinity of expected geothermal brine	It requires study
Fresh water supply from the surface *(water sources)*	Rivers Tisa, Latoritsa, Borzhava, Tereblya and their tributaries, groundwater by hydrogeological wells

2. **CHPM operational characteristics - Environmental, social and political background**

Requested information:

- ✓ toleration to gaseous and solids emissions, water and noise pollution,
- ✓ local competition to land and water availability
- ✓ public acceptance
- ✓ political support
- ✓ presence of supporting legislation, regulatory framework

Notes: all of above refers to the selected area and its surroundings.

CHPM operational characteristics governed by the legislation of Ukraine on the subsoil use, the environment, etc.

Before starting work, it is necessary to obtain permits: mining license, land allotment, mining allotment, etc.

Public acceptance requires public hearings, other social events.

Political support contrary to the legislation of Ukraine - Everyone can be mining.

3. **Financial aspects**

Requested information:

- ✓ list of potential local stakeholders (community, political, companies)

Potential local stakeholders unknown

List of references

1. MINISTRY OF ECOLOGY AND NATURAL RESOURCES OF UKRAINE, DEPARTMENT OF GEOLOGY AND SUBSURFACE USE, SGE "ZAKHIDUKRGEOLOGIYA", STATE GEOLOGICAL MAP OF UKRAINE, Scale 1:200 000, CARPATHIAN SERIES, MAP SHEETS, M-34-XXIX (Snina), M-34-XXXV (Uzhgorod), L-34-V (Satu Mare), Kyiv – 2003
2. Пошуково-оціночні роботи на Берегівському золото-поліметалічному родовищі, 1992-1994 р.р.ДРАЧУК В.П. 1994
3. 10. Звіт про результати пошуків та оцінка рудоносності навколожерлових частин вулканічних апаратів в межах Берегівського рудного поля за 1988-1993 рр.Верхогляд В.М.1993
4. Магматизм Закарпатского внутреннего прогиба и связанная с магматизмом рудоносность.Зайцева В.Н.1991
5. Комплексная металлогеническая карта Закарпатской области масштаба 1:100000.Галахов И.Н.1988

Annexes